

# **ADVANCES IN PULMONARY DISEASES: CELLULAR PATHOLOGY, MOLECULAR TARGETS, NOVEL DIAGNOSIS AND THERAPY**

EDITED BY: Huahao Shen, Dianhua Jiang, Kewu Huang, Min Zhang,  
Kefang Lai, Wen Li and Zhang Qingling

PUBLISHED IN: Frontiers in Molecular Biosciences, Frontiers in Pharmacology  
and Frontiers in Medicine



# frontiers

## Frontiers eBook Copyright Statement

The copyright in the text of individual articles in this eBook is the property of their respective authors or their respective institutions or funders. The copyright in graphics and images within each article may be subject to copyright of other parties. In both cases this is subject to a license granted to Frontiers.

The compilation of articles constituting this eBook is the property of Frontiers.

Each article within this eBook, and the eBook itself, are published under the most recent version of the Creative Commons CC-BY licence.

The version current at the date of publication of this eBook is CC-BY 4.0. If the CC-BY licence is updated, the licence granted by Frontiers is automatically updated to the new version.

When exercising any right under the CC-BY licence, Frontiers must be attributed as the original publisher of the article or eBook, as applicable.

Authors have the responsibility of ensuring that any graphics or other materials which are the property of others may be included in the CC-BY licence, but this should be checked before relying on the CC-BY licence to reproduce those materials. Any copyright notices relating to those materials must be complied with.

Copyright and source acknowledgement notices may not be removed and must be displayed in any copy, derivative work or partial copy which includes the elements in question.

All copyright, and all rights therein, are protected by national and international copyright laws. The above represents a summary only. For further information please read Frontiers' Conditions for Website Use and Copyright Statement, and the applicable CC-BY licence.

ISSN 1664-8714

ISBN 978-2-88974-778-8

DOI 10.3389/978-2-88974-778-8

## About Frontiers

Frontiers is more than just an open-access publisher of scholarly articles: it is a pioneering approach to the world of academia, radically improving the way scholarly research is managed. The grand vision of Frontiers is a world where all people have an equal opportunity to seek, share and generate knowledge. Frontiers provides immediate and permanent online open access to all its publications, but this alone is not enough to realize our grand goals.

## Frontiers Journal Series

The Frontiers Journal Series is a multi-tier and interdisciplinary set of open-access, online journals, promising a paradigm shift from the current review, selection and dissemination processes in academic publishing. All Frontiers journals are driven by researchers for researchers; therefore, they constitute a service to the scholarly community. At the same time, the Frontiers Journal Series operates on a revolutionary invention, the tiered publishing system, initially addressing specific communities of scholars, and gradually climbing up to broader public understanding, thus serving the interests of the lay society, too.

## Dedication to Quality

Each Frontiers article is a landmark of the highest quality, thanks to genuinely collaborative interactions between authors and review editors, who include some of the world's best academicians. Research must be certified by peers before entering a stream of knowledge that may eventually reach the public - and shape society; therefore, Frontiers only applies the most rigorous and unbiased reviews. Frontiers revolutionizes research publishing by freely delivering the most outstanding research, evaluated with no bias from both the academic and social point of view. By applying the most advanced information technologies, Frontiers is catapulting scholarly publishing into a new generation.

## What are Frontiers Research Topics?

Frontiers Research Topics are very popular trademarks of the Frontiers Journals Series: they are collections of at least ten articles, all centered on a particular subject. With their unique mix of varied contributions from Original Research to Review Articles, Frontiers Research Topics unify the most influential researchers, the latest key findings and historical advances in a hot research area! Find out more on how to host your own Frontiers Research Topic or contribute to one as an author by contacting the Frontiers Editorial Office: [frontiersin.org/about/contact](http://frontiersin.org/about/contact)



# ADVANCES IN PULMONARY DISEASES: CELLULAR PATHOLOGY, MOLECULAR TARGETS, NOVEL DIAGNOSIS AND THERAPY

Topic Editors:

**Huahao Shen**, Zhejiang University, China

**Dianhua Jiang**, Cedars Sinai Medical Center, United States

**Kewu Huang**, Capital Medical University, China

**Min Zhang**, Shanghai First People's Hospital, China

**Kefang Lai**, Guangzhou Institute of Respiratory Health, China

**Wen Li**, Zhejiang University, China

**Zhang Qingling**, Guangzhou Institute of Respiratory Health, China

**Citation:** Shen, H., Jiang, D., Huang, K., Zhang, M., Lai, K., Li, W., Qingling, Z., eds. (2022). Advances in Pulmonary Diseases: Cellular Pathology, Molecular Targets, Novel Diagnosis and Therapy. Lausanne: Frontiers Media SA.  
doi: 10.3389/978-2-88974-778-8

# Table of Contents

- 07    *Mechanisms of Pulmonary Hypertension in Acute Respiratory Distress Syndrome (ARDS)***  
Lucy Revercomb, Ankit Hanmandlu, Nancy Wareing, Bindu Akkanti and Harry Karmouty-Quintana
- 21    *Enhancing Extracellular Adenosine Levels Restores Barrier Function in Acute Lung Injury Through Expression of Focal Adhesion Proteins***  
Wei Wang, Ning-yuan Chen, Dewei Ren, Jonathan Davies, Kemly Philip, Holger K. Eltzschig, Michael R. Blackburn, Bindu Akkanti, Harry Karmouty-Quintana and Tingting Weng
- 39    *The Immune System in Transfusion-Related Acute Lung Injury Prevention and Therapy: Update and Perspective***  
Kai Guo and Shuxuan Ma
- 49    *Management and Prognosis of Interstitial Lung Disease With Lung Cancer (ILD-LC): A Real-World Cohort From Three Medical Centers in China***  
Xie Xiaohong, Wang Liqiang, Li Na, Lin Xinqing, Qin Yinyin, Liu Ming, Ouyang Ming, Han Qian, Luo Qun, Li Shiyue, Li Chunyan, Wang Xiaoqian, Yang Shuanying, Huang Wei, Liu Mei, Wang Ping and Zhou Chengzhi
- 59    *High-Flow Nasal Cannula for COVID-19 Patients: A Multicenter Retrospective Study in China***  
Jun Duan, Jia Zeng, Puyu Deng, Zhong Ni, Rongli Lu, Wenxi Xia, Guoqiang Jing, Xiaoping Su, Stephan Ehrmann, Wei Zhang and Jie Li
- 67    *Administration Timing and Efficacy of Tocilizumab in Patients With COVID-19 and Elevated IL-6***  
Pan Li, Zhengmao Lu, Qiang Li, Zhenmeng Wang, Yan Guo, Chen Cai, Shengyun Wang, Peng Liu, Xiaoping Su, Yi Huang, Yuchao Dong, Wenjuan Qiu, Yueming Ling, Lonny Yarmus, Fengming Luo, Li Zeng, Chong Bai and Wei Zhang
- 78    *Pharmacological Mechanisms Underlying the Anti-asthmatic Effects of Modified Guomin Decoction Determined by Network Pharmacology and Molecular Docking***  
Guishu Wang, Bo Zhou, Zheyi Wang, Yufeng Meng, Yaqian Liu, Xiaoqin Yao and Cuiling Feng
- 90    *Serum Cytokine Profiling Identifies Axl as a New Biomarker Candidate for Active Eosinophilic Granulomatosis With Polyangiitis***  
Jianjuan Ma, Cong Dong, Shushan Wei, Minzhi Qiu, Penghui Wu, Changxing Ou, Bomeng Zhang, Xueyan Zhang, Jie Yan, Qingling Zhang and Nanshan Zhong
- 102    *Efficacy and Safety of Combination Treatment With Apatinib and Osimertinib After Osimertinib Resistance in Epidermal Growth Factor Receptor-Mutant Non-small Cell Lung Carcinoma—A Retrospective Analysis of a Multicenter Clinical Study***  
Xue Yang, Yang Xia, Liyan Xu, Li Liang, Minglei Zhuo, Meina Wu, Tongtong An, Ziping Wang, Yuyan Wang, Jianjie Li, Jia Zhong, Hanxiao Chen, Bo Jia, Jingjing Wang and Jun Zhao

- 109 ***Pemetrexed-Platinum With or Without Bevacizumab for Chinese Chemo-Naive Advanced Lung Adenocarcinoma Patients: A Real-World Study***  
Xin Li, Jie Huang, Yao Qiu, Qianyun Zhang, Shaoyu Yang, Kan Wu, Jiaoli Wang, Limin Wang, Jian Ye, Shenglin Ma, Bing Xia and Xueqin Chen
- 117 ***Identification of the Core MicroRNAs and Potential Molecular Mechanisms in Sarcoidosis Using Bioinformatics Analysis***  
Yuan Cao, Hua Zhang, Lulu Zheng and Qiao Li
- 131 ***Comparison of Immediate and Sequential Withdrawal of a Systemic Glucocorticoid in the Treatment of Acute Exacerbations of Chronic Obstructive Pulmonary Disease: A Multicenter, Randomized, Double-Blind, Parallel-Controlled, Open-Label Study***  
Ling Zhou, Yuanyuan Fang, Wei Liu, Jianchu Zhang, Yingnan Wang, Sheng Xie, Minhua Zhong, Zhengyan Wang, Guangcai Li, Hongyan Ai, Hongrong Guo, Fanjun Zeng, Wei Xiao, Chenghong Li, Yi Hu, Yijun Tang and Huiguo Liu
- 142 ***Development and Validation of a Predictive Model for Severe COVID-19: A Case-Control Study in China***  
Zirui Meng, Minjin Wang, Zhenzhen Zhao, Yongzhao Zhou, Ying Wu, Shuo Guo, Mengjiao Li, Yanbing Zhou, Shuyu Yang, Weimin Li and Binwu Ying
- 152 ***Initial PCR Testing Negative, but Chest CT Suggesting for Viral Pneumonia Urges for Repeated Testing for COVID-19 Diagnosis***  
Lingwei Wang, Danting Zhan, Xiaodi Liu, Kai Yang, Shipin Wu, Heng Zhang, Min Yu, Yimin Zha, Weibin Huang, Lei Li, Rongchang Chen and Chen Qiu
- 156 ***An Illustrated Guide to the Imaging Evolution of COVID in Non-Epidemic Areas of Southeast China***  
Lihua Wang, Yeerfan Jiaerken, Qian Li, Peiyu Huang, Zhujiang Shen, Tongtong Zhao, Hanpeng Zheng, Wenbin Ji, Yuantong Gao, Junli Xia, Jianmin Cheng, Jianbing Ma, Jun Liu, Yongqiang Liu, Miaoguang Su, Guixiang Ruan, Jiner Shu, Dawei Ren, Zhenhua Zhao, Weigen Yao, Yunjun Yang and Minming Zhang
- 165 ***ECMO Rescues Patients With Acute Respiratory Failure Related to GPA***  
Rongjun Wan, Wenzhe Yang, Xinhua Ma, Wei Yang, Pinhua Pan, Chengping Hu, Qiong Chen, Yaou Zhou, Rongli Lu, Yimin Fang and Yuanyuan Li
- 178 ***Multi-Dimensional Display of Wang's Lymph Node Map Using Virtual Bronchoscopic Navigation System***  
Fen Lan, Yaling Yue, Hong Shen, Hui Shen, Qiyuan Wang, Xiujing Yu, Laijuan Chen, Qin Li, Kopen Wang, Qinghua Liu and Yang Xia
- 186 ***The Application of Transbronchial Lung Cryobiopsy and Uniportal and Tubeless Video-Assisted Thoracic Surgery in the Multidisciplinary Diagnosis of Interstitial Lung disease—A Real-World Prospective Study***  
Qian Han, Xiaobo Chen, Xin Xu, Weiping Qian, Gui Zhao, Mengmeng Mao, Bingpeng Guo, Shu Xia, Guilin Peng, Jianxing He, Yingying Gu, Shiyue Li and Qun Luo
- 195 ***Gremlin2 Activates Fibroblasts to Promote Pulmonary Fibrosis Through the Bone Morphogenic Protein Pathway***  
Caijuan Huan, Wangting Xu, Yaru Liu, Kexin Ruan, Yueli Shi, Hongqiang Cheng, Xue Zhang, Yuehai Ke and Jianying Zhou

- 210 Identification of Proteomic Signatures in Chronic Obstructive Pulmonary Disease Emphysematous Phenotype**  
Shuang Bai, Rui Ye, Cuihong Wang, Pengbo Sun, Di Wang, Yong Yue, Huiying Wang, Si Wu, Miao Yu, Shuhua Xi and Li Zhao
- 223 Management and Thinking on the Treatment of Cancer Patients During the COVID-19**  
Shuangyue Pan, Jiahong Jiang, Zheling Chen and Liu Yang
- 233 Deep Sequencing of T-Cell Receptors for Monitoring Peripheral CD8<sup>+</sup> T Cells in Chinese Advanced Non–Small-Cell Lung Cancer Patients Treated With the Anti–PD-L1 Antibody**  
Jin Sheng, Huadi Wang, Xiao Liu, Yunyun Deng, Yingying Yu, Pengfei Xu, Jiawei Shou, Hong Pan, Hongsen Li, Xiaoyun Zhou, Weidong Han, Tao Sun, Hongming Pan and Yong Fang
- 244 Expression and Gene Regulation Network of Adenosine Receptor A2B in Lung Adenocarcinoma: A Potential Diagnostic and Prognostic Biomarker**  
Yutong Sui, Jiayin Liu, Jing Zhang, Zena Zheng, Ziwei Wang, Zhenghu Jia and Ziyu Meng
- 259 The Potential Role of Extracellular Vesicles in COVID-19 Treatment: Opportunity and Challenge**  
Yan-yan Yan, Wen-min Zhou, Yu-qing Wang, Qiao-ru Guo, Fu-xi Zhao, Zhuang-yan Zhu, Yan-xia Xing, Hai-yan Zhang, Mohamad Aljofan, Alireza Mosavi Jarrahi, Bolat Makabel and Jian-ye Zhang
- 274 Development and Validation of the Prognostic Index Based on Inflammation-Related Gene Analysis in Idiopathic Pulmonary Fibrosis**  
Yanjiao Lu, Jinkun Chen, Kun Tang, Shanshan Wang, Zhen Tian, Meijia Wang, Jianping Zhao and Jungang Xie
- 283 Management of Coronavirus Disease 2019 Patients With Lung Cancer: Experience From a Thoracic Oncology Center**  
David Barros Coelho, Vanessa Santos, David Araújo, Hélder Novais Bastos, Adriana Magalhães, Venceslau Hespanhol, Henrique Queiroga, Natália Cruz-Martins and Maria Gabriela O. Fernandes
- 289 Multi-Pharmaceutical Activities of Chinese Herbal Polysaccharides in the Treatment of Pulmonary Fibrosis: Concept and Future Prospects**  
Xianbo Wu, Jianli Huang, Jie Wang, Yihua Xu, Xinwei Yang, Minghan Sun and Jianyou Shi
- 304 Targeting M2 Macrophages Alleviates Airway Inflammation and Remodeling in Asthmatic Mice via miR-378a-3p/GRB2 Pathway**  
Qiujie Wang, Luna Hong, Ming Chen, Jiangting Shi, Xiaoling Lin, Linjie Huang, Tiantian Tang, Yimin Guo, Xiaoqing Yuan and Shanping Jiang
- 317 Exhaled Volatile Organic Compounds for Identifying Patients With Chronic Pulmonary Aspergillosis**  
Zheng-Tu Li, Pei-Ying Zeng, Zhao-Ming Chen, Wei-Jie Guan, Tong Wang, Ye Lin, Shao-Qiang Li, Zhi-Juan Zhang, Yang-Qing Zhan, Ming-Die Wang, Guo-Bin Tan, Xue Li and Feng Ye
- 328 Therapeutic Effects of the Bcl-2 Inhibitor on Bleomycin-induced Pulmonary Fibrosis in Mice**  
Yicheng He, Fei Li, Chao Zhang, Xinwei Geng, Madiha Zahra Syeda, Xufei Du, Zhehua Shao, Wen Hua, Wen Li, Zhihua Chen, Songmin Ying and Huahao Shen

- 339**  ***$\Delta$ CT Value of Amplified Refractory Mutation System Predicts Efficacy of EGFR-TKIs in Advanced Non–Small-Cell Lung Cancer: A Multi-Center Retrospective Study***  
Min Chen, Wenqi Huang, Dongyong Yang, Jincheng Huang, Gong Li, Xiaoqing Wang, Nanjie Xiao, Weijian Zhang, Jian Guan, Shuang Wang and Laiyu Liu
- 347** ***STAT3 and IL-6 Contribute to Corticosteroid Resistance in an OVA and Ozone-induced Asthma Model with Neutrophil Infiltration***  
Yishu Xue, Yan Zhou, Wuping Bao, Qiang Fu, Huijuan Hao, Lei Han, Xue Zhang, Xue Tian and Min Zhang
- 361** ***Relationships Between Oral Microecosystem and Respiratory Diseases***  
Jiajia Dong, Wei Li, Qi Wang, Jiahao Chen, Yue Zu, Xuedong Zhou and Qiang Guo



# Mechanisms of Pulmonary Hypertension in Acute Respiratory Distress Syndrome (ARDS)

Lucy Revercomb<sup>1,2†</sup>, Ankit Hanmandlu<sup>2†</sup>, Nancy Wareing<sup>2</sup>, Bindu Akkanti<sup>3</sup> and Harry Karmouty-Quintana<sup>2,3\*</sup>

<sup>1</sup> Department of BioSciences, Rice University, Houston, TX, United States, <sup>2</sup> Department of Biochemistry and Molecular Biology, McGovern Medical School, University of Texas Health Science Center at Houston, Houston, TX, United States, <sup>3</sup> Divisions of Critical Care, Pulmonary and Sleep Medicine, McGovern Medical School, University of Texas Health Science Center at Houston, Houston, TX, United States

## OPEN ACCESS

### Edited by:

Dianhua Jiang,  
Cedars Sinai Medical Center,  
United States

### Reviewed by:

Simon Rowan,  
University College Dublin, Ireland  
Zhiyu Dai,  
University of Arizona, United States

### \*Correspondence:

Harry Karmouty-Quintana  
harry.karmouty@uth.tmc.edu

<sup>†</sup>These authors have contributed  
equally to this work

### Specialty section:

This article was submitted to  
Molecular Diagnostics and  
Therapeutics,  
a section of the journal  
Frontiers in Molecular Biosciences

**Received:** 30 October 2020

**Accepted:** 09 December 2020

**Published:** 18 January 2021

### Citation:

Revercomb L, Hanmandlu A,  
Wareing N, Akkanti B and  
Karmouty-Quintana H (2021)  
Mechanisms of Pulmonary  
Hypertension in Acute Respiratory  
Distress Syndrome (ARDS).  
Front. Mol. Biosci. 7:624093.  
doi: 10.3389/fmolb.2020.624093

**Background:** Acute respiratory distress syndrome (ARDS) is a severe and often fatal disease. The causes that lead to ARDS are multiple and include inhalation of salt water, smoke particles, or as a result of damage caused by respiratory viruses. ARDS can also arise due to systemic complications such as blood transfusions, sepsis, or pancreatitis. Unfortunately, despite a high mortality rate of 40%, there are limited treatment options available for ARDS outside of last resort options such as mechanical ventilation and extracorporeal support strategies.

**Aim of review:** A complication of ARDS is the development of pulmonary hypertension (PH); however, the mechanisms that lead to PH in ARDS are not fully understood. In this review, we summarize the known mechanisms that promote PH in ARDS.

**Key scientific concepts of review:** (1) Provide an overview of acute respiratory distress syndrome; (2) delineate the mechanisms that contribute to the development of PH in ARDS; (3) address the implications of PH in the setting of coronavirus disease 2019 (COVID-19).

**Keywords:** hyaluronan, renin angiotensin system, interleukin-6 (IL-6), vascular dysfunction and inflammation, acute lung injury, vasoconstriction, vascular remodelling

## INTRODUCTION

Acute respiratory distress syndrome (ARDS) is a severe form of lung respiratory failure characterized by diffuse alveolar damage, inflammation, and acute onset of hypoxemia not explained by cardiac failure. Diagnostic criteria for ARDS include (1) presentation within 1 week of a known clinical insult, new, or worsening respiratory symptoms; (2) bilateral opacities consistent with pulmonary edema on chest imaging; (3) respiratory failure not fully explained by cardiac failure or fluid overload; and (4) physiologic values of arterial oxygen partial pressure to fractional inspired oxygen ( $\text{PaO}_2/\text{FIO}_2$ )  $\leq 300$  mmHg and positive end-expiratory pressure (PEEP)  $\geq 5$  cm  $\text{H}_2\text{O}$  (The ARDS Definition Task Force, 2012).

Several chronic disorders have been associated with the development of ARDS; however, the majority of ARDS develops from a pulmonary or non-pulmonary infection (Matthay and Zemans, 2011). ARDS can be triggered by many pathogenic conditions including sepsis, pancreatitis, and respiratory viruses such as the H5N1 avian influenza virus, the 1918 influenza pandemic, the severe acute respiratory syndrome-coronavirus (SARS-CoV), and most recently SARS-CoV-2 that causes coronavirus disease 2019 (COVID-19) (Imai et al., 2010; Rezoagli et al., 2017).



The pathogenesis of ARDS is typically divided into the acute, subacute, and chronic phases (Matthay and Zemans, 2011). The acute phase marks the first 1–6 days and is characterized by interstitial and alveolar edema, endothelial and epithelial injury, and the accumulation of neutrophils, macrophages, and red blood cells in the alveoli (Matthay and Zemans, 2011). The subacute phase marks the next 7–14 days and is characterized by some reabsorption of the edema, evidence of repair attempts by alveolar epithelial type II (AE2) cells, infiltration of fibroblasts, and collagen deposition (Matthay and Zemans, 2011). After 14 days, ARDS is considered to be in the chronic phase and there is often resolution of the acute neutrophilic infiltrate, accumulation of mononuclear cells and alveolar macrophages in the alveoli, and more fibrosis resulting from the alveolar epithelial repair (Matthay and Zemans, 2011).

ARDS is observed in 10–15% of admitted patients in intensive care units and more than 20% of patients undergoing invasive mechanical ventilation (Frutos-Vivar et al., 2004). In addition to this high prevalence and despite best measures, ARDS has a high mortality rate of up to 45% (Bellani et al., 2016). Treatment of ARDS is complex, involving ventilatory and non-ventilatory management strategies including conservative fluid management, low tidal volume ventilation, prone positioning, inhaled vasodilator therapy and in refractory cases, extra corporeal membrane oxygenation (Peek et al., 2009; Calcaianu et al., 2017).

ARDS is frequently complicated by pulmonary hypertension (PH), a pathologic condition involving a progressive increase in pulmonary vascular resistance (PVR) leading to right ventricular dysfunction (RVD) that ultimately results in RV failure (RVF) (Simonneau et al., 2019). PH is clinically defined as mean pulmonary arterial pressure (mPAP) > 20 mmHg measured by right heart catheterization (Simonneau et al., 2019). PH in the setting of ARDS falls under group 3 PH due to the presence of hypoxia and lung injury (Poor et al., 2012).

Potential underlying mechanisms of PH in ARDS include vessel obliteration, pulmonary vasoconstriction, and microthrombosis due to hypoxia, hypercapnia, and an imbalance in vasoactive mediators (Price and Wort, 2017). As an inflammatory condition, ARDS is characterized by endothelial cell injury and dysfunction (Price and Wort, 2017). Early in the pathogenesis of ARDS, thromboembolism, pulmonary vasoconstriction, and interstitial edema contribute to the development of PH by collectively elevating PVR (Moloney and Evans, 2003). Damage to the endothelium of the lung results in the accumulation and activation of neutrophils in the lung microvasculature, leading to degranulation and the release of toxic mediators including proteases, reactive oxygen species, proinflammatory cytokines, and procoagulant molecules, which promote vasoconstriction and an increase in PVR (Matthay and Zemans, 2011). The release of tissue factor (TF), an activator of the extrinsic clotting cascade, by endothelial cells elevates PVR through the local formation of microthrombi which obstruct blood flow (Ryan et al., 2014). Vascular remodeling and proliferation of smooth muscle cells through the release of endothelin-1 (ET-1) in the subacute and chronic phases of ARDS occludes the pulmonary vasculature, further increasing

PVR and the accumulation of interstitial edema, contributing to the development of PH (Moloney and Evans, 2003). In addition, fibrocellular obliteration of the microvasculature in late phase ARDS disrupts blood flow and helps sustain the elevated PVR that leads to PH (Ryan et al., 2014).

Many of these mediators that are triggered after lung damage in ARDS are also central in the pathophysiology of PH, where injury to endothelial cells and increased levels of ET-1 and TF also contribute to increased vascular tone and remodeling in PH (Moloney and Evans, 2003; Tamosiuniene et al., 2011; Antoniuk et al., 2014).

It has been proposed that the increase in inflammation characteristic of ARDS and secondary to ventilator-induced lung injury prompts the pulmonary vascular injury observed in PH (Meduri et al., 2009; Price and Wort, 2017). The incidence of RVD associated with ARDS has declined with the adoption of improvements in mechanical ventilation which lessen the intrathoracic airway pressure in ARDS patients (Vieillard-Baron et al., 2001). The ARDSnet trial has shown significant mortality benefit, with improvement of low tidal volume ventilation for RVD, and improvement of acute cor pulmonale, in severe cases of ARDS (Brower et al., 2000).

Despite advances in the management of ARDS, prevalence of PH in ARDS remains high. A 92% prevalence of PH was reported by Beiderlinden et al. (2006). Namendys-Silva et al. (2014), who used a strict selection criteria excluding any patients with clinical conditions that may have predisposed them to PH before the onset of ARDS, reported a prevalence of 46.6%. Villar et al. (1989) reported a similar prevalence of 54%. These findings are summarized in **Table 1** where mean pulmonary arterial pressure (mPAP) values determined by right-heart catheterization values ranged from 29 to 36 mmHg in patients with PH. The prevalence of acute cor pulmonale, the severest form of RV dysfunction in the setting of ARDS, is still reported to be as high as 20% (Dessap et al., 2016).

ARDS is a complex disease with multifactorial consequences; as such, in addition to elevated mPAP, other parameters have been strongly associated with mortality such as partial pressure of carbon dioxide ( $\text{PaCO}_2$ ), partial pressure of oxygen ( $\text{PaO}_2$ ), or  $\text{PaO}_2$ /fraction of inspired oxygen ( $\text{FiO}_2$ ). Additionally, pulmonary vascular dysfunction, as measured by an increase in transpulmonary pressure gradient and PVR, was associated with increased mortality in ARDS patients (Monchi et al., 1998; Meduri et al., 2009; Bull et al., 2010; Calcaianu et al., 2017). In addition, the composite marker diastolic pulmonary gradient >7 mmHg and  $\text{PVR} > 3$  Wood Units (WU) seemed to provide a better description of hemodynamic and respiratory dysfunction than other measurements, correlating with a more severe illness and worse patient outcomes (Calcaianu et al., 2017). These findings are summarized in **Table 2** and underscore disruptions in the lung vasculature in ARDS as potential disease-amplifying effects that are not fully understood. Although a study showed no correlation between RVF and mortality in ARDS (Osman et al., 2009), other studies have reported an association between RVD and increased morbidity and mortality in ARDS (Monchi et al., 1998; Bull et al., 2010). Further, due to the effects on organ failure in severe ARDS, the severity of organ failure at admission is an

**TABLE 1** | Prevalence of PH in ARDS.

mPAP (mmHg)			Method	Prevalence (%)	References
All patients	Without PH	PH			
35.4 ± 8.8			Right Heart Catheterization	92.2	Beiderlinden et al., 2006*
27.07 ± 10.29	19.19 ± 3.78	36.07 ± 7.50	Right Heart Catheterization	46.6	Ńamendys-Silva et al., 2014
	15 ± 3	29 ± 6	Right Heart Catheterization	54	Villar et al., 1989

\*individual mPAP values for patients with and without PH not provided.

**TABLE 2** | Factors associated with mortality of PH in ARDS.

Variable	Survivors	Non-survivors	P-value	References
PaO <sub>2</sub> (mmHg)	75.95 ± 32.96	74.44 ± 16.47	0.888	Ńamendys-Silva et al., 2014
PaO <sub>2</sub> /FiO <sub>2</sub> (mmHg)	144.64 ± 47.84	135.64 ± 44.81	0.616	
PaCO <sub>2</sub> (mmHg)	34.51 ± 5.15	40.59 ± 8.44	<0.001	
mPAP (mmHg)	28.32 ± 10.98	24.91 ± 9.08		
PaO <sub>2</sub> /FiO <sub>2</sub>	112 ± 39	93 ± 31	<0.05	Osman et al., 2009
PaCO <sub>2</sub>	43 ± 7	48 ± 16	<0.05	
mPAP	27 ± 6	28 ± 8	<0.01	
PaO <sub>2</sub>	88.7 ± 40.1	78.1 ± 38.5	0.002	Squara et al., 1998
PaO <sub>2</sub> /FiO <sub>2</sub>	149 ± 74	120 ± 59	0.0001	
PaCO <sub>2</sub>	37.1 ± 8.2	38.8 ± 9.0	0.02	
mPAP	25.1 ± 7.3	26.8 ± 9.0	0.04	Bull et al., 2010
mPAP	31.3 ± 8.3	32.4 ± 8.3	0.18	
DPG	14.3 (11.3–18.3)	15.7 (12.3–22.3)	0.02	
PVRi	299.9 (199.4–416.1)	326.4 (206.4–518.7)	0.02	Calcaianu et al., 2017
Δ PaO <sub>2</sub> /FiO <sub>2</sub> < 0 (mmHg)			0.007	

important predictor of mortality (Ńamendys-Silva et al., 2014; Bellani et al., 2016).

Although PH is a frequent complication of ARDS, there is not a definitive correlation between the presence of PH and the severity and mortality of ARDS. Regardless, in instances of ARDS with or without PH, the mortality rate is very high. The toll of this mortality rate, and accordingly the need for novel therapies, has been demonstrated by the impact and death resulting from the pandemic of COVID-19 where pulmonary vascular abnormalities are present (Potus et al., 2020). A more comprehensive understanding of the role and mechanism of PH in ARDS is needed to improve therapies. In this review, we discuss the central pathways that contribute to PH in ARDS.

## EXPERIMENTAL METHODOLOGY

We reviewed the current and past literature on ARDS to identify potential mechanisms that promote PH in ARDS.

## RESULTS

### The Renin–Angiotensin System

The renin–angiotensin system (RAS) is a primary cardiovascular regulatory system responsible for the regulation of blood pressure and electrolyte balance. RAS dysfunction has been proposed

as a key pathogenic mechanism of inflammatory lung disease, including ARDS (Imai et al., 2010; Jia, 2016). Genetic variants in the RAS pathway have recently been implicated in the onset and severity of ARDS, specifically angiotensin-converting enzyme (ACE), and its derivatives (Imai et al., 2010). ACE is a peptidase that regulates RAS by cleaving angiotensin I (AngI) to generate angiotensin II (AngII). AngII subsequently binds to AngII receptor type 1 (AT1R) and AngII receptor type II (AT2R) to regulate RAS (Imai et al., 2010). It is primarily through AT1R that AngII causes growth and proliferation of pulmonary artery smooth muscle cells (PASMCs) correlated with pulmonary vascular remodeling (Morrell et al., 1999). This is attributed to AngII-mediated increases in expression of pro-inflammatory genes including interleukin-10 (IL-10), interleukin-6 (IL-6), tumor necrosis factor (TNF-α), and intracellular adhesion molecule-1 (ICAM-1) in fibroblasts and smooth muscle cells (Xianwei et al., 2012). Subsequent vascular remodeling and fibrotic changes contribute to the pathogenesis and progression of pulmonary fibrosis and PH (Kuba et al., 2006). Further, activation of AT1R by AngII promotes vasoconstriction (Iwai and Horiuchi, 2009), adding to the deleterious properties of AngII.

Angiotensin-converting enzyme 2 (ACE2) is an ACE homolog which regulates RAS through counterbalancing ACE activity. This homolog was termed ACE2 after it was identified and cloned from cDNA libraries by two independent groups (Donoghue

et al., 2000; Tipnis et al., 2000). While ACE and ACE2 share 41.8% sequence identity, ACE2 negatively regulates RAS, opposing the role of ACE (Donoghue et al., 2000; Tipnis et al., 2000; Imai et al., 2010). ACE2 cleaves a single residue from AngI to yield angiotensin1–9 (Ang1–9) and removes a single residue from AngII to yield angiotensin1–7 (Ang1–7) (Donoghue et al., 2000; Tipnis et al., 2000), which downregulates AT1R-mediated actions by reducing AngII levels (Ferreira and Santos, 2005). In addition, Ang1–7 and Ang1–9 oppose AT1R through anti-inflammatory and antifibrotic actions, by binding the Mas receptor (MasR) and AT2R, respectively (Kreutz et al., 2020; South et al., 2020). In the pathogenesis of ARDS, ACE, AngII, and AT1R promote inflammation and PH, while ACE2, Ang1–7, and Ang1–9 serve to protect against ARDS and PH (Imai et al., 2005).

There is a polymorphism of ACE defined by the absence (deletion, D) or presence (insertion, I) of a 287-bp repeat in the coding sequence of intron 16 (Rigat et al., 1990). The human ACE D allele results in increased activity of ACE demonstrated by an increase in serum ACE levels. This polymorphism accounts for 47% of the variance in plasma ACE activity (Rigat et al., 1990). There also exists a pronounced correlation between the D allele and the development of ARDS, suggesting the role of RAS activation early in disease (Marshall et al., 2002). In addition, the ACE D/D allele correlates with increased mortality in ARDS especially in comparison with the ACE I/I allele which shows increased survival rate, marking the I/D polymorphism as a significant prognostic factor for ARDS outcome (Jerng et al., 2006). Thus, it is conceivable that the D allele may worsen PH in ARDS.

ACE2 expression has been located on lung alveolar epithelial cells (AECs) and enterocytes of the small intestine, and additionally on arterial smooth muscle cells and arterial and venous endothelial cells in all organs (Hamming et al., 2004). These areas of expression indicate an abundant presence of ACE2 in the lung and small intestine epithelia (Hamming et al., 2004). In addition, increased expression of ACE has been found in the muscularized intra-acinar pulmonary arteries of patients with PH, supporting the proposed role of ACE in PH (Orte et al., 2000), through the upregulation of AngII.

Many experiments have evaluated and found supporting evidence of the role of ACE in PH promoting inflammation and vascular dysfunction, with the activity of ACE2 serving as an important counterbalance. Experimental PH was associated with elevated ACE expression in the endothelial layer of small and elastic pulmonary arteries (Morrell et al., 1995; Orte et al., 2000; Schuster et al., 2012). While a significant decrease in ACE2 activity was observed in human pulmonary arterial hypertension (PAH) patients (Hemnes et al., 2018), ACE2 knockout mice display worsened lung function, increased vascular permeability, enhanced lung edema, and neutrophil accumulation, attributed to a downregulation of ACE2 (Imai et al., 2005). Later treatment of the ACE2-deficient mice with catalytically active recombinant ACE2 protein or ACE knockout resulted in improvement of severe lung failure as measured by lung elastance, edema formation, and histological changes associated with acute lung injury (ALI) (Imai et al., 2005). Administration of a single dose of recombinant human ACE2 (rhACE2) to PAH patients resulted

in improvement of hemodynamic markers of PAH, including cardiac output and PVR (Hemnes et al., 2018). However, no improvement in clinical or physiological measures of ARDS were seen with the addition of exogenous ACE2 in patients with ARDS (Khan et al., 2017); however, these studies did not have the sufficient statistical power to identify potential clinical benefits. In other models of lung diseases, including bleomycin-induced lung fibrosis and monocrotaline-induced PH, it has been demonstrated that ACE2 plays a critical protective role (Ferreira and Santos, 2005; Yamazato et al., 2009; Zhang et al., 2009). The aforementioned findings support the conclusion that increasing ACE2 expression may present a novel approach for ARDS treatment and emphasize the need for a better understanding of the role of RAS in the pathogenesis of ARDS.

In contrast to the results of experimental ACE2 deletion, ACE knockout and AT1Ra-deficient mice showed marked improvement in ALI symptoms (Imai et al., 2005). Similarly, treatment of chronically hypoxic rats and mice with an AngII receptor antagonist or ACE blocker inhibited pulmonary vascular remodeling associated with the pathogenesis of PH (Nong et al., 1996). ACE-deficient mice with 34% of ACE activity exhibit the same remodeling as normal mice to their pulmonary arterioles, associating the presence of ACE with vascular remodeling (Suylen et al., 2001). In LPS and acid-induced ARDS with high-stretch ventilation, treatment with Ang1–7 reduced the acute inflammatory response and subsequent fibrosis and improved oxygenation (Asperen et al., 2011; Zambelli et al., 2015). Collectively, these studies implicate ACE in the pathogenesis of ARDS (Jerng et al., 2006).

In addition to its regulatory role, ACE2 acts as a functional receptor for SARS-CoV (Hamming et al., 2004). SARS-CoV-2 binds to the membrane-bound form of ACE2 leading to the host cell's internalization of the complex (South et al., 2020). Through this mechanism, SARS-CoV-2 and SARS-CoV-1 use ACE2 as a co-receptor for acquiring intracellular entry into the brain and lungs (Kuba et al., 2005; Hoffmann et al., 2020; Wrapp et al., 2020). This internalization of ACE2 results in a decrease of cell surface ACE2, preventing the degradation of disease-promoting AngII and generation of protective Ang1–7 (South et al., 2020). This reduction in pulmonary ACE2 may exacerbate systemic hypertension and PH, fibrosis post-viral infection, and respiratory distress (Imai et al., 2005; Kuba et al., 2005). Potential treatment of COVID-19, with the understanding of the role of ACE2 as a receptor for SARS-CoV-2, could include inhibition of the ACE2 receptor, spike protein-based vaccine, inhibition of transmembrane protease activity, or administration of soluble ACE2 (Cheng et al., 2020). Taken together, these findings support the role of RAS as an important modulator of PH in ARDS where it can modulate both vasoconstriction and vascular remodeling responses (Figure 1).

## The Inflammatory Cascade

Protective mechanical ventilation strategies have improved outcomes of ARDS and PH together, but pulmonary vasculature dysfunction remains in 25% of affected patients and has been increasingly associated with sepsis (Bull et al., 2010; Boissier et al., 2013). Increased flow and ventilatory pressures result

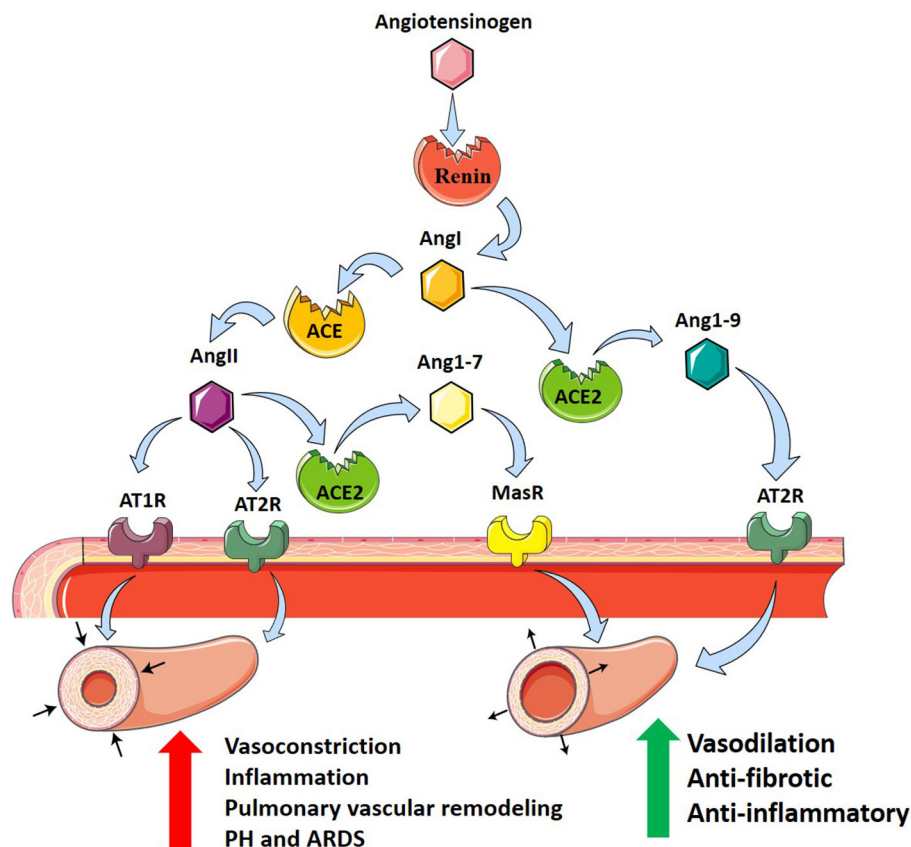


**FIGURE 1 |** The renin-angiotensin system and its contribution to PH in ARDS. Angiotensinogen (pink hexagon) is cleaved by renin (red circle) into angiotensin I (AngI, orange hexagon). Angiotensin-converting enzyme (ACE, orange circle) cleaves AngI producing angiotensin II (AngII, purple hexagon) which binds to angiotensin II receptor type 1 (AT1R, purple receptor) and angiotensin II receptor type 2 (AT2R, teal receptor), resulting in vasoconstriction, inflammation, and pulmonary vascular remodeling promoting PH in ARDS. Alternatively, angiotensin-converting enzyme 2 (ACE2, green circle) cleaves AngI producing angiotensin1-9 (Ang1-9, blue hexagon) which binds to AT2R, or AngII to produce angiotensin1-7 (Ang1-7, yellow hexagon) which binds to Mas receptor (MasR, yellow receptor). ACE2 counterbalances ACE, protecting against PH in ARDS through anti-fibrotic and anti-inflammatory actions and vasodilation.

in elevated cytokines, notably IL-6, which is attenuated with decreased flow (Ranieri et al., 1999; Samary et al., 2015). This is further highlighted by Pandolfi et al. who examined if IL-6 and acid sphingomyelinase (aSMase) contribute to PH in ARDS (Pandolfi et al., 2017). Through an LPS model of ARDS, they identified that the production of ceramide and IL-6 in rat PASMCs resulted in failed hypoxic vasoconstriction (HPV), endothelial dysfunction, and hyperresponsiveness to pulmonary vasoconstriction induced by serotonin (Pandolfi et al., 2017). Interestingly, blockade of aSMase attenuated the progression of PH (Pandolfi et al., 2017). Taken together, it is evident that the upregulation of the inflammatory response after lung injury is a central mechanism in the development of PH in ARDS (Price and Wort, 2017).

There exist a multitude of cytokines that have been implicated in the inflammatory cascade in ALI including interleukins (ILs), interferons (IFNs), tumor necrosis factors (TNFs), chemokines, and colony-stimulating factors (CSFs) (Tisoncik et al., 2012). Many of the cytokines associated with the inflammatory cascade are also implicated in the pathogenesis of PH. The number

of macrophages significantly increases in plexiform lesions of patients with severe PAH due to increased expression of chemokines in the lungs and chemokine receptors on monocytes (Gerasimovskaya et al., 2012; Florentin et al., 2018). Once activated, macrophages then induce the release of IL-6, IL-10, IL-1 $\beta$ , and TNF- $\alpha$  (Stow et al., 2009). This review will focus largely on IL-6, IL-10, and TNF- $\alpha$ .

IL-6 is an acute phase reactant that is produced as part of an inflammatory response perpetuated by the liver (Heinrich et al., 1990). Serum studies of patients with PAH show increased levels of IL-6 compared with healthy patients, and even demonstrate IL-6 levels as a more accurate prognostic marker than traditional clinical tests (Selimovic et al., 2009; Soon et al., 2010). IL-6 overexpression in mice led to increased muscularization of the proximal arterial tree and distal arteriolar vessels (Savale et al., 2009; Steiner et al., 2009). The muscularization presented with occlusive neointimal angioproliferative lesions that contained primarily endothelial and T cells (Savale et al., 2009; Steiner et al., 2009). This vascular remodeling resulted in an elevated right ventricular systolic pressure and increased



right ventricular hypertrophy (Savale et al., 2009; Steiner et al., 2009). Furthermore, IL-6 has also been shown to be involved in the post-transcriptional mechanism of bone morphogenic protein receptor type 2 (BMPR2) downregulation through signal transducer and activator of transcription 3 (STAT3) and the microRNA cluster 17/92 (Brock et al., 2009). IL-6 has also been shown to participate in vascular remodeling by increasing the levels of matrix metalloproteinase 9 (MMP-9) and vascular endothelial growth factor receptor 2 (VEGFR2) that result in the proliferation of PASMCs and trigger the transdifferentiation of pulmonary endothelial cells to PASMCs (Steiner et al., 2009). Most studies have demonstrated that IL-6 exerts a protective effect in ARDS (Groth et al., 2014). This could suggest that the defensive IL-6 response in ARDS can inadvertently result in the development of PH. There are currently multiple clinical trials attempting to elucidate the role of anti-IL6 therapies to attenuate ARDS in COVID-19 (clinicaltrials.gov: NCT00531856; NCT04363853; NCT04335071). Tocilizumab was used to attenuate the cytokine storm in select patients worldwide, but large randomized controlled trials are yet to show efficacy (Xu et al., 2020).

TNF- $\alpha$  is a pro-inflammatory cytokine secreted by macrophages that regulates cellular proliferation, differentiation, apoptosis, and survival (Parameswaran and Patial, 2010). Increased levels of TNF- $\alpha$  were found in patients suffering from PAH (Soon et al., 2010). TNF- $\alpha$  overexpression in experimental models results in the suppression of prostacyclin (PGI<sub>2</sub>: a potent vasodilator) mRNA and increased vascular reactivity (Stevens et al., 1992; Itoh et al., 2003). In addition, TNF- $\alpha$  overexpression in type II AECs led to increased septal destruction, bronchiolitis, pulmonary inflammation, and PH (Fujita et al., 2001). An association has been found between polymorphisms in the surfactant protein-B (SP-B) gene and an increased risk of developing ARDS (Gong et al., 2004). TNF expression has demonstrated potent inhibitory activity of SP-B in a human lung adenocarcinoma cell line and decreased surfactant protein-A (SP-A) expression in lung epithelial cells through the p38/MAPK pathway (Berhane et al., 2000; Miakotina and Snyder, 2002). Therefore, this could imply that TNF- $\alpha$  upregulation in ARDS can co-present with PH by inducing atelectasis of alveoli through decreased surfactant production.

IL-10 is an important anti-inflammatory cytokine released by monocytes, macrophages, and several subsets of T cells including type 1 T helper (Th1) cells and regulatory T (Treg) cells (Sabat et al., 2010). Patients with PAH have elevated levels of IL-10, but interestingly increased levels of IL-10 were also observed in patients receiving PGI<sub>2</sub> for the treatment of PAH (Groth et al., 2014). In a monocrotaline model of PAH in rats, the intramuscular injection of IL-10 prevented the development of PAH (Ito et al., 2007). Moreover, increased IL-10 production has been associated with the IL-10 promoter polymorphism at position -1082 (-1082GG) (Gong et al., 2006). In a study of 211 Caucasian ARDS patients, the -1082GG genotype resulted in decreased mortality and organ failure in comparison with controls (Gong et al., 2006). It is clear that IL-10 serves a protective role in ARDS and PH; to a greater extent in the -1082GG genotype. However, its efforts may be superseded by

a more potent pro-inflammatory response despite persistently elevated IL-10.

Chemokines, or chemotactic cytokines, are a family of 40 low molecular weight proteins that stimulate leukocyte migration and function through their interactions with chemokine receptors (Luster, 1998; Mamazhakypov et al., 2021). There is an elevation in circulating chemokine levels in patients with varying forms of PH which include PH due to chronic obstructive pulmonary disease and lung fibrosis, PAH due to systemic sclerosis, idiopathic PAH, and chronic thromboembolic pulmonary hypertension (CTEPH) (Mamazhakypov et al., 2021). Apart from their roles as biomarkers and in inflammation, chemokines, and their receptors are also involved in pulmonary vascular dysfunction that contributes to PAH (Mamazhakypov et al., 2021). The CCL5-CCR5 axis has been implicated in PAH, most importantly as a mediator of PASM proliferation *in vitro* (Amsellem et al., 2014). When the CCR5 antagonist maraviroc was administered, the proliferation was depleted (Amsellem et al., 2014). Moreover, CXCL10/CXCL4-CXCR3 axis dysregulation in pulmonary artery endothelial cells led to the loss of recanalization of blocked vessels in CTEPH and impaired angiogenesis (Zabini et al., 2012). CCL3 has also been shown to increase endothelin-1 expression in endothelial cells (Molet et al., 2000). In ARDS, chemokines are released by alveolar macrophages in response to bacterial products (Puneet et al., 2005). However, they can also be secreted by other cells in the local environment as part of an inflammatory cascade involving TNF and IL-1 $\beta$  (Puneet et al., 2005). This demonstrates that an initial inflammatory response in ARDS can be strengthened by an inflammatory cascade and potentiate pulmonary vascular dysfunction and eventual PH.

The importance of the inflammatory cascade in the pathogenesis of PH in ARDS is still not fully understood. Here, we present that a heightened pro-inflammatory response in ARDS can contribute to the development of PH through the involvement of TNF, IL-6, chemokines, and IL-10. These cytokines are implicated in a multitude of processes namely HPV failure, decreased surfactant production, imbalance of vasodilators and vasoconstrictors, PASM proliferation, and loss of recanalization in blocked vessels. Conclusively, this can provide a new route for effective therapeutics.

## Thrombosis

Thrombosis is a well-described phenomenon that presents in patients suffering from ARDS (Ryan et al., 2014). In a postmortem study of 22 ARDS patients, 19 patients (86%) exhibited macrothrombi in pulmonary arterial and capillary vessels and evidence of microthrombi (Tomashefski et al., 1983). This results from localized damage to the endothelial cell lining that causes the release of tissue factor (TF) in response to inflammation (Maniatis et al., 2008; Levi and Van Der Poll, 2010; Price et al., 2012). TF is a potent activator of the extrinsic coagulation cascade, and experimental models show inhibition of TF-Factor VIIa-Factor X complex reduces the extent of PH in ARDS (Welty-Wolf et al., 2001; MacKman, 2009). Furthermore, plasminogen activator inhibitor-I (PAI-1) levels are elevated in contrast with decreased levels of protein C and thrombin antithrombin (TAT) complexes in ARDS patients (Ware et al.,

2003, 2007). These markers suggest that ARDS promotes a hypercoagulable state while repressing fibrinolysis and is also associated with increased mortality (Ware et al., 2007).

Interactions between coagulation and an excessive inflammatory response are considered essential in the pathophysiology of ARDS (Frantzeskaki et al., 2017). Activation of coagulation pathways in ARDS results in the overproduction of thrombin that can further ameliorate inflammatory processes through proteinase-activated receptors (Frantzeskaki et al., 2017). Under non-pathological conditions, thrombin production is highly regulated by tissue factor pathway inhibitor, anti-thrombin III, and the protein C system (José et al., 2014). These feedback mechanisms can be diminished in inflammation due to increased consumption and decreased production of anticoagulants (José et al., 2014). It is evident that the formation of microthrombi is due to increased coagulability and can promote PH in ARDS patients through the pathological blockade of vessels.

More recently, ARDS secondary to SARS-CoV-2 infection (COVID-19) has been associated with an increase in the risk of thrombotic complications (mainly pulmonary embolisms) in comparison with non-ARDS SARS-CoV-2 infections (Helms et al., 2020). Longer prothrombin time (PT), increased levels of D-dimer and fibrin degradation products, longer activated partial thromboplastin time (aPTT), and decreased platelets were found in non-survivors of SARS-CoV-2 (Tang et al., 2020b; Xiaofang et al., 2020). These parameters are all related to a poor prognosis in infected patients (Tang et al., 2020b; Xiaofang et al., 2020). While experimental models of SARS-CoV-2 infections have not been widely studied, infection of SARS-CoV with ARDS results in increased fibrin deposition in mice (Gralinski et al., 2013). Furthermore, the use of low molecular weight heparin leads to reduced mortality in severe COVID-19 patients (Tang et al., 2020a). This suggests that a similar balance toward coagulation might exist in patients with ARDS-related SARS-CoV-2 and might provide significant prognostic value in severe infections. How the inflammatory and thrombotic pathways contribute to PH are represented diagrammatically in Figure 2.

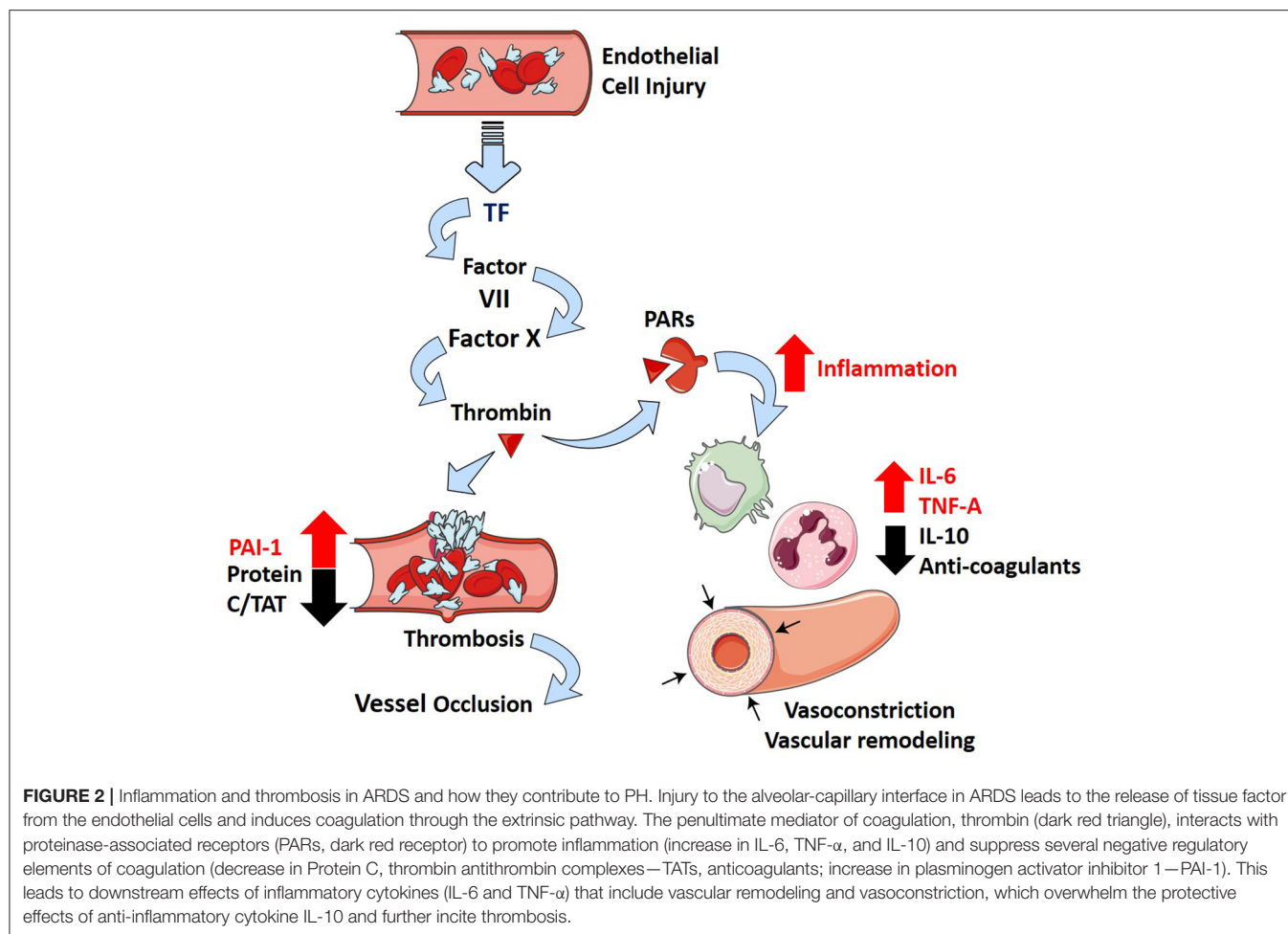
## Hypoxic Pulmonary Vasoconstriction

HPV is a unique and complex feature of the pulmonary circulation whereby hypoxic conditions lead to vasoconstriction, in contrast to the systemic circulation where hypoxia leads to vasodilation (Lumb and Slinger, 2015). HPV has an important physiological role; it acts to match perfusion to ventilation to optimize  $P_{O_2}$  (McLoughlin, 2018). Thus, HPV shunts blood toward areas with high ventilation to maintain efficient gas exchange processes (Sylvester et al., 2012). In ALI settings, both clinically and experimentally, edema as a result of loss of barrier function leads to regional hypoxemia, activating HPV to shunt blood away from hypoxic areas of the lung to ventilated areas (Marshall et al., 1994; Fischer et al., 2004; Spöhr et al., 2007; Sylvester et al., 2012). This beneficial effect of HPV has been shown to be inhibited in experimental models of oleic acid, bleomycin, or endotoxin-induced ALI (Sylvester et al., 2012), underscoring the important role that HPV has in matching

ventilation/perfusion. Herein, studies in mice have revealed that inhibition of ATP-regulated potassium channel Kir6.1, which is elevated after endotoxemia, was able to restore HPV in mice; however, the effects on lung inflammation were not assessed (Turzo et al., 2018). However, prolonged HPV can lead to the development of PH and high-altitude induced pulmonary edema (HAPE) which is characterized by patchy peripheral distribution of edema (Bartsch, 1999). Although this mechanism is distinct to the classic presentation of ARDS that has a strong inflammatory component, HAPE is characterized by the presence of pulmonary edema (Bartsch, 1999). Pulmonary edema is also a feature shared with ARDS that contributes to deficits in gas exchange and lung failure due to fluid accumulation in the alveolar spaces (The ARDS Definition Task Force, 2012). Thus, although distinct to ARDS, HAPE as a result of prolonged HPV represents a mechanism linking PH and the development of edema, a feature of ARDS.

An important downstream molecular consequence of hypoxia is the stabilization of hypoxia-inducible factor (HIF)-1A and HIF-2A. Under normoxic conditions, HIFs are degraded by prolylhydroxylases (PHDs); however, under hypoxia, the PHDs are inactivated allowing HIFs to stabilize (Eltzschig and Carmeliet, 2011). In ALI, the stabilization of HIF1A and HIF2A have been shown to limit injury (Karmouty-Quintana et al., 2013b; Gong et al., 2015; Huang et al., 2019). Deletion of endothelial cell HIF-1A expression inhibited endothelial proliferation and attenuated vascular repair processes in a model of sepsis-induced lung injury (Huang et al., 2019). Similarly, abrogation of endothelial HIF-2A resulted in defective adherens junction that was exacerbated after endotoxin challenge in mice, resulting in worsened lung injury (Gong et al., 2015). The downstream HIF-mediated mechanism is complex and includes many mediators; however, increased expression of ectonucleotidases CD39 and CD73 and the increased expression of the adenosine A2B receptor (ADORA2B) have been implicated in the accumulation of adenosine and subsequent protective effects of adenosine through activation of its receptors (Karmouty-Quintana et al., 2013b). Remarkably, these same mechanisms that are protective in acute lung injury settings have also been linked with the pathophysiology of PH. Genetic deletion of endothelial PHD2 and subsequent stabilization of HIF-2A has been linked with the spontaneous development of PH in mice associated with severe vascular remodeling (Dai Zhiyu et al., 2016). Several studies have also demonstrated an important role for HIF1A, adenosine, and ADORA2B activation as causative mediators in group 3 PH (Karmouty-Quintana et al., 2012, 2013a; Garcia-Morales et al., 2015; Rajagopal et al., 2021). Taken together, these studies illustrate the complexity of hypoxic-adenosinergic responses in the pathophysiology of ARDS and PH, whereas they are protective in ALI settings, they also promote features of PH and chronic lung injury. This duality is perhaps best highlighted by studies that determined the prevalence of HIF2A and PHD2 polymorphisms that are associated with improved adaptation to hypoxia in high-altitude residents in patients with ARDS. This study demonstrated that the PHD2 polymorphism *PHD2 RS516651-TT*, which is associated with increased adaptation to high altitude, was associated with a higher 30-days mortality





risk within 30 days of the onset of ARDS (Dötsch et al., 2017).

## Endothelin

Increased levels of endothelin-1 (ET-1), a potent vasoconstriction agent (Davenport and Maguire, 1994), have been reported clinically in ARDS patients where they contribute not only to pulmonary vasoconstriction but also to promote lung edema (Druml et al., 1993; Sanai et al., 1996; Nakano et al., 2007). These observations are significant because inhibition of ET-1 is an important strategy in the treatment of PH (Clozel et al., 2013). Endothelin receptor antagonists (ERAs) have been used successfully in experimental models of ALI where they inhibited lung edema; unfortunately, pulmonary vascular pressures were not assessed in these studies (Guimarães et al., 2000; Araz et al., 2013). However, due to the effect of ERAs in modulating PH by promoting vasodilation and reducing inflammation in both PH and ALI (Guimarães et al., 2000; Araz et al., 2013; Clozel et al., 2013), its use in ARDS as a front-line therapy has been postulated (Araz, 2020).

## Hyaluronan

PH in the setting of ARDS falls into WHO group 3 PH because it is strongly associated with hypoxia and the presence of lung

injury (Poor et al., 2012). A recent review of mechanisms of group 3 PH associated with lung fibrosis has been recently published (Rajagopal et al., 2021). Interestingly, similar pathways are involved in both PH associated with ARDS and lung fibrosis such as inflammatory mediators, RAS, and endothelins (Rajagopal et al., 2021). In addition, the glycosaminoglycan hyaluronan has been implicated in PH associated with chronic lung diseases (Collum et al., 2017, 2019). Interestingly, hyaluronan is elevated in experimental lung injury (Ni et al., 2018; Bell et al., 2019), and its inhibition has been shown to be effective in models of ALI (McKallip et al., 2013, 2015). Thus, it is conceivable that in addition to promoting lung inflammation, excess hyaluronan in ARDS may also contribute to PH. In line with this, we hypothesize that the hypoxic environment in ARDS leads to increased expression or activity of CD73 and ADORA2B such as in PH in the setting of lung fibrosis (Garcia-Morales et al., 2015) that leads to accumulation of adenosine and subsequent activation of ADORA2B. Activation of this receptor has been shown to promote hyaluronan production through increased expression of hyaluronan synthases (HAS)-1 and 2 (Karmouty-Quintana et al., 2013a; Mertens et al., 2018). Interestingly, many recent publications have linked increased hyaluronan deposition in COVID-19 (Hellman et al., 2020; Kaber et al., 2020), a disease that is more and more associated with

important cardiopulmonary complications (Karmouty-Quintana et al., 2020; Potus et al., 2020). Recent publications from our group have also demonstrated that inhibition of hyaluronan by 4-methylumbelliferone (4MU) attenuated PH by diminishing vascular remodeling (Collum et al., 2017, 2019). 4MU has also been postulated as a therapeutic for COVID-19-induced ARDS where it could not only attenuate the inflammatory effects but also dampen the cardiovascular complications (Karmouty-Quintana et al., 2020; Shi et al., 2020). The main pathways that contribute to PH after vascular injury are summarized in Figure 3.

## CONCLUSIONS

Mechanisms of PH in ARDS are complex and poorly understood. Evidence that PH increases the mortality in patients with ARDS is suggested by some studies, but definitive evidence is thwarted by inconsistent reports (Beiderlinden et al., 2006; Namendys-Silva et al., 2014; Calcaianu et al., 2017). However, it is clear that pulmonary vascular dysfunction is present in patients with ARDS and has indirect associations with mortality (Monchi et al., 1998; Bull et al., 2010). This review summarizes current understanding of the pathways that contribute to PH in ARDS, with specific commentary regarding the implications for the current COVID-19 pandemic.

The renin-angiotensin axis plays an important and multi-dimensional role in pulmonary vascular changes in both acute and chronic lung disease (Jia, 2016). A hyperactive form of ACE correlates with the development of and increased mortality in ARDS (Marshall et al., 2002; Jerng et al., 2006). Further, the increases in ACE and its specific catabolites have been shown to directly contribute to vascular remodeling in PH (Krege et al., 1995; Nong et al., 1996; Suylen et al., 2001). For example, activation of the AngII receptor AT1R directly promotes vasoconstriction and vascular remodeling, prominent drivers of PH (Iwai and Horiuchi, 2009). Conversely, the ACE homolog ACE2 is protective in PH, and increasing its expression would be a novel approach to PH-ARDS treatment (Imai et al., 2005). It is not surprising then that the loss of membrane-associated ACE2 in the lung caused by SARS-CoV has been proposed as a crucial mechanism for the rapidly progressive alveolar damage and vascular changes present in COVID-19 patients (Imai et al., 2005; Kuba et al., 2005). There are multiple clinical trials in the works investigating the prophylactic and therapeutic effect of angiotensin pathway-modulating drugs in preventing and treating patients with COVID-19-associated ARDS (clinicaltrials.gov; NCT04335786; NCT04337190).

Another critical contributing mechanism to ALI is a robust and exaggerated immune response, referred to here as the inflammatory cascade. Acute inflammation characterized by rapid and robust release of inflammatory cytokines such as IL-6, IL-10, and TNF is a central feature of ARDS (Tisoncik et al., 2012). These same mediators are also implicated in PH and may play key roles in the severe and acute inflammation observed in ARDS with PH. Of particular interest, the destructive IL-6 response in ARDS may contribute to the subsequent

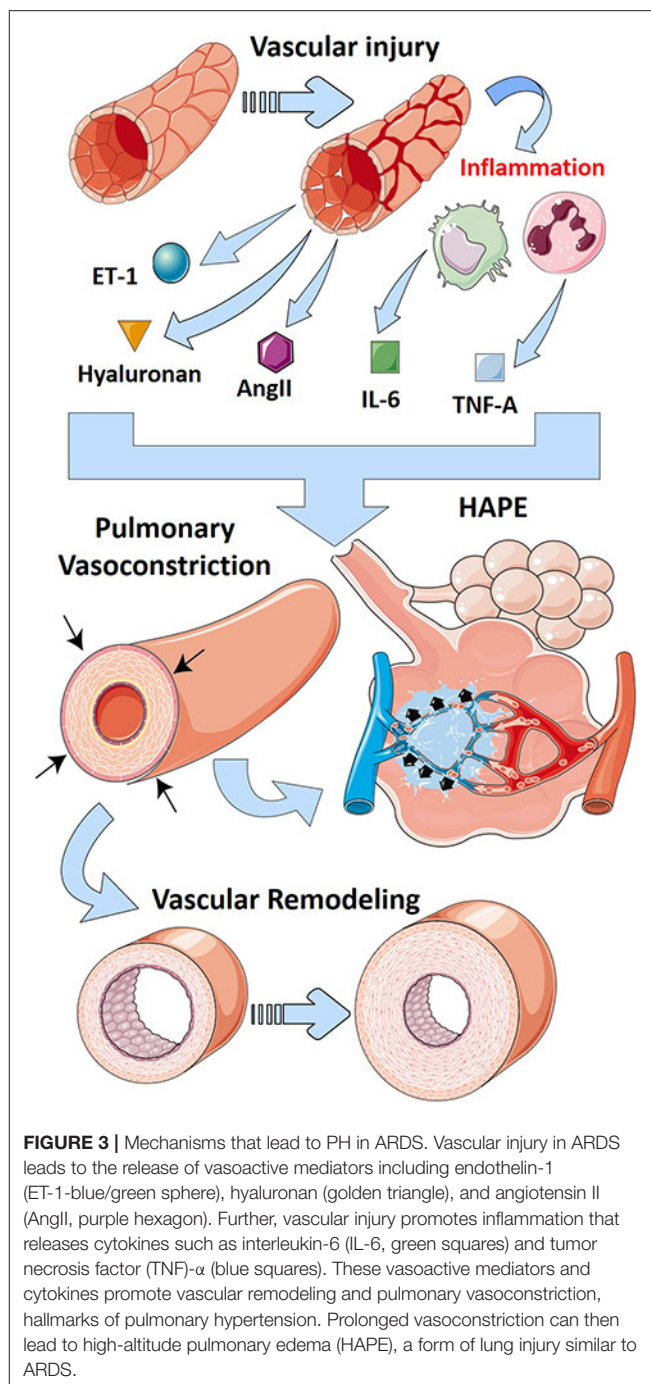


**FIGURE 3 |** Mechanisms that lead to PH in ARDS. Vascular injury in ARDS leads to the release of vasoactive mediators including endothelin-1 (ET-1-blue/green sphere), hyaluronan (golden triangle), and angiotensin II (AngII, purple hexagon). Further, vascular injury promotes inflammation that releases cytokines such as interleukin-6 (IL-6, green squares) and tumor necrosis factor (TNF)- $\alpha$  (blue squares). These vasoactive mediators and cytokines promote vascular remodeling and pulmonary vasoconstriction, hallmarks of pulmonary hypertension. Prolonged vasoconstriction can then lead to high-altitude pulmonary edema (HAPE), a form of lung injury similar to ARDS.

observations of PH in ARDS patients (Groth et al., 2014; Pandolfi et al., 2017). Therapeutics which target these inflammatory pathways are worth serious investigation. The inflammatory cascade, as a component of cytokine release syndrome, is thought to be involved in the development of ARDS in patients infected with SARS-CoV-2, where important changes to the pulmonary vasculature including features of PH have been reported (Potus et al., 2020; Sun et al., 2020). There are currently randomized controlled trials evaluating the efficacy of leronlimab, a CC chemokine receptor 5 (CCR5) modulator,

in patients with mild to severe SARS-CoV-2-induced ARDS (clinicaltrials.gov, NCT04347239).

The ARDS-related inflammatory cascade has also been tied directly to another feature of ARDS: hypercoagulability and thrombosis. An altered thrombotic and fibrinolysis profile has been linked to PH in ARDS (Nieuwenhuizen et al., 2009). Inhibition of the coagulation cascade abrogates ARDS-related PH (Welty-Wolf et al., 2001; MacKman, 2009). In this review, we describe several molecular mechanisms that perpetuate this abnormal hemostatic state, and provide insight into novel diagnostic and therapeutic interventions that can increase positive outcomes in ARDS. The presence of underlying viral infections, in particular COVID-19 infection, in ARDS patients even further increases the risk of thrombotic events. While dysregulation of the coagulation cascade is observed in COVID-19 patients with either or both ARDS and PH, the mechanisms by which this occurs are not fully understood, thwarting the informed use of agents which interfere with hypercoagulability in these patients.

The unique vasoconstrictive response of the lungs to hypoxia presents a particularly complex phenomenon in ARDS and PH (Lumb and Slinger, 2015). Acute pulmonary edema in ALI activates the hypoxic response, which allows the lungs to maximize oxygenation efficiency (Marshall et al., 1994; Fischer et al., 2004; Spöhr et al., 2007; Sylvester et al., 2012). However, if HPV becomes chronic, it can result in the development of PH (Bartsch, 1999). As such, potential therapeutic enhancement of HPV in acute settings must be balanced by consideration of the long-term effects of HPV, which may increase the risk of PH. Viral infections are known to lead to hypoxia through pulmonary vascular and epithelial cell damage (Sun et al., 2020). As such, the role of disrupted vascular regulation in patients with severe COVID-19 warrants further investigation.

Two additional phenomena observed in ARDS are increased circulating ET-1 levels (Nakano et al., 2007) and exacerbated local deposition of hyaluronan in the lung parenchyma (McKallip et al., 2013, 2015; Ni et al., 2018; Bell et al., 2019). Interestingly, inhibition of both ET-1-mediated actions (Guimarães et al., 2000; Araz et al., 2013) and hyaluronan deposition (McKallip et al., 2013, 2015) are beneficial in models of ALI. While hyaluronan has been implicated in the pathogenesis of PH related to chronic lung disease (Collum et al., 2019; World Health Organization, 2020), neither ET-1 nor hyaluronan has been thoroughly investigated in ARDS-related PH.

An important aspect in the pathophysiology of PH in ARDS is the interplay between acute and chronic mediators that may

promote features of PH. In the early stages of ALI, damage to the endothelium and subsequent increase of vasoactive mediators such as ET-1, IL-6, and TNF- $\alpha$  can promote pulmonary vasoconstriction leading to increased PVR. Similarly, loss of ACE2, such as after viral infections, leading to increased AngII and subsequent activation of AT2 receptors can also promote pulmonary vasoconstrictor responses. An important aspect of PH is vascular remodeling. Although it is unclear at what stage vascular remodeling is initiated in ARDS, it is conceivable that the protracted presence of mediators such as HIFs and the accumulation of adenosine initiate vascular remodeling processes that contribute further to the pathogenesis of PH in ARDS. In line with this, chronic phase of ARDS is known for its fibroproliferative milieu, where HIF (Delbrel et al., 2018), adenosine (Karmouty-Quintana et al., 2013b), and hyaluronan (Li et al., 2011) play central roles.

Given the ongoing COVID-19 global pandemic, it is crucial for the authors to address the implications of the aforementioned findings for patients with COVID-19. COVID-19 has infected over 64 million individuals and resulted in over 1.3 million deaths worldwide (<https://coronavirus.jhu.edu/map.html> accessed December 2, 2020). ARDS is the most common clinical course for patients with severe COVID-19 infections (Machhi et al., 2020). Prognosis for patients with ARDS is dismal, and some recent evidence suggests that the patients with COVID-19-related ARDS may face an even higher risk of death. As effective treatments for ARDS are lacking and a vaccine against COVID-19 has yet to be developed, it is critical that targetable mechanisms behind this devastating disease are discovered. A recent review has summarized the known mechanisms to date that promote pulmonary vascular dysfunction in SARS-CoV-2-induced ARDS and identified novel potential treatment options that target the vasculature (Karmouty-Quintana et al., 2020).

## AUTHOR CONTRIBUTIONS

LR and AH contributed equally. All authors read and approved the manuscript.

## FUNDING

We acknowledge the National Heart Lung and Blood Institute: 5R01HL138510 (HK-Q) and The American Heart Association: 18IPA34170220 (HK-Q).

## REFERENCES

- Amsellem, V., Lipskaia, L., Abid, S., Poupel, L., Houssaini, A., Quarck, R., et al. (2014). CCR5 as a treatment target in pulmonary arterial hypertension. *Circulation* 130, 880–891. doi: 10.1161/CIRCULATIONAHA.114.010757
- Antoniak, S., Sparkenbaugh, E., and Pawlinski, R. (2014). Tissue factor, protease activated receptors and pathologic heart remodelling. *Thromb. Haemost.* 112, 893–900. doi: 10.1160/TH14-03-0243
- Araz, O. (2020). Current pharmacological approach to ARDS: the place of bosentan. *Eurasian J. Med.* 52, 81–85. doi: 10.5152/eurasianjmed.2020.19218
- Araz, O., Demirci, E., Ucar, E. Y., Calik, M., Pulur, D., Karaman, A., et al. (2013). Comparison of reducing effect on lung injury of dexamethasone and bosentan in acute lung injury: an experimental study. *Multidiscip. Res. Med.* 8:74. doi: 10.1186/2049-6958-8-74
- Asperen, R. M. W., Lutter, R., Specht, P. A., Moll, G. N., Woensel, J. B., van, Loos, C. M., et al. (2011). Acute respiratory distress syndrome leads to reduced ratio of



- ACE/ACE2 activities and is prevented by angiotensin-(1-7) or an angiotensin II receptor antagonist. *J. Pathol.* 225, 618–627. doi: 10.1002/path.2987
- Bartsch, P. (1999). High altitude pulmonary edema. *Med. Sci. Sports Exerc.* 31, S23–S27. doi: 10.1097/00005768-199901000-00004
- Beiderlinden, M., Kuehl, H., Boes, T., and Peters, J. (2006). Prevalence of pulmonary hypertension associated with severe acute respiratory distress syndrome: predictive value of computed tomography. *Intensive Care Med.* 32, 852–857. doi: 10.1007/s00134-006-0122-9
- Bell, T. J., Brand, O. J., Morgan, D. J., Salek-Ardakani, S., Jagger, C., Fujimori, T., et al. (2019). Defective lung function following influenza virus is due to prolonged, reversible hyaluronan synthesis. *Matrix Biol.* 80, 14–28. doi: 10.1016/j.matbio.2018.06.006
- Bellani, G., Laffey, J. G., Pham, T., Fan, E., Brochard, L., Esteban, A., et al. (2016). Epidemiology, patterns of care, and mortality for patients with acute respiratory distress syndrome in intensive care units in 50 countries. *JAMA* 315, 788–800. doi: 10.1001/jama.2016.0291
- Berhane, K., Margana, R. K., and Boggaram, V. (2000). Characterization of rabbit SP-B promoter region responsive to downregulation by tumor necrosis factor- $\alpha$ . *Am. J. Physiol. Lung Cell Mol. Physiol.* 279, L806–L814. doi: 10.1152/ajplung.2000.279.5.l806
- Boissier, F., Katsahian, S., Razazi, K., Thille, A. W., Roche-Campo, F., Leon, R., et al. (2013). Prevalence and prognosis of cor pulmonale during protective ventilation for acute respiratory distress syndrome. *Intensive Care Med.* 39, 1725–1733. doi: 10.1007/s00134-013-2941-9
- Brock, M., Trenkmann, M., Gay, R. E., Michel, B. A., Gay, S., Fischler, M., et al. (2009). Interleukin-6 modulates the expression of the bone morphogenic protein receptor type ii through a novel STAT3-microRNA cluster 17/92 pathway. *Circ. Res.* 104, 1184–1191. doi: 10.1161/CIRCRESAHA.109.197491
- Brower, R. G., Matthay, M. A., Morris, A., Schoenfeld, D., Thompson, B. T., and Wheeler, A. (2000). Ventilation with lower tidal volumes as compared with traditional tidal volumes for acute lung injury and the acute respiratory distress syndrome. *NEJM* 342, 1301–1308. doi: 10.1056/NEJM200005043421801
- Bull, T. M., Clark, B., McFann, K., and Moss, M. (2010). Pulmonary vascular dysfunction is associated with poor outcomes in patients with acute lung injury. *Am. J. Respir. Crit. Care Med.* 182, 1123–1128. doi: 10.1164/rccm.201002-0250OC
- Calcaianu, G., Calcaianu, M., Gschwend, A., Canuet, M., Meziani, F., and Kessler, R. (2017). Hemodynamic profile of pulmonary hypertension (PH) in ARDS. *Pulm Circ.* 8, 1–8. doi: 10.1177/2045893217753415
- Cheng, H., Wang, Y., and Wang, G.-Q. (2020). Organ-protective effect of angiotensin-converting enzyme 2 and its effect on the prognosis of COVID-19. *J. Med. Virol.* 92, 726–730. doi: 10.1002/jmv.25785
- Clozel, M., Maresta, A., and Humbert, M. (2013). Endothelin receptor antagonists. *Handb. Exp. Pharmacol.* 218, 199–227. doi: 10.1007/978-3-642-38664-0\_9
- Collum, S. D., Chen, N. Y., Hernandez, A. M. M., Hanmandlu, A., Sweeney, H., Mertens, T. C. J. C. J., et al. (2017). Inhibition of hyaluronan synthesis attenuates pulmonary hypertension associated with lung fibrosis. *Br. J. Pharm.* 174, 3284–3301. doi: 10.1111/bph.13947
- Collum, S. D., Molina, J. G., Hanmandlu, A., Bi, W., Pedroza, M., Mertens, T. C. J., et al. (2019). Adenosine and hyaluronan promote lung fibrosis and pulmonary hypertension in combined pulmonary fibrosis and emphysema. *Dis. Models Mech.* 12:dm.038711. doi: 10.1242/dmm.038711
- Davenport, A., and Maguire, J. (1994). Is endothelin-induced vasoconstriction mediated only by ETA receptors in humans? *Trends Pharmacol. Sci.* 15:9–11. doi: 10.1016/0165-6147(94)90120-1
- Delbrel, E., Soumare, A., Naguez, A., Label, R., Bernard, O., Bruhat, A., et al. (2018). HIF-1 $\alpha$  triggers ER stress and CHOP-mediated apoptosis in alveolar epithelial cells, a key event in pulmonary fibrosis. *Sci. Rep.* 8:17939. doi: 10.1038/s41598-018-36063-2
- Dessap, A. M., Boissier, F., Charron, C., Bégot, E., Repessé, X., Legras, A., et al. (2016). Acute cor pulmonale during protective ventilation for acute respiratory distress syndrome: prevalence, predictors, and clinical impact. *Intensive Care Med.* 42, 862–870. doi: 10.1007/s00134-015-4141-2
- Donoghue, M., Hsieh, F., Baronas, E., Godbout, K., Gosselin, M., Stagliano, N., et al. (2000). A novel angiotensin-converting enzyme-related carboxypeptidase (ACE2) converts angiotensin I to angiotensin 1-9. *Circ. Res.* 87, e1–e9. doi: 10.1161/01.RES.87.5.e1
- Dötsch, A., Eisele, L., Rabeling, M., Rump, K., Walstein, K., Bick, A., et al. (2017). Hypoxia inducible factor-2 alpha and prolinhydroxylase 2 polymorphisms in patients with acute respiratory distress syndrome (ARDS). *Int. J. Mol. Sci.* 18:1266. doi: 10.3390/ijms18061266
- Druml, W., Steltzer, H., Waldhäusl, W., Lenz, K., Hammerle, A., Vierhapper, H., et al. (1993). Endothelin-1 in adult respiratory distress syndrome. *Am. Rev. Respir. Dis.* 148, 1169–1173. doi: 10.1164/ajrccm/148.5.1169
- Eltzschig, H. K., and Carmeliet, P. (2011). Hypoxia and inflammation. *N. Engl. J. Med.* 364, 656–665. doi: 10.1056/NEJMra0910283
- Ferreira, A. J., and Santos, R., A. S. (2005). Cardiovascular actions of angiotensin-(1-7). *Braz. J. Med. Biol. Res.* 38, 499–507. doi: 10.1590/s0100-879x2005000400003
- Fischer, L., Freise, H., Hilpert, J.-H., Wendholt, D., Lauer, S., Aken, H., et al. (2004). Modulation of hypoxic pulmonary vasoconstriction is time and nitric oxide dependent in a peritonitis model of sepsis. *Intensive Care Med.* 30, 1821–1828. doi: 10.1007/s00134-004-2351-0
- Florentin, J., Coppin, E., Vasamsetti, S. B., Zhao, J., Tai, Y.-Y., Tang, Y., et al. (2018). Inflammatory macrophage expansion in pulmonary hypertension depends upon mobilization of blood-borne monocytes. *J. Immunol.* 200, 3612–3625. doi: 10.4049/jimmunol.1701287
- Frantzeskaki, F., Armaganidis, A., and Orfanos, S. E. (2017). Immunothrombosis in acute respiratory distress syndrome: cross talks between inflammation and coagulation. *Respiration* 93, 212–225. doi: 10.1159/000453002
- Frutos-Vivar, F., Nin, N., and Esteban, A. (2004). Epidemiology of acute lung injury and acute respiratory distress syndrome. *Curr. Opin. Crit. Care* 10, 1–6. doi: 10.1055/s-2006-948287
- Fujita, M., Shannon, J. M., Irvin, C. G., Fagan, K. A., Cool, C., Augustin, A., et al. (2001). Overexpression of tumor necrosis factor- $\alpha$  produces an increase in lung volumes and pulmonary hypertension. *Am. J. Physiol. Lung Cell Mol. Physiol.* 280, L39–L49. doi: 10.1152/ajplung.2001.280.1.L39
- Garcia-Morales, L. J., Chen, N.-Y., Weng, T., Luo, F., Davies, J., Philip, K., et al. (2015). Altered hypoxic-adenosine axis and metabolism in group iii pulmonary hypertension. *Am. J. Respir. Cell Mol. Biol.* 54, 574–583. doi: 10.1165/rcmb.2015-0145OC
- Gerasimovskaya, E., Kratzer, A., Sidiakova, A., Salys, J., Zamora, M., and Taraseviciene-Stewart, L. (2012). Interplay of macrophages and T cells in the lung vasculature. *Am. J. Physiol. Lung Cell Mol. Physiol.* 302, L1014–L1022. doi: 10.1152/ajplung.00357.2011
- Gong, H., Rehman, J., Tang, H., Wary, K., Mittal, M., Chaturvedi, P., et al. (2015). HIF2 $\alpha$  signaling inhibits adherens junctional disruption in acute lung injury. *J. Clin. Invest.* 125, 652–664. doi: 10.1172/JCI77701
- Gong, M. N., Thompson, B. T., Williams, P. L., Zhou, W., Wang, M. Z., Pothier, L., et al. (2006). Interleukin-10 polymorphism in position-1082 and acute respiratory distress syndrome. *Eur. Respir. J.* 27, 674–681. doi: 10.1183/09031936.06.00046405
- Gong, M. N., Wei, Z., Xu, L. L., Miller, D. P., Thompson, B. T., and Christiani, D. C. (2004). Polymorphism in the surfactant protein-B gene, gender, and the risk of direct pulmonary injury and ARDS. *Chest* 125, 203–211. doi: 10.1378/chest.125.1.203
- Gralinski, L., Bankhead, A. III, Jeng, S., Menachery, V., Prohl, S., Belisle, S., et al. (2013). Mechanisms of severe acute respiratory syndrome coronavirus-induced acute lung injury. *mBio* 4, e00271–13. doi: 10.1128/mBio.00271-13
- Groth, A., Vrugt, B., Brock, M., Speich, R., Ulrich, S., and Huber, L. C. (2014). Inflammatory cytokines in pulmonary hypertension. *Respir. Res.* 15:47. doi: 10.1186/1465-9921-15-47
- Guimarães, C., Da-Silva, S., Couture, R., and Rae, G. (2000). Mixed endothelin ET(A) and ET(B) antagonist bosentan inhibits oleic acid-induced lung plasma extravasation in mouse. *J. Cardiovasc. Pharmacol.* 36, S371–S373. doi: 10.1097/00005344-200036051-00107
- Hamming, I., Timens, W., Bulthuis, M. L. C., Lely, A. T., Navis, G. J., and van Goor, H. (2004). Tissue distribution of ACE2 protein, the functional receptor for SARS coronavirus. A first step in understanding SARS pathogenesis. *J. Pathol.* 203, 631–637. doi: 10.1002/path.1570
- Heinrich, P. C., Castell, J. V., and Andus, T. (1990). Interleukin-6 and the acute phase response. *Biochem. J.* 265, 621–636. doi: 10.1042/bj2650621

- Hellman, U., Karlsson, M. G., Engström-Laurent, A., Cajander, S., Dorofte, L., Ahlm, C., et al. (2020). Presence of hyaluronan in lung alveoli in severe Covid-19: An opening for new treatment options? *J. Biol. Chem.* 295, 15418–15422. doi: 10.1074/jbc.AC120.015967
- Helms, J., Tacquard, C., Severac, F., Leonard-Lorant, I., Ohana, M., and Delabranche, X. (2020). High risk of thrombosis in patients in severe SARS-CoV-2 infection: a multicenter prospective cohort study. *Intensive Care Med.* 46, 1089–1098. doi: 10.1007/s00134-020-06062-x
- Hemnes, A. R., Rathinasabapathy, A., Austin, E. A., Brittain, E. L., Carrier, E. J., Chen, X., et al. (2018). A potential therapeutic role for angiotensin-converting enzyme 2 in human pulmonary arterial hypertension. *Eur. Respir. J.* 51:1702638. doi: 10.1183/13993003.02638-2017
- Hoffmann, M., Kleine-Weber, H., Schroeder, S., Krüger, N., Herrler, T., Erichsen, S., et al. (2020). SARS-CoV-2 cell entry depends on ACE2 and TMPRSS2 and is blocked by a clinically proven protease inhibitor. *Cell* 181, 271–280.e8. doi: 10.1016/j.cell.2020.02.052
- Huang, X., Zhang, X., Zhao, D. X., Yin, J., Hu, G., Evans, C. E., et al. (2019). Endothelial hypoxia-inducible factor-1 $\alpha$  is required for vascular repair and resolution of inflammatory lung injury through forkhead box protein M1. *Am. J. Pathol.* 189, 1664–1679. doi: 10.1016/j.ajpath.2019.04.014
- Imai, Y., Kuba, K., Ohto-Nakanishi, T., and Penninger, J. M. (2010). Angiotensin-converting enzyme 2 (ACE2) in disease pathogenesis. *Circ. J.* 74, 405–410. doi: 10.1253/circj.cj-10-0045
- Imai, Y., Kuba, K., Rao, S., Huan, Y., Guo, F., Guan, B., et al. (2005). Angiotensin-converting enzyme 2 protects from severe acute lung failure. *Nature* 436, 112–116. doi: 10.1038/nature03712
- Ito, T., Okada, T., Miyashita, H., Nomoto, T., Nonaka-Sarukawa, M., Uchibori, R., et al. (2007). Interleukin-10 expression mediated by an adeno-associated virus vector prevents monocrotaline-induced pulmonary arterial hypertension in rats. *Circ. Res.* 101, 734–741. doi: 10.1161/CIRCRESAHA.107.153023
- Itoh, A., Nishihira, J., Makita, H., Miyamoto, K., Yamaguchi, E., and Nishimura, M. (2003). Effects of IL-1 $\beta$ , TNF- $\alpha$  and macrophage migration inhibitory factor on prostacyclin synthesis in rat pulmonary artery smooth muscle cells. *Respirology* 8, 467–472. doi: 10.1046/j.1440-1843.2003.00491.x
- Iwai, M., and Horiuchi, M. (2009). Devil and angel in the renin-angiotensin system: ACE-angiotensin II-AT1 receptor axis vs. ACE2-angiotensin-(1-7)-Mas receptor axis. *Hypertension Res.* 32, 533–536. doi: 10.1038/hr.2009.74
- Jerng, J.-S., Yu, C.-J., Wang, H.-C., Chen, K.-Y., Cheng, S.-L., and Yang, P.-C. (2006). Polymorphism of the angiotensin-converting enzyme gene affects the outcome of acute respiratory distress syndrome. *Crit. Care Med.* 34, 1001–1006. doi: 10.1097/01.CCM.0000206107.92476.39
- Jia, H. (2016). Pulmonary angiotensin-converting enzyme 2 (ACE2) and inflammatory lung disease. *Shock* 46, 239–248. doi: 10.1097/SHK.0000000000000633
- José, R. J., Williams, A. E., and Chambers, R. C. (2014). Proteinase-activated receptors in fibroproliferative lung disease. *Thorax* 69, 190–192. doi: 10.1136/thoraxjnl-2013-204367
- Kaber, G., Kratochvil, M. J., Burgener, E. B., Peltan, E. L., Barlow, G., Yang, S., et al. (2020). Hyaluronan is abundant in COVID-19 respiratory secretions. *medRxiv*, 2020.09.11.20191692. doi: 10.1101/2020.09.11.20191692
- Karmouty-Quintana, H., Thandavarayan, R. A., Keller, S. P., Sahay, S., Pandit, L. M., and Akkanti, B. (2020). Emerging mechanisms of pulmonary vasoconstriction in SARS-CoV-2-induced acute respiratory distress syndrome (ARDS) and potential therapeutic targets. *Int. J. Mol. Sci.* 21:8081. doi: 10.3390/ijms21218081
- Karmouty-Quintana, H., Weng, T., Garcia-Morales, L. J., Chen, N.-Y., Pedroza, M., Zhong, H., et al. (2013a). Adenosine A2B receptor and hyaluronan modulate pulmonary hypertension associated with chronic obstructive pulmonary disease. *Am. J. Respir. Cell Mol. Biol.* 49, 1038–1047. doi: 10.1165/rcmb.2013-0089OC
- Karmouty-Quintana, H., Xia, Y., and Blackburn, M. R. (2013b). Adenosine signaling during acute and chronic disease states. *J. Mol. Med. (Berl)* 91, 173–181. doi: 10.1007/s00109-013-0997-1
- Karmouty-Quintana, H., Zhong, H., Acero, L., Weng, T., Melicoff, E., West, J. D., et al. (2012). The A2B adenosine receptor modulates pulmonary hypertension associated with interstitial lung disease. *FASEB J.* 26, 2546–2557. doi: 10.1096/fj.11-200907
- Khan, A., Benthin, C., Zeno, B., Albertson, T. E., Boyd, J., Christie, J. D., et al. (2017). A pilot clinical trial of recombinant human angiotensin-converting enzyme 2 in acute respiratory distress syndrome. *Crit. Care* 21:234. doi: 10.1186/s13054-017-1823-x
- Krege, J. H., John, S. W. M., Langenbach, L. L., Hodgin, J. B., Hagaman, J. R., Bachman, E. S., et al. (1995). Male–female differences in fertility and blood pressure in ACE-deficient mice. *Nature* 375, 146–148. doi: 10.1038/375146a0
- Kreutz, R., Algharably, E. A. E.-H., Azizi, M., Dobrowolski, P., Guzik, T., Januszewicz, A., et al. (2020). Hypertension, the renin-angiotensin system, and the risk of lower respiratory tract infections and lung injury: implications for COVID-19. *Cardiovasc. Res.* 116, 1688–1699. doi: 10.1093/cvr/cvaa097
- Kuba, K., Imai, Y., and Penninger, J. M. (2006). Angiotensin-converting enzyme 2 in lung diseases. *Curr. Opin. Pharmacol.* 6, 271–276. doi: 10.1016/j.coph.2006.03.001
- Kuba, K., Imai, Y., Rao, S., Gao, H., Guo, F., Guan, B., et al. (2005). A crucial role of angiotensin converting enzyme 2 (ACE2) in SARS coronavirus-induced lung injury. *Nat. Med.* 11, 875–879. doi: 10.1038/nm1267
- Levi, M., and Van Der Poll, T. (2010). Inflammation and coagulation. *Crit. Care Med.* 38, S26–S34. doi: 10.1097/CCM.0b013e3181c98d21
- Li, Y., Jiang, D., Liang, J., Meltzer, E. B., Gray, A., Miura, R., et al. (2011). Severe lung fibrosis requires an invasive fibroblast phenotype regulated by hyaluronan and CD44. *J. Exp. Med.* 208, 1459–1471. doi: 10.1084/jem.20102510
- Lumb, A. B., and Slinger, P. (2015). Hypoxic pulmonary vasoconstriction: physiology and anesthetic Implications. *Anesthesiology* 122, 932–946. doi: 10.1042/BSE0430061
- Luster, A. D. (1998). Mechanisms of disease: chemokines - chemotactic cytokines that mediate inflammation. *N. Engl. J. Med.* 338:436–445. doi: 10.1056/NEJM199802123380706
- Machhi, J., Herskovitz, J., Senan, A. M., Dutta, D., Nath, B., Oleynikov, M. D., et al. (2020). The natural history, pathobiology, and clinical manifestations of SARS-CoV-2 infections. *J. Neuroimmune Pharmacol.* 15:359–386. doi: 10.1007/s11481-020-09944-5
- MacKman, N. (2009). The role of tissue factor and factor VIIa in hemostasis. *Anesth. Analg.* 108, 1447–1452. doi: 10.1213/ane.0b013e31819bceb1
- Mamazhakypov, A., Viswanathan, G., Lawrie, A., Schermuly, R. T., and Rajagopal, S. (2021). The role of chemokines and chemokine receptors in pulmonary arterial hypertension. *Br. J. Pharmacol.* 178:72–89. doi: 10.1111/bph.14826
- Maniatis, N. A., Kotanidou, A., Catravas, J. D., and Orfanos, S. E. (2008). Endothelial pathomechanisms in acute lung injury. *Vascul. Pharmacol.* 49, 119–133. doi: 10.1016/j.vph.2008.06.009
- Marshall, B. E., Hanson, C. W., Frasch, F., and Marshall, C. (1994). Role of hypoxic pulmonary vasoconstriction in pulmonary gas exchange and blood flow distribution. *Intensive Care Med.* 20, 379–389. doi: 10.1007/BF01720916
- Marshall, R. P., Webb, S., Bellingan, G. J., Montgomery, H. E., Chaudhari, B., McNulty, R. J., et al. (2002). Angiotensin converting enzyme insertion/deletion polymorphism is associated with susceptibility and outcome in acute respiratory distress syndrome. *Am. J. Respir. Crit. Care Med.* 166, 646–650. doi: 10.1164/rccm.2108086
- Matthay, M. A., and Zemans, R. L. (2011). The acute respiratory distress syndrome: pathogenesis and treatment. *Annu. Rev. Pathol.* 6, 147–163. doi: 10.1146/annurev-pathol-011110-130158
- McKallip, R., Ban, H., and Uchakina, O. (2015). Treatment with the hyaluronic acid synthesis inhibitor 4-methylumbelliferone suppresses LPS-induced lung inflammation. *Inflammation* 38, 1250–1259. doi: 10.1007/s10753-014-0092-y
- McKallip, R. J., Hagele, H. F., and Uchakina, O. N. (2013). Treatment with the hyaluronic acid synthesis inhibitor 4-methylumbelliferone suppresses SEB-induced lung inflammation. *Toxins* 5, 1814–1826. doi: 10.3390/toxins5101814
- McLoughlin, P. (2018). Hypoxic pulmonary vasoconstriction: Building a solid base [View Point]. *Exp. Physiol.* 103, 1181–1182. doi: 10.1113/EP087179
- Meduri, G. U., Annane, D., Chrousos, G. P., Marik, P. E., and Sinclair, S. E. (2009). Activation and regulation of systemic inflammation in ARDS: rationale for prolonged glucocorticoid therapy. *Chest* 136, 1631–1643. doi: 10.1378/chest.08-2408
- Mertens, T. C. J., Hanmandlu, A., Tu, L., Phan, C., Collum, S. D., Chen, N.-Y., et al. (2018). Switching-off Adora2b in vascular smooth muscle cells halts the development of pulmonary hypertension. *Front. Physiol.* 9:555. doi: 10.3389/fphys.2018.00555

- Miakotina, O. L., and Snyder, J. M. (2002). TNF- $\alpha$  inhibits SP-A gene expression in lung epithelial cells via p38 MAPK. *Am. J. Physiol. Lung Cell Mol. Physiol.* 283, L418–L427. doi: 10.1152/ajplung.00470.2001
- Molet, S., Furukawa, K., Maghazechi, A., Hamid, Q., and Giaid, A. (2000). Chemokine- and cytokine-induced expression of endothelin 1 and endothelin-converting enzyme 1 in endothelial cells. *J. Allergy Clin. Immunol.* 105, 333–338. doi: 10.1016/s0091-6749(00)90084-8
- Moloney, E. D., and Evans, T. W. (2003). Pathophysiology and pharmacological treatment of pulmonary hypertension in acute respiratory distress syndrome. *Eur. Respir. J.* 21, 720–727. doi: 10.1183/09031936.03.00120102
- Monchi, M., Bellenfant, F., Cariou, A., Joly, L.-M., Thebert, D., Laurent, I., et al. (1998). Early predictive factors of survival in the acute respiratory distress syndrome. A multivariate analysis. *Am. J. Respir. Crit. Care Med.* 158, 1076–1081. doi: 10.1164/ajrccm.158.4.9802009
- Morrell, N. W., Morris, K. G., and Stenmark, K. R. (1995). Role of angiotensin-converting enzyme and angiotensin II in development of hypoxic pulmonary hypertension. *Am. J. Physiol. Heart Circ. Physiol.* 269, H1186–H1194. doi: 10.1152/ajpheart.1995.269.4.H1186
- Morrell, N. W., Upton, P. D., Kotecha, S., Huntley, A., Yacoub, M. H., Polak, J. M., et al. (1999). Angiotensin II activates MAPK and stimulates growth of human pulmonary artery smooth muscle via AT1 receptors. *Am. J. Physiol. Lung Cell Mol. Physiol.* 277, L440–L448. doi: 10.1152/ajplung.1999.277.3.L440
- Nakano, Y., Tasaka, S., Saito, F., Yamada, W., Shiraishi, Y., Owaga, Y., et al. (2007). Endothelin-1 level in epithelial lining fluid of patients with acute respiratory distress syndrome. *Respirology* 12, 740–743. doi: 10.1111/j.1440-1843.2007.01115.x
- Namendys-Silva, S. A., Santos-Martínez, L. E., Pulido, T., Rivero-Sigarroa, E., Baltazar-Torres, J. A., Domínguez-Cherit, G., et al. (2014). Pulmonary hypertension due to acute respiratory distress syndrome. *Braz. J. Med. Biol. Res.* 47, 904–910. doi: 10.1590/1414-431X20143316
- Ni, K., Gill, A., Tseng, V., Mikosz, A. M., Koike, K., Beatman, E. L., et al. (2018). Rapid clearance of heavy chain-modified hyaluronan during resolving acute lung injury. *Respir. Res.* 19:107. doi: 10.1186/s12931-018-0812-1
- Nieuwenhuizen, L., De Groot, P. G., Grutters, J. C., and Biesma, D. H. (2009). A review of pulmonary coagulopathy in acute lung injury, acute respiratory distress syndrome and pneumonia. *Eur. J. Haematol.* 82, 413–425. doi: 10.1111/j.1600-0609.2009.01238.x
- Nong, Z., Stassen, J.-M., Moons, L., Collen, D., and Janssens, S. (1996). Inhibition of tissue angiotensin-converting enzyme with quinapril reduces hypoxic pulmonary hypertension and pulmonary vascular remodeling. *Circulation* 94, 1941–1947. doi: 10.1161/01.CIR.94.8.1941
- Orte, C., Polak, J. M., Haworth, S. G., Yacoub, M. H., and Morrell, N. W. (2000). Expression of pulmonary vascular angiotensin-converting enzyme in primary and secondary plexiform pulmonary hypertension. *J. Pathol.* 192, 379–384. doi: 10.1002/1096-9896(2000)9999:9999::AID-PATH715>3.0.CO;2-Q
- Osman, D., Monnet, X., Castelain, V., Anguel, N., Warszawski, J., Teboul, J.-L., et al. (2009). Incidence and prognostic value of right ventricular failure in acute respiratory distress syndrome. *Intensive Care Med.* 35, 69–76. doi: 10.1007/s00134-008-1307-1
- Pandolfi, R., Barreira, B., Moreno, E., Lara-Acedo, V., Morales-Cano, D., Martínez-Ramas, A., et al. (2017). Role of acid sphingomyelinase and IL-6 as mediators of endotoxin-induced pulmonary vascular dysfunction. *Thorax* 72, 460–471. doi: 10.1136/thoraxjnl-2015-208067
- Parameswaran, N., and Patial, S. (2010). Tumor necrosis factor- $\alpha$  signaling in macrophages. *Crit. Rev. Eukaryot. Gene Expr.* 20, 87–103. doi: 10.1615/CritRevEukarGeneExpr.v20.i2.10
- Peek, G. J., Mugford, P. M., Tiruvoipati, R., Wilson, A., Allen, E., Thalanany, M. M., et al. (2009). Efficacy and economic assessment of conventional ventilatory support versus extracorporeal membrane oxygenation for severe adult respiratory failure (CESAR): a multicentre randomised controlled trial. *Lancet* 374, P1351–1363. doi: 10.1016/S0140-6736(09)61069-2
- Poor, H., Gargis, R., and Studer, S. (2012). World Health Organization group III pulmonary hypertension. *Prog. Cardiovasc. Dis.* 55, 119–127. doi: 10.1016/j.pcad.2012.08.003
- Potus, F. F., Mai, V., Lebre, M., Malenfant, S., Breton-Gagnon, E., Lejoie, A. C., et al. (2020). Novel insights on the pulmonary vascular consequences of COVID-19. *Am. J. Physiol. Lung Cell Mol. Physiol.* 319, L277–L288. doi: 10.1152/ajplung.00195.2020
- Price, L. C., McAuley, D. F., Marino, P. S., Finney, S. J., Griffiths, M. J., and Wort, S. J. (2012). Pathophysiology of pulmonary hypertension in acute lung injury. *Am. J. Physiol. Lung Cell Mol. Physiol.* 302, L803–L815. doi: 10.1152/ajplung.00355.2011
- Price, L. C., and Wort, J. S. (2017). Pulmonary hypertension in ARDS: inflammation matters! *Thorax* 72, 396–397. doi: 10.1136/thoraxjnl-2016-209199
- Puneet, P., Moomchala, S., and Bhatia, M. (2005). Chemokines in acute respiratory distress syndrome. *Am. J. Physiol. Lung Cell Mol. Physiol.* 288, L3–L15. doi: 10.1152/ajplung.00405.2003
- Rajagopal, K., Bryant, A. J., Sahay, S., Wareing, N., Zhou, Y., Pandit, L. M., et al. (2021). Idiopathic pulmonary fibrosis and pulmonary hypertension: Heracles meets the Hydra. *Br. J. Pharmacol.* 178, 172–186. doi: 10.1111/bph.15036
- Ranieri, V. M., Suter, P. M., Tortorella, C., De Tullio, R., Dayer, J. M., Brienza, A., et al. (1999). Effect of mechanical ventilation on inflammatory mediators in patients with acute respiratory distress syndrome: a randomized controlled trial. *JAMA* 282, 54–61. doi: 10.1001/jama.282.1.54
- Rezoagli, E., Fumagalli, R., and Bellani, G. (2017). Definition and epidemiology of acute respiratory distress syndrome. *Ann. Transl. Med.* 5, 1–12. doi: 10.21037/atm.2017.06.62
- Rigat, B., Hubert, C., Alhenc-Gelas, F., Cambien, F., Corvol, P., and Soubrier, F. (1990). An insertion/deletion polymorphism in the angiotensin I-converting enzyme gene accounting for half the variance of serum enzyme levels. *JCI* 86, 1343–1346. doi: 10.1172/JCI114844
- Ryan, D., Frohlich, S., and McLoughlin, P. (2014). Pulmonary vascular dysfunction in ARDS. *Ann Intensive Care* 4, 1–11. doi: 10.1186/s13613-014-0028-6
- Sabat, R., Grütz, G., Warszawski, K., Kirsch, S., Witte, E., Wolk, K., et al. (2010). Biology of interleukin-10. *Cytokine Growth Factor Rev.* 21, 331–344. doi: 10.1016/j.cytogfr.2010.09.002
- Samary, C. S., Santos, R. S., Santos, C. L., Felix, N. S., Bentes, M., Barboza, T., et al. (2015). Biological impact of transpulmonary driving pressure in experimental acute respiratory distress syndrome. *Anesthesiology* 123, 423–433. doi: 10.1097/ALN.0000000000000716
- Sanai, L., Haynes, W., MacKenzie, A., Grant, I., and Webb, D. (1996). Endothelin production in sepsis and the adult respiratory distress syndrome. *Intensive Care Med.* 22, 52–56. doi: 10.1007/BF01728331
- Savale, L., Tu, L., Rideau, D., Izziki, M., Maitre, B., Adnot, S., et al. (2009). Impact of interleukin-6 on hypoxia-induced pulmonary hypertension and lung inflammation in mice. *Respir. Res.* 10:6. doi: 10.1186/1465-9921-10-6
- Schuster, D. P., Crouch, E. C., Parks, W. C., Johnson, T., and Botney, M. D. (2012). Angiotensin converting enzyme expression in primary pulmonary hypertension. *Am. J. Respir. Crit. Care Med.* 154, 1087–1091. doi: 10.1164/ajrccm.154.4.8887612
- Selimovic, N., Bergh, C. H., Andersson, B., Sakiniene, E., Carlsten, H., and Rundqvist, B. (2009). Growth factors and interleukin-6 across the lung circulation in pulmonary hypertension. *Eur. Respir. J.* 34, 662–668. doi: 10.1183/09031936.00174908
- Shi, Y., Wang, Y., Shao, C., Huang, J., Gan, J., Huang, X., et al. (2020). COVID-19 infection: the perspectives on immune responses. *Cell Death Differ* 27, 1451–1454. doi: 10.1038/s41418-020-0530-3
- Simonneau, G., Montani, D., Celermajer, D. S., Denton, C. P., Gatzoulis, M. A., Krowka, M., et al. (2019). Haemodynamic definitions and updated clinical classification of pulmonary hypertension. *Eur. Respir. J.* 53, 1–13. doi: 10.1183/13993003.01913-2018
- Soon, E., Holmes, A. M., Treacy, C. M., Doughty, N. J., Southgate, L., MacHado, R. D., et al. (2010). Elevated levels of inflammatory cytokines predict survival in idiopathic and familial pulmonary arterial hypertension. *Circulation* 122, 920–927. doi: 10.1161/CIRCULATIONAHA.109.933762
- South, A. M., Diz, D. I., and Chappell, M. C. (2020). COVID-19, ACE2, and the cardiovascular consequences. *Am. J. Physiol. Heart Circ. Physiol.* 318, H1084–H1090. doi: 10.1152/ajpheart.00217.2020
- Spöhr, F., Busch, C. J., Reich, C., Motsch, J., Gebhard, M. M., Kuebler, W. M., et al. (2007). 4-Aminopyridine restores impaired hypoxic pulmonary vasoconstriction in endotoxemic mice. *Anesthesiology* 107, 597–604. doi: 10.1097/01.anes.0000281897.13703.f3



- Squara, P., Dhainaut, J.-F. A., Artigas, A., Carlet, J., and Group ECAW. (1998). Hemodynamic profile in severe ARDS: results of the European Collaborative ARDS Study. *Intensive Care Med.* 24, 1018–1028. doi: 10.1007/s001340050710
- Steiner, M. K., Syrkin, O. L., Kolliputi, N., Mark, E. J., Hales, C. A., and Waxman, A. B. (2009). Interleukin-6 overexpression induces pulmonary hypertension. *Circ. Res.* 104, 236–244. doi: 10.1161/CIRCRESAHA.108.182014
- Stevens, T., Janssen, P. L., and Tucker, A. (1992). Acute and long-term TNF- $\alpha$  administration increases pulmonary vascular reactivity in isolated rat lungs. *J. Appl. Physiol.* 73, 708–712. doi: 10.1152/jappl.1992.73.2.708
- Stow, J. L., Ching Low, P., Offenhäuser, C., and Sangermani, D. (2009). Cytokine secretion in macrophages and other cells: pathways and mediators. *Immunobiology* 214, 601–612. doi: 10.1016/j.imbio.2008.11.005
- Sun, X., Wang, T., Cai, D., Hu, Z., Chen, J., Liao, H., et al. (2020). Cytokine storm intervention in the early stages of COVID-19 pneumonia. *Cytokine Growth Factor Rev.* 53, 38–42. doi: 10.1016/j.cytofr.2020.04.002
- Suylen, R. J., Van, A. W. M., Smits, J. F., and Daemen, M. J. (2001). Dissociation of pulmonary vascular remodeling and right ventricular pressure in tissue angiotensin-converting enzyme-deficient mice under conditions of chronic alveolar hypoxia. *Am. J. Respir. Crit. Care Med.* 163, 1241–1245. doi: 10.1164/ajrccm.163.5.2003144
- Sylvester, J., Shimoda, L. A., Aaronson, P. I., and Ward, J. P. (2012). Hypoxic pulmonary vasoconstriction. *Physiol. Rev.* 92, 367–520. doi: 10.1152/physrev.00041.2010
- Tamosiuniene, R., Tian, W., Dhillon, G., Wang, L., Sung, Y. K., Gera, L., et al. (2011). Regulatory T cells limit vascular endothelial injury and prevent pulmonary hypertension. *Circ. Res.* 109, 867–879. doi: 10.1161/CIRCRESAHA.110.236927
- Tang, N., Bai, H., Chen, X., Gong, J., Li, D., and Sun, Z. (2020a). Anticoagulant treatment is associated with decreased mortality in severe coronavirus disease 2019 patients with coagulopathy. *J. Thromb. Haemost.* 18, 1094–1099. doi: 10.1111/jth.14817
- Tang, N., Li, D., Wang, X., and Sun, Z. (2020b). Abnormal coagulation parameters are associated with poor prognosis in patients with novel coronavirus pneumonia. *J. Thromb. Haemost.* 18, 1233–1234. doi: 10.1111/jth.14768
- The ARDS and Definition Task Force (2012). Acute respiratory distress syndrome: the Berlin definition. *JAMA* 307, 2526–2533. doi: 10.1001/jama.2012.5669
- Tipnis, S. R., Hooper, N. M., Hyde, R., Karran, E., Christie, G., and Turner, A. J. (2000). A human homolog of angiotensin-converting enzyme cloning and functional expression as a captopril-insensitive carboxypeptidase. *J. Biol. Chem.* 275, 33238–33243. doi: 10.1074/jbc.M002615200
- Tisoncik, J. R., Korth, M. J., Simmons, C. P., Farrar, J., Martin, T. R., and Katze, M. G. (2012). Into the eye of the cytokine storm. *Microbiol. Mol. Biol. Rev.* 76, 16–32. doi: 10.1128/mmbr.05015-11
- Tomashefski, J. F., Davies, P., Boggis, C., Greene, R., Zapol, W. M., and Reid, L. M. (1983). The pulmonary vascular lesions of the adult respiratory distress syndrome. *Am. J. Pathol.* 112, 112–126.
- Turzo, M., Vaith, J., Lasitschka, F., Weigand, M. A., and Busch, C. J. (2018). Role of ATP-sensitive potassium channels on hypoxic pulmonary vasoconstriction in endotoxemia. *Respir. Res.* 19:29. doi: 10.1186/s12931-018-0735-x
- Vieillard-Baron, A., Schmitt, J. M., Augarde, R., Fellahi, J. L., Prin, S., Page, B., et al. (2001). Acute cor pulmonale in acute respiratory distress syndrome submitted to protective ventilation: incidence, clinical implications, and prognosis. *Crit. Care Med.* 29, 1551–1555. doi: 10.1097/00003246-200108000-00009
- Villar, J., Blazquez, M. A., Lubillo, S., Quintana, J., and Manzano, J. L. (1989). Pulmonary hypertension in acute respiratory failure. *Crit. Care Med.* 17, 523–526.
- Ware, L. B., Fang, X., and Matthay, M. A. (2003). Protein C and thrombomodulin in human acute lung injury. *Am. J. Physiol. Lung Cell Mol. Physiol.* 285, L514–L521. doi: 10.1152/ajplung.00442.2002
- Ware, L. B., Matthay, M. A., Parsons, P. E., Thompson, B. T., Januzzi, J. L., Eisner, M. D., et al. (2007). Pathogenetic and prognostic significance of altered coagulation and fibrinolysis in acute lung injury/acute respiratory distress syndrome. *Crit. Care Med.* 35, 1821–1828. doi: 10.1016/s0734-3299(08)70449-0
- Welty-Wolf, K. E., Carraway, M. S., Miller, D. L., Ortel, T. L., Ezban, M., Ghio, A. J., et al. (2001). Coagulation blockade prevents sepsis-induced respiratory and renal failure in baboons. *Am. J. Respir. Crit. Care Med.* 164, 1988–1996. doi: 10.1164/ajrccm.164.10.2105027
- World Health Organization. (2020). WHO Coronavirus Disease (COVID-19) Dashboard. WHO. Available online at: <https://covid19.who.int/>
- Wrapp, D., Wang, N., Corbett, K. S., Goldsmith, J. A., Hsieh, C.-L., Abiona, O., et al. (2020). Cryo-EM structure of the 2019-nCoV spike in the prefusion conformation. *Science* 367, 1260–1263. doi: 10.1126/science.abb2507
- Xianwei, W., Magomed, K., Ding, Z., Sona, M., Jingjun, L., Shijie, L., et al. (2012). Cross-talk between inflammation and angiotensin II: studies based on direct transfection of cardiomyocytes with AT1R and AT2R cDNA. *Exp. Biol. Med.* 237, 1394–1401. doi: 10.1258/ebm.2012.012212
- Xiaofang, Z., Wang, K., Zuo, P., Liu, Y., Zhang, M., Xie, S., et al. (2020). Early decrease in blood platelet count is associated with poor prognosis in COVID-19 patients—indications for predictive, preventive, and personalized medical approach. *EPMA J.* 11, 1–7. doi: 10.1007/s13167-020-00208-z
- Xu, X., Han, M., Li, T., Sun, W., Wang, D., Fu, B., et al. (2020). Effective treatment of severe COVID-19 patients with tocilizumab. *Proc. Natl. Acad. Sci. U.S.A.* 117, 10970–10975. doi: 10.1073/pnas.2005615117
- Yamazato, Y., Ferreira, A. J., Hong, K.-H., Sriramula, S., Francis, J., Yamazato, M., et al. (2009). Prevention of pulmonary hypertension by Angiotensin-converting enzyme 2 gene transfer. *Hypertension* 54, 365–371. doi: 10.1161/HYPERTENSIONAHA.108.125468
- Zabini, D., Nagaraj, C., Stacher, E., Lang, I. M., Nierlich, P., Klepetko, W., et al. (2012). Angiostatic factors in the pulmonary endarterectomy material from chronic thromboembolic pulmonary hypertension patients cause endothelial dysfunction. *PLoS ONE* 7:e43793. doi: 10.1371/journal.pone.0043793
- Zambelli, V., Bellani, G., Borsari, R., Pozzi, F., Grassi, A., Scanziani, M., et al. (2015). Angiotensin-(1-7) improves oxygenation, while reducing cellular infiltrate and fibrosis in experimental acute respiratory distress syndrome. *Intensive Care Med. Exp.* 3:44. doi: 10.1186/s40635-015-0044-3
- Zhang, R., Wu, Y., Zhao, M., Liu, C., Zhou, L., Shen, S., et al. (2009). Role of HIF-1 $\alpha$  in the regulation ACE and ACE2 expression in hypoxic human pulmonary artery smooth muscle cells. *Am. J. Physiol. Lung Cell Mol. Physiol.* 297, L631–L640. doi: 10.1152/ajplung.90415.2008
- Zhiyu, D., Ming, L., John, W., Maggie, M. Z., and You-Yang, Z. (2016). Prolyl-4 Hydroxylase 2 (PHD2) deficiency in endothelial cells and hematopoietic cells induces obliterative vascular remodeling and severe pulmonary arterial hypertension in mice and humans through hypoxia-inducible factor-2 $\alpha$ . *Circulation* 133, 2447–2458. doi: 10.1161/CIRCULATIONAHA.116.021494

**Conflict of Interest:** The authors declare that the research was conducted in the absence of any commercial or financial relationships that could be construed as a potential conflict of interest.

Copyright © 2021 Revercomb, Hanmandlu, Wareing, Akkanti and Karmouty-Quintana. This is an open-access article distributed under the terms of the Creative Commons Attribution License (CC BY). The use, distribution or reproduction in other forums is permitted, provided the original author(s) and the copyright owner(s) are credited and that the original publication in this journal is cited, in accordance with accepted academic practice. No use, distribution or reproduction is permitted which does not comply with these terms.



# Enhancing Extracellular Adenosine Levels Restores Barrier Function in Acute Lung Injury Through Expression of Focal Adhesion Proteins

Wei Wang<sup>1</sup>, Ning-yuan Chen<sup>2</sup>, Dewei Ren<sup>3</sup>, Jonathan Davies<sup>4</sup>, Kemly Philip<sup>2</sup>, Holger K. Eltzschig<sup>5</sup>, Michael R. Blackburn<sup>2,6</sup>, Bindu Akkanti<sup>7</sup>, Harry Karmouty-Quintana<sup>2,6,7\*</sup> and Tingting Weng<sup>2,6\*</sup>

<sup>1</sup>Department of Thoracic Surgery, Renmin Hospital of Wuhan University, Wuhan, China, <sup>2</sup>Department of Biochemistry and Molecular Biology, McGovern Medical School, The University of Texas Health Science Center at Houston, Houston, TX, United States, <sup>3</sup>Houston Methodist J.C. Walter Jr. Transplant Center, Houston Methodist Hospital, Houston, TX, United States, <sup>4</sup>Division of Neonatal-Perinatal Medicine, Department of Pediatrics, Baylor College of Medicine, Houston, TX, United States, <sup>5</sup>Department of Anesthesiology, McGovern Medical School, The University of Texas Health Science Center at Houston, Houston, TX, United States, <sup>6</sup>UTHealth Pulmonary Center of Excellence, Houston, TX, United States, <sup>7</sup>Divisions of Critical Care, Pulmonary and Sleep Medicine, Department of Internal Medicine, McGovern Medical School, The University of Texas Health Science Center at Houston, Houston, TX, United States

## OPEN ACCESS

### Edited by:

Zhang Qingling,  
Guangzhou Institute of Respiratory  
Health, China

### Reviewed by:

Shikha Prasad,  
Feinberg School of Medicine,  
Northwestern University, United States  
Ramya Sivakumar,  
University of Washington, Seattle, WA,  
United States

### \*Correspondence:

Harry Karmouty-Quintana  
harry.karmouty@uth.tmc.edu  
Tingting Weng  
tingting.weng@uth.tmc.edu

### Specialty section:

This article was submitted to  
Molecular Diagnostics and  
Therapeutics,  
a section of the journal  
Frontiers in Molecular Biosciences

**Received:** 01 December 2020

**Accepted:** 01 February 2021

**Published:** 10 March 2021

### Citation:

Wang W, Chen N, Ren D, Davies J, Philip K, Eltzschig HK, Blackburn MR, Akkanti B, Karmouty-Quintana H and Weng T (2021) Enhancing Extracellular Adenosine Levels Restores Barrier Function in Acute Lung Injury Through Expression of Focal Adhesion Proteins. *Front. Mol. Biosci.* 8:636678. doi: 10.3389/fmolb.2021.636678

**Background:** Acute respiratory distress syndrome (ARDS) is a clinical presentation of acute lung injury (ALI) with often fatal lung complication. Adenosine, a nucleoside generated following cellular stress provides protective effects in acute injury. The levels of extracellular adenosine can be depleted by equilibrative nucleoside transporters (ENTs). ENT inhibition by pharmaceutical agent dipyridamole promotes extracellular adenosine accumulation and is protective in ARDS. However, the therapeutic potential of dipyridamole in acute lung injury has not yet been evaluated.

**Methods:** Adenosine acts on three adenosine receptors, the adenosine A1 (Adora1), A2a (Adora2a), the A2b (Adora2b) or the adenosine A3 (Adora 3) receptor. Accumulation of adenosine is usually required to stimulate the low-affinity Adora2b receptor. In order to investigate the effect of adenosine accumulation and the contribution of epithelial-specific ENT2 or adora2b expression in experimental ALI, dipyridamole, and epithelial specific ENT2 or Adora2b deficient mice were utilized. MLE12 cells were used to probe downstream Adora2b signaling. Adenosine receptors, transporters, and targets were determined in ARDS lungs.

**Results:** ENT2 is mainly expressed in alveolar epithelial cells and is negatively regulated by hypoxia following tissue injury. Enhancing adenosine levels with ENT1/ENT2 inhibitor dipyridamole at a time when bleomycin-induced ALI was present, reduced further injury. Mice pretreated with the ADORA2B agonist BAY 60-6583 were protected from bleomycin-induced ALI by reducing vascular leakage ( $558.6 \pm 50.4$  vs.  $379.9 \pm 70.4$ ,  $p < 0.05$ ), total bronchoalveolar lavage fluid cell numbers ( $17.9 \pm 1.8$  to  $13.4 \pm 1.4$  e4,  $p < 0.05$ ), and neutrophil infiltration ( $6.42 \pm 0.25$  vs.  $3.94 \pm 0.29$ ,  $p < 0.05$ ). While mice lacking *Adora2b* in AECs were no longer protected by dipyridamole. We also identified

occludin and focal adhesion kinase as downstream targets of ADORA2B, thus providing a novel mechanism for adenosine-mediated barrier protection. Similarly, we also observed similar enhanced ADORA2B ( $3.33 \pm 0.67$  to  $16.12 \pm 5.89$ ,  $p < 0.05$ ) and decreased occludin ( $81.2 \pm 0.3$  to  $13.3 \pm 0.4$ ,  $p < 0.05$ ) levels in human Acute respiratory distress syndrome lungs.

**Conclusion:** We have highlighted a role of dipyridamole and adenosine signaling in preventing or treating ALI and identified Ent2 and Adora2b as key mediators in important for the resolution of ALI.

**Keywords:** barrier function, pulmonary edema, ARDS, focal adhesion, equilibrative nucleoside transporters (ENTs), alveolar type 2 cell

## INTRODUCTION

Acute respiratory distress syndrome (ARDS) is a clinical presentation of acute lung injury (ALI) characterized by progressive arterial hypoxemia, and dyspnea (Nuckton et al., 2002) caused primarily by pulmonary edema (Ware and Matthay, 2000; Matthay et al., 2012). According to the Berlin definition, ARDS is the presence of bilateral opacities from chest imaging, pulmonary edema not due to cardiac failure or fluid overload, and arterial oxygenation calculated by the  $\text{PaO}_2/\text{FiO}_2$  ratio. A ratio less than 300 mmHg is termed mild, less than 200 is termed moderate, and less than 100 is severe (Ranieri et al., 2012). The etiology of ARDS is complex and multifactorial: sepsis, pneumonia, major trauma, blood transfusion, smoke inhalation, and aspiration of salt water, fresh water or gastric contents can all promote ALI (Ware and Matthay, 2000). ARDS affects approximately 200,000 Americans and has a mortality of approximately 45% (Flori et al., 2005; ). Currently there are no effective treatment options for ARDS (Matthay and Zemans, 2011). This has been painfully apparent in the current COVID-19 pandemic where the vast majority of patients that succumb present with an atypical form of ARDS (Gong et al., 2020; Li and Ma, 2020; Liang et al., 2020), this underscores our need to develop new treatment options for this devastating disease.

Disruption of epithelial and endothelial barrier function is a hallmark of ALI (Ware, 2006). The lung epithelium usually maintains an impermeable network through interactions of numerous structural proteins, including tight junction and focal adhesion proteins. Disruption of tight junction and focal adhesion proteins, including occludins, claudins and focal adhesion kinase (FAK), in epithelial cells promotes the permeability of alveolar epithelium and facilitates the progression of ARDS (Ma et al., 2013; Suzuki, 2013). Preserved epithelial barrier function is inversely associated with mortality of patients with ARDS (Matthay and Zemans, 2011; Fanelli and Ranieri, 2015), suggesting signaling pathways regulating the expression and/or functions of the tight junction and focal adhesion proteins may be a valid therapeutic target for ARDS.

Recently, several studies suggest extracellular adenosine as a potential therapeutic agent for the prevention of lung damage (Kong et al., 2006; Eckle et al., 2009; Eltzschig, 2009; Eltzschig

et al., 2013; Karmouty-Quintana et al., 2013). Extracellular adenosine is enhanced in areas with injury and is generated by the breakdown of precursor nucleotides including ATP, ADP and AMP by nucleotidases CD39 and CD73 (Eltzschig et al., 2013; Karmouty-Quintana et al., 2013; Idzko et al., 2014). Adenosine functions through activation of G-protein-coupled receptors (Adora1, Adora2a, Adora2b, and Adora3), and increased extracellular adenosine is normally associated with enhanced barrier functions and decreased ALI (Blackburn et al., 2009; Eckle et al., 2009). Blocking equilibrative nucleoside transporters (ENTs) with dipyridamole or by genetically deleting *Ent2* significantly enhanced extracellular adenosine in the alveoli, and as a result suppressed pulmonary inflammation and vascular leakage in ventilator-induced lung injury (Eckle et al., 2013; Morote-Garcia et al., 2013). In contrast, genetic depletion of CD73, a nucleotidase that is essential for adenosine generation, increased inflammation as well as pulmonary vascular leakage (Eltzschig et al., 2005; Reutershan et al., 2009; Hasko et al., 2011; Thompson et al., 2011). However, the therapeutic potential of enhancing extracellular adenosine levels at a time when acute injury is already established has not yet been evaluated. In addition, the mechanisms of how extracellular adenosine regulates the integrity of pulmonary epithelium and endothelium are not well understood.

Several mouse models of ALI has been developed, including mechanical ventilation, sepsis, acid aspiration, and ischemia-reperfusion induced ALI (Rosenthal et al., 1998; Matute-Bello et al., 2008). However, none of them truly recapitulate features of human ARDS. Intratracheal (i.t.) bleomycin is one of the most commonly used models of ALI in mice. Bleomycin is a chemotherapeutic agent derived from *Streptomyces verticillus*, and it is clinically used to treat a variety of human cancers. However, one of the adverse effect of bleomycin therapy is lung injury and pulmonary fibrosis (Froudarakis et al., 2013; Martin W. G. et al., 2005). Intratracheal bleomycin induced ALI reproduces many features of ARDS, including neutrophil infiltration and increased levels of pro-inflammatory cytokines such as interleukin (IL)-1 $\beta$ , IL-6, IL-1R1, keratinocyte chemoattractant (KC), tumor necrosis factor (TNF)-A at the early inflammatory stage (Matute-Bello et al., 2008; Williamson et al., 2015). Furthermore, profibrotic cytokines such as Granulocyte colony-stimulating factor (G-CSF),

Granulocyte-macrophage colony-stimulating factor (GM-CSF), interferon (IFN)- $\gamma$ , and IL-4 and the subsequent development of fibrosis at the late stage (Matute-Bello et al., 2008; Williamson et al., 2015). This acute and chronic phases of i.t.- bleomycin instillation reflect the acute and chronic phases of ARDS in human that is characterized by and acute inflammatory onset, hypoxemia and subsequent fibrotic tissue deposition (Matthay and Zemans, 2011).

Accordingly, in the present study, using the intratracheal bleomycin-induced ALI model, we demonstrate that elevating adenosine levels acutely is protective against ALI, both prophylactically and therapeutically. We also demonstrate that activation of *Adora2b* is important to restore barrier function by modulating the expression of focal adhesion proteins.

## MATERIALS AND METHODS

### Generation and Genotyping of Mouse Lines

All of the animal experiments were reviewed and approved by the Animal Welfare Committee at the University of Texas Health Science Center at Houston. *Ent2<sup>fl/fl</sup>* C57BL/6 mice were gifts from Dr Eltzschig's lab at the University of Colorado Denver (Eckle et al., 2013; Grenz et al., 2012a). Conditional SPC-CreER-*Ent2<sup>fl/fl</sup>* and SPC-CreER-*Adora2b<sup>fl/fl</sup>* mice were obtained by crossing *Ent2<sup>fl/fl</sup>* and *Adora2b<sup>fl/fl</sup>* with SPC-CreER mice. Age and gender matched littermate SPC-CreER mice used as controls for SPC-CreER-*Ent2<sup>fl/fl</sup>* and SPC-Cre-*Adora2b<sup>fl/fl</sup>*. All of the mice were housed in a pathogen-free environment with adequate food and water. No evidence of fungal, parasitic, or bacterial infection was observed.

### Mouse Treatment

The SPC-CreER-*Ent2<sup>fl/fl</sup>*, SPC-CreER-*Adora2b<sup>fl/fl</sup>* and control SPC-CreER were injected intraperitoneally (i.p.) with ~75 mg/kg tamoxifen once every 24 h for a total of five consecutive days to induced the cre recombination. A week after the last tamoxifen injection, mice were injected intratracheally with bleomycin as previously described (Zhou et al., 2009). Briefly, 10–12 week old female C57BL/6 mice were anesthetized with freshly made avertin (250 mg/kg) and instilled intratracheally with saline or 2.5 U/kg bleomycin (Teva Parenteral Medicine, Irvine, CA). The lungs and bronchoalveolar lavage fluid (BAL) were collected for analysis on day 3 or day 7 after bleomycin injection.

Dipyridamole (Sigma-Aldrich, St. Louis, MO) was diluted in 400  $\mu$ l DMSO, then 2 ml 100% ethanol and then 18 ml sterile corn oil to a final concentration of 1 mg/ml. For the therapeutic model, two days after bleomycin injection, mice were injected i.p. with 5 mg/kg dipyridamole (Sigma-Aldrich, St. Louis, MO) twice daily or with 500  $\mu$ g/kg BAY 60-6583 (Tocris, Minneapolis, MN) daily (Wang et al., 2013; Zimmerman et al., 2013). Control mice were injected with same volume of vehicle. The lungs and bronchoalveolar lavage fluid (BAL) were collected for analysis on day 7. To avoid animal death, only female mice were used in this study because male mice are more vulnerable to i.t. bleomycin-induced fibrosis.

### Evans Blue Measurement of Vascular Permeability

Mice were i.p. injected with 0.2 ml Evans blue dye (0.5% in PBS) (17). Four hours after dye administration, mice were anesthetized with freshly made avertin (250 mg/kg) and lungs were exposed and perfused with PBS. Lungs were then isolated, weighted and incubated in 1 ml formamide overnight at 55°C to extract dye. Dye concentrations were measured spectrophotometrically at 610 nm. The content of Evans blue dye was determined by generating a standard curve from dye dilutions.

### Quantitative Real-Time PCR

Cells or lung tissues were lysed using TRIZOL Reagent (Thermo Fisher Scientific, Fair Lawn, NJ, United States), and total RNA were extracted using RNeasy mini Kit (Qiagen). Then RNA were treated with Heat&Run gDNA remover kit (ArcticZymes) and reverse transcribed into cDNA using Transcriptor First strand cDNA synthesis (Roche). Real-time PCR was carried out using LightCycler 96 using the following primers: Mouse *Ent1* forward: 5'-CTTGGGATTTCAGGGTCAGAA-3', Mouse *Ent1* reverse: 5'-ATCAGGTCACACGACACCAA-3'; Mouse *Ent2* forward: 5'-CATGGAAACTGAGGGGAAGA-3', Mouse *Ent2* reverse: 5'-GTTCCAAAGGCCTCACAGAG-3'; Mouse  $\beta$ -Actin forward: 5'-GGCTGTATTCCCCTCCATCG-3'; Mouse  $\beta$ -Actin forward: 5'-CCAGTTGGTAACAATGCCATGT-3'. Data was quantified using the comparative Ct method and presented as mean ratio to  $\beta$ -actin.

### BAL Collection and Differential Cell Count

Mice were anesthetized with avertin, the trachea was exposed and lavaged four times with 0.3 ml PBS containing 10  $\mu$ M dipyridamole, 10  $\mu$ M  $\alpha\beta$ -methylene ADP, and 10  $\mu$ M 5'-deoxycoformycin (Sigma-Aldrich), which will pool about 1 ml bronchoalveolar lavage (BAL) fluid. Total number of BAL cells was counted using a hemocytometer. Cellular differentials were determined by cytopinning BAL aliquots onto microscope slides and staining with Diff-Quick (Dade Behring, Deerfield, IL).

### Adenosine Measurement

Adenosine concentration in BAL fluid was measured as described previously (45). Briefly, BAL fluid was centrifuged at highest speed to clear cells and debris. 200  $\mu$ l BAL supernatant was analyzed by reverse-phase high-performance liquid chromatography (HPLC) as described previously (45). Representative peaks were identified and quantified using external standard curves.

### Albumin Measurement

The albumin level in BAL was determined using the mouse albumin ELISA kit (Immunology Consultants Laboratory, Inc., Portland, OR, United States). Briefly, BAL samples and standards were added to predesignated wells coated with anti-albumin antibody for 30 min. After the unbound proteins were rinsed, appropriately diluted Enzyme antibody was added and incubated for an additional 30 min. Then the wells were rinsed again and incubated with TMB Substrate Solution for 10 min. Finally, the



reactions were stopped by adding Stop Solution to each well. The absorbance (450 nm) of the contents of each well was measured by plate reader and albumin concentration was calculated based on the standard curve.

## Cell Culture and Hypoxia Exposure

MLE12 cells (ATCC) were cultured in RPMI Media 1,640 (Life Technologies, Grand Island, NY, United States) containing 10% fetal bovine serum and 100 U/ml penicillin G, and 100 µg/ml. RLE-6 TN was purchased from ATCC and grown in Dulbecco's Modified Eagle's medium, nutrient mixture F-12 Ham (1:1) supplemented with 10% fetal bovine serum, 40 mmol/L HEPES, 100 U/ml penicillin G, and 100 µg/ml. To study the role of Adora2b on junction proteins and transepithelial electric resistance, cells were serum-starved overnight, treated with 10 µg/ml ADA (Roche) for 30 min, followed by incubation in 500 nM BAY 60-6583, and/or 1 µM MRS 1754, and/or 10 µM H89, then the cells were placed in a sealed hypoxia chamber and exposed to 2% oxygen supplied with 95% N<sub>2</sub> and 5% CO<sub>2</sub> for 1–6 h.

To measure calpain activity, cells were serum-starved, treated with different compounds and exposed to normal air or 2% oxygen for 1 h. Calpain activities were determined using the Calpain-Glo™ protease Assay Kit (Promega, Madison, WI, United States). Experiments were repeated 3 times and triplicated.

## Transepithelial Electric Resistance (TEER) Measurement

RLE-6TN cells were seeded on Transwell inserts (0.4-µm pore size, 12-mm inside diameter; Corning Incorporated, Corning, NY) at a density of  $1 \times 10^5$  cells/cm<sup>2</sup>. TEER was measured by EVOM2 (World Precision Instruments, Sarasota, FL, United States). When the electrical resistance between the apical and basolateral surfaces of the monolayers was >400 Ω/cm<sup>2</sup>, cells were serum-starved overnight, treated with 10 µg/ml ADA for 30 min, followed by incubation in 1 nM BAY 60-6583, and/or 100 nM MRS 1754, and/or 10 µM H89, then the cells were placed in a sealed hypoxia chamber and exposed to 2% oxygen supplied with 95% N<sub>2</sub> and 5% CO<sub>2</sub>. TEER was measured 0, 0.5, 1, 2, 4 and 6 h after hypoxia exposure.

## Western Blot

Cells or lung samples were collected and lysed in RIPA lysis buffer (50 mM Tris-HCl PH 7.4, 150 mM NaCl, 1% NP-40) containing both protease and phosphatase inhibitor cocktail (Thermo Fisher Scientific, Fair Lawn, NJ, United States). Western blots were carried out as previously described using primary rabbit anti-ENT1 (Abgent, San Diego, CA, United States), rabbit anti-ENT2 (Abcam), rabbit anti-occludin, rabbit anti-phosphorylated FAK, rabbit anti FAK, rabbit anti ZO-1, rabbit anti claudin-1 (Cell signaling, Boston, MA, United States), mouse anti-CD73 antibodies (ThermoFisher Scientific), mouse anti-Hif-1α antibodies (Novus Biological, Littleton, CO, United States), or mouse anti-β-Actin antibodies (Sigma) and corresponding secondary antibodies conjugated to horseradish peroxidase

(Jackson ImmunoResearch, West Grove, PA, United States). Finally, the membranes were developed with Pierce ECL Western Blotting Substrate (Thermo Fisher scientific, Fair Lawn, NJ, United States).

## H&E Staining and Immunohistochemistry

Mouse lungs were fixed in 10% formaldehyde for at least 24 h. Lungs were then dehydrated, paraffin embedded and sectioned at a thickness of 5 µm. For Hematoxylin and Eosin (H&E), staining sections were rehydrated, incubated with Hematoxylin Solution, Gill No. 3 (Sigma) and then incubated with aqueous 1% Eosin Y solution (Sigma). Finally, slides were dehydrated and mounted in Cytoseal™ XYL (ThermoFisher scientific, Waltham, MA, United States).

For ENT1, ENT2 and neutrophil staining, sections were rehydrated, quenched with 3% hydrogen peroxide, incubated in citric buffer (VectorLabs, Burlingame, CA, United States) for antigen retrieval, and blocked with Avidin/Biotin Blocking System (VectorLabs) and then 5% normal goat serum. After that, the sections were incubated with anti-ENT1, ENT2 (1:200, Abcam), and Anti-Neutrophil antibody NIMP-R14 (1:500, rabbit polyclonal, Abcam, Cambridge, MA, United States) overnight at 4°C. Slides were then incubated with appropriate secondary antibodies (1:1,000, VectorLabs) for 1 h and ABC Elite streptavidin reagents for 30 min at room temperature. Finally, slides were developed with Vector blue (VectorLabs) or 3,3'-diaminobenzidine (Sigma-Aldrich, St. Louis, MO, United States) and counter-stained with methyl green. Stained slides were blindly counted for the numbers of positive stained neutrophils at ×20 objective. Ten random areas per lung were analyzed to get the final average number of infiltrated neutrophil.

## Human Lung Collection

Normal and ARDS lungs were purchased from the International Institute for the Advancement of Medicine (IIAM) Usage of these tissues was performed under IRB: HSC-MS-08-0354. Discarded lungs for transplantation were considered normal if they did not have a history of chronic lung injury, presented with a partial pressure of oxygen (PaO<sub>2</sub>) fraction of inspired oxygen (FIO<sub>2</sub>) ratio PaO<sub>2</sub>/FIO<sub>2</sub> over 300 mmHg and the absence of bilateral opacities by chest imaging. Discarded lungs for transplantation that met the Berlin definition of ARDS: presence of bilateral opacities from chest imaging, pulmonary edema not due to cardiac failure or fluid overload and arterial oxygenation calculated by the PaO<sub>2</sub>/FiO<sub>2</sub> ratio less than 300 mmHg (Ranieri et al., 2012), were used for our study. Samples from four normal and three ARDS lungs were analyzed.

## CD73 Activity Assay

Pulverized normal and ARDS lungs were lysed in NP-40 lysis buffer (1% NP-40, 150 mM NaCl, 50 mM Tris-Cl, PH 8.0) containing protease inhibitor cocktail (ThermoFisher). Protein concentration were determined using the Pierce™ BCA protein assay kit (ThermoFisher). For each assay, five µg lung lysate was mixed with assay buffer (10 mM HEPES, 10 mM MgCl<sub>2</sub>, 10 µM DCF and 200 mM AMP), and immediately incubated at 37°C for 30 min. At the end of the incubation, reaction was inactivated by

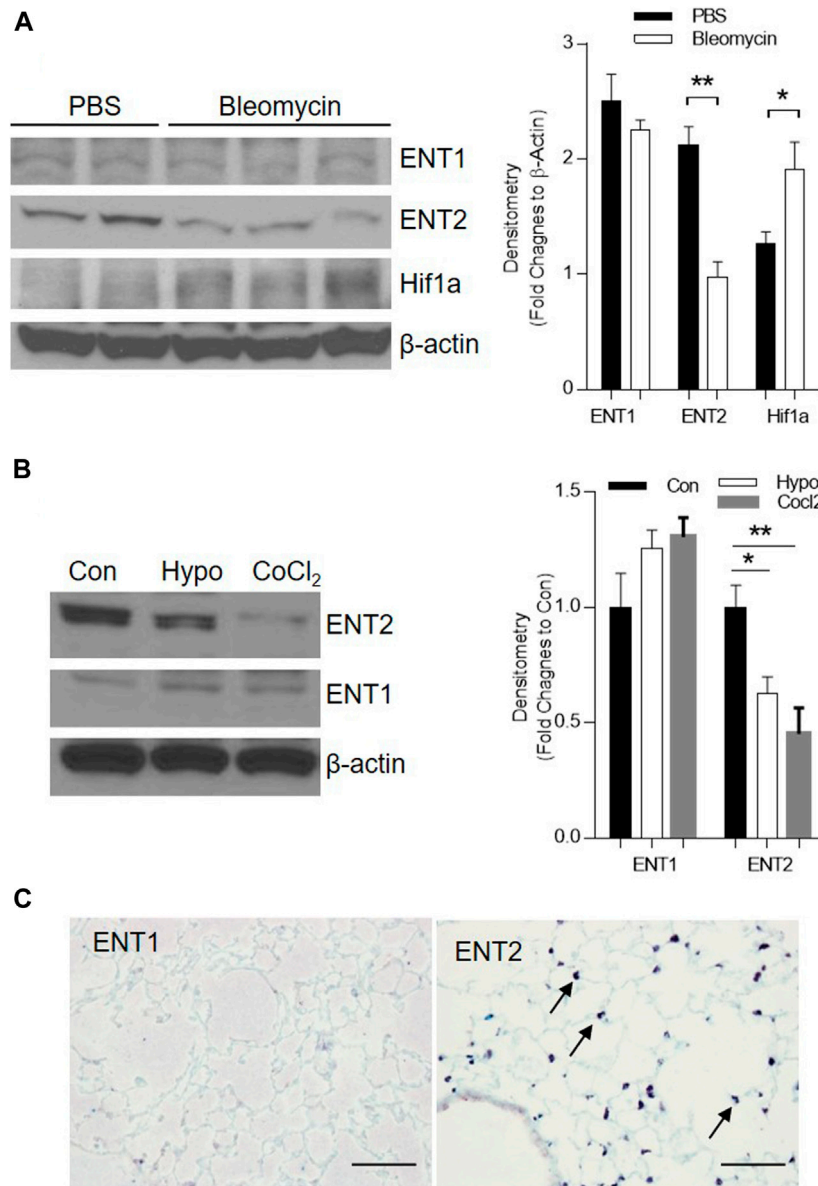


**FIGURE 1** | ENT2 expression is decreased in bleomycin-induced ALI. C57BL/6 mice were i.t. injected with 2.5 U/kg bleomycin and lungs were collected for analysis on day 3. **(A)** Left Panel: The protein expression of ENT1, ENT2, and Hif1a were determined using western blot.  $\beta$ -Actin was used as an internal control. Right Panel: Densitometry of the Western Blot image were analyzed and data were presented as fold changes to  $\beta$ -Actin  $\pm$  MSE. \* $p < 0.05$ , \*\* $p < 0.01$ . **(B)** Primary alveolar epithelial type II (AECII) were isolated from normal mouse lungs and exposed to 2% oxygen, or 100 mM CoCl<sub>2</sub> for 24 h. Right Panel: Densitometry of the Western Blot image were analyzed and data were presented as fold changes to Control (Con)  $\pm$  MSE. \* $p < 0.05$ , \*\* $p < 0.01$ . **(C)** Cellular localization of ENT1 and ENT2 (brown, arrow) was visualized using immunohistochemistry in a normal healthy mouse lung. The protein levels of ENT1, ENT2, and  $\beta$ -Actin were determined using western blot.  $n = 3$ , \* $p < 0.05$  vs. control. Scale bar = 100  $\mu$ m.

incubating the mixture at 95°C for 5 min. Adenosine levels were measured using HPLC as described above. The activities of CD73 were integrated as the amount of adenosine synthesized per minutes per Gram of total protein.

## Statistical Analysis

For scientific rigor, all *in vitro* cell culture experiments were repeated at least three times and each treatment was at least duplicated. For experiments having no more than two treatment

groups, two-tailed student t-tests were used to assess whether the means of two groups were statistically different from each other. Otherwise, one-way or two-way ANOVA were used to determine whether there were significant differences among treatments. If so, Tukey's multiple comparison test were carried out to determine whether there were significant differences between any of the two treatments. The data were considered significant with  $p < 0.05$ . All results were presented as Mean  $\pm$  SEM to indicate variability.



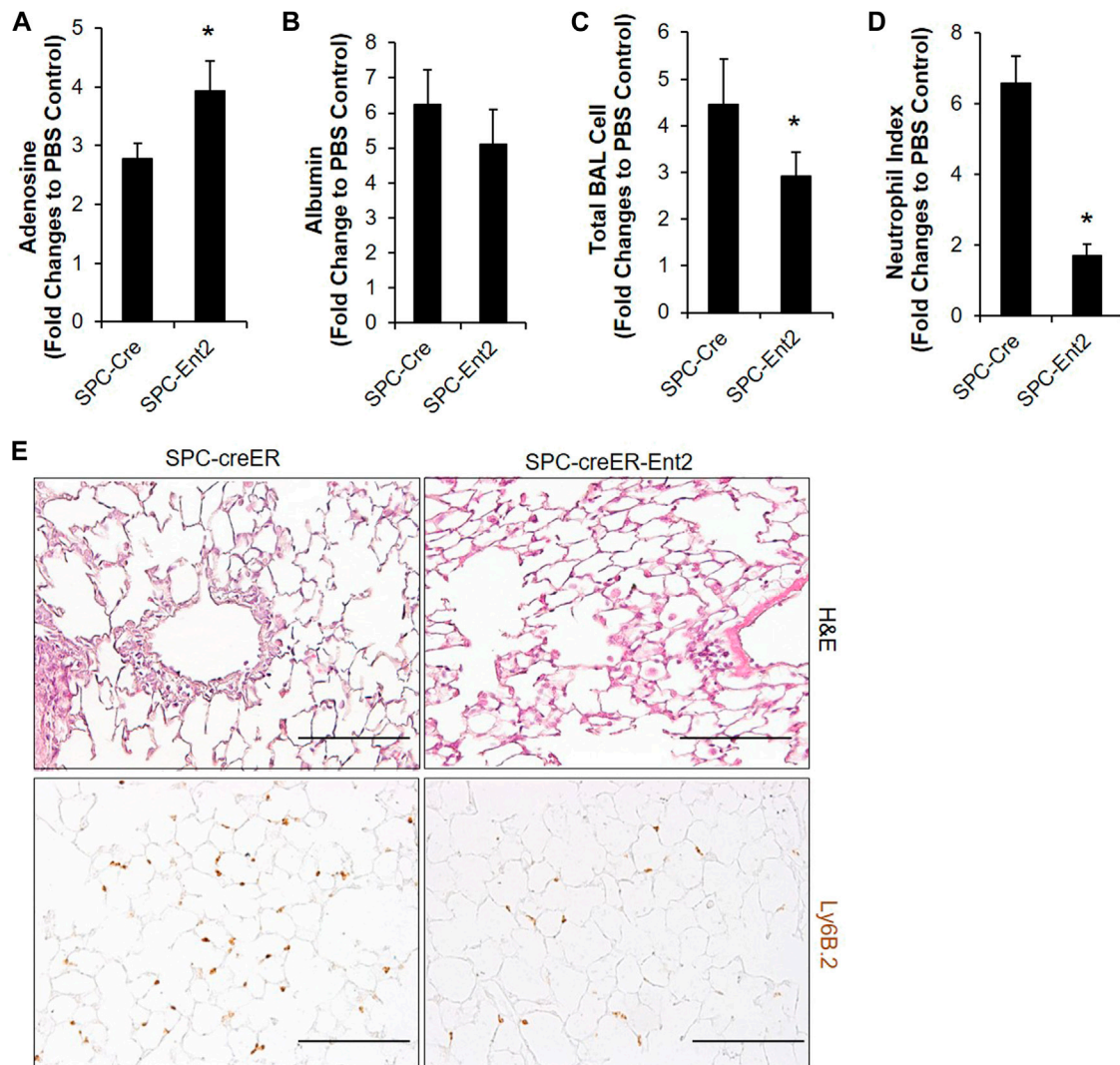


**FIGURE 2 |** Bleomycin-induced ALI is attenuated in mice with epithelial specific deletion of Ent2. SPC-CreER-Ent2<sup>-/-</sup> mice or littermate SPC-CreER controls were i.p. injected with 75 mg/ml tamoxifen daily for 5 days. One week after the first tamoxifen injection, mice were i.t. injected with 2.5 U/kg bleomycin. On day 3, BAL adenosine (A) and albumin levels (B), and total BAL cell number (C) were analyzed. (D) Neutrophil infiltration was determined by staining with anti-Ly6B.2, and cell number per high powered field were counted. (E) Representative H&E and Ly6b staining showing pulmonary inflammation and neutrophil infiltration in different groups of lungs.  $n \geq 4$ , \* $p < 0.05$ , \*\* $p < 0.01$  vs. Control. # $p < 0.05$  vs. wild type bleomycin. Scale bar = 100  $\mu$ m.

## RESULTS

### The Expression of ENT2, but not ENT1, is Negatively Regulated by Hypoxia Following Tissue Injury

Extracellular adenosine is generated following injury and can be transported by ENTs into the cells and then depleted in the extracellular space (Karmouty-Quintana et al., 2013). To understand whether ENT expression is suppressed following bleomycin-induced acute lung injury and partially contributes to the increase of extracellular adenosine levels, we examined the transcript and protein expression of ENTs in the lungs of mice

instilled with bleomycin (i.t.) after 3 days. ENT2 protein levels were decreased in the lungs of mice treated with bleomycin (Figure 1A), suggesting that ENT2 might be the transporter which is more actively regulated following lung injury. Previous studies have demonstrated that hypoxia is one of the important regulators of ENTs (Eckle et al., 2013). Indeed, we observed an increased expression of hypoxia-inducible factor 1 alpha (Hif-1a) following bleomycin treatment (Figure 1A), suggesting that hypoxia is present in the injured lungs and might be the mechanism that leads to decreased ENT expression. To further understand whether hypoxia directly regulates ENT expression, we isolated primary alveolar epithelial type II cells (AECII) from mice and exposed them to 2% oxygen or CoCl<sub>2</sub>, a chemical

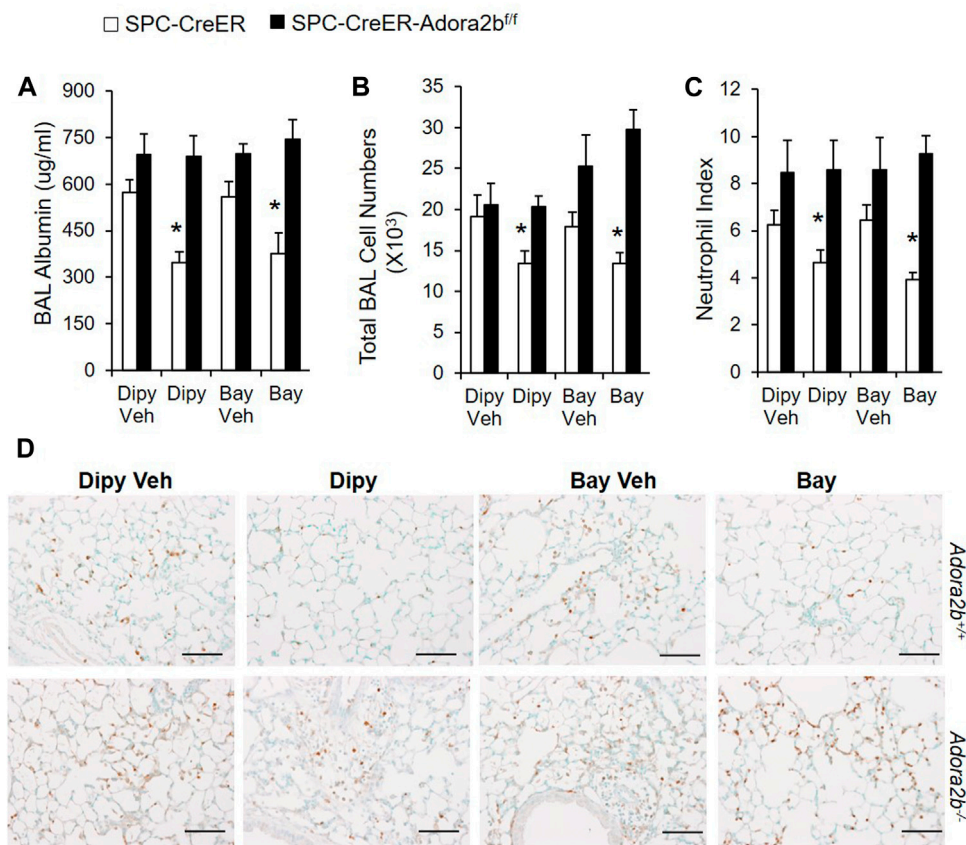


**FIGURE 3 |** Bleomycin-induced ALI in mice with *Adora2b* deletion specially in alveolar epithelial cells. SPC-Cre-*Adora2b*<sup>-/-</sup> mice and littermate controls were i.p. injected with 75 mg/ml tamoxifen daily for 5 days to induce Cre recombination. One week after the first tamoxifen injection, mice were pretreated with vehicle control, 5 mg/kg dipyrindamole or 500 ug/kg BAY 60-6583 1 h before i.t. injected with 2.5 U/kg bleomycin and then continuously injected with dipyrindamole twice daily or BAY 60-6583 once daily until day 3 for analysis. **(A)** BAL albumin levels were measured to show vascular leakage. **(B)** Total BAL cell numbers were counted to determine pulmonary inflammation. **(C)** Neutrophil index was calculated by counting the number of neutrophil per high power field from slides stained with anti-Ly6B.2 antibody.  $n = 5$ , \* $p < 0.05$  vs. corresponding Veh control using student t-test. **(D)** Representative lung sections stained with Ly6B.2 to show neutrophil infiltration.  $n \geq 4$ , \* $p < 0.05$  vs. vehicle using one way ANOVA followed by Bonferroni's multiple comparisons test. Scale bar = 100 μm.

inducer of Hif-1 $\alpha$ . Consistent with the results we observed using whole lung lysates, ENT2 but not ENT1 expression was dramatically down-regulated by both hypoxia and CoCl<sub>2</sub> (**Figure 1B**), suggesting that hypoxia following acute lung injury can suppress ENT2 expression in a Hif-1 $\alpha$  dependent manner. Immunohistochemistry demonstrated that ENT2 is mainly located in alveolar epithelial cells (arrow) in normal mouse lungs (**Figure 1C**). Taken together, our findings demonstrate that ENT2, but not Ent1, is repressed by hypoxia during ALI induced by bleomycin.

## ENT2 Is the Major Transporter to Regulate BAL Adenosine Levels

Our immunostaining mainly located ENT2 in alveolar epithelial cells, suggesting that alveolar epithelial cells might be the key cells to mediate the ENT2 regulation of extracellular adenosine levels. To define this, we crossed SPC-CreER mice with mice carrying a floxed allele of *Ent2* to generate

transgenic mice with *Ent2* deficient specifically in alveolar epithelial cells. Seven days after inducing the cre recombinase with tamoxifen, SPC-CreER-*Ent2* mice were administrated with bleomycin and compared with SPC-CreER controls. SPC-CreER-*Ent2* mice had significantly enhanced extracellular adenosine levels (**Figure 2A**) in association with attenuated vascular leakage (**Figure 2B**) and inflammatory cell infiltration (**Figure 2C**) compared to controls. Further differential cell counts revealed that SPC-CreER-*Ent2* mice presented with reduced neutrophil cell infiltration (**Figure 2D,E**). In summary, these findings demonstrate a selective protective role for epithelial ENT2 in bleomycin-induced lung injury.

## Adenosine Through *Adora2b* Is Important to Protect Lungs From Acute Injury

We have demonstrated that elevation of extracellular adenosine is limited by epithelial ENT2 and is associated with increased

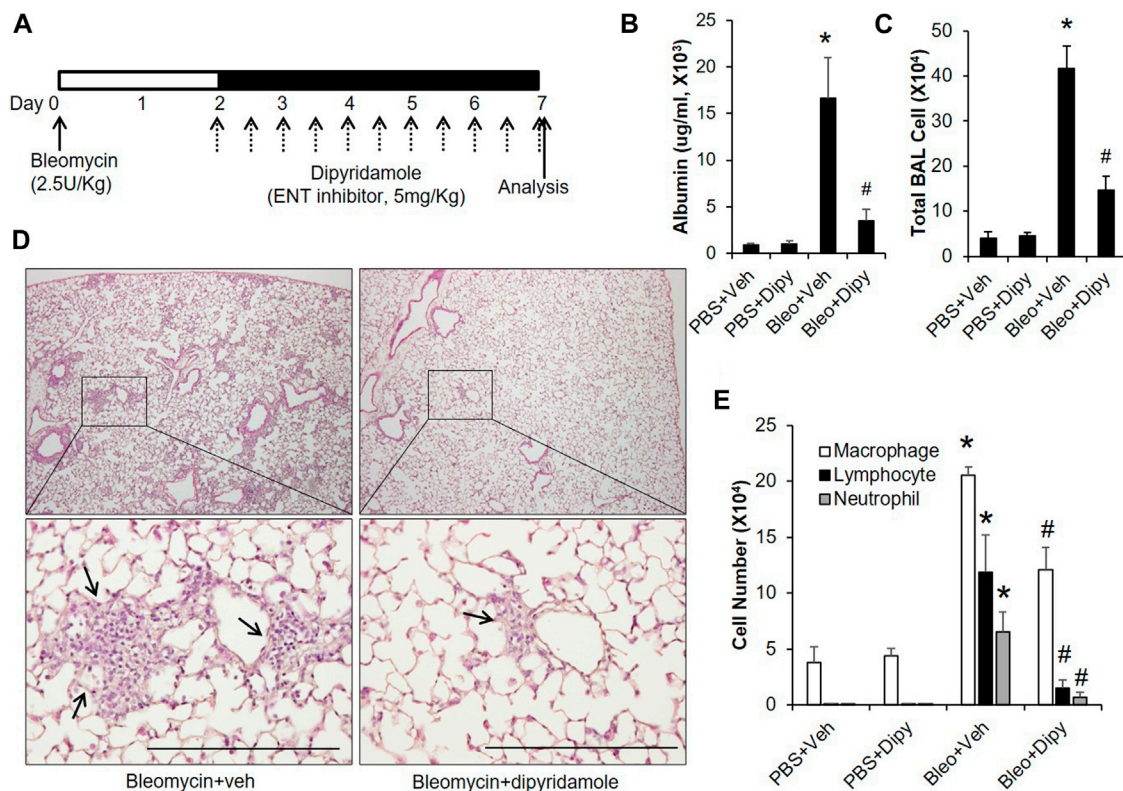


**FIGURE 4 |** Therapeutic effect of dipyrindamole on established ALI. **(A)** A diagram showing how mice were treated with dipyrindamole and bleomycin. Mice injected with same volume of Vehicle were used as control. **(B)** BAL albumin levels were measured from different treatment groups. **(C)** BAL total cell numbers were counted. **(D)** Lungs from bleomycin and/or dipyrindamole treated mice were sectioned and stained with H&E. Representative pictures were shown. Scale bar = 500  $\mu$ M. **(E)** Differential assay was performed to determine the degree of macrophage, lymphocyte and neutrophil trafficking into the lungs.  $n \geq 5$ , \* $p < 0.05$  vs. PBS. # $p < 0.05$  vs. bleomycin using one way ANOVA followed by Bonferroni's multiple comparisons test. Scale bar = 200  $\mu$ m.

protection from lung injury. Next, we want to investigate which adenosine receptor is involved in this protection. Previous studies in a mouse model of VILI indicate that adenosine, through the Adora2b receptor, is the major pathway that promotes barrier protection (Eckle et al., 2013). Based on these notions, we hypothesize that Adora2b is the major adenosine receptor that mediates this protection.

Previous studies shown that Adora2b is mainly expressed in alveolar epithelial cells, and Adora2b in epithelial cells is essential to mediate the protective role of adenosine in ventilation induced acute lung injury (Cagnina et al., 2009; Eckle et al., 2013). To determine whether epithelial Adora2b is also important for the protection of barrier function in our model of acute lung injury, we generated mice with Adora2b deleted specially in alveolar epithelial type II cells by crossing SPC-creER mice with mice carrying a floxed allele of Adora2b, and induced ALI in these mice with bleomycin. Compared to SPC-Cre mice, in SPC-cre-Adora2b<sup>fl/fl</sup> mice, dipyrindamole or BAY 60-6583 (an Adora2B agonist) treatment can no longer alleviate vascular leakage (Figure 3A), inflammation (Figure 3B,D), neutrophil infiltration (Figure 3C,D) after bleomycin exposure. Taken together, our study suggests that epithelial Adora2b is important to mediate the protective role of

extracellular adenosine in bleomycin-induced acute lung injury.

### Inhibiting ENTs at a Time Point When Acute Lung Injury is Already Established Protects Lungs From Bleomycin-Induced Injury

Based on the above findings that extracellular adenosine plays a role in preventing bleomycin-induced injury, we next established another model to see whether adenosine is also beneficial in treating already established ALI. In this model, mice were intratracheally instilled with bleomycin; after 2 days, mice were i.p injected with dipyrindamole twice daily until day 7 for analysis (Figure 4A). Dipyrindamole significantly reduced vascular leakage (Figure 4B) as indicated by the amount of albumin leaking into the BAL. Pulmonary inflammation was also dramatically suppressed as shown by both total BAL cell count (Figure 4C) and H&E staining (Figure 4D). Next, we performed differential assays to understand which inflammatory cells were trafficking into the lungs. We observed that both lymphocytes and neutrophils, which are significantly induced by bleomycin, were repressed by dipyrindamole treatment (Figure 4E). These findings indicate that inhibiting ENTs at a time point when acute



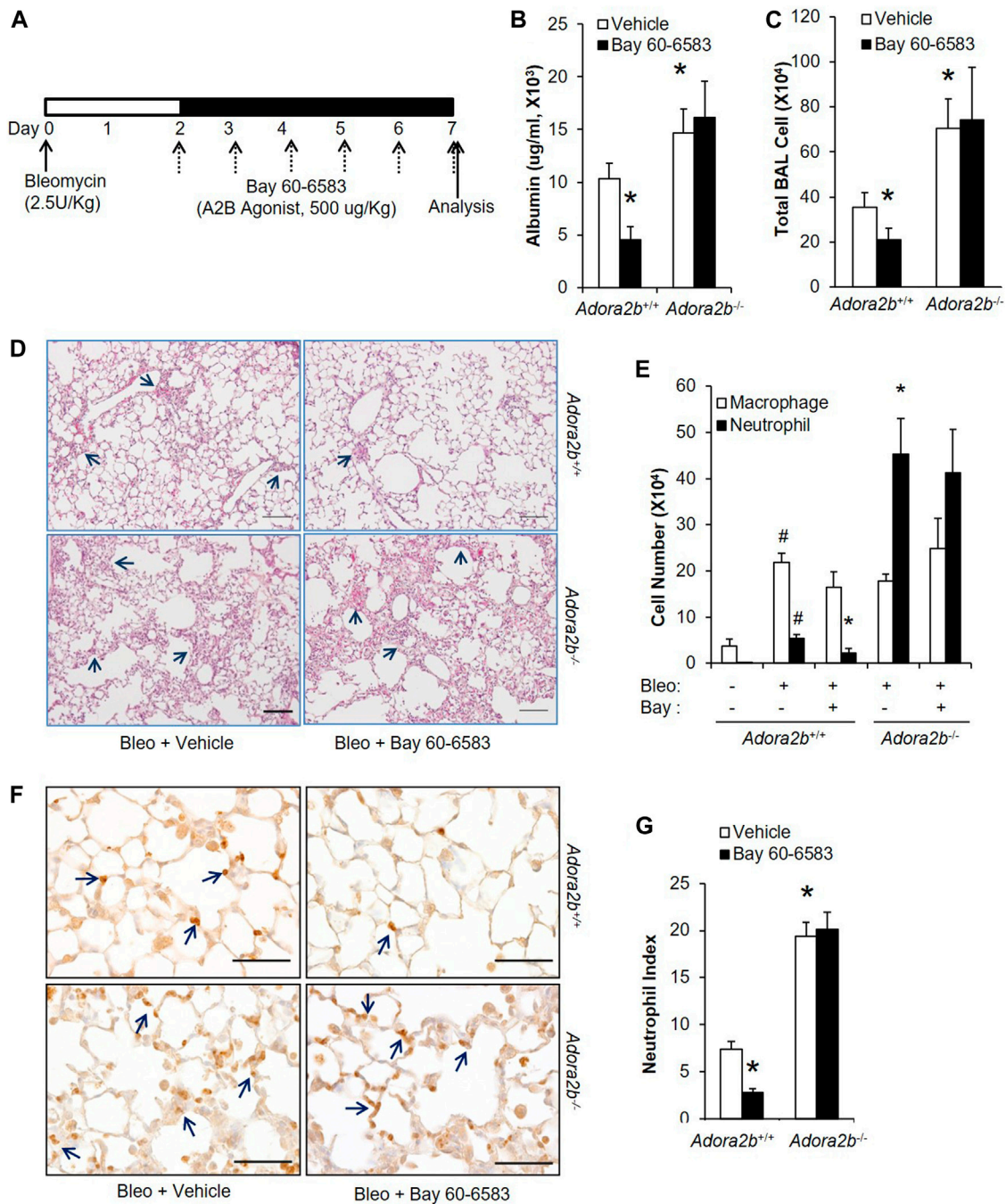


**FIGURE 5 |** Therapeutic effect of BAY 60-6583 on established ALI in *Adora2b*<sup>+/+</sup> and *Adora2b*<sup>-/-</sup> mice. **(A)** A diagram showing how *Adora2b*<sup>+/+</sup> and *Adora2b*<sup>-/-</sup> mice were treated with BAY 60-6583 and bleomycin. **(B)** BAL albumin levels were measured to show the levels of vascular leakage. **(C)** BAL total cell number was counted. **(D)** Representative H&E stainings of lungs from bleomycin and/or dipyrindamole treated mice. Arrows pointing areas with inflammation. Scale bar = 500  $\mu$ m. **(E)** Differential assay was performed to determine the number of macrophage and neutrophil in the lungs. **(F)** Mouse lung sections from different treatment group were stained with anti-Ly6B.2 to visualize neutrophil expression and localization. Arrow: positive stained neutrophils. Scale bar = 100  $\mu$ m. **(G)** The number of neutrophil for each treatment group was quantitated. N = 5, \**p* < 0.05 vs. wildtype bleomycin vehicle. #*p* < 0.05 vs. wild type PBS using one way ANOVA followed by Bonferroni's multiple comparisons test.



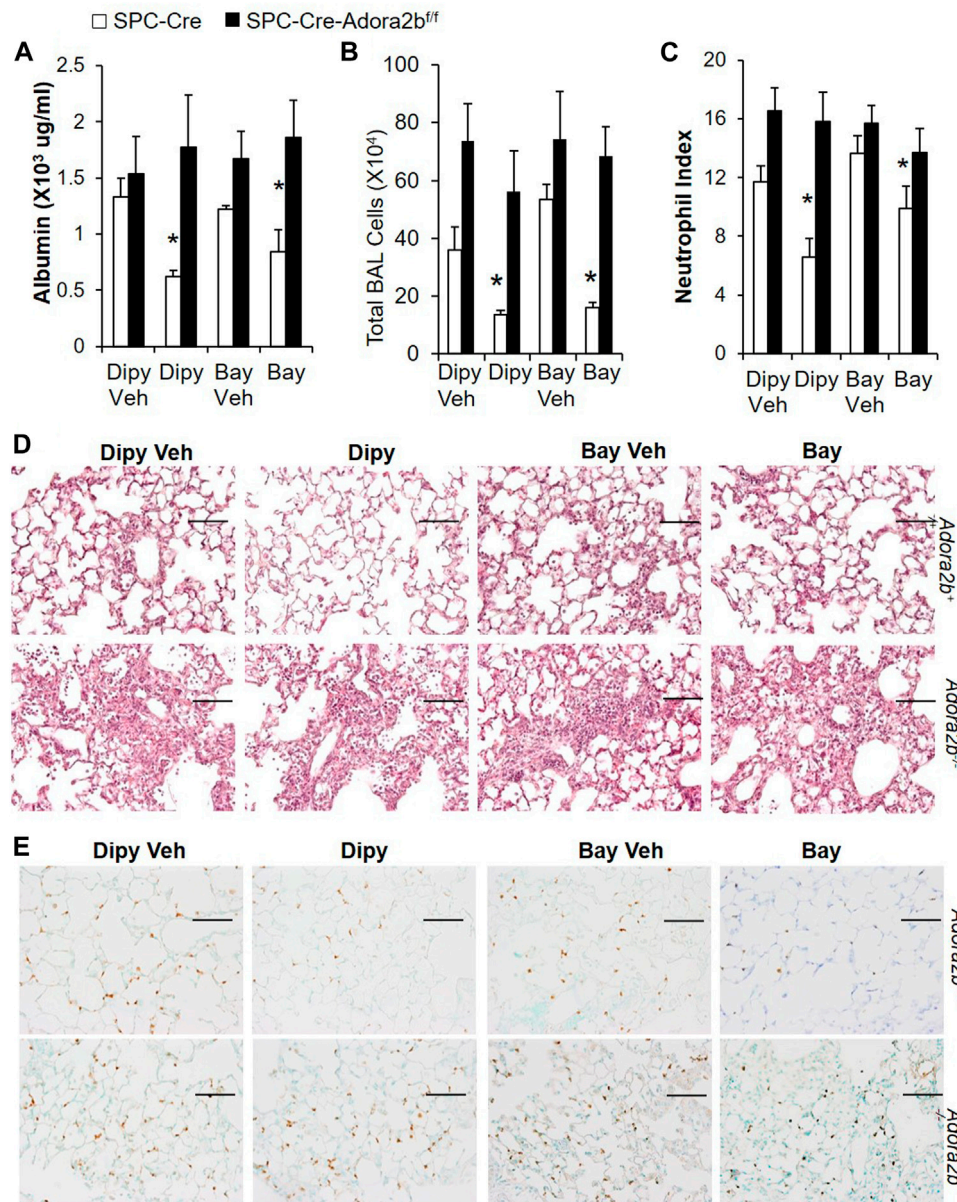


**FIGURE 6 |** Effect of Dipyrindamole and BAY 60-6583 on established ALI in mice with Adora2b knockout specifically in alveolar epithelial cells (SPC-Cre-Adora2b<sup>lox/lox</sup>). SPC-Cre and SPC-Cre-Adora2b<sup>lox/lox</sup> mice were treated with 2.5 U/kg bleomycin through i.t. Two days later, mice were treated with 5 mg/kg dipyrindamole twice daily or 500 ug/kg BAY 60-6583 daily until day 7. BAL albumin (A) and total BAL cells (B) were measured. (C) Lung sections were stained with anti-Ly6B.2 for neutrophil index. (D) Representative H&E staining showed pulmonary inflammation and injury in various groups. (E) Representative lung sections stained with Ly6B.2 to show neutrophil infiltration.  $n = 5$ ,  $p < 0.05$  vs. vehicle using one way ANOVA followed by Bonferroni's multiple comparisons test. Scale bar = 100 μm.

lung injury is already established can also protect lungs from bleomycin-induced injury.

## Adenosine Through Adora2b is Important for Lungs to Recover From Acute Injury

After having shown that adenosine through Adora2b is important to prevent bleomycin-induced acute injury, we wanted to

understand whether Adora2b is also the major adenosine receptor mediating the therapeutic effect of adenosine on established acute lung injury. To study the role of Adora2b in treating acute lung injury, wildtype (Adora2b<sup>+/+</sup>) or Adora2b<sup>-/-</sup> mice were subjected to bleomycin injury, followed by i.p injection of BAY 60-6583 starting on day 2 and continuing daily for 5 days (Figure 5A). BAY 60-6583 dramatically attenuated bleomycin-induced lung injury by reducing vascular leakage (Figure 5A) and

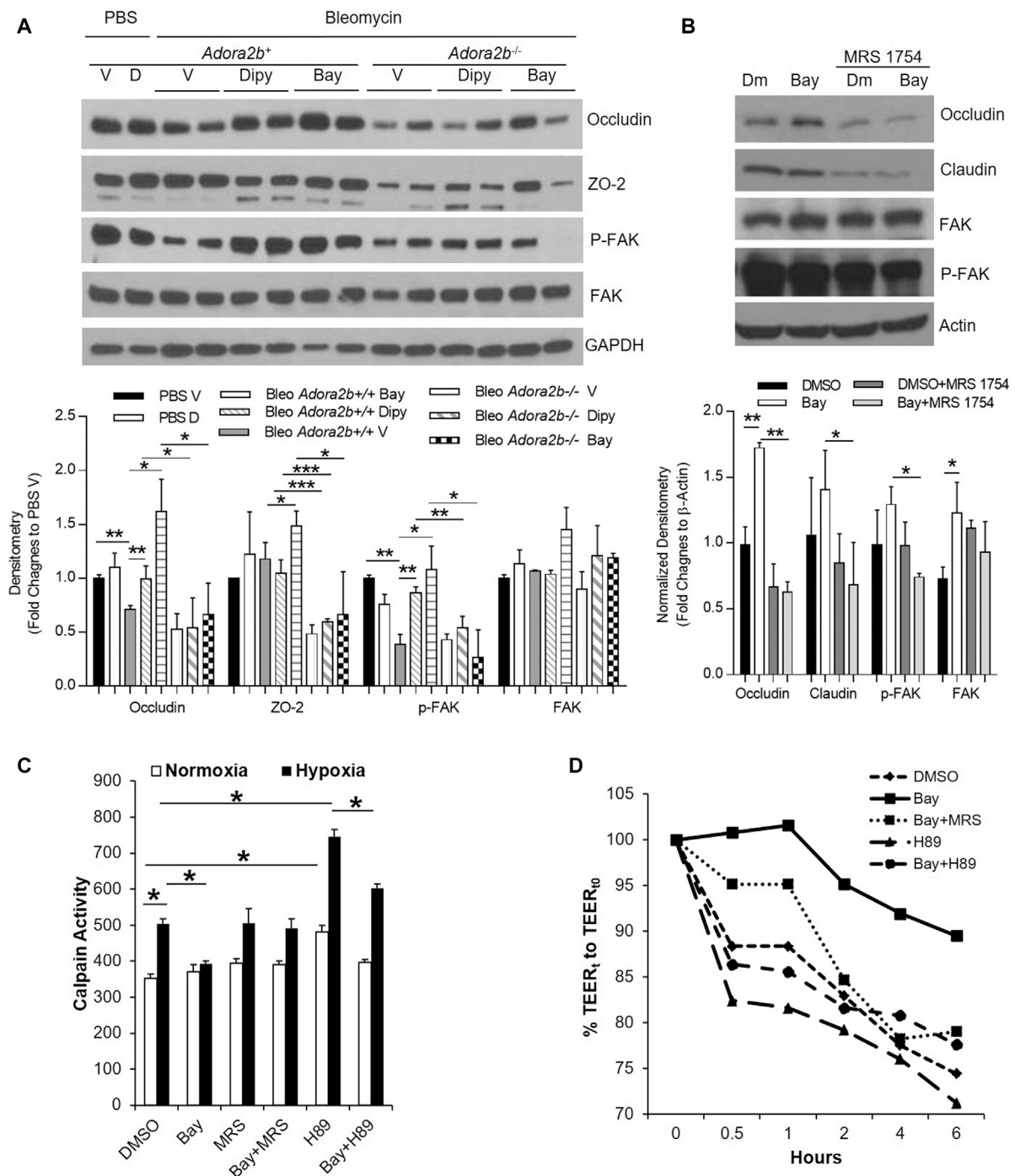


**FIGURE 7 |** The regulation of *Adora2b* on junction proteins. *Adora2b*<sup>+/+</sup> or *Adora2b*<sup>-/-</sup> mice were i.t. injected with 2.5 U/kg bleomycin. Two days later, mice were treated with 5 mg/kg dipyrindimole twice daily or 500 ug/kg BAY 60-6583 daily until day 7 for analysis. **(A)** Upper panel: whole lung samples were collected from different treatment group for western blot analysis of Occludin and ZO-2 or phosphorylated FAK (p-FAK) and FAK. Lower panel: The Densitometry of the Western Blot image were analyzed. Data were presented as Fold Change to PBS Vehicle  $\pm$  SD.  $n \geq 4$ , \* $p < 0.05$ , \*\* $p < 0.01$ , \*\*\* $p < 0.001$ . **(B, D, E)** MLE12 cells were serum starved overnight, pretreated with ADA for 30 min, treated with 500 nM BAY 60-6583 or 1  $\mu$ M MRS 1754 or 10  $\mu$ M H89, and then exposed to 2% oxygen for 6 h for western blot and 1 h for Calpain activity. **(B)** Upper panel: Expression of Occludin and Claudin-1, and p-FAK and FAK were examined using western blot. Lower Panel: Densitometry of the Western Blot image were analyzed. Data were presented as Normalized fold changes to  $\beta$ -Actin  $\pm$  SD. \* $p < 0.05$ , \*\* $p < 0.01$ . **(C)** Calpain activities were measured and quantitated. \* $p < 0.05$  one way ANOVA followed by Bonferroni's multiple comparisons test vs. DMSO control. **(D)** RLE-6TN cells were serum starved overnight, pretreated with ADA for 30 min, treated with 500 nM BAY 60-6583 or 1  $\mu$ M MRS 1754 or 10  $\mu$ M H89, and then exposed to 2% oxygen for 0–6 h, transepithelial electrical resistance (TEER) were measured and normalized to 0 h  $n = 3$  independent experiments.

inflammation (**Figure 5B,C**) in wildtype mice. However, the protection of BAY 60-6583 was completely abolished in the absence of Adora2b (**Figure 5A–C**). Moreover, *Adora2b*<sup>−/−</sup> mice exhibited increased vascular leakage and inflammation compared to *Adora2b*<sup>+/+</sup> mice (**Figure 5A–C**). Differential assay indicated a significant increase in neutrophil trafficking into the lungs in *Adora2b*<sup>−/−</sup> mice compared to wildtype controls, and the inhibition of BAY 60-6583 on neutrophil infiltration that we observed in wildtype mice was completely eliminated in *Adora2b*<sup>−/−</sup> mice (**Figure 5D**). To visualize neutrophil trafficking into the lungs, we stained the lung sections with anti-Neutrophil antibody NIMP-R14. We found the number of neutrophils was significantly increased when Adora2b was deficient (**Figure 5E,F**), and BAY 60-6583 dramatically inhibited neutrophil infiltration in *Adora2b*<sup>+/+</sup> mice but not in *Adora2b*<sup>−/−</sup> mice (**Figure 5E,F**).

We have shown that epithelial Adora2b is important to prevent bleomycin-induced lung injury. Next, we wanted to determine whether epithelial Adora2b is also important for the treatment of established ALI. SPC-Cre or SPC-cre-*Adora2b*<sup>fl/fl</sup> mice were i.t. administrated with bleomycin. After 2 days, mice were i.p. injected with BAY 60-6583 or dipyrindamole for five consecutive days. SPC-Cre mice treated with either BAY 60-6583 or dipyrindamole had better lung recovery with ameliorated vascular leakage (**Figure 6A**), inflammation (**Figure 6B,D**) and neutrophil infiltration (**Figure 6C,E**). However, neither BAY 60-6583 nor dipyrindamole attenuated bleomycin-induced lung injury in mice lacking Adora2b in alveolar epithelial cells (**Figure 6A–C**). Taken together, our findings suggest that epithelial Adora2b is important for lungs to recover from bleomycin-induced acute injury.

## Adenosine Through Adora2b Maintains Epithelial Integrity by Preventing the Degradation of Junction Proteins

Based on the above findings, we know that adenosine through Adora2b is important not only to prevent but also to treat acute lung injury. However, the underlying mechanisms are not known. The lung epithelial monolayer is assembled through the interactions of numerous structural proteins, including occludins, claudins and focal adhesion kinase (FAK). Evidence has suggested that deteriorated expression of these proteins in epithelial cells promotes the permeability of the alveolar epithelium and facilitates the progression of ALI. To understand whether adenosine signaling affects the structural proteins, we first characterized the expression of these structural proteins in bleomycin-induced lung injury in different treatment groups. As shown in **Figure 7A**, the levels of occludin and phosphorylated FAK (*p*-FAK) were decreased in wildtype mice exposed to bleomycin for 7 days. Interestingly, both dipyrindamole and BAY 60-6583 recovered the levels of occludin and *p*-FAK to about the same levels as uninjured controls. Moreover, if Adora2b was absent (*Adora2b*<sup>−/−</sup> mice), the expression of *p*-FAK was more significantly decreased by bleomycin, and dipyrindamole and BAY 60-6583 could no longer recover occludin and *p*-FAK

levels (**Figure 7A**). In addition, the tight junction protein ZO-2 is highly dysregulated in *Adora2b*<sup>−/−</sup> mice, representing massive loss of epithelial integrity in *Adora2b*<sup>−/−</sup> mice. However, dipyrindamole failed and BAY 60-6583 only slightly recover the ZO-2 levels in wildtype mice, indicating that ZO-2 might not directly regulated by the Adenosine through Adora2b receptors (**Figure 7A**). Taking together, these results suggest that adenosine through Adora2b may directly regulate the levels of occludin-1 and *p*-FAK.

To determine whether adenosine through Adora2b directly regulates the levels of occludin and *p*-FAK in epithelial cells, we pretreated MLE12 cells, an immortalized alveolar epithelial type II cell line, with BAY 60-6583 and incubated in 2% oxygen for 6 h. BAY 60-6583 significantly increased the levels of occludin and the effect of BAY 60-6583 on occludin could be fully blocked by MRS 1754, an Adora2b antagonist (**Figure 7B**). Although levels of *p*-FAK and claudin-1 was unaffected by BAY 60-6583, they are largely suppressed in cells treated with MRS 1754 (**Figure 7B**), suggesting a role of adenosine through Adora2b in protecting the protein levels of FAK and claudin-1 under hypoxia exposure. Overall, these findings suggest that a role of Adora2b in regulation of occludin, FAK and *p*-FAK.

Since both occludin and FAK could be degraded by calpain, a protease which can be activated in acute lung injury and under stress conditions such as hypoxia (Liu et al., 2012), we hypothesized that adenosine through Adora2b may maintain occludin and FAK levels in hypoxia and ALI by inhibiting calpain activity. To test this, we measured calpain activity in MLE12 cells pre-treated with BAY 60-6583 and then exposed them to hypoxia for 1 h. Calpain activity was significantly increased after hypoxia exposure and was dramatically inhibited by BAY 60-6583 (**Figure 7C**). The inhibition of BAY 60-6583 could be neutralized by MRS 1754 (**Figure 7C**). Calpain activity has been shown to be repressed by protein kinase A (PKA), a kinase that can be activated by adenosine through Adora2b. To determine whether BAY 60-6583 can suppress calpain activity through PKA activation, we treated MLE12 cells with H89, a PKA inhibitor. H89 significantly increased calpain activity, even in the presence of BAY 60-6583 (**Figure 7C**). Moreover, to examine whether calpain activity is directly correlated with epithelial leakage, we measured transepithelial resistance (TEER) in cells treated with different compounds and exposed to 2% oxygen for 6 h. Since MLE-12 cells can not form monolayer, we chose RLE-6TN for the TEER measurement. As shown in **Figure 7D**, the TEER is negatively correlated with the calpain activity shown in **Figure 7C** (BAY 60-6583 slowed down hypoxia-induced TEER loss, while H89 dramatically accelerated the decrease in TEER compared to control). Moreover, the protection of BAY 60-6583 was attenuated by both MRS 1754 and H89. Taken together, our data provide a novel mechanism for Adora2b-mediated protection in epithelial leakage and demonstrate that adenosine through Adora2b may attenuate occludin and FAK degradation in ALI by inhibiting calpain activity through PKA activation.



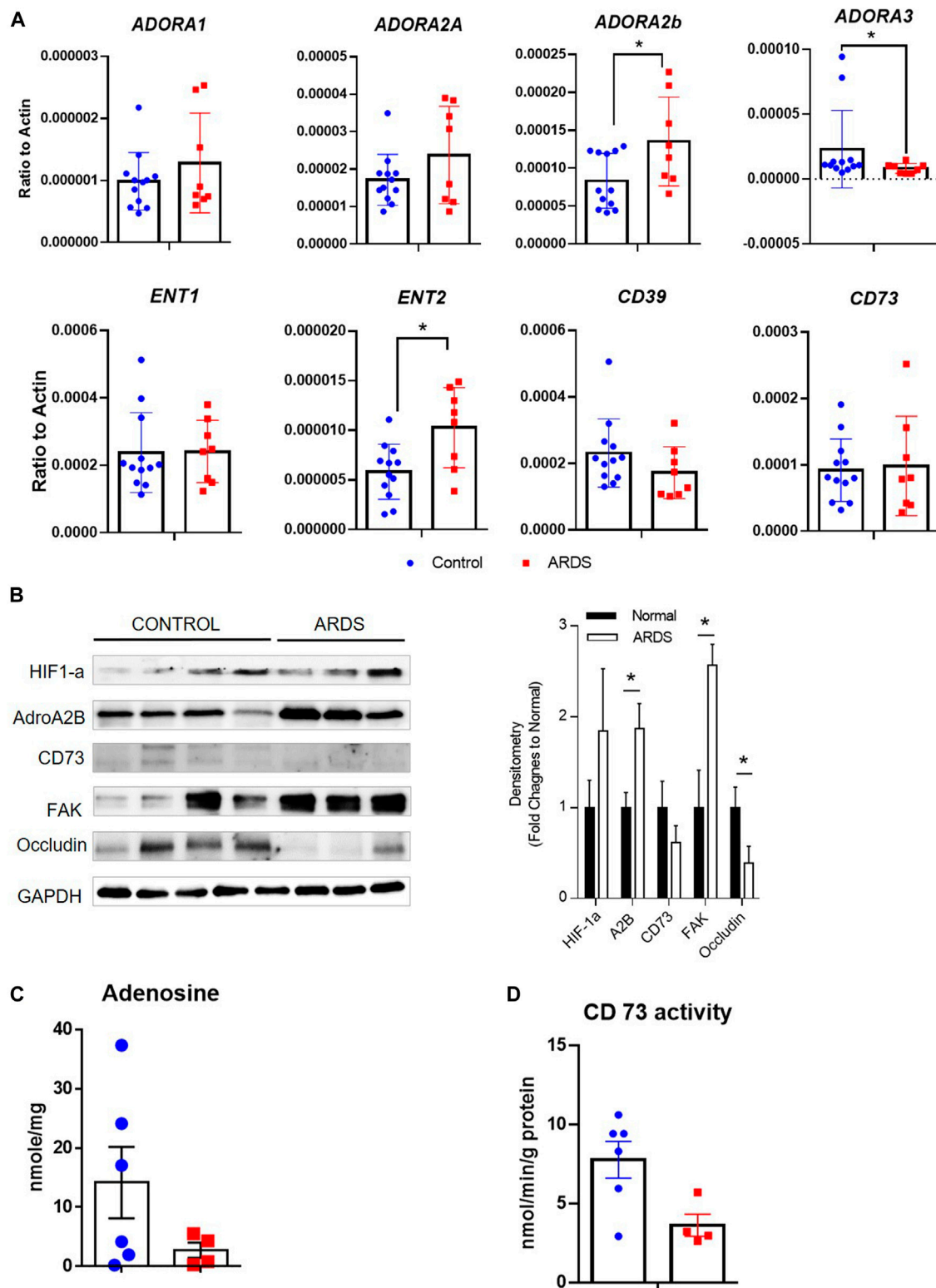


**FIGURE 8** | Expression of adenosine receptors, transporters and enzymes in human ARDS lungs. **(A)** The transcript expression of adenosine receptors (ADORA1, ADORA2A, ADORA2B and ADORA3), transporters (ENT1 and ENT2) as well as enzymes (CD39 and CD73) were determined in human normal and ARDS lungs using realtime PCR. **(B)** Left Panel: The protein expression of HIF-1a, ADORA2B, CD73 as well as tight junction proteins were determined in normal and ARDS lungs using western blot. Right Panel: Densitometry of the Western Blot image were analyzed and data were presented as fold changes to Normal control  $\pm$  MSE.  $*p < 0.05$ . **(C)** The levels of adenosine were measured using HPLC. **(D)** The activities of CD73 were determined in control and ARDS lungs.  $*p < 0.05$  using student t-test.



## Levels of Adenosine Signaling Proteins and Structural Proteins are Differently Expressed in Human ARDS Lungs

Lastly, to understand whether similar adenosine signaling is activated in human ARDS lungs, we examined the levels of adenosine receptors and transporters, as well as enzymes for adenosine synthesis in human normal and ARDS lungs. Consistent with the important roles of Adora2b in acute lung injury in mice, *ADORA2B* was the only adenosine receptor having elevated transcript and protein levels in ARDS lungs, interestingly *ADORA3* levels were attenuated in ARDS lungs (Figure 8A,B). Surprisingly, *ENT2* levels were also increased in ARDS lungs (Figure 8A) in association with reduced adenosine levels (Figure 8C) and decreased CD73 activities (Figure 8D). Moreover, the levels of tight junction protein occludin was decreased in ARDS lungs compared to normal lungs (Figure 8B), suggesting that lost epithelial barrier function is also present in human ARDS lungs. Taken together, our data suggest failed adenosine accumulation in response to injury in ARDS lungs may be the potential reason for dampened barrier functions and severe pulmonary damage in ALI.

## DISCUSSION

ARDS is an inflammatory lung disease that is characterized with noncardiogenic pulmonary edema, massive lung inflammation and severe hypoxemia (Bakowitz et al., 2012). Due to the limited clinical management of this disorder, ALI is among the leading causes of death in intensive care units (Bakowitz et al., 2012). This has been overemphasized in the recent COVID-19 pandemic where patients present with rapid-onset ARDS accompanied by a cytokine release storm, severe hypoxemia (Goh et al., 2020) accounting for mortality rates of up to 88.1% (Richardson et al., 2020). Therefore, novel therapeutic approaches targeted to dampen lung inflammation and pulmonary edema during ALI are urgently needed. The release of adenosine from injury tissue has been highlighted as an endogenous mechanism for tissue protection in several murine models of ALI, including ALI induced by high-pressure mechanical ventilation, lipopolysaccharide (LPS) and bleomycin (Eckle et al., 2009; Karmouty-Quintana et al., 2013). Our study implicates the role of adenosine transport inhibitor dipyridamole, which prevents adenosine re-uptake and enhances extracellular adenosine levels, in tissue protection from bleomycin-induced ALI. We observed that dipyridamole play a therapeutic role in bleomycin-induced ALI. Subsequent studies using epithelial specific Ent2 knockout mice, we demonstrated that epithelial Ent2 is important to regulate extracellular adenosine levels. Moreover, we identified epithelial Adora2b as the major adenosine receptor contributing to the protective effects of dipyridamole, and occludin and focal adhesion kinase (FAK) as potential targets of adenosine through Adora2b, thus providing a novel mechanism for adenosine-mediated barrier protection (Figure 9). Taken together, we have highlighted a role of adenosine signaling in preventing or treating ALI and

identified Ent2 and Adora2b as key mediators in establishing pulmonary protection from bleomycin-induced ALI.

Previous studies identified adenosine as an endogenous protective molecule during lung injury (Eckle et al., 2009; Karmouty-Quintana et al., 2013). In response to tissue injury, ATP and ADP are released from injured cells and quickly metabolized to adenosine monophosphate (AMP) in the extracellular space. Amp is then converted to adenosine by ecto-5'-nucleotidase (CD73). Equilibrative nucleoside transporters can re-uptake extracellular adenosine which allows adenosine to freely cross the extracellular cell membrane according to its concentration gradient (Grenz et al., 2011; Eltzschig et al., 2012; Eckle et al., 2013). Dampened ALI was observed using strategies aiming to inhibit extracellular adenosine levels, including genetic deletion of CD73 or CD39 (Grenz et al., 2007; Hart et al., 2011; Hasko et al., 2011) or treating mice with adenosine deaminase (ADA) which rapidly converts adenosine to inosine. On the other hand, enhancing extracellular adenosine signaling by preventing adenosine re-uptake through ENTs attenuates ALI (Eckle et al., 2013; Morote-Garcia et al., 2013). Our findings are consistent with these studies by targeting ENT as a therapeutic method for the treatment of bleomycin-induced ALI. Inhibiting ENTs with the pharmacological agent dipyridamole ameliorates established lung injury in association with enhanced extracellular adenosine concentrations. Similar protection was also observed in mice with selective deletion of *Ent2* specifically in alveolar epithelial type II cells. Dipyridamole is a FDA-approved medication used as a vasodilator for the treatment of blood clot formation and stroke (De Schryver et al., 2007; Sacco et al., 2008). Compared to mice ENTs, dipyridamole has a more potent inhibition effect on human ENTs (Yao et al., 1997), suggesting that dipyridamole could be an even more beneficial drug in the treatment of patients by lowering the off-target effects.

In this study, we identified Adora2b as the major adenosine receptor involved in the protective effect of dipyridamole mediated lung protection. Adenosine signals through four G-protein coupled receptors (Adora1, Adora2a, Adora2b and Adora3) (Hasko et al., 2008; Blackburn et al., 2009; Eltzschig, 2009; Karmouty-Quintana et al., 2013). Adora2b plays a beneficial role in tissue protection during acute injuries (Csoka et al., 2010; Eltzschig et al., 2009b; Grenz et al., 2012b). The expression levels of Adora2b is elevated as an adaption to hypoxia and inflammation, and it in turn activates a cascade of genes which are implicated in promoting barrier function, attenuating vascular leakage, and preventing inflammation and neutrophil infiltration (Eckle et al., 2009; Koeppen et al., 2011). A study by Eckle and colleagues also suggested that Adora2b promotes fluid clearance from the alveolus and attenuates pulmonary edema (Eckle et al., 2008). Consistent with previous findings, we observed attenuated ALI in mice administrated with Adora2b agonist BAY 60-6583 and enhanced ALI in mice with global deletion of Adora2b. Since Adora2b expression is mainly observed in alveolar epithelial type II cells (Cagnina et al., 2009; Eckle et al., 2013), we also generated mice with Adora2b specifically knocked out in alveolar epithelial cells and detected a similar level of lung injury comparable to global Adora2b

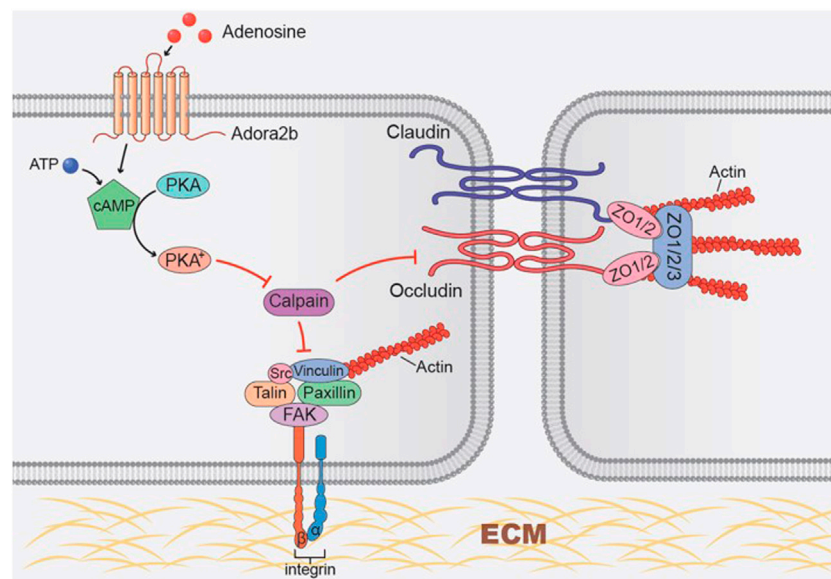


**FIGURE 9 |** Working model of Adora2b activation in regulating tight junction and focal adhesion junction proteins. Adora2b activation increases cAMP levels by activation of adenylyl cyclase, thus activated protein kinase A (PKA). Activated PKA then inhibits hypoxia-induced calpain activity, protects occludin and FAK degradation, and maintains the epithelial integrity.

knockout mice and loss of protection from dipyridamole and BAY 60-6583. Our studies provide important proof for BAY 60-6583 as a therapeutic medicine for the treatment of ALI.

Previous studies provide proof of concept for adenosine signaling in adaption to hypoxia and inflammation in a wide range of injury models (Eltzschig and Carmeliet, 2011; Eltzschig et al., 2014). In response to hypoxia, transcription factor hypoxia-inducible factor (HIF) is stabilized, which subsequently activates several components of the adenosine signaling pathway, including CD39 and CD73 which elevate extracellular adenosine generation (Eltzschig et al., 2009a; Synnestvedt et al., 2002; Thompson et al., 2004) and Adora2b which enhances the protective adenosine signal (Kong et al., 2006; Eltzschig and Carmeliet, 2011; Eckle et al., 2014; Eltzschig et al., 2014). Moreover, hypoxia also suppresses ENT1 and ENT2 expression by promoting the binding of HIF to their promoters, thus inhibiting adenosine re-uptake and enhancing adenosine downstream signaling events (Eltzschig et al., 2005; Eckle et al., 2013; Morote-Garcia et al., 2013). Consistent with these studies, we observed HIF-1 $\alpha$  stabilization following bleomycin exposure in association with a decreased ENT2 expression in the lung. Dampened ENT2 expression is also observed in primary alveolar epithelial cells exposed to hypoxia or HIF-1 $\alpha$  stabilizer CoCl<sub>2</sub>, suggesting the observed down-regulation of ENT2 in ALI could be directly regulated by hypoxia. Taken together, our data provide evidence that the hypoxia-adenosine response is an important mechanism mediating the endogenous protection of ALI. Surprisingly, contrary to the enhanced adenosine levels in response to ALI in mice, we detected decreased adenosine levels in the lungs of ARDS patients. The decreased adenosine levels could be resulted

from decreased CD73 activities and elevated adenosine transportation and elimination by ENT2 in ARDS lungs. It is important to mention that the ARDS lungs were collected from patients that succumbed to ARDS, thus it is conceivable that in these patients, insufficient accumulation of adenosine may have been a factor leading to their demise.

Although the role of extracellular adenosine signaling in inflammation has been explored to some extent (Eltzschig, 2011; Eltzschig and Carmeliet, 2011; Eltzschig et al., 2013; Idzko et al., 2014), the downstream mechanisms that mediate the role of adenosine in preventing epithelial permeability is not well studied. The integrity of the epithelial monolayer is critical for the protection of barrier-function (Kirchner et al., 2005; Lucas et al., 2009). Compared to endothelial damage, epithelial damage has more adverse effects on lung injury due to the destruction of the lung architecture that leads to prolonged changes in gas exchange and disordered repair (Martin T. R. et al., 2005). Studies show that preserved epithelial barrier function is inversely associated with mortality of patients with ALI (Martin T. R. et al., 2005; Matthay and Wiener-Kronish, 1990). These conclusions are consistent with our findings that Adora2b in epithelial cells, but not endothelial cells, prevents vascular leakage. Several tight junction and focal adhesion proteins are involved to maintain the integrity of epithelium, including occludins, claudins and focal adhesion kinase (FAK) (Ma et al., 2013; Suzuki, 2013). Deregulation of these proteins in epithelial cells promotes the permeability of the epithelium and facilitates the progression of injury (Jiang et al., 1998; Koval, 2009; Ma et al., 2013). Under stress conditions, cellular permeability can be accelerated by the activation of calpain protease which promotes the degradation of FAK and tight junction proteins and

disrupts the cell-cell connection (Chun and Prince, 2009; Heijink et al., 2012; Pereira et al., 2014; Wang et al., 2012). In our study, we found the levels of tight junction protein occludin was decreased in both human ARDS lungs and mouse lungs treated with bleomycin, suggesting a loss of epithelial barrier function in both human and mouse ALI. However, the expression of FAK is elevated in ARDS lungs possibly due to increased infiltration of inflammatory cells such as T lymphocyte and macrophages that also have high FAK expression (Chapman and Houtman, 2014; Hart et al., 2011). We also discovered that adenosine through Adora2b inhibits hypoxia-induced calpain activation through the activation of cyclic AMP (cAMP) and protein kinase A (PKA), and as a result prevents occludin-1 degradation and epithelial permeability (Figure 9). Indeed, under hypoxia condition, our data showed that BAY 60-6583 significantly increased the levels of occludin in MLE12 cells, and the effect of BAY 60-6583 on occludin could be fully blocked by Adora2b antagonist MRS 1754. Although levels of *p*-FAK and claudin-1 was unaffected by BAY 60-6583, they were largely suppressed in cells treated with MRS 1754 (Figure 7B), suggesting a role of adenosine through Adora2b in protecting the hypoxia-induced protein degradation of FAK and Claudin-1. FAK protein may be relatively more stable under hypoxia condition, that is probably why it can be slightly upregulated in Bay 606583 treated cells but not obviously affected by MRS 1754. Our results are consistent with previous findings showing improved ALI in mouse treated with a calpain inhibitor (Cuzzocrea et al., 2000; Liu et al., 2012). Although further studies are needed to understand how calpain is activated by hypoxia, and which calpain is directed targeted by adora2b/PKA, our findings identified calpain as a novel downstream target of Adora2b and provide evidence for the development of drugs aimed at targeting adenosine signaling and calpain as a therapeutic treatment of ALI.

In addition to providing evidence for the role of adenosine signaling in preventing ALI, our studies also identified dipyrindamole and BAY 60-6583 as therapeutic agents in the treatment of established ALI. Previous studies showed a beneficial role of adenosine in a wide range of acute injury models, including sepsis (Csoka et al., 2010), and lung (Zhou et al., 2011; Eckle et al., 2013), kidney (Bauerle et al., 2011; Grenz et al., 2012b) and gastrointestinal injuries (Eltzschig et al., 2009b). However, all of these studies initiate adenosine treatment before inducing tissue injury and implicate only the prophylactic role of adenosine signaling in ALI. Here we demonstrate that treating mice with dipyrindamole or BAY 60-6583 two days after bleomycin exposure, a time point when ALI is already established, still improve the barrier function by decreasing inflammation and neutrophil infiltration. Our findings are of particular importance for the treatment of ARDS patients who have already developed symptoms of ALI in the intensive care unit, and provide

important preclinical proof for enhancing adenosine signaling as a therapeutic method for the treatment of ARDS patients.

Taken together, our findings identified adenosine signaling as an important endogenous pathway to not only prevent but also treat ALI. Inhibiting adenosine re-uptake by pharmaceutical agent dipyrindamole could be a therapeutic strategy to enhance adenosine signaling through Adora2b that in turn prevents calpain activity and preserves epithelial integrity. Our results provide important pre-clinical data for the use of dipyrindamole and adenosine receptor agonists in the treatment of ALI.

## DATA AVAILABILITY STATEMENT

The raw data supporting the conclusions of this article will be made available by the authors, without undue reservation.

## ETHICS STATEMENT

The animal study was reviewed and approved by the Animal Welfare Committee of UTHealth. Written informed consent was obtained from the owners for the participation of their animals in this study.

## AUTHOR CONTRIBUTIONS

TW, HKQ, and MRB, designed the study and drafted the manuscript. WW, TW, NC, JD, and KP performed the experiments, collected the data and contributed to the statistical analysis. HKE, DR, and BA interpreted the data, and reviewed the manuscript.

## FUNDING STATEMENT

This study were supported by the National Institutes of Health (MRB: NIH 5R01HL070952, MRB and HKE: NIH P01-HL114457) and American heart association (HKQ: AHA18IPA34170220 and TTW: AHA12POST11810007) for data collection, analysis and interpretation

## ACKNOWLEDGMENTS

We thank Kelly A Volcik from the Department of Biochemistry and Molecular Biology, McGovern Medical School, the University of Texas Health Science Center at Houston for proof-reading the manuscript.

## REFERENCES

- Bakowitz, M., Bruns, B., and McCunn, M. (2012). Acute lung injury and the acute respiratory distress syndrome in the injured patient. *Scand. J. Trauma Resusc. Emerg. Med.* 20, 54. doi:10.1186/1757-7241-20-54
- Bauerle, J. D., Grenz, A., Kim, J.-H., Lee, H. T., and Eltzschig, H. K. (2011). Adenosine generation and signaling during acute kidney injury. *J. Am. Soc. Nephrol.* 22 (1), 14–20. doi:10.1681/ASN.2009121217
- Blackburn, M. R., Vance, C. O., Morschl, E., and Wilson, C. N. (2009). Adenosine receptors and inflammation. *Handb. Exp. Pharmacol.* 193, 215–269. doi:10.1007/978-3-540-89615-9\_8
- Cagnina, R. E., Ramos, S. I., Marshall, M. A., Wang, G., Frazier, C. R., and Linden, J. (2009). Adenosine A2B receptors are highly expressed on murine type II alveolar epithelial cells. *Am. J. Physiol. Lung Cell. Mol. Physiol.* 297 (3), L467–L474. doi:10.1152/ajplung.90553.2008
- Chapman, N. M., and Houtman, J. C. D. (2014). Functions of the FAK family kinases in T cells: beyond actin cytoskeletal rearrangement. *Immunol. Res.* 59 (1–3), 23–34. doi:10.1007/s12026-014-8527-y
- Chun, J., and Prince, A. (2009). TLR2-induced calpain cleavage of epithelial junctional proteins facilitates leukocyte transmigration. *Cell Host and Microbe* 5 (1), 47–58. doi:10.1016/j.chom.2008.11.009
- Csóka, B., Németh, Z. H., Rosenberger, P., Eltzschig, H. K., Spolarics, Z., Pacher, P., et al. (2010). A2B adenosine receptors protect against sepsis-induced mortality by dampening excessive inflammation. *J. Immunol.* 185 (1), 542–550. doi:10.4049/jimmunol.0901295
- Cuzzocrea, S., McDonald, M. C., Mazzon, E., Siriwardena, D., Serrano, I., Dugo, L., et al. (2000). Calpain inhibitor I reduces the development of acute and chronic inflammation. *Am. J. Pathol.* 157 (6), 2065–2079. doi:10.1016/S0002-9440(10)64845-6
- De Schryver, E. L., Algra, A., and van Gijn, J. (2007). Dipyridamole for preventing stroke and other vascular events in patients with vascular disease. *Cochrane Database Syst. Rev.* 3, CD001820. doi:10.1002/14651858.CD001820.pub3
- Eckle, T., Grenz, A., Laucher, S., and Eltzschig, H. K. (2008). A2B adenosine receptor signaling attenuates acute lung injury by enhancing alveolar fluid clearance in mice. *J. Clin. Invest.* 118 (10), 3301–3315. doi:10.1172/JCI34203
- Eckle, T., Hughes, K., Ehrentraut, H., Brodsky, K. S., Rosenberger, P., Choi, D. S., et al. (2013). Crosstalk between the equilibrative nucleoside transporter ENT2 and alveolar Adora2b adenosine receptors dampens acute lung injury. *FASEB J.* 27 (8), 3078–3089. doi:10.1096/fj.13-228551
- Eckle, T., Kewley, E. M., Brodsky, K. S., Tak, E., Bonney, S., Gobel, M., et al. (2014). Identification of hypoxia-inducible factor HIF-1A as transcriptional regulator of the A2B adenosine receptor during acute lung injury. *J. Immunol.* 192 (3), 1249–1256. doi:10.4049/jimmunol.1100593
- Eckle, T., Koeppen, M., and Eltzschig, H. K. (2009). Role of extracellular adenosine in acute lung injury. *Physiology* 24, 298–306. doi:10.1152/physiol.00022.2009
- Eltzschig, H. K. (2011). Targeting hypoxia-induced inflammation. *Anesthesiology* 114 (2), 239–242. doi:10.1097/ALN.0b013e3182070c66
- Eltzschig, H. K., Abdulla, P., Hoffman, E., Hamilton, K. E., Daniels, D., Schönfeld, C., et al. (2005). HIF-1-dependent repression of equilibrative nucleoside transporter (ENT) in hypoxia. *J. Exp. Med.* 202 (11), 1493–1505. doi:10.1084/jem.20050177
- Eltzschig, H. K., Bratton, D. L., and Colgan, S. P. (2014). Targeting hypoxia signalling for the treatment of ischaemic and inflammatory diseases. *Nat. Rev. Drug Discov.* 13 (11), 852–869. doi:10.1038/nrd4422
- Eltzschig, H. K., and Carmeliet, P. (2011). Hypoxia and inflammation. *N. Engl. J. Med.* 364 (7), 656–665. doi:10.1056/NEJMr0910283
- Eltzschig, H. K., Köhler, D., Eckle, T., Kong, T., Robson, S. C., and Colgan, S. P. (2009a). Central role of Sp1-regulated CD39 in hypoxia/ischemia protection. *Blood* 113 (1), 224–232. doi:10.1182/blood-2008-06-165746
- Eltzschig, H. K., Rivera-Nieves, J., and Colgan, S. P. (2009b). Targeting the A2B adenosine receptor during gastrointestinal ischemia and inflammation. *Expert Opin. Ther. Targets* 13 (11), 1267–1277. doi:10.1517/14728220903241666
- Eltzschig, H. K., Sitkovsky, M. V., and Robson, S. C. (2013). Purinergic signaling during inflammation. *N. Engl. J. Med.* 368 (13), 1260. doi:10.1056/NEJMc1300259
- Eltzschig, H. K., Sitkovsky, M. V., and Robson, S. C. (2012). Purinergic signaling during inflammation. *N. Engl. J. Med.* 367 (24), 2322–2333. doi:10.1056/NEJMr1205750
- Eltzschig, H. K. (2009). Adenosine: an old drug newly discovered. *Anesthesiology* 111 (4), 904–915. doi:10.1097/ALN.0b013e3181b060f2
- Fanelli, V., and Ranieri, V. M. (2015). Mechanisms and clinical consequences of acute lung injury. *Ann. ATS* 12 (Suppl. 1), S3–S8. doi:10.1513/AnnalsATS.201407-340MG
- Flori, H. R., Glidden, D. V., Rutherford, G. W., and Matthay, M. A. (2005). Pediatric acute lung injury prospective evaluation of risk factors associated with mortality. *Am. J. Respir. Crit. Care Med.* 171 (9), 995–1001. doi:10.1164/rccm.200404-544OC
- Froudarakis, M., Hatzimichael, E., Kyriazopoulou, L., Lagos, K., Pappas, P., Tzakos, A. G., et al. (2013). Revisiting bleomycin from pathophysiology to safe clinical use. *Crit. Rev. Oncol. Hematol.* 87 (1), 90–100. doi:10.1016/j.critrevonc.2012.12.003
- Goh, K. J., Choong, M. C., Cheong, E. H., Kalimuddin, S., Duu Wen, S., Phua, G. C., et al. (2020). Rapid progression to acute respiratory distress syndrome: review of current understanding of critical illness from COVID-19 infection. *Ann. Acad. Med. Singapore* 49 (1), 1–9. doi:10.47102/annals-acadmedsg.202057
- Gong, Y., Ma, T.-C., Xu, Y.-Y., Yang, R., Gao, L.-J., Wu, S.-H., et al. (2020). Early research on COVID-19: a bibliometric analysis. *Innovation* 1 (2), 100027. doi:10.1016/j.xinn.2020.100027
- Grenz, A., Bauerle, J. D., Dalton, J. H., Ridyard, D., Badulak, A., Tak, E., et al. (2012a). Equilibrative nucleoside transporter 1 (ENT1) regulates postischemic blood flow during acute kidney injury in mice. *J. Clin. Invest.* 122 (2), 693–710. doi:10.1172/JCI60214
- Grenz, A., Kim, J.-H., Bauerle, J. D., Tak, E., Eltzschig, H. K., and Clambey, E. T. (2012b). Adora2b adenosine receptor signaling protects during acute kidney injury via inhibition of neutrophil-dependent TNF- $\alpha$  release. *J. Immunol.* 189 (9), 4566–4573. doi:10.4049/jimmunol.1201651
- Grenz, A., Homann, D., and Eltzschig, H. K. (2011). Extracellular adenosine: a safety signal that dampens hypoxia-induced inflammation during ischemia. *Antioxid. Redox Signaling* 15 (8), 2221–2234. doi:10.1089/ars.2010.3665
- Grenz, A., Zhang, H., Hermes, M., Eckle, T., Klingel, K., Huang, D. Y., et al. (2007). Contribution of E-NTPDase1 (CD39) to renal protection from ischemia-reperfusion injury. *FASEB J.* 21 (11), 2863–2873. doi:10.1096/fj.06-7947com
- Hart, M. L., Grenz, A., Gorzolla, I. C., Schittenhelm, J., Dalton, J. H., and Eltzschig, H. K. (2011). Hypoxia-inducible factor-1 $\alpha$ -dependent protection from intestinal ischemia/reperfusion injury involves ecto-5'-nucleotidase (CD73) and the A2B adenosine receptor. *J. Immunol.* 186 (7), 4367–4374. doi:10.4049/jimmunol.0903617
- Haskó, G., Csóka, B., Koscsó, B., Chandra, R., Pacher, P., Thompson, L. F., et al. (2011). Ecto-5'-Nucleotidase (CD73) decreases mortality and organ injury in sepsis. *J. Immunol.* 187 (8), 4256–4267. doi:10.4049/jimmunol.1003379
- Haskó, G., Linden, J., Cronstein, B., and Pacher, P. (2008). Adenosine receptors: therapeutic aspects for inflammatory and immune diseases. *Nat. Rev. Drug Discov.* 7 (9), 759–770. doi:10.1038/nrd2638
- Heijink, I. H., Brandenburg, S. M., Postma, D. S., and van Oosterhout, A. J. M. (2012). Cigarette smoke impairs airway epithelial barrier function and cell-cell contact recovery. *Eur. Respir. J.* 39 (2), 419–428. doi:10.1183/09031936.00193810
- Idzko, M., Ferrari, D., and Eltzschig, H. K. (2014). Nucleotide signalling during inflammation. *Nature* 509 (7500), 310–317. doi:10.1038/nature13085
- Jiang, W. G., Bryce, R. P., Horrobin, D. F., and Mansel, R. E. (1998). Regulation of tight junction permeability and occludin expression by polyunsaturated fatty acids. *Biochem. Biophys. Res. Commun.* 244 (2), 414–420. doi:10.1006/bbrc.1998.8288
- Karmouty-Quintana, H., Xia, Y., and Blackburn, M. R. (2013). Adenosine signaling during acute and chronic disease states. *J. Mol. Med.* 91 (2), 173–181. doi:10.1007/s00109-013-0997-1
- Kirchner, E. A., Mols, G., Hermle, G., Muehlschlegel, J. D., Geiger, K. K., Guttmann, J., et al. (2005). Reduced activation of immunomodulatory transcription factors during positive end-expiratory pressure adjustment based on volume-dependent compliance in isolated perfused rabbit lungs. *Br. J. Anaesth.* 94 (4), 530–535. doi:10.1093/bja/aei078



- Koeppen, M., Eckle, T., and Eltzschig, H. K. (2011). Interplay of hypoxia and A2B adenosine receptors in tissue protection. *Adv. Pharmacol.* 61, 145–186. doi:10.1016/B978-0-12-385526-8.00006-0
- Kong, T., Westerman, K. A., Faigle, M., Eltzschig, H. K., and Colgan, S. P. (2006). HIF-dependent induction of adenosine A2B receptor in hypoxia. *FASEB J.* 20 (13), 2242–2250. doi:10.1096/fj.06-6419com
- Koval, M. (2009). Tight junctions, but not too tight: fine control of lung permeability by claudins. *Am. J. Physiol. Lung Cell. Mol. Physiol.* 297 (2), L217–L218. doi:10.1152/ajplung.00196.2009
- Li, X., and Ma, X. (2020). Acute respiratory failure in COVID-19: is it “typical” ARDS? *Crit. Care* 24 (1), 198. doi:10.1186/s13054-020-02911-9
- Liang, D., Shi, L., Zhao, J., Liu, P., Sarnat, J. A., Gao, S., et al. (2020). Urban air pollution may enhance COVID-19 case-fatality and mortality rates in the United States. *Innovation* 1 (3), 100047. doi:10.1016/j.xinn.2020.100047
- Liu, D., Yan, Z., Minshall, R. D., Schwartz, D. E., Chen, Y., and Hu, G. (2012). Activation of calpains mediates early lung neutrophilic inflammation in ventilator-induced lung injury. *Am. J. Physiol. Lung Cell. Mol. Physiol.* 302 (4), L370–L379. doi:10.1152/ajplung.00349.2011
- Lucas, R., Verin, A. D., Black, S. M., and Catravas, J. D. (2009). Regulators of endothelial and epithelial barrier integrity and function in acute lung injury. *Biochem. Pharmacol.* 77 (12), 1763–1772. doi:10.1016/j.bcp.2009.01.014
- Ma, Y., Semba, S., Khan, M. R. L., Bochimoto, H., Watanabe, T., Fujiya, M., et al. (2013). Focal adhesion kinase regulates intestinal epithelial barrier function via redistribution of tight junction. *Biochim. Biophys. Acta* 1832 (1), 151–159. doi:10.1016/j.bbdis.2012.10.006
- Martin, T. R., Hagimoto, N., Nakamura, M., and Matute-Bello, G. (2005). Apoptosis and epithelial injury in the lungs. *Proc. Am. Thorac. Soc.* 2 (3), 214–220. doi:10.1513/pats.200504-031AC
- Martin, W. G., Ristow, K. M., Habermann, T. M., Colgan, J. P., Witzig, T. E., and Ansell, S. M. (2005). Bleomycin pulmonary toxicity has a negative impact on the outcome of patients with Hodgkin’s lymphoma. *J. Clin. Oncol.* 23 (30), 7614–7620. doi:10.1200/JCO.2005.02.7243
- Matthay, M. A., Ware, L. B., and Zimmerman, G. A. (2012). The acute respiratory distress syndrome. *J. Clin. Invest.* 122 (8), 2731–2740. doi:10.1172/jci60331
- Matthay, M. A., and Wiener-Kronish, J. P. (1990). Intact epithelial barrier function is critical for the resolution of alveolar edema in humans. *Am. Rev. Respir. Dis.* 142 (6 Pt. 1), 1250–1257. doi:10.1164/ajrccm/142.6.Pt.1.1250
- Matthay, M. A., and Zemans, R. L. (2011). The acute respiratory distress syndrome: pathogenesis and treatment. *Annu. Rev. Pathol. Mech. Dis.* 6, 147–163. doi:10.1146/annurev-pathol-011110-130158
- Matute-Bello, G., Frevert, C. W., and Martin, T. R. (2008). Animal models of acute lung injury. *Am. J. Physiol. Lung Cell. Mol. Physiol.* 295 (3), L379–L399. doi:10.1152/ajplung.00010.2008
- Morote-Garcia, J. C., Köhler, D., Roth, J. M., Mirakaj, V., Eldh, T., Eltzschig, H. K., et al. (2013). Repression of the equilibrative nucleoside transporters dampens inflammatory lung injury. *Am. J. Respir. Cell. Mol. Biol.* 49 (2), 296–305. doi:10.1165/rcmb.2012-0457OC
- Nuckton, T. J., Alonso, J. A., Kallet, R. H., Daniel, B. M., Pittet, J.-F., Eisner, M. D., et al. (2002). Pulmonary dead-space fraction as a risk factor for death in the acute respiratory distress syndrome. *N. Engl. J. Med.* 346 (17), 1281–1286. doi:10.1056/NEJMoa012835
- Pereira, M. B. M., Santos, A. M., Gonçalves, D. C., Cardoso, A. C., Consonni, S. R., Gozzo, F. C., et al. (2014).  $\alpha$ B-crystallin interacts with and prevents stress-activated proteolysis of focal adhesion kinase by calpain in cardiomyocytes. *Nat. Commun.* 5, 5159. doi:10.1038/ncomms6159
- Ranieri, V. M., Ranieri, V. M., Rubenfeld, G. D., Thompson, B. T., Ferguson, N. D., Caldwell, E., et al. (2012). Acute respiratory distress syndrome: the Berlin Definition. *JAMA* 307 (23), 2526–2533. doi:10.1001/jama.2012.5669
- Reutershan, J., Vollmer, I., Stark, S., Wagner, R., Ngamsri, K. C., and Eltzschig, H. K. (2009). Adenosine and inflammation: CD39 and CD73 are critical mediators in LPS-induced PMN trafficking into the lungs. *FASEB J.* 23 (2), 473–482. doi:10.1096/fj.08-119701
- Richardson, S., Hirsch, J. S., Narasimhan, M., Crawford, J. M., McGinn, T., Davidson, K. W., et al. (2020). Presenting characteristics, comorbidities, and outcomes among 5700 patients hospitalized with COVID-19 in the New York city area. *JAMA*, 323, 2052–2059. doi:10.1001/jama.2020.6775
- Rosenthal, C., Caronia, C., Quinn, C., Lugo, N., and Sagy, M. (1998). A comparison among animal models of acute lung injury. *Crit. Care Med.* 26 (5), 912–916. doi:10.1097/00003246-199805000-00027
- Sacco, R. L., Diener, H.-C., Yusuf, S., Cotton, D., Öunpuu, S., Lawton, W. A., et al. (2008). Aspirin and extended-release dipyridamole versus clopidogrel for recurrent stroke. *N. Engl. J. Med.* 359 (12), 1238–1251. doi:10.1056/NEJMoa0805002
- Suzuki, T. (2013). Regulation of intestinal epithelial permeability by tight junctions. *Cell. Mol. Life Sci.* 70 (4), 631–659. doi:10.1007/s00018-012-1070-x
- Synnestvedt, K., Furuta, G. T., Comerford, K. M., Louis, N., Karhausen, J., Eltzschig, H. K., et al. (2002). Ecto-5′-nucleotidase (CD73) regulation by hypoxia-inducible factor-1 mediates permeability changes in intestinal epithelia. *J. Clin. Invest.* 110 (7), 993–1002. doi:10.1172/jci0215337
- Thompson, L. F., Eltzschig, H. K., Ibla, J. C., Van De Wiele, C. J., Resta, R., Morote-Garcia, J. C., et al. (2004). Crucial role for ecto-5′-nucleotidase (CD73) in vascular leakage during hypoxia. *J. Exp. Med.* 200 (11), 1395–1405. doi:10.1084/jem.20040915
- Thompson, L. F., Picher, M., and Blackburn, M. R. (2011). Animal models of airway diseases. *Subcell Biochem.* 55, 195–234. doi:10.1007/978-94-007-1217-1\_8
- Wang, C., Schwab, L. P., Fan, M., Seagroves, T. N., and Buolamwini, J. K. (2013). Chemoprevention activity of dipyridamole in the MMTV-PyMT transgenic mouse model of breast cancer. *Cancer Prev. Res.* 6 (5), 437–447. doi:10.1158/1940-6207.CAPR-12-0345
- Wang, T., Wang, L., Moreno-Vinasco, L., Lang, G. D., Siegler, J. H., Mathew, B., et al. (2012). Particulate matter air pollution disrupts endothelial cell barrier via calpain-mediated tight junction protein degradation. *Part. Fibre Toxicol.* 9, 35. doi:10.1186/1743-8977-9-35
- Ware, L. (2006). Pathophysiology of acute lung injury and the acute respiratory distress syndrome. *Semin. Respir. Crit. Care Med.* 27 (4), 337–349. doi:10.1055/s-2006-948288
- Ware, L. B., and Matthay, M. A. (2000). The acute respiratory distress syndrome. *N. Engl. J. Med.* 342 (18), 1334–1349. doi:10.1056/nejm200005043421806
- Williamson, J. D., Sadofsky, L. R., and Hart, S. P. (2015). The pathogenesis of bleomycin-induced lung injury in animals and its applicability to human idiopathic pulmonary fibrosis. *Exp. Lung Res.* 41 (2), 57–73. doi:10.3109/01902148.2014.979516
- Yao, S. Y. M., Ng, A. M. L., Muzyka, W. R., Griffiths, M., Cass, C. E., Baldwin, S. A., et al. (1997). Molecular cloning and functional characterization of nitrobenzylthioinosine (NBMPR)-sensitive (es) and NBMPR-insensitive (ei) equilibrative nucleoside transporter proteins (rENT1 and rENT2) from rat tissues. *J. Biol. Chem.* 272 (45), 28423–28430. doi:10.1074/jbc.272.45.28423
- Zhou, Y., Schneider, D. J., and Blackburn, M. R. (2009). Adenosine signaling and the regulation of chronic lung disease. *Pharmacol. Ther.* 123 (1), 105–116. doi:10.1016/j.pharmthera.2009.04.003
- Zhou, Y., Schneider, D. J., Morschl, E., Song, L., Pedroza, M., Karmouty-Quintana, H., et al. (2011). Distinct roles for the A2B adenosine receptor in acute and chronic stages of bleomycin-induced lung injury. *J. Immunol.* 186 (2), 1097–1106. doi:10.4049/jimmunol.1002907
- Zimmerman, M. A., Tak, E., Ehrentraut, S. F., Kaplan, M., Giebeler, A., Weng, T., et al. (2013). Retracted: equilibrative nucleoside transporter (ENT)-1-dependent elevation of extracellular adenosine protects the liver during ischemia and reperfusion. *Hepatology* 58 (5), 1766–1778. doi:10.1002/hep.26505

**Conflict of Interest:** The authors declare that the research was conducted in the absence of any commercial or financial relationships that could be construed as a potential conflict of interest.

Copyright © 2021 Wang, Chen, Ren, Davies, Philip, Eltzschig, Blackburn, Akkanti, Karmouty-Quintana and Weng. This is an open-access article distributed under the terms of the Creative Commons Attribution License (CC BY). The use, distribution or reproduction in other forums is permitted, provided the original author(s) and the copyright owner(s) are credited and that the original publication in this journal is cited, in accordance with accepted academic practice. No use, distribution or reproduction is permitted which does not comply with these terms.



# The Immune System in Transfusion-Related Acute Lung Injury Prevention and Therapy: Update and Perspective

Kai Guo\* and Shuxuan Ma\*

Department of Transfusion Medicine, Beijing Children's Hospital, Capital Medical University, National Center for Children's Health, Beijing, China

## OPEN ACCESS

### Edited by:

Wen Li,  
Zhejiang University, China

### Reviewed by:

Ajay Dixit,  
University of Minnesota Twin Cities,  
United States  
John W. Semple,  
Lund University, Sweden

### \*Correspondence:

Kai Guo  
guokai223@outlook.com;  
285647152@qq.com  
Shuxuan Ma  
masxfwyy@sina.com

### Specialty section:

This article was submitted to  
Molecular Diagnostics  
and Therapeutics,  
a section of the journal  
Frontiers in Molecular Biosciences

**Received:** 10 December 2020

**Accepted:** 05 March 2021

**Published:** 24 March 2021

### Citation:

Guo K and Ma S (2021) The  
Immune System  
in Transfusion-Related Acute Lung  
Injury Prevention and Therapy:  
Update and Perspective.  
Front. Mol. Biosci. 8:639976.  
doi: 10.3389/fmolb.2021.639976

As an initiator of respiratory distress, transfusion-related acute lung injury (TRALI) is regarded as one of the rare complications associated with transfusion medicine. However, to date, the pathogenesis of TRALI is still unclear, and specific therapies are unavailable. Understanding the mechanisms of TRALI may promote the design of preventive and therapeutic strategies. The immune system plays vital roles in reproduction, development and homeostasis. Sterile tissue damage, such as physical trauma, ischemia, or reperfusion injury, induces an inflammatory reaction that results in wound healing and regenerative mechanisms. In other words, in addition to protecting against pathogens, the immune response may be strongly associated with TRALI prevention and treatment through a variety of immunomodulatory strategies to inhibit excessive immune system activation. Immunotherapy based on immune cells or immunological targets may eradicate complications. For example, IL-10 therapy is a promising therapeutic strategy to explore further. This review will focus on ultramodern advances in our understanding of the potential role of the immune system in TRALI prevention and treatment.

**Keywords:** transfusion-related acute lung injury, immune system, immune molecule, immunotherapy, prevention

## INTRODUCTION

Transfusion-related acute lung injury (TRALI) is the onset of respiratory distress and acute lung injury due to blood product transfusion (Semple et al., 2019), and it is a life-threatening complication characterized by the sudden onset of hypoxemic respiratory failure with non-cardiogenic pulmonary edema and bilateral lung infiltration that developed within 6 h of blood transfusion (Toy et al., 2005; Gokhale and Hendrickson, 2019). Although TRALI develops within 6 hrs of blood transfusion, most occurrences take place during transfusion or within the first 1 or 2 h. According to Voelker and Spieth (2019) TRALI is defined as more complex for cases of seeming TRALI, such as transfusion-associated circulatory overload (TACO), and further testing and diagnosis may be required. TRALI pathophysiology has been partially elucidated. According to the 2004 Canadian Consensus Conference Panel (Kleinman et al., 2004) and TRALI redefinition

(Vlaar et al., 2019), TRALI can be identified and diagnosed, and the terms TRALI I [without an acute respiratory distress syndrome (ARDS)] and TRALI II (accompanied by ARDS) have been proposed. However, there were some potential TRALI cases did not meet standard clinical definitions (Fuller et al., 2021).

Currently, TRALI is the leading cause of transfusion-related fatalities (Clifford et al., 2015), and the case fatality rate is 5–10% (Swanson et al., 2006). The incidence of TRALI in surgical transfusion patients is 1.3–1.4% (Clifford et al., 2015), and as many as 15% of patients with severe transfusions develop TRALI (Benson et al., 2010). A report from the US FDA showed that 34% of fatalities were due to TRALI from 2012 to 2016 (fatalities reported to FDA following blood collection and transfusion: annual summary for fiscal year 2016: US Food and Drug Administration), which constitutes one of the leading serious adverse reactions to transfusion. Lieberman et al. (2014) suggested that the incidence of TRALI in children is similar to that in adults. Although the numbers are low, there are no differences in outcomes or presentation between adults and children with TRALI.

Generally, the risk factors for blood transfusion can be divided into antibody-independent and antibody-dependent in the context of TRALI. The former is caused by the transfusion of aged red blood cells or platelets, which contain proinflammatory mediators, bioactive lipids, etc. (Mangalmurti et al., 2009; Vlaar et al., 2010; Peters et al., 2015a). The latter is caused by antibody infusions, which mainly contain human leukocyte antigen (HLA) I and II or human neutrophil antigen (HNA) antibodies (Peters et al., 2015b), are mainly obtained from female donors and cause human neutrophil activation (Popovsky et al., 1983). Antibody-dependent TRALI is the most prevalent type (Popovsky and Moore, 1985; Curtis and McFarland, 2006).

Currently, the two-hit model is used to describe the underlying mechanism of TRALI pathology (Peters et al., 2015b; Lorello and Alam, 2018). The predisposing factors of the patient are the first hit, and antibody or non-antibody factors are the second hit (Silliman et al., 1997; Silliman, 2006). Some clinical studies have shown that an inflammatory first hit almost always occurs before TRALI onset and have identified ARDS risk factors that may also be TRALI risk factors in transfusion recipients, including liver surgery, shock, increased peak airway pressure, chronic alcohol abuse and current smoking in the context of immune system balance and inflammation (Toy et al., 2012). Namely, the clinical condition of the patient induces the release of a large number of cytokines, which cause neutrophil activation, accumulation and adhesion to pulmonary microvascular endothelial cells. The second hit is mainly due to HLA or HNA antibodies from the blood products that directly or indirectly activate the recipient's immune system. An increasing number of studies have shown that antibody-dependent TRALI is mediated by the activation of neutrophils, which results in the release of oxygen free radicals and proteases, causes endothelial damage, and increases capillary permeability, ultimately causing pulmonary edema, and inducing TRALI (Silliman, 2006).

According to the classic definition, the immune system is comprised of complement molecules, as well as immune cells and their products, including cytokines, chemokines, antibodies,

and growth factors. The immune system is considered to be responsible for defending the host from invading pathogenic microorganisms. In fact, the immune system is an integral part of fundamental physiological processes and immune cells function beyond host defense (Sattler, 2017). Researchers in an expanding range of areas are beginning to recognize continuously the implications of the immune system in their respective fields. The immune system plays an essential role in reproduction both before and during pregnancy, and leukocytes are found in male and female reproductive tissues (Oakley et al., 2011; Care et al., 2013). In other words, the effects of the immune system are not limited to host defense but extend to tissue homeostasis, regeneration and the repair of tissues such as the liver (Meijer et al., 2000), kidney (Lin et al., 2010; Zhang et al., 2012), skin (Goren et al., 2009; Mirza et al., 2009), skeletal muscle, heart (Arnold et al., 2007; Nahrendorf et al., 2007; Frantz et al., 2012; Gallego-Colon et al., 2015; Tonkin et al., 2015; Sattler and Rosenthal, 2016), gut (Seno et al., 2009), and brain (Glod et al., 2006; London et al., 2013). Both evolutionary development and functional variety strongly support the idea of the immune system as an all-encompassing system to ensure systemic integrity.

More importantly, the immune response is closely associated with transfusion therapy (Passwater, 2018). Landers et al. (1996) showed the immunomodulatory effects of blood transfusion in 1996. The immune response is an important basis for the occurrence of TRALI (Tung, 2019). Specifically, before and after transfusion, TRALI patients exhibited elevated levels of IL-6 and IL-8, which are the main contributors to the development of TRALI (Roubinian et al., 2015). Fung et al. (2010) also suggested the importance of T cells in reducing the severity of antibody-dependent TRALI in a murine model. Furthermore, it is believed that TRALI is the result of imbalances in the body's inflammatory response. During infectious diseases, a variety of immunomodulatory molecular mechanisms are activated, including the induction of regulatory T cells (Tregs), regulatory B cells, alternatively activated M2 macrophages or the anti-inflammatory cytokines IL-10 and TGF- $\beta$  (Taylor et al., 2012; Ziegler et al., 2015; Xu et al., 2016; Loevenich et al., 2017; Soares et al., 2017), which affect all facets of the host immune response to ensure host survival. However, some immune factors, such as B cells, were shown to not play a significant role in the onset of murine antibody-mediated TRALI (Kapur et al., 2017a). Accordingly, in this report, we identified potential immunotherapeutic approaches for TRALI based on immune cells, cytokines and complement molecules by analyzing the literature.

## REGULATORY T CELLS

Tregs are essential for maintaining immune homeostasis by regulating effector T cell responses, thus facilitating pathogen immune evasion (Velavan and Ojuronbe, 2011) and preventing potential pathogenic host pathogenic effects through a variety of mechanisms (Shevach, 2009; Maruyama et al., 2011; Gao et al., 2012). For example, Tregs express receptor molecules

such as CTLA-4, PD-1 and GITR and directly contact target cells to regulate effector cell function, secrete IL-10, TGF- $\beta$  and other inhibitory cytokines to exert immunosuppressive effects, and allow antigen-presenting cells to enter a non-response state; the expression of enzymes such as CD39 and CD73 indirectly affects the metabolism of target cells, and the secretion of granzymes A and B directly kills target cells and affects immune responses (Shevach, 2009; Josefowicz et al., 2012; Gubser et al., 2016; Rueda et al., 2016). Tregs represent an antigen-specific mechanism to inhibit potentially harmful autoreactive responses.

Although Tregs are defined as T cells with immunosuppressive activity, it has been documented that Treg populations remain diverse (Miyara and Sakaguchi, 2007). Tregs expressing CD25 and Foxp3 are naturally present in the immune system and are considered to be negative regulators of the T cell response. These natural Tregs originate during thymic development (Mold et al., 2008). In addition, other cells, such as IL-10-secreting CD4<sup>+</sup>CD25<sup>-</sup>Foxp3<sup>-</sup> (Tr1) cells and TGF- $\beta$ -secreting CD4<sup>+</sup>CD25<sup>-</sup>Foxp3<sup>+</sup> T cells, have also been shown to exert regulatory effects (Lan et al., 2005). While CD4<sup>+</sup>CD25<sup>-</sup>Foxp3<sup>+</sup> T cells, which originate from CD4<sup>+</sup>CD25<sup>-</sup> T cells that develop in the periphery (Wen et al., 2012), CD4<sup>+</sup>CD25<sup>+</sup>Foxp3<sup>+</sup>, CD4<sup>+</sup>CD25<sup>-</sup>Foxp3<sup>+</sup>, and Tr1 Tregs can be activated in different microenvironments. Moreover, CD4<sup>-</sup>CD8<sup>-</sup> Tregs (double-negative Tregs, DN Tregs) express the  $\alpha\beta$  TCR but do not express CD4, CD8, NK cell surface markers or Foxp3, and CD8<sup>+</sup> Tregs have no specific surface markers (Lan et al., 2005; Sakaguchi et al., 2010; Murphy and Weaver, 2016). In recent years, a new subpopulation of Tregs (iT<sub>R35</sub> cells) has been shown to mediate immunosuppression via IL-35 but not IL-10 or TGF- $\beta$  and is independent of Foxp3 (Collison et al., 2010).

Foxp3-expressing Tregs are known to be indispensable for the maintenance of immunological self-tolerance and immune homeostasis (Sakaguchi et al., 2006). IL-10, TGF- $\beta$  and Foxp3 are functional and phenotypic markers of natural Tregs (nTregs) and are associated with inducible Tregs (iTregs) (Fontenot et al., 2003). Tregs expressing Foxp3 are able to suppress the activation, proliferation and effector functions (such as cytokine production) of CD4<sup>+</sup> and CD8<sup>+</sup> T cells, natural killer (NK) cells, NKT cells, B cells and antigen-presenting cells (APCs) *in vitro* and *in vivo* (Sakaguchi et al., 2008). Tregs can also be isolated and expanded *in vitro*; thus far, treatment with this cell product seems safe and well tolerated (Salas and Panes, 2015).

Notably, some researchers have shown that lymphocytes, especially Tregs, are recruited to the lung in response to lung injury. Tregs may play a key role in protecting against TRALI. Tregs can relieve inflammation by regulating immune responses, thereby alleviating lung injury *in vivo* and *in vitro* (D'Alessio et al., 2009). Venet et al. (2009) confirmed that Tregs reduced neutrophil recruitment and activation by producing IL-10 in lipopolysaccharide (LPS)-mediated acute lung injury. Furthermore, Kapur et al. (2017a) demonstrated for the first time that CD4<sup>+</sup>CD25<sup>+</sup>Foxp3<sup>+</sup> Tregs are critical effectors that protect against antibody-dependent murine TRALI via IL-10. Two years later, He et al. (2019) showed that IL-2c and IL-2 derived from CD4<sup>+</sup>CD25<sup>+</sup>Foxp3<sup>+</sup> Tregs increased IL-10 and decreased IL-17A, thereby prophylactically preventing antibody-dependent

murine TRALI. Subsequently, different subtypes of Tregs, such as Tr1 and iT<sub>R35</sub> cells, may play important roles in further studies.

## DENDRITIC CELLS

In general, dendritic cells (DCs) are highly specialized antigen-presenting cells that are important in not only initiating immune responses but also in tuning the quality of the immune response or inhibiting the response (Moll, 2003). DCs play a crucial role in this regulatory work, as these cells can regulate T cell-mediated effector responses by generating anti-inflammatory cytokines or inducing Tregs (Maldonado and von Andrian, 2010). Tolerogenic DCs, in particular, can regulate immune responses through various mechanisms (Steinman et al., 2003). Cell fate is predominantly controlled by cytokines in the microenvironment, and to some extent, by the strength of the interaction between the T cell receptor (such as CD45, CTLA-4, and PD-1) and the antigen (Boyton and Altmann, 2002). Tight regulation of effector T cell responses is required to effectively control infections and avoid autoimmune and immunopathological diseases. Aberrant T cell responses, especially those of Th1 and Th17 cells, may play key roles in organ-specific autoimmunity (Dardalhon et al., 2008) and immunopathology (Rutitzky et al., 2008) in the lung. Previously, Kapur R demonstrated that CD11c<sup>+</sup> DCs protected against antibody-dependent TRALI via IL-10 in mice (Kapur et al., 2017a). The role of DCs may be essential for TRALI immunotherapy.

## MACROPHAGES

Currently, macrophage-targeted therapy has been used in patients (Patel and Janjic, 2015). Alveolar macrophages are central effector cells in the production of proinflammatory mediators. These cells are key in the initiation and resolution of lung inflammation in humans. In the future, the polarization of M1 macrophages may be essential in human TRALI. Lei W et al. (Wang et al., 2020) confirmed that  $\alpha$ 1-antitrypsin expression improved lung injury by regulating IL-6 production in alveolar macrophages and decreased the M1 macrophage polarization. Modulating macrophage polarization may serve as a potential treatment strategy for human TRALI. By establishing an anti-major histocompatibility complex (MHC) class I monoclonal antibody-induced mouse model of TRALI-like disease, Strait et al. (2011) showed that TRALI induction involves monocytes and macrophages in this murine model.

In addition, osteopontin, a recognized proinflammatory molecule that mediates diverse biological functions (Lund et al., 2009), is involved in various pulmonary disorders, such as fibrosis, inflammation, malignancies, and vascular lung disorders (O'Regan, 2003). Osteopontin is also an important protein involved in regulating the migration of immune cells (Lund et al., 2009). The osteopontin-mediated murine TRALI response is dependent on macrophages, which may be possibly the cellular source of osteopontin (Kapur et al., 2019). In summary, targeting macrophage function may be a critical strategy for TRALI treatment or prevention (Zeeuw van der Laan et al., 2020b).



## NEUTROPHILS

Neutrophils, which have diameters of 12–14  $\mu\text{m}$ , are derived from hematopoietic stem cells. As the first line of cellular defense against invading pathogens, neutrophils can rapidly move across the blood-endothelial cell barrier and exert effector functions during inflammation. Neutrophils are the first responders and are recruited in large numbers to the inflammatory microenvironment by the accumulation of lipid mediators, cytokines, and chemokines, as well as changes in the vascular endothelium (Sadik and Luster, 2012; Mocsai et al., 2015). Neutrophil recruitment to inflamed tissues involves elements of neutrophil rolling and firm adhesion (Filippi, 2019). To capture extracellular pathogen-associated molecules and other stimuli, neutrophils release decondensed chromatin coated with granular proteins, which form neutrophil extracellular traps (NETs) (Branzk et al., 2014; Storisteanu et al., 2017; Watanabe and Petri, 2019). However, the secretion of NETs can also cause tissue damage at the expense of the host and has been shown to impair wound healing or facilitate lung injury in diabetes (Wong et al., 2015) and ventilator-induced lung injury (Yildiz et al., 2015). NETs play an essential role in TRALI. Caudrillier et al. (2012) demonstrated that platelets triggered NET formation in an LPS- or anti-MHC class I antibody-based TRALI mouse model. Thomas et al. (2012) showed that NET biomarkers were present in the serum of TRALI patients, as well as in the lungs of LPS- and anti-MHC class I antibody-induced TRALI mice. Treatment with DNase I IV, which disrupts the formation of the extracellular chromatin web (Hakkim et al., 2010), was shown to have beneficial effects in these two studies. Although DNases are associated with cystic fibrosis in the lung (Thornby et al., 2014), and additional studies on NETs are necessary in the context of DNase therapy for human TRALI.

In addition, as the major producers of reactive oxygen species (ROS), neutrophils can damage the endothelium in antibody-dependent TRALI mice (Strait et al., 2011; Bayat et al., 2013) and in human pulmonary microvascular endothelial cells *in vitro* (Silliman et al., 2007). Other studies have shown neutrophil-mediated endothelial cell damage in antibody-independent TRALI (Xie et al., 2015) and antibody-dependent TRALI (Nishimura et al., 2006; Silliman et al., 2007; Khoy et al., 2017). Moreover, neutrophils and ROS were shown to be critical in antibody-mediated murine TRALI, as demonstrated by *in vivo* neutrophil depletion and the use of gp91phox-knockout mice, respectively (Kapur et al., 2017a).

Lipids in blood products also damage endothelial cells via neutrophils in an antibody-independent TRALI model, and in human pulmonary microvascular endothelial cells that were activated by LPS and cocultured with neutrophils (Wyman et al., 2002). Neutrophil-dependent endothelial cell damage also occurred in the presence of soluble CD40L (Khan et al., 2006). The Fc $\gamma$  receptor on neutrophils can recognize the Fc-tail of IgG, which binds to pathogens via the IgG-Fab region (Vidarsson and van de Winkel, 1998; Hogarth and Pietersz, 2012; Kapur et al., 2014). A study by Looney MR (Looney et al., 2006) showed that neutrophils and their Fc $\gamma$  receptors were essential in a TRALI mouse model. Moreover, researchers found that neutrophil Fc $\gamma$  receptors were critically involved in TRALI, as

adoptive transfer of wild-type neutrophils into TRALI-resistant Fc $\gamma$  receptor-knockout mice ameliorated acute lung injury upon challenge with anti-MHC class I antibodies (Looney et al., 2006). Neutrophil depletion can protect against anti-HNA-3a antibody-mediated TRALI in mice, although TRALI was not completely prevented in this context (Bayat et al., 2013).

Neutrophils are key effectors in TRALI pathogenesis (Rebetz et al., 2018). Pulmonary neutrophil infiltration has been shown to occur in multiple murine TRALI models (Looney et al., 2006, 2009; Kelher et al., 2009; Fung et al., 2010; Tung et al., 2011; Semple et al., 2012; Bayat et al., 2013, 2015; McKenzie et al., 2014; Kapur et al., 2015, 2017a, 2018) and human TRALI patients (Dry et al., 1999; Silliman et al., 2005; Akagi et al., 2020). Currently, new evidence clearly points to the plasticity of neutrophils and may present a new strategy for the potential treatment of TRALI.

## IL-10

IL-10 is a member of the IL-10 family of cytokines and a non-covalent homodimeric  $\alpha$  helical cytokine with structural similarities to IFN- $\gamma$ . The IL-10 receptor (IL-10R) is expressed on the surface of most hematopoietic cells, including T and B cells and macrophages. Genetically, the immunological and physiological functions of IL-10 were found to be non-redundant in engineered mouse models that lack IL-10 or IL-10R. IL-10 inhibits the proliferation of CD4<sup>+</sup> T cells and the secretion of many kinds of cytokines (Fiorentino et al., 1989).

IL-10 expression is altered in patients with TRALI relative to that in control patients. Kapur et al. (2017b) showed reduced IL-10 levels in patients with TRALI. In all pulmonary transfusion reactions, the combination of clinical variables and cytokine measurements indicated optimal diagnostic performance, and the model comparing TACO and TRALI correctly classified 92% of cases relative to expert panel diagnoses (Roubinian et al., 2015). Low plasma IL-10 levels were associated with TRALI susceptibility in a mouse model, and IL-10-knockout mice were also hypersensitive to TRALI induction (Kapur et al., 2017a). These results suggested that low IL-10 levels were a risk factor for TRALI in humans (Kapur et al., 2017b). However, despite this beneficial effect, these data were in contrast to the findings in patients who suffered from other inflammatory/transfusion-associated pulmonary disorders, such as sepsis-associated acute lung injury (Kapur et al., 2017b) or transfusion-associated circulatory overload (Roubinian et al., 2015), in which IL-10 levels were often elevated. This finding may indicate that TRALI has a distinct mechanism of injury and may be uniquely characterized by impaired IL-10 production. However, two reports demonstrated that IL-10 levels were increased in TRALI patients (Looney et al., 2006, 2014). However, the study showed the changes that may indicate risk factors before blood transfusion (Looney et al., 2014) and may explain this discrepancy.

Regardless, IL-10 infusion may have a therapeutic effect in human TRALI and may completely prevent and protect against the development of antibody-dependent TRALI without any apparent side effects both prophylactically and therapeutically by ameliorating the TRALI reaction in mice (Kapur et al.,

2017a). Furthermore, the administration of IL-10 to healthy volunteers was documented as a safe intervention, and only mild to moderate side effects, such as flu-like symptoms, were observed (Moore et al., 2001). We therefore hypothesize that IL-10 administration may be an attractive approach for alleviating TRALI, and clinical studies in humans are highly warranted within 6 h of transfusion for acute lung reactions. However, IL-10 may impair host immune system resistance to infection in clinical settings.

In summary, low plasma IL-10 levels were associated with TRALI susceptibility in a mouse model, and IL-10-knockout mice were also hypersensitive to TRALI induction (Kapur et al., 2017a). IL-10 levels are low in TRALI patients (Kapur et al., 2017b), and very importantly, IL-10 therapy both prophylactically and therapeutically alleviates TRALI in mice (Kapur et al., 2017a). Therefore, IL-10 therapy is a promising therapeutic strategy to explore further.

## IL-8

IL-8 is a CXC chemokine that promotes neutrophil chemotaxis and degranulation downstream of CXC-chemokine receptor (CXCR) 1 and CXCR2, which are G protein-coupled receptors (Holmes et al., 1991; Hammond et al., 1995; Waugh and Wilson, 2008). A study by Roubinian NH demonstrated that IL-6 and IL-8 were elevated in patients with TRALI before and after transfusion relative to those in the control group (Roubinian et al., 2015). In H-2Kd/H-2Dd antibody-based severe combined immunodeficient TRALI models, it was demonstrated that the binding of H-2Kd/H-2Dd antibodies to monocytes increased the levels of macrophage inflammatory protein 2 (MIP-2), causing increased pulmonary neutrophil infiltration and subsequently inducing TRALI (McKenzie et al., 2014).

*In vivo*, peripheral blood monocyte depletion or chemokine blockade completely stopped TRALI induction using an MIP-2 receptor antagonist in severe combined immunodeficiency (SCID) mice (McKenzie et al., 2014). Roubinian et al. (2015) showed that IL-8 is a known risk factor for TRALI, and blocking the IL-8 receptor may also be sufficient to suppress neutrophil chemotaxis and degranulation, thereby counteracting TRALI induction. Moreover, in clinical trials, CXCR2 antagonists were evaluated in other pulmonary disorders, such as cystic fibrosis, asthma and chronic obstructive pulmonary disease (Chapman et al., 2009; O'Byrne et al., 2016), and may have potential efficacy in TRALI as well.

## COMPLEMENT CASCADE

One hundred years ago, the complement system was defined based on its ability to “complement” the antibody-dependent and cell-dependent immune responses against pathogens in blood-based antimicrobial system to compared that of global regulators of immunity and tissue homeostasis. Today, many studies have focused on understanding the biology of complement and its mechanisms of action. Our understanding of innate immunity has substantially changed. Complement plays an essential role

in modulating innate and adaptive immunity, supports innate immune responses and the initiation of general inflammatory reactions, contributes to tissue and organ development and promotes tissue repair after injury. In cooperation with other immune and physiological systems, the complement system is key in the recognition and elimination of invading pathogens and mediates the clearance of apoptotic cells, cellular debris and immune complexes to remove self-derived danger signals by integrating innate and adaptive immunity (Ricklin et al., 2010; Arbore et al., 2017).

Distinct mechanisms of the complement cascade are triggered by classic, lectin or alternative signals that converge at the third component (C) and lead to the generation of effectors that make up or supplement the ability of antibodies and phagocytes to clear microbial intruders via the opsonization of C3b, which promotes inflammation via anaphylatoxins C3a and C5a and lyses susceptible pathogens via the C5b-9 membrane attack complex (Ricklin et al., 2010). Complement C5a was shown to play an important role in an anti-MHC class I antibody-based TRALI model in BALB/c mice (Strait et al., 2011). Strait et al. (2011) confirmed that the anti-MHC class I antibody-induced murine TRALI model involved complement activation and C5a production (Strait et al., 2011). However, Looney et al. (2006) described the induction of TRALI 2 h after anti-MHC class I antibody injection in C5a receptor-deficient mice (Looney et al., 2006), and additional validation is needed on the role of C5a as a possible TRALI therapy before the use of C5 inhibitors (Nunn et al., 2005). This further research will shed light on the relevance of the complement system in TRALI, which may open up new therapeutic avenues to explore in combatting TRALI. Cleary SJ demonstrated that complement depletion protected the lungs in endothelial MHC I-deficient mice, and targeting complement cascade activation may be useful for TRALI treatment or prevention (Cleary et al., 2020). Zeeuw van der Laan et al. (2020a) further confirmed that TRALI-inducing murine antibodies have increased abilities to activate the complement system, especially Fc-mediated complement activation, compared to those of antibodies that do not cause TRALI. Complement activation by the endothelium initiates antibody-dependent acute lung injury. Neutrophil responses, including NET release, were intact in endothelial MHC I-deficient mice, whereas complement depletion reduced lung injury (Cleary et al., 2020).

In summary, the complement cascade eradicates invading microorganisms, apoptotic cells, and immune complexes. This evidence should significantly increase our understanding of the role of complement in TRALI and thereby potentially result in promising new treatment strategies. Additional systematic studies are needed to elucidate the role of complement in TRALI (Jongnerius et al., 2019).

## OTHER FACTORS

McKenzie et al. (2014) demonstrated that intact antibody-induced TRALI was abrogated after the depletion of peripheral blood monocytes. However, TRALI was restored upon purified monocyte restoration. Looney et al. (2009) showed that platelet depletion and aspirin treatment protected mice in

an antibody-dependent TRALI model. Cognasse et al. (2020) further showed that although platelet depletion did not prevent the occurrence of TRALI in a mouse model, it did reduce TRALI severity and inhibit TRALI development, and recipient platelets are likely involved in TRALI (Semple and Kapur, 2020). The blockade of sphingomyelinase, extracellular vesicle elimination, or supplementation with sphingosine-1-phosphate during platelet storage may present promising new TRALI prevention strategies (McVey et al., 2021).

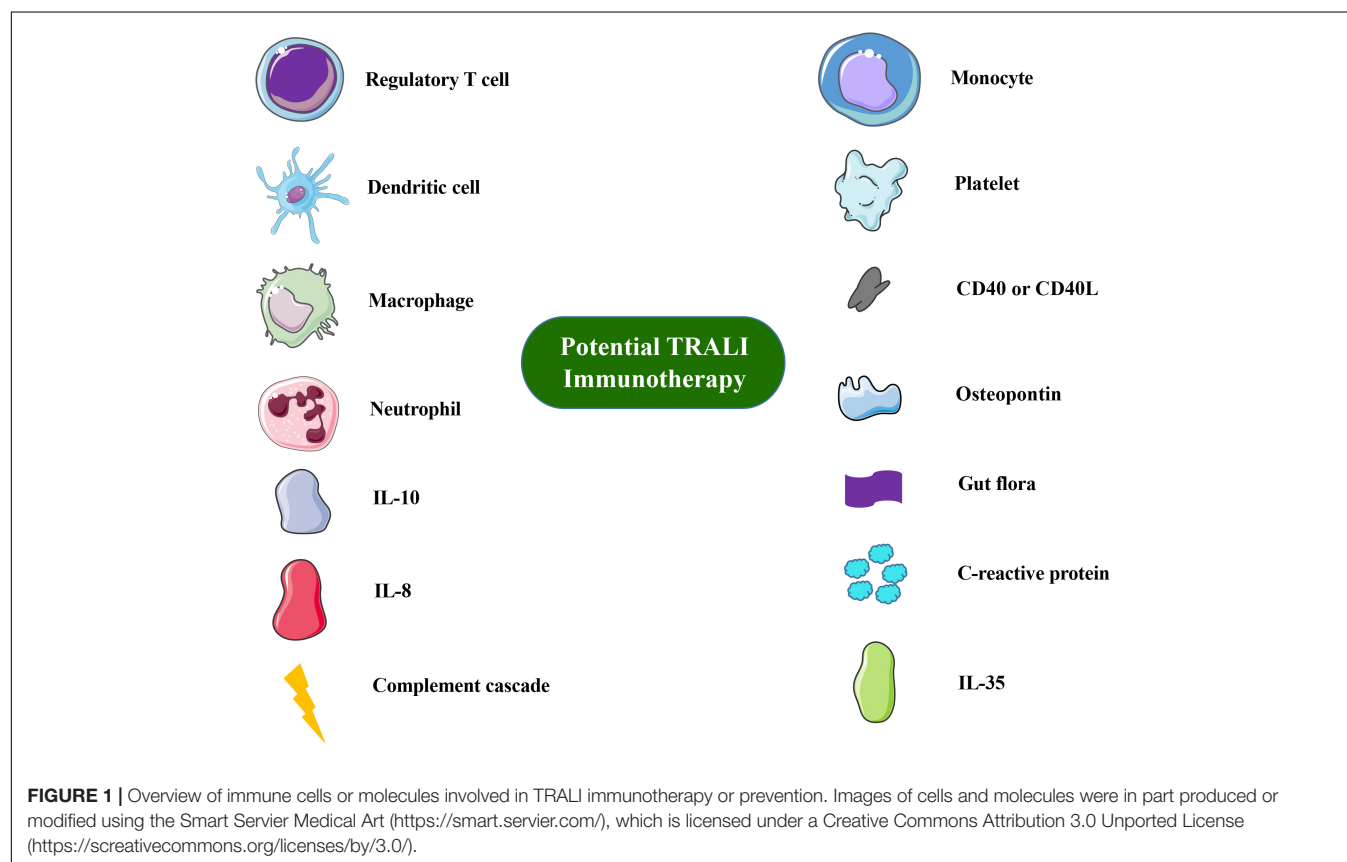
We should also note that C-reactive protein (CRP) enhances antibody-mediated TRALI induction in mice (Kapur et al., 2015) and that CRP levels are elevated in human TRALI patients (Kapur et al., 2016). Some studies have indicated that targeting the CD40-CD40L interaction could be an important method to prevent or protect against TRALI (Tariket et al., 2019; Hu et al., 2020). The importance of the gut flora in TRALI induction (Kapur et al., 2018) is continuously being studied and explored.

In addition, cytokines connect and interact with each other through a crosstalk network. Cytokines play important roles in regulating the immune response, differentiating and developing immune cells, and mediating the inflammatory response. The TRALI model shows that host inflammation develops, and the disease is the first blow, causing endothelial cells to secrete cytokines, which helps the lung attract neutrophils by increasing the surface expression of cell adhesion molecules. Lung endothelial cells release cytokines and chemokines to activate and induce neutrophils to accumulate in pulmonary capillaries, stimulating neutrophil-mediated endothelial cell

interactions and mediating lung injury. Therefore, other than IL-10 and IL-8, other cytokines may be also potential research targets for TRALI prevention and treatment. For example, Qiao et al. (2020) preliminarily confirmed that IL-35 could prevent murine TRALI by inhibiting the activation of endothelial cells. The study of additional immunological factors in combination with previous research findings could shape the field of TRALI research. For example, IL-6, TNF- $\alpha$ , IL-1 $\beta$  and danger-associated molecular patterns (Land, 2013; Tolle and Standiford, 2013; Liu et al., 2017) are factors that induce ARDS.

## DISCUSSION

Overall TRALI remains a significant clinical problem. The development of TRALI animal models is highly important in dissecting the disease pathology because factors other than volume appear to play a significant role in TRALI. Based on previously studies, these immune approaches may significantly contribute to combating these life-threatening complications of blood transfusion. Cell-based therapies, such as those based on Treg or DC administration, seem to be safe and well tolerated. Cytokines or secreted factors have increasingly been utilized to validate risk factors for TRALI, and cytokine concentrations are related to the pathogenesis of TRALI. As Semple et al. (2018, 2019) proposed, the most promising therapeutic strategies to explore are interleukin-10 therapy, down-modulating C-reactive



protein levels, targeting reactive oxygen species, or blocking the interleukin-8 receptor. Innate immune molecules, such as complement, are also important. The immune cells or molecules involvement in TRALI are summarized in **Figure 1**.

These studies focused on the immune system and may provide potential new therapeutic strategies for TRALI. It will be important to expand the investigation of immune-mediated treatments for the clinical diagnosis of and decision making regarding TRALI patients.

## AUTHOR CONTRIBUTIONS

KG and SM conceptualized the review. Both authors wrote the review, prepared the figure, and edited and approved the final manuscript.

## REFERENCES

- Akagi, Y., Murata, S., Yamashita, Y., Tanaka, K., Hiroi, T., Mushino, T., et al. (2020). Two episodes of Transfusion-related Acute Lung Injury (TRALI) occurring within a short period. *Intern. Med.* 59, 2577–2581. doi: 10.2169/internalmedicine.4700-20
- Arbore, G., Kemper, C., and Kolev, M. (2017). Intracellular complement - the complosome - in immune cell regulation. *Mol. Immunol.* 89, 2–9. doi: 10.1016/j.molimm.2017.05.012
- Arnold, L., Henry, A., Poron, F., Baba-Amer, Y., van Rooijen, N., Plonquet, A., et al. (2007). Inflammatory monocytes recruited after skeletal muscle injury switch into antiinflammatory macrophages to support myogenesis. *J. Exp. Med.* 204, 1057–1069. doi: 10.1084/jem.20070075
- Bayat, B., Tjahjono, Y., Berghofer, H., Werth, S., Deckmyn, H., De Meyer, S. F., et al. (2015). Choline transporter-like protein-2: new von willebrand factor-binding partner involved in antibody-mediated neutrophil activation and transfusion-related acute lung injury. *Arterioscler. Thromb. Vasc. Biol.* 35, 1616–1622. doi: 10.1161/ATVBAHA.115.305259
- Bayat, B., Tjahjono, Y., Sydykov, A., Werth, S., Hippenstiel, S., Weissmann, N., et al. (2013). Anti-human neutrophil antigen-3a induced transfusion-related acute lung injury in mice by direct disturbance of lung endothelial cells. *Arterioscler. Thromb. Vasc. Biol.* 33, 2538–2548. doi: 10.1161/ATVBAHA.113.301206
- Benson, A. B., Austin, G. L., Berg, M., McFann, K. K., Thomas, S., Ramirez, G., et al. (2010). Transfusion-related acute lung injury in ICU patients admitted with gastrointestinal bleeding. *Intens. Care Med.* 36, 1710–1717. doi: 10.1007/s00134-010-1954-x
- Boyton, R. J., and Altmann, D. M. (2002). Is selection for TCR affinity a factor in cytokine polarization? *Trends Immunol.* 23, 526–529. doi: 10.1016/s1471-4906(02)02319-0
- Branzk, N., Lubojemska, A., Hardison, S. E., Wang, Q., Gutierrez, M. G., Brown, G. D., et al. (2014). Neutrophils sense microbe size and selectively release neutrophil extracellular traps in response to large pathogens. *Nat. Immunol.* 15, 1017–1025. doi: 10.1038/ni.2987
- Care, A. S., Diener, K. R., Jasper, M. J., Brown, H. M., Ingman, W. V., and Robertson, S. A. (2013). Macrophages regulate corpus luteum development during embryo implantation in mice. *J. Clin. Invest.* 123, 3472–3487. doi: 10.1172/JCI60561
- Caudrillan, A., Kessenbrock, K., Gilliss, B. M., Nguyen, J. X., Marques, M. B., Monestier, M., et al. (2012). Platelets induce neutrophil extracellular traps in transfusion-related acute lung injury. *J. Clin. Invest.* 122, 2661–2671. doi: 10.1172/JCI61303
- Chapman, R. W., Phillips, J. E., Hipkin, R. W., Curran, A. K., Lundell, D., and Fine, J. S. (2009). CXCR2 antagonists for the treatment of pulmonary disease. *Pharmacol. Ther.* 121, 55–68. doi: 10.1016/j.pharmthera.2008.10.005
- Cleary, S. J., Kwaan, N., Tian, J. J., Calabrese, D. R., Mallavia, B., Magnen, M., et al. (2020). Complement activation on endothelium initiates antibody-mediated acute lung injury. *J. Clin. Invest.* 130, 5909–5923. doi: 10.1172/JCI138136

## FUNDING

This work was supported by grants from Cultivation Fund of Capital Medical University (No. PYZ19033), Cultivation Fund Project of the National Natural Science Foundation in Beijing Children's Hospital, Capital Medical University (No. GPY201802), and the Children's Medicine Research Project of Beijing Children's Hospital, Capital Medical University (Nos. YZQN202003 and YZYB202004).

## ACKNOWLEDGMENTS

We thank our colleagues from the Department of Transfusion Medicine, Beijing Children's Hospital, Capital Medical University for all their invaluable efforts.

- Clifford, L., Jia, Q., Subramanian, A., Yadav, H., Wilson, G. A., Murphy, S. P., et al. (2015). Characterizing the epidemiology of postoperative transfusion-related acute lung injury. *Anesthesiology* 122, 12–20. doi: 10.1097/ALN.0000000000000514
- Cognasse, F., Tariket, S., Hamzeh-Cognasse, H., Arthaud, C. A., Eyraud, M. A., Bourlet, T., et al. (2020). Platelet depletion limits the severity but does not prevent the occurrence of experimental transfusion-related acute lung injury. *Transfusion* 60, 713–723. doi: 10.1111/trf.15738
- Collison, L. W., Chaturvedi, V., Henderson, A. L., Giacomini, P. R., Guy, C., Bankoti, J., et al. (2010). IL-35-mediated induction of a potent regulatory T cell population. *Nat. Immunol.* 11, 1093–1101. doi: 10.1038/ni.1952
- Curtis, B. R., and McFarland, J. G. (2006). Mechanisms of transfusion-related acute lung injury (TRALI): anti-leukocyte antibodies. *Crit. Care Med.* 34, S118–S123. doi: 10.1097/01.CCM.0000214293.72918.D8
- D'Alessio, F. R., Tsushima, K., Aggarwal, N. R., West, E. E., Willett, M. H., Britos, M. F., et al. (2009). CD4+CD25+Foxp3+ Tregs resolve experimental lung injury in mice and are present in humans with acute lung injury. *J. Clin. Invest.* 119, 2898–2913. doi: 10.1172/JCI36498
- Dardalhon, V., Korn, T., Kuchroo, V. K., and Anderson, A. C. (2008). Role of Th1 and Th17 cells in organ-specific autoimmunity. *J. Autoimmun.* 31, 252–256. doi: 10.1016/j.jaut.2008.04.017
- Dry, S. M., Bechard, K. M., Milford, E. L., Churchill, W. H., and Benjamin, R. J. (1999). The pathology of transfusion-related acute lung injury. *Am. J. Clin. Pathol.* 112, 216–221. doi: 10.1093/ajcp/112.2.216
- Filippi, M.-D. (2019). Neutrophil transendothelial migration: updates and new perspectives. *Blood* 133, 2149–2158. doi: 10.1182/blood-2018-12-844605
- Fiorentino, D. F., Bond, M. W., and Mosmann, T. R. (1989). Two types of mouse T helper cell. IV. Th2 clones secrete a factor that inhibits cytokine production by Th1 clones. *J. Exp. Med.* 170, 2081–2095.
- Fontenot, J. D., Gavin, M. A., and Rudensky, A. Y. (2003). Foxp3 programs the development and function of CD4+CD25+ regulatory T cells. *Nat. Immunol.* 4, 330–336. doi: 10.1038/ni904
- Frantz, S., Hofmann, U., Fraccarollo, D., Schäfer, A., Kranepuhl, S., Hagedorn, I., et al. (2012). Monocytes/macrophages prevent healing defects and left ventricular thrombus formation after myocardial infarction. *FASEB J.* 27, 871–881. doi: 10.1096/fj.12-214049
- Fuller, C. C., Nambudiri, V. E., Spencer-Smith, C., Curtis, L. H., Shinde, M., Cosgrove, A., et al. (2021). Medical chart validation of inpatient diagnosis codes for transfusion-related acute lung injury 2013–2015. *Transfusion* doi: 10.1111/trf.16251 [Epub ahead of print].
- Fung, Y. L., Kim, M., Tabuchi, A., Aslam, R., Speck, E. R., Chow, L., et al. (2010). Recipient T lymphocytes modulate the severity of antibody-mediated transfusion-related acute lung injury. *Blood* 116, 3073–3079. doi: 10.1182/blood-2010-05-284570
- Gallego-Colon, E., Sampson, R. D., Sattler, S., Schneider, M. D., Rosenthal, N., and Tonkin, J. (2015). Cardiac-restricted IGF-1Ea overexpression reduces the early accumulation of inflammatory myeloid cells and mediates expression



- of extracellular matrix remodelling genes after myocardial infarction. *Med. Inflamm.* 2015:484357. doi: 10.1155/2015/484357
- Gao, Y., Lin, F., Su, J., Gao, Z., Li, Y., Yang, J., et al. (2012). Molecular mechanisms underlying the regulation and functional plasticity of FOXP3(+) regulatory T cells. *Genes Immun.* 13, 1–13. doi: 10.1038/gene.2011.77
- Glod, J., Kobiler, D., Noel, M., Koneru, R., Lehrer, S., Medina, D., et al. (2006). Monocytes form a vascular barrier and participate in vessel repair after brain injury. *Blood* 107, 940–946. doi: 10.1182/blood-2004-11-4403
- Gokhale, A., and Hendrickson, J. E. (2019). “Chapter 66 – Transfusion-Related Acute Lung Injury,” in *Transfusion Medicine and Hemostasis (Third Edition)*, eds B. H. Shaz, C. D. Hillyer and G. M. Reyes (Elsevier), 405–408. doi: 10.1016/B978-0-12-813726-0.00066-0
- Goren, I., Allmann, N., Yogeve, N., Schurmann, C., Linke, A., Holdener, M., et al. (2009). A transgenic mouse model of inducible macrophage depletion: effects of diphtheria toxin-driven lysozyme M-specific cell lineage ablation on wound inflammatory, angiogenic, and contractive processes. *Am. J. Pathol.* 175, 132–147. doi: 10.2353/ajpath.2009.081002
- Gubser, C., Schmalzer, M., Rossi, S. W., and Palmer, E. (2016). Monoclonal regulatory T cells provide insights into T cell suppression. *Sci. Rep.* 6:25758. doi: 10.1038/srep25758
- Hakim, A., Furnrohr, B. G., Amann, K., Laube, B., Abed, U. A., Brinkmann, V., et al. (2010). Impairment of neutrophil extracellular trap degradation is associated with lupus nephritis. *Proc. Natl. Acad. Sci. U.S.A.* 107, 9813–9818. doi: 10.1073/pnas.0909927107
- Hammond, M. E., Lapointe, G. R., Feucht, P. H., Hilt, S., Gallegos, C. A., Gordon, C. A., et al. (1995). IL-8 induces neutrophil chemotaxis predominantly via type I IL-8 receptors. *J. Immunol.* 155, 1428–1433.
- He, R., Li, L., Kong, Y., Tian, L., Tian, X., Fang, P., et al. (2019). Preventing murine transfusion-related acute lung injury by expansion of CD4(+) CD25(+) FoxP3(+) Tregs using IL-2/anti-IL-2 complexes. *Transfusion* 59, 534–544. doi: 10.1111/trf.15064
- Hogarth, P. M., and Pietersz, G. A. (2012). Fc receptor-targeted therapies for the treatment of inflammation, cancer and beyond. *Nat. Rev. Drug Discov.* 11, 311–331. doi: 10.1038/nrd2909
- Holmes, W. E., Lee, J., Kuang, W. J., Rice, G. C., and Wood, W. I. (1991). Structure and functional expression of a human interleukin-8 receptor. *Science* 253, 1278–1280. doi: 10.1126/science.1840701
- Hu, A., Chen, W., Wu, S., Pan, B., Zhu, A., Yu, X., et al. (2020). An animal model of transfusion-related acute lung injury and the role of soluble CD40 ligand. *Vox Sang.* 115, 303–313. doi: 10.1111/vox.12895
- Jongerijs, I., Porcelijn, L., van Beek, A. E., Semple, J. W., van der Schoot, C. E., Vlaar, A. P. J., et al. (2019). The role of complement in transfusion-related acute lung injury. *Transfus. Med. Rev.* 33, 236–242. doi: 10.1016/j.tmr.2019.09.002
- Josefowicz, S. Z., Lu, L. F., and Rudensky, A. Y. (2012). Regulatory T cells: mechanisms of differentiation and function. *Annu. Rev. Immunol.* 30, 531–564. doi: 10.1146/annurev.immunol.25.022106.141623
- Kapur, R., Einarsdottir, H. K., and Vidarsson, G. (2014). IgG-effector functions: “the good, the bad and the ugly”. *Immunol. Lett.* 160, 139–144. doi: 10.1016/j.imlet.2014.01.015
- Kapur, R., Kasetty, G., Rebetz, J., Egesten, A., and Semple, J. W. (2019). Osteopontin mediates murine transfusion-related acute lung injury via stimulation of pulmonary neutrophil accumulation. *Blood* 134, 74–84. doi: 10.1182/blood.2019000972
- Kapur, R., Kim, M., Aslam, R., McVey, M. J., Tabuchi, A., Luo, A., et al. (2017a). T regulatory cells and dendritic cells protect against transfusion-related acute lung injury via IL-10. *Blood* 129, 2557–2569. doi: 10.1182/blood-2016-12-758185
- Kapur, R., Kim, M., Rebetz, J., Rondina, M. T., Porcelijn, L., and Semple, J. W. (2017b). Low levels of interleukin-10 in patients with transfusion-related acute lung injury. *Ann. Transl. Med.* 5:339. doi: 10.21037/atm.2017.04.37
- Kapur, R., Kim, M., Rebetz, J., Hallstrom, B., Bjorkman, J. T., Takabe-French, A., et al. (2018). Gastrointestinal microbiota contributes to the development of murine transfusion-related acute lung injury. *Blood Adv.* 2, 1651–1663. doi: 10.1182/bloodadvances.2018018903
- Kapur, R., Kim, M., Rondina, M. T., Porcelijn, L., and Semple, J. W. (2016). Elevation of C-reactive protein levels in patients with transfusion-related acute lung injury. *Oncotarget* 7, 78048–78054. doi: 10.18632/oncotarget.12872
- Kapur, R., Kim, M., Shanmugabhavanathan, S., Liu, J., Li, Y., and Semple, J. W. (2015). C-reactive protein enhances murine antibody-mediated transfusion-related acute lung injury. *Blood* 126, 2747–2751. doi: 10.1182/blood-2015-09-672592
- Kelher, M. R., Masuno, T., Moore, E. E., Damle, S., Meng, X., Song, Y., et al. (2009). Plasma from stored packed red blood cells and MHC class I antibodies causes acute lung injury in a 2-event in vivo rat model. *Blood* 113, 2079–2087. doi: 10.1182/blood-2008-09-177857
- Khan, S. Y., Kelher, M. R., Heal, J. M., Blumberg, N., Boshkov, L. K., Phipps, R., et al. (2006). Soluble CD40 ligand accumulates in stored blood components, primes neutrophils through CD40, and is a potential cofactor in the development of transfusion-related acute lung injury. *Blood* 108, 2455–2462. doi: 10.1182/blood-2006-04-017251
- Khoy, K., Nguyen, M. V. C., Masson, D., Bardy, B., Drouet, C., and Paclet, M. H. (2017). Transfusion-related acute lung injury: critical neutrophil activation by anti-HLA-A2 antibodies for endothelial permeability. *Transfusion* 57, 1699–1708. doi: 10.1111/trf.14134
- Kleinman, S., Caulfield, T., Chan, P., Davenport, R., McFarland, J., McPhedran, S., et al. (2004). Toward an understanding of transfusion-related acute lung injury: statement of a consensus panel. *Transfusion* 44, 1774–1789. doi: 10.1111/j.0041-1132.2004.04347.x
- Lan, R. Y., Ansari, A. A., Lian, Z. X., and Gershwin, M. E. (2005). Regulatory T cells: development, function and role in autoimmunity. *Autoimmun. Rev.* 4, 351–363. doi: 10.1016/j.autrev.2005.01.007
- Land, W. G. (2013). Transfusion-related acute lung injury: the work of DAMPs. *Transfus. Med. Hemother.* 40, 3–13. doi: 10.1159/000345688
- Landers, D. F., Hill, G. E., Wong, K. C., and Fox, I. J. (1996). Blood transfusion-induced immunomodulation. *Anesth. Analg.* 82, 187–204. doi: 10.1097/0000539-199601000-00035
- Lieberman, L., Petraszko, T., Yi, Q. L., Hannach, B., and Skeate, R. (2014). Transfusion-related lung injury in children: a case series and review of the literature. *Transfusion* 54, 57–64. doi: 10.1111/trf.12249
- Lin, S. L., Li, B., Rao, S., Yeo, E. J., Hudson, T. E., Nowlin, B. T., et al. (2010). Macrophage Wnt7b is critical for kidney repair and regeneration. *Proc. Natl. Acad. Sci. U.S.A.* 107, 4194–4199. doi: 10.1073/pnas.09122228107
- Liu, X., Cao, H., Li, J., Wang, B., Zhang, P., Dong Zhang, X., et al. (2017). Autophagy induced by DAMPs facilitates the inflammation response in lungs undergoing ischemia-reperfusion injury through promoting TRAF6 ubiquitination. *Cell Death Differ.* 24, 683–693. doi: 10.1038/cdd.2017.1
- Loevenich, K., Ueffing, K., Abel, S., Hose, M., Matuschewski, K., Westendorf, A. M., et al. (2017). DC-Derived IL-10 modulates pro-inflammatory cytokine production and promotes induction of CD4(+)IL-10(+) regulatory t cells during *Plasmodium yoelii* infection. *Front. Immunol.* 8:152. doi: 10.3389/fimmu.2017.00152
- London, A., Cohen, M., and Schwartz, M. (2013). Microglia and monocyte-derived macrophages: functionally distinct populations that act in concert in CNS plasticity and repair. *Front. Cell Neurosci.* 7:34. doi: 10.3389/fncel.2013.00034
- Looney, M. R., Nguyen, J. X., Hu, Y., Van Ziffle, J. A., Lowell, C. A., and Matthay, M. A. (2009). Platelet depletion and aspirin treatment protect mice in a two-event model of transfusion-related acute lung injury. *J. Clin. Invest.* 119, 3450–3461. doi: 10.1172/JCI38432
- Looney, M. R., Roubinian, N., Gajic, O., Gropper, M. A., Hubmayr, R. D., Lowell, C. A., et al. (2014). Prospective study on the clinical course and outcomes in transfusion-related acute lung injury. *Crit. Care Med.* 42, 1676–1687. doi: 10.1097/CCM.0000000000000323
- Looney, M. R., Su, X., Van Ziffle, J. A., Lowell, C. A., and Matthay, M. A. (2006). Neutrophils and their Fc gamma receptors are essential in a mouse model of transfusion-related acute lung injury. *J. Clin. Invest.* 116, 1615–1623. doi: 10.1172/JCI27238
- Lorello, G. R., and Alam, A. (2018). Perioperative transfusion-related acute lung injury. *Int. Anesthesiol. Clin.* 56, 47–67. doi: 10.1097/AIA.0000000000000178
- Lund, S. A., Giachelli, C. M., and Scatena, M. (2009). The role of osteopontin in inflammatory processes. *J. Cell Commun. Signal.* 3, 311–322. doi: 10.1007/s12079-009-0068-0
- Maldonado, R. A., and von Andrian, U. H. (2010). How tolerogenic dendritic cells induce regulatory T cells. *Adv. Immunol.* 108, 111–165. doi: 10.1016/S0065-2776(10)08004\_1
- Mangalmurti, N. S., Xiong, Z., Hulver, M., Ranganathan, M., Liu, X. H., Oriss, T., et al. (2009). Loss of red cell chemokine scavenging promotes transfusion-related lung inflammation. *Blood* 113, 1158–1166. doi: 10.1182/blood-2008-07-166264

- Maruyama, T., Konkel, J. E., Zamarron, B. F., and Chen, W. (2011). The molecular mechanisms of Foxp3 gene regulation. *Semin. Immunol.* 23, 418–423. doi: 10.1016/j.smim.2011.06.005
- McKenzie, C. G., Kim, M., Singh, T. K., Milev, Y., Freedman, J., and Semple, J. W. (2014). Peripheral blood monocyte-derived chemokine blockade prevents murine transfusion-related acute lung injury (TRALI). *Blood* 123, 3496–3503. doi: 10.1182/blood-2013-11-536755
- McVey, M. J., Weidenfeld, S., Maishan, M., Spring, C., Kim, M., Tabuchi, A., et al. (2021). Platelet extracellular vesicles mediate transfusion-related acute lung injury by imbalancing the sphingolipid rheostat. *Blood* 137, 690–701. doi: 10.1182/blood.2020005985
- Meijer, C., Wiezer, M. J., Diehl, A. M., Schouten, H. J., Schouten, H. J., Meijer, S., et al. (2000). Kupffer cell depletion by CI2MDP-liposomes alters hepatic cytokine expression and delays liver regeneration after partial hepatectomy. *Liver* 20, 66–77. doi: 10.1034/j.1600-0676.2000.020001066.x
- Mirza, R., DiPietro, L. A., and Koh, T. J. (2009). Selective and specific macrophage ablation is detrimental to wound healing in mice. *Am. J. Pathol.* 175, 2454–2462. doi: 10.2353/ajpath.2009.090248
- Miyara, M., and Sakaguchi, S. (2007). Natural regulatory T cells: mechanisms of suppression. *Trends Mol. Med.* 13, 108–116. doi: 10.1016/j.molmed.2007.01.003
- Mocsai, A., Walzog, B., and Lowell, C. A. (2015). Intracellular signalling during neutrophil recruitment. *Cardiovasc. Res.* 107, 373–385. doi: 10.1093/cvr/cvv159
- Mold, J. E., Michaelson, J., Burt, T. D., Muench, M. O., Beckerman, K. P., Busch, M. P., et al. (2008). Maternal alloantigens promote the development of tolerogenic fetal regulatory T cells in utero. *Science* 322, 1562–1565. doi: 10.1126/science.1164511
- Moll, H. (2003). Dendritic cells and host resistance to infection. *Cell Microbiol.* 5, 493–500. doi: 10.1046/j.1462-5822.2003.00291.x
- Moore, K. W., de Waal Malefyt, R., Coffman, R. L., and O'Garra, A. (2001). Interleukin-10 and the interleukin-10 receptor. *Annu. Rev. Immunol.* 19, 683–765. doi: 10.1146/annurev.immunol.19.1.683
- Murphy, K., and Weaver, C. (2016). *Janeway's Immunobiology: Garland Science*, 9th Edn, New York, NY: W.W. Norton & Company.
- Nahrendorf, M., Swirski, F. K., Aikawa, E., Stangenberg, L., Wurdinger, T., Figueiredo, J. L., et al. (2007). The healing myocardium sequentially mobilizes two monocyte subsets with divergent and complementary functions. *J. Exp. Med.* 204, 3037–3047. doi: 10.1084/jem.20070885
- Nishimura, M., Takanashi, M., Okazaki, H., and Satake, M. (2006). Lung microvascular endothelial cell injury caused by treatment with polymorphonuclear neutrophils and low-IgM serum: a model of transfusion-related acute lung injury. *Lung* 184, 25–32. doi: 10.1007/s00408-005-2559-y
- Nunn, M. A., Sharma, A., Paesen, G. C., Adamson, S., Lissina, O., Willis, A. C., et al. (2005). Complement inhibitor of C5 activation from the soft tick *Ornithodoros moubata*. *J. Immunol.* 174, 2084–2091. doi: 10.4049/jimmunol.174.4.2084
- Oakley, O. R., Frazer, M. L., and Ko, C. (2011). Pituitary-ovary-spleen axis in ovulation. *Trends Endocrinol. Metab.* 22, 345–352. doi: 10.1016/j.tem.2011.04.005
- O'Byrne, P. M., Metev, H., Puu, M., Richter, K., Keen, C., Uddin, M., et al. (2016). Efficacy and safety of a CXCR2 antagonist, AZD5069, in patients with uncontrolled persistent asthma: a randomised, double-blind, placebo-controlled trial. *Lancet Respir. Med.* 4, 797–806. doi: 10.1016/S2213-2600(16)30227-2
- O'Regan, A. (2003). The role of osteopontin in lung disease. *Cytokine Growth Fact. Rev.* 14, 479–488. doi: 10.1016/S1359-6101(03)00055-8
- Passwater, M. (2018). Antibody formation in transfusion therapy. *J. Infus. Nurs.* 41, 87–95. doi: 10.1097/NAN.0000000000000264
- Patel, S. K., and Janjic, J. M. (2015). Macrophage targeted theranostics as personalized nanomedicine strategies for inflammatory diseases. *Theranostics* 5, 150–172. doi: 10.7150/thno.9476
- Peters, A. L., van Hezel, M. E., Juffermans, N. P., and Vlaar, A. P. (2015a). Pathogenesis of non-antibody mediated transfusion-related acute lung injury from bench to bedside. *Blood Rev.* 29, 51–61. doi: 10.1016/j.blre.2014.09.007
- Peters, A. L., van Stein, D., and Vlaar, A. P. (2015b). Antibody-mediated transfusion-related acute lung injury: from discovery to prevention. *Br. J. Haematol.* 170, 597–614. doi: 10.1111/bjh.13459
- Popovsky, M. A., Abel, M. D., and Moore, S. B. (1983). Transfusion-related acute lung injury associated with passive transfer of antileukocyte antibodies. *Am. Rev. Respir. Dis.* 128, 185–189. doi: 10.1164/arrd.1983.128.1.185
- Popovsky, M. A., and Moore, S. B. (1985). Diagnostic and pathogenetic considerations in transfusion-related acute lung injury. *Transfusion* 25, 573–577.
- Qiao, J., He, R., Yin, Y., Tian, L., Li, L., Lian, Z., et al. (2020). rIL-35 prevents murine transfusion-related acute lung injury by inhibiting the activation of endothelial cells. *Transfusion* 60, 1434–1442. doi: 10.1111/trf.15805
- Rebetz, J., Semple, J. W., and Kapur, R. (2018). The pathogenic involvement of neutrophils in acute respiratory distress syndrome and transfusion-related acute lung injury. *Transfus. Med. Hemother.* 45, 290–298. doi: 10.1159/000492950
- Ricklin, D., Hajishengallis, G., Yang, K., and Lambris, J. D. (2010). Complement: a key system for immune surveillance and homeostasis. *Nat. Immunol.* 11, 785–797. doi: 10.1038/ni.1923
- Roubinian, N. H., Looney, M. R., Kor, D. J., Lowell, C. A., Gajic, O., Hubmayr, R. D., et al. (2015). Cytokines and clinical predictors in distinguishing pulmonary transfusion reactions. *Transfusion* 55, 1838–1846. doi: 10.1111/trf.13021
- Rueda, C. M., Jackson, C. M., and Chougnet, C. A. (2016). Regulatory T-cell-mediated suppression of conventional T-cells and dendritic cells by different cAMP intracellular pathways. *Front. Immunol.* 7:216. doi: 10.3389/fimmu.2016.00216
- Rutitzky, L. I., Bazzzone, L., Shainheit, M. G., Joyce-Shaikh, B., Cua, D. J., and Staderker, M. J. (2008). IL-23 is required for the development of severe egg-induced immunopathology in schistosomiasis and for lesional expression of IL-17. *J. Immunol.* 180, 2486–2495.
- Sadik, C. D., and Luster, A. D. (2012). Lipid-cytokine-chemokine cascades orchestrate leukocyte recruitment in inflammation. *J. Leukoc. Biol.* 91, 207–215. doi: 10.1189/jlb.0811402
- Sakaguchi, S., Miyara, M., Costantino, C. M., and Hafler, D. A. (2010). FOXP3+ regulatory T cells in the human immune system. *Nat. Rev. Immunol.* 10, 490–500. doi: 10.1038/nri2785
- Sakaguchi, S., Ono, M., Setoguchi, R., Yagi, H., Hori, S., Fehervari, Z., et al. (2006). Foxp3+ CD25+ CD4+ natural regulatory T cells in dominant self-tolerance and autoimmune disease. *Immunol. Rev.* 212, 8–27. doi: 10.1111/j.0105-2896.2006.00427.x
- Sakaguchi, S., Yamaguchi, T., Nomura, T., and Ono, M. (2008). Regulatory T cells and immune tolerance. *Cell* 133, 775–787. doi: 10.1016/j.cell.2008.05.009
- Salas, A., and Panes, J. (2015). IBD: regulatory T cells for treatment of Crohn's disease. *Nat. Rev. Gastroenterol. Hepatol.* 12, 315–316. doi: 10.1038/nrgastro.2015.68
- Sattler, S. (2017). The role of the immune system beyond the fight against infection. *Adv. Exp. Med. Biol.* 1003, 3–14. doi: 10.1007/978-3-319-57613-8\_1
- Sattler, S., and Rosenthal, N. (2016). The neonate versus adult mammalian immune system in cardiac repair and regeneration. *Biochim. Biophys. Acta* 1863, 1813–1821. doi: 10.1016/j.bbamcr.2016.01.011
- Semple, J. W., and Kapur, R. (2020). The contribution of recipient platelets in TRALI: has the jury reached a verdict? *Transfusion* 60, 886–888. doi: 10.1111/trf.15814
- Semple, J. W., Kim, M., Hou, J., McVey, M., Lee, Y. J., Tabuchi, A., et al. (2012). Intravenous immunoglobulin prevents murine antibody-mediated acute lung injury at the level of neutrophil reactive oxygen species (ROS) production. *PLoS One* 7:e31357. doi: 10.1371/journal.pone.0031357
- Semple, J. W., McVey, M. J., Kim, M., Rebetz, J., Kuebler, W. M., and Kapur, R. (2018). Targeting transfusion-related acute lung injury: the journey from basic science to novel therapies. *Crit. Care Med.* 46, e452–e458. doi: 10.1097/CCM.0000000000002989
- Semple, J. W., Rebetz, J., and Kapur, R. (2019). Transfusion-associated circulatory overload and transfusion-related acute lung injury. *Blood* 133, 1840–1853. doi: 10.1182/blood-2018-10-860809
- Seno, H., Miyoshi, H., Brown, S. L., Geske, M. J., Colonna, M., and Stappenbeck, T. S. (2009). Efficient colonic mucosal wound repair requires Trem2 signaling. *Proc. Natl. Acad. Sci. U.S.A.* 106, 256–261. doi: 10.1073/pnas.0803343106
- Shevach, E. M. (2009). Mechanisms of foxp3+ T regulatory cell-mediated suppression. *Immunity* 30, 636–645. doi: 10.1016/j.immuni.2009.04.010
- Silliman, C. C. (2006). The two-event model of transfusion-related acute lung injury. *Crit. Care Med.* 34, S124–S131. doi: 10.1097/01.CCM.0000214292.62276.8E
- Silliman, C. C., Ambruso, D. R., and Boshkov, L. K. (2005). Transfusion-related acute lung injury. *Blood* 105, 2266–2273. doi: 10.1182/blood-2004-07-2929

- Silliman, C. C., Curtis, B. R., Kopko, P. M., Khan, S. Y., Kelher, M. R., Schuller, R. M., et al. (2007). Donor antibodies to HNA-3a implicated in TRALI reactions prime neutrophils and cause PMN-mediated damage to human pulmonary microvascular endothelial cells in a two-event in vitro model. *Blood* 109, 1752–1755. doi: 10.1182/blood-2006-05-025106
- Silliman, C. C., Paterson, A. J., Dickey, W. O., Stroneck, D. F., Popovsky, M. A., Caldwell, S. A., et al. (1997). The association of biologically active lipids with the development of transfusion-related acute lung injury: a retrospective study. *Transfusion* 37, 719–726. doi: 10.1046/j.1537-2995.1997.37797369448.x
- Soares, R. R., Antinarelli, L. M. R., Abramo, C., Macedo, G. C., Coimbra, E. S., and Scopel, K. K. G. (2017). What do we know about the role of regulatory B cells (Breg) during the course of infection of two major parasitic diseases, malaria and leishmaniasis? *Pathog. Glob. Health* 111, 107–115. doi: 10.1080/20477724.2017.1308902
- Steinman, R. M., Hawiger, D., and Nussenzweig, M. C. (2003). Tolerogenic dendritic cells. *Annu. Rev. Immunol.* 21, 685–711. doi: 10.1146/annurev.immunol.21.120601.141040
- Storisteanu, D. M., Pocock, J. M., Cowburn, A. S., Juss, J. K., Nadesalingam, A., Nizet, V., et al. (2017). Evasion of neutrophil extracellular traps by respiratory pathogens. *Am. J. Respir. Cell Mol. Biol.* 56, 423–431. doi: 10.1165/rcmb.2016-0193PS
- Straat, R. T., Hicks, W., Barasa, N., Mahler, A., Khodoun, M., Kohl, J., et al. (2011). MHC class I-specific antibody binding to nonhematopoietic cells drives complement activation to induce transfusion-related acute lung injury in mice. *J. Exp. Med.* 208, 2525–2544. doi: 10.1084/jem.20110159
- Swanson, K., Dwyre, D. M., Krochmal, J., and Raife, T. J. (2006). Transfusion-related acute lung injury (TRALI): current clinical and pathophysiologic considerations. *Lung* 184, 177–185. doi: 10.1007/s00408-005-2578-8
- Tariket, S., Hamzeh-Cognasse, H., Laradi, S., Arthaud, C. A., Eyraud, M. A., Bourlet, T., et al. (2019). Evidence of CD40L/CD40 pathway involvement in experimental transfusion-related acute lung injury. *Sci. Rep.* 9:12536. doi: 10.1038/s41598-019-49040-0
- Taylor, M. D., van der Werf, N., and Maizels, R. M. (2012). T cells in helminth infection: the regulators and the regulated. *Trends Immunol.* 33, 181–189. doi: 10.1016/j.it.2012.01.001
- Thomas, G. M., Carbo, C., Curtis, B. R., Martinod, K., Mazo, I. B., Schatzberg, D., et al. (2012). Extracellular DNA traps are associated with the pathogenesis of TRALI in humans and mice. *Blood* 119, 6335–6343. doi: 10.1182/blood-2012-01-405183
- Thornby, K. A., Johnson, A., and Axtell, S. (2014). Dornase alfa for non-cystic fibrosis pediatric pulmonary Atelectasis. *Ann. Pharmacother.* 48, 1040–1049. doi: 10.1177/1060028014535199
- Tolle, I. B., and Standiford, T. J. (2013). Danger-associated molecular patterns (DAMPs) in acute lung injury. *J. Pathol.* 229, 145–156. doi: 10.1002/path.4124
- Tonkin, J., Temmerman, L., Sampson, R. D., Gallego-Colon, E., Barberi, L., Bilbao, D., et al. (2015). Monocyte/macrophage-derived IGF-1 orchestrates murine skeletal muscle regeneration and modulates autocrine polarization. *Mol. Ther.* 23, 1189–1200. doi: 10.1038/mt.2015.66
- Toy, P., Gajic, O., Bacchetti, P., Looney, M. R., Gropper, M. A., Hubmayr, R., et al. (2012). Transfusion-related acute lung injury: incidence and risk factors. *Blood* 119, 1757–1767. doi: 10.1182/blood-2011-08-370932
- Toy, P., Popovsky, M. A., Abraham, E., Ambruso, D. R., Holness, L. G., Kopko, P. M., et al. (2005). Transfusion-related acute lung injury: definition and review. *Crit. Care Med.* 33, 721–726. doi: 10.1097/01.ccm.0000159849.94750.51
- Tung, J.-P. (2019). Transfusion-related acute lung injury (Trali): pathogenesis and diagnosis. *Pathology* 51:S44.
- Tung, J. P., Fung, Y. L., Nataatmadja, M., Colebourne, K. I., Esmael, H. M., Wilson, K., et al. (2011). A novel in vivo ovine model of transfusion-related acute lung injury (TRALI). *Vox Sang.* 100, 219–230. doi: 10.1111/j.1423-0410.2010.01381.x
- Velavan, T. P., and Ojuronbe, O. (2011). Regulatory T cells and parasites. *J. Biomed. Biotechnol.* 2011:520940. doi: 10.1155/2011/520940
- Venet, F., Chung, C. S., Huang, X., Lomas-Neira, J., Chen, Y., and Ayala, A. (2009). Lymphocytes in the development of lung inflammation: a role for regulatory CD4+ T cells in indirect pulmonary lung injury. *J. Immunol.* 183, 3472–3480. doi: 10.4049/jimmunol.0804119
- Vidarsson, G., and van de Winkel, J. G. (1998). Fc receptor and complement receptor-mediated phagocytosis in host defence. *Curr. Opin. Infect. Dis.* 11, 271–278. doi: 10.1097/00001432-199806000-00002
- Vlaar, A. P., Hofstra, J. J., Kulik, W., van Lenthe, H., Nieuwland, R., Schultz, M. J., et al. (2010). Supernatant of stored platelets causes lung inflammation and coagulopathy in a novel in vivo transfusion model. *Blood* 116, 1360–1368. doi: 10.1182/blood-2009-10-248732
- Vlaar, A. P. J., Toy, P., Fung, M., Looney, M. R., Juffermans, N. P., Bux, J., et al. (2019). A consensus redefinition of transfusion-related acute lung injury. *Transfusion* 59, 2465–2476. doi: 10.1111/trf.15311
- Voelker, M. T., and Spieth, P. (2019). Blood transfusion associated lung injury. *J. Thorac. Dis.* 11, 3609–3615. doi: 10.21037/jtd.2019.06.61
- Wang, L., Wu, T., Yan, S., Wang, Y., An, J., Wu, C., et al. (2020). M1-polarized alveolar macrophages are crucial in a mouse model of transfusion-related acute lung injury. *Transfusion* 60, 303–316. doi: 10.1111/trf.15609
- Watanabe, K., and Petri, W. A. (2019). Learning from the research on amebiasis and gut microbiome: is stimulation by gut flora essential for effective neutrophil mediated protection from external pathogens? *Gut Microb.* 10, 100–104. doi: 10.1080/19490976.2018.1479626
- Waugh, D. J., and Wilson, C. (2008). The interleukin-8 pathway in cancer. *Clin. Cancer Res.* 14, 6735–6741. doi: 10.1158/1078-0432.CCR-07-4843
- Wen, K., Li, G., Yang, X., Bui, T., Bai, M., Liu, F., et al. (2012). CD4+ CD25-FoxP3+ regulatory cells are the predominant responding regulatory T cells after human rotavirus infection or vaccination in gnotobiotic pigs. *Immunology* 137, 160–171. doi: 10.1111/j.1365-2567.2012.03617.x
- Wong, S. L., Demers, M., Martinod, K., Gallant, M., Wang, Y., Goldfine, A. B., et al. (2015). Diabetes primes neutrophils to undergo NETosis, which impairs wound healing. *Nat. Med.* 21, 815–819. doi: 10.1038/nm.3887
- Wyman, T. H., Bjornsen, A. J., Elzi, D. J., Smith, C. W., England, K. M., Kelher, M., et al. (2002). A two-insult in vitro model of PMN-mediated pulmonary endothelial damage: requirements for adherence and chemokine release. *Am. J. Physiol. Cell Physiol.* 283, C1592–C1603. doi: 10.1152/ajpcell.00540.2001
- Xie, R. F., Hu, P., Wang, Z. C., Yang, J., Yang, Y. M., Gao, L., et al. (2015). Platelet-derived microparticles induce polymorphonuclear leukocyte-mediated damage of human pulmonary microvascular endothelial cells. *Transfusion* 55, 1051–1057. doi: 10.1111/trf.12952
- Xu, A., Liu, Y., Chen, W., Wang, J., Xue, Y., Huang, F., et al. (2016). TGF-beta-induced regulatory T cells directly suppress B cell responses through a noncytotoxic mechanism. *J. Immunol.* 196, 3631–3641. doi: 10.4049/jimmunol.1501740
- Yildiz, C., Palaniyar, N., Otulakowski, G., Khan, M. A., Post, M., Kuebler, W. M., et al. (2015). Mechanical ventilation induces neutrophil extracellular trap formation. *Anesthesiology* 122, 864–875. doi: 10.1097/ALN.0000000000000605
- Zeeuw van der Laan, E. A. N., van der Velden, S., Bentlage, A. E. H., Larsen, M. D., van Osch, T. L. J., Mok, J. Y., et al. (2020a). Biological and structural characterization of murine TRALI antibody reveals increased Fc-mediated complement activation. *Blood Adv.* 4, 3875–3885. doi: 10.1182/bloodadvances.2020002291
- Zeeuw van der Laan, E. A. N., van der Velden, S., Porcelijn, L., Semple, J. W., van der Schoot, C. E., and Kapur, R. (2020b). Update on the pathophysiology of transfusion-related acute lung injury. *Curr. Opin. Hematol.* 27, 386–391. doi: 10.1097/MOH.0000000000000607
- Zhang, M. Z., Yao, B., Yang, S., Jiang, L., Wang, S., Fan, X., et al. (2012). CSF-1 signaling mediates recovery from acute kidney injury. *J. Clin. Invest.* 122, 4519–4532. doi: 10.1172/JCI60363
- Ziegler, T., Rausch, S., Steinfeld, S., Klotz, C., Hepworth, M. R., Kuhl, A. A., et al. (2015). A novel regulatory macrophage induced by a helminth molecule instructs IL-10 in CD4+ T cells and protects against mucosal inflammation. *J. Immunol.* 194, 1555–1564. doi: 10.4049/jimmunol.1401217

**Conflict of Interest:** The authors declare that the research was conducted in the absence of any commercial or financial relationships that could be construed as a potential conflict of interest.

Copyright © 2021 Guo and Ma. This is an open-access article distributed under the terms of the Creative Commons Attribution License (CC BY). The use, distribution or reproduction in other forums is permitted, provided the original author(s) and the copyright owner(s) are credited and that the original publication in this journal is cited, in accordance with accepted academic practice. No use, distribution or reproduction is permitted which does not comply with these terms.





# Management and Prognosis of Interstitial Lung Disease With Lung Cancer (ILD-LC): A Real-World Cohort From Three Medical Centers in China

Xie Xiaohong<sup>1†</sup>, Wang Liqiang<sup>1†</sup>, Li Na<sup>2†</sup>, Lin Xinqing<sup>1</sup>, Qin Yinyin<sup>1</sup>, Liu Ming<sup>1</sup>, Ouyang Ming<sup>1</sup>, Han Qian<sup>1</sup>, Luo Qun<sup>1</sup>, Li Shiyue<sup>1</sup>, Li Chunyan<sup>3</sup>, Wang Xiaoqian<sup>3</sup>, Yang Shuanying<sup>2</sup>, Huang Wei<sup>2</sup>, Liu Mei<sup>2</sup>, Wang Ping<sup>4\*</sup> and Zhou Chengzhi<sup>1\*</sup>

## OPEN ACCESS

### Edited by:

Dianhua Jiang,  
Cedars Sinai Medical Center,  
United States

### Reviewed by:

Liangliang Ren,  
Jiangmen Central Hospital, China  
Dinesh Kumar,  
Centre of Bio-Medical Research  
(CBMR), India

### \*Correspondence:

Wang Ping  
taoybs\_wp@163.com  
Zhou Chengzhi  
zhouchengzhi@gird.cn;  
doctorcz@163.com

<sup>†</sup>These authors have contributed  
equally to this work and share first  
authorship

### Specialty section:

This article was submitted to  
Molecular Diagnostics  
and Therapeutics,  
a section of the journal  
Frontiers in Molecular Biosciences

**Received:** 29 January 2021

**Accepted:** 08 March 2021

**Published:** 31 March 2021

### Citation:

Xiaohong X, Liqiang W, Na L,  
Xinqing L, Yinyin Q, Ming L, Ming O,  
Qian H, Qun L, Shiyue L, Chunyan L,  
Xiaoqian W, Shuanying Y, Wei H,  
Mei L, Ping W and Chengzhi Z (2021)  
Management and Prognosis  
of Interstitial Lung Disease With Lung  
Cancer (ILD-LC): A Real-World Cohort  
From Three Medical Centers in China.  
Front. Mol. Biosci. 8:660800.  
doi: 10.3389/fmolb.2021.660800

<sup>1</sup> State Key Laboratory of Respiratory Disease, National Clinical Research Center of Respiratory Disease, The First Affiliated Hospital of Guangzhou Medical University, Guangzhou Institute of the Respiratory Health, Guangzhou Medical University, Guangzhou, China, <sup>2</sup> Department of Respiratory and Critical Care Medicine, The Second Affiliated Hospital of Xi'an Jiaotong University, Xi'an, China, <sup>3</sup> Department of Respiratory and Critical Care Medicine, The First Medical Center of PLA General Hospital, Beijing, China, <sup>4</sup> Department of Respiratory and Critical Care Medicine, The Eighth Medical Center of PLA General Hospital, Beijing, China

**Background and Objective:** Interstitial lung disease with lung cancer (ILD-LC) is rare and its management has not been fully described. This study aimed to investigate the management and prognosis of ILD-LC patients in China.

**Methods:** The present analysis is a retrospective real-world cohort study. Clinical data of ILD-LC patients were obtained from 3 hospitals in China. The overall survival (OS) of patients was analyzed. Univariate and multivariate regression analyses were performed.

**Results:** One hundred eighty-four ILD-LC patients included were biased toward male (85.3%), smokers (75.5%), idiopathic pulmonary fibrosis (IPF) (58.2%) patients with comorbidities (67.9%) and ECOG-PS score of 1 (65.2%). Most patients were advanced peripheral non-small cell lung cancer. The initial anti-cancer regimen for ILD-LC is mainly chemotherapy, and patients with early-stage LC prefer surgery. In the anti-cancer cohort, the number of ILD-LC patients who underwent the 2nd and 3rd or more anti-cancer regimens were 78 (55.7%) and 32 (22.8%), respectively. In the non-anticancer cohort, the median OS was 3.5 months. In the early-stage cohort, the median OS was 14.2 months in the systematic therapy group; however, the median OS was not reached in the surgery group. In the advanced-stage cohort with systematic therapy, the median OS was 7.2 months. Interstitial pneumonia (IIP) and anti-angiogenesis were associated with OS in the univariate analysis, whereas anti-angiogenesis was an independent protective factor for advanced LC with ILD.

**Conclusion:** Patients with ILD-LC have very poor prognosis. Appropriate anti-tumor treatment can prolong the survival time of patients who can tolerate it. Targeted therapy and immunotherapy are alternative treatments for LC patients with mild ILD. For ILD patients with advanced LC, antiangiogenic regimens significantly improve the prognosis of the disease.

**Keywords:** interstitial lung disease, lung cancer, ILD-LC, prognosis, anti-angiogenesis treatment



## INTRODUCTION

Interstitial lung disease (ILD), especially idiopathic pulmonary fibrosis (IPF) and connective tissue disease (CTD)-ILD, is a risk factor for lung cancer. The incidence of lung cancer is 4.4–48% in IPF patients, while 5.5–9.0% in CTD-ILD patients (Raghu et al., 2004; Tomassetti et al., 2015; Enomoto et al., 2016; Jung et al., 2018; Watanabe et al., 2018). Risk factors for developing ILD with lung cancer (ILD-LC) include male sex, older age, smoking, combined pulmonary fibrosis and emphysema (CPFE) (Usui et al., 2011; Watanabe et al., 2018). In addition, CTD-ILD without immunosuppressive therapy may be a risk factor for cancer (Watanabe et al., 2018).

Recently, the clinical profile of patients with ILD-LC was described. The ILD-LC population comprises individuals who are male, elderly, smokers, have IPF and are at advanced stage of LC (Minegishi et al., 2009). High-resolution computed tomography (HRCT) shows that the tumors are mainly in peripheral areas around ILD (Minegishi et al., 2009; Yoo et al., 2019). Squamous cell carcinoma was considered to be the most common pathological type of ILD-LC (Tomassetti et al., 2015; Watanabe et al., 2018), but there was an increasing trend for adenocarcinoma and small cell carcinoma nowadays (Saijo et al., 2017).

The IPF guidelines recommend that IPF be considered in treatment decisions for LC in IPF-LC patients (Cottin et al., 2017; Homma et al., 2018). However, the LC guidelines have not yet been established for the treatment of these patients. Surgery is recommended for early-stage lung cancer patients with ILD (Homma et al., 2018); however, there is still controversy over whether active anti-tumor strategies are suitable for inoperable ILD-LC patients with pulmonary dysfunction and poor PS score. The acute exacerbation (AE) of ILD (AE-ILD) is the main reason for the difficulty in treating patients with anti-cancer therapy (Minegishi et al., 2011a,b; Sekine et al., 2016; Hanibuchi et al., 2018; Asahina et al., 2019; Fujimoto et al., 2019; Kenmotsu et al., 2019). Although there are a few prospective studies involving chemotherapy and immunotherapy (Minegishi et al., 2009; Naccache et al., 2018), the current researches on inoperable ILD-LC focus on describing the treatments and AE-ILD retrospectively in a small population. Reducing AE-ILD is urgent, and several studies have shown that anti-angiogenic drugs such as nintedanib and bevacizumab can reduce the risk of chemotherapy-related AE-ILD (Richeldi et al., 2014; Hamada et al., 2019). However, there are more anti-angiogenic drugs, such as apatinib, anlotinib and recombinant human endostatin, etc., which have an unknown effect in reducing AE-ILD.

To date, there is no large-scale research on the treatment and prognosis of ILD-LC in China. Besides, the treatment of lung cancer has undergone tremendous changes, so the management of ILD-LC needs to be further described. To better understand the current management and prognosis of ILD-LC in China, we conducted a retrospective study to provide a feasible reference for the follow-up treatment for ILD-LC in real clinical practice.

## PATIENTS AND METHODS

### Patients and Diagnostic Criteria

A systematic search was conducted in the databases of three medical centers, The First Affiliated Hospital of Guangzhou Medical University, Chinese People's Liberation Army General Hospital, and The Second Affiliated Hospital of Xi'an Jiaotong University, located in Southeast, North, and Northwest China. All included cases presented with ILD on chest HRCT scan and were histologically diagnosed with LC from January 1, 2009 to October 1, 2019. Those with missing clinical data, other malignant tumors, drug-related ILD, and cancerous lymphangitis were excluded.

Patients eligible were grouped into idiopathic interstitial pneumonia (IIP) and CTD-ILD groups based on HRCT findings and clinical courses. We classify IIP into two groups: the IPF pattern and non-IPF groups. The IPF pattern group consisted of patients diagnosed as IPF histologically or clinically according to the American Thoracic Society/European Respiratory Society (ATS/ERS) criteria. IPF diagnosed without pathology is mainly based on clinical manifestations and typical chest CT findings: basal and peripheral predominant reticular abnormalities with traction bronchiectasis and honeycombing (ATS and ERS, 2002).

### Data Collection

Data such as demographic characteristics, as well as information on smoking history, comorbidities, the subtype of ILD, pulmonary function test, time to diagnose LC, histology according to World Health Organization (WHO) tumor classification, stage group using the 8th edition of the TNM classification, and regimens for anti-cancer, was obtained retrospectively from the medical record. Two independent pulmonologists evaluated the chest HRCT images taken during the diagnosis of ILD-LC that met the criteria. The imaging evaluation mainly distinguishes the IPF pattern which is mentioned above. The location of the mass is recorded as either peripheral or central. The peripheral location is defined as <3 cm from the pleura. The disagreement between the 2 reviewers has been resolved by consensus.

### Statistical Analysis

SPSS software version 24 (IBM) was used for statistical analysis and Graphpad Prism version 8 for graphing. Patient demographics were compared using the unpaired t-test for continuous variables and Pearson's  $\chi^2$  test for categorical variables. Overall survival (OS) was defined as the time from the date of diagnosis of primary lung cancer to the date of death from any cause. Patients who were alive or had been lost to follow-up at the time of analysis were considered censored. Kaplan-Meier was used for survival analysis and the log-rank test was used to assess differences between groups. Cox's proportional hazards regression analysis was used to identify significant variables that affect the survival of advanced ILD-LC patients and to estimate hazard ratios

(HR) and 95% confidence intervals (CI) for predictors of survival. All tests were two-tailed, and  $p < 0.05$  was considered statistically significant.

## RESULTS

### Patient Characteristics

A total of 236 patients with ILD-LC were identified, and 184 were eventually enrolled in the study (Figure 1). The baseline characteristics of all patients, the anti-cancer group and the non-anticancer group are shown in Table 1. Overall, at the time of LC diagnosis, the majority of the patients were male (85.3%) and smokers (75.5%) with a median age of 68 years (range, 44–90 years). The main subtype of ILD was IPF (58.2%). Most patients were stage III/IV peripheral NSCLC with comorbidities (67.9%) and ECOG-PS scores of 1 (65.2%). There were differences in age, ECOG-PS, and smoking status between the anti-cancer and non-anticancer groups. Patients in the non-anticancer group had older age and worse ECOG-PS scores.

### The Distribution of Various Anti-cancer Regimens at Different Treatment Stages in ILD-LC

Most patients with ILD-LC could not undergo multiple courses of anti-cancer regimens (Table 2). Compared with the initial treatment, the number of patients underwent the 2nd and 3rd or more anti-cancer regimens were 78 (55.7%) and 32 (22.8%), respectively. Chemotherapy accounted for the largest proportion of all treatment stages. In addition to chemotherapy, surgery (17.9%) and radiotherapy (28.2%) were the most common in the first-stage treatment and the second-stage

treatment, respectively. Besides, anti-angiogenic therapy (25.0%) is preferred in the third and above stage therapies.

### The Choice of Anti-cancer Regimens Based on Histological Type, Clinical-Stage, the Subtype of ILD, and ECOG-PS Score

The anti-cancer regimen for ILD-LC is similar to that for lung cancer alone (Table 3). Patients who underwent surgery were early-stage non-small cell lung cancer patients with good ECOG-PS scores and non-IPF can be found for a higher proportion of these patients. Patients with good ECOG-PS score, small cell lung cancer, advanced stage lung cancer, and non-IPF are more inclined to choose chemotherapy. Radiotherapy is mainly used for stage III/IV squamous cell carcinoma and small cell carcinoma with an ECOG-PS score of 1, and IPF accounts for more. Targeted therapy is mainly used for IIP patients with an ECOG-PS score of 2–3 and stage III/IV adenocarcinoma. Immune checkpoint inhibitors have also been used in our ILD-LC patients, who are characterized by advanced IIP-LC with better ECOG-PS scores.

### Survival Data and Prognostic Factors

Patients were followed-up until May 2020. Thirty-four of the one hundred eighty-four patients were lost to follow-up and 23 were still alive. The median follow-up time was 27 months. In the overall population, the median OS for anti-cancer cohort and non-anticancer cohort were 11.1 vs. 3.5 (HR 0.3014, 95%CI: 0.1771 to 0.5130). In the non-anticancer cohort, the 6-month and 1-year OS rates were 25 and 6.8%, respectively. Furthermore, we divided the patients in the anti-cancer cohort into two groups: the early-stage (stage I–IIIA) group ( $n = 48$ ) and the advanced stage (stage IIIB–IV) cohort ( $n = 92$ ). In the early-stage group, 25 patients received surgery and 23 received systematic therapy. The advanced stage group all received systematic therapy. Among the surgical patients, 7 cases died, 13 cases survived, and 5 cases were lost to follow-up. The median OS was not reached for patients who underwent surgery, and the 1, 2, and 3-year OS rates were 80.0, 68.0, and 36.0%, respectively. The median OS for the early-stage group that underwent systematic therapy was 14.2 m, the 1 and 2-year OS rate was 47.8%, and 17.4%, respectively. The median OS of the advanced-stage cohort that underwent systematic therapy was 7.2 m, and the 1-year OS rate was 20.7% (Figure 2). Sixteen advanced-stage LC patients were receiving targeted therapy with a median OS of 6.5 months, while 9 of them with EGFR mutations receiving targeted therapy in the first stage have a median OS of 16.2 months. The median OS of 6 patients with advanced-stage LC receiving immunotherapy was 8.8 months.

Analysis of prognostic factors was conducted to identify significant variables that affect the OS of the advanced stage group (Table 4). Gender, age, smoking status, anatomical type, histological type, stage, the subtype of ILD, the sequence of tumor occurrence, and anti-cancer regimens were included in the study. Univariate analysis revealed that patients with CTD-ILD and antiangiogenic therapy had a significantly better prognosis.

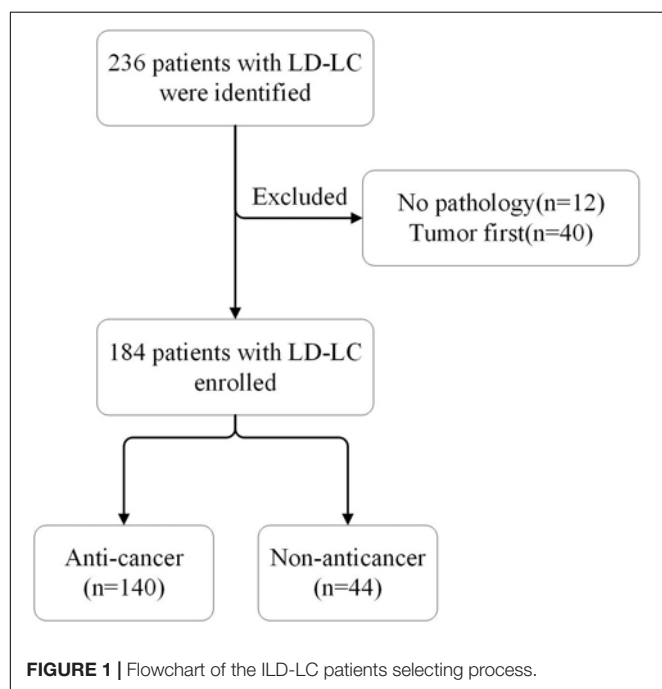


**TABLE 1 |** Characteristics of anti-cancer and non-anticancer patients with interstitial lung disease and lung cancer (ILD-LC).

Characteristics	All patients (N = 184)	Anti-cancer (N = 140)	Non-anticancer (N = 44)	p-value
Gender, male, n (%)	157 (85.3)	121 (86.4)	36 (81.8)	0.451
Age, median (range), year	68.0 (44–90)	66.0 (44–90)	70.5 (46–89)	0.005
ECOG-PS				0.001
1	120 (65.2)	99 (70.7)	21 (47.7)	
2	57 (31.0)	39 (27.9)	18 (40.9)	
3	7 (3.8)	2 (1.4)	5 (11.4)	
Smoking status, current or former, n (%)	139 (75.5)	111 (79.2)	28 (63.6)	0.035
Smoking index	885 ± 514	881 ± 500	901 ± 577	0.850
Comorbidities, yes, n (%)	125(67.9)	93 (66.4)	32 (72.7)	0.435
Histology				0.36
Squamous cell carcinoma	58 (31.5)	42 (30.0)	16 (36.4)	
Adenocarcinoma	69 (37.5)	50 (35.7)	19 (43.2)	
Other NSCLC	17 (9.2)	15 (10.7)	2 (4.5)	
Small cell carcinoma	40 (21.7)	33 (23.6)	7 (15.9)	
Clinical stage				0.536
I	19 (10.3)	17 (12.1)	2 (4.5)	
II	12 (6.5)	9 (6.4)	3 (6.8)	
III	52 (28.3)	38 (27.1)	14 (31.8)	
IV	101 (54.9)	76 (54.3)	25 (56.8)	
Anatomical type				0.776
Peripheral	145 (78.8)	111 (79.3)	34 (77.3)	
Central	39 (21.2)	29 (20.7)	10 (22.7)	
Subtype of ILD				0.107
IPF	107 (58.2)	78 (55.7)	29 (65.9)	
non-IPF	56 (30.4)	48 (34.3)	8 (18.2)	
CTD-ILD	21 (11.4)	14 (10.0)	7 (15.9)	
Time to diagnose LC				0.781
After ILD	87 (47.3)	67 (47.9)	20 (45.5)	
Simultaneous	97(52.7)	73 (52.1)	24 (54.5)	
Disorder of ventilation function (n)	68	47	21	0.071
Normal	15 (22.1)	14 (29.8)	1 (4.8)	
Restrictive	32 (47.1)	20 (42.6)	12 (57.1)	
Mixed	21 (30.9)	13 (27.6)	8 (38.1)	
Degree of ventilation function (n)	68	47	21	0.521
Normal or Mild	42 (61.8)	31 (66.0)	11 (52.4)	
Moderate	17 (25.0)	10 (21.3)	7 (33.3)	
Severe	9 (13.2)	6 (12.8)	3 (14.3)	
Degree of diffusion capacity (n)	61	43	18	0.077
Normal or mild	24 (39.3)	20 (46.5)	4 (22.2)	
Moderate and severe	37 (60.7)	23 (53.5)	14 (77.8)	

ECOG-PS, Eastern Cooperative Oncology Group-Performance Status; ILD, interstitial lung disease; IPF, idiopathic pulmonary fibrosis; CTD, connective tissue disease; NSCLC, non-small cell lung cancer; LC, lung cancer. The p-values refer to comparisons between the anti-cancer and non-anti-cancer groups.

Anti-angiogenic therapy was the independent factor in the Cox regression model. Patients with anti-angiogenic therapy have significantly longer OS compared to those without anti-angiogenesis, with a median OS of 9.3 vs. 6.1 m (HR: 0.5002, 95% CI: 0.2866 to 0.8731,  $p = 0.0148$ ).

## DISCUSSION

The current descriptions of the treatment and prognosis of ILD-LC are mainly derived from retrospective studies involving

a small population, which are insufficient and limited. Here, we conducted a multicenter retrospective study involving 184 ILD-LC patients, with the aim of understanding the clinical profile, management, and prognosis of ILD-LC patients in China. Consistent with previous studies (Minegishi et al., 2009; Tomassetti et al., 2015), patients with ILD-LC in our cohort are mainly elderly, smokers, male. They also had IIP, peripheral NSCLC, poor ECOG-PS, and comorbidities. Half of the patients were diagnosed with lung cancer and ILD at the same time, and most of them had mild to moderate restrictive ventilatory dysfunction and moderate to severe diffuse dysfunction.

**TABLE 2 |** Initial and follow-up anti-cancer regimens for patients with ILD-LC.

Stage of treatment <sup>#</sup>	Total	1st- (n, % <sup>&amp;</sup> )	2nd- (n, %)	≥3rd-or more (n, %)
N	140	140 (100.0)	78 (55.7)	32 (22.8)
Surgery	25	25 (17.9)	0 (0)	0 (0)
Chemotherapy	109	89 (63.6)	45 (57.7)	23 (71.9)
Interventional therapy	6	2 (1.4)	3 (3.8)	1 (3.1)
Radiotherapy	35	10 (7.1)	22 (28.2)	3 (9.4)
Anti-angiogenic therapy <sup>**</sup>	29	13 (9.3)	10 (12.8)	8 (25.0)
Targeted therapy <sup>‡</sup>	20	12 (8.6)	8 (10.3)	3 (9.4)
Immunotherapy	8	5 (3.6)	3 (3.8)	1 (3.1)
Others <sup>‡</sup>	7	7 (5.0)	0 (0)	0 (0)

<sup>#</sup>Patients can receive more than one anti-cancer regimens at every stage of treatment.

<sup>&</sup>The proportion of a regimen in the treatment stage to total events of the regimen.

<sup>\*\*</sup>Anti-angiogenic agents include 11 cases of bevacizumab, 3 cases of apatinib, 5 cases of anlotinib, 9 cases of nintedanib, 1 case of recombinant human endostatin.

<sup>‡</sup>There were 11 patients with EGFR mutations, 10 in the first stage and 1 in the second stage. Two patients in the first stage received EGFR-TKIs without confirming the EGFR status. The remaining patients in the second- and above stage were at an unknown EGFR status for lacking records.

<sup>‡</sup>Oral anti-cancer drugs.

The management of ILD-LC is important and necessary but has not been fully described. The published articles hardly discuss the differences in choosing anti-cancer or not in patients with ILD-LC. In our study, 44 (23.9%) of 184 patients chose the best supportive care (BSC) without anti-cancer regimens. We found that older age, worse ECOG-PS scores, and poor lung function may be reasons for patients choosing the BSC. Furthermore, the

anti-cancer regimens in our cohort are similar to that of patients with lung cancer only. However, the challenge in clinical practice is that AE induced by anti-cancer regimens may interrupt the treatment of LC and even cause the death of patients (Minegishi et al., 2009; Amundson et al., 2019). We did not summarize the AE-ILD in most patients for the lack of clinical data. Therefore, the number of patients who underwent anti-cancer treatment at different stages was used to reflect the tolerance of these patients to anti-cancer treatment. There were 55.7% of patients administered second- and above stage treatments in our study, while 36.3% (32 of 88 in anticancer) in Minegishi et al. (2009). However, only 22.8% of ILD-LC patients underwent a third or more anti-cancer treatment in the anti-cancer group. All this means that many patients have lost the opportunity to receive more anti-cancer treatments because of ILD.

Appropriate anti-cancer measures for ILD-LC are reasonable, which makes patients live longer. Surgery is important and recommended for the management of early-stage LC with ILD due to the high survival rate (Omori et al., 2015; Sato et al., 2015; Homma et al., 2018). We also concluded that the 3-year OS rates of surgery cohort were 36.0%. However, postoperative AE-ILD is a serious complication for patients with surgery. There was one patient who experienced postoperative AE-ILD and died within 2 months in our study. Sato et al. (2014) showed that 9.3% of 1,763 patients suffered postoperative AE-ILD with a mortality rate of 43.9%. Minegishi et al. (2009) reported that 8 of 35 patients who underwent surgery experienced postoperative AE-ILD, and 3 died of AE. Surgical procedures, male sex, history of exacerbation, preoperative steroid use, serum sialylated carbohydrate antigen KL-6 levels, preoperative percent vital capacity plus serum LDH

**TABLE 3 |** Treatment options for the anti-cancer cohort of ILD-LC stratified according to histological type, clinical stage, subtype of ILD, and ECOG-PS score.

	N	Surgery <sup>&amp;</sup>	Chemotherapy	Interventional therapy	Radiotherapy	Anti-angiogenic therapy	Targeted therapy	Immunotherapy	Others
<b>Histology</b>									
Squamous cell carcinoma <sup>#</sup>	42	10 (23.8)	31 (73.8)	3 (7.1)	16 (38.1)	6 (14.3)	2 (4.7)	4 (9.5)	5 (11.9)
Adenocarcinoma	50	8 (16.0)	36 (72.0)	0 (0)	5 (10.0)	14 (28.0)	15 (30.0)	1 (2.0)	1 (2.0)
Other NSCLC	15	4 (26.7)	11 (73.3)	1 (6.7)	2 (13.3)	3 (20.0)	3 (20.0)	1 (6.7)	1 (6.7)
Small cell carcinoma	33	3 (9.1)	31 (93.9)	2 (6.1)	12 (36.4)	6 (18.2)	0 (0)	2 (6.1)	0 (0)
<b>Clinical stage</b>									
I	17	14 (82.4)	10 (58.8)	0 (0)	5 (29.4)	3 (17.6)	1 (5.9)	1 (5.9)	2 (11.8)
II	9	5 (55.6)	8 (88.9)	0 (0)	2 (22.2)	1 (11.1)	0 (0)	0 (0)	0 (0)
III	38	6 (15.8)	30 (78.9)	1 (2.6)	13 (34.2)	8 (21.1)	4 (10.5)	2 (5.3)	3 (7.9)
IV	76	0 (0)	61 (80.3)	5 (6.6)	15 (19.7)	17 (22.4)	15 (19.7)	5 (6.6)	2 (2.6)
<b>ILD classification</b>									
IPF	78	12 (15.4)	60 (76.9)	3 (3.8)	15 (19.2)	17 (21.8)	13 (16.7)	4 (5.1)	6 (7.7)
non-IPF	48	11 (22.9)	40 (83.3)	3 (6.3)	16 (33.3)	6 (12.5)	6 (12.5)	4 (8.3)	1 (2.1)
CTD-ILD	14	2 (14.3)	9 (64.3)	0 (0)	4 (28.6)	6 (42.9)	1 (7.1)	0 (0)	0 (0)
<b>ECOG-PS</b>									
1	99	23 (23.2)	81 (81.8)	2 (2.0)	35 (35.3)	21 (21.2)	8 (8.1)	7 (7.1)	6 (6.1)
2	39	2 (5.1)	27 (69.2)	3 (7.7)	0 (0)	7 (17.9)	12 (30.8)	1 (2.6)	1 (2.6)
3	2	0 (0)	0 (0)	1 (50)	0 (0)	1 (50)	0 (0)	0 (0)	0 (0)

ECOG-PS, Eastern Cooperative Oncology Group-Performance Status; ILD, interstitial lung disease; IPF, idiopathic pulmonary fibrosis; CTD, connective tissue disease; NSCLC, non-small cell lung cancer.

<sup>#</sup>Patients in each stratification may receive one or more treatments.

<sup>&</sup>The proportion of a regimen in each stratification to the total number of the stratification.



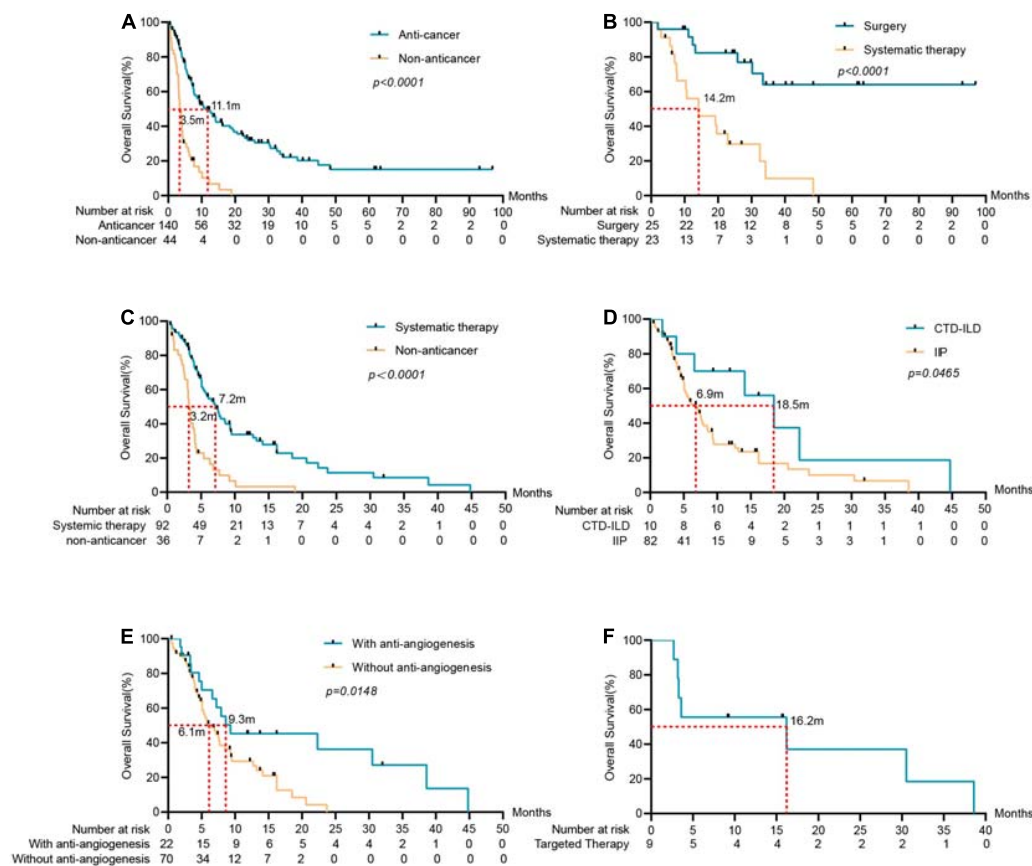


**FIGURE 2 |** Survival analysis of ILD-LC patients in different groups. **(A)** Anti-cancer group ( $n = 140$ ) vs. non-anticancer group ( $n = 44$ ), the mOS of the anti-cancer group was significantly longer than that of the non-anticancer group. **(B)** Surgery group ( $n = 25$ ) and systematic therapy group ( $n = 23$ ) in early-stage LC with ILD. **(C)** Systematic therapy group ( $n = 92$ ) vs. non-anticancer group in advanced stage LC with ILD. **(D)** For patients in advanced stage LC with ILD, OS was associated with the subtype of ILD ( $p = 0.0465$ ). **(E)** OS was associated with anti-angiogenesis ( $p = 0.0148$ ). **(F)** Patients received targeted therapy in advanced stage LC with ILD and the mOS was 16.2 months.

values were risk factors for postoperative AE-ILD after in patients with ILD (Shintani et al., 2010; Sato et al., 2014).

Systematic therapy for inoperable or recurrent LC with ILD is still controversial due to the AE-ILD. As mentioned above, most patients fail to receive multi-stage anti-cancer treatments in our study. However, consistent with the published researches (Kawahara et al., 2019), the present study showed that patients with advanced-stage LC benefit from systematic therapy in OS compared to those without anti-cancer treatment. The options of systematic treatment are diverse, and there is no optimal treatment for ILD-LC. Consistent with the previous study, chemotherapy was the most commonly chosen in our patients. However, the chemotherapy regimen for less AE is still inconclusive and chemotherapy-related exacerbation of ILD was between 9 and 42.8% (Watanabe et al., 2013; Kenmotsu et al., 2015). A series of prospective studies conducted in Japan showed that nab-paclitaxel plus carboplatin in NSCLC and etoposide plus carboplatin in SCLC were safe for patients with mild or moderate ILD (Minegishi et al., 2011a,b; Kenmotsu et al., 2019).

Radiotherapy plays a critical role in unresectable SCLC and NSCLC but should be used with caution in ILD-LC due to severe

radiation pneumonia or AE-ILD (Yamaguchi et al., 2013; Glick et al., 2018). There were 35 patients with mild ILD administered with radiotherapy in our study, and 2 of them suffered grade 3 radiation pneumonia and AE-ILD respectively. The patient with radiation pneumonia received nintedanib monotherapy for more than a year and is still alive. While the patient with AE-ILD received BSC and died with an OS of 8 months. Radiotherapy-related grade 2–5 pneumonitis of patients with ILD-LC was 15.8% (Yamaguchi et al., 2013). Hagiwara et al. (2020) conducted a nationwide survey of radiotherapy in Japan for ILD-LC and found that 5 (7.5%) of 67 patients suffered AE-ILD and 1 died of radiation-induced AE. Kobayashi et al. (2018) revealed that 17 (46%) of 37 patients treated with chemoradiotherapy developed grade 3 and above AE-ILD within 1 year after the last irradiation. Therefore, radiotherapy should be applied cautiously considering the serious side effects.

For patients with driver genes and mutations, tyrosine kinase inhibitors (TKIs) are more effective than traditional chemotherapy. However, the risk of TKI-induced ILD and AE-ILD remind us that TKIs should be applied cautiously in ILD-LC (Shi et al., 2014; Shah, 2016; Gemma et al., 2019). In our cohort,

**TABLE 4 |** Clinical characteristics, univariate and multivariate analysis of 92 advanced lung cancer with ILD for overall survival.

Group	No. patients (%)	Overall survival	
		Univariate analysis: P	Multivariate analysis: P
Gender (male, %)	77 (83.7)	0.058	0.065
Age ( $\geq 65$ , %)	58 (63.0)	0.071	0.163
Smoking status (yes, %)	72 (78.3)	0.47	*
Comorbidities (yes, %)	64 (69.6)	0.103	0.113
Histology (NSCLC, %)	68 (73.9)	0.647	*
Clinical stage (IV, %)	72 (78.3)	0.323	*
Anatomical type (peripheral, %)	70 (76.1)	0.659	*
ECOG-PS (1, %)	62 (67.4)	0.551	*
Subtype of ILD (IIP, %)	82 (89.1)	<b>0.046</b>	0.138
Time to diagnose LC (simultaneous, %)	52 (56.5)	0.17	0.122
Interventional therapy (yes, %)	3 (3.3)	*	*
Radiotherapy (yes, %)	21 (22.8)	0.16	0.133
Chemotherapy (yes, %)	74 (80.4)	0.659	*
Anti-angiogenic therapy (yes, %)	22 (23.9)	<b>0.015</b>	<b>0.011</b>
Targeted therapy (yes, %)	16 (17.4)	0.736	*
Immunotherapy (yes, %)	6 (6.5)	*	*
Others (yes, %)	5 (5.4)	*	*

ECOG-PS, Eastern Cooperative Oncology Group-Performance Status; ILD, interstitial lung disease; CTD, connective tissue disease; NSCLC, non-small cell lung cancer; IIP, idiopathic interstitial pneumonia, including idiopathic pulmonary fibrosis (IPF) and non-IPF.

\*Analysis could not be done.

The bold values means statistically different.

there were 10 patients confirmed with EGFR mutations receiving EGFR-TKIs in first-line treatment. The median OS of the 9 patients with advanced-stage LC was 16.2 months, and 4 (44.4%) of them experienced more than one stage treatments. Besides, preliminary evidence suggests that TKIs can be continued after TKI-induced ILD in the case of steroid coverage and/or dose reduction (Shah, 2016). Considering the long-term survival of ILD-LC patients with driver genes and mutations, TKIs should be administered at the first stage treatments.

The application of immune checkpoint inhibitors (ICIs) is a milestone in lung cancer, and the occurrence of immune-related adverse events (irAEs) such as checkpoint inhibitor-related pneumonitis (CIPs) is inevitable (Jain et al., 2018). The high mortality rate was observed in severe grade CIPs in NSCLC (Suresh et al., 2018; Tone et al., 2019), and pre-existing ILD is a risk factor for developing CIPs (Kanai et al., 2018). Therefore, CIPs maybe a serious threat to patients with ILD-LC though there was no report of AE-ILD induced by ICIs. However, compared with TKIs-related pneumonia, CIPs have a higher response rate to corticosteroid therapy and a lower mortality rate (Beom et al., 2016; Kato et al., 2017). For inoperable patients with mild IIP receiving nivolumab, a pilot study conducted by Fujimoto et al. (2017, 2019) showed no AE-ILD, while a phase II showed that 2 of 18 patients developed grade 2 pneumonitis, which could be treated using corticosteroid therapy. There was no AE-ILD or CIP observed in our advanced stage LC patients receiving

immunotherapy with a median OS of 8.6 months, while 1 of them died of tumor progression within 1 month. This suggests that immunotherapy may be a good choice for these patients, but more clinical studies are needed to confirm it.

For advanced LC with ILD, the most appropriate anti-cancer regimens should bring the fewest AEs rather than the best anti-tumor effect. However, it is still necessary to look for prognostic factors that affect OS. We conducted a prognosis analysis in the advanced anti-cancer cohort and found the IIP was associated with poor prognosis, while anti-angiogenic therapy was an independent protective factor that improves the prognosis of advanced LC with ILD. There was in line with expectations that IIP is a prognostic risk factor of ILD-LC, because IIP, especially IPF, has a worse prognosis compared to CTD-ILD (Lim et al., 2019). Vascular endothelial growth factor (VEGF), a potent stimulator of vascular permeability and angiogenesis, plays an important role in lung diseases, including injury, fibrosis and cancer, as well as AE of IPF (Simler et al., 2004; Weis and Cheresch, 2005; McKeown et al., 2009). Nintedanib, an anti-angiogenic agent targeting VEGF, has been proven to have anti-cancer and anti-pulmonary fibrosis effects and reduce AE-ILD in patients with IPF (Reck et al., 2014; Richeldi et al., 2014; Hilberg et al., 2018; Fabre and Nicholson, 2020). Besides, nintedanib and bevacizumab have been shown to reduce the risk of chemotherapy-related AE-ILD in patients with lung cancer (Shimizu et al., 2014; Enomoto et al., 2015; Hamada et al., 2019). Anlotinib, a new anti-angiogenesis agent approved globally in 2018, has been proven attenuating bleomycin-induced pulmonary fibrosis in mice via the TGF- $\beta$ 1 signaling pathway (Ruan et al., 2020). Recombinant human endostatin and apatinib have not been evaluated to reduce AE in patients with ILD. In our study, anti-angiogenic agents mentioned above were included in the analysis. Although we failed to confirm whether anti-angiogenesis can reduce the acute exacerbation of ILD, we found that patients with advanced-stage LC receiving systematic therapy benefited from anti-angiogenic therapy. The possible reasons for anti-angiogenic therapy as an independent protective factor are as follows: 1. exerting the anti-tumor effect directly; 2. reducing AE-ILD and enabling patients to receive more anti-tumor treatments. Therefore, anti-angiogenic agents may be a good choice for patients with ILD-LC.

ILD-LC is a rare disease with poor prognosis, which is a part of severe lung cancer (Xie et al., 2019). These patients often face challenges in anti-cancer treatment because of poor PS scores or lung function caused by the progression of ILD. Furthermore, they may fail to receive anti-cancer treatment due to the slow progression or treatment-related AE-ILD. However, our research shows that patients with ILD-LC benefit from anti-cancer treatment. Our research shows that patients with ILD-LC benefit from anti-cancer treatment. In particular, these patients can live longer after using anti-angiogenic drugs, which suggests that anti-angiogenic therapy may be an important part of ILD-LC anti-cancer therapy.

Several limitations need to be noted regarding this real-world study. First, this is a retrospective study conducted over a long time. This study failed to reflect the current treatment status of ILD-LC due to the anti-cancer therapy of lung cancer has

undergone great changes. Second, the lack of acute exacerbation and lung function data in most patients makes it impossible for us to analyze the toxicity and true efficacy of anti-cancer treatments. Our interpretation of survival data is inadequate. Third, the present study involves a variety of anti-angiogenic drugs and cannot be analyzed separately due to the limited sample size. Further investigations and larger patient groups are needed to confirm the protective effect of anti-angiogenic agents in patients with ILD-LC treated with anti-cancer therapy.

## CONCLUSION

Patients with ILD-LC have very poor prognosis. Appropriate anti-tumor treatment can prolong the survival time of patients who can tolerate it. Targeted therapy and immunotherapy are alternative treatments for LC patients with mild ILD. For ILD patients with advanced LC, anti-angiogenic regimens significantly improve their prognosis.

## DATA AVAILABILITY STATEMENT

The raw data supporting the conclusions of this article will be made available by the authors, without undue reservation.

## ETHICS STATEMENT

The studies involving human participants were reviewed and approved by the Institutional Review Board of The First Affiliated Hospital of Guangzhou Medical University (Guangzhou, Guangdong, China). Written informed consent for participation

was not required for this study in accordance with the national legislation and the institutional requirements.

## AUTHOR CONTRIBUTIONS

XX, WL, and ZC: conception and design. QY, LMi, OM, HQ, LQ, LS, LC, WX, YS, HW, LMe, WP, and ZC: provision of study materials or patients. LW and LN: collection and assembly of data. XX, LW, LN, LX, LC, WX, YS, and HW: data analysis and interpretation. XX, WL, and LN: manuscript writing. All authors: final approval of the manuscript.

## FUNDING

This study was supported by the Guangdong High Level University Clinical Cultivation Project (No. 2017–21020) and Guangzhou Science and Technology Program key projects (No. 202008010006).

## ACKNOWLEDGMENTS

We appreciate the patients and their families for their contributions to this study.

## SUPPLEMENTARY MATERIAL

The Supplementary Material for this article can be found online at: <https://www.frontiersin.org/articles/10.3389/fmolb.2021.660800/full#supplementary-material>

## REFERENCES

- Amundson, W. H., Racila, E., Allen, T., Dincer, H. E., Tomic, R., et al. (2019). Acute exacerbation of interstitial lung disease after procedures. *Respir. Med.* 150, 30–37. doi: 10.1016/j.rmed.2019.02.012
- Asahina, H., Oizumi, S., Takamura, K., Harada, T., Harada, M., et al. (2019). A prospective phase II study of carboplatin and nab-paclitaxel in patients with advanced non-small cell lung cancer and concomitant interstitial lung disease (HOT1302). *Lung Cancer* 138, 65–71. doi: 10.1016/j.lungcan.2019.09.020
- ATS and ERS (2002). American Thoracic Society/European Respiratory Society International Multidisciplinary Consensus Classification of the Idiopathic Interstitial Pneumonias. This joint statement of the American Thoracic Society (ATS), and the European Respiratory Society (ERS) was adopted by the ATS board of directors, June 2001 and by the ERS Executive Committee, June 2001. *Am. J. Respir. Crit. Care Med.* 165, 277–304. doi: 10.1164/ajrccm.165.2.ats01
- Beom, S. H., Kim, D. W., Sim, S. H., Keam, B., Park, J. H., et al. (2016). Gefitinib-Induced interstitial lung disease in Korean lung cancer patients. *Cancer Res. Treat.* 48, 88–97. doi: 10.4143/crt.2014.201
- Cottin, V., Crestani, B., Cadranet, J., Cordier, J. F., Marchand-Adam, S., et al. (2017). French practical guidelines for the diagnosis and management of idiopathic pulmonary fibrosis - 2017 update. Full-length version. *Rev. Mal. Respir.* 34, 900–968. doi: 10.1016/j.rmr.2017.07.017
- Enomoto, Y., Inui, N., Yoshimura, K., Nishimoto, K., Mori, K., et al. (2016). Lung cancer development in patients with connective tissue disease-related interstitial lung disease: A retrospective observational study. *Medicine* 95:e5716. doi: 10.1097/MD.00000000000005716
- Enomoto, Y., Kenmotsu, H., Watanabe, N., Baba, T., Murakami, H., et al. (2015). Efficacy and safety of combined carboplatin, paclitaxel, and bevacizumab for patients with advanced non-squamous non-small cell lung cancer with pre-existing interstitial lung disease: A retrospective multi-institutional study. *Anticancer Res.* 35, 4259–4263.
- Fabre, A., and Nicholson, A. G. (2020). Nintedanib in progressive fibrosing interstitial lung diseases. *N. Engl. J. Med.* 382:780.
- Fujimoto, D., Morimoto, T., Ito, J., Sato, Y., Ito, M., et al. (2017). A pilot trial of nivolumab treatment for advanced non-small cell lung cancer patients with mild idiopathic interstitial pneumonia. *Lung Cancer* 111, 1–5. doi: 10.1016/j.lungcan.2017.06.008
- Fujimoto, D., Yomota, M., Sekine, A., Morita, M., Morimoto, T., et al. (2019). Nivolumab for advanced non-small cell lung cancer patients with mild idiopathic interstitial pneumonia: A multicenter, open-label single-arm phase II trial. *Lung Cancer* 134, 274–278. doi: 10.1016/j.lungcan.2019.06.001
- Gemma, A., Kusumoto, M., Kurihara, Y., Masuda, N., Banno, S., et al. (2019). Interstitial lung disease onset and its risk factors in Japanese patients with ALK-Positive NSCLC after treatment with crizotinib. *J. Thorac. Oncol.* 14, 672–682. doi: 10.1016/j.jtho.2018.11.022
- Glick, D., Lyen, S., Kandel, S., Shapera, S., Le, L. W., et al. (2018). Impact of pretreatment interstitial lung disease on radiation pneumonitis and survival in patients treated with lung stereotactic body radiation therapy (SBRT). *Clin. Lung Cancer* 19, 219–226. doi: 10.1016/j.clcc.2017.06.021
- Hagiwara, Y., Nakayama, Y., Kudo, S., Hayakawa, T., Nakamura, N., et al. (2020). Nationwide survey of radiation therapy in Japan for lung cancer complicated with interstitial lung disease. *J. Radiat. Res.* 61, 563–574. doi: 10.1093/jrr/rraa018

- Hamada, S., Ichiyasu, H., Ikeda, T., Inaba, M., Kashiwabara, K., et al. (2019). Protective effect of bevacizumab on chemotherapy-related acute exacerbation of interstitial lung disease in patients with advanced non-squamous non-small cell lung cancer. *BMC Pulmonary Med.* 19:72. doi: 10.1186/s12890-019-0838-2
- Hanibuchi, M., Kakiuchi, S., Atagi, S., Ogushi, F., Shimizu, E., et al. (2018). A multicenter, open-label, phase II trial of S-1 plus carboplatin in advanced non-small cell lung cancer patients with interstitial lung disease. *Lung Cancer* 125, 93–99. doi: 10.1016/j.lungcan.2018.09.007
- Hilberg, F., Tontsch-Grunt, U., Baum, A., Le, A. T., Doebele, R. C., et al. (2018). Triple angiokinase inhibitor nintedanib directly inhibits tumor cell growth and induces tumor shrinkage via blocking oncogenic receptor tyrosine kinases. *J. Pharmacol. Exp. Ther.* 364, 494–503. doi: 10.1124/jpet.117.244129
- Homma, S., Bando, M., Azuma, A., Sakamoto, S., Sugino, K., et al. (2018). Japanese guideline for the treatment of idiopathic pulmonary fibrosis. *Respir. Investig.* 56, 268–291. doi: 10.1016/j.resinv.2018.03.003
- Jain, A., Shannon, V. R., and Sheshadri, A. (2018). Immune-Related adverse events: Pneumonitis. *Adv. Exp. Med. Biol.* 995, 131–149. doi: 10.1007/978-3-030-02505-2\_6
- Jung, H. I., Park, J. S., Lee, M., Park, B., Kim, H. J., et al. (2018). Prevalence of lung cancer in patients with interstitial lung disease is higher than in those with chronic obstructive pulmonary disease. *Medicine* 97:e71. doi: 10.1097/MD.00000000000010071
- Kanai, O., Kim, Y. H., Demura, Y., Kanai, M., Ito, T., et al. (2018). Efficacy and safety of nivolumab in non-small cell lung cancer with preexisting interstitial lung disease. *Thorac. Cancer* 9, 847–855. doi: 10.1111/1759-7714.12759
- Kato, T., Masuda, N., Nakanishi, Y., Takahashi, M., Hida, T., et al. (2017). Nivolumab-induced interstitial lung disease analysis of two phase II studies patients with recurrent or advanced non-small-cell lung cancer. *Lung Cancer* 104, 111–118. doi: 10.1016/j.lungcan.2016.12.016
- Kawahara, T., Sakashita, H., Suzuki, T., Tateishi, T., and Miyazaki, Y. (2019). Real world data of combined lung cancer and interstitial lung disease. *J. Thorac. Dis.* 11, 4144–4151. doi: 10.21037/jtd.2019.10.01
- Kenmotsu, H., Naito, T., Mori, K., Ko, R., Ono, A., et al. (2015). Effect of platinum-based chemotherapy for non-small cell lung cancer patients with interstitial lung disease. *Cancer Chemother. Pharmacol.* 75, 521–526. doi: 10.1007/s00280-014-2670-y
- Kenmotsu, H., Yoh, K., Mori, K., Ono, A., Baba, T., et al. (2019). Phase II study of nab-paclitaxel + carboplatin for patients with non-small-cell lung cancer and interstitial lung disease. *Cancer Sci.* 110, 3738–3745. doi: 10.1111/cas.14217
- Kobayashi, H., Naito, T., Omae, K., Omori, S., Nakashima, K., et al. (2018). Impact of interstitial lung disease classification on the development of acute exacerbation of interstitial lung disease and prognosis in patients with stage III Non-Small-Cell lung cancer and interstitial lung disease treated with chemoradiotherapy. *J. Cancer* 9, 2054–2060. doi: 10.7150/jca.24936
- Lim, J. U., Gil, B. M., Kang, H. S., Oh, J., Kim, Y. H., et al. (2019). Interstitial pneumonia with autoimmune features show better survival and less exacerbations compared to idiopathic pulmonary fibrosis. *BMC Pulm. Med.* 19:120. doi: 10.1186/s12890-019-0868-9
- McKeown, S., Richter, A. G., O'Kane, C., McAuley, D. F., and Thickett, D. R. (2009). MMP expression and abnormal lung permeability are important determinants of outcome in IPF. *Eur. Respir. J.* 33, 77–84. doi: 10.1183/09031936.00060708
- Minegishi, Y., Kuribayashi, H., Kitamura, K., Mizutani, H., Kosaihiara, S., et al. (2011a). The feasibility study of Carboplatin plus Etoposide for advanced small cell lung cancer with idiopathic interstitial pneumonias. *J. Thorac. Oncol.* 6, 801–807. doi: 10.1097/JTO.0b013e3182103d3c
- Minegishi, Y., Sudoh, J., Kuribayashi, H., Mizutani, H., Seike, M., et al. (2011b). The safety and efficacy of weekly paclitaxel in combination with carboplatin for advanced non-small cell lung cancer with idiopathic interstitial pneumonias. *Lung Cancer* 71, 70–74. doi: 10.1016/j.lungcan.2010.04.014
- Minegishi, Y., Takenaka, K., Mizutani, H., Sudoh, J., Noro, R., et al. (2009). Exacerbation of idiopathic interstitial pneumonias associated with lung cancer therapy. *Intern. Med.* 48, 665–672. doi: 10.2169/internalmedicine.48.1650
- Naccache, J. M., Gibiot, Q., Monnet, I., Antoine, M., Wislez, M., et al. (2018). Lung cancer and interstitial lung disease: A literature review. *J. Thorac. Dis.* 10, 3829–3844. doi: 10.21037/jtd.2018.05.75
- Omori, T., Tajiri, M., Baba, T., Ogura, T., Iwasawa, T., et al. (2015). Pulmonary resection for lung cancer in patients with idiopathic interstitial pneumonia. *Ann. Thorac. Surg.* 100, 954–960. doi: 10.1016/j.athoracsur.2015.03.094
- Raghu, G., Nyberg, F., and Morgan, G. (2004). The epidemiology of interstitial lung disease and its association with lung cancer. *Br. J. Cancer* 91(Suppl. 2), S3–S10. doi: 10.1038/sj.bjc.6602061
- Reck, M., Kaiser, R., Mellemegaard, A., Douillard, J. Y., Orlov, S., et al. (2014). Docetaxel plus nintedanib versus docetaxel plus placebo in patients with previously treated non-small-cell lung cancer (LUME-Lung 1): A phase 3, double-blind, randomised controlled trial. *Lancet Oncol.* 15, 143–155. doi: 10.1016/S1470-2045(13)70586-2
- Richeldi, L., du Bois, R. M., Raghu, G., Azuma, A., Brown, K. K., et al. (2014). Efficacy and safety of nintedanib in idiopathic pulmonary fibrosis. *N. Engl. J. Med.* 370, 2071–2082. doi: 10.1056/NEJMoa1402584
- Ruan, H., Lv, Z., Liu, S., Zhang, L., Huang, K., et al. (2020). Anlotinib attenuated bleomycin-induced pulmonary fibrosis via the TGF- $\beta$ 1 signalling pathway. *J. Pharm. Pharmacol.* 72, 44–55. doi: 10.1111/jphp.13183
- Saijo, A., Hanibuchi, M., Goto, H., Toyoda, Y., Tezuka, T., et al. (2017). An analysis of the clinical features of lung cancer in patients with connective tissue diseases. *Respir. Investig.* 55, 153–160. doi: 10.1016/j.resinv.2016.11.003
- Sato, T., Teramukai, S., Kondo, H., Watanabe, A., Ebina, M., et al. (2014). Impact and predictors of acute exacerbation of interstitial lung diseases after pulmonary resection for lung cancer. *J. Thorac. Cardiovasc. Surg.* 147, 1604–1611. doi: 10.1016/j.jtcvs.2013.09.050
- Sato, T., Watanabe, A., Kondo, H., Kanzaki, M., Okubo, K., et al. (2015). Long-term results and predictors of survival after surgical resection of patients with lung cancer and interstitial lung diseases. *J. Thorac. Cardiovasc. Surg.* 149, 70–71. doi: 10.1016/j.jtcvs.2014.08.086
- Sekine, A., Satoh, H., Baba, T., Ikeda, S., Okuda, R., et al. (2016). Safety and efficacy of S-1 in combination with carboplatin in non-small cell lung cancer patients with interstitial lung disease: A pilot study. *Cancer Chemother. Pharmacol.* 77, 1245–1252. doi: 10.1007/s00280-016-3040-8
- Shah, R. R. (2016). Tyrosine kinase Inhibitor-Induced interstitial lung disease: Clinical features, diagnostic challenges, and therapeutic dilemmas. *Drug Saf.* 39, 1073–1091. doi: 10.1007/s40264-016-0450-9
- Shi, L., Tang, J., Tong, L., and Liu, Z. (2014). Risk of interstitial lung disease with gefitinib and erlotinib in advanced non-small cell lung cancer: A systematic review and meta-analysis of clinical trials. *Lung Cancer* 83, 231–239. doi: 10.1016/j.lungcan.2013.11.016
- Shimizu, R., Fujimoto, D., Kato, R., Otoshi, T., Kawamura, T., et al. (2014). The safety and efficacy of paclitaxel and carboplatin with or without bevacizumab for treating patients with advanced nonsquamous non-small cell lung cancer with interstitial lung disease. *Cancer Chemother. Pharmacol.* 74, 1159–1166. doi: 10.1007/s00280-014-2590-x
- Shintani, Y., Ohta, M., Iwasaki, T., Ikeda, N., Tomita, E., et al. (2010). Predictive factors for postoperative acute exacerbation of interstitial pneumonia combined with lung cancer. *Gen. Thorac. Cardiovasc. Surg.* 58, 182–185. doi: 10.1007/s11748-009-0569-z
- Simler, N. R., Brenchley, P. E., Horrocks, A. W., Greaves, S. M., Hasleton, P. S., et al. (2004). Angiogenic cytokines in patients with idiopathic interstitial pneumonia. *Thorax* 59, 581–585. doi: 10.1136/thx.2003.009860
- Suresh, K., Voong, K. R., Shankar, B., Forde, P. M., Ettinger, D. S., et al. (2018). Pneumonitis in Non-Small cell lung cancer patients receiving immune checkpoint immunotherapy: Incidence and risk factors. *J. Thorac. Oncol.* 13, 1930–1939. doi: 10.1016/j.jtho.2018.08.2035
- Tomassetti, S., Gurioli, C., Ryu, J. H., Decker, P. A., Ravaglia, C., et al. (2015). The impact of lung cancer on survival of idiopathic pulmonary fibrosis. *Chest* 147, 157–164. doi: 10.1378/chest.14-0359
- Tone, M., Izumo, T., Awano, N., Kuse, N., Inomata, M., et al. (2019). High mortality and poor treatment efficacy of immune checkpoint inhibitors in patients with severe grade checkpoint inhibitor pneumonitis in non-small cell lung cancer. *Thorac. Cancer* 10, 2006–2012. doi: 10.1111/1759-7714.13187
- Usui, K., Tanai, C., Tanaka, Y., Noda, H., and Ishihara, T. (2011). The prevalence of pulmonary fibrosis combined with emphysema in patients with lung cancer. *Respirology* 16, 326–331. doi: 10.1111/j.1440-1843.2010.01907.x
- Watanabe, N., Taniguchi, H., Kondoh, Y., Kimura, T., Kataoka, K., et al. (2013). Efficacy of chemotherapy for advanced non-small cell lung cancer with



- idiopathic pulmonary fibrosis. *Respiration* 85, 326–331. doi: 10.1159/000342046
- Watanabe, S., Saeki, K., Waseda, Y., Murata, A., Takato, H., et al. (2018). Lung cancer in connective tissue disease-associated interstitial lung disease: Clinical features and impact on outcomes. *J. Thoracic Dis.* 10, 799–807. doi: 10.21037/jtd.2017.12.134
- Weis, S. M., and Cheres, D. A. (2005). Pathophysiological consequences of VEGF-induced vascular permeability. *Nature* 437, 497–504. doi: 10.1038/nature03987
- Xie, Z., Zhou, C., Qin, Y., Ouyang, M., Li, S., et al. (2019). [Diagnosis and treatment strategy for advanced severe lung cancer]. *Chin. J. Pract. Internal Med.* 39, 416–419. doi: 10.19538/j.nk2019050106
- Yamaguchi, S., Ohguri, T., Ide, S., Aoki, T., Imada, H., et al. (2013). Stereotactic body radiotherapy for lung tumors in patients with subclinical interstitial lung disease: The potential risk of extensive radiation pneumonitis. *Lung Cancer* 82, 260–265. doi: 10.1016/j.lungcan.2013.08.024
- Yoo, H., Jeong, B. H., Chung, M. J., Lee, K. S., Kwon, O. J., et al. (2019). Risk factors and clinical characteristics of lung cancer in idiopathic pulmonary fibrosis: A retrospective cohort study. *BMC Pulm. Med.* 19:149. doi: 10.1186/s12890-019-0905-8

**Conflict of Interest:** The authors declare that the research was conducted in the absence of any commercial or financial relationships that could be construed as a potential conflict of interest.

Copyright © 2021 Xiaohong, Liqiang, Na, Xinqing, Yinyin, Ming, Ming, Qian, Qun, Shiyue, Chunyan, Xiaoqian, Shuanying, Wei, Mei, Ping and Chengzhi. This is an open-access article distributed under the terms of the Creative Commons Attribution License (CC BY). The use, distribution or reproduction in other forums is permitted, provided the original author(s) and the copyright owner(s) are credited and that the original publication in this journal is cited, in accordance with accepted academic practice. No use, distribution or reproduction is permitted which does not comply with these terms.



# High-Flow Nasal Cannula for COVID-19 Patients: A Multicenter Retrospective Study in China

Jun Duan<sup>1†</sup>, Jia Zeng<sup>2,3†</sup>, Puyu Deng<sup>4†</sup>, Zhong Ni<sup>5</sup>, Rongli Lu<sup>6</sup>, Wenxi Xia<sup>7</sup>, Guoqiang Jing<sup>8</sup>, Xiaoping Su<sup>9</sup>, Stephan Ehrmann<sup>10</sup>, Wei Zhang<sup>3,11\*</sup> and Jie Li<sup>12\*</sup>

<sup>1</sup>Department of Respiratory and Critical Care Medicine, First Affiliated Hospital of Chongqing Medical University, Chongqing, China, <sup>2</sup>Department of Aviation Disease, Naval Medical Center of PLA, Second Military Medical University, Shanghai, China, <sup>3</sup>Hubei Maternal and Child Health Hospital, Wuhan, China, <sup>4</sup>Department of Emergency and Critical Care Medicine, Shanghai General Hospital, Shanghai Jiao Tong University School of Medicine, Shanghai, China, <sup>5</sup>Department of Respiratory and Critical Care Medicine, West China Hospital, Sichuan University, Chengdu, China, <sup>6</sup>Department of Pulmonary and Critical Care Medicine, Xiangya Hospital, Central South University, Changsha, China, <sup>7</sup>Department of Critical Care Medicine, West China Hospital, Sichuan University, Chengdu, China, <sup>8</sup>Department of Pulmonary and Critical Care Medicine, Binzhou Medical University Hospital, Binzhou Medical University, Binzhou, China, <sup>9</sup>School of Basic Medicine, Wenzhou Medical University, Wenzhou Tea Mountain Higher Education Park, Wenzhou, China, <sup>10</sup>CHRU Tours, Médecine Intensive Réanimation, CIC INSERM 1415, CRICS-TriggerSep Network, Tours France, and INSERM, Centre D'étude des Pathologies Respiratoires, Université de Tours, Tours, France, <sup>11</sup>Department of Respiratory and Critical Care Medicine, First Affiliated Hospital, Second Military Medical University, Shanghai, China, <sup>12</sup>Department of Cardiopulmonary Sciences, Division of Respiratory Care, Rush University Medical Center, Chicago, IL, United States

## OPEN ACCESS

### Edited by:

Wen Li,  
Zhejiang University, China

### Reviewed by:

Yuenan Ni,  
Sichuan University, China  
Alessandra Bettiol,  
University of Florence, Italy

### \*Correspondence:

Wei Zhang  
zhangweismmu@126.com  
Jie Li  
jie\_li@rush.edu

<sup>†</sup>These authors have contributed  
equally to this work

### Specialty section:

This article was submitted to  
Molecular Diagnostics and  
Therapeutics,  
a section of the journal  
Frontiers in Molecular Biosciences

**Received:** 08 February 2021

**Accepted:** 08 February 2021

**Published:** 13 April 2021

### Citation:

Duan J, Zeng J, Deng P, Ni Z, Lu R,  
Xia W, Jing G, Su X, Ehrmann S,  
Zhang W and Li J (2021) High-Flow  
Nasal Cannula for COVID-19 Patients:  
A Multicenter Retrospective Study  
in China.  
Front. Mol. Biosci. 8:  
doi: 10.3389/fmolb.2021.639100

**Background:** High-flow nasal cannula (HFNC) may help avoid intubation of hypoxemic patients suffering from COVID-19; however, it may also contribute to delaying intubation, which may increase mortality. Here, we aimed to identify the predictors of HFNC failure among patients with COVID-19.

**Methods:** We performed a multicenter retrospective study in China from January 15 to March 31, 2020. Two centers in Wuhan (resource-limited centers) enrolled 32 patients, and four centers outside Wuhan enrolled 34 cases. HFNC failure was defined as the requirement of escalation therapy (NIV or intubation). The ROX index (the ratio of SpO<sub>2</sub>/FiO<sub>2</sub> to the respiratory rate) was calculated.

**Results:** Among the 66 patients, 29 (44%) cases experienced HFNC failure. The ROX index was much lower in failing patients than in successful ones after 1, 2, 4, 8, 12, and 24 h of HFNC. The ROX index was independently associated with HFNC failure (OR = 0.65; 95% CI: 0.45–0.94) among the variables collected before and 1 h after HFNC. To predict HFNC failure tested by ROX index, the AUC was between 0.73 and 0.79 for the time points of measurement 1–24 h after HFNC initiation. The HFNC failure rate was not different between patients in and outside Wuhan (41% vs. 47%,  $p = 0.63$ ). However, the time from HFNC initiation to intubation was longer in Wuhan than that outside Wuhan (median 63 vs. 22 h,  $p = 0.02$ ). Four patients in Wuhan underwent intubation due to cardiac arrest; in contrast, none of the patients outside Wuhan received intubation (13 vs. 0%,  $p = 0.05$ ). The mortality was higher in Wuhan than that out of Wuhan, but the difference did not reach statistical significance (31 vs. 12%,  $p = 0.07$ ).

**Conclusion:** The ROX index can be used to predict HFNC failure among COVID-19 patients to avoid delayed intubation, which may occur in the resource-limited area.

**Keywords:** coronavirus, high-flow nasal cannula, ROX index, risk factor, delay intubation

## INTRODUCTION

As of January 17, 2021, more than ninety million cases were confirmed with 2019 novel coronavirus disease (COVID-19) worldwide, with a fatality rate of approximately 2% (WHO Coronavirus Disease Dashboard, 2021). Nearly 20% of patients experienced hypoxemia, which was the primary reason for hospitalization (Wu and McGoogan, 2020). Oxygen therapy is the primary treatment for those hypoxemic patients. In recent years, high-flow nasal cannula (HFNC) has been proven to improve oxygenation and ultimately reduce intubation rates for hypoxemic respiratory failure patients of various etiologies (Li et al., 2020a). HFNC provides gas flow higher than the patient's inspiratory flow demand, which enables the delivery of a constant fraction of inspired oxygen ( $\text{FiO}_2$ ) without dilution by room air. It also washes out the dead space and provides, to some extent, positive expiratory pressure (Nishimura, 2016).

Two retrospective studies with a small sample size from China reported that HFNC could improve oxygenation for COVID-19 patients, particularly among patients with  $\text{PaO}_2/\text{FiO}_2 > 200$  mmHg (Geng et al., 2020; Wang et al., 2020). Among moderate-to-severe hypoxemic patients treated with HFNC, 36% of them did not require therapy escalation, such as intubation or noninvasive ventilation (NIV) (Wang et al., 2020). In Wuhan, China, 63.5% of ICU patients suffering from COVID-19 used HFNC (Yang et al., 2020). In Jiangsu, China, HFNC became the standard of care for hypoxemic COVID-19 patients (Sun et al., 2020). In the Seattle region, United States, 42% of critically ill patients received HFNC (Bhatraju et al., 2020). As the risk of virus transmission associated with HFNC is relatively low (Hui et al., 2019; Li et al., 2020b), current Surviving Sepsis Campaign COVID-19 subcommittee guidelines recommend using HFNC in hypoxemic patients with COVID-19 (Alhazzani et al., 2020). However, delayed intubation after HFNC failure is associated with increased mortality (Kang et al., 2015). Therefore, early identification of HFNC failure is essential, particularly in a resource-limited area, where the number of life-saving devices, such as ventilators, is limited; the use of those devices should be prioritized; early decision on the distribution of ventilators, instead of using a ventilator at the last minute, to patients with high possibility of HFNC failure might help reduce mortality (Kang et al., 2015).

The ROX index, the ratio of pulse oximetry ( $\text{SpO}_2$ )/ $\text{FiO}_2$  to the respiratory rate, has been shown to effectively predict HFNC failure in patients with hypoxemia caused by bacterial pneumonia (Roca et al., 2016). However, its value for predicting HFNC failure in COVID-19 patients remains unknown. Albeit not fully elucidated so far, the pathophysiology of COVID-19-associated hypoxemia may differ from that of other diseases, such as bacterial pneumonia (Gattinoni et al., 2020a; Gattinoni et al., 2020b; Ziehr et al., 2020). In addition, the place

where the device, such as the invasive ventilator, was unavailable when the patient required intubation was considered as a resource-limited area. Delayed intubation may occur in this area. As such, we aimed to identify the risk factors associated with HFNC failure in COVID-19 patients, and further explore the relationship between HFNC therapy and delayed intubation in a resource-limited area compared to a normal setting.

## METHODS

A retrospective study was conducted in six Chinese hospitals, after approval by the institutional review board [approval No. FYGG(L)-2020-017], in the central institution (Guanggu, Wuhan). Adult patients with a laboratory-confirmed diagnosis of COVID-19 and treated by HFNC from January 15 to March 31, 2020 were enrolled. Exclusion criteria included 1) use of HFNC as palliative care and 2) use of HFNC for less than 30 min. Patients were identified by the medical record system in each hospital.

HFNC (Fisher & Paykel, Auckland, New Zealand; OH-70B/70C, Micomme Medical Technology, Hunan, China; and HiFent TM, Respirac Medical, Liaoning, China) was implemented according to the current consensus and experts' suggestions (Respiratory and Critical Care Medicine Group of Chinese Thoracic Society, 2019; Critical care committee of Chinese Association of Chest Physician, 2020; Yuan et al., 2020). Flow and  $\text{FiO}_2$  were adjusted to maintain  $\text{SpO}_2$  above 93% and the respiratory rate below 30 breaths/min, while favoring patients' tolerance. Withdrawal of HFNC was considered if  $\text{FiO}_2$  was less than 0.4. In case of respiratory failure worsening, escalation therapy consisting of NIV or intubation was initiated based on the attending physicians' decision.

Patients' demographic data, including age, gender, preexisting chronic diseases such as hypertension, diabetes mellitus, chronic pulmonary diseases, coronary artery disease, and cerebral infarction, and admission comorbidities, were collected. Chronic pulmonary disease included asthma, COPD, and bronchiectasis. Laboratory tests including white blood cell counts, cluster of differentiation 4 (CD4), lymphocyte counts, procalcitonin, IL-6, C-reactive protein, lactate dehydrogenase, lactic acid, and arterial blood gas analysis were also recorded, if available. The data of HFNC utilization including flow and  $\text{FiO}_2$  settings, patients' changes in vital signs, and  $\text{SpO}_2$  at 1, 2, 4, 8, 12, and 24 h of HFNC were extracted from patients' medical records. At the same time, the ROX index was calculated (Roca et al., 2016).

All the patients were followed up until discharge or death in the hospital. Data on HFNC duration, use of NIV as rescue therapy, intubation, survival, and length of stay in the ICU and hospital were collected. HFNC failure was defined as the

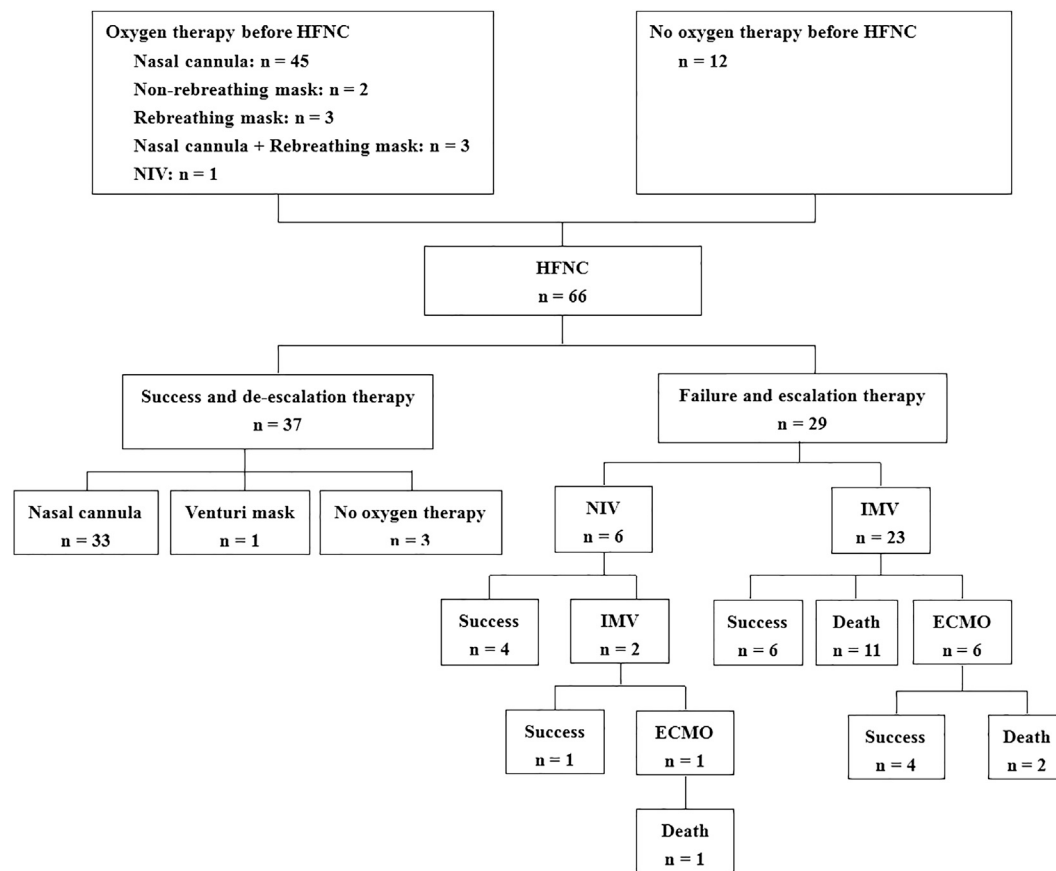


**FIGURE 1 |** Flowchart of the enrolled patients. HFNC, high-flow nasal cannula; NIV, noninvasive ventilation; IMV, invasive mechanical ventilation; ECMO, extracorporeal membranous oxygenation.

requirement of escalation therapy (NIV or intubation) (Geng et al., 2020); HFNC failure in 28 days was recorded.

Among the six centers, two were in Wuhan and four were out of Wuhan. As many COVID-19 patients crowded into hospitals in Wuhan within a short period, the healthcare workers were overwhelmed and a severe shortage of medical devices occurred. Compared to the hospitals outside Wuhan, the resources in Wuhan were relatively inadequate. Thus, we defined the two centers in Wuhan as resource-limited areas, which probably impacted intubation decisions in patients who underwent HFNC.

## Statistical Analysis

Normally distributed continuous variables were reported as mean and standard deviation, and non-normally distributed continuous variables were reported as median and interquartile range (IQR). Differences between the groups of HFNC success and failure were analyzed using the Student's *t*-test or Mann-Whitney *U* test when appropriate. Categorical variables were reported as number and percentage, and differences between groups were analyzed with using chi-square test or Fisher's exact test when appropriate.

The area under the curve (AUC) of receiver operating characteristics was calculated to identify the predictive power

of HFNC failure. The optimal cutoff value was determined at the maximal Youden index (Youden, 1950). Variables with a *p* value less than 0.1 in the univariate analysis were entered in a stepwise multivariate logistic regression analysis to identify independent risk factors associated with HFNC failure. As the respiratory rate, SpO<sub>2</sub>, and PaO<sub>2</sub>/FiO<sub>2</sub> were collinear with the ROX index, they were not included in the regression analysis. A *p* value less than 0.05 was considered to be significant.

## RESULTS

### Data Collected From Hospital Admission to Termination of High-Flow Nasal Cannula

We enrolled 66 patients with COVID-19 (32 in Wuhan and 34 outside Wuhan) in this study (Figure 1). Of them, 29 (44%) patients experienced HFNC failure and required escalation therapy within 28 days. Univariate comparisons of patients with HFNC success and failure are presented in Table 1. HFNC success was associated with younger age, lack of chronic respiratory disease, lower illness severity measured by the sequential organ failure score (SOFA), better oxygenation, less inflammation (lower procalcitonin levels), and immune



**TABLE 1** | Baseline data collected before the use of HFNC.

	HFNC success (N = 37)	HFNC failure (N = 29)	P value
Age, years	63 ± 16	73 ± 14	0.01
Male, n (%)	14 (38)	11 (38)	> 0.99
Oxygen therapy before HFNC, n %	8 (22)	4 (14)	0.53
SOFA score	3.4 ± 2.1	4.5 ± 1.7	0.047
Underlying disease, n %			
Hypertension	21 (57)	19 (66)	0.61
Diabetes mellitus	13 (35)	6 (21)	0.28
Coronary heart disease	4 (11)	4 (14)	0.72
Cerebral infarction	4 (11)	4 (14)	0.72
Chronic respiratory disease	3 (8)	8 (28)	0.048
Hypoproteinemia	6 (16)	7 (24)	0.54
Anemia	5 (14)	4 (14)	> 0.99
Chronic renal dysfunction	2 (5)	3 (10)	0.65
Gastrointestinal bleeding	1 (3)	3 (10)	0.31
Airway secretions, n %			
None	20 (54)	12 (41)	0.33
Mild	16 (43)	17 (59)	0.32
Moderate to abundant	1 (3)	0 (0)	> 0.99
Laboratory tests			
White blood cell counts, × 10 <sup>9</sup> /L	8.5 ± 4.6	8.6 ± 3.5	0.94
Lymphocyte counts, × 10 <sup>9</sup> /L	1.12 ± 0.95	0.59 ± 0.30	0.02
PCT, ng/mL	0.10 (0.05–0.14)	0.42 (0.10–2.37)	< 0.01
IL-6	8 (1–76)	73 (24–192)	0.13
C-reactive protein, mg/L	65 ± 53	96 ± 67	0.08
LDH, U/L	365 ± 114	429 ± 144	0.18
CD4, counts/μL	335 ± 183	152 ± 113	0.06
pH	7.42 ± 0.06	7.42 ± 0.08	0.77
PaCO <sub>2</sub> , mmHg	42 ± 9	37 ± 9	0.06
PaO <sub>2</sub> /F <sub>i</sub> O <sub>2</sub> , mmHg	214 ± 110	168 ± 108	0.15
Lactate, mmol/L	2.6 ± 1.2	2.8 ± 1.5	0.57
Vital signs			
Heart rate, beats/min	90 ± 11	93 ± 21	0.50
Respiratory rate, breaths/min	24 ± 4	26 ± 7	0.17
Systolic blood pressure, mmHg	122 ± 18	132 ± 22	0.07
Diastolic blood pressure, mmHg	70 ± 9	73 ± 10	0.33
SpO <sub>2</sub> , %	94 (92–96)	89 (85–93)	< 0.01
ROX index	9.4 ± 3.1	8.4 ± 4.7	0.32

HFNC, high-flow nasal cannula; SOFA, Sequential Organ Failure Assessment; PCT, procalcitonin; LDH, lactate dehydrogenase; ROX, the ratio of SpO<sub>2</sub>/F<sub>i</sub>O<sub>2</sub> to the respiratory rate. HFNC failure was defined as the requirement of escalation therapy (noninvasive ventilation or intubation).

dysfunction (higher lymphocyte count). However, the PaO<sub>2</sub>/FiO<sub>2</sub> and ROX index did not differ between the two groups at hospital admission and before the use of HFNC (Table 1; Supplementary Table S1).

## Outcomes

As the medical resources and staff were exhausted in the early stage of COVID-19, the data in ROX were missed in 5 patients before HFNC, 8 at 1, 24 at 2, 25 at 4, 25 at 8, 20 at 12, and 14 at 24 h. At 1, 2, 4, 8, 12, and 24 h and HFNC termination, the ROX index was much lower in patients experiencing HFNC failure than in those experiencing success (Figure 2A; Supplementary Table S2). In the multivariate analysis, we observed that the ROX index was independently associated with HFNC failure (odds ratio [OR] = 0.65; 95% confidence interval [CI]: 0.45–0.94) among the variables collected before and at 1 h of HFNC (Table 2). The AUC of the ROX index to predict

HFNC failure was 0.74, 0.73, 0.73, 0.77, 0.75, and 0.79 at 1, 2, 4, 8, 12, and 24 h of HFNC, respectively (Figure 2B). Other variables to predict HFNC failure were summarized in Supplementary Table S3.

The median duration of HFNC therapy was 242 h (IQR: 144–295) in the HFNC success group and 39 h (IQR: 15–117) in the group experiencing HFNC failure (Table 3). Among the patients with HFNC failure, six cases used NIV as a rescue therapy (21%), and 23 cases (79%) were directly intubated for invasive mechanical ventilation (IMV). Among the six NIV patients, two were intubated after NIV failure. Cardiac arrest occurred during HFNC therapy in four patients (6%), and all occurred in the resource-limited setting of Wuhan. Among the intubated patients, seven underwent extracorporeal membranous oxygenation (ECMO). The median time from HFNC initiation to intubation was 41 h (IQR: 19–152). Mortality was higher in patients with HFNC failure than in those with HFNC success (28 vs. 0%,  $p < 0.01$ ).

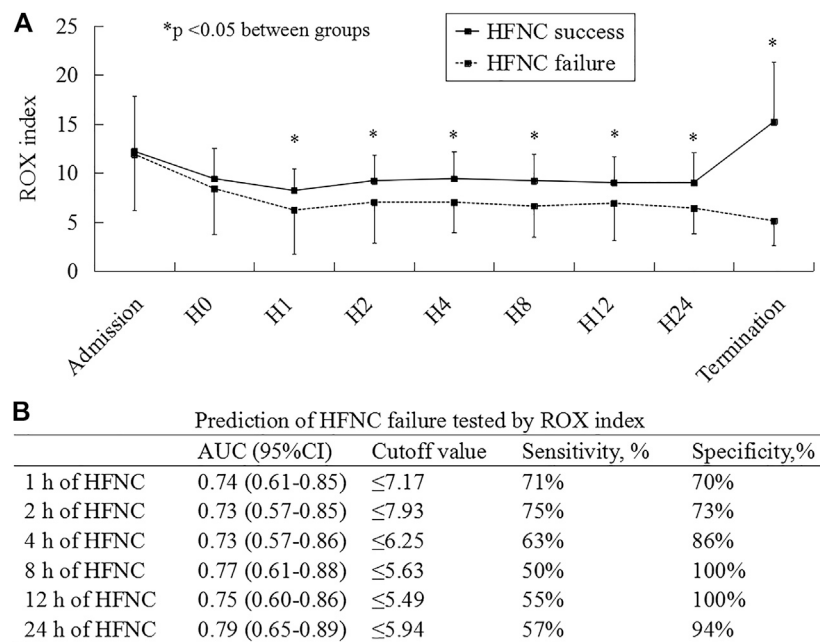


**FIGURE 2 |** ROX index as a risk factor to predict HFNC failure. H0, H1, H2, H4, H8, H12, and H24 mean the data collected before and at 1, 2, 4, 8, 12, and 24 h HFNC, respectively. ROX, the ratio of  $\text{SpO}_2/\text{FIO}_2$  to the respiratory rate; HFNC, high-flow nasal cannula; AUC, area under the curve of receiver operating characteristics; CI, confidence interval.

**TABLE 2 |** Univariate and multivariate analysis for HFNC failure.

	Univariate analysis OR (95%CI)	P value	Multivariate analysis <sup>a</sup> OR (95% CI)	p value
Age, years	1.05 (1.01–1.08)	0.02	–	–
SOFA score	1.39 (0.97–1.98)	0.07	2.16 (1.19–5.53)	0.02
Chronic respiratory disease	4.32 (1.03–18.12)	0.05	–	–
Systolic blood pressure before HFNC, mmHg	1.03 (1.00–1.06)	0.07	–	–
ROX index at 1 h of HFNC	0.68 (0.53–0.88)	<0.01	0.65 (0.45–0.94)	0.02

<sup>a</sup>Due to missing data in some variables, 43 patients (22 HFNC successes and 21 failures) were entered in multivariate analysis.

HFNC, high-flow nasal cannula; OR, odds ratio; CI, confidence interval; SOFA, Sequential Organ Failure Assessment; ROX, the ratio of  $\text{SpO}_2/\text{FIO}_2$  to the respiratory rate. HFNC failure was defined as the requirement of escalation therapy (noninvasive ventilation or intubation).

**TABLE 3 |** Outcomes of patients with HFNC success and failure.

	HFNC success (N = 37)	HFNC failure (N = 29)	P value
Duration of HFNC therapy, h	242 (144–295)	39 (15–117)	<0.01
Duration of NIV, h	–	72 (21–192)	–
Duration of IMV, h	–	120 (48–576)	–
Length of ICU stay, d	16 (13–22)	15 (8–34)	0.92
Length of hospital stay, d	23 (17–33)	23 (8–42)	0.43
Cardiac arrest during HFNC, n %	–	4 (14)	–
NIV as a rescue therapy, n %	–	6 (21)	–
Intubation for IMV, n %	–	25 (86)	–
Time from initiation of HFNC to intubation, h	–	41 (19–152)	–
Use of ECMO, n %	–	7 (24)	–
Mortality, n %	0 (0)	14 (48)	<0.01

HFNC, high-flow nasal cannula; NIV, noninvasive ventilation; IMV, invasive mechanical ventilation; ECMO, extracorporeal membranous oxygenation. HFNC failure was defined as the requirement of escalation therapy (noninvasive ventilation or intubation).

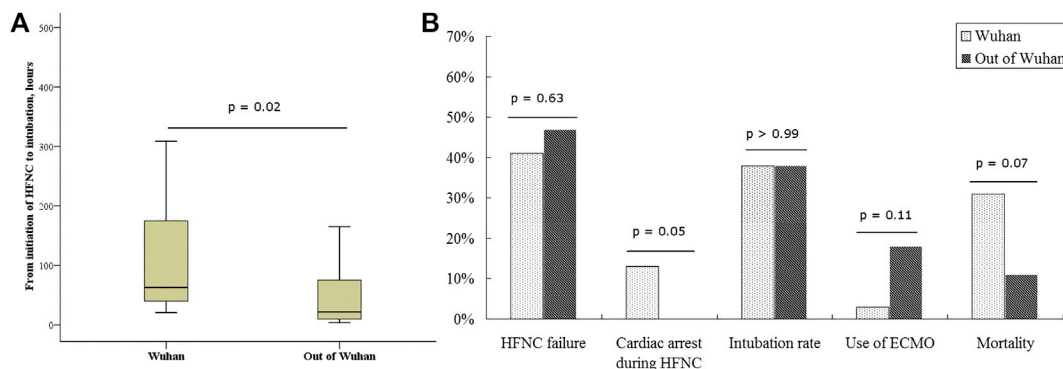


**FIGURE 3 |** The comparisons between patients in and out of Wuhan. HFNC, high-flow nasal cannula; ECMO, extracorporeal membranous oxygenation. In Wuhan, a very large number of patients crowded into hospitals, staff were overwhelmed, and a severe shortage of medical devices occurred; thus, Wuhan is to be considered as a resource-limited area.

## Comparisons Between Patients Inside and Outside Wuhan, China

The rate of HFNC failure and intubation did not differ between patients inside and outside Wuhan (41 vs. 47% for HFNC failure,  $p = 0.63$ ; 38 vs. 38% for intubation,  $p > 0.99$ ). We also observed similar baseline characteristics of patients inside and outside Wuhan before HFNC initiation (**Supplementary Table S4**). However, the duration from HFNC initiation to intubation was longer in Wuhan than that outside Wuhan [63 (IQR: 39–179) vs. 22 (9–78) h,  $p = 0.02$ ; **Figure 3A**]. Furthermore, all instances of cardiac arrests occurring under HFNC before intubation were in Wuhan, and all the cases died. Mortality trended higher in patients treated in Wuhan than in those treated outside Wuhan (31 vs. 12%,  $p = 0.07$ ; **Figure 3B**).

## DISCUSSION

In this study, we found the ROX index had a high predictive value to identify HFNC failure when it was measured within the first 24 h of HFNC therapy. Hospitals in Wuhan, as a resource-limited area, had similar HFNC failure rates but higher mortality than those centers outside Wuhan.

Several studies have reported the use of HFNC in COVID-19 patients (Geng et al., 2020; Wang et al., 2020; Chandel et al., 2020; Hu et al., 2020; Xu et al., 2020a). These studies showed that the rates of HFNC failure were between 38 and 45%, which agreed with the failure rate in our study (44%). We further explored if the resource limitation impacted the patients' outcomes and found that resource limitation was associated with increased mortality. Although HFNC appeared feasible and successful in about half of the patients in a setting with adequate resources, monitoring of the ROX index may enable early identification of patients who are likely to require intubation; conversely, the use of HFNC in resource-limited settings without sufficient monitoring and delayed intubation may be associated with poor outcome, especially among those patients who were intubated at the last minute.

Prior to the COVID-19 pandemic, the ROX index showed high discriminative power to predict HFNC failure in hypoxemic patients (Roca et al., 2016). Recently, this team validated the ROX index in five ICUs in Spain and France (Roca et al., 2019). In our study, we have confirmed that the efficacy of the ROX index can be served as a predictor of HFNC failure among patients with COVID-19. The ROX index showed high discriminative values to predict HFNC failure within 24 h of HFNC use (at 1, 2, 4, 8, 12, and 24 h after HFNC initiation). As the variables required to calculate the ROX index are easy to obtain, even in the resource-limited area, it may be helpful for the physicians to early identify patients with a high likelihood of success and those who will require escalation therapy. Apart from the ROX index, the advanced age, increased SOFA score, and decreased platelets were also reported to be associated with increased HFNC failure (Hu et al., 2020; Xu et al., 2020a). As such, the combined use of these variables and the ROX index might help improve the predictive accuracy.

The surge of patients largely overloaded the healthcare workers and challenged medical resources (Cesari and Proietti, 2020; Solnica et al., 2020; Vergano et al., 2020). In China, most of the COVID-19 patients were in Wuhan. The duration from HFNC initiation to intubation for cases in Wuhan was longer than that outside Wuhan, and four cases with cardiac arrest during HFNC therapy all occurred in Wuhan. The present study did not record the reasons for this difference in duration from HFNC initiation to intubation, but it may indicate that delayed intubation occurred in Wuhan possibly because of lack of life-saving device resources or the overwhelmed staff. This might have contributed to the increased mortality observed in Wuhan compared with the mortality in patients outside Wuhan. Intensive monitoring during HFNC therapy is needed to avoid such delay in escalation therapy, such as awake prone positioning, NIV, or IMV (Tu et al., 2020; Xu et al., 2020b). As the ROX is easily obtained, it can be used to improve the management of COVID-19 patients in resource-limited circumstances to rapidly identify patients who will require escalation therapy, and thus, anticipate the required resources or plan the patient transfer.

Among the patients with COVID-19, Chandel et al. explored the likelihood of death in hospitals among patients with early and late HFNC failure (Chandel et al., 2020). Although the sample size was larger than that of ours, it failed to find the difference between patients with early and late HFNC failure. In Chandel et al.'s study, the patients who required intubation within 48 h of HFNC were classified as early HFNC failure, in contrast to the late HFNC failure in which patients were intubated after 48 h of HFNC. This definition is unable to distinguish the duration of the hypoxemia, especially severe hypoxemia. A longer duration of hypoxemia was more likely to be associated with higher mortality. In our study, we classified the patients with and without resource limitation. The patients in resource-limited areas were bound to experience a longer duration of hypoxemia and delayed escalation care, which might explain the higher mortality in the resource-limited area.

This study has several limitations. First, only 43 patients (65%) were included in the multivariate analysis as some variables were missing due to retrospective design. And data imputation was not deemed feasible, given the small sample size. Consequently, it was not possible to combine several variables to predict HFNC failure with greater accuracy. Second, even though all the centers had built HFNC protocol and keeping SpO<sub>2</sub> above 93% was the goal, it is impossible to guarantee that the goal would be achieved all the time for all the patients, as the data points were not recorded minute by minute in the medical records. Third, delayed therapy may occur due to the bedside treating physician. Fourth, a lack of power may have resulted in the lack of statistically significant mortality between the patients with delayed intubation in Wuhan compared to those promptly intubated in the absence of resource limitation outside Wuhan. Last, HFNC gas flow settings were found to affect the ROX index (Mauri et al., 2019), due to room air entrainment when the gas flow is set below the patient inspiratory flow demand. As such, a constant gas flow setting might enable a more precise ROX index measurement but might not be feasible in a clinical study.

## CONCLUSION

ROX index, calculated by the ratio of SpO<sub>2</sub>/FiO<sub>2</sub> to the respiratory rate, is easily obtained at bedside and can be used to predict HFNC failure among the patients with COVID-19. It may be used to avoid delayed escalation care, which may otherwise occur in resource-limited areas.

## REFERENCES

- Alhazzani, W., Möller, M. H., Arabi, Y. M., Loeb, M., Gong, M. N., Fan, E., et al. (2020). Surviving sepsis campaign: guidelines on the management of critically ill adults with coronavirus disease 2019 (COVID-19). *Intensive Care Med.* 46, 854–887. doi:10.1007/s00134-020-06022-5
- Bhatraju, P. K., Ghassemieh, B. J., Nichols, M., Kim, R., Jerome, K. R., Nalla, A. K., et al. (2020). Covid-19 in critically ill patients in the seattle region—case series. *N. Engl. J. Med.* 382, 2012. doi:10.1056/NEJMoa2004500

## DATA AVAILABILITY STATEMENT

The raw data supporting the conclusions of this article will be made available by the authors, without undue reservation.

## ETHICS STATEMENT

The studies involving human participants were reviewed and approved by Guanggu district, the Maternal and Child Health Hospital of Hubei Province. Written informed consent for participation was not required for this study in accordance with the national legislation and the institutional requirements.

## AUTHOR CONTRIBUTIONS

JL and WZ conceived the study, and joined in study design, study management, data analysis, and manuscript preparation. JD participated in study design, study management, data analysis, data interpretation, and manuscript drafting. JZ, PD, ZN, RL, WX, GJ, and XS joined in study design and data collection. SE joined in data interpretation and manuscript preparation. All authors revised and approved the final version of the manuscript.

## FUNDING

This study was supported by Wenzhou's second batch of SARS-CoV-2 prevention and treatment emergency scientific research project (enterprise) (ZG2020008).

## ACKNOWLEDGMENTS

We thank all the staff for participating in data collection.

## SUPPLEMENTARY MATERIAL

The Supplementary Material for this article can be found online at: <https://www.frontiersin.org/articles/10.3389/fmolb.2021.639100/full#supplementary-material>.

- Cesari, M., and Proietti, M. (2020). COVID-19 in Italy: ageism and decision making in a pandemic. *J. Am. Med. Dir. Assoc.* 21, 576–577. doi:10.1016/j.jamda.2020.03.025
- Chandel, A., Patolia, S., Brown, A. W., Collins, A. C., Sahjwani, D., Khangoora, V., et al. (2020). High-flow nasal cannula in COVID-19: outcomes of application and examination of the ROX index to predict success. *Respir. Care* 66, respcare.08631. doi:10.4187/respcare.08631
- Critical care committee of Chinese Association of Chest Physician (2020). [Conventional respiratory support therapy for severe acute respiratory infections (SARI): clinical indications and nosocomial infection prevention and control]. *Zhonghua Jie He He Hu Xi Za Zhi* 43, 189–194. doi:10.3760/cma.j.issn.1001-0939.2020.03.010



- Gattinoni, L., Coppola, S., Cressoni, M., Busana, M., Rossi, S., and Chiumello, D. (2020a). Covid-19 does not lead to a “typical” acute respiratory distress syndrome. *Am. J. Respir. Crit. Care Med.* 201, 1299. doi:10.1164/rccm.202003-0817LE
- Gattinoni, L., Chiumello, D., Caironi, P., Busana, M., Romitti, F., Brazzi, L., et al. (2020b). COVID-19 pneumonia: different respiratory treatments for different phenotypes?. *Intensive Care Med.* 46, 1099. doi:10.1007/s00134-020-06033-2
- Geng, S., Mei, Q., Zhu, C., Yang, T., Yang, Y., Fang, X., et al. (2020). High flow nasal cannula is a good treatment option for COVID-19. *Heart Lung* 49 (5), 444–445. doi:10.1016/j.hrtlng.2020.03.018
- Hu, M., Zhou, Q., Zheng, R., Li, X., Ling, J., Chen, Y., et al. (2020). Application of high-flow nasal cannula in hypoxemic patients with COVID-19: a retrospective cohort study. *BMC Pulm. Med.* 20, 324. doi:10.1186/s12890-020-01354-w
- Hui, D. S., Chow, B. K., Lo, T., Tsang, O. T. Y., Ko, F. W., Ng, S. S., et al. (2019). Exhaled air dispersion during high-flow nasal cannula therapy versus CPAP via different masks. *Eur. Respir. J.* 53. doi:10.1183/13993003.02339-2018
- Kang, B. J., Koh, Y., Lim, C. M., Huh, J. W., Baek, S., Han, M., et al. (2015). Failure of high-flow nasal cannula therapy may delay intubation and increase mortality. *Intensive Care Med.* 41, 623–632. doi:10.1007/s00134-015-3693-5
- Li, J., Fink, J. B., and Ehrmann, S. (2020a). High-flow nasal cannula for COVID-19 patients: low risk of bio-aerosol dispersion. *Eur. Respir. J.* 55, 2000892. doi:10.1183/13993003.00892-2020
- Li, J., Jing, G., and Scott, J. B. (2020b). Year in review 2019: high-flow nasal cannula oxygen therapy for adult subjects. *Respir. Care* 65, 545–557. doi:10.4187/respcare.07663
- Mauri, T., Carlesso, E., Spinelli, E., Turrini, C., Corte, F. D., Russo, R., et al. (2019). Increasing support by nasal high flow acutely modifies the rox index in hypoxemic patients: a physiologic study. *J. Crit. Care* 53, 183–185. doi:10.1016/j.jcrc.2019.06.020
- Nishimura, M. (2016). High-flow nasal cannula oxygen therapy in adults: physiological benefits, indication, clinical benefits, and adverse effects. *Respir. Care* 61, 529–541. doi:10.4187/respcare.04577
- Respiratory and Critical Care Medicine Group of Chinese Thoracic Society (2019). [Expert consensus of high flow nasal cannula oxygen therapy on clinical application regularity]. *Zhonghua Jie He He Hu Xi Za Zhi* 42, 83–91. doi:10.3760/cma.j.issn.1001-0939.2019.02.003
- Roca, O., Caralt, B., Messika, J., Samper, M., Sztrymf, B., Hernández, G., et al. (2019). An index combining respiratory rate and oxygenation to predict outcome of nasal high-flow therapy. *Am. J. Respir. Crit. Care Med.* 199, 1368–1376. doi:10.1164/rccm.201803-0589OC
- Roca, O., Messika, J., Caralt, B., García-de-Acila, M., Sztrymf, B., Ricard, J. D., et al. (2016). Predicting success of high-flow nasal cannula in pneumonia patients with hypoxemic respiratory failure: the utility of the ROX index. *J. Crit. Care* 35, 200–205. doi:10.1016/j.jcrc.2016.05.022
- Solnica, A., Barski, L., and Jotkowitz, A. (2020). Allocation of scarce resources during the COVID-19 pandemic: a Jewish ethical perspective. *J. Med. Ethics* 46, 444. doi:10.1136/medethics-2020-106242
- Sun, Q., Qiu, H., Huang, M., and Yang, Y. (2020). Lower mortality of COVID-19 by early recognition and intervention: experience from Jiangsu Province. *Ann. Intensive Care* 10, 33. doi:10.1186/s13613-020-00650-2
- Tu, G. W., Liao, Y. X., Li, Q. Y., Dong, H., Yang, L. Y., Zhang, X. Y., et al. (2020). Prone positioning in high-flow nasal cannula for COVID-19 patients with severe hypoxemia: a pilot study. *Ann. Transl. Med.* 8, 598. doi:10.21037/atm-20-3005
- Vergano, M., Bertolini, G., Giannini, A., Gristina, G. R., Livigni, S., Mistraretti, G., et al. (2020). Clinical ethics recommendations for the allocation of intensive care treatments in exceptional, resource-limited circumstances: the Italian perspective during the COVID-19 epidemic. *Crit. Care* 24, 165. doi:10.1186/s13054-020-02891-w
- Wang, K., Zhao, W., Li, J., Shu, W., and Duan, J. (2020). The experience of high-flow nasal cannula in hospitalized patients with 2019 novel coronavirus-infected pneumonia in two hospitals of Chongqing, China. *Ann. Intensive Care* 10, 37. doi:10.1186/s13613-020-00653-z
- WHO Coronavirus Disease Dashboard (2021). WHO Coronavirus Disease Dashboard. Available at: <https://arcg.is/XvuSX> (Accessed January 17, 2021).
- Wu, Z., and McGoogan, J. M. (2020). Characteristics of and important lessons from the coronavirus disease 2019 (COVID-19) outbreak in China. *JAMA* 323, 1239. doi:10.1001/jama.2020.2648
- Xu, J., Yang, X., Huang, C., Zou, X., Zhou, T., Pan, S., et al. (2020a). A novel risk-stratification models of the high-flow nasal cannula therapy in COVID-19 patients with hypoxemic respiratory failure. *Front. Med.* 7, 607821. doi:10.3389/fmed.2020.607821
- Xu, Q., Wang, T., Qin, X., Jie, Y., Zha, L., and Lu, W. (2020b). Early awake prone position combined with high-flow nasal oxygen therapy in severe COVID-19: a case series. *Crit. Care* 24, 250. doi:10.1186/s13054-020-02991-7
- Yang, X., Yu, Y., Xu, J., Shu, H., Xia, J., Liu, H., et al. (2020). Clinical course and outcomes of critically ill patients with SARS-CoV-2 pneumonia in Wuhan, China: a single-centered, retrospective, observational study. *Lancet Respir. Med.* 8 (5), 475–481. doi:10.1016/S2213-2600(20)30079-5
- Youden, W. J. (1950). Index for rating diagnostic tests. *Cancer* 3 (1), 32–35. doi:10.1002/1097-0142(1950)3:1<32::aid-cnrcr2820030106>3.0.co;2-3
- Yuan, X., Mu, J. S., Mo, G. X., Hu, X. S., Yan, P., and Xie, L. X. (2020). [Respiratory support for severe 2019-nCoV pneumonia suffering from acute respiratory failure: time and strategy]. *Zhonghua Jie He He Hu Xi Za Zhi* 43, 177–180. doi:10.3760/cma.j.issn.1001-0939.2020.03.006
- Ziehr, D. R., Alladina, J., Petri, C. R., Maley, J. H., Moskowitz, A., Medoff, B. D., et al. (2020). Respiratory pathophysiology of mechanically ventilated patients with COVID-19: a cohort study. *Am. J. Respir. Crit. Care Med.* 201, 1560. doi:10.1164/rccm.202004-1163LE

**Conflict of Interest:** JL declares receiving research funding from Fisher & Paykel Healthcare Ltd., Aerogen Ltd., and Rice Foundation and lecture honorarium from AARC and Fisher & Paykel Healthcare Ltd. SE reports consultancies from Aerogen Ltd., research support from Aerogen Ltd., Fisher & Paykel Healthcare, and Hamilton medical and travel reimbursements from Aerogen Ltd. and Fisher & Paykel. The companies had no role in the study design, data collection, analysis, preparation of the manuscript, or the decision to publish the findings.

The remaining authors declare that the research was conducted in the absence of any commercial or financial relationships that could be construed as a potential conflict of interest.

Copyright © 2021 Duan, Zeng, Deng, Ni, Lu, Xia, Jing, Su, Ehrmann, Zhang and Li. This is an open-access article distributed under the terms of the Creative Commons Attribution License (CC BY). The use, distribution or reproduction in other forums is permitted, provided the original author(s) and the copyright owner(s) are credited and that the original publication in this journal is cited, in accordance with accepted academic practice. No use, distribution or reproduction is permitted which does not comply with these terms.



# Administration Timing and Efficacy of Tocilizumab in Patients With COVID-19 and Elevated IL-6

Pan Li<sup>1,2†</sup>, Zhengmao Lu<sup>2,3†</sup>, Qiang Li<sup>2,4†</sup>, Zhenmeng Wang<sup>2,5</sup>, Yan Guo<sup>2,6</sup>, Chen Cai<sup>2,7</sup>, Shengyun Wang<sup>2,8</sup>, Peng Liu<sup>2,9</sup>, Xiaoping Su<sup>10</sup>, Yi Huang<sup>11</sup>, Yuchao Dong<sup>11</sup>, Wenjuan Qiu<sup>2,12</sup>, Yueming Ling<sup>2,13</sup>, Lonny Yarmus<sup>14</sup>, Fengming Luo<sup>15</sup>, Li Zeng<sup>2,16\*</sup>, Chong Bai<sup>11,\*</sup> and Wei Zhang<sup>2,11\*</sup>

## OPEN ACCESS

### Edited by:

Huahao Shen,  
Zhejiang University, China

### Reviewed by:

Salva Mena-Mollá,  
University of Valencia, Spain  
Alessandra Bettiol,  
University of Florence, Italy

### \*Correspondence:

Wei Zhang  
zhangweismmu@126.com  
Chong Bai  
bc7878@sohu.com  
Li Zeng  
Zengli111109@163.com

<sup>†</sup> These authors have contributed  
equally to this work and share first  
authorship

### Specialty section:

This article was submitted to  
Molecular Diagnostics  
and Therapeutics,  
a section of the journal  
Frontiers in Molecular Biosciences

**Received:** 10 January 2021

**Accepted:** 17 March 2021

**Published:** 15 April 2021

### Citation:

Li P, Lu Z, Li Q, Wang Z, Guo Y,  
Cai C, Wang S, Liu P, Su X, Huang Y,  
Dong Y, Qiu W, Ling Y, Yarmus L,  
Luo F, Zeng L, Bai C and Zhang W  
(2021) Administration Timing  
and Efficacy of Tocilizumab in Patients  
With COVID-19 and Elevated IL-6.  
Front. Mol. Biosci. 8:651662.  
doi: 10.3389/fmolb.2021.651662

<sup>1</sup> Department of Cardiology, Changhai Hospital, Second Military Medical University, Shanghai, China, <sup>2</sup> Department of Infection Diseases No. 1, The Maternal and Child Health Hospital of Hubei Province, Wuhan, China, <sup>3</sup> Department of Gastrointestinal Surgery, Changhai Hospital, Second Military Medical University, Shanghai, China, <sup>4</sup> Department of Neurosurgery, Changhai Hospital, Second Military Medical University, Shanghai, China, <sup>5</sup> Department of Anesthesia, Third Affiliated Hospital, Second Military Medical University, Shanghai, China, <sup>6</sup> Department of Endocrinology, Changhai Hospital, Second Military Medical University, Shanghai, China, <sup>7</sup> Department of Special Clinic, Changhai Hospital, Second Military Medical University, Shanghai, China, <sup>8</sup> Department of Emergency and Critical Care Medicine, Changzheng Hospital, Second Military Medical University, Shanghai, China, <sup>9</sup> Department of Colorectal Surgery, Changhai Hospital, Second Military Medical University, Shanghai, China, <sup>10</sup> School of Basic Medicine, Wenzhou Medical University, Wenzhou, China, <sup>11</sup> Department of Respiratory and Critical Care Medicine, Changhai Hospital, Second Military Medical University, Shanghai, China, <sup>12</sup> Department of Cardiovascular ICU, Changhai Hospital, Second Military Medical University, Shanghai, China, <sup>13</sup> Department of Clinical Laboratory Science of No. 910 Hospital of PLA Joint Support Force, Quanzhou, China, <sup>14</sup> Division of Pulmonary and Critical Care, Johns Hopkins University School of Medicine, Baltimore, MD, United States, <sup>15</sup> Department of Pulmonary and Critical Care Medicine, West China Hospital, Sichuan University, Chengdu, China, <sup>16</sup> Department of Organ Transplantation, Changhai Hospital, Second Military Medical University, Shanghai, China

**Background:** Tocilizumab (TCZ), an interleukin-6 receptor antibody, has previously been used for treating patients with the coronavirus disease 2019 (COVID-19), but there is a lack of data regarding the administration timing of TCZ.

**Objectives:** This study aimed to evaluate the timing and efficacy of TCZ in the treatment of patients with COVID-19.

**Methods:** Laboratory-confirmed patients with COVID-19 with an elevated interleukin-6 (IL-6) level (>10 pg/ml) were offered TCZ intravenously for compassionate use. Clinical characteristics, laboratory tests, and chest imaging before and after the administration of TCZ were retrospectively analyzed.

**Results:** A total of 58 consecutive patients who met the inclusion criteria and with no compliance to the exclusion criteria were included. Of these 58 patients, 39 patients received TCZ treatment, and 19 patients who declined TCZ treatment were used as the control cohort. In the TCZ-treatment group, 6 patients (15.4%) were in mild condition, 16 (41.0%) were in severe condition, and 17 (43.6%) were in critical condition. After TCZ treatment, the condition of 27 patients (69.2%) improved and 12 (30.8%) died. Compared with the improvement group, patients in the death group had higher baseline levels of IL-6 ( $P = 0.0191$ ) and procalcitonin (PCT) ( $P = 0.0003$ ) and lower lymphocyte percentage (LYM) ( $P = 0.0059$ ). Patients receiving TCZ treatment had better prognoses

than those without TCZ treatment ( $P = 0.0273$ ). Furthermore, patients with a baseline IL-6 level of  $\geq 100$  pg/ml in the TCZ-treatment group had poorer clinical outcomes than those with an IL-6 level of  $< 100$  pg/ml ( $P = 0.0051$ ).

**Conclusion:** The administration of TCZ in an early stage of cytokine storm (IL-6 level  $< 100$  pg/ml) may effectively improve the clinical prognosis of patients with COVID-19 by blocking the IL-6 signal pathway.

**Keywords:** cytokine storm, interleukin-6, SARS-CoV-2, tocilizumab (TCZ), coronavirus – COVID-19

## INTRODUCTION

Ever since the coronavirus disease 2019 (COVID-19) outbreak in December 2019, the disease rapidly continues to spread and has been declared a global pandemic (Wang et al., 2020). According to the real-time statistics released by Johns Hopkins University, the COVID-19 pandemic has led to 77,107,760 confirmed cases with a death toll of 1,696,995 worldwide, as of December 21, 2020. Although the reported incidence rate of COVID-19 is currently lower than that of SARS-CoV and MERS-CoV, the mortality rate among patients with severe COVID-19 is up to 60% (Arabi et al., 2020). More worrisome is the fact that the mechanisms of the underlying pathogenicity of COVID-19 are thus far not fully illustrated. This, in part, has resulted in limited specific antiviral treatments available for COVID-19.

During the SARS-CoV-2 epidemic, it was discovered that the immuno-pathological processes were involved in lung injury (Kuiken et al., 2003). In the biopsy samples of patients with SARS-CoV-2, extensive lung damage revealed the accumulation of monocytes, macrophages, and neutrophils in the lungs, resulting in elevated lung cytokine/chemokine levels (Moore and June, 2020). The levels of serum proinflammatory cytokines and chemokines were also found to increase in patients with COVID-19, including tumor necrosis factor  $\alpha$  (TNF- $\alpha$ ), interferon- $\gamma$  (IFN- $\gamma$ )-induced protein 10 (IP-10), interleukin-6 (IL-6), IL-8, and IL-10 (Chen N. et al., 2020; Huang et al., 2020). Therefore, the clinical deterioration of COVID-19 may partly result from the immunopathology induced by a hypercytokinemia or cytokine storm. Of note is that a large number of studies have shown that the levels of IL-6 were significantly higher in patients with severe COVID-19 as compared to those in uncomplicated individuals (Chen G. et al., 2020; Ye et al., 2020). These findings suggest that IL-6 might play a vital role in the severe deterioration of some patients.

Tocilizumab [TCZ, (Roche Pharma (Schweiz) Ltd., S20171024)], a human monoclonal antibody directed against IL-6, has been commonly used in the therapy of rheumatoid arthritis (RA) (Biggioggero et al., 2018). Recent studies have reported the benefit of TCZ in severely ill patients with COVID-19 (Luo et al., 2020; Stone et al., 2020; Xu et al., 2020). However, to our knowledge, the appropriate timing of the administration of TCZ in patients with COVID-19 is unknown. Herein, this study evaluated the efficacy and timing of the intravenous administration of TCZ for compassionate use in the treatment of patients with COVID-19.

## MATERIALS AND METHODS

### Study Design and Participants

This single-center retrospective cohort study was performed at the Guanggu district, the Maternal and Child Health Hospital of Hubei Province, China, which is a designated hospital for the treatment of patients with COVID-19. The study protocol was approved by the Medical Ethics Committee of the Maternal and Child Health Hospital of Hubei Province [FYGG (L)-2020-018].

From February 19, 2020 to April 7, 2020, consecutive patients with confirmed COVID-19 were evaluated for inclusion in this study. The inclusion criteria were as follows: (1) age  $\geq 18$  years; (2) nasal swab samples that were confirmed to be positive for SARS-CoV-2 nucleic acid by real-time reverse-transcriptase-PCR (RT-PCR) or for serum novel coronavirus-specific IgM and IgG antibodies; and (3) IL-6 level exceeding the upper limit of the normal value ( $> 10$  pg/ml). The exclusion criteria were as follows: (1) allergic reactions to TCZ or any adjuvant and (2) active inflammatory disease, such as hepatitis, tuberculosis, terminal tumor, or rheumatism immunity.

The diagnosis and severity stratification of COVID-19 were made based on the guidelines released by the National Health Commission of China (trial version 7) (National Health Commission, 2020). Patients with moderate or common type of COVID-19 having fever, dyspnea, and other symptoms with the manifestation of pneumonia seen in imaging data were diagnosed as mild cases; patients with respiratory frequency  $\geq 30$ /min, blood oxygen saturation  $\leq 93\%$  at room air, or  $\text{PaO}_2/\text{FiO}_2$  ratio  $\leq 300$  mmHg were defined as severe cases; and patients with respiratory failure requiring mechanical ventilation, shock, or other organ dysfunction/failure in addition to COVID-19 needing a stay in the intensive care unit (ICU) for treatment were diagnosed as critical cases. Comparison of the clinical characteristics among patients with COVID-19 treated with or without TCZ (Table 1) is a cohort study, while comparison between clinical characteristics of patients in the improvement group and in the death group after receiving TCZ (Table 2) is a case-control study.

### TCZ Treatment and Observation

Tocilizumab of 4–8 mg/kg, to a maximum dose of 800 mg, was intravenously administered once within 60 min of patients meeting the inclusion criteria. For patients who still had fever 24 h after the administration of the first dose, TCZ was

**TABLE 1** | Clinical characteristics of the enrolled patients with coronavirus disease 2019 (COVID-19) treated with or without tocilizumab (TCZ).

	Total (N = 58)	TCZ-treatment group (N = 39)	Non-TCZ treatment group (N = 19)	p-value
<b>Age, y</b>	73.9 ± 12.7	74.7 ± 13.4	72.3 ± 11.3	0.2812
<b>Gender, n (%)</b>				0.5685
Male	37 (63.8)	26 (66.7)	11 (57.9)	
Female	21 (36.2)	13 (33.3)	8 (42.1)	
<b>BMI</b>	24.1 ± 2.1	24.3 ± 2.1	23.6 ± 2.0	0.2027
<b>Type, n (%)</b>				0.2034
Mild	12 (20.7)	6 (15.4)	6 (31.6)	
Severe	20 (34.5)	16 (41.0)	4 (21.0)	
Critical	26 (44.8)	17 (43.6)	9 (47.4)	
<b>Symptoms, n (%)</b>				
Fever history	39 (67.2)	23 (59.0)	16 (84.2)	0.0756
Fever at admission (°C)	9 (15.5)	6 (15.4)	3 (15.8)	1.0000
Dyspnea	18 (31.0)	7 (18.0)	11 (57.9)	<b>0.0053</b>
Fatigue	30 (51.7)	18 (46.2)	12 (63.2)	0.2708
Muscle soreness	9 (15.5)	6 (15.4)	3 (15.8)	1.0000
Chills	8 (13.8)	4 (10.3)	4 (21.1)	0.4179
Cough	30 (51.7)	17 (43.6)	13 (68.4)	0.0973
Throat irritation	8 (13.8)	1 (2.6)	7 (36.8)	<b>0.0011</b>
<b>Presence of comorbidities, n (%)</b>				
Hypertension	32 (55.2)	18 (46.1)	14 (73.7)	0.0558
Diabetes	22 (37.9)	10 (25.6)	12 (63.2)	<b>0.0092</b>
CHD	18 (31.0)	10 (25.6)	8 (42.1)	0.2367
Cerebrovascular events	6 (10.3)	3 (7.7)	3 (15.8)	0.5894
COPD Renal insufficiency	7 (12.1) 5 (8.6)	4 (10.3) 2 (5.1)	3 (15.8) 3 (15.8)	0.6726 0.3179
Oxygen saturation%	92 (86–95)	90 (85.0–93.0)	92 (87–96)	0.6416
Systolic blood pressure (mmHg)	132 (120–155)	130 (120–155)	136 (125–156)	0.1587
Diastolic blood pressure (mmHg)	78.5 (70–88) 36.4 (36.2–36.8)	78 (69–86) 36.4 (36.2–36.9)	86 (74–90) 36.5 (36.2–36.6)	0.0861 0.9934
<b>Treatment</b>				
Antiviral treatment, n (%)	37 (63.8)	30 (76.9)	11 (57.9)	0.2181
Antibiotic treatment, n (%)	42 (72.4)	31 (79.5)	11 (57.9)	0.1190
Oxygen therapy				0.5801
Low-flow oxygen	24 (41.4)	14 (35.9)	10 (52.6)	
High-flow oxygen	10 (17.2) 9 (15.5) 15 (25.9)	7 (18.0) 6 (15.4) 12 (30.8)	3 (15.8) 3 (15.8) 3 (15.8)	
Invasive ventilation				
Glucocorticoid, n (%)	22 (37.9)	21 (53.9)	5 (26.3)	0.0558
<b>Laboratory characteristics</b>				
WBC (× 10 <sup>9</sup> /L)	7.4 (5.3–11.6)	6.4 (4.1–11.0)	10.9 (6.9–12.3)	<b>0.0170</b>
PCT (ng/ml)	0.13 (0.07–0.61)	0.09 (0.05–0.28)	0.20 (0.10–0.81)	0.0721
LDH (U/L)	291 (218–343)	285.5 (212–343)	287.5 (234–312)	0.9203
Lymphocyte count (× 10 <sup>9</sup> /L)	0.77 (0.45–1.02)	0.70 (0.44–0.93)	0.83 (0.53–1.36)	0.0635
Lymphocyte percentage (%)	8.7 (5.3–17.6)	9.7 (5.2–17.6)	7.6 (5.3–18.4)	0.9208
Hs-CRP (mg/L)	58.3 (24.4–116.8)	35.4 (9.1–92.8)	82.1 (25.5–101.9)	0.9406
IL-6 (pg/ml)	77.8 (34.1–302.0)	63.4 (36.4–129.7)	25.8 (29.8–82.6)	<b>0.0014</b>
D-dimer (mg/l)	3.7 (1.3–6.5)	2.9 (1.3–5.3)	4.3 (1.4–12.5)	0.3375

Three methods have been used for testing: the Wilcoxon rank-sum test for continuous variables, the Fisher's exact test for dichotomous variables, and the General Linear Model for categorical variables. All continuous variables were expressed as median (interquartile range [IQR]), except for age, which was represented as mean ± SD. CHD, coronary artery heart disease; COPD, chronic obstructive pulmonary disease; hs-CRP, high-sensitivity C-reactive protein; IL-6, interleukin-6; LDH, lactate dehydrogenase; PCT, procalcitonin; WBC, white blood cell. There was statistical difference in bold type.



**TABLE 2 |** Clinical characteristics of the patients with COVID-19 in the improvement group or the death group after receiving TCZ.

	Total (N = 39)	Improvement group (N = 27)	Death group (N = 12)	p-value
<b>Age, y</b>	74.7 ± 13.4	75.0 ± 12.3	73.8 ± 16.1	0.3413
<b>Gender, n (%)</b>				1.0000
Male	26 (66.7)	18 (66.7)	8 (66.7)	
Female	13 (33.3)	9 (33.3)	4 (33.3)	
<b>BMI</b>	24.3 ± 2.1	24.3 ± 2.3	24.3 ± 1.4	0.9747
<b>Type, n (%)</b>				0.0003
Mild	6 (15.4)	6 (22.2)	0	
Severe	16 (41.0)	15 (55.6)	1 (8.3)	
Critical	17 (43.6)	6 (22.2)	11 (91.7)	
<b>Symptoms, n (%)</b>				
Fever History	23 (59.0)	19 (70.4)	4 (33.3)	<b>0.0407</b>
Fever at admission (°C)	6 (15.4)	6 (22.2)	0	0.1508
Dyspnea	7 (18.0)	4 (14.8)	3 (25.0)	0.6536
Fatigue	18 (46.2)	12 (44.4)	6 (50.0)	1.0000
Muscle soreness	6 (15.4)	4 (14.8)	2 (16.7)	1.0000
Chills	4 (10.3)	3 (11.1)	1 (8.3)	1.0000
Cough	17 (43.6)	10 (37.0)	7 (58.3)	0.2994
Throat irritation	1 (2.6)	1 (3.7)	0	1.0000
<b>Presence of comorbidities, n (%)</b>				
Hypertension	18 (46.1)	14 (51.9)	4 (33.3)	0.3221
Diabetes	10 (25.6)	7 (25.9)	3 (25.0)	1.0000
CHD	10 (25.6)	7 (25.9)	3 (25.0)	1.0000
Cerebrovascular events	3 (7.7)	3 (11.1)	0	0.5391
COPD Renal insufficiency	4 (10.3) 2 (5.1)	4 (14.8) 1 (3.7)	0 1 (8.3)	0.2916 0.5263
Oxygen saturation%	90 (85.0–93.0)	92 (88.0–95.0)	86.5 (84.5–92.5)	0.0523
Systolic blood pressure (mmHg)	130 (120–155)	130 (120–155)	128 (120–154)	0.9392
Diastolic blood pressure (mmHg)	78 (69–86) 36.4 (36.2–36.9)	78 (69–84) 36.4 (36.2–36.9)	80 (66.5–88.5) 36.25 (36.15–36.85)	0.7839 0.2983
Body temperature (°C)				
<b>Treatment</b>				
Antiviral treatment, n (%)	30 (76.9)	21 (77.8)	9 (75.0)	1.0000
Antibiotic treatment, n (%)	31 (79.5)	20 (74.1)	11 (91.7)	0.3938
Oxygen therapy				0.0004
Low-flow oxygen	14 (35.9)	14 (51.9)	0	
High-flow oxygen	7 (18.0) 6 (15.4) 12 (30.8)	6 (22.2) 3 (11.1) 4 (14.8)	1 (8.3) 3 (25.0) 8 (66.7)	
Non-invasive ventilation				
Invasive ventilation				
Glucocorticoid, n (%)	21 (53.9)	11 (40.7)	10 (83.3)	<b>0.0180</b>
<b>Laboratory characteristics</b>				
WBC (× 10 <sup>9</sup> /L)	6.4 (4.1–11.0)	6.3 (4.1–8.8)	8.55 (4.9–12.3)	0.3377
PCT (ng/ml)	0.09 (0.05–0.28)	0.07 (0.05–0.11)	0.79 (0.16–1.88)	<b>0.0003</b>
LDH (U/L)	285.5 (212–343)	264.5 (192–310)	499.5 (412–614.5)	<b>0.0056</b>
Lymphocyte count (× 10 <sup>9</sup> /L)	0.7 (0.44–0.93)	0.71 (0.44–0.93)	0.65 (0.49–0.89)	0.9515
Lymphocyte percentage (%)	9.7 (5.2–17.6)	14.6 (6.8–20.5)	6.2 (3.0–7.1)	<b>0.0059</b>
Hs-CRP (mg/L)	35.4 (9.1–92.8)	24.4 (9.1–87.2)	54.7 (23.9–112.7)	0.1709
IL-6 (pg/ml)	63.4 (36.4–129.7)	53.2 (33.8–91.4)	140.4 (69.9–316.5)	<b>0.0191</b>
D-dimer (mg/L)	2.9 (1.3–5.3)	2.7 (1.0–5.1)	3.5 (1.6–6.5)	0.3381

The tests to determine the laboratory characteristics presented in **Table 2** were conducted at baseline. Three methods have been used for testing: the Wilcoxon rank-sum test for continuous variables, the Fisher's exact test for dichotomous variables, and the General Linear Model for categorical variables. All continuous variables were expressed as median [interquartile range (IQR)], except for age, which was represented as mean ± SD. CHD, coronary artery heart disease; COPD, chronic obstructive pulmonary disease; hs-CRP, high-sensitivity C-reactive protein; IL-6, interleukin-6; LDH, lactate dehydrogenase; PCT, procalcitonin; WBC, white blood cell. There was statistical difference in bold type.

readministered with an interval of  $\geq 12$  h between the two administrations. Other routine treatments such as antiviral, antibiotic, corticosteroid treatment, and oxygen therapy were continued as per physician discretion.

The clinical data including medical history, clinical symptoms, comorbidities, imaging data, treatment measures, and clinical outcomes were collected and analyzed. Laboratory examinations, including complete blood count, liver and renal function, IL-6 levels, high-sensitive C-reactive protein (hs-CRP), procalcitonin (PCT), myocardial enzymes, and coagulation analysis, were collected and analyzed. Elevated IL-6 level was defined to be  $>10$  pg/ml (Pylon immunoassay system); elevated hs-CRP was defined to be  $>10$  mg/L; and elevated PCT was defined to be  $>0.05$  ng/ml, as per the specifications of the manufacturer. The nasopharyngeal swab test for SARS-CoV-2 (Shanghai ZJ Bio-Tech Co., Ltd.) was performed when the patients were admitted to the isolation ward, and it was repeated twice with an interval of at least 24 h before discharge using RT-PCR.

## Statistical Analysis

All variables were expressed as the mean  $\pm$  SD or median (interquartile range [IQR]) or number (%). The Wilcoxon rank-sum test was used for continuous variables, the Fisher's exact test was used for dichotomous variables, and the general linear model was used for categorical variables. The Wilcoxon signed-rank test was used for paired data analysis before and after treatment with TCZ for both patients in the improvement group and those in the death group. The difference of median IL-6 and of median hs-CRP categorized by the outcomes and the difference of median lymphocyte (LYM) count categorized by the baseline IL-6 level were tested by using the Wilcoxon rank-sum test. The Kaplan–Meier methodology was used to estimate the probability of survival. The survival rate was compared between the groups treated with and without TCZ (IL-6, LYM%, hs-CRP, and PCT) using the log-rank test at the two-sided significance level. The multivariable Cox proportional-hazards model analysis was used to explore the role of TCZ in clinical outcomes when adjusted

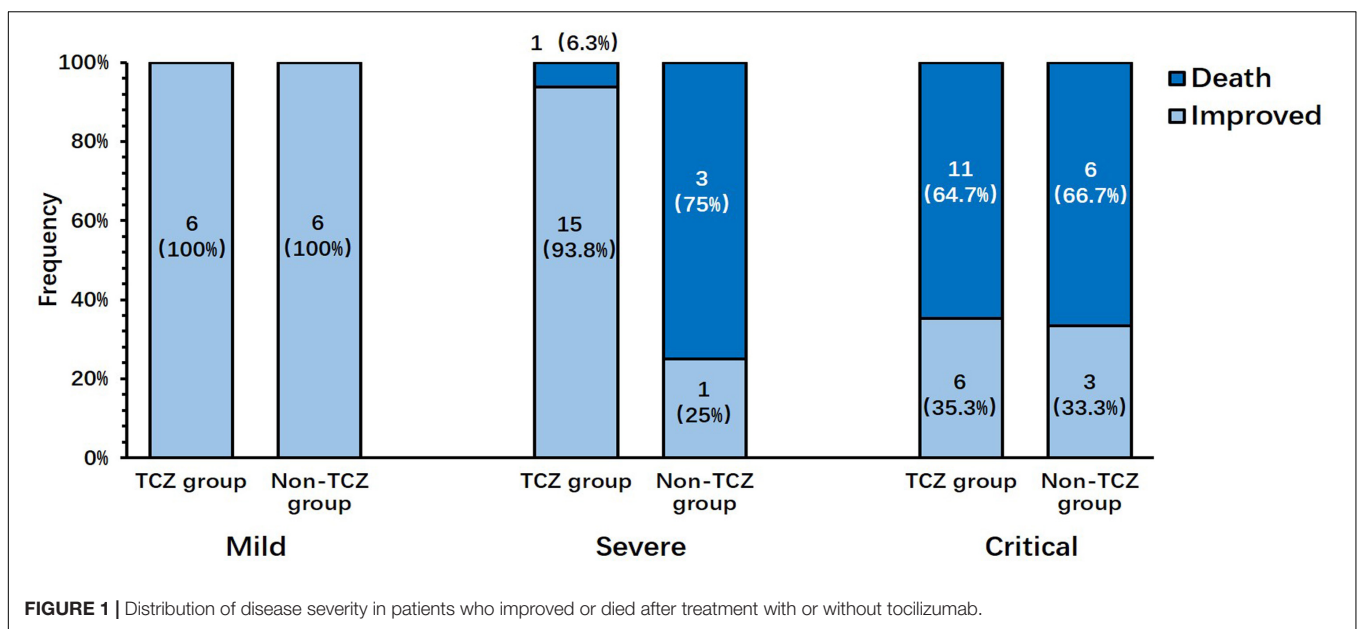
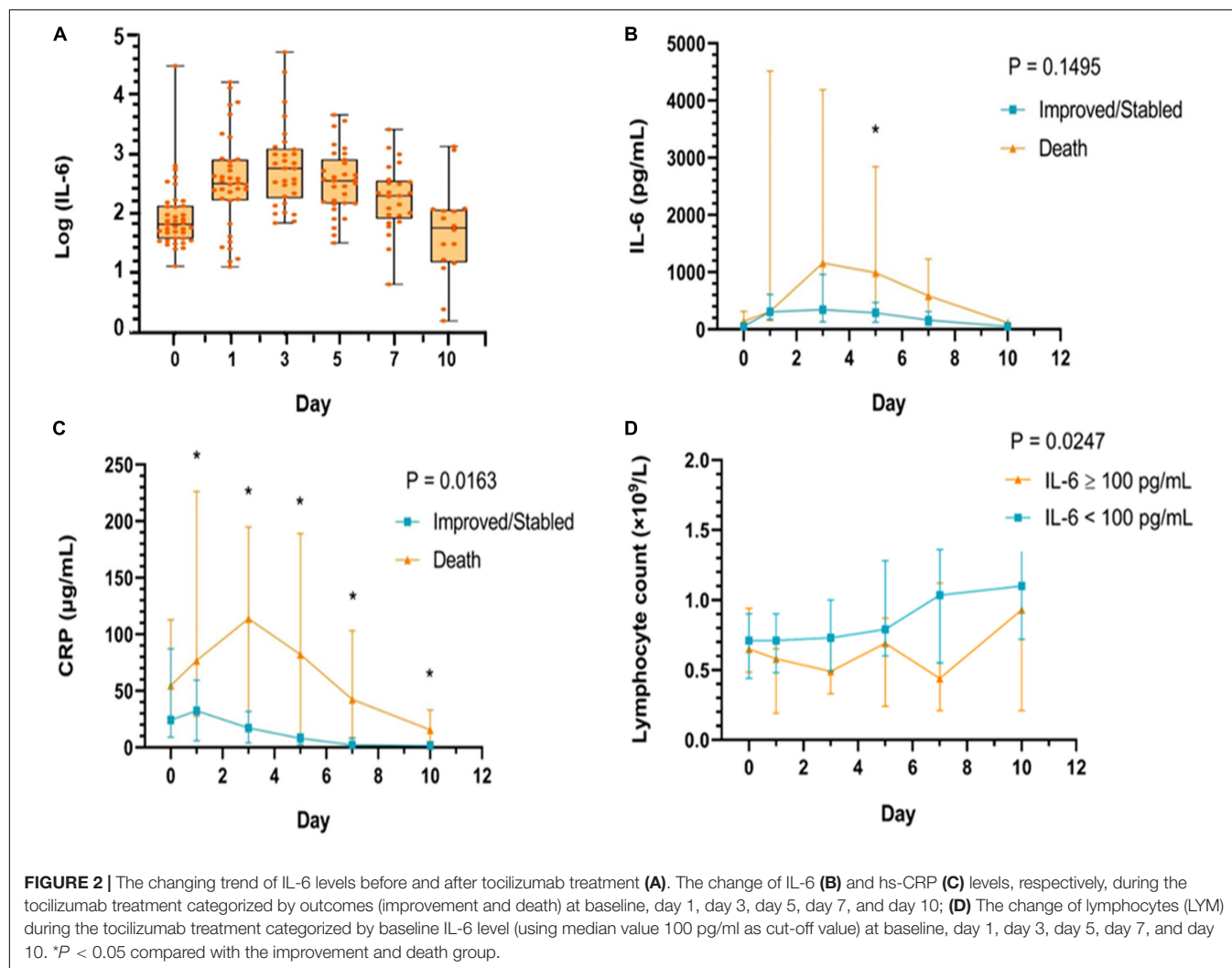


**TABLE 3 |** Laboratory tests before and after the administration of tocilizumab in the improvement group and the death group.

	Improvement group (N = 27)		p-value	Death group (N = 12)		p-value
	Before TCZ	After TCZ		Before TCZ	After TCZ	
WBC ( $\times 10^9/L$ )	6.3 (4.1–8.8)	4.8 (3.9–6.2)	0.0746	8.55 (4.9–12.3)	9.8 (4.6–14.0)	0.8311
PCT (ng/ml)	0.07 (0.05–0.11)	0.05 (0.04–0.06)	0.3088	0.79 (0.16–1.9)	1.75 (0.44–5.5)	0.3750
LDH (U/L)	264.5 (192–310)	219 (193–234)	<b>0.0096</b>	499 (412–614.5)	537 (488.5–626.5)	0.8750
Lymphocyte count ( $\times 10^9/L$ )	0.71 (0.44–0.93)	1.3 (1.1–1.5)	<b>&lt;0.0001</b>	0.65 (0.49–0.89)	0.265 (0.12–0.81)	<b>0.0269</b>
Lymphocyte percentage (%)	14.6 (6.8–20.5)	24.6 (15.9–29.9)	<b>&lt;0.0001</b>	6.15 (3.00–7.05)	7.05 (3.4–11.4)	1.0000
Hs-CRP (mg/L)	24.4 (9.07–87.2)	1.42 (0.56–5.06)	<b>&lt;0.0001</b>	54.7 (23.9–112.2)	20.67 (9.5–125.9)	0.7910
IL-6 (pg/ml)	53.2 (33.8–91.4)	110.5 (16.0–3327.1)	<b>0.0132</b>	140.4 (69.9–316.5)	1216 (584.9–3504.0)	<b>0.0059</b>
D-dimer (mg/L)	2.7 (1.0–5.1)	1.2 (0.73–2.7)	<b>&lt;0.0001</b>	3.51 (1.6–6.5)	10.17 (2.8–21.9)	<b>0.0371</b>
Oxygen saturation%	92 (88–95)	98 (97–99)	<b>&lt;0.0001</b>	86.5 (84.5–92.5)	85 (80–92.5)	0.6240

CHD, coronary artery heart disease; COPD, chronic obstructive pulmonary disease; hs-CRP, high-sensitive C-reactive protein; IL-6, interleukin-6; LDH, lactate dehydrogenase; PCT, procalcitonin; TCZ, tocilizumab; WBC, white blood cell. There was statistical difference in bold type.



for clinical covariates, including age, body mass index (BMI), diabetes, and glucocorticoid. Statistical analyses were performed using the SAS Studio version 3.7 software. A  $P$ -value of  $< 0.05$  was considered statistically significant.

## RESULTS

### Demographic Characteristics

Between February 19, 2020 and April 7, 2020, a total of 58 patients met the inclusion criteria, and no patients who met the exclusion criteria (Table 1) were screened. Of these 58 patients, 39 patients signed informed consent and received TCZ treatment and 19 patients, who declined TCZ treatment, were used as the control cohort. The majority of patients (37, 63.8%) were male, with a mean age of  $73.9 \pm 12.7$  years. There were 12 (20.7%) mild cases, 20 (34.5%) severe cases, and 26 (44.8%) critical cases. A total of 39 consecutive patients receiving TCZ treatment were divided into two groups: the improvement group (27 cases, 69.2%) and the death group (12 cases, 30.8%; Table 2). Six (22.2%) mild cases, 15 (55.6%) severe cases, and 6 (22.2%) critical cases were observed in

the improvement group; meanwhile, 1 (8.3%) severe case and 11 (91.7%) critical cases were present in the death group; no patients with mild cases were present in the death group ( $P = 0.0003$ ). The majority of patients (97.4%) received TCZ once. One patient (2.6%) received a second dose with the same dosage due to the occurrence of fever within 12 h. In contrast, patients in the non-TCZ treatment group had a higher death rate trend (9/19, 47.4%), especially those in the severe case group (3/4, 75%; Figure 1).

### Clinical Presentations and Safety

A total of 67.2% of the patients presented with fever at the onset, followed by fatigue (51.7%), dry cough (51.7%), dyspnea (31.0%), muscle soreness (15.5%), and chills (13.8%). Among patients treated with TCZ, no significant differences were found between the improvement group and the death group in terms of blood oxygen saturation, blood pressure, and body temperature at baseline. The most common comorbidity was hypertension (55.2%), followed by diabetes (37.0%), coronary heart disease (31.0%), tumor (20.7%), and chronic obstructive pulmonary disease (COPD) (12.1%). There was no difference in the incidence

of each comorbidity between the improvement group and the death group (all  $P > 0.05$ , **Table 1**).

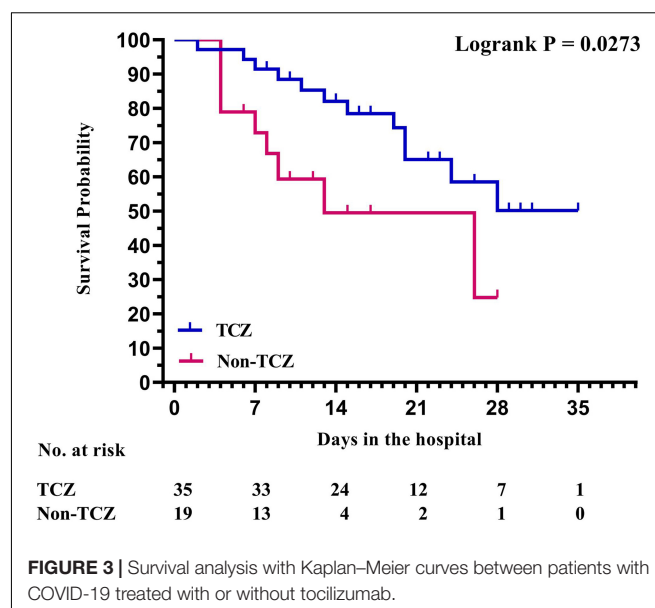
During the hospital stay, 83.3% of patients in the death group and 40.7% of patients in the improvement group received corticosteroids ( $P = 0.018$ , **Table 2**), but there was no difference in the proportion of corticosteroids administered between the TCZ- and the non-TCZ treatment groups. Patients in the death group received a higher rate of invasive ventilation than those in the improvement group ( $P = 0.0004$ , **Table 2**). No differences were observed between the death group and the improvement group on receiving other treatments. No adverse effects, such as rash, nausea, thrombocytopenia, neutropenia, and abnormal liver and kidney function, were observed after treatment with TCZ.

## Laboratory Examinations

At baseline, patients in the death group had a lower percentage of lymphocytes (6.2 [3.0–7.1]) in comparison to those in the improvement group (14.6 [6.8–20.5],  $P = 0.0059$ ). The values of inflammatory markers including PCT and IL-6 before the use of TCZ were significantly higher in the death group than in the improvement group (PCT: 0.79 [0.16–1.9] vs. 0.07 [0.05–0.11],  $P = 0.0003$ ; IL-6: 140.4 [69.9–316.5] vs. 53.2 [33.8–91.4],  $P = 0.0191$ ). After the treatment with TCZ, the level of lactate dehydrogenase (LDH), hs-CRP, IL-6, and D-dimer decreased significantly (all  $P < 0.05$ ) in the improvement group, while the lymphocyte count and the percentage of lymphocytes increased (all  $P < 0.05$ , **Table 3**). In contrast, in the death group, there was no significant improvement in the laboratory indexes after the use of TCZ.

The level of IL-6 observed after receiving TCZ treatment is shown in **Figure 2A**. From baseline, the level of IL-6 tended to increase on the first day after the use of TCZ and reached a peak on the third day, and then, it started to decrease on the fifth day and returned to baseline on the tenth day. However, the overall trend of the levels of IL-6 between patients in the improved group and those in the death group after TCZ treatment was not associated with the clinical outcome ( $P = 0.1495$ ). Also, there was no significant difference in the level of IL-6 between the groups at each time point (All  $P > 0.05$ ). After TCZ treatment, there was also a significant difference in hs-CRP levels within 10 days between patients in the improved and patients in the death group ( $P = 0.0163$ ), indicating that the overall trend of the levels of hs-CRP after TCZ treatment was associated with the clinical outcome (**Figure 2C**), whereas the overall trend of the levels of IL-6 was not (**Figure 2B**).

In addition, based on the cut-off value of 100 pg/ml for IL-6 at baseline (10 times the upper limit of normal; e.g., 10 pg/ml), all patients in the study were divided into two groups: patients with an IL-6 level of  $\geq 100$  pg/ml and patients with an IL-6 level of  $< 100$  pg/ml. The elevated trend of the level of lymphocytes was found in both groups after receiving TCZ, and there was a significant difference between the two groups ( $P = 0.0247$ , **Figure 2D**). The Kaplan–Meier curves showed that the survival rate of patients in the TCZ treatment group was significantly higher than that of patients in the non-TCZ treatment group ( $P = 0.0273$ , **Figure 3**). The multivariable Cox proportional-hazards model



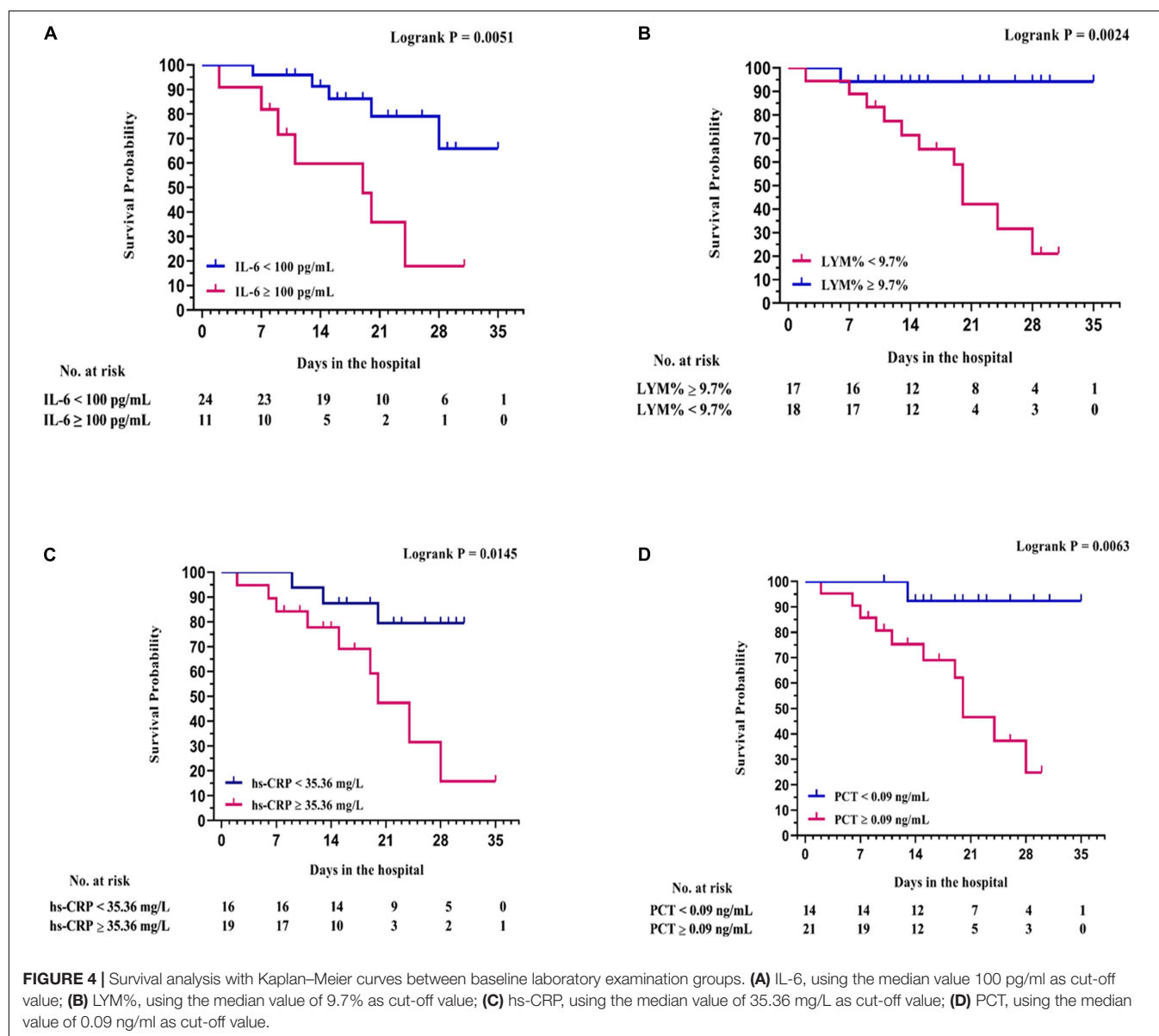
showed that TCZ was significantly associated with a lower risk of death (HR 0.383; 95% CI, 0.157 to 0.935;  $P = 0.035$ ; **Supplementary Figure 2**). Furthermore, for patients receiving TCZ, the survival rate of patients with an IL-6 baseline level  $\geq 100$  pg/ml was worse than that of the patients with an IL-6 level  $< 100$  pg/ml; similar findings were also observed in patients with LYM%  $< 9.7$ , hs-CRP  $> 35.36$  mg/L, and PCT  $\geq 0.09$  ng/ml (**Figure 4**).

## DISCUSSION

This is the first study assessing the optimal timing of intravenous TCZ in patients with COVID-19. The preliminary data presented in this paper showed that, among the 39 patients with COVID-19 who received TCZ treatment, the majority of patients (27, 69.2%) either improved or stabilized without obvious side effects. TCZ, in this cohort, exhibited a good clinical efficacy and safety profile. Twelve patients (30.8%) in this cohort that died after TCZ therapy during hospitalization showed significantly higher IL-6, PCT, and LDH levels and lower lymphocyte percentages at baseline than those with clinical improvement. Patients receiving TCZ treatment had more survival probability than those that did not receive TCZ treatment. IL-6 levels  $\geq 100$  pg/ml, hs-CRP levels  $\geq 35.56$  mg/L, PCT levels  $\geq 0.09$  ng/ml, and LYM%  $< 9.7\%$  were closely associated with poor prognoses after TCZ therapy. These findings collectively suggest that TCZ may be considered in the early stages of a cytokine storm (IL-6 level  $< 100$  pg/ml).

Lymphopenia is a common feature in patients with severe COVID-19 and is also a predictor of poor prognosis (Yang et al., 2020). Specifically, the number of T cells, B cells, and natural killer cells decreased dramatically, while the number of neutrophils increased significantly. A cytokine storm in coronavirus disease results in the formation of cytokines storm, indicating an increase





in proinflammatory cytokines, such as IL-6, IL-1 $\beta$ , IL-8, and IL-17; granulocyte colony-stimulating factor (G-CSF); granulocyte-macrophage colony-stimulating factor (GM-CSF); monocyte chemoattractant protein 1 (MCP-1); macrophage inflammatory protein-1 $\alpha$  (MIP-1 $\alpha$ ); and TNF- $\alpha$  (Cheung et al., 2005; Law et al., 2005). The abundant release of inflammatory cytokines may mediate acute respiratory distress syndrome (ARDS), leading to inflammatory cell infiltration and diffused alveolar damage within a short time. The cytokine storm can then cause further severe inflammatory damage to multiple organs, including the heart, liver, and kidney. The complex immune process induced by the SARS-CoV-2 could explain why some patients deteriorate suddenly at a later stage or during the recovery period (Special Expert Group for Control of the Epidemic of Novel Coronavirus Pneumonia of the Chinese Preventive Medicine Association, 2020).

Previous studies had reported that IL-6 positively correlated with the severity of COVID-19, with higher levels of IL-6 present in patients with severe and critical COVID-19 than those present in patients with common illness (Chen L. et al., 2020). IL-6 has a prominent proinflammatory effect through binding to the membrane-bound IL-6 receptor (mIL-6R) in a complex with gp130; on the other hand, IL-6-related downstream signal path is mediated by JAKs and STAT3 (Kang et al., 2019). An IL-6 antagonist may effectively reduce mortality in autoimmune diseases by inhibiting cytokine storms (Jones et al., 2011; Wolf et al., 2014). There is pre-existing evidence which suggests that TCZ can improve the clinical outcome in patients with severe and critical COVID-19 (Luo et al., 2020; Price et al., 2020; Toniati et al., 2020; Xu et al., 2020). In the current study, 27 patients (69.2%) who received TCZ had an obvious improvement of clinical symptoms, and the release of an *in vivo*

inflammatory response without toxicity or adverse reactions, such as peripheral blood leukocyte decrease or hepatic and renal function abnormality, was observed. The outcomes in the patient cohort in this study suggest that TCZ may be an effective and safe treatment option in patients with COVID-19 with cytokine storms.

Cytokine storm is a highly complex condition, showing an excessive immune response to external stimuli (Davidson et al., 2015). Once a cytokine storm forms during COVID-19 infection and reaches its peak, it may be refractory to treatment. Therefore, the timing of the administration of TCZ is an important factor that affected the prognosis of patients with severe and critical illnesses. In the current study, the rate of death (30.8%) after TCZ treatment is higher than previously reported data. The possible reasons are as follows: (1) the rate of critically ill patients with COVID-19 in the present study is almost 50%, which is higher than that in previously published reports (Xu et al., 2020: 19.0%; Luo et al., 2020: 26.7%; Toniati et al., 2020: 20%; Price et al., 2020: 25%); (2) patients in this study seemed to have a lower baseline oxygen saturation (median SpO<sub>2</sub> 90%) than those in the previous studies (SpO<sub>2</sub> range 91–99%) (Xu et al., 2020), suggesting that patients included in this study may be more seriously ill; (3) about 64.7% of critically ill patients in this study died after TCZ treatment, which suggests that later administration of TCZ in critically ill patients with evidence of an existing cytokine storm may be ineffective. Remarkably, of the 12 patients who died during the TCZ treatment, 58.3% patients had higher baseline levels of IL-6 than the cutoff value of 100 pg/ml; whereas, in the improvement group, only 18.5% patients had IL-6 levels above this cutoff value.

Compared to the TCZ treatment group, patients in the non-TCZ treatment group had a numerically higher death rate (47.4% vs. 30.8%) and were closely associated with a lower survival rate ( $P = 0.0273$ ), indicating the improvement effect of TCZ on the prognoses of patients with COVID-19. In particular, a significant improvement was observed in the majority of severe cases (55.6%) receiving TCZ treatment, whereas the improvement rate of severe cases was only 10% in the non-TCZ group. More importantly, the Kaplan–Meier survival curves showed that the baseline IL-6 level of  $\geq 100$  pg/ml was closely associated with poor prognosis after TCZ treatment whereas at different cutoff values for the IL-6 baseline level, including IL-6 baseline level  $\geq 30$  pg/ml vs.  $< 30$  pg/ml ( $P = 0.454$ ) and IL-6 baseline level  $\geq 50$  pg/ml vs.  $< 50$  pg/ml ( $P = 0.076$ ), both of them have no significant correlation with clinical prognosis (**Supplementary Figure 1**). Accordingly, we recommend that the suitable timing to administer TCZ in patients with COVID-19 is in the early stage of the cytokine storm and, in particular, when the baseline level of IL-6 is less than 100 pg/ml. The early use of TCZ may effectively prevent excessive inflammatory injury and improve the outcome of severely ill patients with COVID-19.

At present, there is no clear conclusion about the time of and dose of administration of TCZ. In this study, based on the guidelines released by the National Health Commission of China, the majority of patients with COVID-19 (97.4%) received TCZ (4–8 mg/kg) once and one patient (2.6%) received a second dose due to the occurrence of fever. The results

presented in this paper showed that the patients receiving TCZ treatment had better prognoses than those that did not receive TCZ treatment. Similarly, Xu et al. (2020) reported that TCZ (intravenous infusion of 400 mg) is an effective treatment for severely ill patients with COVID-19. Toniati et al. (2020) treated 100 patients with COVID-19 with TCZ at a dosage of 8 mg/kg (two consecutive intravenous infusions 12 h apart) and found that the treatment was associated with a clinical improvement in more than three-quarters of the patients. Moreover, Luo et al. (2020) suggested that repeated dose of the TCZ is recommended for critically ill patients with COVID-19 with elevated IL-6 levels. However, controversy remains as to whether the use of TCZ improves survival, shortens hospital stay, or reduces the need for mechanical ventilators. A randomized controlled study reported by Salama et al. (2021) demonstrated that TCZ reduced the likelihood of progression to mechanical ventilation or death by day 28 efficiently but that it did not improve the incidence of death from any cause. It appears that the timing of administration of TCZ is a critical factor that affects the prognosis.

The present study has several limitations. Previous data (Zhang et al., 2020) showed that D-dimer on admission could effectively predict the in-hospital mortality of patients with COVID-19. Although the improvement group had a numerically higher D-dimer level at baseline than that of the death group, no statistical difference was observed between the two groups, which may be due to the limited sample size in this study. Moreover, the results of a prospective meta-analysis (Sterne et al., 2020) showed that the administration of systemic corticosteroids among critically ill patients with COVID-19, compared with usual care or placebo, was associated with lower 28-day all-cause mortality. However, in the present study, there was no statistical difference in the use of corticosteroids between the improvement group and the death group after receiving TCZ. This study was conducted in the early stages of the COVID-19 epidemic, and there is a lack of clinical experience in the application of corticosteroids. We believe that the possible reason for the inconsistency of the results presented in this study compared with the reported data may be the different timing and dosages of glucocorticoids among the patients, as well as the limited sample size. Because this is a retrospective study, we did not compare the different dosages and the timing of administration of TCZ prospectively in this study. Therefore, the clinical practice value of the cutoff points of IL-6 in predicting the timing of TCZ administration needs further evaluation in future randomized controlled trials with large sample sizes and long-term clinical follow-up.

## CONCLUSION

This study suggests that TCZ may help to improve the prognosis of patients with COVID-19 with the baseline IL-6 level below the cutoff value of 100 pg/ml with an acceptable safety profile. Further clinical trials are required to confirm the observed findings and evaluate the efficacy of TCZ and its scope of clinical application and timing.

## DATA AVAILABILITY STATEMENT

The raw data supporting the conclusions of this article will be made available by the authors, without undue reservation.

## ETHICS STATEMENT

The studies involving human participants were reviewed and approved by the study protocol was approved by the Medical Ethics Committee of the Maternal and Child Health Hospital of Hubei Province [FYGG (L)-2020-018]. The patients/participants provided their written informed consent to participate in this study.

## AUTHOR CONTRIBUTIONS

PaL: data collection and writing. ZL: data collection and analysis. QL: data interpretation and analysis. ZW and WQ: literature search. YG and LY: manuscript preparation. CC: preparation of figures. SW: preparation of tables. PeL and YD: data interpretation. YH: literature search. YL: data collection. LZ: statistical analysis. CB: data analysis. WZ: study design and

writing the manuscript. All authors: contributed to the article and approved the submitted version.

## FUNDING

This study received the following funding: the San Hang Program of the Second Military Medical University; the Chinese Natural Science Foundation (81870356); and the Shanghai Rising-Star Program (20QA1409000).

## SUPPLEMENTARY MATERIAL

The Supplementary Material for this article can be found online at: <https://www.frontiersin.org/articles/10.3389/fmolb.2021.651662/full#supplementary-material>

**Supplementary Figure 1** | Survival analysis with Kaplan–Meier curves between baseline laboratory examination groups. **(A)** IL-6, using the median value of 30 pg/ml as cut-off value; **(B)** IL-6, using the median value of 50 pg/ml as cut-off value.

**Supplementary Figure 2** | Multivariable Cox proportional-hazards model analysis used to explore the role of tocilizumab on clinical outcomes when adjusted for clinical covariates, including age, Bmi, diabetes, and administration of glucocorticoids.

## REFERENCES

- Arabi, Y. M., Murthy, S., and Webb, S. (2020). Covid-19: a novel coronavirus and a novel challenge for critical care. *Intens. Care Med.* 46, 833–836. doi: 10.1007/s00134-020-05955-1
- Biggioggero, M., Crotti, C., Becciolini, A., and Favalli, E. G. (2018). Tocilizumab in the treatment of rheumatoid arthritis: an evidence-based review and patient selection. *Drug Des. Dev. Ther.* 13, 57–70. doi:10.2147/DDDT.S150580
- Chen, G., Wu, D., Guo, W., Cao, Y., Huang, D., Wang, H., et al. (2020). Clinical and immunological features of severe and moderate coronavirus disease 2019. *J. Clin. Invest.* 130, 2620–2629. doi: 10.1172/JCI137244
- Chen, L., Liu, H.-G., Liu, W., Liu, J., Liu, K., Shang, J., et al. (2020). Analysis of clinical features of 29 patients with 2019 novel coronavirus pneumonia. *Chin. J. Tuberc. Respir. Dis.* 43, 203–208.
- Chen, N., Zhou, M., Dong, X., Qu, J., Gong, F., Han, Y., et al. (2020). Epidemiological and clinical characteristics of 99 cases of 2019 novel coronavirus pneumonia in Wuhan, China: a descriptive study. *Lancet* 395, 507–513. doi: 10.1016/S0140-6736(20)30211-7
- Cheung, C. Y., Poon, L. L., Ng, I. H., Luk, W., Sia, S. F., Wu, M. H., et al. (2005). Cytokine responses in severe acute respiratory syndrome coronavirus-infected macrophages in vitro: possible relevance to pathogenesis. *J. Virol.* 79, 7819–7826. doi: 10.1128/JVI.79.12.7819-7826.2005
- Davidson, S., Maini, M. K., and Wack, A. (2015). Disease-promoting effects of type I interferons in viral, bacterial, and coinfections. *J. Interf. Cytokine Res.* 35, 252–264. doi: 10.1089/jir.2014.0227
- Huang, C., Wang, Y., Li, X., Ren, L., Zhao, J., Hu, Y., et al. (2020). Clinical features of patients infected with 2019 novel coronavirus in Wuhan, China. *Lancet* 395, 497–506. doi: 10.1016/S0140-6736(20)30183-5
- Jones, S. A., Scheller, J., and Rose-John, S. (2011). Therapeutic strategies for the clinical blockade of IL-6/gp130 signaling. *J. Clin. Invest.* 121, 3375–3383. doi: 10.1172/JCI57158
- Kang, S., Tanaka, T., Narazaki, M., and Kishimoto, T. (2019). Targeting interleukin-6 signaling in clinic. *Immunity* 50, 1007–1023. doi: 10.1016/j.immuni.2019.03.026
- Kuiken, T., Fouchier, R. A. M., Schutten, M., Rimmelzwaan, G. F., van Amerongen, G., van Riel, D., et al. (2003). Newly discovered coronavirus as the primary cause of severe acute respiratory syndrome. *Lancet* 362, 263–270. doi: 10.1016/S0140-6736(03)13967-0
- Law, H. K., Cheung, C. Y., Ng, H. Y., Sia, S. F., Chan, Y. O., Luk, W., et al. (2005). Chemokine up-regulation in SARS-coronavirus-infected, monocyte-derived human dendritic cells. *Blood* 106, 2366–2374. doi: 10.1182/blood-2004-10-4166
- Luo, P., Liu, Y., Qiu, L., Liu, X., Liu, D., and Li, J. (2020). Tocilizumab treatment in COVID-19: a single center experience. *J. Med. Virol.* 92, 814–818. doi: 10.1002/jmv.25801
- Moore, J. B., and June, C. H. (2020). Cytokine release syndrome in severe COVID-19. *Science* 368, 473–474. doi: 10.1126/science.abb8925
- National Health Commission (2020). *Diagnosis and Treatment Protocol for Novel Coronavirus Pneumonia*. China NHCOTPSRO, 7th Interim Edn, Available online at: <http://www.nhc.gov.cn/yzygj/s7653p/202003/46c9294a7dfe4cef80dc7f5912eb1989/files/ce3e6945832a438eae415350a8ce964.pdf> (accessed March 3, 2020).
- Price, C. C., Altice, F. L., Shyr, Y., Koff, A., Pischel, L., Goshua, G., et al. (2020). Tocilizumab treatment for cytokine release syndrome in hospitalized COVID-19. *Chest* doi: 10.1016/j.chest.2020.06.006 [Epub ahead for print],
- Salama, C., Han, J., Yau, L., Reiss, W. G., Kramer, B., Neidhart, J. D., et al. (2021). Tocilizumab in patients hospitalized with Covid-19 pneumonia. *N. Engl. J. Med.* 384, 20–30. doi: 10.1056/NEJMoa2030340
- Special Expert Group for Control of the Epidemic of Novel Coronavirus Pneumonia of the Chinese Preventive Medicine Association (2020). An update on the epidemiological characteristics of novel Coronavirus pneumonia (COVID-19). *Chin. J. Epidemiol.* 41, 139–144.
- Sterne, J. A. C., Murthy, S., Diaz, J. V., Slutsky, A. S., Villar, J., Angus, D. C., et al. (2020). Association between administration of systemic corticosteroids and mortality among critically ill patients with COVID-19: a meta-analysis. *JAMA* 324, 1330–1341. doi: 10.1001/jama.2020.17023
- Stone, J. H., Frigault, M. J., Serling-Boyd, N. J., Fernandes, A. D., Harvey, L., Foulkes, A. S., et al. (2020). Efficacy of Tocilizumab in patients hospitalized with Covid-19. *N. Engl. J. Med.* 383, 2333–2344. doi: 10.1056/NEJMoa2028836

- Toniati, P., Piva, S., Cattalini, M., Garrafa, E., Regola, F., Castelli, F., et al. (2020). Tocilizumab for the treatment of severe COVID-19 pneumonia with hyperinflammatory syndrome and acute respiratory failure: a single center study of 100 patients in Brescia, Italy. *Autoimmun. Rev.* 19:102568. doi: 10.1016/j.autrev.2020.102568
- Wang, C., Horby, P. W., Hayden, F. G., and Gao, G. F. (2020). A novel coronavirus outbreak of global health concern. *Lancet* 395, 470–473. doi: 10.1016/S0140-6736(20)30185-9
- Wolf, J., Rose-John, S., and Garbers, C. (2014). Interleukin-6 and its receptors: a highly regulated and dynamic system. *Cytokine* 70, 11–20. doi: 10.1016/j.cyt.2014.05.024
- Xu, X., Han, M., Li, T., Sun, W., Wang, D., Fu, B., et al. (2020). Effective treatment of severe COVID-19 patients with tocilizumab. *Proc. Natl. Acad. Sci. U.S.A.* 117, 10970–10975. doi: 10.1073/pnas.2005615117
- Yang, X., Yu, Y., Xu, J., Shu, H., Xia, J., Liu, H., et al. (2020). Clinical course and outcomes of critically ill patients with SARS-CoV-2 pneumonia in Wuhan, China: a single-centered, retrospective, observational study. *Lancet Respir. Med.* 8, 475–481. doi: 10.1016/S2213-2600(20)30079-5
- Ye, Q., Wang, B., and Mao, J. (2020). The pathogenesis and treatment of the 'Cytokine Storm' in COVID-19. *J. Infect.* 80, 607–613. doi: 10.1016/j.jinf.2020.03.037
- Zhang, L., Yan, X., Fan, Q., Liu, H., Liu, X., Liu, Z., et al. (2020). D-dimer levels on admission to predict in-hospital mortality in patients with Covid-19. *J. Thromb. Haemost.* 18, 1324–1329. doi: 10.1111/jth.14859

**Conflict of Interest:** The authors declare that the research was conducted in the absence of any commercial or financial relationships that could be construed as a potential conflict of interest.

Copyright © 2021 Li, Lu, Li, Wang, Guo, Cai, Wang, Liu, Su, Huang, Dong, Qiu, Ling, Yarmus, Luo, Zeng, Bai and Zhang. This is an open-access article distributed under the terms of the Creative Commons Attribution License (CC BY). The use, distribution or reproduction in other forums is permitted, provided the original author(s) and the copyright owner(s) are credited and that the original publication in this journal is cited, in accordance with accepted academic practice. No use, distribution or reproduction is permitted which does not comply with these terms.





# Pharmacological Mechanisms Underlying the Anti-asthmatic Effects of Modified Guomin Decoction Determined by Network Pharmacology and Molecular Docking

Guishu Wang<sup>1,2†</sup>, Bo Zhou<sup>3†</sup>, Zheyi Wang<sup>1†</sup>, Yufeng Meng<sup>2</sup>, Yaqian Liu<sup>1</sup>, Xiaolin Yao<sup>4,5\*</sup> and Cuiling Feng<sup>2,5\*</sup>

## OPEN ACCESS

### Edited by:

Huahao Shen,  
Zhejiang University, China

### Reviewed by:

Zhihua Chen,  
Zhejiang University, China  
Kai Yang,

State Key Laboratory of Respiratory  
Diseases, First Affiliated Hospital  
of Guangzhou Medical University,  
China

### \*Correspondence:

Cuiling Feng  
fengcuiling@sina.com  
Xiaolin Yao  
yaoxiaolin@pku.edu.cn

<sup>†</sup> These authors have contributed  
equally to this work

### Specialty section:

This article was submitted to  
Molecular Diagnostics  
and Therapeutics,  
a section of the journal  
Frontiers in Molecular Biosciences

**Received:** 21 December 2020

**Accepted:** 29 March 2021

**Published:** 22 April 2021

### Citation:

Wang G, Zhou B, Wang Z,  
Meng Y, Liu Y, Yao X and Feng C  
(2021) Pharmacological Mechanisms  
Underlying the Anti-asthmatic Effects  
of Modified Guomin Decoction  
Determined by Network  
Pharmacology and Molecular  
Docking.  
Front. Mol. Biosci. 8:644561.  
doi: 10.3389/fmolb.2021.644561

<sup>1</sup> Dongzhimen Hospital Affiliated to Beijing University of Chinese Medicine, Beijing, China, <sup>2</sup> Department of TCM, Peking University People's Hospital, Beijing, China, <sup>3</sup> Xiyuan Hospital Affiliated to China Academy of Chinese Medical Sciences, Beijing, China, <sup>4</sup> Department of TCM, Peking University International Hospital, Beijing, China, <sup>5</sup> Department of Integration of Chinese and Western Medicine, School of Basic Medical Sciences, Peking University, Beijing, China

**Background:** Asthma is a chronic inflammatory disease characterized by Th2-predominant inflammation and airway remodeling. Modified Guo Min decoction (MGMD) has been an extensive practical strategy for allergic disorders in China. Although its potential anti-asthmatic activity has been reported, the exact mechanism of action of MGMD in asthma remains unexplored.

**Methods:** Network pharmacology approach was employed to predict the active components, potential targets, and molecular mechanism of MGMD for asthma treatment, including drug-likeness evaluation, oral bioavailability prediction, protein-protein interaction (PPI) network construction and analysis, Gene Ontology (GO) terms, and Reactome pathway annotation. Molecular docking was carried out to investigate interactions between active compounds and potential targets.

**Results:** A total of 92 active compounds and 72 anti-asthma targets of MGMD were selected for analysis. The GO enrichment analysis results indicated that the anti-asthmatic targets of MGMD mainly participate in inflammatory and in airway remodeling processes. The Reactome pathway analysis showed that MGMD prevents asthma mainly through regulation of the IL-4 and IL-13 signaling and the specialized pro-resolving mediators (SPMs) biosynthesis. Molecular docking results suggest that each bioactive compounds (quercetin, wogonin, luteolin, naringenin, and kaempferol) is capable to bind with STAT3, PTGS2, JUN, VEGFA, EGFR, and ALOX5.

**Conclusion:** This study revealed the active ingredients and potential molecular mechanism by which MGMD treatment is effective against airway inflammation and remodeling in asthma through regulating IL-4 and IL-13 signaling and SPMs biosynthesis.

**Keywords:** asthma, airway inflammation, airway remodeling, Chinese medicine, network pharmacology

## INTRODUCTION

Asthma is a globally prevalent chronic inflammatory pulmonary disease, with an estimated 358 million affected individuals (Soriano et al., 2017). Persistent airway inflammation is the hallmark of asthma, which is infiltrated eosinophils, T lymphocytes, mast cells, and release of pro-inflammatory cytokines and lipid mediators. Lipid mediators, such as specialized pro-resolving mediators (SPMs), play a decisive role in the resolution of inflammation in asthma (Schett and Neurath, 2018; Kytikova et al., 2019). Actions of SPMs generated from polyunsaturated fatty acids (PUFAs) include inhibition of eosinophil and neutrophil migration, and decrease of T helper 2 (Th2) cytokine production (e.g., IL-4, IL-5, and IL-13) (Barnig et al., 2018). SPMs are originated via lipoxygenase (LOX)-catalyzed reaction. SPMs include omega-6 PUFA arachidonic acid derived lipoxins, as well as omega-3 PUFA eicosapentaenoic acid (EPA) and docosahexaenoic acid (DHA) derived resolvins, protectins and maresins. Arachidonic acid also forms a range of pro-inflammatory mediators in asthma, such as prostaglandins via cyclooxygenase (COX)-2, and the leukotrienes via 5-LOX actions (Krishnamoorthy et al., 2018).

Airway remodeling is another key pathological features of asthma. It is characterized by thickening of basement membrane, goblet cell metaplasia, smooth muscle cell hyperplasia and hypertrophy, deposition of extracellular matrix proteins, vascular activation and angiogenesis (Jeffery, 2001; James and Wenzel, 2007). Synthesis of extracellular matrix components and collagen is promoted by epidermal growth factor (EGF) released by airway epithelial cells and TGF- $\beta$  produced by myofibroblasts (Flood-Page et al., 2003; Le Cras et al., 2011). Under the influence of airway epithelial cells-derived endothelial growth factor (VEGF)-A, angiogenesis allow for extravasation of more inflammatory cells (Lambrecht and Hammad, 2012).

Traditional Chinese medicine (TCM) has been used to treat allergic diseases in Asia for hundreds of years (Liu L. et al., 2018). “Guo Min” means allergy in Chinese and Guo Min decoction (GMD) is a compound recipe composed by herbs, that raised by a well-known Chinese physician, Zhu Shenyu (Zhu and Liang, 1985). GMD has been widely used for allergic diseases treatment in China (Tao et al., 2018). The Modified Guo Min decoction (MGMD) comprises Fang Feng (*Radix Saposhnikoviae divaricate*, FF), Wu Mei (*Fructus Mume*, WM), Wu Wei Zi (*Schisandra chinensis*, WWZ), Yin Chai Hu (*Radix Stellariae*, YCH), Qian Hu (*radix Peucedani*, QH), and Jie Geng (*Radix*

*Platycodi*, JG). Previous studies showed that prescriptions based on GMD increased the proportion of Th1 cells in the spleen tissue of asthmatic mice, reduced the Th2 subset of T cells, and balanced the number of Treg and Th17 cells (Qin et al., 2017). However, the therapeutic mechanisms of MGMD in asthma remain unclear. In this study, network pharmacology approach was used to explore the multi-components, multi-targets, and multi-pathways closely related to the anti-asthma effect of MGMD. The molecular docking method was also used to verify the binding of the active substance to the target of action to reveal and predict the efficacy of MGMD in asthma. The work scheme is shown in **Figure 1**.

## MATERIALS AND METHODS

### Active Compounds Collection

The compounds of MGMD were extracted from the HERB database<sup>1</sup> (Fang et al., 2020) and the encyclopedia of traditional Chinese medicine (ETCM)<sup>2</sup> (Xu et al., 2019). HERB contains a comprehensive list of 7263 TCM herbs and 49258 ingredients by integrating multiple TCM databases included SymMap (Wu et al., 2019), TCMID 2.0 (Huang et al., 2018), TCMSP 2.3 (Ru et al., 2014), and TCM-ID (Chen et al., 2006). Oral bioavailability (OB)  $\geq 30\%$  and drug-likeness (DL)  $\geq 0.18$  were set as the thresholds to screen the active compounds from the TCMSP<sup>3</sup>. The properties of the other ingredients collected from the HERB were retrieved from the Swiss absorption, distribution, metabolism, and excretion (ADME) database<sup>4</sup>. The SMILES format files of the compounds were obtained from the PubChem<sup>5</sup> database (Kim et al., 2019). The screening criterion for gastrointestinal GI absorption was set as high, and DL was satisfied with both “yes” at the same time (Daina et al., 2017). Active ingredients from ETCM were retrieved as DL Grading “Good” (Xu et al., 2019).

### Target Fishing

#### Identification of Predicted Targets of MGMD

The active ingredients in drugs exert their biological effects via molecular targets. The targets related to the active compounds presented in MGMD were searched from ETCM (Xu et al., 2019) and Similarity ensemble approach (SEA)<sup>6</sup> (Keiser et al., 2007). ETCM predicts targets by MedChem Studio and only outputs these targets with confidence score at least 0.8. The threshold of “human” and Tanimoto coefficients (Tc)  $> 0.57$  were set to filter results predicted by SEA. The key targets corresponding to the compounds in such six herbs were obtained.

### Building the Disease Target Database

Asthma-related targets were identified by integrating data from these databases: Comparative Toxicogenomics Database (CTD)<sup>7</sup>

**Abbreviations:** AD, anti-allergic decoction; ADME, absorption, distribution, metabolism, and excretion; ALOX5, arachidonate 5-lipoxygenase; BP, biological process; H-C-T, herb-compound-target; DHA, docosahexaenoic acid; DL, drug-likeness; FF, Fangfeng (*Saposhnikovia Radix*); EPA, Eicosapentaenoic acid; GO, Gene ontology; HL, Half-life; JG, Jiegeng (*Platycodon grandiflorus*); JUN, c-Jun NH2-terminal kinase; MGMD, Modified Guo Min decoction; MF, molecular function; OB, oral bioavailability; PPI, Protein-protein interaction; PUFA, polyunsaturated fatty acid; QH, Qianhu (*Peucedanum praeruptorum*); SPM, Specialized pro-resolving mediator; TCM, traditional Chinese medicine; TCMSP, traditional Chinese medicine system pharmacology database; VEGFA, vascular endothelial growth factor A; WM, Wumei (*Prunus mume*); WWZ, Wuweizi (*Schisandra chinensis*); YCH, Yinchaihu (*Stellaria dichotoma L. var. lanceolata* Bge).

<sup>1</sup><http://herb.ac.cn>

<sup>2</sup><http://www.tcmip.cn/ETCM/index.php/Home/Index/>

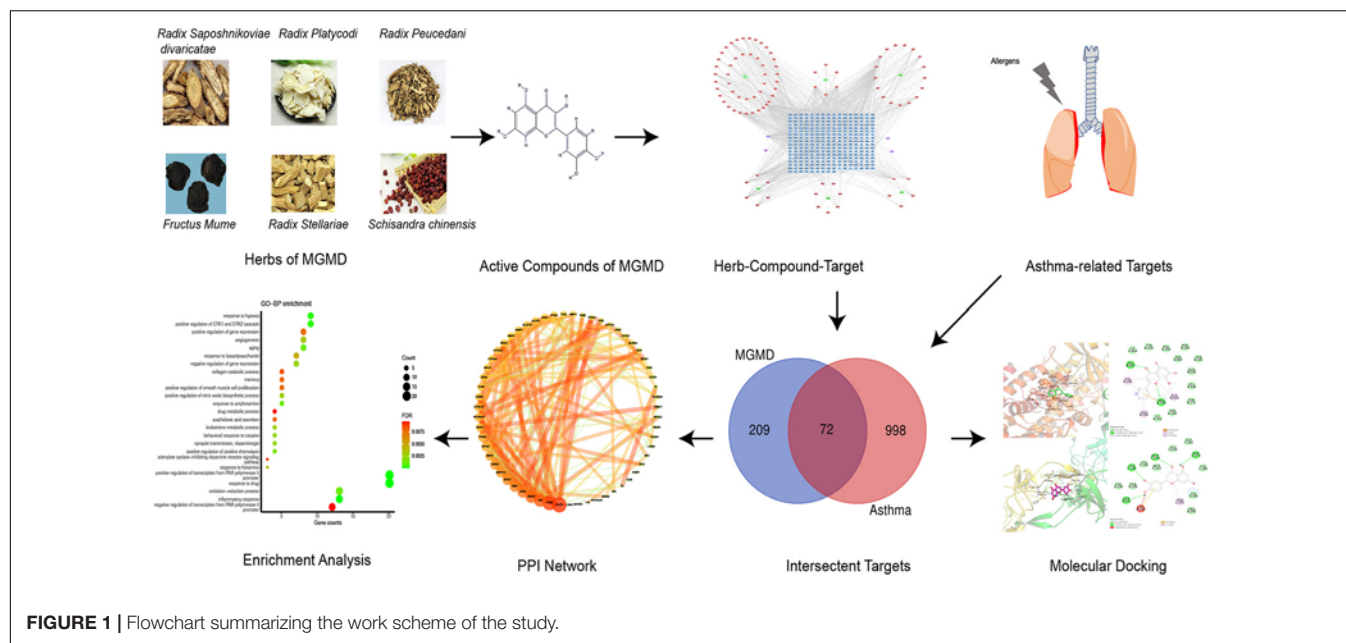
<sup>3</sup><http://tcmispw.com/tcmisp.php>

<sup>4</sup><http://www.swissadme.ch/>

<sup>5</sup><https://pubchem.ncbi.nlm.nih.gov/>

<sup>6</sup><http://sea.bkslab.org>

<sup>7</sup><http://ctdbase.org/>



(Grondin et al., 2018), Online Mendelian Inheritance in Man (OMIM)<sup>8</sup> (Amberger and Hamosh, 2017), and the Human Gene Database (GeneCards)<sup>9</sup> (Safran et al., 2010). For filtering the targets, “asthma” was defined as the key word and results were restricted to human genes/proteins. Targets with a relevance score above the median were selected in GeneCards database. The overlapping targets between MGMD and asthma were likely to be potential action targets of MGMD in the treatment of asthma.

### PPI Network Construction and Analysis

To obtain the data of protein–protein interaction (PPI), the candidate targets were inputted to STRING<sup>10</sup> with a minimum required interaction score > 0.7 and limited to “Homo sapiens” specie (von Mering et al., 2005). The visual network graphs were created by Cytoscape (version 3.7.1)<sup>11</sup>, an open-source software platform for visualizing complex networks (Shannon et al., 2003). The target interaction network parameters were calculated by NetworkAnalyzer.

Molecular Complex Detection (MCODE) of Cytoscape was used to searching the highly connected sub-networks in the PPI network. In the illustrations depicting MCODE results, a vertex-weighting-based scheme was used to identify local high-density areas in the graph. Density was generally defined based on the connection level of the graph (Bader and Hogue, 2003).

### Protein Functional Enrichment Analysis

To reveal the potential biological functions of MGMD in the treatment of asthma, functional enrichment analyses were performed by the Database for Annotation, Visualization and

Integrated Discovery (DAVID, v6.8)<sup>12</sup> and Reactome<sup>13</sup> (Fabregat et al., 2018). The results for Gene ontology (GO) biological processes (BPs) and Reactome pathway enrichment were saved and sorted by the adjusted *P* value corrected by the false discovery rate (FDR) algorithm for each term.

### Network Construction

To demonstrate the multi-compound therapeutic features of MGMD, network constructions were performed as follows: (1) herb-compound-target Network (H-C-T network) was constructed to explore the active compounds and their potential targets. The core compounds were obtained through the H-C-T network. (2) PPI networks were built to analyze the target interactions. Hub targets involved in MGMD treatment of asthma were selected from the PPI network. (3) BP sub-networks were established for classification analysis of BPs in MGMD treatment for asthma. (4) Target pathway network (T-P network) was constructed to show the functional pathways of MGMD for the therapy of asthma.

### Molecular Docking

Molecular docking was conducted to validate if MGMD's compounds could bind to these targets. The 2D structures of the top five core compounds were downloaded from the TCMSP database (Ru et al., 2014). The structures were added charge and displayed rotatable keys by AutoDock Tools (version 1.5.6). The protein crystal structures corresponding to the core target genes were downloaded from the Protein Data Bank database (PDB)<sup>14</sup> (Burley et al., 2017). Water and hetero molecules of the proteins were removed by Pymol. Hydrogen atoms and charge operations

<sup>8</sup><https://omim.org/>

<sup>9</sup><https://www.genecards.org/>

<sup>10</sup><http://string-db.org>

<sup>11</sup><http://www.cytoscape.org/>

<sup>12</sup><https://david.ncifcrf.gov/>

<sup>13</sup><https://reactome.org/>

<sup>14</sup><http://www1.rcsb.org/>



with 55, naringenin with 51, and kaempferol with 40. The properties of the H-C-T network were suitable for displaying complex ingredients, multiple targets, and close interactions between ingredients and targets. Detailed information about the active compounds and targets identified in MGMD is shown in **Supplementary Table 1**.

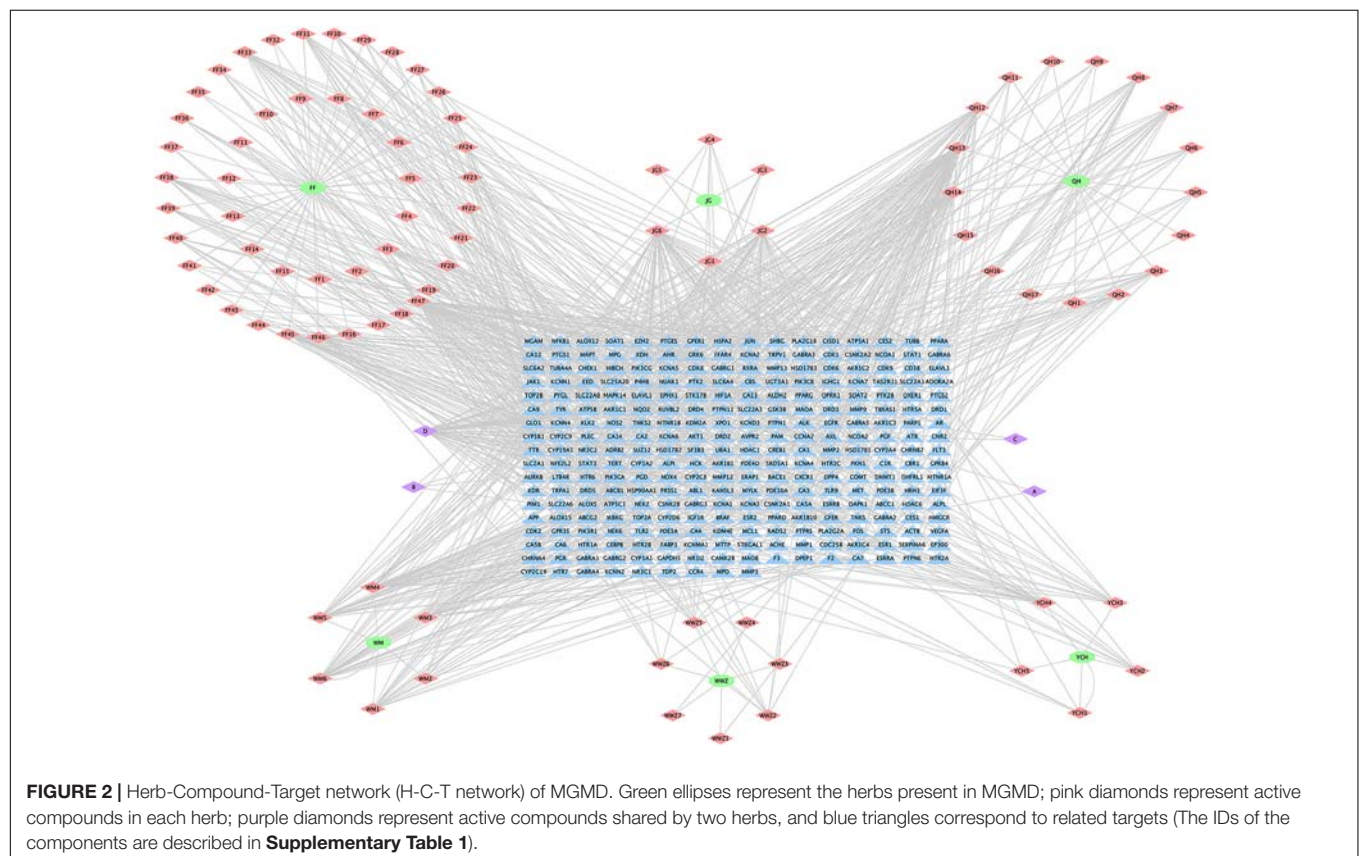
## Potential Asthma Targets

The targets for asthma were integrated from multi-source databases and a final list of 1,070 disease-related targets obtained after eliminating duplicates (**Supplementary Table 2**). 72 overlapping targets were identified as the key targets for studying the anti-asthmatic activity of the MGMD compounds (**Supplementary Table 3**).

## Analysis of the Network of Overlapping Targets

### Protein-Protein Interaction (PPI) Network

The STRING database was used to acquire PPI relationships of 72 potential protein targets of MGMD as related to the treatment of asthma. The visualized PPI network was constructed by Cytoscape 3.7.1, constructing by 72 nodes represented proteins and 205 edges represented the interactions between the proteins (**Figure 3A** and **Supplementary Table 4**). The average node degree value of the PPI network was 6.508. 28 protein targets had significantly higher node degree than the average in the PPI network, including STAT3, PTGS2,





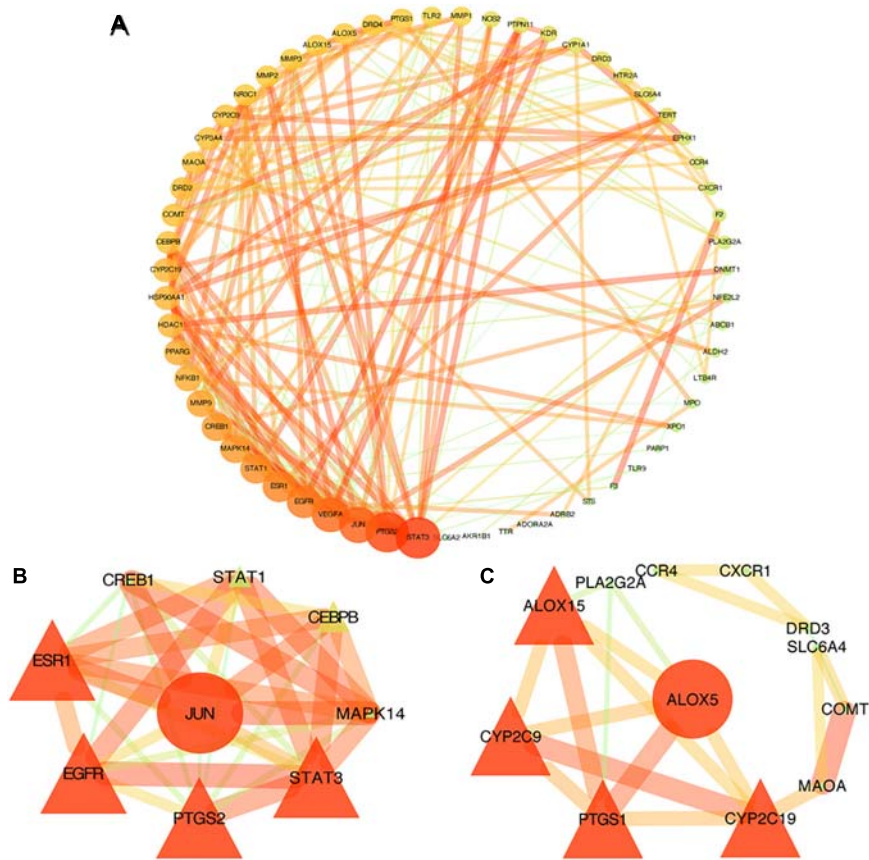


**FIGURE 3 |** PPI networks of MGMD for asthma treatment. Each node represents a protein target and each line represents the interaction between two nodes. Nodes in red are important and nodes in green are less important in the network. Panel (A) is the PPI network diagram arranged according to the df. Two clusters detected in the MGMD-asthma PPI network. Panels (B,C) show clusters 1 and 2, respectively. The ellipses are seed nodes of each cluster.

JUN, vascular endothelial growth factor A (VEGFA), EGFR, ESR1, STAT1, CREB1, MAPK14, MMP9, NFKB1, PPARG, CYP2C19, HDAC1, HSP90AA1, CYP3A4, COMT, MAOA, CYP2C9, DRD2, CEBPB, ALOX15, PTGS1, arachidonate 5-lipoxygenase (ALOX5), DRD4, NR3C1, MMP3, and MMP2. These 28 targets showed the preliminary relationships between active compound and potential protein targets of MGMD treatment in asthma.

### Clustering Analysis of the PPI Network

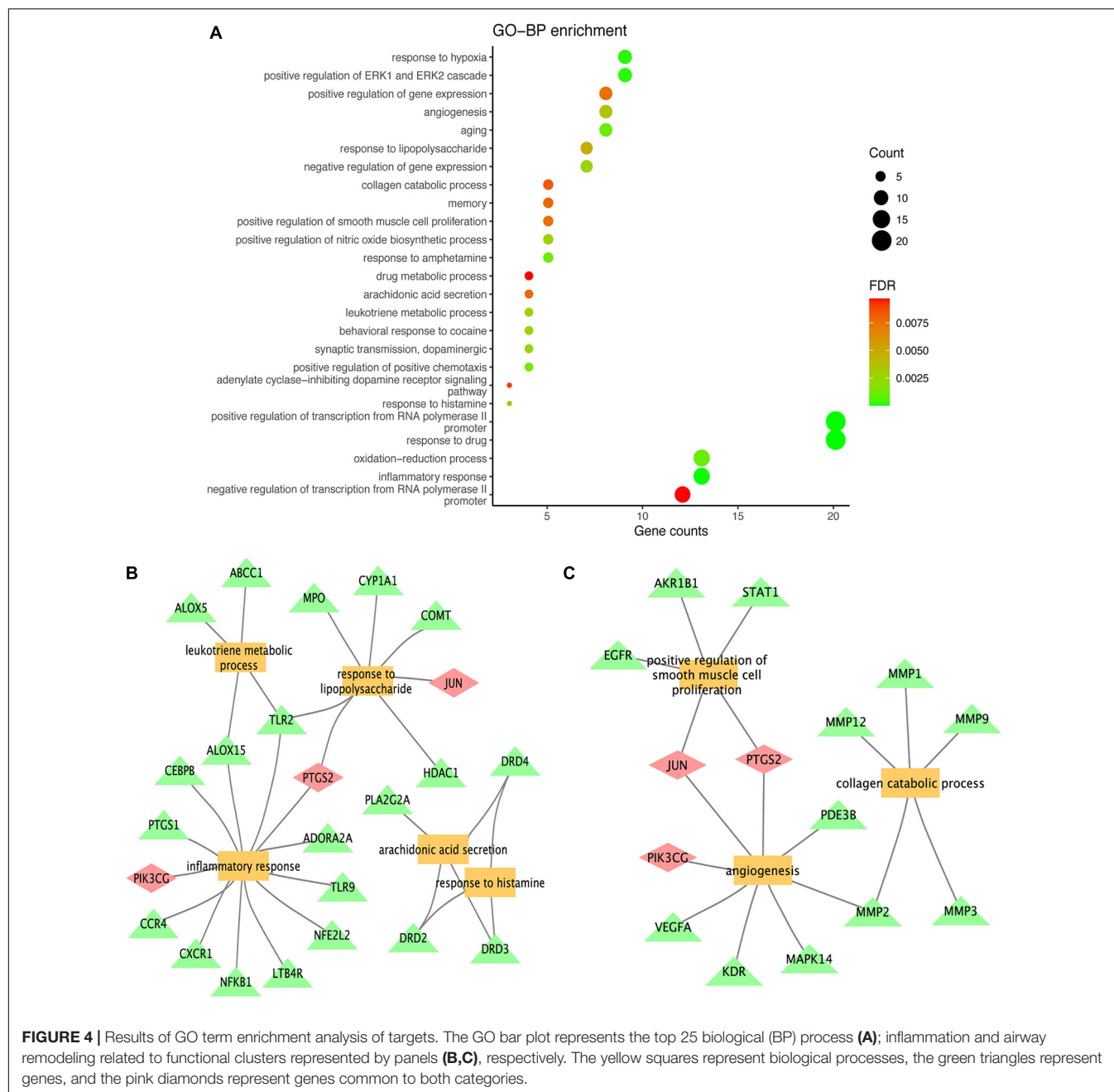
Similar function clusters of the PPI network were selected by MCODE analysis based on topology to find densely interconnected regions using Cytoscape software. 2 clusters of functional modules were detected ( $K\text{-core} = 4$ ) and the attribute values of the cluster were shown in **Figures 3B,C**.

Clusters in a PPI network are often protein complexes and parts of pathways, while clusters in a protein similarity network represent protein families. Cluster 1 comprised nine nodes and 33 edges with a score of 8.250 (**Figure 3B**). The seed node of this cluster was JUN (Jun proto-oncogene, also known as AP-1, cJUN, c-Jun), which involved in cell proliferation, differentiation, migration, transformation, and programmed cell death (Liu and Lin, 2007). Cluster 2 comprised 12 nodes

and 21 sides with a score of 3.818 (**Figure 3C**). The seed node of this cluster was ALOX5 (arachidonate 5-lipoxygenase, also known as 5-LO, 5-LOX), an essential enzyme in the metabolism of arachidonic acid, which initiates the biosynthesis of leukotrienes (Bruno et al., 2018). Leukotrienes are powerful immune-regulating lipid mediators with established pathogenic roles in asthma. The connected proteins of ALOX5 in cluster 2 participating in the biosynthetic pathways of SPMs (Barnig et al., 2018; Kytikova et al., 2019), such as ALOX15 (15-LOX), cytochrome P450 proteins CYP2C9 and CYP2C19, are among the 28 protein targets which had higher node degree than the average in our PPI network. Thus, the constructed PPI network and the further functional clustering both indicate that MGMD intervene asthma by regulating SPMs biosynthesis.

### GO Enrichment Analysis

To further explore the biological functions of the 72 potential targets of MGMD, GO enrichment analysis was constructed on DAVID website and obtained 76 terms ( $FDR < 0.05$ ) of BPs. We found the top 25 most enriched BP terms represented in a bubble chart (**Figure 4A** and **Supplementary Table 5**). BP analysis



revealed that the potential targets of MGMD were remarkably enriched in inflammation and airway remodeling.

As shown in **Figure 4B**, the potential targets of MGMD were involved in inflammatory response (GO ID: 0006954), response to lipopolysaccharide (GO ID: 0032496), leukotriene metabolic process (GO ID: 0006691), arachidonic acid secretion (GO ID: 0050482) and positive regulation of nitric oxide biosynthetic process (GO ID: 0045429). In addition, the BPs of airway remodeling were mainly enriched in positive regulation of smooth muscle cell proliferation (GO ID: 0048661), angiogenesis (GO ID: 0001525) and collagen catabolic process (GO ID: 0030574) (**Figure 4C**).

## Pathway Enrichment Analysis

Reactome pathway enrichment analysis obtained 123 items (FDR < 0.05) and the top 16 pathways at a significance threshold of FDR <  $10^{-5}$  were displayed (**Figure 5A** and **Table 1**). The pathways result was intensively enriched in SPMs biosynthesis and inflammatory and immune response, including arachidonic acid metabolism, metabolism of lipids, biosynthesis of EPA-derived SPMs, biosynthesis of DHA-derived SPMs, biosynthesis of DPA-n-3 SPMs, interleukin-4 and interleukin-13 signaling, and signaling by interleukins and immune system.

The T-P network showed the associations of the top 16 pathways with 75 nodes and 187 edges (**Figure 5B**). The results

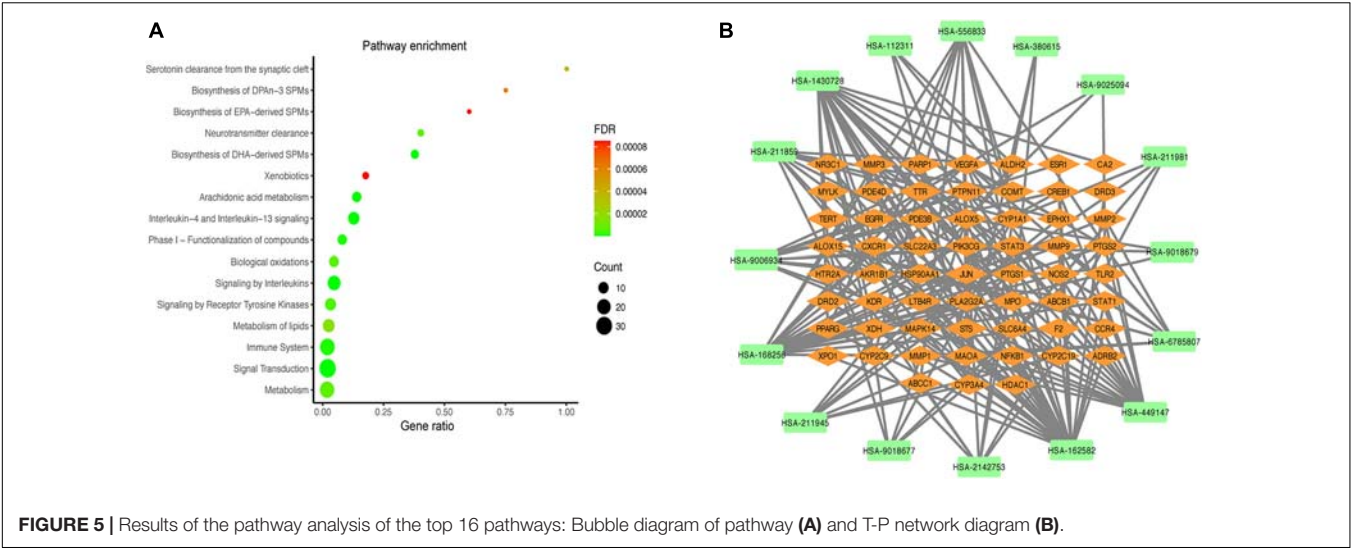


**TABLE 1 |** Information on enrichment analysis based on Reactome.

Term ID	Pathway	Counts	FDR	Genes
HSA-6785807	Interleukin-4 and Interleukin-13 signaling	13	2.47E-13	MMP2, STAT3, MMP3, MMP1, NOS2, HSP90AA1, MAOA, STAT1, PTGS2, MMP9, ALOX5, ALOX15, VEGFA
HSA-449147	Signaling by Interleukins	18	1.16E-11	MMP2, NFKB1, MAPK14, STAT3, MMP3, MMP1, NOS2, HSP90AA1, MAOA, PTPN11, STAT1, PTGS2, JUN, MMP9, ALOX5, CREB1, ALOX15, VEGFA
HSA-162582	Signal Transduction	33	4.72E-09	NFKB1, MAPK14, NR3C1, TTR, KDR, STAT3, EGFR, PDE3B, PPARG, CXCR1, MMP3, ADRB2, F2, TERT, CCR4, HSP90AA1, PTPN11, PDE4D, PIK3CG, MYLK, STAT1, DRD2, PARP1, JUN, MMP9, HDAC1, DRD3, LTB4R, XPO1, CREB1, ESR1, HTR2A, VEGFA
HSA-2142753	Arachidonic acid metabolism	8	1.49E-08	CYP2C9, PTGS1, PTGS2, CYP2C19, ALOX5, CYP1A1, ABCC1, ALOX15
HSA-9018677	Biosynthesis of DHA-derived SPMs	6	1.49E-08	CYP2C9, CYP3A4, PTGS2, ALOX5, CYP1A1, ALOX15
HSA-211945	Phase I - Functionalization of compounds	8	6.39E-07	CYP2C9, ALDH2, CYP3A4, MAOA, PTGS1, CYP2C19, CYP1A1, EPHX1
HSA-168256	Immune System	25	7.37E-07	MMP2, MPO, NFKB1, MAPK14, TTR, TLR2, STAT3, CXCR1, MMP3, F2, MMP1, NOS2, HSP90AA1, MAOA, PTPN11, STAT1, PTGS2, JUN, MMP9, ALOX5, XDH, PLA2G2A, CREB1, ALOX15, VEGFA
HSA-9006934	Signaling by Receptor Tyrosine Kinases	12	4.85E-06	MAPK14, KDR, STAT3, EGFR, PDE3B, HSP90AA1, PTPN11, STAT1, MMP9, CREB1, ESR1, VEGFA
HSA-211859	Biological oxidations	9	6.89E-06	CYP2C9, ALDH2, CYP3A4, MAOA, COMT, PTGS1, CYP2C19, CYP1A1, EPHX1
HSA-1430728	Metabolism	24	7.31E-06	STS, TTR, CYP2C9, ALDH2, SLC22A3, CA2, AKR1B1, PPARG, HSP90AA1, CYP3A4, MAOA, PIK3CG, COMT, PTGS1, PTGS2, CYP2C19, ALOX5, XDH, CYP1A1, ABCC1, PLA2G2A, ALOX15, ABCB1, EPHX1
HSA-112311	Neurotransmitter clearance	4	7.71E-06	SLC6A4, ALDH2, MAOA, COMT
HSA-556833	Metabolism of lipids	14	1.54E-05	STS, CYP2C9, AKR1B1, PPARG, CYP3A4, PIK3CG, PTGS1, PTGS2, CYP2C19, ALOX5, CYP1A1, ABCC1, PLA2G2A, ALOX15
HSA-380615	Serotonin clearance from the synaptic cleft	3	3.63E-05	SLC6A4, ALDH2, MAOA
HSA-9025094	Biosynthesis of DPAn-3 SPMs	3	5.97E-05	PTGS2, ALOX5, ALOX15
HSA-211981	Xenobiotics	4	8.52E-05	CYP2C9, CYP3A4, CYP2C19, CYP1A1
HSA-9018679	Biosynthesis of EPA-derived SPMs	3	8.52E-05	PTGS2, ALOX5, ALOX15

revealed that the active compounds of the MGMD had effects on asthma through regulating various pathways, in particular through improving airway inflammatory infiltration resulted from Th2 cytokine production and lipid mediators.

## Molecular Docking Verification of Core Compounds and Core Protein Targets

Furthermore, we verified the binding affinity between core compounds and protein targets of MGMD by molecular docking. As screened in H-C-T network, quercetin, wogonin, luteolin, naringenin, and kaempferol were the core compounds of MGMD. The hub protein targets were identified by top 5 node degree of PPI network and seed node of clusters, included STAT3, PTGS2, JUN, VEGFA, EGFR, and ALOX5.

The results obtained by the molecular docking software were shown in **Table 2**. The Grid box was centered to cover the active binding site and all essential residues. For the STAT3, grid box ( $126\text{\AA} \times 60\text{\AA} \times 126\text{\AA}$ ) centered at (0.233, 28.877, 33.555)  $\text{\AA}$ , for the PTGS2, grid box ( $76\text{\AA} \times 94\text{\AA} \times 90\text{\AA}$ ) centered at (33.269, -4.946, 7.759)  $\text{\AA}$ , for the JUN, grid box ( $90\text{\AA} \times 72\text{\AA} \times 70\text{\AA}$ ) centered at (-16.564, 23.05, 26.225)  $\text{\AA}$ , for the VEGFA, grid box ( $58\text{\AA} \times 40\text{\AA} \times 40\text{\AA}$ ) centered at (2.965, -4.946, 7.759)  $\text{\AA}$ , for

the EGFR, grid box ( $126\text{\AA} \times 126\text{\AA} \times 126\text{\AA}$ ) centered at (80.339, 11.821, 66.594)  $\text{\AA}$ , for the ALOX5, grid box ( $70\text{\AA} \times 90\text{\AA} \times 96\text{\AA}$ ) centered at (4.01, 45.829, 3.32)  $\text{\AA}$ . As seen from **Table 2**, the binding affinity for the five core compounds and protein crystal structures corresponding to the core target genes were all greater than -5 kcal/mol, indicating that the compound had a certain affinity for the protein crystal structure. Wogonin showed the high binding affinity of -8.8 kcal/mol in ALOX5, -6.2 kcal/mol in JUN and -6.2 kcal/mol in VEGFA. Luteolin showed the high binding affinity of -8.3 kcal/mol in EGFR, -9.3 kcal/mol in PTGS2 and -7.9 kcal/mol in STAT3. The small-molecule compounds were tightly bound to the protein residues via various interactions (**Figure 6** and **Table 2**).

## DISCUSSION

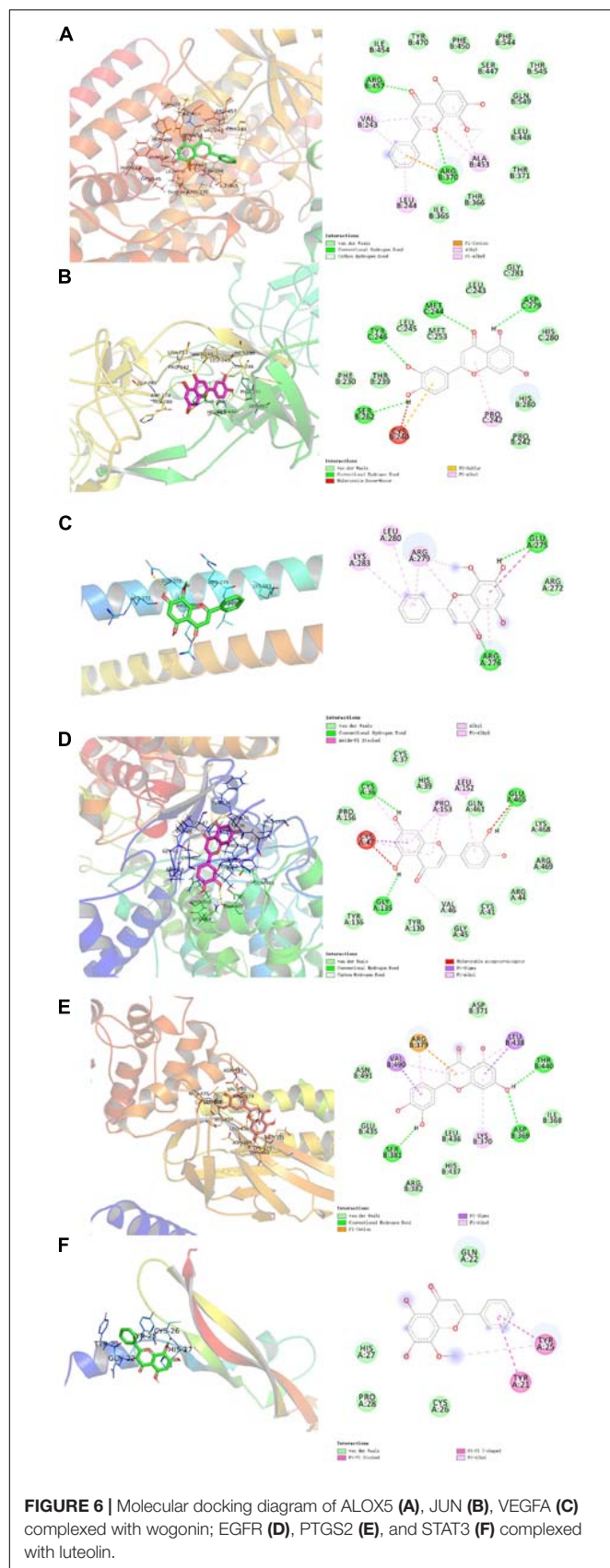
Asthma is a major public health challenge in China that affecting 45.7 million adults aged 20 years or older (Huang et al., 2019). TCM has a long history of clinical practice with available records, which provides a considerable number of classical herbal formulas widely used for disease treatment and represents a unique resource for drug development (Chao et al., 2017). Among the complex mixtures of compounds present in herbal medicines, unique combinations in the traditional complex formulas may exert major efficacy by targeting specific nodes of cellular signaling to intervene a specific chronic disease (Stermitz et al., 2000). Network pharmacology is used to study the intervention mechanism of drugs on diseases by constructing a biological interaction network (Yang et al., 2013). It systematically reveals the therapeutic effects of drugs on diseases from the interaction relationship between drugs, targets, and disease (Liu J. et al., 2018; Zhang et al., 2018). In a previous clinical study, we have found that MGMD had significant efficacy on respiratory symptoms (Zhang, 2016). To provide further insight of underlying mechanisms, we used the systematic pharmacology method and molecular docking to explore the potential molecular mechanism of the bioactive compounds.

We obtained 92 active compounds of MGMD from HERB, ECTM, SEA databases. A total of 72 putative anti-asthmatic targets of MGMD were selected by overlapping the targets between the MGMD-associated targets and the predicted asthma targets. According the H-C-T network topological analysis, we found the core compounds contained quercetin, wogonin, luteolin, naringenin, and kaempferol. Intriguingly, these compounds have all been reported to have therapeutic effects on inflammatory disease in previous studies. It had been demonstrated that all of the five core ingredients can reduce the allergic airway inflammation, inhibit levels of Th2 cytokine, including IL-4, IL-5, and IL-13, in OVA-sensitized and-challenged animals (Park et al., 2009; Shi et al., 2014; Bui et al., 2017; Jang et al., 2017; Molitorisova et al., 2021). Moreover, quercetin can inhibit human neutrophil elastase-induced MUC5AC expression in human airway epithelial cells through PKC/EGFR/ERK signal transduction pathway (Li et al., 2012). Both wogonin and luteolin had effect on reduction of airway mucus production (Lucas et al., 2015; Wang et al., 2021),

**TABLE 2 |** The binding energy values of core compounds of MGMD and core targets.

Target	Compounds	binding affinity/(kcal/mol)
STAT3(6tlc)	Quercetin	-7.5
	Wogonin	-7.5
	Luteolin	-7.9
	Naringenin	-7.3
	Kaempferol	-7.7
PTGS2(5lkr)	Quercetin	-9.1
	Wogonin	-8.9
	Luteolin	-9.3
	Naringenin	-9
	Kaempferol	-9
JUN(5T01)	Quercetin	-5.9
	Wogonin	-6.2
	Luteolin	-5.9
	Naringenin	-5.8
	Kaempferol	-6.2
VEGFA(4kzn)	Quercetin	-5.8
	Wogonin	-6.2
	Luteolin	-5.8
	Naringenin	-5.7
	Kaempferol	-6
EGFR(5wb7)	Quercetin	-7.9
	Wogonin	-7.9
	Luteolin	-8.3
	Naringenin	-7.4
	Kaempferol	-7.9
ALOX5(3o8y)	Quercetin	-8.3
	Wogonin	-8.8
	Luteolin	-8.5
	Naringenin	-8.3
	Kaempferol	-8.2



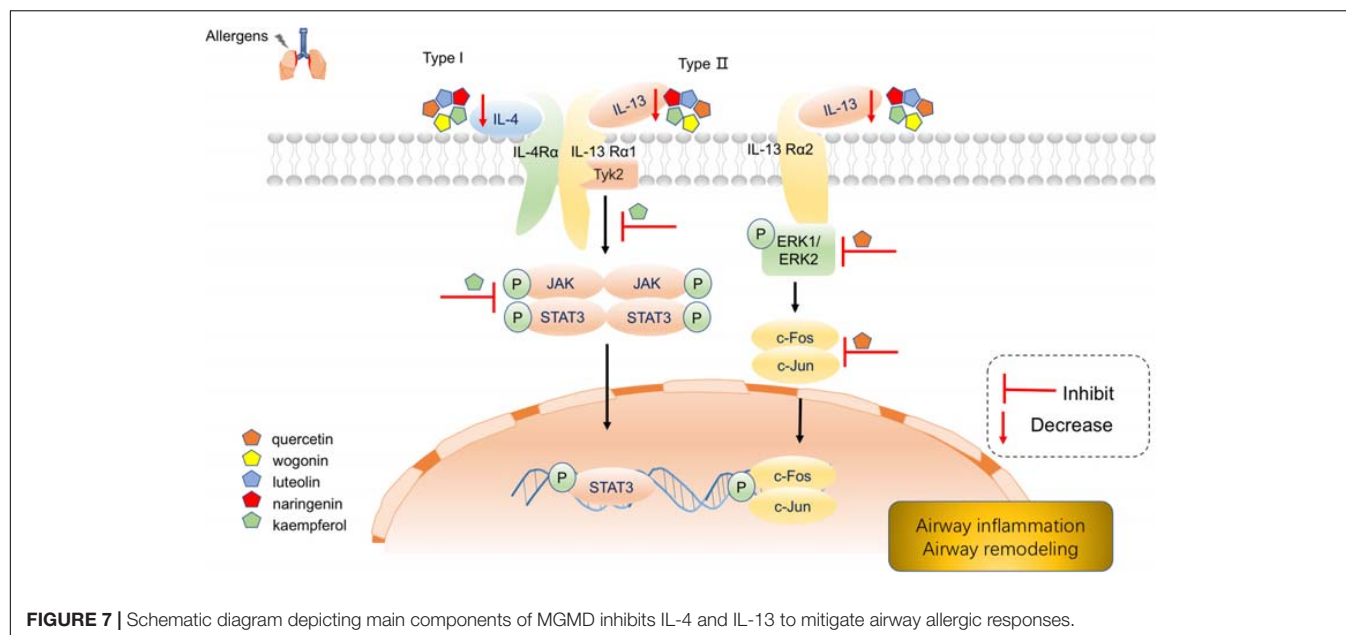


meanwhile luteolin can also decrease collagen deposition *in vivo* (Wang et al., 2021). In addition, it had reported that kaempferol alleviated airway inflammation through modulating Tyk2-STAT1/3 signaling responsive (Gong et al., 2013), and suppressed COX2 expression level in lung tissues in asthmatic mice (Kang et al., 2018). These previous studies suggest that MGMD is likely to decrease Th2 cytokine production in asthma mainly through compound of quercetin, wogonin, luteolin, naringenin, and kaempferol.

The PPI network was constructed by 72 potential targets of MGMD which were involved in asthma, and the network was further analyzed by MCODE clustering to explore the asthma related pathways. Our results suggested that the core potential targets of MGMD were intensively enriched in the pathways related to SPMs biosynthesis, including ALOX5 (5-LOX), ALOX15 (15-LOX), PTGS1 (COX1), PTGS2 (COX2), cytochrome P450 proteins CYP2C9 and CYP2C19, which play pivotal role in the resolution of inflammation in asthma (Schett and Neurath, 2018; Kytikova et al., 2019). 5-LOX is a crucial enzyme which helps in the conversion of arachidonic acid to leukotrienes. With the increasing number of indications for anti-leukotriene drugs, the development of 5-LOX inhibitor agents for asthma becomes increasingly important (Bruno et al., 2018; Sinha et al., 2019). Our results argue a potential that MGMD is a 5-LOX inhibitor for the treatment of asthma, in turn suggest a promising mechanism by which MGMD intervene asthma.

Furthermore, STAT3, JUN, EGFR, and VEGFA were also the core potential targets in our PPI network results. STAT3 and JUN are closely related to the pathological process of asthma (Simeone-Penney et al., 2007; Garcia-Menaya et al., 2019). STAT3 can induce gene expression of cytokines, chemokines, and adhesion molecules with an important role in directing the inflammatory response and act as a novel epithelial regulator of the allergic response by altering Th2 cell recruitment and effector function (Schumann et al., 1996; Simeone-Penney et al., 2007). JUN activation appears to be implicated in airway inflammation by contributing to regulate the expression of Th2 cytokines, chemokines, growth factors, and adhesion molecules, which is associated with several inflammation related disorders such as asthma and allergy (Haeggström and Funk, 2011). There are extensive studies focusing on the relation among EGFR, VEGFA and asthma pathophysiology, which describe airway remodeling, airway hypermucus secretion, as well as immunological responses of airway inflammation (Hoshino et al., 2001; Lee et al., 2004; Burgel and Nadel, 2008; Inoue et al., 2020). MGMD compounds may exert anti-inflammatory and anti-remodeling activity through regulating STAT3, JUN, EGFR, and VEGFA.

The GO enrichment results strengthen the evidence that candidate protein targets of MGMD are involved in airway inflammation and remodeling. The enriched BPs of anti-inflammatory in our results included inflammatory response, leukotriene metabolic process and arachidonic acid secretion, suggesting that MGMD could influenced the lipid mediators, both pro-inflammatory mediators and SPMs, to ameliorate the airway inflammation in asthma patients. Moreover, the typical airway remodeling processes, including positive regulation of



smooth muscle cell proliferation, angiogenesis and collagen catabolic process, were also enriched by MGMD related targets. Combined with the PPI network results, we propose that MGMD regulates SPMs biosynthesis by ALOX5 to reduce airway inflammation and relieve airway remodeling process by suppressing the EGFR and VEGFA signaling.

Our Reactome pathway enrichment results consistently argue that MGMD reduces allergic airway inflammation through the biosynthetic pathways of SPMs. Arachidonic acid metabolism, metabolism of lipids, biosynthesis of EPA-derived SPMs, biosynthesis of DHA-derived SPMs and biosynthesis of DPAn-3 SPMs were all enriched in Reactome pathway enrichment analysis. Additionally, interleukin-4 and interleukin-13 signaling, signaling by interleukins and immune system pathways were also enriched in our results. IL-4 and IL-13 are principal regulatory cytokines mainly secreted by activated Th2 cells, crucially important during the immune response in allergy and asthma (Nelms et al., 1999; Hershey, 2003). The receptors of allergic cytokines, including IL-4, IL-5, and IL-13, trigger the JAK/STAT pathway (Hsieh et al., 2011; Howell et al., 2018). Therefore, we propose that MGMD compounds targets the IL-4 and IL-13 pathway, which in turn activate transcription factors to modulate clinical symptoms of asthma (Figure 7).

According to the compound-target interaction analysis, six targets with higher degrees on the PPI network (STAT3, PTGS2, JUN, VEGFA, EGFR, and ALOX5) were identified. In our molecular docking analysis, the binding mode with the best docking score was selected to analyze the interaction between the protein receptor and its predicted active compounds. The docking scores of all compound-target pairs are lower than  $-5$  kcal/mol, indicating that each of the five core compounds (quercetin, wogonin, luteolin, naringenin, and kaempferol) has good binding affinity to all six targets. These results suggested that the core ingredients of MGMD could relieve airway

inflammation and remodeling through binding STAT3, PTGS2, JUN, VEGFA, EGFR, and ALOX5.

## CONCLUSION

On the ground of the above, network pharmacology strategy was presented to investigate the active compounds, potential anti-asthmatic targets and involved regulatory pathways in MGMD. Our results revealed the active ingredients and potential molecular mechanism by which MGMD treatment is effective against airway inflammation and remodeling in asthma through regulating IL-4 and IL-13 signaling and SPMs biosynthesis. These findings were partially validated previous studies. Our subsequent molecular docking showed that each bioactive compounds (quercetin, wogonin, luteolin, naringenin, and kaempferol) of MGMD has favorable binding abilities with STAT3, PTGS2, JUN, VEGFA, EGFR, and ALOX5, further arguing the potential molecular mechanism of action of MGMD in asthma. Our results will serve as a comprehensive reference for investigation of the mechanism by which MGMD intervene asthma.

## DATA AVAILABILITY STATEMENT

The datasets presented in this study can be found in online repositories. The names of the repository/repositories and accession number(s) can be found in the article/Supplementary Material.

## AUTHOR CONTRIBUTIONS

GW, BZ, and ZW: conceptualization. GW and BZ: methodology and visualization. BZ: software. GW and ZW: writing—original

draft preparation. BZ, YM, YL, and XY: writing–review and editing. XY and CF: supervision and project administration. All authors have read and agreed to the published version of the manuscript.

## FUNDING

This research was funded by the National Natural Science Foundation of China (No. 81673921 to CF and No. 81804015 to XY).

## REFERENCES

- Amberger, J. S., and Hamosh, A. (2017). Searching Online Mendelian Inheritance in Man (OMIM): a Knowledgebase of Human Genes and Genetic Phenotypes. *Curr. Protoc. Bioinformatics* 58, 1.2.1–1.2.12. doi: 10.1002/cpbi.27
- Bader, G. D., and Hogue, C. W. V. (2003). An automated method for finding molecular complexes in large protein interaction networks. *BMC Bioinformatics* 4:2. doi: 10.1186/1471-2105-4-2
- Barnig, C., Frossard, N., and Levy, B. D. (2018). Towards targeting resolution pathways of airway inflammation in asthma. *Pharmacol. Ther.* 186, 98–113. doi: 10.1016/j.pharmthera.2018.01.004
- Bruno, F., Spaziano, G., Liparulo, A., Roviezzo, F., Nabavi, S. M., Sureddi, A., et al. (2018). Recent advances in the search for novel 5-lipoxygenase inhibitors for the treatment of asthma. *Eur. J. Med. Chem.* 153, 65–72. doi: 10.1016/j.ejmech.2017.10.020
- Bui, T. T., Piao, C. H., Song, C. H., Lee, C.-H., Shin, H. S., and Chai, O. H. (2017). Baicalin, wogonin, and Scutellaria baicalensis ethanol extract alleviate ovalbumin-induced allergic airway inflammation and mast cell-mediated anaphylactic shock by regulation of Th1/Th2 imbalance and histamine release. *Anat. Cell Biol.* 50, 124–134. doi: 10.5115/acb.2017.50.2.124
- Burgel, P.-R., and Nadel, J. A. (2008). Epidermal growth factor receptor-mediated innate immune responses and their roles in airway diseases. *Eur. Respir. J.* 32, 1068–1081. doi: 10.1183/09031936.00172007
- Burley, S. K., Berman, H. M., Kleywegt, G. J., Markley, J. L., Nakamura, H., and Velankar, S. (2017). Protein Data Bank (PDB): the Single Global Macromolecular Structure Archive. *Methods Mol. Biol.* 1607, 627–641. doi: 10.1007/978-1-4939-7000-1\_26
- Chao, J., Dai, Y., Verpoorte, R., Lam, W., Cheng, Y.-C., Pao, L.-H., et al. (2017). Major achievements of evidence-based traditional Chinese medicine in treating major diseases. *Biochem. Pharmacol.* 139, 94–104. doi: 10.1016/j.bcp.2017.06.123
- Chen, X., Zhou, H., Liu, Y. B., Wang, J. F., Li, H., Ung, C. Y., et al. (2006). Database of traditional Chinese medicine and its application to studies of mechanism and to prescription validation. *Br. J. Pharmacol.* 149, 1092–1103. doi: 10.1038/sj.bjp.0706945
- Daina, A., Michielin, O., and Zoete, V. (2017). SwissADME: a free web tool to evaluate pharmacokinetics, drug-likeness and medicinal chemistry friendliness of small molecules. *Sci. Rep.* 7:42717. doi: 10.1038/srep42717
- Fabregat, A., Jupe, S., Matthews, L., Sidiropoulos, K., Gillespie, M., Garapati, P., et al. (2018). The Reactome Pathway Knowledgebase. *Nucleic Acids Res.* 46, D649–D655. doi: 10.1093/nar/gkx1132
- Fang, S., Dong, L., Liu, L., Guo, J., Zhao, L., Zhang, J., et al. (2020). HERB: a high-throughput experiment- and reference-guided database of traditional Chinese medicine. *Nucleic Acids Res.* 49, D1197–D1206. doi: 10.1093/nar/gkaa1063
- Flood-Page, P., Menzies-Gow, A., Phipps, S., Ying, S., Wangoo, A., Ludwig, M. S., et al. (2003). Anti-IL-5 treatment reduces deposition of ECM proteins in the bronchial subepithelial basement membrane of mild atopic asthmatics. *J. Clin. Invest.* 112, 1029–1036. doi: 10.1172/JCI17974
- García-Menaya, J. M., Cordobés-Durán, C., García-Martín, E., and Agúndez, J. A. G. (2019). Pharmacogenetic Factors Affecting Asthma Treatment Response. Potential Implications for Drug Therapy. *Front. Pharmacol.* 10:520. doi: 10.3389/fphar.2019.00520

## ACKNOWLEDGMENTS

We would like to thank Editage (www.editage.cn) for English language editing.

## SUPPLEMENTARY MATERIAL

The Supplementary Material for this article can be found online at: <https://www.frontiersin.org/articles/10.3389/fmolb.2021.644561/full#supplementary-material>

- Gong, J.-H., Shin, D., Han, S.-Y., Park, S.-H., Kang, M.-K., Kim, J.-L., et al. (2013). Blockade of Airway Inflammation by Kaempferol via Disturbing Tyk-STAT Signaling in Airway Epithelial Cells and in Asthmatic Mice. *Evid. Based Complement. Alternat. Med.* 2013:250725. doi: 10.1155/2013/250725
- Grondin, C. J., Davis, A. P., Wiegers, T. C., Wiegers, J. A., and Mattingly, C. J. (2018). Accessing an Expanded Exposure Science Module at the Comparative Toxicogenomics Database. *Environ. Health Perspect.* 126:014501. doi: 10.1289/EHP2873
- Haeggström, J. Z., and Funk, C. D. (2011). Lipoxygenase and leukotriene pathways: biochemistry, biology, and roles in disease. *Chem. Rev.* 111, 5866–5898. doi: 10.1021/cr200246d
- Hershey, G. K. K. (2003). IL-13 receptors and signaling pathways: an evolving web. *J. Allergy Clin. Immunol.* 111, 677–690. doi: 10.1067/mai.2003.1333
- Hoshino, M., Takahashi, M., and Aoike, N. (2001). Expression of vascular endothelial growth factor, basic fibroblast growth factor, and angiogenin immunoreactivity in asthmatic airways and its relationship to angiogenesis. *J. Allergy Clin. Immunol.* 107, 295–301. doi: 10.1067/mai.2001.111928
- Howell, M. D., Fitzsimons, C., and Smith, P. A. (2018). JAK/STAT inhibitors and other small molecule cytokine antagonists for the treatment of allergic disease. *Ann. Allergy Asthma Immunol.* 120, 367–375. doi: 10.1016/j.anai.2018.02.012
- Hsieh, Y.-Y., Chang, C.-C., Hsu, C.-M., Wan, L., Chen, S.-Y., Lin, W.-H., et al. (2011). JAK-1 rs2780895 C-related genotype and allele but not JAK-1 rs10789166, rs4916008, rs2780885, rs17127114, and rs3806277 are associated with higher susceptibility to asthma. *Genet. Test. Mol. Biomarkers* 15, 841–847. doi: 10.1089/gtmb.2011.0002
- Huang, K., Yang, T., Xu, J., Yang, L., Zhao, J., Zhang, X., et al. (2019). Prevalence, risk factors, and management of asthma in China: a national cross-sectional study. *Lancet* 394, 407–418. doi: 10.1016/S0140-6736(19)31147-X
- Huang, L., Xie, D., Yu, Y., Liu, H., Shi, Y., Shi, T., et al. (2018). TCMID 2.0: a comprehensive resource for TCM. *Nucleic Acids Res.* 46, D1117–D1120. doi: 10.1093/nar/gkx1028
- Inoue, H., Akimoto, K., Homma, T., Tanaka, A., and Sagara, H. (2020). Airway Epithelial Dysfunction in Asthma: relevant to Epidermal Growth Factor Receptors and Airway Epithelial Cells. *J. Clin. Med.* 9:3698. doi: 10.3390/jcm9113698
- James, A. L., and Wenzel, S. (2007). Clinical relevance of airway remodelling in airway diseases. *Eur. Respir. J.* 30, 134–155. doi: 10.1183/09031936.00146905
- Jang, T. Y., Jung, A.-Y., Kyung, T.-S., Kim, D.-Y., Hwang, J.-H., and Kim, Y. H. (2017). Anti-allergic effect of luteolin in mice with allergic asthma and rhinitis. *Cent. Eur. J. Immunol.* 42, 24–29. doi: 10.5114/cej.2017.67315
- Jeffery, P. K. (2001). Remodeling in Asthma and Chronic Obstructive Lung Disease. *Am. J. Respir. Crit. Care Med.* 164, S28–38. doi: 10.1164/ajrccm.164.supplement\_2.2106061
- Kang, D. R., Belal, S. A., Choe, H. S., Shin, D. K., and Shim, K. S. (2018). Effect of Kaempferol on Cyclooxygenase 2 (Cox2) and Cytosolic Phospholipase A2 (cPLA2) Protein Expression in BALB/c Mice. *Iran. J. Allergy Asthma Immunol.* 17, 428–435. doi: 10.18502/ijaa.v17i5.301
- Keiser, M. J., Roth, B. L., Armbruster, B. N., Ernsberger, P., Irwin, J. J., and Shoichet, B. K. (2007). Relating protein pharmacology by ligand chemistry. *Nat. Biotechnol.* 25, 197–206. doi: 10.1038/nbt1284
- Kim, S., Chen, J., Cheng, T., Gindulyte, A., He, J., He, S., et al. (2019). PubChem 2019 update: improved access to chemical data. *Nucleic Acids Res.* 47, D1102–D1109. doi: 10.1093/nar/gky1033



- Krishnamoorthy, N., Abdounour, R.-E. E., Walker, K. H., Engstrom, B. D., and Levy, B. D. (2018). Specialized Proresolving Mediators in Innate and Adaptive Immune Responses in Airway Diseases. *Physiol. Rev.* 98, 1335–1370. doi: 10.1152/physrev.00026.2017
- Kytikova, O., Novgorodtseva, T., Denisenko, Y., Antonyuk, M., and Gvozdenko, T. (2019). Pro-Resolving Lipid Mediators in the Pathophysiology of Asthma. *Medicina* 55:284. doi: 10.3390/medicina55060284
- Lambrecht, B. N., and Hammad, H. (2012). The airway epithelium in asthma. *Nat. Med.* 18, 684–692. doi: 10.1038/nm.2737
- Le Cras, T. D., Acciani, T. H., Mushaben, E. M., Kramer, E. L., Pastura, P. A., Hardie, W. D., et al. (2011). Epithelial EGF receptor signaling mediates airway hyperreactivity and remodeling in a mouse model of chronic asthma. *Am. J. Physiol. Lung Cell. Mol. Physiol.* 300, L414–21. doi: 10.1152/ajplung.00346.2010
- Lee, C. G., Link, H., Baluk, P., Homer, R. J., Chapoval, S., Bhandari, V., et al. (2004). Vascular endothelial growth factor (VEGF) induces remodeling and enhances TH2-mediated sensitization and inflammation in the lung. *Nat. Med.* 10, 1095–1103. doi: 10.1038/nm1105
- Li, N., Li, Q., Zhou, X. D., Kolosov, V. P., and Perelman, J. M. (2012). The effect of quercetin on human neutrophil elastase-induced mucin5AC expression in human airway epithelial cells. *Int. Immunopharmacol.* 14, 195–201. doi: 10.1016/j.intimp.2012.07.008
- Liu, J., and Lin, A. (2007). Wiring the cell signaling circuitry by the NF- $\kappa$ B and JNK1 crosstalk and its applications in human diseases. *Oncogene* 26, 3267–3278. doi: 10.1038/sj.onc.1210417
- Liu, J., Liu, J., Shen, F., Qin, Z., Jiang, M., Zhu, J., et al. (2018). Systems pharmacology analysis of synergy of TCM: an example using saffron formula. *Sci. Rep.* 8:380. doi: 10.1038/s41598-017-18764-2
- Liu, L., Wang, L., He, S., and Ma, Y. (2018). Immune Homeostasis: effects of Chinese Herbal Formulae and Herb-Derived Compounds on Allergic Asthma in Different Experimental Models. *Chin. J. Integr. Med.* 24, 390–398. doi: 10.1007/s11655-018-2836-2
- Lucas, C. D., Dorward, D. A., Sharma, S., Rennie, J., Felton, J. M., Alessandri, A. L., et al. (2015). Wogonin Induces Eosinophil Apoptosis and Attenuates Allergic Airway Inflammation. *Am. J. Respir. Crit. Care Med.* 191, 626–636. doi: 10.1164/rccm.201408-1565OC
- Molitorisova, M., Sutovska, M., Kazimierova, I., Barborikova, J., Joskova, M., Novakova, E., et al. (2021). The anti-asthmatic potential of flavonol kaempferol in an experimental model of allergic airway inflammation. *Eur. J. Pharmacol.* 891:173698. doi: 10.1016/j.ejphar.2020.173698
- Nelms, K., Keegan, A. D., Zamorano, J., Ryan, J. J., and Paul, W. E. (1999). The IL-4 receptor: signaling mechanisms and biologic functions. *Annu. Rev. Immunol.* 17, 701–738. doi: 10.1146/annurev.immunol.17.1.701
- Park, H., Lee, C.-M., Jung, I. D., Lee, J. S., Jeong, Y., Chang, J. H., et al. (2009). Quercetin regulates Th1/Th2 balance in a murine model of asthma. *Int. Immunopharmacol.* 9, 261–267. doi: 10.1016/j.intimp.2008.10.021
- Qin, L., Lan, Y., and Ma, S. (2017). Effects of Modified Guomin Decoction on Treg Cell Specific Transcription Factor in Mice with Allergic Asthma. *Tradit. Chin. Drug Res. Clin. Pharmacol.* 28, 332–335.
- Ru, J., Li, P., Wang, J., Zhou, W., Li, B., Huang, C., et al. (2014). TCMSP: a database of systems pharmacology for drug discovery from herbal medicines. *J. Cheminform.* 6:13. doi: 10.1186/1758-2946-6-13
- Safra, M., Dalah, I., Alexander, J., Rosen, N., Iny Stein, T., Shmoish, M., et al. (2010). GeneCards Version 3: the human gene integrator. *Database* 2010:baq020. doi: 10.1093/database/baq020
- Schett, G., and Neurath, M. F. (2018). Resolution of chronic inflammatory disease: universal and tissue-specific concepts. *Nat. Commun.* 9:3261. doi: 10.1038/s41467-018-05800-6
- Schumann, R. R., Kirschning, C. J., Unbehauen, A., Aberle, H. P., Knope, H. P., Lamping, N., et al. (1996). The lipopolysaccharide-binding protein is a secretory class 1 acute-phase protein whose gene is transcriptionally activated by APRE/STAT3 and other cytokine-inducible nuclear proteins. *Mol. Cell. Biol.* 16, 3490–3503. doi: 10.1128/mcb.16.7.3490
- Shannon, P., Markiel, A., Ozier, O., Baliga, N. S., Wang, J. T., Ramage, D., et al. (2003). Cytoscape: a software environment for integrated models of biomolecular interaction networks. *Genome Res.* 13, 2498–2504. doi: 10.1101/gr.1239303
- Shi, Y., Tan, Y., Mao, S., and Gu, W. (2014). Naringenin inhibits allergen-induced airway remodeling in a murine model of asthma. *Mol. Med. Rep.* 9, 1204–1208. doi: 10.3892/mmr.2014.1940
- Simeone-Penney, M. C., Severgnini, M., Tu, P., Homer, R. J., Mariani, T. J., Cohn, L., et al. (2007). Airway epithelial STAT3 is required for allergic inflammation in a murine model of asthma. *J. Immunol.* 1950, 6191–6199. doi: 10.4049/jimmunol.178.10.6191
- Sinha, S., Doble, M., and Manju, S. L. (2019). 5-Lipoxygenase as a drug target: a review on trends in inhibitors structural design, SAR and mechanism based approach. *Bioorg. Med. Chem.* 27, 3745–3759. doi: 10.1016/j.bmc.2019.06.040
- Soriano, J. B., Abajobir, A. A., Abate, K. H., Abera, S. F., Agrawal, A., Ahmed, M. B., et al. (2017). Global, regional, and national deaths, prevalence, disability-adjusted life years, and years lived with disability for chronic obstructive pulmonary disease and asthma, 1990–2015: a systematic analysis for the Global Burden of Disease Study 2015. *Lancet Respir. Med.* 5, 691–706. doi: 10.1016/S2213-2600(17)30293-X
- Stermitz, F. R., Lorenz, P., Tawara, J. N., Zenewicz, L. A., and Lewis, K. (2000). Synergy in a medicinal plant: antimicrobial action of berberine potentiated by 5'-methoxyhydnocarpin, a multidrug pump inhibitor. *Proc. Natl. Acad. Sci. U. S. A.* 97, 1433–1437. doi: 10.1073/pnas.030540597
- Tao, T., Zhang, Y., Li, J., and Mei, C. (2018). Review of experiments and clinical application research on Guomin Decoction. *China J. Tradit. Chin. Med. Pharm.* 33, 242–244.
- Trott, O., and Olson, A. J. (2010). AutoDock Vina: improving the speed and accuracy of docking with a new scoring function, efficient optimization, and multithreading. *J. Comput. Chem.* 31, 455–461. doi: 10.1002/jcc.21334
- von Mering, C., Jensen, L. J., Snel, B., Hooper, S. D., Krupp, M., Foglierini, M., et al. (2005). STRING: known and predicted protein–protein associations, integrated and transferred across organisms. *Nucleic Acids Res.* 33, D433–7. doi: 10.1093/nar/gki005
- Wang, S., Wuniquemu, T., Tang, W., Teng, F., Bian, Q., Yi, L., et al. (2021). Luteolin inhibits autophagy in allergic asthma by activating PI3K/Akt/mTOR signaling and inhibiting Beclin-1-PI3KC3 complex. *Int. Immunopharmacol.* 94:107460. doi: 10.1016/j.intimp.2021.107460
- Wu, Y., Zhang, F., Yang, K., Fang, S., Bu, D., Li, H., et al. (2019). SymMap: an integrative database of traditional Chinese medicine enhanced by symptom mapping. *Nucleic Acids Res.* 47, D1110–D1117. doi: 10.1093/nar/gky1021
- Xu, H.-Y., Zhang, Y.-Q., Liu, Z.-M., Chen, T., Lv, C.-Y., Tang, S.-H., et al. (2019). ETCM: an encyclopaedia of traditional Chinese medicine. *Nucleic Acids Res.* 47, D976–D982. doi: 10.1093/nar/gky987
- Yang, M., Chen, J.-L., Xu, L.-W., and Ji, G. (2013). Navigating traditional chinese medicine network pharmacology and computational tools. *Evid. Based Complement. Alternat. Med.* 2013:731969. doi: 10.1155/2013/731969
- Zhang, G.-X., Zhang, Y.-Y., Zhang, X.-X., Wang, P.-Q., Liu, J., Liu, Q., et al. (2018). Different network pharmacology mechanisms of Danshen-based Fangjis in the treatment of stable angina. *Acta Pharmacol. Sin.* 39, 952–960. doi: 10.1038/aps.2017.191
- Zhang, X. (2016). *Clinical And Animal Experimental Study Of Allergy Decoction Combined With Cough Suppressant To Interfere With Pm2.5*. Available online at: <https://kns.cnki.net/kcms/detail/detail.aspx?dbcode=CMFD&dbname=CMFD201602&filename=1016071173.nh&v=THPQPTs5AmVKWk3lTRAFLU2OZN63qJJsXUW1RC1V3QQsD67MWJgqLm9VNc7mE1mF> (accessed March 21, 2021).
- Zhu, S., and Liang, X. (1985). Discussion on disease differentiation and medication based on syndrome differentiation from the application of Guomin Decoction. *Chin. J. Med.* 59:1985,

**Conflict of Interest:** The authors declare that the research was conducted in the absence of any commercial or financial relationships that could be construed as a potential conflict of interest.

Copyright © 2021 Wang, Zhou, Wang, Meng, Liu, Yao and Feng. This is an open-access article distributed under the terms of the Creative Commons Attribution License (CC BY). The use, distribution or reproduction in other forums is permitted, provided the original author(s) and the copyright owner(s) are credited and that the original publication in this journal is cited, in accordance with accepted academic practice. No use, distribution or reproduction is permitted which does not comply with these terms.





# Serum Cytokine Profiling Identifies Axl as a New Biomarker Candidate for Active Eosinophilic Granulomatosis With Polyangiitis

Jianjuan Ma<sup>1,2,3†</sup>, Cong Dong<sup>2†</sup>, Shushan Wei<sup>2</sup>, Minzhi Qiu<sup>2</sup>, Penghui Wu<sup>2</sup>, Changxing Ou<sup>2</sup>, Bomeng Zhang<sup>2</sup>, Xueyan Zhang<sup>4</sup>, Jie Yan<sup>5</sup>, Qingling Zhang<sup>2\*</sup> and Nanshan Zhong<sup>1,2\*</sup>

<sup>1</sup> Department of Pathophysiology, School of Basic Medical Sciences, Guizhou Medical University, Guiyang, China,

<sup>2</sup> Pulmonary and Critical Care Medicine, Guangzhou Institute of Respiratory Health, National Clinical Research Center for Respiratory Disease, National Center for Respiratory Medicine, State Key Laboratory of Respiratory Diseases, The First Affiliated Hospital of Guangzhou Medical University, Guangzhou, China, <sup>3</sup> Department of Pediatric Hematology, Affiliated Hospital of Guizhou Medical University, Guiyang, China, <sup>4</sup> School of Basic Medical Sciences, The Second Affiliated Hospital, State Key Laboratory of Respiratory Disease, Guangdong Provincial Key Laboratory of Allergy & Clinical Immunology, Guangzhou Medical University, Guangzhou, China, <sup>5</sup> The Second Affiliated Hospital, State Key Laboratory of Respiratory Disease, Guangdong Provincial Key Laboratory of Allergy & Clinical Immunology, Guangzhou Medical University, Guangzhou, China

## OPEN ACCESS

### Edited by:

Huahao Shen,  
Zhejiang University, China

### Reviewed by:

Sanjay Mishra,  
The Ohio State University,  
United States  
Xiaodong Wu,  
Tongji University, China

### \*Correspondence:

Nanshan Zhong  
nanshan@vip.163.com  
Qingling Zhang  
zqling68@hotmail.com

<sup>†</sup> These authors have contributed  
equally to this work and share first  
authorship

### Specialty section:

This article was submitted to  
Molecular Diagnostics  
and Therapeutics,  
a section of the journal  
Frontiers in Molecular Biosciences

**Received:** 14 January 2021

**Accepted:** 06 April 2021

**Published:** 27 April 2021

### Citation:

Ma J, Dong C, Wei S, Qiu M,  
Wu P, Ou C, Zhang B, Zhang X,  
Yan J, Zhang Q and Zhong N (2021)  
Serum Cytokine Profiling Identifies Axl  
as a New Biomarker Candidate  
for Active Eosinophilic Granulomatosis  
With Polyangiitis.  
Front. Mol. Biosci. 8:653461.  
doi: 10.3389/fmolb.2021.653461

**Background:** Eosinophilic granulomatosis with polyangiitis (EGPA) prognosis is generally favorable and is treated with combined corticosteroids/immunosuppressor(s) therapy. However, disease flares increase the number of clinical visits. Therefore, discovering new serum biomarkers for early identification of active EGPA is crucial.

**Objective:** To identify reliable serum biomarkers to measure EGPA activity.

**Methods:** The expression of 160 proteins was compared in sera from 15 inactive and 13 active EGPA patients by antibody-based microarray. Network-based analysis identified patterns in the different groups. Differentially expressed proteins (DEPs) in active disease were identified, and the correlation between their serum levels and clinical parameters was assessed. DEPs were further analyzed for GO enrichment and KEGG pathways. Finally, DEP marker candidates were validated by ELISA and Bio-plex as well as against a second cohort of 22 inactive and 18 active EGPA patients.

**Results:** The active group presented higher peripheral and sputum eosinophil counts, FeNO, and FEV1 (% predicted) ( $P < 0.05$ ). Network-based analysis showed scattered expression patterns in active subjects, but no significant bias in inactive subjects. Significant differences were observed in serum levels of 19 candidate markers, all of which were higher in active EGPA ( $P < 0.05$ ). KEGG analysis indicated that DEPs were mainly involved in the MAPK, PI3K-Akt, RAS and Rap1 related pathways. Nine out of 19 candidate markers were positively correlated with peripheral eosinophil counts including FGF-7, SCF, GDNF,  $\beta$ -NGF, IGFBP-4, Axl, PIGF, Insulin, NT-4, ErbB3, OPN and BMP-4 ( $r = 0.693$ ,  $r = 0.692$ ,  $r = 0.687$ ,  $r = 0.683$ ,  $r = 0.671$ ,  $r = 0.606$ ,  $r = 0.571$ ,  $r = 0.570$ ,  $r = 0.516$ , respectively;  $P < 0.05$ ), while two, CD14 and MCP-3, were negatively correlated ( $r = -0.644$  and  $r = -0.515$ ;  $P < 0.05$ ). The higher expression of Axl, OPN, HCC-4, GDNF, and MCP-3 in active EGPA subjects was confirmed by ELISA and Custom Multiplex Bio-plex analyses.

**Conclusion:** The serum protein profiles were significantly different between active and inactive EGPA. The expression of the candidate proteins correlated with peripheral blood eosinophil count. Serum Axl, OPN, HCC-4, GDNF, and MCP-3 levels were consistently higher in active EGPA, independent of the assessment methods. Finally, Axl had the largest AUC, indicating that this cytokine may serve as novel biomarker for the diagnosis of active EGPA.

**Keywords:** eosinophilic granulomatosis with polyangiitis, antibody array, biomarkers, active, serum

## INTRODUCTION

Eosinophilic granulomatosis with polyangiitis (EGPA), formerly called Churg-Strauss syndrome, is a systemic necrotizing vasculitis affecting small- and medium-size vessels; it is characterized by asthma, peripheral eosinophilia, eosinophil-rich inflammation, and vascular and/or extravascular granulomas. Since 1951, when EGPA was first reported by Churg and Strauss, there have been several definitions and classification criteria for EGPA (Churg and Strauss, 1951). In 1990, the American College of Rheumatology (ACR) proposed the first EGPA classification criteria including the following six items (Lightfoot et al., 1990; Masi et al., 1990): (1) asthma; (2) paranasal sinus abnormality; (3) peripheral blood eosinophilia ( $>10\%$ ); (4) unfixated pulmonary infiltration; (5) mononeuropathy or polyneuropathy; and (6) extravascular eosinophils on histology. When four or more items are satisfied, a patient can be classified as EGPA. The sensitivity and specificity of the 1990 ACR criteria for EGPA have been reported were 85% and 99.75% respectively (Masi et al., 1990).

However, there are no definitive diagnosis criteria for EGPA. EGPA diagnosis remains clinical and is based on the existence of vasculitis. Moreover, discriminating disease activity from worsening underlying asthma is challenging. Thus, biomarkers to diagnose EGPA disease flares would be extremely valuable. Further, to improve EGPA management, researchers have attempted to identify biomarkers that discriminate active and inactive EGPA. Some studies have established associations between common laboratory readouts, e.g., serum IgE, erythrocyte sedimentation rate and C-reactive protein (CRP) (Peter C. Grayson et al., 2015), and disease activity, but these have limitations as longitudinal biomarkers to monitor disease activity. In addition, the eosinophil cationic protein was correlated with disease activity in small series. Other studies examined several novel biomarkers, e.g., CCL17/TARC (Dallos et al., 2010; Dejaco et al., 2015), IgG4 (Augusto Vaglio et al., 2012; Dejaco et al., 2015) and CCL26/eotaxin-3 (Polzer et al., 2008; Dejaco et al., 2015; Zagvozdina et al., 2016), but their use for routine diagnosis has not yet been implemented. These findings suggest that novel biomarkers to monitor disease activity in EGPA are still needed.

High throughput protein expression studies, such as microarray analyses, are increasingly used to identify changes in protein profiles during the onset and progression of complex diseases. In this study, we integrated microarray data from EGPA and sought to identify protein expression profiles and signaling pathways that can mark pathogenetic changes in active EGPA.

This study led to the identification of new diagnostic markers and therapeutic targets.

## METHODS

### Study Design and Subjects

In the current study, we conducted a prospective observational study in which 2 groups of patients were recruited, including 31 patients with active EGPA, and 37 patients with inactive EGPA, all treated at the Department of Allergy and Clinical Immunology at The First Affiliated Hospital of Guangzhou Medical University, China. Among them, an exploration subgroup included 15 inactive patients and 13 active patients. Other 22 inactive patients and 18 active patients were recruited in the validation study.

All EGPA subjects met four or more ACR items (Masi et al., 1990), including (1) asthma; defined as a history of wheezing or diffuse high-pitched rales on expiration; (2) peripheral blood eosinophilia ( $>10\%$ ); (3) mononeuropathy or polyneuropathy; defined as the development of mononeuropathy, multiple mononeuropathies, or polyneuropathy (i.e., glove stocking distribution) attributable to a systemic vasculitis; (4) unfixated pulmonary infiltration; defined as migratory or transitory pulmonary infiltrates on radiographs (not including fixed infiltrates), attributable to a systemic vasculitis; (5) paranasal sinus abnormality; defined as a history of acute or chronic paranasal sinus pain or tenderness or radiographic opacification of the paranasal sinuses and (6) extravascular eosinophils on histology; defined as biopsy including artery, arteriole, or venule, showing accumulations of eosinophils in extravascular areas. All EGPA subjects had vasculitis manifestations and met ACR criteria. Disease activity was assessed at diagnosis using the original 1994 Birmingham Vasculitis Activity Score (BVAS) (Luqmani et al., 1994) and was recorded in the database. Patients with a score under 15 were recruited to the inactive group, whereas they joined the active group above a score of 15. All subjects underwent a standardized clinical assessment, including pulmonary function test, sputum induction, inflammatory cell differentiation test, allergy status or serum (Se)-specific-IgE measurement, fractional exhaled nitric oxide (FeNO), anti-neutrophil cytoplasmic antibodies (ANCA) test and complete blood count (CBC).

The study was approved by the Ethics Review Board of the First Affiliated Hospital of Guangzhou Medical University

[Medical research ethics review 2018,No.35]. All participants provided written informed consent.

## Lung Function

Lung function was measured by spirometer (MasterScreen PFT; Jaeger<sup>TM</sup>, CareFusion, Hoechst, Germany), in accordance with the American Thoracic Society/European Respiratory Society guidelines (Miller et al., 2005). Parameters, including percent of predicted forced vital capacity (FVC%) and forced expiratory volume in 1 second of predicted (FEV<sub>1</sub>%), percent of predicted peak expiratory flow (PEF%) and maximum mid expiratory flow (MMEF75/25), were recorded.

## Blood Sample

Five milliliters of venous blood sample were collected into vacutainer tubes containing no additive. Sera were prepared by centrifugation and stored at  $-80^{\circ}\text{C}$  for protein microarray analysis, ELISA and Bio-Plex assay.

## Protein Microarray Analysis

RayBiotech Human Cytokine Antibody Array 3000 (RayBiotech, Inc., Cat# QAH-CAA-3000) was used to analyze serum protein profiles. This antibody array simultaneously detects 160 human cytokines shared between 4 non-overlapping arrays (Supplementary Table 1). The samples were read by the Guangzhou Biotech Company. The experimental procedure was carried out in accordance with the manufacturer's instructions. Briefly, antibody pre-coated array membranes were incubated with coating buffer for 30 min. The blocking buffer was then decanted and replaced with dilutions of the samples, for overnight incubation at  $4^{\circ}\text{C}$  under shaking. The next day, the membranes were washed and incubated with a mix of biotin-conjugated antibodies for 2 h. The biotin-conjugated antibodies were removed, and Streptavidin-Fluor was added to each subarray. The incubation chambers were covered with adhesive film and incubated for 2 h. After washing, signals were read with a GenePix 4000B system (Axon Instruments, Foster City, CA, United States). GenePix Pro 6.0 software (Axon Instruments) was used for densitometric analysis of the spots. The values were normalized to the signals obtained for the positive controls of each sample. The total normalized fluorescence values of the replicates were averaged and are expressed as the fold increase compared to the control samples.

## Gene Ontology and KEGG Pathway Analysis

The Database for Annotation, Visualization and Integrated Discovery (DAVID<sup>1</sup>) is an online biological information database for gene functional analysis (Huang et al., 2007). To predict the possible functions of the overlapping differentially expressed proteins (DEPs) and their neighboring genes, and the potential pathways in which they intervene, we performed Gene Ontology (GO) enrichment and KEGG pathway analyses in DAVID.  $P < 0.05$  was considered statistically significant.

<sup>1</sup> <https://david.ncifcrf.gov/>

## ELISA

ELISA kits (Thermo/Invitrogen Carlsbad, CA, United States) were used to validate the results obtained from the antibody arrays, following the manufacturer's instructions. Briefly, serum samples were diluted at different dilution factors based on individual serum biomarker characteristics. Samples were coated on the plates for 1 to 2.5 h at room temperature. The plates were washed, and a biotin-conjugated antibody specific for each kit was added and incubated for 1 h under gentle shaking. Horse Radish Peroxidase (HRP)-conjugated streptavidin was added to catalyze the 3,3',5,5'-Tetramethylbenzidine (TMB) chromogenic reagent. Finally, the catalytic reaction was stopped by addition of sulfuric acid. At each step, the reactional volume in each well was of 100  $\mu\text{l}$ . Finally, the OD450 was read using a microplate reader (Multiskan GO, Thermo Scientific, Carlsbad, CA, United States).

**TABLE 1 |** Clinical manifestations in patients with EGPA.

Subjects' characteristics	Inactive (n = 31)	Active (n = 37)	P-value
Age, mean $\pm$ SD years*	42.1 $\pm$ 12.7	42.8 $\pm$ 18.1	0.903
Gender (female, %)#	58	53	0.063
Body Mass Index*	21.9 $\pm$ 2.9	19.8 $\pm$ 1.6	0.055
Smoking history (> 10 packs/year, n)*	11	13	0.603
Atopic status (n)*	15	21	0.804
Asthma diagnosis (n)*	31	37	–
Duration of asthma (years)*	5.2 $\pm$ 4.8	4.1 $\pm$ 2.7	0.466
Presence of rhinosinusitis (%)#	91	93	0.828
Peripheral eosinophil count*	5.8 $\pm$ 5.2	20.3 $\pm$ 9.8	<b>0.000</b>
Sputum eosinophil percent (%)#	5.4 $\pm$ 8.0	40.7 $\pm$ 30.1	<b>0.000</b>
<b>Parameters of lung function</b>			
·FEV1% Pred*	76.3 $\pm$ 22.6	57.7 $\pm$ 18.5	<b>0.030</b>
·FVC % Pred*	87.3 $\pm$ 21.2	82.1 $\pm$ 15.9	0.497
·FEV1/FVC*	77.8 $\pm$ 18.9	55.8 $\pm$ 15.9	0.066
·PEF% Pred*	77.5 $\pm$ 35.7	61.0 $\pm$ 11.7	0.158
·MMEF75/25*	22.6 $\pm$ 22.7	27.6 $\pm$ 22.7	0.526
FeNO (ppb)*	39.3 $\pm$ 26.3	87.6 $\pm$ 53.2	<b>0.015</b>
<b>Organ involvement</b>			
·Arthralgia/Arthritis, n (%)#	0	0	1.000
·Myalgia/Myositis, n (%)#	3 (9.6)	3 (8.8)	0.959
·Skin, n (%)#	12 (38.7)	19 (53.4)	0.087
·Ear/nose/throat, n (%)#	128 (80.6)	31 (83.8)	0.828
·Cardiovascular Events, n (%)#	0 (0)	3 (8.1)	0.060
·Gastrointestinal, n (%)#	5 (16.1)	10 (27.2)	0.128
·Pulmonary, n (%)#	31 (100)	37 (100)	–
·Kidney, n (%)#	3 (9.6)	5 (13.5)	0.603
·Peripheral neuropathy, n (%)#	5 (16.1)	5 (13.5)	0.939
BVAS score*	6 $\pm$ 2.95	20.0 $\pm$ 3.7	<b>0.000</b>

Data expressed as mean  $\pm$  standard deviation, median (interquartile range) or number (%). The P-value was calculated from the  $\chi^2$  test and ANOVA, between the 2 groups. FVC, forced vital capacity; FEV1, forced expiratory volume in 1 s; PEF% Pred, percent of predicted peak expiratory flow; MMEF75/25, maximum mid expiratory flow; FeNO, fractional exhaled nitric oxide; BVAS, Birmingham Vasculitis Activity Score. \*Values are expressed as means  $\pm$  SEM, #Values are expressed as percentage. Bold values means P-value < 0.05.



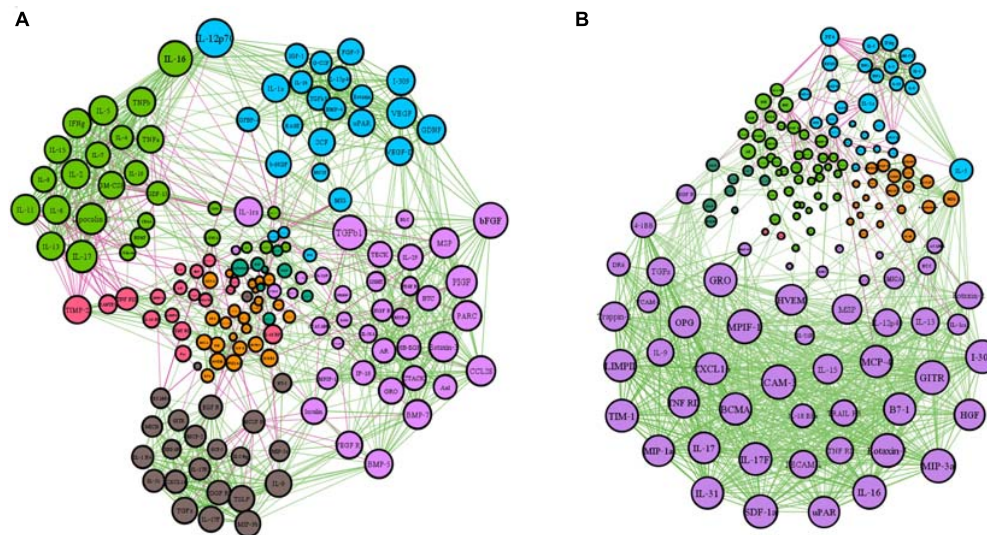


**FIGURE 1 |** Network-based analysis of protein expression in active and inactive EGPA. The network graphs were constructed with the expression data of 160 proteins. Each protein is represented by a specific node whose color represents a specific cluster. Different colors represent the different weighting degrees of nodes and edges. The size of the node is proportional to the to the number of connections (i.e., degree). Edges between nodes represent a statistically significant association ( $P < 0.05$ ). Edge thickness represents the strengths of association between two nodes (correlation coefficient, Spearman's correlation). The correlation coefficient is represented by a color code, green and purple indicating positive and negative relationships, respectively. **(A)** Inactive EGPA; **(B)** Active EGPA

## Bio-Plex Assay

The levels of 13 cytokines were assessed in the sera by the Custom Multiplex Kit featuring Axl, GDNF, HB-EGF, MCP-3, NGF beta, PDGF-BB, PlGF-1 and SCF (Thermo/Invitrogen Carlsbad, CA, United States; Cat#PPX-08), and the Custom Multiplex Kit featuring BMP-4, ErbB3, IGFBP-4, Insulin and NT-4 (Thermo/Invitrogen Carlsbad, CA, United States; Cat#LSAHM-05). The experimental procedure was carried out according to the manufacturer's instructions. Briefly, beads coated with capture antibodies were incubated with premixed standards or sample supernatants for 120 min at room temperature under 500-rpm agitation. Following incubation, premixed detection antibodies were added and incubated for 30 min at room temperature under 500-rpm agitation. After washing, Phycoerythrin (PE)-conjugated streptavidin was added and incubated as before. After washing, the beads were resuspended in Bio-Plex cytokine assay buffer and read on the Bio-Plex 200 system using Low PMT setting. Data were analyzed with Bio-Plex Manager™ software version 2.0.

## Statistical Analysis and Visualization

Statistical analysis was performed using the SPSS software package (version 22.0; IBM Corp., Armonk, NY, United States). Continuous variables are expressed as number (%) or means  $\pm$  standard deviation (SD). Comparisons between groups were made using the *t*-test or Mann-Whitney *U*-test for continuous endpoints, and the  $\chi^2$  test for categorical endpoints. *P*-values were corrected using the Benjamini-Hochberg false discovery rate (FDR). Correlations were assessed using Pearson's or Spearman's correlation test. A *P*-value of  $< 0.05$  was considered significant.

Network analysis based on the Spearman analysis was performed using Gephi V0.9.2 open source software<sup>2</sup> output showing the 160 serum soluble proteins from the different subjects. Each serum soluble protein is represented by a specific node whose color represents a specific cluster. The size of the node is proportional to the sum of the edges that connects to them. Edges connecting nodes represent statistically significant correlations ( $P < 0.05$ ). The edge's thickness represents the strengths of their association (Spearman's correlation). We used the existence of modules represented by highly interlinked to pological clusters in the network using the computational algorithm proposed by Blonde et al. (Lancichinetti and Fortunato, 2009) and included in the Gephi statistical module. Modularity is the fraction of the edges that fall within the given groups of nodes minus the expected fraction if the edges were distributed at random. The value of the modularity lies in the range of  $-1$  to  $1$ . If positive then the number of edges within groups exceeds the number expected on the basis of chance.

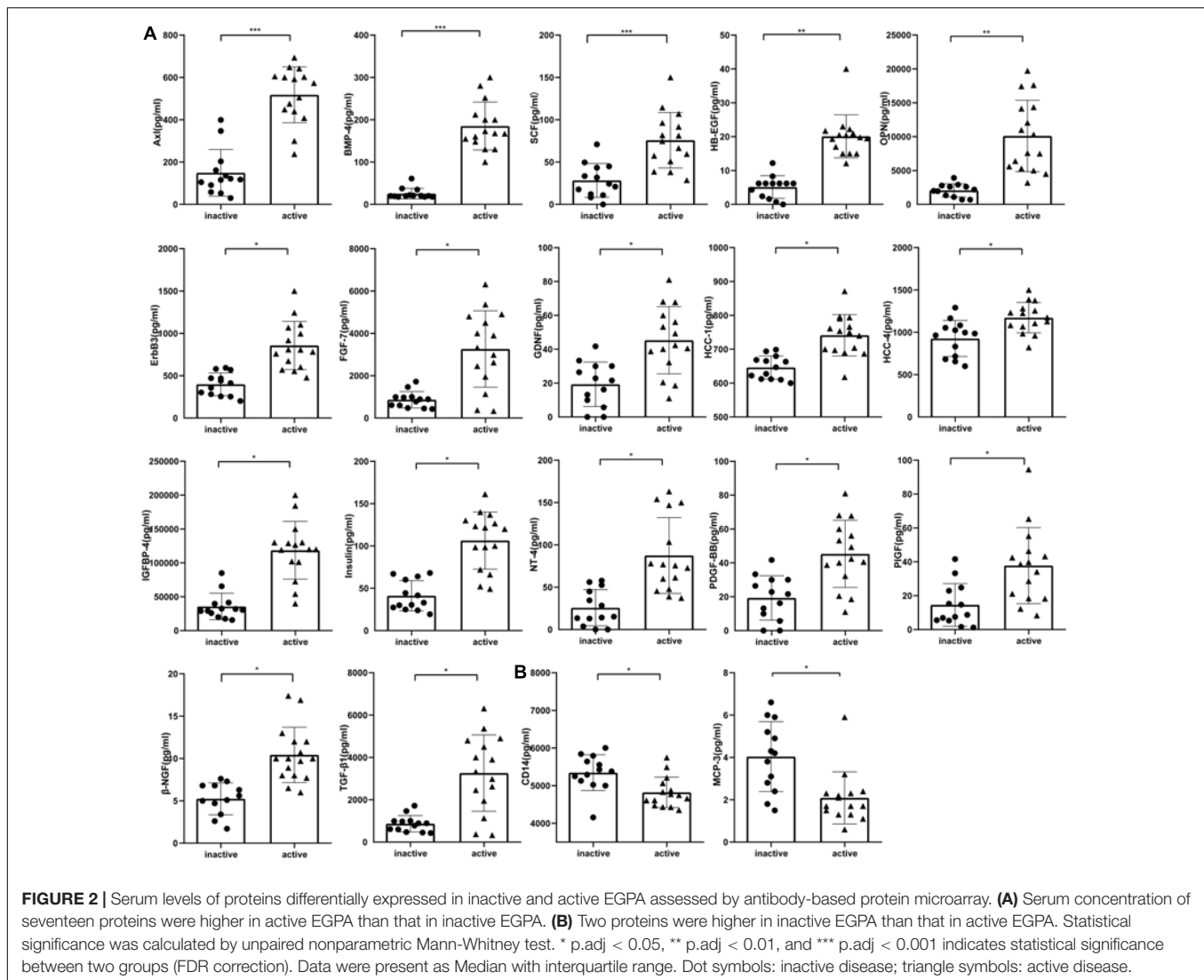
## RESULTS

### Patient Characteristics

After screening, we recruited 37 patients with inactive EGPA and 31 patients with active EGPA. All subjects had a definitive EGPA diagnosis, presented more than two organs involvement, and tested negative for ANCA. There were no significant clinical differences among all EGPA subjects regarding lung function indices (FVC (% predicted), FEV1/FVC, PEF (% predicted), MMEF75/25) and organ involvement ( $P > 0.05$ ). However, the

<sup>2</sup><https://gephi.org/>



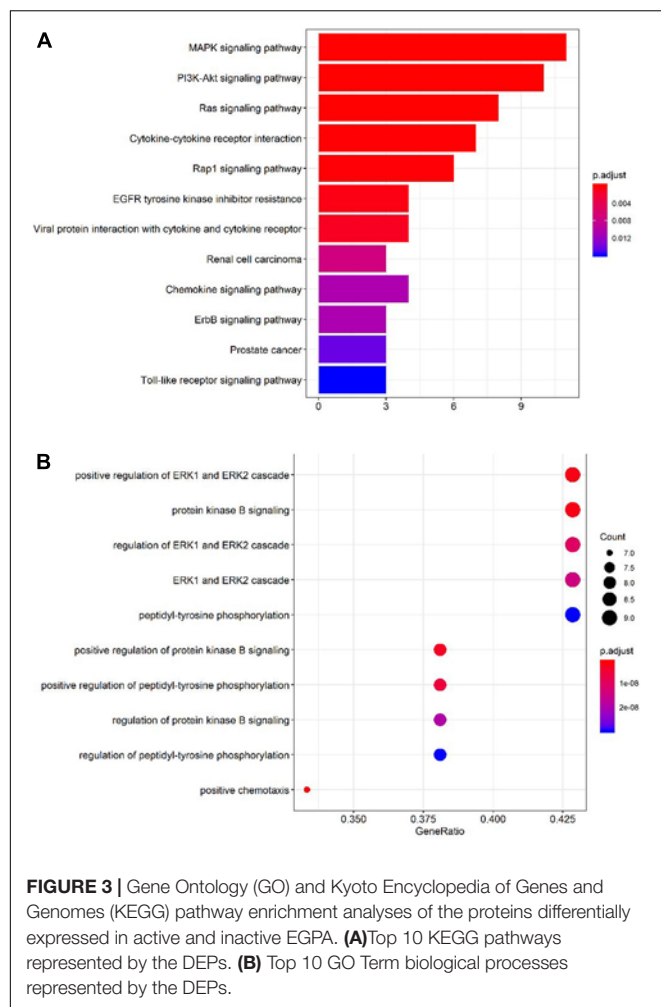


EGPA active group presented higher peripheral and sputum eosinophil counts, FeNO and FEV1 (% predicted) ( $P = 0.000$ ,  $P = 0.000$ ,  $P = 0.015$ ,  $P = 0.030$ , respectively). The demographics and characteristics of the subjects are shown in **Table 1**.

## Network-Based Analysis

The patterns of serum proteins in active and inactive EGPA patients were characterized by network-based analysis (**Figure 1**). The active network graphs comprise 152 nodes, each representing a serum protein concentration, and a total of 1174 links representing correlations between nodes scoring a  $P$ -value  $< 0.05$ . The active EGPA network contains 4 clusters of highly interlinked nodes: cluster 1 gathers 51 nodes (purple) corresponding to 51 serum proteins (**Supplementary Table 2**); cluster 2, 21 nodes (or serum proteins; orange), cluster 3, 28 nodes (or serum proteins; blue); and cluster 4, 42 nodes (or serum proteins; green). The inactive network graphs comprise 160 nodes, each representing a serum protein concentration, and a total of 1209 links representing correlations between nodes scoring a  $P$ -value  $< 0.05$ . The inactive EGPA network

contains 4 clusters of highly interlinked nodes: cluster 1 gathers 37 nodes (purple) corresponding to 37 serum proteins (**Supplementary Table 3**); cluster 2, 23 nodes (or serum proteins; brown), cluster 3, 24 nodes (or serum proteins; blue); and cluster 4, 27 nodes (or serum proteins; green). In active EGPA, cluster 1 has the largest number of nodes, suggesting that the proteins in cluster 1 are most closely related to other clusters, which may be related to disease activity. Specifically, featured cytokines associate with endothelial (PECAM-1, HVEM, VCAM-1, ICAM-3), immune cells including macrophage (CXCL16, MIP-3a, MIP-3b, MCP-4), eosinophil (Eotaxin-2, Eotaxin-3, CCL28), lymphocyte (TARC, GITR, IL-31, IL-17F, IL-9, IL-17, IL-16, IL-15, IL-13, IL-10 Rb, IL-18 BPa, IL21R) in cluster1 might robustly suggest that EGPA active stage involves the activation of multiple immune cells and vascular endothelium. But in inactive EGPA, the size of the nodes in the four clusters is similar, which indicates that during the inactive stage the proteins in the clusters are in balance with each other and might maintain the body's homeostasis.



## Comparison of the Serum Levels of 160 Proteins in Inactive and Active EGPA

To identify accurate and predictive biomarkers of disease activity, we first compared the serum levels of 160 serum proteins in active and inactive EGPA. Twenty-one serum proteins displayed differential levels between active and inactive disease ( $P < 0.05$ ) (Supplementary Table 4, unpaired nonparametric Mann-Whitney test). To further strengthen our selection criteria,  $P$ -values were corrected using the Benjamini-Hochberg false discovery rate (FDR). Finally, 19 DEPs were identified (Figure 2). These DEPs can mainly be divided into three categories: growth factors and related receptors (BMP4, SCF, HB-EGF, OPN, FGF-7, TGF- $\beta$ , IGFBP4, insulin, PDGF-BB, PIGF, ErbB3), many of which have firmly correlation with vascular remodeling; neurotrophic factor (GDNF, NT-4,  $\beta$ -NGF) and chemokines (HCC-1; HCC-4, CD14, MCP-3). The results probably demonstrated that multifaceted biological events engaged including neurotrophic, immune cells, and vascular activation during active disease phase. Following via using short-listed proteins, i.e., scoring  $FDR < 0.5$ , we performed KEGG pathway and GO enrichment analyses to gain insights into the potential functions involved in

the clinical evolution of EGPA. Five major signaling pathways were represented by the DEPs during active EGPA, i.e., MAPK signaling pathway, PI3K-Akt signaling pathway, RAS signaling pathway, cytokine-cytokine receptor interaction and Rap1 signaling pathway. Four major biological processes were found, i.e., positive regulation of ERK1 and ERK2 cascade, protein kinase B signal, regulation of ERK1 and ERK2 cascade, ERK1 and ERK2 cascade and positive regulation of peptide-tyrosine phosphorylation (Figure 3).

## Correlations Between the Serum Level of the DEPs and Peripheral Eosinophil Cell Count in Patients With Inactive and Active EGPA

To evaluate the clinical relevance of the variation in serum level of the candidate proteins, we performed a correlation analysis between protein levels and peripheral eosinophil counts in all patients. Importantly, 15 serum proteins were significantly correlated with peripheral eosinophil count ( $P < 0.05$ ) (Figure 4). Precisely, 13 of the proteins positively correlated with eosinophil count, while another two proteins (CD14 and MCP3) negatively correlated with eosinophil count. Results were objectively credible because CD14 and MCP3 are two chemokines with monocyte/macrophage. And The results might suggest that eosinophils participated in the process of vascular remodeling during EGPA active phase.

## Correlations Between the Serum Level of the DEPs and BVAS With Inactive and Active EGPA

To evaluate the relationship between DEPs and disease activity, we performed a correlation analysis between protein levels and BVAS in all patients. Nine the DEPs were significantly correlated with BVAS ( $P < 0.05$ ) (Figure 5). Serum level of Axl, IGFBP4, PIGF, OPN, SCF,  $\beta$ -NGF, and NT-4 (Figure 5A) positively correlated with BVAS, while MCP-3 and CD14 (Figure 5B) negatively.

## Evaluation of the Sensitivity and Specificity of the Candidate Protein Biomarkers

Receiver operating characteristic (ROC) analysis is the standard approach to evaluate the sensitivity and specificity of diagnostic procedures (Song, 1997). We evaluated the sensitivity and specificity of the 15 differentially expressed serum proteins by ROC curve analysis ( $P < 0.001$ ) (Figure 6; Supplementary Table 5). Axl has the largest AUC (0.94), specificity was 100% and sensitivity was 86.7%.

## Validation of the Differential Expression of the Biomarker Candidates by ELISA and Custom Multiplex Bio-plex Assay

To further consolidate the data on the variation of candidate biomarkers levels between inactive and active EGPA, we measured serum levels of the 19 DEPs by ELISA and Custom

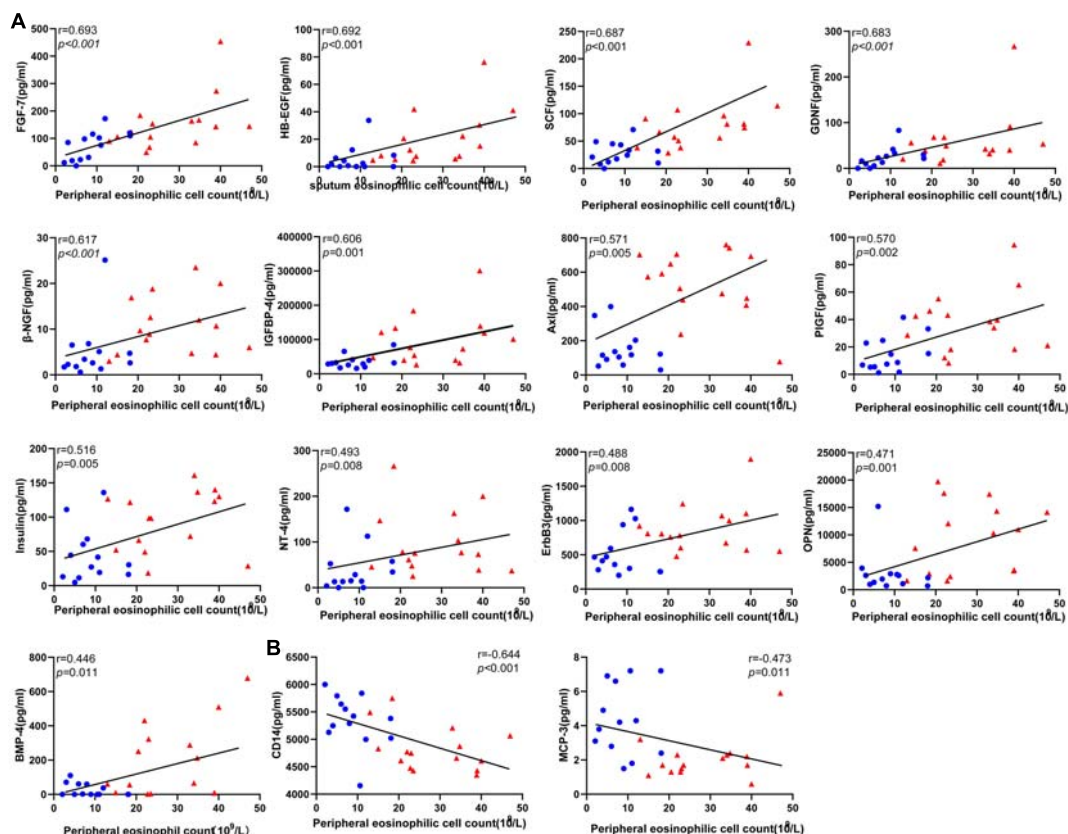


**FIGURE 4 |** Correlations between the level of the differentially expressed protein candidates and peripheral eosinophil count in EGPA patients (Spearman correlation). Only the significant correlations are shown in dot plots. Fifteen protein markers had serum levels correlated with eosinophil cell counts. **(A)** Thirteen protein markers had a level of expression positively correlated with blood eosinophil count. **(B)** Two protein markers had level of expression negatively correlated with blood eosinophil count. Blue dots represent data from patients with inactive disease. Red triangles represent data from patients with active disease.  $P$ -values and Spearman correlation coefficients are displayed.

Multiplex assay (Figure 7A). The variation of serum levels of Axl, GDNF, HCC-4, MCP-3 and OPN were consistent with the array results, confirming their differential expression in inactive and active EGPA (Figures 7B–F).

## Follow-up of Serum Level of Axl

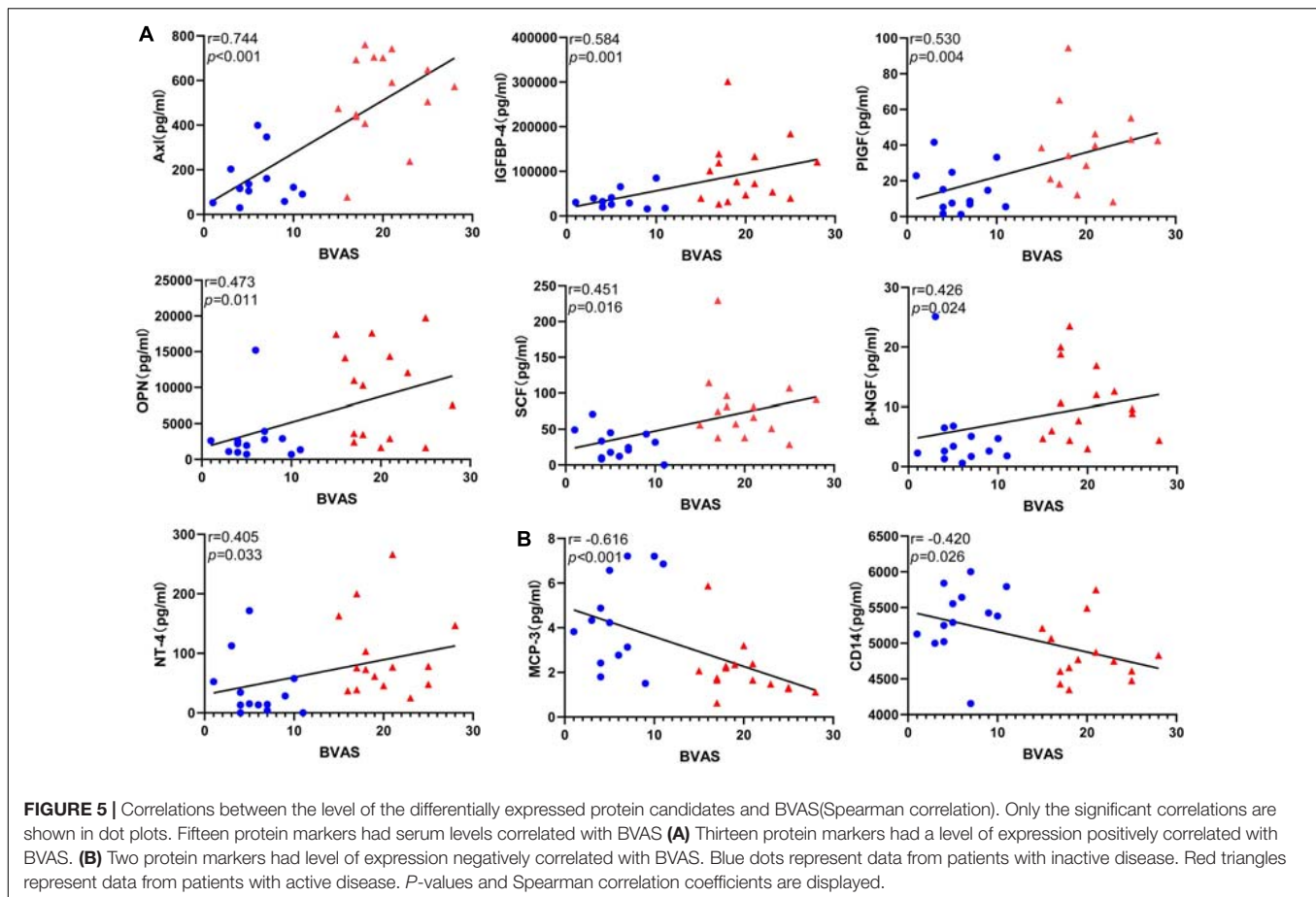
Furthermore, to confirm the faithfully clinical diagnosis significance of Axl, we followed up the longitudinal Axl expressions for paired 12 enrolled patients in active and remission disease stage. Specifically, the serum Axl levels decreased significantly in the inactive disease compared with the baseline. Moreover, 10/12 patients showed descending tendency, suggesting that the high expression of Axl is related to the disease activity. (Figure 8).

## DISCUSSION

In EGPA, identifying active disease is often challenging, especially when non-specific symptoms occur, such as worsening asthma or rhinosinusitis. The development of predictive biomarkers would greatly improve the ability to identify patients likely to

enter an active phase of the disease. To this aim, we screened 160 soluble proteins to identify those presenting differential serum levels in inactive and active EGPA, and tested their associations with clinical characteristics. Network-based analysis defined 4 clusters of serum proteins characteristic of patients with active disease, and containing 51, 21, 28, and 42 serum proteins, respectively. Among the 160 screened proteins, 19 were significantly upregulated in the sera of patients with active disease compared with sera from patients in the inactive phase ( $P < 0.05$ ). Spearman's correlation analysis indicated that 16 of these DEFs were significantly correlated with peripheral eosinophil count in active and inactive EGPA patients ( $P < 0.05$ ). Finally, we verified the differential levels of the candidate markers by ELISA and bio-plex assay. With these methods, Axl, OPN, HCC-4, GDNF and MCP-3 were further validated, and among them, Axl scored the largest AUC, indicating its superior diagnostic value above the other candidates. Thus, our study uncovered Axl as a candidate biomarker to discriminate active from inactive disease in EGPA.

Eosinophilic granulomatosis with polyangiitis is considered a Th2-mediated disease. Previous studies on the differential expression of serum ECP, CCL17/ TARC, eotaxin-3, periostin and IgG4, representing Th2 features, were reported to correlate



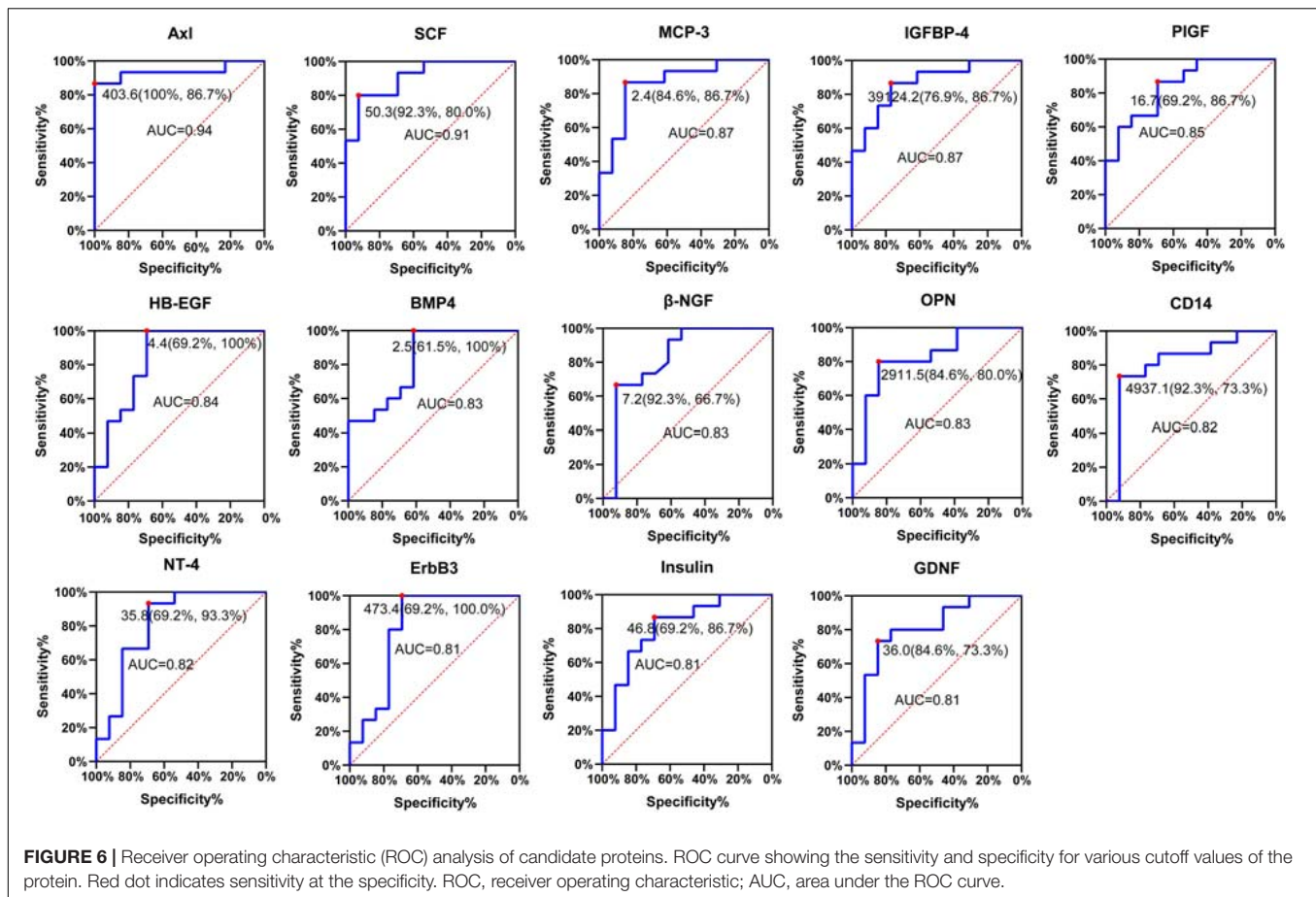
with disease activity, but could not distinguish between different phases of the disease (Guilpain et al., 2007; Dallos et al., 2010; Vaglio et al., 2012; Rhee et al., 2018). The clinical value of absolute eosinophil count, serum IgE, ESR and CRP also showed their limitations as longitudinal biomarkers of disease activity or predictors of flare in EGPA (Grayson et al., 2015). Therefore, it is urgent to uncover new serum biomarkers of active and inactive EGPA. The clinical phenotype of EGPA cannot be explained by exaggerated Th2 response alone. Pagnoux et al. (2019) explored a panel of 54 serum cytokines and chemokines involved in Th1/Th2, Th9/Th17/Th22/Treg, and inflammatory responses, but did not detect clear differences in the serum levels of these proteins, indistinguishable between active or inactive EGPA. Some of the non-differential proteins found in this previous study were also non-differential in our study. However, contrary to what Pagnoux and colleagues reported, we found the MCP-3 level was significantly different between active and inactive EGPA. The reason for this discrepancy remains unclear. In our study, all patients were treated with glucocorticoid, and 75% (51 / 68) of them were treated with glucocorticoid combined with immunosuppressors. In the cohort studied by Pagnoux et al. (2019), only 45% (18/40) of the patients were treated with glucocorticoids. These different treatments likely affected the expression of serum cytokines. In addition, ethnic differences cannot be excluded to explain the different results.

Our findings also suggest that, whereas most emphasis has been given to eosinophils and some cytokines in the pathophysiology of EGPA, more attention should be paid to a possible role of monocytes/macrophages. Decision making for treatments should not rely solely on cytokine level.

Network analysis was used to compare the expression profiles of 160 soluble serum proteins in patients with active and inactive EGPA. Result showed that serum samples with different disease activity have a distinguishable expression pattern, suggesting that distinct disease activity have different target proteins.

Pathogenesis of EGPA remains largely unknown. However, like many other autoimmune diseases, genetic predisposition and environmental factors appear to contribute to the development of EGPA (Nguyen and Guillevin, 2018). Eosinophilic inflammation and ANCA-mediated vasculitis are both cardinal features of EGPA (Furuta et al., 2019). Our study found that peripheral blood eosinophils, induced sputum eosinophils and FeNO were significantly higher in patients with active EGPA than in those with inactive disease. The reasons for these differences were mainly related to the pathogenesis of the disease itself. IL-5, a main eosinophil activator, seems involved in EGPA pathogenesis. IL-5 is produced by Th2 cells and induces the differentiation and maturation of human eosinophils (Sanderson, 1988). Following activation, eosinophils release granules containing stored cytotoxic proteins and toxins such as eosinophil-derived





neurotoxin, major basic protein (MBP), eosinophil peroxidase, and eosinophil cationic protein (ECP), all causing tissue damage (Guilpain et al., 2006). These pathophysiological differences explain the differential network between active and inactive EGPA. There were 19 DEPs between active and inactive EGPA, and some of these DEPs were related to eosinophil count in peripheral blood. This suggests that the differences between the two groups may be related to eosinophilic inflammation. To better understand the potential biological functions of these DEPs in active EGPA, GO and KEGG pathways analyses were performed. This analysis revealed the prominence of biological pathways involving ERK1 and ERK2. These proteins are related protein-serine/threonine kinases that participate in the Ras-Raf-MEK-ERK signal transduction cascade, regulating a broad variety of processes including cell adhesion, cell cycle progression, cell migration, cell survival, differentiation, metabolism, proliferation, and transcription (Roskoski, 2012). Robins et al. (2011) proposed ERK1/ERK2 MAPK cascade as a novel and attractive target in severe asthma, because this pathway is resistant to glucocorticoids, while it contributes the inflammation by neutrophil recruitment. This observation supports that the ERK1/ERK2 MAPK cascade may be also functionally involved in the active phase of EGPA, but this hypothesis needs further confirmation. Previous studies comparing biomarkers in serum of patients with active and

inactive EGPA did not address the signaling pathways and biological functions related to the different biomarkers. In this study, GO and KEGG analyses were used for the first time to further explore the biological functions and signaling pathways of DEPs, and discover the possible mechanisms and biological roles involving the cytokines in active EGPA. It is expected that follow-up on these candidate pathways in *in vitro* and *in vivo* experiments will help better explain disease etiology and variations underlying different phases of EGPA.

The concentration of Axl and IGFBP-4 were significantly correlated with eosinophil counts in peripheral blood and sputum (Supplementary Figure 1). The reasons for this difference may be explained by the fact that the samples used for differential screening were from the peripheral blood, and not from the respiratory tract. Thus, differences may exist between the pathogenesis of the acute phase in peripheral blood and in the respiratory tract. ROC analysis showed that Axl had the highest diagnostic efficiency and significantly correlation with eosinophil counts in both peripheral blood and induced sputum, and meanwhile it has a significantly correlation with BVAS. Axl serum levels were significantly diminished in follow-up inactive patients. Therefore, Axl may be a better biomarker to distinguish active and inactive EGPA. Furthermore, Axl combined with BMP-4 and SCF could improve the diagnostic sensitivity (93.3%) (Supplementary Figure 2).

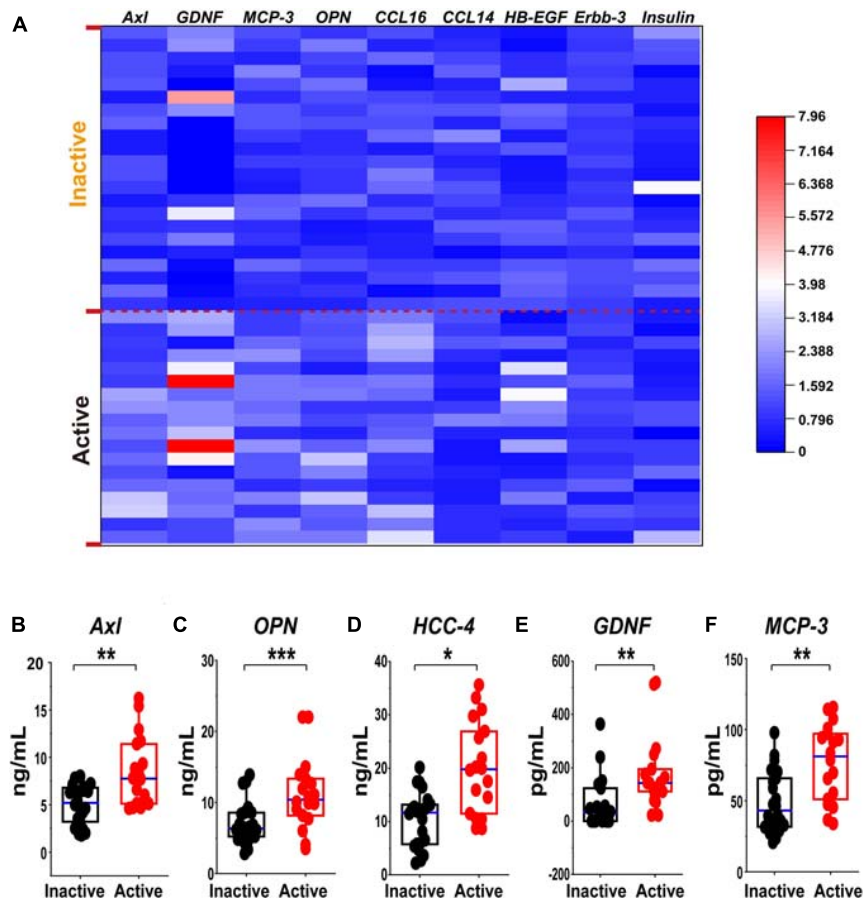


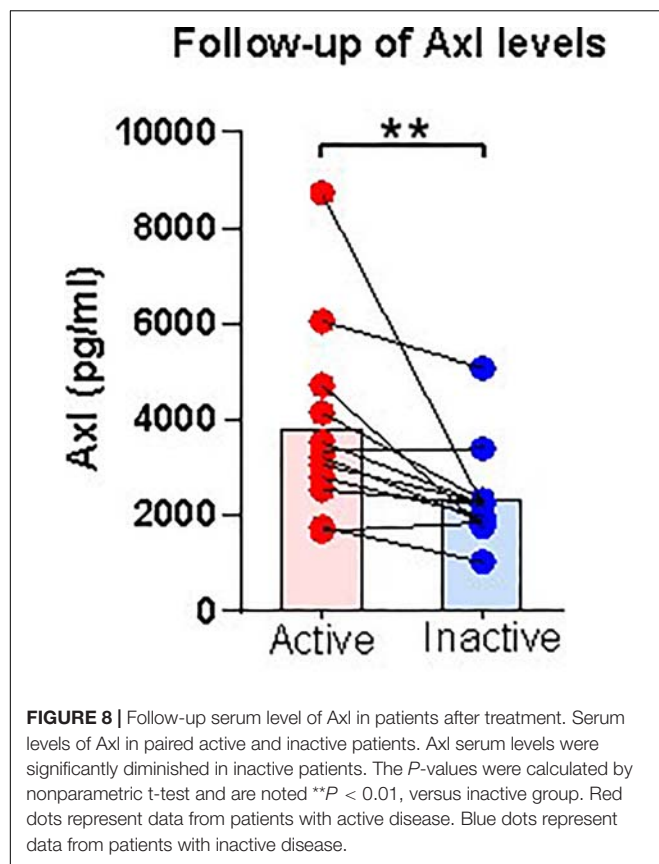
**FIGURE 7 |** Validation of the differential expression of the serum protein marker candidates for active EGPA by ELISA and Custom Multiplex. **(A)** Heatmap comparison of the expression level of the serum protein marker candidates in inactive and active EGPA by ELISA and Bio-plex. Nine of 13 were highly expressed. **(B-F)** Scatter plots representing the median values of the expression level of the serum protein marker candidates in inactive and active EGPA assessed ELISA and Bio-plex. Five of 9 were significant difference in the group. The P values were calculated by nonparametric t-test and are noted \* $P < 0.05$ , \*\* $P < 0.01$ , \*\*\* $P < 0.001$ , versus inactive group. Black dots represent data from patients with inactive disease. Red dots represent data from patients with active disease.

Axl is a receptor tyrosine kinase that transduces signals from the extracellular matrix to the cytoplasm by binding the growth factor GAS6. Thus, Axl regulates many physiological processes including cell survival, cell proliferation, migration and differentiation (Korshunov, 2012; Brown et al., 2016). GAS6/Axl signaling plays a role in processes such as endothelial cell survival during acidification by preventing apoptosis, optimal cytokine signaling during human natural killer cell development, hepatic regeneration, gonadotropin-releasing hormone neuron survival and migration, platelet activation, or regulation of thrombotic responses (Sasaki et al., 2006). The mechanism underlying Axl upregulation is not clear but continuous stimulation of macrophages by apoptotic debris may increase its expression and release (Lee and Chun, 2019). Axl is critical for phagocytosis of apoptotic cells and regulation of the immune system (Di Stasi et al., 2020).

Shuai Wang et al. (2021) found that, consistent with ACE2, SARS-CoV-2 can cause infection through the Axl receptor of the lung epithelium, while knocking out Axl significantly reduces the effect of SARS-CoV-2 on H1299 lung cells and human primary

lung epithelial cells. Besides, Milena S. Espindola et al. (2018) found that Axl activation is obviously related to the process of pulmonary fibrosis, and pulmonary fibrosis is significantly reduced after Axl inhibition. These studies showed that Axl plays very important roles in inflammatory diseases. Therefore, further investigations on the role of the Gas6/Axl pathway in EGPA and the development of specific antagonists targeting this pathway are necessary.

The present study has limitations. First, we limited our investigation to the study of the level of expression of 160 soluble proteins in peripheral blood of patients with active and inactive subjects. Although this approach validated our strategy of identification of a new marker for active EGPA, it could be extended to whole proteomes, using broader proteomics screening. Thus, while we identified candidate cytokine markers, our study did not provide a comprehensive view on the proteomic differences distinguishing active and inactive EGPA. Second, although we uncovered correlations between some of the differentially expressed proteins and clinical features, we did not further explore the molecular mechanisms linking the



protein markers to the pathology. Functional approaches will be endeavored in the future, using a broader range of clinical samples (e.g., sputum, bronchoalveolar lavage, etc.), to further verify the consistency of the results, and validate the use of the biomarker candidates in diagnostic and prognosis. The development of *in vitro* models and/or *in vivo* animal models of the disease will help verify the reliability of the functional results.

In conclusion, we identified a new cytokine, Axl, related to active EGPA, and demonstrated a high degree of correlation between its serum level and peripheral blood and induced sputum eosinophil counts. This is the first report of this biomarker in EGPA. Further studies involving higher numbers of clinical samples will help strengthen its clinical value for the diagnosis and prognosis of active EGPA and other vasculitis.

## DATA AVAILABILITY STATEMENT

The original contributions presented in the study are included in the article/Supplementary Material, further inquiries can be directed to the corresponding author/s.

## ETHICS STATEMENT

The studies involving human participants were reviewed and approved by Ethics Review Board of The First Affiliated Hospital of Guangzhou Medical University (Medical Research Ethics

Review 2018, No. 35). The patients/participants provided their written informed consent to participate in this study.

## AUTHOR CONTRIBUTIONS

JM and CD performed the experiments and drafted the manuscript. SW, MQ, PW, CO, and BZ interpreted the patient data and collected the samples. XZ and JY co-designed the experiment strategy. NZ and QZ critically revised the manuscript. All authors read and approved the final manuscript.

## FUNDING

This study was supported partly by the Natural Science Foundation of Guangdong Province (2019A1515010622), the Foundation of Featured Clinical Technique of Guangzhou (2019TS24), the Foundation for high-level University Construction of Guangzhou Medical University (B195002010041), and the Clinical Independent Exploration Project Foundation of Guangzhou Institute of Respiratory Health/National Clinical Research Center for Respiratory Disease (2019GIRHZ02).

## ACKNOWLEDGMENTS

We thank LetPub ([www.letpub.com](http://www.letpub.com)) for its linguistic assistance and scientific consultation during the preparation of this manuscript.

## SUPPLEMENTARY MATERIAL

The Supplementary Material for this article can be found online at: <https://www.frontiersin.org/articles/10.3389/fmolb.2021.653461/full#supplementary-material>

**Supplementary Figure 1 |** Correlations between Axl or IGFBP-4 protein levels and sputum eosinophilic cell count in EGPA patients (Spearman correlation). Only the significant correlations are shown in dot plots. Two protein markers had serum levels correlated with eosinophil cell counts. Blue dots represent data from patients with inactive disease. Red triangles represent data from patients with active disease. *P* values and Spearman correlation coefficients are displayed.

**Supplementary Figure 2 |** ROC combination analysis of Axl, BMP-4 and SCF. Combination ROC curve showing the sensitivity and specificity for cutoff values of Axl with BMP-4 and SCF. Red dot indicates sensitivity at the specificity. ROC, receiver operating characteristic; AUC, area under the ROC curve.

**Supplementary Table 1 |** Information of 160 soluble proteins.

**Supplementary Table 2 |** The nodes or serum proteins of each cluster of network in active EGPA.

**Supplementary Table 3 |** The nodes or serum proteins of each cluster of network in inactive EGPA.

**Supplementary Table 4 |** Differentially expressed proteins from unpaired nonparametric Mann-Whitney test.

**Supplementary Table 5 |** Summary of the ROC curve analysis.

## REFERENCES

- Brown, M., Black, J. R., Sharma, R., Stebbing, J., and Pinato, D. J. (2016). Gene of the month: Axl. *J. Clin. Pathol.* 69, 391–397. doi: 10.1136/jclinpath-2016-203629
- Churg, J., and Strauss, L. (1951). Allergic granulomatosis, allergic angiitis, and periarteritis nodosa. *Am. J. Pathol.* 27, 277–301.
- Dallos, T., Heiland, G. R., Strehl, J., Karonitsch, T., Gross, W. L., Moosig, F., et al. (2010). CCL17/thymus and activation-related chemokine in Churg-Strauss syndrome. *Arthritis Rheum.* 62, 3496–3503. doi: 10.1002/art.27678
- Dejaco, C., Oppl, B., Monach, P., Cuthbertson, D., Carette, S., Hoffman, G., et al. (2015). Serum biomarkers in patients with relapsing eosinophilic granulomatosis with polyangiitis (Churg-Strauss). *PLoS One* 10:e121737. doi: 10.1371/journal.pone.0121737
- Di Stasi, R., De Rosa, L., and D'Andrea, L. D. (2020). Therapeutic aspects of the Axl/Gas6 molecular system. *Drug Discov. Today* 25, 2130–2148. doi: 10.1016/j.drudis.2020.09.022
- Espindola, M. S., Habel, D. M., Narayanan, R., Jones, I., Coelho, A. L., Murray, L. A., et al. (2018). Targeting of TAM receptors ameliorates fibrotic mechanisms in idiopathic pulmonary fibrosis. *Am. J. Respir. Crit. Care Med.* 197, 1443–1456. doi: 10.1164/rccm.201707-1519OC
- Furuta, S., Iwamoto, T., and Nakajima, H. (2019). Update on eosinophilic granulomatosis with polyangiitis. *Allergol. Int.* 68, 430–436. doi: 10.1016/j.alit.2019.06.004
- Grayson, P. C., Monach, P. A., Pagnoux, C., Cuthbertson, D., Carette, S., Hoffman, G. S., et al. (2015). Value of commonly measured laboratory tests as biomarkers of disease activity and predictors of relapse in eosinophilic granulomatosis with polyangiitis. *Rheumatology* 54, 1351–1359. doi: 10.1093/rheumatology/keu427
- Guilpain, P., Auclair, J. F., Tamby, M. C., Servetaz, A., Mahr, A., Weill, B., et al. (2007). Serum eosinophil cationic protein: a marker of disease activity in Churg-Strauss syndrome. *Ann. N. Y. Acad. Sci.* 1107, 392–399. doi: 10.1196/annals.1381.041
- Guilpain, P., Guillevin, L., and Mouthon, L. (2006). [Eosinophil granule cationic proteins: eosinophil activation markers]. *Rev. Med. Internet* 27, 406–408. doi: 10.1016/j.revmed.2006.01.008
- Huang, D. W., Sherman, B. T., Tan, Q., Kir, J., Liu, D., Bryant, D., et al. (2007). DAVID bioinformatics resources: expanded annotation database and novel algorithms to better extract biology from large gene lists. *Nucleic Acids Res.* 35, W169–W175. doi: 10.1093/nar/gkm415
- Korshunov, V. A. (2012). Axl-dependent signalling: a clinical update. *Clin. Sci.* 122, 361–368. doi: 10.1042/CS20110411
- Lancichinetti, A., and Fortunato, S. (2009). Community detection algorithms: a comparative analysis. *Phys. Rev. E Stat. Nonlin. Soft Matter Phys.* 80(5 Pt 2), 56117. doi: 10.1103/PhysRevE.80.056117
- Lee, C. H., and Chun, T. (2019). Anti-inflammatory role of TAM family of receptor tyrosine kinases via modulating macrophage function. *Mol. Cells* 42, 1–7. doi: 10.14348/molcells.2018.0419
- Lightfoot, R. J., Michel, B. A., Bloch, D. A., Hunder, G. G., Zvaifler, N. J., McShane, D. J., et al. (1990). The american college of rheumatology 1990 criteria for the classification of polyarteritis nodosa. *Arthritis Rheum.* 33, 1088–1093. doi: 10.1002/art.1780330805
- Lugmani, R. A., Bacon, P. A., Moots, R. J., Janssen, B. A., Pall, A., Emery, P., et al. (1994). Birmingham Vasculitis Activity Score (BVAS) in systemic necrotizing vasculitis. *QJM* 87, 671–678.
- Masi, A. T., Hunder, G. G., Lie, J. T., Michel, B. A., Bloch, D. A., Arend, W. P., et al. (1990). The American College of Rheumatology 1990 criteria for the classification of Churg-Strauss syndrome (allergic granulomatosis and angiitis). *Arthritis Rheum.* 33, 1094–1100. doi: 10.1002/art.1780330806
- Miller, M. R., Hankinson, J., Brusasco, V., Burgos, F., Casaburi, R., Coates, A., et al. (2005). Standardisation of spirometry. *Eur. Respir. J.* 26, 319–338. doi: 10.1183/09031936.05.00034805
- Nguyen, Y., and Guillevin, L. (2018). Eosinophilic granulomatosis with polyangiitis (Churg-Strauss). *Semin. Respir. Crit. Care Med.* 39, 471–481. doi: 10.1055/s-0038-1669454
- Pagnoux, C., Nair, P., Xi, Y., Khalidi, N. A., Carette, S., Cuthbertson, D., et al. (2019). Serum cytokine and chemokine levels in patients with eosinophilic granulomatosis with polyangiitis, hypereosinophilic syndrome, or eosinophilic asthma. *Clin. Exp. Rheumatol.* 37(Suppl. 117), 40–44.
- Polzer, K., Karonitsch, T., Neumann, T., Eger, G., Haberler, C., Soleiman, A., et al. (2008). Eotaxin-3 is involved in Churg-Strauss syndrome—a serum marker closely correlating with disease activity. *Rheumatology* 47, 804–808. doi: 10.1093/rheumatology/ken033
- Rhee, R. L., Holweg, C., Wong, K., Cuthbertson, D., Carette, S., Khalidi, N. A., et al. (2018). Serum periostin as a biomarker in eosinophilic granulomatosis with polyangiitis. *PLoS One* 13:e205768. doi: 10.1371/journal.pone.0205768
- Robins, S., Roussel, L., Schachter, A., Risse, P. A., Mogas, A. K., Olivenstein, R., et al. (2011). Steroid-insensitive ERK1/2 activity drives CXCL8 synthesis and neutrophilia by airway smooth muscle. *Am. J. Respir. Cell Mol. Biol.* 45, 984–990. doi: 10.1165/rcmb.2010-0450OC
- Roskoski, R. J. (2012). ERK1/2 MAP kinases: structure, function, and regulation. *Pharmacol. Res.* 66, 105–143. doi: 10.1016/j.phrs.2012.04.005
- Sanderson, C. J. (1988). Interleukin-5: an eosinophil growth and activation factor. *Dev. Biol. Stand.* 69, 23–29.
- Sasaki, T., Knyazev, P. G., Clout, N. J., Cheburkin, Y., Gohring, W., Ullrich, A., et al. (2006). Structural basis for Gas6-Axl signalling. *EMBO J.* 25, 80–87. doi: 10.1038/sj.emboj.7600912
- Song, H. H. (1997). Analysis of correlated ROC areas in diagnostic testing. *Biometrics* 53, 370–382.
- Vaglio, A., Strehl, J. D., Manger, B., Maritati, F., Alberici, F., Beyer, C., et al. (2012). IgG4 immune response in Churg-Strauss syndrome. *Ann. Rheum. Dis.* 71, 390–393. doi: 10.1136/ard.2011.155382
- Wang, S., Qiu, Z., Hou, Y., Deng, X., Xu, W., Zheng, T., et al. (2021). AXL is a candidate receptor for SARS-CoV-2 that promotes infection of pulmonary and bronchial epithelial cells. *Cell Res.* 31, 126–140. doi: 10.1038/s41422-020-00460-y
- Zagvozdina, E. S., Moiseev, S. V., and Novikov, P. I. (2016). Eotaxin-3 as a biomarker of activity in established eosinophilic granulomatosis with polyangiitis. *J. Rheumatol.* 43, 2082–2083. doi: 10.3899/jrheum.160576

**Conflict of Interest:** The authors declare that the research was conducted in the absence of any commercial or financial relationships that could be construed as a potential conflict of interest.

The handling editor declared a past collaboration with several of the authors MQ, NZ, and QZ.

Copyright © 2021 Ma, Dong, Wei, Qiu, Wu, Ou, Zhang, Zhang, Yan, Zhang and Zhong. This is an open-access article distributed under the terms of the Creative Commons Attribution License (CC BY). The use, distribution or reproduction in other forums is permitted, provided the original author(s) and the copyright owner(s) are credited and that the original publication in this journal is cited, in accordance with accepted academic practice. No use, distribution or reproduction is permitted which does not comply with these terms.





# Efficacy and Safety of Combination Treatment With Apatinib and Osimertinib After Osimertinib Resistance in Epidermal Growth Factor Receptor-Mutant Non-small Cell Lung Carcinoma—A Retrospective Analysis of a Multicenter Clinical Study

## OPEN ACCESS

### Edited by:

Huahao Shen,  
Zhejiang University, China

### Reviewed by:

Paromita Raha,  
Bold Therapeutics, Canada  
Jianchun Duan,

Cancer Hospital, Chinese Academy  
of Medical Sciences and Peking  
Union Medical College, China  
Wenfeng Fang,  
Sun Yat-sen University Cancer Center  
(SYSUCC), China

### \*Correspondence:

Jun Zhao  
ohjerry@163.com

† These authors have contributed  
equally to this work

### Specialty section:

This article was submitted to  
Molecular Diagnostics  
and Therapeutics,  
a section of the journal  
Frontiers in Molecular Biosciences

**Received:** 10 December 2020

**Accepted:** 12 April 2021

**Published:** 05 May 2021

### Citation:

Yang X, Xia Y, Xu L, Liang L,  
Zhuo M, Wu M, An T, Wang Z,  
Wang Y, Li J, Zhong J, Chen H, Jia B,  
Wang J and Zhao J (2021) Efficacy  
and Safety of Combination Treatment  
With Apatinib and Osimertinib After  
Osimertinib Resistance in Epidermal  
Growth Factor Receptor-Mutant  
Non-small Cell Lung Carcinoma—A  
Retrospective Analysis of a  
Multicenter Clinical Study.  
Front. Mol. Biosci. 8:639892.  
doi: 10.3389/fmolb.2021.639892

Xue Yang<sup>1†</sup>, Yang Xia<sup>2†</sup>, Liyan Xu<sup>3</sup>, Li Liang<sup>4</sup>, Minglei Zhuo<sup>1</sup>, Meina Wu<sup>1</sup>, Tongtong An<sup>1</sup>,  
Ziping Wang<sup>1</sup>, Yuyan Wang<sup>1</sup>, Jianjie Li<sup>1</sup>, Jia Zhong<sup>1</sup>, Hanxiao Chen<sup>1</sup>, Bo Jia<sup>1</sup>,  
Jingjing Wang<sup>1</sup> and Jun Zhao<sup>1\*</sup>

<sup>1</sup> Key Laboratory of Carcinogenesis and Translational Research (Ministry of Education), Department of Thoracic Medical  
Oncology, Peking University Cancer Hospital and Institute, Beijing, China, <sup>2</sup> Key Laboratory of Respiratory Disease  
of Zhejiang Province, Department of Respiratory and Critical Care Medicine, Second Affiliated Hospital of Zhejiang University  
School of Medicine, Hangzhou, Zhejiang, China, <sup>3</sup> Department of Medical Oncology, Beijing Chest Hospital, Capital Medical  
University, Beijing, China, <sup>4</sup> Department of Tumor Chemotherapy and Radiation Sickness, Peking University Third Hospital,  
Beijing, China

Currently, there are limited treatment options for patients who developed resistance to osimertinib, a third-generation epidermal growth factor receptor (EGFR) inhibitor. Resistance to EGFR inhibitors is frequently associated with enhanced vascular endothelial growth factor (VEGF) levels. This multicenter, retrospective study aimed to evaluate the efficacy of the combination treatment with apatinib and osimertinib in 39 patients with EGFR-mutant non-small cell lung carcinoma (NSCLC) who developed osimertinib resistance. The patients received the combination of oral apatinib 250 mg qd and osimertinib 80 mg qd. The efficacy was evaluated after the first month then every 2 months thereafter. The primary endpoint was progression-free survival (PFS). The overall response rate (ORR) and the disease control rate (DCR) of the combination of apatinib and osimertinib was 12.8% (5/39) and 79.5% (31/39), respectively. The median PFS was 4 months [95% confidence interval (CI): 3.5–4.5 months]. Fourteen patients were administered with at least 6 months of combination therapy, and 11 of them remained on treatment programs. The 6-month PFS rate was 38%. Nine patients underwent biopsies after failing osimertinib treatment, and five of six patients with TP53 mutations had PFS of less than 3 months. The spectrum of resistance to osimertinib mechanisms included c-mesenchymal-epithelial transition factor (c-Met) amplification, phosphatidylinositol-4,5-bisphosphate 3-kinase catalytic subunit alpha (PIK3CA) gain-of-function mutation, phosphatase and tensin homolog (PTEN) loss-of-function mutation, Erb-B2 receptor tyrosine kinase 2 (ERBB2) amplification, and insulin-like growth factor 1 receptor (IGF1R) mutation. The most

common adverse events were hypertension (30.7%, 12/39), diarrhea (15.4%, 6/39), and proteinuria (12.8%, 5/39). The combination of apatinib and osimertinib improved the ORR and the DCR of patients with osimertinib-refractory EGFR-positive NSCLC, thus making it a reasonable treatment choice after the development of osimertinib resistance.

**Keywords:** osimertinib, apatinib, EGFR, NSCLC, resistance

## INTRODUCTION

Osimertinib, a third-generation epidermal growth factor receptor-tyrosine kinase inhibitor (EGFR-TKI), can selectively block mutations that are sensitive to EGFR-TKI. It is resistant to EGFR T790M mutation. In patients with non-small cell lung carcinoma (NSCLC) who had EGFR T790M mutations that are resistant to both first- and second-generation EGFR-TKIs, it can help achieve a median progression-free survival (PFS) of approximately 10 months (Mok et al., 2017). However, some patients are becoming resistant to osimertinib, which presents additional challenges. Currently, there are limited treatment options for patients who developed osimertinib resistance (Planchard et al., 2015; Ou et al., 2016; Zhou et al., 2019).

Resistance to EGFR inhibitors is frequently associated with enhanced vascular endothelial growth factor (VEGF) levels. Dual inhibition of the VEGF receptor (VEGFR) and EGFR signaling pathways shows the potential to overcome osimertinib resistance (Naumov et al., 2009; Larsen et al., 2011). Apatinib is an oral tyrosine kinase inhibitor that targets VEGFR-2 (Mi et al., 2010). We previously reported good efficacy and prolonged PFS benefit of using the combination of apatinib and a first-generation EGFR-TKI in cases of EGFR mutation-positive NSCLC (Li et al., 2017) progression. However, there are no data about the efficacy of the combination of a VEGFR inhibitor and osimertinib after third-generation EGFR-TKI failure. Thus, this study aimed to evaluate the efficacy of the combination of apatinib and osimertinib in patients with EGFR-mutant NSCLC who developed osimertinib resistance.

## MATERIALS AND METHODS

### Study Population

In this analysis, 39 patients were enrolled from four participating institutions, namely, Peking University Cancer Hospital ( $n = 24$ ), Second Affiliated Hospital of Zhejiang University School of Medicine ( $n = 9$ ), Beijing Chest Hospital ( $n = 4$ ), and Peking University Third Hospital ( $n = 2$ ), between March 1, 2018 and November 1, 2019 (Figure 1). Every patient who displayed resistance to osimertinib during treatment

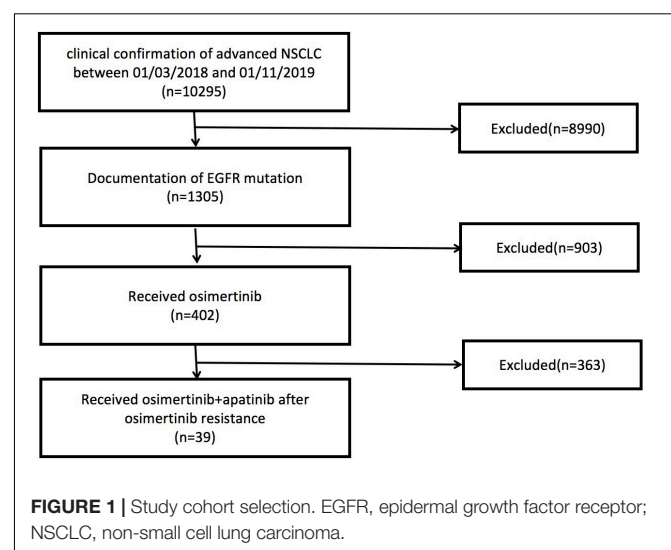
for advanced lung adenocarcinoma was identified from the databases of the four institutions. All the patients received the combination of osimertinib and apatinib after progression of osimertinib resistance. None of the enrolled patients received other types of antiangiogenic therapy except for apatinib prior to or during combination therapy. This multicenter, retrospective study was approved by the ethics committee of the four participating institutions. All the patients provided informed consent for treatment in this protocol.

### Treatment Regimens

The patients received osimertinib at a dose of 80 mg and apatinib at a dose of 250 mg, taken orally once daily. The treatment would be discontinued in the event of disease progression, unacceptable toxicity, or if the physician or patient opted to end the treatment.

### Efficacy and Safety Assessments

Tumor response was radiographically evaluated according to RECIST guidelines version 1.1. Efficacy evaluation was conducted after the first month, then every two months thereafter. The primary endpoint was PFS, which is defined as the time from the first administration of the combination of osimertinib and apatinib to the first documentation of progression of disease according to RECIST guidelines version 1.1. The ORR was calculated as the sum of CR and PR rates, whereas the DCR was calculated as the sum of SD, CR, and PR rates. Toxicities during osimertinib and apatinib combination treatment were assessed



**Abbreviations:** CR, complete response; CI, confidence interval; DCR, disease control rate; EGFR, epidermal growth factor receptor; EGFR-TKI, epidermal growth factor receptor-tyrosine kinase inhibitor; NGS, next-generation sequencing; NSCLC, non-small cell lung carcinoma; ORR, overall response rate; PR, partial response; PFS, progression-free survival; RECIST, response evaluation criteria in solid tumors; SD, stable disease; VEGF, vascular endothelial growth factor; VEGFR, vascular endothelial growth factor receptor.

according to the Common Terminology Criteria for Adverse Events (CTCAE) 4.0 classification.

### Capture-Based Targeted Next-Generation Sequencing

A subgroup of the patients ( $n = 9$ ) enrolled in the study was subjected to several biopsies (liquid or tumor) once osimertinib resistance progressed and prior to the administration of apatinib. We obtained a biopsy of the tumor of a patient from a lesion, after which we performed targeted next-generation sequencing (NGS) according to previously described methods (Lin et al., 2018; Zhuo et al., 2020). Eight patients underwent liquid biopsy using targeted NGS as previously described (Zhuo et al., 2020). The collected samples of liquid biopsy included peripheral blood ( $n = 6$ ), pleural effusion ( $n = 1$ ), and cerebrospinal fluid ( $n = 1$ ).

**TABLE 1 |** Baseline clinical features of patients enrolled in the study ( $n = 39$ ).

Characteristic	Value
<b>Sex</b>	
Male	18 (46%)
Female	21 (54%)
<b>Age (years)</b>	
Median	54
<65	31 (79%)
≥65	8 (21%)
<b>Smoking history</b>	
Yes	9 (24%)
No	30 (76%)
<b>ECOG performance status</b>	
≤1	31 (79%)
2	8 (21%)
<b>Stage</b>	
Iva	14 (36%)
IVb	25 (64%)
<b>Metastasis site</b>	
Brain	18 (46%)
Bone	17 (44%)
Liver	12 (31%)
<b>EGFR mutation status</b>	
EGFR exon 19 del	16 (41%)
EGFR exon 21 L858R	17 (44%)
EGFR exon 18 G719X	6 (15%)
<b>Osimertinib treatment</b>	
First line	4 (10%)
Second line	25 (64%)
Beyond second line	10 (26%)
<b>Previous treatment</b>	
Radiotherapy	5 (13%)
Chemotherapy	10 (26%)
<b>Osimertinib disease progression model</b>	
Intrathoracic progression	24 (62%)
Extrathoracic progression	15 (38%)

ECOG, Eastern Cooperative Oncology Group; EGFR, epidermal growth factor receptor.

### Statistical Analysis

The Kaplan–Meier method was used to estimate the median PFS, while we produced 95% CIs with a log–log transformation. Safety analyses were done through descriptive methods as well as percentages. SPSS version 22.0 (IBM, Armonk, NY, United States) was used to calculate and produce the results of all statistical analyses performed in this study.  $P < 0.05$  was considered statistically significant.

## RESULTS

### Patient Characteristics

Of the 39 patients, 18 were male and 21 were female. Thirty patients were never smokers, while nine of them were current or former smokers. Every patient was a carrier of EGFR mutations; and according to their TKI-naïve samples, there were 16 exon 19 deletion, 17 exon 21 L858R mutation, and 6

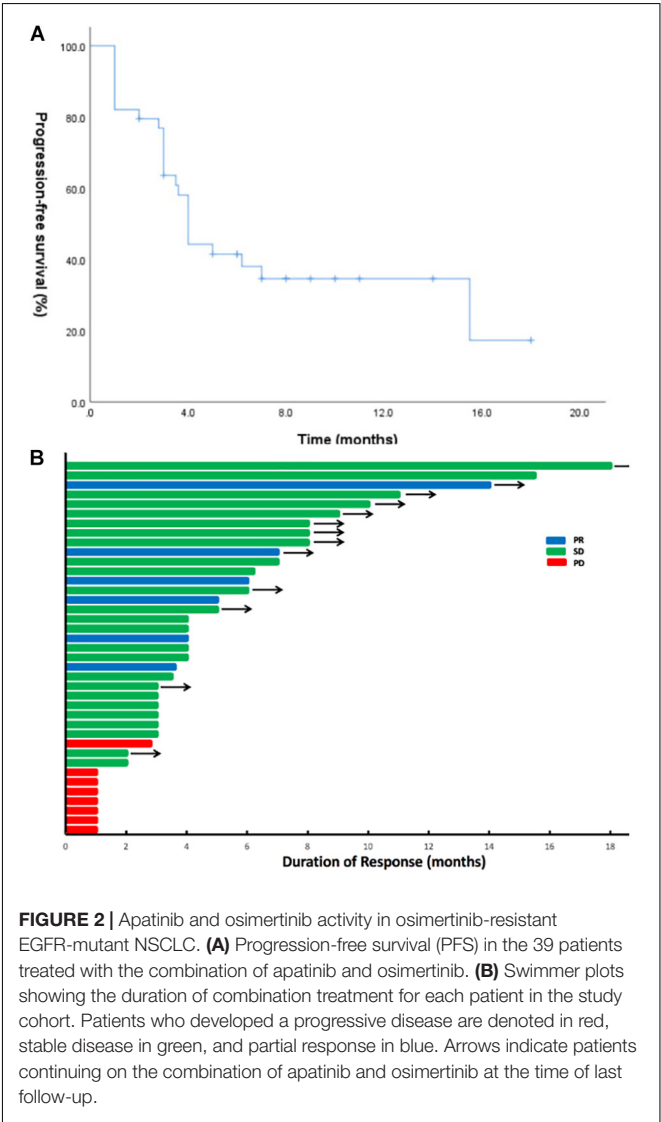


**FIGURE 2 |** Apatinib and osimertinib activity in osimertinib-resistant EGFR-mutant NSCLC. **(A)** Progression-free survival (PFS) in the 39 patients treated with the combination of apatinib and osimertinib. **(B)** Swimmer plots showing the duration of combination treatment for each patient in the study cohort. Patients who developed a progressive disease are denoted in red, stable disease in green, and partial response in blue. Arrows indicate patients continuing on the combination of apatinib and osimertinib at the time of last follow-up.

exon 18 G719X mutation cases. In total, 4, 25, and 10 patients received osimertinib as first-, second-, and later-line treatment, respectively. The median PFS for osimertinib was 8 months (95% CI: 7.1–8.9). NGS data from 9 patients who developed osimertinib resistance were available for analysis. The clinical characteristics of the patients are listed in **Table 1**.

### Molecular Characteristics of Post-osimertinib/Pre-combination Treatment Specimens

Rebiopsy for NGS was performed in nine patients during osimertinib treatment and prior to the combination treatment. We found that of all somatic variations in nine patients, mutations related to EGFR sensitivity were the most common. TP53 mutation was found in seven of nine patients (77.8%), whereas T790M mutation was identified in four of nine patients (44.4%). The spectrum of resistance to osimertinib mechanisms included c-Met amplification ( $n = 1$ ), PIK3CA gain-of-function mutation ( $n = 1$ ), PTEN loss-of-function mutation ( $n = 1$ ), ERBB2 amplification ( $n = 1$ ), and IGF1R mutation ( $n = 1$ ).

### Outcomes of Combination of Apatinib and Osimertinib Treatment

Until the last follow-up on April 1, 2020, the disease progressed in 25 patients (64.1%), and the remaining 14 patients (35.9%) were still being treated with combination therapy (**Figure 2**). The median follow-up time was 9.8 months (range: 4.8–24.8 months). The ORR and the DCR for the combination of apatinib and osimertinib were 12.8% (5/39) and 79.5% (31/39), respectively. Median PFS was 4 months (95% CI: 3.5–4.5). Fourteen patients had received at least a 6-month combination therapy, and 11 of them were still on treatment. The 6-month PFS rate was 38%. The data are based on treatment length and patient response to the profiling of mutations after the development of osimertinib resistance and are shown in **Figure 3**. Among the 6 patients whose PFS less than 3 months, 5 had pathogenic mutations of TP53 and 3 had maintained T790M (**Table 2**). Examples of three cases with different resistance mechanisms demonstrated various therapeutic effects (**Figure 4**).

The most frequently observed adverse events were hypertension (30.7%, 12/39), diarrhea (15.4%, 6/39), and proteinuria (12.8%, 5/39). Other less common adverse events

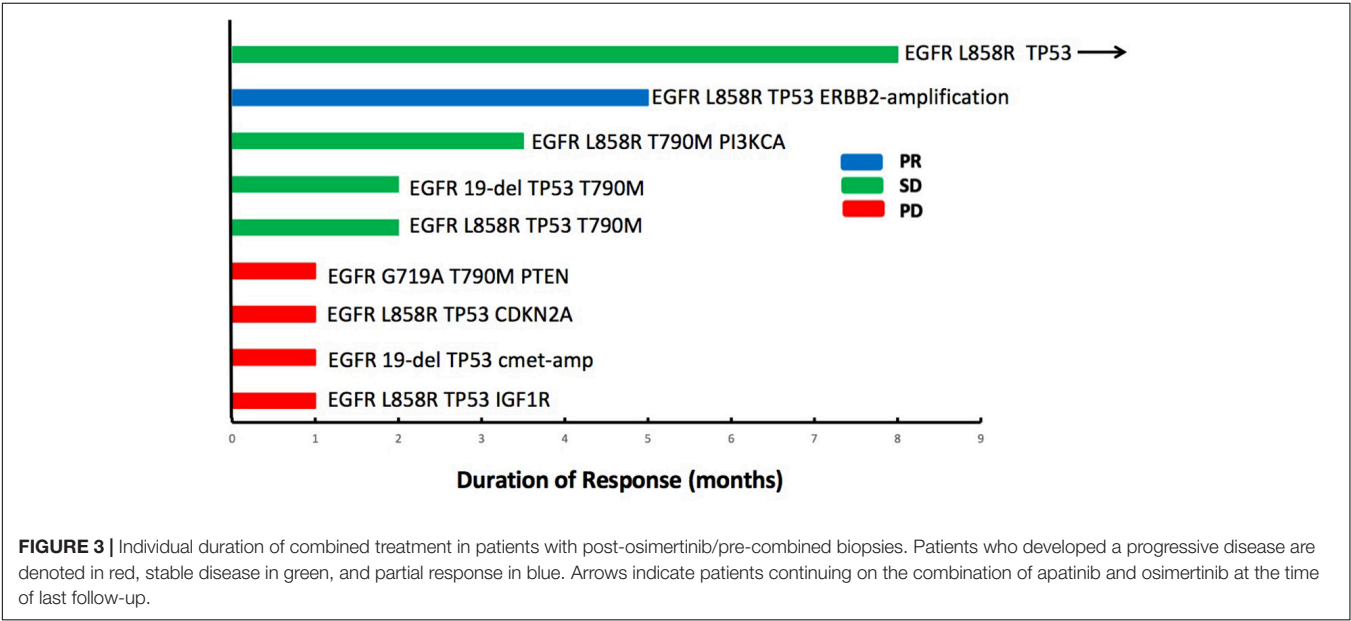


**TABLE 2 |** Basic characteristics of nine patients with NGS testing.

Patient No.	Gender	Age	Smoking history	ECOG	Stage	EGFR mutation	PFS of Osimertinib (months)	Osimertinib PD model
1	M	61	No	1	IVa	L858R	8	Extrathoracic
2	M	62	No	2	IVb	19-del	8	Extrathoracic
3	F	55	No	1	IVa	L858R	12	Intrathoracic
4	F	44	No	1	IVb	G719A	6	Intrathoracic
5	F	54	No	1	IVa	L858R	2	Intrathoracic
6	F	66	No	2	IVa	19-del	11	Intrathoracic
7	M	35	No	1	IVb	L858R	6	Intrathoracic
8	M	62	No	1	IVb	L858R	12	Extrathoracic
9	F	53	No	1	IVb	L858R	8	Intrathoracic



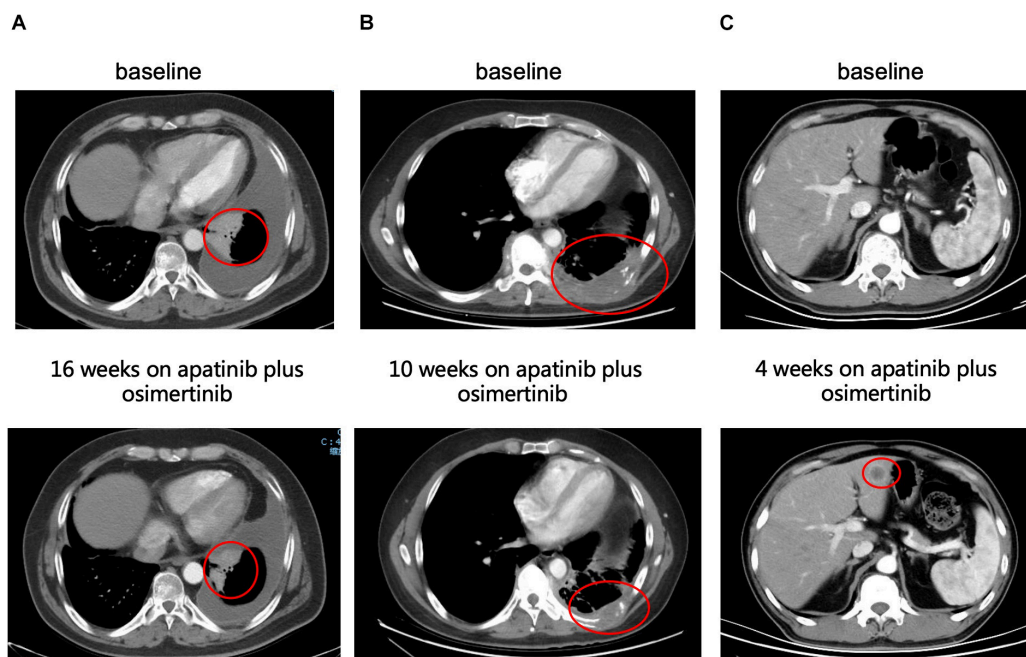


**FIGURE 4 |** Examples of tumor response to the combination of apatinib and osimertinib in EGFR-positive cases with osimertinib resistance. **(A)** Partial response of a left lung mass to combination therapy in a patient with TP53 mutation detected post-osimertinib/pre-combined treatment biopsy. This patient remained on treatment at the time of last follow-up. **(B)** Partial response of a left chest wall mass to combination therapy in a patient with TP53 mutation and ERBB2-amplification detected post-osimertinib/pre-combined treatment biopsy. **(C)** Progressive disease demonstrated with new hepatic metastases after 1 month of combination treatment in a patient with TP53 and PTEN loss-of-function mutations detected in the post-osimertinib/pre-combined treatment biopsy.

**TABLE 3 |** Treatment-related adverse events in all patients ( $n = 39$ ).

	Any grade*	Grades 1–2*	Grade 3*
Adverse event	35 (90%)	31 (79%)	4 (11%)
Hypertension	12 (31%)	10 (26%)	2 (5%)
Diarrhea	6 (15%)	6 (15%)	–
Proteinuria	5 (13%)	5 (13%)	–
Rash	3 (8%)	2 (5%)	1 (3%)
Hand–foot syndrome	3 (8%)	3 (8%)	–
Hoarseness	2 (5%)	2 (5%)	–
Thrombocytopenia	2 (5%)	2 (5%)	–
Liver dysfunction	1 (3%)	1 (3%)	–
Decreased left ventricular ejection fraction	1 (3%)	–	1 (3%)

\*Grading per the Common Terminology Criteria for Adverse Events, version 4.0.

included rash ( $n = 3$ ), hand–foot syndrome ( $n = 3$ ), hoarseness ( $n = 2$ ), thrombocytopenia ( $n = 2$ ), and liver dysfunction ( $n = 1$ ). Notably, a patient achieved partial response; however, the combination therapy was terminated because of tachycardia and markedly decreased left ventricular ejection fraction (Table 3).

## DISCUSSION

Significant research has been conducted on osimertinib resistance, and treatment strategies after osimertinib treatment failure have been evaluated (Le et al., 2018; Leonetti et al., 2019; Zhao et al., 2020). However, there are limited data on the use

of apatinib after the development of osimertinib resistance. Given the broad range of resistance mechanisms currently emerging with osimertinib, the potential role of combination therapy in certain osimertinib-refractory settings warrants further investigation. This multicenter retrospective analysis demonstrated that treating patients with the combination of osimertinib and apatinib resulted in a 13% ORR and a median PFS of 4 months, together with a safety profile (Lin et al., 2018). In the scope of our knowledge, this is the first large-scale study to assess the clinical nature of administering combination therapy with osimertinib and apatinib under osimertinib-refractory conditions.

Resistance to osimertinib is related to genomic alterations that are both dependent and independent of EGFR and includes an acquired tertiary mutation related to EGFR resistance (EGFR C797S mutation), MET amplification, aberrations in downstream signaling pathways (mutations in the RAS and RAF genes), and epithelial–mesenchymal transition (Ricordel et al., 2018). For patients with EGFR C797S found alongside T790M, the PFS for the combination treatment of erlotinib and osimertinib was almost 3 months (Wang et al., 2017). Treatment using a combination of cetuximab and brigatinib showed promising results for patients with EGFR-T790M-*cis*-C797S mutations; however, in this study, only few patients were assessed.

To date, For MET-driven acquired resistance, the longest PFS for combination treatment with c-Met inhibitor and osimertinib has been almost 5 months (Sequist et al., 2020). Aside from these types of targeted therapy, the addition of antiangiogenic inhibitors to EGFR-TKI therapy after progression of EGFR-TKI therapy is also an attractive strategy. Preclinical and clinical evidence suggests that EGFR-TKIs may work synergistically with VEGF inhibitors (Naumov et al., 2009; Larsen et al., 2011). We previously showed that apatinib, together with gefitinib, displayed significant antitumor properties in patients with NSCLC because of EGFR-TKI resistance related to T790M, under both *in vitro* and *in vivo* conditions (Li et al., 2017). Moreover, a previous retrospective analysis of patients with advanced NSCLC who failed icotinib treatment showed that the combination of apatinib and icotinib reached a median PFS of 5.33 months (95% CI: 3.63–7.03 months) (Xu et al., 2017). Additionally, patients with EGFR-mutant NSCLC who were first treated with a combination therapy using apatinib and gefitinib demonstrated prolonged PFS inclinations, indicating that the therapy was a reasonable treatment (Zhang et al., 2019). Collectively, these findings support that treatments using the combination of apatinib and a first-generation EGFR-TKI is well tolerated and has good efficacy.

This study produced results similar to those of Liu et al., who assessed three patients afflicted with T790M-positive lung adenocarcinoma. After progression of osimertinib resistance, their patients responded to sustained therapy combining osimertinib and apatinib within a PFS range of 5–7 months (Liu et al., 2019). This suggests that the particular mechanism related to resistance could alter patient response to the apatinib and osimertinib treatment in osimertinib-refractory tumors. EGFR-mutant NSCLC could be affected by changes in TP53, which would result in reduced genomic stability. Previous studies have shown that concomitant TP53 mutations were correlated with lower survival rates in patients with EGFR alterations (Blakely et al., 2017). In our study, we also found that pathogenic TP53 mutation was the most common mutation after the development of osimertinib resistance. In addition to TP53 mutation, maintained T790M mutation was also associated with heterogeneous mechanisms of resistance (PI3KCA mutation and PTEN loss). This finding indicated that subclones with T790M mutants can be found alongside subclones with specific mechanisms related to resistance (Zhao et al., 2020). In this case, targeting T790M alone is unlikely to result in clinical benefit. Among the three of four patients who barely benefited from the combination therapy, with PFS of less than 1 month, T790M loss was related to the progression of other mechanisms

related to resistance, such as c-Met amplification and IGF1R and CDKN2A mutations. Our findings underscore the value of conducting multiple biopsies (Lin et al., 2018) in patients who develop progression during osimertinib treatment. In addition, it is essential to explore novel biomarkers predictive of treatment response to the combination of osimertinib and apatinib in patients with osimertinib resistance.

This retrospective study had several limitations and lacked a control group. Moreover, while a multicenter analysis was performed to identify patient eligibility, selection bias was still a potential problem. Thus, further multicenter prospective research is required to validate the experiment results.

In summary, the combination of apatinib and osimertinib in osimertinib-refractory EGFR-positive NSCLC improved the ORR and the DCR. The results promote combination treatment therapy in patients with osimertinib resistance, especially in ones with a non-targetable resistance mechanism. Further studies are warranted to determine biomarkers predictive of treatment response to anti-VEGF therapy for patients with osimertinib-resistant EGFR-mutant NSCLC.

## DATA AVAILABILITY STATEMENT

The data used to produce the results of this study are not publicly available due to ethical and privacy restrictions. However, the data are available from the corresponding author upon request.

## ETHICS STATEMENT

This multicenter, retrospective study was approved by the ethics committee of four participating institutions. All patients provided informed consent for treatment in this protocol.

## AUTHOR CONTRIBUTIONS

XY and JZa: conception and design. XY, YX, LX, LL, MZ, MW, TA, ZW, YW, and JL: acquisition of data (provided acquired and managed patients, provided facilities, etc.). XY, JZo, HC, BJ, and JW: analysis and interpretation of data (e.g., statistical analysis, biostatistics). XY, YX, LX, LL, and JZa: writing, review, and/or revision of the manuscript. All authors contributed to the article and approved the submitted version.

## FUNDING

The study was supported by Wu Jieping medical foundation Research Fund (320.6750.19094-2), by Beijing Hospitals Authority Research Incubation Program (PX2020044), and by AiYou Foundation (KY201701).

## ACKNOWLEDGMENTS

The authors would like to thank Liting Guo for editing the manuscript. The number of patients and results have been expanded since the data first appeared as conference manuscripts on WCLC 2019.

## REFERENCES

- Blakely, C. M., Watkins, T. B. K., Wu, W., Gini, B., Chabon, J. J., McCoach, C. E., et al. (2017). Evolution and clinical impact of co-occurring genetic alterations in advanced-stage EGFR-mutant lung cancers. *Nat. Genet.* 49, 1693–1704. doi: 10.1038/ng.3990
- Larsen, A. K., Ouaret, D., El Quadrani, K., and Petitprez, A. (2011). Targeting EGFR and VEGF(R) pathway cross-talk in tumor survival and angiogenesis. *Pharmacol. Ther.* 131, 80–90. doi: 10.1016/j.pharmthera.2011.03.012
- Le, X., Puri, S., Negrao, M. V., Nilsson, M. B., Robichaux, J., Boyle, T., et al. (2018). Landscape of EGFR-dependent and -independent resistance mechanisms to osimertinib and continuation therapy beyond progression in EGFR-mutant NSCLC. *Clin. Cancer Res.* 24, 6195–6203. doi: 10.1158/1078-0432.ccr-18-1542
- Leonetti, A., Sharma, S., Minari, R., Perego, P., Giovannetti, E., and Tiseo, M. (2019). Resistance mechanisms to osimertinib in EGFR-mutated non-small cell lung cancer. *Br. J. Cancer.* 121, 725–737. doi: 10.1038/s41416-019-0573-8
- Li, F., Zhu, T., Cao, B., Wang, J., and Liang, L. (2017). Apatinib enhances antitumor activity of EGFR-TKIs in non-small cell lung cancer with EGFR-TKI resistance. *Eur. J. Cancer.* 84, 184–192. doi: 10.1016/j.ejca.2017.07.037
- Lin, J. J., Zhu, V. W., Schoenfeld, A. J., Yeap, B. Y., Saxena, A., Ferris, L. A., et al. (2018). Brigatinib in Patients With Alectinib-Refractory ALK-Positive NSCLC. *J. Thorac. Oncol.* 13, 1530–1538. doi: 10.1016/j.jtho.2018.06.005
- Liu, Y., Xiong, Z.-C., Sun, X., Sun, L., Zhang, S.-L., Ma, J.-T., et al. (2019). Impact of apatinib in combination with osimertinib on EGFR T790M-positive lung adenocarcinoma. *Trans Cancer Res.* 8, 2151–2163. doi: 10.21037/tcr.2019.09.35
- Mi, Y. J., Liang, Y. J., Huang, H. B., Zhao, H. Y., Wu, C. P., Wang, F., et al. (2010). Apatinib (YN968D1) reverses multidrug resistance by inhibiting the efflux function of multiple ATP-binding cassette transporters. *Cancer Res.* 70, 7981–7991. doi: 10.1158/0008-5472.can-10-0111
- Mok, T. S., Wu, Y. L., Ahn, M. J., Garassino, M. C., Kim, H. R., Ramalingam, S. S., et al. (2017). Osimertinib or platinum-pemetrexed in EGFR T790M-positive lung cancer. *N. Engl. J. Med.* 376, 629–640. doi: 10.1056/NEJMoa1612674
- Naumov, G. N., Nilsson, M. B., Cascone, T., Briggs, A., Straume, O., Akslen, L. A., et al. (2009). Combined vascular endothelial growth factor receptor and epidermal growth factor receptor (EGFR) blockade inhibits tumor growth in xenograft models of EGFR inhibitor resistance. *Clin. Cancer Res.* 15, 3484–3494. doi: 10.1158/1078-0432.ccr-08-2904
- Ou, S. I., Agarwal, N., and Ali, S. M. (2016). High MET amplification level as a resistance mechanism to osimertinib (AZD9291) in a patient that symptomatically responded to crizotinib treatment post-osimertinib progression. *Lung Cancer.* 98, 59–61. doi: 10.1016/j.lungcan.2016.05.015
- Planchard, D., Loriot, Y., Andre, F., Gobert, A., Auger, N., Lacroix, L., et al. (2015). EGFR-independent mechanisms of acquired resistance to AZD9291 in EGFR T790M-positive NSCLC patients. *Ann. Oncol.* 26, 2073–2078. doi: 10.1093/annonc/mdv319
- Ricordel, C., Friboulet, L., Facchinetti, F., and Soria, J. C. (2018). Molecular mechanisms of acquired resistance to third-generation EGFR-TKIs in EGFR T790M-mutant lung cancer. *Ann. Oncol.* 29, i28–i37. doi: 10.1093/annonc/mdx705
- Sequist, L. V., Han, J. Y., Ahn, M. J., Cho, B. C., Yu, H., Kim, S. W., et al. (2020). Osimertinib plus savolitinib in patients with EGFR mutation-positive, MET-amplified, non-small-cell lung cancer after progression on EGFR tyrosine kinase inhibitors: interim results from a multicentre, open-label, phase 1b study. *Lancet Oncol.* 21, 373–386. doi: 10.1016/s1470-2045(19)30785-5
- Wang, Z., Yang, J. J., Huang, J., Ye, J. Y., Zhang, X. C., Tu, H. Y., et al. (2017). Lung adenocarcinoma harboring EGFR T790M and in trans C797S responds to combination therapy of first- and third-generation EGFR TKIs and shifts allelic configuration at resistance. *J. Thorac. Oncol.* 12, 1723–1727. doi: 10.1016/j.jtho.2017.06.017
- Xu, J., Liu, X., Yang, S., Zhang, X., and Shi, Y. (2017). Apatinib plus icotinib in treating advanced non-small cell lung cancer after icotinib treatment failure: a retrospective study. *Oncol. Targets Ther.* 10, 4989–4995. doi: 10.2147/ott.s142686
- Zhang, Z., Luo, F., Zhang, Y., Ma, Y., Hong, S., Yang, Y., et al. (2019). The ACTIVE study protocol: apatinib or placebo plus gefitinib as first-line treatment for patients with EGFR-mutant advanced non-small cell lung cancer (CTONG1706). *Cancer Commun.* 39:69. doi: 10.1186/s40880-019-0414-4
- Zhao, J., Lin, G., Zhuo, M., Fan, Z., Miao, L., Chen, L., et al. (2020). Next-generation sequencing based mutation profiling reveals heterogeneity of clinical response and resistance to osimertinib. *Lung Cancer* 141, 114–118. doi: 10.1016/j.lungcan.2019.10.021
- Zhou, Z., Zhao, Y., Shen, S., Gu, L., Niu, X., Xu, Y., et al. (2019). Durable clinical response of lung adenocarcinoma harboring EGFR 19Del/T790M/in trans-C797S to combination therapy of first- and third-generation EGFR tyrosine kinase inhibitors. *J. Thorac. Oncol.* 14, e157–e159. doi: 10.1016/j.jtho.2019.04.020
- Zhuo, M., Guan, Y., Yang, X., Hong, L., Wang, Y., Li, Z., et al. (2020). The prognostic and therapeutic role of genomic subtyping by sequencing tumor or cell-free DNA in pulmonary large-cell neuroendocrine carcinoma. *Clin. Cancer Res.* 26, 892–901. doi: 10.1158/1078-0432.CCR-19-0556

**Conflict of Interest:** The authors declare that the research was conducted in the absence of any commercial or financial relationships that could be construed as a potential conflict of interest.

The reviewer JD declared a past co-authorship with several of the authors XY, JZo, HC, JZa, TA, and YW to the handling editor.

Copyright © 2021 Yang, Xia, Xu, Liang, Zhuo, Wu, An, Wang, Wang, Li, Zhong, Chen, Jia, Wang and Zhao. This is an open-access article distributed under the terms of the Creative Commons Attribution License (CC BY). The use, distribution or reproduction in other forums is permitted, provided the original author(s) and the copyright owner(s) are credited and that the original publication in this journal is cited, in accordance with accepted academic practice. No use, distribution or reproduction is permitted which does not comply with these terms.



# Pemetrexed-Platinum With or Without Bevacizumab for Chinese Chemo-Naive Advanced Lung Adenocarcinoma Patients: A Real-World Study

Xin Li<sup>1†</sup>, Jie Huang<sup>2†</sup>, Yao Qiu<sup>3</sup>, Qianyun Zhang<sup>3</sup>, Shaoyu Yang<sup>1</sup>, Kan Wu<sup>2</sup>, Jiaoli Wang<sup>4</sup>, Limin Wang<sup>4</sup>, Jian Ye<sup>4</sup>, Shenglin Ma<sup>2,5</sup>, Bing Xia<sup>2\*</sup> and Xueqin Chen<sup>1,3\*</sup>

<sup>1</sup>Department of Thoracic Oncology, Key Laboratory of Clinical Cancer Pharmacology and Toxicology Research of Zhejiang Province, Affiliated Hangzhou First People's Hospital, Zhejiang University School of Medicine, Hangzhou, China, <sup>2</sup>Department of Thoracic Oncology, Hangzhou Cancer Hospital, Zhejiang University School of Medicine, Hangzhou, China, <sup>3</sup>Department of Thoracic Oncology, Nanjing Medical University Affiliated Hangzhou Hospital, Hangzhou, China, <sup>4</sup>Department of Respiratory Disease, Affiliated Hangzhou First People's Hospital, Zhejiang University School of Medicine, Hangzhou, China, <sup>5</sup>Cancer Center, Zhejiang University, Hangzhou, China

## OPEN ACCESS

### Edited by:

Zhang Qingling,  
Guangzhou Institute of Respiratory  
Health, China

### Reviewed by:

Salva Mena-Mollá,  
University of Valencia, Spain  
Jianchun Duan,  
Chinese Academy of Medical  
Sciences and Peking Union Medical  
College, China

### \*Correspondence:

Bing Xia  
bingxia\_hzch@163.com  
Xueqin Chen  
chenxueqin@zju.edu.cn

<sup>†</sup>These authors have contributed  
equally to this work

### Specialty section:

This article was submitted to  
Pharmacology of Anti-Cancer Drugs,  
a section of the journal  
Frontiers in Pharmacology

**Received:** 04 January 2021

**Accepted:** 19 April 2021

**Published:** 07 May 2021

### Citation:

Li X, Huang J, Qiu Y, Zhang Q, Yang S,  
Wu K, Wang J, Wang L, Ye J, Ma S,  
Xia B and Chen X (2021) Pemetrexed-  
Platinum With or Without Bevacizumab  
for Chinese Chemo-Naive Advanced  
Lung Adenocarcinoma Patients: A  
Real-World Study.  
Front. Pharmacol. 12:649222.  
doi: 10.3389/fphar.2021.649222

Despite recent advances in the treatment of advanced non-small-cell lung cancer (NSCLC), bevacizumab plus platinum-based doublet chemotherapy remains a commonly used first-line regimen. This study was conducted to compare the efficacy and safety of pemetrexed-platinum with or without bevacizumab in Chinese chemo-naive advanced lung adenocarcinoma patients in a real-world setting. We retrospectively collected 100 patients who received pemetrexed-platinum with or without bevacizumab (PP,  $n = 46$ ; Bev+PP,  $n = 54$ ) until disease progression or unacceptable toxicity. Clinical characteristics of patients were balanced, except for the proportion of stage IV b+c (Bev+PP and PP: 67.4 vs. 37.0%,  $p = 0.0066$ ). Bev+PP significantly improved the objective response rate (ORR, 65 vs. 30%,  $p = 0.0004$ ) and progression-free survival (PFS, 7.4 vs. 6.8 months,  $p = 0.009$ ), but not overall survival (OS, 17.5 vs. 15.0 months,  $p = 0.553$ ) compared with PP. Treatment ( $p = 0.001$ ), gender ( $p = 0.008$ ), adrenal metastasis ( $p = 0.001$ ), and liver metastasis ( $p = 0.013$ ) were independent risk factors for PFS. Patients with adrenal metastasis tended to be at the highest risk of not benefiting from bevacizumab addition (HR [95% CI]: 2.244 [0.6495–7.753]). The safety profile was acceptable, and grade  $\geq 3$  toxicity occurred similarly. This study showed that pemetrexed-platinum plus bevacizumab was effective compared to chemotherapy alone in Chinese patients with advanced NSCLC.

**Keywords:** bevacizumab, pemetrexed, platinum, lung adenocarcinoma, adrenal metastasis

## INTRODUCTION

Lung cancer is the most common cancer in the world (Ferlay et al., 2019), and China is also faced with a heavy burden of lung cancer (Cao et al., 2020; Yang et al., 2020) which is linked to tobacco smoking, outdoor air pollution, household air pollution, etc. (Vermeulen et al., 2019; Guan et al., 2020). The rapid development of the pharmaceutical industry and molecular biology research,



especially on the tumor-associated immune microenvironment, has resulted in a variety of treatment options for lung adenocarcinoma patients including small-molecule tyrosine kinase inhibitors (TKIs) that target the EGFR/ALK/ROS1 (EAR) gene (Pakkala and Ramalingam, 2018) and immune checkpoint inhibitors that block the PD1/PD-L1 and B7/CTLA4 pathways (Bansal et al., 2016). However, for patients lacking the EAR mutations and PD-L1 expression, or in patients where these therapeutic strategies fail, platinum-based chemotherapy regimens have been commonly used in clinical practice.

Bevacizumab is a widely researched monoclonal antibody that inhibits VEGF-A and has been approved in combination with chemotherapy for the treatment of chemo-naïve non-small-cell lung cancer patients (Assoun et al., 2017; Garcia et al., 2020). Previous studies have shown that VEGF-A functions as a high-risk factor dampening the prognosis of lung cancer patients (Hu et al., 2013). Serum VEGF attenuates the efficacy of platinum-based chemotherapy in non-small-cell lung cancer (NSCLC) patients (Zang et al., 2017). Blockade of VEGF-A by bevacizumab decreases the microvessel structure density in tumors, reduces tumor volumes (Zhao et al., 2012), and reprograms the tumor immune microenvironment (Tamura et al., 2019), thus providing a rationale for combination strategies.

Previous observational cohort studies mainly explored the use of paclitaxel/platinum plus bevacizumab versus paclitaxel/platinum therapy in advanced NSCLC and demonstrated improved response and survival benefits of bevacizumab (Sandler et al., 2006; Zhou et al., 2015). A pointbreak study directly compared pemetrexed or paclitaxel combined with carboplatin and bevacizumab in patients with previously untreated stage IIIB or IV non-squamous NSCLC and reported significantly improved progression-free survival (PFS) but not overall survival (OS) (Patel et al., 2013). However, studies on pemetrexed-based chemotherapy with or without bevacizumab mostly focus on the maintenance therapy (Barlesi et al., 2013; Paz-Ares et al., 2013). The association between clinicopathologic characteristics and treatment outcomes of patients receiving pemetrexed-platinum doublet plus bevacizumab and specific populations which might or might not achieve tumor remission remains unclear.

Therefore, studies on whether pemetrexed-based chemotherapy plus antiangiogenesis agents can indeed prolong patients' survival with tolerable safety profiles in real-world settings are needed. In this study, we conducted a retrospective real-world study comparing pemetrexed-platinum doublet plus bevacizumab (Bev+PP) with doublet alone (PP) in Chinese chemo-naïve advanced lung adenocarcinoma patients.

## MATERIALS AND METHODS

### Study Design and Patient Enrollment

This retrospective study collected clinical data from patients with advanced lung adenocarcinoma who received at least one cycle of first-line pemetrexed-platinum chemotherapy with or without bevacizumab between April 2014 and June 2020 in our own

hospital. The study was approved by the Hangzhou Cancer Hospital Ethics Review Board. This study is observational and presents no more than minimal risk of harm to subjects and involves no procedures for which written consent is normally required outside the research context. The Hangzhou Cancer Hospital Ethics Review Board approved the waiver of informed consents for this study according to section 39 of Measures for the Ethical Review of Biomedical Research Involving Humans published by the National Health Commission of the People's Republic of China (CLI4.282697). The inclusion criteria were as follows: 1) pathologic and radiographic confirmation of stage IIIB-IV (AJCC 7th edition) lung adenocarcinoma patients; 2) patients with no history of prior chemotherapy or antiangiogenesis drugs administration; 3) recipients of Bev+PP or PP; 4) recipients of  $\geq 1$  cycles of chemotherapy; and 5) complete medical records. Patients were excluded if they 1) were receiving other categories of antitumor therapy during the indicated treatments, 2) were given bevacizumab after the progression of pemetrexed-platinum-based chemotherapy, or 3) were lost to follow-up.

### Data Collection

Patients' private information remained confidential; however, the characteristics including age, gender, smoking history, baseline Eastern Cooperative Oncology Group Performance Score (ECOG PS), pathological diagnosis and staging, medical history, and imaging data were captured from the electronic health system. The follow-up was conducted using both outpatient and telephone appointments. Treatment responses were assessed as complete response (CR), partial response (PR), stable disease (SD), or progressive disease (PD), by comparing the imaging data before and after treatment using the Response Evaluation Criteria in Solid Tumors (RECIST) version 1.1. The objective response rate (ORR) was calculated as CR + PR/total cases, while the disease control rate (DCR) was calculated as CR + PR + SD/total cases. PFS was defined as the time from treatment initiation to the first confirmation of disease progression or death, while OS was defined as the time from treatment initiation until death. Adverse events were graded according to the National Cancer Institute—Common Toxicity Criteria for Adverse Events version 4.0. Two professional oncologists performed the grading of the treatment responses and adverse events independently, which were later recorded in the database.

### Statistical Analysis

A chi-square test or Fisher's exact test was used to assess for independence between the categorical variables in the two treatment groups with or without bevacizumab. The Kaplan-Meier method and log-rank test were used to compare the efficacy of combination therapy with chemotherapy alone. Multivariate Cox analyses were employed to estimate the factors affecting the efficacy of treatment (PFS and OS). For matched factors affecting PFS, the patients were divided on that factor and further analyzed whether the strength of one treatment could still be present in the subgroup. All analyses were performed with IBM SPSS Statistics 26.0. Survival curves were drawn using Prism GraphPad 8.0.

**TABLE 1 |** Clinical characteristics of lung adenocarcinoma patients.

Characteristic	Bev+PP (n = 46)		PP (n = 54)		p-value
	N	%	N	%	
Age (years)	62 [38–75]		63 [18–83]		
≥60	28	60.9	34	63.0	0.8298
<60	18	39.1	20	37.0	
Gender					
Male	33	71.7	32	59.3	0.2133
Female	13	28.3	22	40.7	
Smoking					
Never	20	43.5	11	20.4	0.08
Ever	26	56.5	43	79.6	
ECOG PS					
0	3	6.5	3	5.6	0.9648
1	41	89.1	49	90.7	
2	2	4.3	2	3.7	
Tumor stage					
III <sub>b</sub>	2	4.3	9	16.7	0.0066*
IV <sub>a</sub>	13	28.3	25	46.3	
IV <sub>b+c</sub>	31	67.4	20	37.0	
Site of metastasis					
Lung	17	37.0	20	37.0	0.5052
Bone	20	43.5	21	38.9	
Pleura	11	23.9	15	27.8	
Brain	14	30.4	13	24.1	
Adrenal glands	9	19.6	3	5.6	
Liver	6	13.0	4	7.4	
Driver gene status					
EAR negative	26	56.5	37	68.5	0.3418
EGFR mutation	12	26.1	13	24.1	
ALK or ROS1 fusion	2	4.3	2	3.7	
Unknown	6	13.0	2	3.7	

## RESULTS

### Clinicopathologic Characteristics

Between April 2014 and June 2020, a total of 100 chemotherapy-naïve patients with advanced lung adenocarcinoma at our institute met the inclusion criteria and were enrolled on our retrospective real-world study comparing the efficacy and safety of pemetrexed–platinum with or without bevacizumab (46 patients in the Bev+PP group and 54 patients in the PP group).

The median age was 62 (38–75) years in the Bev+PP group and 63 (18–83) years in the PP group. Bev+PP and PP groups enrolled similar proportions of male (71.7 vs. 59.3%,  $p = 0.2133$ ), elder (60.9 vs. 63.0%,  $p = 0.8298$ ), ever smoking (56.5 vs. 79.6%,  $p = 0.08$ ), ECOG PS = 1 (89.1 vs. 90.7%,  $p = 0.9648$ ), and EAR-negative (56.5 vs. 68.5%,  $p = 0.3418$ ) patients. The occurrence rates of metastasis in organs including the lung, bone, pleural, brain, adrenal glands, and liver, and the EAR gene mutation status were distributed evenly between the two groups ( $p = 0.5052$ , 0.3418, respectively). However, the Bev+PP group reported more later stage lung adenocarcinoma patients than PP group (IV<sub>b+c</sub> 67.4 vs. 37.0%,  $p = 0.0066$ ). (Detailed data are shown in **Table 1**.) The pre- and post-line treatment history information are presented in **Supplementary Table S1**; in brief, the Bev+PP group enrolled a higher number of patients reporting failed prior TKI treatments than the PP group (26.1 vs. 14.8%,  $p = 0.160$ ).

### Treatment and Efficacy

In brief, patients were intravenously injected with 500 mg/m<sup>2</sup> pemetrexed on d1, 37.5 mg/m<sup>2</sup> cisplatin on d1–2, or carboplatin (area under the curve, 4–5) on d1, with or without 7.5 mg/kg bevacizumab on d1 during induction therapy. Pemetrexed plus bevacizumab or pemetrexed monotherapy was administered during maintenance therapy. Patients in the two groups received similar cycles of induction therapy (mean cycle 4.1 [2–7] vs. 4.2 [1–6] for PP and Bev+PP groups, respectively,  $p = 0.9740$ ). However, patients receiving Bev+PP were more likely to receive more cycles of maintenance therapy than patients in the PP group (5.3 [0–22] vs. 2.5 [0–18],  $p = 0.0015$ ). Although none of the patients achieved complete clearance of cancer, 65% of patients in the Bev+PP group had PR, obviously higher than only 30% in the PP group (same with ORR,  $p = 0.0004$ ). And surprisingly, only one patient experienced PD after administration of bevacizumab and pemetrexed–platinum, with the DCR of the Bev+PP group reaching 98% (45/46), compared with 87% in the PP group ( $p = 0.0663$ ) (**Table 2**). Patients in the Bev+PP group achieved superior PFS than those in the PP group (median PFS, 7.4 vs. 6.8 months; HR [95% CI]: 0.59 [0.39–0.90],  $p = 0.0093$ ) (**Figure 1A**). However, addition of bevacizumab did not cause any significant improvement in OS (median OS for Bev+PP and PP, 17.5 vs. 15.0 months; HR [95% CI]: 0.86 [0.50–1.47],  $p = 0.5531$ ) (**Figure 1B**). When we merely looked at EAR-negative patients, bevacizumab addition also tended to improve PFS (median PFS, 8.9 vs. 7.0 months; HR [95% CI]: 0.63 [0.37–1.07],  $p = 0.0836$ ), but not OS (median OS, 17.5 vs. 16.2 months; HR [95% CI]: 0.99 [0.51–1.91],  $p = 0.9638$ ) (**Supplementary Figures S1A,B**). Multivariate Cox regression analysis showed that treatment with or without bevacizumab ( $p = 0.001$ ), gender ( $p = 0.008$ ), and adrenal metastasis ( $p = 0.001$ ) as well as liver metastasis ( $p = 0.013$ ) were independent risk factors for the PFS in lung adenocarcinoma patients (**Table 3**), reaffirming that bevacizumab addition improved the PFS of chemo-naïve lung adenocarcinoma patients.

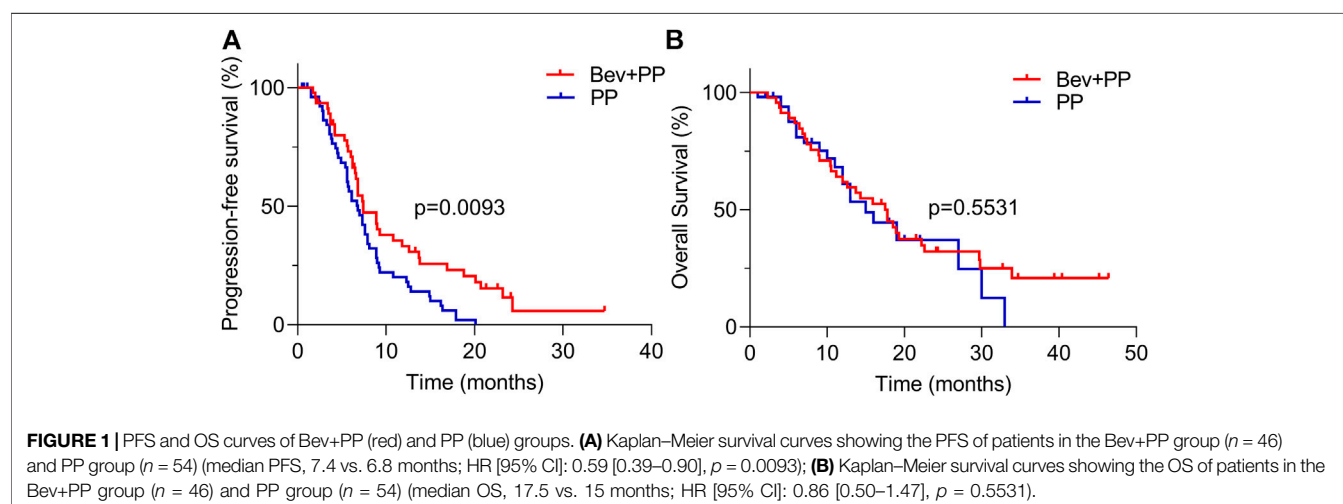
The relationship between the baseline clinicopathologic characteristics of enrolled patients and PFS or OS was further analyzed by multivariate Cox analyses to screen out a specific population of patients who could optimally benefit from Bev+PP treatment and risk factors that reduced the efficacy. As listed in **Table 4**, female patients had superior OS than male patients (Bev+PP, HR [95% CI]: 0.18 [0.04–0.87]; PP, HR [95% CI]: 0.08 [0.01–0.53]). EGFR or ALK/ROS1 status did not affect the efficacy of Bev+PP ( $p = 0.899$  and 0.984) on OS. Additionally, adrenal metastasis severely reduce the PFS of patients receiving Bev+PP (HR [95% CI]: 10.17 [2.99–34.62]).

### Subgroup Analysis

To further confirm whether adrenal metastasis or other characteristics may favor Bev+PP or PP on PFS, we conducted a subgroup analysis of hazard ratios for progression of enrolled patients after Bev+PP or PP administration using the Kaplan–Meier method. As shown in

**TABLE 2 |** Efficacy profile and treatment cycles of the two groups.

	Bev+PP ( <i>n</i> = 46)	PP ( <i>n</i> = 54)	<i>p</i> -value
	N (%)	N (%)	
Best response			
CR	0 (0)	0 (0)	
PR	30 (65)	16 (30)	
SD	15 (33)	31 (57)	
PD	1 (2)	7 (13)	
ORR	30 (65)	16 (30)	0.0004*
DCR	45 (98)	47 (87)	0.0663
Induction cycle mean (range)	4.1 [2–7]	4.2 [1–6]	0.9740
Maintenance cycle mean (range)	5.3 [0–22]	2.5 [0–18]	0.0015*

**TABLE 3 |** Multivariate analysis of PFS in all patients.

Characteristic	<i>p</i> -value	HR	95% CI	
			Lower limit	Upper limit
Bev+PP	0.001*	0.42	0.25	0.71
Gender = female	0.008*	0.43	0.23	0.80
Age (years)	0.746	1.00	0.97	1.02
Smoking	0.750	0.89	0.44	1.79
Lung metastasis	0.671	0.89	0.52	1.52
Pleura metastasis	0.488	1.24	0.67	2.30
Adrenal metastasis	0.001*	3.80	1.77	8.18
Bone metastasis	0.981	0.99	0.55	1.81
Brain metastasis	0.188	1.49	0.82	2.71
Liver metastasis	0.013*	2.67	1.23	5.77
Distant metastasis	0.118	0.47	0.18	1.21
ECOG ≥ 2	0.232	2.17	0.61	7.68
EGFR mutation	0.149	1.56	0.85	2.85
ALK/ROS1 fusion	0.998	1.00	0.30	3.36
Unknown status	0.882	0.93	0.38	2.30

**Figure 2**, the effect of bevacizumab on the pemetrexed-platinum chemotherapy was generally consistent in subgroups including gender, age, smoking, stage, distant metastasis, and EAR status. However, adrenal metastasis tended to be relatively in favor of

pemetrexed-platinum doublet alone (HR [95% CI]: 2.244 [0.6495–7.753]).

## Adverse Events

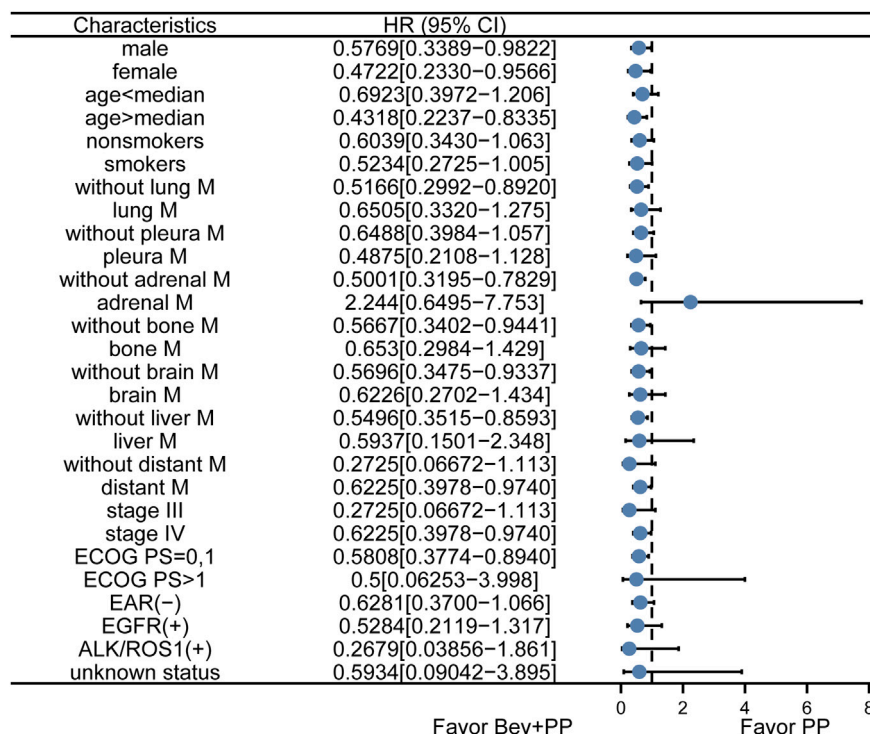
The prevalence of all adverse events (AEs), including grade ≥3 adverse events in the two groups was similar (all AEs, *p* = 0.465; all grade ≥3 AEs, *p* = 0.652). The top three frequent AEs of patients in Bev+PP and PP groups were leukopenia (63.0%, 59.3%), fatigue (45.7%, 38.9%), and nausea (37.0%, 33.3%) (Table 5). Grade 3–4 leukopenia was the most common grade ≥3 AE occurring in 19.6 and 18.5% of patients in Bev+PP and PP groups, respectively, while other grade ≥3 AEs were rare in the two groups. The safety profiles in both groups were acceptable, and no new unexpected AEs were observed.

## DISCUSSION

In the current real-world study, the addition of bevacizumab in first-line pemetrexed-platinum (either cisplatin or carboplatin) doublet significantly improved PFS compared to doublet alone, with similar and tolerable adverse events, although no differences in OS was observed between the two groups. Multivariate Cox regression

**TABLE 4 |** Multivariate Cox regression analysis of OS and PFS in the Bev+PP group.

Category	OS		PFS	
	HR	p-value	HR	p-value
Gender = female	0.18 [0.04–0.87]	0.032*	0.25 [0.07–0.90]	0.034*
Age (years)	1.00 [0.95–1.06]	0.899	0.99 [0.95–1.04]	0.796
Smoking	0.81 [0.23–2.77]	0.731	0.85 [0.28–2.64]	0.784
Distant metastasis	0.95 [0.09–9.83]	0.65	0.82 [0.08–8.33]	0.65
Lung metastasis	2.23 [0.79–6.27]	0.130	1.57 [0.65–3.82]	0.318
Pleura metastasis	0.51 [0.17–1.58]	0.245	0.58 [0.22–1.54]	0.273
Adrenal metastasis	2.18 [0.70–6.82]	0.179	10.17 [2.99–34.62]	0.000*
Bone metastasis	0.90 [0.36–2.25]	0.813	0.77 [0.33–1.81]	0.551
Brain metastasis	0.62 [0.24–1.62]	0.329	1.50 [0.59–3.85]	0.395
Liver metastasis	4.34 [0.99–18.91]	0.051	3.04 [0.88–10.58]	0.080
ECOG $\geq 2$	1.10 [0.16–7.49]	0.919	2.27 [0.33–15.39]	0.402
EGFR mutation	1.08 [0.33–3.56]	0.899	1.28 [0.43–3.78]	0.660
ALK/ROS1 fusion	0.00 [0.00–NA]	0.984	0.69 [0.09–5.38]	0.720
Unknown status	0.28 [0.06–1.25]	0.095	0.34 [0.09–1.32]	0.118

**FIGURE 2 |** Subgroup analysis of PFS in enrolled patients. Dots and horizontal lines represent the mean value and confidence intervals, respectively. Bev+PP denotes bevacizumab plus pemetrexed-platinum, and PP denotes pemetrexed-platinum.

analyses confirmed that pemetrexed-platinum doublet with bevacizumab was an independent favorable factor of PFS. This study confirmed that pemetrexed-platinum doublet combined with bevacizumab was safe and effective for Chinese chemo-naïve lung adenocarcinoma patients.

Bevacizumab plus pemetrexed-platinum doublet chemotherapy has become a standard first-line treatment for advanced lung adenocarcinoma patients with negative results of detecting PD-L1 expression, EGFR mutations, and ALK/ROS1 gene fusions, or after the

failure of targeted therapies for patients with EGFR mutations or ALK/ROS1 fusions, as recommended in NCCN NSCLC guidelines (Ettinger et al., 2019) and pan-Asian adapted ESMO NSCLC guideline (Wu et al., 2019), based on several large phase III clinical trials, including SAiL and ARIES (Crinò et al., 2010; Lynch Jr et al., 2014) and several other clinical trials comparing paclitaxel-based chemotherapy with or without bevacizumab. Consistent with the ORR and PFS benefits of bevacizumab addition found in these clinical trials, our study also demonstrated similar PFS and ORR improvements.



**TABLE 5 |** Safety profile of the two groups.

	All AEs			Grade $\geq 3$ AEs		
	Bev+PP ( <i>n</i> = 46)	PP ( <i>n</i> = 54)	<i>p</i> -value	Bev+PP ( <i>n</i> = 46)	PP ( <i>n</i> = 54)	<i>p</i> -value
	N (%)	N (%)		N (%)	N (%)	
Leukopenia	29 (63.0)	32 (59.3)	0.837	9 (19.6)	10 (18.5)	0.999
Abnormal liver function	12 (26.1)	9 (16.7)	0.326	1 (2.2)	2 (3.7)	0.999
Fatigue	21 (45.7)	21 (38.9)	0.546	1 (2.2)	2 (3.7)	0.999
Nausea	17 (37.0)	18 (33.3)	0.834	0 (0.0)	1 (1.9)	0.999
Anemia	12 (26.1)	14 (25.9)	0.999	1 (2.2)	3 (5.6)	0.622
Thrombocytopenia	10 (21.7)	8 (14.8)	0.438	1 (2.2)	0 (0.0)	0.460
Thrombosis and hemorrhage	2 (4.3)	1 (1.9)	0.593	1 (2.2)	0 (0.0)	0.460
Hypertension	2 (4.3)	0 (0.0)	0.209	0 (0.0)	0 (0.0)	NA
Anorexia	2 (4.3)	5 (9.3)	0.447	0 (0.0)	0 (0.0)	NA
Headache	1 (2.2)	0 (0.0)	0.460	0 (0.0)	0 (0.0)	NA
Rash	1 (2.2)	1 (1.9)	0.999	0 (0.0)	0 (0.0)	NA
Increased creatinine	2 (4.3)	0 (0.0)	0.209	0 (0.0)	0 (0.0)	NA
Total	41 (89.1)	51 (94.4)	0.465	11 (23.9)	16 (29.6)	0.652

AVAPERL (Barlesi et al., 2013) and COMPASS (Seto et al., 2020) studies compared pemetrexed plus bevacizumab with single-agent bevacizumab in the maintenance and whole phases, respectively, which showed elevated PFS but not OS with bevacizumab addition. A Japanese clinical trial published in 2016 reported a nonsignificant beneficial PFS in the pemetrexed–platinum plus bevacizumab group compared with pemetrexed–platinum alone (mPFS 11.5 vs. 7.3 months,  $p = 0.198$ ) (Karayama et al., 2016). The 2016 Japanese study and another Japanese study SAKK19\_09 (Gautschi et al., 2015) all reported no significant improvement in OS when comparing Bev+Pem–platinum with chemo-monotherapy (24.4 vs. 21.3 months,  $p = 0.63$ ; 14.7 vs. 14.6 months,  $p = 0.890$ ; respectively). However, Stephen J et al. conducted a large sample retrospective cohort study including 4,724 patients with 58% receiving carboplatin–pemetrexed and 42% receiving carboplatin–pemetrexed–bevacizumab. The study demonstrated an OS benefit from 8.6 to 12.1 months ( $p < 0.001$ ) and also showed that female patients had longer OS than male patients after the triple-reagent administration (Bagley et al., 2019). In our study, more patients received longer maintenance cycles of pemetrexed plus bevacizumab treatment, which might have contributed to the longer PFS and also indicated that the safety profile of combination therapy was tolerable in the real-world setting. Although the addition of bevacizumab or not was a constant factor in both induction and maintenance therapies, the final OS was not significantly altered in our study, which was consistent with findings from the abovementioned clinical studies but not the large-sample retrospective cohort study. We also found that female patients treated with pemetrexed–platinum with bevacizumab responded better than male patients. The limited PFS and insignificant OS improvement in our study might be due to a higher percent of patients with stage IV b+c lung adenocarcinoma. Besides, the limited population size may also cause the restricted application of our findings, and uncontrolled post-line treatments in the real-world may have an impact on the OS.

Several other studies have also reported the use of combination therapies in real-world settings. For instance, Katherine B. Winfree retrospectively compared maintenance therapies for non-squamous

lung cancer patients in the United States and found that pemetrexed–bevacizumab treatment could improve patients' PFS compared to pemetrexed treatment alone (Winfree et al., 2019). However, the PFS was calculated from the first day of induction therapy, while the induction therapies included many different regimens such as platinum + bevacizumab, and platinum + other chemo-reagents. Thus, the improvement may be all attributed to the specific maintenance regimen. In our study, we specifically focused on pemetrexed–platinum doublet with or without bevacizumab, and the comparison was intended to investigate whether the addition of bevacizumab could benefit Chinese chemo-naïve lung adenocarcinoma patients during the entire treatment, and we did observe an improvement in PFS but not in OS. Fei Qi et al. (Qi et al., 2019) and Xiaoyou Li et al. (Li et al., 2019) performed similar comparisons with ours and also found that the median PFS was significantly prolonged in the bevacizumab addition group compared with the chemo-only group (9.8 vs. 7.8 months,  $p = 0.006$ ; 10.97 vs. 6.67 months,  $p = 0.0002$ ), as well as ORR, which were consistent with our findings. More than 4 months of PFS improvement may not be all attributed to bevacizumab addition since the combination group enrolled significantly fewer patients with brain or pleural metastasis than the chemo-group, whereas in our study, a higher percent of patients enrolled in the pemetrexed–platinum treatment group were absent of distant metastasis, than the combination group.

The MAP study showed that when receiving platinum/pemetrexed/bevacizumab, patients with EGFR mutation had higher OS than patients with EGFR-negative status (NR vs. 20.7 months,  $p = 0.004$ ). However, only 8 out of 23 patients had prior TKIs (Tsutani et al., 2018). The 2016 Japanese study also enrolled patients with failure from EGFR or ALK/ROS1 tyrosine kinase inhibitors; however, the authors failed to compare the survival difference between negative and positive patients (Karayama et al., 2016). EGFR-negative patients in the COMPASS study obtained a better OS with bevacizumab addition (HR [95% CI], 0.82 [0.68–0.99]) (Seto et al., 2020). In this study, we assessed the treatment efficacy in subgroups using outcome PFS, but not OS because the OS of the total samples did not show any significant tendency to either treatment. Bevacizumab addition tended to be beneficial to both EGFR-negative and -positive patients.

Our study also compared combination therapy with pemetrexed–platinum doublet in subgroup analysis, and surprisingly, the findings demonstrated that it tended to be favoring chemotherapy alone for patients with adrenal metastasis. However, to the best of our knowledge, no clinical trials or other retrospective studies analyzing such a specific population have been reported. Only the ECOG4599 study comparing paclitaxel–carboplatin doublet plus bevacizumab with chemotherapy alone in NSCLC reported the hazard ratio for OS (0.97 [0.65–1.46]) of patients with adrenal metastasis, with the largest value in analyses of all sites of metastasis, indicating the highest risk not benefiting from the addition of bevacizumab (Sandler et al., 2006). We have to admit that limited patients with adrenal metastasis were enrolled in our study, which might cause false discovery. However, to avoid the economic burden of bevacizumab addition, we cautiously suggest that clinical trials or retrospective studies with a large sample size be conducted to further investigate the effect of bevacizumab addition in patients with adrenal metastasis.

The combination treatment was well-tolerated, and no unexpected findings were reported in our real-world study. The two groups shared similar adverse effects, including severe adverse effects. Leukopenia (also categorized as neutropenia in clinical trials), fatigue, and nausea were found to be the most frequent AEs in the two groups, which are reported as common adverse effects of chemotherapy treatment (Zinner and Herbst, 2004), and bevacizumab addition in this study did not significantly augment those side effects. The ECOG-ACRIN 5508 study investigating the strategies for maintenance therapies revealed that the incidence of grade  $\geq 3$  AEs was obviously elevated in the combination regimen, from 37 to 51% (Ramalingam et al., 2019). However, such an increase in the incidence of grade  $\geq 3$  AEs was not demonstrated in the abovementioned clinical trials and retrospective studies and in the current study. Besides, patients in the ECOG-ACRIN 5508 study were administered with paclitaxel–carboplatin plus bevacizumab as induction therapy before randomization into pemetrexed or pemetrexed plus bevacizumab groups, which might cause late impact on grade  $\geq 3$  AEs during maintenance therapy.

In conclusion, although the survival benefit associated with bevacizumab addition is reported limited in our study, the overall response is increased and the safety profile is acceptable. The addition of bevacizumab is currently recommended and has been demonstrated to be a better treatment option in chemo-naïve lung adenocarcinoma patients with PD-L1–negative scores in many clinical trials and real-world studies including this study. However, we carefully suggest that medical oncologists should be cautious with bevacizumab addition in patients with adrenal metastasis, unless large clinical studies focusing on this specific population are performed and show clear evidence.

## REFERENCES

- Assoun, S., Brosseau, S., Steinmetz, C., Gounant, V., and Zalcman, G. (2017). Bevacizumab in Advanced Lung Cancer: State of the Art. *Future Oncol.* 13, 2515–2535. doi:10.2217/fon-2017-0302

## DATA AVAILABILITY STATEMENT

The raw data supporting the conclusions of this article will be made available by the authors, without undue reservation.

## ETHICS STATEMENT

The studies involving human participants were reviewed and approved by Ethics Review Board of Hangzhou Cancer Hospital. Written informed consent for participation was not required for this study in accordance with the national legislation and the institutional requirements.

## AUTHOR CONTRIBUTIONS

Conceptualization: XC and BX; methodology: XL, JH, QZ, and YQ; validation: KW; formal analysis: JH; investigation: XL and YQ; resources: XL, SY, KW, JW, JY, and LW; data curation: JH; writing—original draft preparation: JH and QZ; writing—review and editing: JH and XC; visualization: JH; supervision: SM; project administration: XC; funding acquisition: XC and SM. All authors have read and agreed to the published version of the manuscript.

## FUNDING

This research was funded by the National Natural Science Foundation of China (grant number 81773242); Science and Technology Development Project of Hangzhou (grant numbers 20180417A01 and 20180533B98); the Zhejiang Provincial Natural Science Foundation of China (grant number LY19H160030); Zhejiang Provincial Traditional Chinese Medicine Science and Technology Project (grant number 2018ZY009).

## SUPPLEMENTARY MATERIAL

The Supplementary Material for this article can be found online at: <https://www.frontiersin.org/articles/10.3389/fphar.2021.649222/full#supplementary-material>

**Supplementary Figure S1** | PFS and OS curves of EAR negative patients in Bev+PP (red) and PP 418 (blue) groups. (A) Kaplan-Meier survival curves showed the PFS of EAR negative patients in Bev+PP 419 group ( $n = 26$ ) and PP group ( $n = 37$ ) (median PFS, 8.9 vs. 7.0 months; HR[95%CI]: 0.63[0.37–1.07], 420  $p = 0.0836$ ); (B) Kaplan-Meier survival curves showed the OS of EAR negative patients in Bev+PP 421 group ( $n = 26$ ) and PP group ( $n = 37$ ) (median OS, 17.5 vs. 16.2 months; HR [95%CI]: 0.99[0.51–1.91], 422  $p = 0.9638$ ).

- Bagley, S. J., Talento, S., Mitra, N., Meropol, N. J., Cohen, R. B., Langer, C. J., et al. (2019). Comparative Effectiveness of Carboplatin/Pemetrexed with versus without Bevacizumab for Advanced Nonsquamous Non-small Cell Lung Cancer. *J. Natl. Compr. Cancer Netw.* 17, 469–477. doi:10.6004/jnccn.2018.7102

- Bansal, P., Osman, D., Gan, G. N., Simon, G. R., and Boucher, Y. (2016). Recent Advances in Immunotherapy in Metastatic NSCLC. *Front. Oncol.* 6, 239. doi:10.3389/fonc.2016.00239
- Barlesi, F., Scherpereel, A., Rittmeyer, A., Pazzola, A., Ferrer Tur, N., Kim, J.-H., et al. (2013). Randomized Phase III Trial of Maintenance Bevacizumab with or without Pemetrexed after First-Line Induction with Bevacizumab, Cisplatin, and Pemetrexed in Advanced Nonsquamous Non-small-cell Lung Cancer: AVAPERL (MO22089). *J. Clin. Oncol.* 31, 3004–3011. doi:10.1200/jco.2012.42.3749
- Cao, M., Li, H., Sun, D., and Chen, W. (2020). Cancer Burden of Major Cancers in China: A Need for Sustainable Actions. *Cancer Commun.* 40, 205–210. doi:10.1002/cac2.12025
- Crinò, L., Dansin, E., Garrido, P., Griesinger, F., Laskin, J., Pavlakis, N., et al. (2010). Safety and Efficacy of First-Line Bevacizumab-Based Therapy in Advanced Nonsquamous Non-small-cell Lung Cancer (SAiL, MO19390): a Phase 4 Study. *Lancet Oncol.* 11, 733–740. doi:10.1016/s1470-2045(10)70151-0
- Ettinger, D. S., Wood, D. E., Aggarwal, C., Aisner, D. L., Akerley, W., Bauman, J. R., et al. (2019). NCCN Guidelines Insights: Non-small Cell Lung Cancer, Version 1.2020. *J. Natl. Compr. Cancer Netw.* 17, 1464–1472. doi:10.6004/jnccn.2019.0059
- Ferlay, J., Colombet, M., Soerjomataram, I., Mathers, C., Parkin, D. M., Piñeros, M., et al. (2019). Estimating the Global Cancer Incidence and Mortality in 2018: GLOBOCAN Sources and Methods. *Int. J. Cancer* 144, 1941–1953. doi:10.1002/ijc.31937
- García, J., Hurwitz, H. I., Sandler, A. B., Miles, D., Coleman, R. L., Deurloo, R., et al. (2020). Bevacizumab (Avastin) in Cancer Treatment: A Review of 15 Years of Clinical Experience and Future Outlook. *Cancer Treat. Rev.* 86, 102017. doi:10.1016/j.ctrv.2020.102017
- Gautschi, O., Mach, N., Rothschild, S. I., Li, Q., Stahel, R. A., Zippelius, A., et al. (2015). Bevacizumab, Pemetrexed, and Cisplatin, or Bevacizumab and Erlotinib for Patients with Advanced Non-small-cell Lung Cancer Stratified by Epidermal Growth Factor Receptor Mutation: Phase II Trial SAKK19/09. *Clin. Lung Cancer* 16, 358–365. doi:10.1016/j.clcc.2015.02.007
- Guan, Y., Wang, G., Fails, D., Nagarajan, P., and Ge, Y. (2020). Unraveling Cancer Lineage Drivers in Squamous Cell Carcinomas. *Pharmacol. Ther.* 206, 107448. doi:10.1016/j.pharmthera.2019.107448
- Hu, P., Liu, W., Wang, L., Yang, M., and Du, J. (2013). High Circulating VEGF Level Predicts Poor Overall Survival in Lung Cancer. *J. Cancer Res. Clin. Oncol.* 139, 1157–1167. doi:10.1007/s00432-013-1425-1
- Karayama, M., Inui, N., Fujisawa, T., Enomoto, N., Nakamura, Y., Kuroishi, S., et al. (2016). Maintenance Therapy with Pemetrexed and Bevacizumab versus Pemetrexed Monotherapy after Induction Therapy with Carboplatin, Pemetrexed, and Bevacizumab in Patients with Advanced Nonsquamous Non-small Cell Lung Cancer. *Eur. J. Cancer* 58, 30–37. doi:10.1016/j.ejca.2016.01.013
- Li, X., Abbas, M., Li, Y., Teng, Y., Fang, Y., Yu, S., et al. (2019). Comparative Effectiveness of Pemetrexed-Platinum Doublet Chemotherapy with or without Bevacizumab as First-Line Therapy for Treatment-Naïve Patients with Advanced Nonsquamous Non-small-cell Lung Cancer in China. *Clin. Ther.* 41, 518–529. doi:10.1016/j.clinthera.2019.02.004
- Lynch, T. J., Jr, Spigel, D. R., Brahmer, J., Fischbach, N., Garst, J., Jahanzeb, M., et al. (2014). Safety and Effectiveness of Bevacizumab-Containing Treatment for Non-small-cell Lung Cancer: Final Results of the ARIES Observational Cohort Study. *J. Thorac. Oncol.* 9, 1332–1339. doi:10.1097/jto.0000000000000257
- Pakkala, S., and Ramalingam, S. S. (2018). Personalized Therapy for Lung Cancer: Striking a Moving Target. *JCI Insight* 3, e120858. doi:10.1172/jci.insight.120858
- Patel, J. D., Socinski, M. A., Garon, E. B., Reynolds, C. H., Spigel, D. R., Olsen, M. R., et al. (2013). PointBreak: a Randomized Phase III Study of Pemetrexed Plus Carboplatin and Bevacizumab Followed by Maintenance Pemetrexed and Bevacizumab versus Paclitaxel Plus Carboplatin and Bevacizumab Followed by Maintenance Bevacizumab in Patients with Stage IIIB or IV Nonsquamous Non-small-cell Lung Cancer. *J. Clin. Oncol.* 31, 4349–4357. doi:10.1200/jco.2012.47.9626
- Paz-Ares, L. G., de Marinis, F., Dediu, M., Thomas, M., Pujol, J.-L., Bidoli, P., et al. (2013). PARAMOUNT: Final Overall Survival Results of the Phase III Study of Maintenance Pemetrexed versus Placebo Immediately after Induction Treatment with Pemetrexed Plus Cisplatin for Advanced Nonsquamous Non-small-cell Lung Cancer. *J. Clin. Oncol.* 31, 2895–2902. doi:10.1200/jco.2012.47.1102
- Qi, F., Hu, X., Hu, X., Liu, Y., Wang, Z., Duan, J., et al. (2019). First-line Pemetrexed-Platinum Doublet Chemotherapy with or without Bevacizumab in Nonsquamous Non-small Cell Lung Cancer: A Real-World Propensity Score-Matched Study in China. *Chin J Cancer Res.* 31, 749–758. doi:10.21147/j.issn.1000-9604.2019.05.05
- Ramalingam, S. S., Dahlberg, S. E., Belani, C. P., Saltzman, J. N., Pennell, N. A., Nambudiri, G. S., et al. (2019). Pemetrexed, Bevacizumab, or the Combination as Maintenance Therapy for Advanced Nonsquamous Non-small-cell Lung Cancer: ECOG-ACRIN 5508. *J. Clin. Oncol.* 37, 2360–2367. doi:10.1200/jco.19.01006
- Sandler, A., Gray, R., Perry, M. C., Brahmer, J., Schiller, J. H., Dowlati, A., et al. (2006). Paclitaxel-carboplatin Alone or with Bevacizumab for Non-small-cell Lung Cancer. *N. Engl. J. Med.* 355, 2542–2550. doi:10.1056/nejmoa061884
- Seto, T., Azuma, K., Yamanaka, T., Sugawara, S., Yoshioka, H., Wakuda, K., et al. (2020). Randomized Phase III Study of Continuation Maintenance Bevacizumab with or without Pemetrexed in Advanced Nonsquamous Non-small-cell Lung Cancer: COMPASS (WJOG5610L). *J. Clin. Oncol.* 38, 793–803. doi:10.1200/jco.19.01494
- Tamura, R., Tanaka, T., Ohara, K., Miyake, K., Morimoto, Y., Yamamoto, Y., et al. (2019). Persistent Restoration to the Immunosuppressive Tumor Microenvironment in Glioblastoma by Bevacizumab. *Cancer Sci.* 110, 499–508. doi:10.1111/cas.13889
- Tsutani, Y., Miyata, Y., Masuda, T., Fujitaka, K., Doi, M., Awaya, Y., et al. (2018). Multicenter Phase II Study on Cisplatin, Pemetrexed, and Bevacizumab Followed by Maintenance with Pemetrexed and Bevacizumab for Patients with Advanced or Recurrent Nonsquamous Non-small Cell Lung Cancer: MAP Study. *BMC cancer* 18, 1231. doi:10.1186/s12885-018-5146-3
- Vermeulen, R., Downward, G. S., Zhang, J., Hu, W., Portengen, L., Bassig, B. A., et al. (2019). Constituents of Household Air Pollution and Risk of Lung Cancer Among Never-Smoking Women in Xuanwei and Fuyuan, China. *Environ. Health Perspect.* 127, 097001. doi:10.1289/ehp4913
- Winfrey, K. B., Torres, A. Z., Zhu, Y. E., Muehlenbein, C., Aggarwal, H., Woods, S., et al. (2019). Treatment Patterns, Duration and Outcomes of Pemetrexed Maintenance Therapy in Patients with Advanced NSCLC in a Real-World Setting. *Curr. Med. Res. Opin.* 35, 817–827. doi:10.1080/03007995.2018.1547273
- Wu, Y.-L., Planchard, D., Lu, S., Sun, H., Yamamoto, N., Kim, D.-W., et al. (2019). Pan-Asian Adapted Clinical Practice Guidelines for the Management of Patients with Metastatic Non-small-cell Lung Cancer: a CSCO-ESMO Initiative Endorsed by JSMO, KSMO, MOS, SSO and TOS. *Ann. Oncol.* 30, 171–210. doi:10.1093/annonc/mdy554
- Yang, D., Liu, Y., Bai, C., Wang, X., and Powell, C. A. (2020). Epidemiology of Lung Cancer and Lung Cancer Screening Programs in China and the United States. *Cancer Lett.* 468, 82–87. doi:10.1016/j.canlet.2019.10.009
- Zang, J., Hu, Y., Xu, X., Ni, J., Yan, D., Liu, S., et al. (2017). Elevated Serum Levels of Vascular Endothelial Growth Factor Predict a Poor Prognosis of Platinum-Based Chemotherapy in Non-small Cell Lung Cancer. *Onco Targets Ther.* 10, 409–415. doi:10.2147/ott.s124124
- Zhao, Y.-Y., Xue, C., Jiang, W., Zhao, H.-Y., Huang, Y., Feenstra, K., et al. (2012). Predictive Value of Intratumoral Microvascular Density in Patients with Advanced Non-small Cell Lung Cancer Receiving Chemotherapy Plus Bevacizumab. *J. Thorac. Oncol.* 7, 71–75. doi:10.1097/jto.0b013e31823085f4
- Zhou, C., Wu, Y.-L., Chen, G., Liu, X., Zhu, Y., Lu, S., et al. (2015). BEYOND: A Randomized, Double-Blind, Placebo-Controlled, Multicenter, Phase III Study of First-Line Carboplatin/Paclitaxel Plus Bevacizumab or Placebo in Chinese Patients with Advanced or Recurrent Nonsquamous Non-small-cell Lung Cancer. *J. Clin. Oncol.* 33, 2197–2204. doi:10.1200/jco.2014.59.4424
- Zinner, R. G., and Herbst, R. S. (2004). Pemetrexed in the Treatment of Advanced Non-small-cell Lung Cancer: A Review of the Clinical Data. *Clin. Lung Cancer* 5, S67–S74. doi:10.3816/clc.2004.s.006

**Conflict of Interest:** The authors declare that the research was conducted in the absence of any commercial or financial relationships that could be construed as a potential conflict of interest.

Copyright © 2021 Li, Huang, Qiu, Zhang, Yang, Wu, Wang, Wang, Ye, Ma, Xia and Chen. This is an open-access article distributed under the terms of the Creative Commons Attribution License (CC BY). The use, distribution or reproduction in other forums is permitted, provided the original author(s) and the copyright owner(s) are credited and that the original publication in this journal is cited, in accordance with accepted academic practice. No use, distribution or reproduction is permitted which does not comply with these terms.



# Identification of the Core MicroRNAs and Potential Molecular Mechanisms in Sarcoidosis Using Bioinformatics Analysis

Yuan Cao<sup>1†</sup>, Hua Zhang<sup>2†</sup>, Lulu Zheng<sup>1</sup> and Qiao Li<sup>3\*</sup>

<sup>1</sup> Department of Pulmonary and Critical Care Medicine, The Second Affiliated Hospital of Xi'an Jiaotong University (Xibei Hospital), Xi'an, China, <sup>2</sup> Department of Respiratory Medicine, Zhangjiakou First Hospital, Zhangjiakou, China, <sup>3</sup> Clinical Laboratory, The Affiliated Children Hospital of Xi'an Jiaotong University, Xi'an, China

## OPEN ACCESS

### Edited by:

Wen Li,  
Zhejiang University, China

### Reviewed by:

Carlos Romá-Mateo,  
University of Valencia, Spain  
Yan Du,  
Second Affiliated Hospital, School  
of Medicine, Zhejiang University,  
China

### \*Correspondence:

Qiao Li  
liqiao@csu.edu.cn

<sup>†</sup> These authors have contributed  
equally to this work and share first  
authorship

### Specialty section:

This article was submitted to  
Molecular Diagnostics  
and Therapeutics,  
a section of the journal  
Frontiers in Molecular Biosciences

**Received:** 20 December 2020

**Accepted:** 19 April 2021

**Published:** 13 May 2021

### Citation:

Cao Y, Zhang H, Zheng L and Li Q  
(2021) Identification of the Core  
MicroRNAs and Potential Molecular  
Mechanisms in Sarcoidosis Using  
Bioinformatics Analysis.  
Front. Mol. Biosci. 8:644232.  
doi: 10.3389/fmolb.2021.644232

Sarcoidosis is a systemic heterogeneous inflammatory disease; however, the etiology and pathogenesis of sarcoidosis are still unknown. Herein, we investigated the core microRNAs and potential molecular mechanisms in sarcoidosis. The DE-miRNAs were diagnosed using the LIMMA software package. DIANA-mirPath was employed to perform pathway and GO enrichment analysis of the DE-miRNAs. PPI networks and miRNA-target gene regulatory networks were used to obtain insight into the actions of DE-miRNAs. Expression of the hub genes along with miRNAs was validated in clinical specimens. Overall, 266 DE-miRNAs were screened. Among these DE-miRNAs, hsa-miR-144, hsa-miR-126, as well as hsa-miR-106a were the upmost upregulated miRNAs; hsa-miR-151-3p, hsa-miR-320d, and hsa-miR-324-3p were the top downregulated miRNAs. *NR3C1*, *ZBTB7A*, *NUFIP2*, *BZW1*, *ERGIC2*, and *VEGFA* were mapped as the most targeted hub genes in the upregulation of miRNAs, and *MCL1* and *SAE1* were the most targeted hub genes in the downregulation of miRNA. *VEGFA* and *NR3C1* were selected and potentially modulated by hsa-miR-20b, hsa-miR-126, and hsa-miR-106a. In sarcoidosis pathological tissue, hsa-miR-126 was highly expressed, and *VEGFA* and *NR3C1* were overexpressed. In conclusion, our results revealed the dysregulation of hsa-miR-126 and a potential regulatory mechanism for pathogenesis in sarcoidosis.

**Keywords:** sarcoidosis, bioinformatics analysis, microRNA-126, *VEGFA*, *NR3C1*

## INTRODUCTION

Sarcoidosis is a systemic heterogeneous inflammatory disease that usually leads to a multisystemic granulomatous disorder (Iannuzzi et al., 2007; Jain et al., 2020). It can affect any organ; however, at least 90% of cases occur in intrathoracic lymph nodes, as well as the lungs (Ungprasert et al., 2019). The annual incidence of sarcoidosis changes with race and ethnicity and is highest in African Americans (17 to 35/100,000) and lowest in Asians (1/100,000). However, the incidence may be underestimated, as almost 50% of the sarcoidosis patients are asymptomatic, especially those in the early stage of the disease. Epidemiologic studies have reported that the maximum incidence of sarcoidosis occurs in female non-smokers with an average age of 30 (Jain et al., 2020).



The characteristic pathologic lesion of pulmonary sarcoidosis is a non-necrotizing granuloma (Iannuzzi et al., 2007). The etiology and pathogenesis of sarcoidosis are still unknown, and genetic susceptibility, autoimmunity, and environmental factors are all considered to be involved in the development of sarcoidosis.

MicroRNAs (miRNAs) are small, single-stranded, non-coding RNAs approximately 22 nucleotides long, some of which have been discovered to perform significant modulatory functions in animals through targeting the messages of protein-coding genes for translational inhibition. Research has documented that changes in the expression levels of miRNAs participate in multiple pathologies, as well as diseases. A previous study evaluated the expression trend of multiple miRNAs in sarcoidosis, and selected miRNAs were identified. However, regulatory miRNAs, their target genes, and the correlated protein expression have seldom been explored (Pattnaik et al., 2020). In this regard, we examined the microarray data of the gene expression profile of GSE26409 by a series of biological informatics approaches. The potential target genes of the upmost up-regulated, as well as down-regulated miRNAs were prognosticated by miRTarBase, and their potential functions were evaluated by DIANA-mirPath. Then, a protein-protein interaction (PPI) and miRNA-gene modulatory network were established by Cytoscape. Moreover, we validated the expression status of these hub genes and their modulated microRNAs in sarcoidosis samples by immunohistochemistry (IHC) along with fluorescence *in situ* hybridization (FISH). Based on a gene chip array, we used biological information technology to reveal the potential pathway in the etiology of sarcoidosis and yield additional information for its diagnosis, prognosis and treatment.

## MATERIALS AND METHODS

### Microarray Data

The microarray GSE26409 cohort was selected for further study and abstracted from the National Center for Biotechnology Information GEO (Gene Expression Omnibus) website<sup>1</sup>, which is available online. This data set was based on the GPL9040 platform (febit Homo Sapiens miRBase 13.0) and included 45 samples from sarcoidosis patients and 55 from normal controls.

### Screening for DE-miRNAs

First, normalization of the downloaded data was performed using the Normalize Between Array function in the Bioconductor R package “LIMMA” (available online: <http://www.bioconductor.org/>). Then, the unpaired Student's *t*-test was employed in comparing the sarcoidosis group with the control group. The cut-off criterion for screening differentially expressed miRNAs (DE-miRNAs) were  $p < 0.05$  along with  $|\text{fold change (FC)}| > 1$ . Additionally, the GEO2R online analytic tool based on GEO data platform was employed further to validate the DE-miRNAs.

<sup>1</sup><http://www.ncbi.nlm.nih.gov/geo>

### Prediction of Target Genes of DE-miRNAs

MiRTarBase (available online: <http://mirtarbase.mbc.nctu.edu.tw/php/index.php>) is extensively employed to search for miRNA target genes. The microRNA-target interactions in this database were experimentally validated. Herein, miRTarBase was employed to identify the target genes of DE-miRNAs.

### GO Annotation and KEGG Pathway Enrichment Analyses of DE-miRNAs

DIANA-mirPath (available online: <https://microrna.gr/mirPathv3/>) constitutes a miRNA pathway analysis web-platform that provides accurate statistics and at the same time accommodates advanced pipelines (Vlachos et al., 2015). The functional, as well as pathway enrichment of the candidate miRNAs were explored and annotated by mirPath v2.0 based on the database Tarbase v7. The GO (Gene Ontology) was annotated through the DIANA-mirPath online tool on the selected DE-miRNAs. The KEGG (Kyoto Encyclopedia of Genes and Genomes) pathway analysis of DE-miRNAs was also performed by using DIANA-mirPath.  $p < 0.05$  signified statistical significance.

### PPI Network Integration

To analyze the connection among proteins, the identify target genes of the upmost 5 most up and downregulated DE-miRNAs were uploaded to the STRING data resource<sup>2</sup>, and the results were visualized in Cytoscape 3.7.1 (Damian et al., 2015). Furthermore, we screened the significant nodes or hub genes based on degree, and then the miRNA-hub gene networks were mapped with Cytoscape 3.7.1.

### Immunohistochemistry (IHC)

Immunohistochemistry was used to further validate the paraffin sections of mediastinal lymph node tissues from pulmonary sarcoidosis patients and tuberculosis patients (control group), which came from the Second Affiliated Hospital of Xi'an Jiaotong University, with ethical approval. All specimens were obtained by endobronchial ultrasound-guided transbronchial needle aspiration (EBUS-TBNA), and all the patients in the study group and the control group have been screened, and those with cardiovascular and cerebrovascular diseases, endocrine, infectious diseases, tumor diseases, etc., have been excluded. The diagnosis was made based on guidelines (Costabel and Hunninghake, 1999). The tissue paraffin sections were first deparaffinized with dimethylbenzene and ethyl alcohol for 15 min, repaired by boiling for 8 min in the repairing solution with EDTA (pH 9.0), digested for 10 min by 3% H<sub>2</sub>O<sub>2</sub> at 37°C, washed with PBS solution and blocked for 30 min with 3% BSA at room temperature (RT). Afterward, the sections were overnight-incubated with the primary antibody (NR3C1, VEGFA) at 4°C (Abcam, Cambridge, United States). The next day, the tissues were inoculated with the horseradish-peroxidase (HRP) and incubated at RT for 60 min and incubated with diaminobenzidine

<sup>2</sup><http://string-db.org/>

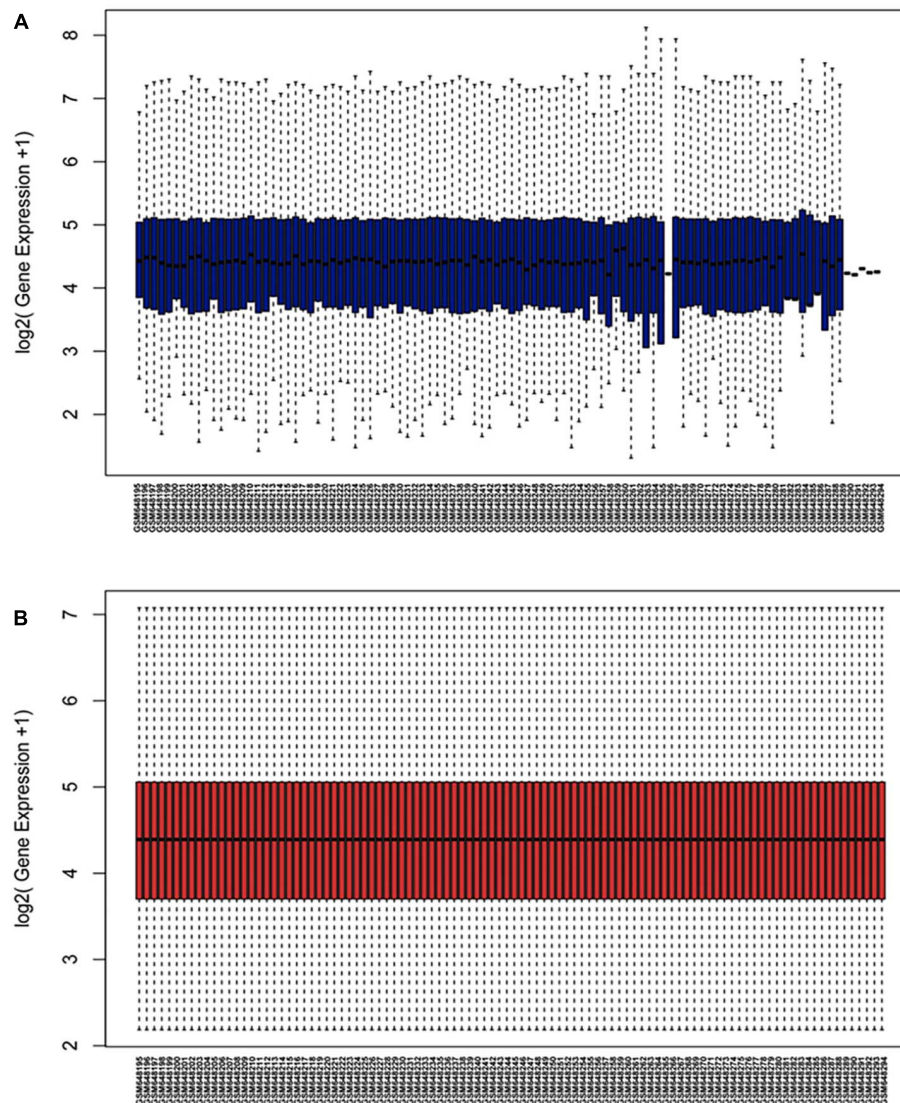


**FIGURE 1 |** Normalization of dataset GSE26409 (A) raw data of GSE26409; (B) standardization of GSE26409.

(DAB) color liquid after washing. Afterward, the tissues were counterstained using Harris hematoxylin, 1% hydrochloric acid alcohol, and lithium carbonate blue sequentially, and then visualized using an optical microscope (10 $\times$ , 40 $\times$ , Nikon, Japan) after routine cleaning and drying.

### Fluorescence *in situ* Hybridization (FISH)

*In situ* hybridization was carried out on the clinical samples using a FISH kit (Servicebio, Wuhan, China). First, tissue paraffin sections were deparaffinated with dimethylbenzene and 100% ethyl alcohol for 15 min, repaired by boiling for 8 min, digested by protein kinase K at 37°C for 10 min, washed 2 $\times$  with a saline-sodium citrate (2 $\times$  SSC) solution and dried before hybridization. Then, the prepared tissues were prehybridized at 37°C for 60 min, and hybridized with a hsa-miR-126, hsa-miR-20b, or hsa-miR-106a oligodeoxynucleotide

probe (Shenggong, Shanghai, China) in the hybridization solution at 37°C overnight in the dark. Hsa-miR-126 probe: 5'-FAM-UCGUACCGUGAGUAAUAAUGCG-FAM-3' (Entrez Gene 574032, Xq26.2); hsa-miR-20b probe: 5'-FAM-CTACCTGCACTATGAGCACTTTG-FAM-3' (Entrez Gene 406913, 9q34.3); hsa-miR-106a: 5'-FAM-ATCTGCACTGTCAGCACTTTA-FAM-3' (Entrez Gene 406899, Xq26.2). The next day, the tissues were washed by 2 $\times$  SSC solution and 3% BSA employed to block the tissues for 30 min at RT, then counterstained with anti-digoxigenin antibody and DAPI (4',6-diamidino-2-phenylindole, dihydrochloride), all from Servicebio, and imaged using a fluorescence microscope (400 $\times$ , Nikon, Japan) and measured using Image-J software at two to three fields after routine cleaning and drying. Mean fluorescence intensity (MFI) was calculated. All measured intensities were normalized to the respective channel in control tissues.



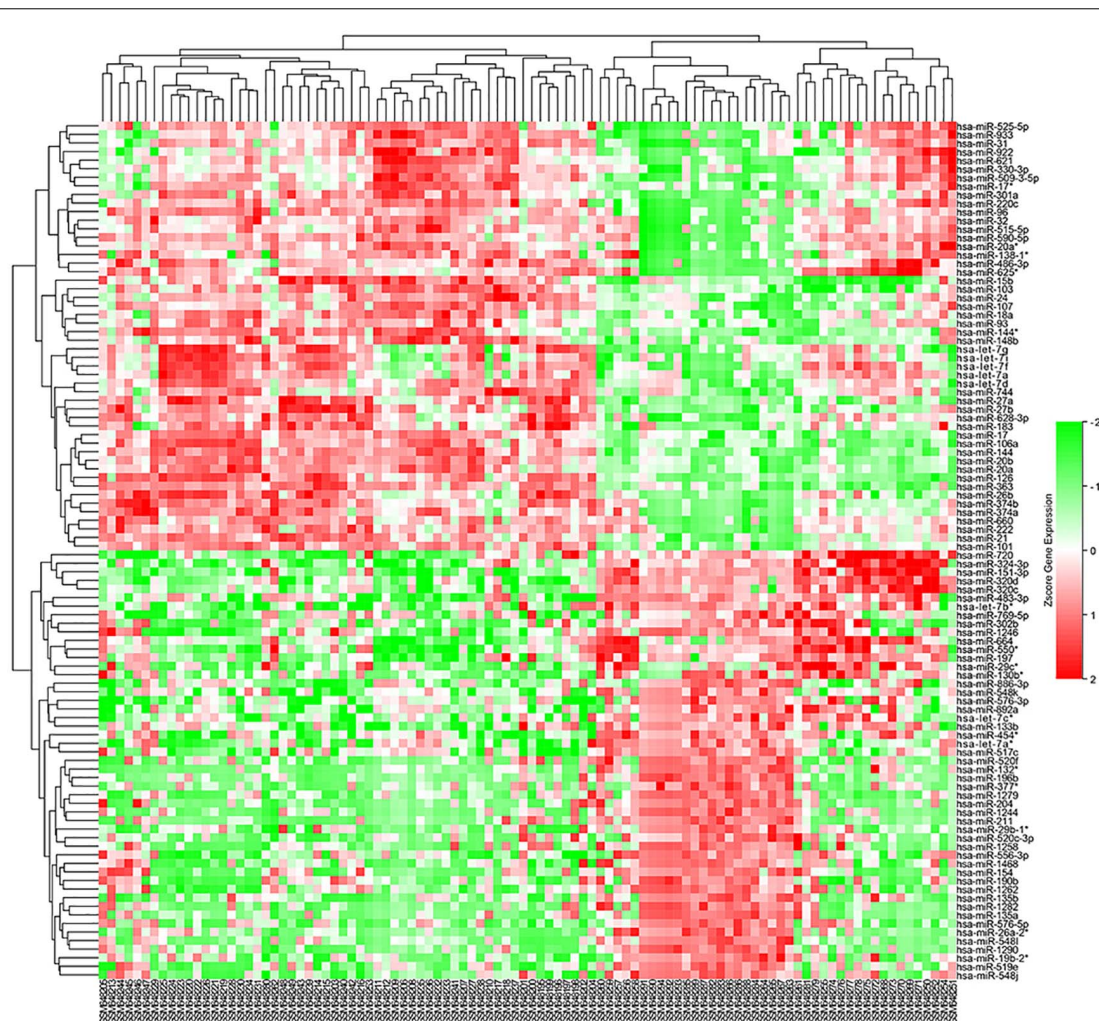


**FIGURE 2 |** Heatmap of DE-miRNAs: DE miRNAs (differentially expressed miRNAs) in 45 cases of sarcoidosis and 55 cases of normal controls.

## RESULTS

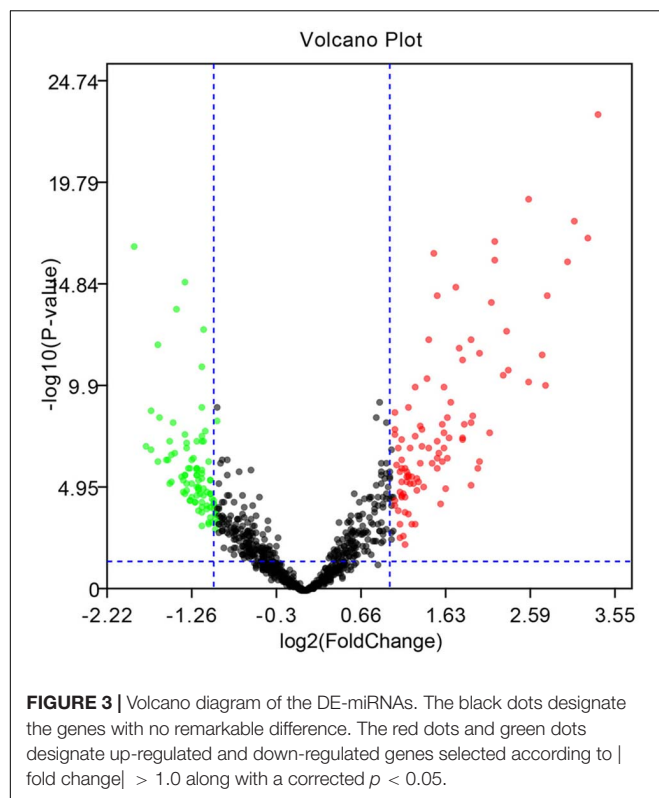
### Identification of DE-miRNAs and Prediction of Target Genes

The microarray GSE26409 cohort was acquired from the GEO website, and this cohort consisted of 45 cases of sarcoidosis (GSM648250-GSM648294) and 55 normal controls (GSM648195-GSM648249). After normalization (**Figure 1**), processing of the data was conducted via unpaired *t*-test, with the cutoff criterion of  $P < 0.05$  along with  $|\log_2FC| > 1$ . Overall, 266 DE-miRNAs were finally screened (**Figures 2, 3**), which constituted 132 and 134 upregulated and downregulated miRNAs, respectively. The top ten most upregulated, as well as downregulated miRNAs are indicated in **Table 1**. On the basis of the fold change (FC), hsa-miR-144, hsa-miR-126, and hsa-miR-106a were the upmost 3 upregulated miRNAs and hsa-miR-151-3p, hsa-miR-320d, and hsa-miR-324-3p were the upmost 3 downregulated miRNAs. For the three upregulated miRNAs, 580 potential target genes were investigated, and 543

genes were predicted for the 3 downregulated miRNAs via the miRTarBase platform.

### Functional Enrichment Analysis

To determine the enriched pathways and process enrichment of these target genes, we afterward carried out a KEGG pathway enrichment and GO functional annotation. The KEGG pathway analysis included non-small cell lung cancer, proteoglycans in cancer, viral carcinogenesis, *etc.* (**Figure 4A, Table 2**). We selected 3 GO categories consisting of biological pathway (BP), cellular component (CC), along with molecular function (MF) for functional annotation. The top ten GO terms of the target genes of the 10 upmost up-regulated DE-miRNAs are indicated in **Figures 4B–D** and **Table 3**, including the responses to stress, catabolic process, gene expression, *etc.* in the BP category; cellular component, nucleoplasm, cytosol, *etc.* in the CC category; and enzyme binding, nucleic acid binding transcription factor activity, RNA binding, *etc.* in the MF category. Subsequently, the target genes of the ten



upmost downregulated DE-miRNAs were analyzed in the same way, and the results are shown in **Figures 5A–D** and **Tables 4, 5**.

## Development and Analysis of the PPI Network and miRNA-Target Network

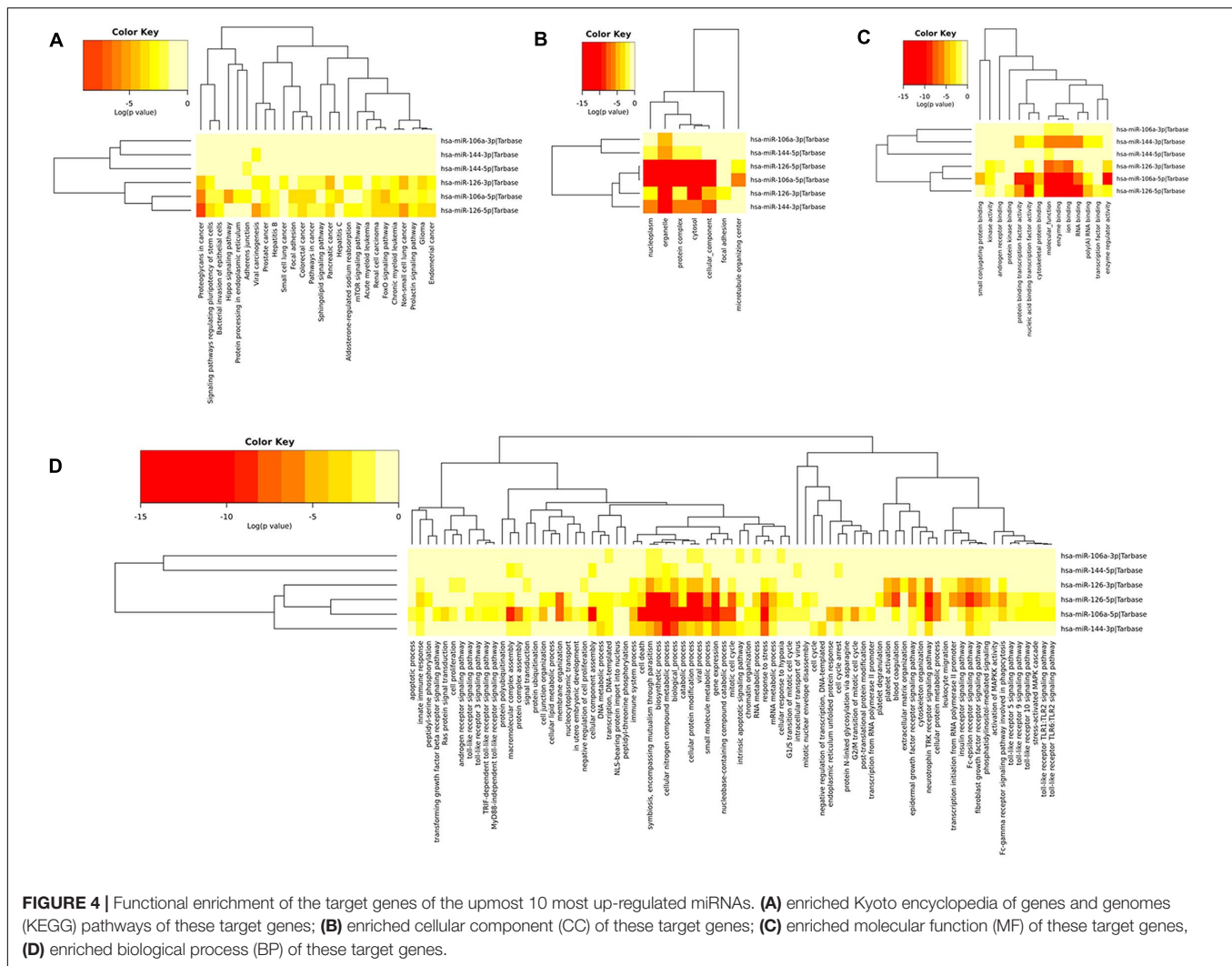
The STRING online data resource was used to develop the PPI network complex of the filtered target genes of the 5 upmost upregulated and downregulated miRNAs. By using Cystoscape software, the hub nodes were screened out and further developed the miRNA-hub gene network (**Supplementary Figures 1, 2**). After simplification, a concise relationship between miRNAs and hub genes was achieved. As shown in **Figure 6A**, *NR3C1*, *ZBTB7A*, *NUFIP2*, *BZW1*, *ERGIC2*, *VEGFA*, *BTG2*, and *BCL2L11* were the eight most targeted hub genes in the upregulation of miRNAs. Among these, four hub genes could potentially be modulated by the upregulation of hsa-miR-144. Six hub genes and eight hub genes could potentially be modulated by hsa-miR-126 and hsa-miR-106a, respectively. Eight and five hub genes could potentially be modulated by hsa-miR-20b and hsa-miR-363, respectively. Moreover, *MCL1* and *SAE1* were the two most targeted hub genes in the downregulation of miRNA. *MCL1* could potentially be targeted by hsa-miR-30d, hsa-miR-320d, and hsa-miR-151-3p; *SAE1* could potentially be regulated by hsa-miR-324-3p, hsa-miR-30d, as well as hsa-miR-151-3p (**Figure 6B**).

To further identify reliable hub genes, the targeted hub genes of miRNAs were screened in the gene nodes of the PPI network, and only two overlapping genes (*NR3C1*, *VEGFA*) were found with a relatively high degree (19 and 18, respectively) in the up and downregulated hub genes. After combining the above results, *NR3C1* and *VEGFA* were selected and potentially modulated by hsa-miR-126, hsa-miR-20b, and hsa-miR-106a. Of note, these three miRNAs might be potential regulators in manipulating the pathogenesis and development of sarcoidosis.

**TABLE 1 |** Top ten up-regulated and down-regulated differentially expressed miRNAs between sarcoidosis and normal control.

Row names(tT)	logFC	AveExpr	t	P Value	Adj. P Val	B	Regulated
hsa-miR-144	3.550863	9.313051	13.49568	9.40E-25	4.05E-22	45.78095	Up-Regulated
hsa-miR-126	3.320719	9.096936	13.12656	5.97E-24	1.72E-21	43.9572	Up-Regulated
hsa-miR-106a	2.530724	11.62744	11.24603	8.78E-20	1.90E-17	34.4828	Up-Regulated
hsa-miR-20b	3.063342	10.19364	10.80117	8.78E-19	1.52E-16	32.20948	Up-Regulated
hsa-miR-363	3.221189	10.27816	10.42804	6.08E-18	8.75E-16	30.29805	Up-Regulated
hsa-miR-15b	1.469123	13.24834	10.08452	3.62E-17	3.47E-15	28.53664	Up-Regulated
hsa-miR-103	2.156385	11.94484	9.951238	7.24E-17	6.25E-15	27.85326	Up-Regulated
hsa-miR-20a	2.986091	10.55733	9.923751	8.35E-17	6.55E-15	27.71235	Up-Regulated
hsa-miR-27a	1.718716	7.379181	9.366076	1.51E-15	1.00E-13	24.85707	Up-Regulated
hsa-miR-17	2.75136	11.48185	9.189665	3.75E-15	2.31E-13	23.95629	Up-Regulated
hsa-miR-151-3p	-2.12643	9.873969	-13.827	1.81E-25	1.56E-22	47.40578	Down-Regulated
hsa-miR-320d	-1.93278	10.06991	-10.2473	1.56E-17	1.68E-15	29.37113	Down-Regulated
hsa-miR-324-3p	-1.36532	9.917577	-9.47768	8.45E-16	6.08E-14	25.42768	Down-Regulated
hsa-miR-720	-1.46921	12.4055	-8.86408	2.02E-14	1.02E-12	22.29872	Down-Regulated
hsa-miR-30d	-1.15751	13.04519	-8.42283	1.94E-13	9.15E-12	20.06631	Down-Regulated
hsa-miR-550	-1.67819	9.709234	-8.11338	9.40E-13	3.69E-11	18.51341	Down-Regulated
hsa-miR-132	-2.22146	4.350623	-7.72266	6.76E-12	2.16E-10	16.57212	Down-Regulated
hsa-miR-320b	-1.17778	11.65868	-7.62165	1.12E-11	3.46E-10	16.07431	Down-Regulated
hsa-miR-30c	-1.16476	11.15127	-6.68633	1.11E-09	2.51E-08	11.56764	Down-Regulated
hsa-miR-483-3p	-1.75494	5.540333	-6.5849	1.80E-09	3.78E-08	11.09214	Down-Regulated





## Verification of the Expression of Hub Genes and miRNAs in Clinical Specimens

To validate the expression of *VEGFA* and *NR3C1*, we performed IHC to examine 12 mediastinal lymph node tissues from pulmonary sarcoidosis patients and 13 mediastinal lymph node tissues from tuberculosis patients. Ten of the twelve sections showed moderate to strong dark brown staining of VEGFA in both the epithelioid cells and lymphocytes (Figures 7C,D), and negative to very weak staining for control group (Figures 7A,B). Nine of the twelve sections presented weak to moderate staining expression of NR3C1 (Figures 7G,H) comparing the control sections which present negative to very weak staining (Figures 7E,F).

The expression contents of hsa-miR-126, hsa-miR-20b, and hsa-miR-106a were further analyzed via FISH on the 12 mediastinal lymph node tissues of pulmonary sarcoidosis patients versus the 13 control tissues. Typical results were shown in Figure 8. The staining revealed strong enrichment of hsa-miR-126 along the edge of the non-caseating granulomas (Figure 8B),

presenting higher expression than the controls (Figure 8A), while hsa-miR-20b (Figures 8D,E) and hsa-miR-106a had low expression (Figures 8G,H) in both groups. Quantification of fluorescence for hsa-miR-126, hsa-miR-20b, and hsa-miR-106a were measured, and it demonstrated that hsa-miR-126 significantly increased in mediastinal lymph node tissues of pulmonary sarcoidosis patients (Figures 8C,E,I).

## DISCUSSION

Sarcoidosis, a multisystem disease, is typified by non-caseating granulomas. Up to 50% of sarcoidosis cases are diagnosed by chest radiographs during a routine examination. Clinically, approximately 1/4 of pulmonary sarcoidosis cases are atypical with non-specific clinical symptoms, atypical radiological manifestations, and non-unique pathology, which easily lead to misdiagnosis (Aryal and Nathan, 2019). The etiology and pathogenesis are still uncertain. Although intensive studies have revealed genetic factors, inflammation, and immune responses in the risk and clinical development of sarcoidosis, the regulation

**TABLE 2 |** KEGG pathway analysis of unregulated DE-miRNAs in sarcoidosis.

KEGG pathway	p-value	Genes	miRNAs
Proteoglycans in cancer (hsa05205)	7.77E-16	PIK3R2, PIK3CD, CTNNB1, AKT1, PIK3CA, SDC2, VEGFA, MAPK1, ITGB1, PTCH1, WNT5A, PIK3R2, FRS2, RDX, KRAS, FZD4, PIK3CD, CCND1, CTNNB1, AKT1, FLNB, GAB1, PIK3CA, SDC2, PDPK1, VEGFA, MAPK1, GRB2, MDM2, RPS6KB1, PDCD4, ITGB1, EZR, CBL, NRAS, CAV1, ROCK2, FRS2, IGF1R, RHOA, PPP1R12B, CAV2, FZD3, PPP1R12A, CCND1, CTNNB1, FLNB, TIMP3, PIK3R1, SOS1, DDX5, GAB1, AKT3, CDKN1A, VEGFA, MAPK1	hsa-miR-126-3p, hsa-miR-126-5p, hsa-miR-106a-5p
Viral carcinogenesis (hsa05203)	8.91E-08	CCND2, YWHAB, DDX3X, CASP3, JUN, EP300, USP7, HIST2H2BE, GTF2A1, PIK3R2, HIST1H2BD, PIK3CD, GTF2H3, CCNE1, PIK3CA, IL6ST, HDAC8, MAPK1, ATF2, RASA2, DLG1, PIK3R2, CDK1, KRAS, CDK6, PMAIP1, PIK3CD, CCND1, YWHAZ, HDAC2, RBPJ, ACTN4, CCNE1, PIK3CA, USP7, MAPK1, CREBBP, GRB2, JAK1, MDM2, CCND3	hsa-miR-144-3p, hsa-miR-126-3p, hsa-miR-126-5p
Non-small cell lung cancer (hsa05223)	4.87E-07	E2F1, PIK3R2, PIK3CD, E2F3, AKT1, PIK3CA, MAPK1, RXRA, PIK3R2, KRAS, CDK6, PIK3CD, CCND1, E2F3, AKT1, PIK3CA, PDPK1, MAPK1, GRB2, E2F1, NRAS, STK4, CCND1, PIK3R1, RB1, SOS1, AKT3, MAPK1, RASSF5	hsa-miR-126-3p, hsa-miR-126-5p, hsa-miR-106a-5p
Pancreatic cancer (hsa05212)	5.51E-06	E2F1, PIK3R2, PIK3CD, E2F3, AKT1, PIK3CA, VEGFA, MAPK1, PIK3R2, KRAS, CDK6, PIK3CD, CCND1, E2F3, AKT1, PIK3CA, VEGFA, MAPK1, TGFBF2, JAK1, STAT3, E2F1, SMAD3, CCND1, SMAD4, MAPK8, PIK3R1, RB1, AKT3, VEGFA, MAPK1, TGFBF2, JAK1	hsa-miR-126-3p, hsa-miR-126-5p, hsa-miR-106a-5p
Colorectal cancer (hsa05210)	9.75E-06	PIK3R2, PIK3CD, CTNNB1, AKT1, PIK3CA, MAPK1, GSK3B, PIK3R2, BCL2, KRAS, PIK3CD, CCND1, CTNNB1, AKT1, PIK3CA, MAPK1, TGFBF2, TCF7L1, SMAD3, RHOA, APPL1, CCND1, SMAD4, CTNNB1, MAPK8, PIK3R1, AKT3, LEF1, MAPK1, TGFBF2	hsa-miR-126-3p, hsa-miR-126-5p, hsa-miR-106a-5p
Glioma (hsa05214)	1.33E-05	PIK3R2, KRAS, CDK6, PIK3CD, CCND1, E2F3, AKT1, PIK3CA, MAPK1, GRB2, MDM2, PDGFRA, E2F1, NRAS, IGF1R, CCND1, PIK3R1, RB1, SOS1, AKT3, CDKN1A, MAPK1	hsa-miR-126-3p, hsa-miR-126-5p, hsa-miR-106a-5p
FoxO signaling pathway (hsa04068)	1.34E-05	IRS2, PIK3R2, STK11, PIK3CD, AKT1, PLK2, IRS1, PIK3CA, MAPK1, SGK1, IRS2, CCNB1, SIRT1, PIK3R2, KRAS, PIK3CD, CCND1, AKT1, IRS1, PRKAA1, BCL6, PRKAB2, SOD2, PIK3CA, USP7, PDPK1, MAPK1, CREBBP, GRB2, CCNG2, TGFBF2, MDM2, RBL2, STAT3, CCNB1, NRAS, STK4, SIRT1, SETD7, CCND2, STK11, SMAD3, IGF1R, NLK, CCND1, SMAD4, MAPK8, PLK2, PIK3R1, SOS1, IRS1, PRKAB2, CSNK1E, AKT3, SOD2, CDKN1A, MAPK1, CCNG2, TGFBF2	hsa-miR-126-3p, hsa-miR-126-5p, hsa-miR-106a-5p
Renal cell carcinoma (hsa05211)	1.64E-05	CRK, CUL2, PIK3R2, RAP1A, ETS1, KRAS, PIK3CD, AKT1, GAB1, PIK3CA, VEGFA, MAPK1, CREBBP, GRB2, NRAS, CRK, PAK2, ARNT, ETS1, EPAS1, EGLN3, PIK3R1, SOS1, GAB1, AKT3, VEGFA, MAPK1, EGLN1	hsa-miR-126-3p, hsa-miR-126-5p, hsa-miR-106a-5p
Chronic myeloid leukemia (hsa05220)	4.95E-05	E2F1, CRK, PIK3R2, CTBP2, PIK3CD, E2F3, AKT1, PIK3CA, MAPK1, KRAS, CDK6, CCND1, HDAC2, GRB2, TGFBF2, MDM2, CBL, NRAS, RUNX1, SMAD3, SMAD4, PIK3R1, RB1, SOS1, AKT3, CDKN1A	hsa-miR-126-3p, hsa-miR-126-5p, hsa-miR-106a-5p
Pathways in cancer (hsa05200)	5.12E-05	E2F1, CRK, PIK3R2, GNA13, ETS1, CTBP2, PIK3CD, CTNNB1, E2F3, AKT1, CCNE1, PIK3CA, ITGA6, VEGFA, MAPK1, ADCY9, RXRA, GSK3B, ITGB1, CRK, PTCH1, CUL2, WNT5A, PIK3R2, GNA13, ETS1, BCL2, KRAS, CDK6, FZD4, PIK3CD, CCND1, CTNNB1, E2F3, AKT1, HDAC2, CCNE1, PIK3CA, VEGFA, MAPK1, CREBBP, GRB2, TGFBF2, JAK1, MDM, STAT3, PDGFRA, E2F1, ITGB1, CXCL8, CBL, CXCR4, NRAS, STK4, CRK, RUNX1, ROCK2, TCF7L1, ARNT, ETS1, SMAD3, IGF1R, RHOA, APPL1, FZD3, TPM3, EPAS1, CCND1, SMAD4, CTNNB1, COL4A2, MAPK8, EGLN3, PIK3R1, RB1, SOS1, HSP90B1, AKT3, LEF1, CDKN1A, ITGA6, VEGFA, MAPK1, TGFBF2, JAK1, EGLN1, COL4A1, RASSF5	hsa-miR-126-3p, hsa-miR-126-5p, hsa-miR-106a-5p

of miRNAs is rarely involved. Our study indicated that multiple complex signal transduction pathways and factors participate in the pathogenic mechanisms of sarcoidosis. The microarray and bioinformatics analysis provides us with a comprehensive map of the biological functions and interactions of sarcoidosis-related genes, this will not only provide us with pivotal information to reveal the pathogenesis of the disease, but also help us to find novel preventive and therapeutic interventions.

Herein, we explored the gene expression profile of GSE26409 consisting of 45 sarcoidosis blood samples and 55 normal blood samples, to identify the molecular mechanism of sarcoidosis. Totally, 266 DE-miRNAs were filtered, consisting of 132 upregulated and 134 downregulated miRNAs. Among these, hsa-miR-144, hsa-miR-126 along with hsa-miR-106a were the most upregulated miRNAs; hsa-miR-151-3p, hsa-miR-320d, and hsa-miR-324-3p were the most downregulated miRNAs.

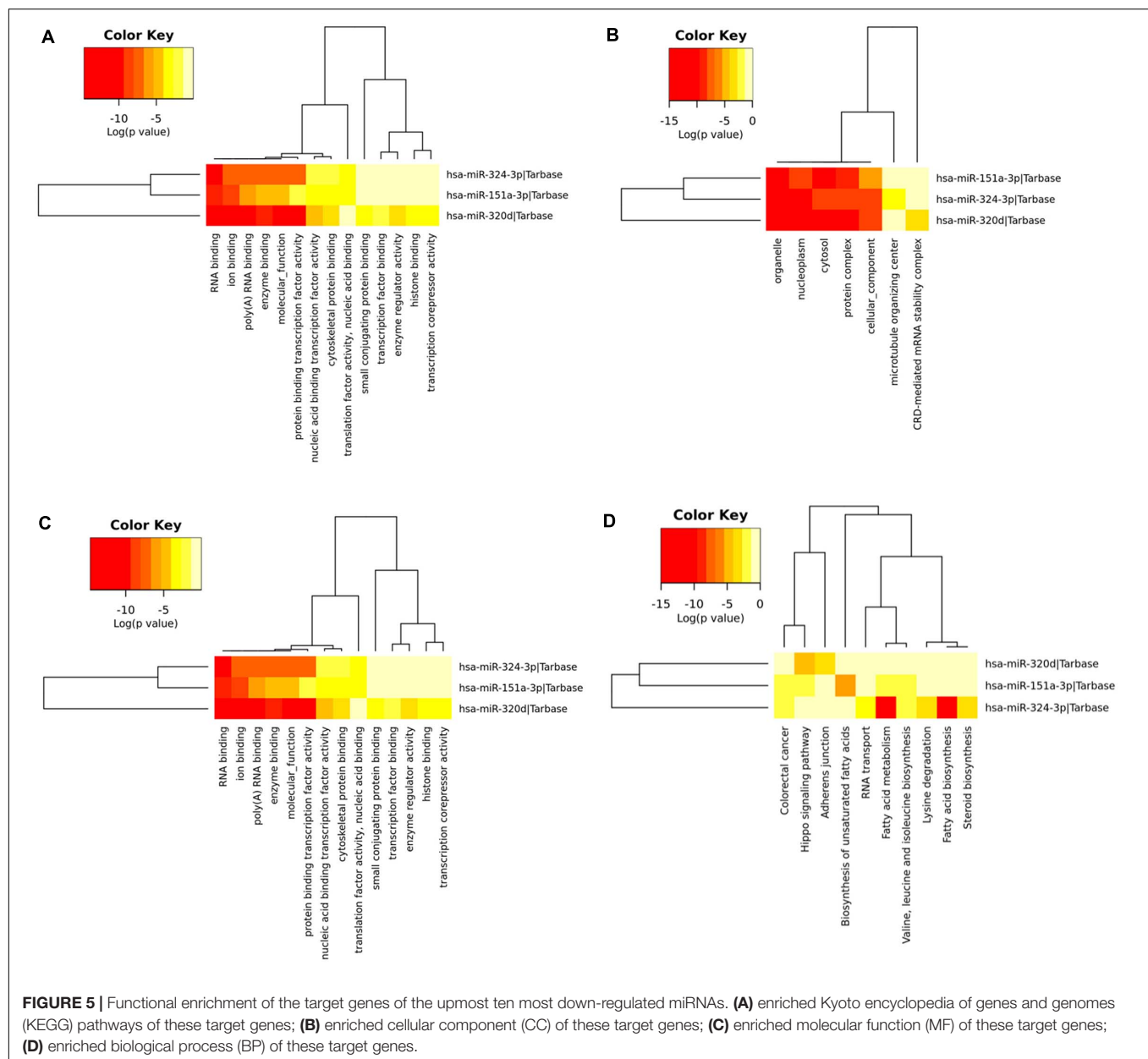
At the molecular level, prediction of the miRNA target genes was performed, then GO annotation and associated cascades were analyzed. Furthermore, by constructing the protein-protein interaction (PPI) networks, *NR3C1*, *ZBTB7A*, *NUFIP2*, *BZW1*, *ERGIC2*, *VEGFA*, *BTG2*, and *BCL2L11* were mapped as the most targeted hub genes in the upregulation of miRNAs, and *MCL1* and *SAE1* were the most targeted hub genes in the downregulation of miRNA. *NR3C1* and *VEGFA* were selected and are potentially modulated by hsa-miR-126, hsa-miR-20b, and hsa-miR-106a. To validate the bioinformatics analysis data, immunohistochemistry along with fluorescence *in situ* hybridization were employed to assess gene expression in clinical specimens. Among the identified miRNAs involved in sarcoidosis, hsa-miR-126 was highly expressed, and the two target genes *VEGFA* and *NR3C1* were also highly expressed in lymph node samples of sarcoidosis.

**TABLE 3 |** GO analysis of unregulated DE-miRNAs associated with sarcoidosis.

GO Category	Gene function (Term)	Gene count	miRNAs	p-value
BP	Response to stress (GO:0006950)	313	hsa-miR-144-3p, hsa-miR-126-3p, hsa-miR-126-5p, hsa-miR-106a-5p	<1e-325
BP	Catabolic process (GO:0009056)	249	hsa-miR-144-3p, hsa-miR-126-3p, hsa-miR-126-5p, hsa-miR-106a-5p	<1e-325
BP	Gene expression (GO:0010467)	119	hsa-miR-144-3p, hsa-miR-126-3p, hsa-miR-126-5p, hsa-miR-106a-5p	<1e-325
BP	Fc-epsilon receptor signaling pathway (GO:0038095)	38	hsa-miR-144-3p, hsa-miR-126-3p, hsa-miR-126-5p, hsa-miR-106a-5p	<1e-325
BP	Neurotrophin TRK receptor signaling pathway (GO:0048011)	58	hsa-miR-144-3p, hsa-miR-126-3p, hsa-miR-126-5p, hsa-miR-106a-5p	<1e-325
BP	Cellular protein modification process (GO:0006464)	376	hsa-miR-144-3p, hsa-miR-126-3p, hsa-miR-126-5p, hsa-miR-106a-3p, hsa-miR-106a-5p	<1e-325
BP	Biological_process (GO:0008150)	1711	hsa-miR-144-3p, hsa-miR-144-5p, hsa-miR-126-3p, hsa-miR-126-5p, hsa-miR-106a-5p	<1e-325
BP	Viral process (GO:0016032)	101	hsa-miR-144-3p, hsa-miR-126-3p, hsa-miR-126-5p, hsa-miR-106a-3p, hsa-miR-106a-5p	<1e-325
BP	Cellular nitrogen compound metabolic process (GO:0034641)	647	hsa-miR-144-3p, hsa-miR-144-5p, hsa-miR-126-3p, hsa-miR-126-5p, hsa-miR-106a-5p	<1e-325
BP	biosynthetic process (GO:0009058)	536	hsa-miR-144-3p, hsa-miR-144-5p, hsa-miR-126-3p, hsa-miR-126-5p, hsa-miR-106a-3p, hsa-miR-106a-5p	<1e-325
CC	cellular component (GO:0005575)	1729	hsa-miR-144-3p, hsa-miR-126-3p, hsa-miR-126-5p, hsa-miR-106a-5p	<1e-325
CC	nucleoplasm (GO:0005654)	196	hsa-miR-144-3p, hsa-miR-144-5p, hsa-miR-126-3p, hsa-miR-126-5p, hsa-miR-106a-5p	<1e-325
CC	cytosol (GO:0005829)	419	hsa-miR-144-3p, hsa-miR-144-5p, hsa-miR-126-3p, hsa-miR-126-5p, hsa-miR-106a-5p	<1e-325
CC	protein complex (GO:0043234)	483	hsa-miR-144-3p, hsa-miR-144-5p, hsa-miR-126-3p, hsa-miR-126-5p, hsa-miR-106a-5p	<1e-325
CC	organelle (GO:0043226)	1324	hsa-miR-144-3p, hsa-miR-144-5p, hsa-miR-126-3p, hsa-miR-126-5p, hsa-miR-106a-3p, hsa-miR-106a-5p	<1e-325
CC	microtubule organizing center (GO:0005815)	64	hsa-miR-126-5p, hsa-miR-106a-5p	3.37E-06
CC	focal adhesion (GO:0005925)	13	hsa-miR-126-3p	0.013148
MF	nucleic acid binding transcription factor activity (GO:0001071)	161	hsa-miR-144-3p, hsa-miR-126-3p, hsa-miR-126-5p, hsa-miR-106a-5p	<1e-325
MF	RNA binding (GO:0003723)	266	hsa-miR-144-3p, hsa-miR-126-3p, hsa-miR-126-5p, hsa-miR-106a-5p	<1e-325
MF	enzyme binding (GO:0019899)	233	hsa-miR-144-3p, hsa-miR-126-3p, hsa-miR-126-5p, hsa-miR-106a-3p, hsa-miR-106a-5p	<1e-325
MF	ion binding (GO:0043167)	756	hsa-miR-144-3p, hsa-miR-126-3p, hsa-miR-126-5p, hsa-miR-106a-3p, hsa-miR-106a-5p	<1e-325
MF	molecular_function (GO:0003674)	1767	hsa-miR-144-3p, hsa-miR-144-5p, hsa-miR-126-3p, hsa-miR-126-5p, hsa-miR-106a-3p, hsa-miR-106a-5p	<1e-325
MF	protein binding transcription factor activity (GO:0000988)	90	hsa-miR-144-3p, hsa-miR-126-5p, hsa-miR-106a-5p	2.22E-16
MF	enzyme regulator activity (GO:0030234)	109	hsa-miR-126-3p, hsa-miR-126-5p, hsa-miR-106a-5p	3.56E-12
MF	poly(A) RNA binding (GO:0044822)	205	hsa-miR-144-3p, hsa-miR-126-5p, hsa-miR-106a-5p	6.95E-08
MF	cytoskeletal protein binding (GO:0008092)	102	hsa-miR-144-3p, hsa-miR-126-5p, hsa-miR-106a-5p	1.82E-07
MF	transcription factor binding (GO:0008134)	46	hsa-miR-144-3p, hsa-miR-126-5p	0.000592

The GO annotation and KEGG pathway analysis have identified more cancer related pathways that were closely related to upregulated DE-miRNAs in sarcoidosis, which

including proteoglycans in cancer, viral carcinogenesis, non-small cell lung cancer, pancreatic cancer, colorectal cancer, glioma, etc. The relationship between sarcoidosis



and cancer is complex, and meta-analyses have concluded that an increased risk of neoplasia in sarcoidosis (El Jammal et al., 2020). Fatty acid biosynthesis and metabolism also participated in the biological functions of miRNA in sarcoidosis. The mismatch of myocardial fatty acid metabolism and myocardial perfusion under positron emission tomography computed tomography (PET-CT) could diagnosis and detection of myocardial injury in cardiac sarcoidosis (Momose et al., 2015).

VEGFA (Vascular endothelial growth factor-A) is a PDGF/VEGF growth factor family member, and by triggering the proliferation, as well as the migration of vascular endothelial cells, it is vital for physiological and pathological of angiogenesis (Tamura et al., 2019). A previous clinical study confirmed

that the serum levels of VEGF were higher in sarcoidosis subjects than in normal controls (Mirzaei et al., 2018). Further research evaluated the VEGFA level in serum, as well as bronchoalveolar lavage (BAL) and found similar results: VEGFA was remarkably higher in individuals with sarcoidosis relative to the healthy controls ( $p = 0.0002$ ). The results also showed that the immunoexpression of VEGFA was higher in serum in contrast to the BAL fluid. However, the levels of VEGFA had no correlation with the clinical phenotype (acute onset or insidious onset), stage, or lung function (Piotrowski et al., 2015). Immunohistochemistry analyses on VATS (video-assisted thoracoscopic surgery) lung biopsy samples of sarcoidosis lesions were very consistent with our findings that VEGF was upregulated compared to the control group (Tzouveleakis et al., 2012).



**TABLE 4 |** KEGG pathway analysis of downregulated DE-miRNAs in sarcoidosis.

KEGG pathway	p-value	Genes	miRNAs
Fatty acid biosynthesis (hsa00061)	<1e-325	FASN	hsa-miR-324-3p
Fatty acid metabolism (hsa01212)	1.12E-09	PTPLB, ELOVL5, SCD, ACACA, FASN, CPT2	hsa-miR-151a-3p, hsa-miR-324-3p
Hippo signaling pathway (hsa04390)	6.90E-05	APC, PPP2CA, PPP1CC, SNAI2, YWHAB, CCND1, SMAD4, PPP2CB, LATS1, PARD6B, PPP2CA, YWHAG, CCND2, GIL2, SMAD3, WWTR1, CDH1, CTNNB1, CSNK1E, WNT2, SMAD7, LATS1	hsa-miR-151a-3p, hsa-miR-320d
Biosynthesis of unsaturated fatty acids (hsa01040)	0.000417325	PTPLB, ELOVL5, SCD	hsa-miR-151a-3p
Colorectal cancer (hsa05210)	0.001949491	BRAF, APC, RHOA, PIK3R3, CCND1, SMAD4, MSH6, GSK3B, PIK3CB, BIRC5, CCND1, SMAD4, CTNNB1	hsa-miR-151a-3p, hsa-miR-324-3p
Adherens junction (hsa04520)	0.00509092	SMAD3, TJP1, CDH1, CTNNB1, RAC1, INSR, SSX2IP, MAPK1	hsa-miR-320d
RNA transport (hsa03013)	0.01706858	PAIP1, NUP160, EIF3B, NUP214, RNPS1, EIF2B3, EIF4B, EIF4G1, EEF1A1, NDC1, EIF4, BP2, NUP155, RAN, EIF4G2	hsa-miR-324-3p
Lysine degradation (hsa00310)	0.02839269	WHSC1L1, ALDH3A2, SETD2, ASH1L, KMT2C	hsa-miR-324-3p
Steroid biosynthesis (hsa00100)	0.02915267	DHCR24	hsa-miR-324-3p
Valine, leucine and isoleucine biosynthesis (hsa00290)	0.04059014	BCAT2	hsa-miR-151a-3p, hsa-miR-324-3p

NR3C1 (Nuclear receptor subfamily 3 group C member-1) codes for the glucocorticoid receptor and extensively participates in cellular proliferation, differentiation of target tissues, as well as inflammatory responses. Mutations that occurred in NR3C1 are related to generalized glucocorticoid resistance. Glucocorticoids (GCs) are the most common therapeutic agents in clinical use, and due to the fundamental regulatory roles in suppression of inflammation, GCs were widely used for autoimmune and inflammatory diseases (Ghahesouran et al., 2018). GWAS (Genome-wide association studies) have found that SNPs (single nucleotide polymorphisms) located in *NR3C1* were positively replicated in the corticosteroid drug pathway of asthma (Keskin et al., 2019). After evaluating the SNPs of *NR3C1* in *in vivo* and *in vitro* models, the results showed that it was closely associated with hypersensitivity to glucocorticoids in asthma (Cuzzoni et al., 2012). In this study, *NR3C1* was upregulated in sarcoidosis and expressed in pathological specimens, which may be related to the sensitivity of sarcoidosis to glucocorticoid therapy. Simultaneously, we found that NR3C1 is not always highly expressed, which may be related to the insensitivity of some sarcoidosis patients to glucocorticoid treatment in clinical practice. It can finally be seen that the DNA polymorphism reflects the heterogeneity of the disease.

At present, the role of miRNA in sarcoidosis remains unclear. Kiszalkiewicz et al. investigated the expression of ten screened miRNAs in 94 pulmonary sarcoidosis patients and 50 controls, and remarkable differences were discovered between the sarcoidosis patients and healthy controls in the expression of diverse detected miRNAs in peripheral blood lymphocytes (miR-27b, miR-let-7f, miR-15b, miR-192, miR-130a, miR-221, miR-222). Three miRNAs were merely reported to differ in BALF cells (miR-15b, miR-192, as well as miR-221) (Kiszalkiewicz et al., 2016). A subgroup analysis further observed several correlations among the levels of expression

of miRNA, lung function parameters (FVC, FEV<sub>1</sub>/FVC), and selected laboratory molecular markers (CD4<sup>+</sup>/CD8<sup>+</sup>, serum Ca<sup>2+</sup> concentration). The results showed only gender was not related to the expression of miRNA in BALF (Kiszalkiewicz et al., 2016). Nevertheless, in our study, we did not evaluate the relationship of some clinical indicators to miRNAs expression. We summarized the following reasons. Firstly, the expression of miRNA in peripheral blood is affected by various factors throughout the body, so is the alveolar lavage fluid. For patients with lung infection, COPD, asthma, and tumors, the detected miRNA itself is not accurate enough, subsequently, error in correlation analysis is even greater. Secondly, for early stage sarcoidosis, the lung function is hardly affected, especially FVC, FEV<sub>1</sub>/FVC, and diffusion function parameters. And, changes in lung function cannot reflect the true situation of patients with sarcoidosis. Thirdly, our study is a retrospective study, not all included patients had lung function tests and samples of alveolar lavage fluid, thus, some of these parameters could not be tested.

To elucidate the function of miRNAs in sarcoidosis, Jazwa et al. (2015) compared the expression levels of selected inflammatory miRNAs in patients with sarcoidosis and healthy individuals. After screening the miRNA transcriptome, miR-34a was isolated from sarcoidosis patients in peripheral blood mononuclear cells, which suggested that it may be involved in the pathology of sarcoidosis. Additionally, miR-155 was shown to be one of the miRNAs that are differentially expressed in macrophages, which are considered to have a role in formation of granuloma in sarcoidosis (Zhang et al., 2013). A study on the mechanism of miRNA in pulmonary sarcoidosis proved that miR-34a along with miR-155 enhance the secretion of interferon-gamma and negatively modulate SIRT-1, therefore inhibiting NF-κB transcription, as well as deacetylate the p53 protein, ultimately inactivating

**TABLE 5 |** GO analysis of downregulated DE-miRNAs associated with sarcoidosis.

GO Category	Gene function (Term)	Gene count	miRNAs	p-value
BP	Cellular protein modification process (GO:0006464)	231	hsa-miR-151a-3p, hsa-miR-320d, hsa-miR-324-3p	<1e-325
BP	Biosynthetic process (GO:0009058)	363	hsa-miR-151a-3p, hsa-miR-320d, hsa-miR-324-3p	<1e-325
BP	Gene expression (GO:0010467)	110	hsa-miR-151a-3p, hsa-miR-320d, hsa-miR-324-3p	<1e-325
BP	Cellular nitrogen compound metabolic process (GO:0034641)	461	hsa-miR-151a-3p, hsa-miR-320d, hsa-miR-324-3p	<1e-325
BP	Symbiosis, encompassing mutualism through parasitism (GO:0044403)	72	hsa-miR-151a-3p, hsa-miR-320d, hsa-miR-324-3p	7.99E-14
BP	Viral process (GO:0016032)	65	hsa-miR-151a-3p, hsa-miR-320d, hsa-miR-324-3p	1.59E-13
BP	Mitotic cell cycle (GO:0000278)	57	hsa-miR-151a-3p, hsa-miR-320d, hsa-miR-324-3p	3.04E-12
BP	Cell death (GO:0008219)	104	hsa-miR-151a-3p, hsa-miR-320d, hsa-miR-324-3p	9.11E-12
BP	Neurotrophin TRK receptor signaling pathway (GO:0048011)	40	hsa-miR-151a-3p, hsa-miR-320d, hsa-miR-324-3p	4.37E-11
BP	Biological_process (GO:0008150)	1138	hsa-miR-151a-3p, hsa-miR-320d, hsa-miR-324-3p,	1.42E-10
CC	Cellular_component (GO:0005575)	1189	hsa-miR-151a-3p, hsa-miR-320d, hsa-miR-324-3p	<1e-325
CC	Nucleoplasm (GO:0005654)	157	hsa-miR-151a-3p, hsa-miR-320d, hsa-miR-324-3p	<1e-325
CC	Cytosol (GO:0005829)	279	hsa-miR-151a-3p, hsa-miR-320d, hsa-miR-324-3p	<1e-325
CC	Organelle (GO:0043226)	889	hsa-miR-151a-3p, hsa-miR-320d, hsa-miR-324-3p	<1e-325
CC	Protein complex (GO:0043234)	349	hsa-miR-151a-3p, hsa-miR-320d, hsa-miR-324-3p	<1e-325
CC	CRD-mediated mRNA stability complex (GO:0070937)	5	hsa-miR-320d	0.006458676
CC	Microtubule organizing center (GO:0005815)	20	hsa-miR-324-3p	0.00699504
MF	Protein binding transcription factor activity (GO:0000988)	73	hsa-miR-151a-3p, hsa-miR-320d, hsa-miR-324-3p	<1e-325
MF	Molecular_function (GO:0003674)	1174	hsa-miR-151a-3p, hsa-miR-320d, hsa-miR-324-3p	<1e-325
MF	RNA binding (GO:0003723)	223	hsa-miR-151a-3p, hsa-miR-320d, hsa-miR-324-3p	<1e-325
MF	Enzyme binding (GO:0019899)	144	hsa-miR-151a-3p, hsa-miR-320d, hsa-miR-324-3p	<1e-325
MF	Ion binding (GO:0043167)	478	hsa-miR-151a-3p, hsa-miR-320d, hsa-miR-324-3p	<1e-325
MF	Poly(A) RNA binding (GO:0044822)	195	hsa-miR-151a-3p, hsa-miR-320d, hsa-miR-324-3p	<1e-325
MF	Nucleic acid binding transcription factor activity (GO:0001071)	93	hsa-miR-151a-3p, hsa-miR-320d, hsa-miR-324-3p	7.76E-07
MF	Cytoskeletal protein binding (GO:0008092)	76	hsa-miR-151a-3p, hsa-miR-320d, hsa-miR-324-3p	1.46E-05
MF	Translation factor activity, nucleic acid binding (GO:0008135)	15	hsa-miR-151a-3p, hsa-miR-324-3p	0.000339
MF	Enzyme regulator activity (GO:0030234)	38	hsa-miR-320d	0.002755

p53-regulated transcription and apoptosis (Kachamakova-Trojanowska et al., 2018). On the other hand, by establishing a murine model, Barna et al. (2016) found that elevated miRNA-33 promoted the formation of granuloma through

the inhibition of the alveolar macrophage lipid transporters ABCA1 and ABCG1.

In our study, the lymphatic tissue of tuberculosis patients was used as a control group. This is why we raise the

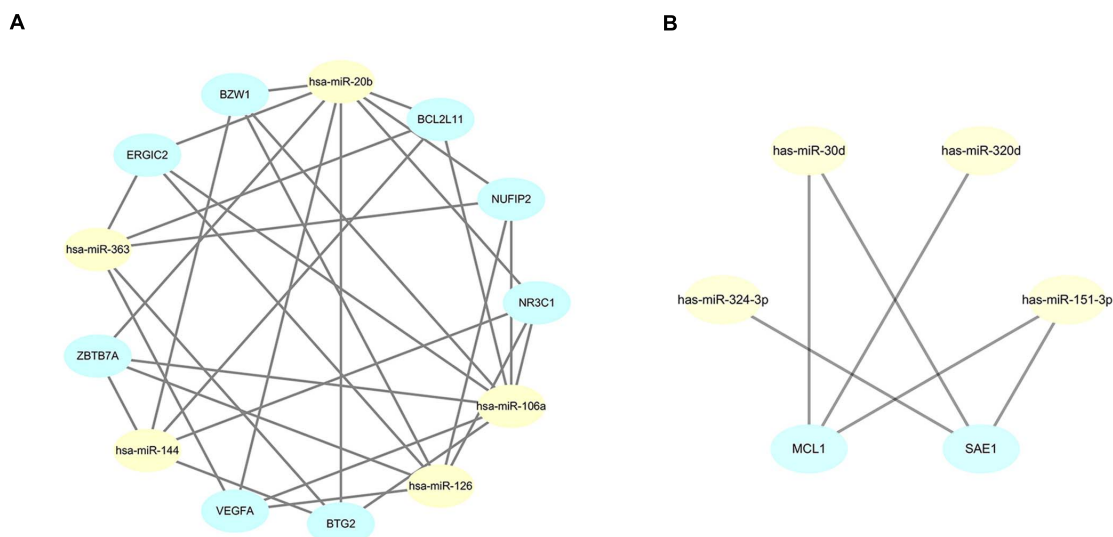


**FIGURE 6 |** Simplified miRNA-gene network. **(A)** miRNA-gene network of upregulated miRNAs after simplified by interaction at degree  $\geq 4$ ; **(B)** miRNA-gene network of downregulated miRNAs after simplified by interaction at degree  $\geq 3$ .

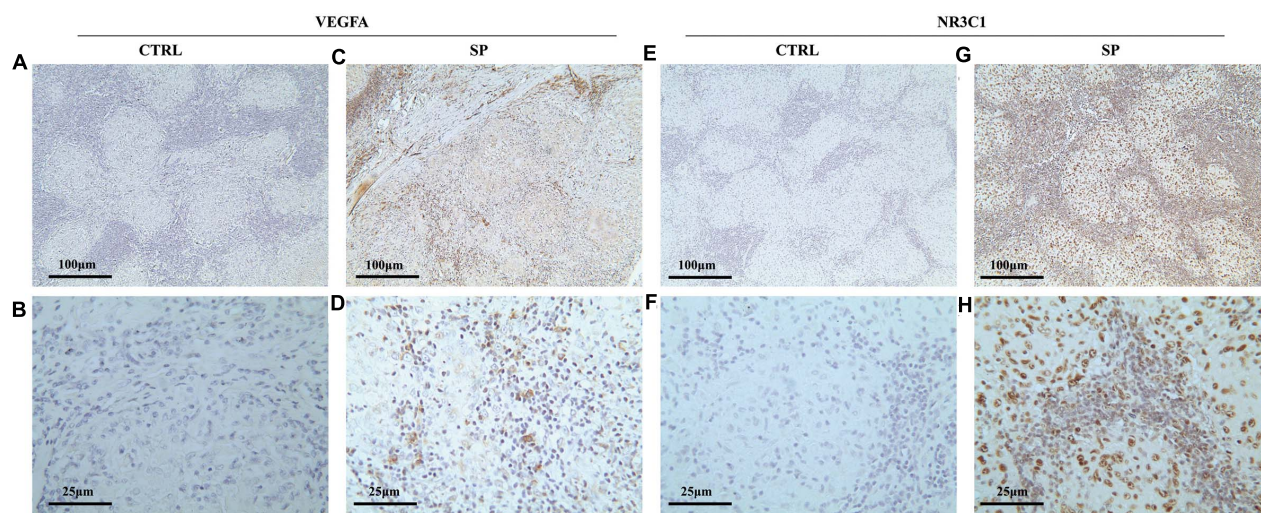


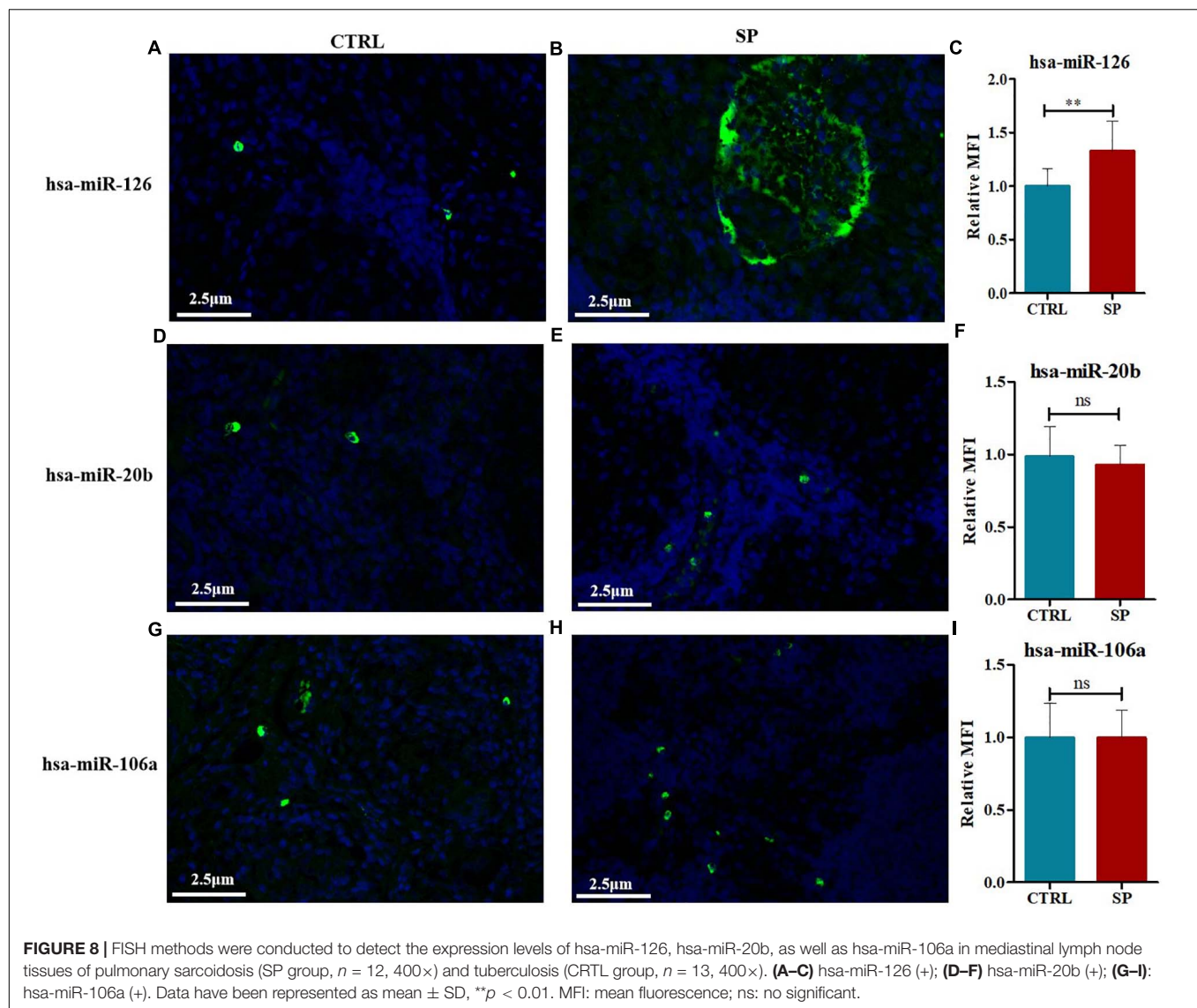
**FIGURE 7 |** Immunohistochemical methods were employed to assess the cellular localization and expression levels of NR3C1 and VEGFA in mediastinal lymph node tissues of pulmonary sarcoidosis (SP group,  $n = 12$ ) and tuberculosis (CTRL group,  $n = 13$ ). **(A–D)** VEGFA (+); **(E–H)** NR3C1 (+). (10 $\times$ : ACEG; 40 $\times$ : BDFH).

question from clinic and return to clinic through this research. Pulmonary sarcoidosis and tuberculosis are the most difficult to distinguish in clinical practice. Even if they have the gold standard of pathological diagnosis, it still needs experienced pathologists to give a definite diagnosis. Sometimes, for the small tissue, it can interfere with the definitive diagnosis of sarcoidosis. At the same time, the treatments for these two diseases are completely opposite. For treatment of sarcoidosis requires glucocorticoids, but the use of glucocorticoids for tuberculosis often causes the spread of disease. More significantly, the mediastinal lymph node of healthy people is not enlarged, and it is not available

or difficult to obtain, which also violates ethical principles. Therefore, we used lymphatic tissue of tuberculosis as control group in this study.

There are still several limitations in this study. First of all, in the section of clinical specimen verification, the sample size we included is still small. Although immunohistochemistry and FISH have obtained positive results, a large sample study is still needed to further corroborate our results. Secondly, the specific regulatory mechanism of miR-126 in the pathogenesis and development of sarcoidosis still needs to be explored *in vitro* and *in vivo*. Finally, the incidence of sarcoidosis in different races is slightly different. In this study,





we only included Asian individuals. This may bring certain limitations to our results.

From our results, we found that VEGFA and NR3C1 were overexpressed in the pathological tissue of sarcoidosis, which was mainly regulated by hsa-miR-126. To our knowledge, miRNAs are small non-coding RNAs that function as negative gene expression regulators. However, emerging evidences have shown that its function was switching from repression to activation, and its gene-activation function can up-regulate translation in nuclear (Vasudevan et al., 2007; Xiao et al., 2017). The GO annotation of our study comprised the molecular function on current biological knowledge of miRNA in sarcoidosis, which showed nucleic acid binding transcription factor activity has a pronounced gene count. This novel finding was also worth exploring for the study of the role of miRNAs in the regulation of sarcoidosis.

In summary, this work sheds further light on understanding the pathogenesis of sarcoidosis and might indicate novel diagnostic markers and treatment targets in the clinical practice

of sarcoidosis. Nevertheless, further studies should be conducted to clarify the role of miRNAs and their related pathways in the pathogenesis of sarcoidosis.

## DATA AVAILABILITY STATEMENT

The original contributions presented in the study are included in the article/Supplementary Material, further inquiries can be directed to the corresponding author/s.

## ETHICS STATEMENT

The studies involving human participants were reviewed and approved by Biomedical Ethics Committee of Second Affiliated Hospital of Xi'an Jiaotong University. The patients/participants provided their written informed consent to participate in this study.



## AUTHOR CONTRIBUTIONS

YC, HZ, and QL performed the experiments, contributed to data analyses, as well as wrote the manuscript. YC, HZ, and LZ conceptualized the study design, contributed equally to data analyses and experimental materials. All authors contributed to the article and approved the submitted version.

## FUNDING

This work was funded by Fundamental Research Funds for the Central Universities under Grant xzy012019129, Natural

Science Basic Research Plan in Shaanxi Province of China (ProgramNo.2020JQ-543 and 2020JQ-927).

## SUPPLEMENTARY MATERIAL

The Supplementary Material for this article can be found online at: <https://www.frontiersin.org/articles/10.3389/fmolb.2021.644232/full#supplementary-material>

**Supplementary Figure 1** | miRNA-gene network of upregulated miRNAs (before simplified).

**Supplementary Figure 2** | miRNA-gene network of downregulated miRNAs (before simplified).

## REFERENCES

- Aryal, S., and Nathan, S. D. (2019). Contemporary optimized practice in the management of pulmonary sarcoidosis. *Ther. Adv. Respir. Dis.* 13:1753466619868935. doi: 10.1177/1753466619868935
- Barna, B. P., Mcpeek, M., Malur, A., Fessler, M. B., Wingard, C. J., Dobbs, L., et al. (2016). Elevated MicroRNA-33 in sarcoidosis and a carbon nanotube model of chronic granulomatous disease. *Am. J. Respir. Cell Mol. Biol.* 54, 865–871. doi: 10.1165/rcmb.2015-0332OC
- Costabel, U., and Hunninghake, G. W. (1999). ATS/ERS/WASOG statement on sarcoidosis. sarcoidosis statement committee. american thoracic society. European respiratory society. world association for sarcoidosis and other granulomatous disorders. *Eur. Respir. J.* 14, 735–737. doi: 10.1034/j.1399-3003.1999.14d02.x
- Cuzzoni, E., De Iudicibus, S., Bartoli, F., Ventura, A., and Decorti, G. (2012). Association between BclI polymorphism in the NR3C1 gene and in vitro individual variations in lymphocyte responses to methylprednisolone. *Br. J. Clin. Pharmacol.* 73, 651–655. PMID:NOPMIDdoi: 10.1111/j.1365-2125.2011.04130.x
- Damian, S., Andrea, F., Stefan, W., Kristoffer, F., Davide, H., Jaime, H. C., et al. (2015). STRING v10: protein-protein interaction networks, integrated over the tree of life. *J. Nucleic Acids Res.* 43:D447.
- El Jammal, T., Pavic, M., Gerfaud-Valentin, M., Jamilloux, Y., and Sève, P. (2020). Sarcoidosis and cancer: a complex relationship. *Front. Med.* 7:594118. doi: 10.3389/fmed.2020.594118
- Ghahesouran, J., Taheri, M., Sayad, A., Ghafouri-Fard, S., Mazdeh, M., and Omrani, M. D. (2018). The growth arrest-specific transcript 5 (GAS5) and nuclear receptor subfamily 3 group C member 1 (NR3C1): novel markers involved in multiple sclerosis. *Int. J. Mol. Cell Med.* 7, 102–110. doi: 10.22088/ijmcm.Bums.7.2.102
- Iannuzzi, M. C., Rybicki, B. A., and Teirstein, A. S. (2007). Sarcoidosis. *N. Engl. J. Med.* 357, 2153–2165. doi: 10.1056/NEJMra071714
- Jain, R., Yadav, D., Puranik, N., Guleria, R., and Jin, J.-O. (2020). Sarcoidosis: causes, diagnosis, clinical features, and treatments. *J. Clin. Med.* 9:1081. doi: 10.3390/jcm9041081
- Jazwa, A., Kasper, L., Bak, M., Sobczak, M., Szade, K., Jozkowicz, A., et al. (2015). Differential inflammatory microRNA and cytokine expression in pulmonary sarcoidosis. *Arch. Immunol. Ther. Exp.* 63, 139–146. doi: 10.1007/s00005-014-0315-9
- Kachamakova-Trojanowska, N., Jazwa-Kusior, A., Szade, K., Kasper, L., Soja, J., Andrychiewicz, A., et al. (2018). Molecular profiling of regulatory T cells in pulmonary sarcoidosis. *J. Autoimmun.* 94, 56–69. doi: 10.1016/j.jaut.2018.07.012
- Keskin, O., Farzan, N., Birben, E., Akel, H., Karaaslan, C., Maitland-Van Der Zee, A. H., et al. (2019). Genetic associations of the response to inhaled corticosteroids in asthma: a systematic review. *Clin. Transl. Allergy* 9:2. doi: 10.1186/s13601-018-0239-2
- Kiszkiewicz, J., Piotrowski, W. J., Pastuszak-Lewandoska, D., Górski, P., Antczak, A., Górski, W., et al. (2016). Altered miRNA expression in pulmonary sarcoidosis. *BMC Med. Genet.* 17:2. doi: 10.1186/s12881-016-0266-6
- Mirsaeidi, M., Omar, H. R., Calzadilla, A., Khatib, A. E., Whitney, P., Sweiss, N., et al. (2018). Circulatory TGF-beta1 is significantly higher in early stage of pulmonary sarcoidosis. *Sarcoidosis Vasculitis Diffuse Lung Dis.* 35, 213–217. doi: 10.36141/svdl.v35i3.6112
- Momose, M., Fukushima, K., Kondo, C., Serizawa, N., Suzuki, A., Abe, K., et al. (2015). Diagnosis and detection of myocardial injury in active cardiac sarcoidosis—significance of myocardial fatty acid metabolism and myocardial perfusion mismatch. *Circ. J.* 79, 2669–2676. doi: 10.1253/circj.CJ-15-0681
- Pattnaik, B., Sryma, P. B., Mittal, S., Agrawal, A., Guleria, R., and Madan, K. (2020). MicroRNAs in pulmonary sarcoidosis: a systematic review. *Respir. Investig.* 58, 232–238. doi: 10.1016/j.resinv.2020.02.008
- Piotrowski, W. J., Kiszkiewicz, J., Górski, P., Antczak, A., Górski, W., Pastuszak-Lewandoska, D., et al. (2015). Immunoeexpression of TGF-β/Smad and VEGF-A proteins in serum and BAL fluid of sarcoidosis patients. *BMC Immunol.* 16:58. doi: 10.1186/s12865-015-0123-y
- Tamura, R., Tanaka, T., Akasaki, Y., Murayama, Y., Yoshida, K., and Sasaki, H. (2019). The role of vascular endothelial growth factor in the hypoxic and immunosuppressive tumor microenvironment: perspectives for therapeutic implications. *Med. Oncol.* 37:2. doi: 10.1007/s12032-019-1329-2
- Tzouveleakis, A., Ntoliou, P., Karameris, A., Koutsopoulos, A., Boglou, P., Koulelidis, A., et al. (2012). Expression of hypoxia-inducible factor (HIF)-1α-vascular endothelial growth factor (VEGF)-inhibitory growth factor (ING)-4- axis in sarcoidosis patients. *BMC Res. Notes* 5:654. doi: 10.1186/1756-0500-5-654
- Ungrasert, P., Ryu, J. H., and Matteson, E. L. (2019). Clinical manifestations, diagnosis, and treatment of sarcoidosis. *Mayo Clin. Proc. Innov. Qual. Outcomes* 3, 358–375. doi: 10.1016/j.mayocpiqo.2019.04.006
- Vasudevan, S., Tong, Y., and Steitz, J. A. (2007). Switching from repression to activation: microRNAs can up-regulate translation. *Science* 318, 1931–1934. doi: 10.1126/science.1149460
- Vlachos, I. S., Zagganas, K., Paraskevopoulou, M. D., Georgakilas, G., Karagkouni, D., Vergoulis, T., et al. (2015). DIANA-miRPath v3.0: deciphering microRNA function with experimental support. *Nucleic Acids Res.* 43, W460–W466. doi: 10.1093/nar/gkv403
- Xiao, M., Li, J., Li, W., Wang, Y., Wu, F., Xi, Y., et al. (2017). MicroRNAs activate gene transcription epigenetically as an enhancer trigger. *RNA Biol.* 14, 1326–1334. doi: 10.1080/15476286.2015.1112487
- Zhang, Y., Zhang, M., Zhong, M., Suo, Q., and Lv, K. (2013). Expression profiles of miRNAs in polarized macrophages. *Int. J. Mol. Med.* 31, 797–802. doi: 10.3892/ijmm.2013.1260

**Conflict of Interest:** The authors declare that the research was conducted in the absence of any commercial or financial relationships that could be construed as a potential conflict of interest.

Copyright © 2021 Cao, Zhang, Zheng and Li. This is an open-access article distributed under the terms of the Creative Commons Attribution License (CC BY). The use, distribution or reproduction in other forums is permitted, provided the original author(s) and the copyright owner(s) are credited and that the original publication in this journal is cited, in accordance with accepted academic practice. No use, distribution or reproduction is permitted which does not comply with these terms.



# Comparison of Immediate and Sequential Withdrawal of a Systemic Glucocorticoid in the Treatment of Acute Exacerbations of Chronic Obstructive Pulmonary Disease: A Multicenter, Randomized, Double-Blind, Parallel-Controlled, Open-Label Study

## OPEN ACCESS

### Edited by:

Wen Li,  
Zhejiang University, China

### Reviewed by:

Rakesh Pathak,  
National Institutes of Health Clinical  
Center (NIH), United States  
Xiaodong Wu,  
Tongji University, China

### \*Correspondence:

Huiguo Liu  
huiguol@163.com

### Specialty section:

This article was submitted to  
Molecular Diagnostics  
and Therapeutics,  
a section of the journal  
Frontiers in Molecular Biosciences

**Received:** 08 December 2020

**Accepted:** 07 April 2021

**Published:** 20 May 2021

### Citation:

Zhou L, Fang Y, Liu W, Zhang J,  
Wang Y, Xie S, Zhong M, Wang Z,  
Li G, Ai H, Guo H, Zeng F, Xiao W,  
Li C, Hu Y, Tang Y and Liu H (2021)  
Comparison of Immediate  
and Sequential Withdrawal of a  
Systemic Glucocorticoid  
in the Treatment of Acute  
Exacerbations of Chronic Obstructive  
Pulmonary Disease: A Multicenter,  
Randomized, Double-Blind,  
Parallel-Controlled, Open-Label  
Study. *Front. Mol. Biosci.* 8:639079.  
doi: 10.3389/fmolb.2021.639079

Ling Zhou<sup>1</sup>, Yuanyuan Fang<sup>1</sup>, Wei Liu<sup>2</sup>, Jianchu Zhang<sup>3</sup>, Yingnan Wang<sup>4</sup>, Sheng Xie<sup>5</sup>,  
Minhua Zhong<sup>6</sup>, Zhengyan Wang<sup>7</sup>, Guangcai Li<sup>8</sup>, Hongyan Ai<sup>9</sup>, Hongrong Guo<sup>10</sup>,  
Fanjun Zeng<sup>11</sup>, Wei Xiao<sup>12</sup>, Chenghong Li<sup>13</sup>, Yi Hu<sup>14</sup>, Yijun Tang<sup>15</sup> and Huiguo Liu<sup>1\*</sup>

<sup>1</sup> Department of Respiratory and Critical Care Medicine, Tongji Hospital, Tongji Medical College, Huazhong University of Science and Technology, Wuhan, China, <sup>2</sup> Department of Respiratory and Critical Care Medicine, Renmin Hospital of Wuhan University, Wuhan, China, <sup>3</sup> Department of Respiratory and Critical Care Medicine, Union Hospital, Tongji Medical College, Huazhong University of Science and Technology, Wuhan, China, <sup>4</sup> Department of Respiratory and Critical Care Medicine, The People's Hospital of China Three Gorges University, The First People's Hospital of Yichang, Yichang, China, <sup>5</sup> Department of Respiratory and Critical Care Medicine, Huangshi Central Hospital, Affiliated Hospital of Hubei Polytechnic University, Huangshi, China, <sup>6</sup> Department of Respiratory and Critical Care Medicine, Xiaogan Hospital Affiliated to Wuhan University of Science and Technology, The Central Hospital of Xiaogan, Xiaogan, China, <sup>7</sup> Department of Respiratory Medicine, Suizhou Hospital, Hubei University of Medicine, Suizhou, China, <sup>8</sup> Department of Respiratory and Critical Care Medicine, The Central Hospital of Enshi Tujia and Miao Autonomous Prefecture, Enshi Clinical College of Wuhan University, Enshi Tujia and Miao Autonomous Prefecture, Hubei, China, <sup>9</sup> Department of Respiratory and Critical Care Medicine, Hanyang Hospital Affiliated to Wuhan University of Science and Technology, Wuhan, China, <sup>10</sup> Department of Respiratory and Critical Care Medicine, Wuhan Third Hospital, Tongren Hospital of Wuhan University, Wuhan, China, <sup>11</sup> Department of Respiratory and Critical Care Medicine, The First College of Clinical Medicine Science, China Three Gorges University, Yichang Central People's Hospital, Yichang, China, <sup>12</sup> Department of Respiratory and Critical Care Medicine, The First People's Hospital of Jingzhou, Jingzhou, China, <sup>13</sup> Department of Respiratory and Critical Care Medicine, The Sixth Hospital of Wuhan, Jiangnan University, Wuhan, China, <sup>14</sup> Department of Respiratory and Critical Care Medicine, The Central Hospital of Wuhan, Tongji Medical College, Huazhong University of Science and Technology, Wuhan, China, <sup>15</sup> Department of Respiratory and Critical Medical, Taihe Hospital, Affiliated Hospital of Hubei University of Medicine, Shiyan, China

Patients with acute exacerbations of chronic obstructive pulmonary disease (AECOPD) were treated with immediate or sequential withdrawal after 5 days of systemic glucocorticoids. The effects of the two withdrawal methods on the prognosis of patients were compared at 30, 90, 180, and 360 days after discharge. A multicenter, randomized, double-blind, parallel-controlled, open-label study was conducted in the respiratory department of tertiary hospitals in Central China. Patients met inclusion criteria for AECOPD and needed to use systemic glucocorticoids. They were randomly assigned to immediate and sequential withdrawal groups at a 1:1 ratio. The study was completed in August 2020 and is registered at the China Clinical Trials Registry (ChiCTR.org) (ChiCTR1800018894). According to general data and clinical characteristics, there were no statistically significant differences between the 329 patients in the

immediate withdrawal group and the 310 patients in the sequential withdrawal group ( $P > 0.05$ ). At the 30, 90, 180, and 360-days follow-up, the acute exacerbation frequency, rehospitalization rate, mortality, and intensive care unit (ICU) treatment rate were not significantly different between the immediate withdrawal group and sequential withdrawal group ( $P > 0.05$ ). The modified Medical Research Council (mMRC) and COPD assessment test (CAT) scores were also not significantly different between the two groups. At the 180- and 360-day follow-up, forced expiratory volume in 1 s (FEV1%) and peak expiratory flow (PEF) were not significantly different between the two groups ( $P > 0.05$ ). The time from discharge to first acute exacerbation was significantly lower in the immediate withdrawal group (46.12 days) than in sequential withdrawal group (49.02 days) ( $P < 0.05$ ). The time of stay in the hospital for the first time after discharge was not significantly different between the two groups ( $P > 0.05$ ). Adverse events were not significantly different between the immediate withdrawal group and sequential withdrawal group ( $P < 0.05$ ). Subgroup analysis was performed according to age, degree of disease, and relevant indicators. At the 30-day follow-up, the acute exacerbation frequency of patients with advanced age, high global strategy for chronic obstructive lung disease (GOLD), and high fractional exhaled nitric oxide was significantly higher in the immediate withdrawal group than in the sequential withdrawal group ( $P < 0.05$ ). In addition, according to receiver operating characteristic (ROC) curve analysis, the frequency of acute exacerbations at the 30-day follow-up was significantly higher in patients with age  $> 63.5$  years or GOLD  $> 3$  in the immediate withdrawal group than in the sequential withdrawal group, suggesting that the short-term efficacy was poor.

**Keywords:** glucocorticoids, immediately withdrawal, sequential withdrawal, acute exacerbations of chronic obstructive pulmonary disease, prognosis, methyl prednolone, Central China

## INTRODUCTION

Chronic obstructive pulmonary disease (COPD) is a chronic, non-specific disease in which inflammation of the airways activates inflammatory epithelial and smooth muscle cells and the release of inflammatory mediators (Doumas et al., 2020). Considering its high rates of morbidity and disability, COPD can pose a serious threat to human health (Rabe et al., 2020). Acute exacerbations of chronic obstructive pulmonary disease (AECOPD) occur when COPD patients show rapid changes within a short period (Vermeersch et al., 2019), with obvious aggravation of clinical symptoms such as cough, sputum production, dyspnea, and shortness of breath. In the absence of timely treatment, the life of the patient may be in jeopardy (Berenyi et al., 2020).

The Global Strategy for Chronic Obstructive Lung Disease (GOLD) guide indicates that glucocorticoids can shorten recovery time and improve lung function and hypoxia during acute exacerbations, in addition to reducing the risk of recurrence and disease progression (Burns et al., 2020). However, the long-term use of glucocorticoids causes a variety of adverse events, such as hyperglycemia, necrosis of the femoral head, reduction in immunity, and increased risk of infection (Lucafo et al., 2020). The GOLD guide recommends methyl prednisone at 40 mg/d for 5 days in cases of AECOPD (Leuppi et al., 2013).

The United Kingdom National Institute for Health and Care Excellence (NICE) recommended that COPD be treated with systemic glucocorticoids for 7–14 days (National Collaborating Centre for Chronic, 2004). The Australian and New Zealand guidelines for the diagnosis and treatment of COPD recommend an optimal course of systemic glucocorticoids for 10–14 days (McKenzie et al., 2003). Thus, there is still no consensus on the treatment time and dose of systemic glucocorticoids in the treatment of AECOPD. In this study, a randomized controlled trial was used to compare the short-term efficacy and long-term prognosis of immediate and sequential withdrawal of methyl prednisone treatment of AECOPD.

## MATERIALS AND METHODS

### Study Design and Subjects

A multicenter, randomized, double-blind, parallel-controlled study was conducted in tertiary hospitals in Central China to compare the effects of systemic glucocorticoid immediate or sequential withdrawal on the prognosis of AECOPD patients at 30, 90, 180, and 360 days after discharge. Patients admitted from July 2017 to August 2019 were randomly assigned to the immediate and sequential withdrawal groups at a 1:1 ratio. Patients in the immediate withdrawal group received intravenous

injections of methyl prednone at 40 mg/d for five consecutive days, then withdrawal on day six. Patients in the sequential withdrawal group received the same 5-day treatment, but the dose was reduced to 30 mg/d on days six and seven, to 20 mg/d on days eight and nine, and then stopped completely on day 10. The immediate group received the same amount of saline injection as the sequential withdrawal group from 6 to 10 days. To evaluate the efficacy and prognosis of the two treatment regimens, patient follow-ups were conducted for 1 year from the discharge date. The competent authorities of participating hospitals and the Medical Ethics Committee of Tongji Medical College of Huazhong University of Science and Technology approved the study (2018-S301). The study is registered at the China Clinical Trials Registry (ChiCTR.org) (ChiCTR1800018894).

All patients agreed to participate in the study and signed the informed consent. The inclusion criteria were as follows: (1) age between 40 years and 70 years; (2) diagnosis of AECOPD: sudden changes in clinical symptoms, including dyspnea, cough, and expectoration of sputum; (3) COPD beyond the range of daily variation; (4) pulmonary function examination indicating that forced expiratory volume in 1 s (FEV1%) < 0.70 after previous use of a bronchodilator. Patients suffering from the following diseases or lesions were excluded: (1) those critically ill patients with assisted respiratory muscle involvement in respiratory movement, thoracic and abdominal contradictory breathing, cyanosis, or need for invasive mechanical ventilation; (2) those with edema, right heart failure, or hemodynamic instability; (3) those with changes in mental state; (4) those with malignant tumors or other serious diseases.

## Randomization, Double Blindness, and Follow-ups

The study leader LHG placed the subjects in order of inclusion in either the sequential withdrawal or the immediate withdrawal group. The study leader did not participate in subject recruitment and kept the randomization form confidential. Since the subjects signed the consent form, the researchers and the subjects were informed of the grouping.

Baseline measurements were taken on the day of recruitment, and clinical symptoms were assessed daily during hospitalization (cough assessment score, sputum viscosity, sputum volume, mMRC score). Discharge decisions were made by the attending physician. Clinical symptoms, mMRC score, and CAT score were assessed on days 30, 90, 180, and 360 after discharge, with the frequency of acute exacerbations from the last follow-up recorded. Pulmonary function (FEV1%, PEF) was measured on days 180 and 360 after discharge. There was a focus on adverse events (hypertension, kidney injury, electrolyte disturbance, infection, edema, plasma glucose, and osteoporosis) during and after therapy.

## Endpoints

The primary endpoint was the frequency of acute exacerbations at 30, 90, 180, and 360 days after discharge. The key secondary endpoint was mortality. Other secondary endpoints were the

mMRC score, CAT score, rehospitalization rate, and ICU treatment rate at 30, 90, 180, and 360 days after discharge and FEV1% and PEF at 180 and 360 days after discharge.

## Statistical Analyses

Categorical variables were presented as numbers (percentages) and analyzed using a chi-squared test or Fisher's exact test. Continuous variables with a normal distribution were expressed as the mean  $\pm$  standard deviation and analyzed using the independent samples *t*-test, whereas those with a skewed distribution were shown as the median (Q<sub>1</sub>, Q<sub>3</sub>) and analyzed using the Mann-Whitney U test. COX regression analyses were adopted to identify risk factors of prognosis. Receiver operating characteristic (ROC) curves were used to calculate the area under the curve (AUC) of a single continuous variable and the cutoff value. The SPSS software v 25.0 (SPSS Inc., Chicago, IL, United States) was used for statistical analyses. Differences at *P* < 0.05 (two-sided) were considered statistically significant.

## RESULTS

### General Data and Clinical Characteristics

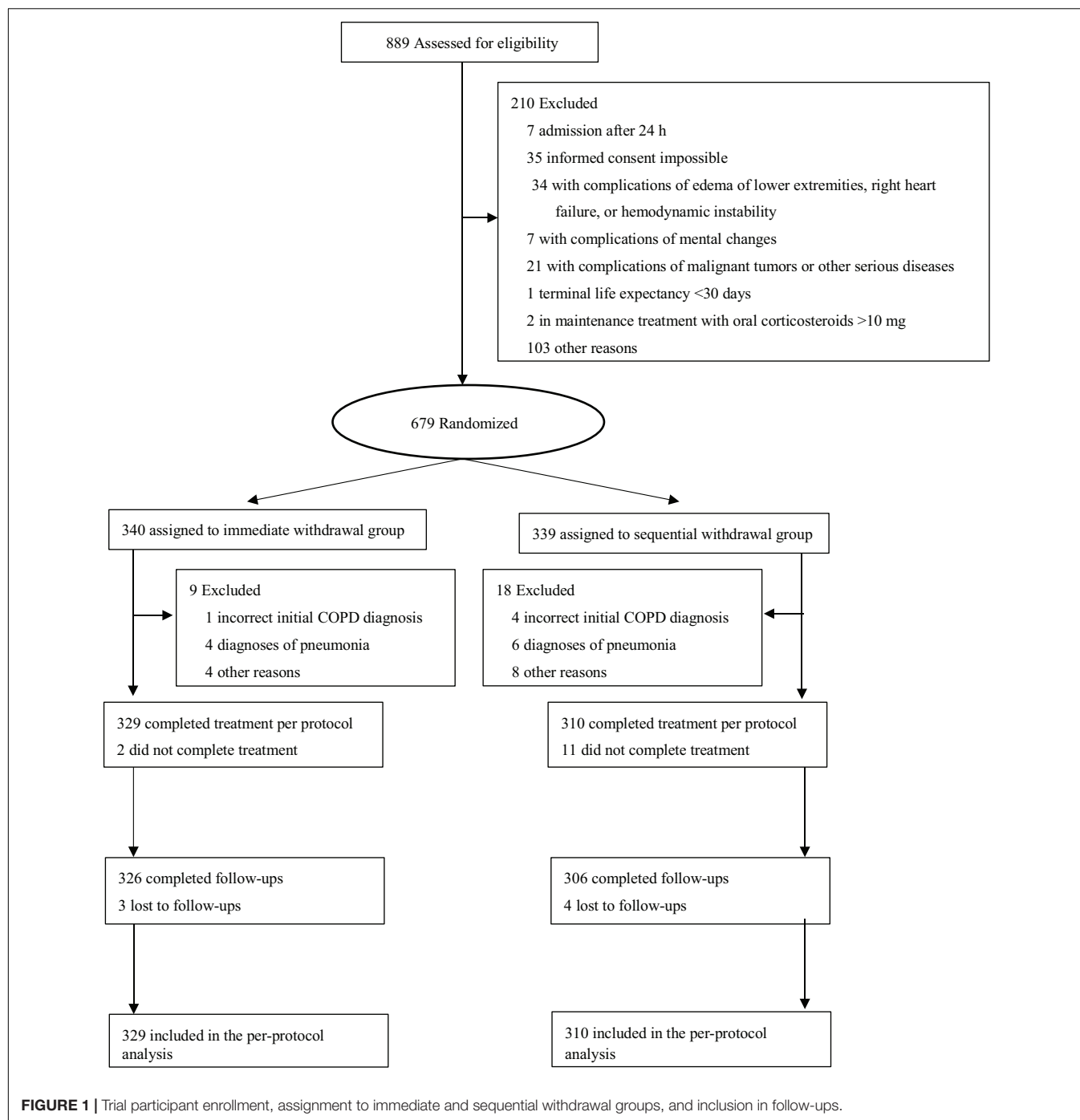
Trial participant assignment to immediate and sequential withdrawal groups, and inclusion in follow-ups are shown in **Figure 1**. There were 639 COPD patients, including 349 males and 290 females. The average age was 61.02 years, and the average body mass index was 26.03. There were 230 patients that had smoked in the past and 62 patients that were smoking at the time of the study, with 14.93 years being the average time of smoking. Forty-nine cases had COPD exacerbations more than three times in the previous year. Fifteen cases had a history of exposure to biofuels. Among these indicators, there were no statistically significant differences between the immediate and sequential withdrawal group (*P* > 0.05). In addition, the Charlson comorbidity index, admission characteristics, pulmonary function indicators, GOLD grade, mMRC score, CAT score, laboratory indicators, and use of home oxygen therapy were not significantly different between the two groups (*P* > 0.05). We focus on hypertension, kidney injury, electrolyte disturbance, infection, edema, plasma glucose, and osteoporosis in this study, but there were no statistically significant differences between the immediate withdrawal group and sequential withdrawal group (*P* > 0.05, **Table 1**).

### Endpoints

The primary endpoint was the frequency of acute exacerbations in the follow-ups at 30, 90, 180, and 360 days after discharge. The frequency of acute exacerbations was not significantly different between immediate and sequential withdrawal groups at 30, 90, 180, and 360 days after discharge (*P* > 0.05, **Figure 2**).

The key secondary endpoint was mortality. Mortality was not significantly different between immediate and sequential withdrawal groups at 30, 90, 180, and 360 days (*P* > 0.05). The other secondary endpoints were mMRC score, CAT score, admission rate, and ICU treatment rate at 30, 90, 180, and 360 days after discharge and FEV1% and PEF at 180 and 360 days





after discharge. There were no statistically significant differences in these indicators between the two groups ( $P > 0.05$ ). The time from discharge to first acute exacerbation was significantly lower in the immediate withdrawal group (46.12 days) than in the sequential withdrawal group (49.02 days) ( $P < 0.05$ ). The time of stay in the hospital for the first time after discharge was longer in the immediate withdrawal group (6.28 days) than in the sequential withdrawal group (6.17 days), but the difference was not statistically significant ( $P > 0.05$ , **Table 2**).

## Subgroup Analysis

### Subgroup Analysis at the 30-day Follow-Up

Prognostic evaluation was defined according to acute exacerbation frequency in the follow-up at 30 days after discharge. Subgroup analysis was performed according to the history of frequent acute exacerbations, C-reactive protein (CRP), eosinophils, fractional exhaled nitric oxide (FeNO), GOLD grade, and age (**Figure 3**). In patients with either frequent or infrequent acute exacerbation history, high CRP or low CRP,

**TABLE 1 |** Baseline characteristics of the intention-to-treat population.

Items	Total (n = 639)	Immediate withdrawal (n = 329)	Sequential withdrawal (n = 310)	Statistic	P
Age (y)	61.02 ± 0.19	61.19 ± 0.28	60.87 ± 0.27	0.802*	0.423
<b>Sex</b>					
Male	349 (54.6)	177 (53.8)	172 (55.5)	0.183 <sup>†</sup>	0.669
Female	290 (45.4)	152 (46.2)	138 (44.5)		
BMI	26.30 ± 0.18	26.00 ± 0.26	26.61 ± 0.27	1.597*	0.111
<b>Smokers</b>					
Never	347 (54.3)	178 (54.1)	169 (54.5)	0.779 <sup>†</sup>	0.677
Past	230 (36.0)	122 (37.1)	108 (34.8)		
Current	62 (9.7)	29 (8.8)	33 (10.7)		
Pack-years smoked (y)	14.93 ± 0.48	14.85 ± 0.70	15.01 ± 0.65	0.167*	0.868
Course of COPD (y)	3.38 ± 0.06	3.38 ± 0.08	3.36 ± 0.09	0.217*	0.829
Number of AECOPD in previous year				2.837 <sup>†</sup>	0.586
0	45 (7.0)	24 (7.3)	21 (6.8)		
1	74 (11.6)	41 (12.5)	33 (10.6)		
2	292 (45.7)	156 (47.4)	136 (43.9)		
3	179 (28.0)	83 (25.2)	96 (31.0)		
> 3	49 (7.7)	25 (7.6)	24 (7.7)		
History of biofuel use	15 (2.3)	6 (1.8)	9 (2.9)	0.811 <sup>†</sup>	0.368
Charlson comorbidity index	2.86 ± 0.03	2.87 ± 0.04	2.86 ± 0.05	0.834*	0.834
<b>Admission presentation</b>					
Cough symptom score	2.05 ± 0.04	2.09 ± 0.05	2.01 ± 0.04	1.207*	0.228
Sputum viscosity	1.98 ± 0.03	2.02 ± 0.06	1.92 ± 0.05	1.393*	0.164
Sputum volume	1.66 ± 0.02	1.62 ± 0.03	1.70 ± 0.04	1.195*	0.232
Pulmonary function					
FEV1%	60.34 ± 0.27	59.99 ± 0.40	60.71 ± 0.35	1.360*	0.174
PEF	7.76 ± 0.08	7.62 ± 0.11	7.91 ± 0.10	1.852*	0.065
GOLD				7.273 <sup>†</sup>	0.064
GOLD1	30 (4.6)	14 (4.3)	16 (5.2)		
GOLD2	229 (35.9)	105 (31.9)	124 (40.0)		
GOLD3	275 (43.0)	158 (48.0)	117 (37.7)		
GOLD4	105 (16.5)	52 (15.8)	53 (17.1)		
mMRC score	1.99 ± 0.03	1.96 ± 0.04	2.03 ± 0.05	0.997*	0.319
CAT score	18.21 ± 0.29	18.11 ± 1.15	17.18 ± 0.46	0.814*	0.416
<b>Laboratory</b>					
Leucocytes (10 <sup>9</sup> /L)	6.83 ± 0.11	6.66 ± 0.16	7.02 ± 0.14	1.687*	0.092
Eosinophils (10 <sup>9</sup> /L)	0.55 ± 0.05	0.55 ± 0.03	0.56 ± 0.11	0.129*	0.897
C-reactive protein (mg/L)	2.50 ± 0.16	2.22 ± 0.18	2.69 ± 0.24	1.475*	0.141
FeNO	29.62 ± 0.71	31.05 ± 1.08	28.10 ± 0.91	0.454*	0.224
PaCO <sub>2</sub> (kPa)	40.32 ± 0.31	39.91 ± 0.401	40.92 ± 0.50	1.589*	0.114
PaO <sub>2</sub> (kPa)	66.82 ± 1.35	67.11 ± 1.95	66.38 ± 1.73	0.265*	0.791
Home oxygen therapy	76 (11.9)	34 (10.3)	42 (13.5)	1.573*	0.209
<b>Clinical findings</b>					
Diastolic blood pressure (mm Hg)	79 ± 0.36	78 ± 0.56	80 ± 0.44	1.273*	0.204
Systolic blood pressure (mm Hg)	116 ± 0.32	116 ± 0.42	117 ± 0.49	1.168*	0.243
Heart rate (beats/min)	92 ± 0.47	91 ± 0.67	92 ± 0.46	0.659*	0.510
Oxygen saturation (%)	94 ± 0.24	94 ± 0.39	95 ± 0.27	1.931*	0.054
Respiratory rate (breaths/min)	21 ± 0.71	21 ± 0.34	20 ± 0.35	0.863*	0.389
<b>Adverse events</b>					
Hypertension	0	0	0	—	—
Electrolyte disturbance	3 (0.5)	2 (0.6)	1 (0.3)	0.278 <sup>†</sup>	0.598
Kidney injury	0	0	0	—	—

(Continued)

TABLE 1 | Continued

Items	Total (n = 639)	Immediate withdrawal (n = 329)	Sequential withdrawal (n = 310)	Statistic	P
Infection	0	0	0	–	–
Edema	4 (0.6)	1 (0.3)	3 (1.0)	1.131 <sup>†</sup>	0.287
Elevated plasma glucose	6 (0.9)	2 (0.6)	4 (1.3)	0.667 <sup>†</sup>	0.414
Osteoporosis	0	0	0	–	–

Data are shown as the mean  $\pm$  standard deviation or n (%). \*t-test; <sup>†</sup> $\chi^2$ -value. BMI, Body Mass Index; COPD, chronic obstructive pulmonary disease; AECOPD, acute exacerbation of chronic obstructive pulmonary disease; FEV1, forced expiratory volume in 1 s; PEF, peak expiratory flow; GOLD, global initiative for chronic obstructive lung disease; mMRC, Modified Medical Research Council Dyspnea Scale; CAT, COPD Assessment Test; FeNO, Fractional exhaled nitric oxide; PaO<sub>2</sub>, partial pressure of oxygen; PaCO<sub>2</sub>, partial pressure of carbon dioxide. Degree of sputum viscosity: (1), sputum clings to the wall of phlegm cup during rotation; (2), sputum slides slowly along the wall of phlegm cup during rotation; (3), sputum can be poured out quickly but some remains attached to the wall of phlegm cup; (4), sputum can be poured out quickly and completely. Sputum volume: 1, mild, with less than 10 mL/day; 2, moderate, with 10–150 mL/day; 3, severe, with more than 150 mL/day.

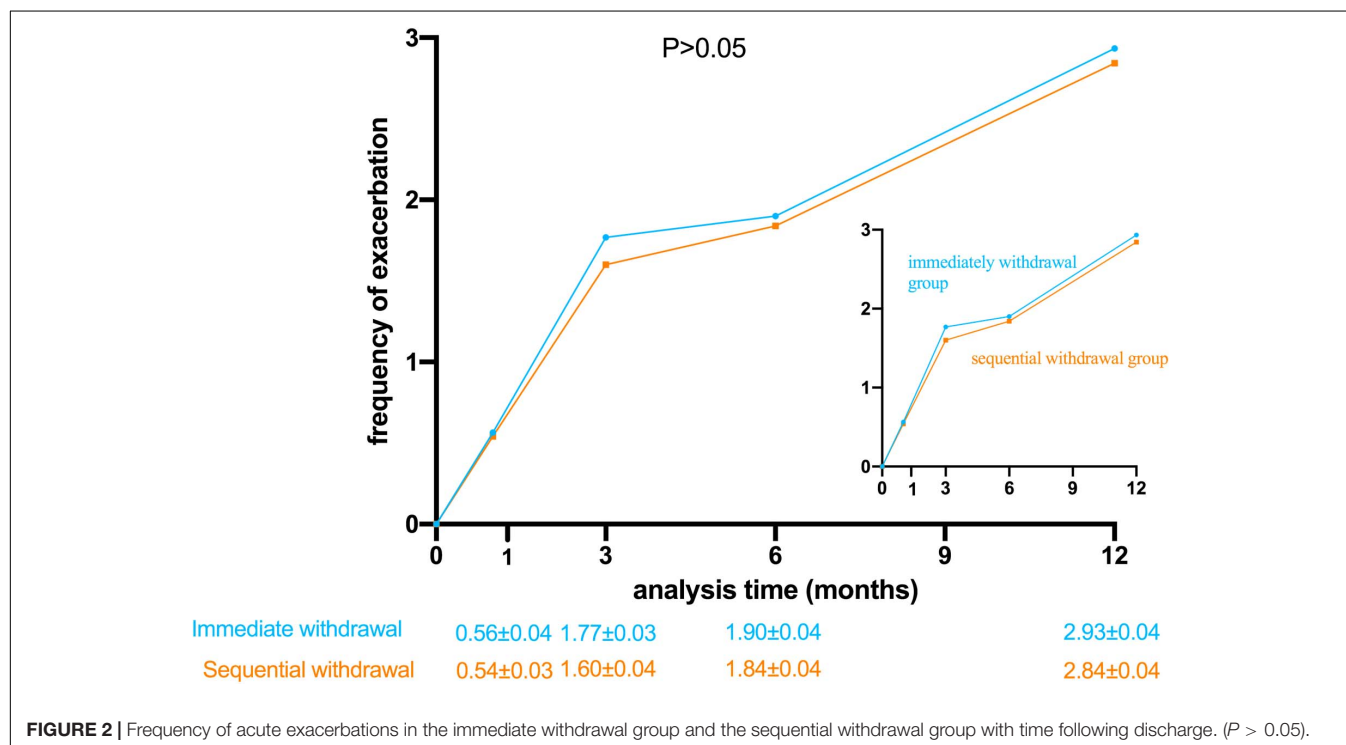


FIGURE 2 | Frequency of acute exacerbations in the immediate withdrawal group and the sequential withdrawal group with time following discharge. ( $P > 0.05$ ).

high eosinophils or low eosinophils, there was no statistically significant difference in acute exacerbation frequency between immediate and sequential withdrawal groups at the 30-day follow-up ( $P > 0.05$ ). Although the acute exacerbation frequency of patients with high FeNO showed no statistically significant difference between the two groups ( $P > 0.05$ ), in patients with low FeNO, the difference was significant between immediate and sequential withdrawal groups ( $P < 0.05$ ). Although the acute exacerbation frequency of patients with a low GOLD grade was not different between the two withdrawal groups, in patients with a high GOLD grade, the difference was significant between immediate and sequential withdrawal groups at the 30-day follow-up ( $P < 0.05$ ). The acute exacerbation frequency in patients with age  $\leq 59$  years showed no statistically significant difference between the immediate and sequential withdrawal groups ( $P > 0.05$ ). However, in patients with age  $> 59$  years, the difference between withdrawal methods was significant ( $P < 0.05$ ). Thus, the results of the 30-day follow-up show acute

exacerbation frequency in patients with advanced age, high GOLD grade, and low FeNO, and was significantly higher in the immediate withdrawal group than in the sequential withdrawal group ( $P < 0.05$ , Figure 3).

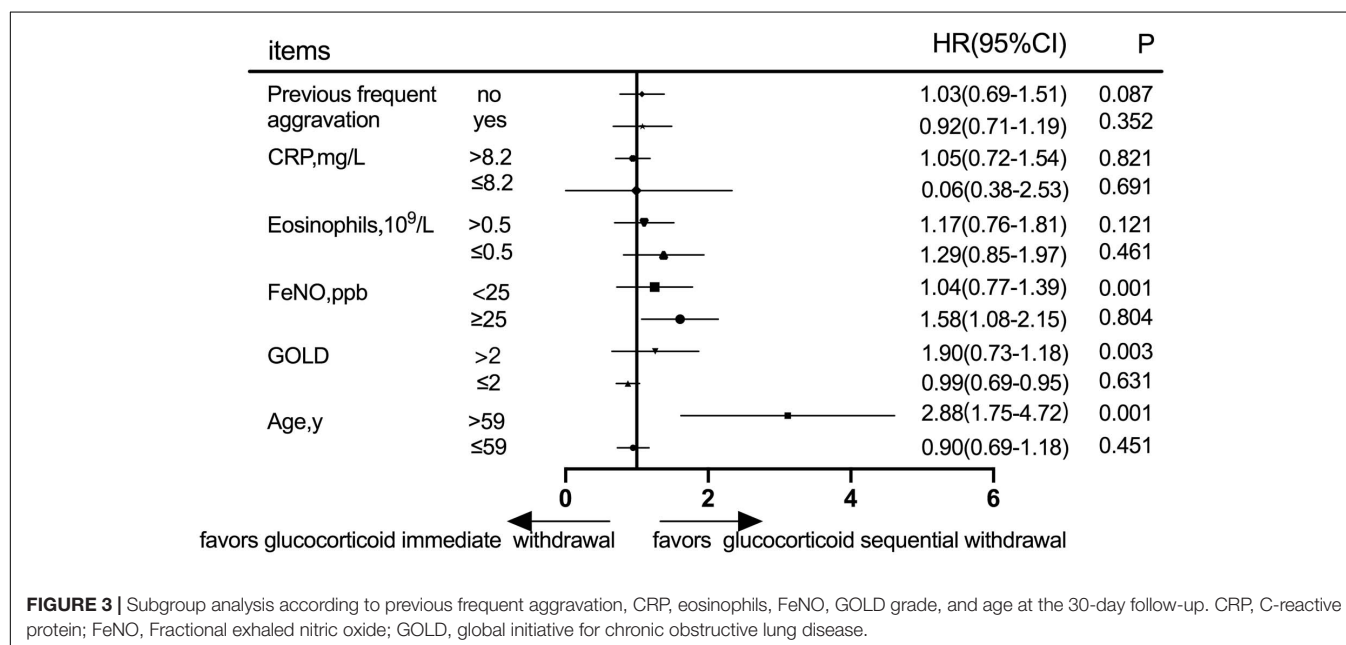
### Subgroup Analysis at the 360-day Follow-up

Prognostic evaluation was defined according to acute exacerbation frequency in the follow-up at 360 days. Subgroup analysis was performed according to the history of frequent acute exacerbations, CRP, eosinophils, FeNO, GOLD grade, and age (Figure 4). In patients with a history of either previous frequent aggravation or infrequent aggravation, there was no statistically significant difference in acute exacerbation frequency between immediate and sequential withdrawal groups at the 360-day follow-up ( $P > 0.05$ ). Similarly, in patients with either high or low CRP, high or low eosinophils, high or low FeNO, high or low GOLD grade, age  $\leq 59$  years or age  $> 59$  years, there was no statistically significant difference

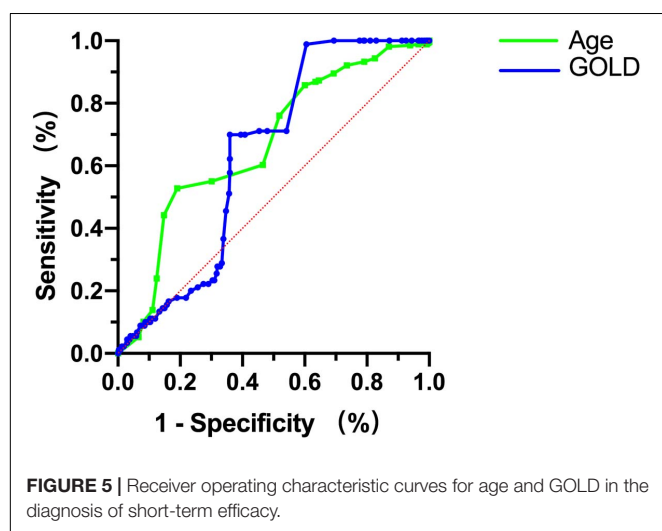
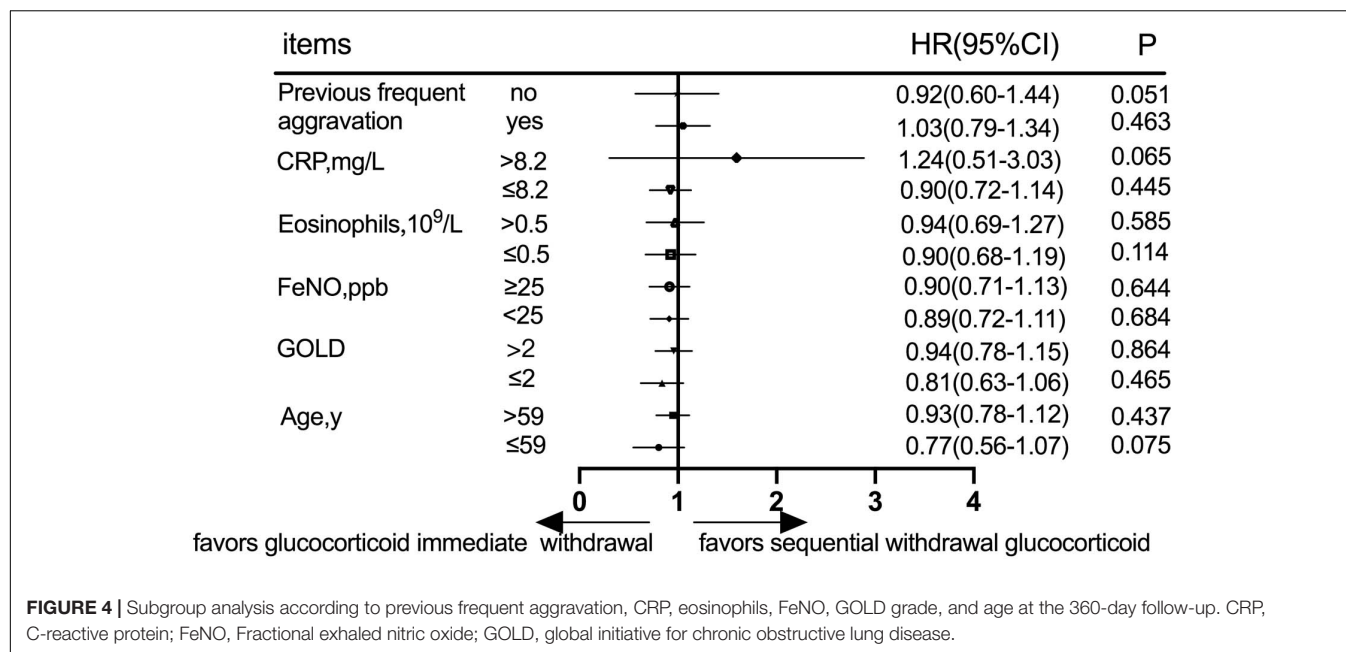
**TABLE 2 |** Secondary endpoints.

	Visit time (days)	Immediate withdrawal group	Sequential withdrawal group	Statistic	P-value
<b>Key secondary endpoint</b>					
Mortality	30	0	0	–	–
	90	3 (0.9)	3 (1)	0.073*	0.942
	180	5 (1.5)	6 (1.9)	1.163 <sup>†</sup>	0.686
	360	7 (2.1)	8 (2.6)	0.143 <sup>†</sup>	0.705
<b>Other secondary endpoints</b>					
mMRC score	30	1.97 ± 0.05	1.99 ± 0.05	0.380 <sup>‡</sup>	0.704
	90	2.01 ± 0.05	2.06 ± 0.05	0.679 <sup>‡</sup>	0.497
	180	1.95 ± 0.04	2.08 ± 0.05	1.923 <sup>‡</sup>	0.055
	360	1.96 ± 0.05	2.04 ± 0.05	0.997 <sup>‡</sup>	0.319
CAT score	30	18.93 ± 0.38	17.15 ± 0.44	3.045 <sup>‡</sup>	0.770
	90	19.31 ± 0.37	17.61 ± 0.45	2.875 <sup>‡</sup>	0.841
	180	19.04 ± 0.36	17.35 ± 0.47	2.854 <sup>‡</sup>	0.312
	360	19.09 ± 0.36	17.66 ± 0.49	2.354 <sup>‡</sup>	0.162
Rehospitalization rate	30	63 (19.1)	44 (14.2)	2.811 <sup>†</sup>	0.094
	90	107 (32.5)	90 (29.0)	0.912 <sup>†</sup>	0.339
	180	123 (37.4)	132 (42.6)	1.796 <sup>†</sup>	0.180
	360	144 (43.8)	145 (46.8)	0.582 <sup>†</sup>	0.446
ICU treatment rate	30	3 (0.9)	6 (1.9)	1.097*	0.328
	90	12 (3.6)	15 (4.8)	0.559 <sup>†</sup>	0.454
	180	25 (7.6)	26 (8.4)	0.135 <sup>†</sup>	0.713
	360	47 (14.3)	45 (14.5)	0.007 <sup>†</sup>	0.934
FEV1%	180	61.00 ± 0.48	61.80 ± 0.42	1.501 <sup>‡</sup>	0.134
	360	62.92 ± 0.51	61.57 ± 0.47	1.665 <sup>‡</sup>	0.097
PEF	180	7.54 ± 0.11	7.89 ± 0.14	1.263 <sup>‡</sup>	0.207
	360	7.73 ± 0.15	7.89 ± 0.14	1.075 <sup>‡</sup>	0.283
Time from discharge to first acute exacerbation	–	46.12 ± 1.28	49.02 ± 1.33	0.489 <sup>‡</sup>	0.030
Time of stay in hospital for the first time after discharge	–	6.28 ± 0.07	6.17 ± 0.05	1.275 <sup>‡</sup>	0.203

Data are shown as the mean ± standard deviation or n (%). \*Fisher's test; <sup>†</sup>χ<sup>2</sup>-value; <sup>‡</sup>t-test. mMRC, Modified Medical Research Council Dyspnea Scale; CAT, COPD Assessment Test; ICU, intensive-care unit; FEV1, forced expiratory volume in 1 s; PEF, peak expiratory flow.







(95%CI: 0.586–0.689) were risk factors for short-term efficacy (Figure 5 and Table 3).

## DISCUSSION

The treatment goal for AECOPD is to minimize the adverse effects of the current deterioration of the disease as soon as possible and prevent the development of subsequent events (Zhang et al., 2020). Standardized diagnosis and treatment measures play an important role in the prognosis of patients. Current recommendations from the Global Initiative for Chronic Obstructive Lung Disease suggest that patients who continue to have exacerbations should initially step up to glucocorticoid therapy (Terry and Dhand, 2019, 2020). GOLD point out AECOPD treatment strategies: “A dose of 40 mg prednisone per day for 5 days is recommended.” and “Intensified combination therapy with ICS/LABA for 10 days at Upper Respiratory Tract Infection onset could be associated with a reduction of exacerbations, particularly in patients with severe disease” (Singh et al., 2019). Immediate withdrawal for 5-days can reduce the treatment dose of glucocorticoid, but rapid withdrawal or dose reduction may result in a rebound effect, causing aggravation and deterioration of the original disease. Prolonged use of glucocorticoid can reverse severe illness and reduce the acute exacerbation frequency in specific subgroups. Some diseases, such as hypopituitarism, adrenocortical dysfunction, nephrotic syndrome, systemic lupus erythematosus, rheumatoid arthritis and other diseases need long-term use, or even lifelong use. Long-term use of glucocorticoids may cause some adverse events, such as obesity, peptic ulcer, or even gastrointestinal bleeding, which can also cause high blood pressure, high plasma glucose, osteoporosis, and aseptic necrosis of the femoral head. In this study, a randomized controlled trial comparing the short-term

in acute exacerbation frequency between immediate and sequential withdrawal groups at the 360-day follow-up ( $P > 0.05$ , Figure 4).

## Efficacy Analysis of Each Indicator at the 30-day Follow-up

Subgroup analysis showed that different ages, GOLD grading, and FeNO values could affect short-term efficacy. ROC curve analysis was performed based on the significant index values (age, GOLD, FeNO) to analyze short-term efficacy. Although FeNO had no diagnostic value for short-term efficacy ( $P > 0.05$ ), age and GOLD grading had diagnostic value in evaluating the short-term efficacy ( $P < 0.05$ ). Thus, age  $> 63.5$  years with an AUC = 0.668 (95%CI: 0.627–0.711) and GOLD  $> 3$  with an AUC = 0.638

**TABLE 3 |** Efficacy analysis of each indicator at the 30-day follow-up.

Items	AUC (95%CI)	P-value	Cut-off	Sensitivity (%)	Specificity (%)	Yoden index
Age	0.668 (0.627–0.711)	0.001	63.5	52.81	81.96	0.347
GOLD	0.638 (0.586–0.689)	0.007	3	40.47	98.89	0.393
FeNO	0.541 (0.497–1.586)	0.067	/	/	/	/

efficacy and long-term prognosis of immediate and sequential withdrawal of methyl prednisone was performed.

The trial included more than 600 patients with COPD, and all patients were randomly assigned to either the immediate withdrawal group or the sequential withdrawal group. The general data were analyzed to ensure there were no statistically significant differences between the immediate and sequential withdrawal groups ( $P > 0.05$ ). Follow-up results show the frequency of acute exacerbations had no statistically significant differences between the immediate and sequential withdrawal groups at 30, 90, 180, and 360 days after discharge ( $P > 0.05$ ). The mMRC dyspnea score is a 5-point (0–4) scale based on the severity of dyspnea (Cheng et al., 2019), and the CAT score is a patient-completed instrument used to assess and quantify health-related quality of life and symptom burden in COPD patients (Jones et al., 2009). As indicators of prognosis, mMRC and CAT scores were not statistically significant difference between the immediate and sequential withdrawal groups during follow-up ( $P > 0.05$ ). The 2011 GOLD consensus report uses symptoms, exacerbation history, and FEV1% to improve the clinical assessment and to guide treatment of COPD patients (Vestbo et al., 2012). In this study, there were no statistically significant differences in FEV1% and PEF between immediate and sequential withdrawal groups at 180 and 360 days ( $P > 0.05$ ). The time from discharge to first acute exacerbation was significantly lower ( $P < 0.05$ ) in the immediate withdrawal group (46.12 days) than in the sequential withdrawal group (49.02 days), indicating that sequential withdrawal of glucocorticoid can hold a longer disease stabilization time.

Different studies recommend different durations of glucocorticoid application, Yui et al. (2019) found that a history of frequent acute exacerbations is a strong and independent predictor of prognosis. In addition, the history of exacerbations is independent of severe exacerbations (Han et al., 2017). Moreover, Motegi et al. (2013) found that no index was significantly better than history of exacerbation alone to predict future exacerbations. In this study, subgroup analysis was performed according to the history of frequent acute exacerbation, but there was no statistically significant difference between the two withdrawal groups ( $P > 0.05$ ).

The CRP is a type of acute protein that increases sharply in the plasma when the body is infected or damaged (Aksu et al., 2013). It can activate, complement, and enhance phagocytosis of phagocytes and play a regulatory role in clearing invading pathogenic microorganisms and injured, necrotic, and apoptotic cells (Sacks, 2019). The value of CRP as a prognostic biomarker in AECOPD patients has been extensively investigated (Sneh et al., 2020). The association of blood eosinophil levels with rehospitalization rates is a question that remains to be answered:

some studies show increased rehospitalizations (Vedel-Krogh et al., 2016; Couillard et al., 2017), whereas others find no significant effect (Bafadhel et al., 2016). In this study, subgroup analysis was performed according to CRP and eosinophils, but there was no statistically significant difference between the two methods of withdrawal ( $P > 0.05$ ). This result might be due to CRP having a half-life of 19 h and therefore there is no significant difference in a long-term follow-up. Thus, the study was expanded to identify the relevant indicators. The GOLD was developed to spread awareness of COPD as a major public health problem and facilitate its prevention and treatment (Nowak et al., 2020). To explore the effect of the GOLD on patient prognosis, patients were divided into high or low GOLD grade groups, and the difference was significant ( $P < 0.05$ ). The GOLD attempts to promote spirometry not only as a case-finding and prognostication tool for airflow obstruction but also as a marker for good health (Bhatt et al., 2019). According to this study, patients with an elevated GOLD grade should be treated with sequential withdrawal.

The FeNO measurement was considered to be a biomarker for airway eosinophilic inflammation (Zhou et al., 2020), because its concentration is highly correlated with the number of inflammatory cells (Hogman et al., 2019). In this study, subgroup analysis was performed according to FeNO, and the difference was not statistically significant ( $P > 0.05$ ). FeNO is significantly elevated in asthmatic patients (Heaney et al., 2019), and FeNO values in stable COPD patients were slightly higher than those in healthy individuals (Matsunaga et al., 2020). The relationship between FeNO and AECOPD needs to be explored further. The elderly are the main patients with chronic diseases (Zhou et al., 2019), COPD is one of the major chronic diseases. In this study, subgroup analysis was performed according to age, and the difference was significant ( $P < 0.05$ ). The ROC curve analysis showed sequential withdrawal at age  $> 59$  years could decrease acute exacerbation frequency at the 30-day follow-up. Elderly patients are likely to have many complications that affect treatment (Rydberg et al., 2020). Clinicians should consider increasing age as a key risk factor in the management of COPD and develop correct treatment to improve the therapeutic effect (Stone et al., 2012). Because there was no consensus for the time and dose of systemic glucocorticoids in treating AECOPD, they should be explored in further studies.

The study had some deficiencies: (1) although the study was a randomized, double-blind, controlled trial, the open labeling might have affected clinical decisions and outcome endpoints; (2) the number of patients were insufficient to distinguish causes of death, and mortality assessment was not targeted, therefore, adverse reactions of glucocorticoid therapy might not have been detected.

## CONCLUSION

In this study, the glucocorticoid schemes for AECOPD treatment were analyzed. sequential withdrawal of glucocorticoid can hold a longer disease stabilization time. The frequency of acute exacerbations at the 30-day follow-up was significantly higher in patients with age > 63.5 years or GOLD > 3 in the immediate withdrawal group than in the sequential withdrawal group, suggesting that the short-term efficacy was poor. AECOPD patients who are elderly or with a high GOLD grade should be treated with glucocorticoid sequential withdrawal to reduce the acute exacerbation frequency of the 30-day follow-up.

## DATA AVAILABILITY STATEMENT

The original contributions presented in the study are included in the article/supplementary material, further inquiries can be directed to the corresponding author/s.

## REFERENCES

- Aksu, F., Capan, N., Aksu, K., Ofuoglu, R., Canbakan, S., Yavuz, B., et al. (2013). C-reactive protein levels are raised in stable Chronic obstructive pulmonary disease patients independent of smoking behavior and biomass exposure. *J. Thorac. Dis.* 5, 414–421.
- Bafadhel, M., Greening, N. J., Harvey-Dunstan, T. C., Williams, J. E., Morgan, M. D., Brightling, C. E., et al. (2016). Blood eosinophils and outcomes in severe hospitalized exacerbations of COPD. *Chest* 150, 320–328. doi: 10.1016/j.chest.2016.01.026
- Berenyi, F., Steinfert, D. P., Abdelhamid, Y. A., Bailey, M. J., Pilcher, D. V., Bellomo, R., et al. (2020). Characteristics and outcomes of critically ill patients with acute exacerbation of Chronic obstructive pulmonary disease in Australia and New Zealand. *Ann. Am. Thorac. Soc.* 17, 736–745. doi: 10.1513/annalsats.201911-821oc
- Bhatt, S. P., Balte, P. P., Schwartz, J. E., Cassano, P. A., Couper, D., Jacobs, D. R., et al. (2019). Discriminative accuracy of FEV1:FVC thresholds for COPD-related hospitalization and mortality. *JAMA* 321, 2438–2447. doi: 10.1001/jama.2019.7233
- Burns, R. B., Anandaiah, A., Rice, M. B., and Smetana, G. W. (2020). Should you recommend inhaled corticosteroids for this patient with chronic obstructive pulmonary disease: grand rounds discussion from Beth Israel deaconess medical center. *Ann. Intern. Med.* 172, 735–742. doi: 10.7326/m20-1058
- Cheng, S. L., Lin, C. H., Wang, C. C., Chan, M. C., Hsu, J. Y., Hang, L. W., et al. (2019). Comparison between COPD assessment test (CAT) and modified medical research council (mMRC) dyspnea scores for evaluation of clinical symptoms, comorbidities and medical resources utilization in COPD patients. *J. Formos. Med. Assoc.* 118, 429–435. doi: 10.1016/j.jfma.2018.06.018
- Couillard, S., Larivee, P., Courteau, J., and Vanasse, A. (2017). Eosinophils in COPD exacerbations are associated with increased readmissions. *Chest* 151, 366–373. doi: 10.1016/j.chest.2016.10.003
- Doumas, M., Imprialos, K. P., and Stavropoulos, K. (2020). Metoprolol for the prevention of exacerbations of COPD. *N. Engl. J. Med.* 382, 1374–1375. doi: 10.1056/nejmc2000638
- Han, M. K., Quibrera, P. M., Carretta, E. E., Barr, R. G., Bleeker, E. R., Bowler, R. P., et al. (2017). Frequency of exacerbations in patients with chronic obstructive pulmonary disease: an analysis of the SPIROMICS cohort. *Lancet Respir. Med.* 5, 619–626.
- Heaney, L. G., Busby, J., Bradding, P., Chaudhuri, R., Mansur, A. H., Niven, R., et al. (2019). Remotely monitored therapy and Nitric Oxide suppression identifies

## ETHICS STATEMENT

The studies involving human participants were reviewed and approved by the Huazhong University of Science and Technology Institutional Review Board. The patients/participants provided their written informed consent to participate in this study.

## AUTHOR CONTRIBUTIONS

All authors contributed to data analysis, drafting or revising the article, gave final approval of the version to be published, and agreed to be accountable for all aspects of the work.

## FUNDING

This work was supported by the National key Research and Development Program of China (Project No. 2016YFC1304203) and the National Natural Science Foundation of China (No. 81770088).

- nonadherence in severe asthma. *Am. J. Respir. Crit. Care Med.* 199, 454–464. doi: 10.1164/rccm.201806-1182oc
- Hogman, M., Thornadtsen, A., Broms, K., Janson, C., Lisspers, K., Stallberg, B., et al. (2019). Different relationships between FENO and COPD characteristics in smokers and Ex-Smokers. *COPD* 16, 227–233. doi: 10.1080/15412555.2019.1638355
- Jones, P. W., Harding, G., Berry, P., Wiklund, I., Chen, W. H., and Kline Leidy, N. (2009). Development and first validation of the COPD assessment test. *Eur. Respir. J.* 34, 648–654. doi: 10.1183/09031936.00102509
- Leuppi, J. D., Schuetz, P., Bingisser, R., Bodmer, M., Briel, M., Drescher, T., et al. (2013). Short-term vs conventional glucocorticoid therapy in acute exacerbations of chronic obstructive pulmonary disease: the REDUCE randomized clinical trial. *JAMA* 309, 2223–2231. doi: 10.1001/jama.2013.5023
- Lucafo, M., Franzin, M., Decorti, G., and Stocco, G. (2020). A patent review of anticancer glucocorticoid receptor modulators (2014-present). *Expert Opin. Ther. Pat.* 30, 313–324. doi: 10.1080/13543776.2020.1740206
- Matsunaga, K., Kuwahira, I., Hanaoka, M., Saito, J., Tsuburai, T., Fukunaga, K., et al. (2020). An official JRS statement: the principles of fractional exhaled nitric oxide (FeNO) measurement and interpretation of the results in clinical practice. *Respir. Investig.* 59, 34–52. doi: 10.1016/j.resinv.2020.05.006
- McKenzie, D. K., Frith, P. A., Burdon, J. G., Town, G. I., Australian Lung Foundation, Thoracic Society of Australia and New Zealand, et al. (2003). The COPDX plan: Australian and New Zealand guidelines for the management of Chronic obstructive pulmonary disease 2003. *Med. J. Aust.* 178, S1–S39.
- Motegi, T., Jones, R. C., Ishii, T., Hattori, K., Kusunoki, Y., Furutate, R., et al. (2013). A comparison of three multidimensional indices of COPD severity as predictors of future exacerbations. *Int. J. Chron. Obstruct. Pulmon. Dis.* 8, 259–271. doi: 10.2147/COPD.S42769
- National Collaborating Centre for Chronic (2004). Chronic obstructive pulmonary disease. national clinical guideline on management of chronic obstructive pulmonary disease in adults in primary and secondary care. *Thorax* 59(Suppl. 1), 1–232.
- Nowak, M., Brozek, G. M., Zejda, J. E., Jankowski, M., and Pierzchala, W. (2020). Impact of changing GOLD guidelines (2007–2011–2017) on assignment of a COPD patient to disease severity category. *Postępy Dermatol. Alergol.* 37, 221–228. doi: 10.5114/ada.2018.79143
- Rabe, K. F., Martinez, F. J., Ferguson, G. T., Wang, C., Singh, D., Wedzicha, J. A., et al. (2020). Triple inhaled therapy at two glucocorticoid doses in moderate-to-severe COPD. *N. Engl. J. Med.* 383, 35–48. doi: 10.1056/nejmoa1916046
- Rydberg, D. M., Linder, M., Malmstrom, R. E., and Andersen, M. (2020). Risk factors for severe bleeding events during warfarin treatment: the influence of

- sex, age, comorbidity and co-medication. *Eur. J. Clin. Pharmacol.* 76, 867–876. doi: 10.1007/s00228-020-02856-6
- Sacks, H. S. (2019). In primary care, CRP testing reduced antibiotic use in COPD exacerbations without worsening health. *Ann. Intern. Med.* 171:JC51.
- Singh, D., Agusti, A., Anzueto, A., Barnes, P. J., Bourbeau, J., Celli, B. R., et al. (2019). Global strategy for the diagnosis, management, and prevention of Chronic obstructive lung disease: the GOLD science committee report 2019. *Eur. Respir. J.* 53:1900164.
- Sneh, A., Pawan, T., Randeep, G., Anant, M., Mani, K., Hadda, V., et al. (2020). Acute phase proteins as predictors of survival in patients with acute exacerbation of Chronic obstructive pulmonary disease requiring mechanical ventilation. *COPD* 17, 22–28. doi: 10.1080/15412555.2019.1698019
- Stone, R. A., Lowe, D., Potter, J. M., Buckingham, R. J., Roberts, C. M., and Pursey, N. J. (2012). Managing patients with COPD exacerbation: does age matter? *Age Ageing* 41, 461–468. doi: 10.1093/ageing/afs039
- Terry, P. D., and Dhand, R. (2020). Inhalation therapy for stable COPD: 20 Years of GOLD reports. *Adv. Ther.* 37, 1812–1828. doi: 10.1007/s12325-020-01289-y
- Vedel-Krogh, S., Nielsen, S. F., Lange, P., Vestbo, J., and Nordestgaard, B. G. (2016). Blood Eosinophils and Exacerbations in Chronic obstructive pulmonary disease: the Copenhagen general population study. *Am. J. Respir. Crit. Care Med.* 193, 965–974. doi: 10.1164/rccm.201509-1869oc
- Vermeersch, K., Gabrovska, M., Aumann, J., Demedts, I. K., Corhay, J. L., Marchand, E., et al. (2019). Azithromycin during acute Chronic obstructive pulmonary disease exacerbations requiring hospitalization (BACE): a multicenter, randomized, double-blind, placebo-controlled trial. *Am. J. Respir. Crit. Care Med.* 200, 857–868. doi: 10.1164/rccm.201901-0094oc
- Vestbo, J., Hurd, S. S., and Rodriguez-Roisin, R. (2012). The 2011 revision of the global strategy for the diagnosis, management and prevention of COPD (GOLD)—why and what? *Clin. Respir. J.* 6, 208–214. doi: 10.1111/crj.12002
- Yii, A. C. A., Loh, C. H., Tiew, P. Y., Xu, H., Taha, A. A. M., Koh, J., et al. (2019). A clinical prediction model for hospitalized COPD exacerbations based on “treatable traits”. *Int. J. Chron. Obstruct. Pulmon. Dis.* 14, 719–728. doi: 10.2147/COPD.S194922
- Zhang, R., Zhu, J., Liu, Y., Li, Y., Liu, W., Zhang, M., et al. (2020). Optimization of Nebulized Budesonide in the treatment of Acute Exacerbation of Chronic obstructive pulmonary disease. *Int. J. Chron. Obstruct. Pulmon. Dis.* 15, 409–415. doi: 10.2147/copd.s235125
- Zhou, A., Zhou, Z., Deng, D., Zhao, Y., Duan, J., Cheng, W., et al. (2020). The value of FENO measurement for predicting treatment response in patients with acute exacerbation of Chronic obstructive pulmonary disease. *Int. J. Chron. Obstruct. Pulmon. Dis.* 15, 2257–2266. doi: 10.2147/copd.s263673
- Zhou, M., Wang, H., Zeng, X., Yin, P., Zhu, J., and Chen, W. (2019). Mortality, morbidity, and risk factors in China and its provinces, 1990–2017: a systematic analysis for the global burden of disease study 2017. *Lancet* 394, 1145–1158. doi: 10.1016/s0140-6736(19)30427-1

**Conflict of Interest:** The authors declare that the research was conducted in the absence of any commercial or financial relationships that could be construed as a potential conflict of interest.

Copyright © 2021 Zhou, Fang, Liu, Zhang, Wang, Xie, Zhong, Wang, Li, Ai, Guo, Zeng, Xiao, Li, Hu, Tang and Liu. This is an open-access article distributed under the terms of the Creative Commons Attribution License (CC BY). The use, distribution or reproduction in other forums is permitted, provided the original author(s) and the copyright owner(s) are credited and that the original publication in this journal is cited, in accordance with accepted academic practice. No use, distribution or reproduction is permitted which does not comply with these terms.





# Development and Validation of a Predictive Model for Severe COVID-19: A Case-Control Study in China

Zirui Meng<sup>1†</sup>, Minjin Wang<sup>1†</sup>, Zhenzhen Zhao<sup>1</sup>, Yongzhao Zhou<sup>2</sup>, Ying Wu<sup>2</sup>, Shuo Guo<sup>1</sup>, Mengjiao Li<sup>1</sup>, Yanbing Zhou<sup>1</sup>, Shuyu Yang<sup>1</sup>, Weimin Li<sup>2\*</sup> and Binwu Ying<sup>1\*</sup>

<sup>1</sup> Department of Laboratory Medicine, West China Hospital, Sichuan University, Chengdu, China, <sup>2</sup> Department of Respiratory and Critical Care Medicine, West China Hospital, Sichuan University, Chengdu, China

## OPEN ACCESS

### Edited by:

Huahao Shen,  
Zhejiang University, China

### Reviewed by:

Chuan Hu,  
Qingdao University Medical  
College, China  
Chayan Kanti Nandi,  
Indian Institute of Technology  
Mandi, India

### \*Correspondence:

Binwu Ying  
binwuyin@126.com  
Weimin Li  
weimin003@163.com

<sup>†</sup>These authors have contributed  
equally to this work

### Specialty section:

This article was submitted to  
Pulmonary Medicine,  
a section of the journal  
Frontiers in Medicine

**Received:** 02 February 2021

**Accepted:** 12 April 2021

**Published:** 25 May 2021

### Citation:

Meng Z, Wang M, Zhao Z, Zhou Y, Wu Y, Guo S, Li M, Zhou Y, Yang S, Li W and Ying B (2021) Development and Validation of a Predictive Model for Severe COVID-19: A Case-Control Study in China. *Front. Med.* 8:663145. doi: 10.3389/fmed.2021.663145

**Background:** Predicting the risk of progression to severe coronavirus disease 2019 (COVID-19) could facilitate personalized diagnosis and treatment options, thus optimizing the use of medical resources.

**Methods:** In this prospective study, 206 patients with COVID-19 were enrolled from regional medical institutions between December 20, 2019, and April 10, 2020. We collated a range of data to derive and validate a predictive model for COVID-19 progression, including demographics, clinical characteristics, laboratory findings, and cytokine levels. Variation analysis, along with the least absolute shrinkage and selection operator (LASSO) and Boruta algorithms, was used for modeling. The performance of the derived models was evaluated by specificity, sensitivity, area under the receiver operating characteristic (ROC) curve (AUC), Akaike information criterion (AIC), calibration plots, decision curve analysis (DCA), and Hosmer–Lemeshow test.

**Results:** We used the LASSO algorithm and logistic regression to develop a model that can accurately predict the risk of progression to severe COVID-19. The model incorporated alanine aminotransferase (ALT), interleukin (IL)-6, expectoration, fatigue, lymphocyte ratio (LYMR), aspartate transaminase (AST), and creatinine (CREA). The model yielded a satisfactory predictive performance with an AUC of 0.9104 and 0.8792 in the derivation and validation cohorts, respectively. The final model was then used to create a nomogram that was packaged into an open-source and predictive calculator for clinical use. The model is freely available online at <https://severeconid-19predction.shinyapps.io/SHINY/>.

**Conclusion:** In this study, we developed an open-source and free predictive calculator for COVID-19 progression based on ALT, IL-6, expectoration, fatigue, LYMR, AST, and CREA. The validated model can effectively predict progression to severe COVID-19, thus providing an efficient option for early and personalized management and the allocation of appropriate medical resources.

**Keywords:** COVID-19, severe COVID-19, predictive model, laboratory findings, cytokines, online predictive calculator

## INTRODUCTION

The current outbreak of coronavirus disease 2019 (COVID-19) has spread rapidly and widely across the world, causing panic and major public health challenges in the international community (1). COVID-19 presents a wide clinical manifestation, including asymptomatic infection, mild upper respiratory tract illness, and severe viral pneumonia, with respiratory failure. Only a small proportion of the total number of cases progress to a severe condition (~15–20%); however, ~40% of patients with severe disease die (2–5). Although some research has shown that initial therapy with remdesivir or non-invasive positive pressure ventilation (NIPPV) is very efficient for severe cases, there is currently a lack of accepted recommendations for severe patients with regard to individualized treatment (6–8). Therefore, the rapid deterioration of patients with severe COVID-19 deserves special attention. There is an urgent need to develop options for the personalized diagnosis and treatment of such patients, particularly with regard to protecting the relative shortage of medical resources.

Fever, cough, and fatigue are commonly present in patients with mild COVID-19 (9, 10). As the disease progresses further, patients may also experience respiratory failure, acute respiratory distress syndrome, heart failure, metabolic acidosis, and septic shock (11). Besides the well-defined clinical characteristics of COVID-19, previous studies have shown that abnormal laboratory findings and cytokine levels are often associated with disease progression, including coagulation-related markers such as D-dimer and fibrinogen (FIB), neutrophil count, lymphocyte count, and high-sensitivity C-reactive protein (HsCRP) (5, 12–15). In addition, research has identified that a cytokine storm could be the primary driver of severe progression in COVID-19 patients (16, 17). However, the application of these independent indicators is limited by many factors, including insufficient information, individual differences, the experience of the attending physician, and the complexity of disease. Thus, there is an urgent need for advanced multivariable prediction models (18, 19). Although several studies have attempted to develop prediction models, most of the existing models were developed in a single center and based on retrospective data; in some cases, only partial datasets were used, and there was a clear lack of validation. These factors may lead to the omission of key variables and the risk of over-fitting, thus limiting the clinical application of such models. Therefore, there is a critical need to develop more effective prediction models (14, 15, 20, 21).

Here, we prospectively and consecutively enrolled a cohort of COVID-19 patients with a complete set of demographic data, clinical characteristics, laboratory findings, and cytokine information, and we then constructed a multiparameter prediction model for the early identification of severe COVID-19. Our model could help to monitor and guide precision medicine.

## METHODS

### Participants

COVID-19 patients were prospectively and consecutively enrolled from regional medical institutions by the West China

Medical Center between December 20, 2019, and April 10, 2020. The patients were divided into severe and non-severe groups according to the China National Health Commission Guidelines for Diagnosis and Treatment of COVID-19 infection (Versions 5 and 7). Serum samples were collected from patients within 3 days of infection confirmation and stored at  $-80^{\circ}\text{C}$  for the subsequent detection of cytokine levels. Demographic data, clinical characteristics, and laboratory findings were acquired from electronic medical records (Figure 1). Two independent researchers reviewed the data collection forms.

### Diagnostic and Severity Classification Criteria

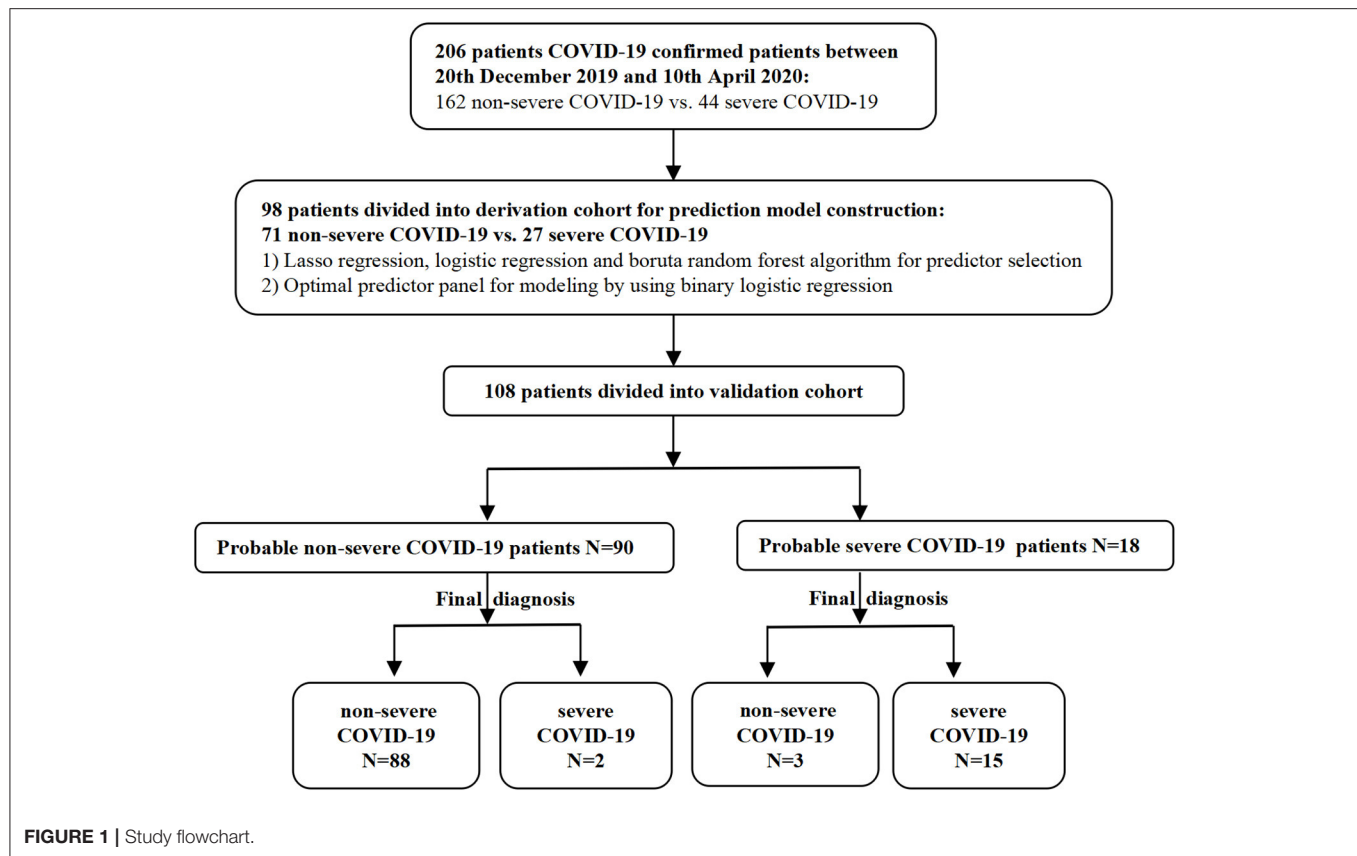
Patients with pneumonia, typical findings on computed tomography (CT) chest scan, and positive severe acute respiratory syndrome coronavirus 2 (SARS-CoV-2) nucleic acid results, as determined by real-time fluorescent reverse transcription-polymerase chain reaction assessment from bronchoalveolar lavage (BAL) or sputum, were considered as COVID-19 “cases” according to the diagnosis and treatment guidelines released by the China Health and Medical Commission (22). Patients with at least one of the following symptoms during hospitalization were allocated into the severe group: (1) respiratory distress, respiratory rate  $\geq 30$  times/min; (2) oxygen saturation  $\leq 93\%$  at rest; and (3) oxygen partial pressure ( $\text{PaO}_2$ )/oxygen concentration ( $\text{FiO}_2$ ) in arterial blood  $\leq 300$  mmHg. All patients were discharged or had died by the time the model was developed.

### The Detection of Cytokines

Circulating levels of interferon (IFN)- $\alpha 2$ , IFN- $\beta$ , IFN- $\gamma$ , tumor necrosis factor (TNF)- $\alpha$ , interleukin (IL)-1 $\alpha$ , IL-1 $\beta$ , IL-2, IL-4, IL-6, IL-8, IL-10, IL-17A, IL-17E, IL-17F, IL-22, and IL-33 in serum samples were measured by a multiplexed flow cytometric assay using Human Cytokine Kits on a Luminex<sup>®</sup> system (MAGPIX<sup>®</sup> with xPONENT) according to the manufacturer's instructions (MILLIPLEX<sup>®</sup> Analyst 5.1). All samples were measured in duplicate. Based on standard curves, we calculated the coefficient of variation (CV); this did not exceed 20%.

### Construction of the Predictive Model and Internal Validation

Patients from the Chengdu region were divided into a derivation cohort, including a training set for modeling and a testing set for internal validation. Stepwise selection was based on  $p$ -values; least absolute shrinkage and selection operator (LASSO) and the Boruta algorithm were used to select variables (23, 24). Stepwise selection, as based on  $p$ -values, is a classic regression-based method. A variable's value with a  $p < 0.05$  was regarded as significant and was retained. This practice generally achieves a better performance in smaller datasets and has been extensively used in previous research. LASSO regression can compress the coefficients of the features *via* penalty function to obtain optimal constraint models; this practice has been used effectively to avoid over-fitting and co-linearity in classical analysis methods based on significance differences and also enhances the ability of a model to be generalized. Boruta algorithm is a wrapper algorithm



that uses random forest classification. This practice can iteratively remove features that prove to be less relevant than random probes and thus aims to retain relevant variables for the function of a response variable. In addition, these two algorithms are particularly suitable for a dataset with a small sample size but with a large number of variables. By using these three different variable selection methods, we were able to select three candidate predictor panels to construct different binary logistic regression models, which were then verified internally by 10-fold cross-validation. The optimal model was then selected by comparing the area under the curve (AUC) and the Akaike information criterion (AIC) in order to generate a nomogram that could be encapsulated as an open-source online predictive calculator.

### Independent Validation

The independent validation cohort consisted of patients from outside Chengdu; this was used for external verification to predict the generalization ability of the model by comparing the predicted results with a set of follow-up results to calculate several metrics: sensitivity, specificity, positive predictive value (PPV), and negative predictive value (NPV). AUCs and decision curve analysis (DCA) were used to comprehensively evaluate the model's discrimination and net clinical benefits (25).

### Statistical Analysis

Continuous variables and categorical variables are presented as the median (upper and lower quartiles) and as a frequency,

respectively. The chi-squared test for categorical variables and the Student *t*-test or Mann–Whitney *U*-test for continuous variables were used to test the data between groups. Pearson correlation was used to determine the linear correlation between two variables. The diagnostic performance of equations was then displayed by AIC and receiver operating characteristic (ROC) curve and quantified by AUCs. An open-source online predictive calculator was then created using the Shiny tool in the R environment (version 1.2.0). All statistical analyses were completed using R 3.5.0 version. All statistical tests were two-tailed, and  $p \leq 0.05$  was considered to indicate statistical significance.

### Standard Protocol Approvals, Registrations, and Patient Consent

The protocol for this study was approved by the West China Hospital, Sichuan University Medical Ethics Committee (reference no. 193, 2020), and conformed to the principles of the Declaration of Helsinki. Written informed consent was obtained from all participants.

## RESULTS

### Epidemiological Characteristics

We recruited 206 patients with a confirmed diagnosis of COVID-19; of these, 44 patients progressed to severe COVID-19, and 162 patients were classified as having non-severe COVID-19.

**TABLE 1 |** Patients' characteristics in training set.

	Non-severe COVID-19 71 patients	Severe COVID-19 27 patients	P-value		Non-severe COVID-19 71 patients	Severe COVID-19 27 patients	P-value
Demographics				Cytokines			
Age	46 (33, 51)	50 (42, 65)	0.005*	IFN- $\beta$	8.87 (8.08, 8.87)	8.87 (8.08, 8.87)	0.403
Sex	53.50%	63.00%	0.4	IFN- $\gamma$	10.58 (1.71, 24.88)	17.07 (3.67, 54.26)	0.161
Diabetes	4.20%	29.60%	<0.001*	Laboratory findings			
Hypertension	16.90%	40.70%	0.013*	WBC	5.41 (4.40, 7.15)	6.31 (4.40, 7.67)	0.148
Clinical features				HB	137.00 (126.00, 156.00)	134.00 (125.00, 151.00)	0.239
Temperature	36.7 (36.5, 37.4)	37.2 (36.7, 37.7)	0.115	PLT	180.00 (141.00, 244.00)	146.00 (120.00, 223.00)	0.131
Heart rate	88 (78, 97)	90 (84, 105)	0.196	LYMR	23.80 (18.80, 30.90)	15.20 (5.10, 23.40)	<0.001*
Respiratory rate	20 (20, 21)	20 (20, 22)	0.008*	NEUTR	65.80 (57.60, 71.00)	77.00 (67.20, 87.60)	<0.001*
SBP	130 (120, 140)	139 (123, 150)	0.183	EOSR	0.20 (0.09, 0.90)	0.00 (0.00, 0.20)	0.003*
DBP	82 (77, 89)	84 (76, 94)	0.619	BASOR	0.20 (0.10, 0.30)	0.20 (0.10, 0.30)	0.977
SBP-DBP	48 (42, 58)	50 (44, 63)	0.202	MONOR	8.30 (6.80, 10.80)	7.00 (4.20, 9.10)	0.028*
Fever	60.60%	74.10%	0.212	HCT	39.80 (35.60, 45.40)	36.60 (29.50, 44.10)	0.215
Cough	45.10%	81.50%	0.001*	D-dimer	1.90 (0.32, 62.44)	5.46 (0.83, 31.00)	0.75
Dry cough	25.40%	25.90%	0.954	FIB	3.59 (2.84, 4.32)	4.03 (3.20, 4.86)	0.045*
Expectoration	16.90%	51.90%	<0.001*	APTT	31.82 (27.20, 37.80)	32.70 (31.20, 35.20)	0.578
Dyspnea	2.80%	25.90%	<0.001*	PT	12.40 (11.70, 13.40)	12.70 (11.90, 13.30)	0.559
Asthma	4.20%	18.50%	0.021*	INR	1.02 (0.97, 1.10)	1.05 (1.00, 1.15)	0.379
Chest distress	7.00%	11.10%	0.511	TBIL	10.70 (7.11, 14.90)	6.78 (4.00, 13.35)	0.043*
Nasal obstruction	2.80%	0.00%	$P = 0.378$	DBIL	3.40 (2.20, 4.60)	3.90 (2.64, 6.40)	0.272
Nasal discharge	5.60%	3.70%	$P = 0.698$	IBIL	6.60 (4.50, 11.70)	5.47 (2.70, 9.33)	0.158
Earache	0.00%	3.70%	0.103	ALT	29.50 (18.00, 48.01)	41.17 (21.00, 74.14)	0.147
Sore throat	11.30%	18.50%	0.344	AST	26.00 (19.60, 35.70)	37.00 (23.70, 70.62)	0.022*
Headache	16.90%	7.40%	0.23	TP	75.00 (70.70, 79.00)	68.41 (63.20, 77.30)	0.014*
Myalgia	8.50%	11.10%	0.684	ALB	44.30 (41.00, 46.67)	39.60 (34.90, 44.27)	0.001*
Arthralgia	1.40%	3.70%	0.473	GLB	30.20 (27.06, 33.05)	29.31 (23.80, 32.75)	0.057
Chest wall invagination	0.00%	0.00%	—	TG	1.66 (0.94, 2.28)	1.44 (0.84, 2.37)	0.507
Fatigue	4.20%	25.90%	0.002*	CHOL	4.20 (3.42, 4.80)	3.85 (2.87, 4.58)	0.088
Diarrhea	11.30%	14.80%	0.632	HDL-C	1.20 (1.03, 1.39)	1.04 (0.92, 1.43)	0.231
Cytokines				LDL-C	2.30 (1.84, 2.84)	1.87 (1.33, 2.60)	0.054
IL-1 $\alpha$	2.91 (1.47, 7.80)	7.05 (2.91, 11.53)	0.025*	CK	93.00 (56.80, 216.00)	217.76 (64.00, 314.30)	0.053
IL-1 $\beta$	1.60 (0.66, 4.86)	3.24 (1.37, 7.80)	0.06	CK-MB	11.83 (5.32, 14.73)	12.34 (3.76, 17.00)	0.688
IL-2	0.21 (0.10, 0.45)	0.36 (0.14, 0.61)	0.343	Glu	5.63 (5.07, 6.97)	6.80 (5.44, 9.15)	0.044*
IL-4	1.94 (0.48, 3.91)	1.73 (0.78, 6.47)	0.181	Na	140.10 (137.10, 143.00)	138.00 (133.14, 141.80)	0.097
IL-6	1.19 (0.66, 3.54)	5.03 (2.12, 18.61)	<0.001*	K	3.97 (3.60, 4.30)	3.94 (3.40, 4.33)	0.519
IL-8	3.72 (2.18, 6.98)	5.56 (3.82, 9.44)	0.074	Ca	2.27 (2.16, 2.39)	2.09 (1.96, 2.19)	<0.001*
IL-10	1.13 (0.34, 2.47)	3.76 (0.92, 14.15)	0.001*	Mg	0.87 (0.82, 0.99)	0.85 (0.79, 1.02)	0.741
IL-17A	0.97 (0.52, 4.12)	1.45 (0.80, 4.37)	0.083	Urea	3.70 (2.90, 5.30)	4.31 (3.30, 7.20)	0.076
IL-17E	28.56 (17.37, 90.70)	24.36 (9.85, 80.88)	0.203	CREA	71.60 (56.00, 83.30)	69.40 (52.00, 192.90)	0.735
IL-17F	7.66 (5.75, 13.53)	7.66 (6.22, 10.75)	0.817	URIC	348.00 (258.00, 427.00)	276.00 (183.00, 379.00)	0.038*
IL-22	36.67 (2.05, 86.54)	11.20 (1.42, 91.01)	0.874	Myo	125.00 (21.89, 583.83)	166.40 (23.72, 1247.00)	0.245
IL-33	8.76 (7.51, 8.76)	8.76 (8.76, 10.11)	0.161	HsCRP	10.00 (2.58, 23.28)	27.60 (6.80, 55.14)	0.004*
TNF- $\alpha$	41.15 (21.84, 71.55)	45.50 (17.29, 89.73)	0.525	PCT	0.09 (0.04, 4.10)	0.48 (0.04, 7.42)	0.362
IFN- $\alpha$ 2	6.46 (4.00, 20.38)	6.46 (4.00, 33.26)	0.92				

Data are presented as *n* (%) for categorical variables and as median (upper and lower quartile) for continuous variables. \* $P < 0.05$ .

Patients in the severe group were significantly older (50 vs. 46,  $p = 0.005$ ) and had a significantly higher frequency of underlying diseases (diabetes and hypertension) than the non-severe group

( $p < 0.001$  and  $p = 0.013$ , respectively). There were no differences between the two groups in terms of gender (male: 54.940 vs. 56.810%,  $p = 0.400$ ). With regard to epidemiological exposure,



most of the patients (79.000%) in the severe group had been overseas or had visited Wuhan or surrounding regions within 14 days of disease onset; patients who had been overseas accounted for 50% of the patients with non-severe COVID-19. As of April 28, 2020, the time for the reversal of a negative nucleic acid test result in the non-severe and severe groups was 11 and 18 days (median) except for three patients who died from multiple organ failure (MOF).

## Differences in Characteristics and Correlation Analysis

Demographic data, clinical characteristics, laboratory findings, and cytokine levels are shown in **Table 1** and **Supplementary Figures 1, 2**. Several cytokines were significantly elevated in the severe COVID-19 group ( $p \leq 0.010$ ). The predictive value of each single cytokine, and a combined

panel of cytokines, were evaluated by ROC curve analysis and quantified by AUC (**Supplementary Figure 3**). Results showed that the AUCs were 0.830, 0.796, 0.729, 0.707, 0.694, 0.667, 0.656, and 0.653 for single IL-10, IL-6, IL-1 $\alpha$ , IL-1 $\beta$ , IL-17A, IL-4, TNF- $\alpha$ , and IL-2 and that the binary logistic model had a similar AUC (0.796–0.848). These data indicated that IL-10 and IL-6 may represent potential biomarkers for patients with severe COVID-19. We found significant differences between the severe and non-severe COVID-19 group with regard to a range of clinical characteristics, including respiratory rate, cough, expectoration, dyspnea, asthma, and debilitation. Significant differences were also identified in several laboratory findings; lymphocyte ratio (LYMR), eosinophil ratio (EOSR), monocyte ratio (MONOR), total bilirubin (TBIL), total protein (TP), albumin (ALB), Ca, and URIC were all significantly lower in the severe COVID-19 group, while neutrophil ratio (NEUTR), FIB, aspartate transaminase (AST), glucose (GIU), and HsCRP were all significantly higher. However, the AUCs for these indicators when used to predict severe COVID-19 were all  $<0.690$ . Simple logistic analysis was not suited for the severe COVID-19 group, owing to the feature selection of such a large number of indicators.

We identified significant correlations between each pair for all cytokines except IL-33 and IFN- $\beta$ . In addition, IL-6, IL-10, and IFN- $\beta$  were closely associated with certain laboratory indicators of hepatobiliary function. Similarly, hematocrit (HCT), tBIL, direct bilirubin (DBIL), indirect bilirubin (IBIL), TP, creatine kinase (CK), and myoglobin (Myo) were significantly associated with most cytokines except IL-33, which was not correlated with any of the indices.

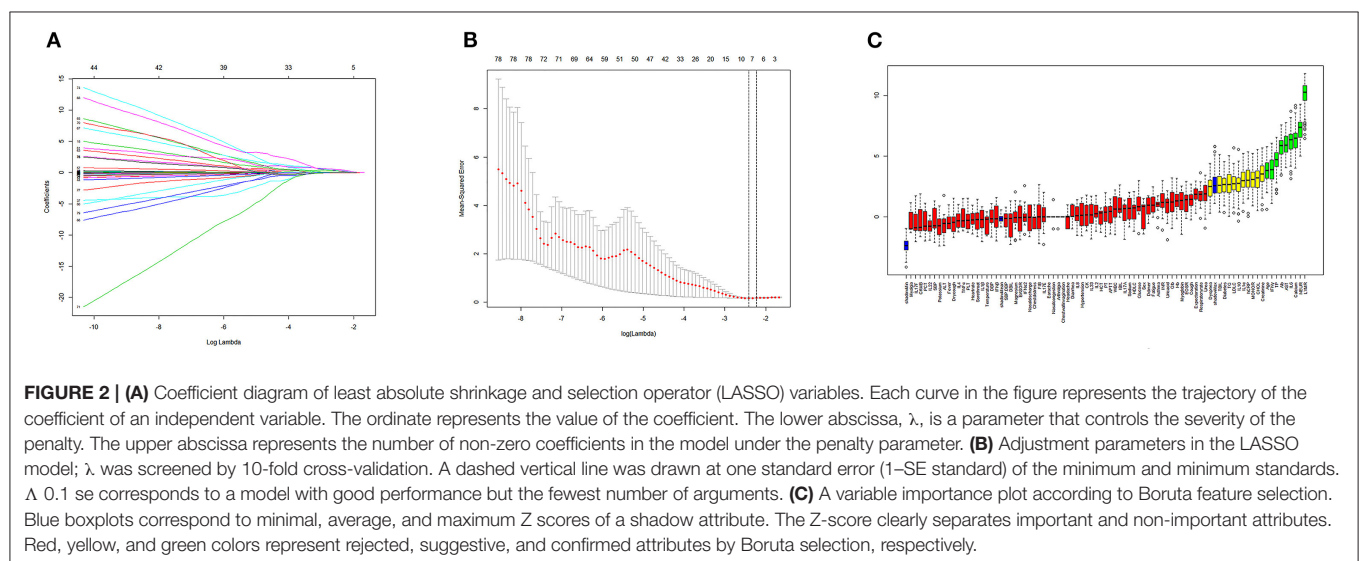
## The Selection of Predictors and Model Construction

Next, we used variation analysis, LASSO regression, and the Boruta algorithm, to select three predictive panels and construct

**TABLE 2 |** Comprehensive performance of three prediction models.

	Model A	Model B	Model C
Variables	IL-6, LYMR, HsCRP, expectoration, dyspnea	ALT, IL-6, expectoration, fatigue, LYMR, AST, CREA	Dyspnea, diabetes, age, IFN- $\gamma$ , IL-6, IL-10, LYMR, NEUR, AST, TP, Alb, Ca
AUC	0.8811	0.9104	0.8574
AIC	80.977	76.582	83.909
Cut-off	0.237	0.256	0.468
Specificity	0.831	0.842	0.958
Sensitivity	0.889	0.897	0.667
Hosmer-Lemeshow test ( $P$ -value)	0.1178	0.4989	0.2986

AIC, Akaike's information criterion; AUC, area under the ROC curve.



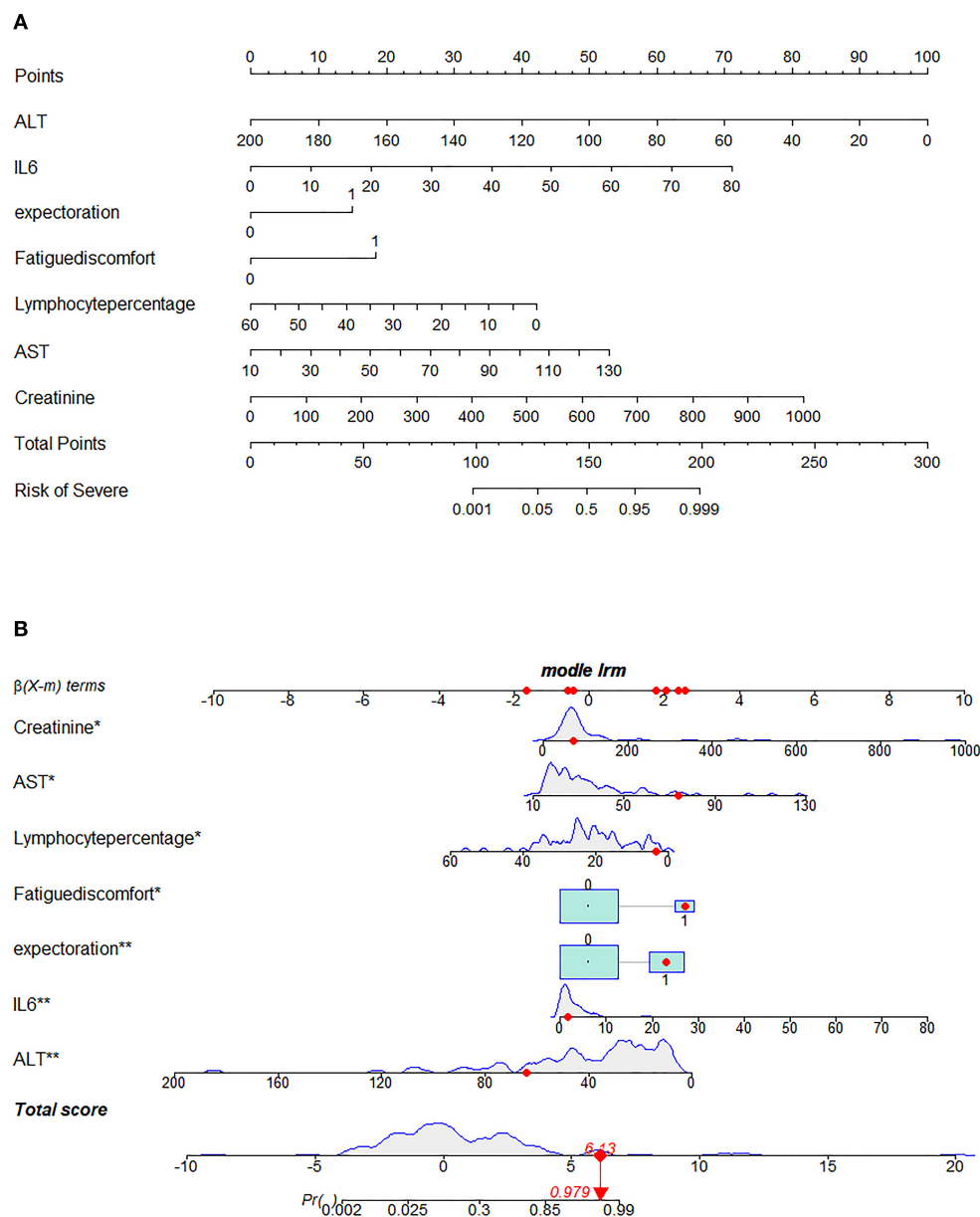


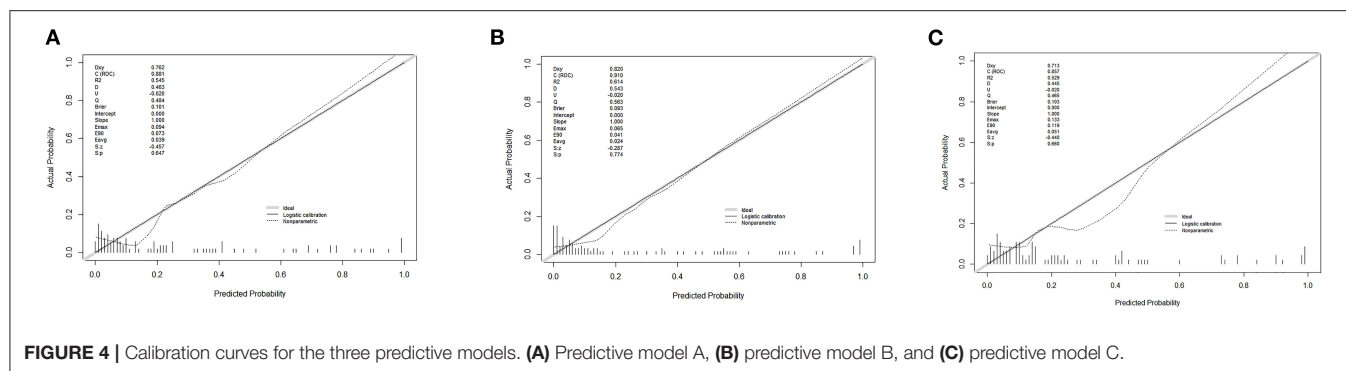
**FIGURE 3 |** Nomogram for predicting severe coronavirus disease 2019 (COVID-19). **(A)** To use the nomogram for an individual patient, the points (top gridline) for each predictor variable are first assigned and the total points calculated. A vertical line from this value on the Total Points gridline then provides a probability for predicting severe COVID-19. The results of the binary variable are encoded as 0 and 1, representing the absence and presence of this symptom, respectively. The calculation is further illustrated in **(B)**, which shows the results of a patient with certain laboratory findings; the probability of this patient progressing to severe COVID-19 is 97.9%.

corresponding predictive models (predictive models A, B, and C, respectively) (Table 2, Figure 2). Predictive model B exhibited a better performance than the other two models in terms of sensitivity, specificity, discrimination, calibration, and clinical net benefit. In addition, the predictors included in this model are objective and universal. An optimal model, with seven features, alanine aminotransferase (ALT), IL-6, expectoration, fatigue, LYMR, AST, and serum creatinine (CREA), were used to generate a nomogram (Figure 3) and were encapsulated as an open-source

online predictive calculator with R/Shiny (<https://severeconid-19prediction.shinyapps.io/SHINY/>).

### Validation of the Online Predictive Model

Finally, we predicted the disease progression of the 108 patients in the validation cohort using our model. The model predicted that 18 patients would progress to severe COVID-19 while the remaining 90 would not. Compared with the follow-up results (91 patients with non-severe COVID-19 and 17 patients with



severe COVID-19), the sensitivity, specificity, PPV, and NPV of our assay were 0.882 (95% CI; 0.622–0.979), 0.967 (95% CI; 0.890–0.991), 0.833 (95% CI; 0.747–0.896), and 0.978 (95% CI; 0.914–0.996), respectively. The model also achieved excellent discrimination (AUC = 0.879), calibration, and clinical net benefit (Figures 4, 5).

## DISCUSSION

The accurate and individualized assessment of a patient who may progress to severe COVID-19 will promote the efficiency of clinical intervention and improve the rational use of medical resources. In the present study, we recruited 206 patients (162 patients with non-severe COVID-19 and 44 patients with severe COVID-19). We analyzed a range of indicators associated with severe COVID-19 and developed a novel predictive model that included ALT, IL-6, expectoration, fatigue, LYMR, AST, and CREA. This model proved to have excellent ability to predict the progression of COVID-19 during hospitalization, in both the derivation and validation cohorts.

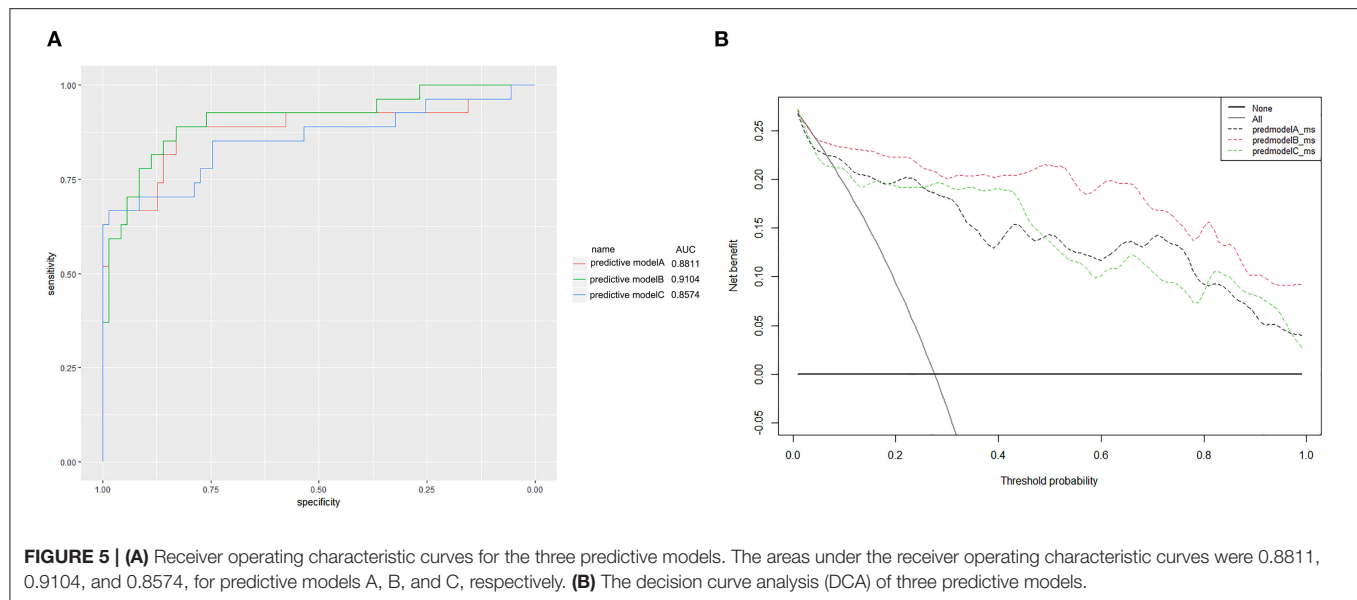
Our final model was visualized in the form of a nomogram and was then packaged into an open-source and free predictive calculator (<https://severeconid-19predction.shinyapps.io/SHINY/>). The model represents a powerful tool with which to aid decision-making and guide treatment strategies for target patients who are at high risk of developing severe progression. The model could also be used to facilitate personalized management.

Previous research reported wide differences in the levels of a large number of cytokines from patients with non-severe and severe COVID-19 (26–28). Our present results identified obvious elevations of various cytokines in patients with severe COVID-19, including IL-1 $\alpha$ , IL-1 $\beta$ , IFN- $\gamma$ , TNF- $\alpha$ , IL-2, IL-4, IL-6, IL-10, and IL-17A. Of these cytokines, IL-6 and IL-10 showed the highest fold-change, thus indicating the presence of a strong inflammatory reaction; this could be a sufficient response to trigger a cytokine storm. Univariate logistic analysis showed that a number of cytokines can be used as predictors for patients with severe illness, although their predictive efficacies can vary considerably; these cytokines could not be used individually. We

also found that underlying diseases (diabetes and hypertension), initial clinical characteristics (cough, expectoration, dyspnea, asthma, and debilitation), and laboratory findings [LYMR ALT, AST, CK, GIU, and procalcitonin (PCT)] were also significantly associated with disease progression, although these were non-specific. The extensive correlation between cytokines and the clinical response spectrum may be explained by multiple organ damage caused by the over-exuberant inflammatory response in severe COVID-19 (12, 29).

Univariate logistic analysis indicated that using a certain evaluation index could not provide sufficient evidence for the prediction of progression and that modeling by data mining may be a more efficient and viable tool with which to compensate for the lack of a single source of information (30). We used the LASSO algorithm and logistic regression and compared different modeling approaches. Finally, we selected a predictive model that included ALT, IL-6, expectoration, fatigue, LYMR, AST, and CREA. Our model achieved satisfactory predictive performance with AUCs of 0.910 and 0.879 in the derivation and validation cohorts, respectively. We also packaged this model into an open-source online format for clinical use. Although several predictive models have been published previously, these studies were associated with obvious limitations, including the fact that they were retrospective reviews or were associated with suboptimal predictive abilities or were not validated externally (31–33). Taking these limitations into account, our study is superior in several respects. First, we considered potential predictors for severe COVID-19 and included a comprehensive dataset retrospectively. Second, our shrinking model, featuring representative key variables, may exhibit better levels of performance than a complex model. This can be supported by the fact that our predictive model was established by comparing several different methods; the optimal method had a significantly higher AUC than the other models; this finding was reconfirmed in the validation cohort. Third, the predictive model was used to create a nomogram that was then used to generate an open-source online calculator format with visualization and maneuverability function.

There are also some limitations associated with our study that need to be considered. For example, we mainly focused on the changes of symptoms and the levels of key indicators



in patients after SARS-CoV-2 infection and did not consider the influence of individual differences on the progression of disease. More in-depth investigations and longitudinal dynamic monitoring studies now need to be conducted to explain the specific characteristics of the potential predictors. Furthermore, the predictive model needs to be validated in a larger patient cohort and other populations outside of China.

## CONCLUSION

In this study, we developed and validated an online predictive calculator that provides personalized probability for the progression of disease based on seven commonly used variables. The model will be vital for early personalized management, to promote the appropriate allocation of medical resources, and to ensure that patients who may develop severe COVID-19 can receive appropriate treatment as soon as possible.

## DATA AVAILABILITY STATEMENT

The original contributions presented in the study are included in the article/**Supplementary Material**, further inquiries can be directed to the corresponding author/s.

## ETHICS STATEMENT

The studies involving human participants were reviewed and approved by West China Hospital, Sichuan University Medical Ethics Committee. The patients/participants provided their written informed consent to participate in this study.

## AUTHOR CONTRIBUTIONS

ZM and MW designed the research and wrote the manuscript. ZZ and YoZ responsible for the recruitment of COVID-19 patients and clinical treatment. YW and SG responsible for the detection of candidate biomarkers. ML, SY, and YaZ responsible for collecting and organizing data. All authors contributed to the article and approved the submitted version.

## FUNDING

This study was supported by the Sichuan Provincial Department of Science and Technology Program (References: 2020YFS0002 and 2020YFS0004) and the Science and Technology Project of West China Hospital (Reference: HX-2019-nCov-066).

## ACKNOWLEDGMENTS

The authors would like to express their gratitude to EditSprings (<https://www.editsprings.com/>) for the expert linguistic services provided.

## SUPPLEMENTARY MATERIAL

The Supplementary Material for this article can be found online at: <https://www.frontiersin.org/articles/10.3389/fmed.2021.663145/full#supplementary-material>

**Supplementary Figure 1 |** Box plots of continuous variables.

**Supplementary Figure 2 |** Bar plots of categorical variables.

**Supplementary Figure 3 |** ROC curves for each single cytokine and a combined panel of cytokines.



## REFERENCES

1. Yao D, Yan K, Duan J, Zhang X, Zhou L. Coronavirus disease 2019 (COVID-19): prevention and control in gynecological outpatient clinic. *Front Public Health*. (2020) 8:618494. doi: 10.3389/fpubh.2020.618494
2. Zhou F, Yu T, Du R, Fan G, Liu Y, Liu Z, et al. Clinical course and risk factors for mortality of adult inpatients with COVID-19 in Wuhan, China: a retrospective cohort study. *Lancet*. (2020) 395:1054–62. doi: 10.1016/S0140-6736(20)30566-3
3. Sun L, Song F, Shi N, Liu F, Li S, Li P, et al. Combination of four clinical indicators predicts the severe/critical symptom of patients infected COVID-19. *J Clin Virol*. (2020) 128:104431. doi: 10.1016/j.jcv.2020.104431
4. Zheng YL, He YK, Ma XQ, Gao ZC. Feasibility of coronavirus disease 2019 eradication. *Chin Med J*. (2020) 133:1387–9. doi: 10.1097/CM9.0000000000000936
5. Kim SR, Nam SH, Kim YR. Risk factors on the progression to clinical outcomes of COVID-19 patients in South Korea: using national data. *Int J Environ Res Public Health*. (2020) 17:8847. doi: 10.3390/ijerph17238847
6. Alhazzani W, Moller MH, Arabi YM, Loeb M, Gong MN, Fan E, et al. Surviving sepsis campaign: guidelines on the management of critically ill adults with coronavirus disease 2019 (COVID-19). *Crit Care Med*. (2020). 48:E440–69. doi: 10.1097/CCM.00000000000004363
7. Hossein-khannazer N, Shokoohian B, Shpichka A, Aghdaei HA, Timashev P, Vosough M. Novel therapeutic approaches for treatment of COVID-19. *J Mol Med*. (2020) 98:789–803. doi: 10.1007/s00109-020-01927-6
8. Yadav P, Vats R, Bano A, Bhardwaj R. Mesenchymal stem cell immunomodulation and regeneration therapeutics as an ameliorative approach for COVID-19 pandemics. *Life Sci*. (2020) 263:8588. doi: 10.1016/j.lfs.2020.118588
9. Xu R, Hou KK, Zhang K, Xu HY, Zhang N, Fu H, et al. Performance of two risk-stratification models in hospitalized patients with coronavirus disease. *Front Med-Lausanne*. (2020) 7:518. doi: 10.3389/fmed.2020.00518
10. Jamwal S, Gautam A, Elsworth J, Kumar M, Chawla R, Kumar P. An updated insight into the molecular pathogenesis, secondary complications and potential therapeutics of COVID-19 pandemic. *Life Sci*. (2020) 257:118105. doi: 10.1016/j.lfs.2020.118105
11. Wiersinga WJ, Rhodes A, Cheng AC, Peacock SJ, Prescott HC. Pathophysiology, transmission, diagnosis, and treatment of coronavirus disease 2019 (COVID-19) A review. *JAMA-J Am Med Assoc*. (2020) 324:782–93. doi: 10.1001/jama.2020.12839
12. Tian JB, Yuan XL, Xiao J, Zhong Q, Yang CG, Liu B, et al. Clinical characteristics and risk factors associated with COVID-19 disease severity in patients with cancer in Wuhan, China: a multicentre, retrospective, cohort study. *Lancet Oncol*. (2020) 21:893–903. doi: 10.1016/S1470-2045(20)30309-0
13. Luo Y, Mao LY, Yuan X, Xue Y, Lin Q, Tang GX, et al. Prediction model based on the combination of cytokines and lymphocyte subsets for prognosis of SARS-CoV-2 infection. *J Clin Immunol*. (2020) 40:960–9. doi: 10.1007/s10875-020-00821-7
14. Gong J, Ou JY, Qiu XP, Jie YS, Chen YQ, Yuan LX, et al. A tool for early prediction of severe coronavirus disease 2019 (COVID-19): a multicenter study using the risk Nomogram in Wuhan and Guangdong, China. *Clin Infect Dis*. (2020). 71:833–40. doi: 10.1093/cid/ciaa443
15. Hu CY, Liu ZQ, Jiang YF, Shi OM, Zhang X, Xu KL, et al. Early prediction of mortality risk among patients with severe COVID-19, using machine learning. *Int J Epidemiol*. (2020) 49:1918–29. doi: 10.1101/2020.04.13.20064329
16. Edalatfard M, Akhtari M, Salehi M, Naderi Z, Jamshidi A, Mostafaei S, et al. Intravenous methylprednisolone pulse as a treatment for hospitalised severe COVID-19 patients: results from a randomised controlled clinical trial. *Eur Respir J*. (2020) 56:2002808. doi: 10.1183/13993003.02808-2020
17. Marfia G, Navone S, Guarnaccia L, Campanella R, Mondoni M, Locatelli M, et al. Decreased serum level of sphingosine-1-phosphate: a novel predictor of clinical severity in COVID-19. *Embo Mol Med*. (2021) 13:e13424. doi: 10.15252/emmm.202013424
18. Michel-Kabamba N, Ngatu NR, Leon-Kabamba N, Katumbo-Mukemo A, Mukuku O, Ngoyi-Mukonkole J, et al. Occupational COVID-19 prevention among congolese healthcare workers: knowledge, practices, PPE compliance, and safety imperatives. *Trop Med Infect Dis*. (2021) 6:6. doi: 10.3390/tropicalmed6010006
19. Wynants L, Van Calster B, Bonten MMJ, Collins GS, Debray TPA, De Vos M, et al. Prediction models for diagnosis and prognosis of covid-19 infection: systematic review and critical appraisal. *Bmj-Brit Med J*. (2020) 369:m1328. doi: 10.1101/2020.03.24.20041020
20. Li Q, Zhang JL, Ling Y, Li WX, Zhang XY, Lu HZ, et al. A simple algorithm helps early identification of SARS-CoV-2 infection patients with severe progression tendency. *Infection*. (2020) 48:577–84. doi: 10.1007/s15010-020-01446-z
21. Dong YL, Zhou HF, Li MY, Zhang ZL, Guo WN, Yu T, et al. A novel simple scoring model for predicting severity of patients with SARS-CoV-2 infection. *Transbound Emerg Dis*. (2020) 67:2823–9. doi: 10.1111/tbed.13651
22. Shen B, Yi X, Sun YT, Bi XJ, Du JP, Zhang C, et al. Proteomic and metabolomic characterization of COVID-19 patient sera. *Cell*. (2020) 182:59. doi: 10.1016/j.cell.2020.05.032
23. MacWilliam D, Kowalewski J, Kumar A, Pontrello C, Ray A. Signaling mode of the broad-spectrum conserved CO<sub>2</sub> receptor is one of the important determinants of odor valence in drosophila. *Neuron*. (2018) 97:1153. doi: 10.1016/j.neuron.2018.01.028
24. Rubbens P, Schmidt ML, Props R, Biddanda BA, Boon N, Waegeman W, et al. Randomized lasso links microbial taxa with aquatic functional groups inferred from flow cytometry. *Msystems*. (2019) 4:e00093-19. doi: 10.1128/mSystems.00093-19
25. Muntner P, Colantonio LD, Cushman M, Goff DC, Howard G, Howard VJ, et al. Validation of the atherosclerotic cardiovascular disease pooled cohort risk equations. *JAMA-J Am Med Assoc*. (2014) 311:1406–15. doi: 10.1001/jama.2014.2630
26. Udomsinprasert W, Jittikoon J, Sangroongruangsri S, Chaikledkaew U. Circulating levels of interleukin-6 and interleukin-10, but not tumor necrosis factor-alpha, as potential biomarkers of severity and mortality for COVID-19: systematic review with meta-analysis. *J Clin Immunol*. (2021) 41:11–22. doi: 10.1007/s10875-020-00899-z
27. Ahmad T, Chaudhuri R, Joshi MC, Almatroudi A, Rahmani AH, Ali SM. COVID-19: the emerging immunopathological determinants for recovery or death. *Front Microbiol*. (2020) 11:588409. doi: 10.3389/fmicb.2020.588409
28. Mannino F, Bitto A, Irrera N. Severe acute respiratory syndrome coronavirus-2 induces cytokine storm and inflammation during coronavirus disease 19: perspectives and possible therapeutic approaches. *Front Pharmacol*. (2020) 11:592169. doi: 10.3389/fphar.2020.592169
29. Reznik SE, Tiwari AK, Ashby CR. Edaravone: a potential treatment for the COVID-19-induced inflammatory syndrome? *Pharmacol Res*. (2020) 160:105055. doi: 10.1016/j.phrs.2020.105055
30. Wang W, Zhang YF, Liu MX, Wang Y, Yang T, Li DS, et al. TIMP2 is a poor prognostic factor and predicts metastatic biological behavior in gastric cancer. *Sci Rep-Uk*. (2018) 8:9629. doi: 10.1038/s41598-018-27897-x
31. Bello-Chavolla OY, Antonio-Villa NE, Ortiz-Brizuela E, Vargas-Vazquez A, Gonzalez-Lara ME, de Leon AP, et al. Validation and repurposing of the MSL-COVID-19 score for prediction of severe COVID-19 using simple clinical predictors in a triage setting: The Nutri-CoV score. *PLoS ONE*. (2020) 15:244051. doi: 10.1371/journal.pone.0244051
32. Xiao LS, Li P, Sun FL, Zhang YP, Xu CH, Zhu HB, et al. Development and validation of a deep learning-based model using computed tomography imaging for predicting disease severity of coronavirus disease 2019. *Front Bioeng Biotech*. (2020) 8:898. doi: 10.3389/fbioe.2020.00898
33. Xiao LS, Zhang WF, Gong MC, Zhang YP, Chen LY, Zhu HB, et al. Development and validation of the HNC-LL score for predicting the severity of coronavirus disease 2019. *Ebiomedicine*. (2020) 57:102880. doi: 10.1016/j.ebiom.2020.102880

**Conflict of Interest:** The authors declare that the research was conducted in the absence of any commercial or financial relationships that could be construed as a potential conflict of interest.

Copyright © 2021 Meng, Wang, Zhao, Zhou, Wu, Guo, Li, Zhou, Yang, Li and Ying. This is an open-access article distributed under the terms of the Creative Commons Attribution License (CC BY). The use, distribution or reproduction in other forums is permitted, provided the original author(s) and the copyright owner(s) are credited and that the original publication in this journal is cited, in accordance with accepted academic practice. No use, distribution or reproduction is permitted which does not comply with these terms.

## GLOSSARY

AIC, Akaike information criterion; ALB, albumin; ALT, alanine aminotransferase; APTT, activated partial thromboplastin time; AST, aspartate transaminase; AUC, area under the ROC curve; BASOR, basophil ratio; CHOL, cholesterol; CK, creatine kinase; CREA, serum creatinine; DBIL, direct bilirubin; DBP, diastolic blood pressure; DCA, decision curve analysis; DM, diabetes; EOSR, eosinophil ratio; FIB, fibrinogen; GLB, globulin; GLU, glucose; Hb, hemoglobin; HCT, hematocrit; HDL-C, high-density lipoprotein cholesterol; HLP, hyperlipidemia; HP, hypertension; HsCRP, high-sensitivity C reactive protein; IBIL, indirect bilirubin; IFN, interferon; IL, interleukins; INR, International Normalized Ratio; LDL-C, low-density lipoprotein cholesterol; LYMR, lymphocyte ratio; MONOR, monocyte ratio; Myo, myoglobin; NEUTR, neutrophil ratio; PCT, procalcitonin; PLT, platelets; PT, prothrombin time; ROC, receiver operating characteristic; SBP, systolic blood pressure; TBIL, total bilirubin; TG, triglyceride; TNE, tumor necrosis factor; TP, total protein; URIC, uric acid; WBC, white blood cell.



# Initial PCR Testing Negative, but Chest CT Suggesting for Viral Pneumonia Urges for Repeated Testing for COVID-19 Diagnosis

Lingwei Wang<sup>1,2†</sup>, Danting Zhan<sup>1,2†</sup>, Xiaodi Liu<sup>3†</sup>, Kai Yang<sup>1,2†</sup>, Shipin Wu<sup>3</sup>, Heng Zhang<sup>1,2</sup>, Min Yu<sup>1,2</sup>, Yimin Zha<sup>1,2</sup>, Weibin Huang<sup>1,2</sup>, Lei Li<sup>4\*</sup>, Rongchang Chen<sup>1,2\*</sup> and Chen Qiu<sup>1,2\*</sup>

<sup>1</sup>The Department of Respiratory Diseases and Critic Care Unit, Shenzhen Institute of Respiratory Diseases, Shenzhen People's Hospital (The Second Clinical Medical College, Jinan University; The First Affiliated Hospital, Southern University of Science and Technology), Shenzhen, China, <sup>2</sup>Shenzhen Key Laboratory of Respiratory Diseases, Shenzhen Major Respiratory Diseases's Prevention and Treatment Center, Shenzhen, China, <sup>3</sup>Department of Infectious Diseases, Shenzhen People's Hospital (The Second Clinical Medical College, Jinan University; The First Affiliated Hospital, Southern University of Science and Technology), Shenzhen, China, <sup>4</sup>Guangdong Provincial Key Laboratory of Brain Connectome and Behavior, CAS Key Laboratory of Brain Connectome and Manipulation, The Brain Cognition and Brain Disease Institute (BCBDI), Shenzhen Institutes of Advanced Technology, Chinese Academy of Sciences, Shenzhen-Hong Kong Institute of Brain Science-Shenzhen Fundamental Research Institutions, Shenzhen, China

## OPEN ACCESS

### Edited by:

Wen Li,  
Zhejiang University, China

### Reviewed by:

Chao Zhang,  
Zhejiang University, China  
Jun Gang Xie,  
Huazhong University of Science and  
Technology, China

### \*Correspondence:

Lei Li  
saralilei@siat.ac.cn  
Rongchang Chen  
chenrc@vip.163.com  
Chen Qiu  
szcheater@163.com

<sup>†</sup>These authors have contributed  
equally to this work

### Specialty section:

This article was submitted to  
Molecular Diagnostics  
and Therapeutics,  
a section of the journal  
Frontiers in Molecular Biosciences

**Received:** 12 December 2020

**Accepted:** 30 April 2021

**Published:** 26 May 2021

### Citation:

Wang L, Zhan D, Liu X, Yang K, Wu S,  
Zhang H, Yu M, Zha Y, Huang W, Li L,  
Chen R and Qiu C (2021) Initial PCR  
Testing Negative, but Chest CT  
Suggesting for Viral Pneumonia Urges  
for Repeated Testing for COVID-19  
Diagnosis.  
Front. Mol. Biosci. 8:640788.  
doi: 10.3389/fmolb.2021.640788

**Keywords:** COVID-19, chest CT, PCR test, pneumonia, diagnosis

## INTRODUCTION

The COVID-19 pandemic has become one of the major health crises worldwide (Guan et al., 2020). PCR testing of SARS-CoV-2 is generally used as the gold standard of confirmation for diagnostics of COVID-19. With the growing awareness of the high false-negative rates of PCR testing (Ai et al., 2020; Yang et al., 2020b), whether and which subgroup of patients with initial negative results should be subjected to repeated testing is a matter that requires more clinical data.

Under this circumstance, the value of chest CT as a screening tool in COVID-19 has been vigorously discussed (Ai et al., 2020; Bao et al., 2020; ; Merkus and Klein, 2020). A recent report with 1,014 cases (Ai et al., 2020; Bao et al., 2020) proposed that chest CT has a high sensitivity for the diagnosis of COVID-19 and may be considered as a primary tool for COVID-19 screening. Others have called for caution regarding the usage of CT due to its ionizing radiation, and some have specified its unsuitability as a screening tool for pediatric patients (Merkus and Klein, 2020). After evaluation, our triaging procedure and diagnostic practice for a total of 358 outpatients (149 COVID-19-suspected cases including 13 confirmed) at Shenzhen People's Hospital, Shenzhen, China, we found that chest CT can distinguish COVID-19 patients from suspected cases (AUC = 0.85) much better than other indicators (AUCs < 0.65) without PCR testing, including epidemiological history, symptoms, white blood cell (WBC) count, and lymphocyte count. Therefore, we propose chest CT as a main tool in determining which subgroup of suspected patients should be subjected to repeated tests after their initial negative PCR testing for SARS-CoV-2.

The first COVID-19 patient was admitted on January 9, 2020 in Shenzhen, an international city with a population of 13.43 million. Different levels of responsive strategies were quickly developed under the pressure of the highly contagious pandemic (Yang et al., 2020a). We received 358 patients at the emergency department and fever clinic with fever or upper respiratory syndromes from January 2020 to March 2020 in our hospital. Among them, 149 were classified as COVID-19-suspected cases according to the criteria complying with the guidelines for the diagnosis and treatment of novel coronavirus pneumonia issued by the

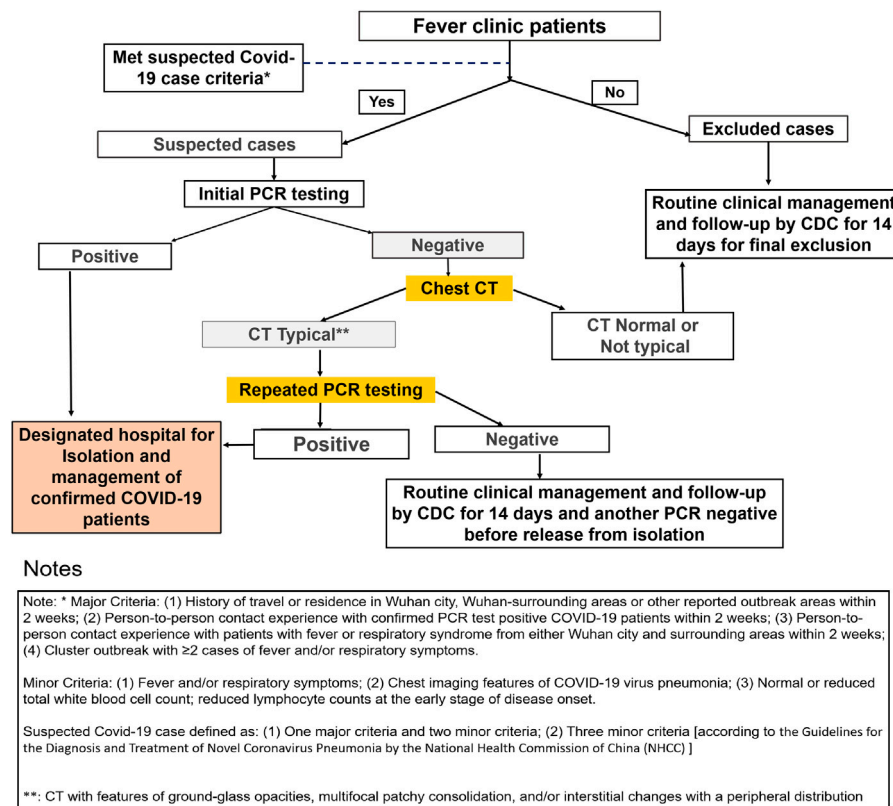


**FIGURE 1 |** Fever clinic patients were efficiently triaged and diagnosed for COVID-19. The false-negative rate for initial PCR testing is 30.8% (4 out of 13). A high percentage (8.9%) of the initial PCR testing-negative patients with typical CT signature were confirmed to be COVID-19 positive after repeated testing. Initial PCR testing-negative results but chest CT-positive results for viral pneumonia urges for repeated testing for COVID-19 diagnosis.

National Health Commission of China (NHCC) (National Health Commission and State Administration of Traditional Chinese Medicine, 2020) and required by at least two COVID-19 specialists, and they were subjected to our triaging procedure for suspected cases. Among all 149 patients, after tests and evaluation, 22 patients who were confirmed or highly suspected with COVID-19 were transferred to a special neighboring hospital in Shenzhen that has a special ward for the COVID-19 outbreak.

Our initial oropharyngeal swab PCR testing confirmed 9 SARS-CoV-2-positive patients and 140 negative patients. Expert consultation, chest CT scan, blood WBC counting, epidemiology investigation, and further repeated PCR tests revealed that four patients of the 140 with initial negative PCR tests were false-negative, making the final COVID-19 patient number up to 13. The false-negative initial PCR testing accounts for 30.8% (4 out of 13) of the total confirmed cases (**Figure 1**), with a true-positive rate of initial PCR test of 69.2% (9 out of 13). This is in line with the reported positive rate from 30 to 60% (Ai et al., 2020) and suggests that additional diagnostic procedures should be carried out after initial negative PCR testing before patients are being subjected to routine clinical follow-up.

## SUBSECTIONS RELEVANT FOR THE SUBJECT

### The Description of Four Patients With Positive Computed Tomography and Initial Negative Reverse-Transcription Polymerase Chain Reaction Test

**Patient 1:** A 35-year-old male with fever for 6 days, with a recent travel history to Wuhan, China, where the pandemic was going on at that time, visited the hospital. Although the initial PCR test for SARS-CoV-2 was negative, the chest CT (January 26, 2020) showed multifocal ground-glass opacity (GGO) and parenchyma consolidation, predominantly involving subpleural regions of both the lungs. A routine blood test showed that the WBC count was  $5.24 \times 10^9/L$ , and the absolute value of the lymphocyte count was  $0.87 \times 10^9/L$ . However, the patient met the diagnostic criteria for a suspected COVID-19 patient and was quarantined at the hospital. The PCR test was repeated with bronchoalveolar lavage fluid (BALF), and the result was positive.

**Patient 2:** A 76-year-old female with fatigue and drowsiness, and with no fever visited the hospital. She had a travel history to Wuhan during the COVID-19 outbreak period. Although the



initial PCR test for SARS-CoV-2 was negative, the chest CT (January 23, 2020) showed multifocal parenchyma. A routine blood test showed that the WBC count was  $6.96 \times 10^9/L$ , while the absolute value of the lymphocyte count was  $1.09 \times 10^9/L$ . The second throat swab test was positive. Patient 3: A 66-year-old female appeared with cough and sputum but had no fever. She had a travel history from Wuhan in January 2020. The first swab test was negative. The chest CT (January 25, 2020) showed a bit of GGO. A routine blood test showed that the WBC count was  $4.9 \times 10^9/L$ , and the absolute value of the lymphocyte count was  $1.27 \times 10^9/L$ . A repeated nasopharyngeal swab for the PCR test was positive, and follow-up chest CT showed typical GGO consistent with COVID-19. Patient 4: A 78-year-old male with fever, cough, and sputum, and a recent travel history to Wuhan, China, visited the hospital in January 2020. The first throat swab test was negative. The chest CT (January 25, 2020) showed multifocal GGO. A routine blood test showed that the WBC count was  $4.53 \times 10^9/L$ , and the absolute value of the lymphocyte count was  $0.96 \times 10^9/L$ . However, the patient met the diagnostic criteria for suspected COVID-19 and was quarantined in the hospital. A repeated nasopharyngeal swab for the PCR test was positive.

## Influence of Different Indexes on the Diagnosis of COVID-19

Variable positive rates of the PCR test may be associated with sample collection, PCR methodology, and developing stages of COVID-19 in patients (Ai et al., 2020). Two articles reported using specimens from nasopharyngeal swabs showed a higher positive PCR test rate than oropharyngeal swabs (Tan et al., 2020; Xiao et al., 2020). For the high false-negative rate of the initial PCR test (30.8%), it is necessary to do repeated tests. To avoid occupation of limited hospital resources and speed up the screening procedure, it is not practical to test all the initial PCR-negative patients repeatedly. One parameter or a cluster of test parameters would help in selecting the most possible COVID-19 patients among all the initial PCR test-negative cases.

Typical chest CT refers to ground-glass opacities, multifocal patchy consolidation, and/or interstitial changes with a peripheral distribution (National Health Commission and State Administration of Traditional Chinese Medicine, 2020). The sensitivity and the specificity of typical chest CT in suggesting COVID-19 among all 149 suspected cases are 100% (13/13) and 69.85% (95/136), respectively. A positive WBC parameter means a normal or decreased WBC count (National Health Commission and State Administration of Traditional Chinese Medicine, 2020; National Institutes of Health, 2020). The sensitivity and the specificity of WBC counting in suggesting COVID-19 among all 149 suspected cases are 100% (13/13) and 0.74% (1/136), respectively. The specificity of WBC counting is much lower than that of chest CT. The sensitivity and the specificity of the combination of chest CT positive and WBC counting are 100% (13/13) and 70.59% (96/136), respectively, with not much improvement compared with using chest CT alone as a parameter. When we used the strict parameter combinations in our study according to the guideline of the NHCC, which includes fever/cough, positive result of chest CT

manifestations, and WBC counting, along with epidemiology characteristic (history of traveling to Wuhan or being in close contact with COVID-19 patients), the sensitivity and the specificity in suggesting COVID-19 among all suspected cases are 84.62% (11/13) and 88.24% (120/136), respectively. Although the specificity increases from 69.85 to 88.24%, the sensitivity decreases from 100 to 84.62% when compared with using chest CT alone as a parameter.

## DISCUSSION

Among the 140 initial PCR test-negative patients, 95 showed normal chest CT, and they were excluded from the diagnosis of COVID-19 and released after another PCR test confirmation complying with the NHCC guideline. For the 45 cases with pneumonia CT features, 40 were classified as not typical COVID-19 CT presentation, and four were classified as typical COVID-19 CT presentation. In these four cases, repeated PCR tests revealed all positive results (**Figure 1**), which account for 8.9% (4 out of 45) of the “initial PCR testing negative but chest CT positive for viral pneumonia” group. This is quite a high percentage considering the high contagious nature of SARS-CoV-2. We strongly suggest that for patients with initial PCR testing-negative results but chest CT positive, repeated PCR tests should be carried out. Here we are not considering chest CT as an alternative screening tool to replace the PCR test for COVID-19 but rather proposing that chest CT serves well as a tool in determining which subgroup of suspected patients should be subjected to repeated tests after their negative initial PCR testing for SARS-CoV-2.

Among our 140 initial PCR-negative cases, the sensitivity and the specificity of chest CT in suggesting COVID-19 are 100% (4/4) and 69.85% (95/136), respectively; the sensitivity and the specificity of WBC counting are 100% (4/4) and 0.74% (1/136), respectively; and the sensitivity and the specificity of combined parameters (fever/cough, chest CT, WBC counting, and epidemiology characteristic) are 50.0% (2/4) and 88.24% (120/136), respectively. Considering both the sensitivity and the specificity, chest CT proves to be the most powerful parameter in suggesting COVID-19 among initial PCR-negative cases. In our study, upon using chest CT as a parameter, the repeated PCR testing pressure was reduced by 67.9% (95 out of 145) (**Figure 1**). All of the CT nontypical cases among the initial negative testing cases were excluded from COVID-19 diagnosis (confirmed by repeat PCR before releasing and then followed up). Altogether, in our study, chest CT serves well as a tool in determining what kind of suspected patients should be subjected to repeated tests after their negative initial PCR testing for SARS-CoV-2.

As demonstrated in **Figure 1**, our triage operation process showed a high performance, with a screening rate of 14.77% (22/149) in COVID-19-suspected patients to be sent to the special ward, while the screening rate was 0% (0/209) for non-suspected outpatients. For all 149 suspected cases, the top four diagnoses were upper respiratory tract infection (54/149), community-acquired pneumonia (53/149), COVID-19 (13/149), and gastroenteritis (5/149). This suggests that upper respiratory

tract infection and community-acquired pneumonia should be emphasized and excluded from the COVID-19 diagnostic process to avoid the occupation of hospital resources. Till date, all 13 confirmed patients have recovered and were discharged.

Our clinical practice showed that with an initial PCR positive rate of 69.2% in those finally confirmed COVID-19 cases, further testing and repeated PCR testing for subgroups of the initial PCR test–negative patients should be emphasized. In a recently published article, it was stated that to compensate for the potential risk of false-negative PCR, chest CT should be applied for clinically suspected patients with negative initial RT-PCR (He et al., 2020), and repeated swab tests should be carried out (Xie et al., 2020). In terms of chest imaging findings, the less pulmonary consolidation found *via* CT scan, the greater the possibility of negative initial RT-PCR results (Chen et al., 2021).

Our study had limitations. First, the limitation of the hospital and the confirmed patient resources is an unavoidable problem for this study. However, from another perspective, as the vaccines are developed and applied, suspected or confirmed patients of COVID-19 infection will be reduced in number. The idea in this opinion article is to somehow provide clinical instruction. Second, the PCR result is affected by many factors, such as laboratory reagents, test methods, and subjective performance. However, at this time, the nucleic acid detection method is not mature yet, and our research results are more important. We try to provide evidence to support the importance of chest CT scan in

“work protocol for fever clinic” in detection of COVID-19 patients. In our protocol, chest CT does not serve as a screening tool but as an important indicator for follow-up and repeated PCR testing after initial PCR-negative results. We provide more evidence to show that this work protocol could provide high sensitivity and acceptable specificity, which are better than other criteria and able to reduce the missed diagnosis of false-negative nucleic acid patients.

## AUTHOR CONTRIBUTIONS

All authors listed have made a substantial, direct, and intellectual contribution to the work and approved it for publication.

## FUNDING

This work was supported by the emergency research project of coronavirus 2019 infection of Zhejiang University (No. 2020XGZX024), the National Natural Science Foundation of China (NSFC31971072, NSFC31471109), the Guangdong International Cooperation grant (2019A050510032), the China Shenzhen Science Technology and Innovative Commission (SZSTI JCYJ20180508152336419 and 20170307095633450), and the grant of Shenzhen Health commission (SZLY 2017024).

## REFERENCES

- Ai, T., Yang, Z., Hou, H., Zhan, C., Chen, C., Chen, C., et al. (2020). Correlation of Chest CT and RT-PCR Testing in Coronavirus Disease 2019 (COVID-19) in China: A Report of 1014 Cases. *Radiology* 296, E32–E40. doi:10.1148/radiol.2020200642
- Bao, C., Liu, X., Zhang, H., Li, Y., and Liu, J. (2020). Coronavirus Disease 2019 (COVID-19) CT Findings: A Systematic Review and Meta-Analysis. *J. Am. Coll. Radiol.* 17, 701–709. doi:10.1016/j.jacr.2020.03.006
- Chen, D., Jiang, X., Hong, Y., Wen, Z., Wei, S., Peng, G., et al. (2021). Can Chest CT Features Distinguish Patients with Negative from Those with Positive Initial RT-PCR Results for Coronavirus Disease (COVID-19)? *AJR Am. J. Roentgenol* 216, 66–70. doi:10.2214/AJR.20.23012
- Guan, W., Ni, Z., Hu, Y., Liang, W., Ou, C., He, J., et al. (2020). Clinical Characteristics of Coronavirus Disease 2019 in China. *N. Engl. J. Med.* 382, 1708–1720. doi:10.1056/NEJMoa2002032
- He, J. L., Luo, L., Luo, Z. D., Lyu, J. X., Ng, M. Y., Shen, X. P., et al. (2020). Diagnostic Performance between CT and Initial Real-Time RT-PCR for Clinically Suspected 2019 Coronavirus Disease (COVID-19) Patients outside Wuhan, China. *Respir. Med.* 168, 105980. doi:10.1016/j.rmed.2020.105980
- Merkus, P. J., and Klein, W. M. (2020). Value of Chest CT as COVID 19 Screening Tool in Children. *Eur. Respir. J.* 55, 2001241. doi:10.1183/13993003.01241-2020
- National Health Commission and State Administration of Traditional Chinese Medicine (2020). Diagnosis and Treatment Protocol for Novel Coronavirus Pneumonia (Trial Version 7). Available online at: <http://www.nhc.gov.cn/yzygj/s7653p/202003/46c9294a7dfe4cef80dc7f59> (Accessed March 3, 2020).
- National Institutes of Health (2020). Coronavirus Disease 2019 (COVID-19) Treatment Guidelines. Available online at: <https://www.covid19treatmentguidelines.nih.gov/> (Accessed March 3, 2020).
- Tan, L., Wang, X., Liu, W., Lu, Y., Cheng, L., and Sun, Z. (2020). Comparison of Nasopharyngeal and Oropharyngeal Swabs for SARS-CoV-2 Detection in 353 Patients Received Tests with Both Specimens Simultaneously. *Int. J. Infect. Dis.* 94, 107–109. doi:10.1016/j.ijid.2020.04.023
- Xiao, A., Tong, Y., Gao, C., Zhu, L., Zhang, Y., and Zhang, S. (2020). Dynamic Profile of RT-PCR Findings from 301 COVID-19 Patients in Wuhan, China: A Descriptive Study. *J. Clin. Virol.* 127, 104346. doi:10.1016/j.jcv.2020.104346
- Xie, X., Zhong, Z., Zhao, W., Zheng, C., Wang, F., and Liu, J. J. R. (2020). Chest CT for Typical 2019-nCoV Pneumonia: Relationship to Negative RT-PCR Testing. *Radiology* 296, 200343. doi:10.1148/radiol.2020200343
- Yang, K., Wang, L., Li, F., Chen, D., Li, X., Qiu, C., et al. (2020a). The Influence of Preventive Strategies on the COVID-2019 Epidemic in Shenzhen, China. *Eur. Respir. J.* 55, 2000599. doi:10.1183/13993003.00599-2020
- Yang, Y., Yang, M., Shen, C., Wang, F., Yuan, J., Li, J., et al. (2020b). Evaluating the Accuracy of Different Respiratory Specimens in the Laboratory Diagnosis and Monitoring the Viral Shedding of 2019-nCoV Infections. doi:10.1101/2020.02.11.20021493

**Conflict of Interest:** The authors declare that the research was conducted in the absence of any commercial or financial relationships that could be construed as a potential conflict of interest.

Copyright © 2021 Wang, Zhan, Liu, Yang, Wu, Zhang, Yu, Zha, Huang, Li, Chen and Qiu. This is an open-access article distributed under the terms of the Creative Commons Attribution License (CC BY). The use, distribution or reproduction in other forums is permitted, provided the original author(s) and the copyright owner(s) are credited and that the original publication in this journal is cited, in accordance with accepted academic practice. No use, distribution or reproduction is permitted which does not comply with these terms.



# An Illustrated Guide to the Imaging Evolution of COVID in Non-Epidemic Areas of Southeast China

Lihua Wang<sup>1</sup>, Yeerfan Jiaerken<sup>1</sup>, Qian Li<sup>1</sup>, Peiyu Huang<sup>1</sup>, Zhuqing Shen<sup>1</sup>, Tongtong Zhao<sup>2</sup>, Hanpeng Zheng<sup>3</sup>, Wenbin Ji<sup>4</sup>, Yuantong Gao<sup>5</sup>, Junli Xia<sup>6</sup>, Jianmin Cheng<sup>7</sup>, Jianbing Ma<sup>8</sup>, Jun Liu<sup>9</sup>, Yongqiang Liu<sup>10</sup>, Miaoguang Su<sup>11</sup>, Guixiang Ruan<sup>12</sup>, Jiner Shu<sup>13</sup>, Dawei Ren<sup>14</sup>, Zhenhua Zhao<sup>15</sup>, Weigen Yao<sup>16</sup>, Yunjun Yang<sup>17</sup> and Minming Zhang<sup>1\*</sup>

<sup>1</sup>Department of Radiology, Second Affiliated Hospital, School of Medicine, Zhejiang University, Hangzhou, China, <sup>2</sup>Fuyang Second People's Hospital, Fuyang, China, <sup>3</sup>Yueqing People's Hospital, Yueqing, China, <sup>4</sup>Zhejiang Taizhou Hospital, Taizhou, China, <sup>5</sup>Radiology Department, Third Affiliated Hospital of Wenzhou Medical University, Wenzhou, China, <sup>6</sup>Bozhou Bone Trauma Hospital Image Center, Bozhou, China, <sup>7</sup>Department of Radiology, Second Affiliated Hospital and Yuying Children's Hospital of Wenzhou Medical University, Wenzhou, China, <sup>8</sup>First Hospital of Jiaxing, Jiaxing, China, <sup>9</sup>Second Xiangya Hospital, Central South University, Changsha, China, <sup>10</sup>Quzhou Kecheng People's Hospital, Quzhou, China, <sup>11</sup>Pingyang County People's Hospital, Wenzhou, China, <sup>12</sup>Yuhang First People's Hospital, Hangzhou, China, <sup>13</sup>Jinhua Central Hospital, Jinhua, China, <sup>14</sup>Ningbo First Hospital, Ningbo, China, <sup>15</sup>Shaoxing People's Hospital, Shaoxing, China, <sup>16</sup>Yuyao People's Hospital, Yuyao, China, <sup>17</sup>Radiology Department, First Affiliated Hospital of Wenzhou Medical University, Wenzhou, China

## OPEN ACCESS

### Edited by:

Wen Li,  
Zhejiang University, China

### Reviewed by:

Zeliha Selamoglu,  
Niğde Ömer Halisdemir University,  
Turkey  
Youmin Guo,  
Xi'an Jiaotong University, China

### \*Correspondence:

Minming Zhang  
zhangminming@zju.edu.cn

### Specialty section:

This article was submitted to  
Molecular Diagnostics and  
Therapeutics,  
a section of the journal  
Frontiers in Molecular Biosciences

**Received:** 31 December 2020

**Accepted:** 30 April 2021

**Published:** 28 May 2021

### Citation:

Wang L, Jiaerken Y, Li Q, Huang P, Shen Z, Zhao T, Zheng H, Ji W, Gao Y, Xia J, Cheng J, Ma J, Liu J, Liu Y, Su M, Ruan G, Shu J, Ren D, Zhao Z, Yao W, Yang Y and Zhang M (2021) An Illustrated Guide to the Imaging Evolution of COVID in Non-Epidemic Areas of Southeast China. *Front. Mol. Biosci.* 8:648180. doi: 10.3389/fmolb.2021.648180

**Purpose:** By analyzing the CT manifestations and evolution of COVID in non-epidemic areas of southeast China, analyzing the developmental abnormalities and accompanying signs in the early and late stages of the disease, providing imaging evidence for clinical diagnosis and identification, and assisting in judging disease progression and monitoring prognosis.

**Methods:** This retrospective and multicenter study included 1,648 chest CT examinations from 693 patients with laboratory-confirmed COVID-19 infection from 16 hospitals of southeast China between January 19 and March 27, 2020. Six trained radiologists analyzed and recorded the distribution and location of the lesions in the CT images of these patients. The accompanying signs include crazy-paving sign, bronchial wall thickening, microvascular thickening, bronchogram sign, fibrous lesions, halo and reverse-halo signs, nodules, atelectasis, and pleural effusion, and at the same time, they analyze the evolution of the abovementioned manifestations over time.

**Result:** There were 1,500 positive findings in 1,648 CT examinations of 693 patients; the average age of the patients was 46 years, including 13 children; the proportion of women was 49%. Early CT manifestations are single or multiple nodular, patchy, or flaky ground-glass-like density shadows. The frequency of occurrence of ground-glass shadows (47.27%), fibrous lesions (42.60%), and microvascular thickening (40.60%) was significantly higher than that of other signs. Ground-glass shadows increase and expand 3–7 days after the onset of symptoms. The distribution and location of lesions were not significantly related to the appearance time. Ground-glass shadow is the most common lesion, with an average absorption time of 6.2 days, followed by consolidation, with an absorption time of about 6.3 days. It takes about 8 days for pure ground-glass lesions to absorb. Consolidation change into ground glass or pure ground glass takes

10–14 days. For ground-glass opacity to evolve into pure ground-glass lesions, it takes an average of 17 days. For ground-glass lesions to evolve into consolidation, it takes 7 days, pure ground-glass lesions need 8 days to evolve into ground-glass lesions. The average time for CT signs to improve is 10–15 days, and the first to improve is the crazy-paving sign and nodules; while the progression of the disease is 6–12 days, the earliest signs of progression are air bronchogram signs, bronchial wall thickening, and bronchiectasis. There is no severe patient in this study.

**Conclusion:** This study depicts the CT manifestation and evolution of COVID in non-epidemic origin areas, and provides valuable first-hand information for clinical diagnosis and judgment of patient's disease evolution and prediction.

**Keywords:** COVID, image, CT, evolution, multicenter

## INTRODUCTION

Coronavirus disease 2019 (COVID-19), an acute respiratory infectious disease in 2019–2020, is becoming more and more serious. Although the epidemic situation in China has been well controlled, the number of cases in the world is increasing, and it is still in a pandemic state. With the continuous accumulation and comprehensive understanding of disease prevention, control, diagnosis, and treatment experience, research on the disease evolution, including the risk factors for patients progressed from mild-to-severe even critical illness, risk factors for death and related early warning models, is actively processing. Imaging plays an important role in disease diagnosis, clinical decision-making, treatment, and clinical outcome evaluation. The occurrence and development of imaging is of great significance for us to understand the characteristics of the disease and to guide clinical practice. The combination of imaging findings and the nucleic acid test as a means of diagnosis program aimed to make up for missed diagnosis of early nucleic acid-negative cases, and can also be used to evaluate curative effect, and it has now become a consensus in the treatment of COVID-19. This study collects imaging and clinical data of patients with confirmed COVID-19 in 16 hospitals in southeast China outside of the epidemic area; uses big data analysis to find the early and late development; explores the correlation among imaging performance, developmental trend, and patient basic diseases; describes the characteristics and evolution of the imaging manifestations with the time of onset; displays the imaging map of new coronary pneumonia; provides imaging clues for clinical diagnosis and identification; and provides assistance in disease progression and prognostic monitoring.

## METHODS

### Patients Information

The study was conducted in accordance with the Declaration of Helsinki (as revised in 2013). This retrospective multicenter study was approved by the Institutional Review Board of each participating hospital. Written informed consent was waived. A total of 693 patients came from the southeastern region of

China outside of the epidemic-intensive areas, with an average age of 46 years, including 13 children; the proportion of women was 49%. They were all imported second-generation confirmed cases. This study included 1,648 chest CT examinations at 16 hospitals between January 19 and March 27, 2020. The median CT follow-up period was 10 days from symptom onset (IQR, 6–16; range, 0–58 days). All patients were recovered after treatment, and there are no clinically critically ill patients in this study.

### CT Protocol

CT examinations were performed using 16-slice to 128-slice CT scanners of different manufacturers, including SIEMENS, GE, TOSHIBA, and PHILIPS. Chest CT examinations were performed with a varying slice thickness from 1 to 5 mm. Standard lung algorithm settings were used as follows: tube voltage, 100–130 kV; tube current, 100–440 mAs; section thickness, 1–5 mm; and reconstruction matrix, 512 × 512.

### CT Image Recording Method

All CT images were read by six attending doctors with qualifications. The density of lesions was divided into pure ground-glass shadow (completely ground-glass density), ground-glass lesions (referring to ground-glass lesions containing consolidation lesions not exceeding one-half of the total volume), and consolidation lesions (completely solidified lesions or contained ground-glass opacity not exceeding one-half of the total volume). At the same time, the lobe location and distribution characteristics of the lesions were recorded: subpleural distribution pattern defined as lesions distributed within 2 cm of the subpleural area on both sides; diffuse distribution refers to the involvement of multiple lobes in both lungs; distribution along the bronchial vascular bundle pattern refers to the lesions distributed along the bronchial vascular bundle. Signs within the lesion were recorded, such as bronchogram sign, paving stone sign (shown as mosaic ground-glass shadow with thickened interlobular septum), thickened microvessels, halo and reversal halo signs, nodules, fibrous foci, and other manifestations such as pleural effusion and pericardium effusion, and old lesions. In the follow-up CT, the outcome of the above-observed lesion was recorded once more, in



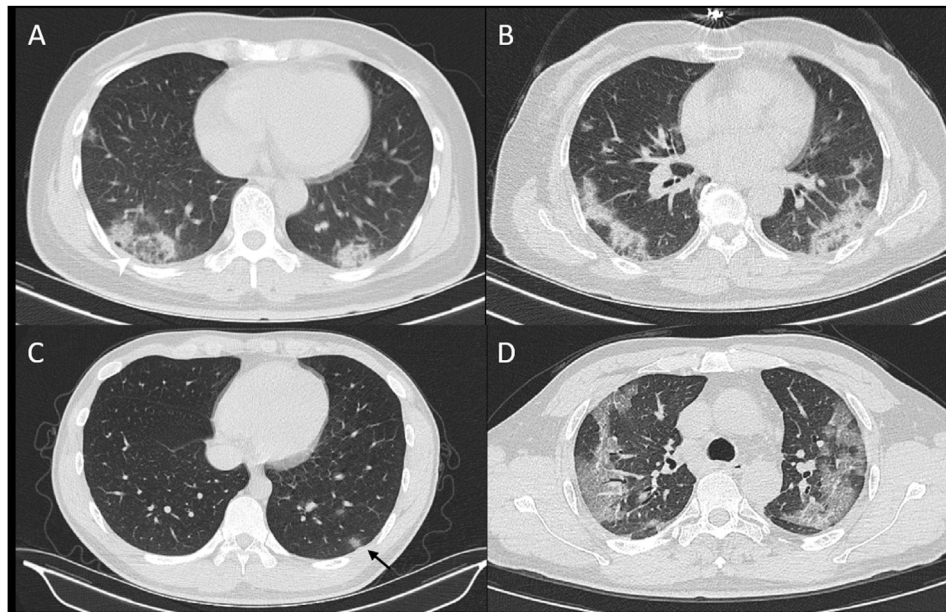


**FIGURE 1 |** CT signs of reversed hollow sign (A), bilateral distribution of lesion (B), and nodule with hollow sign (C), and crazy-paving sign (D).

addition to the improvement and progress of the lesion. The form of lesion improvement is explained as the reduction of lesion area and density, including ground-glass and consolidation shadow absorption, and any kinds of density decreased and area reduced. The form of lesion progression is explained as the increase in the range and/or density of the original lesion, including pure ground-glass lesions that progress to ground-glass lesions, and ground-glass lesions that progress to consolidation lesions; disappearance of signs means improvement, and reappearance of signs means progress. The first examination was negative, and the reexamination showed that the lesion appeared and was recorded as a new lesion. The days of improvement, absorption, and progression of different density lesions and signs were recorded.

## Statistical Analysis

The differences in the frequency of the CT signs were tested with the chi-square test. The differences between the days of the onset between different CT signs were tested with the ANOVA test. The differences in the demographic data between groups were also tested with the ANOVA test. Data normality was tested with the K-W test. All statistical analyses were performed with MATLAB 2019b on windows platform. A corrected  $p$  value of  $< 0.05$  was considered as statistically significant.

## RESULT

### Examination Information

The average time for the first CT examination was 6.5 days after the onset of the disease, and the longest CT examination was 58 days after the onset of the disease; the median number of

follow-ups was two, and the maximum number of follow-ups was 10; the average follow-up interval was 5.3 days; and there were positive findings in 1,500 CT examinations.

### Basic CT Manifestations

All 1,500 CT examinations with positive signs were included, and the distribution, density, accompanying signs, and extrapulmonary manifestations were analyzed. The basic CT manifestations are as follows: 1. The distribution is mainly under the pleura, more often on the dorsal side or the lower lobes of the lungs. The lesions are mostly localized, mainly subsegmental or segmental. 2. Single or multiple nodular, patchy, or ground-glass density shadows, with or without intralobular reticular shadows, thickening of the lobular septa, and thickened microvessels and paving stone sign inside (Figures 1A–D). Consolidation was accompanied by bronchogram, internal bronchiectasis, and with or without subsegmental or lobular atelectasis, which was manifested as a fusiform, flat, or strip-shaped shadow connected to the bronchovascular bundle under the pleura (Figure 2). 3. As the course of the disease progresses and treatment measures follow-up, the ground-glass shadow or consolidation completely or partially absorbed, and was transformed into lobular atelectasis or fibrosis. Extrapulmonary manifestations including pleural effusion, pericardial effusion, and lymphadenopathy are rare.

### Frequency Analysis of Lesions

CT lesion distribution and imaging manifestation frequency analysis are shown in Table 1. The results of the chi-square test showed that the distribution of lesions was mainly subpleural (82.33%), which was significantly more than the distribution of bronchial vascular bundles or diffuse distribution, and diffuse

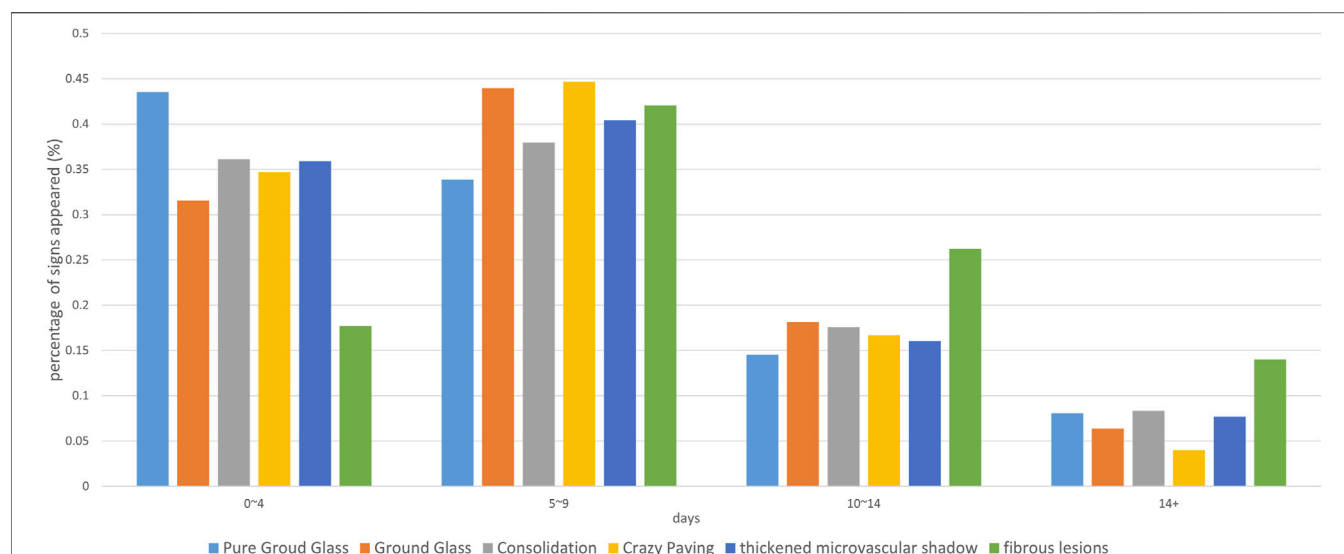


**FIGURE 2 |** The percentage of time at each CT sign. The horizontal axis is the date of onset, and the vertical axis represents the percentage of the number of positive cases with the corresponding sign to all cases with the sign on that date.

**TABLE 1 |** The frequency of CT lesion distribution, location, intensity, and signs.

CT lesion description	Number (%)
CT lesion distribution	
Under the pleura	1,235 (82.33) <sup>a</sup>
Along bronchovascular bundle	573 (38.20) <sup>b</sup>
Diffused distribution	102 (6.80) <sup>c</sup>
CT lesion location	
Right upper lobe	920 (61.33) <sup>a</sup>
Left upper lobe	993 (66.20) <sup>a</sup>
Right middle lobe	773 (51.53) <sup>b</sup>
Right lower lobe	1,279 (85.27) <sup>c</sup>
Left lower lobe	1,251 (83.40) <sup>c</sup>
CT lesion intensity	
Ground-glass opacity	709 (47.27) <sup>a</sup>
Consolidation	507 (33.80) <sup>b</sup>
Pure ground-glass opacity	378 (25.20) <sup>c</sup>
CT signs of changes in the lung	
Fibrous lesions	639 (42.60) <sup>a</sup>
Thickened small vessel	609 (40.60) <sup>a</sup>
Air bronchogram	478 (31.87) <sup>b</sup>
Bronchial dilating and wall thickening	383 (25.53) <sup>c</sup>
Halo sign	309 (20.60) <sup>c</sup>
Crazy-paving sign	264 (17.60) <sup>d</sup>
Nodule	231 (15.40) <sup>d</sup>
Inversed halo	60 (4.00) <sup>e</sup>
Lobular atelectasis	29 (1.93) <sup>f</sup>
Pulmonary fibrosis	23 (1.53) <sup>f</sup>
Pulmonary emphysema	33 (2.20) <sup>e,f</sup>
CT signs of changes outside the lung	
Pleural effusion	21 (1.40) <sup>a</sup>
Pericardial effusion	3 (0.20) <sup>b</sup>
Enlargement of lymph nodes	32 (2.13) <sup>b</sup>

Frequency (%) of CT lesion distribution, location, intensity, and signs of changes in and outside the lung were shown. Within a same sub-table, the pair with the same superscript letter (a,b,c...) showed no statistically significant differences, while the pair with different superscript letter had significant differences (chi-square test, Bonferroni corrected  $p < 0.05$ ).

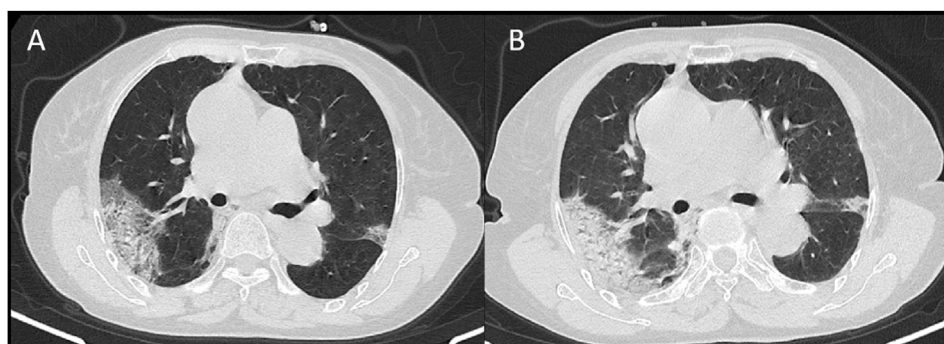
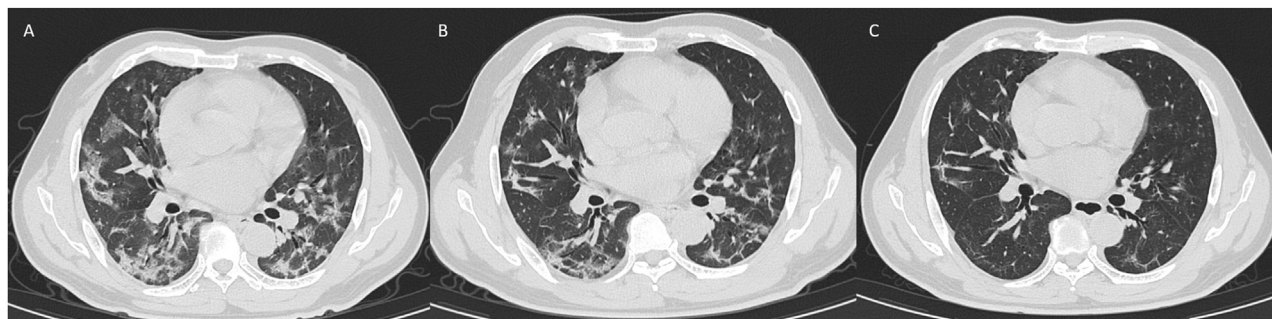
distribution was rare. The lesions are mainly seen in the two lower lungs, and there is no obvious difference between the left and right lungs. The frequency of lesions in the middle lobe of the right lung is relatively low (51.53%); the most common manifestation is ground-glass density shadow (47.27%). The first three signs with higher frequency were fibrous lesions (42.60%), microvascular thickening (40.60%), and air bronchogram (31.87%). There was no significant difference among the three. In other accompanying signs, the paving stone sign is about 17%, and the antihalo sign is less, which is about 4%.

## Analysis of Follow-Up Outcome

The first CT examination showed significant differences in the appearance time of lesions and signs with different densities ( $p = 0.014$ ). The average time of appearance of pure ground-glass, ground-glass lesions, and consolidation and accompanying signs including paving stone, bronchogram, thickened microvessels, nodules, halo and reversed halo signs was about 6–7 days (Table 2); among them, pure ground-glass lesions appear earliest, with the highest peak at 0–4 days (43.54% of pure ground-glass lesions appear in this period), and it took about 8 days for pure ground-glass lesions to absorb, while progress into consolidation needs 11 days (Figure 3). It takes 8 days for pure ground-glass disease to progress to ground-glass lesions. The first examination was negative, and among them, 18 patients showed original pure ground-glass lesions after 16 days of reexamination (Figure 4), 16 cases showed ground-glass lesions, and 24 cases showed consolidation lesions in about 13 days. The number of ground-glass lesions was the largest (216 cases), and the peak appeared on the sixth day. The average absorption time was 6.2 days, or

**TABLE 2 |** Comparison of time and clinical data between different outcome groups.

Trend	Lesion development	Mean days between visit	Number of cases
Recovery	Consolidation turned negative	6.37	181
	Consolidation to ground-glass opacity	10.66	71
	Consolidation to pure ground-glass opacity	13.78	23
	Ground-glass opacity turned negative	6.21	216
	Ground-glass opacity to pure ground-glass opacity	17.14	29
	Pure ground-glass opacity turned negative	7.99	78
Progressed	New pure ground-glass opacity	15.78	18
	Pure ground-glass opacity to ground glass opacity	8.73	13
	Pure ground-glass opacity to consolidation	11.07	15
	New ground-glass opacity	11.75	16
	Ground-glass opacity to consolidation	7.35	54
	New consolidation lesion	12.92	24

**FIGURE 3 |** CT signs of a 74-year-old female showed subpleural distributed ground-glass opacity in 13 days (A) and 16 days (B) from onset.**FIGURE 4 |** CT signs of a 47-year-old male on day 1 (A), day 5 (B), and day 17 (C) showed bilateral ground-glass opacity absorbed and fibrosis formation.

it progressed to consolidation in 7 days. There were 29 cases of ground-glass lesions that evolved into pure ground-glass lesions, and the lesions took the longest time to be absorbed, which is about 17 days. Among the 29 cases, 11 patients had underlying diseases (37.93%), which was significantly higher than the other groups, including two cases of diabetes, two cases of hypertension with diabetes, two cases of hypertension, two cases of tuberculosis, two cases of spinal surgery, and one case of chronic urticaria. As for age, gender, body temperature, and the proportion of neutrophils and lymphocytes, there was no significant difference between

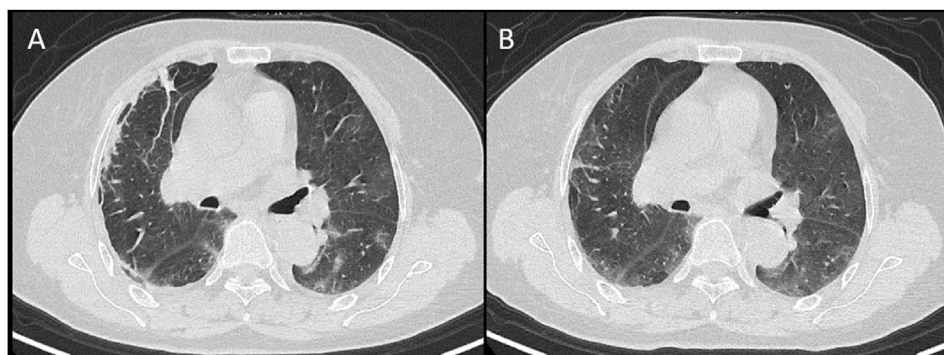
these 29 patients compared with the ground-glass absorption group.

The absorption time of consolidation lesions is about 6.3 days. It takes 10–14 days for consolidation to transform into ground-glass or pure ground-glass lesions. Most of the peaks of accompanying signs are on the 5th to 9th days, such as paving stone sign, microvascular thickening, and fibrous lesions (Table 3). The average time for improvement is 10–15 days. The first improvement is the paving stone sign and nodules; the time for signs to progress is 6–12 days. The earliest signs of progress are bronchogram, bronchial wall thickening, and



**TABLE 3 |** Development of CT signs.

CT signs	From positive to negative		From negative to positive	
	Mean days between visit	Number of cases (%)	Mean days between visit	Number of cases (%)
Crazy-paving	10.14 a	62 (19.50)	10.15 b	17 (6.67)
Air bronchogram	11.32 a	79 (24.84)	6.20 b	23 (9.02)
Fibrous lesions	15.08 a	13 (4.09)	10.12 b	133 (52.15)
Bronchial dilating and wall thickening	12.88 a	56 (17.61)	9.12 b	34 (13.33)
Thickened small vessel	13.26 a	74 (23.27)	8.56 b	25 (9.80)
Nodule	10.82 a	34 (10.69)	11.48 a,b	23 (9.02)
Halo sign	11.44	54 (14.52)	9.78	16 (6.40)

**FIGURE 5 |** A 68-year-old female showed lobular atelectasis in the subpleural area of the right upper lobe on day 3 from onset (A) and disappeared on day 6 (B).

bronchiectasis. Fibrous lesions appear less frequently in 0–4 days (17.68%), but the duration is long, and there is still 26.12% in 10–14 days, which is higher than other signs (Figure 5).

## DISCUSSION

This article summarizes and analyzes the imaging manifestation in non-epidemic areas, summarizes the image characteristics and evolution time of sporadic cases, describes the accompanying signs of the images, provides clinical diagnosis for sporadic cases and mild patients, and provides comprehensive imaging data for efficacy clinical evaluation.

### Selection of Imaging Methods

Chest CT is the first choice for screening and evaluating new coronary pneumonia (Wong et al., 2019). It is recommended to use a volumetric CT scan, the scan thickness is 5 mm (16-slice CT and above are acceptable), and the reconstruction is a thin layer of 1.0–1.5 mm. Multi-planar reconstruction (cross-sectional, sagittal, and coronal) was based on thin-slice CT. At present, the latest guidelines have not yet reached a consensus on the timing of the use of low-dose CT (LDCT) examination and the time interval for reexamination of CT. Early CT findings of some patients with new coronary pneumonia are negative, and positive findings gradually appear in the lungs as the disease progresses (Minming and Bin, 2020). We agree with opinions as follows: reports of the various CT features of

COVID-19 pneumonia are an important first step in helping radiologists identify patients who may have COVID-19 pneumonia in the appropriate clinical environment. CT should be reserved for evaluation of complications of COVID-19 pneumonia or for assessment if alternative diagnoses are suspected (Raptis et al., 2020).

## CT Manifestations

### Density Change and Evolution

Density changes include ground-glass opacity and consolidation; ground-glass opacity indicated slight increase in density as a hazy cloud-like change that does not cover the accompanying pulmonary vascular shadows in the lungs. Consolidation means a significant increase in the density of lung parenchyma, and the pulmonary blood vessels and airway walls are unclear due to the lack of alveolar gas contrast (Adam et al., 2020). The imaging manifestations depend on the pathology. The pathology of COVID-19 shows that the lungs exhibited different degrees of consolidation, mainly showing diffuse alveolar injury and exudative alveolitis. Pulmonary lesions in different areas are complex and diverse, with the new and the old lesions alternating. The formation of serous/fibrinous exudate and transparent membrane in the alveolar cavity can show consolidation of different densities in imaging. Infiltrating cells are mainly monocytes and macrophages. Type-II alveolar epithelial cell hyperplasia, alveolar septal hyperemia and edema, and some alveolar hyperinflation, forming airspace-containing cavity, can form



lobular septal thickening and paving stone signs. Bronchioles and small bronchi are easy to see mucus thrombosis, pulmonary vasculitis and thrombosis, and embolism, which can explain the signs of microvascular thickening. With the development of the disease, it can be seen that the alveolar cavity exudate is organized (meat change) and the pulmonary interstitial fibrosis, so the later stage could find the formation of fibrous bands (Minming and Bin, 2020).

The results showed that the lesions were mainly distributed under the two lower lobes, followed by the two upper lobes, and the right middle lobe was the least involved (Fan et al., 2020; Minming and Bin, 2020; Salehi et al., 2020). The frequency of ground-glass opacity is the highest, and the peak time is 0–4 days, which is consistent with many literature reports outside Hubei Province and can have no clinical symptoms (Ai et al., 2020; Xiong et al., 2020; Zhao et al., 2020). Meng et al. (2020) reported asymptomatic cases with normal laboratory findings confirmed by nucleic acid testing show CT findings as ground-glass opacity (GGO) (94.8%) with peripheral (75.9%) distribution, unilateral location (58.6%), and mostly involving one or two lobes (65.5%).

The most rapid absorption of lesion density evolution was ground glass–based lesions, with an average transformation time of 6.2 days, followed by consolidation, with an absorption time of about 6.3 days, which was also the shortest absorption time, which did not match the 3.5-day average prognosis time reported by Li et al. (2020). Shi et al. (2020) reported a case of Wuhan with pure ground-glass shadow absorption for 13 days, which the author believes is related to clinical treatment and individual differences in patients and virus virulence. It may be due to different areas of the patient. Xiong et al. (2020) reported that in Wuhan, 83% of patients, which is more than that in our observation, progressed to opacifications, consolidation, interstitial thickening, fibrous strips, and air bronchogram signs during a mean follow-up period of 4.5 and 11.6 days.

According to our result, it takes about 7–11 days for ground-glass or pure ground-glass lesions to switch to consolidation. Wang et al. (2020) reported that the ground-glass lesions progressed to a mixed type for about 12–17 days. The progression of the lesion is based on pure ground-glass opacity and develops into ground glass in turn, followed by consolidation. It is speculated that density increase is related to the increase in exudate and cells in the lung, the thickening of the interlobular septum, and the formation of fibrosis. It takes about 10–14 days for consolidation absorption to turn into ground-glass or pure ground-glass opacity; ground-glass lesions evolve into pure ground-glass and also indicate that the lesions improve absorption, but it takes as long as 17 days. The reason is that this group of patients has underlying diseases, such as hypertension, diabetes, or a history of surgery. It is speculated that the immune function of the patients may delay the absorption of the lesion. Relevant literature on clinical indicators predicting lesion progression predicted that patients with imaging progression had significantly higher frequency of chronic inflammatory manifestation than those without imaging progression (Yang et al., 2020). This may be related to the pathological basis of pulmonary edema, protein exudation, and thickening of pulmonary interstitium, which may play a role,

resulting in the formation of ground-glass opacity. Among them, edema and protein exudation are absorbed faster, while the lung interstitium thickness process is relatively slow, which can explain the different results of ground-glass shadow absorption in some patients. Similarly, consolidation may be caused by multiple pathological factors. After pulmonary edema and exudation are absorbed, the density of the lesion decreases, and the interstitial thickening maintains the ground-glass density and enters a slow absorption period, which can evolve into fibrotic lesions in the later stage.

### Accompanying Signs and Evolution

Accompanying signs include paving stone sign, microvascular thickening, bronchogram sign, halo sign, reversed halo sign, tree-in-bud sign, nodules, and traction bronchiectasis. Most signs merged in 5–9 days and accompanied with the absorption and evolution of the lesions; only fibrotic lesions appear on the 9th day. The average time for improvement is 10–15 days, and the first to get better is the paving stone sign. The progression time of signs is 6–12 days, and the relatively earlier signs are bronchogram, bronchial wall thickening, and traction bronchiectasis.

What needs to be emphasized is the paving stone sign. Some researchers believe that this sign indicates the progress of the disease; we have different opinions. The crazy-paving pattern demonstrates as thickened interlobular septa and intralobular lines with superimposition on a GGO background, resembling irregular paving stones (Cheng et al., 2020; Fan et al., 2020; Qi et al., 2020; Raptis et al., 2020; Wang et al., 2020; Ye et al., 2020). The early pathological changes of COVID-19 include pulmonary edema, protein exudation, thickening of the lung interstitium, and infiltration of multinucleated giant cells and macrophages in the alveolar cavity. Pan et al. (2020) mentioned that in 22 cases of observation, the paving stone sign appeared in 5–8 days from the symptom and continued to be absorbed after 13 days, and the lesion progression was accompanied by more paving stone signs. Salehi et al. (2020) indicated follow-up CT in the intermediate stage of disease shows an increase in the number and size of GGOs and progressive transformation of GGO into multifocal consolidative opacities, septal thickening, and development of a crazy-paving pattern, with the greatest severity of CT findings visible around day 10 after the symptom onset. There were no severe cases in this study, the paving stone sign improved in about 10 days in 20% of the patients, only 6% cases progressed, and the average progression time was also about 10 days. Relatively speaking, bronchial wall thickening appeared more frequently. In many progressive cases, thickening of the bronchial wall and microvessel signs had larger frequency and may be predictive signs of critically ill patients. The paving stone sign has been used to distinguish it from viral pneumonia. While a cluster-like pattern and bronchial wall thickening were more frequently seen in influenza pneumonia (Wang et al., 2020), we considered that the imaging manifestations of COVID and avian influenza, influenza B, and influenza A have a large

overlap, and the performance is similar, and the differential diagnosis depends on clinical microbiological tests. YU reported (Yu et al., 2020) interlobular septal thickening (75%), air bronchogram (70%), and pleural effusion (40%) were more likely to manifest in patients with severe form. Wang et al. (2020) also reported heavy/critical-type COVID-19 was associated with multiple lobe involvement and the presence of consolidation, the crazy-paving sign, interlobular septal thickening, pleural thickening, and pleural effusion.

Halo sign, reversed-halo sign, tree-in-bud sign, and nodules are rare manifestations. Halo sign refers to a circle of ground-glass density shadow around the nodules or patchy opacity on CT. It was first used to describe the exudation around the focal invasive *Aspergillus* nodule. The pathological mechanism is bleeding around the lesion and so was a nonspecific sign. To COVID-19, it shows ill-defined cloud-like inflammatory exudation around the lesion, which is similar to other opacity. As for reversed-halo sign, there is a certain difference between the traditional appearance and COVID-19. The center of the reversed-halo sign showed a ground-glass density shadow, the surrounding appearance is ring or crescent, and the density of the ring in COVID-19 is lower than that of the ring in others, such as organized pneumonia. The pathological mechanism of GGO-like banding needs further explanation (Guan et al., 2020). It is reported that reversed halo sign was observed in approx. 5% of patients (Hamer et al., 2020). In the early CT images, nodules with a diameter of  $\leq 3$  cm can be solid nodules, partial solid nodules, and pure ground-glass nodules, with clear or fuzzy boundaries. As for the tree-in-bud sign, the initial lesion was a solitary sub-centimeter ground-glass nodule distributed in the boundary between the outer one-third and inner two-thirds of pulmonary lobes, along with adjacent bronchovascular bundles, and the lesion progressed over a period of 2–3 days, presenting as an enlarged nodule with a blurred margin on CT (Xia et al., 2020). Current pathological studies believe that COVID-19 mainly causes inflammatory reactions characterized by deep airway and alveolar damage. However, individual COVID-19 cases showed tree-in-bud signs, suggesting that the disease involves bronchioles (Güneyli et al., 2020).

Fibrous lesions appeared with a low frequency (17.68%) in 0–4 days, and 26.12% in 10–14 days, which is higher than that in other signs. The frequency of fibrotic lesions in the disease outcome of this study was higher, which may be due to different interpretations: some fiber streaks disappeared in the later period, and two cases of streaks were reported to be absorbed in 19 days (Jiang et al., 2020). Guan et al. (2020) reported a delay in the changes on CT and evidence of lesion absorption. During the absorption period, the patchy lung consolidations gradually absorbed and shrank, but the subpleural line was still present 22 days after admission. It is suggested that the stripe shadow displayed in the previous stage is atelectasis or segmental atelectasis. Lobular atelectasis refers to complete atelectasis or results in swelling of the lung caused by bronchial obstruction or contraction of scar tissue in the lung, which is caused by bronchiolitis. The resulting

inflammation is absorbed, the lumen of the bronchioles reopens, and the lung is recruited to expand. The unabsorbable fiber strips are the real scars. Pleural effusion and enlargement of lymph nodes appear less generally. Traction bronchiectasis may appear in the consolidation area on CT or in the fibrous cord shadow.

## RESEARCH LIMITATIONS

This study mainly describes the imaging manifestations and evolution of COVID-19, and does not include the treatment and the clinical evolution of the patient. The reason is that the current treatment is basically the same, and the difference is the patient's individual response and immune status. Therefore, the image analysis of big data shows that the overall development of new coronary pneumonia has a certain degree of representativeness.

## SUMMARY

This study describes the CT manifestation and evolution of COVID-19 in non-epidemic areas of southeast China, and provides valuable first-hand information for clinical diagnosis and judgment of disease evolution and prediction.

## DATA AVAILABILITY STATEMENT

The raw data supporting the conclusions of this article will be made available by the authors, without undue reservation.

## ETHICS STATEMENT

The studies involving human participants were reviewed and approved by the Ethics Board of the Second Affiliated Hospital, Zhejiang University School of Medicine. The patients/participants provided their written informed consent to participate in this study.

## AUTHOR CONTRIBUTIONS

All authors listed have made a substantial, direct, and intellectual contribution to the work and approved it for publication.

## FUNDING

This research was supported by Zhejiang University special scientific research fund for COVID-19 prevention and control (No. 2020XGZX036).

## REFERENCES

- Adam, B., Mei, X., Huang, M., Yang, Y., Fayad, Z. A., Zhang, N., et al. (2020). Chest CT Findings in Coronavirus Disease-19 (COVID-19): Relationship to Duration of Infection. *Radiol.* 295, 200463. doi:10.1148/radiol.202000463
- Ai, T., Yang, Z., Hou, H., Zhan, C., Chen, C., Lv, W., et al. (2020). Correlation of Chest CT and RT-PCR Testing for Coronavirus Disease 2019 (COVID-19) in China: A Report of 1014 Cases. *Radiol.* 296, E32, 2020. Online ahead of print. doi:10.1148/radiol.202000642
- Cheng, Z., Qin, L., Cao, Q., Dai, J., Pan, A., Yang, W., et al. (2020). Quantitative Computed Tomography of the Coronavirus Disease 2019 (COVID-19) Pneumonia. *Radiol. Infect. Dis.* 7 (2), 55–61. Epub 2020 Apr 28. doi:10.1016/j.rid.2020.04.004
- Fan, N., Fan, W., Li, Z., Shi, M., and Liang, Y. (2020). Imaging Characteristics of Initial Chest Computed Tomography and Clinical Manifestations of Patients with COVID-19 Pneumonia. *Jpn. J. Radiol.* 38 (6), 533–538. doi:10.1007/s11604-020-00973-x
- Guan, C. S., Lv, Z. B., Yan, S., Du, Y. N., Chen, H., Wei, L. G., et al. (2020b). Imaging Features of Coronavirus Disease 2019 (COVID-19): Evaluation on Thin-Section CT. *Acad. Radiol.* 27, 609–613. doi:10.1016/j.acra.2020.03.002
- Guan, W., Liu, J., and Yu, C. (2020a). CT Findings of Coronavirus Disease (COVID-19) Severe Pneumonia. *Am. J. Roentgenol.* 214, W85–W86. doi:10.2214/ajr.20.23035 0361–803X/20/2145–W85.
- Güneyli, S., Atçeken, Z., Atçeken, Z., Dogan, H., Altinmakas, E., and Atasoy, K. C. (2020). Radiological Approach to COVID-19 Pneumonia with an Emphasis on Chest CT. *Diagn. Interv. Radiol.* 26 (4), 323–332. doi:10.5152/dir.2020.20260
- Hamer, O. W., Salzberger, B., Gebauer, J., Stroszczyński, C., and Pfeifer, M. (2020). CT Morphology of COVID-19: Case Report and Review of Literature. *Fortschr Röntgenstr* 192, 386–392. Published online: 26.3.2020. doi:10.1055/a-1142-4094
- Jiang, X., Yin, Z., Wang, T., Zhai, N., Lu, F., Zhan, C., et al. (2020). COVID-19 Dynamic Computed Tomography (CT) Performance and Observation of Some Laboratory Indicators. *Med. Sci. Monit.* 26, e924403. doi:10.12659/MSM.924403
- Li, X., Zeng, W., Li, X., Chen, H., Shi, L., Li, X., et al. (2020). CT Imaging Changes of Corona Virus Disease 2019(COVID-19): A Multi-Center Study in Southwest China. *J. Transl. Med.* 18 (1), 154. doi:10.1186/s12967-020-02324-w
- Meng, H., Xiong, R., He, R., Lin, W., Hao, B., Zhang, L., et al. (2020). CT Imaging and Clinical Course of Asymptomatic Cases with COVID-19 Pneumonia at Admission in Wuhan, China. *J. Infect.* 81 (1), e33–e39. Epub 2020 Apr 12. doi:10.1016/j.jinf.2020.04.004
- Minning, Z., and Bin, L. (2020). *Diagnostic Imaging of Novel Coronavirus Pneumonia* | SpringerLink. Singapore: Springer.
- Pan, F., Ye, T., Sun, P., Gui, S., Liang, B., Li, L., et al. (2020). Time Course of Lung Changes at Chest CT during Recovery from Coronavirus Disease 2019 (COVID-19). *Radiol.* 295, 715–721. Online ahead of print. doi:10.1148/radiol.202000370
- Qi, X., Lei, J., Yu, Q., Xi, Y., Wang, Y., and Ju, S. (2020). CT Imaging of Coronavirus Disease 2019 (COVID-19): from the Qualitative to Quantitative. *Ann. Transl. Med.* 8 (5), 256. doi:10.21037/atm.2020.02.91
- Raptis, C. A., Hammer, M. M., Short, R. G., Shah, A., Bhalla, S., Bierhals, A. J., et al. (2020). Chest CT and Coronavirus Disease (COVID-19): A Critical Review of the Literature to Date. *AJR* 215, 1–4. doi:10.2214/AJR.20.23202 0361–803X/20/2154–1.
- Salehi, S., Abedi, A., Balakrishnan, U., and Ali, G. (2020). Coronavirus Disease 2019 (COVID-19): A Systematic Review of Imaging Findings in 919 Patients. *AJR* 215, 1–7. doi:10.2214/AJR.20.23034
- Shi, H., Han, X., and Zheng, C. (2020). Evolution of CT Manifestations in a Patient Recovered from 2019 Novel Coronavirus (2019-nCoV) Pneumonia in Wuhan, China. *Radiol.* 295, 20. doi:10.1148/radiol.202000269
- Wang, H., Wei, R., Rao, G., Zhu, J., and Song, B. (2020a). Characteristic CT Findings Distinguishing 2019 Novel Coronavirus Disease (COVID-19) from Influenza Pneumonia. *Eur. Radiol.* 30, 4910–4917. doi:10.1007/s00330-020-06880-z
- Wang, J., Xu, Z., Wang, J., Feng, R., An, Y., Ao, W., et al. (2020b). CT Characteristics of Patients Infected with 2019 Novel Coronavirus: Association with Clinical Type. *Clin. Radiol.* 75 (6), 408–414. Epub 2020 Apr 7. doi:10.1016/j.crad.2020.04.001
- Wang, Y., Dong, C., Hu, Y., Li, C., Ren, Q., Zhang, X., et al. (2020c). Temporal Changes of CT Findings in 90 Patients with COVID-19 Pneumonia: A Longitudinal Study. *Radiol.* 296, E55–E64. Online ahead of print. doi:10.1148/radiol.202000843
- Wong, H. Y. F., Lam, H. Y. S., Fong, A. H., Leung, S. T., Chin, T. W., Lo, C. S. Y., et al. (2019). Frequency and Distribution of Chest Radiographic Findings in COVID-19 Positive Patients. *Radiol.* 296, 201160. doi:10.1148/radiol.202001160
- Xia, T., Li, J., Gao, J., and Xu, X. (2020). Small Solitary Ground-Glass Nodule on CT as an Initial Manifestation of Coronavirus Disease 2019 (COVID-19) Pneumonia. *Korean J. Radiol.* 21 (5), 545–549. doi:10.3348/kjr.2020.0240
- Xiong, Y., Sun, D., Liu, Y., Fan, Y., Zhao, L., Li, X., et al. (2020). Clinical and High-Resolution CT Features of the COVID-19 Infection. *Invest. Radiol.* 55 (6), 332–339. doi:10.1097/RLI.0000000000000674
- Yang, Z., Shi, J., He, Z., Lü, Y., Xu, Q., Ye, C., et al. (2020). Predictors for Imaging Progression on Chest CT from Coronavirus Disease 2019 (COVID-19) Patients. *Aging* 12 (7), 6037–6048. Epub 2020 Apr 10. doi:10.18632/aging.102999
- Ye, Z., Zhang, Y., Wang, Y., Huang, Z., and Song, B. (2020). Chest CT Manifestations of New Coronavirus Disease 2019 (COVID-19): a Pictorial Review. *Eur. Radiol.* 30 (8), 4381–4389. doi:10.1007/s00330-020-06801-0
- Yu, M., Xu, D., Lan, L., Tu, M., Liao, R., Cai, S., et al. (2020). Thin-section Chest CT Imaging of Coronavirus Disease 2019 Pneumonia: Comparison between Patients with Mild and Severe Disease. *Radiol.* 2 (2), e200126. doi:10.1148/ryct.202000126
- Zhao, W., Zhong, Z., Xie, X., Yu, Q., and Liu, J. (2020). Relation between Chest CT Findings and Clinical Conditions of Coronavirus Disease (COVID-19) Pneumonia: A Multicenter Study. *Am. J. Roentgenol.* 214, 1072–1077. doi:10.2214/ajr.20.22976

**Conflict of Interest:** The authors declare that the research was conducted in the absence of any commercial or financial relationships that could be construed as a potential conflict of interest.

Copyright © 2021 Wang, Jiaerken, Li, Huang, Shen, Zhao, Zheng, Ji, Gao, Xia, Cheng, Ma, Liu, Liu, Su, Ruan, Shu, Ren, Zhao, Yao, Yang and Zhang. This is an open-access article distributed under the terms of the Creative Commons Attribution License (CC BY). The use, distribution or reproduction in other forums is permitted, provided the original author(s) and the copyright owner(s) are credited and that the original publication in this journal is cited, in accordance with accepted academic practice. No use, distribution or reproduction is permitted which does not comply with these terms.



# ECMO Rescues Patients With Acute Respiratory Failure Related to GPA

Rongjun Wan<sup>1,2</sup>, Wenzhe Yang<sup>1</sup>, Xinhua Ma<sup>3</sup>, Wei Yang<sup>1</sup>, Pinhua Pan<sup>1</sup>, Chengping Hu<sup>1</sup>, Qiong Chen<sup>2</sup>, Yaou Zhou<sup>4</sup>, Rongli Lu<sup>1</sup>, Yimin Fang<sup>1</sup> and Yuanyuan Li<sup>1\*</sup>

<sup>1</sup> Department of Respiratory Medicine (Department of Respiratory and Critical Care Medicine), Xiangya Hospital, Central South University, Changsha, China, <sup>2</sup> National Clinical Research Center for Geriatric Disorders, Xiangya Hospital, Central South University, Changsha, China, <sup>3</sup> Department of Critical Care Medicine, Xiangya Hospital, Central South University, Changsha, China, <sup>4</sup> Department of Rheumatology and Immunology, Xiangya Hospital, Central South University, Changsha, China

## OPEN ACCESS

### Edited by:

Huahao Shen,  
Zhejiang University, China

### Reviewed by:

Ying Liang,  
Peking University Third Hospital, China  
Alvise Berti,  
Santa Chiara Hospital, Italy

### \*Correspondence:

Yuanyuan Li  
leeround@csu.edu.cn

### Specialty section:

This article was submitted to  
Pulmonary Medicine,  
a section of the journal  
Frontiers in Medicine

**Received:** 23 February 2021

**Accepted:** 22 April 2021

**Published:** 28 May 2021

### Citation:

Wan R, Yang W, Ma X, Yang W, Pan P,  
Hu C, Chen Q, Zhou Y, Lu R, Fang Y  
and Li Y (2021) ECMO Rescues  
Patients With Acute Respiratory  
Failure Related to GPA.  
Front. Med. 8:671396.  
doi: 10.3389/fmed.2021.671396

Granulomatosis with polyangiitis (GPA) is a subtype of anti-neutrophil cytoplasmic antibody-associated vasculitis with a wide range of clinical symptoms related to the systemic involvement of small blood vessels. The respiratory system is one of the most frequently involved, and life-threatening acute respiratory failure could occur due to diffusive alveolar hemorrhage and tracheal stenosis. When maximum mechanical ventilation is unable to maintain oxygenation, extracorporeal membrane oxygenation (ECMO) should be considered as the final respiratory supportive method, if available. Here we present a 32-year-old male patient with acute respiratory failure (ARF) related to GPA, who was rescued by winning time for accurate diagnosis and appropriate treatment. Additionally, we reviewed more than 60 GPA-related ARF cases on multiple online databases, summarized the clinical manifestations of these patients, and concluded that ECMO plays an important role in further respiratory support for ARF patients with GPA and assists in accurate and timely diagnosis and appropriate treatment, thus helping them recuperate.

**Keywords:** diffuse alveolar hemorrhage, ANCA-associated vasculitis, extracorporeal membrane oxygenation, acute respiratory failure, granulomatosis with polyangiitis

## INTRODUCTION

Granulomatosis with polyangiitis (GPA), formerly termed Wegener's granulomatosis, is the most common pathogenesis of anti-neutrophil cytoplasmic antibody (ANCA)-associated vasculitis (AAV) and highly relate to PR3-ANCA (1). The diversiform characteristics of GPA can refer to almost all body systems, particularly the lungs and kidneys (2). Pulmonary hemorrhagic nephritis syndrome is the most frequent cause of acute respiratory failure (ARF), and intensive care unit (ICU) supervision with advanced respiratory support and renal replacement treatment is necessary to help those patients recuperate (3, 4).

Extracorporeal membrane oxygenation (ECMO) is the final respiratory support technique for severe acute respiratory distress syndrome (ARDS) after maximum mechanical ventilation fails to provide optimal oxygen levels in the blood (5, 6). Although systemic anticoagulation is required during ECMO, with the advancement of technology, diffuse alveolar hemorrhage (DAH) has become a potential indication of ECMO as well.



According to a literature review, only the respiratory system is involved in patients with GPA, and ARF at the onset of symptoms is rare (7). Here we report a case of GPA with ARF at the onset of the disease. The disease progressed from shortness of breath to severe respiratory failure in 3 weeks, and maximum mechanical ventilation could not maintain oxygenation. The patient eventually recovered after venovenous extracorporeal membrane oxygenation (VV-ECMO), plasmapheresis, and immunosuppressive treatment (**Figure 1**). Within 2 years of follow-up, the patient showed a great prognosis.

In this study, we also reviewed 60 cases of ARF caused by GPA as published in academic journals; among this series, 22 patients recovered successfully after ECMO support.

## CASE REPORT

On March 13, 2018, a 32-year-old male patient was admitted to the respiratory acute ICU (RICU) at our hospital owing to cough, expectoration, dyspnea for 3 weeks, and fever for 1 week. At 3 weeks before admission, he developed a dry cough and fever sequentially, and the fever was irregular with the highest temperature of 38.0°C, and it was difficult to get a reduction through centrifugation. In a local hospital, a computed tomography (CT) scan showed multiple shadows, and physicians prescribed demethylvancomycin, meropenem, and oseltamivir based on an empirical diagnosis of community-acquired pneumonia (CAP). However, the anti-microorganism treatment was ineffective, and the patient progressed into expectorating blood-stained sputum and dyspnea. For improved treatment, the patient was transferred to the emergency department on March 9. Before he became ill, he worked as a metal mechanical processing engineer for 8 years and had a history of metallic dust and chemical aerosol inhalation. He also had a smoking history of 1.25 pack-years.

After admission to our hospital, the patient reported aggravation of dyspnea with white mucus sputum. Physical examination showed that his body temperature was between 38.0 and 39.0°C without downtrend; the respiratory rate was 30 times/min, auscultation demonstrated only a reduction of breath sound at both sides of the lung, and no rales were revealed. There were no hemorrhagic spots or rashes on the skin. Laboratory examinations showed elevated procalcitonin, C-reactive protein, and erythrocyte sedimentation rate. On CT re-scan in this patient, multiple cavities emerged in his right lung. An empirical diagnosis of severe CAP was established. On estimation, methicillin-resistant *Staphylococcus aureus* or fungus was the most probable pathogen; thus, the patient was treated using linezolid, voriconazole, and levofloxacin. However, the patient continued to develop dyspnea and hyperpyrexia, indicating the probability of incorrect diagnosis. Simultaneously, the patient's blood gas analysis revealed a type I respiratory failure, with an oxygenation index of approximately 100. Although high-flow mask oxygen inhalation and non-invasive positive pressure ventilation (NIPPV) were administered sequentially, the blood oxygenation worsened, and the patient was transferred to our RICU on March 8. Considering that NIPPV did not improve

oxygenation, a bedside chest film revealed consolidation in the lungs bilaterally, and the oxygenation index dropped to 60. Hence, bedside bronchoscope-guided intubation and invasive ventilation were performed. Although maximum ventilatory support was provided under sedation and analgesia, the oxygenation index did not show any improvement at 5 h later. Based on the small amount of hemorrhagic secretion in the trachea under bronchoscopy and consolidation of the gravity areas of the lower lungs by critical ultrasonic imaging, DAH was suspected, and more advanced life support systems were planned. Thus, our team performed VV-ECMO through the internal jugular and femoral veins. The ventilator was changed to synchronized intermittent mandatory ventilation sequentially, and blood gas analysis improved immediately (**Table 1**). Thus, the diagnosis of potential connective tissue diseases such as pulmonary vasculitis was made.

On the day after ECMO was established, the patient's immune disorder-related test results were back, with negative anti-nucleic antibody and anti-dsDNA antibody and positive cytoplasmic anti-neutrophil cytoplasmic antibody (c-ANCA) and proteinase3 (PR3) antibodies; we confirmed the patient's diagnosis as GPA. Considering medical images, airway hemorrhagic secretion, and results of positive autoantibodies, the ARF of this patient was suspected to be due to DAH. Immunosuppressive therapy immediately replaced the antibiotics. Methylprednisolone impact therapy (March 16–18, 500 mg Qd) and maintenance therapy (March 20 and later, 40 mg Qd), cyclophosphamide (0.2 g, Qod), and plasmapheresis (March 19, 21, and 27; three times in total) were administered. Subsequently, the oxygenation and lung conditions of this patient gradually improved (**Figure 1**, **Table 1**). On the 12th day after ECMO, the latter was removed after interrupting the oxygen source of ECMO for 4 h. At 1 day later, intubation was removed after evaluation. High-flow nasal cannula oxygen therapy (HFNC) was observed to be sufficient to maintain oxygenation. On April 3, the patient was transferred to the rheumatology department and treated for another 4 days. On April 6, the patient was discharged in a good respiratory condition.

During follow-up, methylprednisolone and cyclophosphamide were maintained, and the dosages were gradually reduced, and the patient showed a stable condition. Multiple CT scans showed diminishing cavities; however, fibrosis persisted (**Figure 2**).

## METHODS

### Data Collection

A literature search was performed in MEDLINE/PUBMED, Embase, and Scopus databases using the terms, “respiratory failure,” “Wegener's granulomatosis,” and “granulomatosis with polyangiitis.” The article type was limited to case reports when eligible literature was collected from Embase. Furthermore, wild retrieval was performed through Google Scholar. All conference papers and reports that were not in English were excluded, owing to a lack of medical details. By reading the abstract and full text, we collected data on patients with respiratory failure related to GPA, and the inclusion criteria were as follows: (1)

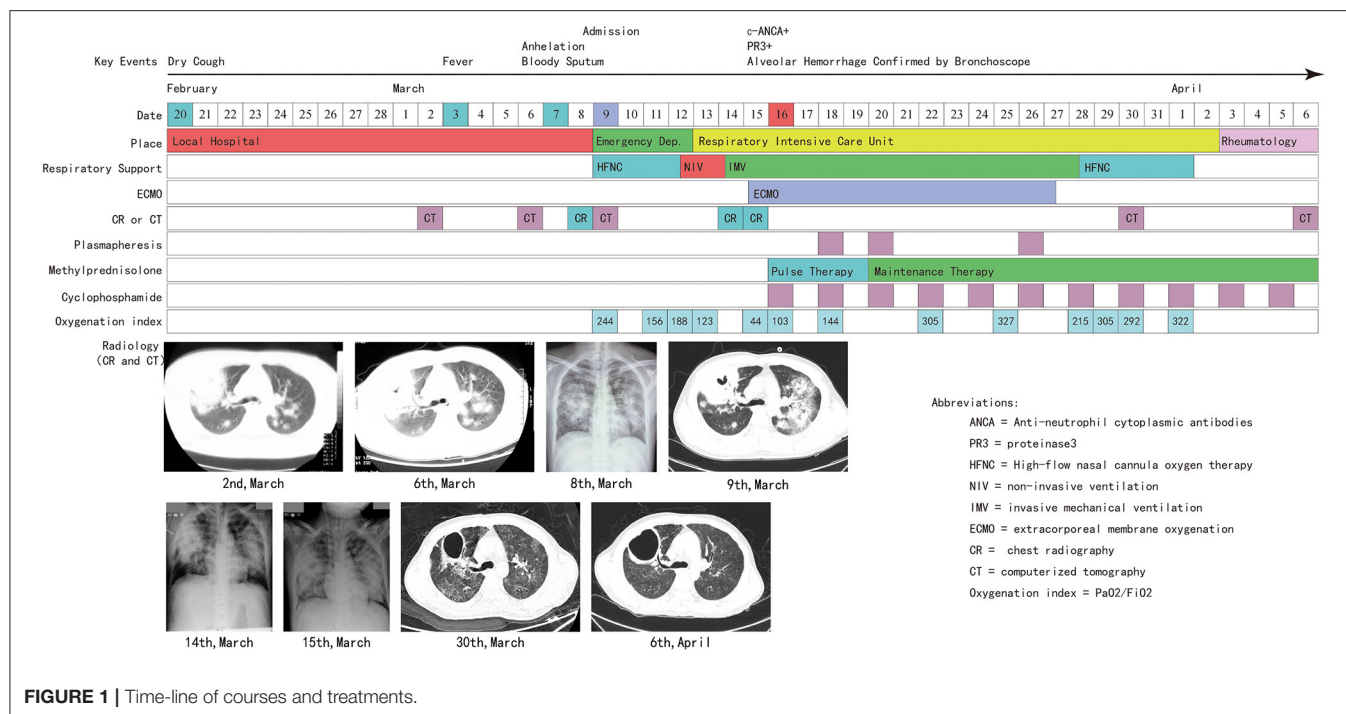


**FIGURE 1 |** Time-line of courses and treatments.

diagnosed with GPA, (2) acute respiratory failure and mechanical ventilation, and (3) the patient's medical history was described in detail. We reviewed the basic information, clinical characteristics, laboratory results, radiology characteristics, ECMO application and type, treatment, and prognosis among these patients.

## Statistical Analysis

We used the Wilcoxon rank-sum test to assess the statistical difference in the age between patients who were administered ECMO or not. We also used Fisher's exact test to examine differences of other clinical characteristics between the two groups. Patients who lacked specific items were excluded when performing statistical analyses on relative items.  $P < 0.05$  was considered significant. All the analyses were performed in R software (version 3.6.3).

## RESULTS

The overall schematic general information and clinical manifestations are presented in **Table 2**. Among the 61 cases in this review (including our case), 32 were women (32/61). The mean age was 35.0 years (interquartile range, IQR: 32.0–57.0). However, the mean age of patients who received ECMO was 27.0 years (IQR, 20.8–33.8), those who did not receive ECMO was 51.0, and their IQR was 30.0–61.5, much higher than that of patients who received ECMO treatment (**Table 3**).

In this series, 41 patients had respiratory symptoms at the onset of their disorders (41/61); among them, patients who received ECMO treatment had a higher proportion (18/22 vs. 23/39), but without statistical significance. Except for our patients and the patient reported by Falk et al.

(58), all patients in this series presented with symptoms of extrapulmonary involvement (59/61). Regarding respiratory failure, DAH was the main reason for GPA patients developing ARF (59/61), while in the other two cases, airway stenosis-related ventilation dysfunction was considered to be the etiology. There were three cases infected with cytomegalovirus, one with pneumocystis jirovecii pneumonia, and one with mucormycosis after immunosuppressive treatment.

By examining imaging manifestations, after excluding patients without radiological information, we found that the extent of involvement was related to the severity of the respiratory failure. Patients with DAH mainly displaying infiltration (45/58) and other imaging findings such as cavities (9/58), consolidation (13/58), and nodules (15/58) were relatively rare. Comparing patients who received and did not receive ECMO (**Table 3**), the infiltration proportion was much higher in those who received ECMO treatment (15/18 vs. 30/39), while the number of nodules was much lower (3/19 vs. 12/39). Among the two cases of airway stenosis, stenosis was detected in the radiological image directly in one patient, while another displayed pneumothorax and emphysema, which indirectly indicated airway stenosis. However, there were no statistical differences between the two groups in terms of radiological manifestations.

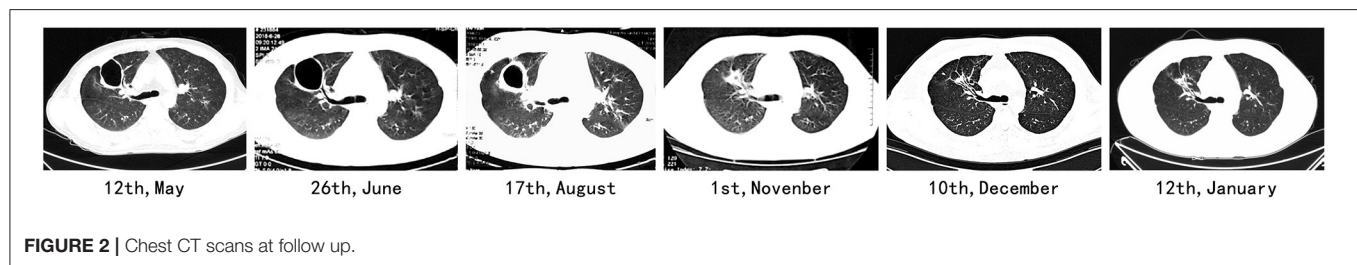
Except for cases not mentioned, tested, or classified, most of the patients in the series had a positive c-ANCA (42/46), and the most frequent antigen type was PR3 (35/38). P-ANCA (2/46) and MPO (2/38) were positive in only two patients, while c/p-ANCA double-positive and PR3/MPO double-positive were found in one patient each.

About ECMO, 22 patients received ECMO support in this series (22/61). Among those ECMO patients, 17 received

**TABLE 1** | Extracorporeal membrane oxygenation (ECMO) and SIMV parameters and results of arterial blood gas analysis.

Time	ECMO				SIMV					Blood gas analysis			
	Pump (rpm)	Blood flow (L/min)	Air flow (L/min)	Air FiO <sub>2</sub> (%)	RR (/min)	TV (ml)	Pressure (cmH <sub>2</sub> O)	PEEP (cmH <sub>2</sub> O)	Air FiO <sub>2</sub> (%)	pH	pCO <sub>2</sub>	pO <sub>2</sub>	OI (pO <sub>2</sub> /FiO <sub>2</sub> )
1st day (before ECMO)	–	–	–	–	44–54 (SPONT)	–	12	8–20	100	7.29	59	44	44
1st day (after ECMO)	3,485	3.8	5	100	14	380	10	12	60	7.43	36	65	65
2nd day	3,510	4.34	7	100	14	240	10	12	50	7.45	41	62	103
3rd day	3,555	4.33	6	100	–	–	–	–	–	–	–	–	–
4th day	–	–	–	–	14	223	10	12	50	7.41	48	72	144
6th day	3,555	4.32	8	100	–	–	–	–	50	–	–	–	–
7th day	3,555	4.23	7.5	100	–	–	–	–	50	–	–	–	–
8th day	3,500	4.02	8	100	–	–	–	–	50	7.49	43	120	305
9th day	–	–	–	–	14	244	10	10	40	–	–	–	–
10th day	3,480	4	8	100	–	–	–	–	40	–	–	–	–
11th day	3,480	3.64	8	100	14	240	10	10	40	7.46	44	131	327
12th day (removal of ECMO)	3,480	4	6.5	40	14	380	10	14	60	7.51	40	129	215
13th day (HFNC)	–	–	–	–	–	–	–	–	–	7.47	38	146	292
15th day	–	–	–	–	–	–	–	–	–	7.48	38	129	322

SIMV, synchronized intermittent mandatory ventilation; RR, respiratory rate; TV, tide volume; OI, oxygenation index; PEEP, positive end-expiratory pressure; SPONT, continuous spontaneous ventilation; HFNC, high-flow nasal cannula oxygen therapy; –, not applicable or no data or not changed.

**FIGURE 2** | Chest CT scans at follow up.

VV-ECMO (20/22), one received VA-ECMO (1/22), and one received VA-ECMO and VV-ECMO (1/22) sequentially. All patients, except the one who died before diagnosis, were administered glucocorticoids (60/61); cyclophosphamide was another important immunosuppressive drug for combinational utilization (52/61), while other immunosuppressive drugs such as methotrexate (1/61) and mycophenolate mofetil (1/61) were seldom used. Ten patients in this series received rituximab, a drug developed in recent years. Additionally, plasma exchange was also widely used in this series (34/61), and the proportion of patients receiving ECMO was 16/22, while that in non-ECMO was 18/39 (Table 3).

Finally, 14 patients died in this series due to ARF (14/61); none of them received ECMO support (Table 3), and the results showed a higher survival rate of patients in the ECMO group.

## DISCUSSION

GPA is a type of AAV; 85% of the patients with GPA show positive ANCA, mainly PR3-ANCA, and only a few demonstrate

MPO-ANCA (62). GPA is a multisystem vasculitis syndrome characterized by granulomatous lesions and necrotizing vasculitis, and all small blood vessels could be involved. The clinical symptoms of GPA vary and cover a wide range of symptoms, including fever, fatigue, weight loss, poor appetite, anorexia, arteritis, night sweats, cough, and dyspnea (63). Treatment strategies generally involve 3–6 months of remission induction plus more than 24 months of maintenance treatment using glucocorticoids in combination with immunosuppressors; sometimes, rituximab is added during the induction, and maintenance period (7).

More than 90% of patients with GPA have upper or lower respiratory tract involvement; however, the clinical manifestations can be asymptomatic to life-threatening respiratory failure. Among them, DASH and subglottic stenosis are the most common characteristics of GPA respiratory tract involvement (64, 65). Including the case, we reported that the main cause of respiratory failure was DASH in our series, and subglottic stenosis was relatively rare. It is noteworthy that patients with GPA may be

**TABLE 2 |** Case reports of respiratory failure due to granulomatosis with polyangiitis.

Case	Author	Publication year	Age	Gender	Respiratory onset	Extrapulmonary involvement	Reason of respiratory failure	ANCA		Radiology	ECMO		Immune-suppression	Plasma pheresis	Rituximab	Outcome
								Type	Antigen		Use and type	Duration (days)				
1	Leak et al. (8)	1967	61	Female	No	Yes	DAH	–	–	Infiltration, nodule	Not used	–	GC	No	No	Death
2	Leak et al. (8)	1967	45	Female	Yes	Yes	DAH	–	–	Cavity, infiltration	Not used	–	GC	No	No	Discharged
3	Hensley et al. (9)	1979	57	Female	No	Yes	DAH	–	–	Infiltration	Not used	–	GC, Cyc	No	No	Discharged
4	Feinstein et al. (10)	1985	22	Male	No	Yes	DAH	–	–	Cavity, infiltration	Not used	–	GC, Cyc	Yes	No	Discharged
5	Grupe and Colvin (11)	1986	15	Male	No	Yes	DAH	–	–	Infiltration	Not used	–	GC, Cyc	Yes	No	Death
6	Lenclud et al. (12)	1989	69	Female	Yes	Yes	DAH	p	–	Infiltration	Not used	–	GC, Cyc	No	No	Death
7	Lenclud et al. (12)	1989	70	Male	Yes	Yes	DAH	Positive	–	Infiltration	Not used	–	GC, Cyc	No	No	Discharged
8	Coggins et al. (13)	1989	56	Male	Yes	Yes	DAH	p/c	PR3/MPO	Infiltration	Not used	–	GC, Cyc	Yes	No	Death
9	Sanchez et al. (14)	1989	82	Female	Yes	Yes	DAH	–	–	Infiltration	Not used	–	GC, Cyc	No	No	Death
10	Misset et al. (15)	1991	35	Female	Yes	Yes	DAH	Negative	–	Infiltration	Not used	–	GC, Cyc	No	No	Discharged
11	Yoshimura et al. (16)	1992	58	Male	No	Yes	DAH	c	–	Nodule	Not used	–	GC, Cyc	No	No	Death
12	Odeh, M. et al. (17)	1993	75	Female	No	Yes	DAH	–	–	Consolidation	Not used	–	GC, Cyc	No	No	Death
13	Pradhan et al. (18)	2000	15	Female	Yes	Yes	DAH	p	MPO	Nodule	Not used	–	GC, Cyc	No	No	Discharged
14	Ullmer et al. (19)	2000	62	Male	Yes	Yes	DAH/PCP	c	–	Nodule, infiltration	Not used	–	GC, Cyc	No	No	Discharged
15	Hermon et al. (20)	2003	17	Female	No	Yes	DAH	c	PR3	Infiltration	Not used	–	GC, Cyc	No	No	Discharged
16	Senf et al. (21)	2003	35	Male	No	Yes	DAH/hydro thorax	c	PR3	Nodule, infiltration	Not used	–	GC, Cyc	Yes	Yes	Discharged
17	Prutkin et al. (22)	2003	56	Male	Yes	Yes	DAH	c	PR3	Infiltration, consolidation	Not used	–	GC, Cyc	No	No	Discharged

(Continued)



TABLE 2 | Continued

Case	Author	Publication year	Age	Gender	Respiratory onset	Extrapulmonary involvement	Reason of respiratory failure	ANCA		Radiology	ECMO		Immune-suppression	Plasma pheresis	Rituximab	Outcome
								Type	Antigen		Use and type	Duration (days)				
18	Griffith et al. (23)	2003	28	Male	Yes	Yes	DAH	c	PR3	Infiltration	Not used	–	GC, Cyc	Yes	No	Discharged
19	Steinau et al. (24)	2003	19	Male	Yes	Yes	DAH	c	PR3	Infiltration	Not used	–	GC, Cyc	No	No	Discharged
20	Nguyen et al. (25)	2005	20	Male	No	Yes	DAH	c	–	Infiltration	Not used	–	GC, Cyc	Yes	No	Discharged
21	Mera et al. (26)	2007	19	Male	Yes	Yes	DAH	c	PR3	Cavity, nodule	Not used	–	GC, Cyc	No	No	Discharged
22	Mukhopadhyay et al. (27)	2010	37	Male	Yes	Yes	DAH	c	PR3	Consolidation	Not used	–	(Death)	No	No	Death
23	Esposito et al. (28)	2010	7	Female	Yes	Yes	DAH	c	PR3	Infiltration, consolidation	Not used	–	GC, Cyc	No	No	Discharged
24	Berthoux et al. (29)	2011	54	Male	No	Yes	DAH	c	PR3	Consolidation	Not used	–	GC, Cyc	Yes	Yes	Discharged
25	Mahajan et al. (30)	2011	35	Male	Yes	Yes	DAH	c	–	Infiltration	Not used	–	GC, Cyc	No	No	Discharged
26	Marina et al. (31)	2011	64	Female	Yes	Yes	DAH/ mucormy cosis	c	PR3	Infiltration, nodule	Not used	–	GC, Cyc	Yes	No	Death
27	Cardenas–Garcia et al. (32)	2012	51	Female	Yes	Yes	DAH	c	–	Infiltration	Not used	–	GC, Cyc	Yes	No	Discharged
28	Ishiguro et al. (33)	2012	73	Female	No	Yes	DAH/CMV	Positive	PR3	Infiltration, nodule	Not used	–	GC, Cyc	No	No	Death
29	Kaya et al. (34)	2013	48	Male	No	Yes	DAH	c	PR3	Infiltration, nodule	Not used	–	GC, Cyc	Yes	No	Death
30	Powers et al. (35)	2013	32	Male	Yes	Yes	DAH	c	PR3	Infiltration, consolidation, nodule	Not used	–	GC, Cyc	Yes	Yes	Discharged
31	Haupt et al. (36)	2013	14	Female	Yes	Yes	DAH	c	PR3	Infiltration	Not used	–	GC	Yes	No	Discharged
32	Pinto et al. (37)	2014	65	Female	Yes	Yes	DAH/ pneumo thorax	c	PR3	Cavity	Not used	–	GC, Cyc	No	No	Death
33	Kaya et al. (34)	2014	60	Male	No	Yes	DAH	c	PR3	Infiltration	Not used	–	GC, Cyc	Yes	No	Discharged
34	Moreno-González et al. (38)	2014	42	Male	Yes	Yes	DAH/PTE	Positive	PR3	Infiltration, nodule	Not used	–	GC, Cyc	Yes	Yes	Discharged

(Continued)

TABLE 2 | Continued

Case	Author	Publication year	Age	Gender	Respiratory onset	Extrapulmonary involvement	Reason of respiratory failure	ANCA		Radiology	ECMO		Immune-suppression	Plasma pheresis	Rituximab	Outcome
								Type	Antigen		Use and type	Duration (days)				
35	Hilal et al. (39)	2015	55	Female	Yes	Yes	DAH/CMV c	PR3		Infiltration	Not used	–	GC	Yes	Yes	Death
36	Fukui et al. (40)	2015	69	Male	No	Yes	DAH/CMV c	MPO		Consolidation	Not used	–	GC, Cyc	Yes	No	Death
37	Tajarernmuang et al. (41)	2016	48	Female	No	Yes	Airway stenosis c	PR3		Stenosis	Not used	–	GC, Cyc	No	No	Discharged
38	Ning et al. (42)	2018	70	Female	Yes	Yes	DAH c	PR3		Nodule, infiltration, cavity	Not used	–	GC, MMF	Yes	No	Discharged
39	Sattar et al. (43)	2019	60	Female	No	Yes	DAH c	PR3		Cavity, infiltration	Not used	–	GC, Cyc	Yes	No	Discharged
40	Hartmann et al. (44)	1994	20	Female	No	Yes	DAH c	–		Infiltration	VV	6	GC, Cyc	Yes	No	Discharged
41	Loscar et al. (45)	1997	19	Female	No	Yes	DAH c	PR3		–	VV	10	GC, Cyc	No	No	Discharged
42	Matsumoto et al. (46)	2000	29	Female	Yes	Yes	DAH c	–		Nodule, infiltration	VA	3.4	GC, Cyc	No	No	Discharged
43	Rosengarten et al. (47)	2002	27	Female	Yes	Yes	DAH c	PR3		Infiltration	VV	15	GC, Cyc	No	No	Discharged
44	Hernandez et al. (48)	2002	13	Male	Yes	Yes	DAH c	–		Infiltration	VV	9	GC, Cyc	Yes	No	Discharged
45	Ahmed et al. (49)	2004	26	Female	Yes	Yes	DAH c	–		Cavity, infiltration	VV	14	GC, Cyc	Yes	No	Discharged
46	Gay et al. (50)	2005	26	Female	Yes	Yes	DAH c	–		Cavity, infiltration	VV	10	GC, Cyc	Yes	No	Discharged
47	Balasubramanian et al. (51)	2005	53	Male	No	Yes	DAH c	PR3		Infiltration	VV	NA	GC, Cyc	Yes	No	Discharged
48	Joseph et al. (52)	2011	13	Male	Yes	Yes	DAH Positive	PR3		Infiltration	VV	7	GC	Yes	No	Discharged
49	Barnes et al. (53)	2012	50	Female	Yes	Yes	DAH c	PR3		Consolidation	VV	1.5	GC, Cyc	Yes	No	Discharged
50	Hohenforst et al. (54)	2013	65	Female	Yes	Yes	DAH Positive	PR3		Infiltration	VV	10	GC, Cyc	Yes	No	Discharged
51	Yusuff et al. (55)	2015	23	Female	Yes	Yes	DAH c	PR3		–	VV	13	GC, Cyc	No	No	Discharged

(Continued)

TABLE 2 | Continued

Case	Author	Publication year	Age	Gender	Respiratory onset	Extrapulmonary involvement	Reason of respiratory failure	ANCA		Radiology	ECMO		Immune-suppression	Plasma pheresis	Rituximab	Outcome
								Type	Antigen		Use and type	Duration (days)				
52	Yusuff et al. (55)	2015	27	Male	Yes	Yes	DAH	c	–	Infiltration	VV	21	GC, Cyc	Yes	Yes	Discharged
53	Rawal et al. (56)	2016	28	Male	Yes	Yes	DAH	Positive	PR3	Infiltration	VV	21	GC, Cyc	Yes	No	Discharged
54	Vanoli et al. (57)	2017	33	Male	Yes	Yes	DAH	c	PR3	Consolidation, infiltration	VV	NA	GC, Cyc	Yes	Yes	Discharged
55	Falk et al. (58)	2017	17	Female	Yes	No	Airway stenosis	c	PR3	Emphysema	VA and VV	21	GC, Cyc	Yes	Yes	Discharged
56	Delvino et al. (59)	2019	45	Male	Yes	Yes	DAH	c	PR3	Infiltration	VV	6	GC, Cyc	Yes	No	Discharged
57	Delvino et al. (59)	2019	45	Male	No	Yes	DAH	c	PR3	Nodule, consolidation	VV	14	GC, MTX	No	Yes	Discharged
58	Goel et al. (60)	2020	34	Female	Yes	Yes	DAH	c	PR3	Nodule, consolidation	VV	7	GC, Cyc	Yes	No	Discharged
59	Yin et al. (61)	2020	25	Female	Yes	Yes	DAH	Positive	–	Infiltration, consolidation	VV	52	GC, Cyc	No	No	Discharged
60	Yin et al. (61)	2020	18	Female	Yes	Yes	DAH	Positive	–	–	VV	123	GC	Yes	Yes	Lung transplant
61	This case	2020	32	Male	Yes	No	DAH	c	PR3	Cavity, infiltration, consolidation	VV	12	GC, Cyc	Yes	No	Discharged

PTE, pulmonary thromboembolism.

**TABLE 3 |** Summary of cases of respiratory failure due to GPA.

	<b>Total (IQR/%)</b> <b>(n = 61)</b>	<b>ECMO (IQR/%)</b> <b>(n = 22)</b>	<b>Non-ECMO (IQR/%)</b> <b>(n = 39)</b>	<b>P-value</b>
Publication time				0.08
Before 2000	17 (27.87)	3 (13.64)	14 (35.90)	–
After 2000	44 (72.13)	19 (86.36)	25 (64.10)	–
Age	35.00 (23.00–57.00)	27.00 (20.75–33.75)	51.00 (30.00–61.50)	<0.01
Female	32 (52.45)	13 (52.63)	19 (53.13)	0.59
Respiratory onset	41 (67.21)	18 (81.82)	23 (58.97)	0.09
ANCA				0.80
No information	7 (11.48)	0	7 (17.95)	–
Negative	1 (1.64)	0	1 (2.56)	–
Unknown type	8 (13.11)	5 (22.72)	3 (7.69)	–
c-ANCA	42 (68.85)	17 (77.27)	25 (64.10)	–
p-ANCA	2 (3.28)	0	2 (5.13)	–
p + c-ANCA	1 (1.64)	0	1 (2.56)	–
ANCA antigen				0.69
No information	23 (37.70)	8 (36.36)	15 (38.46)	–
PR3	35 (57.38)	14 (63.64)	21 (53.85)	–
MPO	2 (3.28)	0	2 (5.13)	–
PR3 + MPO	1 (1.64)	0	1 (2.56)	–
<b>Radiology</b>				
No information	3 (4.92)	3 (13.64)	0	–
Infiltration	45 (73.77)	15 (68.18)	30 (76.92)	0.55
Consolidation	13 (21.31)	6 (27.27)	7 (17.95)	0.07
Cavity	9 (14.75)	3 (13.64)	6 (15.38)	1
Nodule	15 (24.59)	3 (13.64)	12 (30.77)	0.22
Stenosis	1 (1.64)	0	1 (2.56)	1
Emphysema	1 (1.64)	1 (4.55)	0	0.36
Treatment				
GC	60 (98.36)	22 (100.00)	38 (97.44)	1
CYC	52 (85.25)	19 (86.36)	33 (84.62)	1
MTX	1 (1.64)	1 (4.54)	0	0.34
MMF	1 (1.64)	0	1 (2.56)	1
Plasmapheresis	34 (55.74)	16 (72.73)	18 (46.15)	0.06
Rituximab	10 (16.39)	5 (22.73)	5 (12.82)	0.47
Death				<0.01 (total death)
Before 2000	7 (11.48)	0	7 (17.95)	0.55
After 2000	7 (11.48)	0	7 (17.95)	0.03

–, not applicable.

associated with opportunistic infections of the lungs due to immunosuppressive therapy.

GPA-related DAH occurs in 7–45% of patients with GPA (65, 66). Fewer than 10% of cases with DAH are serious with life-threatening conditions (29); most of them are GPA patients with alveolar hemorrhage, and their mortality rate is six times that of those without alveolar hemorrhage (67). Among patients with GPA, 60% are caused by DAH (43). Any degree of DAH should be considered a serious manifestation of the disease as it can quickly progress to respiratory failure (62). The underlying pathophysiological mechanism of GPA-related DAH is linked to antibodies related to ANCA, which

interact with inflammatory cells (neutrophils, monocytes, and lymphocytes) and cytokines (particularly Th1 cytokines, namely, tumor necrosis factor and interferon- $\gamma$ ) and then initiate and perpetuate vasculitis (68, 69). The basement membrane of capillaries is destroyed during these processes, and erythrocytes are allowed to enter the alveolar space with fluid (69). These processes damage the gas exchange of the affected lung area. However, the symptoms of DAH, including dyspnea, hypoxia, anemia, and lack of imaging findings of diffuse alveolar filling, are not specific; however, hemoptysis is relatively rare in DAH. In clinical practice, when a case with imaging findings indicates extensive infiltration but is refractory to anti-infective treatment,



bronchial alveolar lavage under bronchoscopy is recommended to ascertain the occurrence of DAH (62), and immunological examination should also be conducted to obtain a definitive diagnosis that can help clinicians arrange immunosuppressive treatment earlier.

Moreover, similar to DAH, the symptoms of subglottic stenosis lack specificity, ranging from coughing and dyspnea to life-threatening stridor (65). Unlike DAH, subglottic stenosis generally does not show any positive findings on radiology, bronchoscopy is needed to confirm the diagnosis, and the severity of respiratory involvement is related to the location, length, and degree of stenosis (65). In addition, rapid progress to respiratory failure may occur among these patients soon after admission (41, 58).

Our patient has a severe case of the disease that progressed rapidly to respiratory failure within 3 days of admission, and respiratory support was upgraded from HFNC and NIPPV to intermittent mandatory ventilation (IMV) and ECMO in a short period. Additionally, the patient had no extrapulmonary manifestations, and severe infective pneumonia was the first clinical diagnosis. GPA was not diagnosed until a positive ANCA result was reported. At this time, ECMO was used for approximately 12 h. This case showed that GPA may present with unspecified clinical symptoms and radiological manifestations with rapid progress into respiratory failure, which leads to difficulties in early diagnosis and proper treatment.

Therefore, when respiratory symptoms occur in patients with GPA, etiological treatment and powerful respiratory support should be provided as soon as possible. Glucocorticoids and cyclophosphamide are the first-line drugs for impact and maintenance treatment. Rituximab and plasmapheresis should be considered when feasible (7). Respiratory support should be chosen based on oxygenation conditions, and HFNC should be upgraded early to IMV or ECMO when necessary and available (5) to further timely diagnose and treat. In this case series, all patients received ECMO as they were unable to maintain oxygenation through basic respiratory support; among them, one patient received VV-ECMO and VA-ECMO sequentially due to circulatory dysfunction related to mediastinal emphysema.

ARF is one of the indications for ECMO support. Since the first patient with ARDS was rescued using ECMO in 1972 (70), it has been increasingly used in ARF (71). Without ECMO support, our patient would not have survived. In our series, none of the patients could maintain oxygenation under mechanical ventilation before ECMO, indicating that ECMO can improve the prognosis of respiratory failure caused by GPA (59) and provide the possibility of later recovery. In other studies, such as the conventional ventilatory support vs. extracorporeal membrane oxygenation for severe acute respiratory failure in 2009, ECMO significantly improved the disability-free survival rate of patients with severe ARF (72). ECMO to rescue lung injury in severe ARDS (EOLIA) in 2008 showed that ECMO can significantly reduce the probability of 60-day treatment failure in patients with severe ARDS and increase the days of improved oxygenation, and no renal failure has occurred

(73). However, whether ECMO can improve the prognosis of ARF remains controversial. There was no statistical significance in terms of prognosis between ECMO and non-ECMO users among patients with ARDS in the EOLIA study (73). Among patients with immune-related DAH, ECMO did not improve the survival rates (20 vs. 38%,  $p = 0.323$ ) (74). Although these studies showed negative results, we should note that the early termination of the EOLIA study and the high proportion of patients who received remedial treatments from the traditional treatment group transferred to the ECMO group may lead to no statistically significant difference in mortality between the two groups. In studies of patients with ARDS owing to DAH (74), those who required ECMO generally had a lower oxygenation index (87 vs. 62,  $p = 0.017$ ), more days of mechanical ventilation (21 vs. 9.5,  $p < 0.001$ ), and higher alveolar-arterial gradient (450 vs. 586,  $p = 0.017$ ), which indicates that even if these two groups of patients are included in the study under the same criteria, the oxygenation index may be much worse in patients who used ECMO, which may generate negative results.

Hence, regardless of the conclusions of future clinical studies on whether ECMO can improve the prognosis of patients with GAP-related respiratory failure, we recommend ECMO as a transitional method for those with respiratory failure caused by GPA who cannot maintain oxygenation through mechanical ventilation. Moreover, ECMO could win some time for these patients to be correctly diagnosed and treated later (74).

## CONCLUSION

ECMO provides the final respiratory support for GPA-related critical respiratory failure and assists patients who cannot maintain oxygenation using mechanical ventilation for further definitive diagnosis and treatment. However, whether it can improve the clinical outcomes of GPA-related respiratory failure remains to be further studied.

## DATA AVAILABILITY STATEMENT

The original contributions presented in the study are included in the article/supplementary material, further inquiries can be directed to the corresponding author/s.

## ETHICS STATEMENT

Ethical review and approval was not required for the study on human participants in accordance with the local legislation and institutional requirements. The patients/participants provided their written informed consent to participate in this study.

## AUTHOR CONTRIBUTIONS

RW and YL reviewed the lectures and wrote the manuscript. WenY, XM, WeiY, YZ, RL, and YF collected and arranged the materials. CH, QC, and PP viewed the complete manuscript.

All authors contributed to the article and approved the submitted version.

## FUNDING

This work was supported by grants from the Natural Science Foundation of Hunan Province (2019JJ50939), the National

Natural Science Foundation of China (81873406), and the National Key R&D Program of China (2018YFC1311900).

## ACKNOWLEDGMENTS

We would like to thank Editage (www.editage.cn) for English language editing.

## REFERENCES

- Nasser M, Cottin V. Alveolar hemorrhage in vasculitis (Primary and Secondary). *Semin Respir Crit Care Med.* (2018) 39:482–93. doi: 10.1055/s-0038-1668533
- Lamprecht P, Kerstein A, Klapa S, Schinke S, Karsten CM, Yu X, et al. Pathogenetic and clinical aspects of anti-neutrophil cytoplasmic autoantibody-associated vasculitides. *Front Immunol.* (2018) 9:680. doi: 10.3389/fimmu.2018.00680
- Geri G, Terrier B, Heshmati F, Moussaoui H, Massot J, Mira JB, et al. Effect of plasma exchange in acute respiratory failure due to Anti-neutrophil cytoplasmic antibody-associated vasculitis. *Critic Care.* (2018) 22:328. doi: 10.1186/s13054-018-2264-x
- Demiselle J, Auchabie J, Beloncle F, Gatault P, Grange S, Du Cheyron D, et al. Patients with ANCA-associated vasculitis admitted to the intensive care unit with acute vasculitis manifestations: a retrospective and comparative multicentric study. *Ann Intensive Care.* (2017) 7:39. doi: 10.1186/s13613-017-0262-9
- Goligher EC, Ferguson ND, Brochard LJ. Clinical challenges in mechanical ventilation. *Lancet.* (2016) 387:1856–66. doi: 10.1016/S0140-6736(16)30176-3
- Combes A, Pesenti A, Ranieri VM. Fifty years of research in ARDS. Is extracorporeal circulation the future of acute respiratory distress syndrome management? *Am J Respir Crit Care Med.* (2017) 195:1161–70. doi: 10.1164/rccm.201701-0217CP
- Salvador F. ANCA associated vasculitis. *Eur J Intern Med.* (2020) 74:18–28. doi: 10.1016/j.ejim.2020.01.011
- Leak D, Klein GP. Acute Wegener's granulomatosis. *Thorax.* (1967) 22:437–43. doi: 10.1136/thx.22.5.437
- Hensley MJ, Feldman NT, Lazarus JM, Galvanek EG. Diffuse pulmonary hemorrhage and rapidly progressive renal failure. an uncommon presentation of Wegener's granulomatosis. *Am J Med.* (1979) 66:894–8. doi: 10.1016/0002-9343(79)91149-5
- Feinstein EI, Kitt D, Collins JF, Boylen T, Koss M. Hemoptysis and acute renal failure in a young man. *Am J Nephrol.* (1985) 5:64–70. doi: 10.1159/000166908
- Grupe WE, Colvin RB. Case records of the Massachusetts General Hospital. Weekly clinicopathological exercises. Case 12-1986. A 15-year-old boy with hemoptysis and occult blood in the urine. *N Engl J Med.* (1986) 314:834–44. doi: 10.1056/NEJM198603273141307
- Lenclud C, De Vuyst P, Dupont E, Depierreux M, Ketelbant P, Goldman M. Wegener's granulomatosis presenting as acute respiratory failure with anti-neutrophil-cytoplasm antibodies. *Chest.* (1989) 96:345–7. doi: 10.1378/chest.96.2.345
- Coggins CH, Niles JL, Fienberg R. Case records of the Massachusetts General Hospital. Weekly clinicopathological exercises. Case 25-1989. A 56-year-old man with hemoptysis and microscopic hematuria. *N Engl J Med.* (1989) 320:1677–86. doi: 10.1056/NEJM198906223202508
- Sanchez-Masiques J, Etensohn DB. Alveolar hemorrhage in Wegener's granulomatosis. *Am J Med Sci.* (1989) 297:390–3. doi: 10.1097/0000441-198906000-00013
- Misset B, Glotz D, Escudier B, Nochy D, Bosq J, Gilles E, et al. Wegener's granulomatosis presenting as diffuse pulmonary hemorrhage. *Intensive Care Med.* (1991) 17:118–20. doi: 10.1007/BF01691435
- Yoshimura N, Matsubara O, Tamura A, Kasuga T, Mark EJ. Wegener's granulomatosis. associated with diffuse pulmonary hemorrhage. *Acta Pathol Jpn.* (1992) 42:657–61. doi: 10.1111/j.1440-1827.1992.tb03047.x
- Odeh M, Best LA, Kerner H, Bassan H, Oliven A. Localized Wegener's granulomatosis relapsing as diffuse massive intra-alveolar hemorrhage. *Chest.* (1993) 104:955–6. doi: 10.1378/chest.104.3.955
- Pradhan M, Meyers KE, Guttenberg M, Kaplan BS. Wegener granulomatosis—an atypical case. *Pediatr Nephrol.* (2000) 14:862–71. doi: 10.1007/PL00013445
- Ullmer E, Mayr M, Binet I, Ebnother-Staub C, Dalquen P, Soler M, et al. Granulomatous Pneumocystis carinii pneumonia in Wegener's granulomatosis. *Eur Respir J.* (2000) 15:213–6. doi: 10.1183/09031936.00.15121300
- Herman MM, Golej J, Emminger W, Puig S, Szeplafusi Z, Trittenwein G. Acute hemorrhagic respiratory failure caused by Wegener's granulomatosis successfully treated by bronchoalveolar lavage with diluted surfactant. *Wien Klin Wochenschr.* (2003) 115:793–6. doi: 10.1007/BF03040505
- Senf R, Jürgensen JS, Teichgräber U, Kampf D, Schindler R. Ruptured arterial aneurysm of the kidney in a patient with Wegener's granulomatosis. *Nephrol Dialysis Transp.* (2003) 18:2671–3. doi: 10.1093/ndt/gfg380
- Prutkin JM, Barry P, Zaas D. Cases from the osler medical service at Johns Hopkins University. *Am J Med.* (2003) 115:150–3. doi: 10.1016/S0002-9343(03)00356-5
- Griffith M, Brett S. The pulmonary physician in critical care · illustrative case 3: pulmonary vasculitis. *Thorax.* (2003) 58:543–6. doi: 10.1136/thorax.58.6.543
- Steinau F, Deja M, Weber-Carstens S, Busch T, Kaisers U. Onset of acute respiratory distress syndrome following severe pulmonary hemorrhage in a patient with anti-neutrophil cytoplasmic antibody associated vasculitis. *Intensive Care Med.* (2003) 29:504. doi: 10.1007/s00134-003-1647-9
- Nguyen T, Martin MK, Indrikovs AJ. Plasmapheresis for diffuse alveolar hemorrhage in a patient with Wegener's granulomatosis: case report and review of the literature. *J Clin Apher.* (2005) 20:230–4. doi: 10.1002/jca.20069
- Mera A, Wada M, Miyajima M. [A case of Wegener's granulomatosis presenting as severe acute respiratory failure]. *Nihon Kokyuki Gakkai Zasshi.* (2007) 45:262–6.
- Mukhopadhyay S, Hensley RG, Tazelaar HD. Cardiac involvement in Wegener granulomatosis diagnosed at autopsy. *Cardiovasc Pathol.* (2010) 19:312–5. doi: 10.1016/j.carpath.2009.06.011
- Esposito S, Corona F, Defilippi A, Petaccia A, Chidini G, Dell'Era L, et al. Wegener's granulomatosis presenting with life-threatening lung hemorrhage in a 7-year-old child. *Rheumatol Int.* (2010) 30:1665–8. doi: 10.1007/s00296-009-1132-z
- Berthoux E, Padilla M, Chavez L, Colombe B, Bosseray A, Massot C. Unusual evolution in Wegener's granulomatosis: recovery of pulmonary involvement while renal disease progressed to end-stage. *Ren Fail.* (2011) 33:1032–6. doi: 10.3109/0886022X.2011.610547
- Mahajan V, Whig J, Kashyap A, Gupta S. Diffuse alveolar hemorrhage in Wegener's granulomatosis. *Lung India.* (2011) 28:52–5. doi: 10.4103/0970-2113.76302
- Marina M, Maria A. A fatal case of treatment-related adverse effects in granulomatosis with polyangiitis (Wegener's Granulomatosis). *Open J Rheumatol Autoimmune Dis.* (2011) 1:5–9. doi: 10.4236/ojra.2011.12002
- Cardenas-Garcia J, Farmakiotis D, Baldovino BP, Kim P. Wegener's granulomatosis in a middle-aged woman presenting with dyspnea, rash, hemoptysis and recurrent eye complaints: a case report. *J Med Case Rep.* (2012) 6:335. doi: 10.1186/1752-1947-6-335
- Ishiguro T, Takayanagi N, Yamaguchi S, Shimizu Y, Yanagisawa T, Sugita Y, et al. Pulmonary capillaritis in Wegener's granulomatosis

- detected via transbronchial lung biopsy. *Intern Med.* (2012) 51:905–9. doi: 10.2169/internalmedicine.51.6518
34. Kaya H, Yilmaz S, Sezgi C, Abakay O, Taylan M, Sen H, et al. Two cases of extrapulmonary onset granulomatosis with polyangiitis which caused diffuse alveolar haemorrhage. *Respir Med Case Rep.* (2014) 13:32–6. doi: 10.1016/j.rmcr.2014.09.002
  35. Powers B, Uppalapati A, Gogineni S, Jamkhana ZA. Rituximab—a drug with many facets and cures: a treatment for acute refractory hypoxemic respiratory failure secondary to severe granulomatosis with polyangiitis. *Case Rep Crit Care.* (2013) 2013:123134. doi: 10.1155/2013/123134
  36. Haupt ME, Pires-Ervoes J, Brannen ML, Klein-Gitelman MS, Prestidge AL, Nevin MA. Successful use of plasmapheresis for granulomatosis with polyangiitis presenting as diffuse alveolar hemorrhage. *Pediatr Pulmonol.* (2013) 48:614–6. doi: 10.1002/ppul.22666
  37. Pinto B, Dhir V, Singh PK, Gowda KK, Sharma A. Granulomatosis with polyangiitis and severe respiratory involvement. *J Emerg Med.* (2014) 47:e79–81. doi: 10.1016/j.jemermed.2014.01.037
  38. Moreno-González G, Corral-Ansa L, Sabater-Riera J, Solanich-Moreno X, Mañez-Mendiluce R. Pulmonary thromboembolism and diffuse alveolar hemorrhage in granulomatosis with polyangiitis vasculitis. *Respiratory Care.* (2014) 59:e206–e9. doi: 10.4187/respcare.03162
  39. Hilal T. Fatal cytomegalovirus disease after combination therapy with corticosteroids and rituximab for granulomatosis with polyangiitis. *Case Rep Rheumatol.* (2015) 2015:538137. doi: 10.1155/2015/538137
  40. Fukui S, Iwamoto N, Tsuji S, Umeda M, Nishino A, Nakashima Y, et al. Diffuse alveolar hemorrhage emerging one week after starting high-dose corticosteroid therapy for granulomatosis with polyangiitis (GPA) with systemic lupus erythematosus (SLE). *Intern Med.* (2015) 54:2681–6. doi: 10.2169/internalmedicine.54.5299
  41. Tajarernmuang P, Limsukon A, Liwsrisakun C, Wannasopha Y. Severe bilateral bronchial stenosis with acute respiratory failure from granulomatosis with polyangiitis. *Respirol Case Rep.* (2016) 4:e00189. doi: 10.1002/rcr2.189
  42. Ning S, Zhang X, Xu C, Dang X, Cheng H, Zhu K, et al. Methylprednisolone and plasmapheresis are effective for life-threatening diffuse alveolar hemorrhage and gastrointestinal hemorrhage in granulomatosis with polyangiitis: a case report and literature review. *Medicine.* (2018) 97:e0592. doi: 10.1097/MD.00000000000010592
  43. Sattar Y, Susheela AT, Ullah W, Usman N, Zafrullah F. Use of plasmapheresis and immunosuppressants to treat diffuse alveolar hemorrhage in a patient with granulomatosis with polyangiitis. *Medicina.* (2019) 55:378. doi: 10.3390/medicina55070378
  44. Hartmann A, Nordal KP, Svennevig J, Noddeland H, Pedersen T, Skarbovik AJ, et al. Successful use of artificial lung (ECMO) and kidney in the treatment of a 20-year-old female with Wegener's syndrome. *Nephrol Dial Transplant.* (1994) 9:316–9.
  45. Loscar M, Hummel T, Haller M, Briegel J, Wiebecke B, Samtleben W, et al. [ARDS and Wegener granulomatosis]. *Anaesthesist.* (1997) 46:969–73. doi: 10.1007/s001010050494
  46. Matsumoto T, Ueki K, Tamura S, Ideura H, Tsukada Y, Maezawa A, et al. Extracorporeal membrane oxygenation for the management of respiratory failure due to ANCA-associated vasculitis. *Scand J Rheumatol.* (2000) 29:195–7. doi: 10.1080/030097400750002111
  47. Rosengarten A, Elmore P, Epstein J. Long distance road transport of a patient with Wegener's Granulomatosis and respiratory failure using extracorporeal membrane oxygenation. *Emerg Med.* (2002) 14:181–7. doi: 10.1046/j.1442-2026.2002.00315.x
  48. Hernandez ME, Lovrekovic G, Schears G, Helfaer M, Friedman D, Stafford P, et al. Acute onset of Wegener's granulomatosis and diffuse alveolar hemorrhage treated successfully by extracorporeal membrane oxygenation. *Pediatric Criti Care Med.* (2002) 3:63–6. doi: 10.1097/00130478-200201000-00014
  49. Ahmed SH, Aziz T, Cochran J, Highland K. Use of extracorporeal membrane oxygenation in a patient with diffuse alveolar hemorrhage. *Chest.* (2004) 126:305–9. doi: 10.1378/chest.126.1.305
  50. Gay SE, Ankney N, Cochran JB, Highland KB. Critical care challenges in the adult ECMO patient. *Dimens Crit Care Nurs.* (2005) 24:157–62; quiz 63–4. doi: 10.1097/00003465-200507000-00001
  51. Balasubramanian SK, Tiruvoipati R, Chatterjee S, Sosnowski A, Firmin RK. Extracorporeal membrane oxygenation with lepirudin anticoagulation for Wegener's granulomatosis with heparin-induced thrombocytopenia. *Asaio J.* (2005) 51:477–9. doi: 10.1097/01.mat.00000169123.21946.31
  52. Joseph M, Charles AG. Early extracorporeal life support as rescue for Wegener granulomatosis with diffuse alveolar hemorrhage and acute respiratory distress syndrome: a case report and literature review. *Pediatr Emerg Care.* (2011) 27:1163–6. doi: 10.1097/PEC.0b013e31823b01a2
  53. Barnes SL, Naughton M, Douglass J, Murphy D. Extracorporeal membrane oxygenation with plasma exchange in a patient with alveolar haemorrhage secondary to Wegener's granulomatosis. *Intern Med J.* (2012) 42:341–2. doi: 10.1111/j.1445-5994.2012.02720.x
  54. Hohenforst-Schmidt W, Petermann A, Visouli A, Zarogoulidis P, Darwiche K, Kougioumtzi I, et al. Successful application of extracorporeal membrane oxygenation due to pulmonary hemorrhage secondary to granulomatosis with polyangiitis. *Drug Des Devel Ther.* (2013) 7:627–33. doi: 10.2147/DDDT.S47156
  55. Yusuf H, Malagon I, Robson K, Parmar J, Hamilton P, Falter F. Extracorporeal membrane oxygenation for Life-threatening ANCA-positive pulmonary capillaritis. a review of UK experience. *Heart Lung Vessel.* (2015) 7:159–67.
  56. Rawal G, Kumar R, Yadav S. ECMO rescue therapy in diffuse alveolar haemorrhage: a case report with review of literature. *J Clin Diagn Res.* (2016) 10:Od10–1. doi: 10.7860/JCDR/2016/20649.7969
  57. Vanoli J, Riva M, Vergnano B, D'Andrea G, L'Imperio V, Pozzi MR, et al. Granulomatosis with polyangiitis presenting with diffuse alveolar hemorrhage requiring extracorporeal membrane oxygenation with rapid multiorgan relapse: A case report. *Medicine.* (2017) 96:e6024. doi: 10.1097/MD.00000000000006024
  58. Falk L, Broman LM. Extracorporeal membrane oxygenation rescue in adolescent with bronchiolitis obliterans-organizing pneumonia like Wegener's granulomatosis. *Clin Case Rep.* (2017) 5:29–34. doi: 10.1002/ccr3.752
  59. Delvino P, Monti S, Balduzzi S, Belliato M, Montecucco C, Caporali R. The role of extra-corporeal membrane oxygenation (ECMO) in the treatment of diffuse alveolar haemorrhage secondary to ANCA-associated vasculitis: report of two cases and review of the literature. *Rheumatol Int.* (2019) 39:367–75. doi: 10.1007/s00296-018-4116-z
  60. Goel MK, Chauhan M, Kumar A, Wadwa P, Maitra G, Talegaonkar M, et al. A case of refractory hypoxemic respiratory failure due to antineutrophil cytoplasmic antibodies-associated diffuse alveolar hemorrhage rescued by extracorporeal membrane oxygenation. *Indian J Crit Care Med.* (2020) 24:879–81. doi: 10.5005/jp-journals-10071-23585
  61. Yin K, March RJ, Hoopes CW, Balk RA, Raman J, Lateef OB, et al. Extracorporeal membrane oxygenation in the management of granulomatosis with polyangiitis. *J Cardiac Surg.* (2021) 36:743–7. doi: 10.1111/jocs.15252
  62. Thompson GE, Specks U. Update on the management of respiratory manifestations of the antineutrophil cytoplasmic antibodies-associated vasculitides. *Clin Chest Med.* (2019) 40:573–82. doi: 10.1016/j.ccm.2019.05.012
  63. Almouhawis HA, Leao JC, Fedele S, Porter SR. Wegener's granulomatosis: a review of clinical features and an update in diagnosis and treatment. *J Oral Pathol Med.* (2013) 42:507–16. doi: 10.1111/jop.12030
  64. Wick MR. Pulmonary disorders that are potentially associated with anti-neutrophilic cytoplasmic antibodies: a brief review. *Semin Diagn Pathol.* (2018) 35:304–14. doi: 10.1053/j.semdp.2018.08.005
  65. Thickett DR, Richter AG, Nathani N, Perkins GD, Harper L. Pulmonary manifestations of anti-neutrophil cytoplasmic antibody (ANCA)-positive vasculitis. *Rheumatology.* (2006) 45:261–8. doi: 10.1093/rheumatology/kei217
  66. Quartuccio L, Bond M, Isola M, Monti S, Felicetti M, Furini F, et al. Alveolar haemorrhage in ANCA-associated vasculitis: long-term outcome and mortality predictors. *J Autoimmun.* (2020) 108:102397. doi: 10.1016/j.jaut.2019.102397
  67. Caetano J, Fernandes das Neves M, Oliveira S, Delgado Alves J. Refractory Wegener's granulomatosis presenting with alveolar haemorrhage, treated with rituximab. *BMJ Case Rep.* (2014) 2014:bcr2014208510. doi: 10.1136/bcr-2014-208510

68. Scapa JV, Fishbein GA, Wallace WD, Fishbein MC. Diffuse alveolar hemorrhage and pulmonary vasculitides: histopathologic findings. *Semin Respir Crit Care Med.* (2018) 39:425–33. doi: 10.1055/s-0038-1669412
69. Martinez-Martinez MU, Oostdam DAH, Abud-Mendoza C. Diffuse alveolar hemorrhage in autoimmune diseases. *Curr Rheumatol Rep.* (2017) 19:27. doi: 10.1007/s11926-017-0651-y
70. Hill JD, O'Brien TG, Murray JJ, Dontigny L, Bramson ML, Osborn JJ, et al. Prolonged extracorporeal oxygenation for acute post-traumatic respiratory failure (shock-lung syndrome). use of the Bramson membrane lung. *N Engl J Med.* (1972) 286:629–34. doi: 10.1056/NEJM197203232861204
71. Parekh M, Abrams D, Brodie D, Yip NH. Extracorporeal membrane oxygenation for ARDS: optimization of lung protective ventilation. *Respir Care.* (2018) 63:1180–8. doi: 10.4187/respcare.06262
72. Peek GJ, Mugford M, Tiruvoipati R, Wilson A, Allen E, Thalanany MM, et al. Efficacy and economic assessment of conventional ventilatory support versus extracorporeal membrane oxygenation for severe adult respiratory failure (CESAR): a multicentre randomised controlled trial. *Lancet.* (2009) 374:1351–63. doi: 10.1016/S0140-6736(09)61069-2
73. Combes A, Hajage D, Capellier G, Demoule A, Lavoue S, Guervilly C, et al. Extracorporeal membrane oxygenation for severe acute respiratory distress syndrome. *N Engl J Med.* (2018) 378:1965–75. doi: 10.1056/NEJMoa1800385
74. Seeliger B, Stahl K, Schenk H, Schmidt JJ, Wiesner O, Welte T, et al. Extracorporeal membrane oxygenation for severe ARDS due to immune diffuse alveolar hemorrhage: a retrospective observational study. *Chest.* (2020) 157:744–7. doi: 10.1016/j.chest.2019.10.021

**Conflict of Interest:** The authors declare that the research was conducted in the absence of any commercial or financial relationships that could be construed as a potential conflict of interest.

Copyright © 2021 Wan, Yang, Ma, Yang, Pan, Hu, Chen, Zhou, Lu, Fang and Li. This is an open-access article distributed under the terms of the Creative Commons Attribution License (CC BY). The use, distribution or reproduction in other forums is permitted, provided the original author(s) and the copyright owner(s) are credited and that the original publication in this journal is cited, in accordance with accepted academic practice. No use, distribution or reproduction is permitted which does not comply with these terms.





# Multi-Dimensional Display of Wang's Lymph Node Map Using Virtual Bronchoscopic Navigation System

Fen Lan<sup>1†</sup>, Yaling Yue<sup>2†</sup>, Hong Shen<sup>3†</sup>, Hui Shen<sup>1,4†</sup>, Qiyuan Wang<sup>5†</sup>, Xiuqing Yu<sup>6</sup>, Laijuan Chen<sup>6</sup>, Qin Li<sup>1</sup>, Kopen Wang<sup>7</sup>, Qinghua Liu<sup>8\*</sup> and Yang Xia<sup>1\*</sup>

<sup>1</sup>Key Laboratory of Respiratory Disease of Zhejiang Province, Department of Respiratory and Critical Care Medicine, Second Affiliated Hospital of Zhejiang University School of Medicine, Hangzhou, China, <sup>2</sup>Department of Medical Oncology, Handan Central Hospital, Handan, China, <sup>3</sup>Department of Respiratory and Critical Care Medicine, Second Affiliated Hospital of Nanjing Medical University, Nanjing, China, <sup>4</sup>Department of Respiratory and Critical Care Medicine, Huzhou Central Hospital, Huzhou, China, <sup>5</sup>Department of Radiology, Second Affiliated Hospital of Zhejiang University School of Medicine, Hangzhou, China, <sup>6</sup>Department of Endoscopic Center, Second Affiliated Hospital of Zhejiang University School of Medicine, Hangzhou, China, <sup>7</sup>Division of Pulmonary and Critical Care Medicine, Johns Hopkins University School of Medicine, Baltimore, MD, United States, <sup>8</sup>Department of Respiratory and Critical Care Medicine, Shanghai East Hospital, Tongji University, Shanghai, China

## OPEN ACCESS

### Edited by:

Dianhua Jiang,  
Cedars Sinai Medical Center,  
United States

### Reviewed by:

Yan Yin,  
China Medical University, China  
Jiayuan Sun,  
Shanghai Jiaotong University, China  
Suqin Ben,  
Shanghai General Hospital, China

### \*Correspondence:

Yang Xia  
yxia@zju.edu.cn  
Qinghua Liu  
lzlqhlz@163.com

<sup>†</sup>These authors share first authorship

### Specialty section:

This article was submitted to  
Molecular Diagnostics and  
Therapeutics,  
a section of the journal  
Frontiers in Molecular Biosciences

**Received:** 11 March 2021

**Accepted:** 11 May 2021

**Published:** 07 June 2021

### Citation:

Lan F, Yue Y, Shen H, Shen H, Wang Q, Yu X, Chen L, Li Q, Wang K, Liu Q and Xia Y (2021) Multi-Dimensional Display of Wang's Lymph Node Map Using Virtual Bronchoscopic Navigation System. *Front. Mol. Biosci.* 8:679442. doi: 10.3389/fmolb.2021.679442

**Background:** Transbronchial needle aspiration (TBNA) is a classical technique for diagnosing mediastinal-hilar lymph node enlargement. However, the diagnostic value of conventional TBNA (cTBNA) is limited in small lymph nodes.

**Methods:** Here, we generated an innovative multi-dimensional virtual lymph node map on top of Wang's lymph node map using a Lungpoint Virtual Bronchoscopic Navigation System.

**Results:** The virtual bronchoscopic navigation (VBN) system was combined with computed tomography (CT) images to generate extrabronchial, endobronchial, sagittal, coronal as well as horizontal views of the 11 intrathoracic lymph node stations and their adjacent tissues and blood vessels. We displayed the specific puncture site of each lymph node station. The 11 stations were divided into four groups: right mediastinal stations, left mediastinal stations, central mediastinal stations and hilar stations.

**Conclusion:** The VBN system provides a precise view of the intrabronchial landmarks, which may increase the diagnostic accuracy of intrathoracic lymph node adenopathy and assist bronchoscopists with practicing TBNA.

**Keywords:** lymph node map, TBNA, mediastinal-hilar lymph node, virtual navigation system, bronchoscopy

## INTRODUCTION

Transbronchial needle aspiration (TBNA) is a classical bronchoscopic technique for diagnosing benign and malignant mediastinal-hilar lymph node enlargement. With technological progress, endobronchial ultrasound-guided TBNA (EBUS-TBNA) provides real-time ultrasound imaging, resulting in a higher diagnostic yield than conventional TBNA (cTBNA) and has been widely practiced in clinical settings worldwide (Herth et al., 2004; Bonifazi et al., 2017; Madan et al., 2017). However, even with ultrasound guidance, the diagnostic yield of TBNA varies, largely due to the skill and experience of the operator (Rodriguez de Castro et al., 1997; Hsu et al., 2004). Therefore, whether

the operator can accurately locate the target lymph nodes is of great importance, and requires a comprehensive understanding of the anatomy of mediastinal-hilar lymph nodes.

The International Association for the Study of Lung Cancer (IASLC) lymph node map and Wang's lymph node map are the two most commonly used lymph node maps (Wang, 1994; Rusch et al., 2009). The eighth edition of the IASLC map was introduced in 2009 and most of the lymph node stations are defined according to the positions of blood vessels (El-Sherief et al., 2014). Without ultrasound, it is challenging to identify the blood vessels under bronchoscopy. Wang's map was proposed in 1994 and the targeted lymph nodes are located by airway landmarks under endoscopic view, which is more practical for practitioners (Wang, 1994).

Electromagnetic navigation bronchoscopy (ENB) was first applied in human subjects in 2006 (Schwarz et al., 2006). Compared with traditional bronchoscopy, ENB improved the diagnostic accuracy for peripheral pulmonary lesions (PPLs) and mediastinal lymph nodes (Gildea et al., 2006). However, the ENB process requires expensive equipment and special training for operators, and therefore it can only be applied in qualified medical centers. On the other hand, virtual bronchoscopy can simulate a three-dimensional view of the bronchi and adjacent structures using. The reported diagnostic yield of virtual bronchoscopic navigation (VBN) system for peripheral pulmonary lesions was 70.9%–76.8% for peripheral pulmonary lesions, that of thin bronchoscopy combined with computed tomography (CT) and VBN was 65.4%–81.6% and that of X-ray fluoroscopy plus VBN was 62.5%–78.7% (Asano et al., 2014). Electromagnetic navigation and virtual navigation could also be used as advanced lymph node localisation systems. Previously, we reported the intrabronchial display of hilar-mediastinal lymph nodes by the SPiN Thoracic Navigation System (Wu et al., 2018). However, only an endobronchial map of mediastinal-hilar lymph nodes was generated, without demonstration of the extrabronchial anatomical position of each lymph node. Here, we further devised a virtual extrabronchial and endobronchial map together with horizontal, coronal and sagittal views on chest CT for each mediastinal and hilar lymph node using the Lungpoint Virtual Bronchoscopic Navigation System, in accordance with the recommended lymph node puncture site in Wang's map. Therefore, clinicians can gain an overall impression of the three-dimensional (3D) spatial structure of the most frequently punctured lymph nodes, thus improving the accuracy and safety of TBNA.

## METHODS

CT images 1 mm thick were acquired and transferred to a workstation where the Lungpoint Virtual Bronchoscopic Navigation System (Broncus Technologies, Inc., Mountain View, CA, United States) automatically generated a 3D model of the airway. We set up 3D markers of the locations of intrathoracic lymph nodes. The extrabronchial anatomical positions of each target lymph node were shown as green

spheres. The positions and borders of 11 target lymph nodes were described according to Wang's lymph node map.

## RESULTS

We generated an overall view of 11 lymph node stations in Wang's map under 3D reconstruction (**Figure 1**). Next, we collected the horizontal, coronal and sagittal views of chest CT, labeled extrabronchial 3D anatomical locations of the 11 nodal stations in terms of Wang's lymph node map and generated a virtual view from an extrabronchial perspective. We classified the 11 stations into four groups: right mediastinal stations (**Figure 2**), left mediastinal stations (**Figure 3**), central mediastinal stations (**Figure 4**) and hilar stations (**Figure 5**). The recommended TBNA puncture sites of particular lymph nodes were also described in detail (Wang, 1994; Wang, 1995; Xia and Wang, 2013) (see **Supplementary Table S1**).

W1 station, anterior carina (correlated with IASLC 4R).

Location: In front and between the proximal portions of the right and left main bronchi.

Posterior border: The carina of the trachea.

Puncture point: The first trachea cartilage ring gap at 12–1 o'clock.

W2 station, posterior carina (correlated with IASLC-7).

Location: Behind and between the proximal portions of the right and left main bronchi or directly behind the right main bronchus.

Upper border: tip of the carina.

Lower border: The superior portion of the opening of the right upper lobe bronchus.

Puncture point: The opposite side of W1, 5–6 o'clock at the posterior wall of the carina.

W3 station, right paratracheal (correlated with IASLC-4R).

Location: Behind the superior vena cava and in front of the anterolateral aspect of the lower trachea near the azygous arch.

Upper border: The inferior margin of the brachiocephalic vein or superior margin of the aortic arch.

Lower border: The superior margin of the azygous arch.

Puncture point: Second to fourth trachea cartilage ring gaps at 1–2 o'clock.

W4 station, left paratracheal (A-P window, correlated with IASLC-4L).

Location: Lateral to trachea near the tracheobronchial angulation, below the aortic arch and above the left main pulmonary artery.

The W4 lymph nodes are divided into interior, middle and exterior windows.

Puncture point: First or second cartilage ring gap from the distal trachea at 9 o'clock or one trachea cartilage ring distal or proximal from the tracheobronchial angle.

W5 station, right main bronchus (distal W5 correlated with IASLC-10R, proximal W5 correlated with IASLC-4R).

Location: In front of the proximal proportion of the right main bronchus.

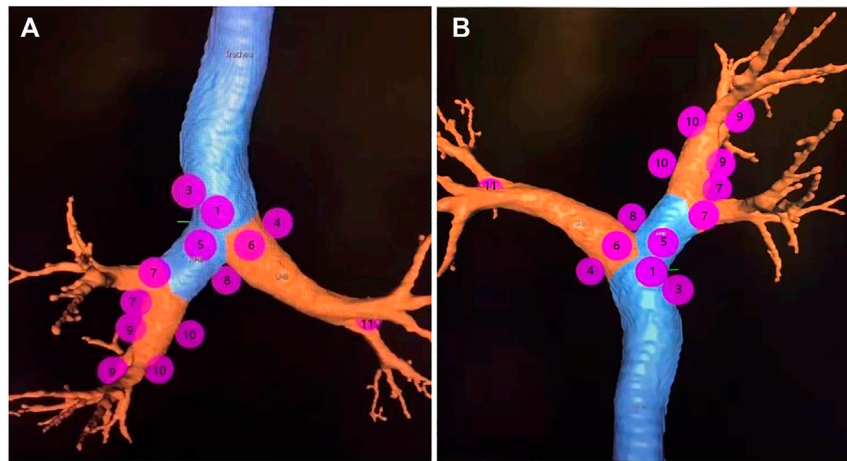


**FIGURE 1** | Note: The overall view of eleven lymph node stations of Wang's map in a 3D reconstructed imaging.

Puncture point: The first or second trachea cartilage ring gap of the right main bronchus at 12 o'clock.

W6 station, left main bronchus (correlated with IASLC-10L).

Location: In front of the proximal proportion of the left main bronchus. The W6 lymph node is a mediastinal lymph node.

Puncture point: The first or second trachea cartilage ring gap of the left main bronchus at 12 o'clock.

W7 station, right upper hilar (correlated with IASLC-11Rs).

Location: In front and between the right upper lobe bronchus and bronchus intermedius.

Puncture point: Anterolateral direction of the right upper lobe crest.

W8 station, subcarina (correlated with IASLC-7).

Location: Between the right and left main bronchi, at or near the level of the right upper lobe bronchus.

Upper border: The superior margin of the opening of the right upper lobe bronchus.

Lower border: The opening of the right intermediate bronchus.

Puncture point: Right main bronchus at the level of the opening of the right upper lobe bronchus, at 9 o'clock.

W9 station, right lower hilar (correlated with IASLC-11Ri).

Location: Lateral or in front of the bronchus intermedius, at or near the level of the right middle lobe bronchus. The W9 lymph nodes consist of lymph nodes at the right lateral side of the right intermediate bronchus and near the ridge of the right middle and lower lobe bronchi.

Puncture point: Lateral side of the right intermediate bronchus.

W10 station, subsubcarina (correlated with the lower part of IASLC-7).

Location: Between the bronchus intermedius and the left main bronchus, at or near the level of the right middle lobe bronchus.

Upper border: The opening of the right intermediate bronchus.

Lower border: The distal end of the right intermediate bronchus, extending to the inferior side of the opening of the right middle lobe.

Puncture point: Right intermediate bronchus at 9 o'clock.

W11 station, left hilar (correlated with IASLC-11L).

Location: Between the left upper lobe and the left lower lobe bronchus.

Puncture point: The opening of the dorsal segment of the left lower lobe at 9 o'clock.

## DISCUSSION

In the present study, we introduced a virtual map of lymph node landmarks under the assistance of a VBN system. Our map displays the intrabronchial and extrabronchial spatial relationships of 11 lymph node stations and their recommended puncture sites corresponding to Wang's map.

The VBN system in combination with CT of the 11 mediastinal and hilar lymph nodes and their surrounding structures from extrabronchial and endobronchial, sagittal, coronal as well as horizontal views provided a full understanding of the thoracic lymph nodes and their intrabronchial and extrabronchial relationships with adjacent tissues and blood vessels. A detailed view of the lymph nodes and their adjacent tissues can reinforce the understanding of the anatomy and assist in training of operators for TBNA.

There are two major differences between Wang's map and the IASLC map (Xia et al., 2015). First, stations five and six in Wang's map are located in front of the proximal proportion of the right and left main bronchi, respectively. Both W5 and W6 stations are defined as mediastinal lymph nodes. Second, W5 covers two IASLC lymph nodal stations: the distal end of

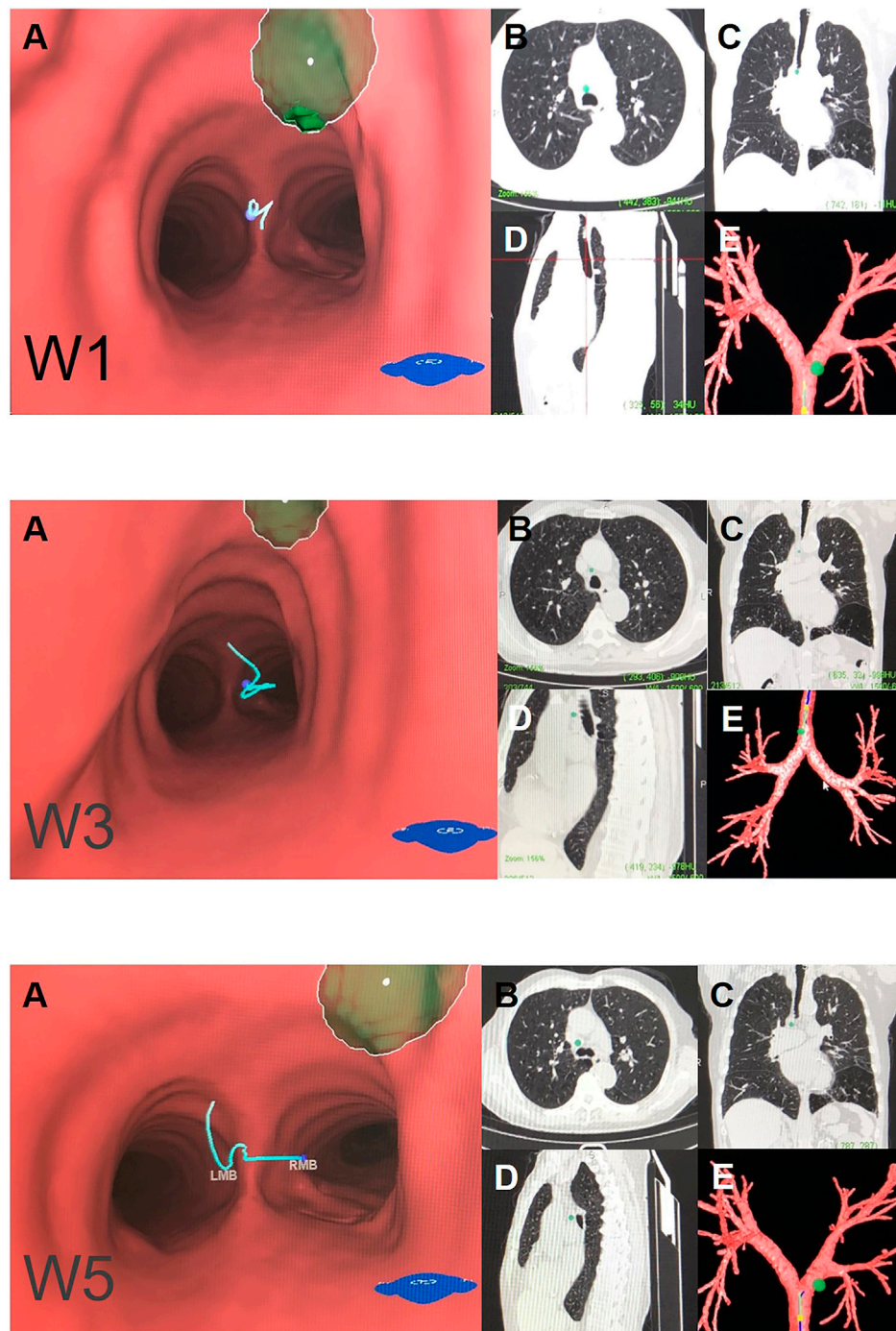


**FIGURE 2 |** Right mediastinal lymph node (N2) Note: (W1) anterior carina lymph nodes. (W3) right paratracheal lymph nodes. (W5) right main bronchus lymph nodes. (A) Intraluminal view and puncture sight (green). (B) Axial view. (C) Coronal view. (D) Sagittal view. (E) Reconstruction image.

4R as well as 10R station. Third, compared with the previous edition of the IASLC lymph node map, the lower border is extended to the azygos vein on the right, which fits the principle of Wang's map that 4R is correlated with station W1 and W3 as well as proximal W5 station. Similarly, the lower border of station seven in the IASLC map is extended

to the upper border of the lower lobe bronchus on the left and the lower border of the bronchus intermedius on the right. This changed definition is also correlated with the definitions of W8 and W10.

VBN is generally conducted for guidance in treatment of PPLs. PPLs cannot be accessed easily by cTBNA because they are



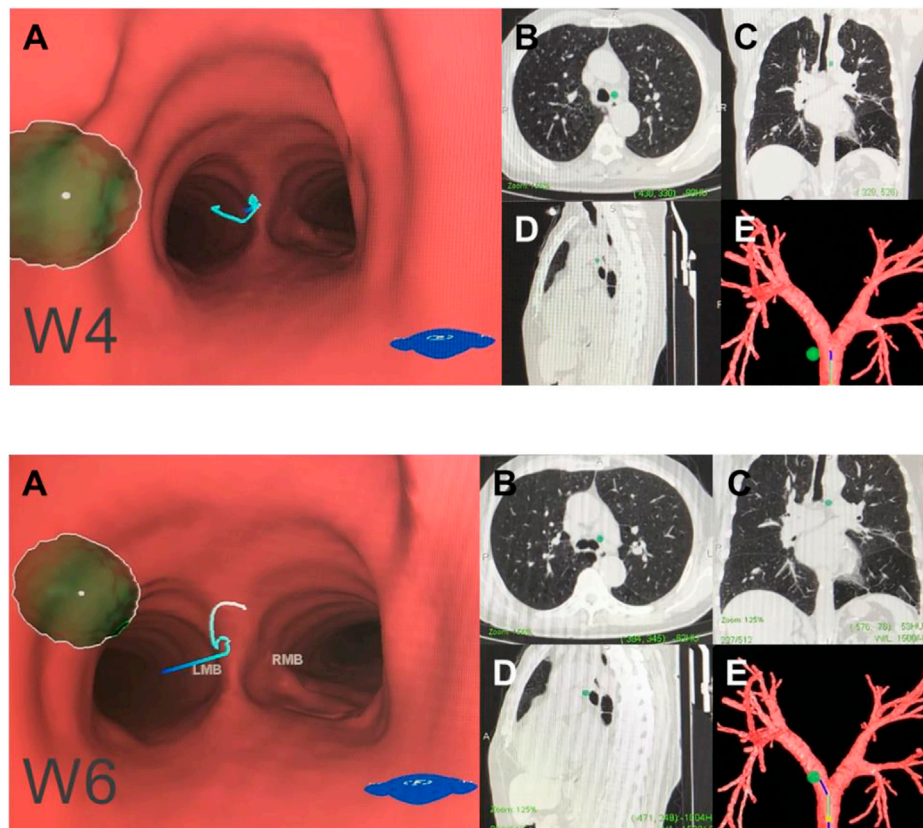


**FIGURE 3 |** Left mediastinal lymph node (N2). Note: (W4) left paratracheal lymph nodes or aortic pulmonary (A-P) window lymph nodes. (W6) left main bronchus lymph nodes. (A) Intraluminal view and puncture sight (green). (B) Axial view. (C) Coronal view. (D) Sagittal view. (E) Reconstruction image.

distinct from the trachea and central bronchus. The development of image-guided bronchoscopy techniques significantly enhances the diagnostic accuracy of PPLs. The VBN system was designed to reach and guide aspiration of PPLs with a diagnostic value of 72.0%–73.8% (Wang Memoli et al., 2012; Asano et al., 2014), and the diagnostic value reached 67.4% for lesions <2 cm in diameter (Asano et al., 2014). In combination with CT-guided ultrathin bronchoscopy, the diagnostic value of VBN increases to 65.4%–81.6% (Asano et al., 2014). On the other hand, the VBN system has also been applied in diagnosis of thoracic lymph node adenopathy. The sensitivity and diagnostic accuracy are both significantly increased for mediastinal lymph nodes by VBN (McAdams et al., 1998; Fiorelli et al., 2017), suggesting that the VBN system is also valuable in cases of mediastinal lymph node enlargement.

Aside from the advantages of the VBN system, the bronchoscopist still has to perform cTBNA blindly in clinical practice, as the exact puncture site cannot be confirmed in real-time. In general, the main purpose of

generating our multi-dimensional virtual Wang's lymph node map is for training junior interventional pulmonology fellows or bronchoscopists. Compared with EBUS-TBNA, our approach does not require the use of a regular scope for the airway survey. In addition, although EBUS-TBNA allows real-time visualisation of a punctured lymph node, the operator cannot precisely identify the puncture site. In contrast, our system probes the 3D anatomy of each lymph node station with the puncture site. We expect that our multi-dimensional virtual Wang's lymph node map would allow precise targeting of lymph nodes 1–2 cm in diameter. Hence, the two methods are not competitive but complementary for bronchoscopists within the learning curve. The diagnostic yield is satisfactory upon combining virtual endobronchial ultrasound with EBUS-TBNA bronchoscopy when diagnosing mediastinal-hilar lymph node enlargement (Sato et al., 2013), but its necessity is doubtful. In addition, rapid on-site evaluation (ROSE) may be a good alternative to EBUS for combination with the VBN system. In addition, we recommend a probe designed to determine whether the needle is aligned in the

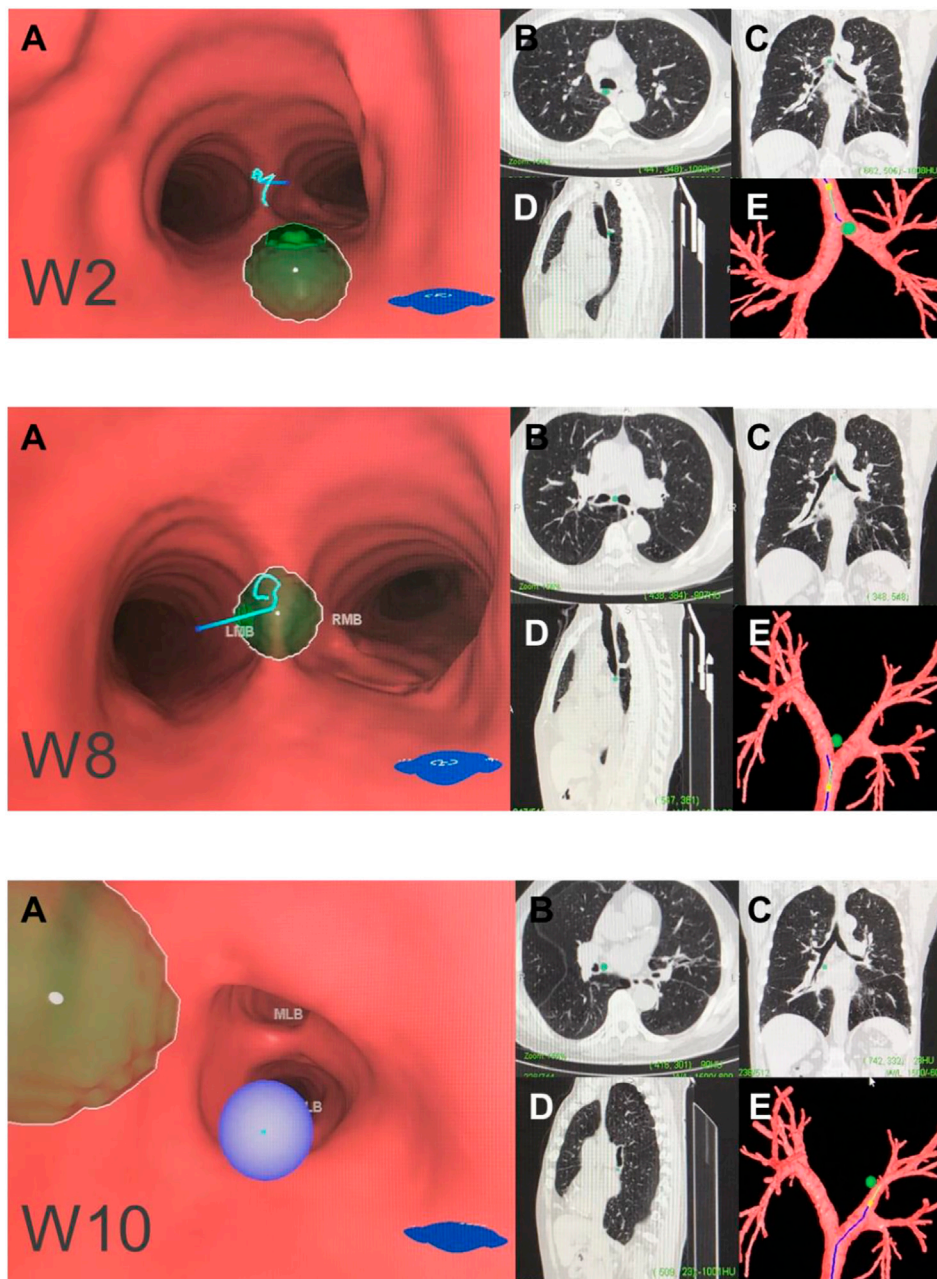


**FIGURE 4 |** Central mediastinal lymph node (N2). Note: (W2) posterior carina lymph nodes. (W8) subcarinal lymph nodes. (W10) subsubcarinal lymph nodes. (A) Intraluminal view and puncture sight (green). (B) Axial view. (C) Coronal view. (D) Sagittal view. (E) Reconstruction image.

puncture site. When it is aligned properly, the inducer could turn from green to red to alert the practitioner of puncture. Such a device may further improve the diagnostic value of VBN-guided TBNA.

There was a significant limitation of this study in that the diagnostic yield of this particular VBN-assisted TBNA has not yet been verified. A clinical trial is required to examine the

validity of this VBN plus TBNA system. In addition, the quality of the CT image can also affect the accuracy of the derived 3D images.

Overall, we have proposed a virtual map for intra- and extrabronchial landmarks of hilar and mediastinal lymph nodes based on the Lungpoint VBN system. This map can help in training bronchoscopists as well as enhancing the



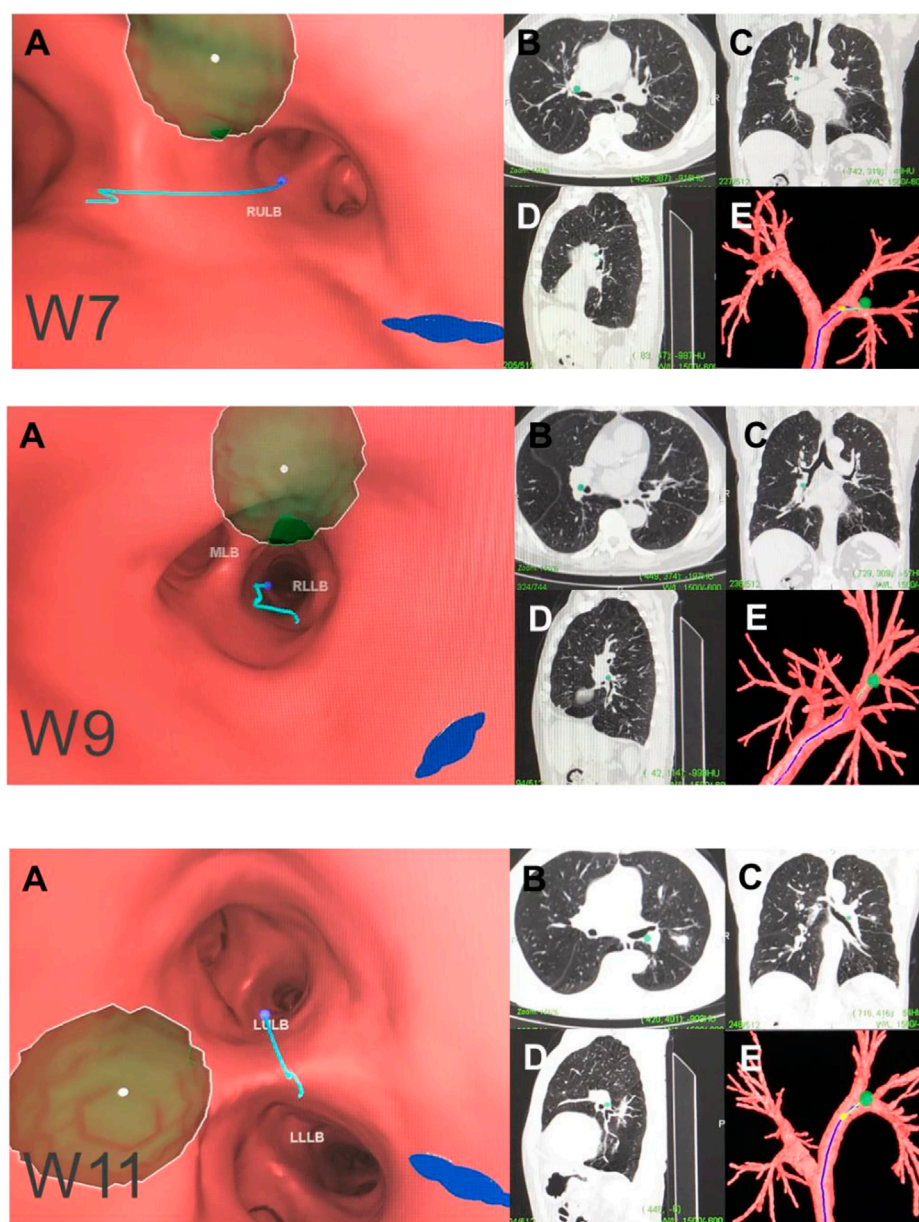


**FIGURE 5 |** Hilar lymph node (N1). Note: (W7) right upper hilar lymph nodes. (W9) right lower hilar lymph nodes. (W11) left hilar lymph nodes. (A) Intraluminal view and puncture sight (green). (B) Axial view. (C) Coronal view. (D) Sagittal view. (E) Reconstruction image.

diagnostic value of the VBN system. Further clinical trials are required to determine the efficacy of this strategy.

## DATA AVAILABILITY STATEMENT

The original contributions presented in the study are included in the article/**Supplementary Material**, further inquiries can be directed to the corresponding authors.

## AUTHOR CONTRIBUTIONS

KW, QLi, HoS, and YX contributed to study conception and design. FL, YY, HuS, QW, XY, QLi, LC, and YX conducted data collection and data analysis. QLi, HoS, HuS, KW, YY, FL, and YX drafted the manuscript. All authors contributed to revision of the manuscript, and confirmed the final approval of manuscript.

## FUNDING

This work was supported by the National Natural Science Foundation of China (81870022) and the Zhejiang Provincial Natural Science Foundation (LY20H010004).

## REFERENCES

- Asano, F., Eberhardt, R., and Herth, F. J. F. (2014). Virtual bronchoscopic navigation for peripheral pulmonary lesions. *Respiration* 88 (5), 430–440. doi:10.1159/000367900
- Bonifazi, M., Tramacere, I., Zuccatosta, L., Mei, F., Sediari, M., Paonessa, M.C., et al. (2017). Conventional versus Ultrasound-Guided Transbronchial Needle Aspiration for the Diagnosis of Hilar/Mediastinal Lymph Adenopathies: A Randomized Controlled Trial. *Respiration*. 94 (2), 216–223. doi:10.1159/000475843
- El-Sherief, A. H., Lau, C. T., Wu, C. C., Drake, R. L., Abbott, G. F., and Rice, T. W. (2014). International association for the study of lung cancer (IASLC) lymph node map: radiologic review with CT illustration. *Radiographics* 34 (6), 1680–1691. doi:10.1148/rg.346130097
- Fiorelli, A., Raucci, A., Cascone, R., Reginelli, A., Di Natale, D., Santoriello, C., et al. (2017). Three-dimensional virtual bronchoscopy using a tablet computer to guide real-time transbronchial needle aspiration. *Interact Cardiovasc Thorac Surg* 24 (4), ivw404–575. doi:10.1093/icvts/ivw404
- Gildea, T. R., Mazzone, P. J., Karnak, D., Mezziane, M., and Mehta, A. C. (2006). Electromagnetic Navigation Diagnostic Bronchoscopy. *Am J Respir Crit Care Med* 174 (9), 982–989. doi:10.1164/rccm.200603-344OC
- Herth, F., Becker, H. D., and Ernst, A. (2004). Conventional vs Endobronchial Ultrasound-Guided Transbronchial Needle Aspiration. *Chest* 125 (1), 322–325. doi:10.1378/chest.125.1.322
- Hsu, L.-H., Liu, C.-C., and Ko, J.-S. (2004). Education and Experience Improve the Performance of Transbronchial Needle Aspiration. *Chest* 125 (2), 532–540. doi:10.1378/chest.125.2.532
- Madan, K., Dhungana, A., Mohan, A., Hadda, V., Jain, D., Arava, S., et al. (2017). Conventional Transbronchial Needle Aspiration Versus Endobronchial Ultrasound-guided Transbronchial Needle Aspiration, With or Without Rapid On-Site Evaluation, for the Diagnosis of Sarcoidosis: A Randomized Controlled Trial. *J Bronchology Interv Pulmonol* 24 (1), 48–58. doi:10.1097/LBR.0000000000000339
- McAdams, H. P., Goodman, P. C., and Kussin, P. (1998). Virtual bronchoscopy for directing transbronchial needle aspiration of hilar and mediastinal lymph nodes: a pilot study. *American Journal of Roentgenology* 170 (5), 1361–1364. doi:10.2214/ajr.170.5.9574616
- Rodriguez de Castro, F., López, F. D., Serdá, G. J., Navarro, P. C., López, A. R., and Gilart, J. F. (1997). Relevance of training in transbronchial fine-needle aspiration technique. *Chest* 111 (1), 103–105. doi:10.1378/chest.111.1.103
- Rusch, V. W., Asamura, H., Watanabe, H., Giroux, D. J., Rami-Porta, R., Goldstraw, P., et al. (2009). The IASLC lung cancer staging project: a proposal for a new international lymph node map in the forthcoming seventh edition of the TNM classification for lung cancer. *Journal of Thoracic Oncology* 4 (5), 568–577. doi:10.1097/JTO.0b013e3181a0d82e
- Sato, M., Chen, F., Aoyama, A., Yamada, T., Ikeda, M., Bando, T., et al. (2013). Virtual endobronchial ultrasound for transbronchial needle aspiration. *The Journal of Thoracic and Cardiovascular Surgery* 146 (5), 1204–1212. doi:10.1016/j.jtcvs.2013.01.019
- Schwarz, Y., Greif, J., Becker, H. D., Ernst, A., and Mehta, A. (2006). Real-Time Electromagnetic Navigation Bronchoscopy to Peripheral Lung Lesions Using Overlaid CT Images. *Chest* 129 (4), 988–994. doi:10.1378/chest.129.4.988
- Wang, K.-P. (1994). Staging of bronchogenic carcinoma by bronchoscopy. *Chest* 106 (2), 588–593. doi:10.1378/chest.106.2.588
- Wang, KP (1995). Transbronchial needle aspiration and percutaneous needle aspiration for staging and diagnosis of lung cancer. *Clin Chest Med* 16 (3), 535–52.
- Wang Memoli, J. S., Nietert, P. J., and Silvestri, G. A. (2012). Meta-analysis of guided bronchoscopy for the evaluation of the pulmonary nodule. *Chest* 142 (2), 385–393. doi:10.1378/chest.11-1764
- Wu, X., Shi, L., Xia, Y., Wang, K.-p., and Li, Q. (2018). Intrabronchial display of hilar-mediastinal lymph nodes by virtual bronchoscopic navigation system. *Thorac Cancer* 9 (3), 415–419. doi:10.1111/1759-7714.12555
- Xia, Y., Ma, Y., Arias, S., Lee, H., and Wang, K.-P. (2015). Utilization of the International Association for the Study of Lung Cancer and Wang's nodal map for the identification of mediastinum and hilar lymph nodes. *Thoracic Cancer* 6 (4), 464–468. doi:10.1111/1759-7714.12206
- Xia, Y., and Wang, KP (2013). Transbronchial needle aspiration: where are we now? *J Thorac Dis* 5 (5), 678–82. doi:10.3978/j.issn.2072-1439.2013.09.11

## SUPPLEMENTARY MATERIAL

The Supplementary Material for this article can be found online at: <https://www.frontiersin.org/articles/10.3389/fmolb.2021.679442/full#supplementary-material>

**Conflict of Interest:** The authors declare that the research was conducted in the absence of any commercial or financial relationships that could be construed as a potential conflict of interest.

Copyright © 2021 Lan, Yue, Shen, Shen, Wang, Yu, Chen, Li, Wang, Liu and Xia. This is an open-access article distributed under the terms of the Creative Commons Attribution License (CC BY). The use, distribution or reproduction in other forums is permitted, provided the original author(s) and the copyright owner(s) are credited and that the original publication in this journal is cited, in accordance with accepted academic practice. No use, distribution or reproduction is permitted which does not comply with these terms.





# The Application of Transbronchial Lung Cryobiopsy and Uniportal and Tubeless Video-Assisted Thoracic Surgery in the Multidisciplinary Diagnosis of Interstitial Lung disease—A Real-World Prospective Study

## OPEN ACCESS

### Edited by:

Wen Li,  
Zhejiang University, China

### Reviewed by:

Tao Wang,  
Huazhong University of Science and  
Technology, China  
Gang Hou,  
China-Japan Friendship Hospital,  
China

### \*Correspondence:

Qun Luo  
luoqunx@163.com  
Shiyue Li  
lishiyue@188.com

<sup>†</sup>These authors have contributed  
equally to this work

### Specialty section:

This article was submitted to  
Molecular Diagnostics and  
Therapeutics,  
a section of the journal  
Frontiers in Molecular Biosciences

**Received:** 17 March 2021

**Accepted:** 02 June 2021

**Published:** 16 June 2021

### Citation:

Han Q, Chen X, Xu X, Qian W, Zhao G,  
Mao M, Guo B, Xia S, Peng G, He J,  
Gu Y, Li S and Luo Q (2021) The  
Application of Transbronchial Lung  
Cryobiopsy and Uniportal and  
Tubeless Video-Assisted Thoracic  
Surgery in the Multidisciplinary  
Diagnosis of Interstitial Lung  
disease—A Real-World  
Prospective Study.  
Front. Mol. Biosci. 8:681669.  
doi: 10.3389/fmolb.2021.681669

Qian Han<sup>1,2†</sup>, Xiaobo Chen<sup>1,2†</sup>, Xin Xu<sup>2,3†</sup>, Weiping Qian<sup>1,2</sup>, Gui Zhao<sup>1,2</sup>, Mengmeng Mao<sup>1,2</sup>,  
Bingpeng Guo<sup>1,2</sup>, Shu Xia<sup>1,2</sup>, Guilin Peng<sup>2,3</sup>, Jianxing He<sup>2,3</sup>, Yingying Gu<sup>2,4</sup>, Shiyue Li<sup>1,2\*</sup> and  
Qun Luo<sup>1,2\*</sup>

<sup>1</sup>Department of Respiratory Medicine, The First Affiliated Hospital of Guangzhou Medical University, Guangzhou, China, <sup>2</sup>National  
Clinical Research Center for Respiratory Disease, Guangzhou Institute of Respiratory Health, Guangzhou, China, <sup>3</sup>Department of  
Cardio-thoracic Surgery, The First Affiliated Hospital of Guangzhou Medical University, Guangzhou, China, <sup>4</sup>Department of  
Pathology, Guangzhou Institute of Respiratory Health, Guangzhou, China

The application of transbronchial lung cryobiopsy (TBLC) and uniportal and tubeless video-assisted thoracic surgery (UT-VATS) in the multidisciplinary diagnosis of interstitial lung disease (ILD) has not been demonstrated in real-world clinical practice. This prospective study included 137 patients with no definitive diagnosis who were the subject of two multidisciplinary discussion (MDD) sessions. As indicated in the first MDD, 67 patients underwent UT-VATS and 70 underwent TBLC. The specificity of biopsy information and its contribution to final MDD diagnosis were evaluated in the second MDD. The post-operative complications and hospitalization costs associated with the two biopsy methods were compared. UT-VATS was favored for patients initially diagnosed with idiopathic pulmonary fibrosis (IPF), bronchiolitis-associated interstitial lung disease (RB-ILD)/desquamative interstitial pneumonia (DIP) and undefined idiopathic interstitial pneumonia (UIIP), while TBLC was preferred for pulmonary lymphangioleiomyomatosis (PLAM) and pulmonary alveolar proteinosis (PAP). The spirometry parameters were better in patients who underwent UT-VATS than those who underwent TBLC. UT-VATS provided more specific pathological results than TBLC (85.7 vs 73.7%,  $p = 0.06$ ). In patients initially diagnosed with UIIP, pathological information from UT-VATS was more clinically useful than that obtained from TBLC, although both tests contributed similarly to cases initially diagnosed as interstitial pneumonia with auto-immune features (IPAF)/connective tissue disease-related ILD (CTD-ILD). The safety of UT-VATS was comparable with TBLC although TBLC was cheaper during hospitalization (US\$4,855.7 vs US\$3,590.9,  $p < 0.001$ ). multidisciplinary discussion decisions about biopsies were driven by current knowledge of sampling and diagnosis capacity as well as potential risks of different

biopsy methods. The current MDD considered UT-VATS more informative than TBLC in cases initially diagnosed as UIP although they were equally valuable in patients initially diagnosed with IPAF/CTD-ILD.

**Keywords:** multidisciplinary diagnosis, interstitial lung disease, cryobiopsy, uniportal and tubeless video-assisted thoracic surgery, pathological diagnosis

## INTRODUCTION

Interstitial lung diseases (ILDs) represent a heterogeneous group of non-neoplastic pulmonary disorders that manifest with varying patterns of parenchymal inflammation and fibrosis of the lungs (Demedts and Costabel, 2002). A specific diagnosis is essential to determine appropriate therapeutic interventions and prognosis. Diagnosis following multidisciplinary discussion (MDD) is considered the gold standard in ILD diagnosis (Flaherty et al., 2004; Chaudhuri et al., 2016; De Sadeleer et al., 2018). Nonetheless MDD pathways are largely heterogeneous due to the absence of specific guidelines. The American Thoracic Society (Raghu et al.)/European Respiratory Society (ERS) joint statement recommends a two-round MDD process and emphasizes the necessity for lung biopsy and utilization of histopathologic information in reaching a final diagnosis (Raghu et al., 2018).

Current guidelines emphasize the significant role of surgical lung biopsy (SLB) in the diagnosis of undefined ILDs, with video-assisted thoracic surgery (VATS) preferred to open thoracotomy (Raghu et al., 2011; Raghu et al., 2018; Travis et al., 2013). Nonetheless traditional VATS is burdened by relatively high morbidity and mortality (Han et al., 2015; Luo et al., 2013; Fibla et al., 2012a; Fibla et al., 2012b; Sigurdsson et al., 2009). The development of uniportal and tubeless VATS (UT-VATS) under spontaneous ventilation anesthesia offers a safe and feasible option in the diagnosis of ILDs (Peng et al., 2017). Recent studies suggest that transbronchial lung cryobiopsy (TBLC) may be an alternative method for obtaining large and well-preserved samples of lung parenchyma. It is less invasive and associated with fewer complications and a lower mortality rate than SLB (Colella et al., 2018; Tomassetti et al., 2016; Johansson et al., 2016).

Little is known about how this two-round MDD model is implemented in real-world practice. It is unclear what proportion of cases require biopsy; and how much pathological information, with different biopsies performed, contributes to the final MDD diagnosis and patient management. In this prospective study, we aimed to evaluate the application of UT-VATS and TBLC, under the current MDD schema, in the diagnostic algorithm of undefined ILDs. The option by the MDD on biopsy methods was described, and the contribution of different biopsy methods in a spectrum of certain ILD subtypes was evaluated by MDD.

## METHODS

### Patient Selection and Data Archiving

This was a single center, non-randomized, prospective study that involved consecutive patients referred to the ILD Center, First

Affiliated Hospital of Guangzhou Medical University, between June 1st and Dec 1st, 2019. According to the patient triage algorithm at our Center, all referred patients were reviewed at MDD sessions (see below) and the initial diagnosis of ILD was based on clinical-radiological information. Prior to this, complete data (clinical and imaging findings) of each patient were collated.

To ensure integrity and consistency of clinical data, case report forms (CRFs) were used to record patient information, including general information (age, sex, smoking status), exposure history (environmental, occupational, medications), history of physician-diagnosed connective tissue disease (CTD), CTD-related symptoms, signs and serological results, and spirometry. The CRFs were a modified form of the American College of Chest Physicians (ACCP) ILD questionnaire (with CHEST copyright permission) and an ILD questionnaire adopted by the Firestone Institute for Respiratory Health in Canada (by courtesy of MK).

### Study Protocol

The MDD session was held online via a regional research network, and hosted by an expert panel that comprised one pulmonologist (LQ), one respiratory radiologist (ZQS), one thoracic pathologist (GY) and one rheumatologist (YSH) from our institute, each with recognized expertise in the management of ILDs for at least 10 years.

As per our practice, two MDD sessions were usually needed to agree a final diagnosis of ILD. The first MDD session produced an initial diagnosis but where histological data were required for accurate diagnosis, a multidisciplinary decision would be made to perform a biopsy with careful scrutiny of the indications for VATS or TBLC based on dominant distribution of lesions on high-resolution CT (HRCT) and spirometry data (**Figure 1**). All patients gave informed consent. The eligibility and exclusion criteria are described in the supplemental materials (**Supplementary Table S1**).

Following biopsy, a second MDD session was conducted to review complete clinical, radiological and pathological data and agree a final diagnosis. The evaluation of the pathological diagnosis by the MDD produced one of four grades: Grade 1, histological information was specific to indicate a definitive ILD subtype and sufficient to alter the initial clinical-radiological diagnosis; grade 2, histological information was specific and sufficient to support the initial clinical-radiological diagnosis; grade 3, albeit non-specific, the histological information provided supplementary information for ILD subtype and thereby aided treatment decision, i.e., germinal center formation, lymphoid aggregates, vasculitis; grade 4, the histological information failed to provide diagnostic or therapeutic clues for a given case. The detailed "Pathological evaluation form" is shown in the supplemental materials (**Supplementary Table S2**).

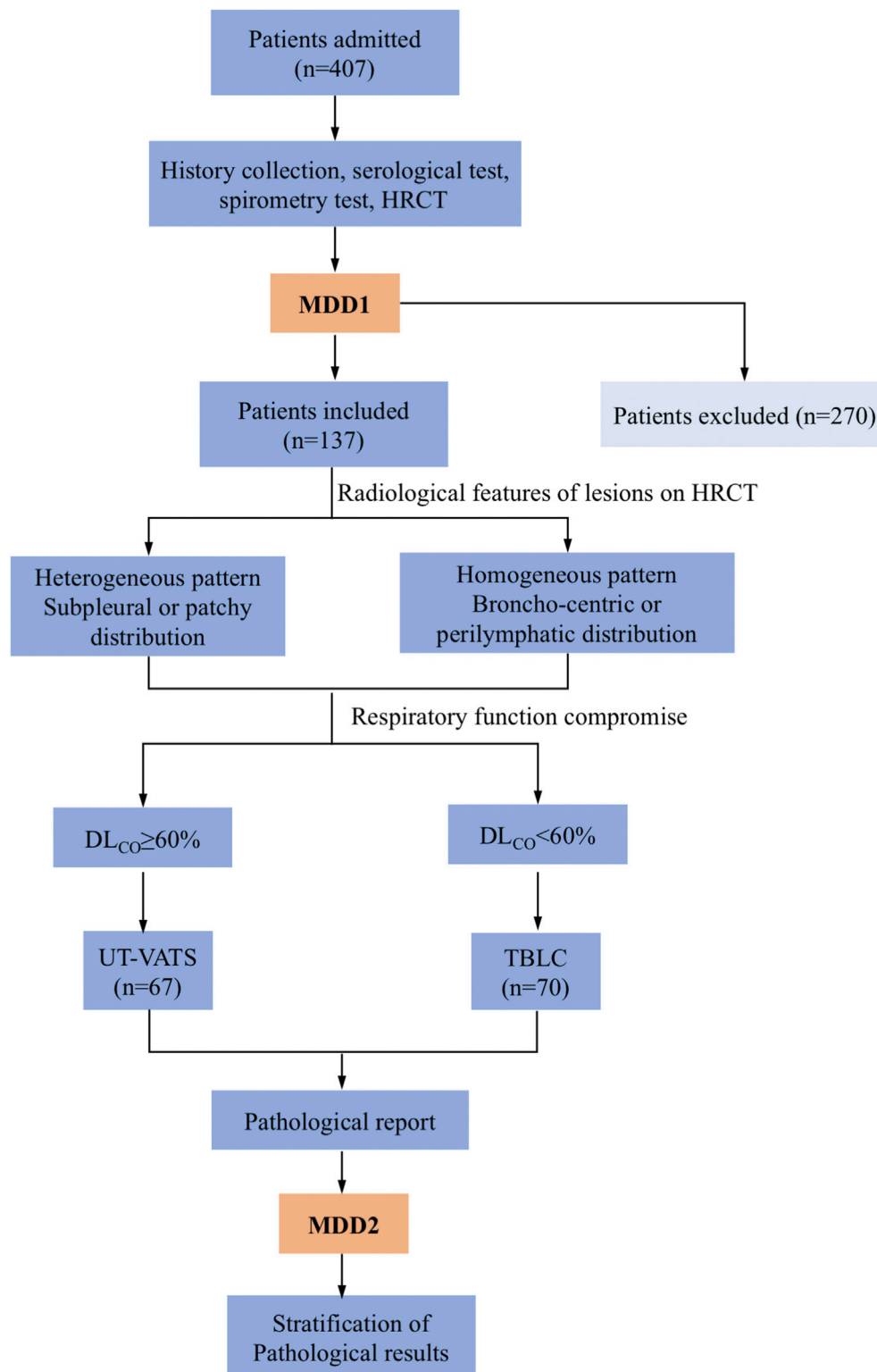


**FIGURE 1 |** Flowchart of the study. Patients admitted to the institute underwent MDD1 after history collection, serological testing, spirometry and HRCT. A decision was made whether to perform a biopsy and which method (UT-VATS or TBLC) to utilize, the latter based on radiological features of lesions as well as respiratory compromise of patients. MDD2 was held with pathological reports available. Stratification of pathological results was performed based on specificity as well as their contribution to the final MDD diagnosis. MDD: multidisciplinary discussion, HRCT: high resolution computed tomography. UT-VATS: uniportal and tubeless-video-assisted thoracic surgery, TBLC: transbronchial lung cryobiopsy, FVC: forced vital capacity,  $DL_{CO}$ : carbon-monoxide diffusion coefficient.

## Uniportal and Tubeless Video-Assisted Thoracic Surgery and Transbronchial Lung Cryobiopsy

The biopsy location for both procedures was confirmed by the pulmonologist and radiologist on the MDD panel following review of a pre-operative HRCT. Two specimens from different lobes were routinely harvested for UT-VATS; in TBLC, several samples from different segments of the selected lobe were collected. Sample characteristics were evaluated by individual sample size as well as sample number.

The UT-VATS was performed as previously described (Peng et al., 2017) by an experienced cardiothoracic team in our institute (XX and PGL). Briefly, under intravenous anesthesia with a laryngeal mask airway, a 30°/5 mm thoracoscope (Stryker, United States) was inserted into the pleural cavity to exclude any dense or extensive lung-pleura adhesions. Ring-forceps were used to hold the targeted pulmonary segment and the parenchyma gently pulled out of the chest wall. Wedge resection was performed for biopsy and the residual lung tissue sutured. A chest tube was placed into the chest cavity followed by subcutaneous tissue closure. After expansion of the lung through the chest tube and laryngeal mask, the “tubeless” state was realized by rapid removal of the chest tube and subsequent suture of the skin incision.

TBLC was performed by two experienced bronchoscopists (LSY and CXB) under general sedation using an endotracheal tube airway. Samples were obtained using a flexible cryoprobe with a diameter of 1.9 mm (Erbokryo CA, Erbe, Germany) under fluoroscopic guidance. The gas source of the cryosurgical system was CO<sub>2</sub> with a working pressure of 55–60 bar. The freezing time was 3–6 s, adjusted according to the sample size. Samples were harvested from different bronchopulmonary segments of selected lobes.

The study was registered at clinicaltrials.gov (NCT03958162) and approved by the local independent ethics committee (The First Affiliated Hospital of Guangzhou Medical University; reference number: 2018-85).

## Statistical Analysis

Statistical analyses were performed using IBM SPSS Statistics 20.0 (IBM Corporation, Armonk, NY, United States). Qualitative values are presented as numbers with percentages and compared by Chi-Square test or Fisher's exact test. Quantitative values are expressed as mean with standard error of mean (SEM) or median with interquartile range and compared by independent t-test or Mann-Whitney test. Kappa coefficient ( $\kappa$ ) was used to determine the agreement between pathological results or initial clinical-radiological diagnoses and final diagnoses. A  $p$  value < 0.05 was considered statistically significant.

## RESULTS

### General Conditions of the Study Population

Between June and Dec 2019, 407 consecutive patients who visited our institute for the first time were initially determined to have ILD.

**TABLE 1 |** Characteristics of patients undergoing UT-VATS or TBLC.

	UT-VATS (n = 67)	TBLC (n = 70)	p value
Age <sup>b</sup>	54.0 (20–70)	50.0 (21–72)	0.27
Male/female, n	39/28	28/42	0.04
Smoking history, no/yes, n	28/39	16/54	0.03
FVC% <sup>a</sup>	81.3 (2.7)	71.8 (2.8)	0.01
FEV1% <sup>a</sup>	80.7 (2.6)	73.0 (2.8)	0.05
DL <sub>CO</sub> % <sup>a</sup>	68.7 (2.4)	47.2 (2.5)	<0.001
Biopsy location, n	–	–	–
LUL	10	NA	–
LL(lingular)L	42	NA	–
LL(lower)L	53	44	–
RUL	1	4	–
RML	9	NA	–
RLL	8	295	–
Sample number, n	–	–	–
1	14 (20.9)	1 (1.4)	–
2	50 (74.6)	1 (1.4)	–
3	3 (4.5)	8 (11.4)	–
4	–	9 (12.9)	–
5	–	31 (44.3)	–
>5	–	20 (28.6)	–
Sample number <sup>b</sup>	2 (1–3)	5 (1–8)	–
Sample size <sup>b</sup> , cm <sup>2</sup> /mm <sup>2</sup>	5.3 (1–32.0) <sup>c</sup>	9.0 (1–40.0) <sup>d</sup>	–

Values are presented as

<sup>a</sup>mean (SEM)

<sup>b</sup>median (interquartile range) where appropriate.

<sup>c</sup>: cm<sup>2</sup>

<sup>d</sup>: mm<sup>2</sup>

UT-VATS: uniportal and tubeless-video-assisted thoracic surgery, TBLC: transbronchial lung cryobiopsy, FVC: forced vital capacity, FEV1: forced expiratory volume in 1 s, DL<sub>CO</sub>: carbon-monoxide diffusion coefficient. LUL: left upper lobe, RUL: right upper lobe, RML: right middle lobe, RLL: right lower lobe.

Of these, 137 (33.7%) were eligible and included in this study. As indicated by the first MDD session, 67 patients underwent UT-VATS and 70 underwent TBLC. The two cohorts did not differ significantly in age but there were more female and never-smoking patients in the TBLC compared with the UT-VATS cohort, and spirometry parameters (FVC, FEV1 and DL<sub>CO</sub>%) in the UT-VATS were better than those in the TBLC cohort (Table 1).

## Biopsy Specimens

As shown in Table 1, a total of 123 samples (median: 2, range: 1–3) were obtained by UT-VATS and 343 (median: 5, range: 1–8) by TBLC. The mean individual sample size was 5.3 (range: 1–32) cm<sup>2</sup> for UT-VATS and 9.0 (range: 1–40.0) mm<sup>2</sup> for TBLC. The VATS samples were mainly from the left lobe, especially the left lingular and lower lobes; TBLC samples were mainly from the lower lobes, especially the right lower lobe.

## Multidisciplinary Discussion Choice of Biopsy Methods

The choice of biopsy method and altered MDD diagnosis following the addition of pathological information are listed in Table 2. The multidisciplinary team was inclined to select UT-VATS as the biopsy method where the initial diagnosis was idiopathic pulmonary fibrosis (IPF) (76.9%, 10/13), respiratory bronchiolitis-associated interstitial lung disease (RB-ILD)/



**TABLE 2 |** The alteration of MDD diagnosis after the addition of pathological information.

Pre-biopsy dx	Post-biopsy dx		p value
	UT-VATS (n = 67)	TBLC (n = 70)	
IPF (n = 13)	IPF 8 RBILD/DIP 2	IPF 3 –	0.40
COP (n = 1)	NA	COP 1	–
RBILD/DIP (n = 7)	RBILD/DIP 2 IPF 2 HP 1	RBILD/DIP 2 – –	0.15
LIP (n = 2)	NSIP 1	LIP 1	–
UIIP (n = 37)	UIIP 9 HP 4 IPF 3 RBILD/DIP 2 IPAF 1 LIP 1 Vasculitis 1 ACIF 1	UIIP 8 IPF 3 NSIP 1 Pneumoconiosis 1 HP 1 ACIF 1 – –	0.46
IPAF (n = 34)	IPAF 12 Sarcoidosis 1 HP 1	IPAF 20 – –	0.10
–	–	–	–
CTD-ILD (n = 22)	CTD-ILD 9	CTD-ILD 12	0.43
HP (n = 3)	IPAF 1 –	IPF 1 HP 1 Infection 1	–
Sarcoidosis (n = 1)	Sarcoidosis 1	NA	–
PAP (n = 5)	PAP 1	PAP 4	–
PLAM (n = 4)	NA	PLAM 4	–
Vasculitis (n = 1)	Vasculitis 1	NA	–
Pneumoconiosis (n = 1)	Lipid pneumonia 1	–	–
PLCH (n = 2)	UIIP 1	PLCH 1	–
IPH (n = 1)	NA	IPH 1	–
PAM (n = 1)	NA	PAM 1	–
Infection (n = 1)	NA	Infection 1	–

UT-VATS: uniportal and tubeless-video-assisted thoracic surgery, TBLC: transbronchial lung cryobiopsy, IPF: idiopathic pulmonary fibrosis, NSIP: non-specific interstitial pneumonia, COP: cryptogenic organizing pneumonia, RB-ILD: respiratory bronchiolitis interstitial lung disease, DIP: desquamative interstitial pneumonia, LIP: lymphocyte interstitial pneumonia, ACIF: airway-lefted interstitial fibrosis, UIIP: undefined interstitial pneumonia, IPAF: interstitial pneumonia with autoimmune features, CTD-ILD: connective tissue disease-related ILD, HP: hypersensitivity pneumonitis, PAP: pulmonary alveolar proteinosis, PLAM: pulmonary lymphangioleiomyomatosis, PLCH: pulmonary Langerhans cell histiocytosis, IPH: idiopathic pulmonary hemosiderosis, PAM: pulmonary alveolar microlithiasis.

desquamative interstitial pneumonia (DIP) (71.4%, 5/7) or unclassifiable idiopathic interstitial pneumonia (UIIP) (59.5%, 22/37); TBLC was more likely to be selected when the initial diagnosis was pulmonary lymphangioleiomyomatosis (PLAM) (100%, 4/4), pulmonary alveolar proteinosis (PAP) (80%, 4/5), connective tissue disease-related ILD (CTD-ILD) (59.1%, 13/22) or interstitial pneumonia with auto-immune features (IPAF) (58.8%, 20/34).

## Pathological Diagnoses

There was a borderline significant increase in specific pathological diagnosis for the UT-VATS compared with TBLC cohort (85.7 vs 73.7%,  $p = 0.06$ ). For UT-VATS, the most common pathological diagnosis was usual interstitial pneumonia (UIP), followed by non-specific interstitial pneumonia (NSIP) and RB-ILD/DIP; for TBLC, UIIP was most commonly encountered, followed by NSIP and UIP

(Figure 2). The kappa coefficient between pathological result and final diagnosis was 0.8 (95% CI: 0.7–0.9) for UT-VATS and 0.7 (95% CI: 0.6–0.8) for TBLC.

A total of 42.5% (65 out of 153) of pathological diagnoses were derived from patients diagnosed with IPAF/CTD-ILD, with NSIP as the dominant pattern (38.5%, 25/65), followed by UIP (33.8%, 22/65) (Supplementary Figure S1). The spectrum of connective tissue diseases in this study encompassed idiopathic inflammatory myopathy (IIM), rheumatoid arthritis (RA) and systemic sclerosis (SSc). The distribution of pathological patterns was not significantly different between the two cohorts ( $p = 0.26$ ) (Table 3).

## Stratification of the Pathological Information

As mentioned above, the pathological information was stratified based on its specificity as well as its contribution to the final MDD diagnosis. The grade distribution of pathological results was significantly different for UT-VATS and TBLC ( $p = 0.02$ ): compared with TBLC, UT-VATS was more likely to alter the initial clinical-radiological diagnosis (grade1: 34.3 vs 12.9%,  $p = 0.003$ ) and provide more informative results (grade 4: 9.0 vs 20.0%,  $p = 0.06$ ) to the second MDD session. As shown in Figure 2, among cases with specific pathological diagnoses, those initially diagnosed as UIIP accounted for a majority of diagnosis-altered cases (62.5%, 20/32), followed by RB-ILD/DIP (9.4%, 3/32). Those initially diagnosed as IPAF accounted for a great proportion of diagnosis-unchanged cases (35.1%, 26/74), followed by CTD-ILD (24.3%, 18/74) and IPF (13.5%, 10/74). A subgroup analysis based on ILD subtype and focused on cases initially diagnosed as UIIP and IPAF/CTD-ILD showed that histological information from UT-VATS appeared more informative than that obtained from TBLC for cases initially diagnosed as UIIP (grade 4: 13.6 vs 40.0%,  $p = 0.06$ ). Nonetheless UT-VATS and TBLC contributed similarly to the final diagnosis for cases initially diagnosed as IPAF/CTD-ILD (total  $p = 0.14$ , grade 4: 8.7 vs 15.2%,  $p = 0.47$ ) (Table 4).

## Safety and Cost

Pneumothorax occurred in 5.7% (4/70) of patients who underwent TBLC. There were no significant differences in severe bleeding, acute exacerbation or 90-days mortality between UT-VATS and TBLC cohorts. The total and post-operative length of hospital stay were comparable for both methods although the hospitalization cost of UT-VATS was much higher (US\$4,855.7 vs US\$3,590.9,  $p < 0.001$ ) (Table 5).

## DISCUSSION

This prospective study illustrated the two-round MDD decision-making process in the diagnostic algorithm of ILD. The first MDD reflected the choice of experts on candidates and methods of biopsies, and the second revealed the performance of different biopsy methods in patients with distinct ILD subtypes: pathological information via UT-VATS was more clinically useful than that from TBLC for cases initially diagnosed as UIIP, although both methods contributed similarly to cases

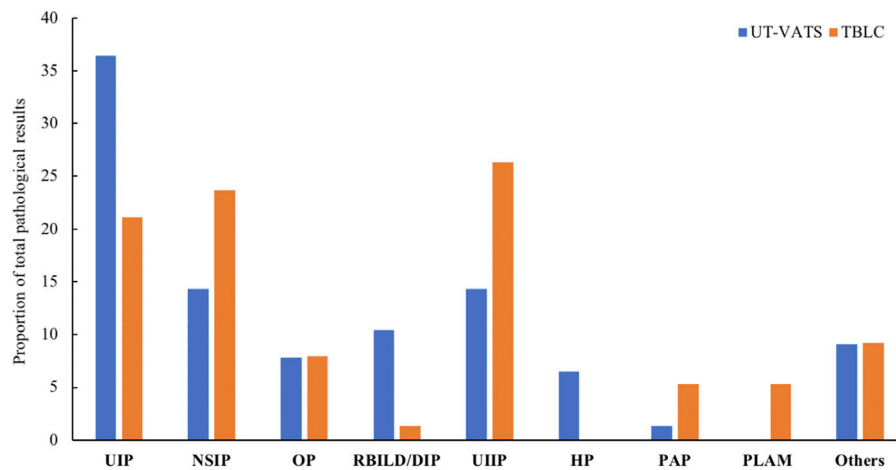


**FIGURE 2 |** The distribution of pathological diagnoses by different biopsy methods. UT-VATS: uniportal and tubeless-video-assisted thoracic surgery, TBLC: transbronchial lung cryobiopsy, UIP: usual interstitial pneumonia, NSIP: non-specific interstitial pneumonia, OP: organizing pneumonia, RB-ILD: respiratory bronchiolitis interstitial lung disease, DIP: desquamative interstitial pneumonia, UIIP: undefined interstitial pneumonia, HP: hypersensitivity pneumonitis, PAP: pulmonary alveolar proteinosis, PLAM: pulmonary lymphangioleiomyomatosis, Others: including LIP (lymphocyte interstitial pneumonia), sarcoidosis, PLCH (pulmonary Langerhans cell histiocytosis), IPH (idiopathic pulmonary hemosiderosis) and PAM (pulmonary alveolar microlithiasis).

**TABLE 3 |** The distribution of pathological diagnosis in IPAF/CTD-ILD patients.

	UT-VATS (n = 29)				–	TBLC (n = 36)			
	UIP	NSIP	OP	DIP		UIIP	UIP	NSIP	OP
IPAF	8	4	1	1	1	6	11	2	4
IIM-ILD	1	4	2	0	1	1	4	2	1
RA-ILD	3	2	0	0	0	1	0	0	1
SSc-ILD	1	0	0	0	0	1	0	1	1
Total	13	10	3	1	2	9	15	5	7

UT-VATS: uniportal and tubeless-video-assisted thoracic surgery, TBLC: transbronchial lung cryobiopsy, UIP: usual interstitial pneumonia, NSIP: non-specific interstitial pneumonia, OP: organizing pneumonia, DIP: desquamative interstitial pneumonia, UIIP: undefined idiopathic interstitial pneumonia, IPAF: interstitial pneumonia with autoimmune features, IIM-ILD: idiopathic inflammatory myositis-related interstitial lung disease, RA-ILD: rheumatoid arthritis-related interstitial lung disease, SSc-ILD: systemic sclerosis-related interstitial lung disease.

initially diagnosed as IPAF/CTD-ILD. The safety of UT-VATS was comparable with that of TBLC although the latter appeared to cost less during the hospitalization.

MDD is considered the gold standard in the diagnosis of ILD given its improvement of diagnostic confidence. Although different pathways that follow a multidisciplinary approach to ILD are largely heterogeneous and need further validation, the two-round MDD method is recommended in the ATS/ERS joint statement (Raghu et al., 2018). We implemented this mode in real-world practice and included a pulmonologist, radiologist, pathologist and rheumatologist in the MDD team. The first round MDD aimed to confirm which patients required a biopsy along with the appropriate biopsy method. SLB is regarded as the most reliable tool to provide diagnostic and prognostic information but is associated with substantial morbidity and mortality. In recent years, TBLC has been proposed as an alternative to SLB in the diagnosis of ILD, with a comparable diagnostic yield and less invasive nature (Tomassetti et al., 2016; Johansson et al., 2016;

**TABLE 4 |** The stratification of pathological information with different biopsy methods

	UT-VATS	TBLC	p value
Total, n	67	70	0.02
Grade 1	23 (34.3)	9 (12.9)	0.003
Grade 2	33 (49.3)	41 (58.6)	0.27
Grade 3	5 (7.5)	6 (8.6)	0.81
Grade 4	6 (9.0)	14 (20.0)	0.06
Initial dx UIIP, n	22	15	0.27
Grade 1	13 (59.1)	7 (46.7)	0.46
Grade 2	1 (4.5)	0 (0)	0.40
Grade 3	5 (22.7)	2 (13.3)	0.47
Grade 4	3 (13.6)	6 (40.0)	0.06
Initial dx IPAF/CTD-ILD, n	23	33	0.14
Grade 1	2 (8.7)	0 (0)	0.08
Grade 2	19 (82.6)	25 (75.8)	0.54
Grade 3	0 (0)	3 (9.1)	0.14
Grade 4	2 (8.7)	5 (15.2)	0.47

Values are presented as number (%) unless specified. UT-VATS: uniportal and tubeless-video-assisted thoracic surgery, TBLC: transbronchial lung cryobiopsy, UIIP: undefined interstitial pneumonia, IPAF: interstitial pneumonia with autoimmune features, CTD-ILD: connective tissue disease-related interstitial lung disease. Grade 1: specific diagnosis with final diagnosis altered; grade 2: specific diagnosis without final diagnosis altered; grade 3: non-specific diagnosis with supplementary information provided; grade 4: non-informative diagnosis.

Ravaglia et al., 2016; Kronborg-White et al., 2017), although results are conflicting (Troy et al., 2020; Romagnoli et al., 2019). In the present study, the counterpart of TBLC was uniportal and tubeless VATS (UT-VATS), characterized by spontaneous ventilation anesthesia and absence of postoperative chest tube drainage, thereby mitigating the peri-procedure risk and postoperative discomfort (Peng et al., 2017). Based on current knowledge of the utility and safety of biopsy procedures, our MDD team was inclined to select UT-VATS in cases initially diagnosed as IPF and RB-ILD/DIP; TBLC appeared to be favored more in cases initially

**TABLE 5 |** Complications and hospitalization costs for different biopsy methods.

	UT-VATS (n = 67)	TBLC (n = 70)	p value
Pneumothorax, n	NA	4 (5.7)	NA
Severe bleeding, n	0 (0)	0 (0)	NA
Acute exacerbation, n	2 (3.0)	3 (4.3)	0.68
90-days mortality, n	0 (0)	0 (0)	NA
Hospitalization days <sup>a</sup>	13.0 (4.0)	13.0 (5.5)	0.57
Post-operative hospitalization days <sup>a</sup>	6.0 (3.0)	5.0 (3.0)	0.2
Total expense <sup>a</sup> , US\$	4885.7 (1586.0)	3590.9 (2927.0)	0.001

Values are presented as number (%) or

<sup>a</sup>median (interquartile range).

UT-VATS: uniportal and tubeless-video-assisted thoracic surgery, TBLC: transbronchial lung cryobiopsy.

diagnosed as PLAM and PAP. This choice may be related to the radiological features of lesions: SLB is preferred in the presence of a heterogeneous pattern with subpleural or patchy distribution, while TBLC is preferred in the presence of a homogeneous pattern with broncho-centric or perilymphatic distribution (Colby et al., 2017).

The major concern raised for TBLC is that a smaller sample from a single locus may not provide the representative data that are obtained from multiple biopsies from multiple lobes via SLB, especially for UIP pattern (Raparia et al., 2016; Patel et al., 2016). Tomassetti et al. reported the comparable change of initial clinical-radiological diagnosis with the addition of histological information from TBLC or SLB (26 vs 36%), and more cases were finally diagnosed as IPF on TBLC (50 vs 39%), albeit with lower inter-pathologist agreement (Tomassetti et al., 2016); similarly, Troy et al. showed a higher proportion of probable UIP relative to UIP pattern in TBLC, while the converse was observed with SLB samples (Troy et al., 2020), indicating that the heterogeneous pattern of IPF may be more reliable on SLB samples. A smoking history combined with typical radiological changes, i.e. bronchial thickening followed by centrilobular nodules and ground-glass opacity (GGO) in RB-ILD and extensive bilateral GGO with a peripheral and basal predominance in DIP, is usually sufficient to diagnose these ILD subtypes causally associated with smoking (Kumar et al., 2018). Nonetheless it should be noted that there is a high chance of overlap of various smoking-related ILDs, such as RB-ILD/DIP and IPF, in which cases confirmation of the dominant lesion is essential for diagnosis orientation and patient management (Bak and Lee, 2017). We identified an altered diagnosis of RB-ILD/DIP and IPF in four cases with UT-VATS samples, raising the possibility that a representative area of the disease or a coexistent fibrotic process could be presented in a higher proportion of SLB samples.

Another concern in decision-making relates to safety. Since low pulmonary function has been suggested to be associated with a higher rate of complications (Ravaglia et al., 2016), the MDD team adopted DL<sub>CO</sub><45% predicted to exclude biopsy candidates and DL<sub>CO</sub><60% to refuse UT-VATS. These cut-off values may partly explain the comparable incidence of procedure-related complications between UT-VATS and TBLC groups. The improved surgical technique with less injury and fast track compared with conventional VATS procedure would increase safety for these selected patients (Peng et al., 2017). Among the adverse events

related to TBLC, pneumothorax was the most common (5.7%) but the lower incidence compared with many previous studies (Tomassetti et al., 2016; Ravaglia et al., 2016) seems to correlate with the distribution of dominant lesions in the TBLC group, i.e., broncho-centric or perilymphatic distribution. No severe bleeding occurred in our cohort, partly due to intubation with the rigid bronchoscope and prophylactic placement of a Fogarty balloon.

The second round MDD evaluated the pathological information in terms of its specificity as well as its contribution to the final MDD diagnosis. In line with previous data (Colby et al., 2017), the majority of UT-VATS samples were obtained from two lobes and TBLC samples were from different segments of one lobe (mostly lower lobes). There were one to three biopsies with average size of 5.3cm<sup>2</sup> and one to eight samples with average size of 9.0 mm<sup>2</sup> in UT-VATS and TBLC groups, respectively. The specific pathological yield in the UT-VATS cohort was borderline higher than that in the TBLC group (85.7 vs 73.7%,  $p = 0.06$ ). The final diagnosis agreed more with UT-VATS than with TBLC ( $\kappa = 0.8$  vs  $\kappa = 0.7$ ), indicating a considerably higher diagnostic confidence for UT-VATS over TBLC.

Apart from histological specificity, biopsy information, albeit non-specific, is valuable if it provides diagnostic clues or suggests a management strategy: the observation of lymphoid aggregates, germinal centers, lymphoplasmacytic inflammation, vasculitis or pleuritis may indicate the underlying “CTD color” (Fischer and Richeldi, 2014), while multiple foci of peribronchiolar metaplasia may favor HP to a great extent (Churg et al., 2017). We therefore stratified the pathological information into four grades based on non-diagnostic supplementary information provided as well as histological specificity, and grades 1–3 were deemed clinically helpful. We found that UT-VATS samples appeared more informative than TBLC samples across the whole ILD spectrum (91.0 vs 80.0%,  $p = 0.06$ ) as well as in cases initially diagnosed as UIIP (86.4 vs 60.0%,  $p = 0.06$ ). These data indicated that following the first round MDD options, pathological information derived from UT-VATS contributed more to the final MDD diagnosis than information obtained from TBLC.

The proportion of patients who underwent biopsy at our institute was relatively higher than previously reported (33.7 vs 7.5–40.3%) (Singh et al., 2017). This may have been attributable to the great number of patients diagnosed with CTD-ILD or IPAF (23/67, 34.3% in UT-VATS and 33/70, 47.1% in TBLC groups, respectively). The necessity for lung biopsy in ILD patients with

autoimmune features remains controversial: although the UIP pattern may offer SSc-ILD patients a comparable prognosis to those with a NSIP pattern (Bouros et al., 2002), it may indicate a worse outcome in patients with RA-ILD, IIM-ILD and IPAF (Antoniou et al., 2009) (Kim et al., 2015; Oldham et al., 2016). Recently, it was revealed in the INBUILD trial that nintedanib could slow the decline in FVC in patients with progressive fibrosing ILD other than IPF, and benefits were observed only when those with a UIP-like pattern were grouped together (Flaherty et al., 2019). These results led pulmonologists and rheumatologists to propose a combination therapy of anti-inflammatory and anti-fibrotic agents in patients with autoimmune diseases characterized by a UIP-pattern. In the current study, we found that most histopathological data for IPAF/CTD-ILD patients, albeit specific, did not alter the diagnosis. Although patients with UIP pattern were prescribed the combination therapy mentioned before and closely monitored, the response to therapy and disease behavior are the subject of another study. Regarding biopsy methods, UT-VATS and TBLC contributed similarly to the final MDD diagnosis in providing clinically useful pathological information, and the distribution of histological pattern was similar between UT-VATS and TBLC groups ( $p = 0.26$ ). This may be partly explained by the distribution of lung injury pattern for this subtype: usually symmetrical, basilar and non-subpleural predominant, thus allowing good sampling with TBLC.

There was no significant difference between UT-VATS and TBLC groups in post-operative hospitalization days, although this may be relatively longer compared with previous data because we usually advise our patients to wait for 3–4 days after the procedure for pathological results and a final MDD decision. The hospitalization expense was higher in the UT-VATS group, mainly attributable to the cost of the procedure, so a patient's ability to pay may also affect choice of biopsy method.

Our study has several limitations. Although it was recommended that the MDD team should decide candidates for biopsy and the biopsy method, there remains no consensus or guideline on how to make the decision. The non-randomized nature of this study may have led to a selection bias. Direct comparison of the techniques is also difficult since they were performed in different patients. Nonetheless our objective was to evaluate TBLC and UT-VATS, each with well-known advantages and disadvantages for sampling and safety, in the real-world clinical practice within the context of MDD. The organizational scheme of this study may provide additional information for the application of biopsy methods in different ILD subtypes, rather than just emphasizing priority or alteration. Second, this study included a limited number of patients so subgroup analysis was difficult to perform in most ILD subtypes. Future studies that focus on a certain subgroup may better inform the application of different biopsy methods under different circumstances. Finally, this study involved patients and MDD experts from only one center, and the counterpart of TBLC in our study was a highly sophisticated surgical technique that has not been widely implemented in other institutes. Results may differ for other institutes. It should be remembered though that improving conventional procedures is just as important, possibly more so, than developing new ones.

## CONCLUSION

In conclusion, this prospective study demonstrated the option and evaluation of different biopsy methods in the ILD diagnostic algorithm within the two-round MDD context. MDD decisions about biopsies are driven by the current knowledge of risk-benefit of different biopsy methods as well as the working diagnosis of a given patient. Our study provides a robust rationale for future studies investigating the MDD implementation regarding the selection of biopsy methods in ILD diagnostic schema.

## DATA AVAILABILITY STATEMENT

The original contributions presented in the study are included in the article/**Supplementary Material**, further inquiries can be directed to the corresponding authors.

## ETHICS STATEMENT

The studies involving human participants were reviewed and approved by The First Affiliated Hospital of Guangzhou Medical University. The patients/participants provided their written informed consent to participate in this study.

## AUTHOR CONTRIBUTIONS

QH, XC, XX, SL, JH, and QL designed the study. QH, XC, XX, SL, and QL coordinated the study. QH, WQ, GZ, and QL included patients. XC and SL performed transbronchial lung cryobiopsy. XX, GP, and JH performed tubeless video-assisted thoracic surgery. QH, XC, SL, XX, YG, and QL participated in multidisciplinary discussion. YG performed blinded tissue pathology. WQ, GZ, BG, and SX participated in data collection. QH, XC, XX, and MM performed statistical analyses. QH, XC, XX, SL, and QL wrote the first draft of the manuscript. All authors critically revised the manuscript for intellectually important content. All authors gave final approval for the publication of the work, and all accepted responsibility for the integrity of the work.

## FUNDING

This work is supported by National Key Research Project-Accurate Medical Research (No. 2016YFC0905701 to QL) and Foundation for Young Scholars of Guangzhou Medical University (No. 2019GIRHZ05 to QH).

## SUPPLEMENTARY MATERIAL

The Supplementary Material for this article can be found online at: <https://www.frontiersin.org/articles/10.3389/fmolb.2021.681669/full#supplementary-material>



## REFERENCES

- Antoniou, K. M., Margaritopoulos, G., Economidou, F., and Siafakas, N. M. (2009). Pivotal Clinical Dilemmas in Collagen Vascular Diseases Associated with Interstitial Lung Involvement. *Eur. Respir. J.* 33 (4), 882–896. doi:10.1183/09031936.00152607
- Bak, S. H., and Lee, H. Y. (2017). Overlaps and Uncertainties of Smoking-Related Idiopathic Interstitial Pneumonias. *Copd* 12, 3221–3229. doi:10.2147/COPD.S146899
- Bouros, D., Wells, A. U., Nicholson, A. G., Colby, T. V., Polychronopoulos, V., Pantelidis, P., et al. (2002). Histopathologic Subsets of Fibrosing Alveolitis in Patients with Systemic Sclerosis and Their Relationship to Outcome. *Am. J. Respir. Crit. Care Med.* 165 (12), 1581–1586. doi:10.1164/rccm.2106012
- Chaudhuri, N., Spencer, L., Greaves, M., Bishop, P., Chaturvedi, A., and Leonard, C. (2016). A Review of the Multidisciplinary Diagnosis of Interstitial Lung Diseases: A Retrospective Analysis in a Single UK Specialist Centre. *Jcm* 5 (8), 66. doi:10.3390/jcm5080066
- Churg, A., Wright, J. L., and Ryerson, C. J. (2017). Pathologic Separation of Chronic Hypersensitivity Pneumonitis from Fibrotic Connective Tissue Disease-Associated Interstitial Lung Disease. *Am. J. Surg. Pathol.* 41 (10), 1403–1409. doi:10.1097/PAS.0000000000000885
- Colby, T. V., Tomassetti, S., Cavazza, A., Dubini, A., and Poletti, V. (2017). Transbronchial Cryobiopsy in Diffuse Lung Disease: Update for the Pathologist. *Arch. Pathol. Lab. Med.* 141 (7), 891–900. doi:10.5858/arpa.2016-0233-RA
- Colella, S., Haentschel, M., Shah, P., Poletti, V., and Hetzel, J. (2018). Transbronchial Lung Cryobiopsy in Interstitial Lung Diseases: Best Practice. *Respiration* 95 (6), 383–391. doi:10.1159/000488910
- De Sadeleer, L. J., Meert, C., Yserbyt, J., Slabbynck, H., Verschakelen, J. A., Verbeken, E. K., et al. (2018). Diagnostic Ability of a Dynamic Multidisciplinary Discussion in Interstitial Lung Diseases. *Chest* 153 (6), 1416–1423. doi:10.1016/j.chest.2018.03.026
- Demedts, M., and Costabel, U. (2002). ATS/ERS International Multidisciplinary Consensus Classification of the Idiopathic Interstitial Pneumonias. *Eur. Respir. J.* 19 (5), 794–796. doi:10.1183/09031936.02.00492002
- Fibla, J. J., Brunelli, A., Cassivi, S. D., and Deschamps, C. (2012a). Aggregate Risk Score for Predicting Mortality after Surgical Biopsy for Interstitial Lung Disease. *Interactive CardioVascular Thorac. Surg.* 15 (2), 276–279. doi:10.1093/icvts/ivs174
- Fibla, J. J., Molins, L., Blanco, A., Royo, I., Martínez Vallina, P., Martínez, N., et al. (2012b). Video-assisted Thoracoscopic Lung Biopsy in the Diagnosis of Interstitial Lung Disease: a Prospective, Multi-center Study in 224 Patients. *Arch. Bronconeumol. (English Edition)* 48 (3), 81–85. doi:10.1016/j.arbres.2011.11.002
- Fischer, A., and Richeldi, L. (2014). Cross-disciplinary Collaboration in Connective Tissue Disease-Related Lung Disease. *Semin. Respir. Crit. Care Med.* 35 (2), 159–165. doi:10.1055/s-0034-1371530
- Flaherty, K. R., King, T. E., Jr., Raghu, G., Lynch, J. P., 3rd, Colby, T. V., Travis, W. D., et al. (2004). Idiopathic Interstitial Pneumonia. *Am. J. Respir. Crit. Care Med.* 170 (8), 904–910. doi:10.1164/rccm.200402-147OC
- Flaherty, K. R., Wells, A. U., Cottin, V., Devaraj, A., Walsh, S. L. F., Inoue, Y., et al. (2019). Nintedanib in Progressive Fibrosing Interstitial Lung Diseases. *N. Engl. J. Med.* 381 (18), 1718–1727. doi:10.1056/NEJMoa1908681
- Han, Q., Luo, Q., Xie, J.-X., Wu, L.-L., Liao, L.-Y., Zhang, X.-X., et al. (2015). Diagnostic Yield and Postoperative Mortality Associated with Surgical Lung Biopsy for Evaluation of Interstitial Lung Diseases: A Systematic Review and Meta-Analysis. *J. Thorac. Cardiovasc. Surg.* 149 (5), 1394–1401.e1. doi:10.1016/j.jtcvs.2014.12.057
- Johannson, K. A., Marcoux, V. S., Ronksley, P. E., and Ryerson, C. J. (2016). Diagnostic Yield and Complications of Transbronchial Lung Cryobiopsy for Interstitial Lung Disease: A Systematic Review and Meta-Analysis. *Ann. ATS* 13 (10), 1828–1838. doi:10.1513/AnnalsATS.201606-461SR
- Kim, H.-C., Ji, W., Kim, M. Y., Colby, T. V., Jang, S. J., Lee, C.-K., et al. (2015). Interstitial Pneumonia Related to Undifferentiated Connective Tissue Disease. *Chest* 147 (1), 165–172. doi:10.1378/chest.14-0272
- Kronborg-White, S., Folkersen, B., Rasmussen, T. R., Voldby, N., Madsen, L. B., Rasmussen, F., et al. (2017). Introduction of Cryobiopsies in the Diagnostics of Interstitial Lung Diseases - Experiences in a Referral center. *Eur. Clin. Respir. J.* 4 (1), 1274099. doi:10.1080/20018525.2016.1274099
- Kumar, A., Cherian, S. V., Vassallo, R., Yi, E. S., and Ryu, J. H. (2018). Current Concepts in Pathogenesis, Diagnosis, and Management of Smoking-Related Interstitial Lung Diseases. *Chest* 154 (2), 394–408. doi:10.1016/j.chest.2017.11.023
- Luo, Q., Han, Q., Chen, X., Xie, J., Wu, L., and Chen, R. (2013). The Diagnosis Efficacy and Safety of Video-Assisted Thoracoscopy Surgery (VATS) in Undefined Interstitial Lung Diseases: a Retrospective Study. *J. Thorac. Dis.* 5 (3), 283–288. doi:10.3978/j.issn.2072-1439.2013.04.12
- Oldham, J. M., Adegunsoye, A., Valenzi, E., Lee, C., Witt, L., Chen, L., et al. (2016). Characterisation of Patients with Interstitial Pneumonia with Autoimmune Features. *Eur. Respir. J.* 47 (6), 1767–1775. doi:10.1183/13993003.01565-2015
- Patel, N. M., Borczuk, A. C., and Lederer, D. J. (2016). Cryobiopsy in the Diagnosis of Interstitial Lung Disease. A Step Forward or Back? *Am. J. Respir. Crit. Care Med.* 193 (7), 707–709. doi:10.1164/rccm.201511-2313ED
- Peng, G., Liu, M., Luo, Q., Chen, H., Yin, W., Wang, W., et al. (2017). Spontaneous Ventilation Anesthesia Combined with Uniportal and Tubeless Thoracoscopic Lung Biopsy in Selected Patients with Interstitial Lung Diseases. *J. Thorac. Dis.* 9 (11), 4494–4501. doi:10.21037/jtd.2017.10.76
- Raghu, G., Collard, H. R., Egan, J. J., Martinez, F. J., Behr, J., Brown, K. K., et al. (2011). An Official ATS/ERS/JRS/ALAT Statement: Idiopathic Pulmonary Fibrosis: Evidence-Based Guidelines for Diagnosis and Management. *Am. J. Respir. Crit. Care Med.* 183 (6), 788–824. doi:10.1164/rccm.2009-040GL
- Raghu, G., Remy-Jardin, M., Myers, J. L., Richeldi, L., Ryerson, C. J., Lederer, D. J., et al. (2018). Diagnosis of Idiopathic Pulmonary Fibrosis. An Official ATS/ERS/JRS/ALAT Clinical Practice Guideline. *Am. J. Respir. Crit. Care Med.* 198 (5), e44–e68. doi:10.1164/rccm.201807-1255ST
- Raparia, K., Aisner, D. L., Allen, T. C., Beasley, M. B., Borczuk, A., Cagle, P. T., et al. (2016). Transbronchial Lung Cryobiopsy for Interstitial Lung Disease Diagnosis: A Perspective from Members of the Pulmonary Pathology Society. *Arch. Pathol. Lab. Med.* 140 (11), 1281–1284. doi:10.5858/arpa.2016-0258-SA
- Ravaglia, C., Bonifazi, M., Wells, A. U., Tomassetti, S., Gurioli, C., Piciucchi, S., et al. (2016). Safety and Diagnostic Yield of Transbronchial Lung Cryobiopsy in Diffuse Parenchymal Lung Diseases: A Comparative Study versus Video-Assisted Thoracoscopic Lung Biopsy and a Systematic Review of the Literature. *Respiration* 91 (3), 215–227. doi:10.1159/000444089
- Romagnoli, M., Colby, T. V., Berthet, J.-P., Gamez, A. S., Mallet, J.-P., Serre, I., et al. (2019). Poor Concordance between Sequential Transbronchial Lung Cryobiopsy and Surgical Lung Biopsy in the Diagnosis of Diffuse Interstitial Lung Diseases. *Am. J. Respir. Crit. Care Med.* 199 (10), 1249–1256. doi:10.1164/rccm.201810-1947OC
- Sigurdsson, M. I., Isaksson, H. J., Gudmundsson, G., and Gudbjartsson, T. (2009). Diagnostic Surgical Lung Biopsies for Suspected Interstitial Lung Diseases: a Retrospective Study. *Ann. Thorac. Surg.* 88 (1), 227–232. doi:10.1016/j.athoracsurg.2009.04.002
- Singh, S., Collins, B. F., Sharma, B. B., Joshi, J. M., Talwar, D., Katiyar, S., et al. (2017). Interstitial Lung Disease in India. Results of a Prospective Registry. *Am. J. Respir. Crit. Care Med.* 195 (6), 801–813. doi:10.1164/rccm.201607-1484OC
- Tomassetti, S., Wells, A. U., Costabel, U., Cavazza, A., Colby, T. V., Rossi, G., et al. (2016). Bronchoscopic Lung Cryobiopsy Increases Diagnostic Confidence in the Multidisciplinary Diagnosis of Idiopathic Pulmonary Fibrosis. *Am. J. Respir. Crit. Care Med.* 193 (7), 745–752. doi:10.1164/rccm.201504-0711OC
- Travis, W. D., Costabel, U., Hansell, D. M., King, T. E., Jr., Lynch, D. A., Nicholson, A. G., et al. (2013). An Official American Thoracic Society/European Respiratory Society Statement: Update of the International Multidisciplinary Classification of the Idiopathic Interstitial Pneumonias. *Am. J. Respir. Crit. Care Med.* 188 (6), 733–748. doi:10.1164/rccm.201308-1483ST
- Troy, L. K., Grainge, C., Corte, T. J., Williamson, J. P., Valley, M. P., Cooper, W. A., et al. (2020). Diagnostic Accuracy of Transbronchial Lung Cryobiopsy for Interstitial Lung Disease Diagnosis (COLDICE): a Prospective, Comparative Study. *Lancet Respir. Med.* 8 (2), 171–181. doi:10.1016/S2213-2600(19)30342-X

**Conflict of Interest:** The authors declare that the research was conducted in the absence of any commercial or financial relationships that could be construed as a potential conflict of interest.

Copyright © 2021 Han, Chen, Xu, Qian, Zhao, Mao, Guo, Xia, Peng, He, Gu, Li and Luo. This is an open-access article distributed under the terms of the Creative Commons Attribution License (CC BY). The use, distribution or reproduction in other forums is permitted, provided the original author(s) and the copyright owner(s) are credited and that the original publication in this journal is cited, in accordance with accepted academic practice. No use, distribution or reproduction is permitted which does not comply with these terms.



# Gremlin2 Activates Fibroblasts to Promote Pulmonary Fibrosis Through the Bone Morphogenic Protein Pathway

Caijuan Huan<sup>1†</sup>, Wangting Xu<sup>1†</sup>, Yaru Liu<sup>2</sup>, Kexin Ruan<sup>1</sup>, Yueli Shi<sup>3</sup>, Hongqiang Cheng<sup>2</sup>, Xue Zhang<sup>2</sup>, Yuehai Ke<sup>2</sup> and Jianying Zhou<sup>1\*</sup>

<sup>1</sup>Department of Respiratory Medicine, The First Affiliated Hospital, Zhejiang University School of Medicine, Hangzhou, China, <sup>2</sup>Department of Pathology and Pathophysiology, Zhejiang University School of Medicine, Hangzhou, China, <sup>3</sup>The Fourth Affiliated Hospital, Zhejiang University School of Medicine, Yiwu, China

## OPEN ACCESS

### Edited by:

Dianhua Jiang,  
Cedars Sinai Medical Center,  
United States

### Reviewed by:

Huaiyong Chen,  
Tianjin Haihe Hospital, China  
Wen Ning,  
Nankai University, China

### \*Correspondence:

Jianying Zhou  
zyjhz@zju.edu.cn

<sup>†</sup>These authors have contributed  
equally to this work and share first  
authorship

### Specialty section:

This article was submitted to  
Molecular Diagnostics  
and Therapeutics,  
a section of the journal  
Frontiers in Molecular Biosciences

**Received:** 20 March 2021

**Accepted:** 16 June 2021

**Published:** 28 June 2021

### Citation:

Huan C, Xu W, Liu Y, Ruan K, Shi Y,  
Cheng H, Zhang X, Ke Y and Zhou J  
(2021) Gremlin2 Activates Fibroblasts  
to Promote Pulmonary Fibrosis  
Through the Bone Morphogenic  
Protein Pathway.  
Front. Mol. Biosci. 8:683267.  
doi: 10.3389/fmolb.2021.683267

Idiopathic pulmonary fibrosis (IPF) is a progressive lung disease causing unremitting extracellular matrix deposition. Transforming growth factor- $\beta$  (TGF- $\beta$ ) superfamily involves bone morphogenetic proteins (BMPs) and TGF- $\beta$ , and the balance between the activation of TGF- $\beta$ -dependent SMADs (Smad2/3) and BMP-dependent SMADs (Smad1/5/8) is essential for fibrosis process. *GREM2*, initially identified as a TGF- $\beta$ -inducible gene, encodes a small secreted glycoprotein belonging to a group of matricellular proteins, its role in lung fibrosis is not clear. Here, we identified Gremlin2 as a key regulator of fibroblast activation. Gremlin2 was highly expressed in the serum and lung tissues in IPF patients. Bleomycin-induced lung fibrosis model exhibited high expression of Gremlin2 in the bronchoalveolar lavage fluid (BALF) and lung tissue. Isolation of primary cells from bleomycin-induced fibrosis lung showed a good correlation of Gremlin2 and Acta2 ( $\alpha$ -SMA) expressions. Overexpression of Gremlin2 in human fetal lung fibroblast 1 (HFL-1) cells increased its invasion and migration. Furthermore, Gremlin2 regulates fibrosis functions through mediating TGF- $\beta$ /BMP signaling, in which Gremlin2 may activate TGF- $\beta$  signaling and inhibit BMP signaling. Therefore, we provided *in vivo* and *in vitro* evidence to demonstrate that Gremlin2 may be a potential therapeutic target for the treatment of IPF.

**Keywords:** IPF (idiopathic pulmonary fibrosis), gremlin2, BMP antagonists, P-smad1, fibroblast

## INTRODUCTION

Idiopathic pulmonary fibrosis (IPF), is the most common form of interstitial pneumonia (ATS/ERS, 2000), which deteriorates rapidly in a short period of time (Martinez et al., 2005) and the median survival is only 2–3 years (Raghu et al., 2011). Tissue fibrosis is an increasing cause of severe morbidity and mortality with limited therapeutic options, and IPF is characterized by patchy subpleural parenchymal fibrosis with pathological features including the accumulation of myofibroblasts, the formation of fibroblast foci, distortion of pulmonary architecture, and increased collagen deposition (Noble et al., 2012). Mechanisms leading to severe and progressive fibrosis are not entirely understood. Previous studies demonstrated that fibroblasts from patients

with IPF acquire an invasive phenotype that is essential for severe fibrogenesis (Li et al., 2011; Lovgren et al., 2011; Ahluwalia et al., 2016; Chen et al., 2016).

Fibroblasts are the main effector cells in fibrosis. They migrate from different sources to damaged sites, such as resident stromal fibroblasts, circulating fibroblasts, as well as epithelial cells and pericytes, and they are eventually activated as myofibroblasts (Andersson-Sjöland et al., 2008; Fernandez and Eickelberg, 2012; Wolters et al., 2014; Bagnato and Harari, 2015), which secrete excessive extracellular matrix (ECM), resulting in increased tissue hardness and loss of alveolar tissue function.

The progression of fibrosis is regulated by the transforming growth factor- $\beta$  (TGF- $\beta$ )/bone morphogenic protein (BMP) family.

After an injury to the airway epithelium, important profibrotic mediators, such as TGF- $\beta$ , are released from many types of lung cells, involving myofibroblasts and epithelial cells (Li et al., 2017). Their regulation on progenitor cells also affects fibrosis progression. TGF- $\beta$  is very important for the progression of pulmonary fibrosis in mice, as it regulates fibroblast proliferation, collagen synthesis and myofibroblast differentiation (Bonnaud et al., 2004; Bonnaud et al., 2005; Kang et al., 2007). The other important fibrosis regulator is BMP family, especially BMP4/7, which is considered to be an important regulatory molecule for anti-fibrosis (Hinck and Huang, 2013; Huan et al., 2015; Chanda et al., 2019). In recent years, antagonists of the BMP family gradually become the center of research for fibrosis treatment. For example, Gremlin1 and Follistatin-like 1 were proved to participate in and affect pulmonary fibrosis (Dong et al., 2015; Church et al., 2017; Myllärniemi, et al., 2008a; Mezzano et al., 2018).

Overall, the balance between the activation of BMP-dependent SMADs (SMAD1/5/8) and TGF- $\beta$ -dependent (SMAD2/3) plays a great role in fibrosis process.

Gremlin2 (*GREM2*), also known as PRDC, located on human chromosome 1Q43 (CKTSF1B2) (Katoh and Katoh, 2004), is a highly conserved secretory glycoprotein in the DAN region. Gremlin2 was first discovered as a protein associated with embryonic development (Hsu et al., 1998; Stanley et al., 1998). In recent years, its highly stable dimer structure formed via non-disulfide bonds has led scientists to further explore its structure (Kattamuri et al., 2012; Hinck and Huang, 2013; Nolan et al., 2016). Heparin-competitive antagonistic combination of Gremlin2 and BMP provides a new idea for Gremlin2 targeted therapy and the exploration of its structure (Nolan et al., 2013; Kattamuri et al., 2017). As a development-related protein, Gremlin2 is highly expressed during embryonic development but its high levels in adults may imply a severe disease state. It is known that Gremlin2 plays a crucial role in kidney development and kidney injury (Wen et al., 2019). Furthermore, as a strong antagonist of the BMP family, Gremlin2 has a strong effect on gastric cancer and myocardial fibrosis, but its effect on pulmonary fibrosis has not been reported (Sanders et al., 2016; Ran et al., 2019). However, the ability of Gremlin2 to regulate fibroblast activity in pathological settings has not been investigated.

Our previous study showed that Gremlin2 is highly expressed in myofibroblasts in single-cell sequencing (Xie et al., 2018). Data

showed Gremlin2 expression is significantly high in myofibroblasts, which is consistent with specific myofibroblast markers *Acta2* and *Myh11* (Hsia et al., 2016; Hinz et al., 2007). Meanwhile, in other mesenchymal cells, Gremlin2 expression is low, indicating that Gremlin2 has a functional role in myofibroblasts.

Therefore, here, we aimed to show the effect of Gremlin2 in IPF via *in vivo* and *in vitro* studies, as well as through database investigations and understand the potential of it as a therapeutic target.

## MATERIALS AND METHODS

### Mice

C57/BL6 male mice (6–8 weeks old) were purchased from GemPharmatech Co., Ltd., Jiangsu, China. All mice were housed and cared for in a pathogen-free facility at Zhejiang University. All animal protocols were approved by the animal care and use committee of the Zhejiang University School of Medicine.

Lungs were removed from mice at the age of 8–12 weeks after appropriate treatment. The tissues were minced, digested, and cultured in DMEM supplemented with 10% fetal bovine serum (FBS) and antibiotics-antimycotics (Thermo Fisher Scientific).

### Idiopathic Pulmonary Fibrosis Samples From Patients

Lung tissue samples were obtained from surgical lung biopsies or lung transplant explants from patients with IPF or other types of pulmonary fibrosis. IPF diagnosis was performed according to standard accepted American Thoracic Society recommendations (ATS/ERS, 2000). Human blood samples were obtained from the Clinical Laboratory. All samples were collected from the First Affiliated Hospital of Zhejiang University.

### Bleomycin Administration and Bronchoalveolar Lavage Fluid

Bleomycin was injected intratracheally at 2.5 U/kg body weight. Mice exposed to the same volume of PBS were used as controls and sacrificed via pentobarbital injection after 7, 14, and 21 days. Lungs were harvested for RNA preparation, protein isolation or fibroblast isolation. For bronchoalveolar lavage, the trachea was lavaged three times with 0.8 ml sterile saline at room temperature. Samples were centrifuged at 1,500 rpm for 5 min, and the supernatant was collected and stored at  $-80^{\circ}\text{C}$  until further use.

### Enzyme-Linked Immunosorbent Assay of Serum and Bronchoalveolar Lavage Fluid

The mice were anesthetized with 1% pentobarbital at a dose of 50 mg/kg, and the apical blood was obtained in a sterile environment and kept at  $4^{\circ}\text{C}$  overnight. The next day, the blood was centrifuged at  $4^{\circ}\text{C}$  for 15 min at  $3,000 \times g$ . The supernatant was removed and stored separately below  $-70^{\circ}\text{C}$ .

**TABLE 1 |** Reagent and antibody.

Product name	Company	Catalog	Lot
Rabbit polyclonal to PRDC-C-terminal GREM2 antibody	Abcam, cambridge, MA	Cat#ab228736	Lot# GR3209267-6
Rabbit polyclonal to fibronectin	CUSABIO	Catalog#CSB-PA107590	Lot#10902Y
Anti-alpha smooth muscle actin antibody	Abcam, cambridge, MA	Cat# ab2413, RRID:AB_2262874	Lot#GR3323518-2
Mouse PRDC/GREM2 antibody	Abcam, cambridge, MA	Cat# ab7817, RRID:AB_262054	Lot# GR3257713-10
Mouse PRDC/GREM2 biotinylated antibody	R And D systems	Cat# AF 2069, RRID:AB_2263614	Lot#USW0114091
Phospho-Smad1(Ser463/465)	R And D systems	Cat# BAF 2069, RRID:AB_2279268	Lot#UUB0112051
/Smad5(Ser463/465)	Cell signaling TECHNOLOGY	Cat# 13820T	Lot#3
/Smad9(Ser465/467)			
(D5B10)Rabbit mAb			
Smad1(D59D7)Rabbit mAb	Cell signaling TECHNOLOGY	Cat# 6944T	Lot#5
Phospho-SMAD2(Ser465/467) (E8F3R)	Cell signaling TECHNOLOGY	Cat# 188338T	Lot#3
Smad2 (D43B4) XP <sup>®</sup> rabbit mAb	Cell signaling TECHNOLOGY	Cat#5339T	Lot#6
Rabbit anti-P-Smad3(S423/425)		Cat# ET1609	Lot#HM0708
Human Gremlin-2 ELISA kit	Biolebo, beijing, China	ZN2207	Lot#TF0611
Recombinant human PRDC/GREM2 protein, CF	R&D systems	Catalog #8436-PR-050	Lot#DEUB0220071
HRP labeled goat anti-rabbit IgG(H + L)	BIOKER BIOTECHNOLOGY	Catalog #BK-R050	Lot#2313

before detection. BALF from each mouse was collected as mentioned in 2.3. Before measurement, the BALF supernatant of each mouse was stored at  $-70^{\circ}\text{C}$ . Gremlin2 levels in the serum and BALF supernatant were measured using Mouse Gremlin-2 ELISA Kit (Biolebo, Beijing, China), according to the manufacturer's instructions.

## Lung Histology and Immunohistochemistry

Mice were sacrificed at different time points after bleomycin treatment under anesthesia. The left lung of each mouse was fixed with 10% neutral buffer formalin overnight, then embedded in paraffin using standard procedures. Tissues were sectioned to 5  $\mu\text{m}$  slices for hematoxylin and eosin, Masson's Trichrome, and Gremlin2 staining (Table 1).

The alveolar wall thickness and alveolar space were photographed and measured using DP2-BSW software (Olympus, Tokyo, Japan). Slides were screened in a blinded manner and six lungs were observed in areas that did not contain bronchi or major pulmonary vessels. A total of 20 random measurements of alveolar wall thickness were recorded in each field.

## Immunohistochemistry Score

We selected five sections randomly from each slide at 200 $\times$  magnification for IHC score statistics as follows: negative, 1 point (less than 5% of cells); weak positive 2 points (5–25% of cells); positive, 3 points (25–50% of cells); strong positive, 4 points (50–75% of cells). IHC score staining degree and multiple cell ratio score of each section were added, the average of the five visual fields was accepted as the IHC score of the slide, and the average score of each slide was taken after two investigators agreed.

## Immunofluorescence

For cell immunofluorescence, after 48 h of TGF- $\beta$ 1 stimulation, fibroblasts were washed in PBS preheated at  $37^{\circ}\text{C}$ , fixed in 4% paraformaldehyde for 20 min, and permeated with 0.1% Triton

X-100 for 20 min. Cells were blocked in 10% FBS at room temperature for 1 h, and fibroblasts were incubated overnight with antibodies against Gremlin2 or  $\alpha$ -SMA (Table 1). On the second day, fibroblasts were washed with PBS, and 488 goat anti-rabbit/rat IgG (Invitrogen, Fisher Scientific, California, United States) was added for 1 h at room temperature. Cells were then washed with PBS, then immersed in DAPI to stain the nuclei. The staining was performed using a positive two-photon confocal microscope (Olympus BX61).

For tissue immunofluorescence, paraffin sections were baked, dewaxed, and hydrated after microwave antigen repair. They were then incubated in 0.5% Triton-TBS for 20 min and 5% goat serum for 30 min. Anti-Gremlin2 and  $\alpha$ -SMA antibodies were added at  $4^{\circ}\text{C}$  overnight. The next day, slides were washed with PBS and incubated for 2 h at room temperature with 488/576 goat anti-rabbit/rat IgG (Invitrogen, Fisher Scientific, California, United States), then washed with PBS, and immersed in DAPI to observe the nuclei. Imaging was performed using a positive two-photon confocal microscope (Olympus BX61).

## Quantitative Real-Time Polymerase Chain Reaction

Total RNA was extracted from tissues or cells using TRIzol (Invitrogen, Carlsbad, CA, United States) according to the manufacturer's protocol. RNA concentration was measured using a spectrophotometer (Eppendorf, Hamburg, Germany). Reverse transcription of total RNA (2 g) 20  $\mu\text{L}$  was performed using PrimeScript II 1st Strand cDNA Synthesis Kit (Takara, Otsu, Japan). Quantitative real-time PCR was performed using FastStart universal SYBR Green Master Kit (Mannheim Roche, Germany). Sequences of specific primers used are shown in Table 2.

## Western Blotting

The cells were washed with cold PBS and lysed with NP-40, then 6X loading buffer was added. Equivalent proteins were separated



**TABLE 2 |** Sequences of specific primers.

	Sense strand (5' to 3')	Anti-sense strand (5' to 3')
Gremlin2(mouse)	GGTAGCTGAAACACGGAAGAA	TCTTGACACAGTCACCTCTTGA
GAPDH(mouse)	AATGGATTGGACGCGATTGGT	TTTGCACTGGTACGTGTTGAT
Col1a1(mouse)	CCAAGAAGACATCCCTGAAGTCA	TGCACGTCATCGCACACA
Col1a2(mouse)	CGGAGAAGCTGGATCTGC	CAGGAGGACCCATTACACCA
Gremlin2(human)	ATCCCCTCGCCTTACAAGGA	TCTTGACACAGTCACCTCTTGA
GAPDH(human)	TGTGGGCATCAATGGATTTGG	ACACCATGTATTCCGGGTCAAT
Col1(human)	GTTGCTGCTGCAGTAACCTT	AGGGCCAAGTCCAACTCCTT
ACTA2(human)	GACAATGGCTCTGGGCTCTGTAA	CTGTGCTTCGTCAACCCACGTA
Fibronectin(human)	CAGGATCACTTACGGAGAAACAG	GCCAGTGACAGCATACACAGTG

via SDS-PAGE, then transferred to a cellulose nitrate membrane (Pall, Port Washington, NY) and incubated with the relevant primary antibodies (anti-Gremlin2, anti- $\alpha$ -Tubulin, anti-fibronectin, anti-collagen1, anti- $\alpha$ -SMA). This protocol was performed in three replicates. Shorter exposures were selected for optical density analysis to ensure that the band strength was within the linear range, and the integral density of the specified band was calculated using the ImageJ software.

### Transwell Assay

For cell migration,  $5 \times 10^4$  cells were resuspended in 200  $\mu$ l starvation medium and seeded into the upper chamber. In the lower chamber, 600  $\mu$ l of complete medium containing 10% FBS was added. After 24 h, the medium was removed, the upper chamber was washed twice with PBS, and cells were fixed with 4% PFA at room temperature for 30 min. The cells were stained with crystal violet. Three fields were randomly selected under 100 $\times$  magnification and cells were counted in each field for statistical analysis.

For cell invasion, the matrigel was diluted in Ham's F-12K (Kaighn's) Medium (1:32) (Gibco, Thermo Fisher, United States), added to the upper chamber one day in advance, and blow-dried overnight under ultraviolet light.  $2 \times 10^5$  cells were resuspended in 100  $\mu$ l starvation medium and added to the superior lumen. Exactly 600  $\mu$ l of medium containing 10% FBS was added to the lower chamber. After 48 h, the cells were collected, and the same steps were performed as the migration experiment.

### GEO Database Analysis

The original data in the GEO database were homogenized. We used R language (R i386 3.6.1.Ink) and GEO2R analysis software provided by the GEO website for group analysis. Then, the data for different groups were plotted using GraphPad Prism (version 5) and paired t-test was performed for statistical analysis.

### Lentiviral Infection

To knock out *GREM2* in fibroblasts, shRNA-Gremlin2-plko.1 and a control lentiviral vector [(RRID:Addgene\_23,260), Sigma-Aldrich] were obtained. 293T (RRID:CVCL\_LF41) cells were transfected with pMD2. G and psPAX2 were prepared using Lipofectamine 3,000 reagent (Invitrogen, Addgene, Cambridge, MA). After 48 and 72 h, the virus superfluids were collected and filtered through a 0.22  $\mu$ m filter, and added to fibroblasts. After

12 h, the culture medium was changed to allow the cells to grow until treatment and analysis.

### Statistical Analysis

All the results were expressed as the mean  $\pm$  SD, calculated using the statistical program of GraphPad Prism version 5. Student's t-test (two-tailed) was used and  $p < 0.05$  was considered statistically significant.

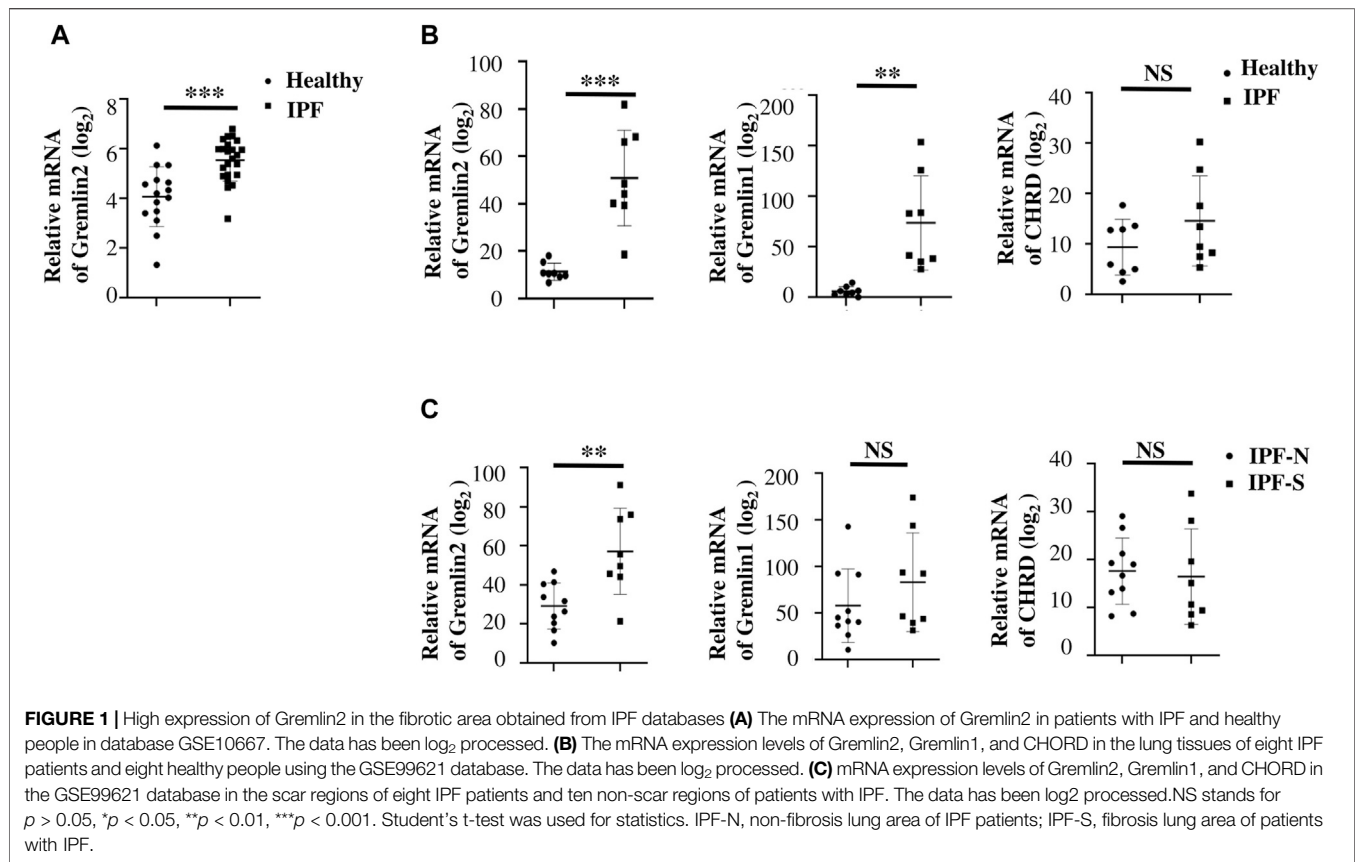
## RESULTS

### High Expression of Gremlin2 has a Strong Correlation With Idiopathic Pulmonary Fibrosis in the Fibrotic Area

To discern the importance of Gremlin2 in pulmonary fibrosis, we evaluated the expression of Gremlin2 using the GEO database and selected two fibrosis-related databases, GSE99621 (<https://www.ncbi.nlm.nih.gov/geo/query/acc.cgi?acc=GSE99621>) and GSE10667 (<https://www.ncbi.nlm.nih.gov/geo/query/acc.cgi>). GSE10667 exhibited that the transcription level of Gremlin2 in the lung tissues of patients with IPF was significantly higher than that of healthy people (Figure 1A,  $p < 0.001$ ). In GSE99621, we divided the data into Group1 (Figure 1B), patients with fibrosis, and healthy controls, and Group2 (Figure 1B), fibrosis foci and non-fibrosis foci of patients. Gremlin1 ( $p = 0.0011$ ) (Myllärniemi et al., 2008a; Myllärniemi et al., 2008b) and Gremlin2 ( $p < 0.001$ ) expressions in Group 1 (Figure 1B) were significantly high in the lung tissues of patients with fibrosis, while there was no difference in the expression of another BMP strong antagonist CHRD ( $p = 0.1819$ ) between healthy people and patients with fibrosis. In Group2 (Figure 1C), only Gremlin2 ( $p = 0.032$ ) expression was significantly higher in the fibrotic scar area than that in the non-fibrotic scar area of patients with IPF. Meanwhile, Gremlin1 ( $p = 0.2622$ ) and CHRD ( $p = 0.7755$ ) expressions showed no statistical significance. These two databases suggested that there was a strong relationship between Gremlin2 and IPF.

### Gremlin2 Expression is Increased in Patients With Idiopathic Pulmonary Fibrosis

To verify the data obtained from databases, we collected blood samples from four patients with non-IPF fibrosis and three



patients with IPF, and measured the concentration of Gremlin2 in the blood serum. These IPF patients were first diagnosed with IPF and had not received anti-fibrosis therapy. The concentration of Gremlin2 in the peripheral blood serum was detected using ELISA (**Figure 2A**), which showed that Gremlin2 expression was high in patients with IPF and low in non-IPF patients.

To further detect the expression of Gremlin2 in the lung tissue, IHC was performed using the lung tissue samples from 20 patients with fibrosis, and the expression of Gremlin2 was compared with that of 16 healthy lung tissues. The patient information is shown in **Table 3**. Gremlin2 expression was hardly detected in healthy lung tissues but was high in the fibrotic foci (**Figure 2B**). IHC score (**Figure 2C**) showed that Gremlin2 expression was statistically high in fibrotic lung tissues ( $p < 0.001$ ). To verify whether myofibroblasts are the main effector cells of Gremlin2, we detected the morphology of cells with high Gremlin2 expression (**Figure 2D**) and co-stained cells with a myofibroblasts marker. We observed the strong positive cells, which showed the long spindle shape characteristic of myofibroblast cells and were concentrated in the fibroblast lesions (**Figure 2D**). At the same time, Gremlin2 and  $\alpha$ -SMA expressions were observed in the adjacent regions (**Figure 2E**). The precise localization of Gremlin2 is somewhat difficult, as it is a secreted protein, just like another secreted protein IL-11 (Ng et al., 2019).

These clinical data were consistent with the databases analysis results, suggesting the possibility of clinical transformation of Gremlin2.

## Gremlin2 Expression is High in Bleomycin-Induced Mice Lung Tissues

We treated C57BL/6 mice with bleomycin (Tashiro et al., 2017) and detected the expression levels of Gremlin2 at mRNA and protein levels in the lung tissue. Since Gremlin2 is a secretory glycoprotein, we collected mouse alveolar lavage fluid for the detection of Gremlin2 concentration using ELISA.

Bleomycin airway infusion (2.5 U/kg) was used to induce pulmonary fibrosis in mice, we detected fibrosis induction using Masson trichromatic staining (**Figure 3A**). The blue area represented collagen accumulation, suggesting a fibrotic condition. The expression of Gremlin2 in the lung tissue was detected using western blotting (**Figure 3B**). Compared with the commonly used fibrosis indexes involving collagen1 (Col1) and fibronectin (FN), we found that the Gremlin2 expression level in the fibrosis model mice group increased more significantly, and was even more sensitive and indicative than the international indexes.

By detecting the mRNA level of Gremlin2 in the lung tissues at different time points, we found that the transcription level of Gremlin2 increased significantly on day 14, while there was no statistical difference between the pulmonary tissues of fibrotic

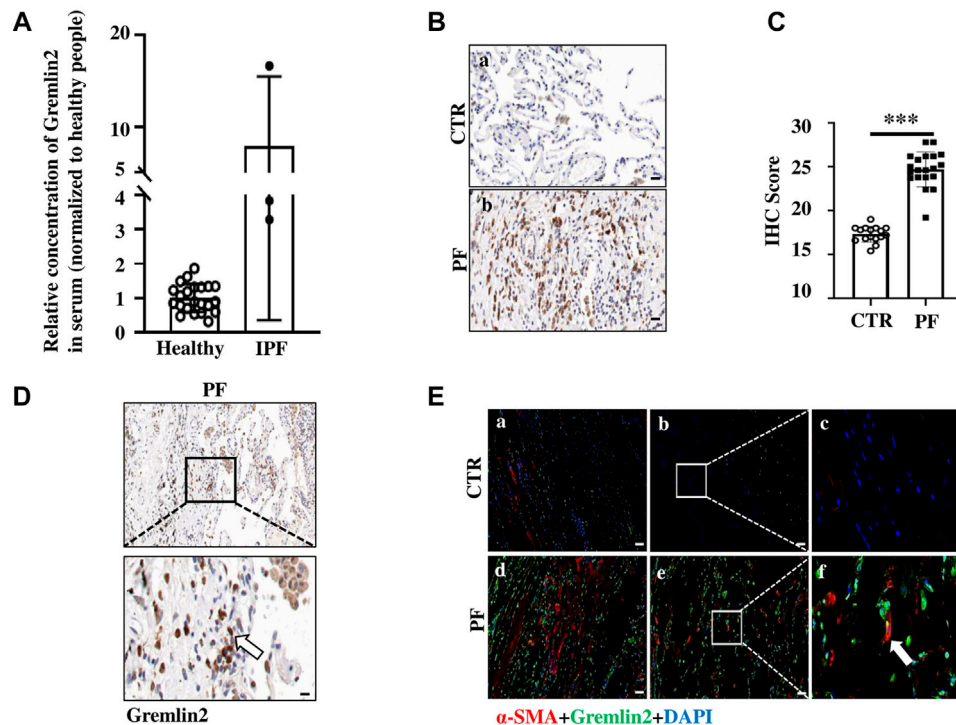


**FIGURE 2 |** Gremlin2 expression is increased in patients with IPF **(A)** Expression of Gremlin2 in the blood serum detected using ELISA, CTR (healthy control)  $n = 22$ , IPF  $n = 3$ . **(B)** Representative pictures of IHC showing Gremlin2 expression in the lung tissue. Scale Bar = 50  $\mu$ m. **(C)** IHC score of patients via immunohistochemical staining grading, CTR (normal)  $n = 16$ , PF  $n = 20$ , \*\*\* $p < 0.001$ , paired t-test. **(D)** Representative photos of Gremlin2 immunohistochemical staining in the fibrotic lung tissue samples of the patient. Lower graph shows the strong positive area of Gremlin2 magnified from upper graph, white arrow shows the strong positive cells of Gremlin2. Scale Bar = 20  $\mu$ m. **(E)** Gremlin2 was co-localized with  $\alpha$ -SMA in fibrotic foci. Representative images of immunofluorescence detection for  $\alpha$ -SMA (red) and gremlin2 (green), and merged (yellow) images of normal subjects and patients with IPF. Graph (2Ea–c) showed the pulmonary tissue in the fibrotic area of normal lung tissues near the fibrotic area of patients with IPF; graph (2Ed,e), f showed the fibrotic lung tissue of patients with IPF; graph (2Ec,f) showed the locally enlarged view in the white box in graph (2Eb,e); white arrow points to the cells with high co-expression of  $\alpha$ -SMA and Gremlin2. CTR is the normal tissue around the pulmonary tissue of patients with fibrosis, and PF is the lung tissue section of patients with lung fibrosis. Scale Bar = 50  $\mu$ m. NS stands for  $p > 0.05$ , \* $p < 0.05$ , \*\* $p < 0.01$ , \*\*\* $p < 0.001$ . Student's t-test was used for statistics.

mice and the control group on day 21 (**Figure 3C**,  $p = 0.0534$ ). This suggested that the transcription level of Gremlin2 increased during the acute progression of fibrosis, thus affecting the process. Gremlin2 content of mouse alveolar lavage fluid was traced using ELISA. As shown in **Figure 3D**, the concentration of Gremlin2 in the alveolar lavage fluid was significantly increased ( $p = 0.0102$ ). Using IHC, we observed that the expression of Gremlin2 in the fibrotic lung tissue was significantly increased (**Figure 3E**). The time course (day 0, day 7, day 14, day 21) data of Gremlin2 mRNA, protein, and BALF were shown in **Supplementary Figure S2**. Overall, Gremlin2 expression was high in the bleomycin-induced pulmonary fibrosis mouse model.

## Myfibroblasts Express High Levels of Gremlin2 in Bleomycin-Induced Lung Fibrosis Mouse Model

To investigate whether the cells with high Gremlin2 expression were activated fibroblasts or not, immunofluorescence staining was used. It was difficult to identify the precise location of Gremlin2, as it is secreted. Co-localization of  $\alpha$ -SMA and

Gremlin2 in bleomycin-induced fibrosis lung of mice was observed (**Figure 4A**).

Then we isolated lung fibroblasts on day 14 after treatment with PBS or bleomycin to detect Gremlin2 expression. After culturing for 5 days, we examined the expression of  $\alpha$ -SMA and Gremlin2 in lung fibroblasts through western blotting (**Figure 4B**) and immunofluorescence detection (**Figure 4C**). **Figures 4B,C** both show the high relevance between the expressions of  $\alpha$ -SMA and Gremlin2, indicating myofibroblasts were the effector cells of Gremlin2 expression.

## Gremlin2 is an Activated Regulator to Fibroblasts

We used TGF- $\beta$ 1 (Li et al., 2014; Meng et al., 2016) to stimulate fibroblasts and mimic the activation of fibroblasts *in vivo* (Xie et al., 2018). Protein and mRNA levels of Gremlin2 were measured after TGF- $\beta$ 1 treatment in fibroblasts (**Figures 5A,B**). Gremlin2 expression increased significantly upon activation of fibroblasts, and the mRNA levels increased in line with the ECM production ( $p < 0.05$ ). The well-known

**TABLE 3 |** Patients' information of IPF and other types of pulmonary fibrosis.

IHC of patients' slices				
Pathology number	Gender	Age (years old)	Pathological diagnosis	Sample site
2019106687-5	Male	51	Pulmonary fibrosis nodules with charcoal deposition	Middle lobe of right lung
2019106687-6				Adjacent area of fibrosis
2019112471-3	Male	40	Fibrotic nodules	Inferior lobe of right lung
2019112471-5				Adjacent area of fibrosis
2019112971-3	Female	56	Chronic inflammatory fibrosis	Upper lobe of left lung
2019112971-4				Adjacent area of fibrosis
2019116608-9	Female	72	Fibrotic nodules	Inferior lobe of right lung
2019116608-8				Adjacent area of fibrosis
2019117672-9	Male	67	Chronic mucosal inflammation with pulmonary fibrosis nodules	Upper lobe of right lung
2019117672-13				Adjacent area of fibrosis
2020000937-3	Female	65	Fibrotic nodules	Middle lobe of right lung
2020000937-4				Adjacent area of fibrosis
2020001297-2	Female	49	Fibrotic nodules	Upper lobe of left lung
2020001297-5				Adjacent area of fibrosis
2020003176-2	Female	69	Fibrotic collagenous nodules	The proper segment of the upper lobe of the left lung
2020003176-3				Adjacent area of fibrosis
2020006458-10	Male	55	Chronic inflammation of lung tissue with collagen fibrotic nodules	Inferior lobe of left lung
2020006458-11				Adjacent area of fibrosis
2020009101-2	Male	44	Chronic inflammation of lung tissue with fibrotic nodules	Inferior lobe of right lung
2020009101-3				Adjacent area of fibrosis
2020009493-3	Male	51	Fibrotic nodules	Upper lobe of right lung
2020009493-8				Adjacent area of fibrosis
2020009765-3	Female	74	Chronic inflammatory fibrosis	Upper lobe of right lung
2020009765-7				Adjacent area of fibrosis
2020012831-1	Male	55	Fibrosis and degenerative necrotic nodules	Inferior lobe of right lung
2020012831-2				Adjacent area of fibrosis
2020020563-3	Male	70	Fibrotic nodules with charcoal deposition	Upper lobe of left lung
2020020563-4				Adjacent area of fibrosis
2020037421-1	Male	68	Interstitial pulmonary fibrosis	Inferior lobe of right lung
2020037421-2				Adjacent area of fibrosis
201651141	Male	64	Chronic interstitial pneumonia with fibrosis	Right lung
201709433	Female	69	Chronic interstitial pneumonia with fibrosis	Right lung
201713228	Male	67	Chronic interstitial pneumonia with fibrosis	Right lung
201722515	Male	58	Interstitial pulmonary fibrosis	Right lung
Blood serum of IPF patients				
Medical record number	Gender	Age (years old)	Clinical diagnosis	Illness stage
5057536	Female	62	IPF	Recurring fever with fatigue for a year, acute exacerbation
3165154	Female	66	IPF	Repeated cough for three years, chest tightness for two years, aggravation for half a year, with respiratory failure
4141982	Male	83	IPF	Repeated shortness of breath for three years, acute exacerbation with respiratory failure for one week

markers of fibroblast activation, including FN, Col1, and  $\alpha$ -SMA (ACTA2) were chosen to verify the activation. Similarly,  $\alpha$ -SMA and Gremlin2 staining was used to detect expression levels with or without TGF- $\beta$ 1 treatment (Figure 5C). We obtained similar results using immunofluorescence and western blotting, where TGF- $\beta$ 1 activated fibroblasts showed upregulated Gremlin2 expression.

Next, we wanted to explore whether Gremlin2 expression affected the activation of fibroblasts. First,  $\alpha$ -SMA expression was detected in fibroblast via cellular immunofluorescence (Figure 5D). We found that after Gremlin2 overexpression, fibroblasts were spontaneously activated into myofibroblasts. The expression of  $\alpha$ -SMA in human fetal lung fibroblast 1 (HFL-1) (ATCC Cat# CCL-153, RRID:CVCL\_0298) cells or MRC-5 (ATCC Cat# CCL-171, RRID:CVCL\_0440) showed

high fluorescence intensity after Gremlin2 overexpression. However, fluorescence intensity did not increase further in Gremlin2-overexpressing HFL-1 cells after TGF- $\beta$ 1 stimulation, which might indicate that Gremlin2 and TGF- $\beta$ 1 counteract each other in fibroblast activation, as shown in Supplementary Figure S3.

To explore the effect of Gremlin2 deficiency, we used an adenovirus containing shGremlin2 and detected changes in fibroblasts stimulated by TGF- $\beta$ 1 after Gremlin2 knockdown (Figure 5E). After knockdown of Gremlin2,  $\alpha$ -SMA expression decreased simultaneously, and fibroblasts were significantly less activated by TGF- $\beta$ 1 than control fibroblasts. Overall, these might indicate that the presence of Gremlin2 was crucial for fibroblast activation.



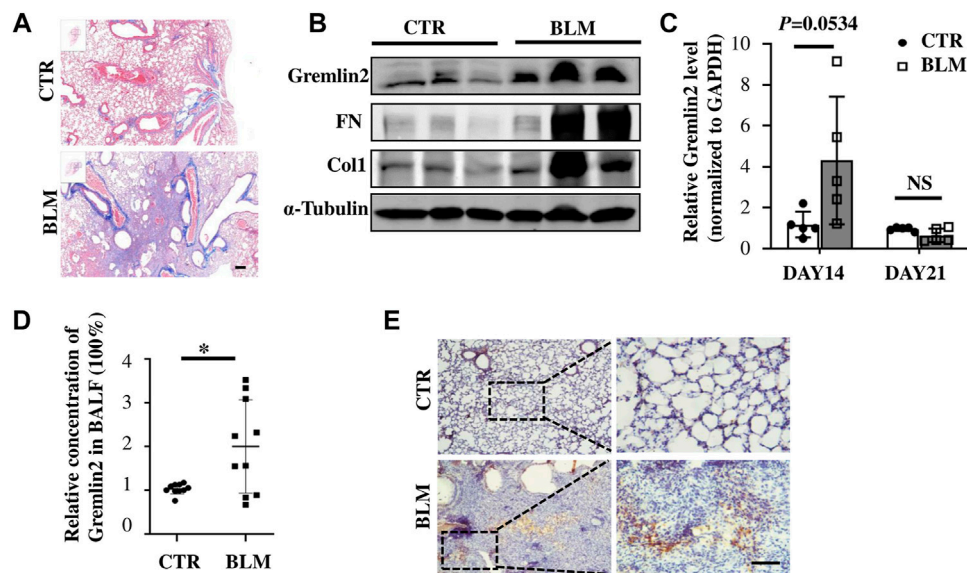


**FIGURE 3 |** Increased expression of Gremlin2 in the lung tissue of bleomycin-induced pulmonary fibrosis mice **(A)** Masson's trichrome staining of the lung tissue in the bleomycin-treated mice and PBS-treated control mice. **(B)** 21 days after bleomycin (BLM) or PBS (CTR) treatment mice were sacrificed. Western blotting was performed using the lung tissue homogenates.  $\alpha$ -tubulin was used as a reference collagen1 (Col1) and fibronectin (FN) were detected as indicators of fibrosis, and Gremlin2 (Grem2) was used as the target protein. **(C)** Following the same operation method as **(B)**, the corresponding mRNA was extracted from the lung tissue of mice treated for 14 and 21 days, and real-time-quantitative PCR was used to detect the mRNA expression levels of Gremlin2. Day 14 CTR  $n = 5$ , BLM  $n = 5$ ,  $p = 0.0534$ , student's paired t-test; day 21 CTR  $n = 5$ , BLM  $n = 5$ , NS  $p > 0.05$ , student's paired t-test. **(D)** Expression level of Gremlin2 in alveolar lavage fluid. CTR  $n = 10$ , BLM  $n = 10$ ,  $*p = 0.0102$ , student t paired test. **(E)** Representative images of control lung tissue sections (CTR) and fibrotic lung tissue (BLM) assessed using immunohistochemical staining with anti-Gremlin2 antibody. The right two pictures are 10 x magnified versions of the left two corresponding pictures. The relative content of Gremlin2 was obtained after standardized numerical treatment. Use the Student's bilateral t-test. Scale bar = 50  $\mu$ m. CTR, control with PBS-treated group; and BLM, bleomycin-treated group.

We obtained the same results from primary lung fibroblasts of bleomycin-induced lung fibrosis mouse model and activated HFL-1 cells. We observed the same upward trend in  $\alpha$ -SMA and Gremlin2 expressions. Compared to classic lung biopsy for IPF diagnosis, it was more convenient to detect Gremlin2 expression from BALF, which could be used as a detection method to indicate the occurrence and development of fibrosis.

## Gremlin2 Regulates Migration and Invasion of Fibroblasts

Next, we identified the functional role of Gremlin2 in lung fibroblasts by investigating whether Gremlin2 expression regulates the invasion and migration of fibroblasts. Gremlin2 overexpression in lung fibroblasts showed a significant increase in fibroblast migration (**Figures 6A,B**;  $p = 0.0024$ ) and invasion (**Figures 6C,D**;  $p = 0.0054$ ). We also examined Col1 mRNA expression levels and found that there was a strong correlation between Gremlin2 and Col1 expression (**Figure 6E**). This suggested that Gremlin2 might control migration and invasion by increasing ECM production. To identify the function of Gremlin2, we used the recombinant human Gremlin2/rPRDC to stimulate HFL-1 cells. Gremlin2/rPRDC activated fibroblasts, inducing high expression of FN and Col1 (**Figure 6F**).  $\alpha$ -SMA expression also increased, which was similar to TGF- $\beta$ 1 stimulation (**Figure 6G**). These results revealed that high expression of Gremlin2 in the activated fibroblasts affected

their migration and invasion, and Gremlin2 acted on the inactive fibroblasts after secretion, exerting a positive feedback effect.

## Gremlin2 Activates Fibroblasts Through the Bone Morphogenic Protein Signaling Pathway

We used Gremlin2 overexpression plasmid in fibroblasts and verified it at mRNA and protein levels (**Figures 7A,B**;  $p < 0.001$ ). When Gremlin2 was overexpressed in fibroblasts, phosphorylation of Smad1 was decreased, while phosphorylation of Smad2 was not significantly changed (**Figure 7C**). To visualize the changes in Smad1 and Smad2 phosphorylation, we detected  $p$ -Smad1 and  $p$ -Smad2 through immunofluorescence. The fluorescence intensity in the nucleus represented the level of phosphorylation. The results showed that Gremlin2 overexpression affected the Smad1 phosphorylation, leading to low expression of  $p$ -Smad1. However, Gremlin2 overexpression had an insignificant effect on Smad2 phosphorylation (**Figure 7D**).

To explore the effect of Gremlin2 deficiency, we infected fibroblasts with Gremlin2-specific adenovirus and validated the knockdown efficiency at transcription and translation levels (**Figures 7E,F**). When Gremlin2 was knocked down, Smad1 phosphorylation increased, while Smad2 phosphorylation did not significantly change. To visualize the change in Smad1 and

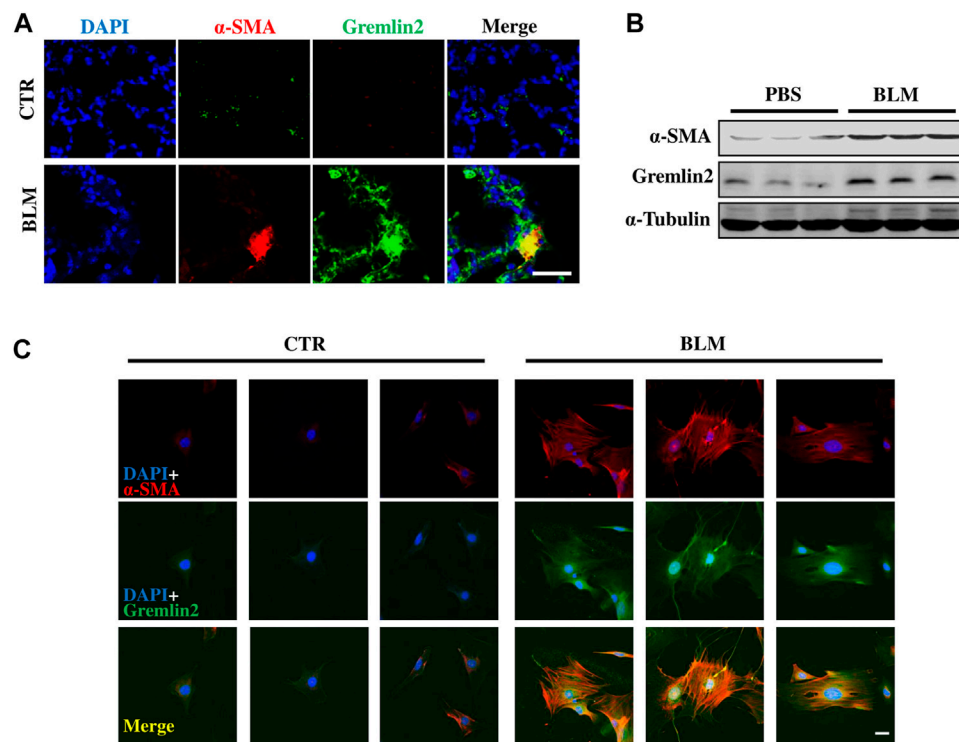


**FIGURE 4 |** Myofibroblast expresses high level of Gremlin2 in bleomycin induced lung fibrosis model through co-localization (A) Immunofluorescence shows co-localization of fibroblast activation marker ( $\alpha$ -SMA) and Gremlin2 in lungs of bleomycin-induced fibrosis mice, Gremlin2 (Green), and  $\alpha$ -SMA (Red), DAPI (Blue), Yellow (Merge), scale bar = 10  $\mu$ m. (B) Fibroblasts were isolated from mice after PBS or bleomycin treatment on day 14, then western blotting was performed to detect the expression of Gremlin2, and  $\alpha$ -SMA. Every group contained three mice. CTR  $n = 3$ , BLM  $n = 4$ . (C) Following the same operation method as (B), then immunofluorescence was performed to detect the expression of Gremlin2 (Green), and  $\alpha$ -SMA (Red). DAPI (Blue) indicated the nucleus. Scale bar = 20  $\mu$ m. CTR  $n = 3$ , BLM  $n = 4$ . CTR, control with PBS-treated group; and BLM, bleomycin-treated group.

Smad2 phosphorylation, we located  $p$ -Smad1 and  $p$ -Smad2 through immunofluorescence. The results showed that Gremlin2 knockdown upregulated the phosphorylation of Smad1, but had little effect on the phosphorylation level of Smad2 (Figure 7H). As shown in Figures 7E–H, the HFL-1 fibroblast cell line was selected for Gremlin2 knockdown, and fibroblast activation was not performed during this process. Even in the inactive state, Gremlin2 knockdown also affected the Smad1 phosphorylation level, indicating that baseline Gremlin2 expression might regulate the BMP signaling. To prove that Gremlin2 affects Smad1 phosphorylation, we knocked down Gremlin2 in TGF- $\beta$ 1-activated HFL-1 cells, and the same trend was observed (Figure 7G). Smad1 phosphorylation was upregulated in activated fibroblasts (Supplementary Figure S4).

Overall, overexpression of Gremlin2 in HFL-1 cells affected the phosphorylation of Smad1 to mediate the BMP signaling pathway.

## DISCUSSION

Here, we achieved overexpression of Gremlin2 (gain of function) and downregulation of Gremlin2 using specific shRNA (loss of

function), which showed that Gremlin2 knockdown upregulated the phosphorylation of Smad1 and Gremlin2 overexpression downregulated the phosphorylation of Smad1. In the mice model, the phosphorylation of Smad1 in primary lung fibroblast was upregulated in the bleomycin treatment group shown in Supplementary Figures S6E–G. These results suggest that Gremlin2 might regulate fibrosis via controlling the phosphorylation of Smad1 to mediate the BMP signaling pathway.

IPF is a progressive, fatal disorder that presents a major challenge for clinicians, and the mechanisms that control IPF are not fully understood (King et al., 2011). The main pathological manifestations of IPF are characteristic fibroblast foci composed of major effector fibroblasts (ATS/ERS, 2000). There have been many studies on fibroblasts, including the senescence phenotype of fibroblasts (Waters et al., 2018), tumor-related fibroblasts (Woodcock et al., 2019), and activation of fibroblasts. Myofibroblasts are key effector cells involved in ECM deposition in various fibrotic conditions, including IPF. Our studies demonstrated the profibrotic role of Gremlin2 in pulmonary fibrosis. We provided data at the cellular, molecular, and animal levels to support a role of Gremlin2 as a therapeutic target candidate for lung fibrosis.

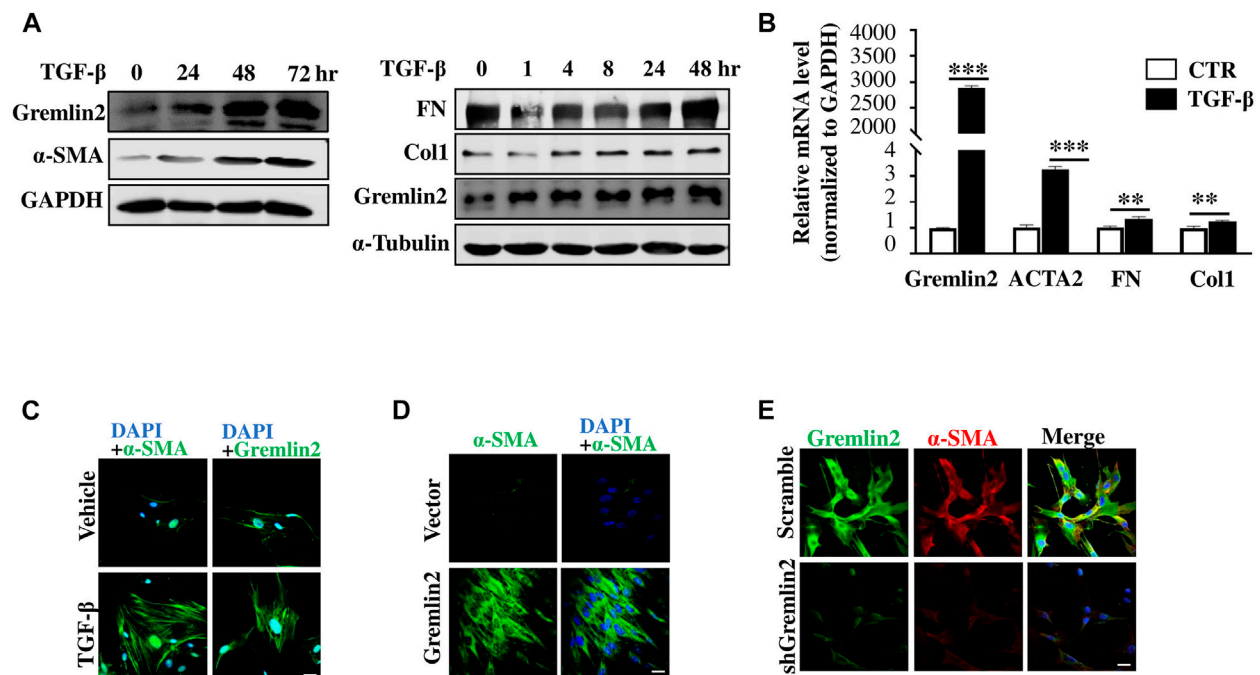


**FIGURE 5 |** Gremlin2 is an activated regulator to fibroblast **(A)** HFL-1 were collected after treatment with TGF-β1 at 5 ng/mL for 0, 24, 48, and 72 h. Protein expression was detected using western blotting, with GAPDH as a quantitative indicator protein, α-SMA as an indicator of fibroblast activation, and Gremlin2 as a target protein (this experiment was repeated three times). The same treatment applied to HFL-1 cells with TGF-β1 at 5 ng/mL for 0, 1, 4, 8, 24, and 48 h. Western blotting was used to detect fibronectin and collagen1 expression. α-Tubulin was used as the quantitative indicator protein. **(B)** The mRNA was extracted after treatment of HFL-1 cells with TGF-β1 (5 ng/mL) for 24 h, and then real-time quantitative PCR was performed to detect the corresponding mRNA expression levels. α-SMA (ACTA2), fibronectin (FN), and collagen1 (Col1) were used as indicators of fibroblast activation (this experiment was repeated three times). Gremlin2 \*\*\* $p < 0.0001$ , Acta2 \*\*\* $p = 0.0002$ , FN \*\* $p = 0.0037$ , Col1 \*\* $p = 0.0069$ . **(C)** Immunofluorescence staining was performed on HFL-1 cells were treated with 5 ng/mL TGF-β1 for 24 h to reveal the content of target antigens in the cells. Blue (DAPI) represents the nucleus, green represents the target antigen (α-SMA/Gremlin2). The control group (CTR) received the same treatment without TGF-β1 (the same experiment was performed using HFL-1). Scale bar = 20 μm. **(D)** Gremlin2 was overexpressed in HFL-1, the control group was transfected with empty-load pcDNA3.1, and TGF-β1 stimulation was performed. Immunofluorescence staining was used to detect the content of target antigens in the cells, with DAPI representing the nucleus and α-SMA representing the target antigen in green as an indicator of fibroblast activation. Scale bar = 20 μm. **(E)** Gremlin2 knockdown in MRC-5 cells using shGremlin2, the control group transfected with plko.1. Immunofluorescence staining showed DAPI in blue indicating the nucleus, Gremlin2 in green, and α-SMA in red. Scale bar = 20 μm. All the experiments have been repeated three times.

First, through the known databases GSE10667 and GSE99621, we found that the expression of Gremlin2 in the fibrotic lung tissue was significantly higher than that in the healthy tissue. Second, Gremlin2 mRNA and protein levels were high in IPF lung tissues and blood serum compared to healthy people. The data collected from the GEO database, including GSE10667 and GSE99621, are shown in **Figure 1**, while all the samples collected from patients primarily diagnosed with IPF or those who had a lung transplant due to interstitial pulmonary disease with fibrosis are shown in **Figure 2**. The GSE10667, the dataset contained data of samples collected after a biopsy or lung transplant from patients with IPF at the University of Pittsburgh Health Sciences Tissue Bank. The GSE99621 dataset contained the samples of healthy lung tissues from healthy controls and affected or unaffected lung tissues from patients with IPF. Because of the low incidence of IPF (2–60 cases per 100,000 persons per year) (Martinez et al., 2017), it was difficult to collect enough samples of lung tissue samples to meet the IPF diagnosis standard. As the focus of our research was Gremlin2 expression in myofibroblasts and fibroblasts around fibrotic lesions, which are

pathological features of the fibrotic region, we collected the fibrotic lesion transplant samples not only from patients with IPF but also from those with other types of lung fibrosis. Therefore, we defined the collective tissue samples as pulmonary fibrosis (PF) samples. Third, when fibroblasts were treated with TGF-β1, Gremlin2 expression increased, which correlated with ECM production. When the expression of Gremlin2 was inhibited through shRNA knockdown, ECM production decreased. We verified the function of upregulating Gremlin2 in mice lung fibroblast in **Supplementary Figure S6**. The primary lung fibroblasts in bleomycin treatment mice lung showed the high capacity of migration and invasion shown in **Supplementary Figures S6A–D**. One hypothesis has emerged that links IPF and cancer due to their similar hallmark pathological alterations, such as aberrant myofibroblast proliferation and apoptosis and ECM invasion (Vancheri et al., 2010). Studies showed that cell invasion increases in IPF fibroblasts (Li et al., 2011). Moreover, IPF lung fibroblasts have an increased migratory capacity compared to healthy lung fibroblasts (Cai et al., 2010). We showed here that Gremlin2

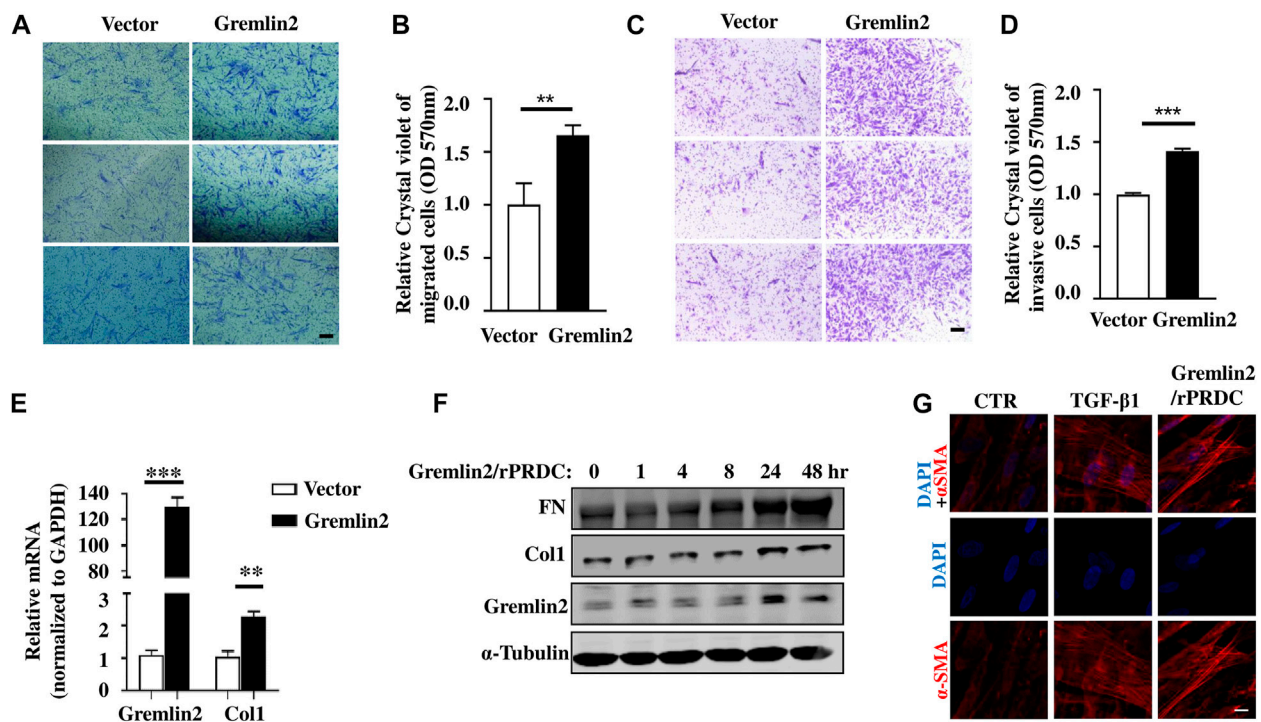


**FIGURE 6 |** Overexpression of Gremlin2 increases the migration and invasion of fibroblasts. **(A)** Transwell cell migration experiment after Gremlin2 overexpression in fibroblasts. The lower chamber was stained with crystal violet 24 h later, and three fields were randomly selected for imaging under 100× magnification. Scale bar = 100 μm. The experiment was repeated three times. **(B)** The value of OD570 after elution of crystal violet, normalized to that of the control group, \*\* $p = 0.072$ . Unpaired student t test. **(C)** Transwell cell invasion experiment after 1:32 matrix glue was laid. After 48 h, crystal violet staining was carried out on the lower layer of the chamber. Scale bar = 100 μm. The experiment was repeated three times. **(D)** The value of OD570 after elution of crystal violet, normalized to that of the control group. \*\*\* $p < 0.001$ . Unpaired student t test. **(E)** HFL-1 cells transfected with Gremlin2 expression plasmid for 24 h, and mRNA was extracted. Then, real-time quantitative PCR was performed to detect the corresponding mRNA expression levels. Using student's t-test, \*\*\* $p < 0.001$ , \*\* $p < 0.01$ . Scale bar = 100 μm. **(F)** Recombinant human PRDC (rPRDC)/GREM2 was added to HFL-1 cells for 0, 1, 4, 8, 24, and 48 h, then western blotting was performed to detect the expression of fibronectin, collagen1, and Gremlin2. **(G)** TGF-β1 or recombinant human PRDC (rPRDC)/GREM2 was added to HFL-1 cells for 48 h, then immunofluorescence was performed to detect the expression of α-SMA (Red). DAPI (Blue) shows the nucleus. Scale bar = 20 μm. All the experiments have been repeated three times.

overexpression in lung fibroblasts increased the migration and invasion of them. Although we showed that Gremlin2 was upregulated in IPF lung tissues and myofibroblasts, but the role of Gremlin2 in alveolar type II cells was not investigated.

Co-labeling via immunofluorescence showed that Gremlin2 was expressed not only in myofibroblasts but also in the injured epithelial cells. Based on the results of **Figure 4A**, these α-SMA-negative cells expressing gremlin2 might have involved epithelial cells, shown in **Supplementary Figure S1**. We used E-Cadherin as an indicator of epithelial cells and co-localized it with Gremlin2 immunofluorescence staining in mice fibrosis lung tissue. **Supplementary Figure S1** showed epithelial cells could express Gremlin2. We selected different visual fields for analysis. **Supplementary Figure S1A** showed some epithelial cells expressed Gremlin2 with the white arrow pointing to the merge part. **Supplementary Figure S1B** was hardly any cell co-expressed Gremlin2 and E-Cadherin, indicating that there were other types of cells expressing Gremlin2 in the fibrotic area and not all epithelial can express Gremlin2. Overall, the epithelial cells, possibly the injured epithelial expressed Gremlin2, indicating that injured epithelial cells might play role in the

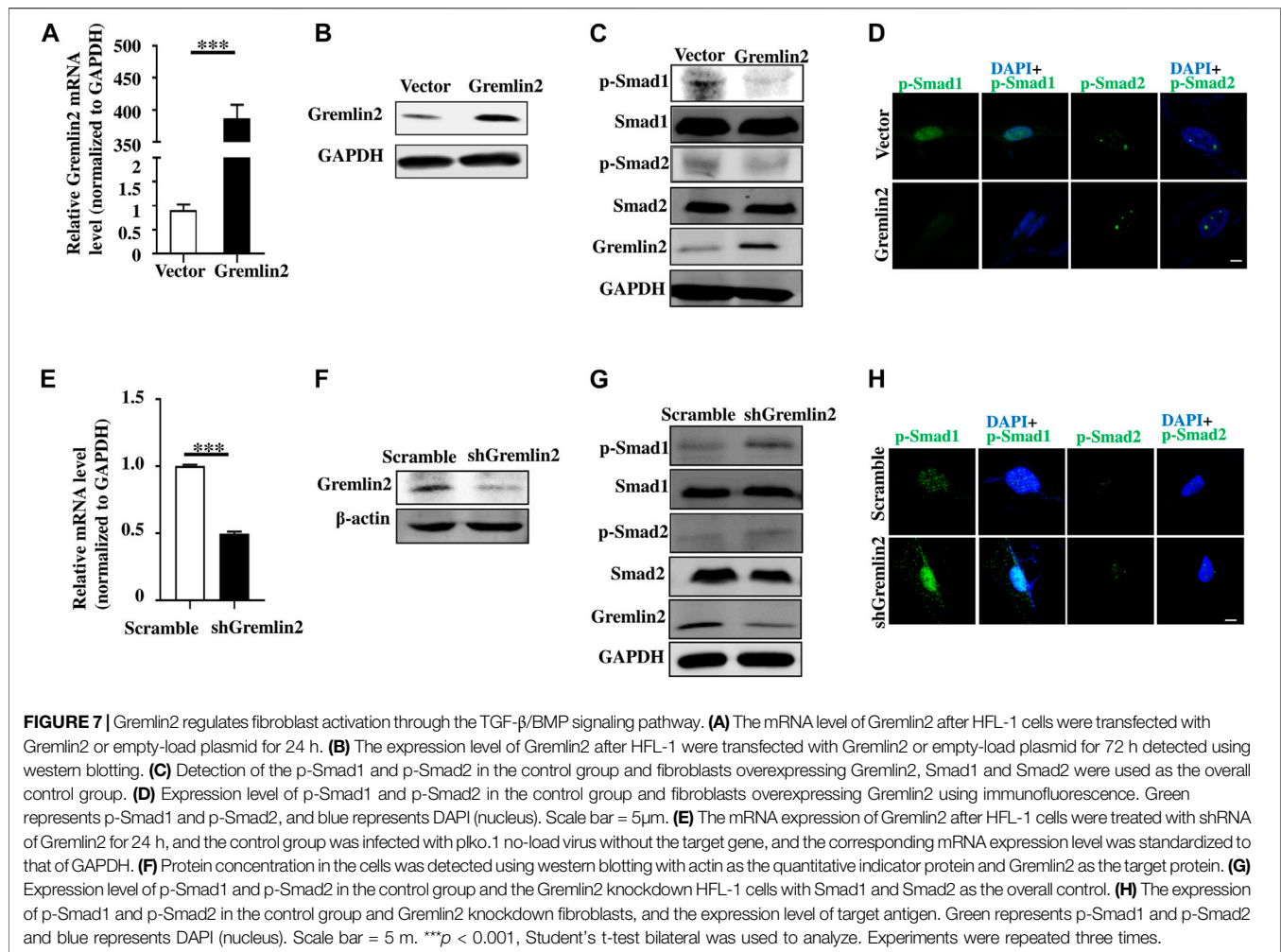
process of fibrosis. This suggested that Gremlin2 might cause the process of pulmonary fibrosis through the migration and invasion of fibroblasts and epithelial injury repair. In this article, we focused on the function of Gremlin2 in fibroblasts; meanwhile, the role of Gremlin2 in epithelial injury repair should also be investigated.

Type II alveolar epithelial (AT-II) cells play a key role in the regulation of alveolar physiology (Zhang et al., 2012). Dysfunctional AEC2 should regenerate damaged cells, leading to insufficient repair ability. Persistent epithelial injury is a key mechanism of severe fibrosis in patients with IPF (Liang et al., 2016). Therefore, exploring the function of Gremlin2 in alveolar epithelial cells might reveal if Gremlin2 is involved in other aspects of fibrosis as well.

Here, we provided another hypothesis that injured epithelial cells expressing Gremlin2 might be another possible mechanism of IPF.

The TGF-β superfamily, which includes the BMP family, is an important regulator of fibrosis (Henderson et al., 2020). In bleomycin-induced lung fibrosis, TGF-β and BMP signaling follow an inverse course, with dynamic activation of TGF-β





signaling and repression of BMP signaling. Modulating the balance between BMP and TGF- $\beta$  may be a therapeutic target in fibrotic lung disease (De Langhe et al., 2015). BMP-7 expression decreases in patients with IPF (Gu et al., 2014) and BMP-7 supplementation significantly reduces the hydroxyproline content in mice treated with aseptic materials (Myllärniemi et al., 2008a). Strong antagonists of the BMP family also include Gremlin1 and CHORD. Previous studies have shown that Pirfenidone can reduce the activity of fibroblasts induced by TGF- $\beta$ , and the upregulation of BMP4/Gremlin1 can be detected (Jin et al., 2019), while Gremlin-1 regulates the recruitment of inflammatory cells and the production of anti-fibrosis chemokines in the lung (Koli et al., 2016).

However, we also recognized there are a few limitations to the current investigation. Studies showed that Fstl1 promoted TGF- $\beta$  signaling and inhibits BMP signaling in epithelial cells, whereas in fibroblasts Fstl1 promotes TGF- $\beta$  signaling without altering BMP signaling (Geng et al., 2011; Zheng et al., 2017). Therefore, further investigation into the mechanisms under which Gremlin2 regulates lung fibrosis could provide a novel target for the development of therapeutics for patients with pulmonary fibrosis. Gremlin2 is a secreted glycoprotein, meaning that it is

not only expressed in a specific area but also can be detected in the bloodstream. As a development-related protein, it is highly expressed during embryonic development but its expression is low in adulthood. The high expression of it in adults might imply a severe disease state. We detected the concentration of Gremlin2 in the blood serum of healthy control samples, and the low expression verified that Gremlin2 low-expression was stable in the healthy control group. The increase in the expression of Gremlin2 can be easily detected via its increased secretion into the bloodstream. Moreover, compared to the golden criteria of a lung biopsy for IPF diagnosis, the detection of biomarkers in the blood serum is more convenient for patients. Less invasive techniques are more applicable in IPF screening at the early stage, therefore, biomarkers, such as Gremlin2, should be further investigated for their potential clinical application.

Besides, in mice model, we found that Gremlin2 showed an upregulated tendency after 2.5 units of bleomycin treatment with time going on. More interestingly, the concentration of Gremlin2 in BALF after 5 units of bleomycin treatment showed an exaggerated increase on day 7 shown in **Supplementary Figure S5A**. We tried to explore the origin by immunohistochemistry and cell immunofluorescence. By

immunofluorescence co-staining CD11b and Gremlin2, we found a significant co-staining relationship between them showed in **Supplementary Figure S5B** in the 5 units bleomycin-treated 7 days group. But the control group treated with PBS showed no this phenomenon shown in **Supplementary Figure S5C**. Furthermore, we got the cells in BALF from the bleomycin-treated mouse group, the Giemsa staining showed a great amount of macrophage shown in **Supplementary Figure S5D**. Cell immunofluorescence co-staining CD11b and Gremlin2 also showed the great consistency shown in **Supplementary Figure S5E**. Besides, we constructed the one-day model treated by LPS for the acute inflammation model to explore the neutrophils would express Gremlin2 or not. The result showed in **Supplementary Figure S5F** may indicate the low expression of Gremlin2 in neutrophils. In all, we found the macrophage may contribute to the high expression of Gremlin2 in BALF of the 5-units bleomycin-treated group. Mice treated with 5 units of bleomycin began to die after 7 days showed high expression of Gremlin in BALF. Gremlin2 was first found as a development-related protein, the high expression of Gremlin2 in adulthood might indicate a severe disease condition. Our experiments have confirmed that fibroblasts can be activated by Gremlin2 to form myofibroblasts shown in **Figures 6F,G**, and a large amount of Gremlin2 production in early macrophages may contribute to the activation of fibroblasts and the progression of fibrosis.

We have constructed Gremlin2 knockout mice and will continue to explore the role of Gremlin2 in pulmonary fibrosis in future studies. Further, we have confirmed that Gremlin2 caused the increased invasive fibroblasts phenotypes, but more *in vivo* evidence is needed to verify that it affects mouse lung fibrosis through myofibroblasts.  $\alpha$ -SMA-positive myofibroblasts or Col1a1-positive fibroblasts both originate from cells expressing Tbx4, can be applied as a general marker of fibroblasts (Xie et al., 2016). TBX4-creER, Gremlin2<sup>flox/flox</sup> mouse model would further verify the role of Gremlin2 in promoting fibrosis through mesenchymal cells.

## DATA AVAILABILITY STATEMENT

The datasets presented in this study can be found in online repositories. The names of the repository/repositories and accession number(s) can be found in the article/**Supplementary Material**.

## ETHICS STATEMENT

The studies involving human participants were reviewed and approved by Clinical Trial Ethics Committee of the First Hospital of Zhejiang University. The patients/participants provided their written informed consent to participate in this study. The animal study was reviewed and approved by animal care and use committee of the Zhejiang University School of Medicine. Written informed consent was obtained from the owners for the participation of their animals in this study. Written informed

consent was obtained from the individual(s) for the publication of any potentially identifiable images or data included in this article.

## AUTHOR CONTRIBUTIONS

CH and WX co-wrote the manuscript. YL contributed to statistical work and rechecked the text composition. KR collected patient information and samples. YS, XZ, HC, and YK were occupied for logical comments of the article. WX accomplished all experimental design and operation. CH and JZ designed and directed the article.

## FUNDING

This work was supported by grants from the National Natural Science Foundation of China (81700064 to CH).

## SUPPLEMENTARY MATERIAL

The Supplementary Material for this article can be found online at: <https://www.frontiersin.org/articles/10.3389/fmolb.2021.683267/full#supplementary-material>

**Supplementary Figure S1** | Epithelial cells express Gremlin2. Immunofluorescence shows the co-localization of the epithelial cell marker E-Cadherin and Gremlin2 in the lungs of bleomycin-induced fibrosis mice. Gremlin2 (Green), and E-Cadherin (Red), DAPI (Blue), Yellow (Merge), scale bar = 20  $\mu$ m. **(A)** The white arrow pointed to the co-labeled cells. **(B)** The high expression of Gremlin2 or E-Cadherin.

**Supplementary Figure S2** | Gremlin2 expression at mRNA and protein levels and its levels in BALF of mice on day 0, 7, 14, 21 after bleomycin treatment. The relative concentration of Gremlin2 in the BALF, and its expression at mRNA and protein levels in the lung tissues of mice on **(A)** day 0 (CTR,  $n = 5$ ; BLM,  $n = 5$ ), **(B)** day 7 (CTR,  $n = 5$ ; BLM,  $n = 4$ ), **(C)** day 14 (CTR,  $n = 5$ ; BLM,  $n = 5$ ), **(D)** day 21 (BALF CTR,  $n = 10$ ; BLM,  $n = 10$ , mRNA and protein levels CTR  $n = 5$ , BLM  $n = 5$ ) after bleomycin (BLM) or PBS (CTR) treatment. Student's unpaired t-test.

**Supplementary Figure S3** | Gremlin2 is overexpressed in HFL-1 cells. The control group was transfected with empty-load pcDNA3.1 with or without TGF- $\beta$ 1 treatment. Immunofluorescence staining was used to detect the content of target antigens in the cells, with DAPI representing the nucleus and  $\alpha$ -SMA representing the target antigen in green as an indicator of fibroblast activation. Scale bar = 20  $\mu$ m.

**Supplementary Figure S4** | Gremlin2 activates fibroblasts through the BMP signaling pathway. Expression level of p-Smad1 and p-Smad2 in the control group and the Gremlin2-knockdown HFL-1 cells after 48 h of TGF- $\beta$ 1 treatment with Smad1 and Smad2, as the overall control.

**Supplementary Figure S5** | Macrophages contribute to the high expression of Gremlin2 in BALF. **(A)** The relative concentration of Gremlin2 in BALF at day7 days after 5 units bleomycin (BLM) or PBS (CTR) treatment mice were sacrificed. CTR  $n = 5$ , BLM  $n = 4$ , student's unpaired t-test,  $p = 0.0073$ . **(B)** Gremlin2 (Green) and CD11b (Red) were co-stained by immunofluorescence of bleomycin **(a)** or PBS **(b)** treated mouse lungs. The right pictures are the enlargement of the white frame area in the left picture. White scale bar = 100  $\mu$ m, yellow scale bar = 20  $\mu$ m. **(C)** The Giemsa staining of cells from mice BALF. Black scale bar = 20  $\mu$ m. **(D)** Gremlin2 (Green) and CD11b (Red) were co-stained by immunofluorescence of cells in BALF from bleomycin treated mice. The right pictures are the enlargement of the white frame area in the left picture. White scale bar = 40  $\mu$ m, yellow scale bar = 10  $\mu$ m. **(E)** Gremlin2 (Green) and CD11b (Red) were co-stained by immunofluorescence of cells in BALF from one-day LPS treated mice. The right pictures are the enlargement of the white frame area in the left picture. White scale bar = 40  $\mu$ m, yellow scale bar = 10  $\mu$ m.

**Supplementary Figure S6** | *p*-Smad1 is upregulated in activated mice lung fibroblasts after bleomycin treatment. **(A)** Transwell cell migration experiment of mice lung fibroblasts after PBS or bleomycin treatment. The lower chamber was stained with crystal violet 24 h later, and three fields were randomly selected for imaging under 100x magnification. Scale bar = 100  $\mu$ m. CTR *n* = 2, BLM *n* = 2. **(B)** The value of OD570 after elution of crystal violet, normalized to that of the control group, \*\**p* = 0.001. Unpaired student *t* test. **(C)** Transwell cell invasion experiment of mice lung fibroblasts after PBS or bleomycin treatment. The lower chamber was stained with crystal violet 24 h later, and three fields were randomly selected for imaging under 100x magnification. Scale bar = 100  $\mu$ m. CTR *n* = 2, BLM *n* = 2. **(D)** The value of OD570 after elution of crystal violet, normalized to that of the control

group, \*\*\**p* < 0.001. Unpaired student *t* test. **(E)** Detection of the *p*-Smad1 and *p*-Smad2 in the fibroblasts from PBS or bleomycin treatment group, Smad1 and Smad2 were used as the overall control group. CTR *n* = 3, BLM *n* = 3. Paired student *t* test was used, *p* = 0.0011. **(F)** Expression level of *p*-Smad1 in the fibroblasts from PBS or bleomycin treatment group using immunofluorescence. Green represents *p*-Smad1 and *p*-Smad2, and blue represents DAPI (nucleus). Scale bar = 10  $\mu$ m. CTR *n* = 3, BLM *n* = 5. Scale bar = 10  $\mu$ m. **(G)** Expression level of *p*-Smad2 in the fibroblasts from PBS or bleomycin treatment group using immunofluorescence. Green represents *p*-Smad1 and *p*-Smad2, and blue represents DAPI (nucleus). Scale bar = 10  $\mu$ m. CTR *n* = 3, BLM *n* = 5. Scale bar = 10  $\mu$ m. CTR presented as PBS treatment group, BLM presented as the bleomycin treatment group.

## REFERENCES

- Ahluwalia, N., Grasberger, P. E., Mugo, B. M., Feghali-Bostwick, C., Pardo, A., Selman, M., et al. (2016). Fibrogenic Lung Injury Induces Non-cell-autonomous Fibroblast Invasion. *Am. J. Respir. Cell Mol. Biol.* 54, 831–842. doi:10.1165/rcmb.2015-0040OC
- Andersson-Sjöland, A., de Alba, C. G., Nihlberg, K., Becerril, C., Ramirez, R., Pardo, A., et al. (2008). Fibrocytes Are a Potential Source of Lung Fibroblasts in Idiopathic Pulmonary Fibrosis. *Int. J. Biochem. Cell Biol.* 40, 2129–2140. doi:10.1016/j.biocel.2008.02.012
- ATS/ERS (2000). American Thoracic Society. Idiopathic Pulmonary Fibrosis: Diagnosis and Treatment. International Consensus Statement. American Thoracic Society (ATS), and the European Respiratory Society (ERS). *Am. J. Respir. Crit. Care Med.* 161, 646–664. doi:10.1164/ajrccm.161.2.ats3-00
- Bagnato, G., and Harari, S. (2015). Cellular Interactions in the Pathogenesis of Interstitial Lung Diseases. *Eur. Respir. Rev.* 24, 102–114. doi:10.1183/09059180.00003214
- Bonniaud, P., Kolb, M., Galt, T., Robertson, J., Robbins, C., Stampfli, M., et al. (2004). Smad3 Null Mice Develop Airspace Enlargement and Are Resistant to TGF- $\beta$ -Mediated Pulmonary Fibrosis. *J. Immunol.* 173, 2099–2108. doi:10.4049/jimmunol.173.3.2099
- Bonniaud, P., Margetts, P. J., Kolb, M., Schroeder, J. A., Kapoun, A. M., Damm, D., et al. (2005). Progressive Transforming Growth Factor  $\beta$ 1-induced Lung Fibrosis Is Blocked by an Orally Active ALK5 Kinase Inhibitor. *Am. J. Respir. Crit. Care Med.* 171, 889–898. doi:10.1164/rccm.200405-612OC
- Cai, G.-q., Zheng, A., Tang, Q., White, E. S., Chou, C.-F., Gladson, C. L., et al. (2010). Downregulation of FAK-Related Non-kinase Mediates the Migratory Phenotype of Human Fibrotic Lung Fibroblasts. *Exp. Cell Res.* 316, 1600–1609. doi:10.1016/j.yexcr.2010.01.021
- Chanda, D., Otoupalova, E., Smith, S. R., Volckaert, T., De Langhe, S. P., and Thannickal, V. J. (2019). Developmental Pathways in the Pathogenesis of Lung Fibrosis. *Mol. Aspects Med.* 65, 56–69. doi:10.1016/j.mam.2018.08.004
- Chen, H., Qu, J., Huang, X., Kurundkar, A., Zhu, L., Yang, N., et al. (2016). Mechanosensing by the  $\alpha$ 6-integrin Confers an Invasive Fibroblast Phenotype and Mediates Lung Fibrosis. *Nat. Commun.* 7, 12564. doi:10.1038/ncomms12564
- Church, R. H., Ali, I., Tate, M., Lavin, D., Krishnakumar, A., Kok, H. M., et al. (2017). Gremlin1 Plays a Key Role in Kidney Development and Renal Fibrosis. *Am. J. Physiology-Renal Physiol.* 312, F1141–F1157. doi:10.1152/ajprenal.00344.2016
- De Langhe, E., Cailotto, F., De Vooght, V., Aznar-Lopez, C., Vanoirbeek, J. A., Luyten, F. P., et al. (2015). Enhanced Endogenous Bone Morphogenetic Protein Signaling Protects against Bleomycin Induced Pulmonary Fibrosis. *Respir. Res.* 16, 38. doi:10.1186/s12931-015-0202-x
- Dong, Y., Geng, Y., Li, L., Li, X., Yan, X., Fang, Y., et al. (2015). Blocking Follistatin-like 1 Attenuates Bleomycin-Induced Pulmonary Fibrosis in Mice. *J. Exp. Med.* 212, 235–252. doi:10.1084/jem.20121878
- Fernandez, I. E., and Eickelberg, O. (2012). New Cellular and Molecular Mechanisms of Lung Injury and Fibrosis in Idiopathic Pulmonary Fibrosis. *The Lancet* 380, 680–688. doi:10.1016/s0140-6736(12)61144-1
- Geng, Y., Dong, Y., Yu, M., Zhang, L., Yan, X., Sun, J., et al. (2011). Follistatin-like 1 (Fstl1) Is a Bone Morphogenetic Protein (BMP) 4 Signaling Antagonist in Controlling Mouse Lung Development. *Proc. Natl. Acad. Sci.* 108, 7058–7063. doi:10.1073/pnas.1007293108
- Gu, P., Luo, B., Yi, X., Zhu, H., Li, S., Yu, X., et al. (2014). The Expressions and Meanings of BMP-7 and TGF- $\beta$  in Idiopathic Pulmonary Fibrosis and Idiopathic Nonspecific Interstitial Pneumonia. *Zhonghua Jie He He Hu Xi Za Zhi* 37, 664–670.
- Henderson, N. C., Rieder, F., and Wynn, T. A. (2020). Fibrosis: from Mechanisms to Medicines. *Nature* 587, 555–566. doi:10.1038/s41586-020-2938-9
- Hinck, A. P., and Huang, T. (2013). TGF- $\beta$  Antagonists: Same Knot, but Different Hold. *Structure* 21, 1269–1270. doi:10.1016/j.str.2013.07.015
- Hinz, B., Phan, S. H., Thannickal, V. J., Galli, A., Bochaton-Piallat, M.-L., and Gabbiani, G. (2007). The Myofibroblast. *Am. J. Pathol.* 170, 1807–1816. doi:10.2353/ajpath.2007.070112
- Hsia, L.-t., Ashley, N., Ouaret, D., Wang, L. M., Wilding, J., and Bodmer, W. F. (2016). Myofibroblasts Are Distinguished from Activated Skin Fibroblasts by the Expression of AOC3 and Other Associated Markers. *Proc. Natl. Acad. Sci. USA*. 113, E2162–E2171. doi:10.1073/pnas.1603534113
- Hsu, D. R., Economides, A. N., Wang, X., Eimon, P. M., and Harland, R. M. (1998). The Xenopus Dorsalizing Factor Gremlin Identifies a Novel Family of Secreted Proteins that Antagonize BMP Activities. *Mol. Cell*. 1, 673–683. doi:10.1016/s1097-2765(00)80067-2
- Huan, C., Yang, T., Liang, J., Xie, T., Cheng, L., Liu, N., et al. (2015). Methylation-mediated BMPER Expression in Fibroblast Activation *In Vitro* and Lung Fibrosis in Mice *In Vivo*. *Sci. Rep.* 5, 14910. doi:10.1038/srep14910
- Jin, J., Togo, S., Kadoya, K., Tulafu, M., Namba, Y., Iwai, M., et al. (2019). Pirfenidone Attenuates Lung Fibrotic Fibroblast Responses to Transforming Growth Factor- $\beta$ 1. *Respir. Res.* 20, 119. doi:10.1186/s12931-019-1093-z
- Kang, H.-R., Cho, S. J., Lee, C. G., Homer, R. J., and Elias, J. A. (2007). Transforming Growth Factor (TGF)- $\beta$ 1 Stimulates Pulmonary Fibrosis and Inflammation via a Bax-dependent, Bid-Activated Pathway that Involves Matrix Metalloproteinase-12. *J. Biol. Chem.* 282, 7723–7732. doi:10.1074/jbc.M610764200
- Katoh, M., and Katoh, M. (2004). Identification and Characterization of Human CKTSF1B2 and CKTSF1B3 Genes *In Silico*. *Oncol. Rep.* 12, 423–427.
- Kattamuri, C., Luedeke, D. M., Nolan, K., Rankin, S. A., Greis, K. D., Zorn, A. M., et al. (2012). Members of the DAN Family Are BMP Antagonists that Form Highly Stable Noncovalent Dimers. *J. Mol. Biol.* 424, 313–327. doi:10.1016/j.jmb.2012.10.003
- Kattamuri, C., Nolan, K., and Thompson, T. B. (2017). Correction: Analysis and Identification of the Grem2 Heparin/heparan Sulfate-Binding Motif. *Biochem. J.* 474, 1529. doi:10.1042/bcj-2016-1050\_cor
- King, T. E., Jr., Pardo, A., and Selman, M. (2011). Idiopathic Pulmonary Fibrosis. *The Lancet* 378, 1949–1961. doi:10.1016/s0140-6736(11)60052-4
- Koli, K., Sutinen, E., Rönty, M., Rantakari, P., Fortino, V., Pulkkinen, V., et al. (2016). Gremlin-1 Overexpression in Mouse Lung Reduces Silica-Induced Lymphocyte Recruitment - A Link to Idiopathic Pulmonary Fibrosis through Negative Correlation with CXCL10 Chemokine. *PLoS One* 11, e0159010. doi:10.1371/journal.pone.0159010
- Li, S., Wang, L., Zhao, Q., Liu, Y., He, L., Xu, Q., et al. (2014). SHP2 Positively Regulates TGF $\beta$ 1-Induced Epithelial-Mesenchymal Transition Modulated by its Novel Interacting Protein Hook1\*. *J. Biol. Chem.* 289, 34152–34160. doi:10.1074/jbc.M113.546077
- Li, X., Wang, L., Sun, X., Wu, J., Li, Y., Zhang, Q., et al. (2017). The Role of TGF $\beta$ -HGF-Smad4 axis in Regulating the Proliferation of Mouse Airway Progenitor Cells. *Mol. Med. Rep.* 16, 8155–8163. doi:10.3892/mmr.2017.7636
- Li, Y., Jiang, D., Liang, J., Meltzer, E. B., Gray, A., Miura, R., et al. (2011). Severe Lung Fibrosis Requires an Invasive Fibroblast Phenotype Regulated by

- Hyaluronan and CD44. *J. Exp. Med.* 208, 1459–1471. doi:10.1084/jem.20102510
- Liang, J., Zhang, Y., Xie, T., Liu, N., Chen, H., Geng, Y., et al. (2016). Hyaluronan and TLR4 Promote Surfactant-Protein-C-Positive Alveolar Progenitor Cell Renewal and Prevent Severe Pulmonary Fibrosis in Mice. *Nat. Med.* 22, 1285–1293. doi:10.1038/nm.4192
- Lovgren, A. K., Kovacs, J. J., Xie, T., Potts, E. N., Li, Y., Foster, W. M., et al. (2011). -Arrestin Deficiency Protects against Pulmonary Fibrosis in Mice and Prevents Fibroblast Invasion of Extracellular Matrix. *Sci. Translational Med.* 3, 74ra23. doi:10.1126/scitranslmed.3001564
- Martinez, F. J., Collard, H. R., Pardo, A., Raghu, G., Richeldi, L., Selman, M., et al. (2017). Idiopathic Pulmonary Fibrosis. *Nat. Rev. Dis. Primers* 3, 17074. doi:10.1038/nrdp.2017.74
- Martinez, F. J., Safrin, S., Weycker, D., Starko, K. M., Bradford, W. Z., King, T. E., Jr., et al. (2005). The Clinical Course of Patients with Idiopathic Pulmonary Fibrosis. *Ann. Intern. Med.* 142, 963–967. doi:10.7326/0003-4819-142-12\_part\_1-200506210-00005
- Meng, X.-m., Nikolic-Paterson, D. J., and Lan, H. Y. (2016). TGF- $\beta$ : the Master Regulator of Fibrosis. *Nat. Rev. Nephrol.* 12, 325–338. doi:10.1038/nrneph.2016.48
- Mezzano, S., Droguett, A., Lavozy, C., Krall, P., Egido, J., and Ruiz-Ortega, M. (2018). Gremlin and Renal Diseases: Ready to Jump the Fence to Clinical Utility? *Nephrol. Dial. Transpl.* 33, 735–741. doi:10.1093/ndt/gfx194
- Myllärniemi, M., Lindholm, P., Ryyänänen, M. J., Kliment, C. R., Salmenkivi, K., Keski-Oja, J., et al. (2008a). Gremlin-mediated Decrease in Bone Morphogenetic Protein Signaling Promotes Pulmonary Fibrosis. *Am. J. Respir. Crit. Care Med.* 177, 321–329. doi:10.1164/rccm.200706-945OC
- Myllärniemi, M., Vuorinen, K., Pulkkinen, V., Kankaanranta, H., Aine, T., Salmenkivi, K., et al. (2008b). Gremlin Localization and Expression Levels Partially Differentiate Idiopathic Interstitial Pneumonia Severity and Subtype. *J. Pathol.* 214, 456–463. doi:10.1002/path.2300
- Ng, B., Dong, J., D'Agostino, G., Viswanathan, S., Widjaja, A. A., Lim, W.-W., et al. (2019). Interleukin-11 Is a Therapeutic Target in Idiopathic Pulmonary Fibrosis. *Sci. Transl. Med.* 11, eaaw1237. doi:10.1126/scitranslmed.aaw1237
- Noble, P. W., Barkauskas, C. E., and Jiang, D. (2012). Pulmonary Fibrosis: Patterns and Perpetrators. *J. Clin. Invest.* 122, 2756–2762. doi:10.1172/jci60323
- Nolan, K., Kattamuri, C., Luedeke, D. M., Deng, X., Jagpal, A., Zhang, F., et al. (2013). Structure of Protein Related to Dan and Cerberus: Insights into the Mechanism of Bone Morphogenetic Protein Antagonism. *Structure* 21, 1417–1429. doi:10.1016/j.str.2013.06.005
- Nolan, K., Kattamuri, C., Rankin, S. A., Read, R. J., Zorn, A. M., and Thompson, T. B. (2016). Structure of Gremlin-2 in Complex with GDF5 Gives Insight into DAN-Family-Mediated BMP Antagonism. *Cel Rep.* 16, 2077–2086. doi:10.1016/j.celrep.2016.07.046
- Raghu, G., Collard, H. R., Egan, J. J., Martinez, F. J., Behr, J., Brown, K. K., et al. (2011). An Official ATS/ERS/JRS/ALAT Statement: Idiopathic Pulmonary Fibrosis: Evidence-Based Guidelines for Diagnosis and Management. *Am. J. Respir. Crit. Care Med.* 183, 788–824. doi:10.1164/rccm.2009-040GL
- Ran, A., Guan, L., Wang, J., and Wang, Y. (2019). GREM2 Maintains Stem Cell-like Phenotypes in Gastric Cancer Cells by Regulating the JNK Signaling Pathway. *Cell Cycle* 18, 2414–2431. doi:10.1080/15384101.2019.1646561
- Sanders, L. N., Schoenhard, J. A., Saleh, M. A., Mukherjee, A., Ryzhov, S., McMaster, W. G., Jr., et al. (2016). BMP Antagonist Gremlin 2 Limits Inflammation after Myocardial Infarction. *Circ. Res.* 119, 434–449. doi:10.1161/circresaha.116.308700
- Stanley, E., Biben, C., Kotecha, S., Fabri, L., Tajbakhsh, S., Wang, C.-C., et al. (1998). DAN Is a Secreted Glycoprotein Related to Xenopus Cerberus. *Mech. Develop.* 77, 173–184. doi:10.1016/s0925-4773(98)00139-7
- Tashiro, J., Rubio, G. A., Limper, A. H., Williams, K., Elliot, S. J., Ninou, I., et al. (2017). Exploring Animal Models that Resemble Idiopathic Pulmonary Fibrosis. *Front. Med.* 4, 118. doi:10.3389/fmed.2017.00118
- Vancheri, C., Failla, M., Crimi, N., and Raghu, G. (2010). Idiopathic Pulmonary Fibrosis: a Disease with Similarities and Links to Cancer Biology. *Eur. Respir. J.* 35, 496–504. doi:10.1183/09031936.00077309
- Waters, D. W., Blokland, K. E. C., Pathinayake, P. S., Burgess, J. K., Mutsaers, S. E., Prele, C. M., et al. (2018). Fibroblast Senescence in the Pathology of Idiopathic Pulmonary Fibrosis. *Am. J. Physiology-Lung Cell Mol. Physiol.* 315, L162–L172. doi:10.1152/ajplung.00037.2018
- Wen, H., Kumar, V., Mishra, A., Song, S., Aslam, R., Hussain, A., et al. (2019). Grem2 Mediates Podocyte Apoptosis in High Glucose Milieu. *Biochimie* 160, 113–121. doi:10.1016/j.biochi.2019.02.015
- Wolters, P. J., Collard, H. R., and Jones, K. D. (2014). Pathogenesis of Idiopathic Pulmonary Fibrosis. *Annu. Rev. Pathol. Mech. Dis.* 9, 157–179. doi:10.1146/annurev-pathol-012513-104706
- Woodcock, H. V., Eley, J. D., Guillotin, D., Platé, M., Nanthakumar, C. B., Martufi, M., et al. (2019). The mTORC1/4E-BP1 axis Represents a Critical Signaling Node during Fibrogenesis. *Nat. Commun.* 10, 6. doi:10.1038/s41467-018-07858-8
- Xie, T., Liang, J., Liu, N., Huan, C., Zhang, Y., Liu, W., et al. (2016). Transcription Factor TBX4 Regulates Myofibroblast Accumulation and Lung Fibrosis. *J. Clin. Invest.* 126, 3063–3079. doi:10.1172/jci85328
- Xie, T., Wang, Y., Deng, N., Huang, G., Taghavifar, F., Geng, Y., et al. (2018). Single-Cell Deconvolution of Fibroblast Heterogeneity in Mouse Pulmonary Fibrosis. *Cel Rep.* 22, 3625–3640. doi:10.1016/j.celrep.2018.03.010
- Zhang, X., Zhang, Y., Tao, B., Teng, L., Li, Y., Cao, R., et al. (2012). Loss of Shp2 in Alveoli Epithelia Induces Deregulated Surfactant Homeostasis, Resulting in Spontaneous Pulmonary Fibrosis. *FASEB j.* 26, 2338–2350. doi:10.1096/fj.11-200139
- Zheng, X., Qi, C., Zhang, S., Fang, Y., and Ning, W. (2017). TGF- $\beta$ 1 Induces Fstl1 via the Smad3-C-Jun Pathway in Lung Fibroblasts. *Am. J. Physiology-Lung Cell Mol. Physiol.* 313, L240–L251. doi:10.1152/ajplung.00523.2016

**Conflict of Interest:** The authors declare that the research was conducted in the absence of any commercial or financial relationships that could be construed as a potential conflict of interest.

Copyright © 2021 Huan, Xu, Liu, Ruan, Shi, Cheng, Zhang, Ke and Zhou. This is an open-access article distributed under the terms of the Creative Commons Attribution License (CC BY). The use, distribution or reproduction in other forums is permitted, provided the original author(s) and the copyright owner(s) are credited and that the original publication in this journal is cited, in accordance with accepted academic practice. No use, distribution or reproduction is permitted which does not comply with these terms.





# Identification of Proteomic Signatures in Chronic Obstructive Pulmonary Disease Emphysematous Phenotype

Shuang Bai<sup>1</sup>, Rui Ye<sup>1</sup>, Cuihong Wang<sup>1</sup>, Pengbo Sun<sup>1</sup>, Di Wang<sup>1</sup>, Yong Yue<sup>2</sup>, Huiying Wang<sup>2</sup>, Si Wu<sup>3</sup>, Miao Yu<sup>3</sup>, Shuhua Xi<sup>4\*†</sup> and Li Zhao<sup>1\*†</sup>

<sup>1</sup>Department of Pulmonary and Critical Care Medicine, Shengjing Hospital of China Medical University, Shenyang, China,

<sup>2</sup>Department of Radiology, Shengjing Hospital of China Medical University, Shenyang, China, <sup>3</sup>Department of Biobank, Shengjing Hospital of China Medical University, Shenyang, China, <sup>4</sup>Department of Environmental and Occupational Health, School of Public Health, China Medical University, Shenyang, China

## OPEN ACCESS

### Edited by:

Kewu Huang,  
Capital Medical University, China

### Reviewed by:

Claudia Landi,  
University of Siena, Italy  
Kechao Nie,  
Guangzhou University of Chinese  
Medicine, China

### \*Correspondence:

Shuhua Xi  
shxi@cmu.edu.cn  
Li Zhao  
lzhao1@163.com

<sup>†</sup>These authors have contributed  
equally to this work

### Specialty section:

This article was submitted to  
Molecular Diagnostics and  
Therapeutics,  
a section of the journal  
Frontiers in Molecular Biosciences

Received: 07 January 2021

Accepted: 20 May 2021

Published: 01 July 2021

### Citation:

Bai S, Ye R, Wang C, Sun P, Wang D,  
Yue Y, Wang H, Wu S, Yu M, Xi S and  
Zhao L (2021) Identification of  
Proteomic Signatures in Chronic  
Obstructive Pulmonary Disease  
Emphysematous Phenotype.  
Front. Mol. Biosci. 8:650604.  
doi: 10.3389/fmolb.2021.650604

Chronic obstructive pulmonary disease (COPD) is a highly heterogeneous disease. Emphysematous phenotype is the most common and critical phenotype, which is characterized by progressive lung destruction and poor prognosis. However, the underlying mechanism of this structural damage has not been completely elucidated. A total of 12 patients with COPD emphysematous phenotype (COPD-E) and nine patients with COPD non-emphysematous phenotype (COPD-NE) were enrolled to determine differences in differential abundant protein (DAP) expression between both groups. Quantitative tandem mass tag-based proteomics was performed on lung tissue samples of all patients. A total of 29 and 15 lung tissue samples from patients in COPD-E and COPD-NE groups, respectively, were used as the validation cohort to verify the proteomic analysis results using western blotting. Gene ontology (GO) and Kyoto Encyclopedia of Genes and Genomes (KEGG) enrichment analyses were conducted for DAPs. A total of 4,343 proteins were identified, of which 25 were upregulated and 11 were downregulated in the COPD-E group. GO and KEGG analyses showed that wound repair and retinol metabolism-related pathways play an essential role in the molecular mechanism of COPD emphysematous phenotype. Three proteins, namely, KRT17, DHRS9, and FMO3, were selected for validation. While KRT17 and DHRS9 were highly expressed in the lung tissue samples of the COPD-E group, FMO3 expression was not significantly different between both groups. In conclusion, KRT17 and DHRS9 are highly expressed in the lung tissue of patients with COPD emphysematous phenotype. Therefore, these proteins might involve in wound healing and retinol metabolism in patients with emphysematous phenotype and can be used as phenotype-specific markers.

**Keywords:** chronic obstructive pulmonary disease, emphysematous phenotype, proteomics, KRT17, DHRS9

## INTRODUCTION

Chronic obstructive pulmonary disease (COPD) emphysematous phenotype is characterized by lung tissue destruction and distal airspace over inflation (Alford et al., 2010; Camp et al., 2014; Wang et al., 2018). In contrast to patients with other COPD phenotypes, those with emphysematous phenotype typically manifest symptoms such as severe dyspnea, decreased exercise tolerance, and physiological complications. Moreover, patients with emphysematous phenotype have a higher mortality than

those with non-emphysematous phenotype (Fan et al., 2014; Criner et al., 2018; Bai et al., 2020). Some emphysematous smokers do not exhibit airflow limitation (Oelsner et al., 2014), despite showing similar pathophysiological features to those with COPD (Bai et al., 2020). Unfortunately, there are few biomarkers that could be useful to predict the emphysema phenotype in COPD patients. And pharmaceutical intervention to reverse lung destruction or inhibit pulmonary damage is not available for these patients (Vogelmeier et al., 2017; Janssen et al., 2019).

Low blood eosinophils, elevated plasmin-mediated degradation of cross-linked fibrin, and hypermethylation of microRNA-7 are regarded as the features of emphysematous phenotype (Papaioannou et al., 2017; Manon-Jensen et al., 2019; Rosas-Alonso et al., 2020), but their potential to serve as prognostic biomarkers needs further validation. Moreover, the underlying molecular mechanism of COPD emphysematous phenotype remains unclear. Besides, imbalances between proteases/antiproteases and oxidants/antioxidants, enhanced inflammatory response (Lan et al., 2019; Zeng et al., 2020), and dysfunctional tissue repair in the lung parenchyma and interstitium play an important role in the pathogenetic mechanisms of emphysema (Jiang et al., 2017; Belgacemi et al., 2020; Hu et al., 2020). However, the underlying mechanisms remain poorly understood.

Proteomics reflects proteins expression changes, which are occurring in organisms. It is an important tool to understand pathogenesis and identify disease biomarkers. Tandem mass tag (TMT) quantitative proteomics is a reliable approach to measure protein content, and it has been increasingly used to identify pathogenetic mechanisms and human disease biomarkers (Mertins et al., 2018; Dziekan et al., 2020; Wang et al., 2020). While most proteomic studies in patients with COPD have used bronchoalveolar lavage fluid (Tu et al., 2014), sputum (Titz et al., 2015), and blood (Sridhar et al., 2019), only a few have used lung tissue samples. Furthermore, as per our understanding, the studies that specifically addressed COPD emphysematous phenotype are not available. Since COPD is a highly heterogeneous disease, the proteomic analysis focused on its emphysematous phenotype has remarkable significance.

In this study, we conducted proteomic analysis of lung tissue samples using TMT quantitative proteomic techniques to identify key molecules and their underlying mechanisms in patients with COPD emphysematous phenotype.

## MATERIALS AND METHODS

### Patients

Patients with COPD were recruited based on the criteria previously described (Bai et al., 2020). In brief, the inclusion criteria were as follows: 40- to 80-year-old patients diagnosed with COPD, more than 10 pack-years of smoking history, preparing for chest surgery, and read and signed informed consent. Patients with other respiratory diseases, autoimmune diseases, or infections that occurred within 4 weeks before surgery were excluded. All enrolled patients were assigned to two groups:

the COPD emphysematous phenotype (COPD-E) group and the COPD non-emphysematous phenotype (COPD-NE) group, according to the diagnosis of investigators and results of image analysis. Chest computed tomography (CT) scans revealed obvious emphysema in COPD-E patients and almost no emphysema in COPD-NE patients. The patients in both groups were matched for sex, age, and smoking history. The study protocol was approved by the Ethics Committee of Shengjing Hospital of China Medical University (Shenyang, China; Ethical no. 2016PS342K). For each patient included, written informed consent was obtained.

### CT Scanning

Chest CT scans were obtained for all patients using Philips Brilliance iCT 256 (Philips, Surrey, United Kingdom), TOSHIBA Aquilion ONE (Toshiba, Tokyo, Japan), Siemens SOMATOM Definition Flash (Siemens, Forchheim, Germany), or GE Optima CT660 (GE, Milwaukee, WI, United States). All scans were obtained at a deep inspiratory breath hold. The following parameters were applied in the examination: tube voltage, 120 kV; tube current, 180 mA; and reconstruction matrix, 512 × 512. Two radiologists performed radiological measurements. The detailed CT acquisition parameters are shown in **Supplementary Table S1**.

### Emphysema Screening

Chest CT scans of the patients were acquired from the CT workstation (Neusoft, Shenyang, China), and the image analyses were performed using Pulmonary Toolkit in Matlab (R2016a) (The MathWorks, Inc., Natick, MA, United States). The degree of emphysema was determined quantitatively according to our previous study (Bai et al., 2020). In brief, voxels with a CT value less than −950 HU were identified as the emphysematous area. The emphysema index was defined as the lung volume fraction of voxels with a CT value below −950 HU at a full inspiration (Camp et al., 2009; Coxson et al., 2014). The emphysema percentile density was defined as the 15th percentile lung density derived from the distribution histogram of whole lung CT voxel (Dirksen et al., 2009). The raw data of all CT images were entered into the analysis software, following which the results were obtained.

### Sample Preparation

Samples were prepared as described previously (Sun et al., 2019; Bai et al., 2020). In brief, lung tissue samples were obtained as far as possible from the tumor (at least 5 cm from the boundary). Lung parenchyma, pulmonary vessels, and small airways were equal approximately in each sample. Each specimen was cleaned with normal saline and dried. The collected lung tissue samples were frozen with liquid nitrogen immediately and stored at −80°C until use.

The lung tissue samples were lysed using the SDT (4% SDS (w/v); 0.1 M DTT; 100 mM Tris-HCl, pH 7.6) lysis method. The BCA method was used to determine protein concentration. Every three tissue samples of COPD-NE patients were pooled together to form the three biological replicates in the COPD-NE group, and every four tissue samples of COPD-E patients were pooled

together to form the three biological replicates in the COPD-E group. The filter-aided proteome preparation method was used to perform protein collection (Wiśniewski et al., 2009). In brief, lysates were mixed with 8 M urea in the filter unit of Microcon devices (Millipore, Bedford, MA, United States) and centrifuged to remove the low-molecular-weight material. Subsequently, 0.05 M iodoacetamide in 8 M urea was added to the concentrate followed by centrifugation. The resulting concentrate was diluted with 8 M urea and concentrated again. Finally, endoproteinase was added to digest proteins, and the digests were centrifuged to collect peptides. The concentration of peptide was measured at OD280. An equal amount of peptide was used from each sample, and all peptides were labeled using the TMT10 labeling kit (Thermo Fisher Scientific, Waltham, MA, United States) as described in the manufacturer's instructions. Then, the labeled peptides were mixed, and the high-pH reversed-phase peptide fractionation kit was used to perform grading subsequently. Briefly, the fractionation column was equilibrated with acetonitrile and 0.1% trifluoroacetic acid, and the labeled peptides were loaded into the column. After adding pure water, the samples were centrifuged at a low speed for desalination treatment. Finally, the column-bound peptides were gradient-eluted with increasing concentrations of high-pH acetonitrile solutions. Each eluted peptide sample was dried in vacuum and reconstituted in 0.1% formic acid. The peptide concentration of each sample was measured at OD280.

## Liquid Chromatography-Tandem Mass Spectrometry Analysis

A high-performance liquid chromatography liquid-phase system (Thermo Fisher Scientific, Waltham, MA, United States) was used to separate the graded samples passed consecutively through the loading and analytical columns at 300 nl/min. Subsequently, a Q Exactive mass spectrometer (Thermo Fisher Scientific, Waltham, MA, United States) was used to perform LC-MS/MS analysis. The following parameters were applied for detection: positive ion mode; the precursor ion scanning range was 300–1800 m/z; the first-order mass spectrum resolution was 70,000 at 200 m/z; the automatic gain control target was 1e6; maximum IT at 50 ms; and dynamic exclusion at 60 s. The collection method of peptide fragments' mass-to-mass ratio was as follows: 20 fragment spectra (MS2 scans) were collected after each full scan; the MS2 activation type was high-energy collision dissociation; and the isolation window was 2 m/z. In addition, the secondary MS resolution was 35,000 at 200 m/z, with a normalized collision energy of 30 eV and 0.1% underfill.

## Protein Identification and Quantification

Proteins were identified in the UniProt database using Mascot 2.2 and Proteome Discoverer 1.4 software. The selection criteria for the trusted peptides were as follows: FDR < 0.01; peptide mass of  $\pm 20$  ppm; and fragment mass tolerance of 0.1 Da. Protein quantification was performed in accordance with only the unique peptides' median of the protein. By calculating the relative expression ratio of the target protein to the reference protein for all samples in each group, the protein abundant

differences between the two groups were compared. Finally, all peptide ratios were normalized using the median protein ratio.

## Bioinformatics Analysis

Gene ontology (GO) and Kyoto Encyclopedia of Genes and Genomes (KEGG) pathways were analyzed using Blast2GO and KEGG automatic annotation server software, respectively. Fisher's exact test was used to compare the distribution of target proteins in the GO and KEGG pathways and perform enrichment analysis. Protein cluster analysis was conducted using the ComplexHeatmap R package (R version 3.4). The expression matrix of target proteins was normalized prior to the generation of the hierarchical cluster heat map. Protein interaction network analysis of target proteins was based on the STRING database and visualized with Cytoscape software (version 3.6.0). The overall scheme of TMT quantitative proteomics is shown in **Figure 1**.

## Western Blot Analysis

Western blotting was performed according to our previous protocols (Bai et al., 2020). In brief, total protein extracts were prepared using RIPA lysis buffer, and the concentration of protein was estimated using the BCA method. In sodium dodecyl sulfate–polyacrylamide gel electrophoresis, equal amounts of denatured proteins were loaded. Each sample protein was transferred from gel to a polyvinylidene fluoride membrane, blocked with 5% non-fat milk, and incubated overnight with the primary antibody at 4°C. On the following day, secondary antibodies were added to incubate the membrane for 1 h. For chemiluminescence detection, protein bands were revealed using enhanced chemiluminescence reagent. The following primary antibodies were used: anti-KRT17 (ab51056) and anti-FMO3 (ab126711) from Abcam (Cambridge, Cambridgeshire, United Kingdom) and anti-DHRS9 and anti-GAPDH from Proteintech (Chicago, IL, United States).

## Statistical Analysis

All statistical analyses were performed using GraphPad Prism 7 (GraphPad, La Jolla, CA, United States), except for bioinformatics analysis. Bioinformatics-related statistical software and methods are described in *Bioinformatics Analysis*. Student's *t*-test was used to compare means between two groups of normally distributed data. For data with non-normal distribution, the Mann–Whitney U test was used. The comparison of two groups of categorical variable data was analyzed by Fisher's exact probability. Continuous variables are expressed as the mean  $\pm$  standard error of mean. Linear regression analysis was conducted for regression and correlation analyses.  $p < 0.05$  was regarded as statistically significant.

## RESULTS

### Demographic and Radiological Features

In total, 16 patients in the COPD-NE group and 29 patients in the COPD-E group were recruited between September 2016 and June 2019. Lung tissue samples of 9 patients in the COPD-NE group and 12 patients in the COPD-E group were used for proteomic

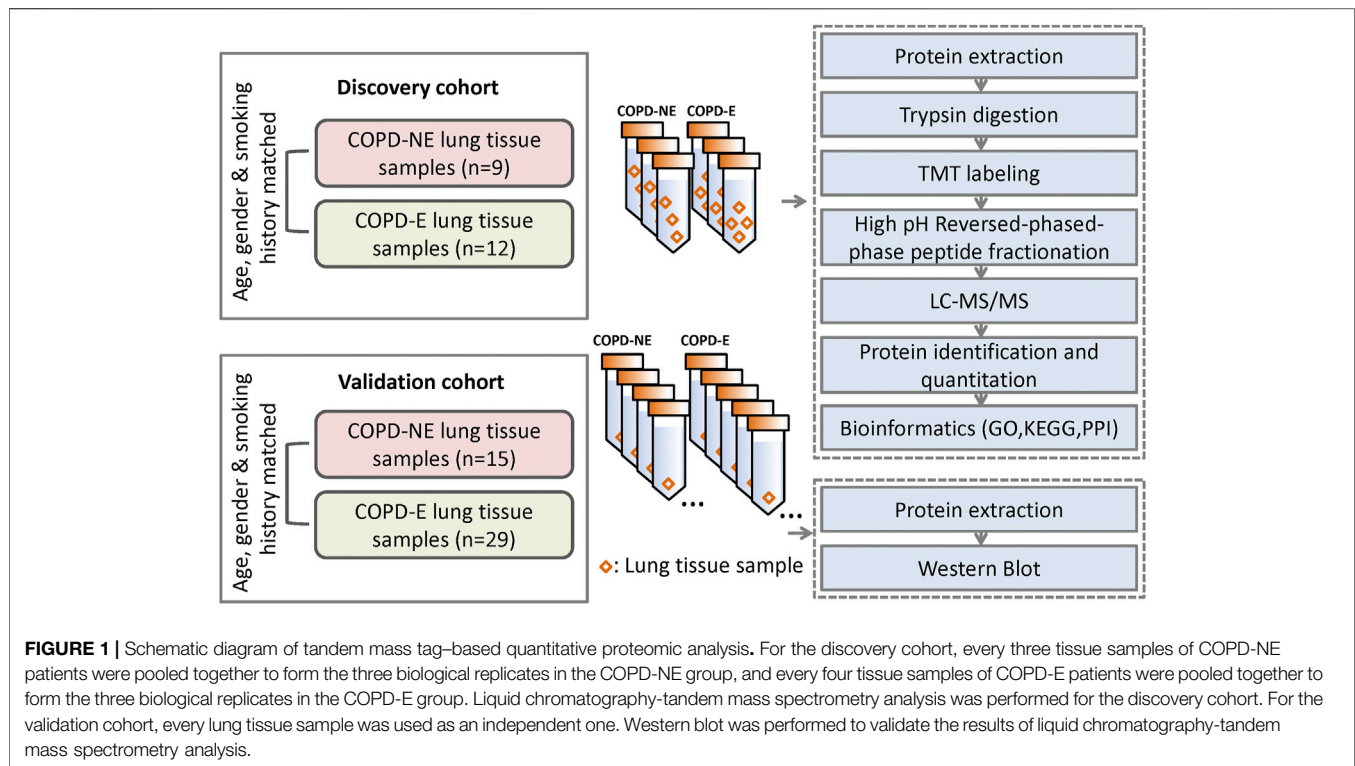


**FIGURE 1 |** Schematic diagram of tandem mass tag-based quantitative proteomic analysis. For the discovery cohort, every three tissue samples of COPD-NE patients were pooled together to form the three biological replicates in the COPD-NE group, and every four tissue samples of COPD-E patients were pooled together to form the three biological replicates in the COPD-E group. Liquid chromatography-tandem mass spectrometry analysis was performed for the discovery cohort. For the validation cohort, every lung tissue sample was used as an independent one. Western blot was performed to validate the results of liquid chromatography-tandem mass spectrometry analysis.

**TABLE 1 |** Demographic and spirometric features of the discovery cohort.

	COPD-NE	COPD-E	p value
Patients, n	9	12	—
Age, years	62.11 ± 2.80	65 ± 1.94	0.39
Gender	—	—	1.00
Male, n (%)	9 (100.0)	12 (100.0)	—
Female, n (%)	0	0	—
Smokers	—	—	0.12
Current, n (%)	5 (55.6)	11 (91.7)	—
Ex-smoker, n (%)	4 (44.4)	1 (8.3)	—
Years of smoking	37.78 ± 4.26	42.75 ± 2.45	0.30
Pack-years	36.11 ± 9.64	46.71 ± 5.59	0.33
Post-bronchodilator (COPD-NE, n = 8; COPD-E, n = 12)			
FEV1 (%)	67.91 ± 7.10	68.29 ± 5.55	0.97
FEV1/FVC	60.89 ± 3.20	57.22 ± 2.58	0.38

Data represent the mean ± SEM of demographic and spirometric features of all patients in each group; COPD, chronic obstructive pulmonary disease; FEV1, forced expiratory volume in 1 s; FVC, forced vital capacity.

**TABLE 2 |** Demographic and spirometric features of the validation cohort.

	COPD-NE	COPD-E	p value
Patients, n	15	29	—
Age, years	62.33 ± 1.90	64.41 ± 1.27	0.36
Gender	—	—	0.60
Male, n (%)	13 (86.67)	27 (93.10)	—
Female, n (%)	2 (13.33)	2 (6.90)	—
Smokers	—	—	0.41
Current, n (%)	11 (73.33)	25 (86.21)	—
Ex-smoker, n (%)	4 (26.67)	4 (13.79)	—
Years of smoking	33.67 ± 3.10	40.28 ± 1.76	0.05
Pack-years	41.00 ± 6.51	43.29 ± 3.50	0.74
Post-bronchodilator (COPD-NE, n = 13; COPD-E, n = 27)			
FEV1 (%)	69.75 ± 4.84	72.25 ± 3.25	0.64
FEV1/FVC	62.17 ± 2.06	60.12 ± 1.57	0.41

Data represent the mean ± SEM of demographic and spirometric features of all patients in each group; COPD, chronic obstructive pulmonary disease; FEV1, forced expiratory volume in 1 s; FVC, forced vital capacity.

analysis. These 21 lung tissues were collected between September 2016 and March 2018 and defined as the discovery cohort. Until June 2019, all samples had been collected and defined as the validation cohort. The validation cohort consisted of 15 COPD-NE lung tissues and 29 COPD-E lung tissues, of which 8 COPD-NE specimens and 12 COPD-E specimens were involved in the discovery cohort. For general features and pulmonary function parameters, there were no significant differences between both groups in the discovery and validation cohorts. However, both cohorts predominantly consisted of male patients, and the

discovery cohort consisted of only male patients. In the validation cohort, patients of the COPD-E group had a longer smoking history than those in the COPD-NE group. However, there were no significant differences in pack-years between the two groups. One patient in the discovery cohort and four in the validation cohort did not have pulmonary function test results after bronchodilator administration (Table 1, Table 2).

In the discovery cohort, patients in the COPD-E group showed a higher emphysema index ( $2.94 \pm 1.12$  vs.  $11.56 \pm 2.78$ ,  $p = 0.02$ ) and lower emphysema percentile density



**TABLE 3 |** Radiological parameters of the discovery and validation cohorts.

	COPD-NE	COPD-E	<i>p</i> value
Discovery cohort			
Patients, <i>n</i>	9	12	—
% of air	82.72 ± 1.57	84.46 ± 0.79	0.30
Volume of air (cm <sup>3</sup> )	2,2419 ± 274.50	2,2635 ± 175.30	0.57
% of tissue	17.28 ± 1.57	15.54 ± 0.79	0.30
Volume of tissue (cm <sup>3</sup> )	467.10 ± 27.20	465.50 ± 22.61	0.96
Emphysema index (%)	2.94 ± 1.12	11.56 ± 2.78	0.02*
Emphysema percentile density (HU)	−911.80 ± 8.30	−944.60 ± 8.40	0.01*
Mean airway lumen radius (mm)	7.02 ± 0.27	6.50 ± 0.28	0.21
Mean airway wall thickness (mm)	3.11 ± 0.21	3.65 ± 0.28	0.16
Ratio of mean airway wall thickness to mean radius	0.44 ± 0.037	0.57 ± 0.06	0.10
Validation cohort			
Patients, <i>n</i>	15	28 <sup>a</sup>	—
% of air	80.59 ± 1.38	83.00 ± 0.78	0.11
Volume of air (cm <sup>3</sup> )	2090 ± 229.70	2,2372 ± 145.30	0.28
% of tissue	19.41 ± 1.38	11.04 ± 0.78	0.11
Volume of tissue (cm <sup>3</sup> )	448.10 ± 21.68	454.70 ± 17.71	0.82
Emphysema index (%)	4.80 ± 1.31	10.93 ± 1.66	0.02*
Emphysema percentile density (HU)	−912.50 ± 7.55	−936.60 ± 5.25	0.01*
Mean airway lumen radius (mm)	6.68 ± 0.27	6.55 ± 0.21	0.70
Mean airway wall thickness (mm)	3.47 ± 0.22	3.69 ± 0.22	0.53
Ratio of mean airway wall thickness to mean radius	0.53 ± 0.06	0.56 ± 0.03	0.62

Data represent the mean ± SEM of radiological parameters for all patients in each group.

<sup>a</sup>Raw radiological data were not available for one patient in the COPD-E group of the validation cohort. COPD, chronic obstructive pulmonary disease.

\**p* < 0.05.

(−911.80 ± 8.30 vs. −944.60 ± 8.40, *p* = 0.01) than those in the COPD-NE group. This result suggested that COPD-E patients had more severe emphysema lesions than COPD-NE patients (Table 3). Other airway-related parameters, including proportion of air and tissue, were not significantly different between both groups. The CT scan results did not show large differences between the validation and discovery cohorts. Raw radiological data were not available for one patient in the validation cohort; this patient was not included in this analysis.

## Protein Identification and Differential Abundant Protein Screening

A total of 31,479 peptides, including 27,157 unique peptides, were identified by mass spectrometry, and 4,343 proteins were finally identified. All identified proteins and related information are shown in Supplementary Table S2. The mass spectrometry proteomics data have been deposited to the ProteomeXchange Consortium (<http://proteomecentral.proteomexchange.org>) via the iProX partner repository with the dataset identifier PXD023900 (Ma et al., 2019). DAPs were identified using the following screening criteria: COPD-E/COPD-NE ratio greater than 1.2-fold (upregulation greater than 1.2-fold or downregulation less than 0.83-fold) and *p* < 0.05. A total of 36 DAPs were identified, of which 25 were upregulated and 11 were downregulated. The type I cytoskeletal 17 (KRT17) protein expression in the COPD-E group was 1.54-fold higher than that in the COPD-NE group, as the protein with the most obvious differences between the two groups. All DAPs are listed in Table 4, and a volcano plot showing the distribution of DAPs is illustrated in Figure 2A. Hierarchical cluster analysis

showed that the samples were clustered into two categories, which were the same groups as the original groups. The clustering results are shown in Figure 2B.

## Functional Enrichment and Protein–Protein Interaction Network of DAPs

GO functional annotation and enrichment analysis was performed for all DAPs, the results of which are shown in Supplementary Table S3. The GO terms were ordered according to the *p* value, and the top 20 enriched GO terms included eight terms in the biological pathway, six terms in the molecular function, and six terms in the cellular component. The biological pathway was mainly related to tissue refactoring and wound healing, including regulation of response to wound, regulation of wound healing, pathways that downregulate wound-related response and healing, response to external stimuli, and defense response. The molecular function was predominantly related to protein binding; protein–lipid complex binding and lipoprotein particle binding had the highest enrichment factor (0.23). For the cellular component, most DAPs were found in the extracellular matrix and some in organelles. Enrichment analysis results of the top 20 enriched GO terms with smallest *p* values are displayed in Figure 3A. GO terms at level 2 are on higher positions in the hierarchy of GO terms. Level 2 GO terms describe the properties of proteins more comprehensively, and all of the level 2 GO terms involved in GO enrichment are shown in Figure 3B. The metabolic process may occupy an important position in emphysematous phenotype-related biological pathways; besides, growth, cell proliferation, and developmental

**TABLE 4 |** Differential abundant proteins in the COPD-E and COPE-NE groups.

Accession	Description	Gene name	COPD-E/COPD-NE ratio	p value
Q04695	Keratin, type I cytoskeletal 17	KRT17	1.54	0.037*
P02745	Complement C1q subcomponent subunit A	C1QA	1.48	<0.001***
Q9BXD5	N-acetylneuraminase lyase	NPL	1.45	0.040*
P02794	Ferritin heavy chain	FTH1	1.38	0.019*
P48061	Stromal cell-derived factor 1	CXCL12	1.38	0.015*
P39900	Macrophage metalloelastase	MMP12	1.35	0.024*
P02747	Complement C1q subcomponent subunit C	C1QC	1.34	0.031*
P0DOX8	Immunoglobulin lambda-1 light chain	—	1.33	0.039*
P02679	Fibrinogen gamma chain	FGG	1.32	<0.001***
P02746	Complement C1q subcomponent subunit B	C1QB	1.31	0.012*
Q9NP78	ATP-binding cassette sub-family B member 9	ABCB9	1.30	0.024*
Q8TED4	Glucose-6-phosphate exchanger SLC37A2	SLC37A2	1.28	0.021*
P0C0L4	Complement C4-A	C4A	1.28	0.020*
P02671	Fibrinogen alpha chain	FGA	1.27	0.003**
MOR2J8	Doublecortin domain-containing protein 1	DCDC1	1.26	<0.001***
P02675	Fibrinogen beta chain	FGB	1.26	0.001**
Q9BPW9	Dehydrogenase/reductase SDR family member 9	DHRS9	1.25	0.005**
P02649	Apolipoprotein E	APOE	1.24	0.041*
P31513	Dimethylaniline monooxygenase [N-oxide-forming] 3	FMO3	1.23	0.022*
P18428	Lipopolysaccharide-binding protein	LBP	1.23	0.028*
Q9BXN1	Asporin	ASPN	1.23	0.038*
P02743	Serum amyloid P-component	APCS	1.22	0.023*
Q5T6F0	DDB1- and CUL4-associated factor 12	DCAF12	1.21	0.004**
P04003	C4b-binding protein alpha chain	C4BPA	1.21	0.036*
P35542	Serum amyloid A-4 protein	SAA4	1.20	0.025*
Q96D46	60S ribosomal export protein NMD3	NMD3	0.83	0.011*
P33764	Protein S100-A3	S100A3	0.83	0.049*
P31415	Calsequestrin-1	CASQ1	0.82	0.007**
P28906	Hematopoietic progenitor cell antigen CD34	CD34	0.81	0.016*
P15090	Fatty acid-binding protein, adipocyte	FABP4	0.81	0.033*
P43155	Carnitine O-acetyltransferase	CRAT	0.80	0.032*
P16671	Platelet glycoprotein 4	CD36	0.79	0.008**
Q96B54	Zinc finger protein 428	ZNF428	0.78	0.017*
P22748	Carbonic anhydrase 4	CA4	0.78	0.014*
P17152	Transmembrane protein 11, mitochondrial	TMEM11	0.76	0.018*
P30486	HLA class I histocompatibility antigen, B-48 alpha chain	HLA-B	0.76	0.014*

\*p &lt; 0.05, \*\*p &lt; 0.01, \*\*\*p &lt; 0.001.

process were also involved. Binding was the most predominant molecular function of DAPs. In addition to the extracellular matrix, organelles may be the portion that DAPs were mainly distributed in.

To understand the mechanisms and signaling pathways that DAPs may participate in the pathogenesis of COPD emphysematous phenotype, we performed KEGG pathway annotation and enrichment analysis of all DAPs; the specific results are shown in **Supplementary Table S4**. KEGG enrichment analysis showed that most DAPs were involved in metabolic and inflammatory pathways, including nitrogen metabolism, PPAR signaling, NF- $\kappa$ B signaling, and cholesterol metabolism. All KEGG terms with *p* values less than 0.05 are shown in **Figure 4A** and ordered according to the *p* value. The top 20 KEGG terms with largest enriched protein numbers are shown in **Figure 4B**.

PPI network analysis was used to analyze the interaction between DAPs. As shown in **Figure 5**, 16 out of 36 DAPs had interaction nodes. Apolipoprotein E is the DAP that has most interactions with other DAPs, which indicates it may

serve as a key molecule in the mechanism of emphysema. Besides, serum amyloid P-component, various chains of fibrinogen, and different subcomponent subunits of the complement interact with each other. These DAPs were related to the pathways in the results of GO and KEGG enrichment analyses. Therefore, these interactions may play roles in the pathogenesis of emphysematous phenotype, as well.

## Validation and Functional Annotation of DAPs

The expression of KRT17, dehydrogenase/reductase short-chain alcohol dehydrogenase/reductase (SDR) family member 9 (DHRS9), and dimethylaniline monooxygenase 3 (FMO3) was determined. Each lung tissue sample obtained from a subject was used as an independent sample in western blot. Western blotting results showing the expression of these proteins in the lung tissue samples of the validation cohort are shown in **Figure 6**. The protein expression of KRT17 (COPD-NE, *n* = 13, COPD-E, *n* =

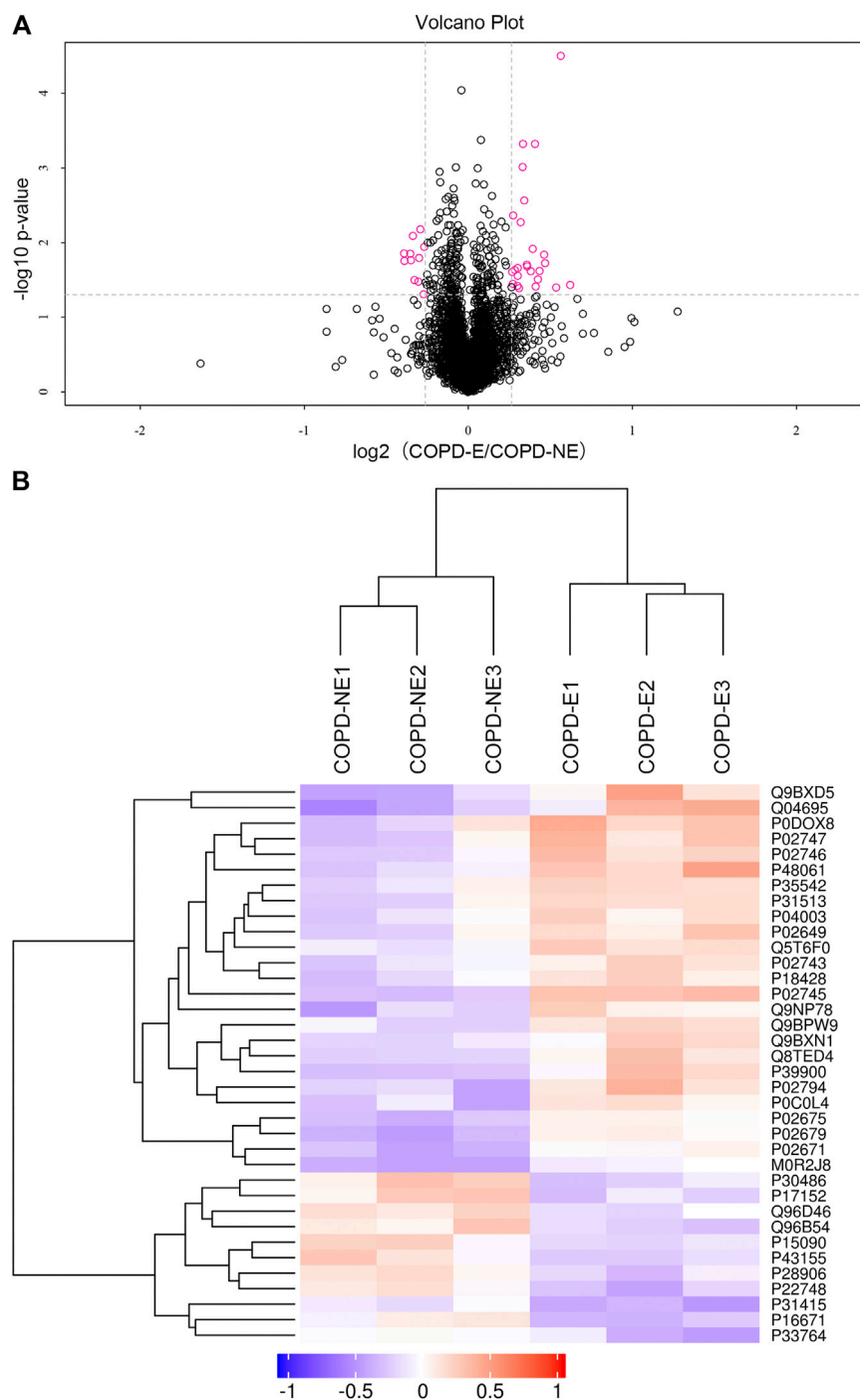


**FIGURE 2 |** Quantification and hierarchical clustering of differential abundant proteins (DAPs) in COPD emphysematous phenotype. **(A)** Volcano plot of DAPs. **(B)** Hierarchical clustering heat map of DAPs.

24;  $p < 0.01$ ) and DHRS9 (COPD-NE,  $n = 13$ , COPD-E,  $n = 24$ ;  $p < 0.01$ ) in the COPD-E group was higher than that in the COPD-NE group. However, the FMO3 expression was not significantly different between both groups. Western blotting results of all lung tissue samples are shown in **Supplementary Figure S1**.

The annotation results showed that KRT17 acts as a cytoskeletal protein and takes part in the process of cell growth and development, while DHRS9 participates in multiple metabolic pathways, such as retinol and steroid hormone biosynthesis (**Table 5**).

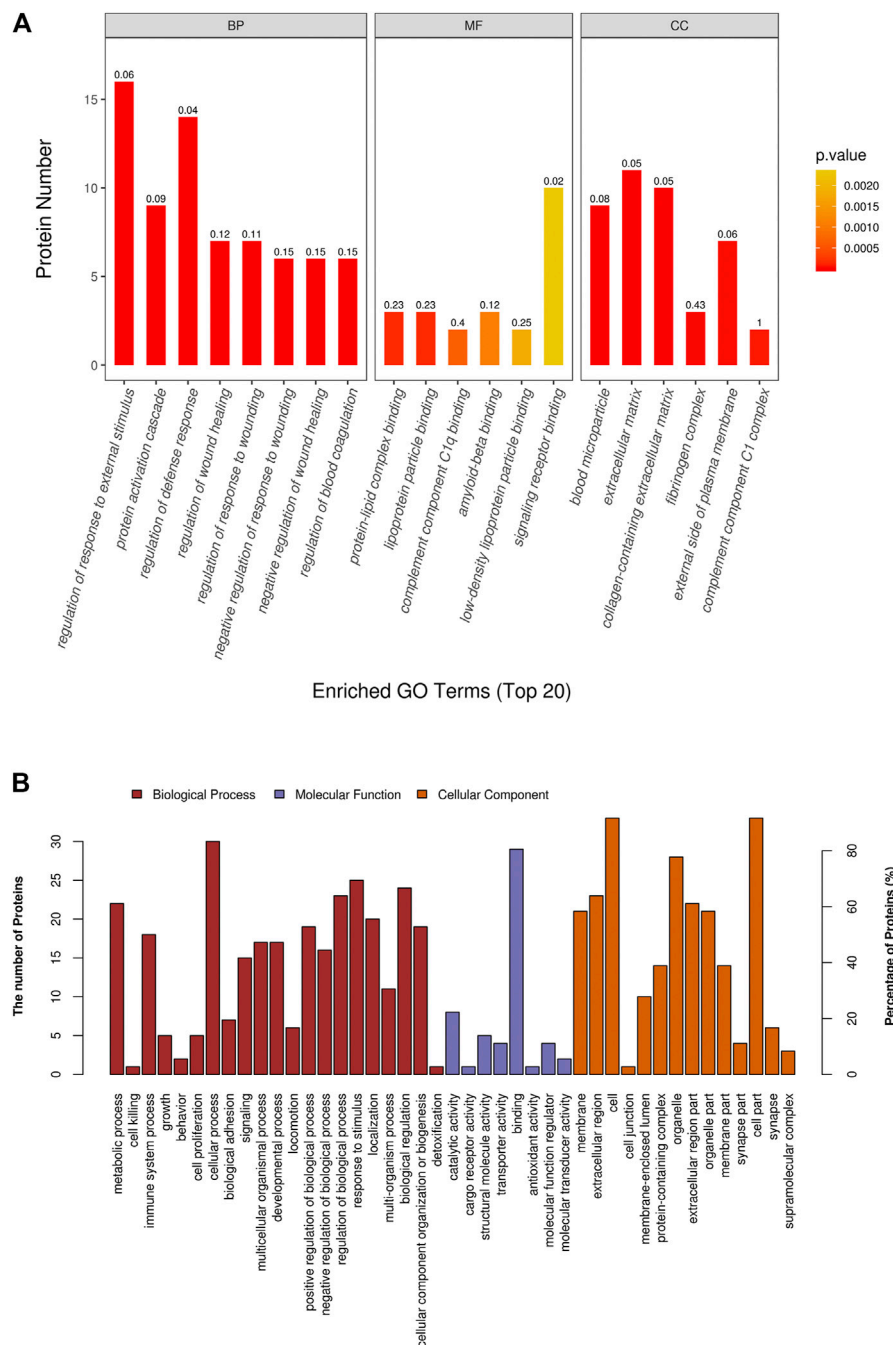


**FIGURE 3 |** Gene ontology (GO) enrichment analysis of differential abundant proteins. **(A)** Top 20 enriched terms with smallest *p* values in GO enrichment analysis. **(B)** All level 2 GO terms involved in GO enrichment analysis.

## DISCUSSION

Patients with COPD emphysematous phenotype account for a considerable portion in clinics. Patients with this phenotype manifest progressive destruction of lung tissue and poor response to current pharmaceutical interventions of COPD (Janssen et al., 2019). With an aim of exploring the specific mechanism underlying the development of this phenotype, the

proteome of lung tissues from patients with COPD emphysematous phenotype was studied using TMT quantitative proteomics. A total of 4,343 proteins were identified, out of which 36 were DAPs. Of these, 25 DAPs were upregulated and 11 DAPs were downregulated. This result was comparable with that of other proteomic analyses on lung tissue (Sun et al., 2019; Wu et al., 2020). Functional enrichment analysis of DAPs showed that tissue repair and cell



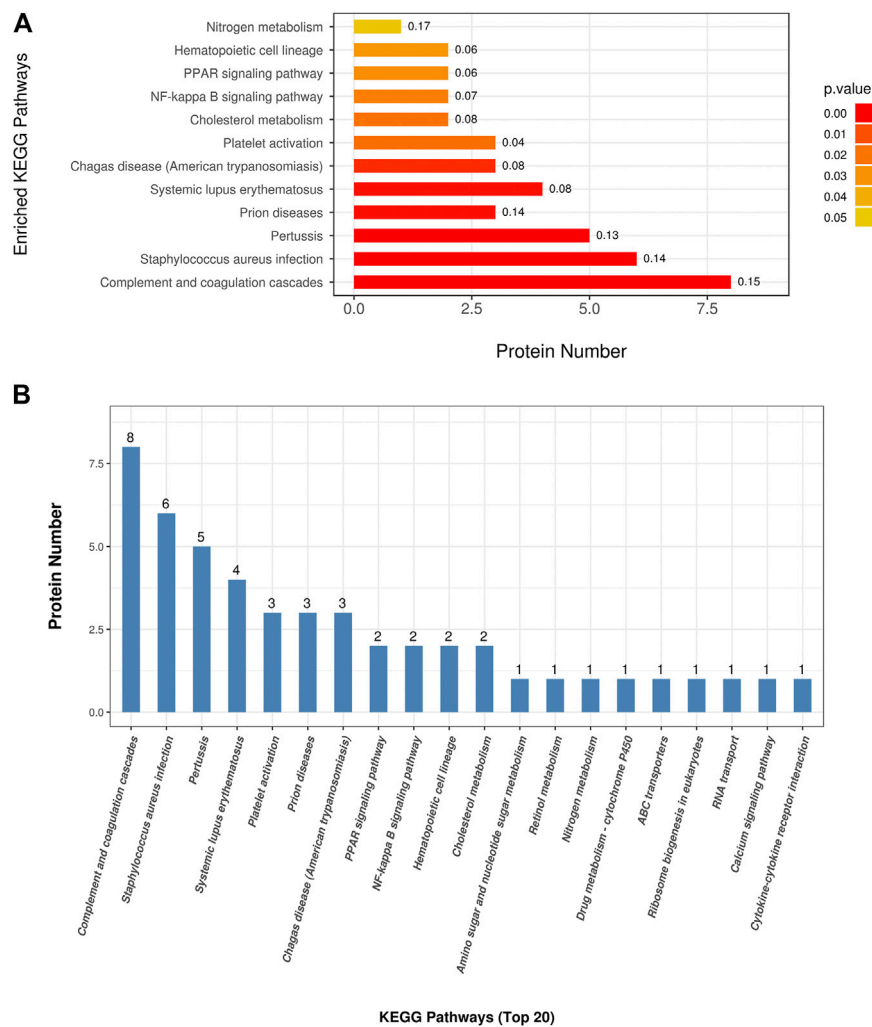


**FIGURE 4 |** Kyoto Encyclopedia of Genes and Genomes (KEGG) enrichment analysis of differential abundant proteins. **(A)** Enriched terms in KEGG enrichment analysis with  $p$  values less than 0.05. **(B)** Top 20 KEGG terms with largest enriched protein numbers in KEGG enrichment results.

proliferation and development were primarily related to the pathogenesis of emphysematous phenotype, in addition to inflammatory response, collagen disruption, and other well-recognized mechanisms in emphysema (Lan et al., 2019). Moreover, cholesterol-related, retinol-related, and other lipid-related metabolic pathways were enriched in KEGG pathway analysis. These results suggested that the impaired ability to repair injured tissue and lipid metabolism disorder might play an essential role in the development of prominent lung tissue destruction in COPD emphysematous phenotype. The differential expression of KRT17 and DHRS9 was validated in the lung tissue samples of patients with COPD emphysematous phenotype. Therefore, KRT17 and DHRS9 might affect the pathogenesis of COPD emphysematous phenotype by regulating tissue repair and lipid metabolism and act as phenotype-specific proteomic signatures.

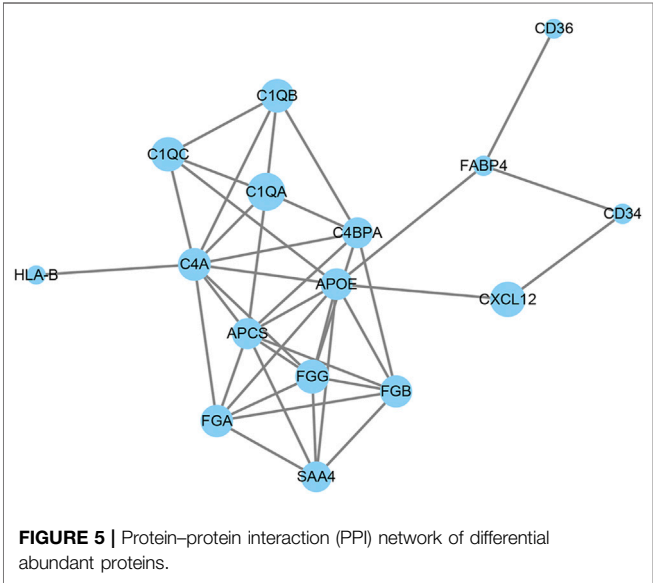
Tissue repair is an essential process for all organisms to protect and maintain the normal structure and function. As structural

destruction and collagen fibril disorder are prominently observed in patients with COPD emphysematous phenotype, the impaired ability to repair lung parenchymal and interstitial cells might play a significant role in its pathogenesis (Hu et al., 2020). The WNT/ $\beta$ -catenin pathway is a classical pathway involved in lung growth and development, and cell proliferation and differentiation (Königshoff and Eickelberg, 2010). Downregulation of this pathway will result in the retardation of tissue repair (Kneidinger et al., 2011; Uhl et al., 2015). Under normal conditions, WNT activates the JNK pathway by forming a complex with small G-proteins to promote cytoskeletal rearrangement during embryonic development (Wiggin and Hamel, 2002; Zhang et al., 2018). Moreover, the canonical WNT signaling pathway promotes the proliferation of type II alveolar epithelial cells (AECIIs) and *trans*-differentiation of AECIIs to type I alveolar epithelial cells (AECIs) that replenish injured ones in the damaged process of emphysema. In contrast, the non-canonical WNT signaling pathway inhibits proliferation

TABLE 5 | Annotation of KRT17 and DHRS9.

Accession	Gene name	ID	Annotation term
Q04695	KRT17	GO:0070268	BP: cornification
		GO:0008544	BP: epidermis development
		GO:0031069	BP: hair follicle morphogenesis
		GO:0045109	BP: intermediate filament organization
		GO:0031424	BP: keratinization
		GO:0030307	BP: positive regulation of cell growth
		GO:0051798	BP: positive regulation of hair follicle development
		GO:0045727	BP: positive regulation of translation
		GO:0007165	BP: signal transduction
		GO:0071944	CC: cell periphery
		GO:0005829	CC: cytosol
		GO:0070062	CC: extracellular exosome
		GO:0005882	CC: intermediate filament
		GO:0045111	CC: intermediate filament cytoskeleton
		GO:0042289	MF: MHC class II protein binding
		GO:0032395	MF: MHC class II receptor activity
		GO:0005200	MF: structural constituent of cytoskeleton
		hsa05150	<i>Staphylococcus aureus</i> infection
		hsa04915	Estrogen signaling pathway
Q9BPW9	DHRS9	GO:0042904	BP: 9-cis-retinoic acid biosynthetic process
		GO:0008209	BP: androgen metabolic process
		GO:0030855	BP: epithelial cell differentiation
		GO:0042448	BP: progesterone metabolic process
		GO:0042572	BP: retinol metabolic process
		GO:0005789	CC: endoplasmic reticulum membrane
		GO:0030176	CC: integral component of endoplasmic reticulum membrane
		GO:0004022	MF: alcohol dehydrogenase (NAD) activity
		GO:0047044	MF: androstan-3- $\alpha$ ,17- $\beta$ -diol dehydrogenase activity
		GO:0047023	MF: androsterone dehydrogenase activity
		GO:0016854	MF: racemase and epimerase activity
		GO:0004745	MF: retinol dehydrogenase activity
		GO:0047035	MF: testosterone dehydrogenase (NAD <sup>+</sup> ) activity
		hsa00830	retinol metabolism

BP: biological pathway; CC: cellular component; MF: molecular function.



and *trans*-differentiation processes (Skronska-Wasek et al., 2017). KRT17 is an important component of cytoskeleton. Functional

annotation of DAPs showed that KRT17 participates in cell growth and development and cytoskeletal composition. Therefore, KRT17 has a potential to serve as an important target of the WNT/ $\beta$ -catenin signaling pathway. Both canonical and non-canonical WNT signaling pathways may rearrange or affect the abundance of cytoskeletal component—KRT17, resulting in the severe tissue destruction in patients with COPD emphysematous phenotype. Some studies have confirmed that the expression of cyclin D1, MMP7, c-Myc, and other vital targets of the WNT/ $\beta$ -catenin pathway is increased in KRT17-overexpressing cells (Wang et al., 2019). However, the mechanism through which canonical and non-canonical WNT signaling pathways interact with KRT17 warrants further studies, and the specific roles of KRT17 in the development of COPD and emphysema are still to be explored.

Retinoic acid is synthesized from retinol, and it regulates lung development and alveolar formation in the human body. Some studies have shown that retinoic acid can inhibit the activation of YAP signaling and epithelial–mesenchymal FGF signaling pathways, which promotes the proliferation and inhibits the differentiation of alveolar epithelial cells (Ng-Blichfeldt et al., 2018). In addition, retinoic acid can downregulate pro-apoptotic

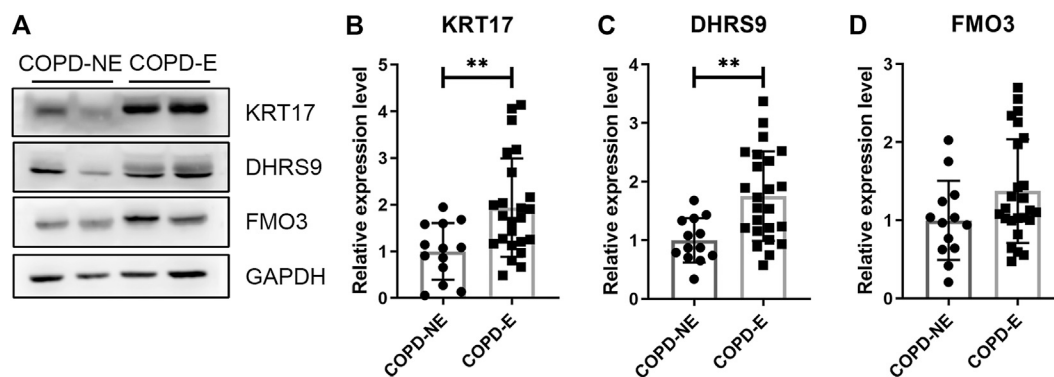


**FIGURE 6 |** Type I cytoskeletal 17 (KRT17) and dehydrogenase/reductase SDR family member 9 (DHRS9) expressions are increased in the lung tissue samples of patients with chronic obstructive pulmonary disease emphysematous phenotype (COPD-E). **(A)** Western blotting results of KRT17, DHRS9, and FMO3 expressions in the lung tissue samples of COPD non-emphysematous phenotype (COPD-NE) and COPD-E groups. **(B–D)** Quantification of KRT17 (COPD-NE,  $n = 13$ ; COPD-E,  $n = 24$ ), DHRS9 (COPD-NE,  $n = 13$ ; COPD-E,  $n = 24$ ), and FMO3 (COPD-NE,  $n = 13$ ; COPD-E,  $n = 25$ ) protein expressions. \*\* $p < 0.01$ .

genes and inhibit the apoptosis of alveolar epithelial cells (Chatterjee and Chatterji, 2017). Therefore, the functional enrichment of DAPs in cholesterol and retinol metabolism in this study suggests aberrant proliferation and differentiation caused by impaired lipid metabolism. DHRS9 is a member of the SDR family. Crosstalk between DHRS9 and retinaldehyde dehydrogenase 1 (Raldh1) exerts important regulatory functions in the synthesis of retinoic acid. Unlike other members of the SDR family (e.g., Rdh10 and Rdh2), DHRS9 knockdown increased retinoic acid synthesis in RALDH1-overexpressing cells (Wang et al., 2011). Combined with the results of functional annotation and enrichment, DHRS9 can modulate the synthesis of retinoic acid, which in turn regulates the proliferation and differentiation of alveolar epithelial cells (Ng-Blichfeldt et al., 2018). Furthermore, clinical studies have confirmed that DHRS9 can regulate inflammation (Morichika et al., 2019) as well as the balance between MMP9 and TIMP1 (Mao et al., 2003) in cells. These results suggest that DHRS9 is predominantly involved in the pathogenic mechanism of emphysema in patients with COPD emphysematous phenotype, but specific molecular mechanisms are still unclear and remain to be explored.

Serum (Sridhar et al., 2019), expectorated sputum (Titz et al., 2015), and bronchoalveolar lavage fluid (Tu et al. 2014) samples have been used in previous proteomic studies to analyze the COPD-related proteome. However, the number of detected DAPs was relatively small and easily influenced by a systemic disease. Lung tissue is the direct affected site of COPD emphysematous phenotype. Therefore, lung tissue samples are the most suitable to identify key molecules involved in the mechanism underlying emphysema pathogenesis. To the best of our knowledge, this is the first proteomic analysis that focuses on emphysematous phenotype, to detect the specific DAPs in this phenotype.

There are some limitations to our study. Due to the fact that only few COPD patients were able to meet the inclusion criteria of our study, there are certain difficulties to collect lung tissue samples and the number of lung tissue samples in the validation cohort was relatively small. Moreover, there was an overlap between lung tissues from the discovery and validation

cohorts. Furthermore, though wound repair and retinol metabolism may be the processes that KRT17 and DHRS9 participated in, they have not yet been demonstrated and explored in this study. In the future, more lung tissue samples from COPD patients should be involved and in-depth research studies should be conducted to explore the mechanism of COPD emphysematous phenotype development, including experiments *in vivo* and *in vitro*.

## CONCLUSION

A total of 36 DAPs were identified in lung tissue samples from patients in the COPD emphysematous phenotype group. Of these, 25 DAPs were upregulated and 11 DAPs were downregulated. KRT17 and DHRS9 were found to take part in the pathogenesis of emphysema. Moreover, wound repair and retinol metabolism may be the processes they participated. Therefore, KRT17 and DHRS9 can be used as phenotype-specific proteomic signatures in patients with COPD emphysematous phenotype.

## DATA AVAILABILITY STATEMENT

The original contributions presented in the study are publicly available. This data can be found here: ProteomeXchange Consortium (<http://proteomecentral.proteomexchange.org>), dataset identifier: PXD023900.

## ETHICS STATEMENT

The studies involving human participants were reviewed and approved by the Ethics Committee of Shengjing Hospital of China Medical University (Shenyang, China; Ethical no. 2016PS342K). The patients/participants provided their written informed consent to participate in this study.

## AUTHOR CONTRIBUTIONS

SB, SX and LZ substantially contributed to the conception and design of the manuscript. SB, RY, CW, PS, DW, YY, HW, SW, MY, SX and LZ contributed to the acquisition, analysis, and interpretation of data. SB, SX and LZ drafted the article, and SB, RY, CW, PS, DW, YY, HW, SW, MY, SX, and LZ revised it critically and substantially. SB, RY, CW, PS, DW, YY, HW, SW, MY, SX, and LZ approved the final version and accepted accountability for all aspects of the study. Corresponding authors SX and LZ contributed equally to this study.

## REFERENCES

- Alford, S. K., van Beek, E. J. R., McLennan, G., and Hoffman, E. A. (2010). Heterogeneity of Pulmonary Perfusion as a Mechanistic Image-Based Phenotype in Emphysema Susceptible Smokers. *Proc. Natl. Acad. Sci.* 107 (16), 7485–7490. doi:10.1073/pnas.0913880107
- Bai, S., Ye, R., Wang, C., Sun, P., and Zhao, L. (2020). Comparative Analysis of Pathophysiological Parameters between Emphysematous Smokers and Emphysematous Patients with COPD. *Sci. Rep.* 10 (1), 420. doi:10.1038/s41598-019-57354-2
- Belgacemi, R., Luczka, E., Ancel, J., Diabasana, Z., Perotin, J.-M., Germain, A., et al. (2020). Airway Epithelial Cell Differentiation Relies on Deficient Hedgehog Signalling in COPD. *EBioMedicine* 51, 102572. doi:10.1016/j.ebiom.2019.11.033
- Camp, P. G., Coxson, H. O., Levy, R. D., Pillai, S. G., Anderson, W., Vestbo, J., et al. (2009). Sex Differences in Emphysema and Airway Disease in Smokers. *Chest* 136 (6), 1480–1488. doi:10.1378/chest.09-0676
- Camp, P. G., Ramirez-Venegas, A., Sansores, R. H., Alva, L. F., McDougall, J. E., Sin, D. D., et al. (2014). COPD Phenotypes in Biomass Smoke- versus Tobacco Smoke-Exposed Mexican Women. *Eur. Respir. J.* 43 (3), 725–734. doi:10.1183/09031936.00206112
- Chatterjee, A., and Chatterji, U. (2017). All -Trans Retinoic Acid Ameliorates Arsenic-Induced Oxidative Stress and Apoptosis in the Rat Uterus by Modulating MAPK Signaling Proteins. *J. Cel. Biochem.* 118 (11), 3796–3809. doi:10.1002/jcb.26029
- Coxson, H. O., Leipsic, J., Parraga, G., and Sin, D. D. (2014). Using Pulmonary Imaging to Move Chronic Obstructive Pulmonary Disease beyond FEV1. *Am. J. Respir. Crit. Care Med.* 190 (2), 135–144. doi:10.1164/rccm.201402-0256PP
- Criner, G. J., Sue, R., Wright, S., Dransfield, M., Rivas-Perez, H., and Wiese, T. (2018). A Multicenter Randomized Controlled Trial of Zephyr Endobronchial Valve Treatment in Heterogeneous Emphysema (LIBERATE). *Am. J. Respir. Crit. Care Med.* 198 (9), 1151–1164. doi:10.1164/rccm.201803-0590OC10.1164/rccm.201808-1477le
- Dirksen, A., Piitulainen, E., Parr, D. G., Deng, C., Wencker, M., Shaker, S. B., et al. (2009). Exploring the Role of CT Densitometry: a Randomised Study of Augmentation Therapy in 1-antitrypsin Deficiency. *Eur. Respir. J.* 33 (6), 1345–1353. doi:10.1183/09031936.00159408
- Dzianan, J. M., Wirjanata, G., Dai, L., Go, K. D., Yu, H., Lim, Y. T., et al. (2020). Cellular thermal Shift Assay for the Identification of Drug-Target Interactions in the Plasmodium Falciparum Proteome. *Nat. Protoc.* 15 (6), 1881–1921. doi:10.1038/s41596-020-0310-z
- Fan, L., Xia, Y., Guan, Y., Zhang, T.-f., and Liu, S.-y. (2014). Characteristic Features of Pulmonary Function Test, CT Volume Analysis and MR Perfusion Imaging in COPD Patients with Different HRCT Phenotypes. *Clin. Respir. J.* 8 (1), 45–54. doi:10.1111/crj.12033
- Hu, Y., Ng-Blichfeldt, J.-P., Ota, C., Ciminieri, C., Ren, W., Hiemstra, P. S., et al. (2020). Wnt/ $\beta$ -catenin Signaling Is Critical for Regenerative Potential of Distal Lung Epithelial Progenitor Cells in Homeostasis and Emphysema. *Stem Cells* 38 (11), 1467–1478. doi:10.1002/stem.3241
- Janssen, R., Pisco, I., Franssen, F. M. E., and Wouters, E. F. M. (2019). Emphysema: Looking beyond Alpha-1 Antitrypsin Deficiency. *Expert Rev. Respir. Med.* 13 (4), 381–397. doi:10.1080/17476348.2019.1580575
- Jiang, J., Xiao, K., and Chen, P. (2017). NOTCH Signaling in Lung Diseases. *Exp. Lung Res.* 43 (4-5), 217–228. doi:10.1080/01902148.2017.1306599
- Kneidinger, N., Yildirim, A. Ö., Callegari, J., Takenaka, S., Stein, M. M., Dumitrescu, R., et al. (2011). Activation of the WNT/ $\beta$ -Catenin Pathway Attenuates Experimental Emphysema. *Am. J. Respir. Crit. Care Med.* 183 (6), 723–733. doi:10.1164/rccm.200910-1560OC
- Königshoff, M., and Eickelberg, O. (2010). WNT Signaling in Lung Disease. *Am. J. Respir. Cell Mol. Biol.* 42 (1), 21–31. doi:10.1165/rcmb.2008-0485TR
- Lan, Y.-W., Yang, J.-C., Yen, C.-C., Huang, T.-T., Chen, Y.-C., Chen, H.-L., et al. (2019). Predifferentiated Amniotic Fluid Mesenchymal Stem Cells Enhance Lung Alveolar Epithelium Regeneration and Reverse Elastase-Induced Pulmonary Emphysema. *Stem Cell Res Ther.* 10 (1), 163. doi:10.1186/s13287-019-1282-1
- Ma, J., Chen, T., Wu, S., Yang, C., Bai, M., Shu, K., et al. (2019). iProX: an Integrated Proteome Resource. *Nucleic Acids Res.* 47 (D1), D1211–D1217. doi:10.1093/nar/gky869
- Manon-Jensen, T., Langholm, L. L., Rønnow, S. R., Karsdal, M. A., Tal-Singer, R., Vestbo, J., et al. (2019). End-product of Fibrinogen Is Elevated in Emphysematous Chronic Obstructive Pulmonary Disease and Is Predictive of Mortality in the ECLIPSE Cohort. *Respir. Med.* 160, 105814. doi:10.1016/j.rmed.2019.105814
- Mao, J. T., Tashkin, D. P., Belloni, P. N., Baileyhealy, I., Baratelli, F., and Roth, M. D. (2003). All- Trans Retinoic Acid Modulates the Balance of Matrix Metalloproteinase-9 and Tissue Inhibitor of Metalloproteinase-1 in Patients with Emphysema \*. *Chest* 124 (5), 1724–1732. doi:10.1378/chest.124.5.1724
- Mertins, P., Tang, L. C., Krug, K., Clark, D. J., Gritsenko, M. A., Chen, L., et al. (2018). Reproducible Workflow for Multiplexed Deep-Scale Proteome and Phosphoproteome Analysis of Tumor Tissues by Liquid Chromatography-Mass Spectrometry. *Nat. Protoc.* 13 (7), 1632–1661. doi:10.1038/s41596-018-0006-9
- Morichika, D., Miyahara, N., Fujii, U., Taniguchi, A., Oda, N., Senoo, S., et al. (2019). A Retinoid X Receptor Partial Agonist Attenuates Pulmonary Emphysema and Airway Inflammation. *Respir. Res.* 20 (1), 2. doi:10.1186/s12931-018-0963-0
- Ng-Blichfeldt, J.-P., Schrik, A., Kortekaas, R. K., Noordhoek, J. A., Heijink, I. H., Hiemstra, P. S., et al. (2018). Retinoic Acid Signaling Balances Adult Distal Lung Epithelial Progenitor Cell Growth and Differentiation. *EBioMedicine* 36, 461–474. doi:10.1016/j.ebiom.2018.09.002
- Oelsner, E. C., Hoffman, E. A., Folsom, A. R., Carr, J. J., Enright, P. L., Kawut, S. M., et al. (2014). Association between Emphysema-like Lung on Cardiac Computed Tomography and Mortality in Persons without Airflow Obstruction. *Ann. Intern. Med.* 161 (12), 863–873. doi:10.7326/m13-2570
- Papaoiannou, A. I., Kostikas, K., Papaportfyriou, A., Angelakis, L., Papathanasiou, E., Hillas, G., et al. (2017). Emphysematous Phenotype Is Characterized by Low Blood Eosinophils: A Cross-Sectional Study. *COPD: J. Chronic Obstructive Pulm. Dis.* 14 (6), 635–640. doi:10.1080/15412555.2017.1386644
- Rosas-Alonso, R., Galera, R., Sánchez-Pascuala, J. J., Casitas, R., Burdiel, M., Martínez-Cerón, E., et al. (2020). Hypermethylation of Anti-oncogenic MicroRNA 7 Is Increased in Emphysema Patients. *Archivos de Bronconeumología (English Edition)* 56 (8), 506–513. doi:10.1016/j.arbres.2019.10.01710.1016/j.arbr.2019.10.019

## ACKNOWLEDGEMENT

The authors would like to thank the Biological Sample Library of Shengjing Hospital for help of getting tissue samples.

## SUPPLEMENTARY MATERIAL

The Supplementary Material for this article can be found online at: <https://www.frontiersin.org/articles/10.3389/fmolb.2021.650604/full#supplementary-material>



- Skronska-Wasek, W., Mutze, K., Baarsma, H. A., Bracke, K. R., Alsafadi, H. N., Lehmann, M., et al. (2017). Reduced Frizzled Receptor 4 Expression Prevents WNT/ $\beta$ -Catenin-driven Alveolar Lung Repair in Chronic Obstructive Pulmonary Disease. *Am. J. Respir. Crit. Care Med.* 196 (2), 172–185. doi:10.1164/rccm.201605-0904OC
- Sridhar, S., Liu, H., Pham, T.-H., Damera, G., and Newbold, P. (2019). Modulation of Blood Inflammatory Markers by Benralizumab in Patients with Eosinophilic Airway Diseases. *Respir. Res.* 20 (1), 14. doi:10.1186/s12931-018-0968-8
- Sun, P., Ye, R., Wang, C., Bai, S., and Zhao, L. (2019). Identification of Proteomic Signatures Associated with COPD Frequent Exacerbators. *Life Sci.* 230, 1–9. doi:10.1016/j.lfs.2019.05.047
- Titz, B., Sewer, A., Schneider, T., Elamin, A., Martin, F., Dijon, S., et al. (2015). Alterations in the Sputum Proteome and Transcriptome in Smokers and Early-Stage COPD Subjects. *J. Proteomics* 128, 306–320. doi:10.1016/j.jprot.2015.08.009
- Tu, C., Mammen, M. J., Li, J., Shen, X., Jiang, X., Hu, Q., et al. (2014). Large-scale, Ion-Current-Based Proteomics Investigation of Bronchoalveolar Lavage Fluid in Chronic Obstructive Pulmonary Disease Patients. *J. Proteome Res.* 13 (2), 627–639. doi:10.1021/pr4007602
- Uhl, F. E., Vierkotten, S., Wagner, D. E., Burgstaller, G., Costa, R., Koch, I., et al. (2015). Preclinical Validation and Imaging of Wnt-Induced Repair in Human 3D Lung Tissue Cultures. *Eur. Respir. J.* 46 (4), 1150–1166. doi:10.1183/09031936.00183214
- Vogelmeier, C. F., Criner, G. J., Martinez, F. J., Anzueto, A., Barnes, P. J., Bourbeau, J., et al. (2017). Global Strategy for the Diagnosis, Management, and Prevention of Chronic Obstructive Lung Disease 2017 Report. GOLD Executive Summary. *Am. J. Respir. Crit. Care Med.* 195 (5), 557–582. doi:10.1164/rccm.201701-0218PP
- Wang, C., de Mochel, N. S. R., Christenson, S. A., Cassandras, M., Moon, R., Brumwell, A. N., et al. (2018). Expansion of Hedgehog Disrupts Mesenchymal Identity and Induces Emphysema Phenotype. *J. Clin. Invest.* 128 (10), 4343–4358. doi:10.1172/jci99435
- Wang, C., Kane, M. A., and Napoli, J. L. (2011). Multiple Retinol and Retinal Dehydrogenases Catalyze All-Trans-Retinoic Acid Biosynthesis in Astrocytes. *J. Biol. Chem.* 286 (8), 6542–6553. doi:10.1074/jbc.M110.198382
- Wang, T., Shen, H., Deng, H., Pan, H., He, Q., Ni, H., et al. (2020). Quantitative Proteomic Analysis of Human Plasma Using Tandem Mass Tags to Identify Novel Biomarkers for Herpes Zoster. *J. Proteomics* 225, 103879. doi:10.1016/j.jprot.2020.103879
- Wang, Z., Yang, M.-Q., Lei, L., Fei, L.-R., Zheng, Y.-W., Huang, W.-J., et al. (2019). Overexpression of KRT17 Promotes Proliferation and Invasion of Non-small Cell Lung Cancer and Indicates Poor Prognosis. *Cmar* 11, 7485–7497. doi:10.2147/cmar.s218926
- Wiggin, O., and Hamel, P. A. (2002). Pax3 Regulates Morphogenetic Cell Behavior *In Vitro* Coincident with Activation of a PCP/non-canonical Wnt-Signaling cascade. *J. Cell Sci.* 115 (Pt 3), 531–541. doi:10.1242/jcs.115.3.531
- Wiśniewski, J. R., Zougman, A., Nagaraj, N., and Mann, M. (2009). Universal Sample Preparation Method for Proteome Analysis. *Nat. Methods* 6 (5), 359–362. doi:10.1038/nmeth.1322
- Wu, M., Wu, Y., Huang, J., Wu, Y., Wu, H., Jiang, B., et al. (2020). Protein Expression Profile Changes of Lung Tissue in Patients with Pulmonary Hypertension. *Peer. J* 8, e8153. doi:10.7717/peerj.8153
- Zeng, H., Li, T., He, X., Cai, S., Luo, H., Chen, P., et al. (2020). Oxidative Stress Mediates the Apoptosis and Epigenetic Modification of the Bcl-2 Promoter via DNMT1 in a Cigarette Smoke-Induced Emphysema Model. *Respir. Res.* 21 (1), 229. doi:10.1186/s12931-020-01495-w
- Zhang, P., Hu, C., Li, Y., Wang, Y., Gao, L., Lu, K., et al. (2018). Vangl2 Is Essential for Myocardial Remodeling Activated by Wnt/JNK Signaling. *Exp. Cell Res.* 365 (1), 33–45. doi:10.1016/j.yexcr.2018.02.012

**Conflict of Interest:** The authors declare that the research was conducted in the absence of any commercial or financial relationships that could be construed as a potential conflict of interest.

Copyright © 2021 Bai, Ye, Wang, Sun, Wang, Yue, Wang, Wu, Yu, Xi and Zhao. This is an open-access article distributed under the terms of the Creative Commons Attribution License (CC BY). The use, distribution or reproduction in other forums is permitted, provided the original author(s) and the copyright owner(s) are credited and that the original publication in this journal is cited, in accordance with accepted academic practice. No use, distribution or reproduction is permitted which does not comply with these terms.



# Management and Thinking on the Treatment of Cancer Patients During the COVID-19

Shuangyue Pan<sup>1,2</sup>, Jiahong Jiang<sup>2</sup>, Zheling Chen<sup>2\*</sup> and Liu Yang<sup>2\*</sup>

<sup>1</sup> The Second Clinical Medical College, Zhejiang Chinese Medical University, Hangzhou, China, <sup>2</sup> Center of Oncology, Department of Medical Oncology, Zhejiang Provincial People's Hospital, People's Hospital of Hangzhou Medical College, Hangzhou, China

## OPEN ACCESS

### Edited by:

Huahao Shen,  
Zhejiang University, China

### Reviewed by:

Wei Zhang,  
Changhai Hospital at Second Military  
Medical University, China  
Daotai Nie,  
Southern Illinois University  
Carbondale, United States  
Xinchun Zhou,  
University of Mississippi Medical  
Center School of Dentistry,  
United States

### \*Correspondence:

Liu Yang  
yangliuqq2003@163.com;  
yangliu@hmc.edu.cn  
Zheling Chen  
383974903@qq.com

### Specialty section:

This article was submitted to  
Molecular Diagnostics  
and Therapeutics,  
a section of the journal  
Frontiers in Molecular Biosciences

**Received:** 27 February 2021

**Accepted:** 20 April 2021

**Published:** 01 July 2021

### Citation:

Pan S, Jiang J, Chen Z and  
Yang L (2021) Management  
and Thinking on the Treatment  
of Cancer Patients During  
the COVID-19.  
Front. Mol. Biosci. 8:673360.  
doi: 10.3389/fmolb.2021.673360

Coronavirus disease-2019 (COVID-19) has spread rapidly around the world and has become a public health emergency of international concern. The weekly epidemiological report issued by the WHO pointed out that new coronavirus variants have appeared in 131 countries and regions, which demonstrates that the current epidemic situation is still severe. As of now, the severe acute respiratory syndrome coronavirus (SARS-CoV-2) has been widespread worldwide for more than one year and poses a serious threat to the health of vulnerable groups such as those with malignancies, the elderly, and the immunocompromised. Compared with the general population, cancer patients with COVID-19 infection are more likely to have serious clinical adverse events, leading to higher mortality. There is no doubt that during the COVID-19 epidemic, whether it is with regards to how to prevent infection or how to continue anti-tumor treatment, cancer patients are in a difficult situation. Meanwhile, an international patient with malignant Hodgkin's lymphoma who was cured after being infected with the new coronavirus surprised us, and it inspires more scientists to explore the relationship between infection, immunity, and tumors. Relevantly, through multi-disciplinary discussion, scientists put forward more new perspectives on the treatment of future tumors and the management of SARS-CoV-2 diseases. In this review, the impact of COVID-19 on cancer patients is discussed in detail and the recommendations for the diagnosis, treatment and management of cancer patients will be put forward under the challenge of the COVID-19 epidemic. Furthermore, the safety and effectiveness of the SARS-CoV-2 vaccine will be discussed, and we will also put forward our insights on cancer immunity.

**Keywords:** COVID-19, SARS-CoV-2, management, cancer patients, vaccine, cancer immunity

## INTRODUCTION

The novel coronavirus disease 2019 (COVID-19) caused by the severe acute respiratory syndrome coronavirus named SARS-CoV-2 occurred in Wuhan, Hubei in December 2019 and has now spread globally (Yu et al., 2020). SARS-CoV-2 virus is an enveloped positive single-stranded RNA virus that can infect both humans and animals (Velavan and Meyer, 2020). Human-to-human transmission has been proven by the infection of 15 medical staff in a Wuhan hospital (Paules et al., 2020). As of Feb 7, 2021, the total number of confirmed cases was 106,277,685 worldwide, and the total number of deaths was 2,316,660 (Real-Time Tracking of New Coronavirus Pneumonia Epidemic, 2021). In a clinical study from China, 81% of the cases were classified as mild pneumonia; 14% of the cases had serious diseases such as dyspnea and decreased blood oxygen saturation and 5% of the cases had respiratory failure, septic shock, or multiple organ failure.

Among them, the overall case fatality rate was 2.3% (1,023 of 44,672 confirmed cases). However, the case fatality rate of patients aged 80 and over has increased to 14.8% (The Novel Coronavirus Pneumonia Emergency Response Epidemiology Team, 2020).

Cancer patients are commonly in a state of systemic immunosuppression due to anti-tumor therapies (such as chemotherapy or radiotherapy), so they are more susceptible to be infected with the SARS-CoV-2 virus (Liang et al., 2020). Nevertheless, anti-tumor therapy is essential for cancer patients to control their condition. Therefore, it is challenging to strengthen the management of anti-tumor treatment while preventing infection. Recently, the vaccination of the SARS-CoV-2 virus has given us full confidence in defeating COVID-19, and the case of a tumor patient cured after being infected with the SARS-CoV-2 virus has triggered our thinking.

This review aims to discuss approaches of management for cancer patients during the pandemic and provide our insights on the cure of tumor patient infected with the SARS-CoV-2 virus.

## CANCER PATIENTS DURING THE COVID-19

### Morbidity and Mortality of Cancer Patients

On the one hand, cancer patients are generally malnourished and have lower ability to fight SARS-CoV-2 virus; on the other hand, cancer patients have immunodeficiency due to the systematic treatment. These factors make cancer patients more susceptible to SARS-CoV-2 virus, and the mortality rate will be higher than normal (Wang and Zhang, 2020). A retrospective study in Zhongnan Hospital of Wuhan University showed that the infection rate of SARS-CoV-2 in cancer patients is 0.79% (12 of 1,524 patients; 95%CI: 0.3–1.2%). However, the cumulative incidence of all COVID-19 cases reported in Wuhan is 0.37% (41,152 of 11,081,000 cases; data cut off on February 17, 2020) (Yu et al., 2020). Cancer patients infected with the SARS-CoV-2 virus have more risk factors than patients without cancer (Heathcote et al., 2020). A study collected and analyzed 2007 confirmed cases of COVID-19 in 575 hospitals in China, of which 1,590 cases of infection are valid data. The study found that patients with cancer are older than patients without cancer (average age 63.1 years old [SD 12.1] vs 48.7 years old [16.2]), more likely to have a history of smoking (four [22%] of 18 patients vs 107 [7%] of 1,572 patients), had more polypnea (eight [47%] of 17 patients vs 323 [23%] of 1,377 patients), and more severe baseline CT manifestation (17 [94%] of 18 patients vs 1,113 [71%] of 1,572 patients) (Liang et al., 2020). These risk factors directly cause the mortality of cancer patients infected with the SARS-CoV-2 virus to be higher than that of the healthy population. A multi-centural study including 105 cancer patients and 536 age-matched non-cancer patients confirmed with COVID-19 showed that compared with COVID-19 patients without cancer, cancer patients have higher observed mortality (OR 2.34, 95% CI [1.15, 4.77];  $p = 0.03$ ), and a higher ICU

hospitalization rate (OR 2.84, 95% CI [1.59, 5.08];  $p < 0.01$ ) (Dai et al., 2020).

### Differentiation of Cancer Patients and COVID-19

Cancer patients have complex conditions, with many non-specific clinical symptoms and signs. For example, lung cancer patients' own lung manifestations, tumor fever, immune-related pneumonia, and other manifestations. During this special period, it is necessary to actively differentiate from COVID-19. Multiple studies have shown that the main clinical manifestations of COVID-19 are fever, cough, and dyspnea (Huang et al., 2020; Jiang et al., 2020; Zhang L. et al., 2020). Although non-cancer and cancer patients with COVID-19 have similar clinical manifestations, a study screened 13,077 SARS-CoV-2 patients and finally compared the clinical characteristics of 232 cancer patients and 519 matched cancer-free patients. Studies have shown that cancer patients infected with the SARS-CoV-2 virus were more likely to have dyspnea and CT scans showed that ground-glass opacity and patchy opacity were more common. Furthermore, the pro-inflammatory cytokines of cancer patients including TNF- $\alpha$ , IL-6, and IL-2R were higher than those of patients without cancer. The lymphocytes, CD4+ T cells, CD8+ T cell counts, and the ratio of CD4+ T cells to CD8+ T cells in cancer patients decreased more significantly (Tian et al., 2020). Special attention should be paid to the appearance of any of these characteristics to minimize the risk of underdiagnosing cancer patients with COVID-19 infection.

In general, the fever of tumor patients can be divided into tumor fever, drug fever, and infection. Tumor fever refers to the response of the immune system to tumor necrosis and stress factors produced by tumors which is generally  $\leq 38.5^{\circ}\text{C}$  with no inducement and lasts for a long time. Experimental treatment with antibiotics is ineffective (Pasikhova et al., 2017). Drug fever means that fever occurs during medication and stops after drug withdrawal. The median time of fever caused by antineoplastic drugs is about 0.5 days after administration (Patel and Gallagher, 2010). Fever caused by infection usually has a higher temperature and can be reflected by blood routine tests.

All patients diagnosed with COVID-19 have varying degrees of lung abnormalities, which can be seen in chest computed tomography (CT) imaging (Huang et al., 2020; **Figure 1**). Most cases of COVID-19 showed bilateral parenchymal ground-glass opacity (GGO) or consolidative pulmonary opacity on CT scans, and the enlargement and consolidation of GGO usually indicate the progression of COVID-19 (Chung et al., 2020). The characteristics of COVID-19 also include reticular pattern, linear subpleural opacity, bronchial dilatation, centrilobular nodules and tree-in-bud (Zhang Y. J. et al., 2020). Through the imaging performance of CT, we can distinguish lung cancer from COVID-19 through the following points. First of all, most COVID-19 patients have bilateral lesions while most cancer patients have unilateral lung lesions. Secondly, most COVID-19 patients have more than one type of lung lesion, while lung cancer patients tend to have either pure GGO or mixed GGO. What is more, COVID-19 shows more patchy lesions, while lung cancer shows more

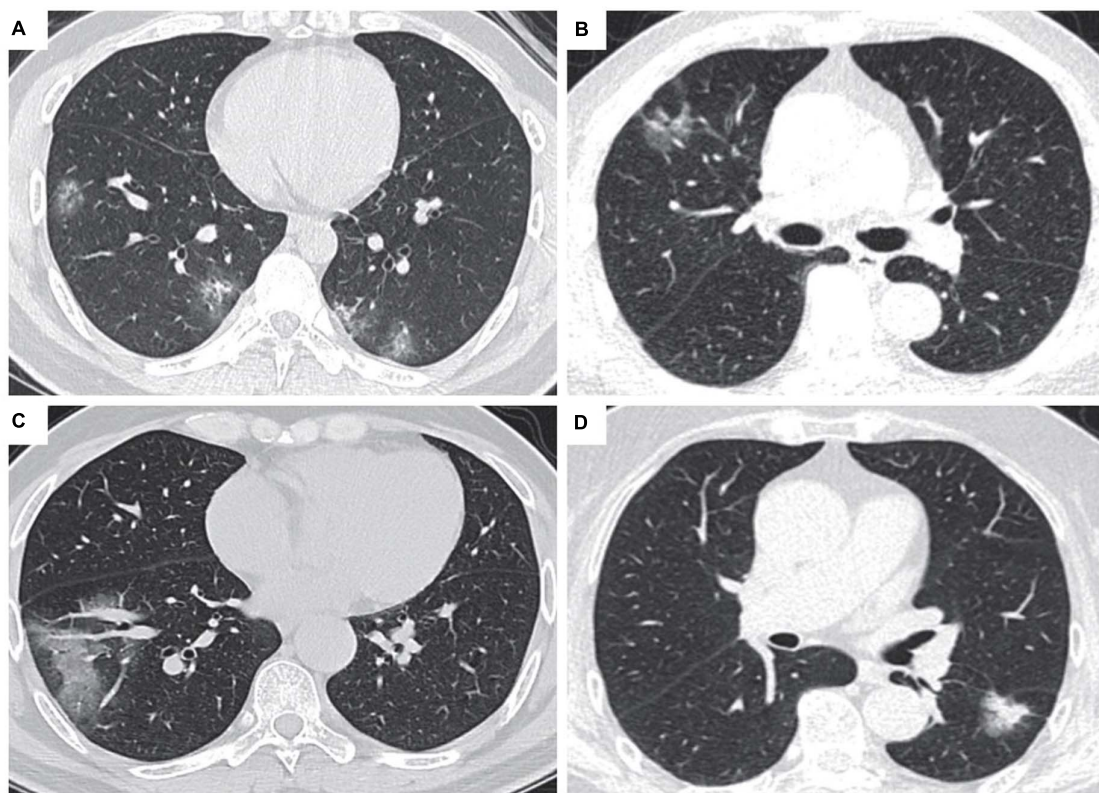


**FIGURE 1 |** CT images of lung cancer patients and COVID-19 (Transl Lung Cancer Res.2020 Aug;9(4):1516-1527.doi: 10.21037/tlcr-20-892). **(A)** CT scan of a patient diagnosed with COVID-19: The lesion is GGO, and there is no sign of pleural retraction or vascular convergence. **(B)** CT scan of a patient diagnosed with lung cancer, with pleural retraction and cystic change. **(C)** CT scan of a patient diagnosed with COVID-19, the lesion showed patchy turbidity, irregular shape, and no pleural retraction. **(D)** CT scan of a patient diagnosed with lung cancer, with pleural retraction, lobulated sign, and spiculate protuberance.

oval lesions (Zhang Y. J. et al., 2020; **Table 1**). There are many types of lung cancer that various imaging manifestations may reveal, therefore, we need to use RT-PCR and next-generation sequencing methods applied to respiratory tract specimens to assist identification when necessary.

## Is Anti-tumor Treatment a Contraindication During the COVID-19?

Cancer patients are at increased risk of death and serious clinical events due to COVID-19 infection. However, risk of

adverse events does not seem to be increased by cancer therapies (Heathcote et al., 2020). Between April 15 and 26, 2020, a total of 1,227 tumor patients were tested for SARS-CoV-2 using RT-qPCR in the tumor clinic, and 78 (6.4%) were positive. Among them, 75 (96.2%) were asymptomatic infections. Fourteen cancer patients out of 75 asymptomatic infections received chemotherapy or immunotherapy ( $\pm 4$  weeks of SARS-CoV-2 test), 48 (61.5%) of 78 patients who tested positive received glucocorticoid combination therapy. None of the patients with asymptomatic infection had unexpected complications caused by SARS-CoV-2 infection. These data indicate that the incidence of symptoms due to COVID-19 is relatively low among patients treated with chemotherapy and other immunosuppressive agents (such as glucocorticoids). Therefore, whether anti-tumor therapy is a contraindication during the epidemic is still inconclusive (Hempel et al., 2020).

Studies have shown that the risk of death in patients infected with COVID-19 is significantly related to the increase in patient age (odds ratio 9.42 [95% CI 6.56–10.02];  $p < 0.0001$ ) and significant correlation with other comorbidities, such as hypertension (1.95 [1.36–2.80];  $p < 0.001$ ) and cardiovascular disease (2.32 [1.47–3.64]). Anti-tumor treatment does not increase the risk of death from new coronary pneumonia in cancer patients (Lee et al., 2020). Therefore, for cancer patients,

**TABLE 1 |** CT differentiation of lung cancer and COVID-19.

	Lung cancer	COVID-19
Lesion(in most cases)	Unilateral	Bilateral
Lesion form	Oval lesions	Patchy lesions
Involved lobes	Less	More
Types of lung disease	Pure GGO or mixed GGO	More than one
Characteristic performance	lobulated signs, pleural retraction, cystic changes and signs of vascular convergence	Air bronchography, reticular pattern, subpleural linear opacity, bronchiectasis, lobular nodules and tree-in-bud



risk-benefit assessment must be carried out. If the benefits outweigh the risks, cancer treatment should continue (Gosain et al., 2020; Zhao Q. et al., 2020; **Figure 2**).

Patients at the priority level 1 do not need to go to the hospital for treatment unless necessary, and can communicate with doctors through telemedicine and other methods; Patients at the priority level 2 can delay treatment appropriately; patients at the priority level 3 should go to the hospital for treatment with protective measures.

## Cancer Patients With Different Treatment Modalities

### Cancer Patients Undergoing Surgery

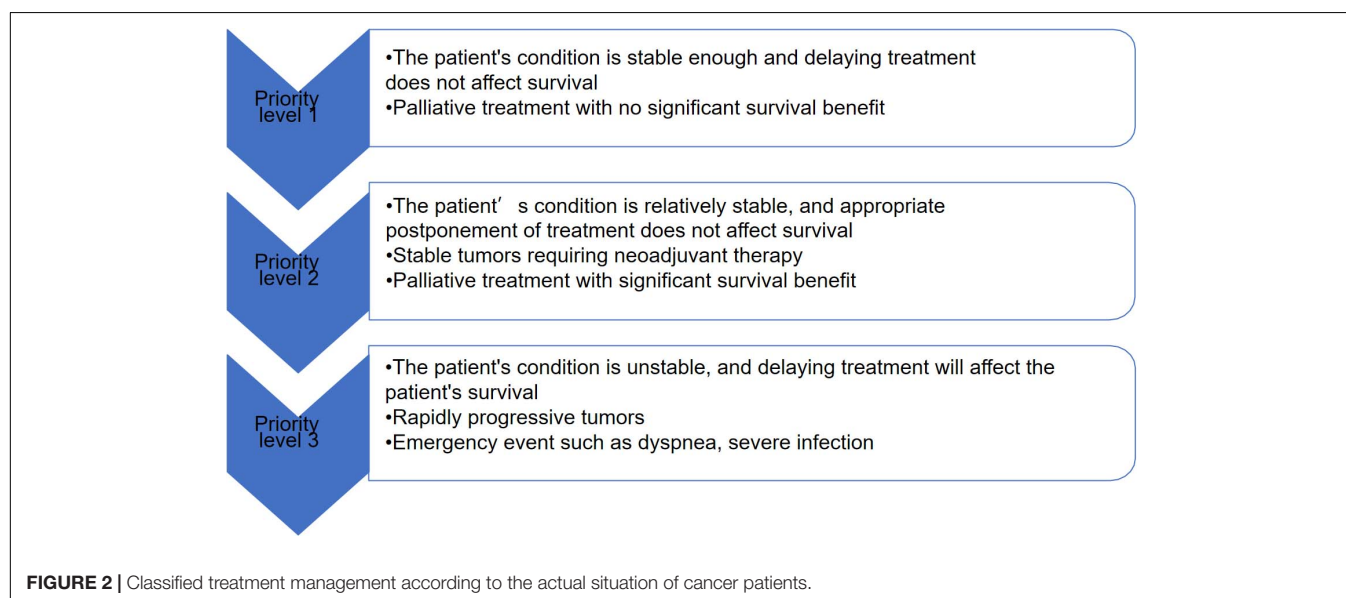
During the COVID-19 pandemic, patients with tumors requiring surgery should be strictly screened for infection with the SARS-CoV-2 Virus, and a comprehensive assessment should be made based on the patient's overall condition as to whether surgery can be performed to avoid serious adverse events. An international study conducted in 235 hospitals in 24 countries/regions included all surgical patients who were confirmed to have SARS-CoV-2 infection. The primary outcome measure was the 30-day mortality rate after surgery, and the secondary outcome measure was pneumonia, acute respiratory distress syndrome, or accidental ventilation after surgery. Among 1,128 patients undergoing surgery, 294 patients (26.1%) were confirmed to have SARS-CoV-2 infection before surgery, their 30-day mortality rate was 23.8% (268 out of 1,128). Pulmonary complications occurred in 577 (51.2%) of 1,128 patients. The 30-day mortality rate of these patients was 38% (219 of 577), accounting for 82.6% of all deaths (219 of 265) (Nepogodiev et al., 2020). Therefore, it is necessary to carefully consider the surgical operation of cancer patients during the epidemic.

If cancer patients do not receive surgery in time, how long will the extension affect the survival rate or the probability of complete resection? Studies have shown that for cancers treated

with surgery first, the median safe postponement period (SPP) is 3 weeks which is 6 weeks from diagnosis. For 48% of cancer types, the SPP was at least 4 weeks. For patients who received neoadjuvant therapy such as chemotherapy or radiotherapy, the median SPP was 8 weeks which is 26 weeks from diagnosis. For 76% of cancer types, the SPP is at least 6 weeks (Kiran and Turaga, 2020). Through this study, we can find that most cancer operations can be postponed for at least 4 weeks without significantly affecting the survival of the patient. The tumor will not progress significantly, and there is no significant difference in the probability of complete tumor resection.

### Cancer Patients Undergoing Routine Chemotherapy

During the COVID-19 pandemic, the main concern of patients receiving chemotherapy was the decrease in anti-tumor efficacy due to the interruption of chemotherapy. While we pay attention to the adverse effects of the epidemic on the delay of chemotherapy for tumor patients, we should also treat the adjustment of chemotherapy regimens rationally (Zhao Z. et al., 2020). Based on the fact that anti-cancer therapy may bring greater risks, some patients may voluntarily choose treatments with lower potential efficacy but a lower degree of myelosuppression (Battershill, 2006). Patients who receive conventional chemotherapy can consider switching from intravenous chemotherapy to oral anticancer drugs, which can reduce the number of visits to the hospital and thus reduce the risk of infection (Gosain et al., 2020). In addition, with the advent of elastic pumps, chemotherapy at home has become more and more common (Shereen and Salman, 2019). In order to reduce the duration of exposure in the hospital, the hospital pharmacy department can deliver medicine to patients by express delivery (Willan et al., 2020). The treatment of lung cancer patients during the COVID-19 pandemic can give us some suggestions: some scholars have proposed that multiple variables should be considered when formulating a diagnosis and treatment plan for lung cancer patients, including virus prevalence, capacity of



local medical institutions, patient infection risk, cancer status, patient comorbidities, age, etc. After considering these factors, the treatment of lung cancer patients is divided into five groups “Should be started when Possible,” “Should not be stopped without justification,” “Can be given preferentially,” “Can be withheld or delayed after careful consideration,” “Should not be started without justification” (Banna et al., 2020). Under the guidance of oncologists, the treatment strategy should be adjusted appropriately according to the progress of tumor patients, the stage and effect of anti-tumor therapy, local epidemic situation, and so on (Zhao Z. et al., 2020).

### Cancer Patients With Radiotherapy

Studies have shown that delayed radiotherapy and interruption of radiotherapy may contribute to inferior local control and overall survival of cancer patients (Yao et al., 2018). Radiotherapy requires specific equipment, and community hospitals have no extra resources to reserve linear accelerators, simulators or mold rooms for patients, the radiotherapy center cannot disperse patients, therefore it will be in a high-risk area (Mukherjee et al., 2003). During the outbreak of COVID-19 in Wuhan, the department of radiotherapy center has taken the following measures: divide the radiotherapy center into different infection control areas and provide different levels of protection; implement daily symptom testing standards for patients receiving treatment; design and implement a revised radiotherapy workflow, special treatment area cleaning and disinfection policies and procedures (Wei et al., 2020).

### Cancer Patients Receiving Immunotherapy

Immune checkpoint inhibitors play an anti-tumor effect by regulating the body's own immune response. Checkpoint antibody inhibitors, such as anti-PD-1/PD-L1, are novel inhibitors that function as tumor suppressors by regulating immune cell-tumor cell interaction (Alsaab et al., 2017). The research team analyzed a total of 800 patients with COVID-19 diagnosed with cancer and symptoms. Among them, 412 (52%) patients had mild COVID-19 symptoms; eventually 226 patients (28%) died. The research team found that in the past 4 weeks, patients using immunotherapy, hormone therapy, targeted therapy, and radiation therapy had no significant impact on mortality (Lee et al., 2020). However, research results published by the famous Memorial Sloan-Kettering Cancer Center (MSKCC) in New York, United States revealed that cancer patients who use immunotherapy (mainly PD-1/PD-L1 inhibitors) were more dangerous after infection with SARS-CoV-2 virus and required a higher proportion of hospitalization, the rate of severe pneumonia was also higher (Robilotti et al., 2020). Cancer immunotherapy can effectively prolong the survival period of cancer patients but also cause some adverse reactions such as organ inflammation, the most common of which is immune-related pneumonia. Distinguishing between COVID-19 pneumonia and immune-related pneumonia is a diagnostic challenge (Suresh et al., 2018). The clinical manifestations of immune-related pneumonia and COVID-19 are similar and they can both show symmetrical patchy GGO and consolidation area in CT imaging. Therefore, a diagnostic algorithm is proposed

to distinguish immune-related pneumonia and COVID-19. The first step is RT-PCR screening. Secondly, laboratory examination and CT imaging features are helpful for identification. There is no obvious specificity in the hemogram of immune-related pneumonia, just CRP and ESR are often increased. In the early stage of COVID-19 patients, peripheral blood leukocytes were normal or decreased, lymphocyte count decreased, CRP and ESR increased in most patients, D-dimer and liver enzymes, LDH, muscle enzymes, myoglobin, and troponin increased in severe patients (Kattan et al., 2020; Wu et al., 2020). Besides, further bronchoscopy is needed if necessary (Dumoulin et al., 2020).

### Cancer Patients Participating in Clinical Trials

During the COVID-19 period, individualized management of clinical trials should be carried out to maximize the protection of patients' interests. Effectively guard against COVID-19 and ensure the scientific nature of clinical experiments at the same time. The Food and Drug Administration (FDA) has issued guidelines for institutions to protect trial participants and administer investigational products by changing monitoring methods (FDA, 2020). The progress of clinical trials may be slowed down due to the impact of the epidemic, because clinical trial subjects have strict standards and time limits for drug administration, efficacy evaluation, safety evaluation, follow-up, and so on. It requires the cooperation of subjects, researchers, sponsors, clinical research coordinators, and other relevant participants under the supervision of ethics. The clinical trial activities during the COVID-19 period should be tailored to the changing epidemic situation. Suspension of some non-therapeutic intervention trials could be considered, and clinical trials that continue after discussion will continue to obtain all the tests and data points needed for the study (Gosain et al., 2020). The researchers can manage according to the different dosage forms used by the subjects, subjects taking oral drugs can be followed up remotely by telephone or Internet, and the researchers can send the drugs to the subjects by express delivery.

## CANCER PATIENTS INFECTED WITH SARS-COV-2 VIRUS

### A Patient Diagnosed With Malignant Hodgkin's Lymphoma Was Cured After Being Infected With the SARS-CoV-2 Virus

Recently, two British doctors reported a special case: a 61-year-old man diagnosed with Hodgkin's lymphoma [EBV viral polymerase chain reaction (PCR) 4,800 copies/ml;  $\log^{10}3.68$ ] infected with SARS-CoV-2 virus and was not given corticosteroids and immunochemotherapy. After 4 months, PET CT showed widespread resolution of the lymphadenopathy and the EBV viral PCR had also fallen to 413 copies/ml ( $\log^{10}2.62$ ) (Challenor and Tucker, 2021). Researchers suspected that the SARS-CoV-2 virus stimulated an anti-tumor immune response, killing the virus while also killing cancer cells. This is not the only case that the tumor is cured after infection. The case in 2012

reported that a 67-year-old woman with lymphoma infected with pneumonia and colitis and the tumor also disappeared completely (Buckner et al., 2012). Although lymphoma does not represent all tumors, it does give us a great inspiration. In fact, there have been similar records dating back hundreds of years. Some doctors even tried to inject pathogens into cancer patients to induce fever to treat cancer. This is actually the original form of immunotherapy. In recent years, PD-1 inhibitors, CTLA-4 inhibitors, CAR-T therapy, CAR-NK therapy, and other modern immunotherapies have been successful, bringing hope to many cancer patients. The idea that activating the immune system can fight cancer has been widely accepted.

## The Contradiction Between the Treatment of Infectious Diseases and Anti-tumor Treatment

Infection is one of the most common complications of anti-tumor therapy. Anti-tumor treatment destroys the patients' immune system, resulting in neutropenia which can lead to more severe infection. The use of antiviral therapy in cancer patients infected with COVID-19 remains controversial. Among cancer patients infected with COVID-19 in a case report, 20 patients (71.4%) were treated with antiviral drugs empirically; 9 patients (32.1%) received a combination of antiviral drugs, 15 patients (53.6%) received systemic corticosteroid therapy, 12 patients (35.7%) received intravenous immunoglobulin. The data from the case did not report that the patient population had benefited from it. Instead, of the 6 cancer patients who received anti-tumor treatment within 14 days of being diagnosed with COVID-19, 5 (83%) had serious incidents (Zhang L. et al., 2020). Although the available information is very limited, it is not recommended to use anticancer drugs and antiviral treatments at the same time outside of clinical trials to avoid unexpected pharmacokinetic interactions and toxicity (Raymond et al., 2020).

## The Impact of Infection on Tumor Prognosis

As mentioned above, a patient with lymphoma had tumor regression after being infected with the SARS-CoV-2 virus. The case of cancer patients whose tumor disappeared after infection has been reported many times. A review of past reports found that self-healing was usually related to acute infections such as bacteria and viruses, fever, and immune stimulation (Buckner et al., 2012; Challenor and Tucker, 2021). The idea of stimulating the human immune response to treat cancer and other diseases has been proven in trials.

Vaccines are a typical example of preventing the invasion of microorganisms by stimulating the human immune response. Bacille Calmette-Guerin (BCG), a live attenuated strain of *Mycobacterium bovis*, is the first live-attenuated vaccine used in humans. BCG provides 80% protection against severe and disseminated tuberculosis in children and can also reduce the risk of adult tuberculosis (Ritz et al., 2008). In the 1980s, BCG became the first choice for the treatment of early *in situ* bladder cancer. As long as the patient's immune system is normal, the tumor burden is small, the BCG vaccine can directly contact

the tumor, and the dosage of the drug is sufficient, the BCG vaccine can eliminate the tumor in 70% of patients (Babaian, 2021). Researchers have found that urothelial cells and immune system cells both play a crucial role in the anti-tumor treatment of BCG. BCG vaccine can stimulate the body's immune response through its internalization, bladder cancer cells up-regulate the expression of MHC class II and ICAM-1 and secrete various cytokines, including IL-6. In addition to bladder cancer cells, dendritic cells may also play a role in the recruitment of immune cells, initially granulocytes, then macrophages and lymphocytes (Redelman-Sidi et al., 2014).

In addition to BCG, oncolytic viruses can achieve anti-tumor effects through the dual mechanism of selective killing of tumor cells and inducing systemic anti-tumor immunity. Oncolytic viruses are attenuated viruses that infect tumor cells to enhance the body's natural immune response. Oncolytic viruses have direct and indirect toxic effects on tumor cells, such as autolysis, honing of immune cells, destruction of vascular supply, and enhancement of other auxiliary anti-cancer therapies (Russell et al., 2012). Currently, the oncolytic virus treatment drug talimogene laherparepvec (T-Vec or Imlygic) for metastatic melanoma has been approved by the FDA.

Therefore, the pathogenic bacterium is not completely harmful to cancer patients, and there are many clinical applications that use the properties of pathogenic bacterium to bring cancer patients benefits such as the use of inactivated pathogenic bacterium to prepare vaccines; the use of genetically engineered viruses as carriers for gene therapy; using viruses to target cancer, etc.

## CANCER PATIENTS AND SARS-COV-2 VACCINES

In order to control the spread of the SARS-CoV-2 virus in a timely and effective manner, researchers have made efforts to develop vaccines (Hodgson et al., 2021). On November 9, 2020, Pfizer and BioNTech announced that the vaccine BNT162b2 against COVID-19 had succeeded in the Phase 3 study. Interim analysis showed that compared with placebo, two vaccination of the mRNA vaccine at 21 days intervals can reduce the infection rate of the symptomatic new coronavirus SARS-CoV-2 by 90% (Pfizer, 2020). The other clinical trial in the United States showed that the effective rate of mRNA-1273 vaccine in preventing COVID-19 diseases was 94.1% (Baden et al., 2021). At present, five COVID-19 vaccines have been approved for marketing or emergency use in China, including three inactivated vaccines and one adenovirus vector vaccine. Vaccines are essential to prevent COVID-19 and to protect patients with high-risk complications. As of April 1, 2021, more than 590 million people have been vaccinated worldwide (Caixin, 2021).

Cancer patients and their families are very concerned about a question: Can cancer patients get the COVID-19 vaccine? Due to the low immune function of cancer patients, the live microorganisms in the live attenuated vaccines will increase the risk; the live vaccines may cause excessive immunity in patients receiving immunotherapy due to the activation of immunity in

the body. Therefore, according to the latest NCCN guidelines, live attenuated vaccines cannot be used for tumor patients with weakened immune function (NCPGI, 2020). However, despite the fact that the vaccines marketed in China are inactivated, patients with malignant tumors are still listed as one of the contraindications due to lack of clinical data. Therefore, it is still necessary to strengthen the management of cancer patients for hospital departments and cancer patients should also pay attention to personal management.

## COVID-19 PREVENTION AND CONTROL MANAGEMENT IN HOSPITAL DEPARTMENTS

All departments of the hospital must provide patients with preventive and control measures, and each department must establish a COVID-19 prevention program within the department, which is composed of the core team of the department and the supervisors of each work link. It is essential to provide infection prevention training and education to all medical staff in the department and develop a clear process that everyone can strictly follow and implement (The Healthcare Infection Control Practices Advisory Committee [HICPAC], 2018). For outpatients, first of all, the number of outpatients

should be controlled to the least level for reducing exposure to infection. Secondly, necessary temperature tests, emphasizing the importance of wearing masks and hand hygiene are effective measures to reduce infections (Al-Shamsi et al., 2020). It is recommended that qualified hospitals actively develop telehealth strategies to provide health care and reduce personnel gathering and unnecessary cross-infection (Centers for Disease Control and Prevention, 2020; Zhao Q. et al., 2020). For hospitalized cancer patients, strict screening must be carried out before anti-cancer treatment (Figure 3). Data from China shows that chest CT is more sensitive than RT-PCR for diagnosing COVID-19, therefore, the screening of the cancer patients for infection requires two examinations of chest CT scan and RT-PCR to consolidate the diagnosis (Ai et al., 2020).

## PERSONAL MANAGEMENT AND SOCIAL ASSISTANCE FOR CANCER PATIENTS

Cancer patients should try to avoid going in and out of public places which is more likely to be exposed to SARS-CoV-2 virus, and ideally wear a mask when in close contact with others to prevent spread of respiratory secretions when they are coughing, sneezing, or talking (Centers for Disease Control and Prevention, 2020). Enhancing immunity and reducing the

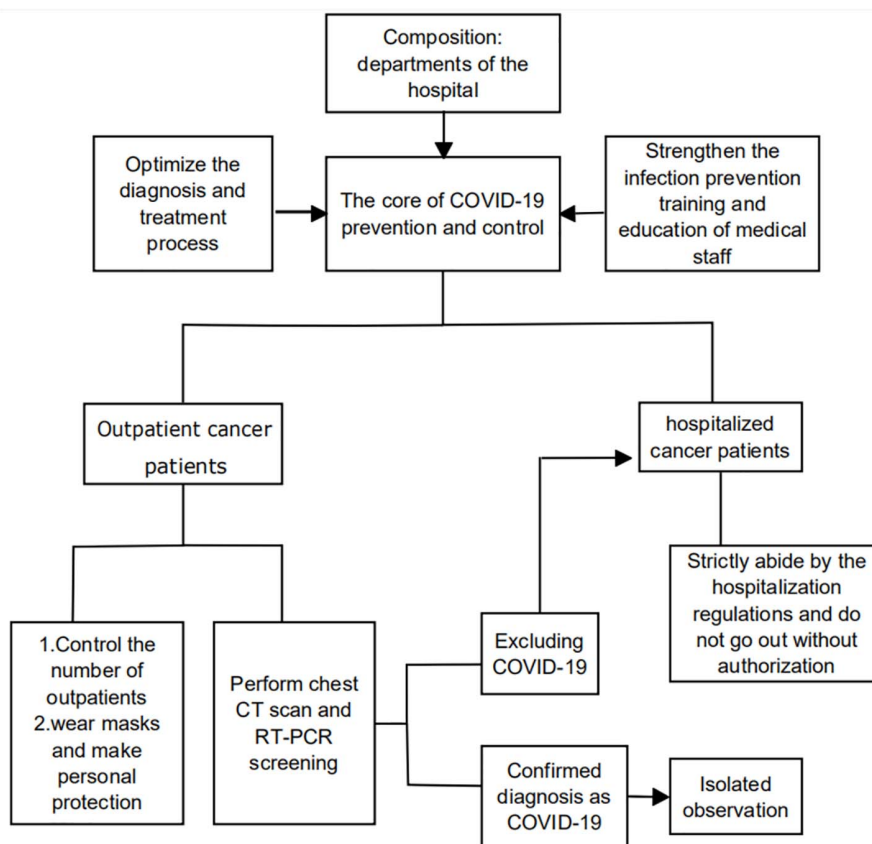


**FIGURE 3 |** COVID-19 prevention and control management in hospital departments.



risk of exposure are important principles for cancer patients to prevent SARS-CoV-2 infections. Supplementation with some of dietary components such as dietary protein, omega-3 fatty acids, vitamin A can improve the conditions of cancer patients and enhance immunity (BourBour et al., 2020). Besides, the psychological bearing capacity of cancer patients is lower than that of normal people, coupled with social distance measures, isolation measures, and visitor restrictions, which limit the mental strength of cancer patients from family support (Al-Shamsi et al., 2020). We believe that while doing a good job in the prevention and control of the epidemic situation, we also need to pay attention to the mental health of tumor patients, and the research and application of related assessment, intervention and treatment measures is extremely urgent. Therefore, hospitals and medical workers should provide mental support to patients, and psychosocial workers should make maximum use of available resources to intervene patients to meet the continuous needs of patients and their families (Wang et al., 2020).

## USE TELEMEDICINE TO ACHIEVE FULL MANAGEMENT OF CANCER PATIENTS

Telemedicine has been shown to reduce medical costs and provide health care to populations with limited access to medical care (Sirintrapun and Lopez, 2020; Tashkandi et al., 2020). Examples of successful telemedicine in oncology include chemotherapy monitoring, symptom management, survival care, palliative care, and clinical trials (Sirintrapun and Lopez, 2020). It has been confirmed in several clinical trials that the outcome of telemedicine is similar to that of face-to-face care (Sirintrapun and Lopez, 2020). We can reduce the number of hospital visits during the COVID-19 pandemic by replacing some clinics with virtual clinics (via videoconferencing or telephone calls) (Tashkandi et al., 2020). In addition, we can also use store-and-forward methods, such as the short message service (SMS), email consultation, or regularly collect and upload data through

networked devices to monitor symptoms and signs (McLean et al., 2013). Patients who do not have access to active treatment during the COVID-19 pandemic are particularly suitable for telemedicine. However, virtual telemedicine management is a developing tool to provide medical services to cancer patients under specific conditions. The main limitations of telemedicine include the jurisdiction of medical practice, restrictions on physical examination, and problems related to telemedicine reimbursement, etc. (Sirintrapun and Lopez, 2020).

## CONCLUSION

The COVID-19 pandemic has caused a huge public health crisis, which has brought tremendous pressure to medical staff and also brought unprecedented challenges to the treatment and management of cancer patients. This review provides detailed suggestions for dealing with COVID-19 from different aspects to help cancer patients affected by the epidemic. The development of the epidemic is very rapid, far beyond our imagination. Therefore, clinicians and medical personnel must strictly follow the epidemic prevention and control measures and modify or adjust the recommendations provided here as needed.

## AUTHOR CONTRIBUTIONS

ZC and LY contributed to the conception and design of the work and data processing and analysis. ZC and SP performed the studies. ZC and SP prepared the majority of the manuscript and LY revised it critically. All authors have given final approvals to the version to be published.

## FUNDING

This work was supported by the National Natural Science Foundation of China (Nos. 81972455 and 81802623).

## REFERENCES

- Ai, T., Yang, Z., Hou, H., Zhan, C., Chen, C., Lv, W., et al. (2020). Correlation of chest CT and RT-PCR testing in Coronavirus. Disease 2019 (COVID-19) in China: a report of 1014 cases. *Radiology* 296:642.
- Alsaab, H. O., Sau, S., Alzhirani, R., Tatiparti, K., Bhise, K., Kashaw, S. K., et al. (2017). PD-1 and PD-L1 checkpoint signaling inhibition for cancer immunotherapy: mechanism, combinations, and clinical outcome. *Front. Pharmacol.* 8:561. doi: 10.3389/fphar.2017.00561
- Al-Shamsi, H. O., Alhazzani, W., Alhurairi, A., Coomes, E. A., Chemaly, R. F., Almuhamma, M., et al. (2020). A practical approach to the management of cancer patients during the novel Coronavirus disease 2019 (COVID-19) pandemic: an international collaborative group. *Oncologist* 25:e0936-45.
- Babaian, K. N. (2021). *Bacillus Calmette-Guérin Immunotherapy for Bladder Cancer Overview of BCG Immunotherapy*. Cham: Springer.
- Baden, L. R., El Sahly, H. M., Essink, B., Kotloff, K., Frey, S., Novak, R., et al. (2021). Efficacy and safety of the mRNA-1273 SARS-CoV-2 vaccine. *N. Engl. J. Med.* 384, 403–416.
- Banna, G., Curioni-Fontecedro, A., Friedlaender, A., and Addeo, A. (2020). How we treat patients with lung cancer during the SARS-CoV-2 pandemic: primus non nocere. *ESMO Open* 4:e000785. doi: 10.1136/esmoopen-2020-000785
- Battershill, P. M. (2006). Influenza pandemic planning for cancer patients. *Curr. Oncol.* 13, 119–120. doi: 10.3390/curroncol13040012
- BourBour, F., Mirzaei Dahka, S., Gholamalizadeh, M., Akbari, M. E., Shadnough, M., Haghighi, M., et al. (2020). Nutrients in prevention, treatment, and management of viral infections; special focus on Coronavirus. *Arch. Physiol. Biochem.* 9, 1–10. doi: 10.1080/13813455.2020.1791188
- Buckner, T. W., Dunphy, C., Fedoriw, Y. D., van Deventer, H. W., Foster, M. C., Richards, K. L., et al. (2012). Complete spontaneous remission of diffuse large B-cell lymphoma of the maxillary sinus after concurrent infections. *Clin. Lymphoma Myeloma Leuk.* 12, 455–458. doi: 10.1016/j.clml.2012.06.007
- Caixin (2021). Available online at: <https://opinion.caixin.com/2021-04-02/101685017.html>. (accessed April 2, 2021).
- Centers for Disease Control and Prevention (2020). *Interim Infection Prevention and Control Recommendations for Healthcare Personnel during the Coronavirus Disease 2019 (COVID-19) Pandemic*. Atlanta, GE: Centers for Disease Control and Prevention.
- Challenor, S., and Tucker, D. (2021). SARS-CoV-2-induced remission of Hodgkin lymphoma. *Haematology* 192:415. doi: 10.1111/bjh.17116

- Chung, M., Bernheim, A., Mei, X., Zhang, N., Huang, M., Zeng, X., et al. (2020). CT imaging features of 2019 novel Coronavirus (2019-nCoV). *Radiology* 295, 202–207.
- Dai, M., Liu, D., Liu, M., Zhou, F., Li, G., Chen, Z., et al. (2020). Patients with Cancer appear more vulnerable to SARS-CoV-2: a multicenter study during the COVID-19 Outbreak. *Cancer Discov.* 10, 783–791.
- Dumoulin, D. W., Gietema, H. A., Paats, M. S., Hendriks, L. E. L., and Cornelissen, R. (2020). Differentiation of COVID-19 pneumonitis and ICI induced pneumonitis. *Front. Oncol.* 10:577696. doi: 10.3389/fonc.2020.577696
- FDA (2020). *FDA Guidance on Conduct of Clinical Trials of Medical Products During COVID-19 Pandemic*. Silver Spring: FDA.
- Gosain, R., Abdou, Y., Singh, A., Rana, N., Puzanov, I., and Ernstoff, M. S. (2020). COVID-19 and cancer: a comprehensive review. *Curr. Oncol. Rep.* 22:53.
- Heathcote, L. C., Zion, S. R., and Crum, A. J. (2020). Cancer survivorship—considering mindsets. *JAMA Oncol.* 6, 1468–1469. doi: 10.1001/jamaoncol.2020.2482
- Hempel, L., Piehler, A., Pfaffl, M. W., Molnar, J., Kirchner, B., Robert, S., et al. (2020). SARS-CoV-2 infections in cancer outpatients—Most infected patients are asymptomatic carriers without impact on chemotherapy. *Cancer Med.* 9, 8020–8028. doi: 10.1002/cam4.3435
- Hodgson, S. H., Mansatta, K., Mallett, G., Harris, V., Emary, K. R. W., and Pollard, A. J. (2021). What defines an efficacious COVID-19 vaccine? A review of the challenges assessing the clinical efficacy of vaccines against SARS-CoV-2. *Lancet Infect. Dis.* 21:e0026–35.
- Huang, C., Wang, Y., Li, X., Ren, L., Zhao, J., Hu, Y., et al. (2020). Clinical features of patients infected with 2019 novel coronavirus in Wuhan, China. *Lancet* 395, 497–506.
- Jiang, F., Deng, L., Zhang, L., Cai, Y., Cheung, C. W., and Xia, Z. (2020). Review of the clinical characteristics of Coronavirus disease 2019 (COVID-19). *J. Gen. Intern. Med.* 35, 1545–1549.
- Kattan, J., Kattan, C., and Assi, T. (2020). Do checkpoint inhibitors compromise the cancer patients' immunity and increase the vulnerability to COVID-19 infection? *Immunotherapy* 12, 351–354. doi: 10.2217/imt-2020-0077
- Kiran, S. G., and Turaga, K. (2020). Are we harming cancer patients by delaying their cancer surgery during the COVID-19 pandemic? *Ann. Surg.* doi: 10.1097/SLA.0000000000003967
- Lee, L. Y. W., Cazier, J.-B., Angelis, V., Arnold, R., Bisht, V., Campton, N. A., et al. (2020). COVID-19 mortality in patients with cancer on chemotherapy or other anticancer treatments: a prospective cohort study. *Lancet* 395, 1919–1926.
- Liang, W., Guan, W., Chen, R., Wang, W., Li, J., Xu, K., et al. (2020). Cancer patients in SARS-CoV-2 infection: a nationwide analysis in China. *Lancet Oncol.* 21, 335–337. doi: 10.1016/s1470-2045(20)30096-6
- McLean, S., Sheikh, A., Cresswell, K., Nurmatov, U., Mukherjee, M., Hemmi, A., et al. (2013) The impact of telehealthcare on the quality and safety of care: a systematic overview. *PLoS One* 8:e71238. doi: 10.1371/journal.pone.0071238
- Mukherjee, R. K., Back, M. F., Lu, J. J., Shakespeare, T. P., and Wynne, C. J. (2003). Hiding in the Bunker: challenges for a radiation oncology department operating in the Severe Acute Respiratory Syndrome outbreak. *Austr. Radiol.* 47, 143–145.
- NCPGI (2020). Oncology, Prevention and Treatment of Cancer-Related Infections. NCCN clinical guidelines. doi: 10.1046/j.0004-8461.2003.01165.x
- Nepogodiev, D., Bhangu, A., Glasbey, J. C., Li, E., Omar, O. M., Simoes, J. F. F., et al. (2020). Mortality and pulmonary complications in patients undergoing surgery with perioperative SARS-CoV-2 infection: an international cohort study. *Lancet* 396, 27–38.
- Pasikhova, Y., Ludlow, S., and Baluch, A. (2017). Fever in patients with cancer. *Cancer Control.* 24, 193–197. doi: 10.1177/107327481702400212
- Patel, R. A., and Gallagher, J. (2010). Drug fever. *Pharmacotherapy* 30, 57–69.
- Paules, C. I., Marston, H. D., and Fauci, A. S. (2020). Coronavirus infections—more than just the common cold. *JAMA* 323, 707–708. doi: 10.1001/jama.2020.0757
- Pfizer (2020). *Pfizer And Biontech Announce Vaccine Candidate Against Covid-19 Achieved Success In First Interim Analysis From Phase 3 Study*. Available online at: <https://www.pfizer.com/news/press-release/press-release-detail/pfizer-and-biontechannounce-vaccine-candidate-against>.
- Raymond, E., Thieblemont, C., Alran, S., and Faivre, S. (2020). Impact of the COVID-19 outbreak on the management of patients with cancer. *Target Oncol.* 15, 249–259. doi: 10.1007/s11523-020-00721-1
- Real-Time Tracking of New Coronavirus Pneumonia Epidemic (2021). *Real-Time Big Data Report on the Novel Coronavirus Pneumonia Outbreak*. News Broadcast.
- Redelman-Sidi, G., Glickman, M. S., and Bochner, B. H. (2014). The mechanism of action of BCG therapy for bladder cancer—a current perspective. *Nat. Rev. Urol.* 11, 153–162. doi: 10.1038/nrurol.2014.15
- Ritz, N., Hanekom, W. A., Robins-Browne, R., Britton, W. J., and Curtis, N. (2008). Influence of BCG vaccine strain on the immune response and protection against tuberculosis. *FEMS Microbiol. Rev.* 32, 821–841. doi: 10.1111/j.1574-6976.2008.00118.x
- Robilotti, E. V., Babady, N. E., Mead, P. A., Rolling, T., Perez-Johnston, R., Bernardes, M., et al. (2020). Determinants of COVID-19 disease severity in patients with cancer. *Nat. Med.* 26, 1218–1223.
- Russell, S. J., Peng, K. W., and Bell, J. C. (2012). Oncolytic virotherapy. *Nat. Biotechnol.* 30, 658–670.
- Shereen, N. G., and Salman, D. (2019). Delivering chemotherapy at home: how much do we know? *Br. J. Commun. Nurs.* 24, 482–484. doi: 10.12968/bjcn.2019.24.10.482
- Sirintrapun, S. J., and Lopez, A. M. (2020). Telemedicine in cancer care. *Am. Soc. Clin. Oncol. Educ. Book* 38, 125–126.
- Suresh, K., Naidoo, J., Lin, C. T., and Danoff, S. (2018). Immune Checkpoint immunotherapy for non-small cell lung cancer: benefits and pulmonary toxicities. *Chest* 154, 1416–1423. doi: 10.1016/j.chest.2018.08.1048
- Tashkandi, E., Zeeneldin, A., AlAbdulwahab, A., Elemam, O., Elsamany, S., Jastaniah, W., et al. (2020). Virtual management of patients with cancer during the COVID-19 pandemic: web-based questionnaire study. *J. Med. Internet Res.* 22:e19691. doi: 10.2196/19691
- The Healthcare Infection Control Practices Advisory Committee [HICPAC] (2018). *Core Infection Prevention and Control Practices for Safe Healthcare Delivery in All Settings –Recommendations of the HICPAC*. Available online at: <https://www.cdc.gov/hicpac/recommendations/core-practices.html>.
- The Novel Coronavirus Pneumonia Emergency Response Epidemiology Team (2020). Vital surveillances: the epidemiological characteristics of an outbreak of 2019 novel Coronavirus diseases (COVID-19) — China, 2020. *China CDC Weekly* 2, 113–122. doi: 10.46234/ccdcw2020.032
- Tian, J., Yuan, X., Xiao, J., Zhong, Q., Yang, C., Liu, B., et al. (2020). Clinical characteristics and risk factors associated with COVID-19 disease severity in patients with cancer in Wuhan, China: a multicentre, retrospective, cohort study. *Lancet Oncol.* 21, 893–903.
- Velavan, T. P., and Meyer, C. G. (2020). The COVID-19 epidemic. *Trop. Med. Int. Health* 25, 278–280.
- Wang, C., Pan, R., Wan, X., Tan, Y., Xu, L., Ho, C. S., et al. (2020). Immediate psychological responses and associated factors during the initial stage of the 2019 coronavirus Disease (COVID-19) epidemic among the general population in China. *Int. J. Environ. Res. Public Health* 17:1729. doi: 10.3390/ijerph17051729
- Wang, H., and Zhang, L. (2020). Risk of COVID-19 for patients with cancer. *Lancet Oncol.* 21:e180.
- Wei, W., Zheng, D., Lei, Y., Wu, S., Verma, V., Liu, Y., et al. (2020). Radiotherapy workflow and protection procedures during the Coronavirus Disease 2019 (COVID-19) outbreak: experience of the Hubei Cancer hospital in Wuhan, China. *Radiother. Oncol.* 148, 203–210. doi: 10.1016/j.radonc.2020.03.029
- Willan, J., King, A. J., Hayes, S., Collins, G. P., and Peniket, A. (2020). Care of haematology patients in a COVID-19 epidemic. *Br. J. Haematol.* 189, 241–243. doi: 10.1111/bjh.16620
- Wu, Q., Chu, Q., Zhang, H., Yang, B., He, X., Zhong, Y., et al. (2020). Clinical outcomes of coronavirus disease 2019 (COVID-19) in cancer patients with prior exposure to immune checkpoint inhibitors. *Cancer Commun.* 40, 374–379. doi: 10.1002/cac2.12077
- Yao, J. J., Jin, Y. N., Wang, S. Y., Zhang, F., Zhou, G. Q., Zhang, W. J., et al. (2018). The detrimental effects of radiotherapy interruption on local control after concurrent chemoradiotherapy for advanced T-stage nasopharyngeal carcinoma: an observational, prospective analysis. *BMC Cancer* 18:740. doi: 10.1186/s12885-018-4495-2

- Yu, J., Ouyang, W., Chua, M. L. K., and Xie, C. (2020). SARS-CoV-2 transmission in patients with cancer at a tertiary care hospital in Wuhan, China. *JAMA Oncol.* 6, 1108–1110. doi: 10.1001/jamaoncol.2020.0980
- Zhang, L., Zhu, F., Xie, L., Wang, C., Wang, J., Chen, R., et al. (2020). Clinical characteristics of COVID-19-infected cancer patients: a retrospective case study in three hospitals within Wuhan, China. *Ann. Oncol.* 31, 894–901. doi: 10.1016/j.annonc.2020.03.296
- Zhang, Y. J., Yang, W. J., Liu, D., Cao, Y. Q., Zheng, Y. Y., Han, Y. C., et al. (2020). COVID-19 and early-stage lung cancer both featuring ground-glass opacities: a propensity score-matched study. *Transl. Lung Cancer Res.* 9, 1516–1527. doi: 10.21037/tlcr-20-892
- Zhao, Q., Meng, M., Kumar, R., Wu, Y., Huang, J., Lian, N., et al. (2020). The impact of COPD and smoking history on the severity of COVID-19: a systemic review and meta-analysis. *J. Med. Virol.* 92, 1915–1921. doi: 10.1002/jmv.25889
- Zhao, Z., Bai, H., Duan, J., and Wang, J. (2020). Recommendations of individualized medical treatment and common adverse events management for lung cancer patients during the outbreak of COVID-19 epidemic. *Thorac. Cancer* 11, 1752–1757. doi: 10.1111/1759-7714.13424
- Conflict of Interest:** The authors declare that the research was conducted in the absence of any commercial or financial relationships that could be construed as a potential conflict of interest.

Copyright © 2021 Pan, Jiang, Chen and Yang. This is an open-access article distributed under the terms of the Creative Commons Attribution License (CC BY). The use, distribution or reproduction in other forums is permitted, provided the original author(s) and the copyright owner(s) are credited and that the original publication in this journal is cited, in accordance with accepted academic practice. No use, distribution or reproduction is permitted which does not comply with these terms.



# Deep Sequencing of T-Cell Receptors for Monitoring Peripheral CD8<sup>+</sup> T Cells in Chinese Advanced Non-Small-Cell Lung Cancer Patients Treated With the Anti-PD-L1 Antibody

Jin Sheng<sup>1,2†</sup>, Huadi Wang<sup>1,2†</sup>, Xiao Liu<sup>3</sup>, Yunyun Deng<sup>4</sup>, Yingying Yu<sup>4</sup>, Pengfei Xu<sup>4</sup>, Jiawei Shou<sup>1,2</sup>, Hong Pan<sup>1,2</sup>, Hongsen Li<sup>1,2</sup>, Xiaoyun Zhou<sup>1</sup>, Weidong Han<sup>1,2</sup>, Tao Sun<sup>4,5\*</sup>, Hongming Pan<sup>1\*</sup> and Yong Fang<sup>1\*</sup>

## OPEN ACCESS

### Edited by:

Kefang Lai,  
Guangzhou Institute of Respiratory  
Health, China

### Reviewed by:

Sudeep Kumar,  
Albany Medical College, United States  
Ninjit Dhanota,  
Weill Cornell Medicine, United States

### \*Correspondence:

Yong Fang  
fangyong@zju.edu.cn  
Hongming Pan  
panhongming@zju.edu.cn  
Tao Sun  
taosun@immuquad.com

<sup>†</sup>These authors have contributed  
equally to this work and share first  
authorship

### Specialty section:

This article was submitted to  
Molecular Diagnostics and  
Therapeutics,  
a section of the journal  
Frontiers in Molecular Biosciences

**Received:** 11 March 2021

**Accepted:** 08 June 2021

**Published:** 09 July 2021

### Citation:

Sheng J, Wang H, Liu X, Deng Y, Yu Y,  
Xu P, Shou J, Pan H, Li H, Zhou X,  
Han W, Sun T, Pan H and Fang Y  
(2021) Deep Sequencing of T-Cell  
Receptors for Monitoring Peripheral  
CD8<sup>+</sup> T Cells in Chinese Advanced  
Non-Small-Cell Lung Cancer Patients  
Treated With the Anti-PD-L1 Antibody.  
Front. Mol. Biosci. 8:679130.  
doi: 10.3389/fmolb.2021.679130

<sup>1</sup>Department of Medical Oncology, School of Medicine, Sir Run Run Shaw Hospital, Zhejiang University, Hangzhou, China,

<sup>2</sup>Laboratory of Cancer Biology, Institute of Clinical Science, School of Medicine, Sir Run Run Shaw Hospital, Zhejiang University, Hangzhou, China, <sup>3</sup>Department of Human Genetics, University of Chicago, Chicago, IL, United States, <sup>4</sup>Hangzhou ImmuQuad Biotechnologies, LLC, Hangzhou, China, <sup>5</sup>Zhejiang-California International Nano-Systems Institute, Zhejiang University, Hangzhou, China

**Background:** Atezolizumab, a high-affinity engineered human anti-PD-L1 antibody, has produced a clinical benefit for patients with advanced non-small-cell lung cancer (NSCLC). However, associated with T-cell regulation, the immunomodulatory effect of PD-L1 blockade and its biomarker in peripheral immunity remains elusive.

**Methods:** In a prospective cohort with 12 Chinese advanced NSCLC patients who received atezolizumab 1,200 mg every 3 weeks as a second-line treatment, blood samples were obtained before and 6 weeks after atezolizumab initiation, and when disease progression was confirmed. Patients were classified into a response or progression group according to response evaluation criteria in solid tumors (RECIST) 1.1. Fresh peripheral blood mononuclear cells (PBMCs) from patients were stained with antihuman CD3, CD8, and PD-1 antibodies for flow cytometry analysis. T-cell receptor (TCR)- $\beta$  chains of CD8<sup>+</sup> T cells were analyzed by next-generation sequencing (NGS) at the deep level. Diversity, clonality, and similarity of TCR have been calculated before and after treatment in both groups.

**Results:** Clonal expansion with high PD-1 expression was detected in all patients' peripheral CD8<sup>+</sup> T cells before the treatment of atezolizumab. Unlike the progression group, the diversity of TCR repertoire and singletons in the TCR $\beta$  pool increased over time with atezolizumab administration, and the TCR repertoire dynamically changes in the response group. The percentage of CD8<sup>+</sup> PD-1<sup>high</sup> terminal exhausted T cells declined in the response group after the PD-L1 blockade. Two patterns of TCR changes among patients who received PD-L1-targeted immunotherapy were observed.

**Conclusions:** Deep sequencing of the T-cell receptors confirmed the existence of CD8<sup>+</sup> PD-1<sup>high</sup> T cells with an exhaustion phenotype in Chinese NSCLC patients. Our study demonstrated that efficient anti-PD-L1 therapy could reshape the TCR repertoire for



antitumor patients. Furthermore, singleton frequency may help us select patients who are sensitive to anti-PD-L1 immunotherapy.

**Keywords:** next-generation sequencing, liquid biopsy, T-cell receptor repertoires, non-small cell lung cancer, anti-PD-L1 immunotherapy

## INTRODUCTION

Non-small cell lung cancer (NSCLC) that accounts for almost 85 percent of total lung cancer patients is still the leading cause of cancer-related mortality, especially in those with advanced disease (Sui et al., 2018; Seigel et al., 2017). Over the past few years, the introduction of the epidermal growth factor receptor (EGFR), tyrosine kinase inhibitors (TKIs), and anaplastic lymphoma kinase (ALK)-based target therapy dramatically improved the therapeutic efficacy for lung cancer patients with specific gene mutations (Califano et al., 2017; Hida et al., 2017; Peters et al., 2017; Kiura et al., 2018; Novello et al., 2018). However, tumor heterogeneity inevitably leads to resistance of targeted therapies from multiple mechanisms (Tsui et al., 2018). Encouragingly, immune checkpoint blockade (ICB) immunotherapy had changed the landscape for treating advanced NSCLC, with a more durable response than targeted therapy and chemotherapy.

Several inhibitory immunoreceptors, including but not limited to CTLA-4, PD-1, TIM3, and LAG3, have been studied in some solid tumors in the past decades. Moreover, the most successfully developed ICB therapy is anti-PD-1/PD-L1 therapy, since atezolizumab, nivolumab, and pembrolizumab have been approved for NSCLC (Ribas and Wolchok, 2018). The PD-1/PD-L1 signaling pathway is one of the self-protection mechanisms of tumors against the endogenous immune response (Taube et al., 2012). Conventionally, the primary PD-1 ligand expressed on the surface of tumor cells or antigen-presenting cells is PD-L1, with PD-1 on T cells to trigger inhibitory signaling (Curiel et al., 2003, 2007; Keir et al., 2008; Lin et al., 2018). T cells respond highly specific to particular antigens as a consequence so that the gene encoding their adaptive immune receptors is generated somatically through a process that creates unique sequences when they encounter the cognate antigen. The generation process of adaptive immune receptor genes results in a tremendously diverse repertoire of distinct T-cell receptors (TCR) to bind the particular antigens (Robins et al., 2010; Warren et al., 2013; Zarnitsyna et al., 2013; Kaplinsky and Arnaut, 2016; Briney et al., 2019). A somatic recombination process of the variable (V), diversity (D, beta chain), and joining (J) exons generates a high degree of TCR diversity and defines the highly variable complementary determining region 3 (CDR3) (Lee and Prins, 2016). CDR3 characterizes the antigen recognition specificity of each T-cell clone. Therefore, deep sequencing data of the T-cell antigen receptor repertoire give us access to a better understanding of T lymphocyte population dynamics in response to therapy (Cowell, 2020).

The application of TCR repertoire deep sequencing to reveal lymphocyte responses in cancer or immunotherapy is widespread

(Kirsch et al., 2015; Schrama et al., 2017). The majority of studies have focused on the T-cell receptor beta locus. Studies of clonal richness and diversity of T lymphocyte population have ranged from tumor-infiltrating T cells and sentinel lymph node T cells to T lymphocytes in peripheral blood. Tumor-infiltrating T cells are the front line of identifying tumor antigens in the tumor microenvironment, resulting in considerable heterogeneity. In NSCLC, abundant TCR sequences have been classified as ubiquitous or regional. As for peripheral blood TCR repertoires, despite that studies found little overlap (from 19 to 25%) between peripheral blood and TIL TCR repertoires so far, evidence confirmed the peripheral TCR repertoire correlated with TILs, and their alteration reflects various aspects of the disease. Moreover, a study (Liu et al., 2019) suggested that peripheral TCR diversity decreases as the disease progresses in lung cancer.

The blockade of PD-1:PD-L1 interactions contains two options: anti-PD-1 and anti-PD-L1. PD-1 is expressed by activated T cells that bind to PD-L1 in the tumor microenvironment. However, during chronic exposure of tumor antigen, T cells undergo exhaustion with upregulation of inhibitory checkpoints, typically PD-1, as one of the tumor escape mechanisms. Blocking of PD-1 is expected to change these exhausted T cells' behavior directly and hopefully reinvigorates them. In contrast, the blockade of PD-L1 produces more possibilities due to broad cell types expressing PD-L1 and the additional ligand B7-1. Intriguingly, the study from Fridman et al. (2017) has given us crucial evidence that anti-PD-L1 treatment during chronic lymphocytic choriomeningitis virus (LCMV) infection induced the interleukin-7 receptor (IL-7R or CD127) on exhausted T cells. IL-7 acts as a pivotal factor for the generation of memory T-cell phenotype (Schluns et al., 2000) and down regulates PD-1 expression on the CD8<sup>+</sup> T cells during chronic LCMV infection. To confirm if similar regulation happens in cancer anti-PD-L1 immunotherapy, monitoring PD-1 expression in peripheral blood could give us a preliminary insight into the invigoration of T-cell exhaustion of anti-PD-L1 in cancer patients.

Collectively, in the present prospective cohort study, the expression of PD-1 and TCR repertoire was analyzed through high-throughput sequencing in blood samples from Chinese advanced NSCLC patients who had received anti-PD-L1 checkpoint blockade immunotherapy, aiming at exploring predictive and monitoring biomarkers before treatment and selecting patients to exhibit better clinical outcomes.

## MATERIALS AND METHODS

### Study Design and Cohort

We performed a prospective cohort study of patients with metastatic lung cancer treated with atezolizumab (MPDL3280A), a PD-L1

**TABLE 1** | Demographic and clinical characteristics of patients.

Patient ID	Gender	Age	Histology	Smoking history	Cycles	Best response	Efficacy group	PFS/months
1	Male	61	SCC	Previous smoker	3	PD	Progression	2.9
2	Male	63	SCC	Previous smoker	4	PD	Progression	2.7
3	Male	59	SCC	Smoker	2	PD	Progression	1.4
4	Male	51	SCC	Previous smoker	11	PR	Response	7.7
5	Male	58	ADN	Previous smoker	8	PD	Progression	5.6
6	Male	52	ADN	Smoker	9	SD	Response	6.3
7	Male	75	SCC	Smoker	6	PD	Progression	4.3
8	Male	45	SCC	Smoker	12	SD	Response	8.3
9	Male	49	SCC	Smoker	6	SD	Response	4.4
10	Male	73	ADN	Previous smoker	3	PD	Progression	2.1
11	Female	58	SCC	Nonsmoker	13	SD	Response	9.3
12	Female	60	ADN	Nonsmoker	8	SD	Response	5.6

SCC refers to squamous carcinoma; ADN refers to adenocarcinoma.

PD: progressive disease; SD: stable disease; PR: partial response.

inhibitor, at Sir Run Run Shaw Hospital, Zhejiang University. This study was approved by the Institutional Review Board (IRB) of the hospital. All patients received atezolizumab 1,200 mg intravenously every 3 weeks. Critical inclusion criteria for this study cohort were cytologically confirmed stage IIIB/IV squamous carcinoma or adenocarcinoma of NSCLC, Eastern Cooperative Oncology Group performance status (ECOG-PS) of 0–1, 18 years old or older measurable lesion confirmed by response evaluation criteria in solid tumors (RECIST) 1.1, and disease recurrence after one prior platinum-containing regimen. Patients with a known autoimmune disease, symptomatic interstitial lung disease, systemic immunosuppression, or prior immune-based therapies were excluded. Smoking status was classified as smokers and nonsmokers. Smokers have been referred to as those patients who smoke more than ten cigarettes per day and with cigarette withdrawal less than 2 years.

## Therapeutic Efficacy Analysis in Response to Atezolizumab

Tumor responses to atezolizumab were evaluated by a CT scan every 6 months. Clinical responses such as complete response (CR), partial response (PR), stable disease (SD), and progressive disease (PD) were determined based on RECIST 1.1. Patients were further categorized into the response group based on tumor shrinkage, while the progression group included patients who achieved PD (Table 1). The median follow-up was 5.0 (IQR 2.75–7.35) months at the endpoint. The median PFS was 4.4 (95% CI: 2.9–5.9) months among all patients.

$$f(x) = a_0 + \sum_{n=1}^{\infty} \left( a_n \cos \frac{n\pi x}{L} + b_n \sin \frac{n\pi x}{L} \right).$$

## PBMC Preparation and CD8<sup>+</sup> T-Cell Isolation

We collected 25 samples of peripheral blood mononuclear cells (PBMCs) from 12 Chinese advanced NSCLC patients. The samples were collected at baseline and 6 weeks after the initiation of treatment within a 3-day time window. PBMCs were immediately isolated from each sample using Ficoll-Hypaque

1077 (Sigma-Aldrich) gradient centrifugation. Total CD8<sup>+</sup> T cells were isolated from PBMCs with the BD IMag<sup>™</sup> Anti-Human CD8 Magnetic Particles kit (catalog no. 557766).

## Flow Cytometry

For the flow cytometry analysis, all antibodies were purchased from BioLegend (San Diego, CA). Cells were stained with antihuman CD3 (HIT3a), CD8 (SK1), and PD-1 (EH12.2H7), and analyzed on a BD LSRFortessa<sup>™</sup> flow cytometer (Becton Dickinson) using FlowJo vX.0.7 software. Gates were set on CD3<sup>+</sup> cells with forward and side scatter, and doublets were gated out (Supplementary Figure S1).

## TCR-β Full-Length Amplification and Sequencing

RNA extraction of pure CD8<sup>+</sup> T cells was performed following the RNeasy Plus Mini Kit (Qiagen). The samples were analyzed by high-throughput sequencing of TCR full length using the ImmuHub<sup>®</sup> TCR profiling system at the deep level (ImmuQuad Biotech, Hangzhou China). Briefly, a 5' RACE unbiased amplification protocol was used. Sequencing was performed on an Illumina MiSeq<sup>®</sup> system with PE300 mode (Illumina), as previously described (Wang et al., 2019). A post-sequencing algorithm was applied to raw sequencing data for PCR and sequencing error correction and V, D, J, and C gene segments mapping with IMGT<sup>®</sup>. The resulting nucleotide and amino acid sequences of CDR3 of TCRβ were determined, and those with out-of-frame and stop codon sequences were removed from the identified TCR-β repertoire. We further defined each TCR-β clonotype's amounts by adding the numbers of TCR-β clones sharing the same nucleotide sequence of CDR3. The TCR-β repertoire analysis algorithm was based on R (version 3.5.1). The total-sequencing reads and the successfully aligned reads are listed in Supplementary Table S1 in detail.

## Diversity, Clonality, and Similarity Calculation

Pielou's evenness index (Pielou, 1966) was calculated to estimate the diversity of TCRβ repertoire, according to the equation:

$$\text{Pielou index} = \frac{\text{Shannon index } H}{\ln N} = \frac{\sum_{i=1}^N p_i (\ln p_i)}{\ln N},$$

$$\text{Clonality index} = 1 - \text{Pielou index},$$

where  $p_i$  is the proportion of sequence,  $i$  is relative to the entire sequences, and  $N$  is the total quantity of clonotypes. The *Pielou index* describes the equability of a TCR repertoire and is positively related to the diversity represented by the *Shannon index*.

Singleton means one unique TCR clone, and the entire singletons in one patient TCR repertoire have shown a strong correlation with the percentage of naive T cells (Britanova et al., 2014), which are the backbone of immune repertoire diversity. *Singleton frequency*, which calculated the proportion of singletons in the total clonotypes, is an essential factor in estimating the total repertoire clonality. In this study, we illustrated *singleton frequency* in donut charts, where the inner layer includes the frequency of singleton (“1,” T-cell clones that only had one sequence read) and high-order (“2+,” T-cell clones that had more than two sequence reads) clonotypes. Repertoire clonality was depicted as the “2+” portion in the donut chart.

Last, to estimate the overlap of TCR- $\beta$  clonotypes between time points or biological compartments, the *Baroni-Urbani and Buser overlap index* (BUB) (Zhang et al., 2017) was calculated according to the following formula:

$$\text{BUB} = \frac{n_{12}}{n_1 + n_2 - n_{12}},$$

where  $n_1$  is the number of clonotypes present at time point 1,  $n_2$  is the number of clonotypes present at time point 2, and  $n_{12}$  is the number of clonotypes presenting in both time points.

## Statistical Analysis

The Student's  $t$ -test (two-tailed) was adopted to compare the Pielou's evenness index, singletons frequency, and BUB overlap index between data before and after treatment. Two-way ANOVA analyzed the differences between repeated-measures data during therapy. A  $p$ -value of 0.05 was considered statistically significant. The Student's  $t$ -test and two-way ANOVA were calculated by GraphPad Prism version 6.0 (La Jolla, CA, United States). The donut chart was made by R (version 3.4.0). A survival analysis was conducted using both Kaplan–Meier log-rank analysis and Cox proportional hazard models.

## RESULTS

### Patient Characteristics and Therapeutic Efficacy

The primary characteristics of the 12 enrolled patients in this study cohort are summarized in **Table 1**. Briefly, eight patients had squamous carcinoma, and the remaining had adenocarcinoma. 83.3 percent of the cohort were current ( $n = 2$ ) or former smokers ( $n = 8$ ). All patients had an ECOG performance status of 1. The response group had a significantly younger average age than the progression group (53.5 vs. 64.8 years,  $p < 0.05$ , **Supplementary Table S2**). In this study, patients received a median of seven cycles of PD-L1

blockade immunotherapy, while half of them progressed after six cycles of treatment (**Figure 1A**). Among the response group, one patient (Patient 4) presented PR (**Figure 1B**), and five patients reached SD as their best response to the treatment during follow-ups (**Table 1**; **Figure 1B**). One patient (Patient 11) in the response group continued to respond to atezolizumab for more than 12 months, although the target lesions did not shrink remarkably as evaluated by computed tomography (**Figure 1C**). Comparing with the progression group (median 2.7 months, 95% CI: 1.7–3.7), the PFS significantly prolonged in the response group (median 6.3 months, 95% CI: 3.8–8.8; Kaplan–Meier estimate  $p < 0.005$ , **Figure 1D**).

### CD8<sup>+</sup>PD-1<sup>high</sup> Terminal Exhausted T Cells Decreased in Response to PD-L1 Blockade

When tumor antigens persist in, exhausted T cells ( $T_{ex}$ ) form with the growing levels of persistent PD-1 expression, inducing a less functional state of exhaustion among cognate antigen-specific T cells.  $T_{ex}$  cells in the early stage retain the capability of renewal and are characterized by intermediate expression of PD-1. Early  $T_{ex}$  cells as a progenitor population give rise to terminal  $T_{ex}$  cells with high expression of PD-1, which loses the ability of proliferation upon tumor antigen stimulation (**Figure 2A**) (McLane et al., 2019). Among the enrolled NSCLC patients, we confirmed PD-1-positive CD8<sup>+</sup> T cells in peripheral blood and further classified them into PD-1<sup>high</sup>, PD-1<sup>low</sup>, and PD-1<sup>neg</sup> subsets by the expression level of PD-1 (**Figure 2B**). The PD-1<sup>high</sup> subsets were regarded as terminal  $T_{ex}$  cells.

The average number of sequencing reads was  $851148 \pm 120135$  (range 69,600–1,892,801), and the average aligned reads were  $638721 \pm 84,218$  (range 45,909–1,385,898). Details of the total sequencing reads and successfully aligned reads are listed in **Supplementary Table S1**. The number of CD8<sup>+</sup>PD-1<sup>high</sup> terminal  $T_{ex}$  cells in the responders' circulation decreased after anti-PD-L1 antibody treatment, whereas there was almost no change of this subset in the progression group (**Figure 2C**). After initiation of atezolizumab, in the response group, the percentage of PD-1<sup>high</sup>CD8<sup>+</sup> terminal  $T_{ex}$  in total CD3<sup>+</sup> T cells dropped from  $12.5 \pm 2.76$  (95% CI: 5.38–19.6) to  $6.38 \pm 1.03$  (95% CI: 3.73–9.02;  $p = 0.0705$  posttreatment vs. pretreatment) after PD-L1 blockade treatment (**Figure 2D**). However, in the progression group, there was no significant difference in the percentage of PD-1<sup>high</sup>CD8<sup>+</sup> T cells before and after treatment (**Figure 2D**;  $8.86 \pm 2.58$  vs.  $8.86 \pm 2.84$ ,  $p > 0.999$ ).

### PD-L1 Blockade Changes TCR Repertoire Diversity

For a given total number of distinct clonotypes in the repertoire, the maximally diverse repertoire consists of uniformly distributed adaptive immune receptors ( $p_i$  are all equal in the formula) (Cowell, 2020). The evenness of the TCR repertoire represented by Pielou's index increased in the response group after treatment ( $p = 0.36$ , paired  $t$ -test; **Figure 3A**); in contrast, those who did not respond to atezolizumab showed no change in the evenness of the TCR repertoire ( $p = 0.98$ , unpaired  $t$ -test). To

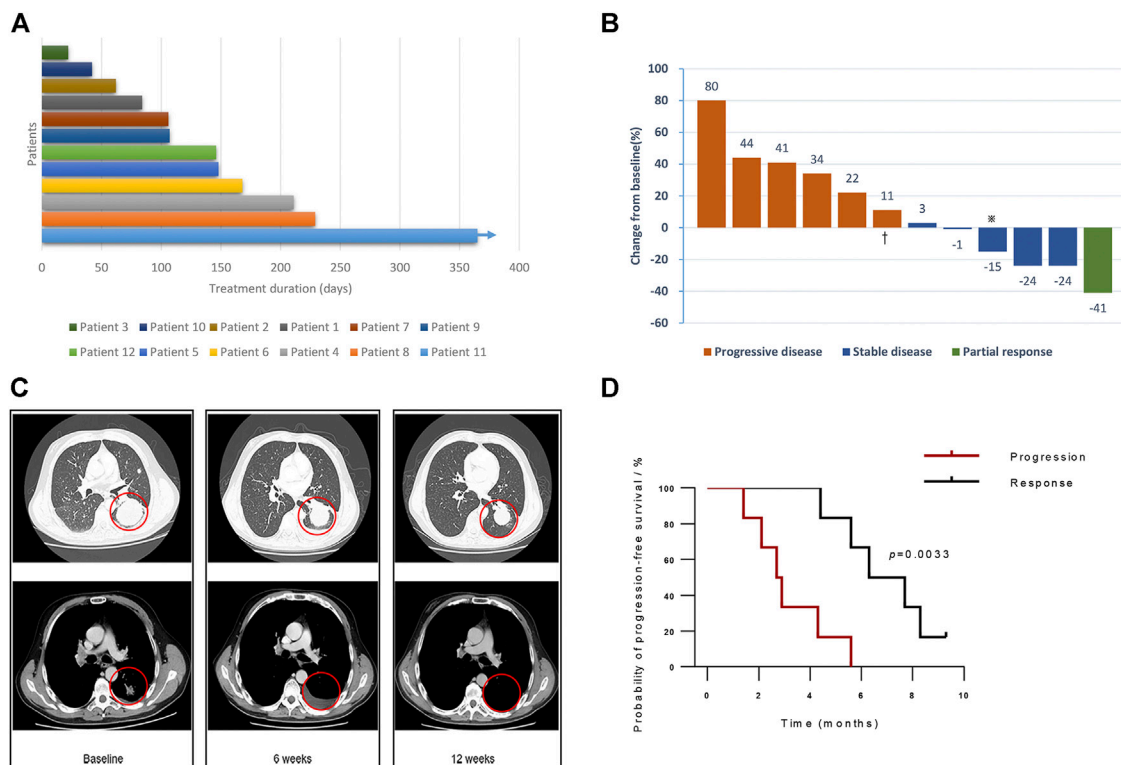


**FIGURE 1 |** Clinical efficacy of PD-L1 blockade. **(A)** Investigator-assessed duration of treatment. The arrow indicates censored patient with follow-up ongoing after one year. **(B)** The confirmed maximum reduction of target lesions, according to the investigator and authorized radiologist. Colors of bars representing the best response confirmed during follow-ups. Red bars represent progressive disease, blue bars represent stable disease, and green bars show partial response. Patient two was confirmed of nontarget lesion progression during the one-year follow-up. **(C)** Representative computed tomography (CT) scans of Patient 11, who achieved a partial response to atezolizumab. **(D)** Comparison of estimated progression-free survival of the response group and the progression group ( $p < 0.005$ ). Note:  $\times$ : Patient 11,  $\dagger$ : Patient 2.

assess the dynamic nature of the TCR repertoire diversity representing the whole course of effective anti-PD-L1 therapy, we collected blood samples from three patients in the response group with their consents when the progressive disease was confirmed. It is noticeable that the evenness of the TCR repertoire maintained or significantly elevated when the targeted lesions continued to respond to atezolizumab. However, Pielou's index dramatically dropped when the disease progressed ( $p < 0.05$ , 2-way ANOVA; **Figure 3B**).

The changes in the singleton frequency reflect the clonal proliferation of the TCR repertoire during anti-PD-L1 immunotherapy. Before treatment, the singleton frequency between the response and the progression group showed no significant difference ( $10.86 \pm 3.67\%$  vs.  $5.22 \pm 1.77\%$ ;  $p = 0.17$ , unpaired  $t$ -test; **Figure 3C**). Nevertheless, after the initiation of atezolizumab, the gap between the mean singleton frequency of the response and progression group grew ( $14.44 \pm 2.25\%$  vs.  $7.51 \pm 1.52\%$ ;  $p < 0.05$ , Welch's  $t$ -test; **Figure 3C**), which interpreted a better T-cell proliferative ability in patients who responded to PD-L1 blockade than in those who did not. Similarly, the singleton frequency of the same three patients in the response group was monitored during follow-ups. The clonal proliferation of the TCR repertoire dramatically elevated after the

initiation of atezolizumab during stable disease. After progression, these three patients all had a decreased singleton frequency, indicating a lower level of richness of the TCR repertoire ( $p < 0.05$ , 2-way ANOVA; **Figure 3D**). There is not a clear correlation between the pretreatment singleton frequency and PFS (**Supplementary Figure S2**).

Also, we calculated the Baroni-Urbani and Buser index to measure the overlap among TCR- $\beta$  clonotypes in the response and progression groups (**Supplementary Figure S3**). The average BUB index is moderately lower in the response group than that in the progression group ( $0.039 \pm 0.0099$  vs.  $0.054 \pm 0.017$ ;  $p = 0.44$ , unpaired  $t$ -test), indicating the TCR similarity of patients in the response group is at a lower level than that of those in the progression group.

## TCR Repertoire Changes due to anti-PD-L1 Treatment Had Typical Patterns Featured by Top Clonotype and Singleton Frequency

According to the clonotype and singleton frequency changes of the TCR repertoire before and after PD-L1 blockade immunotherapy, we summarized two patterns for every group, aiming at exploring a portable way to select proper patients for



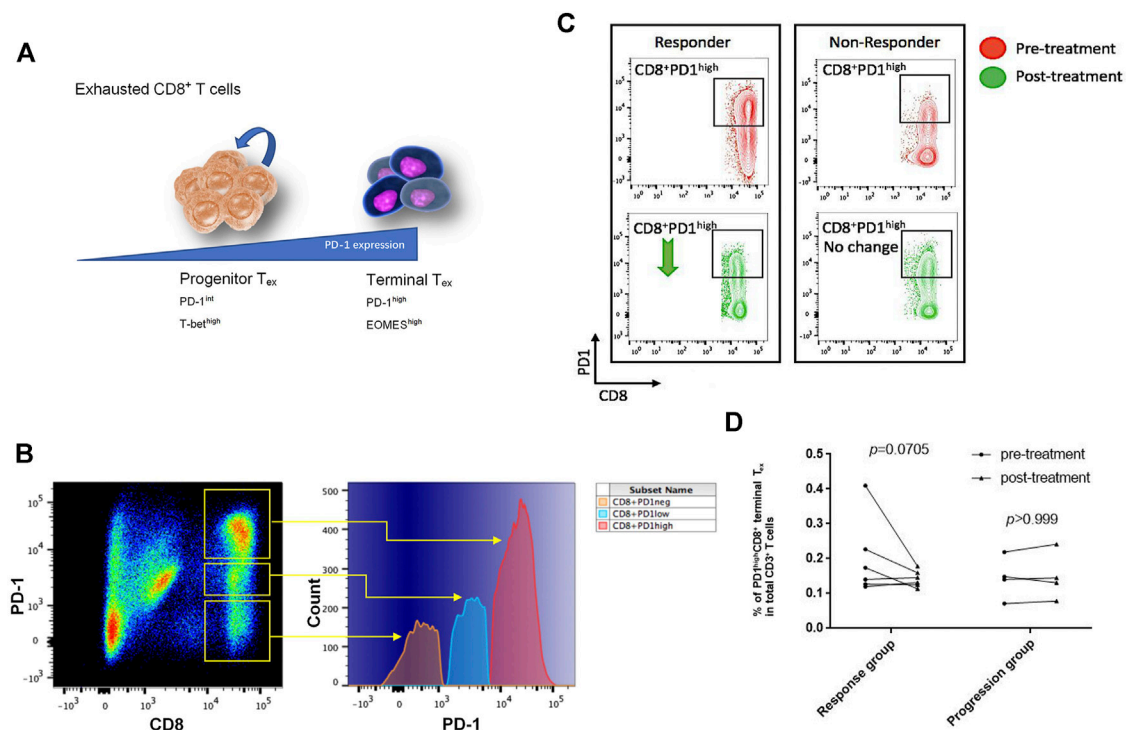


**FIGURE 2 |** CD8<sup>+</sup>PD-1<sup>high</sup> T cells decreased for responding to PD-L1 blockade treatment. **(A)** The CD8<sup>+</sup>PD-1<sup>high</sup> subset was identified as terminal exhausted T cells, which highly expressed the EOMES transcription factor, while CD8<sup>+</sup>PD-1<sup>int/low</sup> population that expressed the T-bet transcription factor was known as progenitor exhausted T cells (Wherry and Kurachi, 2015). **(B)** According to the log-density plot of the PD-1 expression level, three subsets of CD8<sup>+</sup> T cells were found in Chinese non-small-cell lung cancer patients' peripheral blood. There were PD-1<sup>high</sup>, PD-1<sup>low</sup>, and PD-1<sup>neg</sup> CD8<sup>+</sup> T cells. **(C)** Two representatives illustrated that the percentage of CD8<sup>+</sup>PD-1<sup>high</sup> T cells in the response group decreased, whereas it did not have an apparent change in the progression cohort after PD-L1 blockade treatment. **(D)** The percentage of CD8<sup>+</sup>PD-1<sup>high</sup> T cells in each patient before and after treatment ( $p = 0.0705$  in the response group;  $p > 0.999$  in the progression group).

atezolizumab. In the first pattern of the response group, the singleton frequency of the TCR repertoire was increased primarily without variation of the top two clonotypes of CDR3 (Figure 4A). Pattern two had a decent percentage of singletons and was distinguished from the first pattern by the varied top two clones of the amino acid sequence of the CDR3 (Figure 4A). As for the progression group, pattern one had no change in neither singleton frequency nor top two clones of the TCR repertoire; in pattern two, the TCR repertoire of progressed patients maintained a small percentage of singletons in total clonotypes during treatment, but the top two clones changed (Figure 4B). The details of the top two clones of all patients before and after treatment are shown in Table 2. All information is given in Supplementary Table S3.

## DISCUSSION

PD-L1 blockade immunotherapy has been proven to induce durable tumor remissions through T-cell response to cancer, and it remains unclear how these antibodies work in modulating T-cell immunity (Robert et al., 2014). Besides, serial monitoring of checkpoint inhibitors' efficacy needs easily accessible tumor biomarkers. Therefore, the TCR repertoire has become a focus in several studies since checkpoint inhibitor

blockade dramatically changed the treatment for advanced cancer patients. However, exploratory studies of peripheral TCR diversity analysis among advanced cancer patients treated with different checkpoint inhibitors blockade have reached conflicting conclusions. So, we did this pilot study to continue illustrating PD-L1 blockade immunotherapy and exploring peripheral TCR repertoire in advanced NSCLC patients.

In this study, we confirmed the existence of PD-1<sup>high</sup> terminal exhausted T cell and PD-1<sup>low</sup> progenitor exhausted T cell in the enrolled Chinese NSCLC patients, and during treatment, effective anti-PD-L1 immunotherapy was correlated with decreased CD8<sup>+</sup>PD-1<sup>high</sup> exhausted T cells. Multiple influencing factors function during the reform of antitumor immunity. Two main subsets constitute the CD8<sup>+</sup>PD-1-positive T cells: eomes<sup>high</sup>PD-1<sup>high</sup> CD8<sup>+</sup> T cells (terminal T<sub>ex</sub>) respond poorly to the PD-1 pathway blockade; however, T-bet<sup>high</sup>PD-1<sup>int</sup> T cells can reverse exhaustion and produce protective immunity *in vivo* (Blackburn et al., 2008). Furthermore, atezolizumab is the inhibitor of both PD-1/PD-L1 and PD-L1/CD80 pathways (Syn et al., 2017), and CD80 on T cells delivered inhibitory signals as a receptor when engaged by PD-L1 (Butte et al., 2007). J. Park et al. demonstrated that by attenuation of the PD-L1/CD80 pathway through treatment with the anti-PD-L1 monoclonal antibody, blockade of PD-L1/CD80 could enhance T-cell expansion and restore response in the previously anergized

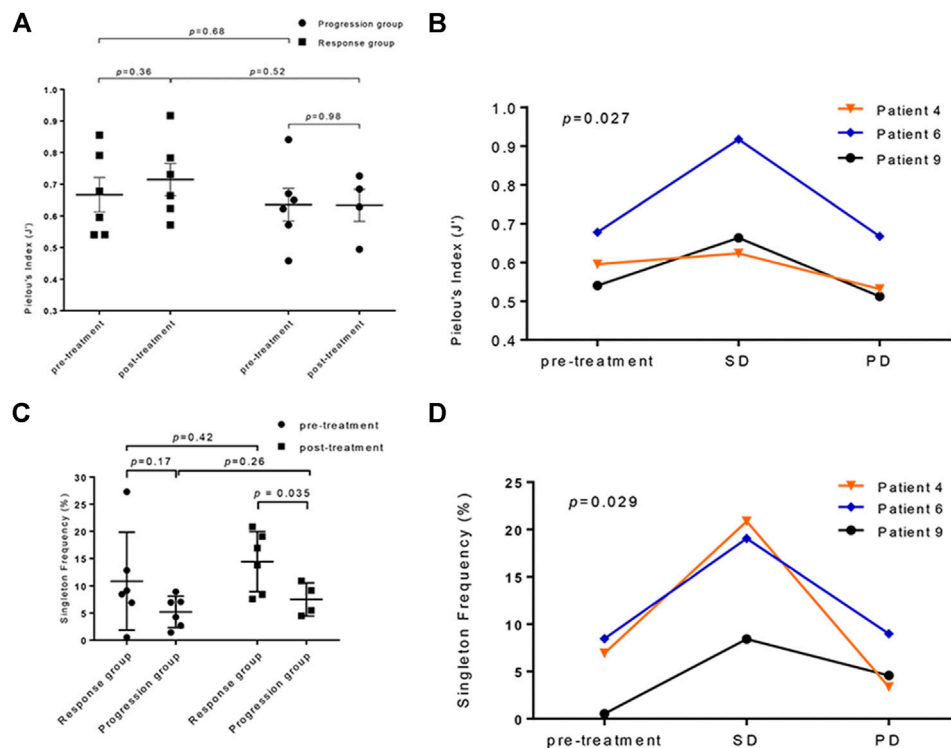


**FIGURE 3 |** The analysis of the T-cell receptor (TCR) repertoires diversity in anti-PD-L1-treated patients. **(A)** The comparison of TCR repertoire evenness changes in the progression and response groups calculated by Pielou's index ( $p = 0.36$  in the response group;  $p = 0.98$  in the progression group; response vs. progression: pretreatment  $p = 0.68$ , posttreatment  $p = 0.52$ ). **(B)** The dynamic observation of TCR repertoire evenness at different disease statuses of three patients who responded to atezolizumab ( $p = 0.027$ ). SD: stable disease; PD: progressive disease. **(C)** The singleton frequency in the response and progression groups before ( $p = 0.17$ ) and after ( $p < 0.05$ ) treatment. (pretreatment vs. posttreatment:  $p = 0.42$  in the response group,  $p = 0.26$  in the progression group). **(D)** The changes of the singleton frequency of the TCR repertoire in three patients responded to atezolizumab during treatment ( $p = 0.029$ ).

T cells. So, we hypothesize that anti-PD-L1 antibodies protect the PD-1-positive T cells from apoptosis and T cells renewed from exhaustion without expression of PD-1, which leads to the decrease of CD8<sup>+</sup> PD-1<sup>high</sup> T cell during effective atezolizumab treatment.

The blockade of PD-L1 makes more T cells survive from apoptosis, and therefore increases the diversity of T cells and TCR repertoires (Figure 5). Low TCR diversity indicates a severely impaired immune status of patients (Teng et al., 2015; Chen and Mellman, 2017; Snyder et al., 2017), and prospective studies in melanoma patients suggested that peripheral tumor-specific clones are likely to be concentrated in the CD8<sup>+</sup>PD-1<sup>+</sup> subset (Gros et al., 2016). Therefore, the diversity of the TCR repertoire may reflect the immune status during treatment, and dynamic monitoring could improve its predictive power (Swanton and Govindan, 2016; Jamal-Hanjani et al., 2017). We dynamically analyzed peripheral TCR repertoire diversity in NSCLC patients, increased TCR repertoire diversity, and clonal proliferation that appeared under situations when patients responded to atezolizumab before progression. The TCR remained at a higher level during stable disease but dropped down after progression, which indicated the potential of peripheral TCR repertoire diversity to be a promising monitoring biomarker for

checkpoint blockade immunotherapy. Similarly, Wieland et al. (2018) reported oligoclonal expansions in the peripheral CD8<sup>+</sup> TCR repertoire after pembrolizumab initiation in melanoma patients and identified the activation of tumor-infiltrating CD8<sup>+</sup> T-cell clones in peripheral blood after anti-PD-1 immunotherapy. In a study containing 29 advanced bladder cancer patients (Snyder et al., 2017), researchers noticed the expansion of circulating tumor-associated TCR 3 weeks after the initiation of atezolizumab, which is correlated with the durable clinical benefit. The further analysis helps us pick two characteristics of the TCR repertoire, the top two clones in CDR3, and singleton frequency (or its percentage), to summarize the changing pattern of the TCR repertoire. No matter the top two clones change or not, the response group always kept a decent or increased percentage of singleton frequency, which increases the possibility of more tumor-specific T cells to control tumor proliferation. Thus, we hypothesize that anti-PD-L1 leads to more tumor antigen presented to T cells, and more tumor-specific T cells survive. Nevertheless, unfortunately, pretreatment singleton frequency of the TCR repertoire could not predict the progression-free survival of NSCLC patients in our study. To further confirm the correlation between TCR repertoire diversity and PFS, a large-scale cohort study is needed.

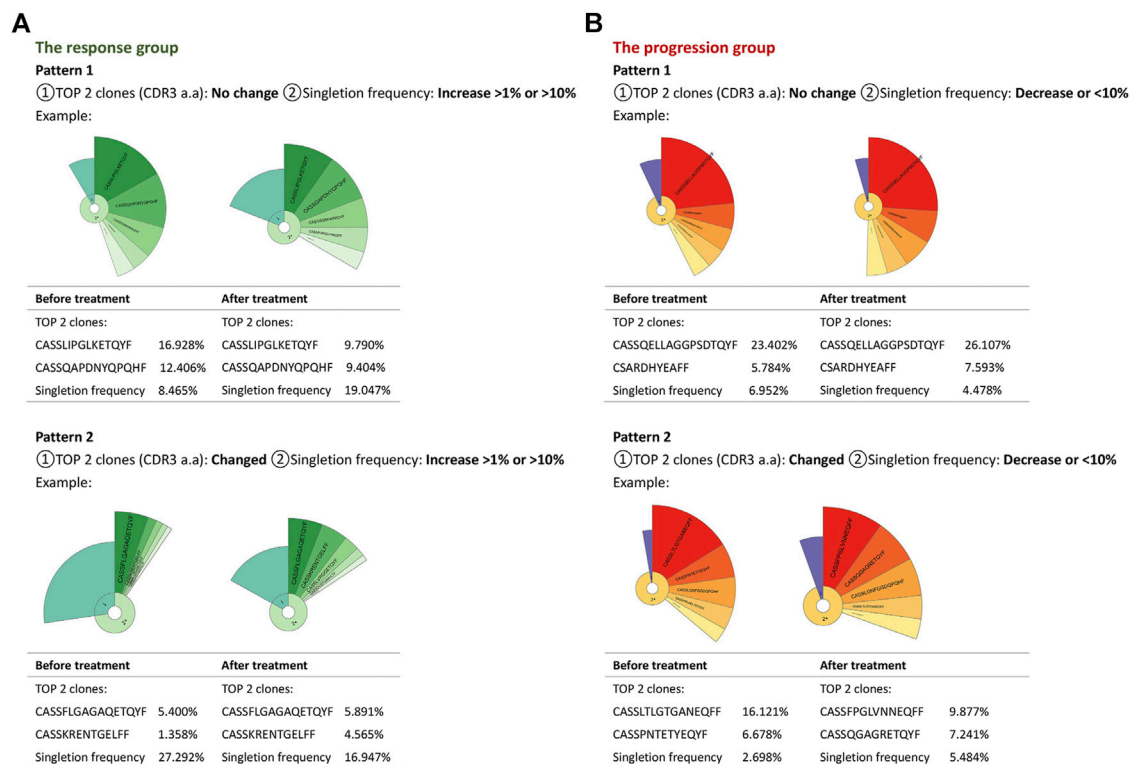
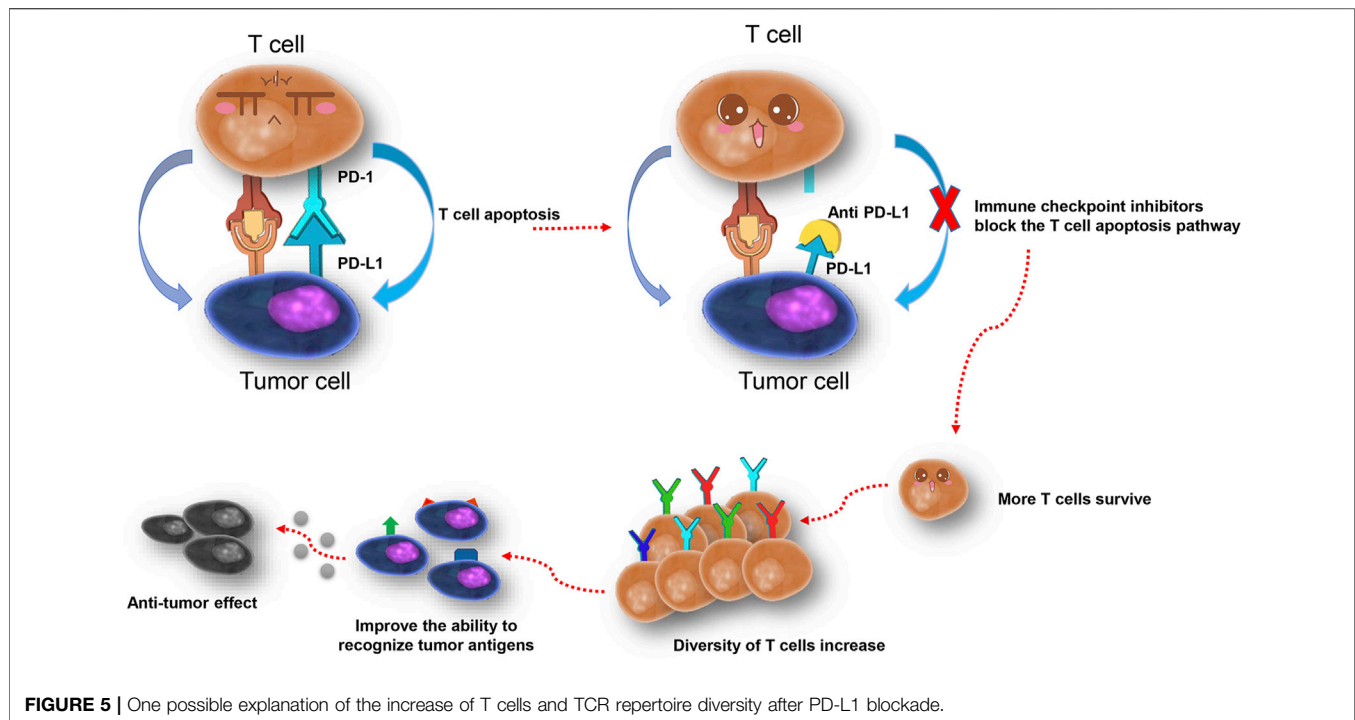


**FIGURE 4 |** Changing patterns of the TCR repertoire in the progression and response groups. Donut charts and tables summarized two patterns in each group. Each pattern took one patient as an example in either group. The fan-shaped area depicts the corresponding clonal frequency. The area of “1” in the donut chart represented the frequency of singletons. “2+” area was the TCR sequences whose reads were more than two. A larger radian meant a higher frequency. The top five clones’ amino acid sequences of complementary determination region 3 (CDR3) of TCR were shown, and the frequencies of the top two clones were listed. The radian marked with the amino acid sequence displayed the frequency of the corresponding T-cell clones.

**TABLE 2 |** The Top two clones’ amino acid sequences of complementary determination region 3 (CDR3) of TCR of each patient before and after treatment.

Group	Patient ID	Time point		Top 1 clone (CDR3)		Top 2 clone (CDR3)
Progression	1	Pretreatment	11.80%	CASHRAGNEYEQYF	8.77%	CASSVAGTADYEQYF
		Posttreatment	NA	NA	NA	NA
	3	Pretreatment	43.09%	CASSFGTFGDGYT	4.45%	CASSLTSEHRTDTQYF
		Posttreatment	NA	NA	NA	NA
	2	Pretreatment	16.12%	CASSLTGTGANEQFF	6.68%	CASSPNTETQYF
		Posttreatment	9.88%	CASSFPLVNEQFF	7.24%	CASSQGAGRETQYF
	10	Pretreatment	8.45%	CASSEWGDTQYF	7.59%	CASRPSGTGGYNEQFF
		Posttreatment	9.04%	CASSEWGDTQYF	4.57%	CASRPSGTGGYNEQFF
	7	Pretreatment	23.40%	CASSQELLAGGPSDTQYF	5.78%	CSARDHYEAF
		Posttreatment	26.11%	CASSQELLAGGPSDTQYF	7.59%	CSARDHYEAF
Response	5	Pretreatment	9.33%	CASSEQSGGYEQYF	2.63%	CASSLNKGYGYTF
		Posttreatment	7.82%	CASSYSYEQYF	3.59%	CASSHPTGVEQYF
	9	Pretreatment	16.93%	CASSLIPGLKETQYF	12.41%	CASSQAPDNYQPQHF
		Posttreatment	9.79%	CASSLIPGLKETQYF	9.40%	CASSQAPDNYQPQHF
	12	Pretreatment	2.73%	CASSVKGSSGPLHF	2.08%	CATSSQDNTEAFF
		Posttreatment	9.94%	CASSVKGSSGPLHF	3.71%	CATSSQDNTEAFF
	6	Pretreatment	11.22%	CASSYSYEQYF	6.43%	CASSFGQGVYNEQFF
		Posttreatment	4.12%	CASRGTYGLNSPLHF	2.58%	CASSQPGQGTGELFF
	4	Pretreatment	19.50%	CSADGTSGNIQYF	14.21%	CASSQGGGQPQHF
		Posttreatment	14.00%	CSADGTSGNIQYF	7.16%	CASSQGGGQPQHF
	8	Pretreatment	5.40%	CASSFLGAGAQTQYF	1.36%	CASSKRENTGELFF
		Posttreatment	5.89%	CASSFLGAGAQTQYF	4.57%	CASSKRENTGELFF
	11	Pretreatment	14.07%	CATQWQQLALHF	12.58%	CATEDGRFRQYF
		Posttreatment	7.79%	CASSEGRGANGYTF	7.08%	CASSFTAGAETQYF



Targeting cancer immunity deficiency is not a single-factor control experiment; multiple factors and unknown events influence the final results of immunotherapy. Our study noticed that patients who responded to anti-PD-L1 therapy are younger than those who progressed (53.5 vs. 64.8 years,  $p < 0.05$ , **Supplementary Table S2**). The impact of age on the therapeutic efficacy of anti-PD-1/PD-L1 treatment is controversial, but phenotypic changes in the adaptive immune system with age certainly include less naïve T cells and more memory T cells, which result in decrease of the TCR repertoire (Nishijima et al., 2016; Daste et al., 2017; Marrone and Forde, 2017).

Several limitations of this study should be noticed. First, all of our patients were from a single institution, and the small cohort restricted the statistical power. So, we focused on describing the features of the TCR repertoire instead of making definite conclusions. Second, considering the patient's willingness and costs, the information of PD-L1 and other inhibitory receptors' expression levels were not recorded in every patient; therefore, more detailed analyses were lacking. Third, the percentage of overlap between tumor-infiltrating lymphocytes (TILs) and peripheral TCR repertoire is still in debate, but TILs are not tested. Further studies are needed to confirm whether circulating T cells can represent TILs. Finally, although we defined TCR repertoire changing patterns for early recognition of atezolizumab-sensitive patients, details of standards need large-scaled and well-organized research to confirm.

In conclusion, our study confirmed the existence of T cells with an exhaustion phenotype in Chinese advanced NSCLC patients, and TCR repertoire diversity is correlated with the

efficacy of anti-PD-L1 therapy. Moreover, monitoring diversity index or patterns of reshaped TCR repertoires by effective PD-L1 blockade treatment may become the biomarkers during immunotherapy.

## DATA AVAILABILITY STATEMENT

The datasets presented in this study can be found in online repositories. The names of the repository/repositories and accession number(s) can be found in the article/**Supplementary Material**.

## ETHICS STATEMENT

The studies involving human participants were reviewed and approved by the Ethics Committee of Sir Run Run Shaw Hospital, School of Medicine, Zhejiang University. The patients/participants provided their written informed consent to participate in this study.

## AUTHOR CONTRIBUTIONS

JS designed the analysis and collected the clinical follow-up data; HW contributed the data analysis, performed the data interpretation, and wrote the article; XL contributed analysis tools and performed the analysis of flow cytometry; YD, YY, and PX performed the analysis of sequencing; JS, HP, HL, and XZ



collected the clinical follow-up data; WH contributed critical revision of the article; TS, HP, and YF approved the final version to be published.

## FUNDING

This work was supported by the National Natural Science Foundation of China (Grant No. 81702809) and the Medical

Science and Technology Project of Zhejiang Province (Grant Nos. 2016ZDB007 and 2017ZD021).

## SUPPLEMENTARY MATERIAL

The Supplementary Material for this article can be found online at: <https://www.frontiersin.org/articles/10.3389/fmolb.2021.679130/full#supplementary-material>

## REFERENCES

- Blackburn, S. D., Shin, H., Freeman, G. J., and Wherry, E. J. (2008). Selective Expansion of a Subset of Exhausted CD8 T Cells by PD-L1 Blockade. *Proc. Natl. Acad. Sci.* 105, 15016–15021. doi:10.1073/pnas.0801497105
- Briney, B., Inderbitzin, A., Joyce, C., and Burton, D. R. (2019). Commonality Despite Exceptional Diversity in the Baseline Human Antibody Repertoire. *Nature* 566, 393–397. doi:10.1038/s41586-019-0879-y
- Britanova, O. V., Putintseva, E. V., Shugay, M., Merzlyak, E. M., Turchaninova, M. A., Staroverov, D. B., et al. (2014). Age-Related Decrease in TCR Repertoire Diversity Measured with Deep and Normalized Sequence Profiling. *J. Immunol.* 192, 2689–2698. doi:10.4049/jimmunol.1302064
- Butte, M. J., Keir, M. E., Phamduy, T. B., Sharpe, A. H., and Freeman, G. J. (2007). Programmed Death-1 Ligand 1 Interacts Specifically with the B7-1 Costimulatory Molecule to Inhibit T Cell Responses. *Immunity* 27, 111–122. doi:10.1016/j.immuni.2007.05.016
- Califano, R., Greystoke, A., Lal, R., Thompson, J., and Popat, S. (2017). Management of Ceritinib Therapy and Adverse Events in Patients with ALK -rearranged Non-small Cell Lung Cancer. *Lung Cancer* 111, 51–58. doi:10.1016/j.lungcan.2017.06.004
- Chen, D. S., and Mellman, I. (2017). Elements of Cancer Immunity and the Cancer-Immune Set point. *Nature* 541, 321–330. doi:10.1038/nature21349
- Cowell, L. G. (2020). The Diagnostic, Prognostic, and Therapeutic Potential of Adaptive Immune Receptor Repertoire Profiling in Cancer. *Cancer Res.* 80, 643–654. doi:10.1158/0008-5472.CAN-19-1457
- Curiel, T. J., Wei, S., Dong, H., Alvarez, X., Cheng, P., Mottram, P., et al. (2003). Blockade of B7-H1 Improves Myeloid Dendritic Cell-Mediated Antitumor Immunity. *Nat. Med.* 9, 562–567. doi:10.1038/nm863
- Curiel, T. J. (2007). Tregs and rethinking cancer immunotherapy. *J. Clin. Invest.* 117, 1167–1174. doi:10.1172/JCI31202
- Daste, A., Domblides, C., Gross-goupil, M., Chakiba, C., Quivy, A., Cochin, V., et al. (2017). Immune Checkpoint Inhibitors and Elderly People: A Review. *Eur. J. Cancer* 82, 155–166. doi:10.1016/j.iejca.2017.05.044
- Fridman, W. H., Zitvogel, L., Sautès-Fridman, C., and Kroemer, G. (2017). The Immune Contexture in Cancer Prognosis and Treatment. *Nat. Rev. Clin. Oncol.* 14, 717–734. doi:10.1038/nrclinonc.2017.101
- Gros, A., Parkhurst, M. R., Tran, E., Pasetto, A., Robbins, P. F., Ilyas, S., et al. (2016). Prospective Identification of Neoantigen-specific Lymphocytes in the Peripheral Blood of Melanoma Patients. *Nat. Med.* 22, 433–438. doi:10.1038/nm.4051
- Hida, T., Nohhara, H., Kondo, M., Kim, Y. H., Azuma, K., Seto, T., et al. (2017). Alectinib versus Crizotinib in Patients with ALK -positive Non-small-cell Lung Cancer (J-ALEX): an Open-Label, Randomised Phase 3 Trial. *The Lancet* 390, 29–39. doi:10.1016/S0140-6736(17)30565-2
- Jamal-Hanjani, M., Wilson, G. A., McGranahan, N., Birkbak, N. J., Watkins, T. B. K., Veeriah, S., et al. (2017). Tracking the Evolution of Non-small-Cell Lung Cancer. *N. Engl. J. Med.* 376, 2109–2121. doi:10.1056/NEJMoa1616288
- Kaplinsky, J., and Arnaout, R. (2016). Robust Estimates of Overall Immune-Repertoire Diversity from High-Throughput Measurements on Samples. *Nat. Commun.* 7, 11881. doi:10.1038/ncomms11881
- Keir, M. E., Butte, M. J., Freeman, G. J., and Sharpe, A. H. (2008). PD-1 and Its Ligands in Tolerance and Immunity. *Annu. Rev. Immunol.* 26, 677–704. doi:10.1146/annurev.immunol.26.021607.090331
- Kirsch, I., Vignali, M., and Robins, H. (2015). T-cell Receptor Profiling in Cancer. *Mol. Oncol.* 9, 2063–2070. doi:10.1016/j.molonc.2015.09.003
- Kiura, K., Imamura, F., Kagamu, H., Matsumoto, S., Hida, T., Nakagawa, K., et al. (2018). Phase 3 Study of Ceritinib vs Chemotherapy in ALK-Rearranged NSCLC Patients Previously Treated with Chemotherapy and Crizotinib (ASCEND-5): Japanese Subset. *Jpn. J. Clin. Oncol.* 48, 367–375. doi:10.1093/jjco/hyy016
- Lee, A. H., and Prins, R. M. (2016). New Applications for Deep Sequencing of the T Cell Receptor Repertoire in Cancer Patients. *Transl. Cancer Res.* 5, S842–S843. doi:10.21037/tcr.2016.10.10
- Lin, H., Wei, S., Hurt, E. M., Green, M. D., Zhao, L., Vatan, L., et al. (2018). Host Expression of PD-L1 Determines Efficacy of PD-L1 Pathway Blockade-Mediated Tumor Regression. *J. Clin. Invest.* 128, 805–815. doi:10.1172/JCI96113
- Liu, Y. Y., Yang, Q. F., Yang, J. S., Cao, R. B., Liang, J. Y., Liu, Y. T., et al. (2019). Characteristics and Prognostic Significance of Profiling the Peripheral Blood T-cell Receptor Repertoire in Patients with Advanced Lung Cancer. *Int. J. Cancer* 145, 1423–1431. doi:10.1002/ijc.32145
- Marrone, K. A., and Forde, P. M. (2017). Cancer Immunotherapy in Older Patients. *Cancer J.* 23, 4. doi:10.1097/00130404-201707000-00005
- McLane, L. M., Abdel-Hakeem, M. S., and Wherry, E. J. (2019). CD8 T Cell Exhaustion During Chronic Viral Infection and Cancer. *Annu. Rev. Immunol.* 37, 457–495. doi:10.1146/annurev-immunol-041015-055318
- Nishijima, T. F., Muss, H. B., Shachar, S. S., and Moschos, S. J. (2016). Comparison of Efficacy of Immune Checkpoint Inhibitors (ICIs) between Younger and Older Patients: A Systematic Review and Meta-Analysis. *Cancer Treat. Rev.* 45, 30–37. doi:10.1016/j.ctrv.2016.02.006
- Novello, S., Mazières, J., Oh, I.-J., de Castro, J., Migliorino, M. R., Helland, Å., et al. (2018). Alectinib versus Chemotherapy in Crizotinib-Pretreated Anaplastic Lymphoma Kinase (ALK)-positive Non-small-cell Lung Cancer: Results from the Phase III ALUR Study. *Ann. Oncol.* 29, 1409–1416. doi:10.1093/annonc/ndy121
- Peters, S., Camidge, D. R., Shaw, A. T., Gadgeel, S., Ahn, J. S., Kim, D.-W., et al. (2017). Alectinib versus Crizotinib in Untreated ALK-Positive Non-small-Cell Lung Cancer. *N. Engl. J. Med.* 377, 829–838. doi:10.1056/NEJMoa1704795
- Pielou, E. C. (1966). The Measurement of Diversity in Different Types of Biological Collections. *J. Theor. Biol.* 13, 131–144. doi:10.1016/0022-5193(66)90013-0
- Ribas, A., and Wolchok, J. D. (2018). Cancer Immunotherapy Using Checkpoint Blockade. *Science* 359, 1350–1355. doi:10.1126/science.aar4060
- Robert, L., Tsoi, J., Wang, X., Emerson, R., Homet, B., Chodon, T., et al. (2014). CTLA4 Blockade Broadens the Peripheral T-Cell Receptor Repertoire. *Clin. Cancer Res.* 20, 2424–2432. doi:10.1158/1078-0432.CCR-13-2648
- Robins, H. S., Srivastava, S. K., Campregher, P. V., Turtle, C. J., Andriesen, J., Riddell, S. R., et al. (2010). Overlap and Effective Size of the Human CD8+ T Cell Receptor Repertoire. *Sci. Translational Med.* 2, 47ra64. doi:10.1126/scitranslmed.3001442
- Schluns, K. S., Kieper, W. C., Jameson, S. C., and Lefrançois, L. (2000). Interleukin-7 Mediates the Homeostasis of Naïve and Memory CD8 T Cells *In Vivo*. *Nat. Immunol.* 1, 426–432. doi:10.1038/80868
- Schrama, D., Ritter, C., and Becker, J. C. (2017). T Cell Receptor Repertoire Usage in Cancer as a Surrogate Marker for Immune Responses. *Semin. Immunopathol* 39, 255–268. doi:10.1007/s00281-016-0614-9
- Siegel, R. L., Miller, K. D., and Jemal, A. (2017). Cancer statistics, 2017. *CA. Cancer J. Clin.* 67, 7–30. doi:10.3322/caac.21387

- Snyder, A., Nathanson, T., Funt, S. A., Ahuja, A., Buros Novik, J., Hellmann, M. D., et al. (2017). Contribution of Systemic and Somatic Factors to Clinical Response and Resistance to PD-L1 Blockade in Urothelial Cancer: An Exploratory Multi-Omic Analysis. *PLOS Med.* 14, e1002309. doi:10.1371/journal.pmed.1002309
- Sui, H., Ma, N., Wang, Y., Li, H., Liu, X., Yu, Y., et al. (2018). Anti-PD-1/PD-L1 Therapy for Non-Small Cell Lung Cancer: Toward Personalized Medicine and Combination Strategies. *J. Immunol. Res.* 2018, 1–17. doi:10.1155/2018/6984948
- Swanton, C., and Govindan, R. (2016). Clinical Implications of Genomic Discoveries in Lung Cancer. *N. Engl. J. Med.* 374, 1864–1873. doi:10.1056/NEJMr1504688
- Syn, N. L., Teng, M. W. L., Mok, T. S. K., and Soo, R. A. (2017). De-novo and Acquired Resistance to Immune Checkpoint Targeting. *Lancet Oncol.* 18, e731–e741. doi:10.1016/S1470-2045(17)30607-1
- Taube, J. M., Anders, R. A., Young, G. D., Xu, H., Sharma, R., McMiller, T. L., et al. (2012). Colocalization of Inflammatory Response with B7-H1 Expression in Human Melanocytic Lesions Supports an Adaptive Resistance Mechanism of Immune Escape. *Sci. Translational Med.* 4, 127ra37. doi:10.1126/scitranslmed.3003689
- Teng, M. W. L., Ngiow, S. F., Ribas, A., and Smyth, M. J. (2015). Classifying Cancers Based on T-Cell Infiltration and PD-L1. *Cancer Res.* 75, 2139–2145. doi:10.1158/0008-5472.CAN-15-0255
- Tsui, D. W. Y., Murtaza, M., Wong, A. S. C., Rueda, O. M., Smith, C. G., Chandrananda, D., et al. (2018). Dynamics of Multiple Resistance Mechanisms in Plasma DNA during EGFR-Targeted Therapies in Non-small Cell Lung Cancer. *EMBO Mol. Med.* 10. doi:10.15252/emmm.201707945
- Wang, X., Hu, Y., Liu, X., Yu, J., Xu, P., Wei, G., et al. (2019). Quantitative Characterization of T-Cell Repertoire Alteration in Chinese Patients with B-Cell Acute Lymphocyte Leukemia after CAR-T Therapy. *Bone Marrow Transpl.* 54, 2072–2080. doi:10.1038/s41409-019-0625-y
- Warren, E. H., Iv, F. A. M., and Chou, J. (2013). High-throughput Sequencing of B- and T-Lymphocyte Antigen Receptors in Hematology. *Blood* 122, 5. doi:10.1182/blood-2013-03-453142
- Wherry, E. J., and Kurachi, M. (2015). Molecular and Cellular Insights into T Cell Exhaustion. *Nat. Rev. Immunol.* 15, 486–499. doi:10.1038/nri3862
- Wieland, A., Kamphorst, A. O., Adsay, N. V., Masor, J. J., Sarmiento, J., Nasti, T. H., et al. (2018). T Cell Receptor Sequencing of Activated CD8 T Cells in the Blood Identifies Tumor-Infiltrating Clones that Expand after PD-1 Therapy and Radiation in a Melanoma Patient. *Cancer Immunol. Immunother.* 67, 1767–1776. doi:10.1007/s00262-018-2228-7
- Zarnitsyna, V. I., Evavold, B. D., Schoettle, L. N., Blattman, J. N., and Antia, R. (2013). Estimating the Diversity, Completeness, and Cross-Reactivity of the T Cell Repertoire. *Front. Immunol.* 4, 485. doi:10.3389/fimmu.2013.00485
- Zhang, L., Cham, J., Paciorek, A., Trager, J., Sheikh, N., and Fong, L. (2017). 3D: Diversity, Dynamics, Differential Testing - a Proposed Pipeline for Analysis of Next-Generation Sequencing T Cell Repertoire Data. *BMC Bioinformatics* 18, 129. doi:10.1186/s12859-017-1544-9

**Conflict of Interest:** Authors YD, YY, PX, and TS were employed by the company Hangzhou ImmuQuad Biotechnologies, LLC.

The remaining authors declare that the research was conducted in the absence of any commercial or financial relationships that could be construed as a potential conflict of interest.

Copyright © 2021 Sheng, Wang, Liu, Deng, Yu, Xu, Shou, Pan, Li, Zhou, Han, Sun, Pan and Fang. This is an open-access article distributed under the terms of the Creative Commons Attribution License (CC BY). The use, distribution or reproduction in other forums is permitted, provided the original author(s) and the copyright owner(s) are credited and that the original publication in this journal is cited, in accordance with accepted academic practice. No use, distribution or reproduction is permitted which does not comply with these terms.



# Expression and Gene Regulation Network of Adenosine Receptor A2B in Lung Adenocarcinoma: A Potential Diagnostic and Prognostic Biomarker

Yutong Sui<sup>1†</sup>, Jiayin Liu<sup>2†</sup>, Jing Zhang<sup>1</sup>, Zena Zheng<sup>1</sup>, Ziwei Wang<sup>1</sup>, Zhenghu Jia<sup>3\*</sup> and Ziyu Meng<sup>4\*</sup>

<sup>1</sup>Shenzhen Hospital, Southern Medical University, Shenzhen, China, <sup>2</sup>Department of Radiation Oncology, Harbin Medical University Cancer Hospital, Harbin, China, <sup>3</sup>The First Affiliated Hospital, Biomedical Translational Research Institute and Guangdong Province Key Laboratory of Molecular Immunology and Antibody Engineering, Jinan University, Guangzhou, China, <sup>4</sup>NHC Key Laboratory of Hormones and Development, Tianjin Key Laboratory of Metabolic Diseases, Chu Hsien-I Memorial Hospital and Tianjin Institute of Endocrinology, Tianjin Medical University, Tianjin, China

## OPEN ACCESS

### Edited by:

Min Zhang,  
Shanghai First People's Hospital,  
China

### Reviewed by:

Jiarong Chen,  
Jiangmen Central Hospital, China  
Xiaoping Li,  
Jiangmen Central Hospital, China

### \*Correspondence:

Zhenghu Jia  
jiazhenghu86@163.com  
Ziyu Meng  
mengziyu@tmu.edu.cn

<sup>†</sup>These authors have contributed  
equally to this work

### Specialty section:

This article was submitted to  
Molecular Diagnostics and  
Therapeutics,  
a section of the journal  
Frontiers in Molecular Biosciences

Received: 02 February 2021

Accepted: 17 June 2021

Published: 19 July 2021

### Citation:

Sui Y, Liu J, Zhang J, Zheng Z, Wang Z,  
Jia Z and Meng Z (2021) Expression  
and Gene Regulation Network of  
Adenosine Receptor A2B in Lung  
Adenocarcinoma: A Potential  
Diagnostic and Prognostic Biomarker.  
Front. Mol. Biosci. 8:663011.  
doi: 10.3389/fmolb.2021.663011

Adenosine receptor A2B (*ADORA2B*) encodes a protein belonging to the G protein-coupled receptor superfamily. Abnormal expression of *ADORA2B* may play a pathophysiological role in some human cancers. We investigated whether *ADORA2B* is a potential diagnostic and prognostic biomarker for lung adenocarcinoma (LUAD). The expression, various mutations, copy number variations, mRNA expression levels, and related network signaling pathways of *ADORA2B* were analyzed using bioinformatics-related websites, including Oncomine, UALCAN, cBioPortal, GeneMANIA, LinkedOmics, KM Plotter, and TIMER. We found that *ADORA2B* was overexpressed and amplified in LUAD, and a high *ADORA2B* expression predicted a poor prognosis for LUAD patients. Pathway analyses of *ADORA2B* in LUAD revealed *ADORA2B*-correlated signaling pathways, and the expression level of *ADORA2B* was associated with immune cell infiltration. Furthermore, *ADORA2B* mRNA and protein levels were significantly higher in human LUAD cell lines (A549 cells and NCI-H1299 cells) than in normal human bronchial epithelial (HBE) cells, and the transcript levels of genes positively or negatively correlated with *ADORA2B* were consistent and statistically significant. siRNA transfection experiments and functional experiments further confirmed these results. *In vitro* results were also consistent with those of bioinformatics analysis. Our findings provide a foundation for studying the role of *ADORA2B* in tumorigenesis and support the development of new drug targets for LUAD.

**Keywords:** *ADORA2B*, lung adenocarcinoma, mRNA expression, functional network analysis, verification experiment

**Abbreviations:** AAMP, angio-associated migratory cell protein; *ADORA2B*, adenosine receptor A2B; ALK, anaplastic lymphoma kinase; ANXA1, annexin A1; CBFA2T2, CBFA2/RUNX1 partner transcriptional co-repressor 2; BRAF, V-raf murine sarcoma viral oncogene homolog B1; DCC, netrin 1 receptor; DPH, diphthamide biosynthesis 1; EGFR, epidermal growth factor receptor; GEO, Gene Expression Omnibus; HER2, human epidermal growth factor receptor 2; ITGA3, integrin subunit alpha 3; KCNJ3, potassium inwardly rectifying channel subfamily J member 3; KDM2B, lysine demethylase 2B; KRAS, Kirsten rat sarcoma viral oncogene; LUAD, lung adenocarcinoma; NEB, nebulin; OS, overall survival; PEX6, peroxisomal biogenesis factor 6; RET, rearranged during transfection; ROS1, ROS proto-oncogene 1; SLC29A2, solute carrier family 29 member 2; SLC9A3R2, solute carrier family 9 member A3 regulator 2; S100A6, S100 calcium binding protein A6; TCGA, The Cancer Genome Atlas; TPD52L2, tumor protein D52-like 2; ZNF267, zinc finger protein 267.

## INTRODUCTION

Lung adenocarcinoma (LUAD) is a common pathological form of lung cancer and is associated with high mortality, leading to more than one million deaths worldwide every year (TCGA, 2018). LUAD is characterized by the presence of heterogeneous tumors that originate in the small airway and spread to the surrounding lung tissue (Yu et al., 2010; Russell et al., 2011). Multiple organ metastasis is the leading cause of death in LUAD patients. Within a few months after diagnosis, metastasis to different organs can occur rapidly. Traditional modalities, such as radiotherapy and chemotherapy, are ineffective for LUAD (Zagryazhskaya et al., 2015), and targeted gene therapy holds potential for the clinical management of LUAD. Epidermal growth factor receptor (EGFR) mutation and anaplastic lymphoma kinase (ALK) fusion are the common gene abnormalities reported in LUAD. Personalized therapy targeting these genes has become a well-designed standard treatment, with erlotinib and gefitinib being the main drugs for LUAD treatment (Yu et al., 2013). Furthermore, mutations in Kirsten rat sarcoma viral oncogene (KRAS), human epidermal growth factor receptor 2 (HER2), and V-raf murine sarcoma viral oncogene homolog B1 (BRAF) as well as other fusions of driver genes, such as rearranged during transfection (RET) and ROS proto-oncogene 1 (ROS1), have been reported in LUAD (Roman et al., 2018; Pillai et al., 2017; Mazieres et al., 2020; Drilon, et al., 2020; Shaw, et al., 2017). These driver genes vary depending on race, sex, and smoking status. The pathogenesis of LUAD is complex and mainly involves cell cycle regulation and signal transduction, reflected in altered gene function at different developmental stages of the disease. New drug targets for LUAD should be identified by screening gene networks associated with tumor formation and progression.

Most of the extracellular adenosine is released from adenine nucleotides in response to various stimuli, including mechanical stress, osmotic stimulation, inflammation, and tissue damage (Borea et al., 2016; Covarrubias et al., 2016; Hamidzadeh and Mosser, 2016). Extracellular adenosine binds to four adenosine receptor subtypes, namely, A1, A2A, A2B, and A3, each of which exhibits unique pharmacological and coupling effects and tissue distribution characteristics. Adenosine receptor A2B (ADORA2B) encodes an adenosine receptor belonging to the G protein-coupled receptor superfamily and is highly expressed in various carcinomas, which leads to the promotion of carcinoma cell proliferation and metastasis (Kasama et al., 2015; Vecchio et al., 2016). ADORA2B also regulates the tumor microenvironment and is involved in peripheral vascular growth, inflammatory cell infiltration, fibroblast proliferation, and extracellular matrix accumulation (Csoka et al., 2012). Therefore, ADORA2B regulates tumor progression and metastasis and could serve as a useful target for cancer therapy or combination therapy.

Recent studies have suggested that ADORA2B is an indispensable target in the regulation of both acute and chronic pulmonary diseases, such as pulmonary hypertension, chronic obstructive pulmonary disease, and pulmonary fibrosis (Karmouty-Quintana et al., 2013; Philip et al., 2017; Mertens et al., 2018; Tian et al., 2021). LUAD is

one of the most lethal pulmonary diseases, with the highest mortality rate; however, the role of ADORA2B in LUAD is still unknown. In this study, we analyzed the expression and mutations of ADORA2B in patients with LUAD using data obtained from various public databases. We also analyzed the genomic variations, survival rates, and functional networks associated with ADORA2B in LUAD. Additionally, human LUAD and normal bronchial epithelial cell lines were used to confirm the role of ADORA2B in LUAD. siRNA transfection experiments and functional experiments further confirmed the obtained results. Therefore, we used bioinformatics analysis in combination with *in vitro* experiments to comprehensively investigate the role of ADORA2B in LUAD.

## MATERIALS AND METHODS

### Oncomine Analysis

The mRNA expression of ADORA2B in LUAD was analyzed using the Oncomine database ([www.oncomine.org](http://www.oncomine.org)). LUAD-based databases established from the Okayama Lung, Landi Lung, Selamat Lung, Stearman Lung, Beer Lung, Su Lung, Bhattacharjee Lung, and Garber Lung datasets were used for this analysis (Bhattacharjee et al., 2001; Garber et al., 2001; Beer et al., 2002; Stearman et al., 2005; Su et al., 2007; Landi et al., 2008; Okayama et al., 2012; Selamat et al., 2012). The difference in the expression of ADORA2B between LUAD tissues and paracarcinoma tissues was considered statistically significant at  $p < 0.01$ .

### UALCAN Analysis

Multiple clinical and pathological features related to the mRNA expression of ADORA2B in LUAD were analyzed by UALCAN (<http://ualcan.path.uab.edu>). ADORA2B expression was analyzed by TCGA Level 3 RNA sequencing in UALCAN, and the clinical data were analyzed to determine ADORA2B expression levels in different tumor subgroups (Chandrashekar et al., 2017).

### cBioPortal Analysis

cBioPortal (<http://cbioportal.org>) was used to analyze ADORA2B alterations observed in The Cancer Genome Atlas (TCGA) LUAD samples. By analyzing various types of mutations, copy number variations, and mRNA expression levels, the tab OncoPrint displayed an overview of the genetic changes in each sample as gene mutations and heat maps of ADORA2B expression. The tab plots displayed an overview of the data type of clinical attributes and mutations, including clinical attributes and group mutations by mutation type.

### GeneMANIA Analysis

GeneMANIA (<http://genemania.org/>) is a web interface that uses large sets of functional association data to identify single genes related to a set of input genes, generating hypotheses on gene function, analyzing gene lists, and prioritizing genes for functional assays. GeneMANIA was used to construct the ADORA2B software for the analysis (Warde-Farley et al., 2010).



## LinkedOmics Analysis

The LinkFinder module of LinkedOmics (<http://www.linkedomics.org/login.php>) was used to identify differentially expressed genes related to *ADORA2B* ( $n = 515$ ) in the TCGA LUAD section. The search and target datasets were obtained by RNA-seq, and the results were analyzed with the Pearson correlation coefficient. The data from the LinkFinder results were labeled and sorted before enrichment analysis was performed for Gene Ontology, KEGG, PANTHER, and Reactome pathway analyses.

## Survival Analysis

We used the Kaplan–Meier (KM) Plotter (<http://kmplot.com>), an online database that contains gene expression data and survival information of 865 LUAD patients, to analyze the prognostic value of *ADORA2B* in LUAD. The patient samples were separated into two groups by median expression (high expression and low expression) to analyze the overall survival (OS) with hazard ratios (HRs) with 95% confidence intervals and log-rank  $p$ -values.

## Immune Infiltration Analysis

Tumor Immune Estimation Resource (TIMER, <https://cistrome.shinyapps.io/timer/>) is a web resource for systematic analysis of the infiltration levels of different subsets of immune cells in different types of cancers. We analyzed the expression of *ADORA2B* in LUAD in relation to tumor purity and the abundance of immune infiltrating cells including B cells, CD8<sup>+</sup> T cells, CD4<sup>+</sup> T cells, macrophages, neutrophils, and dendritic cells. We also analyzed the relationship between the gene copy number variation and the abundance of immune infiltrating cells.

## Cell Culture

A549 cells (human LUAD, ATCC®CCL-185™), NCI-H1299 cells (human LUAD, ATCC®CRL-5803™), and HBE cells (human bronchial epithelial cells, ATCC®CRL-2741™) were obtained from ATCC (Manassas, VA, United States). A549 cells were cultured in Dulbecco's modified Eagle's medium (DMEM, Gibco, Grand Island, NY, United States) containing 10% fetal bovine serum (FBS, Gibco), whereas the culture medium for HBE cells contained 20% FBS. NCI-H1299 cells were cultured in RPMI-1640 medium (Gibco, Grand Island, NY, United States) containing 10% FBS. All the cells were incubated in a humidified incubator at 5% CO<sub>2</sub> and 37°C. The cells that passaged less than five with >70% confluency were used for experiments.

## RNA Extraction and Quantitative Real-time PCR (qRT-PCR)

RNA from A549, NCI-H1299, and HBE cells was isolated using TRIzol Reagent (Invitrogen, Carlsbad, CA, United States) according to the manufacturer's instructions. cDNA synthesis was performed using a cDNA First Strand Synthesis Kit (ABclonal, Wuhan, China), and mRNA expression was quantified by qRT-PCR using the SYBR Green Fast qPCR Mix (ABclonal). Relative mRNA expression levels were normalized to

those of  $\beta$ -actin and measured by the comparative Ct ( $2^{-\Delta\Delta C_t}$ ) method ( $n = 6$  samples/group). Primer sequences used in this study are listed in **Supplementary Table S1**.

## siRNA Transfection

*ADORA2B* siRNAs and negative control siRNA (50 nM) were obtained from GenePharma (Shanghai, China). The siRNAs were transfected with Lipofectamine 2000 (Invitrogen) for 4 h, following the manufacturer's protocol. *ADORA2B* knockdown efficiencies were verified by RT-PCR. The siRNA sequences are listed in **Supplementary Table S1**.

## Western Blotting

A549, NCI-H1299, and HBE cells were cultured as previously described (*Cell Culture*). Total protein was extracted using RIPA buffer (Solarbio, Beijing, China). Protein concentrations were measured using a BCA protein assay kit (Solarbio). Protein extracts (50  $\mu$ g/well) were separated by 10% sodium dodecyl sulfate polyacrylamide gel electrophoresis and transferred onto polyvinylidene fluoride membranes. The membranes were blocked with 5% skim milk for 2 h and incubated with anti- $\beta$ -actin (Bioss, bs-0061R, Beijing, China), anti-*ADORA2B* (Bioss, bs-5900R), anti-cyclin D1 (ABclonal, A2708), anti-PCNA (Proteintech, 10205-2-AP, Wuhan, China), anti-N-cadherin (ABclonal, A0433), and anti-vimentin (ABclonal, A2584) antibodies overnight. The next day, the membranes were incubated with a HRP-conjugated secondary antibody and goat anti-rabbit IgG antibody (ABclonal) for 1 h. A western blot detection ECL kit (Advansta, Menlo Park, United States) was used to detect protein bands. Fold-changes in *ADORA2B* protein expression were normalized to those of  $\beta$ -actin.

## Cell Proliferation Assay

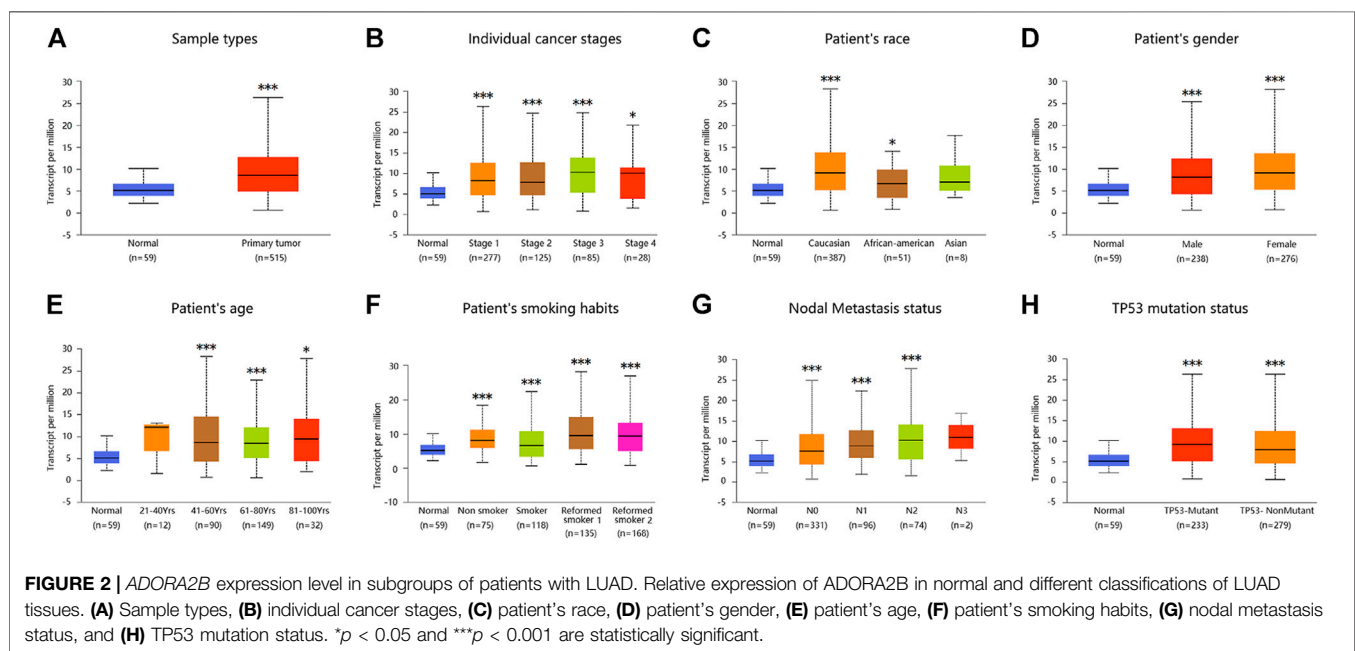
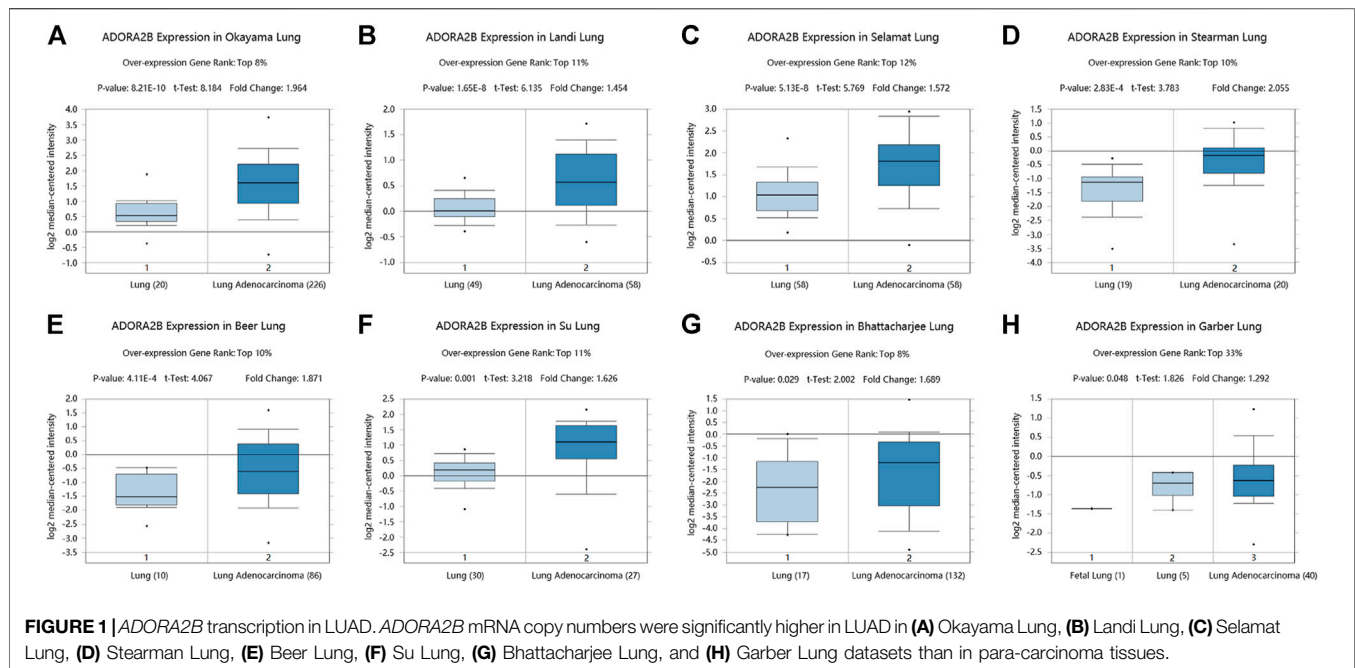
Cell proliferation was measured using cell counting kit-8 (CCK-8, Beyotime, Beijing, China). A549 cells (3000 cells/well) were plated in a 96-well plate and transfected with *ADORA2B* siRNA-2 and negative control siRNA as previously described (*siRNA Transfection*). The cell proliferation rate was detected with CCK-8 at 24, 48, and 72 h. The absorbance at 450 nm was measured using a microplate reader.

## Cell Migration Assay

The cells were transfected with *ADORA2B* siRNA-2 and negative control siRNA using Lipofectamine 2000 as previously described. Transfected cells were grown to 100% confluence, and then wounds were created using pipette tips. Serum-free medium was used instead of complete medium to eliminate the effects of cell proliferation. Images were captured at 0 and 48 h using a microscope. The cell migration rate was calculated by ImageJ software.

## Statistical Analysis

Data are presented as the mean  $\pm$  standard error of the replicates. Comparisons between two groups were performed using Student's  $t$ -test. GraphPad Prism 8.0 software (GraphPad, Inc., La Jolla, CA, United States) was used for statistical analysis.



Results with  $p < 0.05$  were considered statistically significant (\* $p < 0.05$ ; \*\* $p < 0.01$ ; \*\*\* $p < 0.001$ ).

## RESULTS

### Expression of *ADORA2B* in LUAD

We determined *ADORA2B* transcript levels in LUAD patients using data obtained from TCGA and Gene Expression Omnibus (GEO). Data from the Oncomine database showed that the

expression of *ADORA2B* mRNA was significantly upregulated in LUAD tissues when compared with that in para-carcinoma tissues ( $p < 0.01$ ). *ADORA2B* ranked in the top 33% of genes with high mRNA expression, with fold-difference values  $< 2$  (Figures 1A–H).

Similarly, analysis of multiple clinical and pathological features of LUAD patients from the TCGA database revealed elevated *ADORA2B* mRNA expression. Moreover, *ADORA2B* mRNA expression was significantly higher in LUAD tissues than in para-carcinoma tissues in subgroup analyses based on

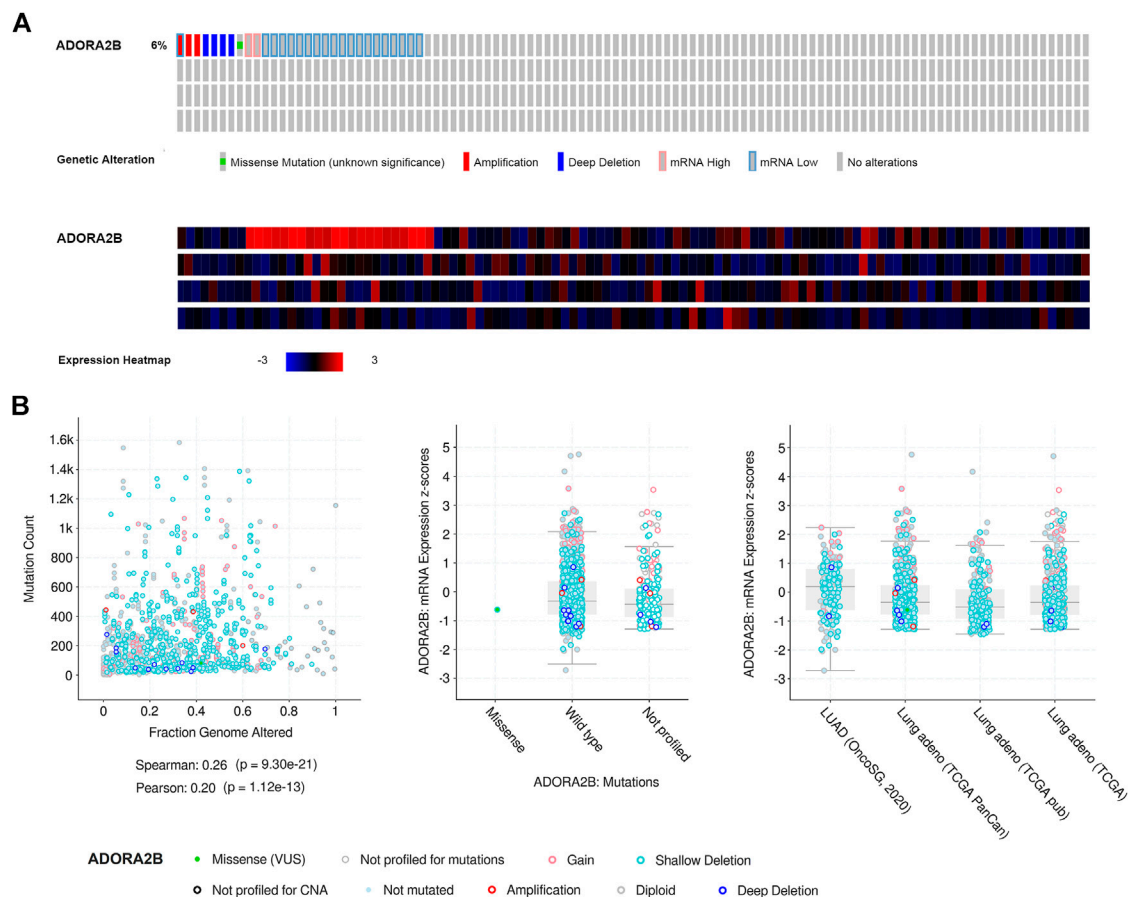


**FIGURE 3 |** Frequency and type of *ADORA2B* alterations in LUAD. **(A)** OncoPrint of *ADORA2B* alterations in LUAD (cBioPortal) and **(B)** plots of *ADORA2B* alterations in LUAD with clinical attributes and mutations (cBioPortal).

sample type, individual cancer stage, ethnicity, gender, age, smoking habits, nodal metastasis status, and TP53 mutation status (Figures 2A–H).

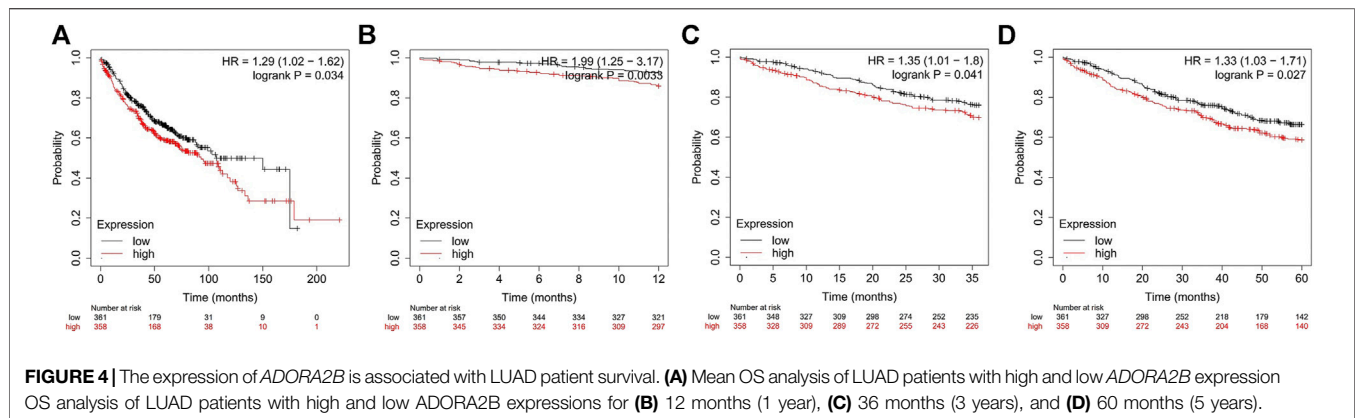
## Frequency and Type of *ADORA2B* Alterations in LUAD

Next, we used the cBioPortal database to evaluate the types and frequencies of *ADORA2B* alterations in LUAD tissues based on sequencing data from patients with LUAD obtained from TCGA's Pan-Cancer Atlas database. *ADORA2B* was altered in 30 out of 503 (6%) patients with LUAD (Figure 3A). These genetic alterations included missense mutations (1, 0.2%), amplification (3, 0.6%), deep deletion (4, 0.8%), mRNA high (2, 0.4%), and mRNA low (20, 4%). The patient order in OncoPrint is shown in **Supplementary Table S2**. Analysis included the type of clinical attribute and mutation, fraction of genome altered, and mutation type, including missense (VUS), not mutated, not profiled for mutations, amplification, gain, diploid, shallow deletion, deep deletion, and not profiled for CNA (Figure 3B). mRNA low, shallow deletion, and diploid were the most

common types of *ADORA2B* genetic alterations found in LUAD.

## Expression of *ADORA2B* Is Associated With the Survival of LUAD Patients

Previous studies have demonstrated that *ADORA2B* participates in the proliferation and metastasis of carcinomas (Kasama et al., 2015; Vecchio et al., 2016). Thus, we further examined the prognostic value of *ADORA2B* in LUAD patients. LUAD patients with a higher expression of *ADORA2B* exhibited poor OS according to the KM Plotter database. Survival analysis showed that the mean OS time in the low *ADORA2B* expression group was longer than that in the high *ADORA2B* expression group ( $p = 0.034$ ) (Figure 4A). The mean OS times for 12 (1 year), 36 (3 years), and 60 months (5 years) in the low *ADORA2B* expression group were significantly longer than those in the high expression group (Figures 4B–D). These results indicated that *ADORA2B* was significantly associated with the prognosis of LUAD patients and that a high *ADORA2B* expression predicted a poor prognosis in LUAD patients.



### Interaction Network of *ADORA2B*

An *ADORA2B* correlation network was constructed to determine the potential mutual effects between *ADORA2B* and cancer-related targets. The results indicated that *ADORA2B* could interact with netrin 1 receptor (*DCC*), solute carrier family 9 member A3 regulator 2 (*SLC9A3R2*), zinc finger protein 267 (*ZNF267*), and tumor protein D52-like 2 (*TPD52L2*); *ADORA2B* was co-expressed with potassium inwardly rectifying channel subfamily J member 3 (*KCNJ3*), angio-associated migratory cell protein (*AAMP*), *TPD52L2*, and solute carrier family 29 member 2 (*SLC29A2*); and *ADORA2B* was co-located with *AAMP*, peroxisomal biogenesis factor 6 (*PEX6*), *SLC29A2*, *ADORA2A*, and diphthamide biosynthesis 1 (*DPH1*). *ADORA2B* was identified to interact with *DCC* and shared protein domains with its isoform *ADORA2A* (Figure 5A).

The LinkedOmics database was used to identify RNA-seq genes co-expressed with *ADORA2B* in LUAD. A volcano plot indicated that the expression of 5,246 genes was negatively correlated with *ADORA2B* expression, whereas the expression of 3,447 genes was positively correlated with *ADORA2B* expression. We confirmed the top 50 genes that negatively or positively interacted with *ADORA2B* (Figure 5B and Supplementary Table S3). The results revealed that multiple differentially expressed genes were correlated with *ADORA2B* expression.

Pearson's correlation coefficient analysis revealed a positive correlation between *ADORA2B* expression levels and those of annexin A1 (*ANXA1*), integrin subunit alpha 3 (*ITGA3*), and S100 calcium binding protein A6 (*S100A6*) and a negative correlation between the expression of *ADORA2B* and that of lysine demethylase 2B (*KDM2B*), nebulin (*NEB*), and CBFA2/RUNX1 partner transcriptional co-repressor 2 (*CBFA2T2*) (Figure 5C).

### Enrichment Analysis of *ADORA2B* Functional Networks in LUAD

Three independent ontologies (biological process, cellular component, and molecular function) were analyzed by gene set enrichment analysis (GSEA). The results indicated that *ADORA2B*-associated differentially expressed genes were

involved in several biological processes (protein targeting, neutrophil mediated immunity, response to IFN- $\gamma$ , etc.), cellular components (ribosome, cell-substrate junction, secretory granule membrane, etc.), and molecular functions (structural constituent of ribosome, cell adhesion molecule binding, enzyme inhibitor activity, etc.) (Figure 6A).

The differentially expressed genes associated with *ADORA2B* were then evaluated for potential functional pathways using KEGG (ribosome, proteoglycans in cancer, fluid shear stress, and atherosclerosis, etc.), PANTHER (FAS, EGF receptor, apoptosis, etc.), and Reactome (influenza infection, major pathway of rRNA processing in the nucleolus and cytosol, cell cycle, etc.) pathway analyses (Figure 6B).

### Relationship Between *ADORA2B* Expression and Infiltrating Immune Cells in LUAD

The tumor microenvironment is a very complex system composed of a variety of cells, enzymes, cytokines, and metabolites and is characterized by low oxygen, low pH, and high pressure. An important immunosuppressive mechanism is mediated by the CD73–adenosine receptor metabolic signaling pathway (Chen et al., 2020). To comprehensively investigate the role of *ADORA2B* in LUAD, we selected the TIMER database to analyze the association of *ADORA2B* expression levels with subsets of infiltrating immune cells. The expression of *ADORA2B* was significantly correlated with the infiltration of B cells, macrophages, neutrophils, and dendritic cells (Figure 7A). In addition, the copy number variation (CNV) of *ADORA2B* was significantly correlated with the infiltration levels of macrophages (Figure 7B).

### Expression Levels of *ADORA2B* and Correlated Genes in Human LUAD Cells

We found that compared with that in normal lung tissues, the expression level of *ADORA2B* was significantly elevated in tumor tissues of LUAD patients with higher morbidity. To confirm that *ADORA2B* expression is related to LUAD, we investigated the *ADORA2B* gene and protein expression in human LUAD (A549



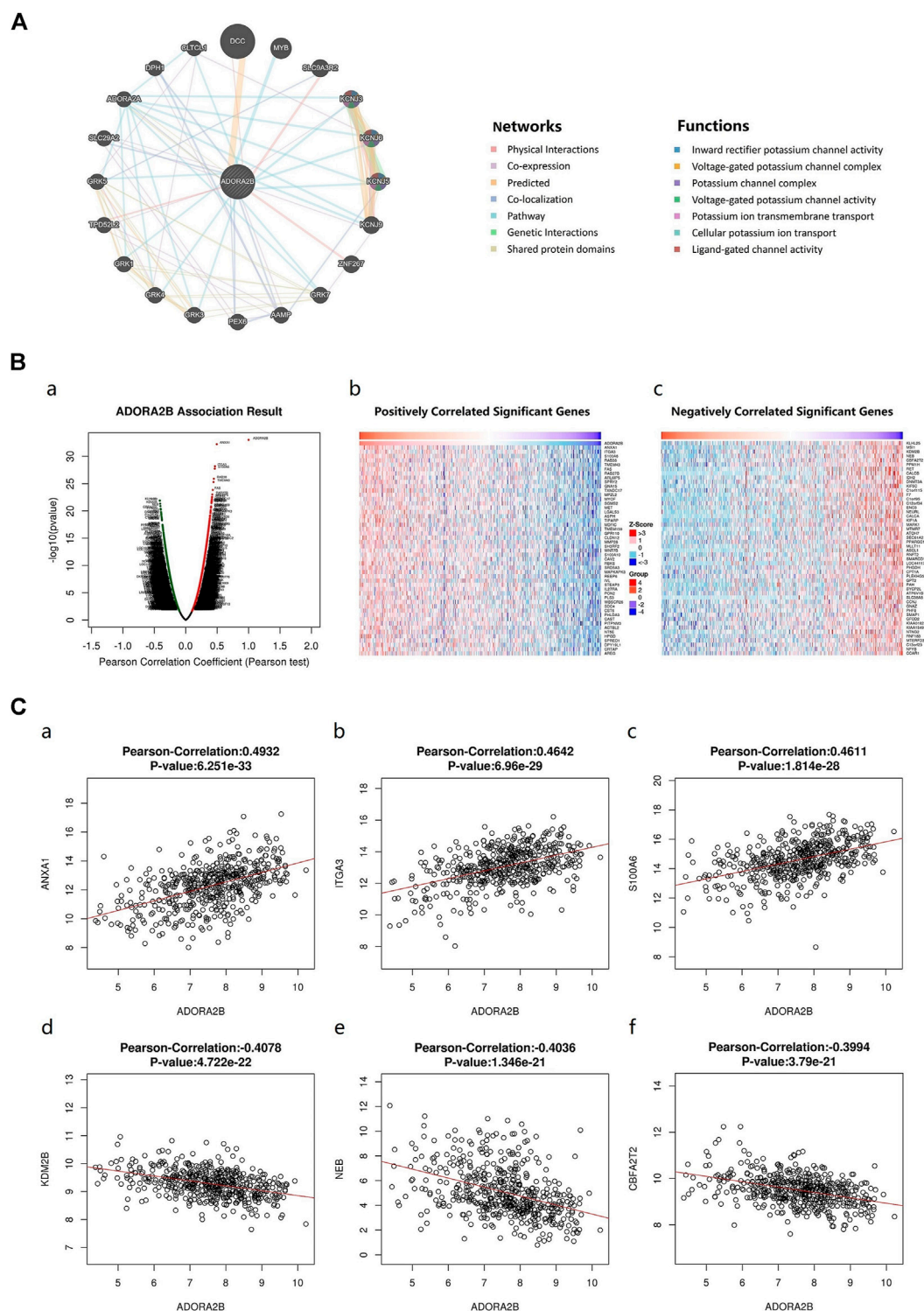
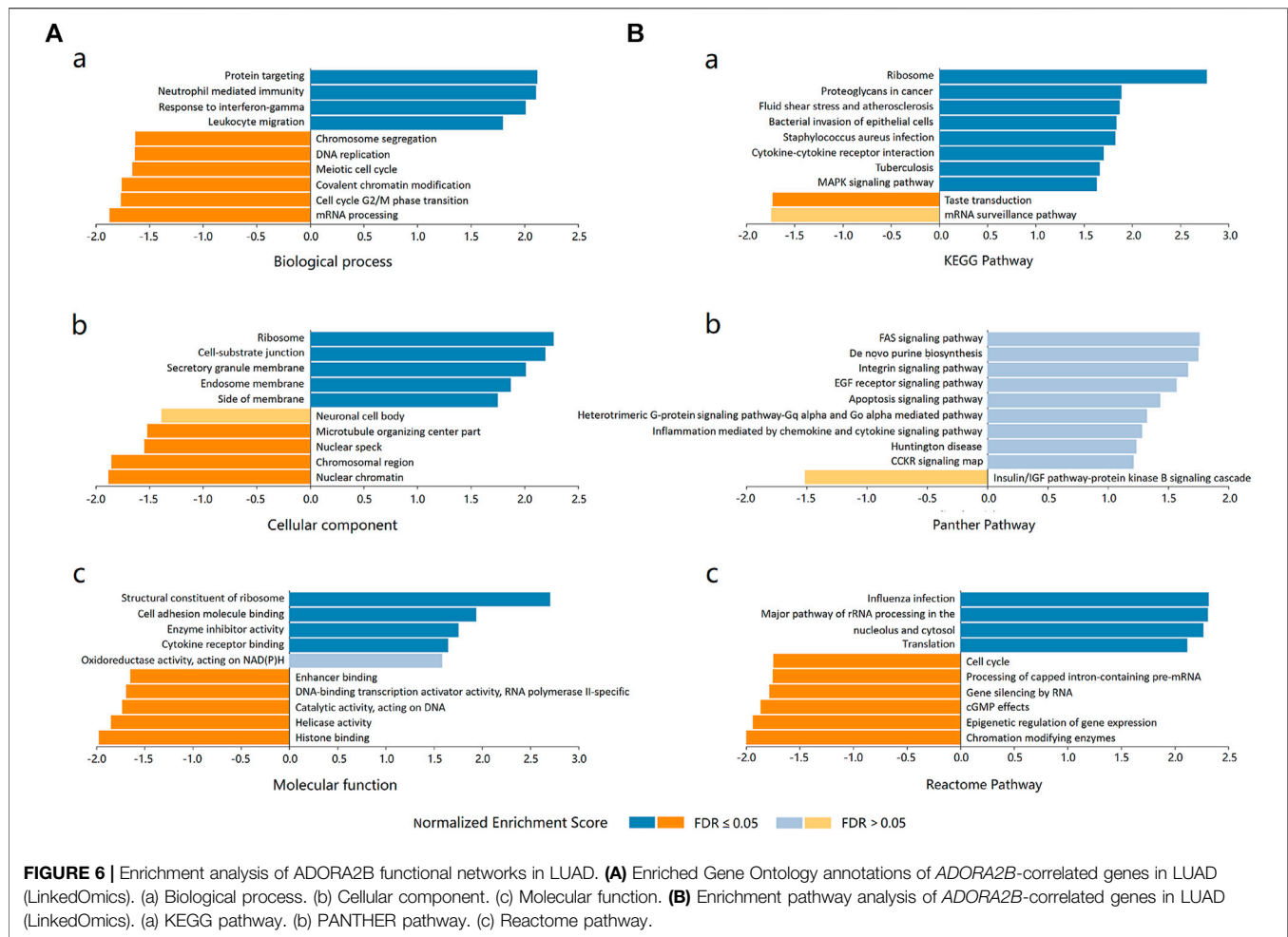


**FIGURE 5 |** Genes associated with *ADORA2B* expression. **(A)** Biological interaction network of *ADORA2B*. **(B)** Differentially expressed genes correlated with *ADORA2B* (LinkedOmics). **(a)** Correlations between *ADORA2B* and differentially expressed genes in LUAD were analyzed with Pearson's correlation coefficient. **(b)** Heat map of genes positively correlated with *ADORA2B* in LUAD. **(c)** Heat map of genes negatively correlated with *ADORA2B* in LUAD. **(C)** Gene expression correlation analysis of *ADORA2B* and *ADORA2B*-correlated genes (LinkedOmics). Pearson correlation of *ADORA2B* expression with that of (a) *ANXA1*, (b) *ITGA3*, (c) *S100A6*, (d) *KDM2B*, (e) *NEB*, and (f) *CBFA2T2* ( $n = 515$ ).



and NCI-H1299) and normal human bronchial epithelial (HBE) cell lines. Western blotting analysis indicated that the relative ADORA2B protein expression levels in A549 cells and NCI-H1299 cells were significantly higher than those in HBE cells (Figures 8A,B). Next, we examined the mRNA expression level of ADORA2B by qRT-PCR and found that the relative ADORA2B mRNA expression level was consistent with the protein expression level in the three cell lines (Figure 8C).

As shown in Figure 5C, LinkedOmics was used to identify the differentially expressed genes related to ADORA2B. The expression levels of ADORA2B-associated genes were positively (ANXA1, ITGA3, and S100A6) or negatively (KDM2B, NEB, and CBFA2T2) correlated with ADORA2B expression in LUAD. To verify these results, we measured the mRNA expression levels of these genes. The expression levels of ANXA1, ITGA3, and S100A6 were significantly higher in A549 cells than in HBE cells and were positively correlated with ADORA2B expression levels (Figure 8D). In contrast, the expression levels of KDM2B, NEB, and CBFA2T2 were significantly lower in A549 cells than in HBE cells and negatively correlated with ADORA2B expression (Figure 8E). These results were consistent with those from our bioinformatics analyses.

To further confirm these findings, specific ADORA2B siRNAs were transfected into A549 cells to inhibit ADORA2B expression. First, we verified the knockdown efficiencies of ADORA2B by qRT-PCR and then selected siRNA-2, which had the highest knockdown efficiency, for subsequent experiments (Figure 8F). Then, we measured the mRNA expression levels of genes that were positively or negatively correlated with ADORA2B expression. The expression levels of ANXA1, ITGA3, and S100A6 were significantly lower in the ADORA2B siRNA group than in the control siRNA group and positively correlated with ADORA2B expression (Figure 8G). The expression levels of KDM2B, NEB, and CBFA2T2 were significantly higher in the ADORA2B siRNA group than in the control siRNA group and negatively correlated with ADORA2B expression (Figure 8H). Taken together, ADORA2B was highly expressed in human LUAD A549 cells and the expression levels of ANXA1, ITGA3, and S100A6 were positively correlated with ADORA2B expression, while those of KDM2B, NEB, and CBFA2T2 were negatively correlated with ADORA2B expression. *In vitro* experimental results were consistent with those of the bioinformatics analyses.

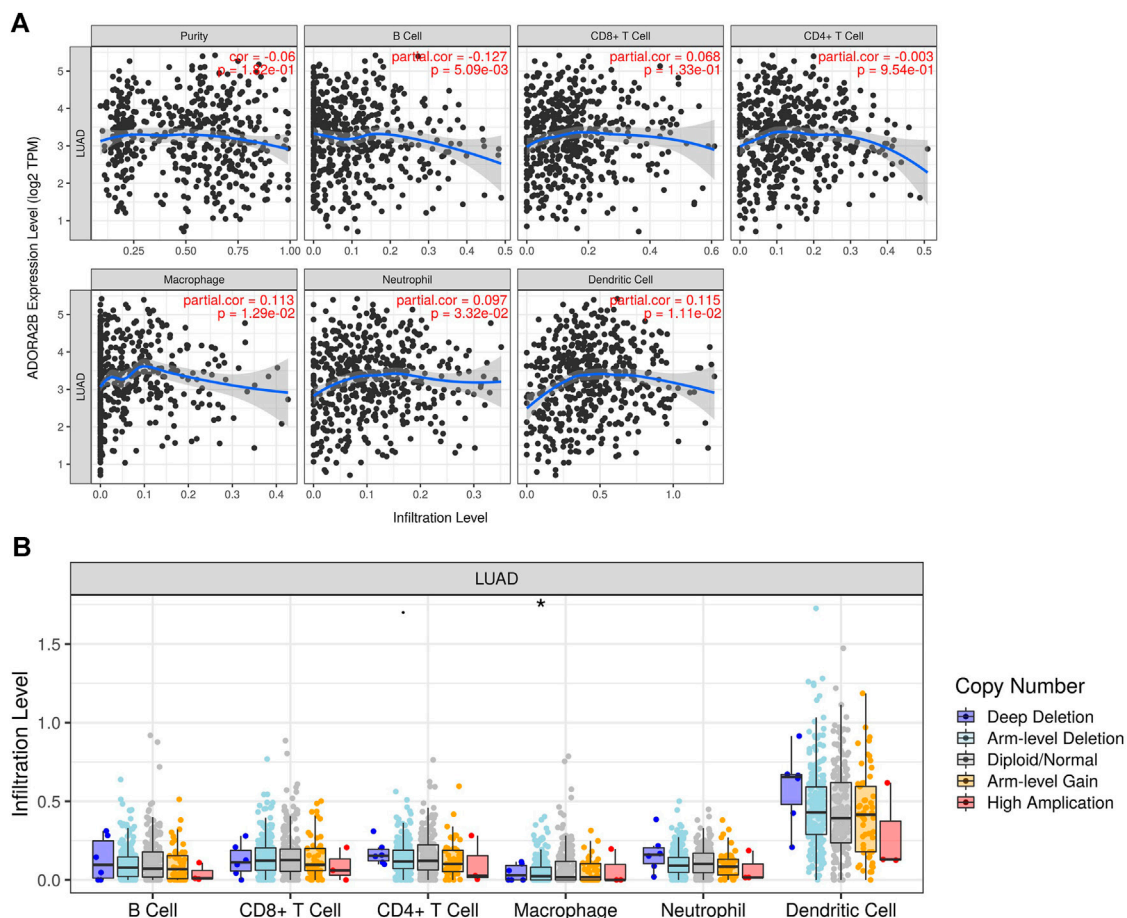


**FIGURE 7 |** Correlation of *ADORA2B* expression with immune cell infiltration in LUAD. **(A)** Correlation of *ADORA2B* with tumor purity and infiltration of different subsets of immune cells. **(B)** Effect of copy number variation of *ADORA2B* on the distribution of various immune cells. \* $p < 0.05$  is statistically significant.

## Knockdown of *ADORA2B* Inhibited the Proliferation and Metastasis of LUAD Cells

Previous studies have demonstrated that *ADORA2B* participates in the proliferation and metastasis of carcinomas, such as prostate and oral cancers (Kasama et al., 2015; Vecchio et al., 2016). To further clarify the role of *ADORA2B* in the progression of LUAD, we performed related functional experiments to verify the function of *ADORA2B*. First, cell proliferation was measured using CCK-8. Compared with that of the control siRNA group, the cell viability of the *ADORA2B* siRNA group was significantly decreased at 24, 48, and 72 h after transfection (Figure 9A). Second, the cell migration rate was evaluated by the wound healing assay, the results of which showed that knockdown of *ADORA2B* reduced the migration capacity of A549 cells after 48 h of induction, partially supporting the role of *ADORA2B* in promoting metastasis in LUAD (Figure 9B). We further examined the protein expression levels of markers of carcinoma cell proliferation and metastasis after *ADORA2B* knockdown. Western blotting analysis indicated that the relative protein expression levels of proliferative (cyclin D1 and PCNA) and metastatic (N-cadherin and vimentin)

markers in the *ADORA2B* siRNA group were significantly lower than those in the control siRNA group (Figures 9C,D). These results demonstrated that knockdown of *ADORA2B* inhibited the proliferation and metastasis of LUAD cells and that *ADORA2B* might participate in the proliferation and metastasis of LUAD cells.

## DISCUSSION

Adenosine is a purinergic molecule that regulates tissue damage and repair. Adenosine receptors belong to the G-protein-coupled receptor superfamily and include A1, A2A, A2B, and A3, which are widely distributed in different human tissues. The expression levels and affinities of adenosine receptors can vary across different tissues and cell types. In addition, these adenosine receptors have different phosphorylation abilities and sensitivities to the G-proteins with which they are conjugated. The A1 receptor is conjugated with the Gi/G0 protein, while the A3 receptor is conjugated with the Gi protein to inhibit the activity of adenylate cyclase and reduce the level of cAMP. In contrast, A2A and A2B receptors are conjugated with Gs proteins

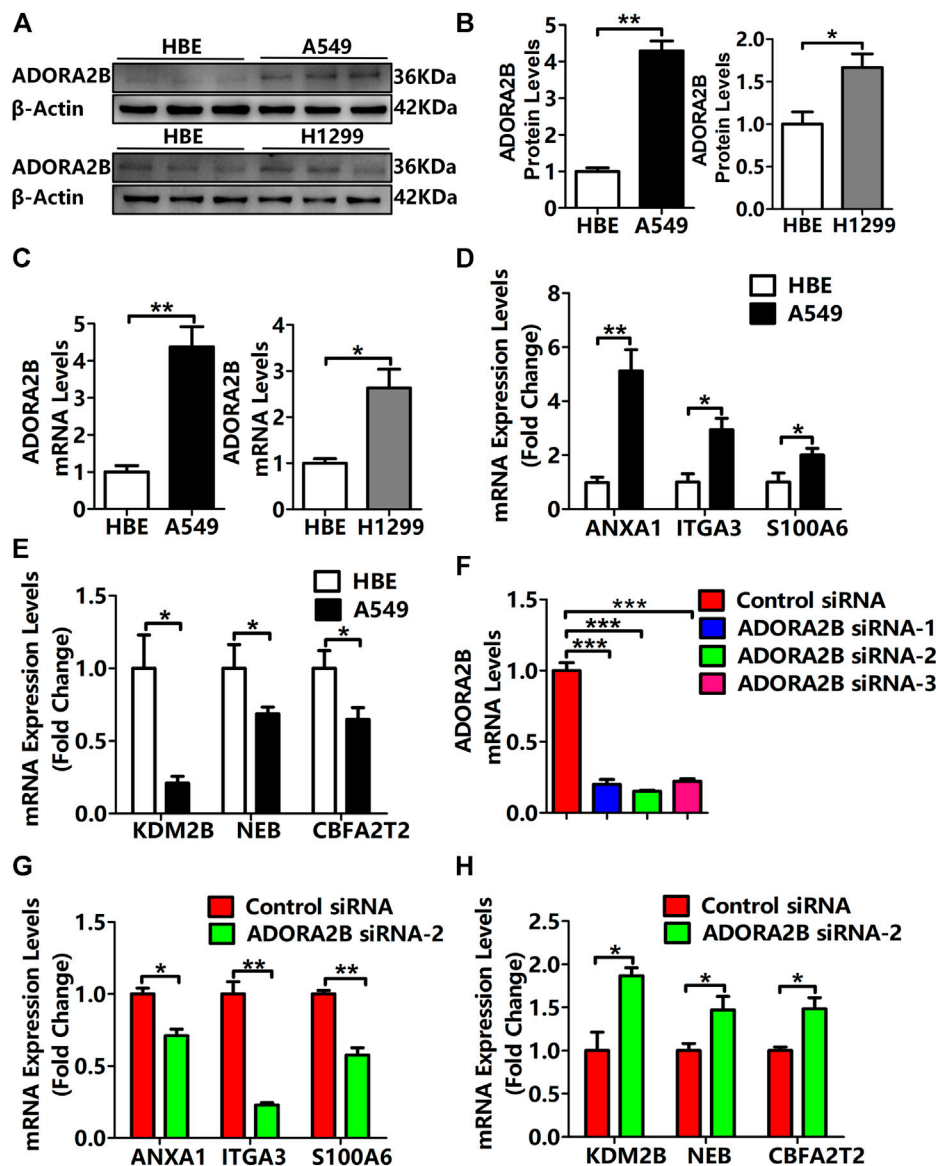


**FIGURE 8 |** Expression levels of *ADORA2B* and correlated genes in human LUAD cells. **(A)** Relative protein expression of *ADORA2B* was determined by western blotting. **(B)** Protein quantitative statistics. **(C)** Relative mRNA expression of *ADORA2B* was determined by qRT-PCR. mRNA expression levels of genes **(D)** positively and **(E)** negatively correlated with *ADORA2B*. **(F)** mRNA expression levels of *ADORA2B* after siRNA transfection. mRNA expression levels of genes **(G)** positively and **(H)** negatively correlated with *ADORA2B* after siRNA transfection. \* $p < 0.05$ , \*\* $p < 0.01$ , and \*\*\* $p < 0.001$  are statistically significant.

to activate the activity of adenylate cyclase and increase the level of cAMP. Low concentrations usually activate the A2A receptor, while higher concentrations of adenosine activate the A2B receptor, which suggests that the basal level of adenosine mainly activates the A2A receptor in a physiological state and that the A2B receptor is activated only when the adenosine level rises above physiological levels or reaches a pathological level (Vecchio et al., 2018; Fenouillet et al., 2019).

Increasing evidence suggests that adenosine receptors are potential diagnostic biomarkers for some diseases, inflammation, and certain types of cancers (Feoktistov and Biaggioni, 2011; Koeppen et al., 2011; Fishman et al., 2012).

Additionally, adenosine receptors are upregulated in various tumors (Fishman et al., 2009). *ADORA2B* plays an important role in the occurrence, development, and metastasis of human tumors and is expressed in a variety of tumor cells. In the present study, to observe the functional network of *ADORA2B* in LUAD, we performed bioinformatics analyses to analyze transcriptional sequencing data from clinical sample data obtained from the Gene Expression Omnibus (GEO) and TCGA databases. To determine the role of *ADORA2B* in LUAD, we evaluated the expression pattern of several genes expressed in the disease. The analysis of the Oncomine database revealed fold-changes in gene expression levels that were similar



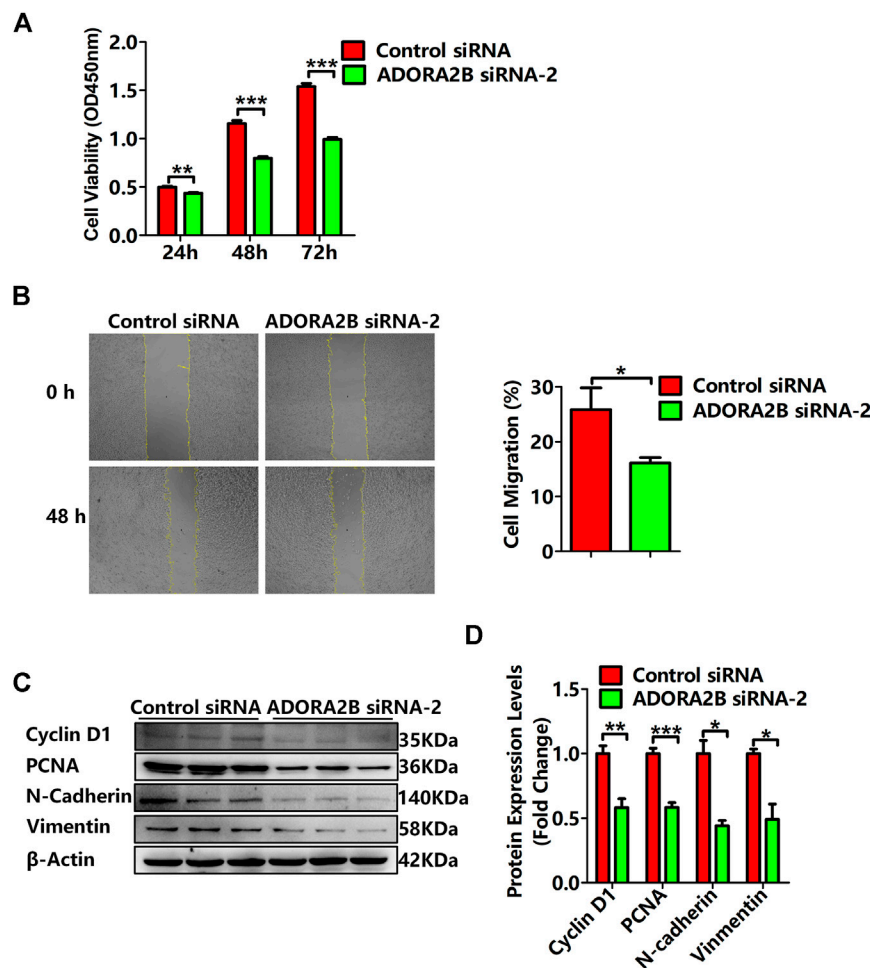


**FIGURE 9 |** Knockdown of *ADORA2B* inhibited the proliferation and metastasis of LUAD cells. **(A)** The cell viability of LUAD cells transfected with control or *ADORA2B* siRNA was detected by the CCK-8 assay. **(B)** The wound healing assay was used to examine the effect of *ADORA2B* siRNA on A549 cell migration for 48 h (magnification:  $\times 40$ ). **(C)** Relative protein expressions of proliferative (cyclin D1 and PCNA) and metastatic (N-cadherin and vimentin) markers were determined by western blotting. **(D)** Protein quantitative statistics. \* $p < 0.05$ , \*\* $p < 0.01$ , and \*\*\* $p < 0.001$  are statistically significant.

to those reported in previous LUAD studies. According to the mRNA expression level, *ADORA2B* ranked among the top 8–33% of all upregulated genes expressed in LUAD, indicating that *ADORA2B* is significantly overexpressed in LUAD (Figure 1). Survival analysis showed that the OS time (including the overall, one-year, three-year, and five-year survival rates) in the low *ADORA2B* expression group was significantly longer than that in the high *ADORA2B* expression group. These results indicated that a high *ADORA2B* expression predicted a poor prognosis for LUAD patients (Figure 4).

Further analysis using the UALCAN database showed that the mRNA expression levels of *ADORA2B* were significantly higher in LUAD samples than in para-carcinoma tissues. Furthermore, the expression varied depending on the cancer stage, age, smoking habit, nodal metastasis status, and TP53 mutation status. In addition, the copy number of *ADORA2B* was significantly increased in LUAD (Figure 2). These associations

indicated the impact of *ADORA2B* expression on human health or the types of biological and social factors that contribute to the pathological process of LUAD.

Cancer progression involves a series of histopathological processes (Xie et al., 2017; Chen et al., 2016) and changes in the functions of specific genes that have potential inhibitory or carcinogenic effects on cancer progression (Cui et al., 2018; Klonowska et al., 2016). Therefore, in the present study, we used the web-based tool, cBioPortal, to detect amplification, mutations, and mRNA expression of *ADORA2B* in LUAD. The major types of *ADORA2B* alterations were mRNA low, deep deletion, and amplification. The fraction of genome altered and mutation type, including not mutated, not profiled for mutations, amplification, gain, diploid, shallow deletion, and deep deletion, were analyzed. These mutations may play key roles in cancer progression and prognosis (Figure 3). Tumorigenesis is an extremely complex process, and new intricate protein–protein interactions and altered signaling pathways accelerate the

pathological process of malignant tumors. *ADORA2B* was reported to be involved in tumor-cell proliferation, tumor-cell metastasis, and tumor microenvironment changes (Desmet et al., 2013; Kasama et al., 2015; Vecchio et al., 2016). To further clarify the role of *ADORA2B* in the progression of LUAD, we performed related functional experiments to verify the function of *ADORA2B*. The results indicated that knockdown of *ADORA2B* inhibited the proliferation and metastasis of LUAD cells and that *ADORA2B* might participate in the proliferation and metastasis of LUAD cells (Figure 9).

To identify the functional proteins in LUAD, we used the GeneMANIA web server. Interacting proteins regulate tumor progression. To determine the hierarchy of interacting proteins, we used the LinkedOmics database and drew a heat map of differentially expressed genes correlated with *ADORA2B* expression. In LUAD, *ADORA2B* was predicted to be associated with several *ADORA2B*-associated genes. Among them, *ANXA1* was highly expressed in various malignant tumors (Huang et al., 2015; Okano et al., 2015), and upregulation of *ANXA1* levels in the serum was related to the pathological grade and clinical stage of patients with particular forms of LUAD. Knockout of *ANXA1* expression inhibited the proliferation, migration, and invasion of lung carcinoma cells (Fang et al., 2016), while the expression level of *ITGA3* can be used as a diagnostic and prognostic marker for several malignant tumors (Koshizuka et al., 2017; Jiao et al., 2019; Ramovs et al., 2019). *S100A6*, which regulates cytoskeleton protein dynamics, cell proliferation, cell differentiation, calcium metabolism, ubiquitination, and acetylation, was found to promote the proliferation, invasion, migration, and angiogenesis of lung carcinoma cells by inhibiting acetylation of *p53* when overexpressed (Li et al., 2019). *KDM2B* can reduce the proliferation of carcinoma cells by inhibiting the expression of oncogenes that play important roles in the self-renewal, differentiation, and apoptosis of stem cells (Hong et al., 2016; Goyama and Kitamura, 2017). Therefore, the findings of the present study validated the significance of *ADORA2B* in LUAD (Figure 5). *ADORA2B* interacts with these proteins that regulate important cellular processes associated with cancers and diseases.

Enrichment analysis of target gene sets using GSEA can identify important networks involved in protein targeting, mRNA processing, and transcription factors. *ADORA2B* was revealed to regulate the FAS signaling pathway, EGF receptor signaling pathway, and apoptosis signaling pathway (Figure 6). The CD73-adenosine receptor signaling pathway can promote the immunosuppressive effect of the tumor microenvironment, which is closely associated with a poor prognosis of multiple tumors (Chen et al., 2020). Immune cell infiltration analysis results suggested that the expression level of *ADORA2B* was associated with infiltrating immune cells in LUAD, including B cells, macrophages, neutrophils, and dendritic cells (Figure 7). These results revealed the indispensable role of *ADORA2B* in the development of LUAD.

The results of our preliminarily bioinformatics analysis suggested that *ADORA2B* can be used as a biomarker for LUAD, and we further confirmed the role of *ADORA2B* in LUAD through *in vitro* experiments. Human LUAD- and

bronchial epithelial cell-derived cells lines were cultured *in vitro*, and mRNA and protein levels of *ADORA2B* were analyzed. Our results showed that both the transcription and protein levels of *ADORA2B* were significantly higher in A549 and NCI-H1299 cells than in HBE cells. The expression of genes positively (*ANXA1*, *ITGA3*, and *S100A6*) or negatively (*KDM2B*, *NEB*, and *CBFA2T2*) correlated with *ADORA2B* was consistent with the transcription level of *ADORA2B*. siRNA *ADORA2B* transfection experiments further confirmed these results (Figure 8). Our *in vitro* experiments confirmed the predictive and diagnostic role of *ADORA2B* in LUAD, but there were some limitations of this study. We tried to obtain human LUAD tissues to verify our *in vitro* results; however, it is difficult to acquire human LUAD tissues owing to ethical and technical reasons. If we get an opportunity to acquire LUAD tissues in the future, we will further investigate the role of *ADORA2B* in LUAD.

## CONCLUSION

In conclusion, we used several public databases to extract data related to mRNA expression and mutations of *ADORA2B* and to the expression of genes associated with *ADORA2B* in LUAD. Furthermore, we predicted the differentially expressed genes correlated with *ADORA2B* expression in LUAD. Survival analysis showed that the OS time in the low *ADORA2B* expression group was longer than that in the high *ADORA2B* expression group. These results indicated that a high expression of *ADORA2B* predicted a poor prognosis for LUAD patients. Enrichment analysis of target gene sets using GSEA revealed important networks of the *ADORA2B* signaling pathway. Immune infiltration analysis results suggested that the expression level of *ADORA2B* was associated with immune cell infiltration in LUAD. *In vitro* experiments revealed that the relative *ADORA2B* expression levels in LUAD cells were significantly higher than those in normal bronchial epithelial cells. Knockdown of *ADORA2B* inhibited the proliferation and metastasis of LUAD cells, indicating that *ADORA2B* might participate in the proliferation and metastasis of LUAD cells. Taken together, our results revealed the significance of *ADORA2B* expression and its interaction networks in LUAD; the results of our *in vitro* experiments were consistent with those of the bioinformatics analysis. Although A549, NCI-H1299, and HBE cell lines were mainly used in the current experiments, we will verify these results with human and murine LUAD tissues in future studies. Our findings provide valuable insights into *ADORA2B* as a potential diagnostic and prognostic marker for LUAD and thus provide a foundation for further research focusing on LUAD biomarker development.

## DATA AVAILABILITY STATEMENT

Okayama Lung data were downloaded from the Oncomine database under Series accession number GSE31210 (<http://www.ncbi.nlm.nih.gov/geo/query/acc.cgi?acc=GSE31210>). Landi Lung

data were downloaded from the Oncomine database under Series accession number GSE10072 (<http://www.ncbi.nlm.nih.gov/geo/query/acc.cgi?acc=GSE10072>). Selamat Lung data were downloaded from the Oncomine database under Series accession number GSE32863 (<http://www.ncbi.nlm.nih.gov/geo/query/acc.cgi?acc=GSE32863>). Stearman Lung data were downloaded from the Oncomine database under Series accession number GSE2514 (<http://www.ncbi.nlm.nih.gov/geo/query/acc.cgi?acc=GSE2514>). Beer Lung data were downloaded from the Oncomine database under the Array Type: HumanGeneFL Array, Measured 5,338 genes, 7,133 reporters (Beer, D. G., Kardia, S. L., Huang, C. C., Giordano, T. J., Levin, A. M., Misek, D. E., et al., 2002). Gene expression profiles predict survival of patients with lung adenocarcinoma (Nat. Med. 8, 816–824. doi: 10.1038/nm733). Su Lung data were downloaded from the Oncomine database under Series accession number GSE7670 (<http://www.ncbi.nlm.nih.gov/geo/query/acc.cgi?acc=GSE7670>). Bhattacharjee Lung data were downloaded from the Oncomine database under the Array Type: Human Genome U95A-Av2 Array, Measured 8,603 genes, 12,651 reporters (Bhattacharjee, A., Richards, W. G., Staunton, J., Li, C., Monti, S., Vasa, P., et al., 2001). Classification of human lung carcinomas by mRNA expression profiling reveals distinct adenocarcinoma subclasses (Proc. Natl. Acad. Sci. U S A 98, 13790–13795. doi: 10.1073/pnas.191502998). Garber Lung data were downloaded from the Oncomine database under Series accession number GSE3398 (<http://www.ncbi.nlm.nih.gov/geo/query/acc.cgi?acc=GSE3398>). OncoPrint data were downloaded from the cBioPortal database Shortened URL <https://bit.ly/3oTsOd5>. Mutation data were downloaded from the cBioPortal database Shortened URL <https://bit.ly/2ObTF7t>. Clinical attribute data were downloaded from the cBioPortal database Shortened URL <https://bit.ly/3rnelHU>. LinkedOmics data were downloaded from the LinkedOmics database under ID number ID-62189.

## REFERENCES

- Beer, D. G., Kardia, S. L. R., Huang, C.-C., Giordano, T. J., Levin, A. M., Misek, D. E., et al. (2002). Gene-expression Profiles Predict Survival of Patients with Lung Adenocarcinoma. *Nat. Med.* 8, 816–824. doi:10.1038/nm733
- Bhattacharjee, A., Richards, W. G., Staunton, J., Li, C., Monti, S., Vasa, P., et al. (2001). Classification of Human Lung Carcinomas by mRNA Expression Profiling Reveals Distinct Adenocarcinoma Subclasses. *Proc. Natl. Acad. Sci.* 98, 13790–13795. doi:10.1073/pnas.191502998
- Borea, P. A., Gessi, S., Merighi, S., and Varani, K. (2016). Adenosine as a Multi-Signalling Guardian Angel in Human Diseases: when, where and How Does it Exert its Protective Effects?. *Trends Pharmacol. Sci.* 37, 419–434. doi:10.1016/j.tips.2016.02.006
- Cancer Genome Atlas Research Network (2018). Author Correction: Comprehensive Molecular Profiling of Lung Adenocarcinoma. *Nature* 559, E12. doi:10.1038/s41586-018-0228-6
- Chandrashekar, D. S., Bashel, B., Balasubramanya, S. A. H., Creighton, C. J., Ponce-Rodriguez, I., Chakravarthi, B. V. S. K., et al. (2017). UALCAN: a portal for Facilitating Tumor Subgroup Gene Expression and Survival Analyses. *Neoplasia* 19, 649–658. doi:10.1016/j.neo.2017.05.002
- Chen, S., Akdemir, I., Fan, J., Linden, J., Zhang, B., and Cekic, C. (2020). The Expression of Adenosine A2B Receptor on Antigen-Presenting Cells Suppresses CD8+ T-Cell Responses and Promotes Tumor Growth.

## AUTHOR CONTRIBUTIONS

YS and JL designed the study, performed the data analysis, and aided in writing the manuscript. JZ, ZZ, and ZW completed the data download and analysis and *in vitro* experiments. ZJ and ZM evaluated and reviewed the manuscript structure, ideas, and science. All authors read and approved the final manuscript.

## FUNDING

This work was supported by the National Natural Science Foundation of China (Grant Number 31800722 to ZM), Tianjin Natural Science Foundation (Grant Number 19JCQNJC11400 to ZM), China Postdoctoral Science Foundation (Grant Number 2019M660030 to YS), Tianjin Health Commission Science and Technology Talent Cultivation Project (Grant Number KJ20040 to ZM), Postdoctoral Fund of the First Affiliated Hospital, Jinan University (Grant Number 809036 to ZJ), and HAI YAN Science Foundation of Harbin Medical University Cancer Hospital (Grant Numbers JJQN 2021-14 and JJMS 2021-30 to JL). We are grateful to the data contributors of Oncomine, UALCAN, cBioPortal, GeneMANIA, LinkedOmics, KM Plotter, and TIMER for providing access to all the data required for this study. We are also grateful to *Editage* for editing the revised manuscript.

## SUPPLEMENTARY MATERIAL

The Supplementary Material for this article can be found online at: <https://www.frontiersin.org/articles/10.3389/fmolb.2021.663011/full#supplementary-material>

*Cancer Immunol. Res.* 8, 1064–1074. doi:10.1158/2326-6066.CIR-19-0833

- Chen, W.-C., Wang, C.-Y., Hung, Y.-H., Weng, T.-Y., Yen, M.-C., and Lai, M.-D. (2016). Systematic Analysis of Gene Expression Alterations and Clinical Outcomes for Long-Chain Acyl-Coenzyme A Synthetase Family in Cancer. *PLoS One* 11, e0155660. doi:10.1371/journal.pone.0155660
- Covarrubias, R., Chepurko, E., Reynolds, A., Huttering, Z. M., Huttering, R., Stanfill, K., et al. (2016). Role of the CD39/CD73 Purinergic Pathway in Modulating Arterial Thrombosis in Mice. *Arterioscler Thromb. Vasc. Biol.* 36, 1809–1820. doi:10.1161/ATVBAHA.116.307374
- Csóka, B., Selmezy, Z., Koscsó, B., Németh, Z. H., Pachter, P., Murray, P. J., et al. (2012). Adenosine Promotes Alternative Macrophage Activation via A2A and A2B Receptors. *FASEB j.* 26, 376–386. doi:10.1096/fj.11-190934
- Cui, X., Jing, X., Yi, Q., Long, C., Tan, B., Li, X., et al. (2018). Systematic Analysis of Gene Expression Alterations and Clinical Outcomes of STAT3 in Cancer. *Oncotarget* 9, 3198–3213. doi:10.18632/oncotarget.23226
- Desmet, C. J., Gallenne, T., Prieur, A., Rey, F., Visser, N. L., Wittner, B. S., et al. (2013). Identification of a Pharmacologically Tractable Fra-1/ADORA2B axis Promoting Breast Cancer Metastasis. *Proc. Natl. Acad. Sci.* 110, 5139–5144. doi:10.1073/pnas.1222085110
- Drilon, A., Oxnard, G. R., Tan, D. S. W., Loong, H. H. F., Johnson, M., Gainor, J., et al. (2020). Efficacy of Selpercatinib in *RET* Fusion-Positive Non-small-cell Lung Cancer. *N. Engl. J. Med.* 383, 813–824. doi:10.1056/NEJMoa2005653

- Fang, Y., Guan, X., Cai, T., Long, J., Wang, H., Xie, X., et al. (2016). Knockdown of ANXA1 Suppresses the Biological Behavior of Human NSCLC Cells *In Vitro*. *Mol. Med. Rep.* 13, 3858–3866. doi:10.3892/mmr.2016.5022
- Fenouillet, E., Mottola, G., Kipson, N., Paganelli, F., Guieu, R., and Ruf, J. (2019). Adenosine Receptor Profiling Reveals an Association between the Presence of Spare Receptors and Cardiovascular Disorders. *Int. J. Mol. Sci.* 20, 5964. doi:10.3390/ijms20235964
- Feoktistov, I., and Biaggioni, I. (2011). Role of Adenosine A2B Receptors in Inflammation. *Adv. Pharmacol.* 61, 115–144. doi:10.1016/B978-0-12-385526-8.00005-9
- Fishman, P., Bar-Yehuda, S., Liang, B. T., and Jacobson, K. A. (2012). Pharmacological and Therapeutic Effects of A3 Adenosine Receptor Agonists. *Drug Discov. Today* 17, 359–366. doi:10.1016/j.drudis.2011.10.007
- Fishman, P., Bar-Yehuda, S., Synowitz, M., Powell, J. D., Klotz, K. N., Gessi, S., et al. (2009). Adenosine Receptors and Cancer. *Handb. Exp. Pharmacol.* 193, 399–441. doi:10.1007/978-3-540-89615-9\_14
- Garber, M. E., Troyanskaya, O. G., Schluens, K., Petersen, S., Thaesler, Z., Pacyna-Gengelbach, M., et al. (2001). Diversity of Gene Expression in Adenocarcinoma of the Lung. *Proc. Natl. Acad. Sci.* 98, 13784–13789. doi:10.1073/pnas.241500798
- Goyama, S., and Kitamura, T. (2017). Epigenetics in normal and Malignant Hematopoiesis: An Overview and Update 2017. *Cancer Sci.* 108, 553–562. doi:10.1111/cas.13168
- Hamidzadeh, K., and Mosser, D. M. (2016). Purinergic Signaling to Terminate TLR Responses in Macrophages. *Front. Immunol.* 7, 74. doi:10.3389/fimmu.2016.00074
- Hong, X., Xu, Y., Qiu, X., Zhu, Y., Feng, X., Ding, Z., et al. (2016). MiR-448 Promotes Glycolytic Metabolism of Gastric Cancer by Downregulating KDM2B. *Oncotarget* 7, 22092–22102. doi:10.18632/oncotarget.8020
- Huang, Y., Zhang, C., Chen, C., Sun, S., Zheng, H., Wan, S., et al. (2015). Investigation of Circulating Antibodies to ANXA1 in Breast Cancer. *Tumor Biol.* 36, 1233–1236. doi:10.1007/s13277-014-2751-x
- Jiao, Y., Li, Y., Liu, S., Chen, Q., and Liu, Y. (2019). ITGA3 Serves as a Diagnostic and Prognostic Biomarker for Pancreatic Cancer. *Ott* 12, 4141–4152. doi:10.2147/OTT.S201675
- Karmouty-Quintana, H., Weng, T., Garcia-Morales, L. J., Chen, N.-Y., Pedroza, M., Zhong, H., et al. (2013). Adenosine A2B Receptor and Hyaluronan Modulate Pulmonary Hypertension Associated with Chronic Obstructive Pulmonary Disease. *Am. J. Respir. Cell Mol. Biol.* 49, 1038–1047. doi:10.1165/rcmb.2013-0089OC
- Kasama, H., Sakamoto, Y., Kasamatsu, A., Okamoto, A., Koyama, T., Minakawa, Y., et al. (2015). Adenosine A2b Receptor Promotes Progression of Human Oral Cancer. *BMC Cancer* 15, 563. doi:10.1186/s12885-015-1577-2
- Klonowska, K., Czubak, K., Wojciechowska, M., Handschuh, L., Zmienko, A., Figlerowicz, G., et al. (2016). Oncogenomic Portals for the Visualization and Analysis of Genome-wide Cancer Data. *Oncotarget* 7, 176–192. doi:10.18632/oncotarget.6128
- Koeppen, M., Eckle, T., and Eltzschig, H. K. (2011). Interplay of Hypoxia and A2B Adenosine Receptors in Tissue protection. *Adv. Pharmacol.* 61, 145–186. doi:10.1016/B978-0-12-385526-8.00006-0
- Koshizuka, K., Hanazawa, T., Kikkawa, N., Arai, T., Okato, A., Kurozumi, A., et al. (2017). Regulation of ITGA 3 by the Anti-tumor miR-199 Family Inhibits Cancer Cell Migration and Invasion in Head and Neck Cancer. *Cancer Sci.* 108, 1681–1692. doi:10.1111/cas.13298
- Landi, M. T., Dracheva, T., Rotunno, M., Figueroa, J. D., Liu, H., Dasgupta, A., et al. (2008). Gene Expression Signature of Cigarette Smoking and its Role in Lung Adenocarcinoma Development and Survival. *PLoS One* 3, e1651. doi:10.1371/journal.pone.0001651
- Li, P., Lv, X., Zhang, Z., and Xie, S. (2019). S100A6/miR193a Regulates the Proliferation, Invasion, Migration and Angiogenesis of Lung Cancer Cells through the P53 Acetylation. *Am. J. Transl. Res.* 11, 4634–4649.
- Mazieres, J., Cropet, C., Montané, L., Barlesi, F., Souquet, P. J., Quantin, X., et al. (2020). Vemurafenib in Non-small-cell Lung Cancer Patients with BRAFV600 and BRAFnonV600 Mutations. *Ann. Oncol.* 31, 289–294. doi:10.1016/j.annonc.2019.10.022
- Mertens, T. C. J., Hanmandlu, A., Tu, L., Phan, C., Collum, S. D., Chen, N.-Y., et al. (2018). Switching-off Adora2b in Vascular Smooth Muscle Cells Halts the Development of Pulmonary Hypertension. *Front. Physiol.* 9, 555. doi:10.3389/fphys.2018.00555
- Okano, M., Kumamoto, K., Saito, M., Onozawa, H., Saito, K., Abe, N., et al. (2015). Upregulated Annexin A1 Promotes Cellular Invasion in Triple-Negative Breast Cancer. *Oncol. Rep.* 33, 1064–1070. doi:10.3892/or.2015.3720
- Okayama, H., Kohno, T., Ishii, Y., Shimada, Y., Shiraiishi, K., Iwakawa, R., et al. (2012). Identification of Genes Upregulated in ALK-Positive and EGFR/KRAS/ALK-negative Lung Adenocarcinomas. *Cancer Res.* 72, 100–111. doi:10.1158/0008-5472.CAN-11-1403
- Philip, K., Mills, W. T., Davies, J., Chen, N. Y., Karmouty-Quintana, H., Luo, F., et al. (2017). HIF1A Up-regulates the ADORA2B Receptor on Alternatively Activated Macrophages and Contributes to Pulmonary Fibrosis. *FASEB J.* 31, 4745–4758. doi:10.1096/fj.201700219R
- Pillai, R. N., Behera, M., Berry, L. D., Rossi, M. R., Kris, M. G., Johnson, B. E., et al. (2017). HER2 Mutations in Lung Adenocarcinomas: a Report from the Lung Cancer Mutation Consortium. *Cancer* 123, 4099–4105. doi:10.1002/cncr.30869
- Ramovs, V., Secades, P., Song, J.-Y., Thijssen, B., Kreft, M., and Sonnenberg, A. (2019). Absence of Integrin  $\alpha\beta 1$  Promotes the Progression of HER2-Driven Breast Cancer *In Vivo*. *Breast Cancer Res.* 21, 63. doi:10.1186/s13058-019-1146-8
- Román, M., Baraibar, I., López, I., Nadal, E., Rolfo, C., Vicent, S., et al. (2018). KRAS Oncogene in Non-small Cell Lung Cancer: Clinical Perspectives on the Treatment of an Old Target. *Mol. Cancer* 17, 33. doi:10.1186/s12943-018-0789-x
- Russell, P. A., Wainer, Z., Wright, G. M., Daniels, M., Conron, M., and Williams, R. A. (2011). Does Lung Adenocarcinoma Subtype Predict Patient Survival?: a Clinicopathologic Study Based on the New International Association for the Study of Lung Cancer/American Thoracic Society/European Respiratory Society International Multidisciplinary Lung Adenocarcinoma Classification. *J. Thorac. Oncol.* 6, 1496–1504. doi:10.1097/ITO.0b013e318221f701
- Selamat, S. A., Chung, B. S., Girard, L., Zhang, W., Zhang, Y., Campan, M., et al. (2012). Genome-scale Analysis of DNA Methylation in Lung Adenocarcinoma and Integration with mRNA Expression. *Genome Res.* 22, 1197–1211. doi:10.1101/gr.132662.111
- Shaw, A. T., Felip, E., Bauer, T. M., Besse, B., Navarro, A., Postel-Vinay, S., et al. (2017). Lorlatinib in Non-small-cell Lung Cancer with ALK or ROS1 Rearrangement: an International, Multicentre, Open-Label, Single-Arm First-In-Man Phase 1 Trial. *Lancet Oncol.* 18, 1590–1599. doi:10.1016/S1470-2045(17)30680-0
- Stearman, R. S., Dwyer-Nield, L., Zerbe, L., Blaine, S. A., Chan, Z., Bunn, P. A., et al. (2005). Analysis of Orthologous Gene Expression between Human Pulmonary Adenocarcinoma and a Carcinogen-Induced Murine Model. *Am. J. Pathol.* 167, 1763–1775. doi:10.1016/S0002-9440(10)61257-6
- Su, L.-J., Chang, C.-W., Wu, Y.-C., Chen, K.-C., Lin, C.-J., Liang, S.-C., et al. (2007). Selection of DDX5 as a Novel Internal Control for Q-RT-PCR from Microarray Data Using a Block Bootstrap Re-sampling Scheme. *BMC Genomics* 8, 140. doi:10.1186/1471-2164-8-140
- Tian, Z., Dixon, J., Guo, X., Deal, B., Liao, Q., Zhou, Y., et al. (2021). Co-inhibition of CD73 and ADORA2B Improves Long-Term Cigarette Smoke Induced Lung Injury. *Front. Physiol.* 12, 614330. doi:10.3389/fphys.2021.614330
- Vecchio, E. A., Baltos, J. A., Nguyen, A. T. N., Christopoulos, A., White, P. J., and May, L. T. (2018). New Paradigms in Adenosine Receptor Pharmacology: Allosteric, Oligomerization and Biased Agonism. *Br. J. Pharmacol.* 175, 4036–4046. doi:10.1111/bph.14337
- Vecchio, E. A., Tan, C. Y. R., Gregory, K. J., Christopoulos, A., White, P. J., and May, L. T. (2016). Ligand-independent Adenosine A2B Receptor Constitutive Activity as a Promoter of Prostate Cancer Cell Proliferation. *J. Pharmacol. Exp. Ther.* 357, 36–44. doi:10.1124/jpet.115.230003
- Warde-Farley, D., Donaldson, S. L., Comes, O., Zuberi, K., Badrawi, R., Chao, P., et al. (2010). The GeneMANIA Prediction Server: Biological Network Integration for Gene Prioritization and Predicting Gene Function. *Nucleic Acids Res.* 38, W214–W220. doi:10.1093/nar/gkq537
- Xie, S., Shen, C., Tan, M., Li, M., Song, X., and Wang, C. (2017). Systematic Analysis of Gene Expression Alterations and Clinical Outcomes of Adenylate Cyclase-Associated Protein in Cancer. *Oncotarget* 8, 27216–27239. doi:10.18632/oncotarget.16111



- Yu, H. A., Arcila, M. E., Rekhtman, N., Sima, C. S., Zakowski, M. F., Pao, W., et al. (2013). Analysis of Tumor Specimens at the Time of Acquired Resistance to EGFR-TKI Therapy in 155 Patients with EGFR-Mutant Lung Cancers. *Clin. Cancer Res.* 19, 2240–2247. doi:10.1158/1078-0432.CCR-12-2246
- Yu, L., Todd, N. W., Xing, L., Xie, Y., Zhang, H., Liu, Z., et al. (2010). Early Detection of Lung Adenocarcinoma in Sputum by a Panel of microRNA Markers. *Int. J. Cancer* 127, 2870–2878. doi:10.1002/ijc.25289
- Zagryazhskaya, A., Gyuraszova, K., and Zhivotovsky, B. (2015). Cell Death in Cancer Therapy of Lung Adenocarcinoma. *Int. J. Dev. Biol.* 59, 119–129. doi:10.1387/ijdb.150044bz

**Conflict of Interest:** The authors declare that the research was conducted in the absence of any commercial or financial relationships that could be construed as a potential conflict of interest.

Copyright © 2021 Sui, Liu, Zhang, Zheng, Wang, Jia and Meng. This is an open-access article distributed under the terms of the Creative Commons Attribution License (CC BY). The use, distribution or reproduction in other forums is permitted, provided the original author(s) and the copyright owner(s) are credited and that the original publication in this journal is cited, in accordance with accepted academic practice. No use, distribution or reproduction is permitted which does not comply with these terms.



# The Potential Role of Extracellular Vesicles in COVID-19 Treatment: Opportunity and Challenge

Yan-yan Yan<sup>1†</sup>, Wen-min Zhou<sup>2†</sup>, Yu-qing Wang<sup>2†</sup>, Qiao-ru Guo<sup>2,3</sup>, Fu-xi Zhao<sup>1</sup>, Zhuang-yan Zhu<sup>1</sup>, Yan-xia Xing<sup>1</sup>, Hai-yan Zhang<sup>1</sup>, Mohamad Aljofan<sup>4</sup>, Alireza Mosavi Jarrahi<sup>5</sup>, Bolat Makabel<sup>3\*</sup> and Jian-ye Zhang<sup>2\*</sup>

<sup>1</sup>School of Medicine, Shanxi Datong University, Datong, China, <sup>2</sup>Key Laboratory of Molecular Target and Clinical Pharmacology and the State Key Laboratory of Respiratory Disease, School of Pharmaceutical Sciences and the Fifth Affiliated Hospital, Guangzhou Medical University, Guangzhou, China, <sup>3</sup>Xinjiang Institute of Materia Medica, Urumqi, China, <sup>4</sup>Department of Biomedical Sciences, School of Medicine, Nazarbayev University, Nur-Sultan, Kazakhstan, <sup>5</sup>School of Medicine, Shahid Beheshti University of Medical Sciences, Tehran, Iran

## OPEN ACCESS

### Edited by:

Wen Li,  
Zhejiang University, China

### Reviewed by:

Jafar Rezaie,  
Urmia University of Medical  
Sciences, Iran  
Lanlan Wei,  
Shenzhen Third People's Hospital,  
China

### \*Correspondence:

Bolat Makabel  
kzkt@163.com  
Jian-ye Zhang  
jianyez@163.com

<sup>†</sup>These authors have contributed  
equally to this work and share first  
authorship.

### Specialty section:

This article was submitted to  
Molecular Diagnostics and  
Therapeutics,  
a section of the journal  
Frontiers in Molecular Biosciences

**Received:** 24 April 2021

**Accepted:** 08 July 2021

**Published:** 21 July 2021

### Citation:

Yan Y, Zhou W, Wang Y, Guo Q,  
Zhao F, Zhu Z, Xing Y, Zhang H,  
Aljofan M, Jarrahi AM, Makabel B and  
Zhang J (2021) The Potential Role of  
Extracellular Vesicles in COVID-19  
Treatment: Opportunity  
and Challenge.  
Front. Mol. Biosci. 8:699929.  
doi: 10.3389/fmolb.2021.699929

SARS-CoV-2 infection has become an urgent public health concern worldwide, severely affecting our society and economy due to the long incubation time and high prevalence. People spare no effort on the rapid development of vaccine and treatment all over the world. Amongst the numerous ways of tackling this pandemic, some approaches using extracellular vesicles (EVs) are emerging. In this review, we summarize current prevalence and pathogenesis of COVID-19, involving the combination of SARS-CoV-2 and virus receptor ACE2, endothelial dysfunction and micro thrombosis, together with cytokine storm. We also discuss the ongoing EVs-based strategies for the treatment of COVID-19, including mesenchymal stem cell (MSC)-EVs, drug-EVs, vaccine-EVs, platelet-EVs, and others. This manuscript provides the foundation for the development of targeted drugs and vaccines for SARS-CoV-2 infections.

**Keywords:** COVID-19, SARS-CoV-2, extracellular vesicles (EVs), mesenchymal stem cell (MSC), immunomodulation, ACE2

## OVERVIEW OF COVID-19

### Current Prevalence of COVID-19

COVID-19, named Coronavirus Infectious Disease 2019 by the World Health Organization (Zhou, et al., 2020a; Zhu, et al., 2020), is an infectious disease caused by the severe acute respiratory syndrome coronavirus type 2 (SARS-CoV-2), which was first reported in Wuhan, China, in December 2019. COVID-19 infection is now a pressing global public health problem. As of today, 23 March 2021, more than 124 million people have been infected with SARS-CoV-2 and more than 2.7 million have died. In addition to having an unprecedented impact on global health care systems, COVID-19 has profound socioeconomic consequences (Nicola, et al., 2020).

Clinically, COVID-19 mainly affects the lungs. Although the majority of COVID-19 victims may show asymptomatic or mild symptoms, interstitial pneumonia (IP) and acute respiratory distress syndrome (ARDS) requiring mechanical ventilation in the intensive care units can occur in approximately 15% of cases (Cascella, et al., 2021), especially in the elderly and individuals with underlying diseases. COVID-19 also has systemic manifestations, affecting multiple organ systems containing cardiovascular, gastrointestinal, hematopoietic, renal, and immune systems (Yi, et al., 2020). In severe cases, COVID-19 can lead to severe cytokine storm or cytokine release syndrome (CRS) (Cascella, Rajnik, 2021), sepsis, multiple organ failure and even death.

SARS-CoV-2 is by far the seventh human coronavirus discovered to date. Four viruses (HCoV-NL63, HCoV-229E, HCoV-OC43, and HKU1) persist in human population and cause mild common cold symptoms (Fung and Liu, 2019). The other two are similar to SARS-CoV-2, named SARS-CoV and Middle East Respiratory Syndrome (MERS)-CoV, and both of them lead to acute respiratory disease (Cui, et al., 2019). SARS-CoV-2 is a spherical or pleomorphic enveloped virus particle with a typical diameter range of 80–120 nm. This virus contains a 30 kB positive single-stranded RNA which surrounded by a membrane embedded with a variety of viral proteins, especially the Spike (S) protein (Mousavizadeh, and Ghasemi, 2020). Studies shown that the Spike protein in SARS-CoV-2 shared a high degree of structural homology with that in SARS-CoV (Li, et al., 2005; Xu, et al., 2020b). SARS-CoV-2 virus infect into human cells by recognizing the angiotensin converting enzyme 2 (ACE2) receptor of host cells. A recent study by Wan et al. reported that SARS-CoV-2 had a stronger binding ability with ACE2 than with SARS-CoV, promoting the infection and transmission capacity of the virus (Wan, et al., 2020).

## Pathogenesis of COVID-19

### ACE2 Plays a Key Role in SARS-CoV-2 Invasion

In 2020, using cryopreserved electron microscopy, Zhou Qiang Laboratory of Westlake University successfully analyzed the full-length structure of ACE2 (Yan, et al., 2020), the receptor protein of SARS-CoV-2. This is the first time of the world that the full-length structure of ACE2 has been resolved. As SARS-CoV-2 invades the body, ACE2 acts like a “doorknob,” the virus grabs it and opens the door to the recipient cells. In addition, interestingly, it has recently been demonstrated that transmembrane protease serine 2 (TMPRSS2) incises the Spike protein during the internalization of SARS-CoV-2 which fuses with host cell membrane (Scheller, et al., 2019). This process is necessary for SARS-CoV-2 to enter into recipient cells (Devaux, et al., 2020). After fusing with the human cell membrane, the virus genome enters into the recipient/host cell. The virus then begins to replicate, mature and leave the host cells to infect new healthy cells. SARS-CoV-2 enters the respiratory system from the upper respiratory tract and eventually infects alveolar cells, causing angiectasis of alveolar cells, increased capillary permeability, decreased pulmonary surface active substances with infiltration of lymphocytes and monocytes. As ACE2 and TMPRSS2 are abundant in type II alveolar and endothelial cells (Hamming, et al., 2004), pulmonary vessels are susceptible to SARS-CoV-2-induced inflammation and injury (Zhao, et al., 2020). Other than the respiratory tract, SARS-CoV-2 infection can cause parts of the body damage, such as the cardiovascular system. Therefore, COVID-19 patients may present with severe forms of myocarditis and endocarditis besides respiratory dysfunction (Guzik, et al., 2020).

ACE2 is located in various types of epithelial cells (lung, kidney, heart, intestinal) and endothelial cells. In recent years, studies have shown that ACE2 played roles in the cardiovascular, renal and respiratory system, and was associated with hypertension and diabetes. ACE2 has a protective effect on a variety of lung diseases, such as acute lung injury, asthma, ARDS,

pulmonary hypertension and chronic obstructive pulmonary disease (Jia, 2016). More importantly, ACE2 was identified as a SARS-CoV and SARS-CoV-2 receptor, which played a protective role in the pathogenesis of SARS and COVID-19. As the first homolog of ACE, ACE2 regulates the renin angiotensin system (RAS) by balancing the ACE activity. The binding complex of Spike protein with ACE2 can induce the cell membrane ACE2 down-regulation (Glowacka, et al., 2010), contributing to the imbalance of ACE and ACE2 activity, and therefore leading to acute lung injury (Zhang, et al., 2020a).

### COVID-19 Is Associated With Endothelial Dysfunction and Micro-thrombosis

Patients with COVID-19 have a high incidence of thrombotic events (Berger, et al., 2020). About the mechanism of thrombosis in COVID-19, there are a lot of speculations, such as coagulation and platelet activation, endothelial cell activation, inflammation and complement system activation, etc (Mackman, et al., 2020). Varga and colleagues demonstrated that SARS-CoV-2 presented in the endothelial cells of various human organs (Varga, et al., 2020). In addition, evidence of alveolar capillary micro-thrombosis and endothelial injury associated with intracellular viruses has been noted in autopsy analyses of infected lungs (Ackermann, et al., 2020). Due to ACE2 show high-expression in vascular endothelial cells, viral infection of the circulatory system directly leads to excessive coagulation in COVID-19 patients (Varga, Flammer, 2020). In addition, the number of peripheral blood mononuclear cells decreased significantly in patients with respiratory failure 7–14 days after the onset of SARS-CoV-2 infection (Yi, Lagniton, 2020). High level of D-dimer was found to presence for the moment, which was associated with severe hypercoagulation and indicated a poor prognosis (Yi, Lagniton, 2020). As a major activator of the coagulation cascade (Grover, and Mackman, 2018), several studies have speculated that the induction of tissue factor (TF) might play an important role in the COVID-19-related thrombosis (Bautista-Vargas, et al., 2020; Grover and Mackman, 2018; Mackman, Antoniak, 2020). Axel Rosell et al. developed a method to determine the activity of TF in plasma EVs in 100 patients with moderate to severe COVID-19. The results showed that the level of EVs-TF activity was significantly higher in COVID-19 patients than in the normal individuals. In addition, the level of EVs-TF activity was associated with disease severity, mortality, and several plasma markers, including D-dimer. These findings suggest that SARS-CoV-2 infection induces the release of TF-positive EVs into the circulation, and possibly cause thrombosis in patients infected with COVID-19 (Rosell, et al., 2020).

### Cytokine Storm: Immune Response to SARS-CoV-2 Is a Major Driving Force of Disease Severity

Because SARS-CoV-2 entry into cells depend on binding to its receptor, ACE2, the RAS and various inflammatory cascades are connected with the pathobiology of COVID-19 (Bourgonje, et al., 2020). The SARS-CoV-2 can also activate the innate and adaptive immune response in patients with COVID-19 (Yang, et al., 2020a). The immune effector cells release a large amount of

proinflammatory cytokines and chemokines (Tukmechi, et al., 2014), such as tumor necrosis factor (TNF), interleukin 1 (IL-1), interleukin 6 (IL-6), interleukin 7 (IL-7) and granulocyte colony stimulating factor (Pedersen and Ho, 2020), inducing an uncontrolled CRS, and leading to various clinical manifestations, such as high fever, hepatosplenomegaly, cytopenia, central nervous system abnormalities, hypoalbuminaemia and capillary leakage (England, et al., 2021; Gao, et al., 2021). A previously published study showed that identifying circulating protein biomarkers in COVID-19 patients used an ultra-high-throughput serum and plasma proteomics technology (Messner, et al., 2020). Recently, Balaji Krishnamachary et al. indicated that EVs from patients affected by the SARS-CoV-2 might alter the pro-inflammatory response, blood coagulation disorders, and endothelium damage. They found that EVs of serious cases of COVID-19 carried higher levels of cytokines, including the IL-6 family, TNF superfamily, chemokines (MCP-1 and CXCL16), and proteases and peptidases (Cathepsin L1), compared with that of patients with moderate COVID-19 or asymptomatic individuals (Krishnamachary, et al., 2020). Therefore, the use of appropriate immunosuppressive and immunomodulatory agents to address the potential inflammatory complications of COVID-19 is currently being explored, which might improve clinical outcomes and ultimately reduce COVID-19 mortality (Stebbing, et al., 2020). Because ACE2 receptors are widely distributed in human alveolar type II cells and capillary endothelial cells (Hamming, Timens, 2004), the lungs are exceptionally sensitive to SARS-CoV-2 infection. In fact, recently published researches have shown that a substantial portion of the lungs were impacted by this disease, leading to an extensive damage that could subsequently result in permanent change of lung function. A recent MRI study in a 59-year-old man who diagnosed with COVID-19, suggested that this disease was not restricted to any specific area in the lung, but spread to the entire lung. In fact, this symptom is not composed directly arouse the SARS-CoV-2 virus, but a host immune response that causes a resistless cytokine storm in lungs. Overexpression of cytokines such as the interleukin family (IL-2, IL-6, IL-7), GSCF, IP10, MCP1, MIP1A, and TNF- $\alpha$  leads to edema and impairs oxygen exchange, which may lead to ARDS with potential acute cardiac injury, secondary infection and death (Huang, et al., 2020a).

## EVS ARE THE PROMISING NEW THERAPEUTIC MEANS OF COVID-19

There is currently no specific therapeutic for COVID-19. Conventional treatment includes infection prevention, supportive care that involving supplement of oxygen and mechanical ventilation support (Grasselli, et al., 2020; Marini, and Gattinoni, 2020). Currently, drugs against COVID-19 are evaluated worldwide, including antiviral drugs, anti-malarial drugs and anti-inflammatory drugs, such as radecevir (Beigel, et al., 2020), chloroquine (Zhou, et al., 2020b) and hydroxychloroquine (HCQ) (Soy, et al., 2020), anthropoized anti-IL-6 receptor antibody tocilizumab (Perrone, et al., 2020; Toniati, et al., 2020; Xu, et al., 2020c), recombinant human IL-1

receptor antagonist Anakinra (Cavalli, et al., 2020; Huet, et al., 2020), etc. Although these treatment strategies improved patient recovery and survival, they do not definitively restore lung damage caused by the virus. In addition, a range of anti-inflammatory drugs have been tested to inhibit the cytokine storm and multiple organ failure caused by the worsening immune response in severe patients, but the effect has not been significant. In recent years, increasing researches reported that the role of EVs in the treatment of inflammation (Lasser, et al., 2016; Martinez-Bravo, et al., 2017), injury (Lanyu, and Feilong, 2019), and lung and respiratory viral infection (Scheller, Herold, 2019; van Dongen, et al., 2016; Yoshikawa, et al., 2019). It was reported that EVs promoted the pathogenesis of diseases such as in infectious diseases and cancers (Fleming, et al., 2014; Han, et al., 2019). The interesting interaction between EVs and the virus provides a new perspective on the treatment of COVID-19 (Dogrammatzis, et al., 2020). Viral infection may affect the exosomal-loading mechanisms of the host cells, resulting in changes in protein and nucleic acid content of EVs. It means the infected cells release modified EVs, not rely on virus contents. Therefore, compared with EVs without infected cells, these modified EVs may modulate the host immune response. Besides, EVs may act as a negatively regulatory element in the transmission of viral infection, and induce the immune system to respond to the virus. There are three types of EVs, including exosomes (20–150 nm), microvesicles (MVs) (100–1,000 nm in diameter), and apoptotic vesicles (1,000–5,000 nm) (Maione, et al., 2020; Raposo and Stoorvogel, 2013). EVs, as a carrier for cell-to-cell transfer of biomolecules, is an important mode of cell-to-cell communication (Huang, et al., 2020b). EVs are present in a variety of biological fluids, such as blood, tissue fluid, pleural fluid, bronchoalveolar lavage fluid (BAL), peritoneal fluid, saliva, urine, breast milk, cerebrospinal fluid, amniotic fluid and so on (Kowal, et al., 2014; Rezaie, et al., 2019). EVs can be transported or accumulated not only in biological liquids but also in solid tissues. In solid tissue, EVs deliver their contents, such as proteins, miRNAs, mRNAs, and lncRNAs, to adjacent or distant cells and reprogram the target cells in fate, function, and morphology, resulting in physiological or pathological effects (Kowal, Tkach, 2014; Maas, et al., 2017; Statello, et al., 2018).

Exosomes, also referred to as intraluminal vesicles (ILVs), are a subtype of EV formed by an endosomal route, which are surrounded by a phospholipid bilayer, and have been found in biological liquids (Raposo and Stoorvogel, 2013). Exosomal vesicles form through inward budding of the limiting membrane of early endosomes, which mature into multivesicular bodies (MVBs) (Huang, Yan, 2020b). MVBs play a significant role in the endocytic and trafficking functions of the cell material, such as protein sorting, recycling, storage, transport, and release (Babaei, and Rezaie, 2021). Release of exosomes into the extracellular space is facilitated by the fusion of the MVB limiting membrane with the plasma membrane. Researches showed that exosomes participated in cell communication, cell maintenance, and tumor progression (Rezaie, et al., 2021). Balaji Krishnamachary et al. explored EVs isolated from plasma of patients with COVID-19 to identify some potential biomarkers



which influence the disease severity and to analyze its role in the pathogenesis of this disease (Krishnamachary, Cook, 2020). Plasma-derived EVs were separated from 53 COVID-19 patients in hospital and compared depending on the severity of their disease. Analysis of inflammation and cardiovascular protein loading in large EVs suggested significant differences in protein expression across disease subgroups. Prominently, the TNF superfamily and IL-6 family members were upregulated in severe and moderate disease patients who need oxygen supplement. EVs in severe patients also shown enhancement of prothrombotic or endothelial injury factors (TF, t-PA, and VWF) and cardiovascular pathology-related proteins (MB, PRSS8, REN, and HGF). There were significantly higher levels of TF, CD163, and EN-RAGE has been observed in EVs from patients with severe disease compared to moderate disease. EVs also play a key role in transmitting viral infection (Owczarek, et al., 2018). It was found that EVs and viruses shared similar physicochemical properties. They are small in size and have common biogenesis and cell entry mechanisms (van Dongen, Masoumi, 2016). The virus enters the uninfected cell *via* the endocytosis pathway and then exits the host cell by budding directly through the cell membrane. A new study found that EVs acted as the tool of virus export to cell, and the EVs depend virus entry mechanisms for cargo transport. EVs are the delivery vectors of viral contents. EVs released from virus-infected cells can infect healthy cells by transferring viral components, for example, virus-derived miRNAs and viral proteins, etc. (Ali, et al., 2010; Arenaccio, et al., 2015; Nolte- $\dot{\text{t}}$  Hoen, et al., 2016). EVs separated from infected cells may also activate humoral and cellular immune responses by transferring viruses and autoantigens in the host (Fleming, Sampey, 2014; Gunasekaran, et al., 2017). In addition, EVs release from virus-infected cells can also transfer viral receptors and pro-inflammatory factors to the recipient cells, leading to the transmitting of viral infection and worsening of tissue damage (Mack, et al., 2000). Studies have shown that the number of EVs secreted from the SARS-CoV-2 infected cells increased significantly during the virus infection, and EVs still played an important role in the pathogenesis of diseases (Yoshikawa, Teixeira, 2019). Lanyu et al. emphasized the role of EVs play which secreted by lung cells and alveolar epithelial cells in lung injury and inflammation (Lanyu and Feilong, 2019). According to report, EVs secreted from broncho alveolar lavage fluid are involved in the pathogenesis of idiopathic pulmonary fibrosis through the signaling regulation mediators such as Wnt5a (Martin-Medina, et al., 2018). The latest research showed EVs derived from epithelial cells which transduced by lentiviral overexpressing SARS-CoV-2 gene could transfer viral genes to recipient cardiomyocytes, leading to increased expression of inflammatory genes (Kwon, et al., 2020).

EVs may contribute to the infection, internalization and transmission of SARS-CoV-2 virus. Some components such as miRNAs, viral proteins and viral receptor ACE2 could be packed into EVs (Wang, et al., 2020), that render the recipient cells sensitive to viral invasion (**Figure 1**). In this review, we discuss the current EVs based COVID-19 treatment strategies, including

MSC and its EVs, EVs based drug delivery systems, EVs based vaccine, platelet EVs and inhibition of EVs intake, etc.

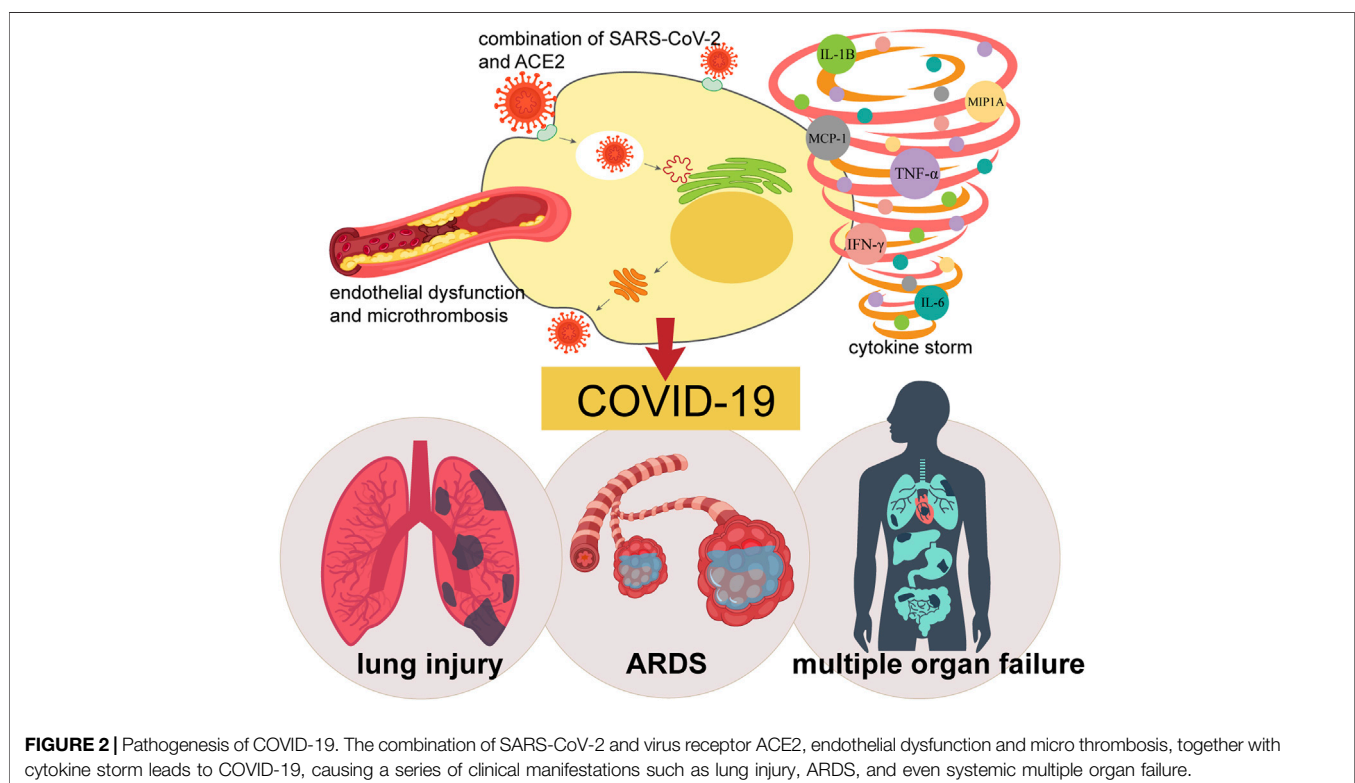
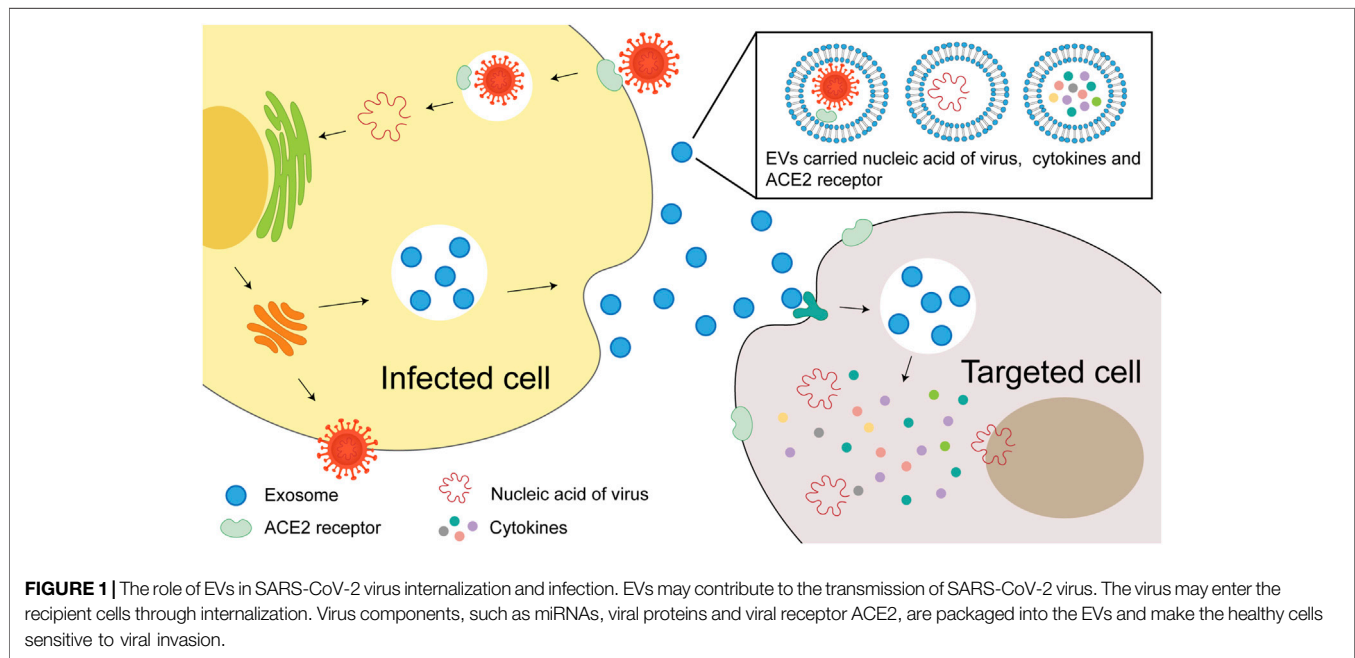
## EVS-BASED COVID-19 THERAPY

### MSC and MSC-EVs

MSCs are heterogeneous cells, including stromal cells, progenitor cells, fibroblasts, and stem cells (Dominici, et al., 2006; Galderisi and Giordano, 2014). The MSCs can be isolated from many tissues, such as bone marrow, placenta, adipose tissue, and umbilical cord blood. They are currently used as therapeutics at the present time, and meanwhile being tested in multiple clinical trials across the world (Meng, et al., 2020). MSCs are safe and possess immunomodulatory and tissue regeneration capabilities (Gao, et al., 2016; Thompson, et al., 2020). Studies suggested that the prospective therapeutic products based on MSCs were success, despite the apparent heterogeneity origin and lacking in specific biomarkers to predict, once implanted, MSCs could show strong regulate ability in immunomodulatory, antioxidant, and angiogenesis. MSCs and MSC-EVs have emerged as promising novel therapies that can not only reduce inflammation, but also regenerate and repair lung damage, and may therefore be used alone or in combination with other therapeutic agents to benefit patients with COVID-19.

Due to MSCs lack the expression of membrane bound molecules involved in immune rejection which enable their allogeneic transplantation, the clinical applications of MSC-based therapy have witnessed an outstanding achievement (Ahmadi and Rezaie, 2021). Nevertheless, in the long-term follow up, safety issues regarding MSCs-based therapy are still a matter of debate. It is worth noting that MSCs have the capacity to differentiate into endothelial cells and to create a capillary network, and the inhibitory effect of MSCs in anti-tumor immune response results an increased tumor growth, which promotes tumor growth and metastasis (Kolios and Moodley, 2013). In addition, it was reported that local microenvironment in which MSCs engraft contained factors that induced unwanted differentiation of transplanted MSCs *in vivo*. Therefore, several factors and signaling pathways regarding MSCs therapy after their *in vivo* administration should be focused. Medical staff should abide by moral and ethical norms, so that the public and government administrators can clearly comprehend the nature and functions of MSCs, and understand the potential risks of treatment, and avoid deviating by non-standard clinical trials (Volarevic, et al., 2018).

The membrane of MSC-EVs is rich in cholesterol, sphingomyelin, ceramide and lipid raft proteins, which enables membrane fusion with target cells. After fusion, MSC-EVs may trigger signaling pathways through the receptor ligand interaction, or be internalized by endocytosis to deliver contents, such as mRNAs, miRNAs, enzymes, cytokines, etc. (Harrell, et al., 2019). Compared with homocellular transport, MSC-EVs overcome safety concerns regarding the long-term survival of engrafted MSCs due to its composition (Rezaie, et al., 2018). Thus, MSC-EVs therapy is a new remedy in cell-free treatment of autoimmune and inflammatory diseases.



### Application of MSCs in Pulmonary Diseases

Inflammatory cytokines play a leading role in the development of COVID-19-caused lung injury (Figure 2). Immunotherapy that reduce the cytokine storm could be the key treatment option. However, traditional immunotherapy usually targeted one or two factors and may not produce enough response. MSCs have been shown to have powerful and extensive immunomodulatory and anti-inflammatory capabilities (Abdi, et al., 2008; Wada, et al., 2000).

Bone marrow MSCs therapy has evolved from preclinical trials to clinical trials for different diseases states in recent years. In animal models, MSCs significantly improve lung pathological change (Cruz and Rocco, 2020) and inhibit immune cell-mediated inflammation induced by influenza virus (Khatri, et al., 2018). Bhattacharya et al. demonstrated that bone marrow MSCs could stabilize endothelial cells and maintain alveolar-capillary barrier function, which is essential for

maintaining or reducing inflammation-induced lung permeability, thereby mitigating the development of interstitial pulmonary edema (Bhattacharya and Matthay, 2013). Li et al. reported that MSCs could alleviate acute lung injury caused by H9N2 and H5N1 viruses in mice by reducing the secretion of pro-inflammatory chemokines and cytokines, and inhibiting migration of inflammatory cells to the lungs (Li, et al., 2016). Currently, there are several ongoing clinical trials using MSCs for a variety of pulmonary diseases, such as obstructive bronchiolitis idiopathic pulmonary fibrosis (NCT02013700), chronic obstructive pulmonary disease (NCT01849159), and bronchial dysplasia (NCT01175655) (Wecht and Rojas, 2016), as well as for ARDS (NCT02097641) (Matthay, et al., 2019) and septic shock (NCT02421484) (McIntyre, et al., 2018). Specifically, Leng et al. found that there were no ACE2 and TMPRSS2 receptors express in MSCs, which indicated that the virus should not infect this cell population (Leng, et al., 2020). In a rat model of hyperoxia-induced lung injury, MSCs reduced overexpression of hyperoxia-induced angiotensin and angiotensin type 1 receptor (AT1R), and reduced ACE to normal level (Chen and Chou, 2018). Recently, Simonson et al. reported a long-term follow-up study on two severe ARDS patients, who required ECMO support and combined mechanical ventilation during the acute phase (Simonson, et al., 2020). After receiving a single systemic infusion of allogeneic MSCs, both patients fully recovered their physical and mental abilities. Remarkably, a dual-energy CT scan showed no signs of pulmonary fibrosis after 5 yr of MSCs treatment.

### Application of MSCs in the Treatment of COVID-19

MSCs therapy is considered a promising strategy for the treatment of COVID-19. The potential of MSCs for the treatment of COVID-19 is based on two benefits: 1) induction of the regenerative program of lung epithelial and endothelial cells, and 2) synchronous modulation of the inflammatory response. MSCs secrete multiple kinds of cytokines and paracrine factors which interact with immune cells directly, including T cells, B cells, dendritic cells, macrophages, and natural killer cells. This combined effect enables MSCs have immunomodulatory capability, which contributes to suppressing overactivation of the immune system. By producing and recruiting different growth factors such as vascular endothelial growth factor (VEGF), epidermal growth factor (EGF) and transforming growth factor (TGF), MSCs promote tissue regeneration and thus improve the microenvironment (Atluri, et al., 2020). It prevents uncontrolled inflammatory cascades while reducing pulmonary fibrosis and pulmonary dysfunction following COVID-19 infection (Mo, et al., 2020; Sun, et al., 2020; Thille, et al., 2013). Particularly, the lacking of ACE2 ensures the injected MSCs achieve immunomodulatory effects free from being destroyed by virus. MSCs from human umbilical cord origin were reported in a recent clinical trial, compared to the placebo group, they were associated with the increase of peripheral lymphocyte count and the decrease of systemic inflammatory biomarkers (ChiCTR2000029990) (Leng, et al., 2020). MSC infusion alleviated cytokine storm syndrome and significantly improved outcomes in patients with severe COVID-19.

### Application of MSC-EVs in Lung Diseases

Most of the therapeutic progress of MSCs are achieved through paracrine mechanisms, including EVs secretion that contain cell protective factors such as keratinocyte growth factor (KGF), anti-inflammatory mediators (PGE2 or lipid A4), anti-osmotic factors (Ang1) and others (Doorn, et al., 2012; Gneccchi, et al., 2008; Li, et al., 2014; Silini, et al., 2017). There have been reports of some limitations of using MSCs. For instance, intravenous administration of MSCs may induce particle aggregation leading to embolism; and some MSCs, especially those from embryonic tissues, may carry a risk of mutagenicity and tumorigenicity. Therefore, MSC derivatives such as SECRETOME (Bari, et al., 2019) and EVs (Tsiapalis and O'Driscoll, 2020) have been suggested as alternatives to MSC therapy. In addition, account of the low immunogenicity and tumorigenicity, simplicity of operation, and low cost, MSC-EVs therapy has significant advantages over MSC therapy. According to the report recently published, MSC-EVs could be administered by inhalation or injection (Bari, Ferrarotti, 2019). Preliminary studies have shown that MSC-EVs might also be effective against COVID-19 (Bari, et al., 2020). MSC-derived EVs have been demonstrated to induce similar influence to parent cells. In animal models, they can be store for a longer time safely without losing their biological function, on the other hand, they have been indicated similar or better indications than MSCs (Tsiapalis and O'Driscoll, 2020).

Some researchers have demonstrated the immunomodulatory effects of MSC-derived EVs *in vitro* (Budoni, et al., 2013; Del Fattore, et al., 2015; Di Trapani, et al., 2016; Henao Agudelo, et al., 2017; Liu, et al., 2012), and have shown significant anti-inflammatory and regenerative abilities in several diseased animal models (Fierabracci, et al., 2015; Phinney and Pittenger, 2017). Specifically, researchers showed demonstration that in animal models of lung injury, the efficacy of MSC-EVs was effective like in hyperoxia (Braun, et al., 2018; Porzionato, et al., 2019; Willis, et al., 2018), severe bacterial pneumonia (Monsel, et al., 2015), and viral pneumonia (Khatri, Richardson, 2018). In addition, MSC-EVs has beneficial effects on lung perfusion *ex vivo* with severe *E. coli* pneumonia (Park, et al., 2011). Finally, MSC-EVs can effectively repair marginal donor lungs through several methods, the first one is dose-dependently increasing the clearance of alveolar fluid; the second one is reducing lung weight after perfusion and ventilation; and the third one is improving airway and hemodynamic parameters (Ragni, et al., 2017). On the basis of these useful and promising results, the role of MSC-EVs in alleviating and repairing ARDS lung injury is gaining increasing attention (Lee, et al., 2019; Li, Huang, 2014; Monsel, Zhu, 2015; Shah, et al., 2019). Notably, fibrosis sequelae with reduced pulmonary function have been reported in patients recovering from COVID-19 pneumonia. Indeed, there is an increased risk of idiopathic pulmonary fibrosis following viral infection (Sheng, et al., 2020), as a long-term complication, it has been reported in parts of SARS infected patients (Zhang, et al., 2020b). MSC-EVs prevent fibrosis following experimental lung injury, which is similar to the cells of their origin (Cargnoni, et al., 2009; Mansouri, et al., 2019). In fact, there is a growing interest in

the new potential application of EV as a disease treatment strategy. EVs are considered safe, easy and cheap to produce, isolate, store and manage (Muraca, et al., 2017), which could reduce costs and improve product availability. It is worth mentioning that EVs seem to be a very generic product that it has application diversity and can be modified by various technologies, for example, manipulating their parent cells use genetic engineering, and then integrated into the secreted EVs by introducing exogenous substances (Armstrong, et al., 2017; Vader, et al., 2016; Wiklander, et al., 2019). A similar method has been demonstrated to deliver exogenous miRNA-Let-7c to alleviate renal fibrosis *via* MSC-EVs in the mice model of unilateral ureteral obstruction (Wang, et al., 2016). On the other hand, studies also suggested that EVs could be loaded with therapeutic molecules form a polymer complex to improve its targeting activity (Cappariello, et al., 2018; Pascucci, et al., 2014; Vader, Mol, 2016; van der Meel, et al., 2014).

The pulmonary pathology of COVID-19 critically ill patients includes the exudation and proliferation phase of diffuse alveolar injury, and microvascular thrombosis that suggest early ARDS (Wichmann, et al., 2020; Xu, et al., 2020d). The pathogenesis includes change of alveolar permeability and neutrophils infiltration (Zemans and Matthay, 2017). Several studies showed that MSC-EVs could reduce alveolar permeability and increase alveolar fluid clearance, in an *in vitro* model of human perfusion lung injury with severe *E. coli* pneumonia (Gennai, et al., 2015; Lee, et al., 2009; Park, et al., 2019). Interestingly, there were antibacterial substances in the culture medium of the bacteria-stimulated MSCs (Krasnodembskaya, et al., 2010). In a mouse sepsis model, treatment with MSCs could increase bacterial clearance, part of the reason is it increased phagocytic activity of host immune cells (Mei, et al., 2010). In addition, MSC-EVs demonstrated antiviral activity *in vitro* by inhibiting replication of influenza virus in lung epithelial cells, meanwhile by reducing viral load in an influenza-induced lung injury model of pigs (Khatri, Richardson, 2018).

### Application of MSC-EVs in the Treatment of COVID-19

Recently, Sengupta, et al. published the safety and efficacy of allogeneic bone marrow MSC-derived EVs in 24 patients with COVID-19 severe pneumonia that they have been treated with hydroxychloroquine and azithromycin (Sengupta, et al., 2020). It was interesting to note that inflammatory biomarkers and absolute neutrophilic counts were decreased prominently, while the counts of total lymphocyte and CD8<sup>+</sup> were increased prominently within 5 days after EVs injection. In addition, D-dimer was significantly reduced. Although this EVs treatment resulted about 71% of patients recovery to health, it is not clear whether the recovery was attributable to EVs treatment, because of the lack of a matched control group and the lack of reported protein or microRNA composition of EVs used in the study. In summary, we would like to underline that there has been currently no approved MSC-based approach in preventing and treating the COVID-19, either with MSCs or MSCs-derived EVs. Clinical trials using EVs should be carried out with great caution, as their cargo determines the functional impact. Consequently, before MSC-derived EVs used in clinic,

standardized protocols need to be developed, including mass production, isolation, functional evaluation, and batch-to-batch consistency. Some clinical trials using MSC-EVs in COVID-19 is currently underway and are summarized in **Table 1**.

Preliminary studies demonstrated that intravenous injection of MSCs and MSC-EVs possessed an enormous potential in treatment for COVID-19 patients. So far, no adverse events were found during MSCs and MSC-EVs treatment and follow-up period, suggesting that this therapy is safe and effective for COVID-19 patients (Akbari and Rezaie, 2020). However, MSCs express tissue factors and accumulate mainly in pulmonary capillaries, which may increase the risk of pulmonary embolism and other thromboembolic events. The effects of administration time, dose, frequency and route of MSCs and MSC-EVs need further study. Though clinical outcomes are promising, the limited literature still warrants more studies to establish safety and efficacy of MSCs and MSC-EVs to treat and manage symptoms associated with COVID-19 infection (Hamdan, et al., 2021).

### Drug-EVs

One interesting approach of using EVs as therapeutic agents is its drug delivery potential (Gnecchi, et al., 2006; Lamichhane, et al., 2016; Lv, et al., 2012). EVs have a cellular origin, such as MSCs, and therefore offer greater safety and stability than other delivery systems such as liposomes (Malhotra, et al., 2016). Selectable compounds or genetically engineered molecules may loading with EVs in the nanocarriers to enhance the targeting ability for tissue/cell infection, suggesting that EVs-based nanocarriers can be used to treat infectious diseases. Some studies have used EV as an effective carrier of tumor-targeted anticancer drugs curcumin, doxorubicin, and paclitaxel (Kim, et al., 2016). Therefore, an EV-based drug delivery system has great potential to increase drug loading in targeting cells and inhibit off-target effects. EVs may be used to deliver therapeutic drugs or biomodulators to inhibiting the spread and replication of virus in the recipient cells (Romagnoli, et al., 2014). The development of safe and efficient nanocarriers is the main goal of nanomedicine. Therefore, the development of EVs-based nanocarriers offers a promising opportunity for therapeutic drug delivery. However, most of the studies have been conducted *in vitro* and *in vivo* experimental models, but it remains a mystery of the safety, specificity, and efficiency of the method in clinical trials.

Another attractive treatment option is to use the blood products of convalescent patients, such as the whole blood, plasma or serum. The EVs containing neutralizing antibodies in convalescent blood products were transferred into patients, and we benefit tremendously with this treatment by promoting immune regulation and lung tissue wound healing. Kesimer et al. proved that EVs derived from culture medium of human tracheobronchial epithelial cells showed a neutralizing effect on human influenza virus (Kesimer, et al., 2009). Studies have proved that plasma-derived EVs also carry an amount of cell growth factors, and these factors could induce the activation of cellular signaling pathways, change vascular reactivity, induce angiogenesis and promote tissue repair (Guo, et al., 2017; Tao, et al., 2017; Torreggiani, et al., 2014).



**TABLE 1 |** Ongoing clinical trials of MSC-EVs in COVID-19.

Registration number	Study title	Number enrolled	Interventions	Purposes
NCT04276987	A pilot clinical study on inhalation of mesenchymal stem cells exosomes treating severe novel coronavirus pneumonia	24	MSCs-derived exosomes	To explore the safety and efficiency of aerosol inhalation of the exosomes derived from allogenic adipose mesenchymal stem cells (MSCs-Exo)
NCT04798716	The use of exosomes for the treatment of acute respiratory distress syndrome or novel coronavirus pneumonia caused by COVID-19	55	MSC-exosomes delivered intravenously	To explore the safety and efficacy of an intravenous injection of MSC derived exosomes
NCT04491240	Evaluation of safety and efficiency of method of exosome inhalation in SARS-CoV-2 associated pneumonia. (COVID-19EXO)	30	EXO inhalation	To explore the safety and efficiency of aerosol inhalation of the exosomes
ChiCTR2000030261	A study for the key technology of mesenchymal stem cells exosomes atomization in the treatment of novel coronavirus pneumonia (COVID-19)	26	Aerosol inhalation of exosomes	To inhibit inflammatory factors and enhance the immunity of the body, promoting the early recovery of patients and reducing complications
ChiCTR2000030484	HUMSCs and exosomes treating patients with lung injury following novel coronavirus pneumonia (COVID-19)	90	Intravenous infusion of HUMSCs and exosomes	To evaluate the safety and efficacy of the treatment of human umbilical cord mesenchymal stem cells (MSCs)

Detailed information can be searched at <https://clinicaltrials.gov> and <http://www.chictr.org.cn>.

## EVs Vaccines

The use of EVs as immunogenicity factors in the treatment of SARS coronavirus infection has been studied. EV might be used as a vaccine with its advantages of high stability, low toxicity and immunogenicity in circulation (Zhou, et al., 2020c). Kuate et al. analyzed exosome-based vaccines which containing the S protein of SARS-CoV-2. The S proteins-containing exosomes were procured by replacing the transmembrane and cytoplasmic domains of the S protein with those of VSV-G, and its immunogenicity and efficacy were tested in mice. After comparing it to an adenoviral vector vaccine expressing the S protein, it has been proved that both of the exosomes and the vaccine could induce neutralizing antibody titers. After priming with the SARS-S protein exosomal vaccine and boosting with the adenoviral vector the neutralizing antibody titers of using SARS-S protein exosomal vaccine exceeded those observed in the convalescent serum of SARS patients (Kuate, et al., 2007). In addition, the treatment of EVs has been shown to be more effective than that of soluble protein subunit vaccines, which might be due to the fact that the expression of multiple copies of the same viral protein exposed on the EVs surface promotes the cross-linking between EVs and the B cell receptor (Gyorgy, et al., 2015).

## Platelet-derived EVs

Platelets are small (2–4 µm), and they are the anuclear cellular fragments of megakaryocytes from bone marrow and lung (Lefrancais, et al., 2017; Machlus, and Italiano, 2013). There are almost one trillion platelets patrol in the blood to hold the vascular system integrity. Once blood vessels are damaged, platelets will form a thrombus to prevent subsequent hemorrhage (Davi and Patrono, 2007). Platelet mediated thrombosis may also involve EVs (micro particles or micro vesicles), that provide anionic phospholipids such as phosphatidylserine to support the blood coagulation cascade (Ridger, et al., 2017). In addition to playing a role in hemostasis and thrombosis, platelets contribute to inducing the immune and inflammatory response (Kapur, et al., 2015; Li, et al., 2012; Morrell, et al., 2014; Semple, et al., 2011). The exosmosis and invasion to inflammatory tissues of neutrophils require interaction

with activated platelets (Imhof, et al., 2016; Sreeramkumar, et al., 2014). The release of extracellular DNA (NETosis) by neutrophils was observed in patients with COVID-19 (Barnes, et al., 2020; Middleton, et al., 2020; Zuo, et al., 2020). NETosis requires platelets and may result in thrombosis (Constantinescu-Bercu, et al., 2020; Martinod, and Wagner, 2014). Some immune and inflammatory molecules have been found to express in platelets, such as IL-1; besides some immune receptors have been detected, such as CD40L, Toll-like receptors (TLR), and Fc receptors (Karas, et al., 1982; Lindemann, et al., 2001; Semple, Italiano, 2011).

Serological findings in patients with symptomatic COVID-19 include severe leukopenia and lymphocytopenia (Arentz, et al., 2020; Connors and Levy, 2020; Tang, et al., 2020). Low platelet count is closely associated with an increased risk of death for the in-hospital COVID-19 patients, although platelet levels are not generally considered clinically relevant. This finding suggests that SARS-CoV-2 infection may decrease platelet production and/or increase the damage of platelet. Patients with COVID-19 are more likely increase platelet consumption because of the platelet activation and thrombosis (Al-Samkari, et al., 2020; Liao, et al., 2020; Lippi and Favalora, 2020a; Lippi, et al., 2020b; Liu, et al., 2020; Xu, et al., 2020a; Yang, et al., 2020b).

Since thrombus and clotting are mainly controlled by platelets (Roberts, et al., 2006), it is critical to determine the status of platelets in COVID-19. Platelet-EVs delivers molecules from the mother platelet. They transport platelet-derived cytokines and other pro-inflammatory molecules, such as damage-associated molecular patterns (DAMPs) (Boudreau, et al., 2014; Maugeri, et al., 2018; Melki, et al., 2017). SARS-CoV-2 enters the ACE2-expressed endothelial cells. The loss of endothelial integrity may facilitate the recruitment of circulating platelets to the infected site, causing platelet activation and degranulation. Through analysis of platelet degranulation and cytokine release, Zaid et al. observed an evident increase in platelet-EVs firstly in platelet-EVs in patients with COVID-19 (Zaid, et al., 2020). This increase may be due to increased production of megakaryocytes or platelets, reduced clearance, or a combination of the two. Surprisingly, the level of

platelet-EVs was significantly lower in severely ill patients than in non-critically ill patients. In severe COVID-19 cases, the number of platelets decreases. They reported that platelets were at the forefront of COVID-19 because they release various molecules at different stages of the disease. Thus, it is possible that platelets, which are associated with SARS-CoV-2 RNA and are highly activated in COVID-19, may be involved in the overwhelming thrombosis of COVID-19. Platelet overactivation may be involved in the systemic inflammatory response and thrombosis events observed in this disease. Therefore, inhibition of pathways associated with platelet activation may improve prognosis during COVID-19.

Giuseppe Cappellano et al. (Cappellano, et al., 2021) showed that platelet-EVs counts were higher in SARS-CoV-2 positive patients compared with SARS-CoV-2-negative patients, while platelet counts were not changed. What is particularly interesting is that the level of PLT-EVs was strongly associated with SARS-CoV-2 infection by a multivariate analysis, which independent from any confounding factors (age, sex, comorbidity, etc.). There was a very good diagnostic performance in ROC curve analysis, with sensitivity of 75% and specificity of 74%.

Platelet-derived EVs can be used to develop novel treatment strategies for COVID-19 patients. A study showed that engineered platelet-derived EVs loaded with TPCA-1 were effective in treating pneumonia (Ma, et al., 2020). In mouse models that selectively target inflammatory sites, platelet-derived EVs suppressed inflammation and reduced local cytokine storms.

## Reduces EVs Secreted by Virus-infected Cells Into Receptor Cells

EVs secreted from virus-infected cells contribute to promoting viral infection and inhibiting immune cell response. Therefore, it may be a new useful method to overcome viral transmission by inhibiting the uptake of EVs (Li, et al., 2019; Schneider, et al., 2017).

## OPPORTUNITIES AND CHALLENGES

Understanding the roles of EVs in COVID-19 infection could increase our knowledge of the dynamics of the virus and help developing effective prevention and treatment modalities. The above-mentioned findings provide a basis for future research on the dynamics of SARS-CoV-2 virus infection and its inhibition. However, it is worth noting that no EVs-based treatment has been approved to date. Significant barriers remain for the development of MSC-EVs as a therapeutic tool (Tsiapalis and O'Driscoll, 2020). Currently, we do not have any information on the possible side effects of EVs treatment against COVID-19. First, there are the similarities between EVs and viruses, both of them interact with the endosomal system which is responsible for synthesis of EVs. Some viruses may use this mechanism to pack viral proteins and RNA into vesicles in infected cells, subsequently released into the extracellular space, then facilitate the spread of the virus to uninfected cells (Gould, et al., 2003). This process has been demonstrated in HIV

infection, but has not been elucidated in coronavirus infection (Arenaccio, Anticoli, 2015; Giannessi, et al., 2020). Second, the heterogeneity of EVs is a big challenge (Tkach, et al., 2018). Up to now, all published studies using heterogeneous EVs in some cases using the part size (<200 nm “small” EVs). Because the origin, size, composition and functional characteristics of the EVs are different, the source selection should be carefully described when using them for treatment. It is important to note that different sizes EVs of dendritic cells can induce the activation of T cells with different polarization mode (Kowal, et al., 2016). Third, due to the lack of standardization for accurate counting EV, as well as the current equipment does not differentiate between vesicles and non-vesicular granules, the quantitation of EV preparation is also an unsolved problems (Tkach, Kowal, 2018). For example, Campanella et al. reported that autologous exosomes were safer than allogeneic plasma exosomes in regenerative medicine (Campanella, et al., 2019). Soni et al. demonstrated that alveolar macrophages produce EVs might have a proinflammatory or anti-inflammatory effects, depending on the separation time of EVs in the process of acute lung injury (Soni, et al., 2016). Fourth, variability of tissue of origin and culture conditions (Patel, et al., 2018; Pittenger, et al., 2019). Although the MSCs from different sources have different immunosuppression and differentiation ability, but the optimal source of immunomodulation has not yet been determined (Gao, Chiu, 2016). Chance et al. reported that MSC-EVs had higher thrombotic activity than BMMSC-EVs (Chance, et al., 2019). Recently, Inal reported a specific EVs subgroup, especially the EVs-TF positive might be associated with venous thromboembolism in COVID-19 patients with hypertension and diabetes (Inal, 2020). Taken together, it is critical to emphasize that care should be taken in using EVs for disease treatment (Borger, et al., 2020). To ensure the curative effect and safety of using EVs for COVID-19, enormous efforts are required to improve the technology for the separation and identification of EVs.

## AUTHOR CONTRIBUTIONS

Y-yY, W-mZ, and Y-qW wrote the first draft of manuscript, Q-rG, F-xZ, and Z-yZ designed the figures, Y-xX and H-yZ finished the table, MA and AMJ amended the text and figures, BM and J-yZ designed and revised the manuscript. All authors read and approved the final manuscript.

## FUNDING

This work was supported by the National Natural Science Foundation of China (81902152, U1903126, 81773888 and 81903467), Open Founding of Key Laboratory Ethnomedicine Ministry of Education (KLEM-KF2019Y03), the Key Medical Science and Technology Project of Shanxi Province (2020 XM33-“Four Batches” of Science and Technology Medical Innovation Project of Shanxi Province), and the Fund of Shanxi Province Higher Education Technology Innovation Project (2019L0753).

## REFERENCES

- Abdi, R., Fiorina, P., Adra, C. N., Atkinson, M., and Sayegh, M. H. (2008). Immunomodulation by Mesenchymal Stem Cells: A Potential Therapeutic Strategy for Type 1 Diabetes. *Diabetes* 57, 1759–1767. doi:10.2337/db08-0180
- Ackermann, M., Verleden, S. E., Kuehnel, M., Haverich, A., Welte, T., Laenger, F., et al. (2020). Pulmonary Vascular Endothelialitis, Thrombosis, and Angiogenesis in Covid-19. *N. Engl. J. Med.* 383, 120–128. doi:10.1056/NEJMoa2015432
- Ahmadi, M., and Rezaie, J. (2021). Ageing and Mesenchymal Stem Cells Derived Exosomes: Molecular Insight and Challenges. *Cell Biochem Funct* 39, 60–66. doi:10.1002/cbf.3602
- Akbari, A., and Rezaie, J. (2020). Potential Therapeutic Application of Mesenchymal Stem Cell-Derived Exosomes in SARS-CoV-2 Pneumonia. *Stem Cell Res. Ther.* 11, 356. doi:10.1186/s13287-020-01866-6
- Al-Samkari, H., Karp Leaf, R. S., Dzik, W. H., Carlson, J. C. T., Fogerty, A. E., Waheed, A., et al. (2020). COVID-19 and Coagulation: Bleeding and Thrombotic Manifestations of SARS-CoV-2 Infection. *Blood* 136, 489–500. doi:10.1182/blood.2020006520
- Ali, S. A., Huang, M.-B., Campbell, P. E., Roth, W. W., Campbell, T., Khan, M., et al. (2010). Genetic Characterization of HIV Type 1 Nef-Induced Vesicle Secretion. *AIDS Res. Hum. Retroviruses* 26, 173–192. doi:10.1089/aid.2009.0068
- Arenaccio, C., Anticoli, S., Manfredi, F., Chiozzini, C., Olivetta, E., and Federico, M. (2015). Latent HIV-1 Is Activated by Exosomes from Cells Infected with Either Replication-Competent or Defective HIV-1. *Retrovirology* 12, 87. doi:10.1186/s12977-015-0216-y
- Arentz, M., Yim, E., Klaff, L., Lokhandwala, S., Riedo, F. X., Chong, M., et al. (2020). Characteristics and Outcomes of 21 Critically Ill Patients with COVID-19 in Washington State. *JAMA* 323, 1612–1614. doi:10.1001/jama.2020.4326
- Armstrong, J. P. K., Holme, M. N., and Stevens, M. M. (2017). Re-Engineering Extracellular Vesicles as Smart Nanoscale Therapeutics. *ACS Nano* 11, 69–83. doi:10.1021/acs.nano.6b07607
- Atluri, S., Manchikanti, L., and Hirsch, J. A. (2020). Expanded Umbilical Cord Mesenchymal Stem Cells (UC-MSCs) as a Therapeutic Strategy in Managing Critically Ill COVID-19 Patients: The Case for Compassionate Use. *Pain Physician* 23, E71–E83. doi:10.36076/ppj.2020/23/e71
- Babaei, M., and Rezaie, J. (2021). Application of Stem Cell-Derived Exosomes in Ischemic Diseases: Opportunity and Limitations. *J. Transl. Med.* 19, 196. doi:10.1186/s12967-021-02863-w
- Bari, E., Ferrarotti, I., Saracino, L., Perteghella, S., Torre, M. L., and Corsico, A. G. (2020). Mesenchymal Stromal Cell Secretome for Severe COVID-19 Infections: Premises for the Therapeutic Use. *Cells* 9, 924. doi:10.3390/cells9040924
- Bari, E., Ferrarotti, I., Torre, M. L., Corsico, A. G., and Perteghella, S. (2019). Mesenchymal Stem/stromal Cell Secretome for Lung Regeneration: The Long Way through "pharmaceuticalization" for the Best Formulation. *J. Control. Release* 309, 11–24. doi:10.1016/j.jconrel.2019.07.022
- Barnes, B. J., Adrover, J. M., Baxter-Stoltzfus, A., Borczuk, A., Cools-Lartigue, J., Crawford, J. M., et al. (2020). Targeting Potential Drivers of COVID-19: Neutrophil Extracellular Traps. *J. Exp. Med.* 217, e20200652. doi:10.1084/jem.20200652
- Bautista-Vargas, M., Bonilla-Abadía, F., and Cañas, C. A. (2020). Potential Role for Tissue Factor in the Pathogenesis of Hypercoagulability Associated with in COVID-19. *J. Thromb. Thrombolysis* 50, 479–483. doi:10.1007/s11239-020-02172-x
- Beigel, J. H., Tomashek, K. M., Dodd, L. E., Mehta, A. K., Zingman, B. S., Kalil, A. C., et al. (2020). Remdesivir for the Treatment of Covid-19 - Final Report. *N. Engl. J. Med.* 383, 1813–1826. doi:10.1056/NEJMoa2007764
- Berger, J. S., Kunichoff, D., Adhikari, S., Ahuja, T., Amoroso, N., Aphinyanaphongs, Y., et al. (2020). Prevalence and Outcomes of D-Dimer Elevation in Hospitalized Patients with COVID-19. *Arterioscler. Thromb. Vasc. Biol.* 40, 2539–2547. doi:10.1161/ATVBAHA.120.314872
- Bhattacharya, J., and Matthay, M. A. (2013). Regulation and Repair of the Alveolar-Capillary Barrier in Acute Lung Injury. *Annu. Rev. Physiol.* 75, 593–615. doi:10.1146/annurev-physiol-030212-183756
- Börger, V., Weiss, D. J., Anderson, J. D., Borràs, F. E., Bussolati, B., Carter, D. R. F., et al. (2020). International Society for Extracellular Vesicles and International Society for Cell and Gene Therapy Statement on Extracellular Vesicles from Mesenchymal Stromal Cells and Other Cells: Considerations for Potential Therapeutic Agents to Suppress Coronavirus Disease-19. *Cytotherapy* 22, 482–485. doi:10.1016/j.jcyt.2020.05.002
- Boudreau, L. H., Duche, A.-C., Cloutier, N., Soulet, D., Martin, N., Bollinger, J., et al. (2014). Platelets Release Mitochondria Serving as Substrate for Bactericidal Group IIA-Secreted Phospholipase A2 to Promote Inflammation. *Blood* 124, 2173–2183. doi:10.1182/blood-2014-05-573543
- Bourgonje, A. R., Abdulle, A. E., Timens, W., Hillebrands, J. L., Navis, G. J., Gordijn, S. J., et al. (2020). Angiotensin-converting Enzyme 2 (ACE2), SARS-CoV-2 and the Pathophysiology of Coronavirus Disease 2019 (COVID-19). *J. Pathol.* 251, 228–248. doi:10.1002/path.5471
- Braun, R. K., Chetty, C., Balasubramaniam, V., Centanni, R., Haraldsdottir, K., Hematti, P., et al. (2018). Intraperitoneal Injection of MSC-Derived Exosomes Prevent Experimental Bronchopulmonary Dysplasia. *Biochem. Biophys. Res. Commun.* 503, 2653–2658. doi:10.1016/j.bbrc.2018.08.019
- Budoni, M., Fierabracci, A., Luciano, R., Petrini, S., Di Ciommo, V., and Muraca, M. (2013). The Immunosuppressive Effect of Mesenchymal Stromal Cells on B Lymphocytes Is Mediated by Membrane Vesicles. *Cell Transplant.* 22, 369–379. doi:10.3727/096368911X58276910.3727/096368911X582769b
- Campanella, C., Caruso Bavisotto, C., Logozzi, M., Marino Gammazza, A., Mizzoni, D., Cappello, F., et al. (2019). On the Choice of the Extracellular Vesicles for Therapeutic Purposes. *Int. J. Mol. Sci.* 20, 236. doi:10.3390/ijms20020236
- Cappariello, A., Loftus, A., Muraca, M., Maurizi, A., Rucci, N., and Teti, A. (2018). Osteoblast-Derived Extracellular Vesicles Are Biological Tools for the Delivery of Active Molecules to Bone. *J. Bone Miner. Res.* 33, 517–533. doi:10.1002/jbmr.3332
- Cappellano, G., Raineri, D., Rolla, R., Giordano, M., Puricelli, C., Vilaro, B., et al. (2021). Circulating Platelet-Derived Extracellular Vesicles Are a Hallmark of Sars-Cov-2 Infection. *Cells* 10, 85. doi:10.3390/cells10010085
- Cargnoni, A., Gibelli, L., Tosini, A., Signoroni, P. B., Nassuato, C., Arienti, D., et al. (2009). Transplantation of Allogeneic and Xenogeneic Placenta-Derived Cells Reduces Bleomycin-Induced Lung Fibrosis. *Cell Transplant.* 18, 405–422. doi:10.3727/096368909788809857
- Cascella, M., Rajnik, M., Cuomo, A., Dulebohn, S. C., and Di Napoli, R. (2021). *Features, Evaluation, and Treatment of Coronavirus (COVID-19)*. Treasure Island, FL: StatPearls.
- Cavalli, G., De Luca, G., Campochiaro, C., Della-Torre, E., Ripa, M., Canetti, D., et al. (2020). Interleukin-1 Blockade with High-Dose Anakinra in Patients with COVID-19, Acute Respiratory Distress Syndrome, and Hyperinflammation: A Retrospective Cohort Study. *Lancet Rheumatol.* 2, e325–e331. doi:10.1016/S2665-9913(20)30127-2
- Chance, T. C., Rathbone, C. R., Kamucheka, R. M., Peltier, G. C., Cap, A. P., and Bynum, J. A. (2019). The Effects of Cell Type and Culture Condition on the Procoagulant Activity of Human Mesenchymal Stromal Cell-Derived Extracellular Vesicles. *J. Trauma Acute Care Surg.* 87, S74–S82. doi:10.1097/TA.0000000000000225
- Chen, C. M., and Chou, H. C. (2018). Human Mesenchymal Stem Cells Attenuate Hyperoxia-Induced Lung Injury through Inhibition of the Renin-Angiotensin System in Newborn Rats. *Am. J. Transl. Res.* 10, 2628–2635.
- Connors, J. M., and Levy, J. H. (2020). COVID-19 and its Implications for Thrombosis and Anticoagulation. *Blood* 135, 2033–2040. doi:10.1182/blood.2020006000
- Constantinescu-Bercu, A., Grassi, L., Frontini, M., Salles-Crawley, I. I., Woollard, K., and Crawley, J. T. (2020). Activated αIIbβ3 on Platelets Mediates Flow-dependent NETosis via SLC44A2. *Elife* 9, e53353. doi:10.7554/eLife.53353
- Cruz, F. F., and Rocco, P. R. M. (2020). The Potential of Mesenchymal Stem Cell Therapy for Chronic Lung Disease. *Expert Rev. Respir. Med.* 14, 31–39. doi:10.1080/17476348.2020.1679628
- Cui, J., Li, F., and Shi, Z.-L. (2019). Origin and Evolution of Pathogenic Coronaviruses. *Nat. Rev. Microbiol.* 17, 181–192. doi:10.1038/s41579-018-0118-9
- Davi, G., and Patrono, C. (2007). Platelet Activation and Atherothrombosis. *N. Engl. J. Med.* 357, 2482–2494. doi:10.1056/NEJMra071014
- Del Fattore, A., Luciano, R., Pascucci, L., Goffredo, B. M., Giorda, E., Scapaticci, M., et al. (2015). Immunoregulatory Effects of Mesenchymal Stem Cell-Derived Extracellular Vesicles on T Lymphocytes. *Cell Transplant.* 24, 2615–2627. doi:10.3727/096368915X687543

- Devaux, C. A., Rolain, J.-M., and Raoult, D. (2020). ACE2 Receptor Polymorphism: Susceptibility to SARS-CoV-2, Hypertension, Multi-Organ Failure, and COVID-19 Disease Outcome. *J. Microbiol. Immunol. Infect.* 53, 425–435. doi:10.1016/j.jmii.2020.04.015
- Di Trapani, M., Bassi, G., Midolo, M., Gatti, A., Takam Kamga, P., Cassaro, A., et al. (2016). Differential and Transferable Modulatory Effects of Mesenchymal Stromal Cell-Derived Extracellular Vesicles on T, B and NK Cell Functions. *Sci. Rep.* 6, 24120. doi:10.1038/srep24120
- Dogrammatzis, C., Waisner, H., and Kalamvoki, M. (2020). Cloaked Viruses and Viral Factors in Cutting Edge Exosome-Based Therapies. *Front. Cell Dev. Biol.* 8, 376. doi:10.3389/fcell.2020.00376
- Dominici, M., Le Blanc, K., Mueller, I., Slaper-Cortenbach, I., Marini, F. C., Krause, D. S., et al. (2006). Minimal Criteria for Defining Multipotent Mesenchymal Stromal Cells. The International Society for Cellular Therapy Position Statement. *Cytotherapy* 8, 315–317. doi:10.1080/14653240600855905
- Doorn, J., Moll, G., Le Blanc, K., van Blitterswijk, C., and de Boer, J. (2012). Therapeutic Applications of Mesenchymal Stromal Cells: Paracrine Effects and Potential Improvements. *Tissue Eng. Part B Rev.* 18, 101–115. doi:10.1089/ten.TEB.2011.0488
- England, J. T., Abdulla, A., Biggs, C. M., Lee, A. Y. Y., Hay, K. A., Hoiland, R. L., et al. (2021). Weathering the COVID-19 Storm: Lessons from Hematologic Cytokine Syndromes. *Blood Rev.* 45, 100707. doi:10.1016/j.blre.2020.100707
- Fierabracci, A., Del Fattore, A., Luciano, R., Muraca, M., Teti, A., and Muraca, M. (2015). Recent Advances in Mesenchymal Stem Cell Immunomodulation: the Role of Microvesicles. *Cell Transplant.* 24, 133–149. doi:10.3727/096368913X675728
- Fleming, A., Sampey, G., Chung, M.-C., Bailey, C., van Hoek, M. L., Kashanchi, F., et al. (2014). The Carrying Pigeons of the Cell: Exosomes and Their Role in Infectious Diseases Caused by Human Pathogens. *Pathog. Dis.* 71, 109–120. doi:10.1111/2049-632X.12135
- Fung, T. S., and Liu, D. X. (2019). Human Coronavirus: Host-Pathogen Interaction. *Annu. Rev. Microbiol.* 73, 529–557. doi:10.1146/annurev-micro-020518-115759
- Galderisi, U., and Giordano, A. (2014). The Gap Between the Physiological and Therapeutic Roles of Mesenchymal Stem Cells. *Med. Res. Rev.* 34, 1100–1126. doi:10.1002/med.21322
- Gao, F., Chiu, S. M., Motan, D. A. L., Zhang, Z., Chen, L., Ji, H.-L., et al. (2016). Mesenchymal Stem Cells and Immunomodulation: Current Status and Future Prospects. *Cell Death Dis.* 7, e2062. doi:10.1038/cddis.2015.327
- Gao, Y. M., Xu, G., Wang, B., and Liu, B. C. (2021). Cytokine Storm Syndrome in Coronavirus Disease 2019: A Narrative Review. *J. Intern. Med.* 289, 147–161. doi:10.1111/joim.13144
- Gennai, S., Monsel, A., Hao, Q., Park, J., Matthay, M. A., and Lee, J. W. (2015). Microvesicles Derived from Human Mesenchymal Stem Cells Restore Alveolar Fluid Clearance in Human Lungs Rejected for Transplantation. *Am. J. Transplant.* 15, 2404–2412. doi:10.1111/ajt.13271
- Giannesi, F., Aiello, A., Franchi, F., Percario, Z. A., and Affabris, E. (2020). The Role of Extracellular Vesicles as Allies of HIV, HCV and SARS Viruses. *Viruses* 12, 571. doi:10.3390/v12050571
- Glowacka, I., Bertram, S., Herzog, P., Pfeifferle, S., Steffen, I., Muench, M. O., et al. (2010). Differential Downregulation of ACE2 by the Spike Proteins of Severe Acute Respiratory Syndrome Coronavirus and Human Coronavirus NL63. *J. Virol.* 84, 1198–1205. doi:10.1128/JVI.01248-09
- Gnecchi, M., He, H., Noiseux, N., Liang, O. D., Zhang, L., Morello, F., et al. (2006). Evidence Supporting Paracrine Hypothesis for Akt-modified Mesenchymal Stem Cell-mediated Cardiac protection and Functional Improvement. *FASEB J.* 20, 661–669. doi:10.1096/fj.05-5211.com
- Gnecchi, M., Zhang, Z., Ni, A., and Dzau, V. J. (2008). Paracrine Mechanisms in Adult Stem Cell Signaling and Therapy. *Circ. Res.* 103, 1204–1219. doi:10.1161/CIRCRESAHA.108.176826
- Gould, S. J., Booth, A. M., and Hildreth, J. E. K. (2003). The Trojan Exosome Hypothesis. *Proc. Natl. Acad. Sci. USA* 100, 10592–10597. doi:10.1073/pnas.1831413100
- Grasselli, G., Zangrillo, A., Zanella, A., Antonelli, M., Cabrini, L., Castelli, A., et al. (2020). Baseline Characteristics and Outcomes of 1591 Patients Infected with SARS-CoV-2 Admitted to ICUs of the Lombardy Region. *Italy. JAMA.* 323, 1574–1581. doi:10.1001/jama.2020.539410.1001/jama.2020.4031
- Grover, S. P., and Mackman, N. (2018). Tissue Factor: An Essential Mediator of Hemostasis and Trigger of Thrombosis. *Arterioscler. Thromb. Vasc. Biol.* 38, 709–725. doi:10.1161/ATVBAHA.117.309846
- Gunasekaran, M., Xu, Z., Nayak, D. K., Sharma, M., Hachem, R., Walia, R., et al. (2017). Donor-Derived Exosomes with Lung Self-Antigens in Human Lung Allograft Rejection. *Am. J. Transplant.* 17, 474–484. doi:10.1111/ajt.13915
- Guo, S.-C., Tao, S.-C., Yin, W.-J., Qi, X., Yuan, T., and Zhang, C.-Q. (2017). Exosomes Derived from Platelet-Rich Plasma Promote the Re-epithelization of Chronic Cutaneous Wounds via Activation of YAP in a Diabetic Rat Model. *Theranostics* 7, 81–96. doi:10.7150/thno.16803
- Guzik, T. J., Mohiddin, S. A., Dimarco, A., Patel, V., Savvatis, K., Marelli-Berg, F. M., et al. (2020). COVID-19 and the Cardiovascular System: Implications for Risk Assessment, Diagnosis, and Treatment Options. *Cardiovasc. Res.* 116, 1666–1687. doi:10.1093/cvr/cvaa106
- György, B., Hung, M. E., Breakefield, X. O., and Leonard, J. N. (2015). Therapeutic Applications of Extracellular Vesicles: Clinical Promise and Open Questions. *Annu. Rev. Pharmacol. Toxicol.* 55, 439–464. doi:10.1146/annurev-pharmtox-010814-124630
- Hamdan, H., Hashmi, S. K., Lazarus, H., Gale, R. P., Qu, W., and El Fakih, R. (2021). Promising Role for Mesenchymal Stromal Cells in Coronavirus Infectious Disease-19 (COVID-19)-Related Severe Acute Respiratory Syndrome? *Blood Rev.* 46, 100742. doi:10.1016/j.blre.2020.100742
- Hamming, I., Timens, W., Bulthuis, M., Lely, A., Navis, G., and van Goor, H. (2004). Tissue Distribution of ACE2 Protein, the Functional Receptor for SARS Coronavirus. A First Step in Understanding SARS Pathogenesis. *J. Pathol.* 203, 631–637. doi:10.1002/path.1570
- Han, L., Lam, E. W.-F., and Sun, Y. (2019). Extracellular Vesicles in the Tumor Microenvironment: Old Stories, but New Tales. *Mol. Cancer* 18, 59. doi:10.1186/s12943-019-0980-8
- Harrell, C. R., Jovicic, N., Djonov, V., Arsenijevic, N., and Volarevic, V. (2019). Mesenchymal Stem Cell-Derived Exosomes and Other Extracellular Vesicles as New Remedies in the Therapy of Inflammatory Diseases. *Cells* 8, 1605. doi:10.3390/cells8121605
- Henao Agudelo, J. S., Braga, T. T., Amano, M. T., Cenedeze, M. A., Cavinato, R. A., Peixoto-Santos, A. R., et al. (2017). Mesenchymal Stromal Cell-Derived Microvesicles Regulate an Internal Pro-inflammatory Program in Activated Macrophages. *Front. Immunol.* 8, 881. doi:10.3389/fimmu.2017.00881
- Huang, C., Wang, Y., Li, X., Ren, L., Zhao, J., Hu, Y., et al. (2020a). Clinical Features of Patients Infected with 2019 Novel Coronavirus in Wuhan, China. *Lancet* 395, 497–506. doi:10.1016/S0140-6736(20)30183-5
- Huang, W., Yan, Y., Liu, Y., Lin, M., Ma, J., Zhang, W., et al. (2020b). Exosomes with Low miR-34c-3p Expression Promote Invasion and Migration of Non-small Cell Lung Cancer by Upregulating Integrin  $\alpha 2 \beta 1$ . *Signal Transduct. Target. Ther.* 5, 39. doi:10.1038/s41392-020-0133-y
- Huet, T., Beaussier, H., Voisin, O., Jouvessomme, S., Dauriat, G., Lazareth, I., et al. (2020). Anakinra for Severe Forms of COVID-19: A Cohort Study. *Lancet Rheumatol.* 2, e393–e400. doi:10.1016/S2665-9913(20)30164-8
- Imhof, B. A., Jemelin, S., Ballet, R., Vesin, C., Schapira, M., Karaca, M., et al. (2016). CCN1/CYR61-mediated Meticulous Patrolling by Ly6Clow Monocytes Fuels Vascular Inflammation. *Proc. Natl. Acad. Sci. USA* 113, E4847–E4856. doi:10.1073/pnas.1607710113
- Inal, J. (2020). COVID-19 Comorbidities, Associated Procoagulant Extracellular Vesicles and Venous Thromboembolisms: A Possible Link with Ethnicity? *Br. J. Haematol.* 190, e218–e220. doi:10.1111/bjh.17011
- Jia, H. (2016). Pulmonary Angiotensin-Converting Enzyme 2 (ACE2) and Inflammatory Lung Disease. *Shock* 46, 239–248. doi:10.1097/SHK.0000000000000633
- Kapur, R., Zufferey, A., Boilard, E., and Semple, J. W. (2015). Nouvelle Cuisine: Platelets Served with Inflammation. *J. Immunol.* 194, 5579–5587. doi:10.4049/jimmunol.1500259
- Karas, S., Rosse, W., and Kurlander, R. (1982). Characterization of the IgG-Fc Receptor on Human Platelets. *Blood* 60, 1277–1282. doi:10.1182/blood.v60.6.1277.bloodjournal6061277
- Kesimer, M., Scull, M., Brighton, B., DeMaria, G., Burns, K., O'Neal, W., et al. (2009). Characterization of Exosome-like Vesicles Released from Human Tracheobronchial Ciliated Epithelium: A Possible Role in Innate Defense. *FASEB J.* 23, 1858–1868. doi:10.1096/fj.08-119131
- Khatri, M., Richardson, L. A., and Meulia, T. (2018). Mesenchymal Stem Cell-Derived Extracellular Vesicles Attenuate Influenza Virus-Induced Acute Lung



- Injury in a Pig Model. *Stem Cell Res. Ther.* 9, 17. doi:10.1186/s13287-018-0774-8
- Kim, M. S., Haney, M. J., Zhao, Y., Mahajan, V., Deygen, I., Klyachko, N. L., et al. (2016). Development of Exosome-Encapsulated Paclitaxel to Overcome MDR in Cancer Cells. *Nanomedicine* 12, 655–664. doi:10.1016/j.nano.2015.10.012
- Kolios, G., and Moodley, Y. (2013). Introduction to Stem Cells and Regenerative Medicine. *Respiration* 85, 3–10. doi:10.1159/000345615
- Kowal, J., Arras, G., Colombo, M., Jouve, M., Morath, J. P., Primdal-Bengtson, B., et al. (2016). Proteomic Comparison Defines Novel Markers to Characterize Heterogeneous Populations of Extracellular Vesicle Subtypes. *Proc. Natl. Acad. Sci. USA* 113, E968–E977. doi:10.1073/pnas.1521230113
- Kowal, J., Tkach, M., and Théry, C. (2014). Biogenesis and Secretion of Exosomes. *Curr. Opin. Cell Biol.* 29, 116–125. doi:10.1016/j.ccb.2014.05.004
- Krasnodembskaya, A., Song, Y., Fang, X., Gupta, N., Serikov, V., Lee, J.-W., et al. (2010). Antibacterial Effect of Human Mesenchymal Stem Cells Is Mediated in Part from Secretion of the Antimicrobial Peptide LL-37. *Stem Cells* 28, 2229–2238. doi:10.1002/stem.544
- Krishnamachary, B., Cook, C., Spikes, L., Chalise, P., and Dhillon, N. K. (2020). The Potential Role of Extracellular Vesicles in COVID-19 Associated Endothelial Injury and Pro-inflammation. medRxiv [Preprint]. Available at: <https://www.ncbi.nlm.nih.gov/pmc/articles/PMC7480053/> (Accessed September 1, 2020). doi:10.1101/2020.08.27.20182808
- Kuate, S., Cinatl, J., Doerr, H. W., and Überla, K. (2007). Exosomal Vaccines Containing the S Protein of the SARS Coronavirus Induce High Levels of Neutralizing Antibodies. *Virology* 362, 26–37. doi:10.1016/j.virol.2006.12.011
- Kwon, Y., Nukala, S. B., Srivastava, S., Miyamoto, H., Ismail, N. I., Rehman, J., et al. (2020). Detection of Viral RNA Fragments in Human iPSC-Cardiomyocytes Following Treatment with Extracellular Vesicles from SARS-CoV-2 Coding-Sequence-Overexpressing Lung Epithelial Cells. bioRxiv [Preprint]. Available at: <https://pubmed.ncbi.nlm.nih.gov/32637965/> (Accessed July 1, 2020). doi:10.1101/2020.05.14.093583
- Lamichhane, T. N., Jeyaram, A., Patel, D. B., Parajuli, B., Livingston, N. K., Arumugasamy, N., et al. (2016). Oncogene Knockdown via Active Loading of Small RNAs into Extracellular Vesicles by Sonication. *Cell. Mol. Bioeng.* 9, 315–324. doi:10.1007/s12195-016-0457-4
- Lanyu, Z., and Feilong, H. (2019). Emerging Role of Extracellular Vesicles in Lung Injury and Inflammation. *Biomed. Pharmacother.* 113, 108748. doi:10.1016/j.biopha.2019.108748
- Lässer, C., O'Neil, S. E., Shelke, G. V., Sihlbom, C., Hansson, S. F., Gho, Y. S., et al. (2016). Exosomes in the Nose Induce Immune Cell Trafficking and Harbour an Altered Protein Cargo in Chronic Airway Inflammation. *J. Transl. Med.* 14, 181. doi:10.1186/s12967-016-0927-4
- Lee, J. H., Park, J., and Lee, J.-W. (2019). Therapeutic Use of Mesenchymal Stem Cell-Derived Extracellular Vesicles in Acute Lung Injury. *Transfusion* 59, 876–883. doi:10.1111/trf.14838
- Lee, R. H., Pulin, A. A., Seo, M. J., Kota, D. J., Ylostalo, J., Larson, B. L., et al. (2009). Intravenous hMSCs Improve Myocardial Infarction in Mice Because Cells Embolized in Lung Are Activated to Secrete the Anti-inflammatory Protein TSG-6. *Cell Stem Cell* 5, 54–63. doi:10.1016/j.stem.2009.05.003
- Lefrançois, E., Ortiz-Muñoz, G., Caudrillier, A., Mallavia, B., Liu, F., Sayah, D. M., et al. (2017). The Lung Is a Site of Platelet Biogenesis and a Reservoir for Haematopoietic Progenitors. *Nature* 544, 105–109. doi:10.1038/nature21706
- Leng, Z., Zhu, R., Hou, W., Feng, Y., Yang, Y., Han, Q., et al. (2020). Transplantation of ACE2- Mesenchymal Stem Cells Improves the Outcome of Patients with COVID-19 Pneumonia. *Aging Dis.* 11, 216–228. doi:10.14336/AD.2020.0228
- Li, C., Li, J., Li, Y., Lang, S., Yougbare, I., Zhu, G., et al. (2012). Crosstalk Between Platelets and the Immune System: Old Systems with New Discoveries. *Adv. Hematol.* 2012, 1–14. doi:10.1155/2012/384685
- Li, F., Li, W., Farzan, M., and Harrison, S. C. (2005). Structure of SARS Coronavirus Spike Receptor-Binding Domain Complexed with Receptor. *Science* 309, 1864–1868. doi:10.1126/science.1116480
- Li, J., Huang, S., Wu, Y., Gu, C., Gao, D., Feng, C., et al. (2014). Paracrine Factors from Mesenchymal Stem Cells: A Proposed Therapeutic Tool for Acute Lung Injury and Acute Respiratory Distress Syndrome. *Int. Wound J.* 11, 114–121. doi:10.1111/iwj.12202
- Li, S., Li, S., Wu, S., and Chen, L. (2019). Exosomes Modulate the Viral Replication and Host Immune Responses in HBV Infection. *Biomed. Res. Int.* 2019, 1–9. doi:10.1155/2019/2103943
- Li, Y., Xu, J., Shi, W., Chen, C., Shao, Y., Zhu, L., et al. (2016). Mesenchymal Stromal Cell Treatment Prevents H9N2 Avian Influenza Virus-Induced Acute Lung Injury in Mice. *Stem Cell Res. Ther.* 7, 159. doi:10.1186/s13287-016-0395-z
- Liao, D., Zhou, F., Luo, L., Xu, M., Wang, H., Xia, J., et al. (2020). Haematological Characteristics and Risk Factors in the Classification and Prognosis Evaluation of COVID-19: A Retrospective Cohort Study. *Lancet Haematol.* 7, e671–e678. doi:10.1016/S2352-3026(20)30217-9
- Lindemann, S., Tolley, N. D., Dixon, D. A., McIntyre, T. M., Prescott, S. M., Zimmerman, G. A., et al. (2001). Activated Platelets Mediate Inflammatory Signaling by Regulated Interleukin 1 $\beta$  Synthesis. *J. Cell Biol.* 154, 485–490. doi:10.1083/jcb.200105058
- Lippi, G., and Favaloro, E. J. (2020a). D-dimer Is Associated with Severity of Coronavirus Disease 2019: A Pooled Analysis. *Thromb. Haemost.* 120, 876–878. doi:10.1055/s-0040-1709650
- Lippi, G., Plebani, M., and Henry, B. M. (2020b). Thrombocytopenia Is Associated with Severe Coronavirus Disease 2019 (COVID-19) Infections: A Meta-Analysis. *Clin. Chim. Acta* 506, 145–148. doi:10.1016/j.cca.2020.03.022
- Liu, F. P., Dong, J. J., Sun, S. J., Gao, W. Y., Zhang, Z. W., Zhou, X. J., et al. (2012). Autologous Bone Marrow Stem Cell Transplantation in Critical Limb Ischemia: A Meta-Analysis of Randomized Controlled Trials. *Chin. Med. J. (Engl)* 125, 4296–4300. doi:10.3760/cma.j.issn.0366-6999.2012.23.024
- Liu, Y., Sun, W., Guo, Y., Chen, L., Zhang, L., Zhao, S., et al. (2020). Association between Platelet Parameters and Mortality in Coronavirus Disease 2019: Retrospective Cohort Study. *Platelets* 31, 490–496. doi:10.1080/09537104.2020.1754383
- Lv, L.-H., Wan, Y.-L., Lin, Y., Zhang, W., Yang, M., Li, G.-L., et al. (2012). Anticancer Drugs Cause Release of Exosomes with Heat Shock Proteins from Human Hepatocellular Carcinoma Cells that Elicit Effective Natural Killer Cell Antitumor Responses In Vitro. *J. Biol. Chem.* 287, 15874–15885. doi:10.1074/jbc.M112.340588
- Ma, Q., Fan, Q., Xu, J., Bai, J., Han, X., Dong, Z., et al. (2020). Calming Cytokine Storm in Pneumonia by Targeted Delivery of TPCA-1 Using Platelet-Derived Extracellular Vesicles. *Matter* 3, 287–301. doi:10.1016/j.matt.2020.05.017
- Maas, S. L. N., Breakefield, X. O., and Weaver, A. M. (2017). Extracellular Vesicles: Unique Intercellular Delivery Vehicles. *Trends Cell Biol.* 27, 172–188. doi:10.1016/j.tcb.2016.11.003
- Machlus, K. R., and Italiano, J. E., Jr. (2013). The Incredible Journey: From Megakaryocyte Development to Platelet Formation. *J. Cell Biol.* 201, 785–796. doi:10.1083/jcb.201304054
- Mack, M., Kleinschmidt, A., Brühl, H., Klier, C., Nelson, P. J., Cihak, J., et al. (2000). Transfer of the Chemokine Receptor CCR5 between Cells by Membrane-Derived Microparticles: A Mechanism for Cellular Human Immunodeficiency Virus 1 Infection. *Nat. Med.* 6, 769–775. doi:10.1038/77498
- Mackman, N., Antoniaki, S., Wolberg, A. S., Kasthuri, R., and Key, N. S. (2020). Coagulation Abnormalities and Thrombosis in Patients Infected with SARS-CoV-2 and Other Pandemic Viruses. *Arterioscler. Thromb. Vasc. Biol.* 40, 2033–2044. doi:10.1161/ATVBAHA.120.314514
- Maione, F., Cappellano, G., Bellan, M., Raineri, D., and Chiocchetti, A. (2020). Chicken-or-egg Question: Which Came First, Extracellular Vesicles or Autoimmune Diseases? *J. Leukoc. Biol.* 108, 601–616. doi:10.1002/JLB.3MR0120-232R
- Malhotra, H., Sheokand, N., Kumar, S., Chauhan, A. S., Kumar, M., Jakhar, P., et al. (2016). Exosomes: Tunable Nano Vehicles for Macromolecular Delivery of Transferrin and Lactoferrin to Specific Intracellular Compartment. *J. Biomed. Nanotechnol.* 12, 1101–1114. doi:10.1166/jbn.2016.2229
- Mansouri, N., Willis, G. R., Fernandez-Gonzalez, A., Reis, M., Nassiri, S., Mitsialis, S. A., et al. (2019). Mesenchymal Stromal Cell Exosomes Prevent and Revert Experimental Pulmonary Fibrosis through Modulation of Monocyte Phenotypes. *JCI Insight* 4, e128060. doi:10.1172/jci.insight.128060
- Marini, J. J., and Gattinoni, L. (2020). Management of COVID-19 Respiratory Distress. *JAMA* 323, 2329–2330. doi:10.1001/jama.2020.6825
- Martin-Medina, A., Lehmann, M., Burgy, O., Hermann, S., Baarsma, H. A., Wagner, D. E., et al. (2018). Increased Extracellular Vesicles Mediate WNT5A Signaling in Idiopathic Pulmonary Fibrosis. *Am. J. Respir. Crit. Care Med.* 198, 1527–1538. doi:10.1164/rccm.201708-1580OC
- Martinez-Bravo, M.-J., Wahlund, C. J. E., Qazi, K. R., Moulder, R., Lukic, A., Rådmark, O., et al. (2017). Pulmonary Sarcoidosis Is Associated with Exosomal

- Vitamin D-Binding Protein and Inflammatory Molecules. *J. Allergy Clin. Immunol.* 139, 1186–1194. doi:10.1016/j.jaci.2016.05.051
- Martinod, K., and Wagner, D. D. (2014). Thrombosis: Tangled up in NETs. *Blood* 123, 2768–2776. doi:10.1182/blood-2013-10-463646
- Matthay, M. A., Calfee, C. S., Zhuo, H., Thompson, B. T., Wilson, J. G., Levitt, J. E., et al. (2019). Treatment with Allogeneic Mesenchymal Stromal Cells for Moderate to Severe Acute Respiratory Distress Syndrome (START Study): A Randomised Phase 2a Safety Trial. *Lancet Respir. Med.* 7, 154–162. doi:10.1016/S2213-2600(18)30418-1
- Maugeri, N., Capobianco, A., Rovere-Querini, P., Ramirez, G. A., Tombetti, E., Valle, P. D., et al. (2018). Platelet Microparticles Sustain Autophagy-Associated Activation of Neutrophils in Systemic Sclerosis. *Sci. Transl. Med.* 10, eaao3089. doi:10.1126/scitranslmed.aao3089
- McIntyre, L. A., Stewart, D. J., Mei, S. H. J., Courtman, D., Watpool, I., Granton, J., et al. (2018). Cellular Immunotherapy for Septic Shock. A Phase I Clinical Trial. *Am. J. Respir. Crit. Care Med.* 197, 337–347. doi:10.1164/rccm.201705-1006OC
- Mei, S. H. J., Haitsma, J. J., Dos Santos, C. C., Deng, Y., Lai, P. F. H., Slutsky, A. S., et al. (2010). Mesenchymal Stem Cells Reduce Inflammation while Enhancing Bacterial Clearance and Improving Survival in Sepsis. *Am. J. Respir. Crit. Care Med.* 182, 1047–1057. doi:10.1164/rccm.201001-0010OC
- Melki, I., Tessandier, N., Zufferey, A., and Boilard, E. (2017). Platelet Microvesicles in Health and Disease. *Platelets* 28, 214–221. doi:10.1080/09537104.2016.1265924
- Meng, F., Xu, R., Wang, S., Xu, Z., Zhang, C., Li, Y., et al. (2020). Human Umbilical Cord-Derived Mesenchymal Stem Cell Therapy in Patients with COVID-19: A Phase 1 Clinical Trial. *Signal Transduct. Target. Ther.* 5, 172. doi:10.1038/s41392-020-00286-5
- Messner, C. B., Demichev, V., Wendisch, D., Michalick, L., White, M., Freiwald, A., et al. (2020). Ultra-High-Throughput Clinical Proteomics Reveals Classifiers of COVID-19 Infection. *Cell Syst.* 11, 11–24. doi:10.1016/j.cels.2020.05.012
- Middleton, E. A., He, X.-Y., Denorme, F., Campbell, R. A., Ng, D., Salvatore, S. P., et al. (2020). Neutrophil Extracellular Traps Contribute to Immunothrombosis in COVID-19 Acute Respiratory Distress Syndrome. *Blood* 136, 1169–1179. doi:10.1182/blood.2020007008
- Mo, X., Jian, W., Su, Z., Chen, M., Peng, H., Peng, P., et al. (2020). Abnormal Pulmonary Function in COVID-19 Patients at Time of Hospital Discharge. *Eur. Respir. J.* 55, 2001217. doi:10.1183/13993003.01217-2020
- Monsel, A., Zhu, Y.-g., Gennai, S., Hao, Q., Hu, S., Rouby, J.-J., et al. (2015). Therapeutic Effects of Human Mesenchymal Stem Cell-Derived Microvesicles in Severe Pneumonia in Mice. *Am. J. Respir. Crit. Care Med.* 192, 324–336. doi:10.1164/rccm.201410-1765OC
- Morrell, C. N., Aggrey, A. A., Chapman, L. M., and Modjeski, K. L. (2014). Emerging Roles for Platelets as Immune and Inflammatory Cells. *Blood* 123, 2759–2767. doi:10.1182/blood-2013-11-462432
- Mousavizadeh, L., and Ghasemi, S. (2021). Genotype and Phenotype of COVID-19: Their Roles in Pathogenesis. *J. Microbiol. Immunol. Infect.* 54, 159–163. doi:10.1016/j.jmii.2020.03.022
- Muraca, M., Piccoli, M., Franzin, C., Tolomeo, A., Jurga, M., Pozzobon, M., et al. (2017). Diverging Concepts and Novel Perspectives in Regenerative Medicine. *Int. J. Mol. Sci.* 18, 1021. doi:10.3390/ijms18051021
- Nicola, M., Alsafi, Z., Sohrabi, C., Kerwan, A., Al-Jabir, A., Iosifidis, C., et al. (2020). The Socio-Economic Implications of the Coronavirus Pandemic (COVID-19): A Review. *Int. J. Surg.* 78, 185–193. doi:10.1016/j.ijsu.2020.04.018
- Nolte-’t Hoen, E., Cremer, T., Gallo, R. C., and Margolis, L. B. (2016). Extracellular Vesicles and Viruses: Are They Close Relatives? *Proc. Natl. Acad. Sci. U S A.* 113, 9155–9161. doi:10.1073/pnas.1605146113
- Owczarek, K., Szczepanski, A., Milewska, A., Baster, Z., Rajfur, Z., Sarna, M., et al. (2018). Early Events During Human Coronavirus OC43 Entry to the Cell. *Sci. Rep.* 8, 7124. doi:10.1038/s41598-018-25640-0
- Park, J., Kim, S., Lim, H., Liu, A., Hu, S., Lee, J., et al. (2019). Therapeutic Effects of Human Mesenchymal Stem Cell Microvesicles in an Ex Vivo Perfused Human Lung Injured with Severe *E. coli* Pneumonia. *Thorax* 74, 43–50. doi:10.1136/thoraxjnl-2018-211576
- Park, J. S., Shim, M.-S., Shim, S. H., Yang, H. N., Jeon, S. Y., Woo, D. G., et al. (2011). Chondrogenic Potential of Stem Cells Derived from Amniotic Fluid, Adipose Tissue, or Bone Marrow Encapsulated in Fibrin Gels Containing TGF- $\beta$ 3. *Biomaterials* 32, 8139–8149. doi:10.1016/j.biomaterials.2011.07.043
- Pascucci, L., Coccè, V., Bonomi, A., Ami, D., Ceccarelli, P., Ciusani, E., et al. (2014). Paclitaxel Is Incorporated by Mesenchymal Stromal Cells and Released in Exosomes that Inhibit In Vitro Tumor Growth: A New Approach for Drug Delivery. *J. Control. Release* 192, 262–270. doi:10.1016/j.jconrel.2014.07.042
- Patel, D. B., Santoro, M., Born, L. J., Fisher, J. P., and Jay, S. M. (2018). Towards Rationally Designed Biomanufacturing of Therapeutic Extracellular Vesicles: Impact of the Bioproduction Microenvironment. *Biotechnol. Adv.* 36, 2051–2059. doi:10.1016/j.biotechadv.2018.09.001
- Pedersen, S. F., and Ho, Y.-C. (2020). SARS-CoV-2: A Storm Is Raging. *J. Clin. Invest.* 130, 2202–2205. doi:10.1172/JCI137647
- Perrone, F., Piccirillo, M. C., Piccirillo, M. C., Ascierto, P. A., Salvarani, C., Parrella, R., et al. (2020). Tocilizumab for Patients with COVID-19 Pneumonia. The Single-Arm TOCIVID-19 Prospective Trial. *J. Transl. Med.* 18, 405. doi:10.1186/s12967-020-02573-9
- Phinney, D. G., and Pittenger, M. F. (2017). Concise Review: MSC-Derived Exosomes for Cell-free Therapy. *Stem Cells* 35, 851–858. doi:10.1002/stem.2575
- Pittenger, M. F., Discher, D. E., Péault, B. M., Phinney, D. G., Hare, J. M., and Caplan, A. I. (2019). Mesenchymal Stem Cell Perspective: Cell Biology to Clinical Progress. *NPJ Regen. Med.* 4, 22. doi:10.1038/s41536-019-0083-6
- Porzionato, A., Zaramella, P., Dedja, A., Guidolin, D., Van Wemmel, K., Macchi, V., et al. (2019). Intratracheal Administration of Clinical-Grade Mesenchymal Stem Cell-Derived Extracellular Vesicles Reduces Lung Injury in a Rat Model of Bronchopulmonary Dysplasia. *Am. J. Physiol. Lung Cell Mol. Physiol.* 316, L6–L19. doi:10.1152/ajplung.00109.2018
- Ragni, E., Banfi, F., Barilani, M., Cherubini, A., Parazzi, V., Larghi, P., et al. (2017). Extracellular Vesicle-Shuttled mRNA in Mesenchymal Stem Cell Communication. *Stem Cells* 35, 1093–1105. doi:10.1002/stem.2557
- Raposo, G., and Stoorvogel, W. (2013). Extracellular Vesicles: Exosomes, Microvesicles, and Friends. *J. Cell Biol.* 200, 373–383. doi:10.1083/jcb.201211138
- Rezaei, J., Aslan, C., Ahmadi, M., Zolbanin, N. M., Kashanchi, F., and Jafari, R. (2021). The Versatile Role of Exosomes in Human Retroviral Infections: From Immunopathogenesis to Clinical Application. *Cell Biosci* 11, 19. doi:10.1186/s13578-021-00537-0
- Rezaei, J., Mehranjani, M. S., Rahbarghazi, R., and Shariatzadeh, M. A. (2018). Angiogenic and Restorative Abilities of Human Mesenchymal Stem Cells Were Reduced Following Treatment with Serum from Diabetes Mellitus Type 2 Patients. *J. Cell. Biochem.* 119, 524–535. doi:10.1002/jcb.26211
- Rezaei, J., Rahbarghazi, R., Pezeshki, M., Mazhar, M., Yekani, F., Khaksar, M., et al. (2019). Cardioprotective Role of Extracellular Vesicles: A Highlight on Exosome Beneficial Effects in Cardiovascular Diseases. *J. Cell. Physiol.* 234, 21732–21745. doi:10.1002/jcp.28894
- Ridger, V. C., Boulanger, C. M., Angelillo-Scherrer, A., Badimon, L., Blanc-Brude, O., Bochaton-Piallat, M.-L., et al. (2017). Microvesicles in Vascular Homeostasis and Diseases. *Thromb. Haemost.* 117, 1296–1316. doi:10.1160/TH16-12-0943
- Roberts, H., Hoffman, M., and Monroe, D. (2006). A Cell-Based Model of Thrombin Generation. *Semin. Thromb. Hemost.* 32 (Suppl. 1), 32–38. doi:10.1055/s-2006-939552
- Romagnoli, G. G., Zelante, B. B., Toniolo, P. C. A., Migliori, I. K., and Barbuto, J. A. M. (2014). Dendritic Cell-Derived Exosomes May Be a Tool for Cancer Immunotherapy by Converting Tumor Cells into Immunogenic Targets. *Front. Immunol.* 5, 692. doi:10.3389/fimmu.2014.00692
- Rosell, A., Havervall, S., von Meijenfildt, F., Hisada, Y., Aguilera, K., Grover, S. P., et al. (2021). Patients with COVID-19 Have Elevated Levels of Circulating Extracellular Vesicle Tissue Factor Activity that Is Associated with Severity and Mortality-Brief Report. *Arterioscler. Thromb. Vasc. Biol.* 41, 878–882. doi:10.1161/ATVBAHA.120.315547
- Scheller, N., Herold, S., Kellner, R., Bertrams, W., Jung, A. L., Janga, H., et al. (2019). Proviral MicroRNAs Detected in Extracellular Vesicles from Bronchoalveolar Lavage Fluid of Patients with Influenza Virus-Induced Acute Respiratory Distress Syndrome. *J. Infect. Dis.* 219, 540–543. doi:10.1093/infdis/jiy554
- Schneider, D. J., Speth, J. M., Penke, L. R., Wettlaufer, S. H., Swanson, J. A., and Peters-Golden, M. (2017). Mechanisms and Modulation of Microvesicle Uptake in a Model of Alveolar Cell Communication. *J. Biol. Chem.* 292, 20897–20910. doi:10.1074/jbc.M117.792416
- Semple, J. W., Italiano, J. E., Jr, and Freedman, J. (2011). Platelets and the Immune Continuum. *Nat. Rev. Immunol.* 11, 264–274. doi:10.1038/nri2956

- Sengupta, V., Sengupta, S., Lazo, A., Woods, P., Nolan, A., and Bremer, N. (2020). Exosomes Derived from Bone Marrow Mesenchymal Stem Cells as Treatment for Severe COVID-19. *Stem Cells Dev.* 29, 747–754. doi:10.1089/scd.2020.0080
- Shah, T. G., Predescu, D., and Predescu, S. (2019). Mesenchymal Stem Cells-derived Extracellular Vesicles in Acute Respiratory Distress Syndrome: A Review of Current Literature and Potential Future Treatment Options. *Clin. Transl. Med.* 8, 25. doi:10.1186/s40169-019-0242-9
- Sheng, G., Chen, P., Wei, Y., Yue, H., Chu, J., Zhao, J., et al. (2020). Viral Infection Increases the Risk of Idiopathic Pulmonary Fibrosis. *Chest* 157, 1175–1187. doi:10.1016/j.chest.2019.10.032
- Silini, A. R., Magatti, M., Cargnoni, A., and Parolini, O. (2017). Is Immune Modulation the Mechanism Underlying the Beneficial Effects of Amniotic Cells and Their Derivatives in Regenerative Medicine? *Cell Transplant.* 26, 531–539. doi:10.3727/096368916X693699
- Simonson, O. E., Stähle, E., Hansen, T., Wedin, J. O., Larsson, A., Mattsson, M., et al. (2020). Five-Year Follow-Up After Mesenchymal Stromal Cell-Based Treatment of Severe Acute Respiratory Distress Syndrome. *Am. J. Respir. Crit. Care Med.* 202, 1051–1055. doi:10.1164/rccm.202003-0544LE
- Soni, S., Wilson, M. R., O'Dea, K. P., Yoshida, M., Katbeh, U., Woods, S. J., et al. (2016). Alveolar Macrophage-Derived Microvesicles Mediate Acute Lung Injury. *Thorax* 71, 1020–1029. doi:10.1136/thoraxjnl-2015-208032
- Soy, M., Keser, G., Atagündüz, P., Tabak, F., Atagündüz, I., and Kayhan, S. (2020). Cytokine Storm in COVID-19: Pathogenesis and Overview of Anti-inflammatory Agents Used in Treatment. *Clin. Rheumatol.* 39, 2085–2094. doi:10.1007/s10067-020-05190-5
- Sreeramkumar, V., Adrover, J. M., Ballesteros, I., Cuartero, M. I., Rossaint, J., Bilbao, I., et al. (2014). Neutrophils Scan for Activated Platelets to Initiate Inflammation. *Science* 346, 1234–1238. doi:10.1126/science.1256478
- Statello, L., Maugeri, M., Garre, E., Nawaz, M., Wahlgren, J., Papadimitriou, A., et al. (2018). Identification of RNA-Binding Proteins in Exosomes Capable of Interacting with Different Types of RNA: RBP-Facilitated Transport of RNAs into Exosomes. *PLoS One* 13, e0195969. doi:10.1371/journal.pone.0195969
- Stebbing, J., Phelan, A., Griffin, I., Tucker, C., Oechsle, O., Smith, D., et al. (2020). COVID-19: Combining Antiviral and Anti-inflammatory Treatments. *Lancet Infect. Dis.* 20, 400–402. doi:10.1016/S1473-3099(20)30132-8
- Sun, P., Qie, S., Liu, Z., Ren, J., Li, K., and Xi, J. (2020). Clinical Characteristics of Hospitalized Patients with SARS-CoV-2 Infection: A Single Arm Meta-analysis. *J. Med. Virol.* 92, 612–617. doi:10.1002/jmv.25735
- Tang, N., Li, D., Wang, X., and Sun, Z. (2020). Abnormal Coagulation Parameters Are Associated with Poor Prognosis in Patients with Novel Coronavirus Pneumonia. *J. Thromb. Haemost.* 18, 844–847. doi:10.1111/jth.14768
- Tao, S.-C., Guo, S.-C., and Zhang, C.-Q. (2017). Platelet-derived Extracellular Vesicles: An Emerging Therapeutic Approach. *Int. J. Biol. Sci.* 13, 828–834. doi:10.7150/ijbs.19776
- Thille, A. W., Esteban, A., Fernández-Segoviano, P., Rodríguez, J.-M., Aramburu, J.-A., Vargas-Errázuriz, P., et al. (2013). Chronology of Histological Lesions in Acute Respiratory Distress Syndrome with Diffuse Alveolar Damage: A Prospective Cohort Study of Clinical Autopsies. *Lancet Respir. Med.* 1, 395–401. doi:10.1016/S2213-2600(13)70053-5
- Thompson, M., Mei, S. H. J., Wolfe, D., Champagne, J., Fergusson, D., Stewart, D. J., et al. (2020). Cell Therapy with Intravascular Administration of Mesenchymal Stromal Cells Continues to Appear Safe: An Updated Systematic Review and Meta-Analysis. *EClinicalMedicine* 19, 100249. doi:10.1016/j.eclinm.2019.100249
- Tkach, M., Kowal, J., and Théry, C. (2018). Why the Need and How to Approach the Functional Diversity of Extracellular Vesicles. *Philos. Trans. R. Soc. Lond. B Biol. Sci.* 373, 20160479. doi:10.1098/rstb.2016.0479
- Toniati, P., Piva, S., Cattalini, M., Garrafa, E., Regola, F., Castelli, F., et al. (2020). Tocilizumab for the Treatment of Severe COVID-19 Pneumonia with Hyperinflammatory Syndrome and Acute Respiratory Failure: A Single center Study of 100 Patients in Brescia, Italy. *Autoimmun. Rev.* 19, 102568. doi:10.1016/j.autrev.2020.102568
- Torreggiani, E., Perut, F., Perut, F., Roncuzzi, L., Zini, N., Baglio, S., et al. (2014). Exosomes: Novel Effectors of Human Platelet Lysate Activity. *Eur. Cell Mater.* 28, 137–151. doi:10.22203/ecm.v028a11
- Tsiapalis, D., and O'Driscoll, L. (2020). Mesenchymal Stem Cell Derived Extracellular Vesicles for Tissue Engineering and Regenerative Medicine Applications. *Cells* 9, 991. doi:10.3390/cells9040991
- Tukmechi, A., Rezaee, J., Nejati, V., and Sheikhzadeh, N. (2013). Effect of Acute and Chronic Toxicity of Paraquat on Immune System and Growth Performance in Rainbow trout, *Oncorhynchus mykiss*. *Aquac. Res.* 45, 1737–1743. doi:10.1111/are.12118
- Vader, P., Mol, E. A., Pasterkamp, G., and Schiffelers, R. M. (2016). Extracellular Vesicles for Drug Delivery. *Adv. Drug Deliv. Rev.* 106, 148–156. doi:10.1016/j.addr.2016.02.006
- van der Meel, R., Fens, M. H. A. M., Vader, P., van Solinge, W. W., Eniola-Adefeso, O., and Schiffelers, R. M. (2014). Extracellular Vesicles as Drug Delivery Systems: Lessons from the Liposome Field. *J. Control. Release* 195, 72–85. doi:10.1016/j.jconrel.2014.07.049
- van Dongen, H. M., Masoumi, N., Witwer, K. W., and Pegtel, D. M. (2016). Extracellular Vesicles Exploit Viral Entry Routes for Cargo Delivery. *Microbiol. Mol. Biol. Rev.* 80, 369–386. doi:10.1128/MMBR.00063-15
- Varga, Z., Flammer, A. J., Steiger, P., Haberecker, M., Andermatt, R., Zinkernagel, A. S., et al. (2020). Endothelial Cell Infection and Endotheliitis in COVID-19. *Lancet* 395, 1417–1418. doi:10.1016/S0140-6736(20)30937-5
- Volarevic, V., Markovic, B. S., Gazdic, M., Volarevic, A., Jovicic, N., Arsenijevic, N., et al. (2018). Ethical and Safety Issues of Stem Cell-Based Therapy. *Int. J. Med. Sci.* 15, 36–45. doi:10.7150/ijms.21666
- Wada, N., Gronthos, S., and Bartold, P. M. (2013). Immunomodulatory Effects of Stem Cells. *Periodontol.* 2000 63, 198–216. doi:10.1111/prd.120242013
- Wan, Y., Shang, J., Graham, R., Baric, R. S., and Li, F. (2020). Receptor Recognition by the Novel Coronavirus from Wuhan: An Analysis Based on Decade-Long Structural Studies of SARS Coronavirus. *J. Virol.* 94, e00127–20. doi:10.1128/JVI.00127-20
- Wang, B., Yao, K., Huuskens, B. M., Shen, H.-H., Zhuang, J., Godson, C., et al. (2016). Mesenchymal Stem Cells Deliver Exogenous MicroRNA-Let7c via Exosomes to Attenuate Renal Fibrosis. *Mol. Ther.* 24, 1290–1301. doi:10.1038/mt.2016.90
- Wang, J., Chen, S., and Bihl, J. (2020). Exosome-Mediated Transfer of ACE2 (Angiotensin-Converting Enzyme 2) from Endothelial Progenitor Cells Promotes Survival and Function of Endothelial Cell. *Oxid. Med. Cell Longev.* 2020, 1–11. doi:10.1155/2020/4213541
- Wecht, S., and Rojas, M. (2016). Mesenchymal Stem Cells in the Treatment of Chronic Lung Disease. *Respirology* 21, 1366–1375. doi:10.1111/resp.12911
- Wichmann, D., Sperhake, J.-P., Lütgehetmann, M., Steurer, S., Edler, C., Heinemann, A., et al. (2020). Autopsy Findings and Venous Thromboembolism in Patients with COVID-19. *Ann. Intern. Med.* 173, 268–277. doi:10.7326/M20-2003
- Wiklander, O. P. B., Brennan, M. Á., Lötvall, J., Breakefield, X. O., and El Andaloussi, S. (2019). Advances in Therapeutic Applications of Extracellular Vesicles. *Sci. Transl. Med.* 11, eaav8521. doi:10.1126/scitranslmed.aav8521
- Willis, G. R., Fernandez-Gonzalez, A., Anastas, J., Vitali, S. H., Liu, X., Ericsson, M., et al. (2018). Mesenchymal Stromal Cell Exosomes Ameliorate Experimental Bronchopulmonary Dysplasia and Restore Lung Function through Macrophage Immunomodulation. *Am. J. Respir. Crit. Care Med.* 197, 104–116. doi:10.1164/rccm.201705-0925OC
- Xu, P., Zhou, Q., and Xu, J. (2020a). Mechanism of Thrombocytopenia in COVID-19 Patients. *Ann. Hematol.* 99, 1205–1208. doi:10.1007/s00277-020-04019-0
- Xu, X., Chen, P., Wang, J., Feng, J., Zhou, H., Li, X., et al. (2020b). Evolution of the Novel Coronavirus from the Ongoing Wuhan Outbreak and Modeling of its Spike Protein for Risk of Human Transmission. *Sci. China Life Sci.* 63, 457–460. doi:10.1007/s11427-020-1637-5
- Xu, X., Han, M., Li, T., Sun, W., Wang, D., Fu, B., et al. (2020c). Effective Treatment of Severe COVID-19 Patients with Tocilizumab. *Proc. Natl. Acad. Sci. USA* 117, 10970–10975. doi:10.1073/pnas.2005615117
- Xu, Z., Shi, L., Wang, Y., Zhang, J., Huang, L., Zhang, C., et al. (2020d). Pathological Findings of COVID-19 Associated with Acute Respiratory Distress Syndrome. *Lancet Respir. Med.* 8, 420–422. doi:10.1016/S2213-2600(20)30076-X
- Yan, R., Zhang, Y., Li, Y., Xia, L., Guo, Y., and Zhou, Q. (2020). Structural Basis for the Recognition of SARS-CoV-2 by Full-Length Human ACE2. *Science* 367, 1444–1448. doi:10.1126/science.abb2762
- Yang, L., Liu, S., Liu, J., Zhang, Z., Wan, X., Huang, B., et al. (2020a). COVID-19: Immunopathogenesis and Immunotherapeutics. *Signal Transduct. Target. Ther.* 5, 128. doi:10.1038/s41392-020-00243-2
- Yang, X., Yang, Q., Wang, Y., Wu, Y., Xu, J., Yu, Y., et al. (2020b). Thrombocytopenia and its Association with Mortality in Patients with COVID-19. *J. Thromb. Haemost.* 18, 1469–1472. doi:10.1111/jth.14848

- Yi, Y., Lagniton, P. N. P., Ye, S., Li, E., and Xu, R.-H. (2020). COVID-19: What Has Been Learned and to Be Learned about the Novel Coronavirus Disease. *Int. J. Biol. Sci.* 16, 1753–1766. doi:10.7150/ijbs.45134
- Yoshikawa, F. S. Y., Teixeira, F. M. E., Sato, M. N., and Oliveira, L. M. d. S. (2019). Delivery of MicroRNAs by Extracellular Vesicles in Viral Infections: Could the News Be Packaged? *Cells* 8, 611. doi:10.3390/cells8060611
- Zaid, Y., Puhm, F., Allaeys, I., Naya, A., Oudghiri, M., Khalki, L., et al. (2020). Platelets Can Associate with SARS-Cov-2 RNA and Are Hyperactivated in COVID-19. *Circ. Res.* 127, 1404–1418. doi:10.1161/CIRCRESAHA.120.317703
- Zemans, R. L., and Matthay, M. A. (2017). What Drives Neutrophils to the Alveoli in ARDS? *Thorax* 72, 1–3. doi:10.1136/thoraxjnl-2016-209170
- Zhang, H., Penninger, J. M., Li, Y., Zhong, N., and Slutsky, A. S. (2020a). Angiotensin-converting Enzyme 2 (ACE2) as a SARS-CoV-2 Receptor: Molecular Mechanisms and Potential Therapeutic Target. *Intensive Care Med.* 46, 586–590. doi:10.1007/s00134-020-05985-9
- Zhang, P., Li, J., Liu, H., Han, N., Ju, J., Kou, Y., et al. (2020b). Long-term Bone and Lung Consequences Associated with Hospital-Acquired Severe Acute Respiratory Syndrome: A 15-year Follow-Up from a Prospective Cohort Study. *Bone Res.* 8, 8. doi:10.1038/s41413-020-0084-5
- Zhao, Y., Zhao, Z., Wang, Y., Zhou, Y., Ma, Y., and Zuo, W. (2020). Single-Cell RNA Expression Profiling of ACE2, the Receptor of SARS-CoV-2. *Am. J. Respir. Crit. Care Med.* 202, 756–759. doi:10.1164/rccm.202001-0179LE
- Zhou, P., Yang, X.-L., Wang, X.-G., Hu, B., Zhang, L., Zhang, W., et al. (2020a). A Pneumonia Outbreak Associated with a New Coronavirus of Probable Bat Origin. *Nature* 579, 270–273. doi:10.1038/s41586-020-2012-7
- Zhou, W., Wang, H., Yang, Y., Chen, Z.-S., Zou, C., and Zhang, J. (2020b). Chloroquine Against Malaria, Cancers and Viral Diseases. *Drug Discov. Today* 25, 2012–2022. doi:10.1016/j.drudis.2020.09.010
- Zhou, X., Xie, F., Wang, L., Zhang, L., Zhang, S., Fang, M., et al. (2020c). The Function and Clinical Application of Extracellular Vesicles in Innate Immune Regulation. *Cell Mol Immunol* 17, 323–334. doi:10.1038/s41423-020-0391-1
- Zhu, F.-C., Guan, X.-H., Li, Y.-H., Huang, J.-Y., Jiang, T., Hou, L.-H., et al. (2020). Immunogenicity and Safety of a Recombinant Adenovirus Type-5-Vectored COVID-19 Vaccine in Healthy Adults Aged 18 Years or Older: A Randomised, Double-Blind, Placebo-Controlled, Phase 2 Trial. *Lancet* 396, 479–488. doi:10.1016/S0140-6736(20)31605-6
- Zuo, Y., Yalavarthi, S., Shi, H., Gockman, K., Zuo, M., Madison, J. A., et al. (2020). Neutrophil Extracellular Traps in COVID-19. *JCI Insight* 5, e138999. doi:10.1172/jci.insight.138999

**Conflict of Interest:** The authors declare that the research was conducted in the absence of any commercial or financial relationships that could be construed as a potential conflict of interest.

Copyright © 2021 Yan, Zhou, Wang, Guo, Zhao, Zhu, Xing, Zhang, Aljofan, Jarrahi, Makabel and Zhang. This is an open-access article distributed under the terms of the Creative Commons Attribution License (CC BY). The use, distribution or reproduction in other forums is permitted, provided the original author(s) and the copyright owner(s) are credited and that the original publication in this journal is cited, in accordance with accepted academic practice. No use, distribution or reproduction is permitted which does not comply with these terms.





# Development and Validation of the Prognostic Index Based on Inflammation-Related Gene Analysis in Idiopathic Pulmonary Fibrosis

Yanjiao Lu<sup>1</sup>, Jinkun Chen<sup>2</sup>, Kun Tang<sup>1</sup>, Shanshan Wang<sup>1</sup>, Zhen Tian<sup>1</sup>, Meijia Wang<sup>1</sup>, Jianping Zhao<sup>1\*</sup> and Jungang Xie<sup>1\*</sup>

<sup>1</sup>Department of Respiratory and Critical Care Medicine, National Clinical Research Center of Respiratory Disease, Tongji Hospital, Tongji Medical College, Huazhong University of Science and Technology, Wuhan, China, <sup>2</sup>Department of science, Western University, London, ON, Canada

## OPEN ACCESS

### Edited by:

Wen Li,  
Zhejiang University, China

### Reviewed by:

Qian Han,  
Guangzhou Medical University, China  
Zhenshun Cheng,  
Wuhan University, China

### \*Correspondence:

Jianping Zhao  
Zhaop88@126.com  
Jungang Xie  
xiejjg@hotmail.com

### Specialty section:

This article was submitted to  
Molecular Diagnostics and  
Therapeutics,  
a section of the journal  
Frontiers in Molecular Biosciences

**Received:** 13 February 2021

**Accepted:** 22 June 2021

**Published:** 22 July 2021

### Citation:

Lu Y, Chen J, Tang K, Wang S, Tian Z,  
Wang M, Zhao J and Xie J (2021)  
Development and Validation of the  
Prognostic Index Based on  
Inflammation-Related Gene Analysis in  
Idiopathic Pulmonary Fibrosis.  
*Front. Mol. Biosci.* 8:667459.  
doi: 10.3389/fmolb.2021.667459

**Background:** Historically, idiopathic pulmonary fibrosis (IPF) was considered a chronic inflammation disorder, but this conception was reassessed in the past decades. Our understanding of the role of inflammation in IPF and its association with clinical significance remained incomplete.

**Methods:** We downloaded mRNA expression data of peripheral blood mononuclear cells (PBMCs) from the Gene Expression Omnibus (GEO) repository. Inflammation-related genes (IRGs) expressed differently between IPF and control (CTRL) were determined. In this study, we systemically analyzed the expression of differently expressed IRGs by comprehensive bioinformatic analysis, and then investigated their potential prognostic values. The related prognostic gene expressions were verified in our cohort.

**Results:** 110 differently expressed IRGs were identified in this study, including 64 upregulated and 46 downregulated IRGs. Three IRGs (*S100A12*, *CCR7*, and *TNFSF4*) were identified as potential hub genes for prognosis. Those genes were subsequently subjected to the construction of the prognostic models. In the results, IPF patients categorized as high risk demonstrated a poor overall survival rate compared to patients categorized as low risk. Based on this prognostic model, the area under the curve (AUC) of the survival-dependent receiver operator characteristic (ROC) for 1-year, 2-year, and 3-year survival rates was 0.611, 0.695, and 0.681, respectively, in the GSE28042 cohort. These observations were validated in the GSE27957 cohort, confirming the good prognostic effect of this model. The expression of the three genes was validated in our cohort. We also conducted a nomogram based on the three IRGs' mRNA for quantitative IPF prognosis.

**Abbreviations:** CCR7: C-C motif chemokine receptor 7, CTRL: control, FC: fold change, FDA: food and drug Administration, FDR: false discovery rate, GEO: gene expression omnibus, ILD: interstitial lung disease, IPF: idiopathic pulmonary fibrosis, IRGs: inflammation-related genes, PBMCs: peripheral blood mononuclear cells, PPT: protein-protein interaction, RA: rheumatoid arthritis, ROC: receiver operator characteristic, S100A12: S100 calcium binding protein A12, STRING: search tool for the retrieval of interacting genes, TOLLIP: toll-interacting protein, TNFSF4: TNF superfamily member 4.

**Conclusion:** Three IRGs (*S100A12*, *CCR7*, and *TNFSF4*) were identified as potential markers for the prognosis of IPF.

**Keywords:** idiopathic pulmonary fibrosis, inflammation, prognostic, interstitial lung disease, gene

## INTRODUCTION

Idiopathic pulmonary fibrosis (IPF), caused by an unknown reason and characterized by poor clinical prognosis, is a progressive, chronic, and irreversible interstitial lung disease (ILD) (Raghu et al., 2011a; Raghu et al., 2015). IPF occurs in elderly and middle-aged adults, and the median survival time from diagnosis is 2–4 years (Ley et al., 2011). Due to the recent advantages in the development of new therapies, the prognosis of IPF has been improved. However, it remains incurable partly due to the complexity and incomprehension of the etiology (Nathan et al., 2016; Richeldi et al., 2016). Therefore, better understandings of the molecular mechanisms of IPF are vital for the improvement of the prognosis of patients with IPF, early screening, and diagnosis.

Historically, IPF is assumed to be caused by chronic inflammation. However, the significance of inflammation in the onset and development of IPF has been strongly challenged. Evidenced by poor response to anti-inflammatory therapy, inflammation has demonstrated to be a nonessential pathogenic event in IPF (Selman et al., 2001; Richeldi, 2013). However, inflammation presents at different stages of IPF as a secondary event due to the activation of the innate and adaptive immune system and participates in IPF development (Mura et al., 2005; Heukels et al., 2019). Gene variants in *TOLLIP* (Toll-interacting protein), directly involved in inflammatory processes, resulted in reduced protein expression, which possibly contributes to an increased pro-inflammatory response observed in IPF patients (Noth et al., 2013). So far, the pathogenic role of inflammation in IPF remains controversial.

Regarding the changes in the understanding of inflammation, some researchers suggest that glucocorticoid treatment, a classic anti-inflammation therapy, is potentially effective in selected IPF patients (Heukels et al., 2019; Khor et al., 2019). Recent advances in precision treatment and increasing awareness of patient subgroup classification indicate a fundamental role of inflammation in IPF (Zhang et al., 2015). Macrophage-targeted lung delivery of dexamethasone improves pulmonary fibrosis therapy *via* regulating the immune microenvironment (Sang et al., 2021). More understanding of inflammation in IPF provides more evidence for the anti-inflammation treatment of IPF patients. Therefore, a systematic functional study of inflammation-related genes (IRGs) in IPF is of critical importance in understanding the roles of inflammation in IPF.

The blood components, including peripheral blood mononuclear cells (PBMCs) and white blood cells, are indicative factors of disease onset, progress, and prognosis of IPF (Richards et al., 2012; Scott et al., 2019). Maya et al. identified a 52-gene signature in PBMCs to stratify IPF patients to different risk levels and validated this signature in a prospective cohort (Herazo-Maya et al., 2013; Herazo-Maya et al., 2017). Studies

using large-scale IRG expression profiles of patients are critically important for stratifying IPF patients and predicting the prognosis of IPF with different inflammation degrees.

The subject of this study was to investigate the roles of inflammation played in IPF and explore the potential clinical utility of IRGs for prognostic stratifications. Therefore, we downloaded the mRNA expression data of PBMCs and the clinicopathological data from the Gene Expression Omnibus (GEO) repository. We identified abnormally expressed IRGs between IPF and control (CTRL) using bioinformatic analysis, and systematically investigated their potential molecular mechanisms and functions. Finally, we analyzed the potential impact of IRGs on prognosis by combining the IRG expression data with clinical information.

## METHODS

### Data Acquisition and Processing

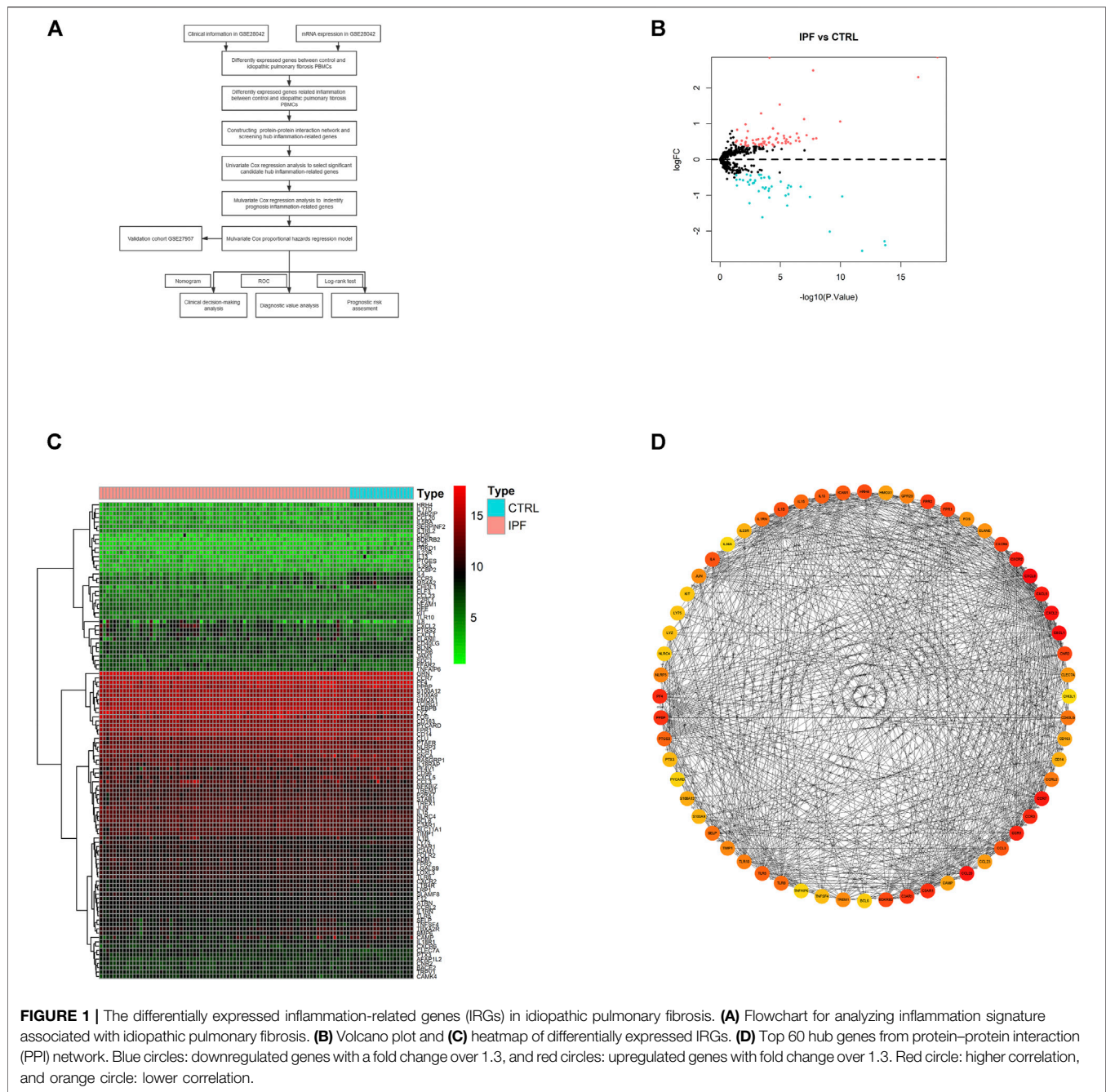
A total of 569 inflammation-related genes were extracted from the Gene Ontology and GO Annotations (<https://www.ebi.ac.uk/QuickGO/>), which provides detailed annotations of genes. We downloaded the microarray expression matrix dataset of 75 IPF and 19 CTRL PBMCs with corresponding clinical data from GSE28042 (<https://www.ncbi.nlm.nih.gov/geo/query/acc.cgi?acc=GSE28042>). To identify differently expressed inflammation-related genes between IPF and CTRL PBMCs, and the limma R package (<http://www.bioconductor.org/packages>) was used to perform the negative binomial distribution method according to the absolute value of fold change (FC) (>1.3) and false discovery rate (FDR) <0.05.

### Protein–Protein Interaction Network and Hub Inflammation-Related Gene Screening

The differently expressed IRGs were submitted to the Search Tool for the Retrieval of Interacting Genes (STRING) (<http://string-db.org>) (version 10.5) for the prediction of the PPI network. Meanwhile, Cytoscape (version 3.8.0) was applied to visualize the PPI networks. The hub genes were identified in the PPI network according to the prediction of cytoHubba plug-in with Nodes' Scores. *p* values less than 0.05 were considered statistically significant.

### Inflammation-Related Prognostic Model Construction

Univariate Cox regression analysis and log-rank tests were applied to analyze the significant risk factors in all hub IRGs using the survival R package. Afterward, we set up a multivariate Cox regression model for the calculation of the risk scores to



estimate the prognosis outcomes of IPF patients. Based on the above significant candidate hub genes, the risk scoring formula for each sample was as follows:

$$\text{Risk Score} = \beta_1 * \text{Exp1} + \beta_2 * \text{Exp2} + \beta_3 * \text{Exp3},$$

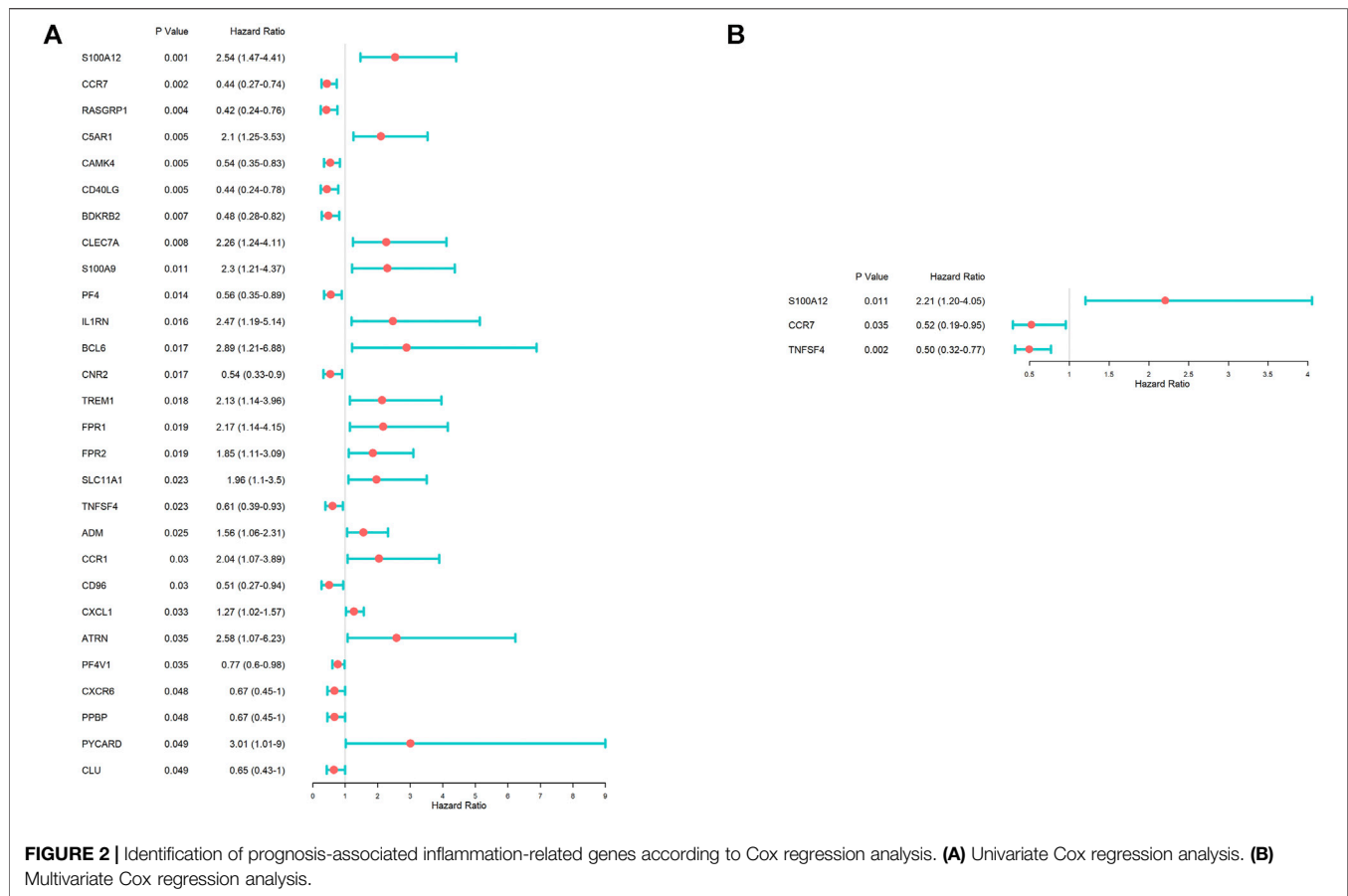
where  $\beta$  represented the coefficient value, while Exp represented the gene expression level.

Based on the median estimated risk score, IPF patients were categorized as high-risk and low-risk subgroups. The log-rank test was carried out for the comparison of the prognostic outcomes

between the two subgroups. Further, the receiver operating characteristic (ROC) analysis was applied to assess the prognostic capabilities of the above model by the SurvivalROC R package.

### Validation of the Prognostic Model

45 samples of IPF patients with the corresponding prognosis from the GSE27957 dataset were used to validate the estimating results to evaluate the accuracy of the model prediction. We also performed expression validation of the three prognostic genes in our cohort by real-time PCR. We collected PBMC samples and



clinical information of IPF patients in Tongji Hospital in Wuhan, China, from July 2020 to November 2020. Adult patients with clinical IPF diagnosis according to the American Thoracic Society/European Respiratory Society guideline (2011) were eligible for this study (Raghu et al., 2011b). This study was approved by the Ethics Committee of Tongji Hospital (IRB ID: 20150503). Results were presented as median with interquartile range (IQR), and nonparametric tests (Kruskal–Wallis or Mann–Whitney test) were used to compare across groups. Finally, a nomogram was conducted using the rms R package to predict the likelihood of a prognostic outcome in IPF patients. *p* values lower than 0.05 were set as statistical significance.

## RESULTS

### Differentially Expressed Inflammation-Related Genes Identification

A systematic analysis was carried out for the critical roles and the potential prognostic values of IRGs played in IPF. As shown in Figure 1A, the study was carried out according to the design. The databases of IPF patients were obtained from GEO-contained 75 IPF and 19 CTRL PBMCs samples. The R packages were used to process the data and discover differently expressed IRGs. According to the screening criteria, 110 IRGs were identified

as differentially expressed between IPF and CTRL, containing 64 upregulated IRGs and 46 downregulated IRGs. The results were illustrated in the heatmap and volcano plot as in Figures 1B,C; details of the results were listed as in Supplementary Table S1.

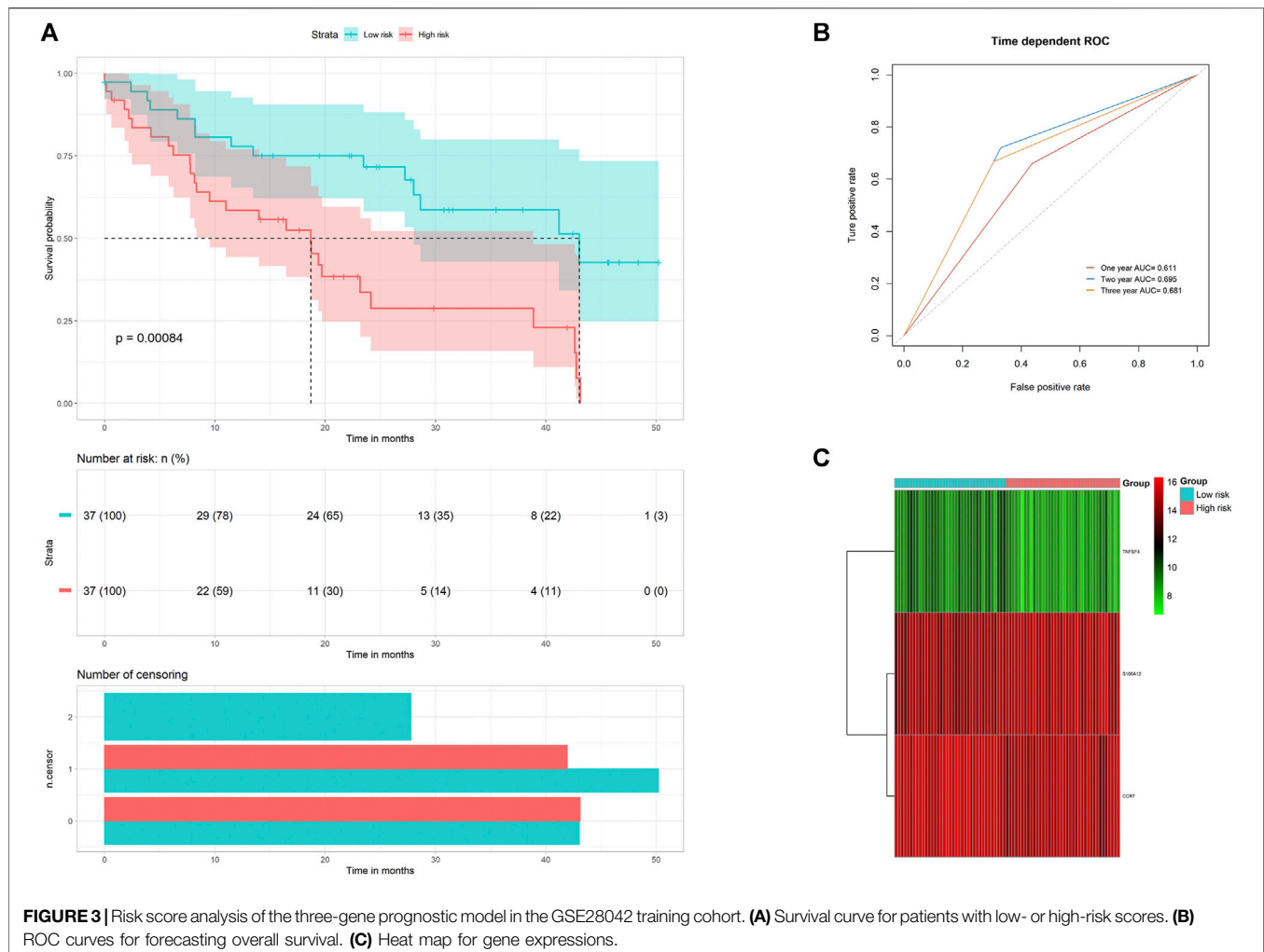
### Protein–Protein Interaction Network Construction and Hub Gene Analysis

Gene network complexes were generated by STRING according to the results of differently expressed IRGs. The PPI network contained 110 nodes and 470 edges (Supplementary Figure S1). The interaction network was operated using cytoHubba tools in Cytoscape to identify top 60 hub IRGs (Figure 1D).

### Prognosis-Related Inflammation-Related Gene Selecting

To identify IRGs of significant correlation with the overall survival, a univariate Cox regression analysis was established based on hub IRGs. As shown in the forest map of the hazard ratio (Figure 2A), 28 IRGs were significantly associated with the prognosis of IPF patients. To estimate the impact of prognostic-associated hub IRGs on the clinical outcomes and survival time, the 28 hub IRGs were further analyzed by multiple stepwise Cox regression. As shown in Figure 2B, S100 calcium binding protein A12 (*S100A12*), C-C motif chemokine receptor 7 (*CCR7*), and





TNF superfamily member 4 (*TNFSF4*) were identified as independent predictors for IPF patients.

## Model Construction and Analysis for Prognosis-Related Genetic Risk Score

The three hub IRGs identified from the above analysis were used for the construction of the inflammation predictive model. The risk score of each IPF patient was calculated as

$$\text{Risk Score} = (0.792 * \text{ExpS100A12}) + (-0.645 * \text{ExpCCR7}) + (-0.704 * \text{ExpTNFSF4}).$$

Then, we performed a survival analysis to evaluate the predictive effect of this model. As the result, 75 IPF patients were categorized as high-risk or low-risk according to the median of risk scores. As revealed by the result, IPF patients with high-risk scores were associated with poor prognosis compared with those with low-risk scores (**Figure 3A**). A survival-dependent ROC analysis was carried out for the assessment of the prognostic abilities (**Figure 3B**). The area under the ROC curve for 1 year, 2 years, and 3 years survival rates were 0.611, 0.695, and 0.681

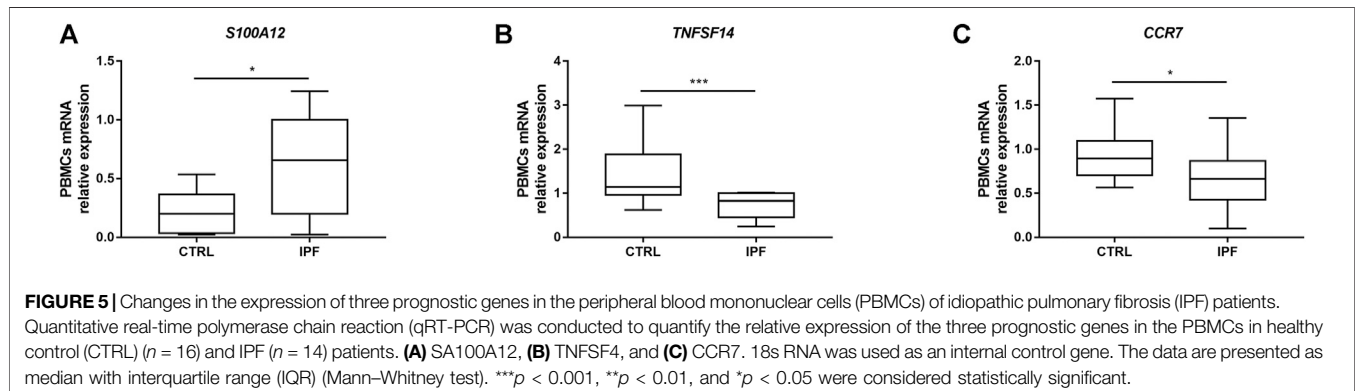
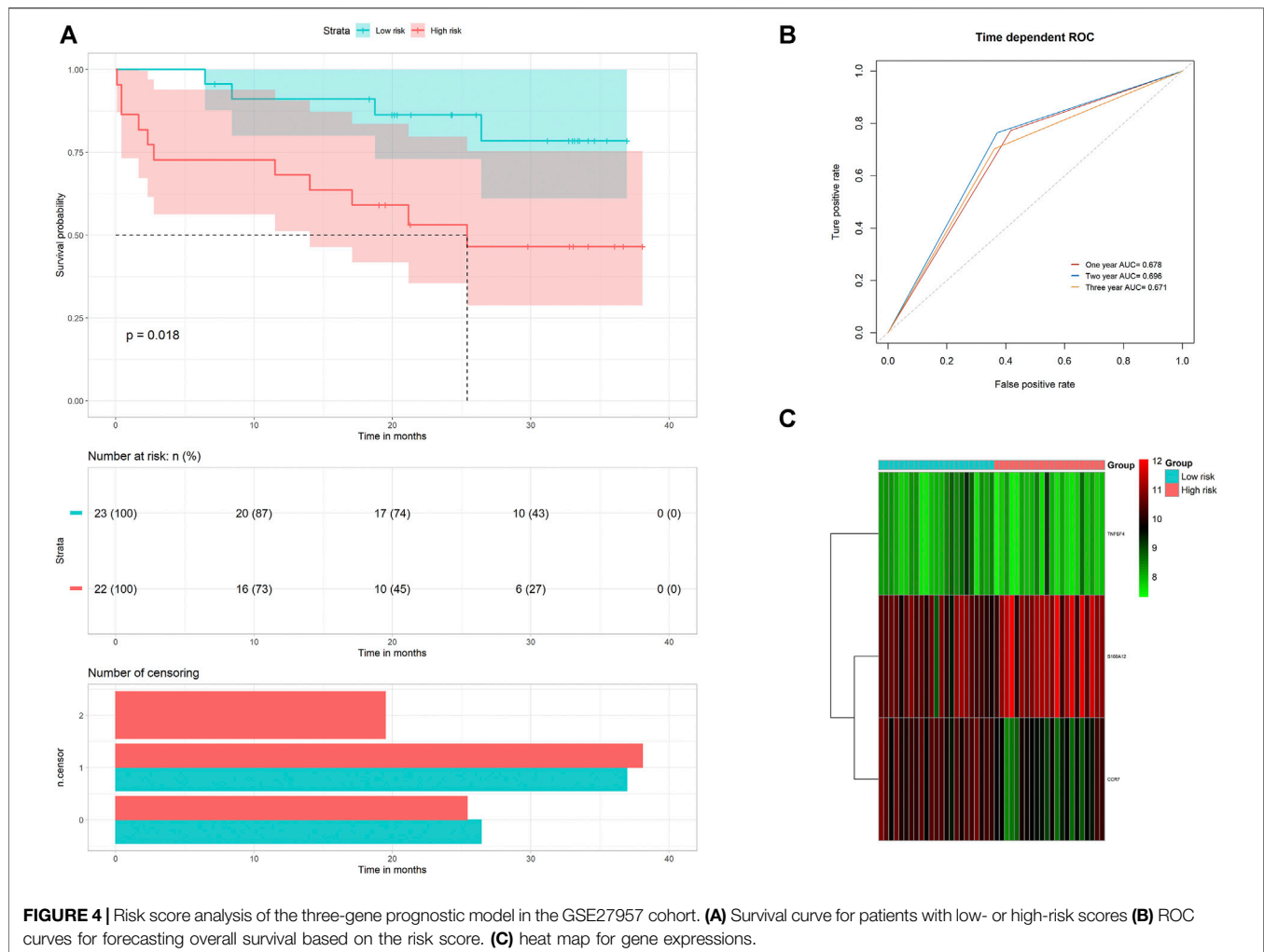
respectively, indicating a moderate prognostic potential of IRGs in the survival prediction of the patients. The expressions heatmap of IRGs between subgroups are shown in **Figure 3C**.

## Validation of the Prognostic Model

On the one hand, to evaluate the prognostic accuracies of the three IRGs' predictive model in IPF cohorts, this formula was applied to GSE27957 datasets. We discovered that high-risk patients had poorer overall survival than low-risk patients in GSE27957 cohorts (**Figure 4**). These results revealed that this prognostic model based on IRGs had better sensitivity and specificity. On the other hand, we performed verification of the three core genes expression in our cohort. As predicted, *S100A12* was significantly increased in IPF patients, while *CCR7* and *TNFSF4* were decreased (**Figure 5**).

## Construction of a Nomogram Based on Three Hub Inflammation-Related Genes

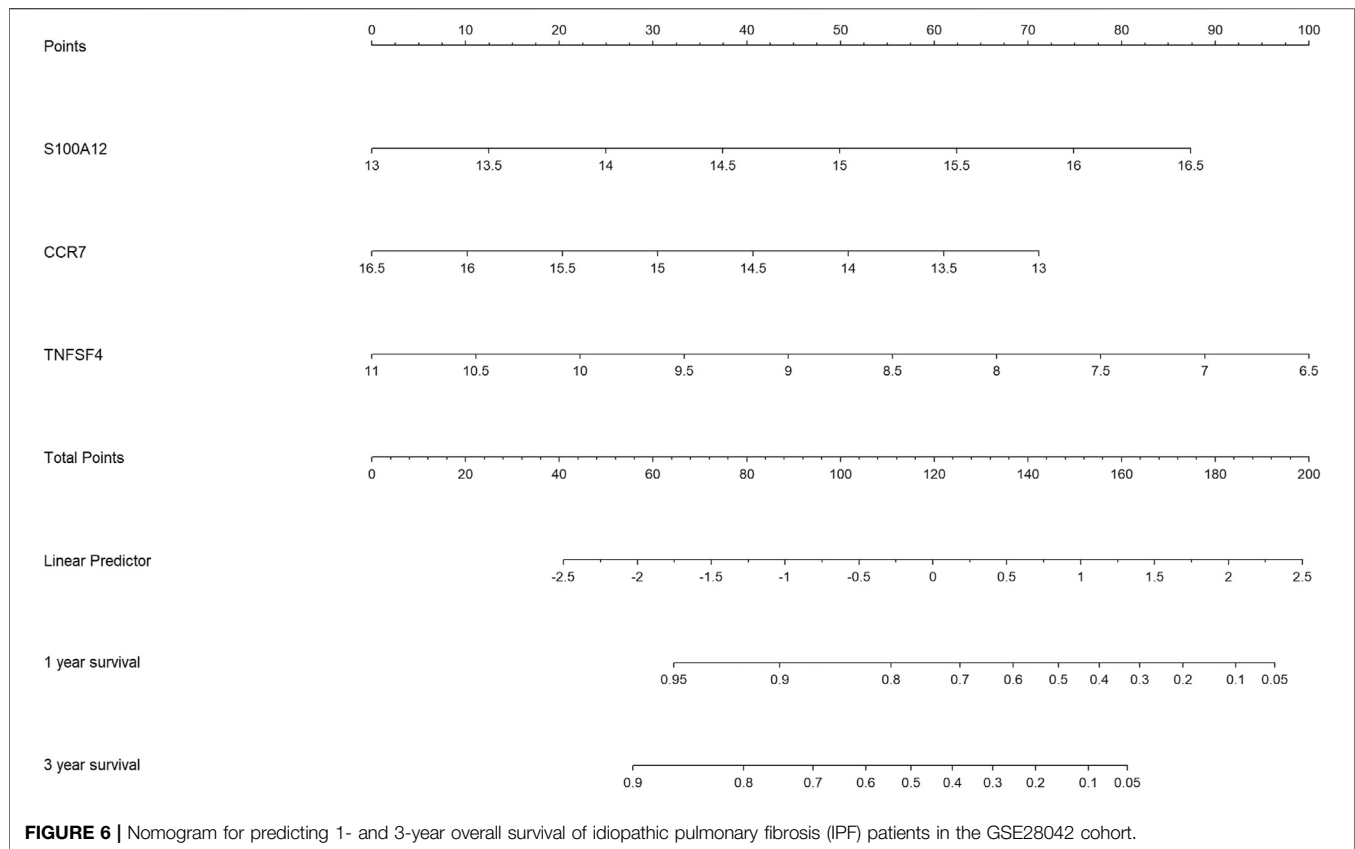
For the establishment of quantitative methods for IPF prognosis, a nomogram was established according to the three hub IRGs (**Figure 6**). Points were distributed to each



variable by the point scale in this nomogram based on the multivariable stepwise Cox regression analysis. We calculated the total points of each IPF patient by summing points of three variables. Next, we could infer the survival rate for IPF patients at 1 and 3 years by matching the total points with below survival rate in our nomogram.

## DISCUSSION

As the contributions of inflammation in the development of IPF were complicated and controversial, a comprehensive analysis of IRGs has not been conducted to explore its clinical significance. From the perspective of inflammation, we identified and



validated three prognostic IRGs. The results indicated that a prognostic model based on three IRGs can be applied for prognostic stratification in IPF patients, helping to provide individualized treatment based on patient risk.

In this study, we identified 110 differently expressed IRGs between IPF and CTRL PBMCs based on GSE28042 from GEO dataset, and constructed a PPI network and co-expression network of these IRGs. As a result, up to 60 hub IRGs were obtained. Many of the hub IRGs had been demonstrated to associate with the development and progression of IPF (Keane et al., 1997; Kowal-Bielecka et al., 2005; Okuda et al., 2015; Yang et al., 2018; Cui et al., 2020). Three IRGs were identified to associate with the prognosis of IPF, including *S100A12*, *CCR7*, and *TNFSF4*.

The increased expression level of *S100A12*, related to neutrophil recruitment and activation, was associated with significantly worse outcomes in IPF. A previous study has reported that *S100A12* levels in the lung, bronchoalveolar lavage fluid (BALF), and serum were increased in acute respiratory distress syndrome (ARDS) patients compared to healthy controls (Lorenz et al., 2008; Kikkawa et al., 2010). Thomas et al. have demonstrated that a high *S100A12* protein level in serum was associated with poor prognosis in the overall survival, transplant-free survival, and progression-free survival in IPF patients (Richards et al., 2012), which was consistent with our findings. *S100A12* could promote inflammation and cell apoptosis in sepsis-induced ARDS while inhibiting fibroblast

migration *via* the receptor for advanced glycation end products (Tanaka et al., 2019; Zhang et al., 2020). The role of *S100A12* in pulmonary fibrosis is still worth investigating.

The decreased level of *CCR7* was related to IPF poor prognosis in this study. But Choi et al. (2006) reported that *CCR7* expression was significantly raised in usual interstitial pneumonia (UIP) relative to biopsies from patients diagnosed with nonspecific interstitial pneumonia (NSIP) or respiratory bronchiolitis/interstitial lung disease (RBILD). *CCR7* was expressed by IPF fibroblasts but not normal fibroblasts and could promote migration and proliferation of IPF fibroblasts (Pierce et al., 2007a; Habel and Hogaboam, 2014). Therapeutic targeting *CCR7* abrogates pulmonary fibrosis induced by the adoptive transfer of human pulmonary fibroblasts to immunodeficient mice (Pierce et al., 2007b). The discrepancy between our result and the previous study might result from the important but opposing roles of *CCR7* in disease. The *CCR7* axis could combat the spread of cancer by trafficking of effector cells involved in mounting an immune response to a growing tumor, while contribute to the expansion of cancer *via* controlling the migration of tumor cells towards the lymphatic system and metastasis (Salem et al., 2021).

The lower level of *TNFSF14* of PBMCs was associated with a worse IPF prognosis. The cytokine *TNFSF14* was demonstrated to be an important factor in the development of lung tissue remodeling in the murine model, which is associated with asthma, IPF, and systemic sclerosis (da Silva Antunes et al.,

2018). Rana Herro et al. demonstrated that *TNFSF14* was upregulated in bleomycin-induced pulmonary fibrosis and is a profibrogenic cytokine (Herro et al., 2015). Considering that *TNFSF14* as an inflammatory indicator was increased in different diseases (Hsu et al., 2019; Fan et al., 2020), the serum protein level of *TNFSF14* should be validated in IPF patients.

Subsequently, a risk model was established for the prediction of IPF prognosis according to multiple stepwise Cox regression analysis of hub IRGs, validated using the GSE27957 cohort. In this study, the ROC curve analysis demonstrated that the IRG signature was better fitted for diagnosis rather than predicting poor prognosis in IPF patients. A nomogram was constructed for intuitively predicting the 1- and 3-year overall survival. This prognostic model based on these three IRGs is financially cost-less and efficient for clinical use.

Nonetheless, limitations were found in this prediction system. First, this prognostic model was constructed according to the GEO database; therefore, further validation in the clinical patient cohort was needed. Second, as a retrospective study, further prospective studies were needed for verification of the outcomes. Finally, functional experiments were needed to further reveal the potential mechanisms of IRGs in the future.

Conclusively, this study identified three IPF prognostic IRGs based on comprehensive bioinformatic analyses in GSE datasets. Our results contributed to the understanding of the roles inflammation played in IPF pathogenesis, and therefore potentially promoted the development of markers for prognosis assessment.

## DATA AVAILABILITY STATEMENT

The datasets presented in this study can be found in online repositories. The names of the repository/repositories and accession number(s) can be found in the article/Supplementary Material.

## ETHICS STATEMENT

The studies involving human participants were reviewed and approved by the Ethics Committee of Tongji Hospital. The

patients/participants provided their written informed consent to participate in this study.

## AUTHOR CONTRIBUTIONS

YL: conceptualization, investigation, formal analysis, and writing—original draft. JC: conceptualization, investigation, formal analysis, and writing—original draft. KT: conceptualization, investigation, formal analysis, and writing—original draft. SW: conceptualization, investigation, formal analysis, and writing—original draft. ZT: formal analysis. MW: formal analysis. Chengfeng Xiao: visualization, writing-review, and editing. JZ: conceptualization and supervision. JX: conceptualization and supervision.

## FUNDING

This study was supported by the National Natural Science Foundation of China (Nos. 81973986 and 81570033), the National key basic research and development program (973 Program, No. 2015CB553403), the National Key R&D Program of China (2016YFC1304500 and 2018YFC1311900), and the National Major Science and Technology Project for the Control and Prevention of Major Infectious Diseases of China (2017ZX10103004).

## ACKNOWLEDGMENTS

We thank all the IPF patients and healthy controls involved in our study.

## SUPPLEMENTARY MATERIAL

The Supplementary Material for this article can be found online at: <https://www.frontiersin.org/articles/10.3389/fmolb.2021.667459/full#supplementary-material>

## REFERENCES

- Choi, E. S., Pierce, E. M., Jakubzick, C., Carpenter, K. J., Kunkel, S. L., Evanoff, H., et al. (2006). Focal Interstitial CC Chemokine Receptor 7 (CCR7) Expression in Idiopathic Interstitial Pneumonia. *J. Clin. Pathol.* 59 (1), 28–39. doi:10.1136/jcp.2005.026872
- Cui, L., Chen, S. Y., Lerbs, T., Lee, J. W., Domizi, P., Gordon, S., et al. (2020). Activation of JUN in Fibroblasts Promotes Pro-fibrotic Programme and Modulates Protective Immunity. *Nat. Commun.* 11 (1), 2795. doi:10.1038/s41467-020-16466-4
- da Silva Antunes, R., Mehta, A. K., Madge, L., Tocker, J., and Croft, M. (2018). *TNFSF14* (LIGHT) Exhibits Inflammatory Activities in Lung Fibroblasts Complementary to IL-13 and TGF- $\beta$ . *Front. Immunol.* 9, 576. doi:10.3389/fimmu.2018.00576
- Fan, H., Lu, B., Cao, C., Li, H., Yang, D., Huang, L., et al. (2020). Plasma *TNFSF13B* and *TNFSF14* Function as Inflammatory Indicators of Severe Adenovirus Pneumonia in Pediatric Patients. *Front. Immunol.* 11, 614781. doi:10.3389/fimmu.2020.614781
- Habel, D. M., and Hogaboam, C. (2014). Heterogeneity in Fibroblast Proliferation and Survival in Idiopathic Pulmonary Fibrosis. *Front. Pharmacol.* 5, 2. doi:10.3389/fphar.2014.00002
- Herazo-Maya, J. D., Noth, I., Duncan, S. R., Kim, S., Ma, S. F., Tseng, G. C., et al. (2013). Peripheral Blood Mononuclear Cell Gene Expression Profiles Predict Poor Outcome in Idiopathic Pulmonary Fibrosis. *Sci. translational Med.* 5 (205), 205ra136. doi:10.1126/scitranslmed.3005964
- Herazo-Maya, J. D., Sun, J., Molyneaux, P. L., Li, Q., Villalba, J. A., Tzouveleakis, A., et al. (2017). Validation of a 52-gene Risk Profile for Outcome Prediction in Patients with Idiopathic Pulmonary Fibrosis: an International, Multicentre, Cohort Study. *Lancet Respir. Med.* 5 (11), 857–868. doi:10.1016/s2213-2600(17)30349-1
- Herro, R., Da Silva Antunes, R., Aguilera, A. R., Tamada, K., and Croft, M. (2015). Tumor Necrosis Factor Superfamily 14 (LIGHT) Controls Thymic Stromal



- Lymphopoietin to Drive Pulmonary Fibrosis. *J. Allergy Clin. Immunol.* 136 (3), 757–768. doi:10.1016/j.jaci.2014.12.1936
- Heukels, P., Moor, C. C., von der Thüsen, J. H., Wijsenbeek, M. S., and Kool, M. (2019). Inflammation and Immunity in IPF Pathogenesis and Treatment. *Respir. Med.* 147, 79–91. doi:10.1016/j.rmed.2018.12.015
- Hsu, C.-Y., Tseng, W.-K., Wu, Y.-W., Lin, T.-H., Yeh, H.-I., Chang, K.-C., et al. (2019). Circulating TNFSF14 (Tumor Necrosis Factor Superfamily 14) Predicts Clinical Outcome in Patients with Stable Coronary Artery Disease. *Atvb* 39 (6), 1240–1252. doi:10.1161/atvbaha.118.312166
- Keane, M. P., Arenberg, D. A., Lynch, J. P., 3rd, Whyte, R. I., Iannettoni, M. D., Burdick, M. D., et al. (1997). The CXC Chemokines, IL-8 and IP-10, Regulate Angiogenic Activity in Idiopathic Pulmonary Fibrosis. *J. Immunol. (Baltimore, Md)* 159 (3), 1437–1443.
- Khor, Y. H., Glaspole, I., and Goh, N. S. L. (2019). Therapeutic burden in Interstitial Lung Disease: Lessons to Learn. *Respirology* 24 (6), 566–571. doi:10.1111/resp.13480
- Kikkawa, T., Sato, N., Kojika, M., Takahashi, G., Aoki, K., Hoshikawa, K., et al. (2010). Significance of Measuring S100A12 and sRAGE in the Serum of Sepsis Patients with Postoperative Acute Lung Injury. *Dig. Surg.* 27 (4), 307–312. doi:10.1159/000313687
- Kowal-Bielecka, O., Kowal, K., Lewszuk, A., Bodzenta-Lukaszyk, A., Walecki, J., and Sierakowski, S. (2005). Beta Thromboglobulin and Platelet Factor 4 in Bronchoalveolar Lavage Fluid of Patients with Systemic Sclerosis. *Ann. Rheum. Dis.* 64 (3), 484–486. doi:10.1136/ard.2004.022970
- Ley, B., Collard, H. R., and King, T. E., Jr (2011). Clinical Course and Prediction of Survival in Idiopathic Pulmonary Fibrosis. *Am. J. Respir. Crit. Care Med.* 183 (4), 431–440. doi:10.1164/rccm.201006-0894ci
- Lorenz, E., Muhlebach, M. S., Tessier, P. A., Alexis, N. E., Duncan Hite, R., Seeds, M. C., et al. (2008). Different Expression Ratio of S100A8/A9 and S100A12 in Acute and Chronic Lung Diseases. *Respir. Med.* 102 (4), 567–573. doi:10.1016/j.rmed.2007.11.011
- Mura, M., Belmonte, G., Fanti, S., Contini, P., Pacilli, A. M. G., Fasano, L., et al. (2005). Inflammatory Activity Is Still Present in the Advanced Stages of Idiopathic Pulmonary Fibrosis. *Respirology* 10 (5), 609–614. doi:10.1111/j.1440-1843.2005.00757.x
- Nathan, S. D., Albera, C., Bradford, W. Z., Costabel, U., du Bois, R. M., Fagan, E. A., et al. (2016). Effect of Continued Treatment with Pirfenidone Following Clinically Meaningful Declines in Forced Vital Capacity: Analysis of Data from Three Phase 3 Trials in Patients with Idiopathic Pulmonary Fibrosis. *Thorax* 71 (5), 429–435. doi:10.1136/thoraxjnl-2015-207011
- Noth, I., Zhang, Y., Ma, S.-F., Flores, C., Barber, M., Huang, Y., et al. (2013). Genetic Variants Associated with Idiopathic Pulmonary Fibrosis Susceptibility and Mortality: a Genome-wide Association Study. *Lancet Respir. Med.* 1 (4), 309–317. doi:10.1016/s2213-2600(13)70045-6
- Okuda, R., Matsushima, H., Aoshiba, K., Oba, T., Kawabe, R., Honda, K., et al. (2015). Soluble Intercellular Adhesion Molecule-1 for Stable and Acute Phases of Idiopathic Pulmonary Fibrosis. *SpringerPlus* 4, 657. doi:10.1186/s40064-015-1455-z
- Pierce, E. M., Carpenter, K., Jakubzick, C., Kunkel, S. L., Evanoff, H., Flaherty, K. R., et al. (2007). Idiopathic Pulmonary Fibrosis Fibroblasts Migrate and Proliferate to CC Chemokine Ligand 21. *Eur. Respir. J.* 29 (6), 1082–1093. doi:10.1183/09031936.00122806
- Pierce, E. M., Carpenter, K., Jakubzick, C., Kunkel, S. L., Flaherty, K. R., Martinez, F. J., et al. (2007). Therapeutic Targeting of CC Ligand 21 or CC Chemokine Receptor 7 Abrogates Pulmonary Fibrosis Induced by the Adoptive Transfer of Human Pulmonary Fibroblasts to Immunodeficient Mice. *Am. J. Pathol.* 170 (4), 1152–1164. doi:10.2353/ajpath.2007.060649
- Raghu, G., Collard, H. R., Egan, J. J., Martinez, F. J., Behr, J., Brown, K. K., et al. (2011). An Official ATS/ERS/JRS/ALAT Statement: Idiopathic Pulmonary Fibrosis: Evidence-Based Guidelines for Diagnosis and Management. *Am. J. Respir. Crit. Care Med.* 183 (6), 788–824. doi:10.1164/rccm.2009-040gl
- Raghu, G., Collard, H. R., Egan, J. J., Martinez, F. J., Behr, J., Brown, K. K., et al. (2011). An Official ATS/ERS/JRS/ALAT Statement: Idiopathic Pulmonary Fibrosis: Evidence-Based Guidelines for Diagnosis and Management. *Am. J. Respir. Crit. Care Med.* 183 (6), 788–824. doi:10.1164/rccm.2009-040gl
- Raghu, G., Rochwerf, B., Zhang, Y., Garcia, C. A. C., Azuma, A., Behr, J., et al. (2015). An Official ATS/ERS/JRS/ALAT Clinical Practice Guideline: Treatment of Idiopathic Pulmonary Fibrosis. An Update of the 2011 Clinical Practice Guideline. *Am. J. Respir. Crit. Care Med.* 192 (2), E3–E19. doi:10.1164/rccm.201506-1063st
- Richards, T. J., Kaminski, N., Baribaud, F., Flavin, S., Brodmerkel, C., Horowitz, D., et al. (2012). Peripheral Blood Proteins Predict Mortality in Idiopathic Pulmonary Fibrosis. *Am. J. Respir. Crit. Care Med.* 185 (1), 67–76. doi:10.1164/rccm.201101-0058oc
- Richeldi, L. (2013). Clinical Trials of Investigational Agents for IPF: a Review of a Cochrane Report. *Respir. Res.* 14 (Suppl. 1), S4. doi:10.1186/1465-9921-14-s1-s4
- Richeldi, L., Cottin, V., du Bois, R. M., Selman, M., Kimura, T., Bailes, Z., et al. (2016). Nintedanib in Patients with Idiopathic Pulmonary Fibrosis: Combined Evidence from the TOMORROW and INPULSIS Trials. *Respir. Med.* 113, 74–79. doi:10.1016/j.rmed.2016.02.001
- Salem, A., Alotaibi, M., Mroueh, R., Basheer, H. A., and Afarinkia, K. (2021). CCR7 as a Therapeutic Target in Cancer. *Biochim. Biophys. Acta (Bba) - Rev. Cancer* 1875 (1), 188499. doi:10.1016/j.bbcan.2020.188499
- Sang, X., Wang, Y., Xue, Z., Qi, D., Fan, G., Tian, F., et al. (2021). Macrophage-Targeted Lung Delivery of Dexamethasone Improves Pulmonary Fibrosis Therapy via Regulating the Immune Microenvironment. *Front. Immunol.* 12, 613907. doi:10.3389/fimmu.2021.613907
- Scott, M. K. D., Quinn, K., Li, Q., Carroll, R., Warsinske, H., Vallania, F., et al. (2019). Increased Monocyte Count as a Cellular Biomarker for Poor Outcomes in Fibrotic Diseases: a Retrospective, Multicentre Cohort Study. *Lancet Respir. Med.* 7 (6), 497–508. doi:10.1016/s2213-2600(18)30508-3
- Selman, M., King, T. E., and Pardo, A. (2001). Idiopathic Pulmonary Fibrosis: Prevailing and Evolving Hypotheses about its Pathogenesis and Implications for Therapy. *Ann. Intern. Med.* 134 (2), 136–151. doi:10.7326/0003-4819-134-2-200101160-00015
- Tanaka, N., Ikari, J., Anazawa, R., Suzuki, M., Katsumata, Y., Shimada, A., et al. (2019). S100A12 Inhibits Fibroblast Migration via the Receptor for Advanced Glycation End Products and P38 MAPK Signaling. *In Vitro Cell.Dev.Biol.-Animal* 55 (8), 656–664. doi:10.1007/s11626-019-00384-x
- Yang, L., Herrera, J., Gilbertsen, A., Xia, H., Smith, K., Benyumov, A., et al. (2018). IL-8 Mediates Idiopathic Pulmonary Fibrosis Mesenchymal Progenitor Cell Fibrogenicity. *Am. J. Physiology-Lung Cell Mol. Physiol.* 314 (1), L127–L136. doi:10.1152/ajplung.00200.2017
- Zhang, H.-T., Fang, S.-C., Wang, C.-Y., Wang, W., Wu, J., Wang, C., et al. (2015). MMP-9 1562C>T Gene Polymorphism and Efficacy of Glucocorticoid Therapy in Idiopathic Pulmonary Fibrosis Patients. *Genet. Test. Mol. biomarkers* 19 (11), 591–597. doi:10.1089/gtmb.2015.0057
- Zhang, Z., Han, N., and Shen, Y. (2020). S100A12 Promotes Inflammation and Cell Apoptosis in Sepsis-Induced ARDS via Activation of NLRP3 Inflammasome Signaling. *Mol. Immunol.* 122, 38–48. doi:10.1016/j.molimm.2020.03.022

**Conflict of Interest:** The authors declare that the research was conducted in the absence of any commercial or financial relationships that could be construed as a potential conflict of interest.

Copyright © 2021 Lu, Chen, Tang, Wang, Tian, Wang, Zhao and Xie. This is an open-access article distributed under the terms of the Creative Commons Attribution License (CC BY). The use, distribution or reproduction in other forums is permitted, provided the original author(s) and the copyright owner(s) are credited and that the original publication in this journal is cited, in accordance with accepted academic practice. No use, distribution or reproduction is permitted which does not comply with these terms.



# Management of Coronavirus Disease 2019 Patients With Lung Cancer: Experience From a Thoracic Oncology Center

David Barros Coelho<sup>1,2\*</sup>, Vanessa Santos<sup>1</sup>, David Araújo<sup>1</sup>, Hélder Novais Bastos<sup>1,2,3</sup>, Adriana Magalhães<sup>1</sup>, Venceslau Hespanhol<sup>1,2,3</sup>, Henrique Queiroga<sup>1,2</sup>, Natália Cruz-Martins<sup>2,3,4</sup> and Maria Gabriela O. Fernandes<sup>1,2,3</sup>

<sup>1</sup> Pulmonology Department, Centro Hospitalar Universitário São João, Porto, Portugal, <sup>2</sup> Faculdade de Medicina, University of Porto, Porto, Portugal, <sup>3</sup> Institute for Research and Innovation in Health (i3S), University of Porto, Porto, Portugal, <sup>4</sup> Laboratory of Neuropsychophysiology, Faculty of Psychology and Education Sciences, University of Porto, Porto, Portugal

## OPEN ACCESS

### Edited by:

Huahao Shen,  
Zhejiang University, China

### Reviewed by:

Alessandra Bettiol,  
University of Florence, Italy  
Marina Sekacheva,  
I. M. Sechenov First Moscow State  
Medical University, Russia

### \*Correspondence:

David Barros Coelho  
david.b.c@hotmail.com

### Specialty section:

This article was submitted to  
Molecular Diagnostics  
and Therapeutics,  
a section of the journal  
Frontiers in Molecular Biosciences

**Received:** 09 December 2020

**Accepted:** 11 March 2021

**Published:** 22 July 2021

### Citation:

Coelho DB, Santos V, Araújo D, Bastos HN, Magalhães A, Hespanhol V, Queiroga H, Cruz-Martins N and Fernandes MGO (2021) Management of Coronavirus Disease 2019 Patients With Lung Cancer: Experience From a Thoracic Oncology Center. *Front. Mol. Biosci.* 8:639676. doi: 10.3389/fmolb.2021.639676

**Background:** Cancer patients appear to be at a higher risk of complications from coronavirus disease 2019 (COVID-19). Specific data related to lung cancer (LC) patient management, active treatment, and/or recent diagnosis are still very limited. Here, we aimed to investigate the clinical presentation, baseline features, and clinical outcomes of LC patients with COVID-19.

**Methods:** A retrospective case study was performed at Centro Hospitalar Universitário de São Joao, a tertiary hospital in the North of Portugal. Data from LC patients diagnosed with COVID-19 were collected during the first 10 months of the COVID-19 pandemic (March 2020–January 2021).

**Results:** Twenty-eight patients with active LC were diagnosed with COVID-19, being adenocarcinoma the most common histological type present ( $n = 13$ , 46.4%). Sixteen patients had metastatic stage IV LC (61.5%). Twenty-five patients (89.3%) had relevant comorbidities including hypertension (39.3%) and chronic obstructive pulmonary disease (32.1%). For patients undergoing antineoplastic treatment, the median time from the last chemotherapy administration to COVID-19 diagnosis was of 16 days (interquartile range = 13–41 days). Half of patients were previously on corticosteroid therapy. Twenty patients (71.4%) needed hospitalization, 18 received oxygen therapy (64.3%), 3 (10.7%) of them received high-flow nasal cannula with good tolerability, and 1 (3.6%) needed non-invasive ventilation. Hydroxychloroquine and antibiotics were given to 4 (14.3%) and 12 (42.9%) patients, respectively. Seven patients (25%) died at a median time of 5 days following COVID-19 diagnosis.

**Conclusion:** This is one of the first studies reporting the adverse outcomes associated with COVID-19 in LC patients at same time that adds evidence regarding the need to create protocols and guidelines to reduce the infection risk in such patients.

**Keywords:** COVID-19, lung cancer, infection, thoracic oncology, clinical management

## INTRODUCTION

Coronavirus disease 2019 (COVID-19) is a viral infection triggered by severe acute respiratory syndrome coronavirus 2 (SARS-CoV-2), with high pulmonary impairment. Although the first cases were reported in Hubei, China, in December 2019, the disease spread rapidly around the world and was recognized as a global pandemic by the World Health Organization (WHO) (Guan et al., 2020; Johns Hopkins University, 2020). Among the main patients with features that confer a higher risk of a serious disease state and a higher mortality rate resulting from infection are the elderly and those with underlying comorbidities (Guan et al., 2020; Johns Hopkins University, 2020).

Regarding oncology, data on clinical outcomes in cancer patients are still scarce, although published case reports indicate that cancer leads to worse outcomes. For example, a study conducted in China found that cancer patients were at higher risk of COVID-19 with a worse prognosis than those without cancer (de Marinis et al., 2020; Liang et al., 2020; Passaro et al., 2020; Yu et al., 2020). In addition, the first report from a global database (TERAVOLT) revealed a 33% mortality rate and a low proportion of patients in intensive care or mechanical ventilation (Garassino et al., 2020), an aspect that has already been highlighted by smaller studies (de Marinis et al., 2020; Liang et al., 2020; Passaro et al., 2020; Yu et al., 2020). In this sense, it is important to understand the clinical context and epidemiological features of cancer patients in order to create or even improve the existing protocols in cancer centers to deal with lung cancer (LC) patients in the COVID-19 era. In addition, and given the scarcity of specific data on LC patient management in active treatment and/or with recent diagnosis, it is also of utmost importance to better understand the global scope to develop clinical guidelines in this regard. Anyway, considering the disease burden, age, comorbidities, smoking, and even the immunosuppression state to which such patients are exposed, we hypothesize that they face a higher risk of COVID-19-related complications and even death. Thus, the present study aims to analyze the incidence of cases and the impact of infection control measures in LC patients at a thoracic oncology center.

## MATERIALS AND METHODS

A retrospective case study was carried out at the Centro Hospitalar Universitário de São João (CHUSJ), a tertiary hospital in the Oporto region, located at the Northern Portugal. In fact, the Oporto region was the epicenter at the time of the first COVID-19 outbreak in Portugal, as it was in the second wave. The first national cases were reported in this region and, according to data from Portuguese public health authorities, six of the 10 most affected municipalities were in the Porto region during the first 2 months of the pandemic.

The Department of Thoracic Oncology is part of the CHUSJ Oncology Unit. Briefly, it is located in an adjacent building to CHUSJ, where consultations, examinations, and radiotherapy and chemotherapy are performed. In

this study, data were collected from LC patients with COVID-19 diagnosis in Portugal from March 2020 to January 2021. Active cancer was defined as LC diagnosed or treated in the previous 6 months or recurrent/metastatic cancer.

During this period, a contingency plan was developed by the CHUSJ and the Department of Thoracic Oncology, aiming to (1) reduce the in-person consultation, establishing telemedicine for non-essential care; (2) COVID-19 screening in patients starting treatment (chemotherapy or radiotherapy); (3) regular and adequate cleaning of surfaces and objects in the Oncology Daycare Unit; and (4) patient engagement in social distancing and proper hand cleaning techniques.

Demographic and clinical features, laboratory findings, and chest computed tomography (CT) or chest X-ray images were collected and analyzed.

Coronavirus disease 2019 diagnosis was based on the criteria published by the WHO and confirmed by reverse transcriptase-polymerase chain reaction assay of nasal and/or pharyngeal specimens. Patients with confirmed COVID-19 diagnosis were treated according to the emergency room policy, and ward treatment and follow-up were done by a dedicated team led by the Infectious Diseases Unit.

The study protocol was approved by the ethics committee of CHUSJ.

## RESULTS

A total of 28 patients with active LC were retrospectively identified and analyzed. Baseline demographic and clinical characteristics of patients are summarized in **Table 1**. Most patients were male ( $n = 20$ , 71.4%), with median age of 68 years [interquartile range (IQR) = 57–76 years]. All cases presented between March 21, 2020, and January 4, 2021.

Regarding LC histological type, adenocarcinoma was the most common ( $n = 13$ , 46.4%), followed by squamous cell carcinoma ( $n = 7$ , 25.0%). Most had stage IV metastatic LC ( $n = 16$ , 61.5%), whereas four had stage IIb (15.4%). The remaining histological types and staging are represented in **Table 1**.

Two patients (7.1%) had a prior history of another cancer, including lymphoma (recently treated with rituximab) and colon cancer. Eleven patients (39.3%) had hypertension, and nine (32.1%) had chronic obstructive pulmonary disease (COPD) (two of them requiring long-term oxygen therapy). Other relevant comorbidities included hypercholesterolemia ( $n = 7$ ), diabetes ( $n = 3$ ), and heart failure ( $n = 3$ ). One patient had organizing pneumonia (OP) undergoing steroid treatment (**Table 1**).

Most patients were on active treatment ( $n = 20$ , 71.4%). The anticancer therapy is detailed in **Table 1**. The median time from the last administration of chemotherapy to COVID-19 diagnosis was of 16 days (IQR = 13–41 days). The patients from the first COVID-19 wave ( $n = 5$ ) had a median time of last treatment to diagnosis of 4 days, whereas the remaining had 18 days (IQR = 13–41 days).

**TABLE 1 |** Characterization of lung cancer (LC) patients with coronavirus disease 2019 (COVID-19) diagnosis.

Disease features	
Median age (IQR), years	73 (64–76)
Male sex, no. (%)	20 (71.4%)
<b>Smoking status, no. (%)</b>	
Non-smoker	6 (23.1%)
Former smoker	9 (34.6%)
Smoker	11 (42.3%)
<b>Comorbidities, no. (%)</b>	
HBP	11 (39.3%)
COPD	9 (32.1%)
Dyslipidemia	7 (25.0%)
Atrial fibrillation	4 (16.0%)
Cardiac failure	4 (16.0%)
Diabetes	3 (10.7%)
Psoriasis	2 (7.1%)
OSA	2 (7.1%)
Alcoholism	2 (7.1%)
Asthma	1 (3.6%)
Stroke	1 (3.6%)
Laryngeal carcinoma	1 (3.6%)
Hypothyroidism	1 (3.6%)
GERD	1 (3.6%)
Ankylosing spondylitis	1 (3.6%)
Colon cancer	1 (3.6%)
Organizing pneumonia	1 (3.6%)
Peripheral arterial disease	1 (3.6%)
Scleroderma	1 (3.6%)
Lymphoma	1 (3.6%)
Non-significant	3 (10.7%)
<b>Histology, no. (%)</b>	
Adenocarcinoma	13 (46.4%)
Squamous cell carcinoma	7 (25.0%)
Small cell lung cancer	3 (10.7%)
Non-small cell lung carcinoma	1 (3.6%)
Neuroendocrine	1 (3.6%)
Poorly differentiated carcinoma	2 (7.1%)
Glomic tumor	1 (3.6%)
<b>Staging, no. (%)</b>	
IV 16/26 (61.5%)	16 (61.5%)
IIIB 4/26 (15.4%)	4 (15.4%)
Ia 1/26 (3.8%)	1 (3.8%)
Ila 1/26 (3.8%)	1 (3.8%)
IIla 1/26 (3.8%)	1 (3.8%)
IIIB 1/26 (3.6%)	1 (3.6%)
<b>Median time since LC diagnosis (IQR), months</b>	
	6 (1–13)
<b>Last LC treatment, no. (%)</b>	
No treatment/recent diagnosis	8 (28.6%)
Carboplatin-vinorelbine	4 (14.3%)
Carboplatin-pemetrexed	3 (10.7%)
Atezolizumab	2 (7.1%)
Docetaxel	2 (7.1%)
Durvalumab	2 (7.1%)
Etoposide	2 (7.1%)

(Continued)

**TABLE 1 |** Continued

Disease features	
Gencitabine	1 (3.6%)
Carboplatin-Paclitxel	1 (3.6%)
Caboplatin-gemcitabine	1 (3.6%)
Nivolumab	1 (3.6%)
Carboplatin + etoposide	1 (3.6%)
Time since last treatment (days)	16 (13–41)

IQR, interquartile range; HBP, high blood pressure; COPD, chronic obstructive pulmonary disease; OSA, obstructive sleep apnea; GERD, gastroesophageal reflux; LC, lung cancer.

Most patients (11/22) were under corticosteroid therapy, namely, for symptom relief and OP treatment. Three patients (60%) were receiving doses  $\geq 20$  mg/day because of OP ( $n = 1$ ), vena cava syndrome ( $n = 1$ ), and for preparing chemotherapy ( $n = 1$ ).

Regarding COVID-19, patients mostly presented with dyspnea ( $n = 12$ , 42.9%) and cough ( $n = 6$ , 21.4%). Seven patients (25.0%) were diagnosed as a screening for treatment, whereas two patients were screened because of hospital admissions for other reasons (e.g., uncontrolled pain and hemoptysis). The median time since symptom onset until COVID-19 diagnosis was of 2 days (IQR = 0–4 days). More information regarding symptoms at presentation is detailed in **Table 2**.

Laboratory findings on admission are shown in **Table 2**. Regarding data from blood cells count, neutrophilia was present in 17 (70.8%) of patients, whereas 16 (66.7%) had lymphopenia (80%). All patients had increased levels of C-reactive protein.

A total of 16 patients (57.1%) had a thorax image at presentation or shortly after diagnosis of COVID-19. The CT scan of patients revealed the presence of bilateral ground-glass opacities, and three patients evidenced consolidations suggestive of coinfection, in addition to baseline radiological manifestations of LC, such as pleural effusion and lung masses. **Figure 1** represents examples of chest CT scan of patients.

Regarding therapeutic intervention, 18 patients (64.3%) received supplemental oxygen, including three (10.7%) who received high-flow nasal cannula at time of intensive care unit admission due to type 1 respiratory failure. One patient (3.6%) needed non-invasive ventilation, and one (3.6%) had continuous positive airway pressure with supplemental oxygen. No patient received mechanical ventilation or extracorporeal membrane oxygenation.

Empirical SARS-CoV-2 treatment with hydroxychloroquine was administered in four cases (14.3%), one of them with concomitant azithromycin. These patients were all treated in the first 3 months. Twelve patients (42.9%) needed empirical antibiotics (two of them in the context of febrile neutropenia). Nine patients (32.1%) were treated with corticosteroids, all in-hospital. One patient remained on corticotherapy at the same dose because of previous OP diagnosis, with CT scan still showing consolidations consistent with the previous diagnosis. This patient developed pulmonary thromboembolism, with no



**TABLE 2 |** Characterization of symptoms, management, and outcomes of COVID-19 in LC patients.

<b>Characterization of COVID-19</b>	
Median symptoms duration (IQR), days	2 (0–4)
<b>Symptoms</b>	
Dyspnea	13 (46.3%)
Cough	9 (32.1%)
Sputum	4 (14.3%)
Anorexia	2 (7.1%)
Odynophagia	1 (3.6%)
Hemoptysis	1 (3.6%)
Prostration	1 (3.6%)
Screening before LC treatment	7 (25.0%)
<b>Biochemical results, median (IQR)</b>	
White blood cells, $\times 10^3/\mu\text{L}$	6.31 (4.2–10.9)
Neutrophils/lymphocytes/eosinophils, $\times 10^3/\mu\text{L}$	3.9; 0.8; 0.01
Hemoglobin, g/dL	11.4 (1.9)
Platelets, $\times 10^3/\mu\text{L}$	173 (140–356)
C-reactive protein, mg/L	61 (33–164)
<b>Treatment, no. (%)</b>	
Supplementary oxygen	18 (64.3%)
Antibiotics	12 (42.9%)
Steroids	9 (32.1%)
HDQ	4 (14.3%)
HFNC	3 (10.7%)
NIV	1 (3.6%)
CPAP	1 (3.6%)
No treatment	10 (35.7%)
<b>Outcome, no. (%)</b>	
Death	7 (25.0%)

IQR, interquartile range; NIV, non-invasive ventilation; HFNC, high-flow nasal cannula; HDQ, hydroxychloroquine; LC, lung cancer; CPAP, continuous positive airway pressure.

signs of right-sided heart failure and with good recovery after hypocoagulation with low-molecular-weight heparin.

Regarding clinical outcomes, seven patients died (25.0%) after a median time of 5 days since the COVID-19 diagnosis (min–max = 0–116 days). The patients who died had metastatic and progressive LC (stage IV); four of them (80.0%) were previously on steroids.

## DISCUSSION

The COVID-19 pandemic has dramatically changed the population's daily life and health support, with an increased risk reported for cancer patients. This current scenario has put in a higher emphasis the need for continuous changes and adaptations of previous routines in oncology care units.

In our sample, a high lethality rate was observed. When considering the cases of the first wave (between March and May), in fact, at the end of April, the rate of COVID-19–positive cases for the general population was 0.24%, linked to a lethality rate of 4.0%. However, in our case, the rate per LC patient was 1.12%, where 60% of patients died. Such differences

can be attributed, in particular, to the oncological process features, age, treatment regimen, and patients' comorbidities. For example, in the TERA-VOLT study, it was found that, in LC patients, poor prognosis was associated with advanced age (>65 years), comorbidities, Eastern Cooperative Oncology Group performance status grade 2 (ECOG2), steroids (>10 mg of prednisolone), anticoagulants, chemotherapy, and chemotherapy plus immunotherapy (Garassino et al., 2020). In this sample, half of patients were on steroid therapy for different reasons. We could speculate that the worse outcome could also be attributed to the immunosuppression state induced by steroids. Indeed, this aspect further raises the need for a careful intervention in these patients, where the use of lower doses of steroids may be an alternative in cancer patients at high risk of COVID-19.

Additionally, one patient was diagnosed with pulmonary thromboembolism. Cancer is a prothrombotic state that *per se* can explain this finding. However, in COVID-19–derived pneumonia, coagulopathy and disseminated intravascular coagulation are common complications and the most common causes of death (Helms et al., 2020; Wu et al., 2020), with the possible benefit of using heparin in selected acute respiratory distress syndrome patients with coagulopathy (Tang et al., 2020). It is therefore essential to monitor LC patients for the development of pulmonary thrombosis, as they are at an even greater risk of thrombotic events.

In this series, all casualties happened in patients with stage IV LC. This suggests that an advanced and progressive lung disease may be responsible for the worst outcomes. Several reasons may explain the worse prognosis observed to these LC patients, such as the immunosuppression status, male gender, smoking, and the presence of cardiovascular and chronic lung diseases, including the COPD (Cai, 2020; Passaro et al., 2020). LC patients often have recurrent respiratory symptoms, which can eventually delay the recognition of a viral infection for both the patient and the clinician. In our sample, the most common symptoms were dyspnea and cough, which can be wrongly attributed to the disease progression, especially at advanced cancer stages. Thus, regular testing, particularly before treatments and when patients regularly visit the hospital for consultation, should be performed, as they are crucial for early detection, at the same time, which also helps to avoid interventions that can aggravate the disease.

Another key issue is to assess the indication for antineoplastic treatment. In this way, a proper discussion in a multidisciplinary team, which can be done by videoconference and other emerging platforms, can help the clinician to adopt the most appropriate therapeutic option, with a consequent reduction in the risk of infection. In fact, this should be a priority in the decision-making process, if case-by-case risk–benefit assessment is high. In reality, what is intended here is to emphasize that the interruption of the necessary and effective anticancer therapy should not be an option, except for low-priority cases, on a case-by-case analysis. The European Society for Medical Oncology (ESMO) has published specific online guidelines for the different therapeutic regimens that should be considered for LC treatment, dividing them into high (should not be delayed), medium (should not be delayed for more than 6 weeks), and low (the patient's condition is stable enough that services can be suspended during

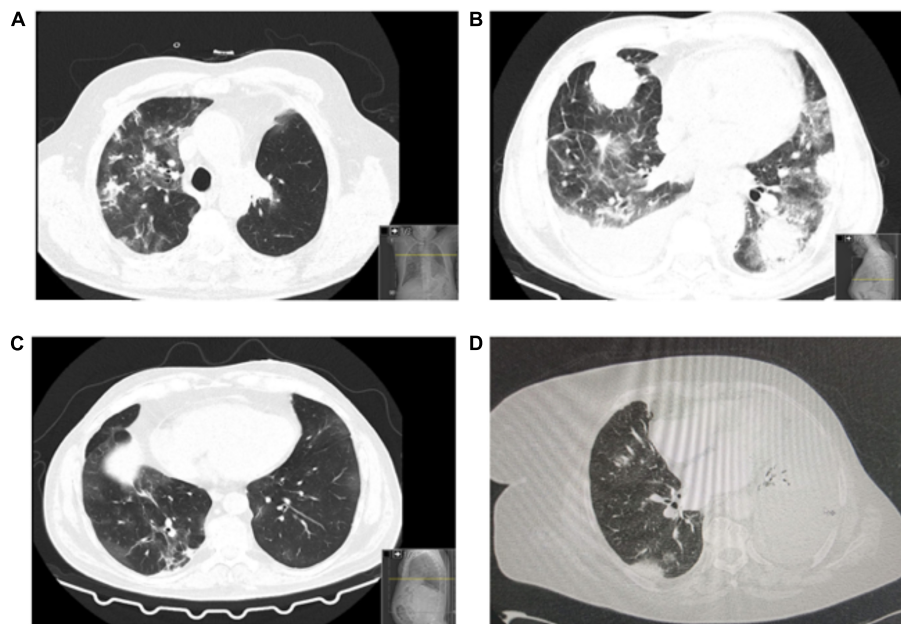


**FIGURE 1 |** Patients' chest CT scans. **(A)** Bilateral predominantly peripheral ground-glass opacities. Asymmetrical consolidations in the right lobes suggestive of concomitant bacterial infection. Left upper lobe lobectomy signs (consistent with recent surgery). **(B)** Patient with multiple findings related to coronavirus disease 2019 (COVID-19) and the underlying lung cancer: bilateral ground-glass opacities, pulmonary mass and pleural implant, right pleural effusion. **(C)** Chest CT: bilateral ground-glass opacities, both central and peripheral, some with nodular shape. Some "band" consolidative opacities in the right upper lobe, middle lobe, and lower inferior lobe opacities suggestive of residual processes. **(D)** Left large-volume pleural effusion with left lung atelectasis. Diffuse ground-glass opacities. Small right pleural effusion. No signs of pulmonary thromboembolism.

the pandemic, or the intervention is unlikely to have a marked benefit) priority.

On the other side, and also worth of note is that hospital transmission was considered a possibility in two of the cases, as they underwent treatment at the daycare oncology unit 4 days before the symptoms developed. However, an epidemiologic link has not been found. Other retrospective studies have indicated the occurrence of hospital transmission in COVID-19 patients. For example, in a retrospective case study in China with 138 patients, 41.3% of patients were reported to have acquired SARS-CoV-2 during hospitalization, five in the oncology department (Wang et al., 2020).

In our particular case, since the beginning of the COVID-19 outbreak, and in line with recommendations from international and national societies, such as ESMO and Direção Geral da Saúde, a specific protocol has been designed to be applied to reduce the patients' access to the oncology unit, promoting telephone screening and consultation. All patients have been screened for COVID-19 symptoms and temperature upon arrival at the entrance to the oncology unit, since the beginning of April. In addition, all patients and staff use a surgical mask inside the hospital. As a result, from May to June 2020, there was no new diagnosis of COVID-19 among LC patients at our institution. This reduction can be in part due to policies adopted to reduce the spread of nosocomial infections. At national level, the peak in the number of active cases was at mid-May (May 15); so, the lack of new cases during the month of May seems to be related to the successful preventive

measures implemented. On the other hand, seven patients had a diagnosis as part of screening for oncologic treatment (chemotherapy or radiotherapy), which could have prevented more serious complications had the patients done treatment. This probably explains the findings regarding time, from the last cancer treatment to the COVID-19 diagnosis, having increased from 4 days in the first wave to 16 days in the following months.

As main study limitations, the reduced sample size is the most prominent one, which limits the conclusions regarding clinical presentation and outcomes to the general population of patients with LC. However, this single-center experience majorly intends to highlight the measures related to infection control and its effects on reducing the likelihood of getting infected by SARS-CoV-2 in our patients. Therefore, this analysis adds to the evidence that strict rules to prevent SARS-CoV-2 infection among LC patients are particularly relevant.

## CONCLUSION

In view of the high vulnerability of LC patients, the death risk associated with COVID-19 is imminent. Thus, and given the data presented in this report, there is urgency in implementing and maintaining protocols at the oncology unit to minimize the viral infection spread and to reduce the consequences in SARS-CoV-2-infected patients.

## DATA AVAILABILITY STATEMENT

The raw data supporting the conclusions of this article will be made available by the authors, without undue reservation.

## ETHICS STATEMENT

The studies involving human participants were reviewed and approved by Centro Hospitalar Universitário de São João, Porto, Portugal.

## REFERENCES

- Cai, H. (2020). Sex difference and smoking predisposition in patients with COVID-19. *Lancet Respir. Med.* 8:e20. doi: 10.1016/S2213-2600(20)30117-X
- de Marinis, F., Attili, I., Morganti, S., Stati, V., Spitaleri, G., Gianoncelli, L., et al. (2020). Results of multilevel containment measures to better protect lung cancer patients from COVID-19: the IEO model. *Front. Oncol.* 10:665. doi: 10.3389/fonc.2020.00665
- Garassino, M. C., Whisenant, J. G., Huang, L.-C., Trama, A., Torri, V., Agustoni, F., et al. (2020). COVID-19 in patients with thoracic malignancies (TERAVOLT): first results of an international, registry-based, cohort study. *Lancet Oncol.* 21, 914–922. doi: 10.1016/S1470-2045(20)30314-4
- Guan, W., Ni, Z., Hu, Y., Liang, W., Ou, C., He, J., et al. (2020). Clinical characteristics of coronavirus disease 2019 in China. *N. Engl. J. Med.* 382, 1708–1720. doi: 10.1056/NEJMoa2002032
- Helms, J., Tacquard, C., Severac, F., Leonard-Lorant, I., Ohana, M., Delabranche, X., et al. (2020). High risk of thrombosis in patients with severe SARS-CoV-2 infection: a multicenter prospective cohort study. *Intensive Care Med.* 46, 1089–1098. doi: 10.1007/s00134-020-06062-x
- Johns Hopkins University (2020). *Coronavirus COVID-19 Global Cases by the Center for Systems Science and Engineering (CSSE) at Johns Hopkins University (JHU)*. Baltimore, MD: Johns Hopkins Univ.
- Liang, W., Guan, W., Chen, R., Wang, W., Li, J., Xu, K., et al. (2020). Cancer patients in SARS-CoV-2 infection: a nationwide analysis in China. *Lancet Oncol.* 21, 335–337. doi: 10.1016/S1470-2045(20)30096-6
- Passaro, A., Peters, S., Mok, T. S. K., Attili, I., Mitsudomi, T., and de Marinis, F. (2020). Testing for COVID-19 in lung cancer patients. *Ann. Oncol.* 31, 832–834. doi: 10.1016/j.annonc.2020.04.002

## AUTHOR CONTRIBUTIONS

All authors listed have made a substantial, direct and intellectual contribution to the work, and approved it for publication.

## ACKNOWLEDGMENTS

NC-M acknowledges the Portuguese Foundation for Science and Technology under the Horizon 2020 Program (PTDC/PSI-GER/28076/2017).

- Tang, N., Bai, H., Chen, X., Gong, J., Li, D., and Sun, Z. (2020). Anticoagulant treatment is associated with decreased mortality in severe coronavirus disease 2019 patients with coagulopathy. *J. Thromb. Haemost.* 18, 1094–1099. doi: 10.1111/jth.14817
- Wang, D., Hu, B., Hu, C., Zhu, F., Liu, X., Zhang, J., et al. (2020). Clinical characteristics of 138 hospitalized patients with 2019 novel coronavirus-infected pneumonia in Wuhan, China. *JAMA* 323, 1061–1069. doi: 10.1001/jama.2020.1585
- Wu, C., Chen, X., Cai, Y., Xia, J., Zhou, X., Xu, S., et al. (2020). Risk factors associated with acute respiratory distress syndrome and death in patients with coronavirus disease 2019 pneumonia in Wuhan, China. *JAMA Intern. Med.* 180, 934–943. doi: 10.1001/jamainternmed.2020.0994
- Yu, J., Ouyang, W., Chua, M. L. K., and Xie, C. (2020). SARS-CoV-2 transmission in patients with cancer at a tertiary care hospital in Wuhan, China. *JAMA Oncol.* 6, 1108–1110. doi: 10.1001/jamaoncol.2020.0980

**Conflict of Interest:** The authors declare that the research was conducted in the absence of any commercial or financial relationships that could be construed as a potential conflict of interest.

Copyright © 2021 Coelho, Santos, Araújo, Bastos, Magalhães, Hespanhol, Queiroga, Cruz-Martins and Fernandes. This is an open-access article distributed under the terms of the Creative Commons Attribution License (CC BY). The use, distribution or reproduction in other forums is permitted, provided the original author(s) and the copyright owner(s) are credited and that the original publication in this journal is cited, in accordance with accepted academic practice. No use, distribution or reproduction is permitted which does not comply with these terms.



# Multi-Pharmaceutical Activities of Chinese Herbal Polysaccharides in the Treatment of Pulmonary Fibrosis: Concept and Future Prospects

Xianbo Wu<sup>1†</sup>, Jianli Huang<sup>2†</sup>, Jie Wang<sup>2</sup>, Yihua Xu<sup>3</sup>, Xinwei Yang<sup>1</sup>, Minghan Sun<sup>4\*</sup> and Jianyou Shi<sup>5\*</sup>

<sup>1</sup>School of Sports Medicine and Health, Chengdu Sport University, Chengdu, China, <sup>2</sup>Guizhou University of Traditional Chinese Medicine, Guiyang, China, <sup>3</sup>Chengdu University of Traditional Chinese Medicine, Chengdu, China, <sup>4</sup>Central of Reproductive Medicine, Department of Obstetrics and Gynecology, School of Medicine, Sichuan Academy of Medical Sciences and Sichuan Provincial People's Hospital, University of Electronic Science and Technology of China, Chengdu, China, <sup>5</sup>Personalized Drug Therapy Key Laboratory of Sichuan Province, Sichuan Academy of Medical Science and Sichuan Provincial People's Hospital, School of Medicine of University of Electronic Science and Technology of China, Chengdu, China

## OPEN ACCESS

### Edited by:

Huahao Shen,  
Zhejiang University, China

### Reviewed by:

Ganesh Prasad Mishra,  
Swami Vivekanand Subharti  
University, India  
Hamed Barabadi,  
Shahid Beheshti University of Medical  
Sciences, Iran

### \*Correspondence:

Jianyou Shi  
shijianyoude@126.com  
Minghan Sun  
sunminghan26@gmail.com

<sup>†</sup>These authors have contributed  
equally to this work and share first  
authorship

### Specialty section:

This article was submitted to  
Respiratory Pharmacology,  
a section of the journal  
Frontiers in Pharmacology

**Received:** 10 May 2021

**Accepted:** 04 August 2021

**Published:** 17 August 2021

### Citation:

Wu X, Huang J, Wang J, Xu Y, Yang X,  
Sun M and Shi J (2021) Multi-  
Pharmaceutical Activities of Chinese  
Herbal Polysaccharides in the  
Treatment of Pulmonary Fibrosis:  
Concept and Future Prospects.  
Front. Pharmacol. 12:707491.  
doi: 10.3389/fphar.2021.707491

Pulmonary fibrosis is a fatal chronic progressive respiratory disease, characterized by continuous scarring of the lung parenchyma, leading to respiratory failure and death. The incidence of PF has increased over time. There are drugs, yet, there are some limitations. Hence, it is of importance to find new therapies and new drugs to replace the treatment of pulmonary fibrosis. In recent years, there have been a great number of research reports on the treatment of traditional Chinese medicine polysaccharides in various system fields. Among them, the treatment of PF has also gained extensive attention. This review summarized the source of polysaccharides, the drug activity of traditional Chinese medicine, and the protective effects on targets of Pulmonary fibrosis. We hope it can inspire researchers to design and develop polysaccharides, serving as a reference for potential clinical therapeutic drugs.

**Keywords:** pulmonary fibrosis, traditional Chinese medicine, polysaccharide, transforming growth factor- $\beta$ , extracellular matrix, collagen-1, biological activity

## INTRODUCTION

Pulmonary fibrosis (PF) is a large category of pulmonary diseases refers to the proliferation of fibroblasts and the accumulation of a large amount of extracellular matrix (ECM), accompanied by inflammatory damage, and tissue structure destruction, which can cause breathing difficulties, cough, hypoxemia, and hinder gas exchange, eventually leading to respiratory failure (Phan et al., 2021). PF's pathogenesis has undergone fibroblast activation, migration, proliferation and differentiation into myofibroblasts, inducing ECM aggregation, destroying the pulmonary parenchyma, changing the expansion of the pulmonary and the diffusion of O<sub>2</sub>/CO<sub>2</sub>, resulting in respiratory abnormalities caused by insufficient gas exchange (limitation reduced pulmonary volume and diffusing capacity) (Ruigrok et al., 2021). The triggering factors for fibrosis include genetic susceptibility and other risk factors, such as persistent viruses, bacterial infections, cigarettes, drug damage, and other medical diseases. Hereditary factors account for the largest proportion among them, one that the cause is unknown and the most common type of the disease is called idiopathic PF. (Richeldi et al., 2017; Majewski and Piotrowski, 2020). Radiology of chest



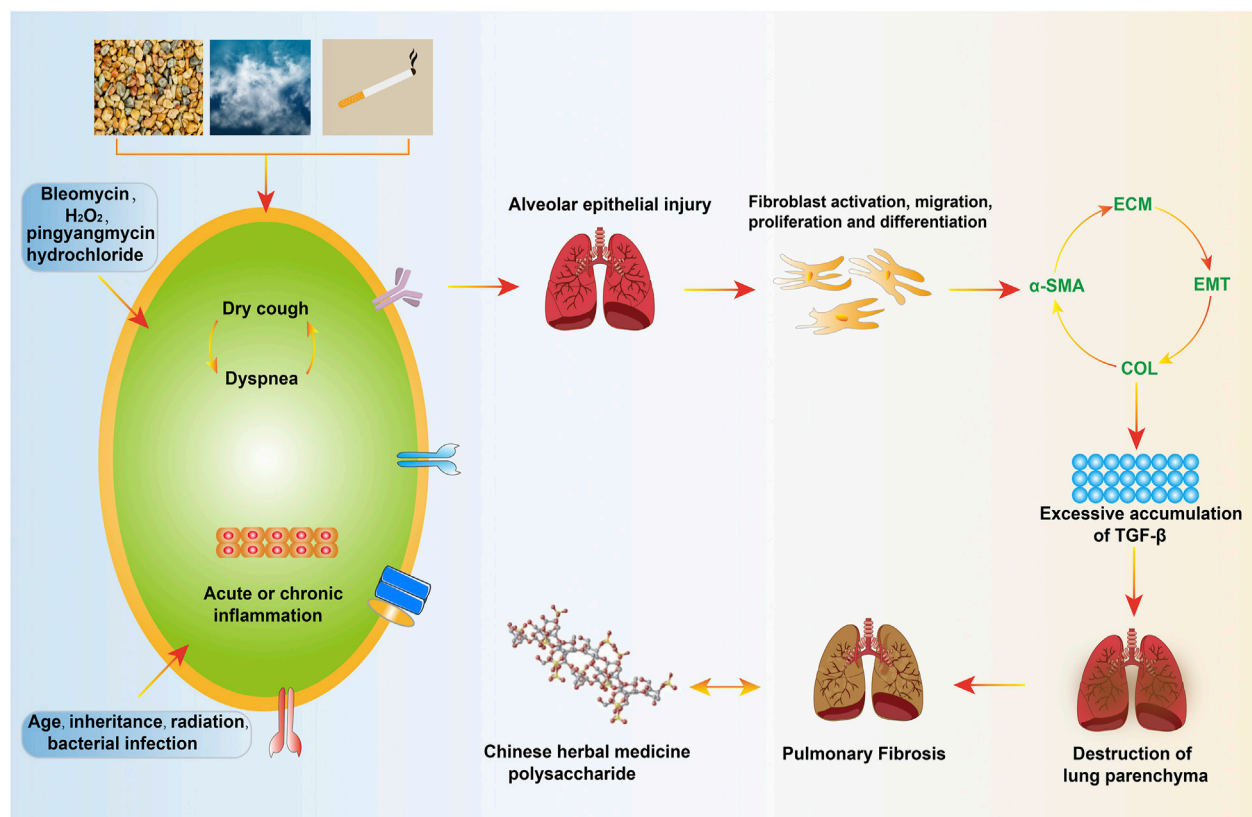
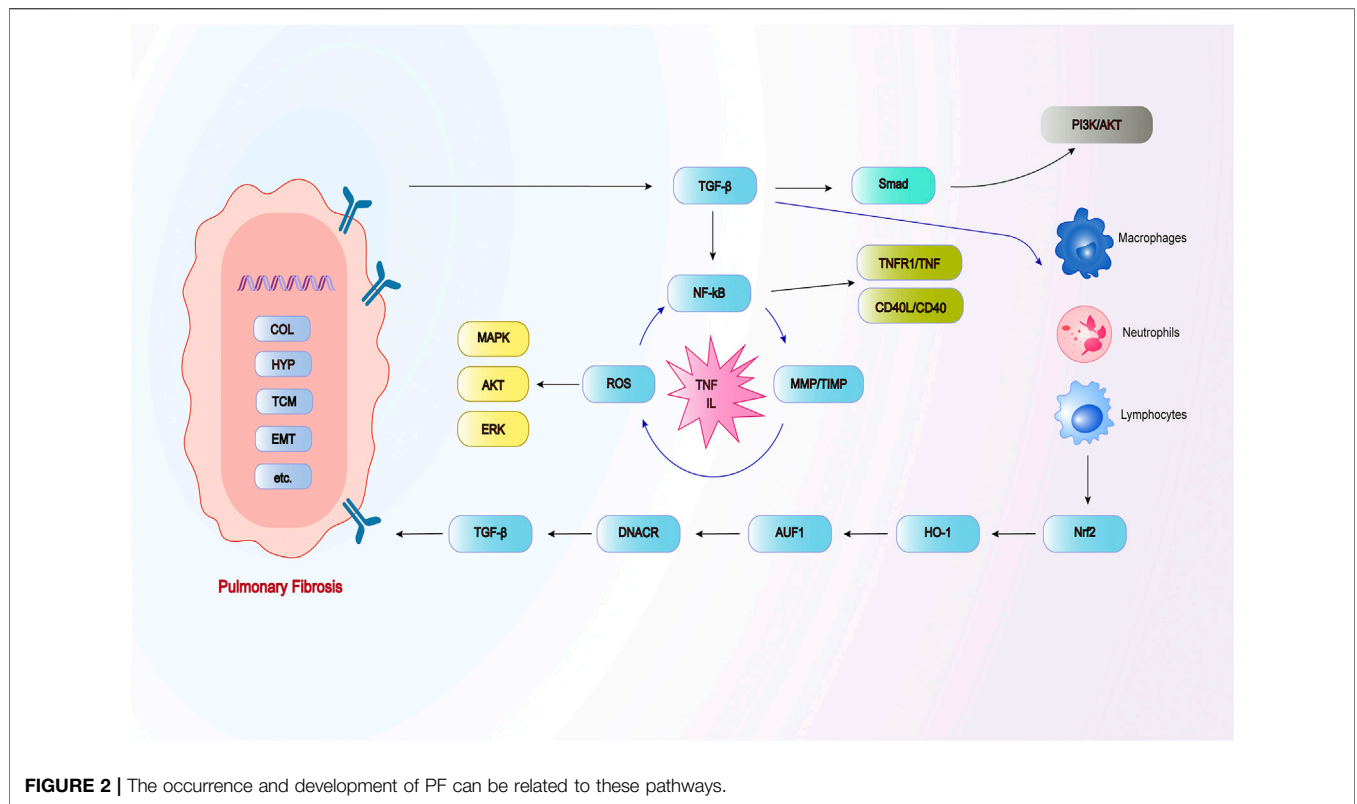


**FIGURE 1 |** Pathogenic factors and development process of pulmonary fibrosis.

high-resolution CT showed that about 90% of patients had interstitial changes, the histology of pulmonary biopsy showed that scar tissue replaced the normal pulmonary parenchyma, which was also used as a standard for the diagnosis of PF (Solomon et al., 2013). The occurrence and development of PF and the decline of pulmonary function are closely related to the survival rate. According to reports, the incidence of PF is increasing year by year and is positively correlated with age, with males higher than females (Hutchinson et al., 2015). With ageing, patients will inevitably experience the gradual loss of physiological integrity, the decrease of steady-state controlling ability and the increase of vulnerability to death. If not taking corresponding treatment measures after diagnosis, most patients' pulmonary function, if not all, will be progressively and irreversibly worsening, and their survival time is within 3–5 years (Lederer and Martinez, 2018) (**Figure 1**).

Currently, only two anti-fibrosis drugs, named pirfenidone and nintedanib, have been approved by the US Food and Drug Administration to treat PF, but, due to their side effects (headache, nausea, diarrhea, skin rash, and impaired liver function) and high cost, they cannot meet the medical needs (Galli et al., 2017). Lung transplantation can improve the survival rate, but the limited organ supply and the complexity of the surgery and medical treatment make it affordable for only a small number of patients (Ryu et al., 2014). Colchicine, prednisone, and cyclophosphamide were also used to reduce the incidence and

mortality of PF, studies on PF reported (Miniati and Matucci Cerinic, 2007; Fiorucci et al., 2008). In the case of acute exacerbations, international guidelines recommend high-dose glucocorticoids, but there are no data to prove its safety and effectiveness (Song et al., 2011). It has also been suggested that the therapeutic effects of prednisolone, cyclophosphamide, interferon-1b, and N-acetylcysteine have no obvious advantages, but various adverse reactions and increase the economic burden of patients (Datta et al., 2011; Canestaro et al., 2016; Raimundo et al., 2016). Therefore, it is critical to developing new therapies and new drugs for PF. Many traditional Chinese medicines (TCM) have played a certain role in the treatment of various systems of diseases (Huang et al., 2018). Chinese herbal extracts also have many effective pharmacological ingredients to treat PF (Ji et al., 2016; Huo et al., 2020). In the past 30 years, the pharmacological activity of polysaccharides has attracted increasing attention (Layek and Mandal, 2020). Japanese scholar, Chihara Hiroo, firstly discovered that lentinan has an anti-tumor effect in 1968, thus striking the research boom of natural active polysaccharides (Chihara et al., 1969). Polysaccharides are natural macromolecular compounds composed of monosaccharides. They, with abundant biological activities and obviously low toxicity, are one of the main active components of Chinese medicine. Polysaccharides have received wide attention thanks to their effective biological activities and multiple molecular targets



(Muhamad et al., 2019; Cao et al., 2020; Mohammed et al., 2021). Studies have shown that polysaccharides have a variety of biological activities, such as anti-tumor, anti-oxidation, anti-radiation, anti-virus, and hypoglycemic effects (Mu et al., 2021; Niu et al., 2021). The development and application of polysaccharides in Chinese herbal medicine have enriched the treatment methods of modern medicine. Nowadays, TCM polysaccharides have been widely used clinically to treat related diseases, such as astragalus polysaccharide injection, ganoderma polysaccharide injection, ginseng polysaccharide injection, etc. (Li et al., 2019b). As expected, TCM polysaccharides have protective effects on PF. For example, astragalus polysaccharides (APS) can reduce the degree of PF by inhibiting transforming growth factor- $\beta$ 1 (TGF- $\beta$ 1) *in vitro* and *in vivo* (Zhang, Xu, 2020). Ganoderma lucidum polysaccharides (GIP) inhibit bleomycin (BLM)-induced adult male SD rats by improving lung antioxidant capacity (Chen et al., 2016). Therefore, Chinese herbal polysaccharides provide a new way to discover and develop anti-PF.

Repeated local micro-injuries play a fatal role in the aging alveolar epithelium, these micro-injuries start the connection of abnormal epithelial cell with fibroblast, induce myofibroblasts that produce matrix, and remodel a large amount of ECM accumulation and lung interstitial. There are many sources of myofibroblasts, including resident mesenchymal cell proliferation, pulmonary interstitial cells, circulating fibroblasts, epithelial-mesenchymal transition (EMT) and endothelial-mesenchymal transition (Todd et al., 2012). The histological characteristics of PF are excessive deposition of matrix collagen, increased fibrosis area and increased hydroxyproline

(HYP) content, which can damage the normal structure and function of the lung. Activated alveolar epithelial cells secrete large amounts of fibrogenic growth factors and cytokines, including TGF- $\beta$ 1 and platelet-derived growth factors. TGF- $\beta$ 1 is an important regulator of fibrogenesis, which can activate fibroblasts and transform them into myofibroblasts (Organ et al., 2015), the initiation and regression of myofibroblasts herald disease progression. TGF- $\beta$ 1 not only promotes ECM deposition, but also concentrates it in the accumulated matrix, thereby accelerating it the pro-fibrotic reaction. The current pathogenesis of PF presumably includes abnormal accumulation of TGF- $\beta$ , cell recruitment, apoptosis, inflammatory factors, oxidative stress, and the imbalance of matrix metalloproteinase/tissue inhibitor of metalloproteinase (MMP/TIMP) (Ryu et al., 2014; Spagnolo et al., 2021) (Figure 2). Therefore, the use of various activities of Chinese herbal polysaccharides brings hope to the treatment of PF through these targets. Chinese herbal polysaccharides can participate in reversing the down-regulation of TGF- $\beta$  and protecting PF, and have broad prospects in the field of anti-PF research.

## Polysaccharides

### Ginseng Polysaccharide (GPS)

GPS is a polysaccharide isolated from ginseng roots, with an average molecular weight (Mw) of  $1.5 \times 10^6$  Da, mainly composed of Glc and Gal (over 90%, w/w) and 5–8% Man and Ara (Chen et al., 2020; Ahn et al., 2011; Ahn et al., 2011; Chen et al., 2020). It makes a variety of immunomodulatory functions, such as anti-oxidation, anti-tumor, anti-cancer and

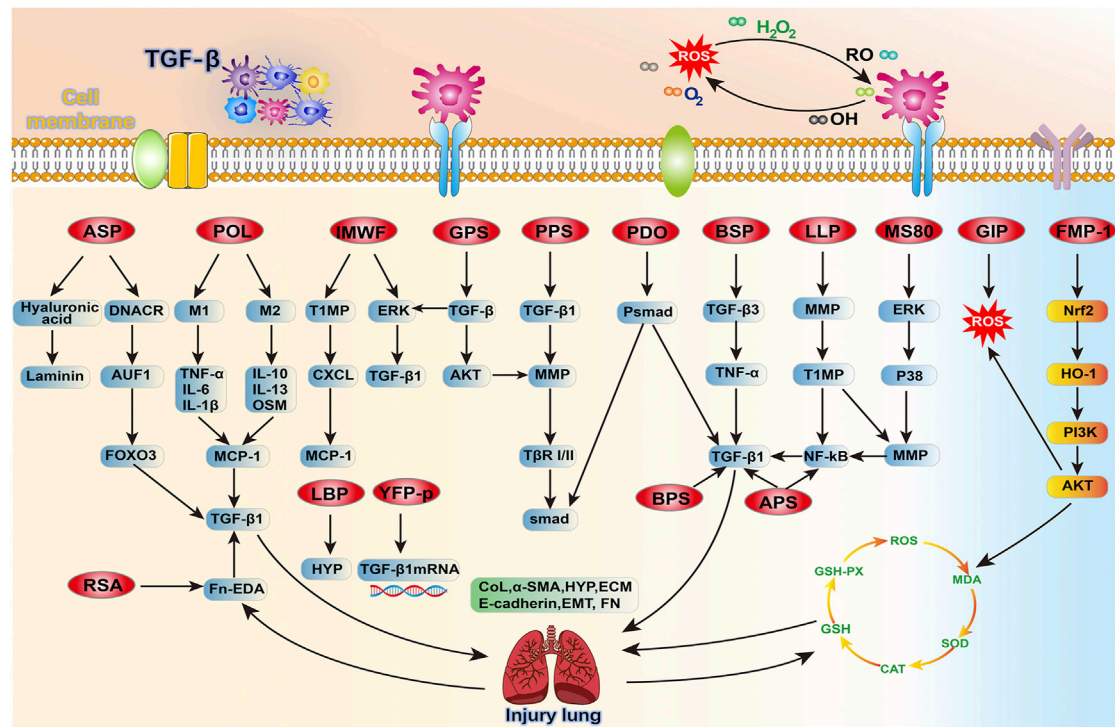


**FIGURE 3** | An overview of the target signaling pathways of 16 Chinese herbal polysaccharides that antagonize PF, mainly by reversing TGF- $\beta$  and improving ROS to treat pulmonary fibrosis, and further linking the relationship with these related pathways.

anti-adhesion (Akhter et al., 2018; Xiong et al., 2019). The Smad pathway is essential for TGF- $\beta$  mediated signal transduction (Wilkes et al., 2005). Studies have shown that GPS inhibits the phosphorylation of Smad2 and Smad3 in fibroblasts through TGF- $\beta$ , but has no response to the levels of Smad6 and Smad7, weakens the phosphorylation level of extracellular signal-regulated kinase/protein kinase B (ERK/AKT) and reverses the synthesis of collagen (COL)-1 and fibronectin (FN) also significantly reduces the protein expression of TGF- $\beta$ 1 receptor (T $\beta$ RI) and T $\beta$ RII in NIH/3T3 cells, preventing T $\beta$ RII from its known that the protein expression of receptor T $\beta$ RIII decreases, and it also inhibits the expression of  $\alpha$ -smooth muscle actin ( $\alpha$ -SMA) in IMR-90 and WI-38 cells (Ahn et al., 2011). Later, studies reported that ginsenosides can reduce EMT of lung tissue by inhibiting TGF- $\beta$ 1/Smad pathway (Guan et al., 2017). There are further reports that ginsenosides can prevent renal fibrosis (Li et al., 2018b). Recent observers have shown that ginseng can prevent liver, lung, kidney and myocardial fibrosis through TGF- $\beta$  (Liu et al., 2020a). Therefore, the possible mechanism of GPS anti-PF is that the downstream Smad2 and Smad3 signals of TGF- $\beta$ 1 and its T $\beta$ RI and T $\beta$ RII can achieve the treatment purpose, and reduce the phosphorylation of ERK and AKT, and reduce the level of MMPs, which is beneficial to lung tissue damage (Figure 3 and Table 1).

### Basil Polysaccharide (BPS)

BPS is extracted from the Chinese herbal medicine basil, basil is a daily dish prepared in summer. BPS is a compound

polysaccharide composed of fructose. It is mainly composed of Man, Rha, Glc, Fru, and Ara, the Mw is  $(8-10) \times 10^4$  Da (Zhan et al., 2020). It has anti-tumor, anti-oxidation, anti-inflammatory, hypolipidemic, anti-diabetic and anti-liver cancer effects (Lv et al., 2013; Feng et al., 2018). Proves have shown that BPS has a potential inhibitory effect on the PF of human A549 cells induced by TGF- $\beta$ , and down-regulates the expression of  $\alpha$ -SMA and COL-1, up-regulates E-cadherin levels, and reduces HYP content (Yan et al., 2017), and proposed that BPS has an inhibitory effect on EMT (Feng et al., 2019). Therefore, BPS can reduce the inflammation of A549 cells by down-regulating TGF- $\beta$  signaling to combat PF.

### Astragalus polysaccharide (APS)

*Astragalus* as a medicinal and tonic food can keep fit and improve health. APS is a water-soluble polysaccharide isolated and purified from astragalus, the Mw is 1,334 kDa, composed of Rha, Ara, Glc, Gal, and GalA, the molar ratio is 0.03:1.00:0.27:0.36:0.30. The backbone of APS consisted of 1,2,4-linked Rhap,  $\alpha$ -1, 4-linked Glcp,  $\alpha$ -1, 4-linked GalAp6Me,  $\beta$ -1, 3, 6-linked Galp, with it branched at O-4 of the 1,2,4-linked Rhap and O-3 or O-4 of  $\beta$ -1, 3, 6-linked Galp. The side chains mainly consisted of  $\alpha$ -T-Araf and  $\alpha$ -1, 5-linked Araf with O-3 as branching points, having trace Glc and Gal, the terminal residues were T-linked Araf, T-linked Glcp, and T-linked Galp (Bao et al., 2018), its chemical structure is 2-(chloromethyl)-4-(4-nitrophenyl)-1,3-thiazole (Liu et al., 2019a). APS has been reported that have a variety of biological activities, including anti-inflammatory,

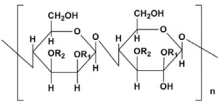
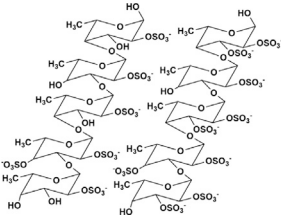
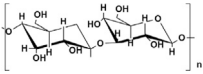
**TABLE 1** | Overview of the research progress of Chinese herbal medicine polysaccharides in the treatment of PF.

Name	Monosaccharides composition	Mw (kDa)	Molecular structure	Experimental model	Anti-PF effect	References
GPS	Glc and Gln (over 90%, w/w) and 5–8% Man and Ara	$1.5 \times 10^6$ Da	—	<i>In vivo</i> : BLM induced male C57BL/6 mice. <i>In vitro</i> : TGF- $\beta$ 1 induced NIH/3T3 cells and IMR-90 and WI-38 cells	Through the downstream Smad2 and Smad3 signals of TGF- $\beta$ 1 and its T $\beta$ R I and T $\beta$ RII, the treatment is achieved, which the levels of COL and $\alpha$ -SMA decreased, weaken the phosphorylation of ERK and AKT, reduce the level of MMPs to reduce lung tissue damage	(Ahn et al., 2011; Akhter et al., 2018; Xiong et al., 2019; Chen et al., 2020)
BPS	Man, Rha, Glc, Fru, Ara	$(8\text{--}10) \times 10^4$ Da	—	<i>In vitro</i> : TGF- $\beta$ induced A549 cells	BPS can reduce the inflammation of A549 cells by down-regulating TGF- $\beta$ signaling to combat PF.it can reduce HYP and COL content, down-regulate the expression of $\alpha$ -SMA, and up-regulate the level of E-cadherin	(Lv et al., 2013; Yan et al., 2017; Feng et al., 2018; Zhan et al., 2020)
APS	Rha:Ara: Glc:Gal:GalA = 0.03:1.00:0.27:0.36:0.30	1,334 kDa	 Chemical structure of APS: 2-(Chloromethyl)-4-(4-nitrophenyl)-1,3-thiazole	<i>In vivo</i> : BLM induced male C57BL/6 mice. <i>In vitro</i> : TGF- $\beta$ 1 induced A549 cells	Regulate EMT and HYP content through the TGF- $\beta$ 1/NF- $\kappa$ B pathway, and reduce the area of $\alpha$ -SMA, COL deposition and fibrosis, and increase E-cadherin	(Bao et al., 2018; Ren et al., 2018; Jia et al., 2019; Liu et al., 2019a; Zhang et al., 2020)
PPS	Component consisting of (1 $\rightarrow$ 3)- $\beta$ -glucan backbone and (1 $\rightarrow$ 6)- $\beta$ -glucopyranose side chains	$1.6 \times 10^5$ Da	 Chemical structure of PPS.	<i>In vivo</i> : BLM induced male C57BL/6 mice. <i>In vitro</i> : TGF- $\beta$ 1 induced in HLFs cells	The further deterioration of PF was prevented by TGF- $\beta$ 1/Smad2/3/T $\beta$ R I and T $\beta$ R II/MMP signaling, resulting in the decrease of $\alpha$ -SMA, MMP2/9, FN, COL-1/3 and ECM.	(Li et al., 2010; Zong et al., 2012; Guo et al., 2019; Jiang et al., 2020)
RSA	Ara:Rha:Xyl: Glc:Gal: GalA = 1.00:3.23:0.26:0.34:0.84:10.24	50,000 Da	—	<i>In vitro</i> : TGF- $\beta$ 1 induced A549 cells	RSA inhibits the process of TGF- $\beta$ 1 inducing A549 cells and down-regulates the expression of Fn-EDA.	(Han et al., 2002; Li et al., 2016; Yang et al., 2016; Song et al., 2019)
PDO	Man:Glc = 5.9:1, it is composed of (1 $\rightarrow$ 4)-linked Man and (1 $\rightarrow$ 4)-linked Glc	$1.78 \times 10^5$ Da	 (1 $\rightarrow$ 4)-linked Man  (1 $\rightarrow$ 4)-connected Glc	<i>In vivo</i> : BLM induced adult male Sprague Dawley rats. <i>In vitro</i> : TGF- $\beta$ 1 induced type II alveolar epithelial cells (RLE-6TN, CRL-2300)	PDO can reduce the number of neutrophils in rat lung tissue induced by BLM, improve inflammation and fibrosis, enhance Smad2/3 and inhibit the expression of pSmad2/3 protein through TGF $\beta$ 1, thereby inhibiting the type II rat alveolar epithelial cells (RLE-6TN, CRL-2300) induced by TGF- $\beta$ 1 fibronectin and COL-1	(He et al., 2016; Wang et al., 2017a; Chen et al., 2018; Yu et al., 2018c; Liu et al., 2019b)
BSP	BSP-1:Man:Glc = 4.0:1.0, BSP-2: Man:Glc = 3.0:1.0, the backbone of BSP-1 and BSP-2 were consisted of $\beta$ -1,4-linked D-Man residues and $\beta$ -1,4-linked D-Glc residues	BSP: $2.23 \times 10^5$ kDa, BSP-1: $8.354 \times 10^4$ Da, BSP-2: $1.26 \times 10^4$ Da	 The main residues sequence of BSP-1 was deduced to be: $\rightarrow$ 4)- $\beta$ -D-Glcp (1 $\rightarrow$ 4)- $\beta$ -D-Manp (1 $\rightarrow$ 4)- $\beta$ -D-Manp (1 $\rightarrow$ 4)- $\beta$ -D-Manp (1 $\rightarrow$ 4)- $\beta$ -D-Manp (1 $\rightarrow$ , The O-acetyl group position was also attached to C-3 of residue B (Man).  The residues sequence of BSP-2 was deduced to be: $\rightarrow$ 4)- $\beta$ -D-Glcp (1 $\rightarrow$ 4)- $\beta$ -D-Manp (1 $\rightarrow$ 4)- $\beta$ -D-Manp (1 $\rightarrow$ 4)- $\beta$ -D-Manp (1 $\rightarrow$	<i>In vivo</i> : BLM induced male SD rats	BSP can reduce cell recruitment to protect lung tissue inflammation, HYP, $\alpha$ -SMA content is significantly reduced, and it also improves TGF- $\beta$ 3 and TNF- $\beta$ 1	(Guo et al., 2016; He et al., 2017; Wang et al., 2019b; Liu et al., 2020b)

(Continued on following page)

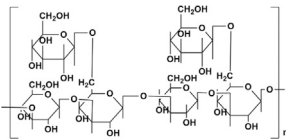


**TABLE 1 |** (Continued) Overview of the research progress of Chinese herbal medicine polysaccharides in the treatment of PF.

Name	Monosaccharides composition	Mw (kDa)	Molecular structure	Experimental model	Anti-PF effect	References
MS80	New type of sulfated oligosaccharide (1→4α-d-Glc)	8,000 Da	 <p>Chemical structure of MS80. R1 = SO<sub>3</sub>Na, R2 = SO<sub>3</sub>Na or H, n = 10~15</p>	<i>In vivo</i> : BLM induced pathogen-free adult Wistar rats. <i>In vitro</i> : TGF-β1 induced HEPF cells	MS80 can improve PF through TGF-β1/MMP/ERK/NF-κB/p38, prevent COL deposition, and reduce COL and EMT content	(Jiang and Guan, 2009; Zhou et al., 2016; Chen et al., 2020)
LMWF	Rha, Fuc, Xly, Man, Glc, Gal, GlcA, Gala, the linkage is backbone →3)-Galp-(1→, →6)-Glc-(1→, →6)-Galp-(1→, →3,6)-manp-(1→ with →3)-Fucp-(1→, →4)-Glc-(1→ and sulfated end units. Consists of (1→3)-linked α-thiopropionyl residues or alternating (13→)- and (→14)-linked α-thiophosphoryl residues	8~10 kDa	 <p>The overview of fucoidan regulation on signaling molecules</p>	<i>In vivo</i> : BLM-induced male C57BL/6 mice. <i>In vitro</i> : TGF-β1 induced A549 cells	LMWF treats PF through TGF-β1/ERK signaling and improving inflammatory cytokines in pathological lung tissue, attenuates the expression of lung EMT phenotype α-SMA and HYP.	(Senthilkumar and Kim, 2014; Haddad et al., 2015; Wang et al., 2019a; Wang et al., 2018; Yu et al., 2018a; Zheng et al., 2018; Chen et al., 2020)
ASP	GalA:Glc:Ara:Gal = 1.00:1.70:1.85:5.02, its main chain is composed of (1→3)-connected Galp, (1→6)-connected Galp and 2-OMe-(1→6)-connected Galp, with three branches connected to 2-OMe-(1→6) link Galp and terminate with GlcPA and Araf	80 kDa, 85 kDa	 <p>Chemically modified with branched LMW PEI (1,200 Da) to obtain cationic ASP.</p>	<i>In vivo</i> : BLM induced healthy Wistar rats and Sprague-Dawley rats. <i>In vitro</i> : TGF-β1 induced alveolar type II epithelial (RLE-6TN) cells	ASP can inhibit EMT and PF through the TGF-β1/DANCR/AUF-1/FOXO3 regulatory axis, reduce and reverse the expression levels of α-SMA, COL and E-cadherin	(Deng et al., 2013a; Zhang et al., 2016; Li et al., 2020a; Qian et al., 2020; Wang et al., 2010; Xu et al., 2021)
POL	Gal: Man:Glc = 5.30:13.38:81.31	3.2 × 10 <sup>5</sup> Da	—	<i>In vivo</i> : BLM induced male C57BL/6 mice	Improve lung inflammation by inhibiting the excessive recruitment of M1 and M2 under TGF-β1 to achieve a therapeutic effect, reducing the levels of MCP-1, TNF-α, IL-1β, IL-6, IL-10, IL-13, and OSM.	(Zhang et al., 2017; Ying-Mei et al., 2020; Zhou et al., 2020)
LBP	Glycan backbone is mainly represented by α-(1→4)-GalA, α-(1→6)-Glc, β-(1→3)-Galp (typical arabinogalactan protein) and β-(1→6)-Giap, other structures that are less representative are α-(1→5)-Ara and β-(1→4)-Galp	10~2,300 kDa	—	<i>In vivo</i> : BLM induced C57BL/6 mice	Inhibit the increase of HYP content in lung tissue when PF occurs, inhibit the increase of ECM, and reduce the expression levels of α-SMA and COL-1	(Liu et al., 2016b; Masci et al., 2018; Huang et al., 2019; Tian et al., 2019)
FMP-1	Man:Glc:Gal = 1.00:7.84:1.24, the main chain is 1,4-linked Glcp and 1,6-connected Galp composition	4.7 × 10 <sup>3</sup> Da	—	<i>In vitro</i> : H2O2 induced human alveolar epithelial cells (A549)	FMP-1 can be used as a natural potential antioxidant to treat PF through the Nrf2/HO-1/PI3K/AKT signaling pathway, which can weaken MDA and ROS levels, increase SOD enzyme activity and total antioxidant capacity	(Liu et al., 2016a; Li et al., 2017; Cai et al., 2018; Li et al., 2018c)

(Continued on following page)

**TABLE 1 |** (Continued) Overview of the research progress of Chinese herbal medicine polysaccharides in the treatment of PF.

Name	Monosaccharides composition	Mw (kDa)	Molecular structure	Experimental model	Anti-PF effect	References
GIP	Gal:Rha:Glc = 1.00:1.15:3.22, backbone structure is mainly composed of 1,2-linked $\beta$ -L Rhap, 1,3,6-linked $\alpha$ D-Galp, 1,2,6-linked $\alpha$ D-Glcp and 1-link $\alpha$ D-Glcp	78 kDa	 Structure of $\beta$ -glucan in GIP.	<i>In vivo</i> : BLM induced adult male SD rats	Improve the status of PF by improving the antioxidant capacity of the lung, reducing inflammatory cell infiltration and collagen deposition, improving the content of CAT and SOD, increasing the levels of GSH, GSH-Px, and reducing the content of MDA and HYP in lung tissue	(Pan et al., 2012; Chen et al., 2016; Wang et al., 2017b; Sohetoglu and Huang, 2018; Zeng et al., 2018; Zeng et al., 2019)
LLP	LLP-1:Glc:Man = 1:2, LLP-2:Glc:Man = 1:1, LLP-3:Ara:Gal: Glc: Man = 2:2:2:1	LLP-1:2.25 $\times$ 10 <sup>6</sup> Da, LLP-2: 2.02 $\times$ 10 <sup>6</sup> Da, LLP-3:2.08 $\times$ 10 <sup>6</sup> Da	—	<i>In vivo</i> : BLM induced SPF Kunming mice	Inhibit MMP-9 and TIMP-2 in lung tissue of BLM pulmonary fibrosis mice, reduce HYP content and COL level, and inhibit the expression of TNF- $\alpha$ , NF- $\kappa$ B in lung tissue of pulmonary fibrosis	(Chen et al., 2014; Hou et al., 2016; Li et al., 2020b; Luo et al., 2013a)
YPF-p	—	—	—	<i>In vivo</i> : pingyangmycin hydrochloride induced Wistar rats and BLM induced healthy adult female Sprague-Dawley rats	YPF-p treats PF by down-regulating the expression of TGF- $\beta$ 1 mRNA and improving the excessive aggregation of fibroblasts induced by TGF- $\beta$ 1, which reduces the expression of HYP, COL and $\alpha$ -SMA in lung tissue	(Wang et al., 2009; Xu et al., 2014; Sun et al., 2016; Fan et al., 2017)

anti-tumor, anti-diabetic and anti-oxidant (Ren et al., 2018; Jia et al., 2019). Previous reports suggested that astragalus injection and astragaloside IV have therapeutic effects on fibrosis (Qian et al., 2018). APS can protect renal fibrosis (Ren et al., 2019). *Astragalus* can improve EMT through  $\beta$ -catenin (Yu et al., 2018b). The overproduction of TGF- $\beta$ 1 is always closely related to PF, and TGF- $\beta$ 1 plays a key role in inducing EMT (Walton et al., 2017), nuclear factor- $\kappa$ B (NF- $\kappa$ B) regulates the expression of a variety of cytokines and inflammatory mediators, by inhibiting the expression of TGF- $\beta$ 1/NF- $\kappa$ B to block related signal pathways and prevent inflammation and reduce liver fibrosis (Li et al., 2018a). A recent observation proposed that APS can reduce PF through the TGF- $\beta$ 1/NF- $\kappa$ B pathway, which can effectively improve the deposition of COL-1, COL-3, and FN *in vivo*, APS reduce the area of fibrosis and HYP content in the matrix, and reduce the expression of  $\alpha$ -SMA neutralizes E-cadherin, it significantly reduces the activation of the EMT and NF- $\kappa$ B pathways of TGF- $\beta$ 1 *in vitro* (Zhang et al., 2020). Therefore, the mechanism of APS protecting PF is the regulation of TGF- $\beta$ 1/NF- $\kappa$ B pathway.

### Polyporus Polysaccharide (PPS)

The pharmaceutical ingredients of polyporus umbellatus include polysaccharides, ergosterol, biotin, protein and other molecules, among which PPS is one of the main biologically active substances of polyporus umbellatus, the main components of PPS are (1–3)- $\beta$ -Glc main chain and (1–6)- $\beta$ -Glc side chain  $\beta$ -glucan, the Mw is about  $1.6 \times 10^5$  Da (Zong et al., 2012). Previous studies have reported various pharmacological activities

of PPS, such as anti-tumor, anti-cancer, anti-oxidation and anti-inflammatory (Li et al., 2010; Guo et al., 2019). In renal fibrosis, PPS can improve the accumulation of TGF- $\beta$ 1, restore the balance of MMP/TIMP factors and improve renal fibrosis (Li et al., 2019a). PPS can significantly inhibit the ECM components in human lung fibrosis (HLFs) cells treated with TGF- $\beta$ 1, and inhibit Smad2/3 phosphorylation even reduce T $\beta$ RI and T $\beta$ RII, but it has no effect on T $\beta$ RIV and can also inhibit medium MMP-2/MMP-9 expression (Jiang et al., 2020). Therefore, PPS prevented the further deterioration of PF through TGF- $\beta$ 1/Smad2/3/T $\beta$ RI, and T $\beta$ RII/MMP level signals.

### Rhodiolasachalinensis Polysaccharide A (RSA)

RSA is an acidic heteropolysaccharide isolated from rhodiola alpina, its mainly composed of Ara, Rha, Xyl, Glc, Gal, and GalA, the molar ratio is 1.00:3.23:0.26:0.34:0.84:10.24, and the relative Mw is about 50,000 Da (Han et al., 2002), has anti-oxidant, anti-viral, anti-oxidant and anti-tumor effects (Yang et al., 2016; Song et al., 2019). Previous evaluations have reported that salidroside protects mice from acute lung injury through the NF- $\kappa$ B pathway by controlling the production of inflammatory cytokines, and is very effective in preventing oxidative stress after exercise in mice (Guan et al., 2012). Studies have suggested that RSA can significantly inhibit the death rate of A549 cells induced by TGF- $\beta$ 1 and the expression of the mesenchymal marker Fibronectin-EDA (Fn-EDA) (Li, et al., 2016). Rhodiola rosea significantly reduced the expression levels of MMP-9 and  $\alpha$ -SMA

in PF in a dose-dependent manner (Zhang et al., 2016). Therefore, RSA can improve the abnormality of Fn-EDA through TGF- $\beta$ 1 to achieve the purpose of treating PF.

## Polysaccharides From *Dendrobium Officinale* (PDO)

*Dendrobium officinale* is an epiphytic herb of the orchid family with mainly grows on semi-shaded moist rocks at an altitude of about 1,600 m in the Nanshan mountains of China. PDO is a neutral heteropolysaccharide isolated from the Chinese medicinal material *dendrobium candidum*, with composed of (1 $\rightarrow$ 4)-linked Man and (1 $\rightarrow$ 4)-linked Glc, the molar ratio is 5.9:1 and the Mw is  $1.78 \times 10^5$  Da (He et al., 2016; Yu W. et al., 2018). It has the effects of anti-oxidation, anti-tumor, anti-viral, anti-aging, lowering blood sugar and promoting hair growth (Wang J.-H. et al., 2017; Liu et al., 2019b), and is often valued in the field of dermatology. *Dendrobium nobile* polysaccharides can improve the antioxidant capacity of rats and reduce liver inflammation, so it has an antagonistic effect on liver fibrosis (Sibinska et al., 2017). Early studies on *dendrobium candidum* can treat myocardial fibrosis (Zhang et al., 2016b; Zeng et al., 2020). PDO can reduce the number of neutrophils in lung tissue induced by BLM, improve inflammation and fibrosis, enhance Smad2/3 and inhibit the expression of pSmad2/3 protein through TGF $\beta$ 1, thereby inhibiting the type II rat alveolar epithelial cells (RLE-6TN, CRL-2300) induced by TGF- $\beta$ 1 fibronectin and COL-1 (Chen et al., 2018). Therefore, PDO treatment of PF lies in the regulation of TGF- $\beta$ 1/Smad2, Smad3/pSmad2/3.

## Bletilla Striata Polysaccharide (BSP)

Two water-soluble polysaccharides, BSP-1 and BSP-2, were extracted and purified from *bacillus striata* tuber, and their Mw are  $8.354 \times 10^4$  and  $1.26 \times 10^4$  Da, both BSP-1 and BSP-2 are composed of Man and Glc, and the molar ratio are 4.0:1.0 and 3.0:1.0. The backbone is mainly composed of repeated  $\beta$ -1,4-linked d-Man residues and  $\beta$ -1, 4-linked d-Glc residue composition. It has anti-ulcer, anti-oxidation, anti-inflammatory, anti-tumor and immunomodulatory activities (He et al., 2017; Liu et al., 2020). BSP can protect renal fibrosis through the down-regulation of T $\beta$ RI, T $\beta$ RII and  $\alpha$ -SMA mediated by TGF- $\beta$  (Wang et al., 2014). Some researchers have confirmed that a Mw of  $2.23 \times 10^5$  kDa, BSP can reduce cell recruitment to protect lung tissue inflammation, the content of HYP is significantly reduced, TGF- $\beta$ 3 and TNF- $\beta$ 1 are also improved, they also proved that bletilla striata extract also has a certain degree of resistance the role of fibrosis (Guo et al., 2016). Therefore, BSP improves lung inflammation and abnormal cell recruitment through TGF- $\beta$ /TNF to improve lung tissue fibrosis.

## Seaweed Sulfated Oligosaccharide (MS80)

Marine macroalgae are mainly divided into four parts, green algae, cyanobacteria, brown algae and red algae. MS80 is a new type of sulfated oligosaccharide (1 $\rightarrow$ 4 $\alpha$ -d-Glc) extracted from seaweed, with the Mw is 8,000 Da, MS80 can anti-cancer, anti-inflammatory and anti-tumor (Chen et al., 2020). MS80 inhibits BLM-induced PF *in vivo*, antagonizes TGF- $\beta$ 1-induced human

embryo pulmonary fibroblast (HEPF) cells proliferation *in vitro*, prevents COL deposition and MMP activity, and inactivates ERK and p38 signaling pathways (Jiang and Guan, 2009). In addition, the MS80 targeting protein is receptor interacting protein 2 (a key component of CD40 signal transduction). MS80 inhibits the activation of NF- $\kappa$ B induced by CD40 linkage, thereby inhibiting the secretion of inflammatory cytokines, COL synthesis and fibrogenesis the excessive proliferation of cells confirms that MS80 has anti-fibrosis effects both *in vivo* and *in vitro* (Du et al., 2010). MS80 can also effectively inhibit standardized TGF- $\beta$ 1/Smad signaling, thereby improving the changes in EMT marker levels (Zhou et al., 2016). Therefore, MS80 can improve PF through TGF- $\beta$ 1/MMP/ERK/NF- $\kappa$ B/p38.

## Low Molecular Weight Fucoidan (LMWF)

LMWF is a sulfated polysaccharide extracted from brown algae, the Mw is 8–10 kDa, containing Rha, Fuc, Xly, Man, Glc, Gal, GlcA and Gala, the linkage is backbone  $\rightarrow$ 3)-Galp-(1 $\rightarrow$ ,  $\rightarrow$ 6)-Glc-(1 $\rightarrow$ ,  $\rightarrow$ 6)-Galp-(1 $\rightarrow$ ,  $\rightarrow$ 3,6)-manp-(1 $\rightarrow$  with  $\rightarrow$ 3)-Fucp-(1 $\rightarrow$ ,  $\rightarrow$ 4)-Glc-(1 $\rightarrow$  and sulfated end units (Chen et al., 2020), consists of (1 $\rightarrow$ 3)-linked  $\alpha$ -thiopropionyl residues or alternating (13 $\rightarrow$ )- and ( $\rightarrow$ 14)-linked  $\alpha$ -thiophosphoryl residues. Depending on previous studies, LMWF can lower blood sugar, anti-inflammatory, and promote angiogenesis (Haddad et al., 2015; Wang et al., 2018; Zheng et al., 2018). LMWF has an antagonistic effect on liver fibrosis through the TGF- $\beta$ 1/Smad3 pathway (Hayashi et al., 2008). Its also inhibit the proliferation of breast cancer cells and the expression of EMT biomarkers (Hsu et al., 2013). In addition, LMWF can reduce inflammation of the inflammatory cytokines TIMP-1, chemokine ligand 1 (CXCL1), monocyte chemotactic protein-1 (MCP-1), and macrophage inflammation protein-2 (MIP-2) of lung tissue, TNF content to improve radiation-induced pneumonia in mice and further PF (Yu H.-H. et al., 2018). LMWF inhibits the morphological changes and proliferation of A549 cells induced by TGF- $\beta$ 1. In the male C57BL/6 mice model, LMWF attenuates the lung EMT phenotype. LMWF down-regulates TGF- $\beta$ 1/ERK signals *in vivo* and *in vitro* to regulate PF (Wang et al., 2019a). Therefore, LMWF treats PF through TGF- $\beta$ 1/ERK signal and improves inflammatory cytokines in pathological lung tissue.

## Angelica Sinensis Polysaccharide (ASP)

ASP is an acidic heteropolysaccharide extracted from the root of angelica sinensis, its composed of GalA, Glc, Ara and Gal with the molar ratio of 1.00:1.70:1.85:5.02, the Mw is 80 kDa. Its main chain is composed of (1 $\rightarrow$ 3)-connected Galp, (1 $\rightarrow$ 6)-connected Galp and 2-OMe-(1 $\rightarrow$ 6)-connected Galp, with three branches connected to 2-OMe-(1 $\rightarrow$ 6) link Galp and terminate with GlcA and Araf (Zhang et al., 2016a). ASP has immune regulation, anti-tumor, anti-oxidation and anti-proliferation functions (Li M. M. et al., 2020; Xu et al., 2021). There is also the ability of the compound Danggui Buxue Decoction total glycosides (containing astragalus and angelica) to inhibit abnormal lung tissue ECM and reverse the expression of MMP/TIMP (Gao et al., 2012). ASP can improve the content of hyaluronic acid and laminin in the lung tissue of rats with PF

induced by BLM (Wang et al., 2010). The latest report points out that ASP inhibits PF by down-regulating the expression of differentiation-antagonizing non-protein coding RNA (DANCR), which inactivates FOXO3 translation after transcription in an AU binding factor 1 (AUF1)-dependent manner (Qian et al., 2020). Therefore, ASP can inhibit EMT and PF through the TGF- $\beta$ 1/DANCR/AUF-1/FOXO3 regulatory axis.

## Total Polysaccharide From *O. Lanpingensis* (POL)

POL is an insect fungal polysaccharide isolated from cordyceps Lanping. It is mainly distributed in northwestern Yunnan, China as a new species reported in recent years, which is closely a relative species of cordyceps sinensis. POL Mw is  $3.2 \times 10^5$  Da, composed of Gal, Man and Glc, and the molar ratio is 5.30:13.38:81.31 (Zhou et al., 2020). It was reported earlier that POL has an anti-inflammatory effect, which can improve liver fibrosis by alleviating the body's oxidative stress, reduce inflammation and anti-apoptosis of liver cells (Zhang et al., 2017). POL can treat renal insufficiency by enhancing antioxidant capacity and improving immune regulation ability (Ying-Mei et al., 2020). *Ophiocordyceps lanpingensis* can treat respiratory diseases. POL can significantly reduce the content of collagen in lung tissue and inflammation of lung tissue by inhibiting classically activated macrophages 1 (M1) and alternately activated M2 in lung tissue. The recruitment of PF inhibits the occurrence of PF (Zhou et al., 2020). Therefore, POL can improve lung inflammation by inhibiting the excessive recruitment of M1 and M2 under TGF- $\beta$ 1 to achieve a therapeutic effect.

## Lycium Barbarum Polysaccharide (LBP)

In the wolfberry extract, LBP isolated from the fruit of lycium barbarum caused the biological activity of the wolfberry. LBP is a group of water-soluble sugar conjugates with a Mw is 10–2,300 kDa, accounting for 5–8% of dried fruit. LBP glycan backbone is mainly represented by  $\alpha$ -(1 $\rightarrow$ 4)-galA,  $\alpha$ -(1 $\rightarrow$ 6)-glc,  $\beta$ -(1 $\rightarrow$ 3)-galp (typical arabinogalactan protein) and  $\beta$ -(1 $\rightarrow$ 6)-giap, other structures that are less representative are  $\alpha$ -(1 $\rightarrow$ 5)-ara and  $\beta$ -(1 $\rightarrow$ 4)-galp, which have different branching and terminal sites (Tian et al., 2019). LBP has the effects of lowering blood sugar, lowering blood lipid, anti-oxidation and anti-tumor effect (Masci et al., 2018; Huang et al., 2019). LBP possibly inhibit the expression of genes such as COL-1 and  $\alpha$ -SMA in inflamed lung tissues, weaken the excessive proliferation of fibroblasts and prevent their differentiation into myofibroblasts, thereby reducing the content of HYP in lung tissues to inhibit the development of PF in C57BL/6 mice (Liu et al., 2016b). Therefore, LBP inhibits PF by improving the degree of fibers in the lung tissue.

## Morel Polysaccharide-1 (FMP-1)

Morels belong to the category of mushrooms, with high nutritional value and delicious taste, both the flavor and the pharmacological effects have been highly regarded (Tietel and

Masaphy, 2018). FMP-1 is a heteropolysaccharide in morel fruiting body, the Mw is  $4.7 \times 10^3$  Da, composed of Man, Glc, and Gal with the molar ratio of 1.00:7.84:1.24, the main chain is 1,4-linked Glcp and 1,6-connected Galp composition (Cai et al., 2018). Previous studies have shown that morel contains many biologically active ingredients, such as polysaccharides, protein, dietary fiber and vitamins. FMP-1 has immunomodulatory, anti-oxidant, anti-value-added and anti-tumor effects (C. Liu et al., 2016a; Li et al., 2017). Controlling oxidative stress after lung injury has been shown to be effective in inhibiting fibrosis, it is proposed that polysaccharides can activate antioxidant defenses and improve oxidative stress damage (Hao et al., 2016; Chen et al., 2017). The phosphatidylinositol 3-kinase (PI3K)/AKT pathway is one of the effective ways to fight oxidative stress (Mozaffari et al., 2010), and it has a protective effect on lung epithelial cell death induced by oxidative stress (Deng et al., 2013b). Many examines have confirmed that the up-regulation of heme oxidase-1 (HO-1) is involved in the cells defense mechanism against the results of oxidation (Lee et al., 2012; Jang et al., 2016). Related research reports that FMP-1 can promote nuclear factor erythroid 2-related factor 2 (Nrf2) phosphorylation and nuclear translocation, and up-regulate downstream protein HO-1 through the PI3K/AKT-Nrf2 signaling pathway, thereby protecting human alveolar epithelial cells (A549) from hydrogen peroxide oxidative stress (Li et al., 2018c). Therefore, FMP-1 can be used as a natural potential antioxidant to treat PF through the Nrf2/HO-1/PI3K/AKT signaling pathway.

## Ganoderma Lucidum Polysaccharide (GIP)

Ganoderma is an edible medicinal mushroom, which has been praised for 2000 years. It can enhance human vitality. GIP is a neutral heteropolysaccharide isolated from ganoderma lucidum. It is composed of Gal, Rha and Glc with the molar ratio of 1.00:1.15:3.22, the Mw is 78 kDa, and the backbone structure is mainly composed of 1,2-linked  $\beta$ -L-Rhap, 1,3,6-linked  $\alpha$ -D-Galp, 1,2,6-linked  $\alpha$ -D-Glcp, and 1-link  $\alpha$ -D-Glcp consisted mainly of 1,2-linked  $\beta$ -L-Rhap, 1,3,6-linked  $\alpha$ -D-Galp, 1,2,6-linked  $\alpha$ -D-Glcp, and 1-linked  $\alpha$ -D-Glcp. (Pan et al., 2012). It is reported that a pure Glc polymer named  $\beta$ -glucan is considered to be one of the active ingredients of GIP (Zeng et al., 2019). GIP has many therapeutic effects on human diseases, including anti-oxidation, anti-inflammatory, anti-tumor, lowering blood sugar, lowering blood lipids, and anti-aging (Wang et al., 2017b; Sohretoglu and Huang, 2018; Zeng et al., 2018). In addition, it has been reported in the literature that GIP 100–300 mg/kg can reverse PF after 28 days. The main mechanism is related to the increase of lung antioxidant capacity. GIP can increase pathological lung tissue CAT (catalase), SOD (superoxide dismutation), GSH (glutathione), and GSH-Px (glutathione peroxidase) levels, simultaneously, reduce the content of MDA (malondialdehyde) and HYP in lung tissue (Chen et al., 2016). Later reports confirmed that ganoderma lucidum has obvious protective effect on oxidative damage caused by oxidants (Laçin et al., 2019; Lin and Deng, 2019). Ganoderic acid can treat renal fibrosis through TGF- $\beta$ /Smad and MAPK signaling (Geng et al., 2020). Therefore, GIP improves the status of PF by improving the lung's antioxidant capacity.



## Lily Polysaccharide (LLP)

LLP-1, LLP-2 and LLP-3 are the three new polysaccharide components in lily, their Mw are estimated to be  $2.25 \times 10^6$ ,  $2.02 \times 10^6$ , and  $2.08 \times 10^6$  Da, LLP-1 and LLP-2 are mainly composed of Glc and Man, with the molar ratio of 1:2 and 1:1, respectively, LLP-3 is mainly composed of Ara, Gal, Glc, and Man, with the molar ratio is 2:2:2:1 (Chen et al., 2014; Hou et al., 2016). LLP has a variety of activities, such as hypoglycemic, anti-oxidant and anti-cancer effects (Li et al., 2020b). LLP can improve the PF alveolar compartment and reduce the infiltration of inflammatory cells. The mechanism is to inhibit the protein expression of MMP-9 and TIMP-2 in the fibrosis model (Luo, et al., 2013a). LLP combined with bone marrow mesenchymal stem cell transplantation inhibits the expression of TNF- $\alpha$  and NF- $\kappa$ B in the lung tissue of PF mice, improves the recruitment of COL and reduces the content of HYP. LLP can reduce the pathological damage of PF (Luo, et al., 2013b). Therefore, LLP treats PF by adjusting the balance of MMP/TIMP in rats, improving the NF- $\kappa$ B signaling pathway and inflammatory TNF- $\alpha$  abnormalities in lung tissue.

## Yupingfeng–Polysaccharide (YPF-p)

Yupingfeng powder is a well-known TCM compound consisting of *Astragalus*, *Atractylodes* and *Fangfeng*. There are many compounds in Yupingfeng powder, including total polysaccharides, total saponins and volatile oil. Among them, YPF-p is one of the important components extracted from Yupingfeng powder, it has anti-inflammatory, anti-allergic, immune-regulating and alleviating effects of lung qi deficiency (Sun et al., 2016; Fan et al., 2017). Anti-fibrosis studies have found that YPF-p can improve the level of HYP in Wistar rats induced by pingyangmycin hydrochloride and the content of COL-3, COL-4, laminin, and hyaluronic acid in serum, and can down-regulate Wistar rats lungs. TGF- $\beta$ 1 mRNA expression in tissues (Wang et al., 2009). The mechanism presumably is that inhibit the increase of TGF- $\beta$ 1 mediated fibroblast activation and thus reduce synthesis (Xu et al., 2014). In addition, the total glycosides of Yupingfeng reduced the protein expression of box1 in the high mobility group, and reversed TGF- $\beta$ 1 to improve PF (Cui et al., 2015; Li et al., 2015). Therefore, YPF-p treats PF by down-regulating the expression of TGF- $\beta$ 1 mRNA and improving the excessive aggregation of fibroblasts induced by TGF- $\beta$ 1.

## CONCLUSION AND FUTURE PROSPECTS

These polysaccharides can significantly improve the abnormal recruitment and apoptosis of various cells in the lung tissue induced by the TGF- $\beta$  signaling pathway, regulate the imbalance of the body caused by lung inflammation, and can control lung tissue damage through oxidative stress, thus confirming these polysaccharides can stabilize PF lung function and prevent further damage.

Our understanding of this evolving deadly disease is constantly improving, but effective treatments are still elusive. PF is also one of the main complications of COVID-19. Studying the properties of polysaccharides and combining polysaccharides

with other drugs may provide medical help for PF patients with COVID-19. The epidemiological risk factors and biological process of PF and COVID-19 are similar. After severe acute respiratory syndrome coronavirus 2 (SARS-CoV-2) induced pneumonia may cause idiopathic PF related to its physical damage. Hence, modulating the mechanism of fibrosis in SARS-CoV-2 infection to exert a therapeutic effect may be acceptable. The chemical structure of Chinese herbal medicine polysaccharides is the basis of biological activity. Using the hydroxyl, carboxyl, amino, and other groups of sugar residues to modify the structure of polysaccharide molecules on the surface of polysaccharide molecules, For example, the GIP isolated from Fudan-Yueyang-G. lucidu has undergone methylation analysis, periodate oxidation, Smith degradation, and NMR characterization analysis to obtain a neutral polysaccharide with four residues A, B, C, and D which is significantly enhanced improve the lung's antioxidant capacity to achieve the purpose of treating PF, The structure determines the activity, can makes the multiple structure of the plant clearer, and seeks the regularity between the nanostructure and the biological activity to improve the immune activity of polysaccharides and reduce toxic effects. Chemical polysaccharides with different structures have great differences in biological activity. Further explore the relationship between the biological effects and efficacy of Chinese herbal medicine polysaccharides to explain the therapeutic mechanism of polysaccharides in PF. It is very important to provide a certain reference for the in-depth study and exploration of the structure-activity relationship of Chinese herbal medicine polysaccharides and the development and application of carbohydrate products. This provides important medical theory and economic value for the development of Chinese herbal polysaccharides to treat fibrotic diseases, and has a very important society. Polysaccharides can be a new type of anti-fibrosis treatment drugs. While, the structure of traditional Chinese medicine polysaccharides is complex and diverse, and its special active mechanism needs to be further studied. The establishment of specific, efficient and practical methods for the stability of polysaccharides is of great significance to the research and development of modern medicine.

## AUTHOR CONTRIBUTIONS

JS guided the experiment. XW and JH collected supporting evidence and wrote the paper. All authors read and approved the final article.

## FUNDING

The authors of this review were supported by the National Natural Science Foundation of China (82073311), the Key Research and Development Projects in Chengdu (2020-YF05-00058-SN), the Key Research and Development Projects in Sichuan Province (2020YFS0399), the Clinical Research and Transformation Foundation of Sichuan Provincial People's

Hospital (2021LZ03), the National Key Research and Development Program of China (2020YFC2005500), and the Key Research and

Development Program of Science and Technology Department of Sichuan Province (2019YFS0514).

## REFERENCES

- Ahn, J.-Y., Kim, M.-H., Lim, M.-J., Park, S., Lee, S.-I. -o., Yun, Y.-S., et al. (2011). The Inhibitory Effect of Ginsan on TGF- $\beta$  Mediated Fibrotic Process. *J. Cel. Physiol.* 226 (5), 1241–1247. doi:10.1002/jcp.22452
- Akhter, K. F., Mumin, M. A., Lui, E. M. K., and Charpentier, P. A. (2018). Fabrication of Fluorescent Labeled Ginseng Polysaccharide Nanoparticles for Bioimaging and Their Immunomodulatory Activity on Macrophage Cell Lines. *Int. J. Biol. Macromolecules* 109, 254–262. doi:10.1016/j.ijbiomac.2017.12.050
- Bao, W.-R., Li, Z.-P., Zhang, Q.-W., Li, L.-F., Liu, H.-B., Ma, D.-L., et al. (2018). Astragalus Polysaccharide RAP Selectively Attenuates Paclitaxel-Induced Cytotoxicity toward RAW 264.7 Cells by Reversing Cell Cycle Arrest and Apoptosis. *Front. Pharmacol.* 9, 1580. doi:10.3389/fphar.2018.01580
- Cai, Z.-N., Li, W., Mehmood, S., Pan, W.-J., Wang, Y., Meng, F.-J., et al. (2018). Structural Characterization, *In Vitro* and *In Vivo* Antioxidant Activities of a Heteropolysaccharide from the Fruiting Bodies of *Morchella Esculenta*. *Carbohydr. Polym.* 195, 29–38. doi:10.1016/j.carbpol.2018.04.069
- Canestaro, W. J., Forrester, S. H., Raghu, G., Ho, L., and Devine, B. E. (2016). Drug Treatment of Idiopathic Pulmonary Fibrosis. *Chest* 149 (3), 756–766. doi:10.1016/j.chest.2015.11.013
- Cao, P., Wu, S., Wu, T., Deng, Y., Zhang, Q., Wang, K., et al. (2020). The Important Role of Polysaccharides from a Traditional Chinese Medicine-Lung Cleansing and Detoxifying Decoction against the COVID-19 Pandemic. *Carbohydr. Polym.* 240, 116346. doi:10.1016/j.carbpol.2020.116346
- Chen, J., Lu, J., Wang, B., Zhang, X., Huang, Q., Yuan, J., et al. (2018). Polysaccharides from *Dendrobium Officinale* Inhibit Bleomycin-Induced Pulmonary Fibrosis via the TGF $\beta$ 1-Smad2/3 axis. *Int. J. Biol. Macromol.* 118 (Pt B), 2163–2175. doi:10.1016/j.ijbiomac.2018.07.056
- Chen, J., Shi, Y., He, L., Hao, H., Wang, B., Zheng, Y., et al. (2016). Protective Roles of Polysaccharides from *Ganoderma Lucidum* on Bleomycin-Induced Pulmonary Fibrosis in Rats. *Int. J. Biol. Macromolecules* 92, 278–281. doi:10.1016/j.ijbiomac.2016.07.005
- Chen, L., Liu, L., Li, C., Hu, C., Su, F., Liu, R., et al. (2017). A Mix of Apple Pomace Polysaccharide Improves Mitochondrial Function and Reduces Oxidative Stress in the Liver of High-Fat Diet-Induced Obese Mice. *Mol. Nutr. Food Res.* 61 (3), 1600433. doi:10.1002/mnfr.201600433
- Chen, R.-r., Li, Y.-j., Chen, J.-j., and Lu, C.-l. (2020). A Review for Natural Polysaccharides with Anti-pulmonary Fibrosis Properties, Which May Benefit to Patients Infected by 2019-nCoV. *Carbohydr. Polym.* 247, 116740. doi:10.1016/j.carbpol.2020.116740
- Chen, Z.-G., Zhang, D.-N., Zhu, Q., Yang, Q.-H., and Han, Y.-B. (2014). Purification, Preliminary Characterization and *In Vitro* Immunomodulatory Activity of Tiger Lily Polysaccharide. *Carbohydr. Polym.* 106, 217–222. doi:10.1016/j.carbpol.2014.02.004
- Chihara, G., Maeda, Y., Hamuro, J., Sasaki, T., and Fukuoka, F. (1969). Inhibition of Mouse Sarcoma 180 by Polysaccharides from *Lentinus Edodes* (Berk.) *Sing. Nature* 222 (5194), 687–688. doi:10.1038/222687a0
- Cui, W., Li, L., Li, D., Mo, X., Zhou, W., Zhang, Z., et al. (2015). Total Glycosides of Yupingfeng Protects against Bleomycin-Induced Pulmonary Fibrosis in Rats Associated with Reduced High Mobility Group Box 1 Activation and Epithelial-Mesenchymal Transition. *Inflamm. Res.* 64 (12), 953–961. doi:10.1007/s00011-015-0878-x
- Datta, A., Scotton, C. J., and Chambers, R. C. (2011). Novel Therapeutic Approaches for Pulmonary Fibrosis. *Br. J. Pharmacol.* 163 (1), 141–172. doi:10.1111/j.1476-5381.2011.01247.x
- Deng, W., Fu, M., Cao, Y., Cao, X., Wang, M., Yang, Y., et al. (2013a). Angelica Sinensis Polysaccharide Nanoparticles as Novel Non-viral Carriers for Gene Delivery to Mesenchymal Stem Cells. *Nanomedicine: Nanotechnology, Biol. Med.* 9 (8), 1181–1191. doi:10.1016/j.nano.2013.05.008
- Deng, X., Rui, W., Zhang, F., and Ding, W. (2013b). PM2.5 Induces Nrf2-Mediated Defense Mechanisms against Oxidative Stress by Activating PI3K/AKT Signaling Pathway in Human Lung Alveolar Epithelial A549 Cells. *Cell. Biol. Toxicol.* 29 (3), 143–157. doi:10.1007/s10565-013-9242-5
- Du, X., Jiang, S., Liu, H., Xin, X., Li, J., Geng, M., et al. (2010). MS80, a Novel Sulfated Polysaccharide, Inhibits CD40-NF-kappaB Pathway via Targeting RIP2. *Mol. Cel. Biochem.* 337 (1–2), 277–285. doi:10.1007/s11010-009-0309-9
- Fan, W., Zheng, P., Wang, Y., Hao, P., Liu, J., and Zhao, X. (2017). Analysis of Immunostimulatory Activity of Polysaccharide Extracted from Yu-Ping-Feng *In Vitro* and *In Vivo*. *Biomed. Pharmacother.* 93, 146–155. doi:10.1016/j.biopha.2017.05.138
- Feng, B., Zhu, Y., Su, Z., Tang, L., Sun, C., Li, C., et al. (2018). Basil Polysaccharide Attenuates Hepatocellular Carcinoma Metastasis in Rat by Suppressing H3K9me2 Histone Methylation under Hepatic Artery Ligation-Induced Hypoxia. *Int. J. Biol. Macromolecules* 107, 2171–2179. doi:10.1016/j.ijbiomac.2017.10.088
- Feng, B., Zhu, Y., Sun, C., Su, Z., Tang, L., Li, C., et al. (2019). Basil Polysaccharide Inhibits Hypoxia-Induced Hepatocellular Carcinoma Metastasis and Progression through Suppression of HIF-1 $\alpha$ -Mediated Epithelial-Mesenchymal Transition. *Int. J. Biol. Macromolecules* 137, 32–44. doi:10.1016/j.ijbiomac.2019.06.189
- Fiorucci, E., Lucantoni, G., Paone, G., Zotti, M., Li, B. E., Serpilli, M., et al. (2008). Colchicine, Cyclophosphamide and Prednisone in the Treatment of Mild-Moderate Idiopathic Pulmonary Fibrosis: Comparison of Three Currently Available Therapeutic Regimens. *Eur. Rev. Med. Pharmacol. Sci.* 12 (2), 105–111. doi:10.1016/S0924-977X(08)70017-8
- Galli, J. A., Pandya, A., Vega-Olivo, M., Dass, C., Zhao, H., and Criner, G. J. (2017). Pirfenidone and Nintedanib for Pulmonary Fibrosis in Clinical Practice: Tolerability and Adverse Drug Reactions. *Respirology* 22 (6), 1171–1178. doi:10.1111/resp.13024
- Gao, J., Feng, L.-j., Huang, Y., Li, P., Xu, D.-j., Li, J., et al. (2012). Total Glucosides of Danggui Buxue Tang Attenuates Bleomycin-Induced Pulmonary Fibrosis via Inhibition of Extracellular Matrix Remodelling. *J. Pharm. Pharmacol.* 64 (6), 811–820. doi:10.1111/j.2042-7158.2012.01490.x
- Geng, X.-q., Ma, A., He, J.-z., Wang, L., Jia, Y.-l., Shao, G.-y., et al. (2020). Ganoderic Acid Hinders Renal Fibrosis via Suppressing the TGF- $\beta$ /Smad and MAPK Signaling Pathways. *Acta Pharmacol. Sin.* 41 (5), 670–677. doi:10.1038/s41401-019-0324-7
- Guan, S., Liu, Q., Han, F., Gu, W., Song, L., Zhang, Y., et al. (2017). Ginsenoside Rg1 Ameliorates Cigarette Smoke-Induced Airway Fibrosis by Suppressing the TGF- $\beta$ 1/Smad Pathway *In Vivo* and *In Vitro*. *Biomed. Res. Int.* 2017, 1–12. doi:10.1155/2017/6510198
- Guan, S., Xiong, Y., Song, B., Song, Y., Wang, D., Chu, X., et al. (2012). Protective Effects of Salidroside from *Rhodiola Rosea* on LPS-Induced Acute Lung Injury in Mice. *Immunopharmacology and Immunotoxicology* 34 (4), 667–672. doi:10.3109/08923973.2011.650175
- Guo, N., Bai, Z., Jia, W., Sun, J., Wang, W., Chen, S., et al. (2019). Quantitative Analysis of Polysaccharide Composition in *Polyporus Umbellatus* by HPLC-ESI-TOF-MS. *Molecules* 24 (14), 2526. doi:10.3390/molecules24142526
- Guo, Q., Meng, Y., Zhao, Y., Cheng, X. C., Lu, Y. X., and Zhang, Q. L. (2016). Therapeutic Effect of Baiji Extract on Pulmonary Fibrosis Induced by Bleomycin in Rats. *J. Int. Pharm. Res.* 43 (3), 518–523. doi:10.13220/j.cnki.jipr.2016.03.022
- Haddad, O., Guyot, E., Marinval, N., Chevalier, F., Maillard, L., Gadi, L., et al. (2015). Heparanase and Syndecan-4 Are Involved in Low Molecular Weight Fucoidan-Induced Angiogenesis. *Mar. Drugs* 13 (11), 6588–6608. doi:10.3390/md13116588
- Han, L. P., Liang, Z. Y., Han, L. M., Gong, R. C., and Ma, X. H. (2002). Isolation, Purification and Composition Analysis of the Polysaccharide RSA of *Rhodiola Alpina*. *Chi. Pharm. J.* 06, 19–22. doi:10.3321/j.issn:1001-2494.2002.06.00610.1142/s0219030302001933
- Hao, L., Sheng, Z., Lu, J., Tao, R., and Jia, S. (2016). Characterization and Antioxidant Activities of Extracellular and Intracellular Polysaccharides from *Fomitopsis Pinicola*. *Carbohydr. Polym.* 141, 54–59. doi:10.1016/j.carbpol.2015.11.048

- Hayashi, S., Itoh, A., Isoda, K., Kondoh, M., Kawase, M., and Yagi, K. (2008). Fucoidan Partly Prevents CCl<sub>4</sub>-Induced Liver Fibrosis. *Eur. J. Pharmacol.* 580 (3), 380–384. doi:10.1016/j.ejphar.2007.11.015
- He, T.-B., Huang, Y.-P., Yang, L., Liu, T.-T., Gong, W.-Y., Wang, X.-J., et al. (2016). Structural Characterization and Immunomodulating Activity of Polysaccharide from *Dendrobium Officinale*. *Int. J. Biol. Macromolecules* 83, 34–41. doi:10.1016/j.ijbiomac.2015.11.038
- He, X., Wang, X., Fang, J., Zhao, Z., Huang, L., Guo, H., et al. (2017). Bletilla Striata: Medicinal Uses, Phytochemistry and Pharmacological Activities. *J. Ethnopharmacology* 195, 20–38. doi:10.1016/j.jep.2016.11.026
- Hou, R., Chen, J., Yue, C., Li, X., Liu, J., Gao, Z., et al. (2016). Modification of Lily Polysaccharide by Selenylation and the Immune-Enhancing Activity. *Carbohydr. Polym.* 142, 73–81. doi:10.1016/j.carbpol.2016.01.032
- Hsu, H.-Y., Lin, T.-Y., Hwang, P.-A., Tseng, L.-M., Chen, R.-H., Tsao, S.-M., et al. (2013). Fucoidan Induces Changes in the Epithelial to Mesenchymal Transition and Decreases Metastasis by Enhancing Ubiquitin-dependent TGF Receptor Degradation in Breast Cancer. *Carcinogenesis* 34 (4), 874–884. doi:10.1093/carcin/bgs396
- Huang, C., Yao, R., Zhu, Z., Pang, D., Cao, X., Feng, B., et al. (2019). A Pectic Polysaccharide from Water Decoction of Xinjiang Lycium Barbarum Fruit Protects against Intestinal Endoplasmic Reticulum Stress. *Int. J. Biol. Macromolecules* 130, 508–514. doi:10.1016/j.ijbiomac.2019.02.157
- Huang, K.-C., Su, Y.-C., Sun, M.-F., and Huang, S.-T. (2018). Chinese Herbal Medicine Improves the Long-Term Survival Rate of Patients with Chronic Kidney Disease in Taiwan: A Nationwide Retrospective Population-Based Cohort Study. *Front. Pharmacol.* 9, 1117. doi:10.3389/fphar.2018.01117
- Huo, J., Lu, Y., Xia, L., and Chen, D. (2020). Structural Characterization and Anticomplement Activities of Three Acidic Homogeneous Polysaccharides from *Artemisia Annuua*. *J. Ethnopharmacology* 247, 112281. doi:10.1016/j.jep.2019.112281
- Hutchinson, J., Fogarty, A., Hubbard, R., and McKeever, T. (2015). Global Incidence and Mortality of Idiopathic Pulmonary Fibrosis: a Systematic Review. *Eur. Respir. J.* 46 (3), 795–806. doi:10.1183/09031936.00185114
- Jang, H. J., Hong, E. M., Kim, M., Kim, J. H., Jang, J., Park, S. W., et al. (2016). Simvastatin Induces Heme Oxygenase-1 via NF-E2-Related Factor 2 (Nrf2) Activation through ERK and PI3K/Akt Pathway in colon Cancer. *Oncotarget* 7 (29), 46219–46229. doi:10.18632/oncotarget.10078
- Ji, S., Li, Z., Song, W., Wang, Y., Liang, W., Li, K., et al. (2016). Bioactive Constituents of Glycyrrhiza uralensis (Licorice): Discovery of the Effective Components of a Traditional Herbal Medicine. *J. Nat. Prod.* 79 (2), 281–292. doi:10.1021/acs.jnatprod.5b00877
- Jia, N., Qiao, H., Zhu, W., Zhu, M., Meng, Q., Lu, Q., et al. (2019). Antioxidant, Immunomodulatory, Oxidative Stress Inhibitory and Iron Supplementation Effect of Astragalus Membranaceus Polysaccharide-Iron (III) Complex on Iron-Deficiency Anemia Mouse Model. *Int. J. Biol. Macromolecules* 132, 213–221. doi:10.1016/j.ijbiomac.2019.03.196
- Jiang, H.-d., and Guan, H.-s. (2009). MS80, a Novel Sulfated Oligosaccharide, Inhibits Pulmonary Fibrosis by Targeting TGF- $\beta$ 1 Both *In Vitro* and *In Vivo*. *Acta Pharmacol. Sin.* 30 (7), 973–979. doi:10.1038/aps.2009.86
- Jiang, J., Wang, F., Luo, A., Lin, S., Feng, X., Yan, W., et al. (2020). Polyporus Polysaccharide Ameliorates Bleomycin-Induced Pulmonary Fibrosis by Suppressing Myofibroblast Differentiation via TGF- $\beta$ /Smad2/3 Pathway. *Front. Pharmacol.* 11, 767. doi:10.3389/fphar.2020.00767
- Layek, B., and Mandal, S. (2020). Natural Polysaccharides for Controlled Delivery of Oral Therapeutics: a Recent Update. *Carbohydr. Polym.* 230, 115617. doi:10.1016/j.carbpol.2019.115617
- Laçın, N., İzol, S. B., İpek, F., and Tuncer, M. C. (2019). Ganoderma Lucidum, a Promising Agent Possessing Antioxidant and Anti-inflammatory Effects for Treating Calvarial Defects with Graft Application in Rats. *Acta Cir. Bras.* 34 (9), e201900904. doi:10.1590/s0102-865020190090000004
- Lederer, D. J., and Martinez, F. J. (2018). Idiopathic Pulmonary Fibrosis. *N. Engl. J. Med.* 378 (19), 1811–1823. doi:10.1056/NEJMra1705751
- Lee, Y.-J., Jeong, H.-Y., Kim, Y.-B., Lee, Y.-J., Won, S. Y., Shim, J.-H., et al. (2012). Reactive Oxygen Species and PI3K/Akt Signaling Play Key Roles in the Induction of Nrf2-Driven Heme Oxygenase-1 Expression in Sulforaphane-Treated Human Mesothelioma MSTO-211H Cells. *Food Chem. Toxicol.* 50 (2), 116–123. doi:10.1016/j.fct.2011.10.035
- Li, D., Li, W., Chen, Y., Liu, L., Ma, D., Wang, H., et al. (2018a). Anti-fibrotic Role and Mechanism of *Periplaneta americana* Extracts in CCl<sub>4</sub>-Induced Hepatic Fibrosis in Rats. *Acta Biochim. Biophys. Sin.* 50 (5), 491–498. doi:10.1093/abbs/gmy024
- Li, H., Yan, Z., Xiong, Q., Chen, X., Lin, Y., Xu, Y., et al. (2019a). Renoprotective Effect and Mechanism of Polysaccharide from Polyporus Umbellatus Sclerotia on Renal Fibrosis. *Carbohydr. Polym.* 212, 1–10. doi:10.1016/j.carbpol.2019.02.026
- Li, L., Li, D., Xu, L., Zhao, P., Deng, Z., Mo, X., et al. (2015). Total Extract of Yupingfeng Attenuates Bleomycin-Induced Pulmonary Fibrosis in Rats. *Phytomedicine* 22 (1), 111–119. doi:10.1016/j.phymed.2014.10.011
- Li, M. M., Zhang, Y., Wu, J., and Wang, K. P. (2020a). Polysaccharide from Angelica Sinensis Suppresses Inflammation and Reverses Anemia in Complete Freund's Adjuvant-Induced Rats. *Curr. Med. Sci.* 40 (2), 265–274. doi:10.1007/s11596-020-2183-3
- Li, N., Yu, X., Yu, Q. H., and Wang, M. (2019b). Research Progress on Stability of Polysaccharides in Traditional Chinese Medicine. *Zhongguo Zhong Yao Za Zhi* 44 (22), 4793–4799. doi:10.19540/j.cnki.cjcm.20190916.309
- Li, S.-s., He, A.-l., Deng, Z.-y., and Liu, Q.-f. (2018b). Ginsenoside-Rg1 Protects against Renal Fibrosis by Regulating the Klotho/TGF- $\beta$ 1/Smad Signaling Pathway in Rats with Obstructive Nephropathy. *Biol. Pharm. Bull.* 41 (4), 585–591. doi:10.1248/bpb.b17-00934
- Li, W., Cai, Z.-N., Mehmood, S., Wang, Y., Pan, W.-J., Zhang, W.-N., et al. (2018c). Polysaccharide FMP-1 from Morchella Esculenta Attenuates Cellular Oxidative Damage in Human Alveolar Epithelial A549 Cells through PI3K/AKT/Nrf2/HO-1 Pathway. *Int. J. Biol. Macromolecules* 120 (Pt A), 865–875. doi:10.1016/j.ijbiomac.2018.08.148
- Li, W., Wang, Y., Wei, H., Zhang, Y., Guo, Z., Qiu, Y., et al. (2020b). Structural Characterization of Lanzhou Lily (Lilium Davidii Var. Unicolor) Polysaccharides and Determination of Their Associated Antioxidant Activity. *J. Sci. Food Agric.* 100 (15), 5603–5616. doi:10.1002/jsfa.10613
- Li, X., Xu, W., and Chen, J. (2010). Polysaccharide Purified from Polyporus Umbellatus (Per) Fr Induces the Activation and Maturation of Murine Bone-Derived Dendritic Cells via Toll-like Receptor 4. *Cell Immunol.* 265 (1), 50–56. doi:10.1016/j.cellimm.2010.07.002
- Li, Y., Yuan, Y., Lei, L., Li, F., Zhang, Y., Chen, J., et al. (2017). Carboxymethylation of Polysaccharide from Morchella Angusticeps Peck Enhances its Cholesterol-Lowering Activity in Rats. *Carbohydr. Polym.* 172, 85–92. doi:10.1016/j.carbpol.2017.05.033
- Li, Z. L., Gao, Y., Zhao, L., and Hong, B. (2016). Study on Rhodiola Polysaccharide against Pulmonary Fibrosis. *J. Mol. Sci.* 32 (01), 34–39. doi:10.13563/j.cnki.jmolsci.2016.01.004
- Lin, Z., and Deng, A. (2019). Antioxidative and Free Radical Scavenging Activity of Ganoderma (Lingzhi). *Adv. Exp. Med.* 1182, 271–297. doi:10.1007/978-981-32-9421-9\_12
- Liu, C., Li, H., Wang, K., Zhuang, J., Chu, F., Gao, C., et al. (2019a). Identifying the Antiproliferative Effect of Astragalus Polysaccharides on Breast Cancer: Coupling Network Pharmacology with Targetable Screening from the Cancer Genome Atlas. *Front. Oncol.* 9, 368. doi:10.3389/fonc.2019.00368
- Liu, C., Sun, Y., Mao, Q., Guo, X., Li, P., Liu, Y., et al. (2016a). Characteristics and Antitumor Activity of Morchella Esculenta Polysaccharide Extracted by Pulsed Electric Field. *Ijms* 17 (6), 986. doi:10.3390/ijms17060986
- Liu, D., Dong, L. J., Lei, T., and Ming, L. G. (2016b). The Interventional Effect and Mechanism of Lycium Barbarum Polysaccharides on Bleomycin-Induced Pulmonary Fibrosis in Mice. *J. Med. Postgraduates* 29 (09), 918–922. doi:10.16571/j.cnki.1008-8199.2016.09.006
- Liu, H., Lv, C., and Lu, J. (2020a). Panax Ginseng C. A. Meyer as a Potential Therapeutic Agent for Organ Fibrosis Disease. *Chin. Med.* 15 (1), 124. doi:10.1186/s13020-020-00400-3
- Liu, J., Li, Y., Liu, W., Qi, Q., Hu, X., Li, S., et al. (2019b). Extraction of Polysaccharide from Dendrobium Nobile Lindl. By Subcritical Water Extraction. *ACS. Omega.* 4 (24), 20586–20594. doi:10.1021/acsomega.9b02550
- Liu, Y., Sun, C., Zhang, G., Wu, J., Huang, L., Qiao, J., et al. (2020b). Bio-responsive Bletilla Striata Polysaccharide-Based Micelles for Enhancing Intracellular Docetaxel Delivery. *Int. J. Biol. Macromolecules* 142, 277–287. doi:10.1016/j.ijbiomac.2019.09.099
- Luo, Y. L., Cheng, X. L., Wang, Y. L., Li, N. L., She, Y. L., and Li, Y. (2013a). Lily Polysaccharide Inhibits the Expression of MMP-9 and TIMP-2 in Lung Tissue of Mice with Bleomycin-Induced Pulmonary Fibrosis. *Basic Clin. Med.* 3, 363–364. doi:10.16352/j.issn.1001-6325.2013.03.002



- Luo, Y. L., Wang, Y. L., Pan, Z., Li, N. L., Li, Y., Yan, X., et al. (2013b). Effect of Lily Polysaccharides Combined with BMSCs Transplantation on Expression of TNF-Alpha and NF-kappaB in Bleomycin-Induced Pulmonary Fibrosis Mice. *J. Third Mil. Med. Univ.* 35 (5), 431–434. doi:10.16016/j.1000-5404.2013.05.004
- Lv, J., Shao, Q., Wang, H., Shi, H., Wang, T., Gao, W., et al. (2013). Effects and Mechanisms of Curcumin and Basil Polysaccharide on the Invasion of SKOV3 Cells and Dendritic Cells. *Mol. Med. Rep.* 8 (5), 1580–1586. doi:10.3892/mmr.2013.1695
- Majewski, S., and Piotrowski, W. J. (2020). Air Pollution-An Overlooked Risk Factor for Idiopathic Pulmonary Fibrosis. *Jcm* 10 (1), 77. doi:10.3390/jcm10010077
- Masci, A., Carradori, S., Casadei, M. A., Paolicelli, P., Petralito, S., Ragno, R., et al. (2018). Lycium Barbarum Polysaccharides: Extraction, Purification, Structural Characterisation and Evidence about Hypoglycaemic and Hypolipidaemic Effects. A Review. *Food Chem.* 254, 377–389. doi:10.1016/j.foodchem.2018.01.176
- Miniati, I., and Matucci Cerinic, M. (2007). Pulmonary Fibrosis in Systemic Sclerosis: Is Treatment with Cyclophosphamide More Effective Than Placebo?. *Nat. Rev. Rheumatol.* 3 (7), 372–373. doi:10.1038/ncprheum0507
- Mohammed, A. S. A., Naveed, M., and Jost, N. (2021). Polysaccharides; Classification, Chemical Properties, and Future Perspective Applications in Fields of Pharmacology and Biological Medicine (A Review of Current Applications and Upcoming Potentialities). *J. Polym. Environ.* 29, 2359–2371. doi:10.1007/s10924-021-02052-2
- Mozaffari, M. S., Liu, J. Y., and Schaffer, S. W. (2010). Effect of Pressure Overload on Cardioprotection via PI3K-Akt: Comparison of Postconditioning, Insulin, and Pressure Unloading. *Am. J. Hypertens.* 23 (6), 668–674. doi:10.1038/ajh.2010.43
- Mu, S., Yang, W., and Huang, G. (2021). Antioxidant Activities and Mechanisms of Polysaccharides. *Chem. Biol. Drug Des.* 97 (3), 628–632. doi:10.1111/cbdd.13798
- MuhamadII, Zulkifli, N., Selvakumaran, S. a. p., and Lazim, N. A. M. (2019). Bioactive Algal-Derived Polysaccharides: Multi-Functionalization, Therapeutic Potential and Biomedical Applications. *Cpd* 25 (11), 1147–1162. doi:10.2174/1381612825666190618152133
- Niu, W., Chen, X., Xu, R., Dong, H., Yang, F., Wang, Y., et al. (2021). Polysaccharides from Natural Resources Exhibit Great Potential in the Treatment of Ulcerative Colitis: A Review. *Carbohydr. Polym.* 254, 117189. doi:10.1016/j.carbpol.2020.117189
- Organ, L., Bacci, B., Koumoundouros, E., Barcham, G., Kimpton, W., Nowell, C. J., et al. (2015). A Novel Segmental challenge Model for Bleomycin-Induced Pulmonary Fibrosis in Sheep. *Exp. Lung Res.* 41 (3), 115–134. doi:10.3109/01902148.2014.985806
- Pan, D., Wang, L., Chen, C., Teng, B., Wang, C., Xu, Z., et al. (2012). Structure Characterization of a Novel Neutral Polysaccharide Isolated from Ganoderma Lucidum Fruiting Bodies. *Food Chem.* 135 (3), 1097–1103. doi:10.1016/j.foodchem.2012.05.071
- Phan, T. H. G., Paliogiannis, P., Nasrallah, G. K., Giordo, R., Eid, A. H., Fois, A. G., et al. (2021). Emerging Cellular and Molecular Determinants of Idiopathic Pulmonary Fibrosis. *Cell. Mol. Life Sci.* 78 (5), 2031–2057. doi:10.1007/s00018-020-03693-7
- Qian, W., Cai, X., Qian, Q., Wang, D., and Zhang, L. (2020). Angelica Sinensis Polysaccharide Suppresses Epithelial-Mesenchymal Transition and Pulmonary Fibrosis via a DANCER/AUF-1/FOXO3 Regulatory Axis. *Aging Dis.* 11 (1), 17–30. doi:10.14336/ad.2019.0512
- Qian, W., Cai, X., Qian, Q., Zhang, W., and Wang, D. (2018). Astragaloside IV Modulates TGF- $\beta$ 1-dependent Epithelial-mesenchymal Transition in Bleomycin-induced Pulmonary Fibrosis. *J. Cel. Mol. Med.* 22 (9), 4354–4365. doi:10.1111/jcmm.13725
- Raimundo, K., Chang, E., Broder, M. S., Alexander, K., Zazzali, J., and Swigris, J. J. (2016). Clinical and Economic burden of Idiopathic Pulmonary Fibrosis: a Retrospective Cohort Study. *BMC. Pulm. Med.* 16, 2. doi:10.1186/s12890-015-0165-1
- Ren, L., Guo, X.-Y., Gao, F., Jin, M.-L., and Song, X.-N. (2019). Identification of the Perturbed Metabolic Pathways Associating with Renal Fibrosis and Evaluating Metabolome Changes of Pretreatment with Astragalus Polysaccharide through Liquid Chromatography Quadrupole Time-Of-Flight Mass Spectrometry. *Front. Pharmacol.* 10, 1623. doi:10.3389/fphar.2019.01623
- Ren, Q., Zhao, S., Ren, C., and Ma, Z. (2018). Astragalus Polysaccharide Alleviates LPS-Induced Inflammation Injury by Regulating miR-127 in H9c2 Cardiomyoblasts. *Int. J. Immunopathol. Pharmacol.* 31, 205873841875918. doi:10.1177/2058738418759180
- Richeldi, L., Collard, H. R., and Jones, M. G. (2017). Idiopathic Pulmonary Fibrosis. *The Lancet* 389 (10082), 1941–1952. doi:10.1016/s0140-6736(17)30866-8
- Ruigrok, M. J. R., Frijlink, H. W., Melgert, B. N., Olinga, P., and Hinrichs, W. L. J. (2021). Gene Therapy Strategies for Idiopathic Pulmonary Fibrosis: Recent Advances, Current Challenges, and Future Directions. *Mol. Ther. - Methods Clin. Dev.* 20, 483–496. doi:10.1016/j.omtm.2021.01.003
- Ryu, J. H., Moua, T., Daniels, C. E., Hartman, T. E., Yi, E. S., Utz, J. P., et al. (2014). Idiopathic Pulmonary Fibrosis: Evolving Concepts. *Mayo Clinic Proc.* 89 (8), 1130–1142. doi:10.1016/j.mayocp.2014.03.016
- Senthilkumar, K., and Kim, S.-K. (2014). Anticancer Effects of Fucoidan. *Adv. Food Nutr. Res.* 72, 195–213. doi:10.1016/b978-0-12-800269-8.00011-7
- Sibinska, Z., Tian, X., Korfei, M., Kojonazarov, B., Kolb, J. S., Klepetko, W., et al. (2017). Amplified Canonical Transforming Growth Factor- $\beta$  Signalling via Heat Shock Protein 90 in Pulmonary Fibrosis. *Eur. Respir. J.* 49 (2), 1501941. doi:10.1183/13993003.01941-2015
- Sohretoglu, D., and Huang, S. (2018). Ganoderma Lucidum Polysaccharides as an Anti-cancer Agent. *Acamc* 18 (5), 667–674. doi:10.2174/187152061766617113121246
- Solomon, J. J., Olson, A. L., Fischer, A., Bull, T., Brown, K. K., and Raghu, G. (2013). Scleroderma Lung Disease. *Eur. Respir. Rev.* 22 (127), 6–19. doi:10.1183/09059180.00005512
- Song, J. W., Hong, S.-B., Lim, C.-M., Koh, Y., and Kim, D. S. (2011). Acute Exacerbation of Idiopathic Pulmonary Fibrosis: Incidence, Risk Factors and Outcome. *Eur. Respir. J.* 37 (2), 356–363. doi:10.1183/09031936.00159709
- Song, J., Wu, Y., Jiang, G., Feng, L., Wang, Z., Yuan, G., et al. (2019). Sulfated Polysaccharides from Rhodiola Sachalinensis Reduce D-Gal-Induced Oxidative Stress in NIH 3T3 Cells. *Int. J. Biol. Macromolecules* 140, 288–293. doi:10.1016/j.jbiomac.2019.08.052
- Spagnolo, P., Distler, O., Ryerson, C. J., Tzouveleakis, A., Lee, J. S., Bonella, F., et al. (2021). Mechanisms of Progressive Fibrosis in Connective Tissue Disease (CTD)-associated Interstitial Lung Diseases (ILDs). *Ann. Rheum. Dis.* 80 (2), 143–150. doi:10.1136/annrheumdis-2020-217230
- Sun, H., Ni, X., Song, X., Wen, B., Zhou, Y., Zou, F., et al. (2016). Fermented Yupingfeng Polysaccharides Enhance Immunity by Improving the Foregut Microflora and Intestinal Barrier in Weaning rex Rabbits. *Appl. Microbiol. Biotechnol.* 100 (18), 8105–8120. doi:10.1007/s00253-016-7619-0
- Tian, X., Liang, T., Liu, Y., Ding, G., Zhang, F., and Ma, Z. (2019). Extraction, Structural Characterization, and Biological Functions of Lycium Barbarum Polysaccharides: A Review. *Biomolecules* 9 (9), 389. doi:10.3390/biom9090389
- Tietel, Z., and Masaphy, S. (2018). True Morels (Morchella)-Nutritional and Phytochemical Composition, Health Benefits and Flavor: A Review. *Crit. Rev. Food Sci. Nutr.* 58 (11), 1888–1901. doi:10.1080/10408398.2017.1285269
- Todd, N. W., Luzina, I. G., and Atamas, S. P. (2012). Molecular and Cellular Mechanisms of Pulmonary Fibrosis. *Fibrogenesis. Tissue Repair* 5 (1), 11. doi:10.1186/1755-1536-5-11
- Walton, K. L., Johnson, K. E., and Harrison, C. A. (2017). Targeting TGF- $\beta$  Mediated SMAD Signaling for the Prevention of Fibrosis. *Front. Pharmacol.* 8, 461. doi:10.3389/fphar.2017.00461
- Wang, J.-H., Zuo, S.-R., and Luo, J.-P. (2017a). Structural Analysis and Immuno-Stimulating Activity of an Acidic Polysaccharide from the Stems of Dendrobium Nobile Lindl. *Molecules* 22 (4), 611. doi:10.3390/molecules22040611
- Wang, L., Zhang, P., Li, X., Zhang, Y., Zhan, Q., and Wang, C. (2019a). Low-molecular-weight Fucoidan Attenuates Bleomycin-Induced Pulmonary Fibrosis: Possible Role in Inhibiting TGF- $\beta$ 1-Induced Epithelial-Mesenchymal Transition through ERK Pathway. *Am. J. Transl. Res.* 11 (4), 2590–2602.
- Wang, S. X., Li, J., and Liu, Y. (2009). Interventional Effect of Yupingfeng Polysaccharide on Pulmonary Fibrosis in Rats and its Partial Mechanism. *J. Anhui Med. Univ.* 44 (05), 586–590. doi:10.3969/j.issn.1000-1492.2009.05.015
- Wang, Y., Han, S., Li, R., Cui, B., Ma, X., Qi, X., et al. (2019b). Structural Characterization and Immunological Activity of Polysaccharides from the



- Tuber of *Bletilla Striata*. *Int. J. Biol. Macromolecules* 122, 628–635. doi:10.1016/j.ijbiomac.2018.10.201
- Wang, Y., Liu, D., Chen, S., Wang, Y., Jiang, H., and Yin, H. (2014). A New Glucomannan from *Bletilla Striata*: Structural and Anti-fibrosis Effects. *Fitoaterapia* 92, 72–78. doi:10.1016/j.fito.2013.10.008
- Wang, Y., Liu, Y., Yu, H., Zhou, S., Zhang, Z., Wu, D., et al. (2017b). Structural Characterization and Immuno-Enhancing Activity of a Highly Branched Water-Soluble  $\beta$ -glucan from the Spores of *Ganoderma Lucidum*. *Carbohydr. Polym.* 167, 337–344. doi:10.1016/j.carbpol.2017.03.016
- Wang, Y. Q., Wang, X. Q., Zhang, X. M., Lin, X. Y., Wang, X. H., and An, Y. F. (2010). Effects Of angelica Polysaccharides on Lung Function and Lung Coefficient in Rats with Pulmonary Fibrosis. *Gansu Traditional Chin. Med.* 23 (011), 28–31. doi:10.3969/j.issn.1004-6852.2010.11.013
- Wang, Z., Liu, T., Chen, X., You, H., Zhang, Q., Xue, J., et al. (2018). Low Molecular Weight Fucoidan Ameliorates Hindlimb Ischemic Injury in Type 2 Diabetic Rats. *J. Ethnopharmacology* 210, 434–442. doi:10.1016/j.jep.2017.09.014
- Wilkes, M. C., Mitchell, H., Penheiter, S. G., Doré, J. J., Suzuki, K., Edens, M., et al. (2005). Transforming Growth Factor- $\beta$  Activation of Phosphatidylinositol 3-Kinase Is Independent of Smad2 and Smad3 and Regulates Fibroblast Responses via P21-Activated Kinase-2. *Cancer Res.* 65 (22), 10431–10440. doi:10.1158/0008-5472.Can-05-1522
- Xiong, X., Huang, G., and Huang, H. (2019). The Antioxidant Activities of Phosphorylated Polysaccharide from Native Ginseng. *Int. J. Biol. Macromolecules* 126, 842–845. doi:10.1016/j.ijbiomac.2018.12.266
- Xu, C., Ni, S., Zhuang, C., Li, C., Zhao, G., Jiang, S., et al. (2021). Polysaccharide from *Angelica Sinensis* Attenuates SNP-Induced Apoptosis in Osteoarthritis Chondrocytes by Inducing Autophagy via the ERK1/2 Pathway. *Arthritis Res. Ther.* 23 (1), 47. doi:10.1186/s13075-020-02409-3
- Xu, L., Li, L.-c., Zhao, P., Qi, L.-w., Li, P., Gao, J., et al. (2014). Total Polysaccharide of Yupingfeng Protects against Bleomycin-Induced Pulmonary Fibrosis via Inhibiting Transforming Growth Factor-B1-Mediated Type I Collagen Abnormal Deposition in Rats. *J. Pharm. Pharmacol.* 66 (12), 1786–1795. doi:10.1111/jphp.12308
- Yan, D. D., Tian, J. Z., Zhang, D., Hou, L., Li, L., Zhang, C. H., et al. (2017). Inhibitory Effect of Basil Polysaccharide on TGF-Beta-Induced Epithelial-Mesenchymal Transition of A549 Cells. *Traditional Chin. Drug Res. Clin. Pharmacol.* 28 (02), 154–159.
- Yang, S.-M., Wang, T., Wen, D.-G., Hou, J.-Q., and Li, H.-B. (2016). Protective Effect of *Rhodiola Rosea* Polysaccharides on Cryopreserved Boar Sperm. *Carbohydr. Polym.* 135, 44–47. doi:10.1016/j.carbpol.2015.08.081
- Ying-Mei, K. E., Min, J., Shu-Bo, Z., Hong, Y. U., Juan, W., and Feng, G. E. (2020). Component Analysis of *Ophiocordyceps Lanpingensis* Polysaccharides and Study on Alleviation of Hepatic Fibrosis in Mice by Polysaccharides. *Zhongguo Zhong Yao Za Zhi* 45 (21), 5256–5264. doi:10.19540/j.cnki.cjcm.20200628.401
- Yu, H.-H., Chengchuan Ko, E., Chang, C.-L., Yuan, K., Wu, A., Shan, Y.-S., et al. (2018a). Fucoidan Inhibits Radiation-Induced Pneumonitis and Lung Fibrosis by Reducing Inflammatory Cytokine Expression in Lung Tissues. *Mar. Drugs* 16 (10), 392. doi:10.3390/md16100392
- Yu, M., Shi, J., Sheng, M., Gao, K., Zhang, L., Liu, L., et al. (2018b). Astragalus Inhibits Epithelial-To-Mesenchymal Transition of Peritoneal Mesothelial Cells by Down-Regulating  $\beta$ -Catenin. *Cell. Physiol. Biochem.* 51 (6), 2794–2813. doi:10.1159/000495972
- Yu, W., Ren, Z., Zhang, X., Xing, S., Tao, S., Liu, C., et al. (2018c). Structural Characterization of Polysaccharides from *Dendrobium Officinale* and Their Effects on Apoptosis of HeLa Cell Line. *Molecules* 23 (10), 2484. doi:10.3390/molecules23102484
- Zeng, J., Li, D., Li, Z., Zhang, J., and Zhao, X. (2020). *Dendrobium Officinale* Attenuates Myocardial Fibrosis via Inhibiting EMT Signaling Pathway in HFD/STZ-Induced Diabetic Mice. *Biol. Pharm. Bull.* 43 (5), 864–872. doi:10.1248/bpb.b19-01073
- Zeng, P., Chen, Y., Zhang, L., and Xing, M. (2019). *Ganoderma Lucidum* Polysaccharide Used for Treating Physical Frailty in China. *Prog. Mol. Biol. Transl. Sci.* 163, 179–219. doi:10.1016/bs.pmbts.2019.02.009
- Zeng, P., Guo, Z., Zeng, X., Hao, C., Zhang, Y., Zhang, M., et al. (2018). Chemical, Biochemical, Preclinical and Clinical Studies of *Ganoderma Lucidum* Polysaccharide as an Approved Drug for Treating Myopathy and Other Diseases in China. *J. Cel. Mol. Med.* 22 (7), 3278–3297. doi:10.1111/jcmm.13613
- Zhan, Y., An, X., Wang, S., Sun, M., and Zhou, H. (2020). Basil Polysaccharides: A Review on Extraction, Bioactivities and Pharmacological Applications. *Bioorg. Med. Chem.* 28 (1), 115179. doi:10.1016/j.bmc.2019.115179
- Zhang, K., Si, X.-P., Huang, J., Han, J., Liang, X., Xu, X.-B., et al. (2016). Preventive Effects of *Rhodiola Rosea* L. On Bleomycin-Induced Pulmonary Fibrosis in Rats. *Ijms* 17 (6), 879. doi:10.3390/ijms17060879
- Zhang, R., Xu, L., An, X., Sui, X., and Lin, S. (2020). Astragalus Polysaccharides Attenuate Pulmonary Fibrosis by Inhibiting the Epithelial-Mesenchymal transition and NF-Kb Pathway Activation. *Int. J. Mol. Med.* 46 (1), 331–339. doi:10.3892/ijmm.2020.4574
- Zhang, Y., Du, Y., Yu, H., Zhou, Y., and Ge, F. (2017). Protective Effects of *Ophiocordyceps Lanpingensis* on Glycerol-Induced Acute Renal Failure in Mice. *J. Immunol. Res.* 2017, 1–8. doi:10.1155/2017/2012585
- Zhang, Y., Zhou, T., Wang, H., Cui, Z., Cheng, F., and Wang, K.-p. (2016a). Structural Characterization and *In Vitro* Antitumor Activity of an Acidic Polysaccharide from *Angelica Sinensis* (Oliv.) Diels. *Carbohydr. Polym.* 147, 401–408. doi:10.1016/j.carbpol.2016.04.002
- Zhang, Z., Zhang, D., Dou, M., Li, Z., Zhang, J., and Zhao, X. (2016b). *Dendrobium officinale* Kimura et Migo attenuates diabetic cardiomyopathy through inhibiting oxidative stress, inflammation and fibrosis in streptozotocin-induced mice. *Biomed. Pharmacother.* 84, 1350–1358. doi:10.1016/j.biopha.2016.10.074
- Zheng, Y., Liu, T., Wang, Z., Xu, Y., Zhang, Q., and Luo, D. (2018). Low Molecular Weight Fucoidan Attenuates Liver Injury via SIRT1/AMPK/PGC1 $\alpha$  axis in Db/db Mice. *Int. J. Biol. Macromolecules* 112, 929–936. doi:10.1016/j.ijbiomac.2018.02.072
- Zhou, J., You, W., Sun, G., Li, Y., Chen, B., Ai, J., et al. (2016). The Marine-Derived Oligosaccharide Sulfate MS80, a Novel Transforming Growth Factor 1 Inhibitor, Reverses Epithelial Mesenchymal Transition Induced by Transforming Growth Factor-1 and Suppresses Tumor Metastasis. *J. Pharmacol. Exp. Ther.* 359 (1), 54–61. doi:10.1124/jpet.116.234799
- Zhou, S., Zhou, Y., Yu, J., Du, Y., Tan, Y., Ke, Y., et al. (2020). *Ophiocordyceps Lanpingensis* Polysaccharides Attenuate Pulmonary Fibrosis in Mice. *Biomed. Pharmacother.* 126, 110058. doi:10.1016/j.biopha.2020.110058
- Zong, A., Cao, H., and Wang, F. (2012). Anticancer Polysaccharides from Natural Resources: a Review of Recent Research. *Carbohydr. Polym.* 90 (4), 1395–1410. doi:10.1016/j.carbpol.2012.07.026

**Conflict of Interest:** The authors declare that the research was conducted in the absence of any commercial or financial relationships that could be construed as a potential conflict of interest.

**Publisher's Note:** All claims expressed in this article are solely those of the authors and do not necessarily represent those of their affiliated organizations, or those of the publisher, the editors and the reviewers. Any product that may be evaluated in this article, or claim that may be made by its manufacturer, is not guaranteed or endorsed by the publisher.

Copyright © 2021 Wu, Huang, Wang, Xu, Yang, Sun and Shi. This is an open-access article distributed under the terms of the Creative Commons Attribution License (CC BY). The use, distribution or reproduction in other forums is permitted, provided the original author(s) and the copyright owner(s) are credited and that the original publication in this journal is cited, in accordance with accepted academic practice. No use, distribution or reproduction is permitted which does not comply with these terms.

## GLOSSARY

**PF** Pulmonary fibrosis

**TCM** Traditional Chinese medicine

**HYP** Hydroxyproline

**ECM** Extracellular matrix

**TGF- $\beta$**  Transforming growth factor- $\beta$

**BLM** Bleomycin

**COL** Collagen

**EMT** Epithelial-mesenchymal transition

**$\alpha$ -SMA**  $\alpha$ -smooth muscle actin

**GPS** Ginseng polysaccharide

**BPS** Basil polysaccharide

**APS** *Astragalus* polysaccharide

**PPS** Polyporus polysaccharide

**RSA** *Rhodiolasachalinensis* polysaccharide A

**PDO** Polysaccharides from *dendrobium officinale*

**BSP** *Bletilla striata* polysaccharide

**MS80** Seaweed sulfated oligosaccharide

**LMWF** Low molecular weight fucoidan

**ASP** *Angelica sinensis* polysaccharide

**POL** Total polysaccharide from *O. lanpingensis*

**LBP** *Lycium barbarum* polysaccharide

**FMP-1** *Morel* polysaccharide-1

**GIP** *Ganoderma lucidum* polysaccharide

**LLP** Lily polysaccharide

**YPF-p** Yupingfeng-polysaccharide

**T $\beta$ R1** Transforming growth factor- $\beta$ 1 receptor

**HLFs** Human lung fibrosis

**HEPF** Human embryo pulmonary fibroblast

**DANCR** Differentiation antagonistic non-protein coding RNA

**Mw** Molecular weight

**Nrf2** Nuclear factor erythroid 2-related factor 2

**AUF1** AU binding factor 1

**MMP** Matrix metalloproteinase

**TIMP**

**Tissue inhibitor of metalloproteinase**

**NF- $\kappa$ B** Nuclear factor- $\kappa$ B

**IL** Interleukin

**MCP-1** Monocyte chemoattractant protein-1

**MDA** Malondialdehyde

**ROS** Reactive oxygen species

**SOD** Superoxide dismutase

**TNF** Tumor necrosis factor

**Ho-1** Heme oxygenase-1

**AKT** Protein kinase B

**ERK** Extracellular signal-regulated kinase

**FN** Fibronectin

**MIP-2** Macrophage inflammatory protein-2

**M1** Macrophages 1

**CXCL1** Chemokine ligand 1

**PI3K** Phosphatidylinositol 3-kinase

**CAT** Catalase

**GSH** Glutathione

**GSH-Px** Glutathione peroxidase

**MAPK** Mitogen -activated protein kinase

**AP-1** Activator protein-1

**Ara** Arabinose

**Glc** Glucose

**Rha** Rhamnose

**Man** Mannose

**Gal** Galactose

**Xyl** Xylose

**Gala** Galacturonic acid

**Fru** Fructose



# Targeting M2 Macrophages Alleviates Airway Inflammation and Remodeling in Asthmatic Mice *via* miR-378a-3p/GRB2 Pathway

Qiujie Wang<sup>1,2,3†</sup>, Luna Hong<sup>1,2,3†</sup>, Ming Chen<sup>1,2,3</sup>, Jiangting Shi<sup>1,2,3</sup>, Xiaoling Lin<sup>1,2,3</sup>, Linjie Huang<sup>1,2,3</sup>, Tiantian Tang<sup>1,2,3</sup>, Yimin Guo<sup>1,2,3</sup>, Xiaoqing Yuan<sup>2,4\*</sup> and Shanping Jiang<sup>1,2,3\*</sup>

<sup>1</sup>Division of Pulmonary and Critical Care Medicine, Sun Yat-sen Memorial Hospital, Sun Yat-sen University, Guangzhou, China, <sup>2</sup>Guangdong Provincial Key Laboratory of Malignant Tumor Epigenetics and Gene Regulation, Medical Research Center, Sun Yat-sen Memorial Hospital, Sun Yat-sen University, Guangzhou, China, <sup>3</sup>Institute of Pulmonary Diseases, Sun Yat-sen University, Guangzhou, China, <sup>4</sup>Breast Tumor Center, Sun Yat-sen Memorial Hospital, Sun Yat-sen University, Guangzhou, China

## OPEN ACCESS

### Edited by:

Wen Li,  
Zhejiang University, China

### Reviewed by:

Rishein Gupta,  
University of Texas at San Antonio,  
United States  
Sudip Banerjee,  
Morehouse School of Medicine,  
United States

### \*Correspondence:

Xiaoqing Yuan  
yuanxq\_1986@163.com  
Shanping Jiang  
jiangshp@mail.sysu.edu.cn

<sup>†</sup>These authors have contributed  
equally to this work and share first  
authorship

### Specialty section:

This article was submitted to  
Molecular Diagnostics and  
Therapeutics,  
a section of the journal  
Frontiers in Molecular Biosciences

**Received:** 31 May 2021

**Accepted:** 31 August 2021

**Published:** 13 September 2021

### Citation:

Wang Q, Hong L, Chen M, Shi J, Lin X,  
Huang L, Tang T, Guo Y, Yuan X and  
Jiang S (2021) Targeting M2  
Macrophages Alleviates Airway  
Inflammation and Remodeling in  
Asthmatic Mice *via* miR-378a-3p/  
GRB2 Pathway.  
Front. Mol. Biosci. 8:717969.  
doi: 10.3389/fmolb.2021.717969

**Background:** Asthma is a complex respiratory disease characterized by airway inflammation and remodeling. MicroRNAs (miRNAs) mediate various cellular processes including macrophage polarization and play an important role in the pathogenesis of asthma. In present study, we aimed to screen miRNA profiling involved in macrophage polarization and investigate its possible functions and mechanisms.

**Methods:** An OVA-sensitized mouse model was established and 2-chloroadenosine (2-CA) was used to interfere with macrophages. The airway inflammation and remodeling were assessed. The identification and function of M2 alveolar macrophages were assessed by flow cytometry, RT-qPCR, arginase activity and co-culture experiment. Microarray screening was used to select miRNAs which were related to macrophage polarization and RNA interference (RNAi) technique was performed to confirm the function of the selected miRNA and its target gene.

**Results:** Alveolar macrophages of asthmatic mice showed significant M2 polarization. 2-CA alleviated airway inflammation and remodeling as well as M2 polarization. *In vitro*, IL-4-induced M2 macrophages promoted the proliferation of  $\alpha$ -SMA-positive cells. And miRNA profiling showed a remarkable increased expression of miR-378a-3p in IL-4 induced M2 macrophages. Dual luciferase reporter assay confirmed growth factor receptor binding protein 2 (GRB2) was a target gene of miR-378a-3p. A miR-378a-3p inhibitor and knockdown of GRB2 repolarized alveolar macrophages from M1 to M2 phenotype.

**Conclusion:** Our findings suggest that miR-378a-3p/GRB2 pathway regulates the polarization of alveolar macrophages which acts as a potential therapeutic target for airway inflammation and remodeling in asthma.

**Keywords:** asthma, airway inflammation, airway remodeling, M2 macrophages, miR-378a-3p, GRB2

**Abbreviations:** AMs, alveolar macrophages; BALF, bronchoalveolar lavage fluid; GRB2, growth factor receptor binding protein 2; miRNAs, microRNAs; MH-S, murine alveolar macrophages; M1, classically activated macrophages; M2, alternatively activated macrophages; OVA, ovalbumin; 2-CA, 2-chloroadenosine.

## INTRODUCTION

Asthma is a chronic inflammatory airway disorder in which eosinophils, neutrophils, macrophages and CD4<sup>+</sup> T cells migrate into the airways and release powerful mediators which lead to airway inflammation and remodeling (Anderson 2008; Holgate 2012; Fehrenbach et al., 2017). One of the most notable features of remodeling is airway smooth muscle cells hyperplasia, which strongly predicts airflow limitation and contributes to narrow airways (Brightling et al., 2012; James et al., 2012; Collaborators 2017).

Alveolar macrophages (AMs) have been recognized to play an important role in maintaining immunological homeostasis and host defense in the lungs. It has been reported that the depletion of AMs in mice with asthma attenuated airway inflammation and remodeling (Lee et al., 2015). 2-CA, a purine analog, might cause a competitive reduction in intracellular adenosine content once phagocytized by macrophages, thus reducing the viability of macrophages (Ohtani et al., 1982; Saito and Yamaguchi 1985). Kubota et al. reported that 2-CA would deplete the number of AMs in the bronchoalveolar lavage fluid of mice without any effect on neutrophil or lymphocyte counts (Kubota et al., 1999). Additionally, Hadjigol et al. found that the depletion of pulmonary macrophages by administration of 2-CA into the lungs suppressed airway hyperresponsiveness and reduced the expression of IL-13, TNF- $\alpha$  and IFN- $\gamma$  (Hadjigol et al., 2020). Macrophages can be polarized into different phenotypes. M1 or 'classically activated' macrophages have high microbicidal and tumoricidal activity, as exemplified by the production of nitric oxide and pro-inflammatory cytokines such as IL-12 and TNF- $\alpha$ , while M2 or 'alternatively activated' macrophages have antiparasitic and tissue remodeling activity, characterized by the production of Arg-1, CD206, FIZZ1, Ym1, CCL17, and CCL24 (Liu and Yang 2013). It has been recognized that M2 macrophages were mainly activated by Th2 cytokines such as IL-4 and IL-13 (Gordon and Martinez 2010; Van Dyken and Locksley 2013). M2 macrophages have been known to facilitate the Th2 immune response and the secretion of chemokines and cytokines which regulate airway inflammation, tissue repair and airway remodeling in the lung (Murray and Wynn 2011; Yang et al., 2012; Byrne et al., 2015). Holtzman reported that the differentiation and accumulation of M2 macrophages might be a hallmark of allergic airway disease (Holtzman 2012).

miRNAs are noncoding small RNAs of 19–25 nucleotide in length which regulate characters of target sites, thus being responsible for diverse biological processes (Shenoy and Belloch 2014). In our previous study, we have identified that miR-142-5p and miR-130a-3p regulated M2 macrophage polarization and promoted the expression of profibrogenic genes in chronic inflammation (Su et al., 2015). The expression of miRNAs in M2 alveolar macrophages and the mechanisms regarding its polarization require further investigation. In the present study, we aimed to screen miRNA profiling involved in macrophage polarization and investigate its possible functions and mechanisms. Through microarray screening, we identified the candidate miRNA responsible for macrophage polarization and confirmed its target gene.

## MATERIALS AND METHODS

### Materials

OVA and 2-CA were purchased from Sigma (Missouri, United States). Recombinant murine IL-4 was sourced from Peprotech (New-Jersey, United States). Anti-CD80-PE, anti-CD206-BV650 and anti-CCR3-BV421 were purchased from Biolegend (California, United States). Antibodies for  $\alpha$ -SMA and GRB2 were purchased from Abcam (Cambridge, England), F4/80 from Servicebio (Hangzhou, China), ECP-1 from Bioss (Beijing, China). The FISH kit, miRNA mimics, miRNA inhibitor and siRNAs were all purchased from GenePharma (Shanghai, China). The primers for PCR were synthesized by BGI (Beijing, China). The lipofectamine RNAiMax was purchased from Invitrogen (California, United States) while the X-tremeGENE HP DNA Transfection Reagent was purchased from Roche (Basel, Switzerland). The arginase assay kit was obtained from BioAssay (California, United States) and the Cell-Light Edu Apollo567 *In Vitro* Kit was purchased from Ribobio (Guangzhou, China). ELISA kits of IL-4 were from BD Biosciences (New-Jersey, United States) and the dual-Glo<sup>®</sup> Luciferase assay system was from Promega (Wisconsin, United States).

### Animals

Male BALB/c mice aged 6–8 weeks were obtained from the Beijing Vital River Laboratory Animal Technology Company and maintained in the Laboratory Animal Center of Sun Yat-sen University. All the experiments were performed in accordance with the protocol approved by the Institutional Animal Care and Use Committee at the Medical College of Sun Yat-sen University (Approval Number: 2017189).

### Establishment of Murine Model With Chronic Asthma

To produce further insights into the macrophage phenotype of asthma, an asthmatic model was established, and 2-CA was used to interfere with macrophages. Male BALB/c mice were randomly divided into three groups with eight mice in each group and treated as follows. 1) The control group were sham sensitized and boosted with normal saline. 2) In OVA group, mice were sensitized and challenged with OVA as previously described (Chen et al., 2011). They were sensitized by intraperitoneal injection (*i.p.*) of 10  $\mu$ g of OVA emulsified in 1 mg of aluminium hydroxide in a total volume of 200  $\mu$ l on Day-1 and Day-14. 7 days after the last sensitization (Day-21), mice were in atomization to 2.5% OVA aerosol for up to 30 min every 3 days for 8 weeks. 3) The 2-CA group was comprised of mice that were sensitized and challenged as in the OVA group described above and were additionally treated with 2  $\mu$ M of 2-CA *via* intratracheal aerosolization using a compressor nebulizer (Dalian, China) before every subsequent three challenges of OVA. The mice were sacrificed 24 h after the final OVA challenge.

### BALF Analysis

Bronchoalveolar lavage fluid (BALF) was collected by lavage of lungs with 5 ml of precooled PBS *via* a tracheal cannula and centrifuged (3,000 rpm, 10 min, 4°C). The cells were used to



detect the expression of CD80, CD206, and CCR3 by flow cytometry and the supernatants were analyzed for IL-4 by ELISA.

## Histology and Blood Analysis

The left lung lobes were harvested for histological analysis and the right lobes were snap-frozen in liquid nitrogen and stored at  $-80^{\circ}\text{C}$  for RNA analysis. The blood was collected within heparinized tubes for flow cytometry analysis, while the plasma was kept at  $-80^{\circ}\text{C}$ .

## Cell Culture and Differentiation

The murine alveolar macrophages (MH-S) purchased from ATCC (Cat. No.: CRL-2019) were maintained in RPMI 1640 containing 10% FBS supplemented with 1% penicillin/streptomycin and incubated at  $37^{\circ}\text{C}$  in a humidified incubator containing 5%  $\text{CO}_2$ . To obtain M2 alveolar macrophages induced by IL-4 as previously described, MH-S cells were seeded into plastic 6-well plates at a concentration of  $1 \times 10^5$  cells/mL and incubated in serum-deprived medium for 12 h followed by treatment with IL-4 at 20 ng/ml for 48 h (Su et al., 2015). Then, the cells were harvested for further analysis.

## Culture of $\alpha$ -SMA-Positive Cells

Primary  $\alpha$ -SMA-positive cells of mice were isolated by the tissue digestion method and purified by differential adhesion as previously described with slight modifications (Chen et al., 2016). Briefly, lungs were removed from 6-8-week-old male BALB/c mice and pulmonary tissues were scraped off. Bronchial tissues were cut into small pieces approximately  $1 \times 1 \times 1$  mm in size and incubated in RPMI 1640 containing 1 mg/ml collagenase I at  $37^{\circ}\text{C}$  for 4 h. Thereafter, the adherent cells within 30 min which were mainly airway fibroblasts were discarded and the suspended  $\alpha$ -SMA-positive cells were pipetted into another culture flask. Successful isolation of  $\alpha$ -SMA-positive cells was determined by immunofluorescence staining of  $\alpha$ -SMA (Wang et al., 2020).  $\alpha$ -SMA-positive cells were cultured in RPMI 1640 containing 10% FBS and passaged every 6–8 days, and cells from 4 to 9 passages were used for further experiments.

## Arginase Activity

To determine the polarization of alveolar macrophages, arginase assay was carried out following the manufacturer's instructions (Ndolo et al., 2010). Total proteins were extracted from MH-S cells using ice-cold RIPA buffer containing 1 mM of PMSF. The supernatants of each sample were added into two separate wells of a 96-well microplate. 5X Substrate Buffer was added into one of the two wells, leaving the other one empty as a blank control. After incubation for 2 h at  $37^{\circ}\text{C}$ , urea reagent was added into all the wells while 5X Substrate Buffer was added into the blank control well. After further incubation for 1 h at room temperature, the optical density (OD) was measured by a microplate reader (Becan, Switzerland) at 430 nm. Additionally, urea standard and  $\text{ddH}_2\text{O}$  were used as standard and control, respectively. Arginase activity is calculated as  $(\text{OD}_{\text{sample}} - \text{OD}_{\text{blank}})/(\text{OD}_{\text{standard}} - \text{OD}_{\text{water}}) \times 10.4$  (U/L).

## Co-Culture Experiment and EdU Incorporation Assay

For the co-culture experiment, transwell assay was carried out using a 24-well transwell apparatus with  $0.4 \mu\text{m}$  pore size (Corning, New York, United States).  $\alpha$ -SMA-positive cells were added into the lower chamber and MH-S cells were added into the upper chamber to explore the effect of M2 macrophages on  $\alpha$ -SMA-positive cells. After co-culture for 48 h, proliferation of  $\alpha$ -SMA-positive cells were determined using EdU kit according to the manufacturer's instructions (Zhao et al., 2019). Cells were incubated with  $50 \mu\text{M}$  5-Ethynyl-2'-deoxyuridine (EdU) for 2 h followed by fixation with 4% paraformaldehyde and permeabilization with 0.5% Triton X-100. The incorporated EdU was visualized using Alexa Fluor 567 and the nuclear DNA was stained by Hoechst 33342. The images were obtained using a fluorescence microscope (Olympus, Tokyo, Japan).

## Flow Cytometry

Cells from BALF and MH-S cells were examined by flow cytometry. The amount of M1 macrophages ( $\text{CD}80^+$ ), M2 macrophages ( $\text{CD}206^+$ ) and eosinophils ( $\text{CCR}3^+$ ) were identified with specific antibodies and analyzed by multicolor flow cytometer (BD Celesta, New-Jersey, United States). The mean fluorescence intensity (MFI) was calculated by FlowJo software version 10 (Stanford, California, United States).

## Enzyme-Linked Immunosorbent Assay

The levels of IL-4 in BALF supernatants and plasma were determined by commercial ELISA kits following the manufacturer's instructions. Briefly, samples were added into a 96-well microplate coated with capture antibody specific for murine IL-4. After incubation overnight at  $4^{\circ}\text{C}$  followed by three washes with washing buffer, detection antibody and streptavidin-peroxidase enzyme were added. After a further incubation for 1 h at room temperature and seven washes, substrate reagents were added, and the reaction was stopped by adding stop solution after 30 min. The intensity of the color was measured by a microplate reader (Tecan, Zurich, Switzerland) at 450 nm, which was subtracted by the absorbance at 570 nm. IL-4 protein levels were calculated with standard curves for each measurement.

## Histological Evaluation

The left lungs were perfused with PBS, fixed in 4% paraformaldehyde, embedded in paraffin and cut into  $4 \mu\text{m}$  thick slices. Sections were stained with H&E, Periodic acid-Schiff (PAS) and Masson's trichrome stain for evaluation of airway inflammation, mucus gland hyperplasia and collagen deposition, respectively. Semi-quantitative morphometric analysis was performed where the degrees of inflammation, mucus and collagen deposition were scored from 0 (absent) to 3 (severe), as modified from a previously described protocol (Stellari et al., 2015). The thickness of the airway wall was determined by morphometric analysis on transverse sections after  $\alpha$ -SMA staining. F4/80 is a general marker for

**TABLE 1 |** The mRNA-specific primer sequences.

mRNA name	Forward (5'-3')	Reverse (5'-3')
IL-6	CCTCTGGTCTTCTGGAGTACC	ACTCCTTCTGTGACTCCAGC
IL-10	TGCCTGCTCTTACTGACTGG	CTCTAGGAGCATGTGGCTCTG
IL-12	CCCTTGCCCTCCTAAACCA	CTAAGACACCTGGCAGGTCCA
CCL5	ATATGGCTCGGACACCACTC	ACTTGGCGGTTCTCTCGAG
OCL24	CTGTCTGTCTGTCCATCTCTGG	GCTGCTGTTGAAATCCTCCGTT
iNOS	TTCACCCAGTTGTGCATCGACCTA	TCCATGGTCACCTCCAACACAAGA
FIZZ1	TGCTGGGATGACTGCTACTG	AGCTGGGTTCTCCACCTCTT
Arg1	TTGGCTTGCTTCGGAACTCA	TTCATGTGGCGCATTACAG
GRB2	AACATCCGTGTCCAGGAACC	AAGTCTCCTCTGCGAAAGCC
$\beta$ -ACTIN	GATCAGCAAGCAGGAGTACGA	CAGCTCAGTAACAGTCCGC

macrophages, and ECP-1 is a marker for eosinophils (Park et al., 2013). Sections were deparaffinized and rehydrated followed by microwave antigen retrieval in citric acid buffer (pH 6.0) and the blocking of endogenous peroxidase with 3% H<sub>2</sub>O<sub>2</sub>. Thereafter, sections were blocked with 5% BSA for 30 min at room temperature and incubated with the appropriate primary antibody overnight at 4°C in a humidified chamber. Staining was revealed followed by incubation with HRP-conjugated secondary antibody for 1 h at room temperature and the diaminobenzidine substrate kit for peroxidase. Counterstaining was performed using hematoxylin in 2 s.

## miRNA Microarray Analysis and Target Prediction

Total RNA from MH-S cells which were treated with or without 20 ng/ml of IL-4 for 48 h was isolated using TRIzol and purified with the RNeasy mini kit according to the manufacturer's instructions. The samples were labelled using the miRCURY Hy3/Hy5 Power labelling kit (Exiqon) and hybridized on the miRCURY LNA Array (v.19.0, Exiqon). The slides were then scanned using the Axon GenePix 4000B microarray scanner. Scanned images were then imported into GenePix Pro 6.0 software (Axon) for grid alignment and data extraction. Replicated miRNAs were averaged and miRNAs with intensities  $\geq 30$  Units in all samples were chosen for calculation of the normalization factor. Expression data were normalized using median normalization. After normalization, differentially expressed miRNAs between two groups were identified through relative quantity, fold change ( $\geq 2.0$ ) and *p*-value ( $< 0.05$ ). Finally, hierarchical clustering was performed to demonstrate distinguishable miRNA expression profiling among samples. The miRNA target prediction tools miRDB, TargetScan7.2 and DIANA-microT were used to identify target genes of candidate miRNAs. Kyoto Encyclopedia of Genes and Genomes (KEGG) analysis of the common target genes were further performed using the DAVID 6.8 website (<https://david.ncifcrf.gov/home.jsp>).

## Quantitative Real-Time PCR

Total RNA from MH-S cells or lungs was extracted using TRIzol according to the manufacturer's instructions. RNA was converted to cDNA with PrimeScript Master Mix for mRNA detection and

**TABLE 2 |** The miRNA-specific primer sequences.

miRNA name	Sequences (5'-3')
Universal primer	GTGCGTGTCTGGAGTTCG
miR-431-5p	AGGTGTCTTGCAGGCCGT
miR-677-3p	AAGCCAGATGCCGTTCC
Let-7i-3p	GGCTCTGCGCAAGCTACTG
miR-3093-5p	CGCGGAGCTCACACTAAAA
miR-378a-3p	GGGCACTGGACTTGGAGTC
miR-370-5p	GGGACAGGTCACGTCTCTGC
U6-Forward	GCTTCGGCAGCACATATACTAAAT
U6-Reverse	CGCTTCACGAATTTGCGTGTCTAT

with Mir-X miRNA First-Strand Synthesis Kit for miRNA evaluation. RT-qPCR was performed using the TB Green Premix Ex Taq II in a LightCycler 480 instrument (Roche, Basel, Switzerland). The fold-change of the transcript mRNA or miRNA was analyzed using the  $2^{-\Delta\Delta C_T}$  method. Expression of mRNA was normalized to that of  $\beta$ -ACTIN, and mature miRNAs were calculated using U6 as an internal control. The gene-specific primer sequences used for mRNA are listed in Table 1 and the primers for miRNAs are listed in Table 2.

## Fluorescence *In situ* Hybridization

Fluorescence *in situ* hybridization was performed on paraffin-embedded sections of lungs according to the manufacturer's instructions. First, the sections were deparaffinized and rehydrated. After rinsing with PBS, the slides were digested with protease K for 20 min at 37°C and then dehydrated by ethanol. The sections were prehybridized in denaturation solution for 8 min at 78°C and dehydrated by ethanol again. Then the sections were hybridized with 20 ng/ $\mu$ l Cy3-labelled LNA miR-378a-3p probe overnight at 37°C. After post-hybridization washes, the nuclei were counterstained with DAPI and the fluorescence images were captured by a confocal microscope (Olympus, Tokyo, Japan).

## Transfection of miRNAs or siRNAs

To determine the effect of miR-378a-3p or GRB2 on polarization of alveolar macrophages or the influence of miR-378a-3p on GRB2, we used RNAi to silence miR-378a-3p or GRB2. MH-S cells were seeded into 6-well plates at a density of  $1 \times 10^5$  cells/ml, and transfection was performed when cells were at 60~70%

**TABLE 3** | Sequences of the specific miRNA and siRNA.

Sequence name	Forward (5'-3')	Reverse (5'-3')
miR-378a-3p mimic	ACUGGACUUGGAGUCAGAAGG	UUCUGACUCCAAGUCCAGUUU
miRNA mimics NC	UUCUCCGAACGUGUCACGUTT	ACGUGACACGUUCCGAGAATT
miR-378a-3p inhibitor	CCUUCUGACUCCAAGUCCAGU	—
miRNA inhibitor NC	CAGUACUUUUUGUGUAGUACAA	—
si-GRB2	GGAACCAGCAGAUUUCUUTT	AAGAAUAUCUGCUGGUUCCTT
siRNA NC	UUCUCCGAACGUGUCACGUTT	ACGUGACACGUUCCGAGAATT

confluence. 100 pmol of miR-378a-3p mimics, miR-378a-3p inhibitor, siRNA specific to GRB2 (si-GRB2) or negative control siRNA (si-NC) were mixed with 250  $\mu$ l Opti-MEM, and 5  $\mu$ l Lipofectamine RNAiMax was mixed with 250  $\mu$ l Opti-MEM for 5 min. Then the RNA complexes and liposome complexes were mixed together, incubated for 20 min and transfected into cells. The cells were harvested 48 h later for further analysis. Sequences of miR-378a-3p inhibitor and si-GRB2 are provided in **Table 3**.

## Western Blot

Protein lysates extracted from lung tissues or MH-S cells which were transfected with miR-378a-3p mimics, miR-378a-3p inhibitor, or si-GRB2 were centrifuged at 16,000  $g$  for 20 min at 4°C and quantified using the BCA method. 20  $\mu$ g of proteins were separated by 10% SDS-PAGE and transferred onto PVDF membranes. After blocking, blots were probed with primary antibodies against GRB2 or  $\beta$ -tubulin at 4°C overnight followed by incubation with HRP-conjugated secondary antibody for 1 h at room temperature. Protein bands were detected by enhanced chemiluminescence assay and the blots were visualized by Minichemi Imaging System (Beijing, China). Densitometric quantitation of band intensity was carried out with ImageJ software version 5.0 (NIH, Maryland, United States).

## Dual Luciferase Reporter Assay

To identify the binding site between miR-378a-3p and GRB2, the 3' untranslated region (UTR) of GRB2 including wild type (WT) or mutant type (MUT) of the binding site was synthesized and cloned into the SV40-firefly Luciferase-MCS vectors (Genechem, Shanghai, China) and 293T cells were used for reporter assays. 293T cells ( $5 \times 10^4$  cells per well) were seeded into 24-well plates and transfected with miR-378a-3p mimics or negative control (20 pmol) for 24 h when the cells reached 60–70% confluence. Then cells were co-transfected with WT or MUT GRB2 3' UTR vector and the control vector coding for Renilla luciferase using X-tremeGENE HP DNA transfection reagent for 48 h. Cells were harvested using 300  $\mu$ l of Passive Lysis Buffer and luciferase activities were measured by a microplate reader (Zeng et al., 2019). The firefly luciferase activity was normalized to that of Renilla luciferase. Sequences of miR-378a-3p mimics and negative control are provided in **Table 3**.

## Statistical Analysis

The quantitative data were presented as the mean  $\pm$  SEM. For quantification analysis, each experiment was performed at least three times. Statistical analysis was conducted using GraphPad

Prism software version 5.0 (GraphPad, California, United States) and SPSS software version 20.0 (SPSS, Chicago, United States). Analysis between two groups was performed using Student's *t*-test and multiple comparisons of continuous variables were analyzed using one-way analysis of variance. Differences were considered statistically significant when the *p*-value was less than 0.05.

## RESULTS

### Airway Inflammation and Remodeling Along With M2 Macrophage Polarization in OVA-Sensitized Mice With Chronic Asthma

In the present study, we have developed an OVA-sensitized mouse model (**Figure 1A**). In asthmatic mice, HE staining revealed inflammatory cell infiltration; a large number of PAS<sup>+</sup> goblet cells were detected by PAS staining; immunohistochemical staining of ECP-1 showed a significant increase of eosinophilic infiltration; the total amount of collagen was significantly increased as defined by Masson staining; and marked airway smooth muscle cell hyperplasia and hypertrophy have been identified by  $\alpha$ -SMA immunohistochemical staining of the lungs (**Figure 1B**). IL-4 levels of plasma and BALF in OVA-challenged mice were significantly increased (**Figure 1C**). The results of flow cytometry analysis showed that the MFI of eosinophils in BALF was increased in OVA-challenged mice (**Figure 1D**). These data showed the airway inflammation and remodeling in OVA-sensitized mice.

A large number of F4/80<sup>+</sup> macrophages were detected around asthmatic airways in the lungs of asthmatic mice (**Figure 1E**). With OVA challenges, a significant downregulation of CD80<sup>+</sup> M1 macrophages and upregulation of CD206<sup>+</sup> M2 macrophages were detected in the BALF of asthmatic mice (**Figure 1F**). In addition, OVA challenge resulted in a significant increase in M2 markers such as FIZZ1, Arg1, and IL-10, with a decrease in M1 markers such as IL-6, IL-12, and iNOS (**Figure 1G**). These results indicated strong M2 macrophage infiltration in the BALF and lungs of asthmatic mice.

### Inhibition of M2 Macrophage Polarization by 2-CA is Accompanied by Alleviation of Airway Inflammation and Remodeling

The timeline in which 2-CA was used to reduce AMs was depicted in **Figure 2A**. Treatment with 2-CA effectively reduced the number of F4/80<sup>+</sup> macrophages in asthmatic mice

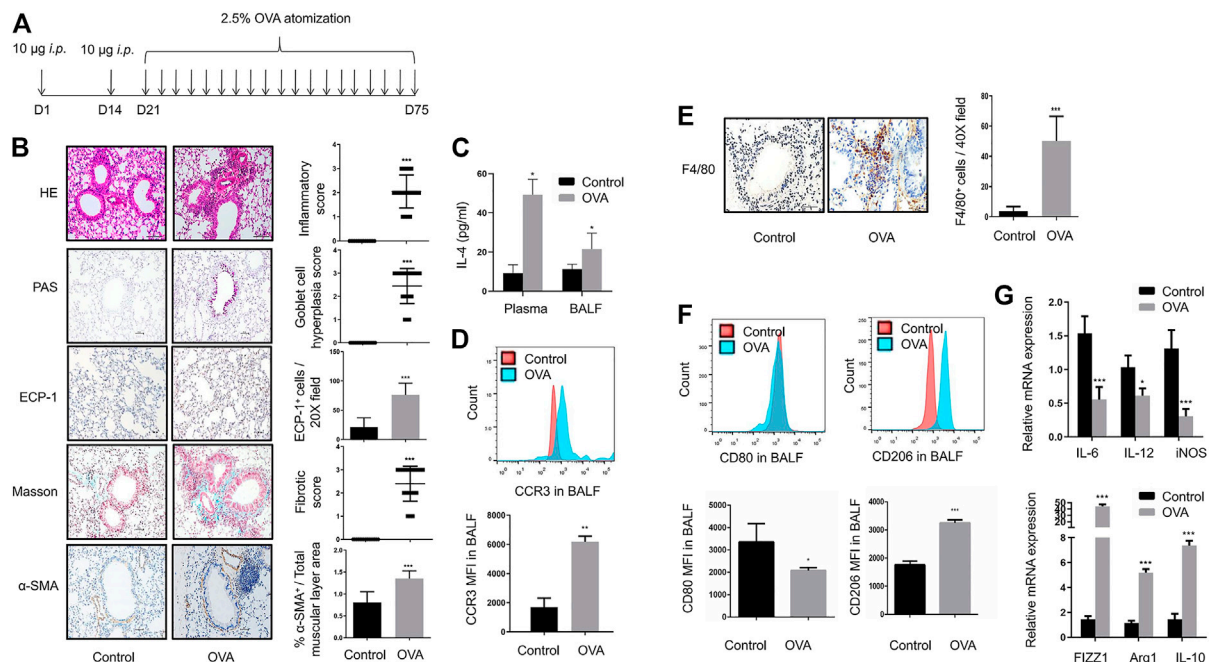


**FIGURE 1 |** Airway inflammation and remodeling along with M2 macrophage polarization in OVA-sensitized mice with chronic asthma **(A)**. Timeline of establishment of the chronic asthma model which was sensitized and challenged with OVA for 8 weeks **(B)**. Representative images of HE, PAS, Masson, ECP-1, and  $\alpha$ -SMA immunohistochemistry staining of lung sections from control and OVA-sensitized mice as shown at a magnification of 20X. Scale bar: 50  $\mu$ m. Bar graph represent morphometric semi-quantitative analysis of histopathological data from HE, PAS, and Masson staining. Quantification of ECP-1<sup>+</sup> cells per 20X field and percentage of  $\alpha$ -SMA<sup>+</sup>/total muscular layer area **(C)**. IL-4 levels in plasma and BALF from control and OVA-sensitized mice assessed by ELISA **(D)**. Expression of CCR3 in BALF from control and OVA-sensitized mice as determined by flow cytometry analysis. The representative histograms and quantitation of the MFI are shown **(E)**. Representative images of F4/80 immunohistochemistry staining of lung sections from control and OVA-sensitized mice as shown at a magnification of 40X. Scale bar: 50  $\mu$ m. Quantification of F4/80<sup>+</sup> cells per 40X field **(F)**. Expression of CD80 and CD206 in alveolar macrophages of BALF from control and OVA-sensitized mice as determined by flow cytometry analysis. The representative histograms and quantitation of the MFI are shown **(G)**. Expression of IL-6, IL-12, iNOS, FIZZ1, Arg1, and IL-10 in lungs from control and OVA-sensitized mice evaluated by RT-qPCR. ( $n = 8$ , \* $p < 0.05$ , \*\* $p < 0.01$ , \*\*\* $p < 0.001$  vs. control mice).

(Figure 2B). With 2-CA management, the downregulation of CD80<sup>+</sup> M1 macrophages and upregulation of CD206<sup>+</sup> M2 macrophages in BALF of asthmatic mice could be reversed (Figure 2C). In addition, 2-CA challenge within asthmatic mice resulted in a decrease in M2 markers such as FIZZ1, Arg1, and IL-10 and an increase in M1 markers such as IL-6, IL-12, and iNOS, which suggested that 2-CA could inhibit M2 polarization in asthmatic mice (Figure 2D). Meanwhile, the inflammatory cell infiltration, goblet cell hyperplasia, eosinophilic infiltration, subepithelial fibrosis, and smooth muscle cell hyperplasia and hypertrophy in the lungs of asthmatic mice could be alleviated by 2-CA treatment (Figure 2E). Consistent with this finding, the increased IL-4 levels of plasma and BALF and MFI of eosinophils in BALF in OVA-challenged mice were reduced by 2-CA (Figures 2F,G). The results suggested that 2-CA could attenuate airway inflammation and remodeling in parallel with the reduction of M2 macrophages in asthmatic mice.

### IL-4-Induced M2 Macrophages Promote the Proliferation of $\alpha$ -SMA-positive Cells *in vitro*

In addition to *in vivo* experiment, macrophage polarization also affects the function of airway cells *in vitro*. After IL-4 induction,

MH-S cells displayed a highly enhanced expression of CD206 and a markedly reduced expression of CD80 by flow cytometry (Figure 3A). Also, the mRNA expression of FIZZ1, Arg1, and CCL24 were largely increased ( $p < 0.05$ ) while IL-6, CCL5, and iNOS were significantly reduced (Figure 3B). Besides, the expression of arginase was significantly increased (Figure 3C). To investigate the effect of M2 macrophages on  $\alpha$ -SMA-positive cells, MH-S cells were stimulated with IL-4 and then co-cultured with  $\alpha$ -SMA-positive cells to evaluate the proliferative ability of  $\alpha$ -SMA-positive cells. As shown in Figure 3D, primary  $\alpha$ -SMA-positive cells were identified by the typical “hill and valley” growth pattern and immunofluorescent staining of  $\alpha$ -SMA. The proliferative ability of  $\alpha$ -SMA-positive cells was strongly enhanced when co-cultured with IL-4-induced M2 macrophages (Figure 3E).

### MiR-378a-3p is Upregulated in IL-4-Induced M2 Macrophages

To explore the important roles of miRNAs in macrophage polarization, we identified differentially expressed miRNAs in murine alveolar macrophages (MH-S) exposed to IL-4 *via* miRNA microarray analysis. The results showed that 13



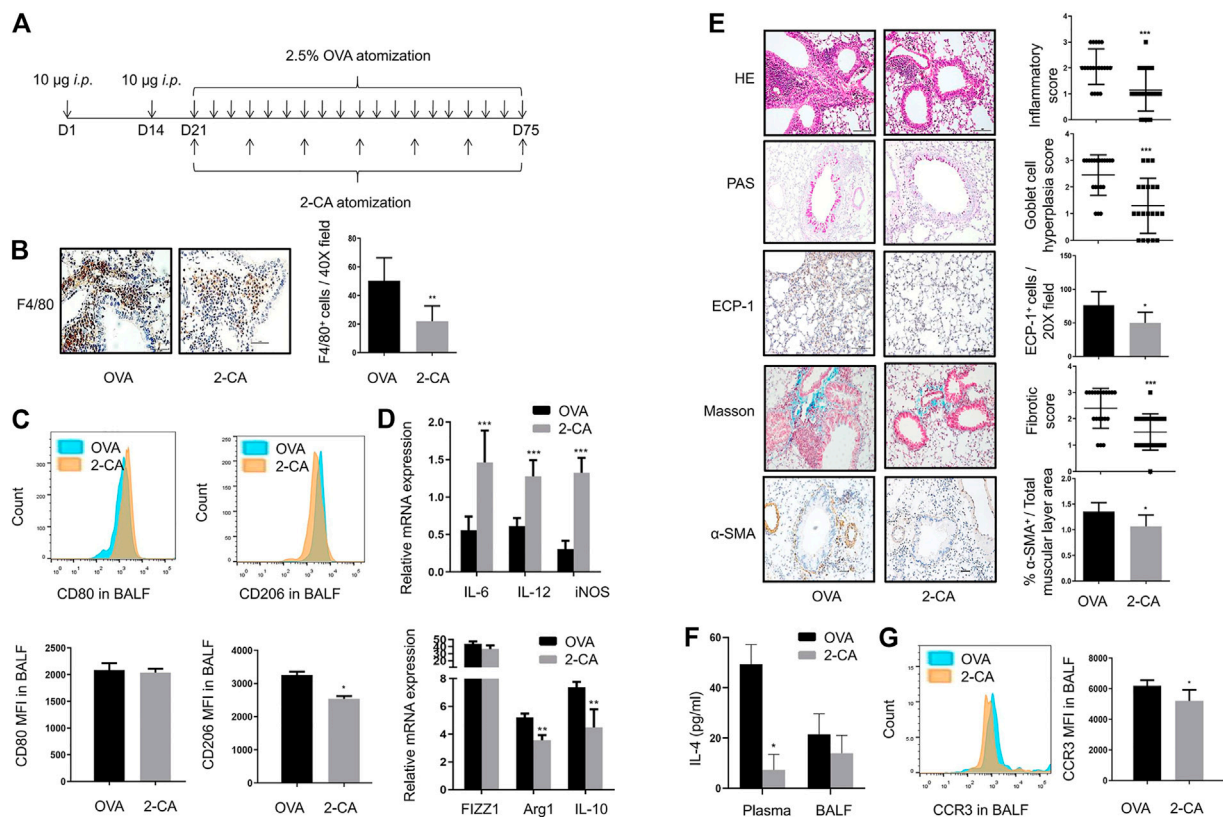


**FIGURE 2 |** Inhibition of M2 macrophage polarization by 2-CA is accompanied by alleviation of airway inflammation and remodeling (A). Timeline of mice with chronic asthma treated with 2-CA before every subsequent three challenges of OVA (B). Representative images of F4/80 immunohistochemistry staining of lung sections from OVA-sensitized and 2-CA-treated mice as shown at a magnification of 40X. Scale bar: 50 µm. Quantification of F4/80<sup>+</sup> cells per 40X field (C). Expression of CD80 and CD206 in alveolar macrophages of BALF from OVA-sensitized and 2-CA-treated mice as determined by flow cytometry analysis. The representative histograms and quantitation of the MFI are shown (D). Expression of IL-6, IL-12, iNOS, FIZZ1, Arg1, and IL-10 in lungs from OVA-sensitized and 2-CA-treated mice evaluated by RT-qPCR (E). Representative images of HE, PAS, Masson, ECP-1, and α-SMA immunohistochemistry staining of lung sections from OVA-sensitized and 2-CA-treated mice as shown at a magnification of 20X. Scale bar: 50 µm. Bar graph represent morphometric semi-quantitative analysis of histopathological data from HE, PAS and Masson staining. Quantification of ECP-1<sup>+</sup> cells per 20X field and percentage of α-SMA<sup>+</sup>/total muscular layer area (F). IL-4 levels in plasma and BALF from OVA-sensitized and 2-CA-treated mice assessed by ELISA (G). Expression of CCR3 in BALF from OVA-sensitized and 2-CA-treated mice as determined by flow cytometry analysis. The representative histograms and quantitation of the MFI are shown. ( $n = 8$ ,  $*p < 0.05$ ,  $**p < 0.01$ ,  $***p < 0.001$  vs. asthmatic mice).

miRNAs were upregulated, and 49 miRNAs were down-regulated between groups (Figure 4A). We further determined the expression of a subset of miRNAs to validate the microarray results by RT-qPCR (Figure 4B). Among these miRNAs, miR-677-3p, miR-3093-5p, miR-378a-3p, and miR-370a-5p were found to be significantly upregulated. The same subset of miRNAs was detected in the lungs of OVA-challenged mice by RT-qPCR (Figure 4B). Notably, miR-378a-3p was the most upregulated miRNA both in IL-4-induced M2 macrophages and the lungs of mice with chronic asthma, which might be involved in M2 polarization of macrophages (Vats et al., 2006; Eichner et al., 2010). In accordance with the results, FISH analysis also showed an increase of miR-378a-3p expression in the lungs of asthmatic mice (Figure 4C). Besides, the correlation coefficient between CD80 MFI in BALF and relative miR-378a-3p expression was negative while the correlation coefficient between CD206 MFI in BALF and relative

miR-378a-3p expression was positive, though both of them didn't achieve statistical significance (Figure 4D).

### MiR-378a-3p Directly Targets GRB2 in Murine Alveolar Macrophages

We used different target-prediction algorithms including miRDB, TargetScan7.2 and DIANA-microT to screen for mRNA targets of miR-378a-3p. 21 target genes were predicted by all three databases (Figure 5A). Among these target genes, KEGG\_PATHWAY analysis suggested that GRB2 might participate in osteoclast differentiation and T cell receptor signaling pathway which was associated with macrophage polarization. Therefore we hypothesized that GRB2 might participate in alveolar macrophage differentiation since osteoclasts acted as a type of macrophage (Figure 5B). Firstly, we found two identical seed-matching sites exist between the 3'-UTR of GRB2 and miR-378a-3p (Figure 5C). And there is no

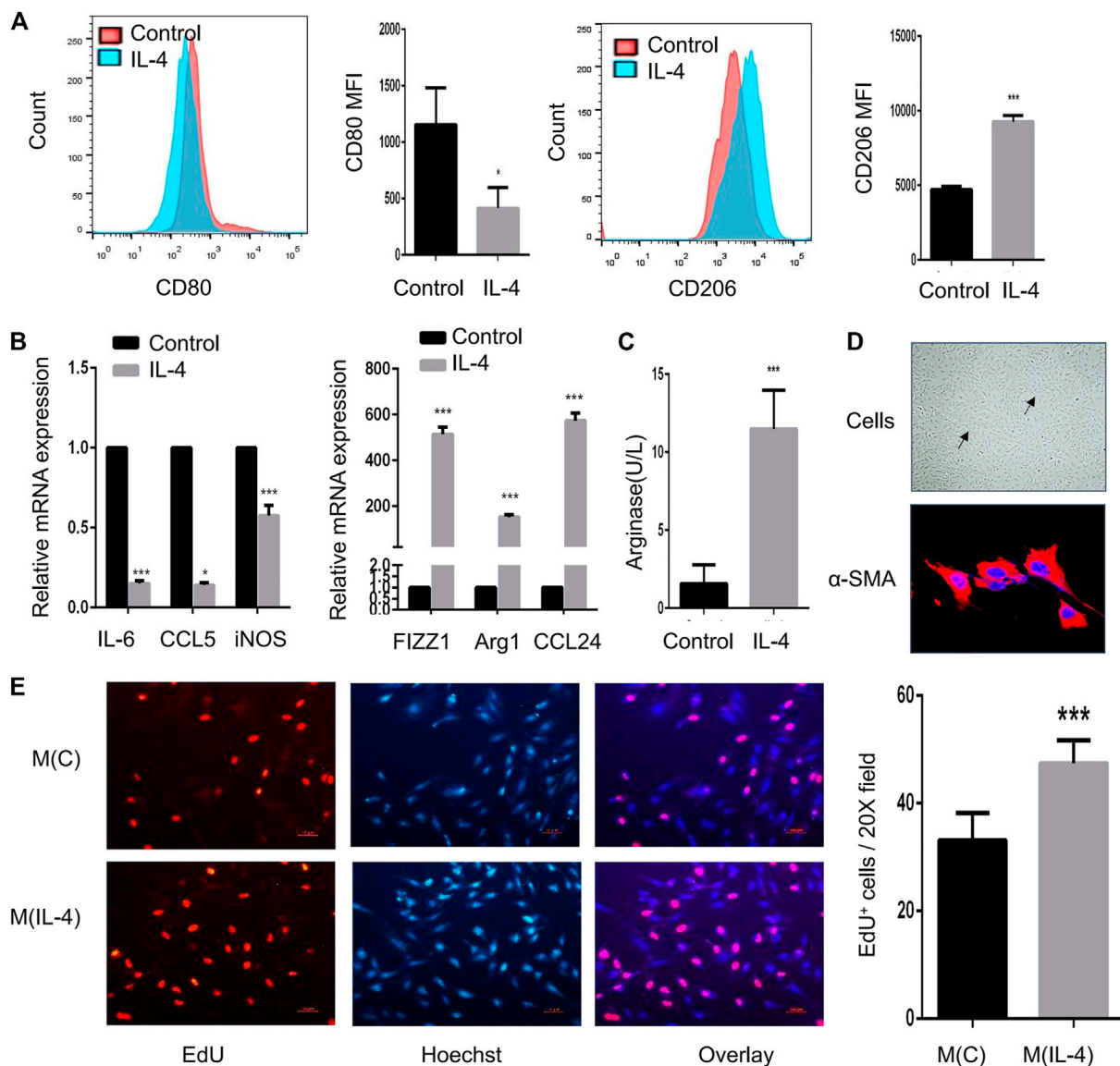
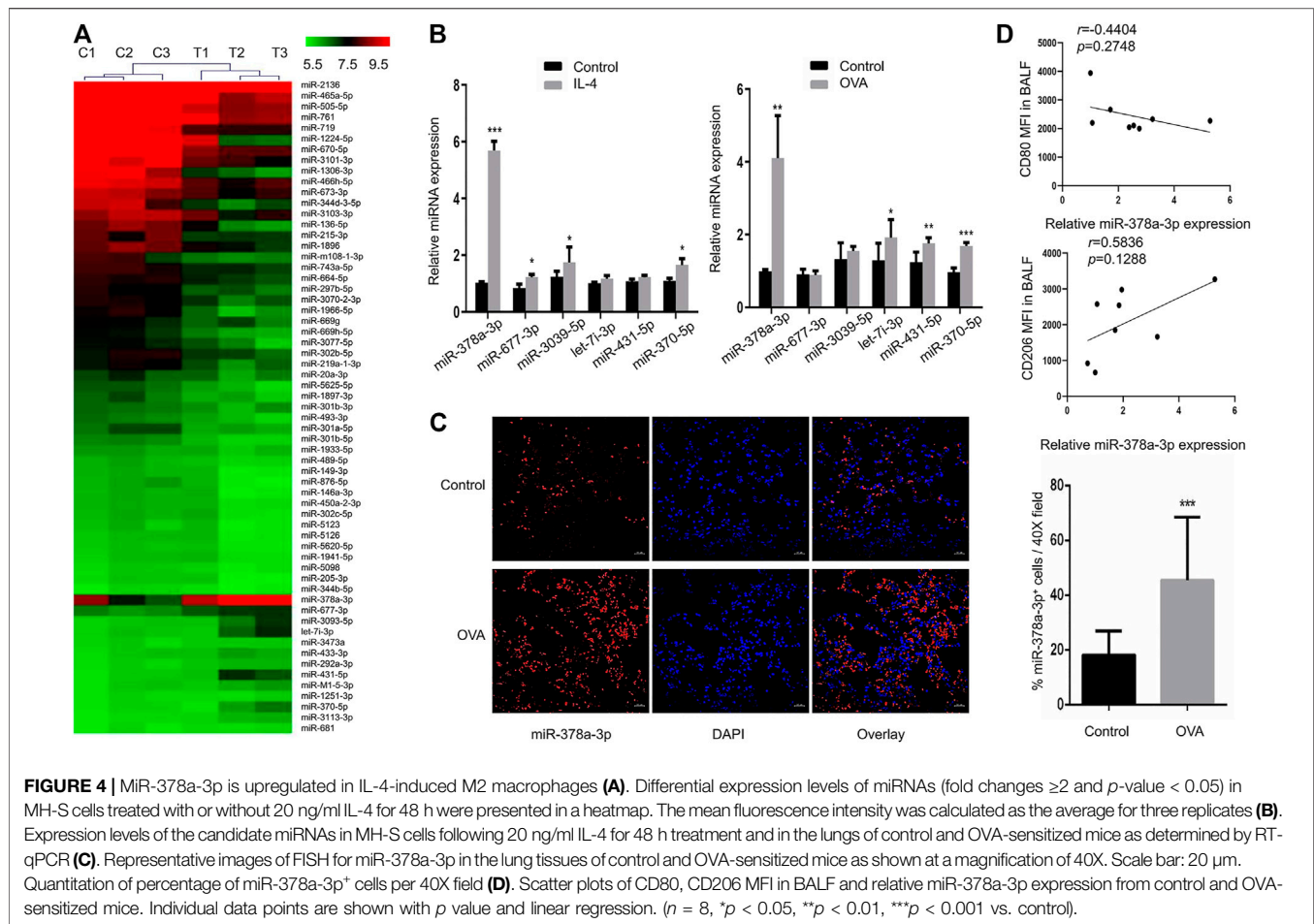


**FIGURE 3** | IL-4-induced M2 macrophages promote the proliferation of  $\alpha$ -SMA-positive cells *in vitro*. MH-S cells were treated for 48 h with 20 ng/ml IL-4, and the identification and function of IL-4-induced M2 macrophages were analyzed **(A–C)** **(A)**. Expression of CD80 and CD206 in IL-4-induced M2 macrophages evaluated by flow cytometry analysis. The representative histograms and quantitation of the MFI are shown **(B)**. Expression of IL-6, CCL5, iNOS, FIZZ1, Arg1, and CCL24 in IL-4-induced M2 macrophages evaluated by RT-qPCR **(C)**. Arginase in IL-4-induced M2 macrophages measured by the arginase assay **(D)**. Representative image of  $\alpha$ -SMA-positive cells under light microscope and immunofluorescent staining of  $\alpha$ -SMA as shown at a magnification of 40X. Scale bar: 50  $\mu$ m. The solid arrow points to the hill and the dotted arrow points to the valley **(E)**. MH-S cells were stimulated with 20 ng/ml IL-4 for 48 h and co-cultured with primary  $\alpha$ -SMA-positive cells for another 48 h. M(C) means MH-S cells treated without IL-4 and M(IL-4) means with IL-4. The proliferation of  $\alpha$ -SMA-positive cells detected by EdU incorporation assay as shown at a magnification of 20X. Scale bar: 10  $\mu$ m. Quantitation of percentage of EdU+ cells per 20X field. (\* $p$  < 0.05, \*\*\* $p$  < 0.001 vs. control).

target site at the 3'UTR of GRB2 for miRNAs identified in microarray analysis besides miR-378a-3p. To validate whether GRB2 was a target gene of miR-378a-3p, we further carried out gain and loss of function analysis as well as dual luciferase reporter assay. The mRNA and protein expression of GRB2 were significantly decreased after MH-S cells were transfected with miR-378a-3p mimics and increased after transfected with miR-378a-3p inhibitor, implying that the reduced transcription

and translation of GRB2 caused by miR-378a-3p was reversed by miR-378a-3p inhibitor **(Figure 5D)**. Furthermore, the results of dual luciferase reporter assay showed that the luciferase activity decreased obviously in cells co-transfected with the wild-type binding site vector in the presence of miR-378a-3p. On the contrary, cells containing the mutated binding sites vector did not show such suppression **(Figure 5E)**. These data confirmed that GRB2 was a specific target of miR-378a-3p.



## MiR-378a-3p Contributes to Alveolar Macrophage Polarization by Targeting GRB2

As showed in **Figure 6A**, M1 markers such as IL-6, IL-12, and iNOS were downregulated while M2 markers such as FIZZ1, Arg1, and IL-10 were upregulated in alveolar macrophages transfected with miR-378a-3p mimics. When alveolar macrophages were transfected with miR-378a-3p inhibitor, M1 markers were upregulated while M2 markers were downregulated (**Figure 6B**), suggesting that miR-378a-3p might promote M2 polarization of alveolar macrophages. The function of GRB2 in alveolar macrophage polarization was evaluated by silencing GRB2 expression with RNAi. As shown in **Figure 6C**, the mRNA and protein expression of GRB2 was significantly repressed after si-GRB2 silencing ( $p < 0.05$ ). Silencing of GRB2 also resulted in a downregulation of IL-6, IL-12, and iNOS mRNA with an upregulation FIZZ1, Arg1, and IL-10 mRNA in alveolar macrophages (**Figure 6D**). These data suggested that miR-378a-3p might contribute to M2 polarization of alveolar macrophages via the direct downregulation of GRB2.

## DISCUSSION

Since M2/M1 imbalance has been a recognized pathology in asthma, studies have been conducted to explore the therapeutic

potential of repolarizing M2 to M1 macrophages. In this study, we found that M2 macrophages were the predominant phenotype in the lungs and BALF of mice with chronic asthma induced by OVA. We also observed that the predominant M2 phenotype could be repolarized to the M1 phenotype by 2-CA in mice with chronic asthma, which was accompanied by the alleviation of airway inflammation and remodeling. These data suggested that 2-CA could reduce airway inflammation and remodeling in asthmatic mice by shifting macrophages from M2 to M1.

Recently, miRNAs have been found to affect the M1/M2 macrophage polarization (Self-Fordham et al., 2017; Li et al., 2018). For example, miRNA-9, miRNA-27, miRNA-155 and miRNA-125b could promote M1 polarization while miRNA-21, miRNA-223, miRNA-34, let-7c, miRNA-146a, and miRNA-511 could promote M2 polarization in various tissues (Feketea et al., 2019). However, the role of miRNAs in M2 alveolar macrophage polarization still needs more explorations. A continuous cell line of murine alveolar macrophages, designated MH-S, has been established and been used in our experiments. In our study, we confirmed that MH-S cells displayed a M2 phenotype after IL-4 induction. Then, differentially expressed miRNAs in M2 MH-S cells were screened, and miR-378a-3p was the most significantly increased miRNA in M2 MH-S cells and the lungs of mice

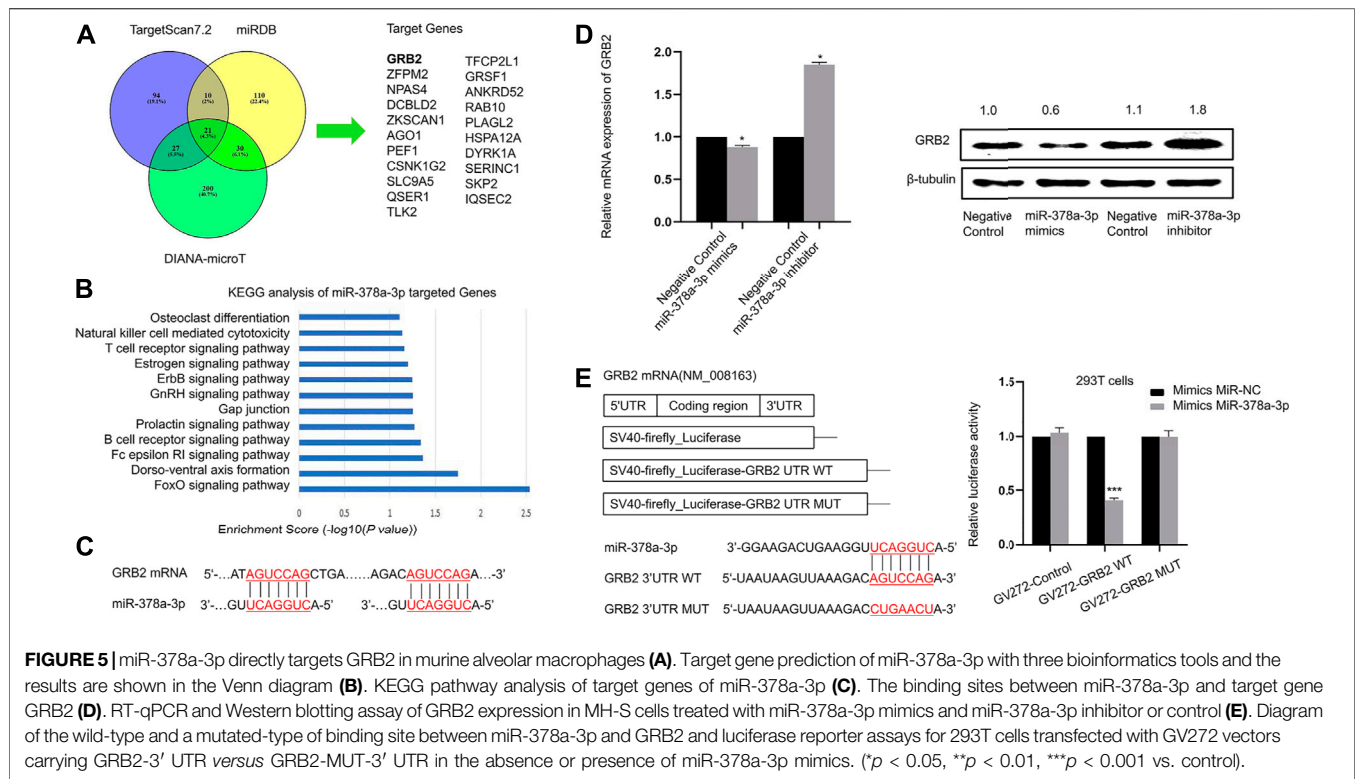


**FIGURE 5 |** miR-378a-3p directly targets GRB2 in murine alveolar macrophages (A). Target gene prediction of miR-378a-3p with three bioinformatics tools and the results are shown in the Venn diagram (B). KEGG pathway analysis of target genes of miR-378a-3p (C). The binding sites between miR-378a-3p and target gene GRB2 (D). RT-qPCR and Western blotting assay of GRB2 expression in MH-S cells treated with miR-378a-3p mimics and miR-378a-3p inhibitor or control (E). Diagram of the wild-type and a mutated-type of binding site between miR-378a-3p and GRB2 and luciferase reporter assays for 293T cells transfected with GV272 vectors carrying GRB2-3' UTR versus GRB2-MUT-3' UTR in the absence or presence of miR-378a-3p mimics. (\* $p < 0.05$ , \*\* $p < 0.01$ , \*\*\* $p < 0.001$  vs. control).

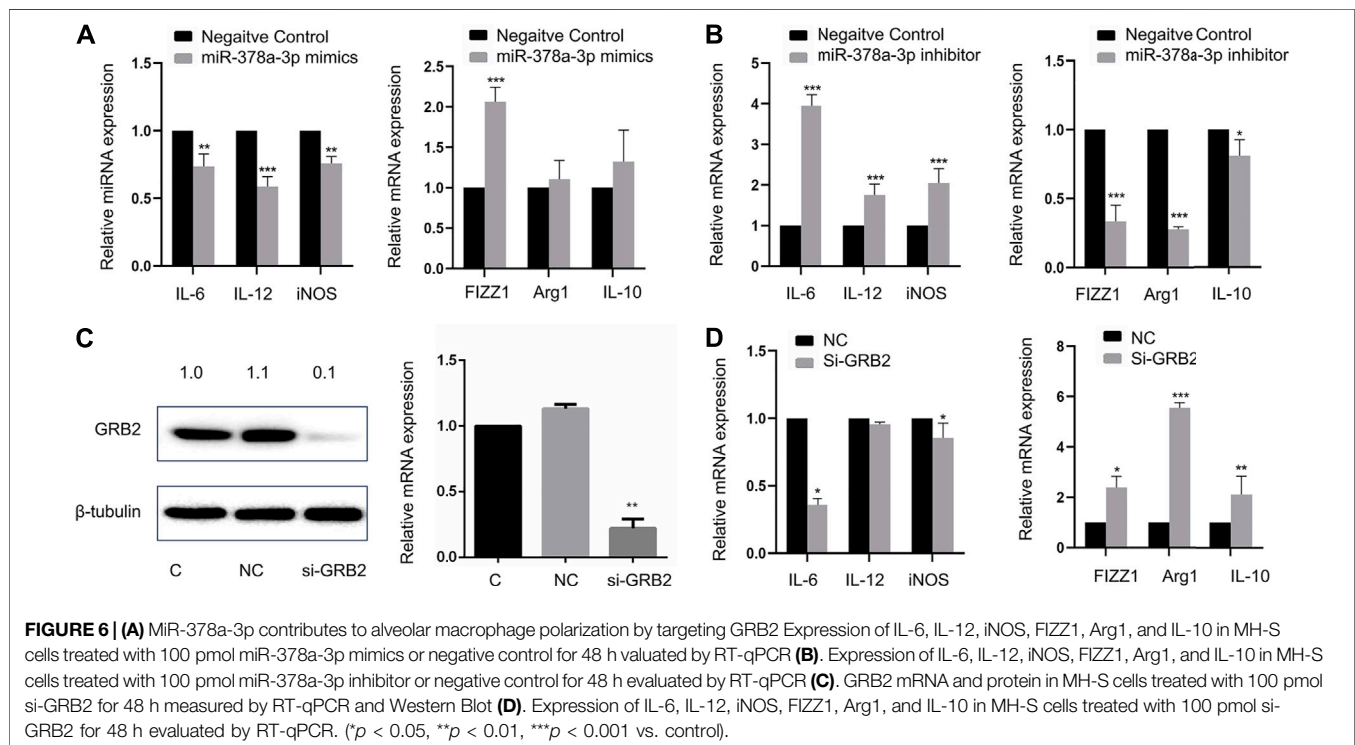


**FIGURE 6 |** (A) miR-378a-3p contributes to alveolar macrophage polarization by targeting GRB2 Expression of IL-6, IL-12, iNOS, FIZZ1, Arg1, and IL-10 in MH-S cells treated with 100 pmol miR-378a-3p mimics or negative control for 48 h evaluated by RT-qPCR (B). Expression of IL-6, IL-12, iNOS, FIZZ1, Arg1, and IL-10 in MH-S cells treated with 100 pmol miR-378a-3p inhibitor or negative control for 48 h evaluated by RT-qPCR (C). GRB2 mRNA and protein in MH-S cells treated with 100 pmol si-GRB2 for 48 h measured by RT-qPCR and Western Blot (D). Expression of IL-6, IL-12, iNOS, FIZZ1, Arg1, and IL-10 in MH-S cells treated with 100 pmol si-GRB2 for 48 h evaluated by RT-qPCR. (\* $p < 0.05$ , \*\* $p < 0.01$ , \*\*\* $p < 0.001$  vs. control).

with chronic asthma. miR-378a-3p is encoded in an intronic region of PPARGC1b, a protein associated with M2 polarization of macrophages (Vats et al., 2006; Eichner et al., 2010). Li et al. reported that miR-378 was increased in the peripheral blood and

lungs of asthmatic children (Li et al., 2019). Rückerl et al. reported that miR-378-3p was significantly upregulated by IL-4 in peritoneal macrophages and was involved in IL-4-driven macrophage proliferation in mice implanted with *Brugia*



*malayi* nematodes (Ruckerl et al., 2012), which didn't mention the role of downstream gene targets. In our study, we found that miR-378a-3p inhibitor promoted a shift from the M2 to M1 phenotype of alveolar macrophages, which meant that miR-378a-3p might participate in M2 polarization of alveolar macrophages.

With online target prediction tools, we have identified GRB2 as a target of miR-378a-3p, which have been verified by gain and loss of function analysis as well as luciferase reporter assay. GRB2 is a receptor-bound protein in various cells which link signaling events initiated by tyrosine kinases to downstream pathways. It can directly bind to activated EGF receptor phosphorylated tyrosine, participate in EGF receptor mediated signal transduction, and indirectly participate in insulin receptor-mediated signal transduction by binding with SHC phosphorylated tyrosine. GRB2 can combine with SHC and SOS at the same time to form SHC-GRB2-SOS complex and activate SOS. The activated SOS can combine with Ras protein on plasma membrane, and activate it to cause signal cascade reaction. (Rao 1996). It is reported that reducing GRB2 expression by shRNA or by gene targeting slowed down the osteoclast-like differentiation of cells (Levy-Apter et al., 2014). CD206 activation mediated GRB2 recruitment to initiate phagocytosis signaling in human monocyte-derived macrophages (Rajaram et al., 2017). Several studies have shown the important effects of GRB2 in eosinophils, mast cells and T cells in allergic diseases (Ben Baruch-Morgenstern et al., 2014; Massoud et al., 2016; Lin et al., 2018). Xu et al. reported that miR-378a-3p sensitized ovarian cancer cells to cisplatin through targeting MAPK1/GRB2 (Xu et al., 2018). Yu et al. suggested that LMV induced osteogenic differentiation of BMSCs through miR-378a-3p/Grb2 pathway to improve bone mineral density and mechanical properties (Yu et al., 2020). However, whether GRB2 participated in alveolar macrophage polarization is still unknown. We demonstrated that the knockdown of GRB2 resulted in repolarization of alveolar macrophages from the M1 to M2 phenotype. Taken together, these findings indicated that the miR-378a-3p/GRB2 axis might act as a mediator of M2 polarization of alveolar macrophages. However, whether other miRNAs or target genes participate in functions of macrophage deserves further experiments.

In conclusion, our study has provided evidences that miR-378a-3p is upregulated in M2 alveolar macrophages which aggravate airway inflammation and remodeling in asthmatic mice. Persistent elevation of miR-378a-3p levels in alveolar macrophages promotes the switch towards the M2 phenotype by suppressing the expression of GRB2. Our results provide the possibility that the inhibition of miR-378a-3p may serve as a promising therapeutic strategy for chronic asthma which deserves further *in vivo* experiments.

## BIOSECURITY STATEMENT

All the experiments were performed in Guangdong Provincial Key Laboratory of Malignant Tumor Epigenetics and Gene

Regulation, Medical Research Center, Sun Yat-Sen Memorial Hospital and in the Laboratory Animal Center of Sun Yat-sen University, which strictly adhered to standard biosecurity and institutional safety procedures.

## DATA AVAILABILITY STATEMENT

The data presented in the study are deposited in the GEO repository, accession number GSE143740.

## ETHICS STATEMENT

The animal study was reviewed and approved by The Institutional Animal Care and Use Committee at the Medical College of Sun Yat-sen University (Approval Number: 2017189).

## AUTHOR CONTRIBUTIONS

SJ and XY conceived the study. QW and JS designed the experiments. QW, LuH, YG, XL, and TT performed the experiments, collected the data and contributed to the statistical analysis. LiH, MC, XY, and SJ interpreted the data. QW drafted the manuscript. QW, XY, and SJ reviewed and edited the manuscript. SJ acquired funding.

## FUNDING

This work was supported by the National Natural Science Foundation of China (81670022, 81700033, 81500018), the Natural Science Foundation of Guangdong Province (2017A030313822), the Novel Coronavirus Disease Prevention and Control Project of Guangdong Province (2020B111105001) and the Guangzhou Science and Technology Program key projects (201704020123, 202008040003).

## ACKNOWLEDGMENTS

The authors would like to thank KC Biotech Co. Ltd. (Shanghai, China) for the library construction and data analysis of miRNA microarray.

## SUPPLEMENTARY MATERIAL

The Supplementary Material for this article can be found online at: <https://www.frontiersin.org/articles/10.3389/fmolb.2021.717969/full#supplementary-material>

## REFERENCES

- Anderson, G. P. (2008). Endotyping Asthma: New Insights Into Key Pathogenic Mechanisms in a Complex, Heterogeneous Disease. *The Lancet*. 372 (9643), 1107–1119. doi:10.1016/s0140-6736(08)61452-x
- Ben Baruch-Morgenstern, N., Shik, D., Moshkovits, I., Itan, M., Karo-Atar, D., Bouffi, C., et al. (2014). Paired Immunoglobulin-Like Receptor A Is an Intrinsic, Self-Limiting Suppressor of IL-5-induced Eosinophil Development. *Nat. Immunol.* 15 (1), 36–44. doi:10.1038/ni.2757
- Brightling, C. E., Gupta, S., Gonen, S., and Siddiqui, S. (2012). Lung Damage and Airway Remodelling in Severe Asthma. *Clin. Exp. Allergy*. 42 (5), 638–649. doi:10.1111/j.1365-2222.2011.03917.x
- Byrne, A. J., Mathie, S. A., Gregory, L. G., and Lloyd, C. M. (2015). Pulmonary Macrophages: Key Players in the Innate Defence of the Airways. *Thorax*. 70 (12), 1189–1196. doi:10.1136/thoraxjnl-2015-207020
- Chen, M., Huang, L., Zhang, W., Shi, J., Lin, X., Lv, Z., et al. (2016). MiR-23b Controls TGF- $\beta$ 1 Induced Airway Smooth Muscle Cell Proliferation via TGF $\beta$ R2/p-Smad3 Signals. *Mol. Immunol.* 70, 84–93. doi:10.1016/j.molimm.2015.12.012
- Chen, M., Lv, Z., and Jiang, S. (2011). The Effects of Triptolide on Airway Remodelling and Transforming Growth Factor- $\beta$ 1/Smad Signalling Pathway in Ovalbumin-Sensitized Mice. *Immunology*. 132 (3), 376–384. doi:10.1111/j.1365-2567.2010.03392.x
- Collaborators, G. B. D. C. R. D. (2017). Global, Regional, and National Deaths, Prevalence, Disability-Adjusted Life Years, and Years Lived With Disability for Chronic Obstructive Pulmonary Disease and Asthma, 1990–2015: a Systematic Analysis for the Global Burden of Disease Study 2015. *Lancet Respir. Med.* 5 (9), 691–706. doi:10.1016/S2213-2600(17)30293-X
- Eichner, L. J., Perry, M.-C., Dufour, C. R., Bertos, N., Park, M., St-Pierre, J., et al. (2010). miR-378 \* Mediates Metabolic Shift in Breast Cancer Cells via the PGC-1 $\beta$ /ERR $\gamma$  Transcriptional Pathway. *Cel. Metab.* 12 (4), 352–361. doi:10.1016/j.cmet.2010.09.002
- Fehrenbach, H., Wagner, C., and Wegmann, M. (2017). Airway Remodeling in Asthma: What Really Matters. *Cell Tissue Res.* 367 (3), 551–569. doi:10.1007/s00441-016-2566-8
- Feketea, G., Bocsan, C. I., Popescu, C., Gaman, M., Stanciu, L. A., and Zdrengea, M. T. (2019). A Review of Macrophage MicroRNAs' Role in Human Asthma. *Cells*. 8 (5), 420. doi:10.3390/cells8050420
- Gordon, S., and Martinez, F. O. (2010). Alternative Activation of Macrophages: Mechanism and Functions. *Immunity*. 32 (5), 593–604. doi:10.1016/j.immuni.2010.05.007
- Hadjigil, S., Netto, K. G., Maltby, S., Tay, H. L., Nguyen, T. H., Hansbro, N. G., et al. (2020). Lipopolysaccharide Induces Steroid-Resistant Exacerbations in a Mouse Model of Allergic Airway Disease Collectively Through IL-13 and Pulmonary Macrophage Activation. *Clin. Exp. Allergy*. 50, 82. doi:10.1111/cea.13505
- Holgate, S. T. (2012). Innate and Adaptive Immune Responses in Asthma. *Nat. Med.* 18 (5), 673–683. doi:10.1038/nm.2731
- Holtzman, M. J. (2012). Asthma as a Chronic Disease of the Innate and Adaptive Immune Systems Responding to Viruses and Allergens. *J. Clin. Invest.* 122 (8), 2741–2748. doi:10.1172/jci60325
- James, A. L., Elliot, J. G., Jones, R. L., Carroll, M. L., Mauad, T., Bai, T. R., et al. (2012). Airway Smooth Muscle Hypertrophy and Hyperplasia in Asthma. *Am. J. Respir. Crit. Care Med.* 185 (10), 1058–1064. doi:10.1164/rccm.201110-1849oc
- Kubota, Y., Iwasaki, Y., Harada, H., Yokomura, I., Ueda, M., Hashimoto, S., et al. (1999). Depletion of Alveolar Macrophages by Treatment With 2-Chloroadenosine Aerosol. *Clin. Diagn. Lab. Immunol.* 6 (4), 452–456. doi:10.1128/cdli.6.4.452-456.1999
- Lee, Y. G., Jeong, J. J., Nyenhuis, S., Berdyshev, E., Chung, S., Ranjan, R., et al. (2015). Recruited Alveolar Macrophages, in Response to Airway Epithelial-Derived Monocyte Chemoattractant Protein 1/CCl $_2$ , Regulate Airway Inflammation and Remodeling in Allergic Asthma. *Am. J. Respir. Cel Mol Biol.* 52 (6), 772–784. doi:10.1165/rcmb.2014-0255oc
- Levy-Apter, E., Finkelshtein, E., Vemulapalli, V., Li, S. S.-C., Bedford, M. T., and Elson, A. (2014). Adaptor Protein GRB2 Promotes Src Tyrosine Kinase Activation and Podosomal Organization by Protein-Tyrosine Phosphatase  $\epsilon$  in Osteoclasts. *J. Biol. Chem.* 289 (52), 36048–36058. doi:10.1074/jbc.m114.603548
- Li, H., Jiang, T., Li, M.-Q., Zheng, X.-L., and Zhao, G.-J. (2018). Transcriptional Regulation of Macrophages Polarization by MicroRNAs. *Front. Immunol.* 9, 1175. doi:10.3389/fimmu.2018.01175
- Li, P., Lang, X., and Xia, S. (2019). Elevated Expression of MicroRNA-378 in Children With Asthma Aggravates Airway Remodeling by Promoting the Proliferation and Apoptosis Resistance of Airway Smooth Muscle Cells. *Exp. Ther. Med.* 17 (3), 1529–1536. doi:10.3892/etm.2018.7141
- Lin, W., Su, F., Gautam, R., Wang, N., Zhang, Y., and Wang, X. (2018). Raf Kinase Inhibitor Protein Negatively Regulates Fc $\epsilon$ R1-Mediated Mast Cell Activation and Allergic Response. *Proc. Natl. Acad. Sci. USA*. 115 (42), E9859–E9868. doi:10.1073/pnas.1805474115
- Liu, G., and Yang, H. (2013). Modulation of Macrophage Activation and Programming in Immunity. *J. Cel. Physiol.* 228 (3), 502–512. doi:10.1002/jcp.24157
- Massoud, A. H., Charbonnier, L.-M., Lopez, D., Pellegrini, M., Phipatanakul, W., and Chatila, T. A. (2016). An Asthma-Associated IL4R Variant Exacerbates Airway Inflammation by Promoting Conversion of Regulatory T Cells to TH17-Like Cells. *Nat. Med.* 22 (9), 1013–1022. doi:10.1038/nm.4147
- Murray, P. J., and Wynn, T. A. (2011). Protective and Pathogenic Functions of Macrophage Subsets. *Nat. Rev. Immunol.* 11 (11), 723–737. doi:10.1038/nri3073
- Ndolo, R. A., Forrest, M. L., and Krise, J. P. (2010). The Role of Lysosomes in Limiting Drug Toxicity in Mice. *J. Pharmacol. Exp. Ther.* 333 (1), 120–128. doi:10.1124/jpet.109.160226
- Ohtani, A., Kumazawa, Y., Fujisawa, H., and Nishimura, C. (1982). Inhibition of Macrophage Function by 2-Chloroadenosine. *J. Reticuloendothel Soc.* 32 (3), 189–200.
- Park, S. Y., Jing, X., Gupta, D., and Dziarski, R. (2013). Peptidoglycan Recognition Protein 1 Enhances Experimental Asthma by Promoting Th2 and Th17 and Limiting Regulatory T Cell and Plasmacytoid Dendritic Cell Responses. *J. I.* 190 (7), 3480–3492. doi:10.4049/jimmunol.1202675
- Rajaram, M. V. S., Arnett, E., Azad, A. K., Guirado, E., Ni, B., Gerberick, A. D., et al. (2017). *M. tuberculosis* -Initiated Human Mannose Receptor Signaling Regulates Macrophage Recognition and Vesicle Trafficking by FcR $\gamma$ -Chain, Grb2, and SHP-1. *Cel Rep.* 21 (1), 126–140. doi:10.1016/j.celrep.2017.09.034
- Rao, G. N. (1996). Hydrogen Peroxide Induces Complex Formation of SHC-Grb2-SOS With Receptor Tyrosine Kinase and Activates Ras and Extracellular Signal-Regulated Protein Kinases Group of Mitogen-Activated Protein Kinases. *Oncogene*. 13 (4), 713–719.
- Rückert, D., Jenkins, S. J., Laqtom, N. N., Gallagher, I. J., Sutherland, T. E., Duncan, S., et al. (2012). Induction of IL-4R $\alpha$ -Dependent MicroRNAs Identifies PI3K/Akt Signaling as Essential for IL-4-driven Murine Macrophage Proliferation *In Vivo*. *Blood*. 120 (11), 2307–2316. doi:10.1182/blood-2012-02-408252
- Saito, T., and Yamaguchi, J. (1985). 2-Chloroadenosine: a Selective Lethal Effect to Mouse Macrophages and its Mechanism. *J. Immunol.* 134 (3), 1815–1822.
- Self-Fordham, J. B., Naqvi, A. R., Uttamani, J. R., Kulkarni, V., and Nares, S. (2017). MicroRNA: Dynamic Regulators of Macrophage Polarization and Plasticity. *Front. Immunol.* 8, 1062. doi:10.3389/fimmu.2017.01062
- Shenoy, A., and Belloch, R. H. (2014). Regulation of MicroRNA Function in Somatic Stem Cell Proliferation and Differentiation. *Nat. Rev. Mol. Cel Biol.* 15 (9), 565–576. doi:10.1038/nrm3854
- Stellari, F., Sala, A., Ruscitti, F., Carnini, C., Mirandola, P., Vitale, M., et al. (2015). Monitoring Inflammation and Airway Remodeling by Fluorescence Molecular Tomography in a Chronic Asthma Model. *J. Transl Med.* 13, 336. doi:10.1186/s12967-015-0696-5
- Su, S., Zhao, Q., He, C., Huang, D., Liu, J., Chen, F., et al. (2015). miR-142-5p and miR-130a-3p Are Regulated by IL-4 and IL-13 and Control Proinflammatory Macrophage Program. *Nat. Commun.* 6, 8523. doi:10.1038/ncomms9523
- Van Dyken, S. J., and Locksley, R. M. (2013). Interleukin-4- and Interleukin-13-Mediated Alternatively Activated Macrophages: Roles in Homeostasis and Disease. *Annu. Rev. Immunol.* 31, 317–343. doi:10.1146/annurev-immunol-032712-095906
- Vats, D., Mukundan, L., Odegaard, J. I., Zhang, L., Smith, K. L., Morel, C. R., et al. (2006). Oxidative Metabolism and PGC-1 $\beta$  Attenuate Macrophage-Mediated Inflammation. *Cel Metab.* 4 (1), 13–24. doi:10.1016/j.cmet.2006.05.011

- Wang, X., Zhang, D., Higham, A., Wolosińska, S., Gai, X., Zhou, L., et al. (2020). ADAM15 Expression Is Increased in Lung CD8+ T Cells, Macrophages, and Bronchial Epithelial Cells in Patients With COPD and Is Inversely Related to Airflow Obstruction. *Respir. Res.* 21 (1), 188. doi:10.1186/s12931-020-01446-5
- Xu, Z.-h., Yao, T.-z., and Liu, W. (2018). miR-378a-3p Sensitizes Ovarian Cancer Cells to Cisplatin Through Targeting MAPK1/GRB2. *Biomed. Pharmacother.* 107, 1410–1417. doi:10.1016/j.biopha.2018.08.132
- Yang, M., Kumar, R. K., Hansbro, P. M., and Foster, P. S. (2012). Emerging Roles of Pulmonary Macrophages in Driving the Development of Severe Asthma. *J. Leukoc. Biol.* 91 (4), 557–569. doi:10.1189/jlb.0711357
- Yu, X., Zeng, Y., Bao, M., Wen, J., Zhu, G., Cao, C., et al. (2020). Low-Magnitude Vibration Induces Osteogenic Differentiation of Bone Marrow Mesenchymal Stem Cells via miR-378a-3p/Grb2 Pathway to Promote Bone Formation in a Rat Model of Age-related Bone Loss. *FASEB J.* 34 (9), 11754–11771. doi:10.1096/fj.201902830rrr
- Zeng, T., Wang, X., Wang, W., Feng, Q., Lao, G., Liang, Y., et al. (2019). Endothelial Cell-Derived Small Extracellular Vesicles Suppress Cutaneous Wound Healing Through Regulating Fibroblasts Autophagy. *Clin. Sci. (Lond.)* 133 (9), CS20190008. doi:10.1042/CS20190008
- Zhao, Y., Tang, X., Huang, Y., Tang, Q., Ma, C., Zheng, F., et al. (2019). Interaction of C-Jun and HOTAIR- Increased Expression of P21 Converge in Polyphyllin I-Inhibited Growth of Human Lung Cancer Cells. *Onco Targets Ther.* Vol. 12, 10115–10127. doi:10.2147/ott.s226830
- Conflict of Interest:** The authors declare that the research was conducted in the absence of any commercial or financial relationships that could be construed as a potential conflict of interest.
- Publisher's Note:** All claims expressed in this article are solely those of the authors and do not necessarily represent those of their affiliated organizations, or those of the publisher, the editors and the reviewers. Any product that may be evaluated in this article, or claim that may be made by its manufacturer, is not guaranteed or endorsed by the publisher.

Copyright © 2021 Wang, Hong, Chen, Shi, Lin, Huang, Tang, Guo, Yuan and Jiang. This is an open-access article distributed under the terms of the Creative Commons Attribution License (CC BY). The use, distribution or reproduction in other forums is permitted, provided the original author(s) and the copyright owner(s) are credited and that the original publication in this journal is cited, in accordance with accepted academic practice. No use, distribution or reproduction is permitted which does not comply with these terms.



# Exhaled Volatile Organic Compounds for Identifying Patients With Chronic Pulmonary Aspergillosis

Zheng-Tu Li<sup>††</sup>, Pei-Ying Zeng<sup>††</sup>, Zhao-Ming Chen<sup>††</sup>, Wei-Jie Guan<sup>1,2†</sup>, Tong Wang<sup>3,4</sup>, Ye Lin<sup>1</sup>, Shao-Qiang Li<sup>1</sup>, Zhi-Juan Zhang<sup>3,4,5</sup>, Yang-Qing Zhan<sup>1</sup>, Ming-Die Wang<sup>1</sup>, Guo-Bin Tan<sup>3,4,6</sup>, Xue Li<sup>3,4\*</sup> and Feng Ye<sup>1\*</sup>

<sup>1</sup> State Key Laboratory of Respiratory Disease, National Clinical Research Center for Respiratory Disease, National Center for Respiratory Medicine, Guangzhou Institute of Respiratory Health, The First Affiliated Hospital of Guangzhou Medical University, Guangzhou, China, <sup>2</sup> Department of Thoracic Surgery, Guangzhou Institute of Respiratory Health, The First Affiliated Hospital of Guangzhou Medical University, Guangzhou, Guangdong, China, <sup>3</sup> Institute of Mass Spectrometry and Atmospheric Environment, Jinan University, Guangzhou, China, <sup>4</sup> Guangdong Provincial Engineering Research Center for On-Line Source Apportionment System of Air Pollution, Guangzhou, China, <sup>5</sup> College of Pharmacy, Hena University of Chinese Medicine, Zhengzhou, China, <sup>6</sup> Guangzhou Hexin Instrument Co., Ltd., Guangzhou, China

## OPEN ACCESS

### Edited by:

Zhang Qingling,  
Guangzhou Institute of Respiratory  
Health, China

### Reviewed by:

Xin Su,  
Nanjing General Hospital of Nanjing  
Military Command, China  
Yi Shi,  
Second People's Hospital of Yunnan  
Province, China

### \*Correspondence:

Xue Li  
tamylee@jnu.edu.cn  
Feng Ye  
tu276025@gird.cn; yefeng@gird.cn

<sup>††</sup>These authors have contributed  
equally to this work and share first  
authorship

### Specialty section:

This article was submitted to  
Pulmonary Medicine,  
a section of the journal  
Frontiers in Medicine

Received: 03 June 2021

Accepted: 31 August 2021

Published: 23 September 2021

### Citation:

Li Z-T, Zeng P-Y, Chen Z-M,  
Guan W-J, Wang T, Lin Y, Li S-Q,  
Zhang Z-J, Zhan Y-Q, Wang M-D,  
Tan G-B, Li X and Ye F (2021) Exhaled  
Volatile Organic Compounds for  
Identifying Patients With Chronic  
Pulmonary Aspergillosis.  
Front. Med. 8:720119.  
doi: 10.3389/fmed.2021.720119

**Background:** Diagnosing chronic pulmonary aspergillosis is a major challenge in clinical practice. The development and validation of a novel, sensitive and specific assay for diagnosing chronic pulmonary aspergillosis is urgently needed.

**Methods:** From April 2018 to June 2019, 53 patients with chronic pulmonary aspergillosis (CPA), 32 patients with community-acquired pneumonia (CAP) and 48 healthy controls were recruited from the First Affiliated Hospital of Guangzhou Medical University. Clinical characteristics and samples were collected at enrollment. All exhaled breath samples were analyzed offline using thermal desorption single-photon ionization time-of-flight mass spectrometry; to analyze the metabolic pathways of the characteristic volatile organic compounds, serum samples were subjected to ultrahigh-performance liquid chromatography.

**Results:** We identified characteristic volatile organic compounds in patients with chronic pulmonary aspergillosis, which mainly consisted of phenol, neopentyl alcohol, toluene, limonene and ethylbenzene. These compounds were assessed using a logistic regression model. The sensitivity and specificity were 95.8 and 96.9% for discriminating patients in the CPA group from those in the CAP group and 95.8 and 97.9% for discriminating patients in the CPA group from healthy controls, respectively. The concentration of limonene ( $m/z$  136) correlated significantly positively with anti-*Aspergillus fumigatus* IgG antibody titers ( $r = 0.420$ ,  $P < 0.01$ ). After antifungal treatment, serum IgG and the concentration of limonene ( $m/z$  136) decreased in the subgroup of patients with chronic pulmonary aspergillosis.

**Conclusions:** We identified VOCs that can be used as biomarkers for differential diagnosis and therapeutic response prediction in patients with chronic pulmonary aspergillosis.

**Keywords:** chronic pulmonary aspergillosis, volatile organic compounds, metabolomics, exhalation, single-photon ionization-mass spectrometry



## IMPORTANCE

In this study, it is promising to apply TD-SPI-TOF-MS to quickly evaluate the possibility of using breath VOCs to fast screen chronic pulmonary aspergillosis (CPA) patients. And several characteristic volatile organic compounds were identified as potential biomarkers for differential diagnosis and therapeutic response prediction in patients with CPA. Furthermore, the serum metabolism also used to preliminarily explore the source of exhaled VOCs. The findings of our study will provide a new, relatively non-invasive and easy to operate diagnostic method for the future clinical diagnosis of CPA.

## INTRODUCTION

Pulmonary aspergillosis is common in immunosuppressed patients and a major global health burden, affecting more than 3 million people worldwide (1, 2). Patients with chronic pulmonary aspergillosis (CPA) frequently have comorbidities and atypical clinical symptoms, making early diagnosis and treatment difficult. To date, the diagnosis of CPA mainly relies on pathology, serology and imaging. However, these diagnostic methods are time consuming and may be invasive, and personnel performing microscopy analyses need to be professional and experienced; therefore, missed or delayed diagnosis occurs in a considerable proportion of patients, which might increase the mortality rate (3, 4).

Recent scientific advances have allowed for the rapid, non-invasive, and convenient diagnosis of respiratory disease with cutting-edge technologies (5). Measuring the patterns of volatile organic compounds (VOCs) in exhaled breath is a novel non-invasive metabolomic approach for studying the molecular signatures of respiratory disease (6–10), and gas chromatography-mass spectrometry (GC-MS) has identified several characteristic VOCs in patients with pulmonary aspergillosis (11–13). Nonetheless, breath analysis of pulmonary aspergillosis is mostly based on *Aspergillus* strains *in vitro*, and there are a limited number of volatile substances that can be detected by GC-MS. Thermal desorption—single-photon ionization—mass spectrometry (TD-SPI-MS) has a high sensitivity, is user-friendly, and can be applied to detect VOCs with a low concentration or a wide range of substances (9, 14). In general, metabolomic analysis can quantitatively analyze all metabolites, which helps in evaluating associations between metabolites and pathophysiological changes (15). Indeed, a number of studies have reported that serum metabolites can be used as biomarkers of infectious diseases for diagnosing and evaluating clinical severity (16–19).

In this study, we aimed to perform broad-spectrum screening of exhaled VOCs and metabolomic analysis by applying TD-SPI-MS for patients with CPA. The metabolic pathways of such metabolites may further reveal the components and biological roles of the characteristic VOCs in exhaled breath associated with pulmonary aspergillosis. Our findings provide a novel tool for the non-invasive, simple and reliable clinical diagnosis of CPA.

## METHODS

### Patients

Between April 2018 and June 2019, patients with CPA, patients with community-acquired pneumonia (CAP) and healthy controls were recruited from the First Affiliated Hospital of Guangzhou Medical University. Patients with CPA according to the guidelines of diagnosis and management of *Aspergillus* diseases were enrolled (group CPA) (20). The diagnosis of CAP was made according to the guidelines of diagnosis and treatment of CAP (group CAP) (21). The healthy controls did not have any documented pulmonary infectious, interstitial or malignant lung diseases (group N). We excluded patients who were younger than 18 years old, declined exhaled breath analysis, had ingested foods or brushed their teeth after 22:00 p.m. the night before sample collection or were currently smokers or had consumed alcohol within 2 months prior to the examination.

The guidelines (20) for the diagnosis and treatment of pulmonary aspergillosis recommend at least 6 months of voriconazole therapy (200 mg every 12 h) for CPA. As the plasma concentration of voriconazole was detected to maintain the recommended effective concentration range (1~5.5 mg/L), four time points were scheduled for follow-up during the antifungal treatment. The patients were followed up for 9 months (before treatment and at 3, 6, and 9 months after treatment).

### VOC Analysis

TD-SPI-MS was performed to obtain qualitative and quantitative data. See **Supplementary Material** for the detailed methods and precautions of exhaled breath collection.

### Serum Metabolite Analysis and Metabolic Pathways

Patients fasted for 8–10 h before exhaled gas collection, followed by venipuncture (4 ml) in the morning to collect peripheral blood. The samples were centrifuged at 3,000 rpm for 15 min, and the serum was stored at  $-80^{\circ}\text{C}$  for subsequent analysis. For each assay, 100  $\mu\text{l}$  serum plus 300  $\mu\text{l}$  methanol and 20  $\mu\text{l}$  internal standard were added to a centrifuge tube. After vortexing for 30 s, the samples were subjected to ultrasonic treatment in an ice bath for 5 min and kept at  $-20^{\circ}\text{C}$  for 2 h. After centrifugation at 13,000 rpm at  $4^{\circ}\text{C}$  for 15 min, 200  $\mu\text{l}$  of the supernatant was transferred to a 2-ml sample vial. All serum metabolites were analyzed using an ultrahigh-performance liquid chromatography-pristine instrument.

### Statistical Analysis

Clinical data were analyzed using IBM SPSS Statistics (version 20, SPSS Inc., USA). A *P*-value of 0.05 or less indicated statistical significance. Categorical data are presented as numbers and percentages and continuous data as medians and ranges or interquartile ranges (IQRs). Comparison of continuous data was performed using Student's *t*-test or Mann-Whitney test. Fisher's exact test was applied to compare categorical variables. Partial least squares discrimination analysis (OPLS-DA) with SIMCA software (version 14.1, MKS Umetrics, Sweden) (22) was adopted. High-dimensional data were further processed

**TABLE 1** | Baseline characteristics of the study participants.

Characteristics	Group CPA ( <i>n</i> = 53)	Group CAP ( <i>n</i> = 32)	Group N ( <i>n</i> = 48)	<i>P</i> -value
Age (year, x ± S)	49.0 ± 15.8	38.0 ± 18.5	26.2 ± 7.0	0.001
Sex, male (No, %)	35 (66.0%)	11 (34.4%)	33 (68.8%)	0.004
Height (cm, x ± S)	162.9 ± 10.0	161.4 ± 9.0	162.2 ± 9.2	0.762
Weight (kg, x ± S)	51.6 ± 10.9	56.3 ± 12.5	59.0 ± 10.6	0.003
<b>Smoking status<sup>a</sup></b>				
Ex-smoker (No, %)	13 (24.5%)	5 (15.6%)	3 (6.3%)	0.010
Never-smoker (No, %)	40 (75.5%)	27 (84.4%)	45 (93.8%)	
<b>Drinking status<sup>a</sup></b>				
Ex-drinker (No, %)	3 (5.8%)	1 (3.1%)	0	0.121
Never-drinker (No, %)	50 (94.3%)	31 (96.9%)	48 (100.0%)	
<b>Eating habits<sup>a</sup></b>				
Light diet (No, %)	45 (83.2%)	30 (93.8%)	43 (89.6%)	0.078
Non-light diet (No, %)	8 (16.8%)	2 (6.3%)	5 (10.4%)	

*a:* Ex-smokers were defined as those who smoked continuously for at least 6 months but had quit smoking for more than 2 months at the time of recruitment; the definitions of ex-drinkers were similar to those of ex-smokers; light diet refers to daily diet habits, including spicy food such as pepper, garlic, and green onion.

through dimensionality reduction, and the variable importance for projection (VIP) in the OPLS-DA model was calculated (23). For VIPs equal to or  $>1.0$ , an array of characteristic ions in the CPA group was selected as potential targets. As each substance may have the same germplasm charge ratio, each  $m/z$  value can correspond to one or more VOCs. The possible ion range can be inferred according to the CAS (Chemical Abstracts Service, USA).

Metabolites were qualitatively evaluated according to the KEGG (Kyoto Encyclopedia of Genes and Genomes) (<http://www.genome.jp/kegg/>) database and a customized database. Multivariate statistical analysis was performed using the normalized data matrix with PCA, PLS-DA, OPLS-DA and sequencing tests. Multivariate (OPLS-DA) and univariate statistical (Student's *t*-test) analyses were applied to screen and cluster differentially expressed metabolites, perform metabolic pathway KEGG enrichment analysis, and construct a metabolite regulation network. Potential metabolic pathways between exhaled breath and blood were explored by performing Venn analysis and enrichment analysis. The digital matrix composed of the selected characteristic VOCs was imported into MATLAB (version R2017b, MathWorks, Inc., USA) to construct different classification models, and the accuracy, sensitivity and characteristics of the models were verified by binary logistic regression analysis. The optimal model was selected for simulation operation, which further confirmed the value of characteristic VOCs for CPA diagnosis. Pearson's correlation analysis was used to analyze correlations between exhaled breath VOC expression levels and anti-*Aspergillus* IgG titers in the CPA group.

## RESULTS

### Baseline Characteristics

We included 53 patients in the CPA group and 32 in the CAP group and 48 subjects in group N. The study flow

chart is provided in **Supplementary Figure 1**, and the baseline characteristics of the included participants are shown in **Table 1**. Most of the subjects were male (59.4%), and the male subjects were significantly older than the female subjects [median: 54 (range 38–65 years) vs. 39 (range 29–54 years)]. Patients in the CPA group rarely smoked or drank alcohol. Additionally, age and sex differed significantly between the CPA group and group N ( $P < 0.01$ ). Both weight and smoking history ( $P < 0.01$ ), but not height, drinking history or eating habits, differed significantly among the three groups.

### Characteristic Exhaled VOCs

To avoid artifacts, the sampling temperature was controlled between 20 and 25°C, and a regular ultraviolet lamp was applied for environmental irradiation to minimize contamination before sample collection. Despite certain differences in demographic characteristics, we recruited study participants without a recent smoking history.

According to the OPLS-DA model of the entire cohort, VOCs in exhaled breath were capable of distinguishing the three groups ( $R^2 = 0.954$ ,  $Q^2 = 0.745$ , **Figures 1A,B**). Therefore, the original data model explained the differences among the CPA, CAP and N groups. The  $m/z$  value of the characteristic VOCs was derived based on the VIP value (**Figure 1C**). After incorporating information from Chemical Abstracts Database (Chemical Abstracts Service, CAS), the characteristic VOCs in patients with CPA were found to be ketones, aldehydes, esters, hydrocarbons and benzenes; the detailed characteristics of these compounds are shown in **Table 2**.

### Characteristic Serum Metabolites and Metabolic Pathways

At present, existing theories show that the exhaled VOCs are the product of blood metabolism after pathogen infection (5, 6, 24). Therefore, the purpose of our study on serum metabolomics is to preliminarily explore the source of exhaled VOCs. To identify

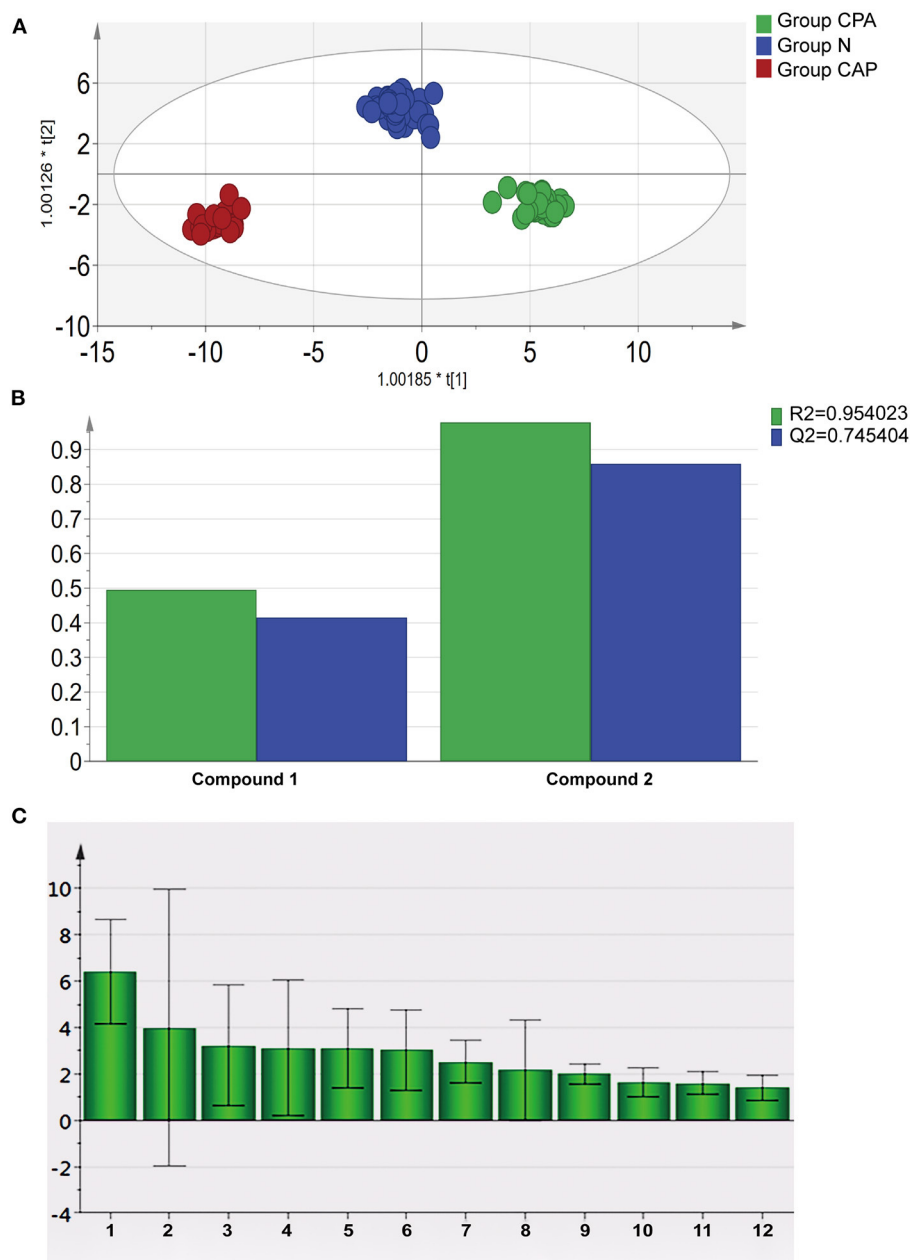


**FIGURE 1 |** Statistical analysis of characteristic VOCs in exhaled breath of patients with CPA. **(A)** OPLS-DA score plot of characteristic VOCs in exhaled breath samples in group CPA, group CAP and group N. **(B)** Parameters of the OPLS-DA model of characteristic VOCs in exhaled breath samples in group CPA, group CAP and group N. **(C)** VIP value of characteristic VOCs in exhaled breath samples of patients with CPA.

characteristic serum metabolites, we randomly selected samples from subjects with paired serum samples (10 cases in group CPA, 5 in group CAP and 5 in group N). Except for a significant difference in age between group CPA and group N, there were no significant differences in sex, weight or height among the three groups ( $P > 0.05$ ).

The OPLS-DA score chart (**Figure 2A**) showed that the original model was able to explain the differences in serum metabolites among the CPA, CAP and N groups.

According to the VIP value of OPLS-DA and between-group comparisons (Student's *t*-test), we identified 24 differentially expressed metabolites between groups CPA and N and 17 differentially expressed metabolites between groups CPA and CAP (**Figure 2B**). A Venn diagram further illustrated 7 metabolites in group CPA that were differentially expressed compared with groups N and CAP (**Figure 2C**).

The same characteristic VOC expressed metabolites between exhaled breath and serum in CPA patients were enriched in

**TABLE 2 |** Reference compounds of characteristic VOCs of patients in the CPA group.

Number	m/z value	Compound name	CAS number
1	m/z 58	Propanone/Acetone	7-64-1
2	m/z 62	Dimethyl sulfide	75-18-3
		Ethylthiol	75-08-1
3	m/z 68	Isoprene/2-Methyl-1,3-Butadiene	78-79-5
4	m/z 69	1,2-Pentadiene	591-95-7
		Ethyl acetate	141-78-6
5	m/z 88	Neopentyl alcohol	75-84-3
		2-Methyl-2-butanol	75-85-5
6	m/z 92	Toluene	108-88-3
7	m/z 94	Phenol	108-95-2
		Methyl disulfide	624-92-0
8	m/z 106	M-Xylene	108-38-3
		P-Xylene	106-42-3
		Ethylbenzene	100-41-4
9	m/z 134	1-Methyl-2-propylbenzene	1074-17-5
		1-Methyl-4-propylbenzene	1074-55-1
10	m/z 136	2-Methyl-3-propylpyrazine	15986-80-8
		3,7-dimethyl-1,3,7-Octatriene	502-99-8
		2-(sec-Butyl)pyrazine	124070-52
		Dipentene	138-86-3
		Phenyl acetate	122-79-2
11	m/z 281	Diphenyl hydrogen phosphate	838-85-7
12	m/z 282	—	—

different metabolic pathways to clarify the source. Pathway analysis based on the latest KEGG database for differentially expressed metabolites was assigned to six level-1 KEGG pathways (**Figure 3A**). Pathway enrichment analysis identified the most significantly altered metabolic pathways related to microbial metabolism in diverse environments (pathway 1,  $P < 0.05$ ) and degradation of aromatic compounds (pathway 2,  $P < 0.05$ ) (**Figure 3B**). In these metabolic pathways, the expression profiles of the characteristic VOCs (including phenol, neopentyl alcohol, toluene, limonene and ethylbenzene) between exhaled breath and serum matched (**Table 3**). These compounds were tested by a logistic regression model, with a sensitivity and specificity of 95.8 and 96.9% for discriminating patients in the CPA group from those in the CAP group and 95.8 and 97.9% for discriminating patients in the CPA group from healthy controls, respectively (**Figures 4A,B**).

### Correlation of Characteristic VOCs With Clinical Parameters

In the CAP group, 13 patients (40.6%) had *Mycoplasma pneumonia*, 11 (34.4%) bacterial pneumonia and 8 (25.0%) viral pneumonia. Among CPA patients, the main presenting symptoms were fever, cough, expectoration, hemoptysis and dyspnea. The dominant radiologic characteristics included cavitation, nodules, patchy shadows and ground-glass opacities. There were no significant differences in the neutrophil

count or hemoglobin and procalcitonin levels ( $P < 0.05$ , **Supplementary Table 1**).

We next further explored the association between characteristic VOCs in exhaled breath and anti-*Aspergillus fumigatus* IgG antibody titers in the serum of those in the CPA group. Although the concentration of characteristic VOCs (neopentyl alcohol, phenol, toluene, ethylbenzene) did not correlate significantly with serum IgG antibody titers ( $P > 0.05$ ), the limonene concentration did correlate positively ( $r = 0.420$ ,  $P < 0.01$ , **Figure 4B**).

We finally evaluated the association between dynamic changes in characteristic VOC expression levels and disease outcomes as well as the efficacy of antifungal treatment. Data were available during longitudinal follow-up four patients (**Figure 4D**). The concentration of VOC  $m/z$  136 (limonene) progressively declined after the initiation of antifungal treatment. After anti-fungal treatment for 9 months, the health status of three patients (PA-13, PA-27 and PA-48) improved, as reflected by the alleviation of cough or hemoptysis, decreased anti-*A. fumigatus* IgG antibody titers (negative in one case, positive in two cases), decreased absorption of lesions on chest computed tomography, and a stable blood voriconazole concentration. In support of these clinical signs, the concentration of exhaled breath limonene was also markedly decreased. After 3 months of treatment, PA-27 was readmitted to the hospital due to the recurrence of hemoptysis. Meanwhile, the anti-*Aspergillus* IgG antibody titer decreased compared with the first clinical visit. In contrast, the



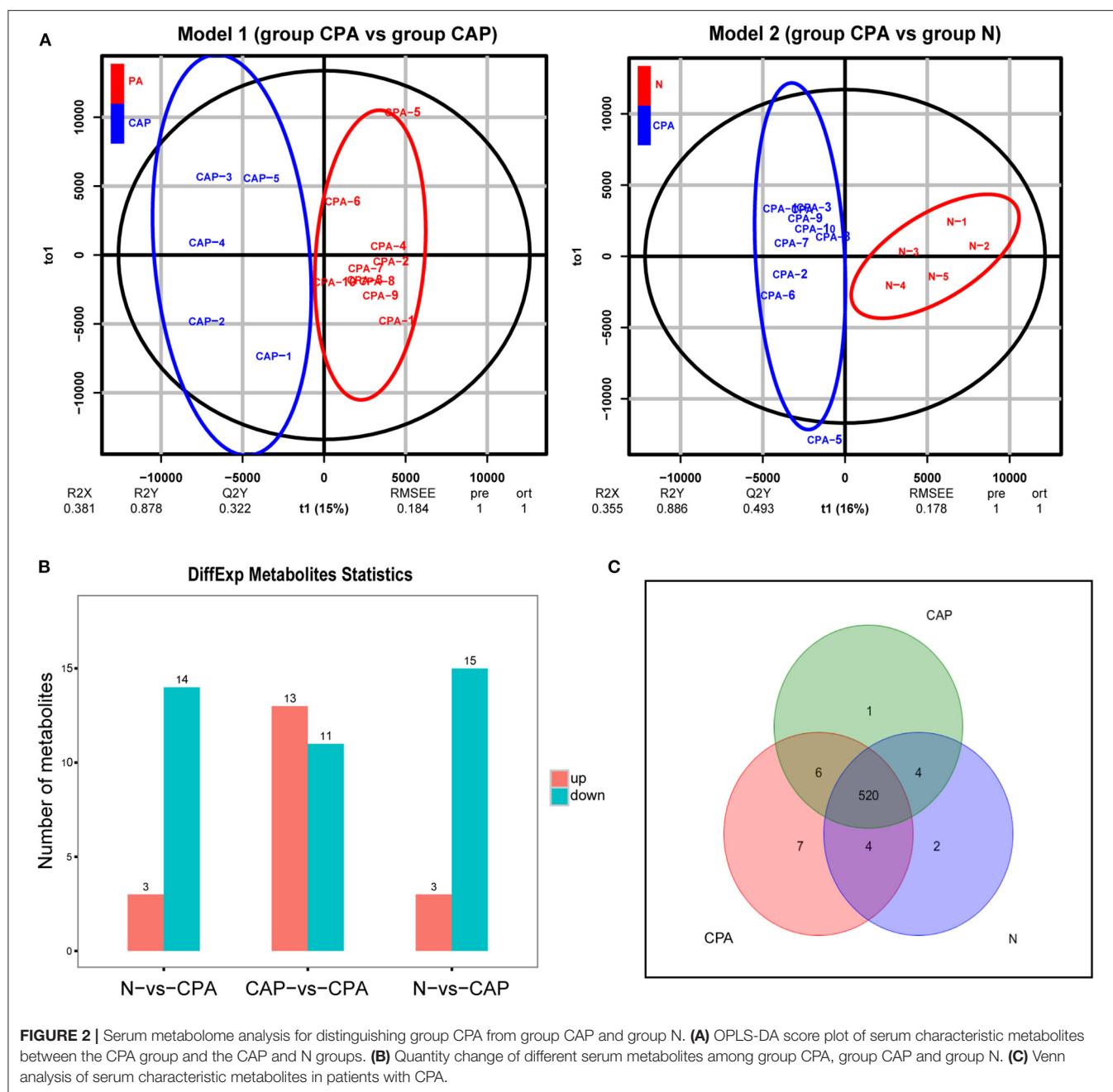


**FIGURE 2 |** Serum metabolome analysis for distinguishing group CPA from group CAP and group N. **(A)** OPLS-DA score plot of serum characteristic metabolites between the CPA group and the CAP and N groups. **(B)** Quantity change of different serum metabolites among group CPA, group CAP and group N. **(C)** Venn analysis of serum characteristic metabolites in patients with CPA.

concentration of exhaled breath limonene increased significantly and then decreased significantly with improvement of the disease. Patient No. PA-20 exhibited disease progression after 9 months of antifungal treatment, with a recurrence of hemoptysis and an increase in pulmonary infiltration, as revealed by chest computed tomography. Nevertheless, negative conversion was achieved for anti-*Aspergillus* IgG antibodies, with the concentration of limonene remaining relatively stable over the course of follow-up (Figure 4C).

## DISCUSSION

We identified several characteristic VOCs by performing TD-SPI-MS in the exhaled breath and serum of patients with CPA, revealing biological pathways associated with microbial metabolism in diverse environments and the degradation of aromatic compounds. Detection of these compounds can effectively distinguish patients with CPA; therefore, some characteristic compounds from exhaled breath or serum VOCs might help with the diagnosis of CPA.

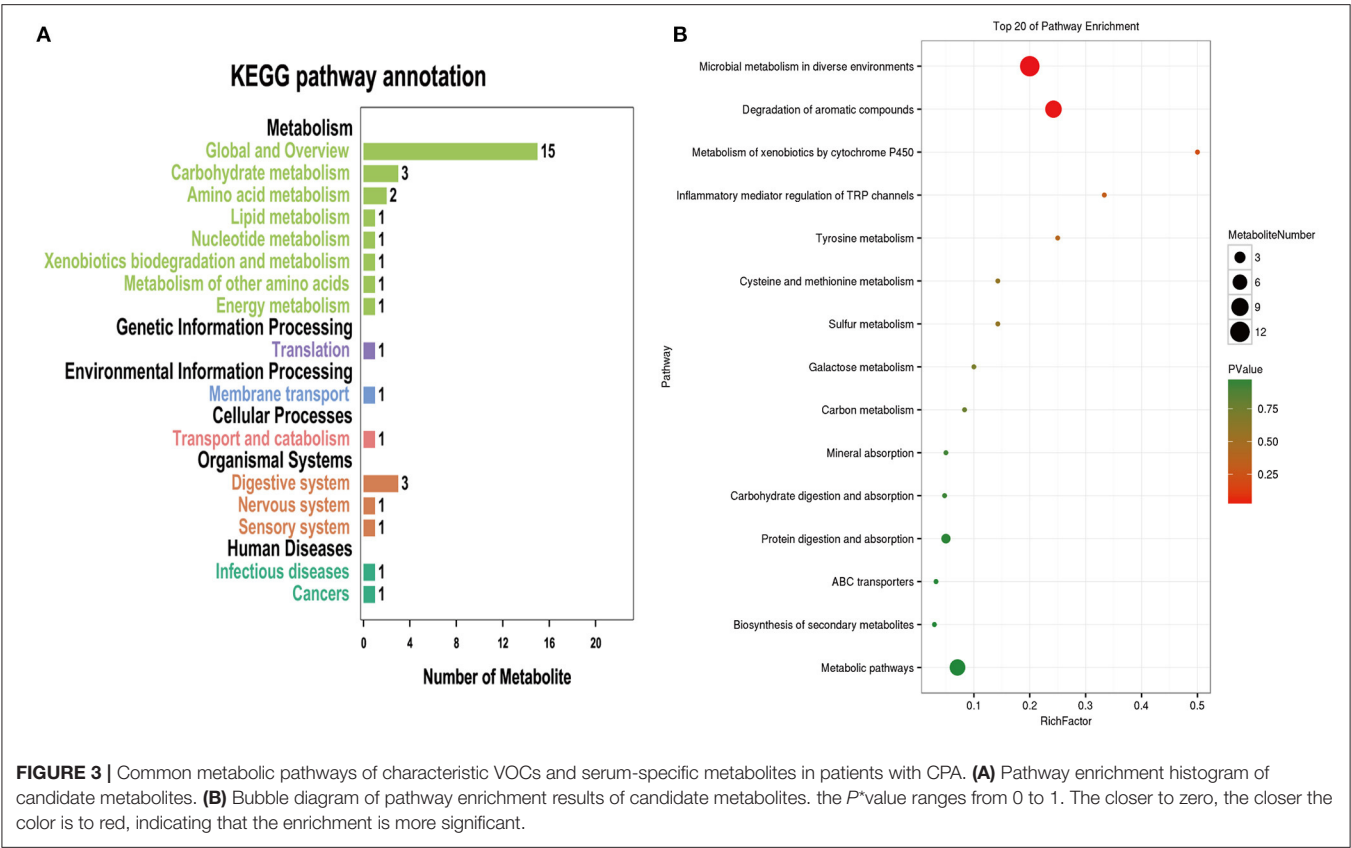


**TABLE 3 |** Common metabolic pathways of characteristic VOCs in exhaled breath and serum metabolites of patients in the CPA group.

KEGG pathway ID	Pathway	P-value	Pathway C-id**	Compound
ko01120	Microbial metabolism in diverse environments	0.0068	C00146	Phenol
			C00556	Neopentyl alcohol*
			C00556	Neopentyl alcohol
			C01455	Toluene
			C06104	Dipentene*
			C07111	Ethylbenzene
ko01220	Degradation of aromatic compounds	0.0140	C00146	Phenol
			C00556	Neopentyl alcohol*
			C01455	Toluene
			C06104	Di pentene*
			C07111	Ethylbenzene

1. \*\*: ID (C number) of metabolites in the KEGG database; 2. \*: serum differential metabolites; 3. Other unmarked metabolites are characteristic VOCs of exhaled breath.

Exhaled breath analysis is prone to bias by environmental or host factors (25, 26). In our study, we conducted rigorous screening for the inclusion of patients, environmental controls and repeated sample collection to minimize measurement bias. The statistical analysis model consistently indicated a good separation of exhaled breath and serum VOCs among the three groups. Our findings confirmed the results from the study by Koo et al. (12), in which alkenes, ketones and alkanes (including limonene) were detected by GC-MS in the exhaled breath of patients with pulmonary aspergillosis. These findings indicate the

value of these compounds as exhaled biomarkers to differentiate pulmonary aspergillosis from other diseases and healthy subjects as well as alkenes and ketones as exhaled breath biomarkers (such as acetone, limonene, isoprene and 1,2-pentadiene). Benzene compounds have not been confirmed as characteristic VOCs of CPA. Our study found that phenol, toluene and ethylbenzene might serve as biomarkers for CPA. The high sensitivity and specificity for differentiating the CPA group might be related to differences in expression levels of benzene, toluene, xylene and chlorobenzene, which are oxidative stress markers of aspergillosis

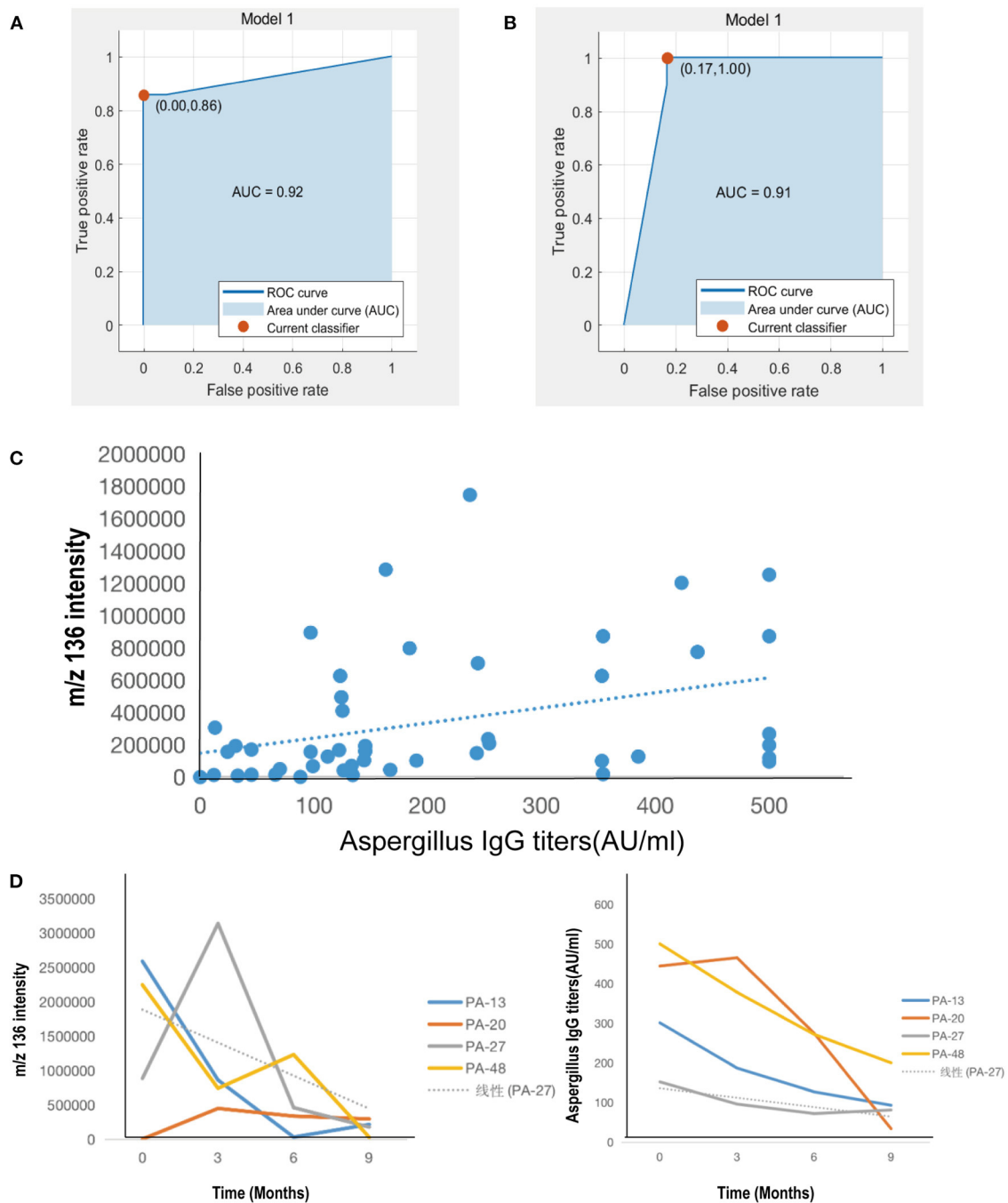


**FIGURE 4 |** Clinical correlation of characteristic VOCs in exhaled breath of patients with CPA. **(A)** Univariate logistic regression model of the CPA group and CAP group. **(B)** Univariate logistic regression model of group CPA and group N. **(C)** Correlation analysis between characteristic VOCs and serum anti-*Aspergillus fumigatus* IgG antibody titers. **(D)** Dynamic changes in levels of breath characteristic VOCs and serum anti-*Aspergillus fumigatus* IgG antibody titers of 4 patients in the CPA group for baseline and follow-up in the third, sixth, and ninth month after voriconazole treatment.

(27). For example, 2-pentyl furan has been considered an important marker of exhaled breath VOCs of patients with *Aspergillus* infection (11, 28, 29). *Aspergillus* spp. produce 2-PF on blood agar, nutrient agar and other media. In our study,

the substance at  $m/z$  128 had a VIP value of  $<1$  and was not confirmed as a characteristic VOC of PA. 2-PF might have originated from hemoglobin, which is produced by blood agar culture medium or pulmonary hemorrhage rather than

*Aspergillus spp. per se* (30). Therefore, it is important to explore the source of these compounds, for instance, by performing metabolomic analysis.

There are more than 200 metabolites related to *Aspergillus sp.* infections (31), most of which are toxins, yet most metabolites produced by interactions with the host are still unknown. In our study, the main metabolic pathways involved in the characteristic VOCs of exhaled breath and the differentially expressed metabolites in serum consisted of microbial metabolism compounds in diverse environments and the products of aromatic compound degradation. Characteristic VOCs in microbial metabolism and metabolic pathways (degradation of aromatic compounds) were shared between the exhaled breath and serum samples. The main metabolites (including phenol, neopentyl alcohol, toluene, limonene and ethylbenzene) suggested that *Aspergillus sp.* infection might result in the production of characteristic metabolites through microbial metabolism and aromatic compound degradation (12, 30). Consistent with this finding, our study also showed limonene to be a potential characteristic compound, thus confirming its value for differential diagnosis based on exhaled breath analysis. It has been reported that aromatic hydrocarbons can regulate inflammatory T cell and dendritic cell (DC) responses (32) and induce oxidative stress and airway tissue injury (33). These compounds in the exhaled breath might also be products of the host's immune response to pathogens (5).

We further confirmed the sensitivity and specificity of the abovementioned characteristic VOCs. According to a previous study, the sensitivity and specificity of exhaled breath VOCs were 95.8 and 96.9% for discriminating patients with CPA from those with CAP and 95.8 and 97.9% for discriminating patients with CPA from healthy controls, respectively. Compared with traditional serologic testing, such as GM tests using serum and bronchoalveolar lavage samples (34), VOC assays via TD-SPI-MS might better indicate candidate biomarkers in the exhaled breath of CPA patients. The current international guidelines suggest that IgG antibody detection is the most sensitive laboratory test for the diagnosis of chronic cavitary pulmonary aspergillosis (CCPA) (3). We also showed that changes in serum anti-*A. fumigatus* IgG antibody titers in patients with CPA before and after antifungal treatment may sensitively reveal the occurrence and progression of CPA. Anti-fungal therapy reportedly decreases levels of serum IgG titers in patients with CPA (35). Importantly, during a 9-month follow-up, the intensity of limonene also decreased significantly. In addition, there were two patients who experienced CPA recurrence. Among them, despite an apparent decrease in IgG titer, the limonene concentration remained relatively high, suggesting that exhaled VOCs might be used for evaluating the therapeutic response. Hence, the concentration of characteristic VOCs might indicate the efficacy of antifungal treatment.

Several limitations need to be acknowledged. First, interpretation of the findings (particularly the follow-up investigation) was limited by the small sample size, and only the conformed CPA patients, was taken as the study group. In the future study, we will recruit all suspected CAP patients as many as possible. Thus, there will be enough remaining suspected CAP

patients which were excluded from the real CPA patients can be used as one of the control groups. Further investigations that take into account different subtypes of pulmonary aspergillosis are also necessary. Second, our study lacks an *in vitro* analysis of *Aspergillus* strains, which will help validate our findings of cell experimental results. Third, although the TD-SPI-MS instrument has a wide detection range and high sensitivity, the findings should be further validated by GC-MS and other mass spectrometry technologies because there is no unified detection standard for exhaled VOCs and detection results among instruments may differ. Finally, heterogeneity in the underlying diseases of the CAP group might have affected the discriminatory capacity of VOCs, though the inclusion of patients with CAP of different pathogens might have increased the generalizability of our findings.

## CONCLUSION

Exhaled breath VOCs (phenol, neopentyl alcohol, toluene, limonene and ethylbenzene), which may help effectively discriminate patients with CPA, are involved in endogenous metabolism. Limonene might be a novel biomarker that reflects the clinical course and treatment response of CPA.

## DATA AVAILABILITY STATEMENT

The data-sets generated and/or analyzed during the current study are not publicly available due to the presence of sensitive (confidential) participants' information. Requests to access the datasets should be directed to [tu276025@gird.cn](mailto:tu276025@gird.cn).

## ETHICS STATEMENT

The studies involving human participants were reviewed and approved by the Ethics Committee of the First Affiliated Hospital of Guangzhou Medical University. The patients/participants provided their written informed consent to participate in this study. Written informed consent was obtained from the individual(s) for the publication of any potentially identifiable images or data included in this article.

## AUTHOR CONTRIBUTIONS

Z-TL, P-YZ, XL, and FY conceived of and designed the study. Z-TL, P-YZ, Z-MC, W-JG, and FY carried out the analyses and wrote the first draft of the manuscript. P-YZ, YL, S-QL, Y-QZ, and M-DW carried out the patient's recruitment, clinical sample collection, and testing. TW, Z-JZ, G-BT, and XL contributed to detection and analysis of VOCs. P-YZ, Z-MC, and YL contributed to the collection of data from the electronic medical records. All authors contributed to data acquisition, data analysis, or data interpretation and reviewed and approved the final version of the manuscript.



## FUNDING

This work was funded by the open fund of State Key Laboratory of Respiratory Diseases (SKLRD-OP-201913); The independent fund of State Key Laboratory of Respiratory Diseases (SKLRD-Z-202019); and The Guangzhou Institute of Respiratory Health Open Project (2019GIRHZ06).

## ACKNOWLEDGMENTS

We thank the patient; the nurses and clinical staff who are providing care for the patient; staff at the respiratory medicine department of hospital; staff at the clinical lab of hospital;

technical staff of the department of State Key Laboratory of Respiratory Disease for excellent assistance. Furthermore, we would also like to thank AJE team for polishing the English language of this manuscript.

## SUPPLEMENTARY MATERIAL

The Supplementary Material for this article can be found online at: <https://www.frontiersin.org/articles/10.3389/fmed.2021.720119/full#supplementary-material>

**Supplementary Figure 1 |** Flow chart of the enrolled participants.

**Supplementary Table 1 |** Clinical characteristics of patients in case group and control group.

## REFERENCES

- Kosmidis C, Denning DW. The clinical spectrum of pulmonary aspergillosis. *Thorax*. (2015) 70: 270–7. doi: 10.1136/thoraxjnl-2014-206291
- Bongomin F, Gago S, Oladele RO, Denning DW. Global and multi-national prevalence of fungal diseases-estimate precision. *J Fungi*. (2017) 3:5247. doi: 10.3390/jof3040057
- Patterson TF, Thompson GR, Denning DW, Fishman JA, Hadley S, Herbrecht R, et al. Practice guidelines for the diagnosis and management of aspergillosis: 2016 update by the infectious diseases society of America. *Clin Infect Dis*. (2016) 63:e1–e60. doi: 10.1093/cid/ciw326
- Bernal-Martinez L, Alastruey-Izquierdo A, Cuenca-Estrella M. Diagnostics and susceptibility testing in *Aspergillus*. *Future Microbiol*. (2016) 11:315–28. doi: 10.2217/fmb.15.140
- van Oort PM, Povoa P, Schnabel R, Dark P, Artigas A, Bergmans D, et al. The potential role of exhaled breath analysis in the diagnostic process of pneumonia—a systematic review. *J Breath Res*. (2018) 12:024001. doi: 10.1088/1752-7163/aaa499
- Tang Z, Liu Y, Duan Y. Breath analysis: technical developments and challenges in the monitoring of human exposure to volatile organic compounds. *J Chromatogr B*. (2015) 1002:285–99. doi: 10.1016/j.jchromb.2015.08.041
- Boots AW, Bos LD, van der Schee MP, van Schooten FJ, Sterk PJ. Exhaled molecular fingerprinting in diagnosis and monitoring: validating volatile promises. *Trends Mol Med*. (2015) 21:633–44. doi: 10.1016/j.molmed.2015.08.001
- Amann A, Costello BL, Miekisch W, Schubert J, Buszewski B, Pleil J, et al. The human volatilome: volatile organic compounds (VOCs) in exhaled breath, skin emanations, urine, feces and saliva. *J Breath Res*. (2014) 8:034001. doi: 10.1088/1752-7155/8/3/034001
- Hong Y, Che X, Su H, Mai Z, Huang Z, Huang W, et al. Exhaled breath analysis using on-line preconcentration mass spectrometry for gastric cancer diagnosis. *J Mass Spectrom*. (2021) 56:e4588. doi: 10.1002/jms.4588
- Ratui IA, Ligor T, Bocos-Bintintan V, Mayhew CA, Buszewski B. Volatile organic compounds in exhaled breath as fingerprints of lung cancer, asthma and COPD. *J Clin Med*. (2020) 10:352. doi: 10.3390/jcm10010032
- Chambers ST, Bhandari S, Scott-Thomas A, Syhre M. Novel diagnostics: progress toward a breath test for invasive *Aspergillus fumigatus*. *Med Mycol*. (2011) 49:S54–61. doi: 10.3109/13693786.2010.508187
- Koo S, Thomas HR, Daniels SD, Lynch RC, Fortier SM, Shea MM, et al. A breath fungal secondary metabolite signature to diagnose invasive aspergillosis. *Clin Infect Dis*. (2014) 59:1733–40. doi: 10.1093/cid/ciu725
- Gerritsen MG, Brinkman P, Escobar N, Bos LD, de Heer K, Meijer M, et al. Profiling of volatile organic compounds produced by clinical *Aspergillus* isolates using gas chromatography–mass spectrometry. *Med Mycol*. (2018) 56:253–6. doi: 10.1093/mmy/myx035
- Huang Y, Li J, Tang B, Zhu L, Hou K, Li H. Development of a portable single photon ionization-photoelectron ionization time-of-flight mass spectrometer. *Int J Anal Chem*. (2015) 2015:581696. doi: 10.1155/2015/581696
- Williams JH, Phillips TD, Jolly PE, Stiles JK, Jolly CM, Aggarwal D. Human aflatoxicosis in developing countries: a review of toxicology, exposure, potential health consequences, and interventions. *Am J Clin Nutr*. (2004) 80:1106–22. doi: 10.1093/ajcn/80.5.1106
- Shen B, Yi X, Sun Y, Bi X, Du J, Zhang C, et al. Proteomic and metabolomic characterization of COVID-19 patient sera. *Cell*. (2020) 182:59–72. e15. doi: 10.1016/j.cell.2020.05.032
- Cho Y, Park Y, Sim B, Kim J, Lee H, Cho SN, et al. Identification of serum biomarkers for active pulmonary tuberculosis using a targeted metabolomics approach. *Sci Rep*. (2020) 10:3825. doi: 10.1038/s41598-020-60669-0
- Albors-Vaquer A, Rizvi A, Matzapetakis M, Lamosa P, Coelho AV, Patel AB, et al. Active and prospective latent tuberculosis are associated with different metabolomic profiles: clinical potential for the identification of rapid and non-invasive biomarkers. *Emerg Microbes Infect*. (2020) 9:1131–9. doi: 10.1080/22221751.2020.1760734
- Cui L, Zheng D, Lee YH, Chan TK, Kumar Y, Ho WE, et al. Metabolomics investigation reveals metabolite mediators associated with acute lung injury and repair in a murine model of influenza pneumonia. *Sci Rep*. (2016) 6:26076. doi: 10.1038/srep26076
- Ullmann AJ, Aguado JM, Arikian-Akdagli S, Denning DW, Groll AH, Lagrou K, et al. Diagnosis and management of *Aspergillus* diseases: executive summary of the 2017 ESCMID-ECMM-ERS guideline. *Clin Microbiol Infect*. (2018) 24 (Suppl 1):e1–e38. doi: 10.1016/j.cmi.2018.01.002
- Cao B, Huang Y, She DY, Cheng QJ, Fan H, Tian XL, et al. Diagnosis and treatment of community-acquired pneumonia in adults: 2016 clinical practice guidelines by the Chinese Thoracic Society, Chinese Medical Association. *Clin Respir J*. (2018) 12:1320–60. doi: 10.1111/crj.12674
- Jang HJ, Lee JD, Jeon HS, Kim AR, Kim S, Lee HS, et al. Metabolic profiling of eccentric exercise-induced muscle damage in human urine. *Toxicol Res*. (2018) 34:199–210. doi: 10.5487/TR.2018.34.3.199
- Wang C, Li P, Lian A, Sun B, Wang X, Guo L, et al. Blood volatile compounds as biomarkers for colorectal cancer. *Cancer Biol Ther*. (2014) 15:200–6. doi: 10.4161/cbt.26723
- Turner C. Techniques and issues in breath and clinical sample headspace analysis for disease diagnosis. *Bioanalysis*. (2016) 8:677–90. doi: 10.4155/bio.16.22
- Hlastala MP, Anderson JC. Alcohol breath test: gas exchange issues. *J Appl Physiol*. (2016) 121:367–75. doi: 10.1152/japplphysiol.00548.2015
- Gaugg MT, Gomez DG, Barrios-Collado C, Vidal-de-Miguel G, Kohler M, Zenobi R, et al. Expanding metabolite coverage of real-time breath analysis by coupling a universal secondary electrospray ionization source and high resolution mass spectrometry—a pilot study on tobacco smokers. *J Breath Res*. (2016) 10:016010. doi: 10.1088/1752-7155/10/1/016010
- Phillips M, Cataneo RN, Condos R, Ring EG, Greenberg J, La Bombardi V, et al. Volatile biomarkers of pulmonary tuberculosis in the breath. *Tuberculosis*. (2007) 87:44–52. doi: 10.1016/j.tube.2006.03.004

28. Chambers ST, Syhre M, Murdoch DR, McCartin F, Epton MJ. Detection of 2-Pentylfuran in the breath of patients with *Aspergillus fumigatus*. *Med Mycol.* (2009) 47:468–76. doi: 10.1080/13693780802475212
29. Syhre M, Scotter JM, Chambers ST. Investigation into the production of 2-Pentylfuran by *Aspergillus fumigatus* and other respiratory pathogens *in vitro* and human breath samples. *Med Mycol.* (2008) 46:209–15. doi: 10.1080/13693780701753800
30. Ahmed WM, Geranios P, White IR, Lawal O, Nijssen TM, Bromley MJ, et al. Development of an adaptable headspace sampling method for metabolic profiling of the fungal volatome. *Analyst.* (2018) 143:4155–62. doi: 10.1039/C8AN00841H
31. Frisvad JC, Rank C, Nielsen KF, Larsen TO. Metabolomics of *Aspergillus fumigatus*. *Med Mycol.* (2009) 47 (Suppl 1):S53–71. doi: 10.1080/13693780802307720
32. O'Driscoll CA, Gallo ME, Hoffmann EJ, Fechner JH, Schauer JJ, Bradfield CA, et al. Polycyclic aromatic hydrocarbons (PAHs) present in ambient urban dust drive proinflammatory T cell and dendritic cell responses via the aryl hydrocarbon receptor (AHR) *in vitro*. *PLoS ONE.* (2018) 13:e0209690. doi: 10.1371/journal.pone.0209690
33. Meldrum K, Gant TW, Macchiarulo S, Leonard MO. Bronchial epithelial innate and adaptive immunity signals are induced by polycyclic aromatic hydrocarbons. *Toxicol Res.* (2016) 5:816–27. doi: 10.1039/C5TX00389J
34. Mennink-Kersten MA, Donnelly JP, Verweij PE. Detection of circulating galactomannan for the diagnosis and management of invasive aspergillosis. *Lancet Infect Dis.* (2004) 4:349–57. doi: 10.1016/S1473-3099(04)01045-X
35. Li H, Rui Y, Zhou W, Liu L, He B, Shi Y, et al. Role of the *Aspergillus*-specific IgG and IgM test in the diagnosis and follow-up of chronic pulmonary aspergillosis. *Front Microbiol.* (2019) 10:1438. doi: 10.3389/fmicb.2019.01438

**Conflict of Interest:** G-BT was employed by company Guangzhou Hexin Instrument Co., Ltd.

The remaining authors declare that the research was conducted in the absence of any commercial or financial relationships that could be construed as a potential conflict of interest.

**Publisher's Note:** All claims expressed in this article are solely those of the authors and do not necessarily represent those of their affiliated organizations, or those of the publisher, the editors and the reviewers. Any product that may be evaluated in this article, or claim that may be made by its manufacturer, is not guaranteed or endorsed by the publisher.

Copyright © 2021 Li, Zeng, Chen, Guan, Wang, Lin, Li, Zhang, Zhan, Wang, Tan, Li and Ye. This is an open-access article distributed under the terms of the Creative Commons Attribution License (CC BY). The use, distribution or reproduction in other forums is permitted, provided the original author(s) and the copyright owner(s) are credited and that the original publication in this journal is cited, in accordance with accepted academic practice. No use, distribution or reproduction is permitted which does not comply with these terms.



# Therapeutic Effects of the Bcl-2 Inhibitor on Bleomycin-induced Pulmonary Fibrosis in Mice

Yicheng He<sup>1</sup>, Fei Li<sup>1</sup>, Chao Zhang<sup>1</sup>, Xinwei Geng<sup>2</sup>, Madiha Zahra Syeda<sup>2</sup>, Xufei Du<sup>1</sup>, Zhehua Shao<sup>1</sup>, Wen Hua<sup>1</sup>, Wen Li<sup>1</sup>, Zhihua Chen<sup>1</sup>, Songmin Ying<sup>1,2\*</sup> and Huahao Shen<sup>1,3\*</sup>

<sup>1</sup>Key Laboratory of Respiratory Disease of Zhejiang Province, Department of Respiratory and Critical Care Medicine, Second Affiliated Hospital of Zhejiang University School of Medicine, Hangzhou, China, <sup>2</sup>Department of Pharmacology, Zhejiang University School of Medicine, Hangzhou, China, <sup>3</sup>State Key Lab of Respiratory Disease, Guangzhou, China

## OPEN ACCESS

### Edited by:

William C Cho,  
QEH, Hong Kong, SAR China

### Reviewed by:

Ravindra K Sharma,  
University of Florida, United States  
Sandeep Kumar Yadav,  
University of Texas MD Anderson  
Cancer Center, United States

### \*Correspondence:

Songmin Ying  
yings@zju.edu.cn  
Huahao Shen  
huahaoshen@zju.edu.cn

### Specialty section:

This article was submitted to  
Molecular Diagnostics and  
Therapeutics,  
a section of the journal  
Frontiers in Molecular Biosciences

**Received:** 24 December 2020

**Accepted:** 21 September 2021

**Published:** 07 October 2021

### Citation:

He Y, Li F, Zhang C, Geng X,  
Syeda MZ, Du X, Shao Z, Hua W, Li W,  
Chen Z, Ying S and Shen H (2021)  
Therapeutic Effects of the Bcl-2  
Inhibitor on Bleomycin-induced  
Pulmonary Fibrosis in Mice.  
Front. Mol. Biosci. 8:645846.  
doi: 10.3389/fmolb.2021.645846

Idiopathic pulmonary fibrosis (IPF) is a distressing lung disorder with poor prognosis and high mortality rates. Limited therapeutic options for IPF is a major clinical challenge. Well-known for its anti-apoptotic properties, B-cell lymphoma 2 (Bcl-2) plays a critical role in the pathology of malignancies and inflammatory diseases, including IPF. In this study, we aimed to investigate the therapeutic effect of a Bcl-2 homology domain 3 mimetic inhibitor, ABT-199, on bleomycin (BLM)-induced pulmonary fibrosis in mice, and explore possible underlying mechanism. The lung inflammation and fibrosis model was established by intratracheal instillation of a single dose of BLM. We observed elevated Bcl-2 in the alveolar macrophages and fibroblasts derived from BLM-instilled mice from day 7. Further, we obtained *in vivo* evidence that early therapeutic treatment with Bcl-2 inhibitor ABT-199 from day 3, and late treatment from day 10, both alleviated airway inflammation and lung fibrosis induced by BLM. Our data suggest that ABT-199 might be an effective antifibrotic agent that interferes with profibrogenic cells, which may be a promising therapy in the treatment of clinical IPF patients.

**Keywords:** idiopathic pulmonary fibrosis, Bcl-2, ABT-199, macrophage, fibroblast

## INTRODUCTION

IPF is an interstitial lung disease characterized pathologically by progressive scarring of lung tissue, increased fibroblast proliferation, excessive accumulation of extracellular matrix (ECM), exacerbation of lung inflammation, diffused destruction of alveolar structure and remodeling of the lung architecture (Todd et al., 2012). The clinical symptoms of IPF are progressive dyspnea, wheezing or panting which finally lead to respiratory failure (Chen et al., 2013). This disease is significantly correlated to a dismal outcome with a median survival time of 2–4 yr after diagnosis (Bjoraker et al., 1998). To date, there is no promising medication to effectively cure this disease, which makes it vital to find novel therapeutic targets to treat IPF.

Apoptosis plays a significant role in wound repair and pulmonary epithelial injury leading to fibrosis. Decreased apoptosis of inflammatory cells and fibroblasts results in chronic inflammation

**Abbreviations:** BALF, bronchial alveolar lavage fluid; Bcl-2, B-cell lymphoma 2; BLM, bleomycin; Collagen I, type I collagen; ECM, extracellular matrix; ELISA, enzyme-linked immunosorbent assay; HE, Hematoxylin-Eosin; HYP, hydroxyproline; IL-1 $\beta$ , interleukin-1 $\beta$ ; IPF, Idiopathic pulmonary fibrosis; NS, normal saline;  $\alpha$ -SMA,  $\alpha$ -smooth muscle actin; SPF, Specific Pathogen Free; TGF- $\beta$ 1, transforming growth factor- $\beta$ 1; TNF- $\alpha$ , tumor necrosis factor- $\alpha$ .

which injures the lung and promotes fibrogenesis (Polunovsky et al., 1993). Notably, a marked reduction in the apoptosis of alveolar macrophages plays an integral role in the pathogenesis of pulmonary fibrosis by triggering an immune response (Larson-Casey et al., 2016). There is evidence that the apoptosis rate of alveolar macrophages in bronchial alveolar lavage fluid (BALF) of IPF patients was decreased compared with normal subjects (Drakopanagiotakis et al., 2012). Further, alveolar macrophages could release important profibrotic mediators, such as transforming growth factor- $\beta$ 1 (TGF- $\beta$ 1) (Jain et al., 2013). Overexpression of active TGF- $\beta$ 1 would extend the survival time of lung fibroblasts, which is known to play a crucial role in the pathogenesis of fibrotic processes and ECM protein synthesis (Huang and Natarajan, 2015). Consequently, the persistent existence of lung fibroblasts induces prolonged and severe interstitial lung fibrosis (Sime et al., 1997; Zhou et al., 2013). Therefore, promoting apoptosis of alveolar macrophages and lung fibroblasts may be a potential strategy to decline proinflammatory cytokine production and accelerate the resolution of IPF.

Bcl-2 family proteins exist in the upstream of apoptotic pathways and have a pivotal role in the regulation of apoptosis. More than 20 members with diverse proapoptotic or anti-apoptotic functions are included in Bcl-2 family (Gross et al., 1999). Mounting evidence revealed that during pulmonary fibrosis, deregulation of Bcl-2 family proteins and imbalance between pro- and anti-apoptotic activities may determine the cellular susceptibility to apoptosis, among which Bcl-2 as an anti-apoptotic protein promotes cell survival. The expression of Bcl-2 differs in different cell types, for example, lower expression of Bcl-2 was observed in alveolar epithelial cell after intratracheally instillation of bleomycin (Oltvai et al., 1993). While in fibroblasts and macrophages, the expression of Bcl-2 increased (Kazufumi et al., 1997; Moodley et al., 2003; Nishimura et al., 2007). Thus, using the inhibitors against antiapoptotic Bcl-2 family proteins might prove a promising treatment option for IPF. One such example is the small molecule BH3 domain peptide mimetic ABT-199, a highly potent bioavailable Bcl-2 specific inhibitor (Oltersdorf et al., 2005). It was approved by the US Food and Drug Administration to treat chronic lymphocytic leukemia (Deeks, 2016). Studies have shown that ABT-199 has remarkable therapeutic effects on steroid-insensitive airway inflammation and particulate matter-induced lung inflammation (Tian et al., 2017; Geng et al., 2018). However, the therapeutic potential of ABT-199 against IPF has not been investigated till now. Hence, in the present study, we sought to explore whether Bcl-2 is a promising target for IPF and evaluate the antifibrotic effect of ABT-199 on BLM-induced pulmonary inflammation and lung fibrosis.

## MATERIALS AND METHODS

### Reagents

ABT-199 was purchased from Selleckchem (TX, United States), and BLM was purchased from Hisun Pfizer Pharmaceuticals Co., Ltd (Zhejiang, China). Hydroxyproline (HYP) assay kit was

purchased from Nanjing Jiancheng Biochemical Institute (Nanjing, China). Mouse TGF- $\beta$ 1 and interleukin-6 (IL-6) enzyme-linked immunosorbent assay (ELISA) kits used were from R&D (Minneapolis, MN, United States). Antibody against Bcl-2 (7382) was purchased from Santa Cruz Biotechnology (TX, United States). Antibodies against  $\alpha$ -SMA (ab5694) and type I collagen (ab34710) were purchased from Abcam Inc. (Cambridge, MA, United States). BCA Protein Assay kit was purchased from Thermo Fisher Scientific (Waltham, MA, United States).

### Animal Model of BLM-induced Pulmonary Fibrosis

8-wk old, male C57BL/6 mice weighing 18–22 g were purchased from the Animal Center of Zhejiang University. The mice were housed in a Specific Pathogen Free (SPF) facility and provided with food and water ad libitum. The pulmonary fibrosis mouse model was established as previously described (Larson-Casey et al., 2016). Briefly, mice were anesthetized *via* intraperitoneal injection of 40 mg/kg pentobarbital sodium solution and then the skin and subcutaneous tissue overlying the proximal portion of the trachea were exposed by a 5 mm transversal incision to allow insertion into the trachea of a needle containing a single dose of BLM 50  $\mu$ l (2.5 U/kg, BLM group) or the same volume of sterile saline (normal saline, NS group). These two groups were respectively divided into two subgroups, a control group, and ABT-199 treatment group. Mice in the latter group were treated through intratracheal administration of 2  $\mu$ g/ $\mu$ l ABT-199, suspended in 50  $\mu$ l PBS, while the mice in control group were treated with an equal volume of PBS. Mice were sacrificed at the indicated times after BLM/saline instillation and their lungs and BALF were collected. The animal study was reviewed and approved by the Institutional Animal Care and Use Committee of Zhejiang University. Experiments with animals were carried out in accordance with the guidelines of the Animal Care and Use Committee of the Zhejiang University School of Medicine.

### BALF Collection and Analysis

BALF was collected and centrifuged at 400 g for 10 min at 4°C. Supernatant was stored at –80°C for the analysis of cytokines, while cell pellets were resuspended in 200  $\mu$ l PBS for total and differential cell counting, numbers of macrophages, lymphocytes and neutrophils in a total of 200 cells were counted and categorized under microscope, according to standard morphological criteria. Total BALF protein was measured using BCA Protein Assay Kit, according to the manufacturer's instructions.

### Histological Examination

Lungs were fixed in 4% paraformaldehyde and embedded in paraffin. Sections were stained with Hematoxylin-Eosin (HE) or Masson's trichrome for evaluation of fibrosis under a microscope. The Szapiel score was used to evaluate the degree of parenchymal alveolitis (Szapiel et al., 1979). The area analysis of fibrotic changes was performed according to Ashcroft scale (Ashcroft



et al., 1988). Five randomly chosen fields within each lung section were observed at a magnification of  $\times 100$  or  $200\times$ . Two independent blind observers scored each specimen. A mean score of Szapiel or Ashcroft for each mouse was used for statistical analysis. For detection of fibroblasts and myofibroblasts, the slides were probed with antibodies against type I collagen (collagen I, 1:500) or  $\alpha$ -smooth muscle actin ( $\alpha$ -SMA, 1:600) as previously described (Rangarajan et al., 2018). Images were acquired on a fluorescence microscope and analyzed using ImageJ software.

### Hydroxyproline Assay

The collagen content of lungs was measured by HYP assay kits according to the manufacturer's instructions. Briefly, 0.1 g of lung tissue was weighed and placed into a test tube, 3 ml of 6 mol/L HCl was added, and lungs were then digested for 12 h at  $110^{\circ}\text{C}$ . Later, the samples were neutralized by adjusting pH to 6.0–6.8 with NaOH. Subsequently, ddH<sub>2</sub>O was added to make a total volume of 10 ml. Absorbance was measured at 560 nm on a spectrophotometer and amount of HYP was calculated.

### Immunofluorescence

BAL cells were collected and fixed in 4% paraformaldehyde for 30 min, permeabilized in 0.2% Triton X-100 (LC262801; Sigma-Aldrich) for 5 min, and then blocked with 5% BSA (Sigma-Aldrich, B2064) for 1 h. Then cells were incubated with the antibody against Bcl-2 (1:1000) at  $4^{\circ}\text{C}$  overnight. Sections were stained with goat anti-mouse IgG secondary antibody (A28180; Invitrogen) (1:5000) for 30 min at room temperature. Slides were then washed and counterstained with DAPI. Finally, slides were observed under a fluorescence microscope (Olympus).

### Enzyme-linked Immunosorbent Assay

The levels of TGF- $\beta$ 1 and IL-6 in BALF and lung homogenate were measured by ELISA kits according to the manufacturer's instructions.

### Real-time Quantitative PCR

Total RNA was extracted from lungs using Trizol reagent (Takara Biotechnology) according to the manufacturer's instructions. RNA was then reverse transcribed into cDNA using Reverse Transcription Reagents (Takara Biotechnology). Real-time PCR was performed with the SYBR Green Master Mix (Takara Biotechnology) on a StepOne real-time PCR system (Applied Biosystems, Foster City, CA, United States). The relative expression of target genes was normalized against  $\beta$ -actin using the  $2^{-\Delta\Delta\text{Ct}}$  method. Primer sequences used were as follows:  $\beta$ -actin (Forward: 5'-GTCCACCGTGTATGCCTTCT-3', Reverse: 5'-CTCCTGGTGTCCGAAGTATGAT-3'); *Il-6* (Forward: 5'-CTGCAAGAGACTTCCATCCAG-3', Reverse: 5'-AGTGGTATAGACAGGTCTGTTGG-3'); *Tgf- $\beta$ 1* (Forward: 5'-GCGCTCACTGCTCTTGTGACA-3', Reverse: 5'-GCAATAGTTGGTATCCAGGGCTCT-3'); *Tnf- $\alpha$*  (Forward: 5'-CAC TTGGTGGTTTGTCTACGA-3', Reverse: 5'-GTGGCCCTGCC ACAAGCAG-3'); *Il-1 $\beta$*  (Forward: 5'-GATCCACACTCTCCA GCTGCA-3', Reverse: 5'-CAACCAACAAGTGATATTCTC CATG-3').

### Statistical Analysis

Results are expressed as mean  $\pm$  SD. All data were analyzed using GraphPad Prism Version 7.0 software. Statistical comparisons were performed using Student t-test for two-group comparison and one or two-way ANOVA with a Tukey's *post hoc* test for multiple comparisons.  $p < 0.05$  was considered to be statistically significant.

## RESULTS

### The Expression of Bcl-2 Increased in BALF Cells and Fibroblasts in BLM-induced Pulmonary Fibrosis

To validate the inflammatory response of IPF *in vivo*, we first established a BLM-induced pulmonary inflammation mouse model by intratracheally instilling a single dose of BLM, BALF and lung tissues was collected on day 3, 7 and 14. The findings revealed that BLM induced lung inflammation was dominated by macrophages on day 7 (Supplementary Figure S1A). In addition, both the total number of BAL cells and the absolute number of differential cells in the BLM group increased significantly relative to the NS group (Supplementary Figure S1B).

We examined the mRNA expression level of Bcl2 in whole lung tissue by qPCR, the results showed no significant statistical difference after BLM administration (Supplementary Figures S2A–C). Of note, the percentage of Bcl-2 positive macrophages examined by immunofluorescence increased after BLM instillation on day 7 and 14 (Figures 1A–C), suggesting that macrophages accumulate in BALF during inflammatory phase with the expression of Bcl-2 increasing significantly. Moreover, fibroblasts began to grow after the instillation of BLM for 7–14 days, we observed that the expression of Bcl-2 in fibroblasts increased on day 14 (Figure 1D).

### Early ABT-199 Treatment Attenuated Lung Inflammation and in the Early Inflammation Phase

To test if targeting Bcl-2 could alleviate the inflammatory response after BLM injury, we applied the Bcl-2 inhibitor ABT-199 *in vivo*. ABT-199 (100  $\mu\text{g}/\text{mouse}$ ) was administrated to mice on day 2 after BLM instillation, and mice were sacrificed on day 3 (Supplementary Figure S3A), the results showed no obvious inflammation induced by BLM and no significant effect following ABT-199 administration (Supplementary Figures S3B–F). Next, ABT-199 was then administrated to mice every 3 days from day 3 after BLM instillation, and mice were sacrificed on days 7 (Figure 2A). Inflammatory cell recruitment and release of cytokines were studied to determine the effects of ABT-199 in BLM-induced lung inflammation. As expected, the number of total cells macrophages in the BALF of ABT-199 treated mice decreased significantly compared to the BLM-only treated group (Figure 2B).

In addition, the percentage of Bcl-2 positive macrophages in BALF decreased after 7 days of treatment with ABT-199 (Figures

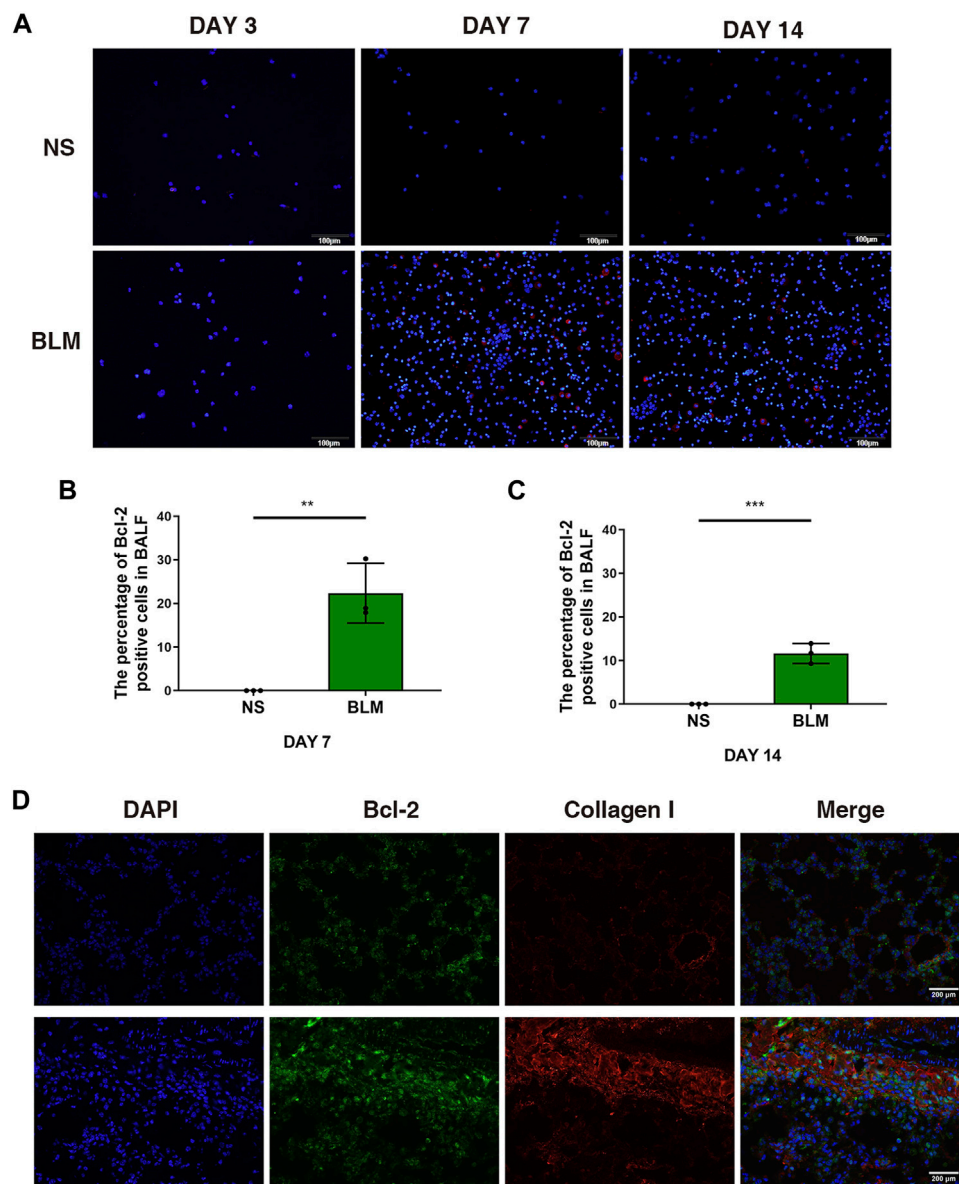


**FIGURE 1 |** The expression of Bcl-2 was increased in BALF cells and fibroblasts in BLM-induced pulmonary fibrosis. **(A–C)** Intracellular Bcl-2 expression of BAL cells was assessed by immunofluorescence assay, and the percentage of Bcl-2 positive macrophages was determined. **(D)** Representative images of collagen I and Bcl-2 show fluorescent staining in lung tissues of mice induced by BLM at day 14. The data are presented as means  $\pm$  SD of an experiment performed three times. \*\* $p < 0.01$ , \*\*\* $p < 0.001$ .  $n = 5$ . BLM, bleomycin; BAL, bronchial alveolar lavage; NS, normal saline; Bcl-2, B-cell lymphoma-2.

2C,D). The attenuation of inflammation in ABT-199-treated mice was further supported by histological analysis by H&E staining (Figures 2E,F), which demonstrated less inflammation and reduced alveolar wall thickness at indicated time points. Results of Masson's trichrome staining revealed that the ABT-199-treated fibrotic mice had a marked reduction in collagen accumulation and preserved lung architecture as shown by the lower Ashcroft scores (Figures 2G,H). To further explore the effect of ABT-199 therapy, we then assessed the level of inflammatory response. Administration of ABT-199 also reduced the BALF protein content in BLM-induced lung injury

(Figure 2I). Moreover, ABT-199 treatment significantly reduced the concentration of TGF- $\beta$ 1 and IL-6 protein in BALF on day 7 (Figures 2J,K).

The continuous attenuation of inflammation in ABT-199-treated mice was further confirmed on day 14 (Figure 3A). Less infiltration of inflammatory cells, in which reduced Bcl2 positive macrophage was observed in BALF (Figures 3B–D). The inflammation score and Ashcroft score for mice which received ABT-199 was much lower compared to that for BLM-only treated mice (Figures 3E–H), accompanied by reduced BALF protein and alleviation of fibrosis factor expression (Figures 3I–M). In

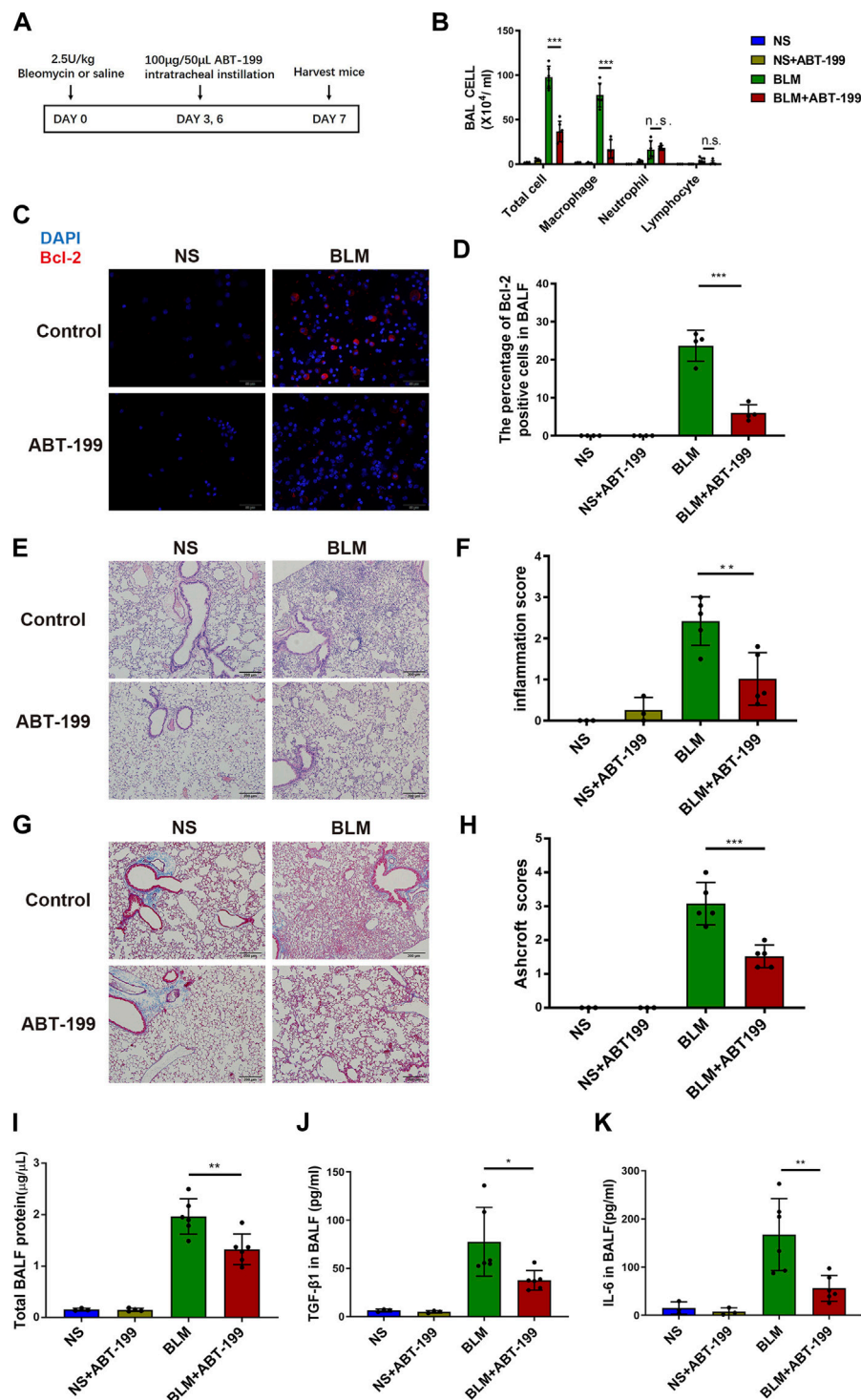


**FIGURE 2 |** Early ABT-199 treatment attenuated BLM-induced lung inflammation at day 7. **(A)** Treatment scheme. **(B)** After 7 days, the total number of inflammatory cells was quantified and the number of differential cells was calculated. **(C)** Intracellular Bcl-2 expression of BAL cells was assessed by immunofluorescence assay on day 7. **(D)** The percentage of Bcl-2 positive macrophages was determined. **(E)** Representative images of lung sections stained with hematoxylin and eosin (H&E). **(F)** Degree of parenchymal alveolitis was evaluated using Szapeli score. **(G)** Representative images of lung sections stained with Masson's trichrome. **(H)** The area analysis of fibrotic changes according to Ashcroft scale. **(I)** Total BALF protein on day 7 was measured using BCA Protein Assay. **(J,K)** Expressions of TGF-β1 and IL-6 levels in BALF on day 7 were determined using ELISA. The data are presented as means ± SD of an experiment performed three times. n.s., not significant, \**p* < 0.05, \*\**p* < 0.01, \*\*\**p* < 0.001. *n* = 3–6. BLM, bleomycin; BAL, bronchial alveolar lavage; NS, normal saline; Bcl-2, B-cell lymphoma-2.

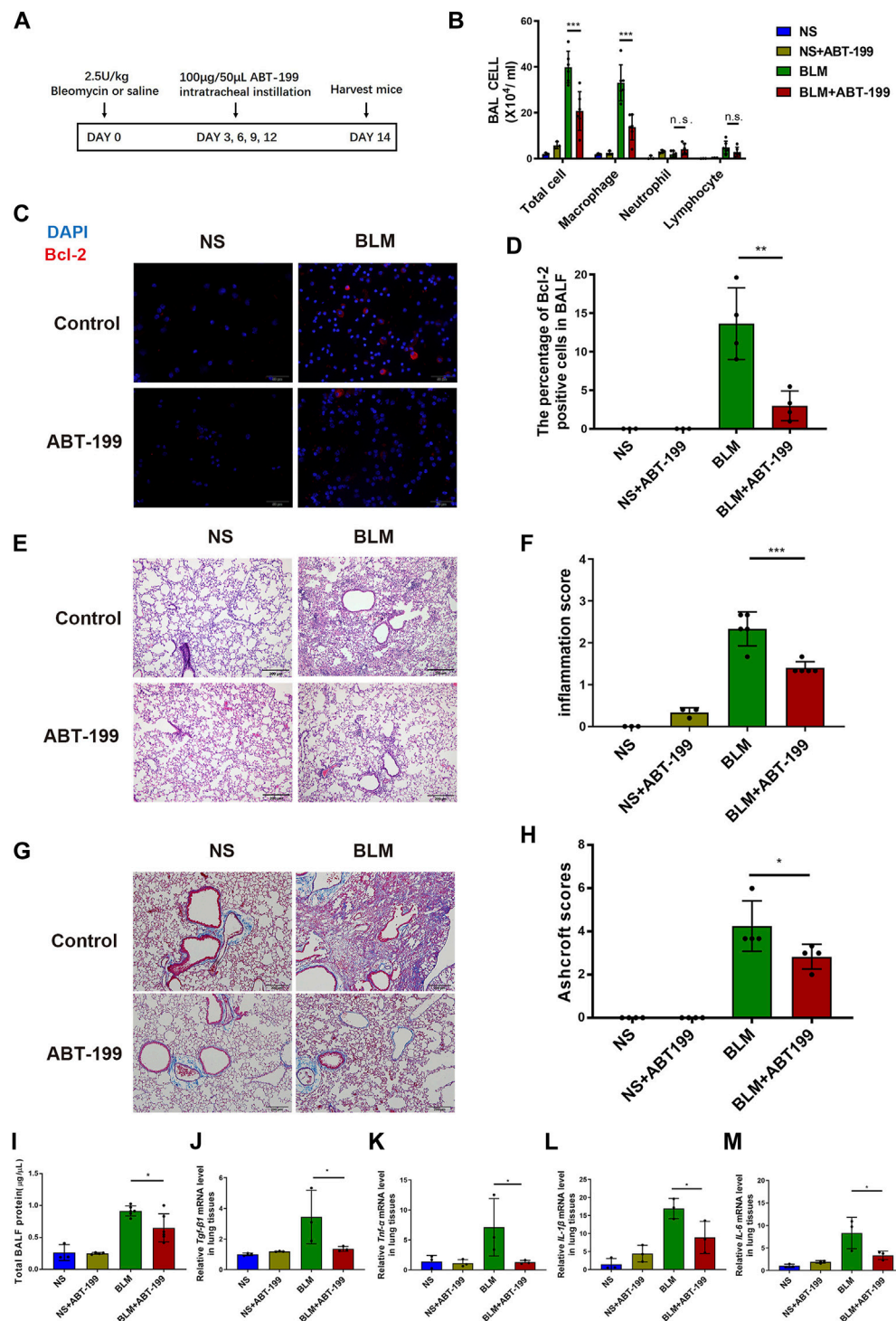


**FIGURE 3 |** Early ABT-199 treatment attenuated BLM-induced lung inflammation at day 14. **(A)** Treatment scheme. **(B)** After 14 days, the total number of inflammatory cells was quantified and the number of differential cells was calculated. **(C)** Intracellular Bcl-2 expression of BAL cells was assessed by immunofluorescence assay on day 14. **(D)** The percentage of Bcl-2 positive macrophages was determined. **(E)** Representative images of lung sections stained with hematoxylin and eosin (H&E). **(F)** Degree of parenchymal alveolitis was evaluated using Szapiel score. **(G)** Representative images of lung sections stained with Masson's trichrome. **(H)** The area analysis of fibrotic changes according to Ashcroft scale. **(I)** Total BALF protein on day 14 was measured using BCA Protein Assay. **(J–M)** The relative levels of *Tgf-β1*, *Tnf-α*, *IL-1β*, and *IL-6* mRNA transcripts were determined using quantitative PCR. The data are presented as means ± SD of an experiment performed three times. n.s., not significant, \* $p < 0.05$ , \*\* $p < 0.01$ , \*\*\* $p < 0.001$ .  $n = 3–6$ . BLM, bleomycin; BAL, bronchoalveolar lavage; NS, normal saline; TGF-β1, transforming growth factor-β1; TNF-α, tumor necrosis factor-α; IL-1β, interleukin-1β; IL-6, interleukin-6.



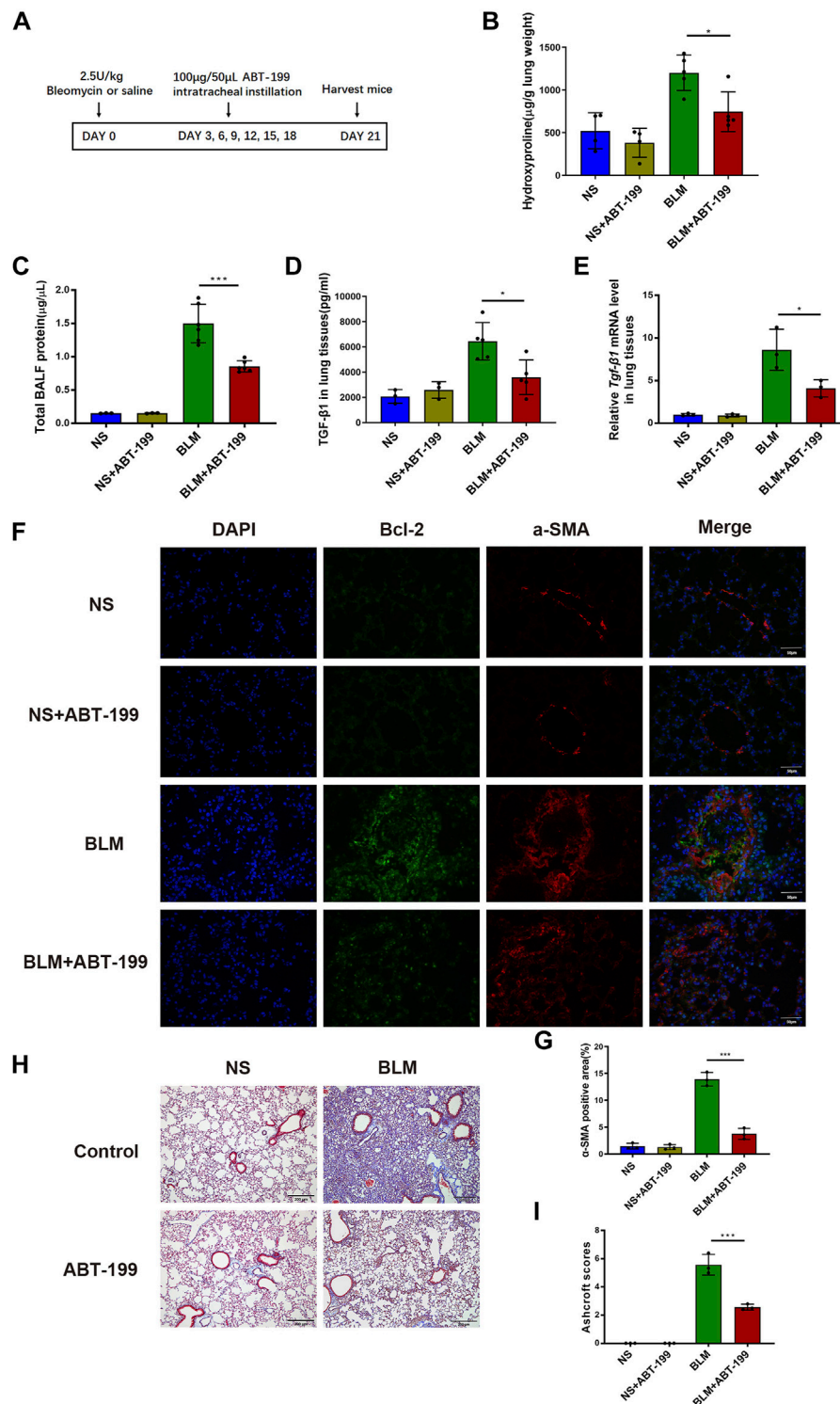


**FIGURE 4 |** ABT-199 alleviates BLM-induced lung fibrosis. **(A)** Treatment scheme. **(B)** Hydroxyproline contents in lung tissues. **(C)** Total BALF protein on day 21 was measured using BCA Protein Assay. **(D,E)** Expression of TGF-β1 level in the lung tissue were determined using ELISA and real-time PCR. **(F)** Representative images of myofibroblasts in lung tissues by immunofluorescence staining of α-SMA and Bcl-2. **(G)** Quantitative analysis of α-SMA positive areas in lung sections. **(H)** Representative images of lung sections stained with Masson's trichrome. **(I)** The area analysis of fibrotic changes according to Ashcroft scale. The data are presented as means ± SD of an experiment performed three times. \* $p < 0.05$ , \*\*\* $p < 0.001$ .  $n = 3-6$ . BLM, bleomycin; BAL, bronchial alveolar lavage; NS, normal saline; TGF-β1, transforming growth factor-β1; α-SMA, alpha smooth muscle actin.

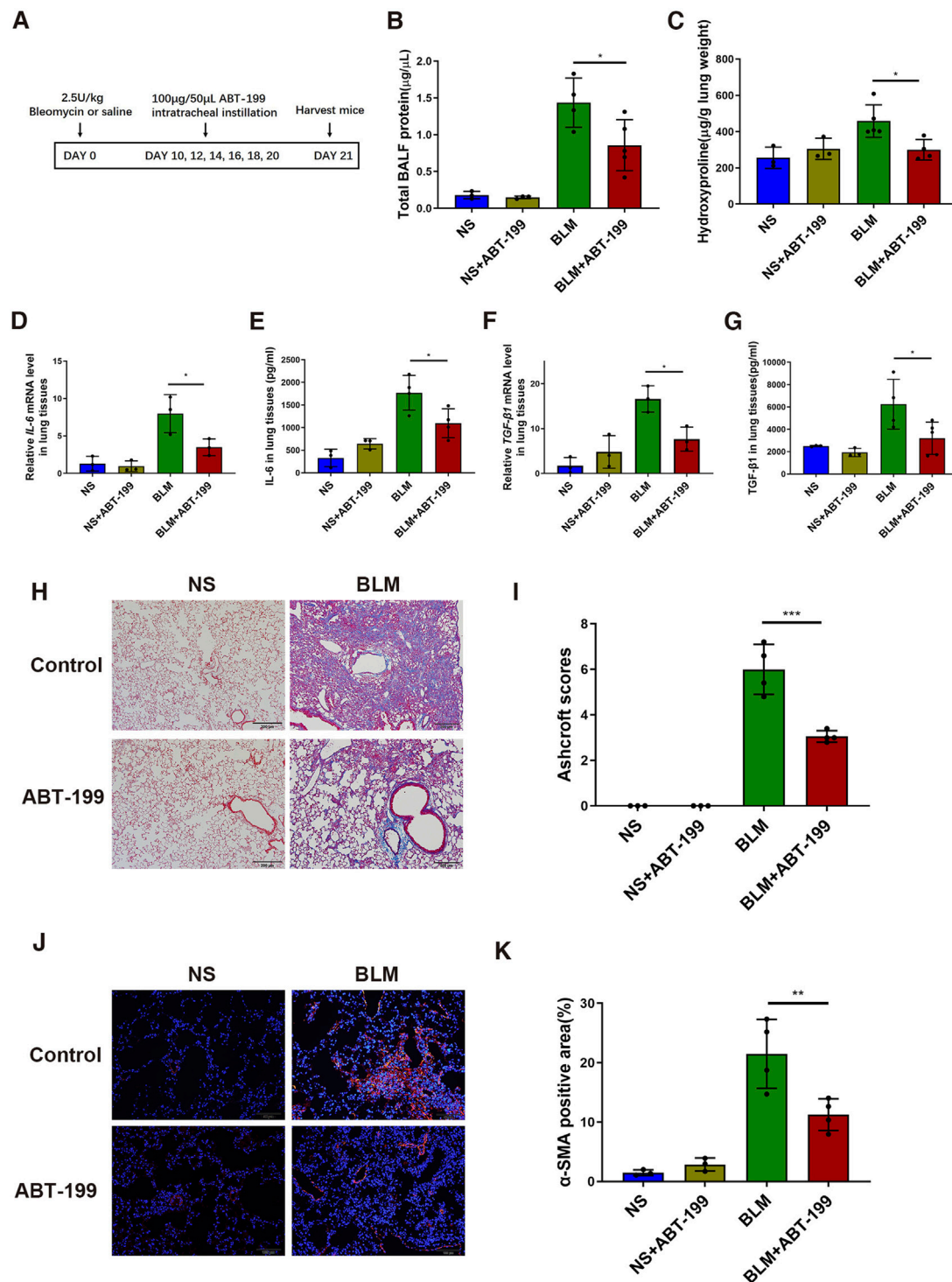


**FIGURE 5 |** ABT-199 reverses the established lung fibrosis in BLM-injured mice. **(A)** Treatment scheme. **(B)** Total BALF protein was measured using BCA Protein Assay. **(C)** Hydroxyproline contents in lung tissues. **(D,E)** Expression level of IL-6 in the lung tissue was determined using real-time PCR and ELISA. **(F,G)** Expression level of TGF-β1 in the lung tissue was determined using real-time PCR and ELISA. **(H)** Representative images of lung sections stained with Masson's trichrome. **(I)** The area analysis of fibrotic changes according to Ashcroft scale. **(J)** Representative images of myofibroblasts in lung tissues by immunofluorescence staining of α-SMA. **(K)** Quantitative analysis of α-SMA positive areas in lung sections. The data are presented as means ± SD of an experiment performed three times. \* $p < 0.05$ , \*\* $p < 0.01$ , \*\*\* $p < 0.001$ .  $n = 3-6$ . BLM, bleomycin; Bcl-2, B-cell lymphoma-2; BAL, bronchial alveolar lavage; NS, normal saline; TGF-β1, transforming growth factor-β1; IL-6, interleukin-6.

*vitro*, we also treated the mouse peritoneal macrophages with ABT-199 and found that 10  $\mu$ M ABT-199 could induce the apoptosis (Supplementary Figures S4A,B). Conclusively, these data indicate that ABT-199 is effective against BLM-induced lung inflammatory response by reducing the number of BAL macrophages.

## ABT-199 Significantly Decreased Bcl-2 and Attenuates BLM-induced Lung Fibrosis in Mice

To evaluate the antifibrotic effects of ABT-199 against BLM-induced pulmonary fibrosis in mice, we established a 21 days BLM-induced pulmonary fibrosis mouse model and intratracheally instilled ABT-199 (100  $\mu$ g/mouse) every 3 days, starting from the third day after BLM administration (Figure 4A). The lung hydroxyproline content and BALF protein concentration of fibrotic mice were significantly reduced by ABT-199 treatment (Figures 4B,C). Analysis of lung extracts revealed decreased mRNA and protein levels of TGF- $\beta$ 1 in mice following treatment with ABT-199 (Figures 4D,E). Furthermore, Bcl2 expression, increased in BLM group and reduced following ABT-199 administration, was shown to be co-localized with  $\alpha$ -SMA (Figure 4F). Also, quantitative analysis showed that the  $\alpha$ -SMA positive areas were smaller in the lungs of ABT-199-treated fibrotic mice than that of fibrotic mice (Figure 4G), suggesting a reduction in myofibroblasts. The results of Masson's trichrome staining revealed that the ABT-199-treated fibrotic mice had a marked reduction in collagen accumulation and preserved lung architecture as shown by the lower Ashcroft scores (Figures 4H,I), which were consistent with the above findings. Collectively, these results confirmed the therapeutic effect of ABT-199 against BLM-induced pulmonary fibrosis in mice.

## ABT-199 Attenuated Established Lung Fibrosis in BLM-injured Mice

To find out whether the inhibition of Bcl-2 protein could attenuate established lung fibrosis during the post-inflammatory phase, we administered ABT-199 every 2 days from day 10 (Figure 5A). ABT-199 administration resulted in decreased number of infiltrating macrophages (Supplementary Figure S5). Notably, even after collagen has already been deposited, ABT-199 significantly reduced the over-production of total BALF protein the over-accumulation of HYP (Figures 5B,C) induced by BLM. Meanwhile, the results of qPCR and ELISA showed that ABT-199 significantly downregulated the expression of pro-fibrotic cytokines (IL-6 and TGF- $\beta$ 1) (Figures 5D–G). Histological analysis of lung by Masson's trichrome staining revealed that ABT-199 could effectively attenuate BLM-induced pulmonary fibrosis, mainly by reducing the thickness of alveolar walls and collagen deposition (Figures 5H,I). Reduction in myofibroblasts was also shown by the  $\alpha$ -SMA positive areas that were smaller in the lungs of ABT-199-treated fibrotic mice than that of fibrotic mice (Figures 5J,K). *In vitro*, we also treated mouse embryonic fibroblasts with ABT-199 and found that 100  $\mu$ M ABT-199 could induce the apoptosis (Supplementary Figures S6A,B). In summary, our data confirm the antifibrotic effect of ABT-199 on established lung fibrosis.

## DISCUSSION

At present, the medications used clinically to treat IPF are insufficient to prevent or reverse the progression of the disease. Therefore, the development of novel therapeutic approaches against IPF is mandatory. Bcl-2, which is known as an inhibitor of apoptosis promotes cell survival (Llambi and Green, 2011). There is a growing body of evidence that suggests a crucial role for Bcl-2 in the pathogenesis of inflammation, apoptosis and fibrosis induced by various factors in the interstitial lung diseases. In this study, we demonstrated that in a mouse model of BLM-induced pulmonary fibrosis, numerous macrophages were recruited to BALF and fibroblasts proliferated in the lungs. Higher expressions of Bcl-2 was detected in alveolar macrophages and lung fibroblasts, which displays similar expression pattern with  $\alpha$ -SMA and the severity of lung fibrosis. Furthermore, we found ABT-199 mediated selective inhibition of Bcl-2 significantly attenuated lung inflammation and fibrosis, even with a late treatment from day 10, when the fibrosis had already been established.

Different experimental models have been developed for understanding the role of Bcl-2 protein in the regulation of apoptosis through fibrosis development, including bleomycin, asbestos, silica, paraquate, chemokine and radiation, among which, the bleomycin model of pulmonary fibrosis is the best characterized murine model. The pathogenesis of IPF is divided into two phases, named the early inflammatory response and the late fibrogenesis. The inflammation phase which is mediated by various inflammatory cells is the initial response after BLM stimulation. In this study, a significant increase in inflammatory cells in BALF from BLM treated mice on day 7 and 14 were detected, especially macrophages, which are known to be the primary source of a variety of pro-inflammatory and fibrogenic cytokines and growth factors (Kendall and Feghali-Bostwick, 2014; Li et al., 2019). Previous studies showed that specific macrophage depletion attenuated lung injury *in vivo* (Redente et al., 2014). Therefore, whether macrophage apoptosis induction be a potential anti-fibrosis therapy remains to be critical and rarely studied.

Our results revealed that the Bcl-2 in alveolar macrophages was increased significantly, suggesting accumulation of macrophages due to their apoptosis resistance in the airway during inflammatory phase. Thus, we wondered if the treatment with Bcl-2 inhibitor ABT-199 would decrease inflammation response in a model of BLM-induced pulmonary fibrosis. Our results confirm that ABT-199 reduced the number of BAL macrophages in the early inflammation phase of lung fibrosis, which might due to direct pro-apoptotic effect on macrophages. In addition, we also observed a decline in the level of various harmful growth factors and cytokines, which is consistent with the fact that macrophages are known to initiate an inflammatory response after injury by secreting these factors, which contribute to the further amplification of inflammatory processes (Bitterman et al., 1982; Lemaire et al., 1986).

Although suppressing inflammatory response has been regarded as an important clinical strategy to treat IPF (Hara et al., 2012). More and more researches proved that anti-

inflammatory treatments may not be effective for all IPF patients. The inflammation is significant in early phase of IPF but relieved in late fibrosis phase, which may lead to the failure of traditional anti-inflammatory therapy. Thus, the anti-fibrosis effect of ABT-199 may not be entirely dependent on the inhibition of inflammatory response. Our observation suggested that the lung fibroblasts were established on day 14 and showed increased apoptosis resistance, with high expression of Bcl-2, indicates that fibroblasts were also a target of ABT-199. Therefore, we aimed to evaluate whether ABT-199 could reverse the already existing fibrosis using a late-ABT199 treatment model. As active fibrosis phase is between 7 and 14 days, significantly increased collagen deposition is observed on day 14 (Peng et al., 2013). For this reason, we intratracheally instilled ABT-199 from 10 days after BLM administration, when lung fibrosis was already established. Our data showed that BLM-induced fibrosis was significantly attenuated. Therefore, a direct effect of ABT-199 on fibroblast could have accounted for the antifibrotic effects observed.

Finally, we originally illustrate the potential therapeutic effect of ABT-199 against BLM-induced pulmonary fibrosis in mice, and emphasized that both early and late treatment with ABT-199 attenuated pulmonary fibrosis through its anti-inflammatory, along with anticoagulant effects. Although we propose that ABT-199 could be used as a new medicinal approach against fibrotic diseases such as IPF, further studies are still required to reveal its more comprehensive effects and mechanism of action.

## DATA AVAILABILITY STATEMENT

The original contributions presented in the study are included in the article/**Supplementary Material**, further inquiries can be directed to the corresponding authors.

## REFERENCES

- Ashcroft, T., Simpson, J. M., and Timbrell, V. (1988). Simple Method of Estimating Severity of Pulmonary Fibrosis on a Numerical Scale. *J. Clin. Pathol.* 41 (4), 467–470. doi:10.1136/jcp.41.4.467
- Bitterman, P. B., Rennard, S. I., Hunninghake, G. W., and Crystal, R. G. (1982). Human Alveolar Macrophage Growth Factor for Fibroblasts. *J. Clin. Invest.* 70 (4), 806–822. doi:10.1172/jci110677
- Bjoraker, J. A., Ryu, J. H., Edwin, M. K., Myers, J. L., Tazelaar, H. D., Schroeder, D. R., et al. (1998). Prognostic Significance of Histopathologic Subsets in Idiopathic Pulmonary Fibrosis. *Am. J. Respir. Crit. Care Med.* 157 (1), 199–203. doi:10.1164/ajrccm.157.1.9704130
- Chen, X., Zhang, X., Li, X., and Wang, Z. (2013). Who and what Should We Rely on in Early Diagnosis of Idiopathic Pulmonary Fibrosis. *Eur. Respir. J.* 41 (1), 249–250. doi:10.1183/09031936.00142012
- Deeks, E. D. (2016). Venetoclax: First Global Approval. *Drugs* 76 (9), 979–987. doi:10.1007/s40265-016-0596-x
- Drakopanagiotakis, F., Xiferti, A., Tsiambas, E., Karameris, A., Tsakanika, K., Karagiannidis, N., et al. (2012). Decreased Apoptotic Rate of Alveolar Macrophages of Patients with Idiopathic Pulmonary Fibrosis. *Pulm. Med.* 2012, 1–9. doi:10.1155/2012/981730
- Geng, X., Wang, X., Luo, M., Xing, M., Wu, Y., Li, W., et al. (2018). Induction of Neutrophil Apoptosis by a Bcl-2 Inhibitor Reduces Particulate Matter-Induced Lung Inflammation. *Aging* 10 (6), 1415–1423. doi:10.18632/aging.101477

## ETHICS STATEMENT

The animal study was reviewed and approved by The Institutional Animal Care and Use Committee of Zhejiang University.

## AUTHOR CONTRIBUTIONS

HS and SY proposed this study and designed the paper. YH, XG, and FL completed the manuscript. YH, FL, WH, and ZS completed the experiments. MS, CZ, and XD analyzed the data. SY, HS, WL, and ZC revised the article. All authors read and approved the final manuscript.

## FUNDING

This work was supported by the State Key Program of National Natural Science Foundation of China (No. 81930003), the National Natural Science Foundation of China (No. 81870007), the Funds for International Cooperation and Exchange of the National Natural Science Foundation of China (No. 81920108001) and the Youth Foundation Project of Natural Science Foundation of Zhejiang Province of China (LQ18H010002).

## SUPPLEMENTARY MATERIAL

The Supplementary Material for this article can be found online at: <https://www.frontiersin.org/articles/10.3389/fmolb.2021.645846/full#supplementary-material>.

- Gross, A., McDonnell, J. M., and Korsmeyer, S. J. (1999). BCL-2 Family Members and the Mitochondria in Apoptosis. *Genes Dev.* 13 (15), 1899–1911. doi:10.1101/gad.13.15.1899
- Hara, A., Sakamoto, N., Ishimatsu, Y., Kakugawa, T., Nakashima, S., Hara, S., et al. (2012). S100A9 in BALF Is a Candidate Biomarker of Idiopathic Pulmonary Fibrosis. *Respir. Med.* 106 (4), 571–580. doi:10.1016/j.rmed.2011.12.010
- Huang, L. S., and Natarajan, V. (2015). Sphingolipids in Pulmonary Fibrosis. *Adv. Biol. Regul.* 57, 55–63. doi:10.1016/j.bior.2014.09.008
- Jain, M., Rivera, S., Monclus, E. A., Synenki, L., Zirk, A., Eisenbart, J., et al. (2013). Mitochondrial Reactive Oxygen Species Regulate Transforming Growth Factor- $\beta$  Signaling. *J. Biol. Chem.* 288 (2), 770–777. doi:10.1074/jbc.M112.431973
- Kazufumi, M., Sonoko, N., Masanori, K., Takateru, I., and Akira, O. (1997). Expression of Bcl-2 Protein and APO-1 (Fas Antigen) in the Lung Tissue from Patients with Idiopathic Pulmonary Fibrosis. *Microsc. Res. Tech.* 38 (5), 480–487. doi:10.1002/(sici)1097-0029(19970901)38:5<480::Aid-jemt4>3.0.Co;2-m
- Kendall, R. T., and Feghali-Bostwick, C. A. (2014). Fibroblasts in Fibrosis: Novel Roles and Mediators. *Front. Pharmacol.* 5, 123. doi:10.3389/fphar.2014.00123
- Larson-Casey, J. L., Deshane, J. S., Ryan, A. J., Thannickal, V. J., and Carter, A. B. (2016). Macrophage Akt1 Kinase-Mediated Mitophagy Modulates Apoptosis Resistance and Pulmonary Fibrosis. *Immunity* 44 (3), 582–596. doi:10.1016/j.immuni.2016.01.001
- Lemaire, I., Beaudoin, H., Massé, S., and Grondin, C. (1986). Alveolar Macrophage Stimulation of Lung Fibroblast Growth in Asbestos-Induced Pulmonary Fibrosis. *Am. J. Pathol.* 122 (2), 205–211.



- Li, G., Jin, F., Du, J., He, Q., Yang, B., and Luo, P. (2019). Macrophage-secreted TSLP and MMP9 Promote Bleomycin-Induced Pulmonary Fibrosis. *Toxicol. Appl. Pharmacol.* 366, 10–16. doi:10.1016/j.taap.2019.01.011
- Llambi, F., and Green, D. R. (2011). Apoptosis and Oncogenesis: Give and Take in the BCL-2 Family. *Curr. Opin. Genet. Dev.* 21 (1), 12–20. doi:10.1016/j.gde.2010.12.001
- Moodley, Y. P., Misso, N. L. A., Scaffidi, A. K., Fogel-Petrovic, M., McAnulty, R. J., Laurent, G. J., et al. (2003). Inverse Effects of Interleukin-6 on Apoptosis of Fibroblasts from Pulmonary Fibrosis and Normal Lungs. *Am. J. Respir. Cell Mol. Biol.* 29 (4), 490–498. doi:10.1165/rcmb.2002-0262OC
- Nishimura, Y., Nishiike-Wada, T., Wada, Y., Miura, Y., Otsuki, T., and Iguchi, H. (2007). Long-Lasting Production of TGF- $\beta$ 1 by Alveolar Macrophages Exposed to Low Doses of Asbestos without Apoptosis. *Int. J. Immunopathol. Pharmacol.* 20 (4), 661–671. doi:10.1177/039463200702000402
- Oltersdorf, T., Elmore, S. W., Shoemaker, A. R., Armstrong, R. C., Augeri, D. J., Belli, B. A., et al. (2005). An Inhibitor of Bcl-2 Family Proteins Induces Regression of Solid Tumours. *Nature* 435 (7042), 677–681. doi:10.1038/nature03579
- Oltvai, Z. N., Millman, C. L., and Korsmeyer, S. J. (1993). Bcl-2 Heterodimerizes In Vivo with a Conserved Homolog, Bax, that Accelerates Programmed Cell Death. *Cell* 74 (4), 609–619. doi:10.1016/0092-8674(93)90509-o
- Peng, R., Sridhar, S., Tyagi, G., Phillips, J. E., Garrido, R., Harris, P., et al. (2013). Bleomycin Induces Molecular Changes Directly Relevant to Idiopathic Pulmonary Fibrosis: a Model for "active" Disease. *PLoS One* 8 (4), e59348. doi:10.1371/journal.pone.0059348
- Polunovsky, V. A., Chen, B., Henke, C., Snover, D., Wendt, C., Ingbar, D. H., et al. (1993). Role of Mesenchymal Cell Death in Lung Remodeling After Injury. *J. Clin. Invest.* 92 (1), 388–397. doi:10.1172/jci116578
- Rangarajan, S., Bone, N. B., Zmijewska, A. A., Jiang, S., Park, D. W., Bernard, K., et al. (2018). Metformin Reverses Established Lung Fibrosis in a Bleomycin Model. *Nat. Med.* 24 (8), 1121–1127. doi:10.1038/s41591-018-0087-6
- Redente, E. F., Keith, R. C., Janssen, W., Henson, P. M., Ortiz, L. A., Downey, G. P., et al. (2014). Tumor Necrosis Factor- $\alpha$  Accelerates the Resolution of Established Pulmonary Fibrosis in Mice by Targeting Profibrotic Lung Macrophages. *Am. J. Respir. Cell Mol. Biol.* 50 (4), 825–837. doi:10.1165/rcmb.2013-0386OC
- Sime, P. J., Xing, Z., Graham, F. L., Csaky, K. G., and Gauldie, J. (1997). Adenovector-mediated Gene Transfer of Active Transforming Growth Factor-Beta1 Induces Prolonged Severe Fibrosis in Rat Lung. *J. Clin. Invest.* 100 (4), 768–776. doi:10.1172/jci119590
- Szapiel, S. V., Elson, N. A., Fulmer, J. D., Hunninghake, G. W., and Crystal, R. G. (1979). Bleomycin-induced Interstitial Pulmonary Disease in the Nude, Athymic Mouse. *Am. Rev. Respir. Dis.* 120 (4), 893–899. doi:10.1164/arrd.1979.120.4.893
- Tian, B.-p., Xia, L.-x., Bao, Z.-q., Zhang, H., Xu, Z.-w., Mao, Y.-y., et al. (2017). Bcl-2 Inhibitors Reduce Steroid-Insensitive Airway Inflammation. *J. Allergy Clin. Immunol.* 140 (2), 418–430. doi:10.1016/j.jaci.2016.11.027
- Todd, N. W., Luzina, I. G., and Atamas, S. P. (2012). Molecular and Cellular Mechanisms of Pulmonary Fibrosis. *Fibrogenesis Tissue Repair* 5 (1), 11. doi:10.1186/1755-1536-5-11
- Zhou, Y., Huang, X., Hecker, L., Kurundkar, D., Kurundkar, A., Liu, H., et al. (2013). Inhibition of Mechanosensitive Signaling in Myofibroblasts Ameliorates Experimental Pulmonary Fibrosis. *J. Clin. Invest.* 123 (3), 1096–1108. doi:10.1172/jci66700

**Conflict of Interest:** The authors declare that the research was conducted in the absence of any commercial or financial relationships that could be construed as a potential conflict of interest.

**Publisher's Note:** All claims expressed in this article are solely those of the authors and do not necessarily represent those of their affiliated organizations, or those of the publisher, the editors and the reviewers. Any product that may be evaluated in this article, or claim that may be made by its manufacturer, is not guaranteed or endorsed by the publisher.

Copyright © 2021 He, Li, Zhang, Geng, Syeda, Du, Shao, Hua, Li, Chen, Ying and Shen. This is an open-access article distributed under the terms of the Creative Commons Attribution License (CC BY). The use, distribution or reproduction in other forums is permitted, provided the original author(s) and the copyright owner(s) are credited and that the original publication in this journal is cited, in accordance with accepted academic practice. No use, distribution or reproduction is permitted which does not comply with these terms.



# $\Delta$ CT Value of Amplified Refractory Mutation System Predicts Efficacy of EGFR-TKIs in Advanced Non-Small-Cell Lung Cancer: A Multi-Center Retrospective Study

Min Chen<sup>1,2†</sup>, Wenqi Huang<sup>3†</sup>, Dongyong Yang<sup>4†</sup>, Jincheng Huang<sup>4</sup>, Gong Li<sup>5</sup>, Xiaoqing Wang<sup>1</sup>, Nanjie Xiao<sup>1</sup>, Weijian Zhang<sup>6</sup>, Jian Guan<sup>1\*</sup>, Shuang Wang<sup>7,8\*</sup> and Laiyu Liu<sup>3\*</sup>

<sup>1</sup>Department of Radiation Oncology, Nanfang Hospital, Southern Medical University, Guangzhou, China, <sup>2</sup>Department of Radiation Oncology, Peking University Shenzhen Hospital, Shenzhen, China, <sup>3</sup>Chronic Airways Diseases Laboratory, Department of Respiratory and Critical Care Medicine, Nanfang Hospital, Southern Medical University, Guangzhou, China, <sup>4</sup>Department of Respiratory and Critical Care Medicine, Second Affiliated Hospital of Fujian Medical University, Quanzhou, China, <sup>5</sup>Guangdong Provincial Hospital of Traditional Chinese Medicine, Guangzhou, China, <sup>6</sup>Department of Radiation Oncology, The First Affiliation Hospital of Fujian Medical University, Fuzhou, China, <sup>7</sup>Department of Pathology, Nanfang Hospital, Southern Medical University, Guangzhou, China, <sup>8</sup>Department of Pathology, School of Basic Medical Sciences, Southern Medical University, Guangzhou, China

## OPEN ACCESS

### Edited by:

Huahao Shen,  
Zhejiang University, China

### Reviewed by:

Tae Jin Lee,  
Augusta University, United States  
Bo Zhang,  
Shanghai Jiaotong University, China

### \*Correspondence:

Jian Guan  
guanjian5461@163.com  
Shuang Wang  
shuangw@126.com  
Laiyu Liu  
liuly5461@163.com

<sup>†</sup>These authors have contributed  
equally to this work and share first  
authorship.

**Received:** 23 March 2021

**Accepted:** 17 August 2021

**Published:** 08 October 2021

### Citation:

Chen M, Huang W, Yang D, Huang J,  
Li G, Wang X, Xiao N, Zhang W,  
Guan J, Wang S and Liu L (2021)  $\Delta$ CT  
Value of Amplified Refractory Mutation  
System Predicts Efficacy of EGFR-TKIs  
in Advanced Non-Small-Cell Lung  
Cancer: A Multi-Center  
Retrospective Study.  
Front. Mol. Biosci. 8:684661.  
doi: 10.3389/fmolb.2021.684661

**Purpose:** This multi-center retrospective study determines whether the  $\Delta$ CT value of the Amplified Refractory Mutation System (ARMS) predicts the efficacy of epidermal growth factor receptor (EGFR) tyrosine kinase inhibitors (TKIs) in EGFR-mutant advanced non-small-cell lung cancer (NSCLC).

**Patients and methods:** Patients who harbored an exon 19 deletion (19Del) or L858R mutation detected by the ARMS and previously received treatment of EGFR-TKIs as a monotherapy were enrolled. A total of 108 NSCLC patients in four hospitals were enrolled. We divided the patients into a high  $\Delta$ CT group (Group H) and a low  $\Delta$ CT group (Group L) by the Martingale residuals analysis and log-rank test. The primary outcome was progression-free survival (PFS). Univariate analysis and multivariable regression were applied to compare the PFS between the groups.

**Result:** The Martingale residuals analysis and log-rank test were applied to find the cutoff  $\Delta$ CT value (0.8). In the 108 patients we enrolled, 59 were in group L and 49 were in group H. Patients' demographics and clinical characteristics, including age, sex, smoking history, pathology, mutation sites, TNM stage, and line of TKIs therapy, were not significantly different between group L and group H. The median PFS was 11.1 months in group L and 6.9 months in group H, and the difference showed statistical significance ( $p < 0.001$ ). Moreover, the objective response rates (ORRs) in group L was significantly higher than in group H (61.0 vs 34.7%,  $p = 0.002$ ). The median OS was 25.0 months in group L and 20.0 months in group H ( $p = 0.046$ ).

**Conclusion:** The  $\Delta$ CT value of ARMS could be an efficacy predictor for EGFR-TKI treatment in advanced EGFR-mutant NSCLC.

**Keywords:**  $\Delta$ CT, ARMS, efficacy, EGFR-TKIs, NSCLC

## INTRODUCTION

Lung cancer is the most common cancer leading to cancer-related deaths worldwide. More than 70% of patients with lung cancer are diagnosed with advanced non-small-cell lung cancer (NSCLC) (Siegel et al., 2017). Many clinical trials have demonstrated the superiority of epidermal growth factor receptor (EGFR) tyrosine kinase inhibitors (TKIs) over chemotherapy in the treatment of patients with advanced NSCLC harboring EGFR mutations (Maemondo et al., 2010; Mitsudomi et al., 2010; Rosell et al., 2012; Yang et al., 2013; Wu et al., 2014). Therefore, EGFR-TKIs have been recommended as the standard of care for first-line treatment for EGFR-mutant NSCLC, especially for those who harbored a drug sensitivity-associated mutation including exon 19 deletion (19Del) and exon 21 L858R. However, these clinical trials also showed that the efficacy of EGFR-TKIs was not so satisfactory in a nonnegligible proportion of NSCLCs harboring sensitive EGFR mutations. In the studies we have mentioned above (Maemondo et al., 2010; Mitsudomi et al., 2010; Rosell et al., 2012; Yang et al., 2013; Wu et al., 2014), 20–44% patients who harbored EGFR mutation had a best response of stable disease (SD) or progressive disease (PD) and 8–15% patients had a best response of PD. Still a significant minority of patients had a primary resistance or poor progression of disease (PFS) to EGFR-TKIs when harbored sensitive EGFR mutations.

Distinguishing patients who are most likely to experience an expected response to EGFR-TKIs from those who are not likely to show a response has emerged as a crucial issue. Although previous studies had reported several resistance mechanisms of EGFR TKIs for EGFR-mutant NSCLC patients, in many cases, the mechanisms remain unclear (Costa et al., 2014; Beau-Faller et al., 2014; Ogino et al., 2007; Engelman et al., 2007). Efforts are still needed to explore the reasons for the various rates of resistance to EGFR-TKIs for EGFR-mutant NSCLC.

The correlation of intratumor heterogeneity of tumor and drug resistance has been widely studied in recent years (Turner and Reis-Filho, 2012; Jamal-Hanjani et al., 2015; Mangano et al., 2015). For the EGFR heterogeneity in lung cancer, recent reports have indicated that tumors are composed of mixed populations of mutant EGFR and wild-type EGFR cells, suggesting that the intratumor heterogeneity does indeed exist (Jiang et al., 2008; Taniguchi et al., 2008; Wei et al., 2014; Cai et al., 2015). Furthermore, several groups have demonstrated that the intratumor heterogeneity of EGFR-mutant NSCLC associated with the efficacy of EGFR-TKIs. They demonstrated that patients with higher relative abundance of EGFR mutation showed longer PFS (Jiang et al., 2008; Taniguchi et al., 2008; Zhou et al., 2011; Zhao et al., 2014a; Zhao et al., 2014b). These reports gave a great inspiration to the development of the therapeutic strategy of EGFR-TKIs. Researchers advised that for patients who harbored a high ratio of EGFR mutation in tumor, EGFR-TKI was effective to control the progression of tumor, but for the low, monotherapy of EGFR-TKIs may be not enough. However, until now, there was not any effective and

convenient ways for clinicians to distinguish whether a patient is harboring a high ratio of EGFR mutation in tumor or not. Therefore, there is an urgent need to develop a method to assess the abundance of EGFR mutations in NSCLC in clinical practice. The Amplified Refractory Mutation System (ARMS) had widely been applied in the detection of EGFR mutation in recent years (Shaiozhang et al., 2014). Mutant allele assays were run with a gene reference assay, which was designed to a mutation-free region of the gene. The mutational status of a sample was determined by calculating the  $\Delta$ CT value between amplification reactions for a mutant allele assay and gene reference assay, as follows:  $\Delta$ CT = Ct (mutant allele assay) – Ct (gene reference assay). Mutation or not is determined by the Ct value and  $\Delta$ CT value. The reference gene was a relatively conserved region of the EGFR gene. Thus, Ct (gene reference assay) could effectively reflect the DNA level of the EGFR gene. For the tumor samples with EGFR mutation, the  $\Delta$ CT value could reflect the relative level of EGFR mutation in the tumor sample. Therefore, we assume that patients with a lower  $\Delta$ CT value may harbor a high ratio of EGFR mutation and may associate with better response to EGFR-TKIs. Furthermore, we divided the EGFR-mutant NSCLC into a low  $\Delta$ CT value and a high  $\Delta$ CT value to explore whether the  $\Delta$ CT value of the tumor sample could be a predictor for the efficacy of EGFR-TKIs in EGFR-mutant NSCLC patients.

## Patients and Methods

### Patients

A total of 108 Chinese patients were enrolled in this study from four medical centers in China including Nanfang Hospital of Southern Medical University, the first affiliated hospital of Fujian Medical University, the second affiliated hospital of Fujian Medical University, and Guangdong Province Traditional Medical Hospital between March 2013 and Jan 2015. The criteria for the patients enrolled in this retrospective study were as follows: 1. Diagnosed with advanced NSCLC and harbored a drug sensitivity-associated mutation site (19Del and L858R). 2. EGFR mutations were tested by ARMS (Shanghai Yuanqi Bio-Pharmaceutical Company Limited, Shanghai, China) and previously received treatment of EGFR-TKIs including gefitinib, erlotinib and icotinib as a monotherapy. The data we collected of all patients were from the electronic medical record system in the four medical centers.

### Epidermal Growth Factor Receptor Mutation Analysis

EGFR mutation testing was performed on formalin-fixed paraffin-embedded (FFPE) specimens from primary tumor obtained from bronchoscopic biopsy or CT-guided core biopsy before any tumor-related treatment. The HE-stained section of FFPE was assessed again to establish the pathological diagnosis. Some of the FFPE samples were trimmed according to the HE-stained section to make sure that the samples we would test were all tumors. The genomic DNA was isolated and purified from tumor specimens using the DNeasy Blood & Tissue Kit (Qiagen,

Valencia, CA, United States) according to the manufacturer's instructions. EGFR mutation detection was performed according to the principles of the ARMS, using the Human EGFR Gene Mutation Detection Kit (PCR Fluorescence Probe) (Shanghai Yuanqi Bio-Pharmaceutical Company Limited, Shanghai, China) on the MX3005P QPCR system (Agilent, Santa Clara, CA, United States), according to manufacturers' recommendations. It covered 23 EGFR mutation hotspots within exons 18, 19, 20 and 21. The results were analyzed according to the criteria defined by the manufacturer's instructions. Positive results were defined as Ct (mutant allele assay) – Ct (gene reference assay) <  $\Delta$ CT (cutoff). We divided the patients into two groups by the media  $\Delta$ CT value.

## Statistical Analyses

The primary end point was progression-free survival (PFS), and the second end points were the objective response rate (ORR) and primary resistance. In patients with measurable disease, the tumor burden was assessed by the Response Evaluation Criteria in Solid Tumor (RECIST) and categorized as a complete response (CR), partial response (PR), stable disease (SD), or progressive disease (PD) (Eisenhauer et al., 2009). PFS was calculated from the time from commencement of EGFR-TKIs treatment to PD according to the RECIST criteria or death resulting from any cause. OS was calculated from the time from commencement of EGFR-TKI treatment to death. The definition of primary resistance to EGFR-TKIs was not uniform among researchers, and in this study, we defined it as patients who had progressive disease to EGFR TKI without initial objective response (Cortot and Janne, 2014). The Kaplan–Meier method was applied to analyze the PFS or OS, and the Cox proportional hazard model was applied to explore the statistical difference in PFS between different groups. A comparison of ORRs and rates of primary resistance in different groups was made using  $\chi^2$  tests. A two-sided  $p$  value of less than 0.05 was considered statistically significant.

## RESULT

### Patient Characteristics

A total of 108 patients who fully met the enrollment criteria were enrolled in the present study. In all the patients, the median age was 61 (ranged from 40 to 83 years); 52 were males and 56 were females; 63 were never smokers and 45 were current or former smokers; three were non-adenocarcinoma and 105 were adenocarcinoma; 57 patients harbored a 19Del mutation and 51 harbored a L858R mutation; and 87 patients received EGFR-TKI as the first-line therapy, 20 patients received EGFR-TKI as the second line therapy, and 1 received EGFR-TKI as the third-line therapy.

### Epidermal Growth Factor Receptor Mutation Groups

Martingale residuals analysis was applied, and a non-linear relationship was noted between the  $\Delta$ CT value and PFS of the

patients (Figures 1A,B). The risk of event went down with an increasing  $\Delta$ CT value when  $\Delta$ CT < –1, remained steadily when –1 >  $\Delta$ CT < 1, and increased when  $\Delta$ CT > 1. Thus, we applied log-ranking analysis to find the cutoff  $\Delta$ CT value. The  $\Delta$ CT value corresponding to the maximum log-rank value was defined as the cutoff  $\Delta$ CT value and was 0.8, which agreed with the tendency in the Martingale residuals analysis (Figure 1C).

59 patients had a  $\Delta$ CT value less than 0.8 (group L), and 49 patients had a  $\Delta$ CT value greater than 0.8 (group H). The median of age was similar between group L and group H (60 vs 61,  $p = 0.499$ ). 49.2% of group L and 55.1% of group H were female ( $p = 0.538$ ). The proportions of never smokers in group L and group H were similar (71.2 vs 71.4%,  $p = 0.978$ ), and 19Del was more frequent in group L than L858R mutation (61.0 vs 42.9%,  $p = 0.060$ ). The TNM stage and line of TKI therapy were all well balanced between the two groups ( $p = 0.356$ ,  $p = 0.818$ ). Treatment with different EGFR-TKIs was balanced between the two groups ( $p = 0.422$ ) (Table 1).

### Efficacy of Different $\Delta$ CT Value Groups

All the patients were received TKIs from Jan 2013 to Dec 2015 in the four hospitals. The last follow-up date was Aug 9, 2021. 100 (92.6%) patients experienced a disease progression, and 36 (33.3%) of the patients were still alive or concord.

The median PFS was 11.1 months (95% CI, 9.8–12.3) in group L and 6.9 months (95% CI, 5.1–8.6) in group H, and the difference showed statistical significance ( $p < 0.001$ ) (Figure 2A). Multivariate analysis shows that the  $\Delta$ CT value was the variable that mostly influences the PFS (Table 2).

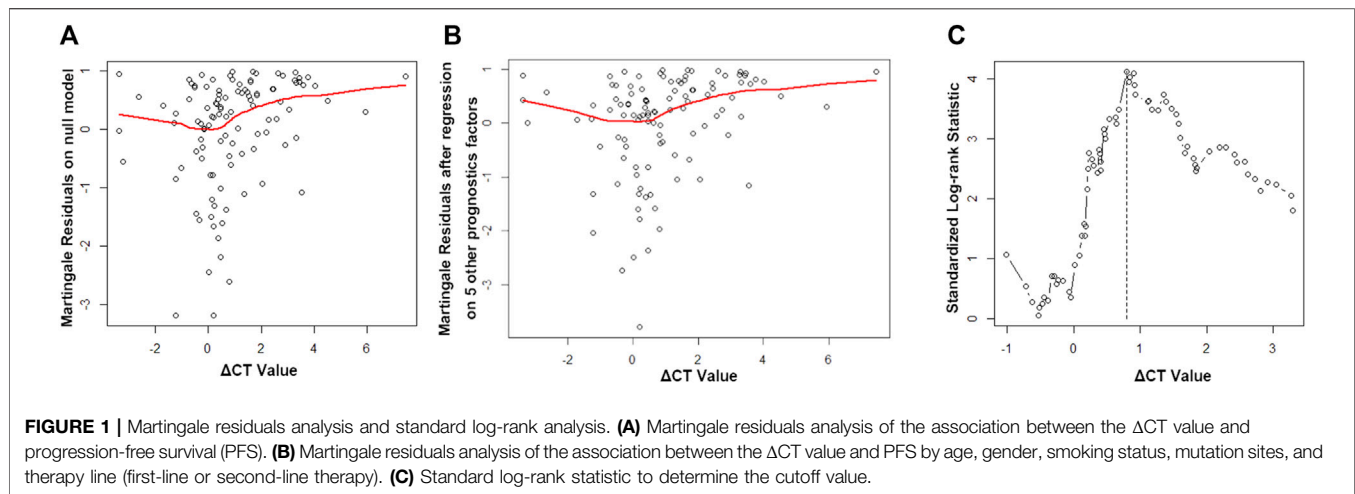
The rate of primary resistance in group H was significantly higher than in group L (26.5% vs 5.1%,  $p = 0.002$ ). ORRs in group L were significantly higher than in group H (61.0% vs 34.7%,  $p = 0.002$ ). The median OS was 24.0 months (95% CI, 19.8–28.2) in group L and 19.0 months in group H (95% CI, 15.4–22.6), which was statistically significant ( $p = 0.046$ ). (Table 3; Figure 2B).

In addition, for patients who either harbored 19Del or L858R mutation, patients in group L had better PFS than those in group H. For patients who harbored 19Del mutation, the median PFS was 10.8 months (95% CI, 10.2–11.4) in group L and 6.8 months (95% CI, 5.3–8.4) in group H, and the difference was statistically significant ( $p = 0.001$ ) (Figure 2C). For patients who harbored L858R mutation, the median PFS was 12.8 months (95% CI, 8.8–16.7) in group L and 6.1 months (95% CI, 3.3–9.1) in group H, and the difference showed statistical significance ( $p < 0.001$ ) (Figure 2D).

### Efficacy of EGFR 19Del and EGFR 21 L858R Mutation

The PFS of patients who harbored 19Del mutation was 9.1 months (95% CI, 7.9–10.2), and in patients who harbored L858R mutation, PFS was 10.6 months (95% CI, 8.5–12.7). The difference between the two group was not significant ( $p = 0.634$ ) (Figure 2A). ORRs in patients who harbored 19Del were higher than in those who harbored L858R mutation, while the difference showed no significance (59.7 vs 39.2%,  $p = 0.034$ ). However, the rate of



**TABLE 1 |** Patient demographics and clinical characteristics.

Variable	Total	ΔCT value				P
		Group L (n = 59)		Group H (n = 49)		
		No. of patients	%	No. of patients	%	
Age, years						0.499
Median (range)	61 (40–83)	60 (40–83)		61 (41–79)		
Sex						0.538
Male	52	30	50.8	22	44.9	
Female	56	29	49.2	27	55.1	
Smoking history						0.978
Never-smoker	77	42	71.2	35	71.4	
Current or former-smoker	31	17	28.8	14	28.6	
Pathology						0.412
Non-adeno	3	2	3.4	1	1.9	
Adeno	105	57	96.6	48	98.1	
Mutation site						0.060
19Del	57	36	61.0	21	42.9	
L858R	51	23	39.0	28	57.1	
TNM stage						0.356
IIIB	7	5	8.5	2	4.1	
IV	101	54	91.5	47	95.9	
Line of therapy						0.818
First	87	48	81.4	39	79.6	
Second	21	11	18.6	10	20.4	
EGFR-TKIs						0.422
Gefitinib	50	26	44.1	24	49.0	
Erlotinib	44	27	45.8	17	34.7	
Icotinib	14	6	10.2	8	16.3	

Group L: patients with a lower  $\Delta$ CT value; group H: patients with a higher  $\Delta$ CT value; adeno: adenocarcinoma.

primary resistance was significantly higher in patients with L858R mutation than those with 19Del (23.5 vs 6.3%,  $p = 0.018$ ) (Table 4).

In addition, for patients in group L, the PFS of the patients who harbored 19Del was 10.8 months (95% CI, 10.2–11.4) and the PFS of the patients who harbored L858R was 12.8 months (95% CI, 8.8–16.7) ( $p = 0.222$ ) (Figure 3B). For patients in group H, the PFS of the patients who harbored 19Del mutation was 6.8 months (95% CI, 5.3–8.4) and the PFS of the patients who harbored L858R was 6.2 months (95% CI, 3.3–9.1) ( $p = 0.551$ ) (Figure 3C).

## DISCUSSION

Our study put forward a new possible predictor for efficacy of EGFR-TKIs. We first put forward that the  $\Delta$ CT value from the ARMS-PCR in EGFR mutation testing could be a predictor for efficacy of EGFR-TKI treatment for advanced EGFR-mutant NSCLC. Patients with a lower  $\Delta$ CT value of EGFR mutations may benefit more than those with a higher  $\Delta$ CT value of EGFR mutations according to the statistically different PFS between the groups, and PFS of the two groups had no overlaps. This might

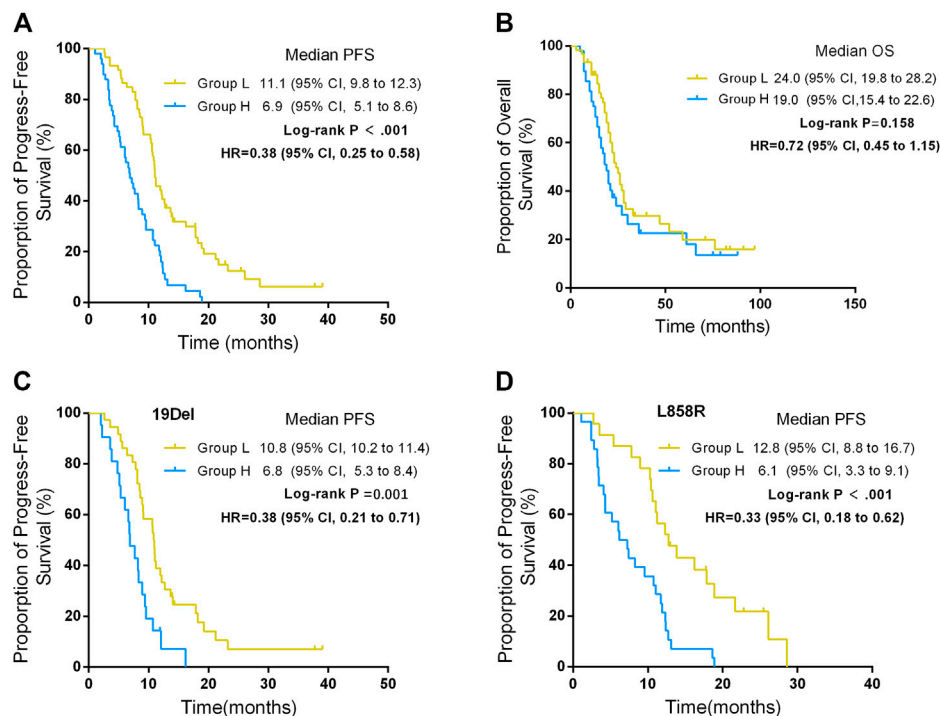


**FIGURE 2 |** Progression-free survival (PFS) and overall survival (OS) between different  $\Delta$ CT value groups. **(A)** PFS between different  $\Delta$ CT value groups. **(B)** OS between different  $\Delta$ CT value groups. **(C)** PFS between different  $\Delta$ CT value groups in patients harboring *EGFR* 19Del. **(D)** PFS between different  $\Delta$ CT value groups in patients harboring *EGFR* L858R.

**TABLE 2 |** Multivariate analyses of PFS by Cox regression analysis.

Variable	HR	95% CI	<i>p</i> Value
<b><math>\Delta</math>CT value groups</b>			
Group L	0.358	0.231–0.555	<0.001
Group H		Reference	
<b>Mutation site</b>			
19Del	1.299	0.848–1.989	0.229
L858R		Reference	
<b>Gender</b>			
Male	1.055	0.612–1.820	0.847
Female		Reference	
<b>Age</b>	0.980	0.956	1.004
<b>Smoking or not</b>			
Never-smoker	1.311	0.727–2.363	0.368
Current or former-smoker		Reference	
<b>Line of therapy</b>			
First	1.311	0.727–2.363	0.096
Second		Reference	

PFS, progression free survival; HR, hazard ratio; CI, confidence interval.

partly explain why some patients who harbored sensitive EGFR mutation did not experience an expected duration of response to EGFR-TKIs. Just like the previous studies, the data of the present study made us not only to focus on whether the patients harbored an EGFR mutation but also to consider the relative abundance of EGFR mutations when making therapeutic strategies for NSCLC (Jiang et al., 2008; Taniguchi et al., 2008; Zhou et al., 2011; Zhao et al., 2014a; Zhao et al., 2014b). What is further than the previous research was that we put forward a predictor that could be conveniently applied in

clinical practice. By relatively quantifying the EGFR mutations in tumor tissue according to  $\Delta$ CT value, patients with a low  $\Delta$ CT value of EGFR mutations could receive EGFR-TKI treatment because they would benefit the most. However, for patients with a high  $\Delta$ CT value of EGFR mutations, monotherapy of EGFR-TKIs may not be enough to control the tumor progression. Owing to the fact that 45.4% of the patients were still alive or concord, overall survival was required further to follow up.

Sheng et al. (2015) conducted a meta-analysis including 26 studies and showed that patients with NSCLC and EGFR exon 19 deletion had a longer PFS, OS, and higher ORR compared with exon 21 L858R mutation after EGFR-TKI therapy. Zhang et al. (2017) thought they may be two distinct diseases. However, it remains unclear why the difference in the outcome exists between the two mutation sites. In our study, ignoring the absence of statistical significance, exon 19Del was more frequent in the group of the low  $\Delta$ CT value and showed higher rate of ORR and lower rate of primary resistance to EGFR-TKIs than exon 21 L858R. Although the PFS showed similarity in the two groups, it may be a clue for researchers to find out the reason why exon 19Del has a better response to EGFR-TKIs. For us, studies with large samples will be conducted to further our findings.

There were some advantages and disadvantages in the present study. The first advantage is that this was a multi-center retrospective study and all the data we recorded were from the electronic medical record system, which made our result more reliable. The second advantage is that the

**TABLE 3 |** Efficacy of different ΔCT value groups.

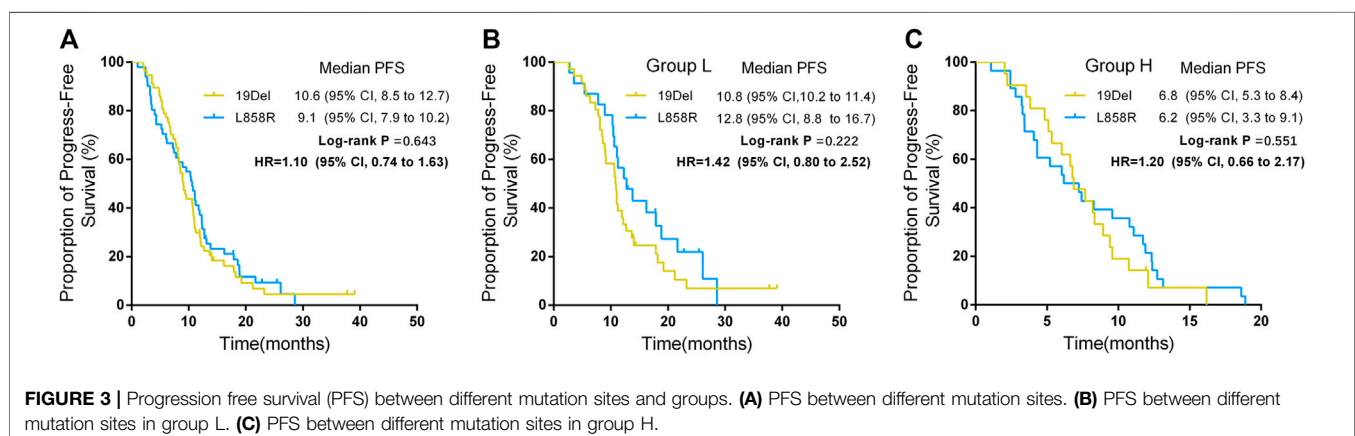
Variable	Total	ΔCT value				P
		Group L (n = 59)		Group H (n = 49)		
		No. of patients	%	No. of patients	%	
PFS, days						<0.001
Median		11.1		6.9		
95% CI		9.8 to 12.3		5.1 to 8.6		
OS, days						0.158
Median		24.0		19.0		
95% CI		19.8–28.2		15.4–22.6		
Primary resistance						0.002
Yes	16	3	5.6	13	24.1	
No	92	56	94.9	36	73.5	
Tumor response						0.002
CR	0	0	0	0	0	
PR	53	36	61.0	17	34.7	
SD	39	20	33.9	19	38.8	
PD	16	3	5.1	13	26.5	

PFS, progression free survival; OS, overall survival; CR, complete response; PR, partial response; SD, stable disease; PD, progressive disease; CI, confidence interval.

**TABLE 4 |** Efficacy of EGFR 19Del and EGFR 21 L858R mutation.

Variable	Total	Mutation sites				P
		E19Del (n = 57)		L858R (n = 51)		
		No. of patients	%	No. of patients	%	
PFS, months						0.643
Median		9.1		10.6		
95% CI		7.9–10.2		8.5–12.7		
OS, months						0.241
Median		25.3		21.6		
95% CI		21.0–29.7		18.0–25.2		
Primary resistance						0.018
Yes	16	4	6.3	12	23.5	
No	92	53	93.7	39	76.5	
Tumor response						0.026
CR	0	0	0	0	0	
PR	54	34	59.7	20	39.2	
SD	38	19	33.3	19	37.3	
PD	16	4	7.0	12	23.5	

PFS, progress free survival; OS, overall survival; CR, complete response; PR, partial response; SD, stable disease; PD, progressive disease; CI, confidence interval.



predictor we found in this study was much more applicable in clinical practice than in other previous studies.

The first limitation of this study is that the patients in our study had a tumor response evaluation per 8–12 weeks after EGFR-TKIs were taken. However, the proportion of patients had an evaluation per 8–10 weeks and per 11–12 weeks, which were not significantly different. The second limitation is that the follow-up of OS was not regular in our study and might lead to a large bias. However, our aim of this study was to explore whether the  $\Delta$ CT value affects the efficacy of EGFR-TKIs. The third one was that only one site of the tumor sample was obtained from each patient. Nonetheless, we trimmed some of the tumor sample to ensure that every sample content is a cancerous cell to make our results more reliable. Wei et al. (2014) have demonstrated that the EGFR mutation ratio showed a high level of concordance in primary tumors and when the tumor content is more than 50% in a tumor sample, a randomly chosen sample would reliably represent the type and ratio of mutations of EGFR in primary tumors.

## CONCLUSION

In summary, our study suggests that the  $\Delta$ CT value of EGFR mutations could predict the efficacy of EGFR-TKI treatment in EGFR mutant NSCLC. We hope this indicator would contribute to more accurate technologies to evaluate the ratio of EGFR mutation in tumors.

## DATA AVAILABILITY STATEMENT

The original contributions presented in the study are included in the article/**Supplementary Material**; further inquiries can be directed to the corresponding authors.

## REFERENCES

- Beau-Faller, M., Prim, N., Ruppert, A.-M., Nanni-Met  llus, I., Lacave, R., Lacroix, L., et al. (2014). Rare EGFR Exon 18 and Exon 20 Mutations in Non-small-cell Lung Cancer on 10 117 Patients: a Multicentre Observational Study by the French ERMETIC-IFCT Network. *Ann. Oncol.* 25, 126–131. doi:10.1093/annonc/mdt418
- Cai, W., Lin, D., Wu, C., Li, X., Zhao, C., Zheng, L., et al. (2015). Intratumoral Heterogeneity of ALK-Rearranged and ALK/EGFR Coaltered Lung Adenocarcinoma. *J. Clin. Oncol.* 33, 3701–3709. doi:10.1200/jco.2014.58.8293
- Cortot, A. B., and Janne, P. A. (2014). Molecular Mechanisms of Resistance in Epidermal Growth Factor Receptor-Mutant Lung Adenocarcinomas. *Eur. Respir. Rev.* 23, 356–366. doi:10.1183/09059180.00004614
- Costa, C., Molina, M. A., Drozdowsky, J., Gim  nez-Capit  n, A., Bertran-Alamillo, J., Karachaliou, N., et al. (2014). The Impact of EGFR T790M Mutations and BIM mRNA Expression on Outcome in Patients with EGFR-Mutant NSCLC Treated with Erlotinib or Chemotherapy in the Randomized Phase III EURTAC Trial. *Clin. Cancer Res.* 20, 2001–2010. doi:10.1158/1078-0432.CCR-13-2233
- Eisenhauer, E. A., Therasse, P., Bogaerts, J., Schwartz, L. H., Sargent, D., Ford, R., et al. (2009). New Response Evaluation Criteria in Solid Tumours: Revised RECIST Guideline (Version 1.1). *Eur. J. Cancer* 45, 228–247. doi:10.1016/j.ejca.2008.10.026

## ETHICS STATEMENT

The studies involving human participants were reviewed and approved by the Ethics Committee of the Nanfang Hospital of Southern Medical University (No. NFEC-2015–11). Written informed consent for participation was not required for this study in accordance with the national legislation and the institutional requirements.

## AUTHOR CONTRIBUTIONS

LL, SW, GJ, and MC contributed to the conception and design of the study. MC, WH and DY performed the statistical analysis and wrote the first draft of the manuscript. JH, GL, XW, NX, and WZ organized the database. All authors contributed to manuscript revision and read and approved the submitted version.

## FUNDING

The National Natural Science Foundation of China No. 81870026; Clinical Research Startup Program of Southern Medical University (LC2016PY015 and LC2019ZD008); Clinical Research Program of Nanfang Hospital, Southern Medical University (2018CR019; 2018CR021 and 2020CR025).

## SUPPLEMENTARY MATERIAL

The Supplementary Material for this article can be found online at: <https://www.frontiersin.org/articles/10.3389/fmolb.2021.684661/full#supplementary-material>

- Engelman, J. A., Zejnullahu, K., Mitsudomi, T., Song, Y., Hyland, C., Park, J. O., et al. (2007). MET Amplification Leads to Gefitinib Resistance in Lung Cancer by Activating ERBB3 Signaling. *Science* 316, 1039–1043. doi:10.1126/science.1141478
- Jamal-Hanjani, M., Quezada, S. A., Larkin, J., and Swanton, C. (2015). Translational Implications of Tumor Heterogeneity. *Clin. Cancer Res.* 21, 1258–1266. doi:10.1158/1078-0432.CCR-14-1429
- Jiang, S. X., Yamashita, K., Yamamoto, M., Piao, C. J., Umezawa, A., Saegusa, M., et al. (2008). EGFR Genetic Heterogeneity of Nonsmall Cell Lung Cancers Contributing to Acquired Gefitinib Resistance. *Int. J. Cancer* 123, 2480–2486. doi:10.1002/ijc.23868
- Maemondo, M., Inoue, A., Kobayashi, K., Sugawara, S., Oizumi, S., Isobe, H., et al. (2010). Gefitinib or Chemotherapy for Non-small-cell Lung Cancer with Mutated EGFR. *N. Engl. J. Med.* 362, 2380–2388. doi:10.1056/NEJMoa0909530
- Mangano, A., Lianos, G. D., Mangano, A., Boni, L., and Dionigi, G. (2015). Intratumor Heterogeneity: Origins, Clinical Significance and Optimal Strategies for Cancer Treatment. *Future Oncol.* 11, 561–564. doi:10.2217/fon.14.296
- Mitsudomi, T., Morita, S., Yatabe, Y., Negoro, S., Okamoto, I., Tsurutani, J., et al. (2010). Gefitinib versus Cisplatin Plus Docetaxel in Patients with Non-small-cell Lung Cancer Harboring Mutations of the Epidermal Growth Factor Receptor (WJTOG3405): an Open Label, Randomised Phase 3 Trial. *Lancet Oncol.* 11, 121–128. doi:10.1016/S1470-2045(09)70364-X



- Ogino, A., Kitao, H., Hirano, S., Uchida, A., Ishiai, M., Kozuki, T., et al. (2007). Emergence of Epidermal Growth Factor Receptor T790M Mutation during Chronic Exposure to Gefitinib in a Non Small Cell Lung Cancer Cell Line. *Cancer Res.* 67, 7807–7814. doi:10.1158/0008-5472.CAN-07-0681
- Rosell, R., Carcereny, E., Gervais, R., Vergnenegre, A., Massuti, B., Felip, E., et al. (2012). Erlotinib versus Standard Chemotherapy as First-Line Treatment for European Patients with Advanced EGFR Mutation-Positive Non-small-cell Lung Cancer (EURTAC): a Multicentre, Open-Label, Randomised Phase 3 Trial. *Lancet Oncol.* 13, 239–246. doi:10.1016/S1470-2045(11)70393-X
- Shaozhang, Z., Ming, Z., Haiyan, P., Aiping, Z., Qitao, Y., Xiangqun, S., et al. (2014). Comparison of ARMS and Direct Sequencing for Detection of EGFR Mutation and Prediction of EGFR-TKI Efficacy between Surgery and Biopsy Tumor Tissues in NSCLC Patients. *Med. Oncol.* 31, 926. doi:10.1007/s12032-014-0926-3
- Sheng, M., Wang, F., Zhao, Y., Li, S., Wang, X., Tao, S., et al. (2015). Comparison of Clinical Outcomes of Patients with Non-small-cell Lung Cancer Harboring Epidermal Growth Factor Receptor Exon 19 or Exon 21 Mutations after Tyrosine Kinase Inhibitors Treatment: a Meta-Analysis. *Eur. J. Clin. Pharmacol.* 72, 1. doi:10.1007/s00228-015-1966-0
- Siegel, R. L., Miller, K. D., and Ahmedin, J. (2017). Cancer Statistics, 2017. *CA Cancer J. Clin.* 67, 7–30. doi:10.3322/caac.21387
- Taniguchi, K., Okami, J., Kodama, K., Higashiyama, M., and Kato, K., (2008). Intratumor Heterogeneity of Epidermal Growth Factor Receptor Mutations in Lung Cancer and its Correlation to the Response to Gefitinib. *Cancer Sci.* 99, 929–935. doi:10.1111/j.1349-7006.2008.00782.x
- Turner, N. C., and Reis-Filho, J. S. (2012). Genetic Heterogeneity and Cancer Drug Resistance. *Lancet Oncol.* 13, e178–e185. doi:10.1016/s1470-2045(11)70335-7
- Wei, B., Yang, K., Zhao, J., Chang, Y., Ma, Z., Dong, B., et al. (2014). Quantification of EGFR Mutations in Primary and Metastatic Tumors in Non-small Cell Lung Cancer. *J. Exp. Clin. Cancer Res.* 33 (5), 5. doi:10.1186/1756-9966-33-5
- Wu, Y.-L., Zhou, C., Hu, C.-P., Feng, J., Lu, S., Huang, Y., et al. (2014). Afatinib versus Cisplatin Plus Gemcitabine for First-Line Treatment of Asian Patients with Advanced Non-small-cell Lung Cancer Harboring EGFR Mutations (LUX-Lung 6): an Open-Label, Randomised Phase 3 Trial. *Lancet Oncol.* 15, 213–222. doi:10.1016/s1470-2045(13)70604-1
- Yang, J. C., Hirsh, V., Schuler, M., Yamamoto, N., O'Byrne, K. J., Mok, T. S., et al. (2013). Symptom Control and Quality of Life in LUX-Lung 3: a Phase III Study of Afatinib or Cisplatin/pemetrexed in Patients with Advanced Lung Adenocarcinoma with EGFR Mutations. *J. Clin. Oncol.* 31, 3342–3350. doi:10.1200/JCO.2012.46.1764
- Zhang, Y., Chen, G., Chen, X., Fang, W., Gao, F., Yang, Y., et al. (2017). The Comparison of EGFR-TKI Failure Modes and Subsequent Management between Exon 19 Deletion and Exon 21 L858R Mutation in Advanced Non-small-cell Lung Cancer. *J. Cancer* 8, 1865–1871. doi:10.7150/jca.19867
- Zhao, J., Wang, X., Xue, L., Xu, N., Ye, X., Zeng, H., et al. (2014). The Use of Mutation-specific Antibodies in Predicting the Effect of EGFR-TKIs in Patients with Non-small-cell Lung Cancer. *J. Cancer Res. Clin. Oncol.* 140, 849–857. doi:10.1007/s00432-014-1618-2
- Zhao, Z.-R., Wang, J.-F., Lin, Y.-B., Wang, F., Fu, S., Zhang, S.-L., et al. (2014). Mutation Abundance Affects the Efficacy of EGFR Tyrosine Kinase Inhibitor Readministration in Non-small-cell Lung Cancer with Acquired Resistance. *Med. Oncol.* 31, 810. doi:10.1007/s12032-013-0810-6
- Zhou, Q., Zhang, X.-C., Chen, Z.-H., Yin, X.-L., Yang, J.-J., Xu, C.-R., et al. (2011). Relative Abundance of EGFR Mutations Predicts Benefit from Gefitinib Treatment for Advanced Non-small-cell Lung Cancer. *J. Clin. Oncol.* 29, 3316–3321. doi:10.1200/jco.2010.33.3757

**Conflict of Interest:** The authors declare that the research was conducted in the absence of any commercial or financial relationships that could be construed as a potential conflict of interest.

**Publisher's Note:** All claims expressed in this article are solely those of the authors and do not necessarily represent those of their affiliated organizations, or those of the publisher, the editors and the reviewers. Any product that may be evaluated in this article, or claim that may be made by its manufacturer, is not guaranteed or endorsed by the publisher.

Copyright © 2021 Chen, Huang, Yang, Huang, Li, Wang, Xiao, Zhang, Guan, Wang and Liu. This is an open-access article distributed under the terms of the Creative Commons Attribution License (CC BY). The use, distribution or reproduction in other forums is permitted, provided the original author(s) and the copyright owner(s) are credited and that the original publication in this journal is cited, in accordance with accepted academic practice. No use, distribution or reproduction is permitted which does not comply with these terms.



# STAT3 and IL-6 Contribute to Corticosteroid Resistance in an OVA and Ozone-induced Asthma Model with Neutrophil Infiltration

Yishu Xue<sup>†</sup>, Yan Zhou<sup>†</sup>, Wuping Bao<sup>†</sup>, Qiang Fu, Huijuan Hao, Lei Han, Xue Zhang, Xue Tian and Min Zhang\*

Department of Respiratory and Critical Care Medicine, Shanghai General Hospital, Shanghai Jiao Tong University School of Medicine, Shanghai, China

## OPEN ACCESS

### Edited by:

Frederico Marianetti Soriani,  
Federal University of Minas Gerais,  
Brazil

### Reviewed by:

Remo Castro Russo,  
Federal University of Minas Gerais,  
Brazil  
Monal Sharma,  
Duke University, United States

### \*Correspondence:

Min Zhang  
maggie\_zhangmin@163.com

<sup>†</sup>These authors have contributed  
equally to this work and share first  
authorship

### Specialty section:

This article was submitted to  
Molecular Diagnostics and  
Therapeutics,  
a section of the journal  
Frontiers in Molecular Biosciences

**Received:** 31 May 2021

**Accepted:** 21 September 2021

**Published:** 25 October 2021

### Citation:

Xue Y, Zhou Y, Bao W, Fu Q, Hao H,  
Han L, Zhang X, Tian X and Zhang M  
(2021) STAT3 and IL-6 Contribute to  
Corticosteroid Resistance in an OVA  
and Ozone-induced Asthma Model  
with Neutrophil Infiltration.  
Front. Pharmacol. 8:717962.  
doi: 10.3389/fmolb.2021.717962

Exposure to high levels of ozone contributes to insensitivity to glucocorticoids in asthma treatment, but the underlying mechanisms are not known. We built two asthma models: a “T2-high” asthma model was established by ovalbumin (OVA) sensitization/challenge and OVA sensitization/challenge combined with ozone exposure (OVA + ozone) was used to induce airway inflammation with increased numbers of neutrophils to simulate “T2-low” asthma. The expression of T-helper (Th)1/2/17-related cytokines was measured by cytokine antibody arrays. Bronchial provocation tests were carried out to evaluate the lung resistance of mice. Hematoxylin and eosin staining, periodic acid-Schiff staining, and immunohistochemical (IHC) analyses of alpha-smooth muscle actin were undertaken to observe morphology changes in lungs. The expression of glucocorticoid receptors (GRs) and phosphorylated-GR (p-GR) was measured by western blotting. *Nr3c1* mRNA was quantified by RT-qPCR. Protein expression of proinflammatory cytokines, signal transducer and activator of transcription 3 (STAT3), suppressor of cytokine signaling 3 (SOCS3), and CXCL1 was measured through ELISAs, western blotting, or IHC analyses. Resected lung tissue from seven asthma patients and 10 healthy controls undergoing thoracotomy for pulmonary nodules was evaluated by IHC analyses and ELISAs. In both asthma models, mucus hypersecretion, as well as inflammation, hyperresponsiveness, and remodeling of the airways, was present compared with the control group, whereas the OVA + ozone group showed severe neutrophil infiltration. The expression of Th17-related cytokines (interleukin (IL)-6, IL-17A, IL-21), GR protein, and CXCL1 increased in the OVA + ozone group, whereas the expression of p-GR decreased. Dexamethasone (Dex) could not totally reverse the expression of p-GR and histone deacetylase-2 in the OVA + ozone group. STAT3 expression increased in the OVA + ozone group and could not be

**Abbreviations:** ACh, acetylcholine chloride;  $\alpha$ -SMA,  $\alpha$ -smooth muscle actin; BALF, bronchoalveolar lavage fluid; CXCL1, chemokine (C-X-C motif) ligand 1; CXCR2, chemokine (C-X-C motif) receptor 2; Dex, dexamethasone; ELISA, enzyme-linked immunosorbent assay; FEV1, forced expiratory volume in one second; FVC, forced vital capacity; GR, glucocorticoid receptor; HDAC2, histone deacetylase 2; H&E, hematoxylin and eosin; IHC, immunohistochemical; OVA, ovalbumin; PAS, periodic acid-Schiff; PC100, the ACh concentration required to increase  $R_L$  by 100% from baseline; p-GR, phosphorylated-GR; p-STAT3, phosphorylated-STAT3;  $R_L$ , lung resistance; SOCS3, suppressor of cytokine signaling 3; STAT3, signal transducer and activator of transcription 3.

completely reversed by Dex, and nor could IL-6 expression. A positive correlation between IL-6 or IL-17A and STAT3 and negative correlation between SOCS3 and STAT3 were shown, suggesting that the IL-6/STAT3 pathway may be involved in OVA + ozone-induced corticosteroid-resistant airway inflammation. In clinical samples, IL-17A expression in lung tissue was positively correlated with percent STAT3-positive area and negatively correlated with SOCS3 expression. The IL-6/STAT3 pathway may contribute to corticosteroid insensitivity in OVA + ozone-induced neutrophilic airway inflammation through regulation of Th17 cells and could provide new targets for individual treatment of corticosteroid resistance in asthma.

**Keywords:** T2-low asthma, STAT3, IL-6, SOCS3, steroid resistance, ozone

## INTRODUCTION

In 2009, Wenzel et al. (1999) defined two distinct inflammatory endotypes of asthma: T-helper type 2 (T2)-high and T2-low. They have remained the most well-recognized and described endotypes of asthma (Svenningsen S and Nair P, 2017).

T2-high asthma is characterized by eosinophilic airway inflammation. It presents with an immune response involving mainly T-helper type 2 (Th2)-related cytokines and, in general, is sensitive to corticosteroid therapy. T2-low asthma is usually characterized by neutrophilic airway inflammation and often exhibits an immune response mediated by interleukin (IL)-17 and Th17 cells (Chung, 2016).

Glucocorticoids are the main choice of asthma treatment due to their significant anti-inflammatory, immunosuppressive, and immunomodulatory effects (Alangari, 2014; Barnes, 2017). However,  $\leq 10\%$  of asthma patients do not respond to glucocorticoids even at high doses or in combination with oral corticosteroids (Chung, 2016). This absence of response makes asthma difficult to control and consumes considerable medical resources.

It has been revealed that proinflammatory cytokines can contribute to corticosteroid resistance in severe asthma and chronic obstructive pulmonary disease. Proinflammatory cytokines (e.g., IL-17A) together with allergens, pathogens, and cigarette smoke can modulate multiple signaling pathways, including nuclear factor, erythroid 2-like 2/histone deacetylase 2/c-Jun (Nrf2/HDAC/c-Jun), and a heightened glucocorticoid receptor (GR) ratio to induce corticosteroid insensitivity (Mei et al., 2019). Neutrophils are involved in corticosteroid insensitivity in asthma and may be regulated by Th17 cells (Chung, 2016; Panettieri, 2018).

An important pathway of initial differentiation of mouse Th17 cells requires IL-6 and signal transducer and activator of transcription 3 (STAT3). Murine and human Th17 cells express IL-17A, IL-17F, IL-21, IL-22, granulocyte-macrophage colony-stimulating factor, and IL-23R (Miossec and Kolls, 2012). STAT3 phosphorylation promotes the transformation of Th0 cells to Th17 cells (Cosmi et al., 2011). Suppressor of cytokine signaling 3 (SOCS3) is a negative regulator of Th17, which usually regulates Th17 cells through the interaction with STAT3 (Rottenberg and Carow, 2014).

STAT3-SOCS3 is an important pathway involved in inflammation modulation (Rottenberg and Carow, 2014). The

role of STAT3 and SOCS3 was investigated in some models of allergic airway inflammation (Santana et al., 2019; Pinheiro et al., 2020), but the results were controversial. Their roles in asthma, especially T2-low asthma, are not clear.

Here, an asthma model with a mixed Th2/Th17 response was constructed by ovalbumin (OVA) sensitization/challenge combined with ozone exposure (OVA + ozone) to simulate some types of T2-low asthma in patients (Last et al., 2004; Zhang J.-h. et al., 2019; Zhang Y. et al., 2019) and show the features of corticosteroid resistance. The expression of total STAT3 was increased in both asthma models, and phosphorylated-STAT3 (p-STAT3) expression increased in the OVA + ozone group, whereas SOCS3 expression was reduced. The expression of STAT3 protein and IL-6 protein in lung tissue did not show an obvious response to corticosteroid intervention. We discovered higher STAT3 expression and lower SOCS3 expression in the lung tissue of asthma patients compared with that of healthy controls (HCs) and observed a correlation between STAT3 expression or SOCS3 expression and the expression of IL-17A protein. The findings from human tissue and mouse models suggested that, by regulating the expression of Th17 cytokines and related cytokines, STAT3 and IL-6 may contribute to corticosteroid insensitivity in an asthma model with a mixed Th2/Th17 response and may become a potential target for treatment of T2-low asthma.

## MATERIALS AND METHODS

### Animals

Male C57BL/6 mice (specific-pathogen-free; 6 weeks) were purchased from SLRC Laboratory (Shanghai, China). They were housed in controlled conditions of temperature (21–25°C) and humidity (40–60%) and had free access to water and food (free from OVA). Mice were acclimatized for 7 days before experimentation and exposed to a 12 h light–dark cycle.

### Induction of Allergic Airway Inflammation and Ozone Exposure

Mice were divided randomly into four groups of eight. OVA sensitization was initiated on day 0 and day 7. OVA sensitization

was achieved by intraperitoneal injection of 20 µg of OVA (grade V; Sigma-Aldrich, Saint Louis, MO, United States) dissolved in 0.2 ml of phosphate-buffered saline (PBS) emulsified in aluminum hydroxide (2 mg; Sigma-Aldrich) as an adjuvant. OVA challenge was undertaken on days 14, 16, 18, 20, and 22, with exposure to 5% aerosolized OVA (20 ml; grade II, Sigma-Aldrich) in a plastic box linked to an ultrasonic nebulizer (Clenny 2 Aerosol; Medel, San Polo di Torrile, Italy) for 30 min. Mice in the control group were sensitized and challenged with an identical volume (0.2 ml for sensitization and 20 ml for challenge) of PBS as a vehicle.

Mice were exposed to ozone (2 ppm) or air in a Perspex™ container 30 min after each OVA/PBS challenge on days 14, 16, 18, 20, and 22. Ozone was produced by an ozonizer (300 series; Aqua Medic, Bissendorf, Germany). Each exposure lasted for 2 h. The ozone concentration was controlled and adjusted by an OS-4 Ozone Switch (Ecosensor; KWJ Engineering, Newark, CA, United States) continuously. Mice in the control group were exposed to air during this time.

In the dexamethasone (Dex)-treated group (OVA + ozone + Dex), mice were injected (i.p.) with Dex (5 mg/kg; Solarbio, Beijing, China) each time before OVA challenge on days 14, 16, 18, 20, and 22.

## Airway Responsiveness

24 h after the last challenge, mice were anesthetized with Zoletil 50 (tiletamine hydrochloride and zolazepam hydrochloride, 25 mg/kg, Virbac S.A., France) and xylazine hydrochloride (10 mg/kg, Chang Sha Best Biological Technology Institute Co., Ltd., China) via IP injection. Mice under anesthesia were then ventilated (MiniVent™; Hugo Sachs Elektronik, March, Germany) at 180 breaths/min and a tidal volume of 210 µl in a whole-body plethysmograph with a pneumotachograph connected to a transducer (Electro-Medical Measurement Systems, Bordon, United Kingdom), as described previously (Bao et al., 2018). Pulmonary airway resistance ( $R_L$ ) was recorded during a 3 min period after increasing concentrations (4–256 mg/ml; 10 µl each time) of acetylcholine chloride (ACh; Sigma-Aldrich).  $R_L$  was expressed as percentage change from baseline  $R_L$  (measured following nebulization with PBS). The ACh concentration required to increase  $R_L$  by 100% from baseline (PC100) was calculated.

## Blood Collection, Bronchoalveolar Lavage, and Protein Isolation From Lung Tissue

After lung-function tests, mice were killed and blood was obtained from the right ventricle. Then, the trachea was exposed, and three aliquots of sterilized saline (0.6 ml each time) were instilled through a PE-60 tube. Bronchoalveolar lavage fluid (BALF) was retrieved (Bao et al., 2020), and the return volume was consistently  $\geq 70\%$  of the instilled volume. Samples of blood and BALF were centrifuged at 3,000 rpm for 10 min at 4°C, and the supernatants were used for measurements.

Lung tissues [for enzyme-linked immunosorbent assays (ELISAs)] were flushed with PBS before freezing. They were homogenized in lysis buffer containing protease and

phosphatase inhibitors and then centrifuged for ELISAs, real-time reverse transcription–quantitative polymerase chain reaction (RT-qPCR), and western blotting.

## ELISAs

ELISAs of serum, BALF, and lung-tissue homogenates were conducted using commercial kits for IgE (Crystal Chem, Chicago, IL, United States), IL-6 and IL-17A (Anogen, Mississauga, Canada), IL-21, p-STAT3 (Tyr705), and total STAT3 (RayBiotech, Peachtree Corners, GA, United States), HDAC2 (EpiGentek, Farmingdale, NY, United States), and hypoxia inducible factor (HIF)-1α (Cell Biolabs, San Diego, CA, United States) according to the manufacturer's instructions.

## Gene Expression

*Nr3c1* is the gene of GRs. Total RNA was isolated from lung tissue by TRIzol™ Reagent (Invitrogen, Carlsbad, CA, United States) and was translated into complementary DNA using the cDNA Reverse Transcription Kit (Applied Biosystems, Foster City, CA, United States) in a PTC-200 Peltier Thermal Cycler (MJ Research, Hercules, CA, United States). Real-time RT-qPCR was undertaken using the ViiA™ 7 Real-Time PCR System (Thermo Fisher, Waltham, MA, United States), as described previously (Bao et al., 2018). The mean fluorescence intensity of the internal reference gene ( $\beta$ -actin) and target gene (*Nr3c1*) was measured. The relative expression of target genes was calculated by the  $2^{-\Delta\Delta C_t}$  method.

The primer sequences (forward and reverse, respectively) used for PCR were 5'-GAA GCA GAT GAG CCA TCA CTT-3' and 5'-CGG TCC TTC TCT GAT AGT GGA-3' for *Nr3c1* and 5'-CCT CTA TGC CAA CAC AGT-3' and 5'-AGC CAC CAA TCC ACA CAG-3' for  $\beta$ -actin.

## Measurement of Cytokine Levels in Serum

Levels of Th1-, Th2-, and Th17-related cytokines in the serum of mice were measured through cytokine antibody arrays (Mouse TH17 Array 1; RayBiotech), as described previously (Zhu et al., 2020), following the manufacturer's instructions.

## Western Blotting

Total protein from lung tissues was extracted using RIPA lysis buffer (Beyotime Biotechnology, Shanghai, China). Extracted proteins were separated by sodium dodecyl sulfate–polyacrylamide gel electrophoresis and transferred to polyvinylidene difluoride (PVDF) membranes. The relative expression of proteins was determined using an ECL detection system (Li et al., 2021). The primary antibodies were those against GR (Cell Signaling Technology, Danvers, MA, United States), p-GR (Ser211; Cell Signaling Technology), SOCS3 (Thermo Scientific), and STAT3 (124H6; Cell Signaling Technology).

## Histology and Morphology

Mouse lungs were dissected out. The left lung was inflated by injecting 4% paraformaldehyde to provide 20 cm of water pressure. Then, it was immersed overnight in paraformaldehyde, embedded in paraffin, and sectioned for staining. Morphologic changes in the epithelia of lungs and



airways were assessed by staining with hematoxylin and eosin (H&E) and periodic acid-Schiff (PAS).

Neutrophils, eosinophils, and lymphocytes located along lobar bronchi and segmental bronchi were counted (magnification = 400×) in a double-blinded manner by two investigators independently, as described previously (Bao et al., 2018). The mean width of the observed area was 100 μm. Peribronchiolar and perivascular inflammation observed in H&E-stained lung slices was scored from 0 to 3, as described previously (Bao et al., 2018).

Blue/purple-stained cells were identified as being PAS-positive. The percent PAS-positive area in the total epithelial area was calculated using ImageJ (National Institutes of Health, Bethesda, MD, United States).

## Immunohistochemical Analyses

IHC staining for α-smooth muscle actin (α-SMA), STAT3, and SOCS3 in lung-tissue sections with mouse α-SMA antibody (Proteintech, Chicago, IL, United States), SOCS3 antibody (Thermo Scientific), STAT3 antibody (124H6; Cell Signaling Technology), chemokine (C-X-C motif) ligand 1 (CXCL1), chemokine (C-X-C motif) receptor 2 (CXCR2) antibody (Proteintech, Chicago, IL, United States), and CXCR2 antibody (Servicebio, Wuhan, China) was done, as described previously (Zhang et al., 2018). The area of positive expression was identified in a double-blinded and independent fashion by two investigators using ImageJ.

## Patient Cohort

### Inclusion Criteria

The inclusion criteria were patients 1) aged 16–75 years; 2) who accepted pneumectomy for lung nodules; 3) who completed spirometry before surgery; 4) had percent forced expiratory volume in one second (FEV<sub>1</sub>%) ≥80% predicted; 5) with FEV<sub>1</sub>/forced vital capacity (FVC) > 0.7 after salbutamol administration; and 6) with the diameter of pulmonary nodules <3 cm.

### Exclusion Criteria

The exclusion criteria were patients 1) who had suffered a respiratory infection in the 8 weeks before screening; 2) who were pregnant; 3) who had concomitant systemic respiratory disease (including chronic obstructive pulmonary disease); and 4) who had other significant medical problems as determined by the principal investigator.

### Grouping

Individuals with a history of asthma, confirmed to have variable symptoms (chronic recurrent wheezing, dyspnea, chest tightness, and/or cough) and variable airflow restriction (positive bronchodilation test or bronchial provocation test), were classified as the “asthma” group. Patients with no symptoms or other pulmonary diseases were classified as the “control” group.

## Statistical Analyses

Statistical analyses and graph creation were undertaken using Prism 8.0 (GraphPad, San Diego, CA, United States). However, the Spearman correlation coefficient matrix and Spearman rank

correlation tests were undertaken using R 3.6.1 (R Institute for Statistical Computing, Vienna, Austria). Data are expressed as mean ± SD unless indicated otherwise. The Kruskal–Wallis one-way analysis of variance with Bonferroni's *post hoc* test (for equal variance) or Dunnett's T3 *post hoc* test (for unequal variance) was used to evaluate differences in variances between multiple groups. A post-test Mann–Whitney analysis was conducted to evaluate differences in variances between two groups. *p* < 0.05 was considered significant.

## RESULTS

### Expression of Th17-Related Cytokines Increased in the OVA Group, but Expression of Th2-Related Cytokines Increased in the OVA + Ozone Group

Cytokine antibody arrays were used to measure the expression of Th1-, Th2-, and Th17-related cytokines in the serum of each group (Figure 1A). The expression of Th1-related cytokines (IFN-γ, IL-2, and TNF-α) showed no significant difference among the two asthma models and control group. The expression of Th2-related cytokines (IL-4, IL-5, and IL-13) increased in the OVA group compared with the control group. IL-13 increased in the OVA + ozone group as well (Supplementary Figure S2). The expression of IL-10 (a cytokine associated with T regulatory cells) in mouse serum was higher in the OVA group. The expression of Th17-related cytokines (IL-17A and IL-21) was significantly higher in the serum of mice in the OVA + ozone group than that in the control group (Figure 1B). IL-6 expression was also increased in the OVA + ozone group. Although often classified as a Th2-related cytokine, IL-6 has an important role in a pathway of the initial differentiation of mouse Th17 cells (Miossec and Kolls, 2012).

Subsequently, the expression of Th17-related cytokines was measured in the BALF and lung-tissue homogenates of mice. Protein expression of IL-6, IL-17A, and IL-21 in the lungs of mice in the OVA + ozone group was significantly higher than that in the control group (Figure 1C). Protein expression of Th17-related cytokines in BALF was similar to that in serum. The expression of IL-6, IL-17A, and IL-21 in the lungs of mice in the OVA + ozone group was significantly higher than that in the control group. The expression of IL-6 and IL-17A in the lungs of mice in the OVA + ozone group was significantly higher than that in the OVA group (Figure 1D). These data suggested that Th17-related cytokines, rather than Th1- or Th2-related cytokines, may have important roles in our OVA + ozone mouse model.

### The OVA + Ozone Group Showed Severe Airway Inflammation, Hypersecretion, and Airway Hyperresponsiveness Compared With Those in the OVA Group

Compared with the control group, the OVA group and OVA + ozone group showed significant airway inflammation (as reflected in airway thickening) as well as infiltration of inflammatory cells (e.g., eosinophils, neutrophils, and lymphocytes) around the

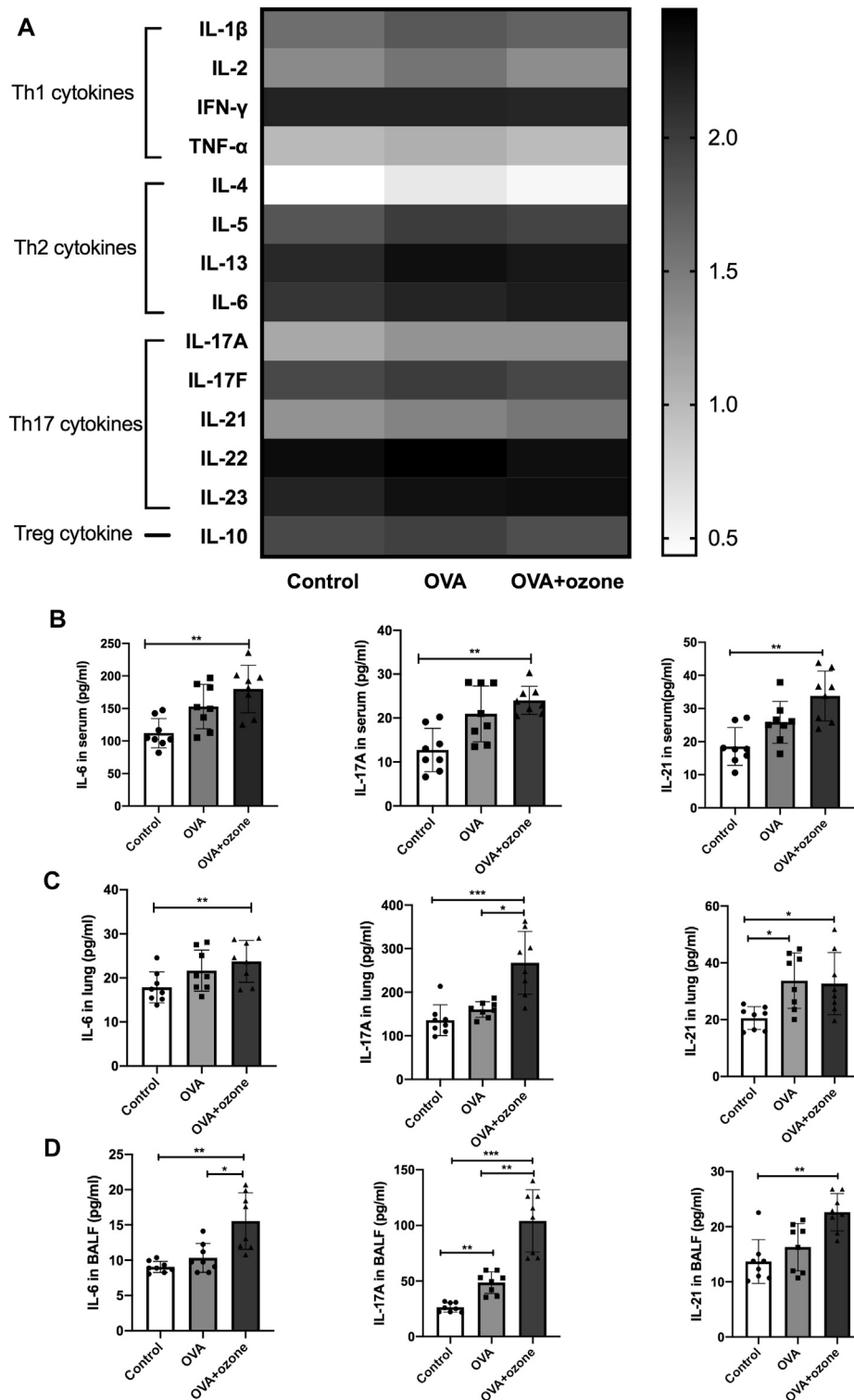


**FIGURE 1** | Expression of Th1-, Th2-, and Th17-related cytokines in the serum of mice and expression of Th17-related cytokines in the lung tissue and BALF of mice. The expression of cytokines in serum was measured by cytokine antibody arrays. The expression of Th17-related cytokines in BALF and lung tissue was measured through ELISAs. **(A)** Expression of different types of cytokines in serum (statistical analysis of cytokines is shown in **Supplementary Figure S1**). **(B)** Expression of Th17-related cytokines in serum. **(C)** Expression of Th17-related cytokines in lung tissue. **(D)** Expression of Th17-related cytokines in BALF. To reduce the difference in expression among different cytokines, the values in panel **(A)** are shown in logarithmic form, whereas the original values of measured protein concentration are used for the remainder of the plates. \* $p < 0.05$ ; \*\* $p < 0.01$ ; \*\*\* $p < 0.001$ .

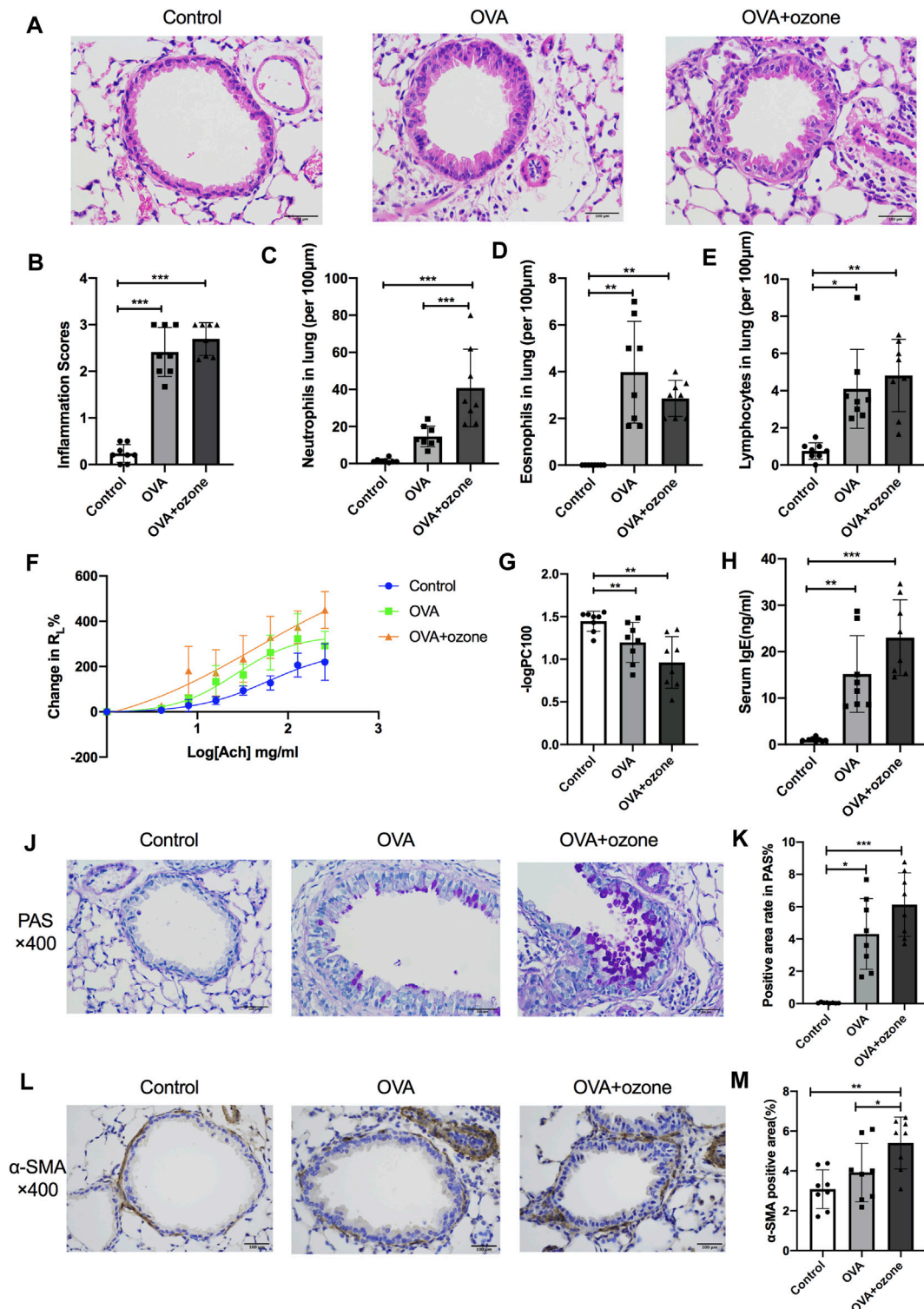


**FIGURE 2 |** Mucus secretion, inflammation, responsiveness, and remodeling of the airways and IgE level of serum in T2-high and T2-low asthma models. Airway inflammation was evaluated through H&E staining. The IgE level in serum was analyzed by ELISAs.  $R_L$  (to acetylcholine chloride) was measured by a commercial setup from Electro-Medical Measurement Systems. **(A)** Representative photomicrographs of the lung with inflammatory-cell infiltration and hyperemia in hematoxylin and eosin-stained sections. **(B)** Airway inflammation scores. **(C)** Density of neutrophil infiltration. **(D)** Density of eosinophil infiltration. **(E)** Density of lymphocyte infiltration. **(F)** Mean percent increase in  $R_L$  in response to increasing concentrations of ACh. **(G)**  $-\log PC_{100}$  (the ACh concentration required to increase  $R_L$  by 100% from baseline). **(H)** IgE level in serum. **(J)** Representative photomicrographs of the lung with airway mucus production and goblet-cell hyperplasia. **(K)** PAS-positive area. **(L)** Representative photomicrographs of immunohistochemistry of  $\alpha$ -SMA in lung-tissue slices. **(M)** Percent SMA-positive area around airways. ACh, acetylcholine chloride;  $R_L$ , lung resistance;  $\alpha$ -SMA,  $\alpha$ -smooth muscle actin. \* $p$  < 0.05; \*\* $p$  < 0.01; \*\*\* $p$  < 0.001. Scale bar = 100  $\mu$ m.

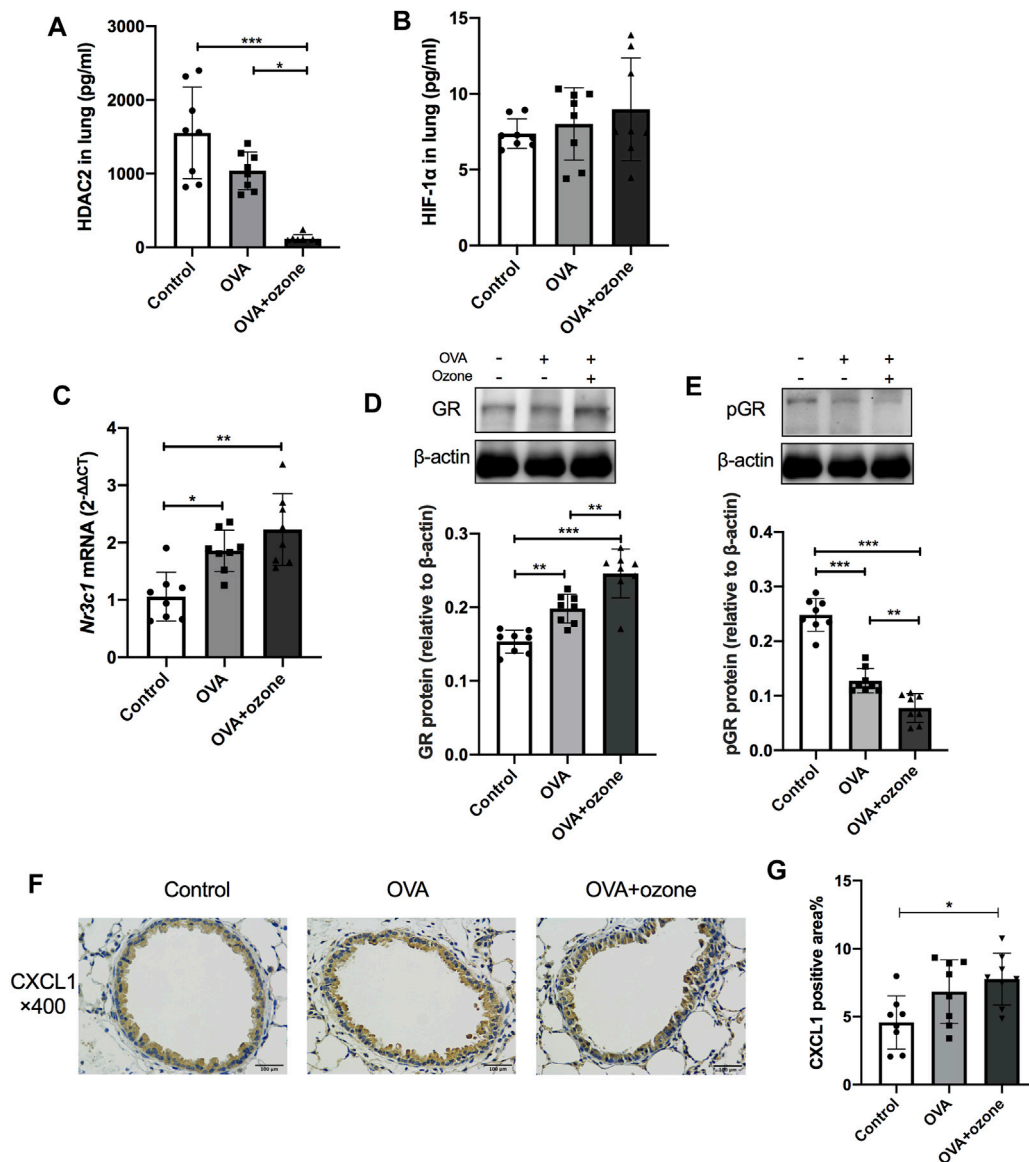


**FIGURE 3 |** Expression of cytokines and receptors related to corticosteroid resistance in the lung tissue of mice suffering from asthma. The expression of HDAC2 and HIF-1α in the lung tissue of mice was measured by ELISAs. *Nr3c1* (gene of GRs) mRNA was detected by RT-qPCR. The expression of GR protein and p-GR protein was measured by western blotting. **(A)** HDAC2 expression in lung tissue. **(B)** HIF-1α expression in lung tissue. **(C)** Expression of *Nr3c1* mRNA in lung tissue. **(D)** Expression of GR protein in lung tissue. **(E)** Expression of p-GR protein in lung tissue. **(F)** Representative photomicrographs of immunohistochemistry of CXCL1 in lung-tissue slices. **(G)** Percent CXCL1-positive area around airways. CXCL1, chemokine (C-X-C motif) ligand 1; GR, glucocorticoid receptor; HDAC2, histone deacetylase 2; p-GR, phosphorylated-GR. \**p* < 0.05; \*\**p* < 0.01; \*\*\**p* < 0.001.

trachea and blood vessels (Figures 2A–E). The OVA + ozone group showed more neutrophil infiltration than that in the OVA group (Figure 2C). Airway hyperresponsiveness (Figures 2F,G) and increased levels of IgE in serum (Figure 2H) were observed in both endotypes of asthma models. The ozone group showed neutrophilic infiltration (Supplementary Figures S4A,B,D) and airway hyperactivity (Supplementary Figures S4E,F) compared to the control group, while its eosinophilic infiltration around the trachea and blood vessels showed no statistical differences from that in the control group (Supplementary Figure S4C).

Airway hypersecretion was observed in mice of both asthma-model groups (Figure 2J). The percent positive PAS-stained area demonstrated that increased mucus secretion occurred in the OVA group and OVA + ozone group compared with that in the control group (Figure 2K).

Airway smooth muscle (ASM) mass (as indicated by the amount of α-SMA around the airways) increased in lung slices from mice treated with OVA + ozone compared with that in the control group (Figures 2L,M). The OVA group had a slightly (but not significantly) thicker ASM mass than control mice. The ASM



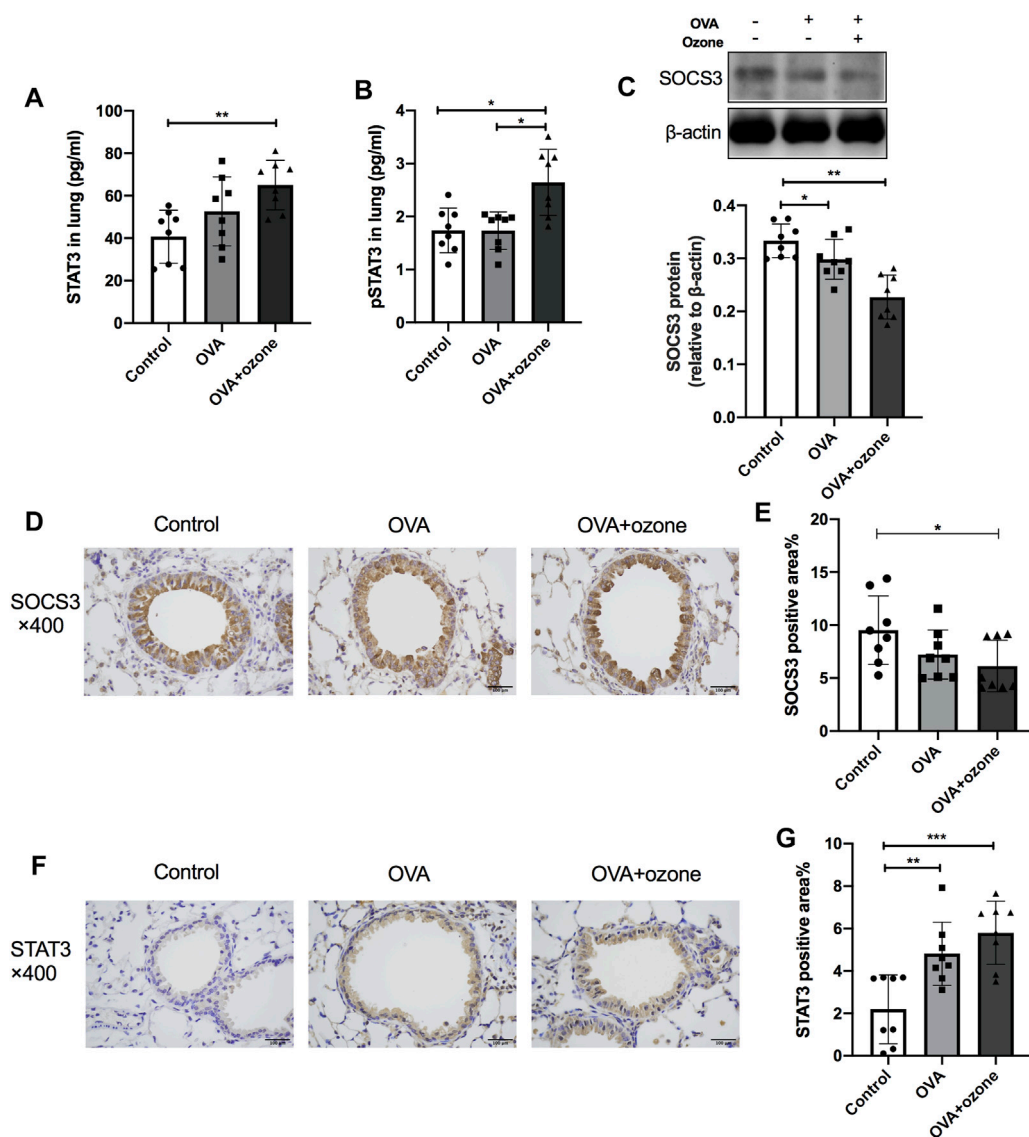


**FIGURE 4 |** Expression of STAT3 and SOCS3 in the lung tissue of mice suffering from asthma. The expression of STAT3 and p-STAT3 in the lung tissue of mice was measured by ELISAs. The expression of SOCS3 protein in the lung tissue of mice was measured by western blotting, and protein expression of STAT3 and SOCS3 in the lung tissue of mice was evaluated by immunohistochemistry. **(A)** Expression of STAT3 protein in lung tissue. **(B)** Expression of p-STAT3 protein in lung tissue. **(C)** Expression of SOCS3 protein in lung tissue. **(D)** Representative photomicrographs of immunohistochemistry of SOCS3 in lung-tissue slices. **(E)** Percent SOCS3-positive area around airways. **(F)** Representative photomicrographs of immunohistochemistry of STAT3 in lung-tissue slices. **(G)** Percent STAT3-positive area around airways. SOCS3, suppressor of cytokine signaling 3; STAT3, signal transducer and activator of transcription 3; p-STAT3, phosphorylated-STAT3. \* $p < 0.05$ ; \*\* $p < 0.01$ ; \*\*\* $p < 0.001$ . Scale bar = 100  $\mu\text{m}$ .

mass in the lung slices of mice of the OVA + ozone group increased more than that of the OVA group (Figure 2M), which indicated severe airway remodeling in the OVA + ozone group.

### The OVA + Ozone Group Showed Features of Corticosteroid Resistance

As mentioned above, the number of neutrophils and expression of Th17-related cytokines were increased in the OVA + ozone group, which could lead to corticosteroid resistance. Protein expression of HDAC2 (which is related to corticosteroid

resistance) decreased in the lung tissues of mice in the OVA + ozone group (Figure 3A). As a model involving neutrophil infiltration induced by oxidative stress, the OVA + ozone group showed a trend of increased HIF-1 $\alpha$  expression, but there was no significant difference between the OVA + ozone group and the control group (Figure 3B). Compared with that in the control group, the expression of *Nr3c1* mRNA in the lung tissue of mice in the OVA + ozone group increased (Figure 3C). Correspondingly, the expression of GR protein increased significantly in the OVA + ozone group (Figure 3D). However, the expression of p-GR in the lung tissue of the OVA

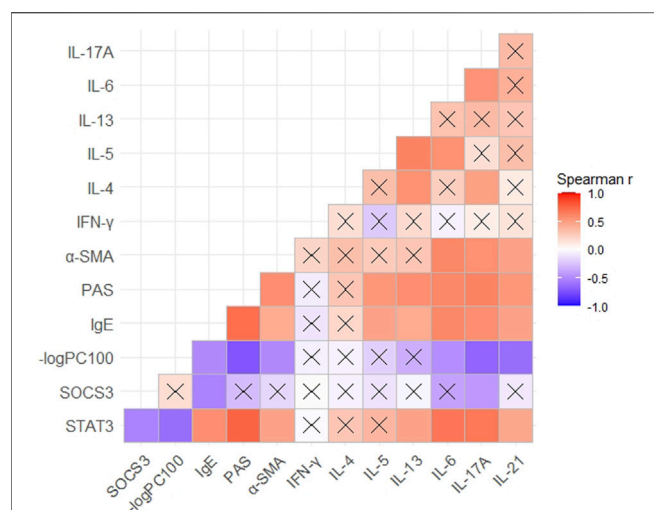


**FIGURE 5 |** Correlation between the expression of STAT3 or SOCS3 and mucus secretion as well as inflammation, responsiveness, and remodeling of the airways in different asthma models. Spearman's correlation coefficient matrix and Spearman's rank correlation tests were conducted. The expression of STAT3, SOCS3, and  $\alpha$ -SMA was discovered from the results of immunohistochemical analyses. The expression of IgE and Th1/Th2/Th17-related cytokines was obtained using ELISAs of serum. A cross indicates no significance. *p*-Values are shown in **Supplementary Table S1**. SOCS3, suppressor of cytokine signaling 3; STAT3, signal transducer and activator of transcription 3;  $\alpha$ -SMA,  $\alpha$ -smooth muscle actin.

+ ozone group decreased more than that in the OVA group (**Figure 3E**). GR phosphorylation may have been involved in corticosteroid resistance observed in the OVA + ozone group.

CXCL1 significantly increased in the lung of the OVA + ozone group compared to the control group (**Figures 3F,G**), while the positive area percentage of CXCR2 showed no statistical difference among the three groups (**Supplementary Figure S2**).

### STAT3 Expression Increased and SOCS3 Expression Decreased in the OVA + Ozone Group

The expression of total STAT3 and p-STAT3 (phosphorylated at Y705) in the lung tissues of mice in the OVA + ozone group increased, and the expression of p-STAT3 showed a significant increase compared with that in the OVA group (**Figures 4A,B**). Simultaneously, the expression of SOCS3 protein decreased in both mouse models of asthma compared with that in the control group (**Figure 4C**). Similar to the results of protein levels, the percent STAT3-positive area in the lung tissues of the OVA group and OVA + ozone group increased compared with that in the control group (**Figures 4F,G**), whereas the percent SOCS3-positive area decreased in the OVA + ozone group (**Figures 4D,E**). Single ozone exposure showed no significant statistical difference from the control group (**Supplementary Figure S5**).

### Expression of STAT3 and SOCS3 Was Correlated With Expression of Th17-Related Cytokines

Correlation was evaluated using Spearman's rank analysis. STAT3 expression and SOCS3 expression showed a strong correlation with each other ( $r = -0.53$ ). The expression of STAT3 and SOCS3 was correlated with the expression of IgE and IL-17A in mouse serum ( $r = 0.57$  and  $0.67$  with STAT3 and  $-0.53$  and  $-0.43$  with SOCS3, respectively) (**Figure 5**). STAT3 expression showed a stronger correlation with the expression of Th17-related cytokines (IL-6, IL-17A, and IL-21) than Th2-related cytokines, in serum. STAT3 expression correlated with the percent stained areas of PAS and  $\alpha$ -SMA ( $r = 0.75$  and  $0.46$ , respectively) and  $-\log PC100$  ( $r = -0.62$ ) (**Figure 5**). Hence, STAT3 may be involved in the hypersecretion, remodeling, and hyperresponsiveness of airways observed in asthma.

### STAT3 and IL-6 Are Involved in the Corticosteroid Resistance of an Asthma Model Induced by OVA and Ozone

The expression of HDAC2 and p-GR protein in the OVA + ozone group could not be restored completely by Dex treatment (**Figures 6A,B**). Protein expression of total STAT3 and p-STAT3 could not be reversed completely by Dex treatment (**Figures 6C,D**). IL-6 (which is important for the differentiation of Th17 cells and may be upstream of STAT3) expression appeared to be corticosteroid-insensitive in mice in the OVA + ozone group (**Figure 6E**). Protein expression of IL-13 (Th2-related cytokine) showed an evident response to this corticosteroid (**Figure 6F**), whereas IL-17A seemed to decline after Dex treatment, but continued to remain higher than that in the control group (**Figure 6G**).

### Expression of STAT3 and SOCS3 Was Altered in the Lung Tissue of Asthma Patients and Showed Correlation With Expression of IL-17A Protein

The normal lung tissues of seven asthma patients and 10 HCs who underwent thoracotomy were evaluated through IHC staining and ELISAs. The STAT3-positive area increased in the lung tissue of asthma patients compared with that in HCs (**Figures 7A,B**), whereas SOCS3 expression decreased in the lung tissue of asthma patients (**Figures 7C,D**). The expression of STAT3 and SOCS3 showed a strong correlation with the expression of IL-17A protein in the lung tissue of patients ( $r = 0.5624$  and  $-0.6553$ , respectively) (**Figures 7E,F**). The characteristics of these patients at baseline are shown in **Supplementary Table S2**.

## DISCUSSION

We established a T2-high asthma model with eosinophil infiltration and increased expression of Th2-related cytokines

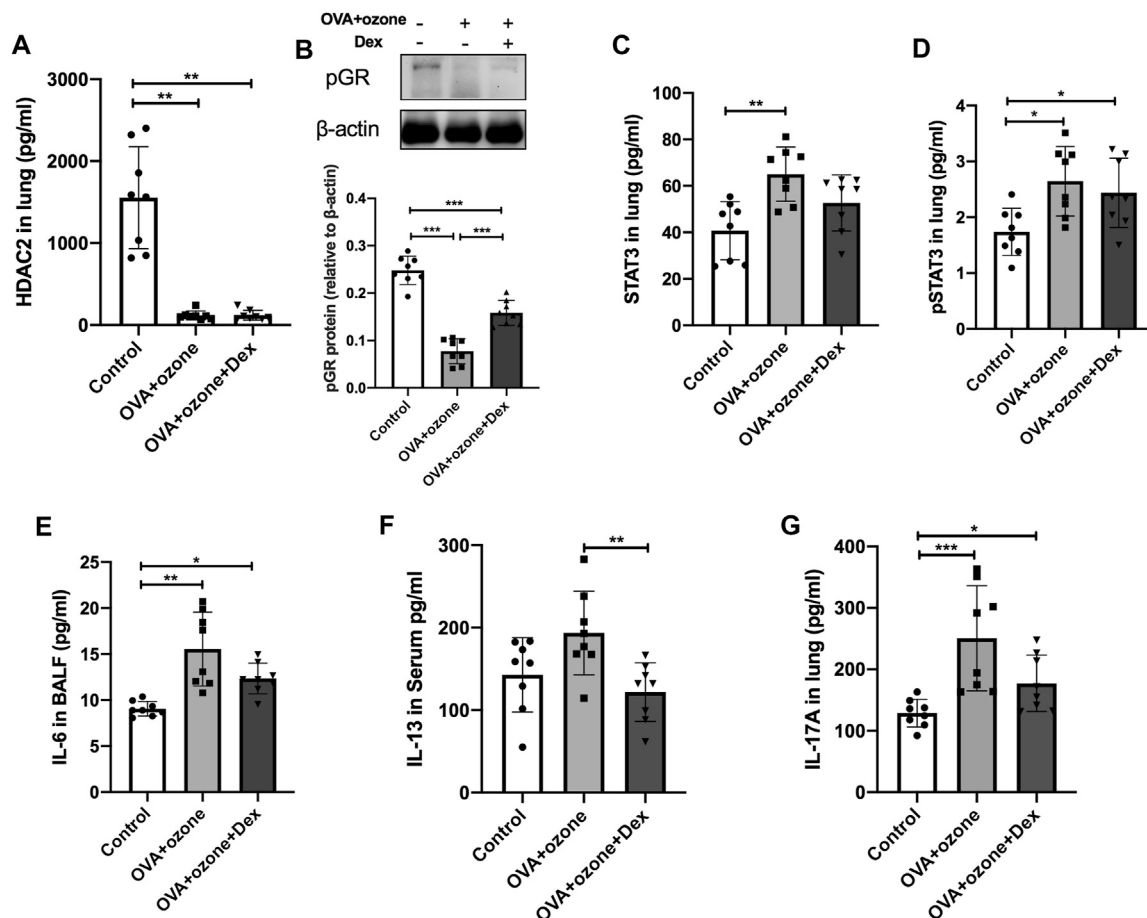


**FIGURE 6 |** Changes in the expression of cytokines and transcription factors after intervention by dexamethasone. The expression of HDAC2, IL-6, IL-13, and IL-17A was measured by ELISAs. The expression of p-GR protein was analyzed by western blotting. **(A)** Expression of HDAC2 protein in lung tissue after Dex treatment. **(B)** Expression of p-GR protein in lung tissue after Dex treatment. **(C)** Expression of STAT3 protein in lung tissue after Dex treatment. **(D)** Expression of p-STAT3 protein in lung tissue after Dex treatment. **(E)** Expression of IL-6 protein in BALF after Dex treatment. **(F)** Expression of IL-13 protein after Dex treatment. **(G)** Expression of IL-17A protein after Dex treatment. Dex, dexamethasone; HDAC2, histone deacetylase 2; p-GR, phosphorylated-GR; STAT3, signal transducer and activator of transcription 3. \* $p < 0.05$ ; \*\* $p < 0.01$ ; \*\*\* $p < 0.001$ .

through OVA sensitization/challenge. We constructed a mixed Th2/Th17 response model with neutrophil infiltration and increased expression of Th17-related cytokines through OVA sensitization/challenge combined with ozone exposure.

The OVA + ozone group showed more severe airway inflammation, airway hyperresponsiveness, and severe airway remodeling than those in the OVA group. Th17-related cytokines have important roles in T2-low asthma (Chung, 2016; Svenningsen and Nair, 2017). To ascertain the differences in endotypes of our mouse models, we adopted cytokine antibody arrays for simultaneous and accurate detection of multiple cytokines.

After establishing models of T2-high asthma or a mixed Th2/Th17 response with neutrophil infiltration-based airway inflammation, we discovered the characteristics of corticosteroid resistance in the OVA + ozone group. Studies using mouse models of asthma and human type II alveolar epithelial cells have shown that exposure to high ozone levels

can reduce the response of asthma patients to glucocorticoid therapy during acute exacerbations (Flayer et al., 2019). In our previous study, a mouse model induced by OVA and ozone showed the traits of corticosteroid resistance (Zhang J.-h. et al., 2019). In the present study, we demonstrated that the expression of HDAC2 and p-GR decreased in the OVA + ozone group, which is a characteristic of corticosteroid resistance. The development of corticosteroid resistance is closely related to the expression and phosphorylation of GRs. Reduced phosphorylation of GRs leads to reduced nuclear translocation, which results in corticosteroid resistance (Irusen et al., 2002). The anti-inflammatory effect of GRs is promoted by HDAC2, and studies have revealed that HDAC2 expression is decreased in patients with severe asthma and may be involved in the development of glucocorticoid resistance (Irvin et al., 2014). The expression of *Nr3c1* (the gene of GRs) (Farrell et al., 2018) was found to be increased, and synchronously, the expression of GR protein increased, in the OVA + ozone

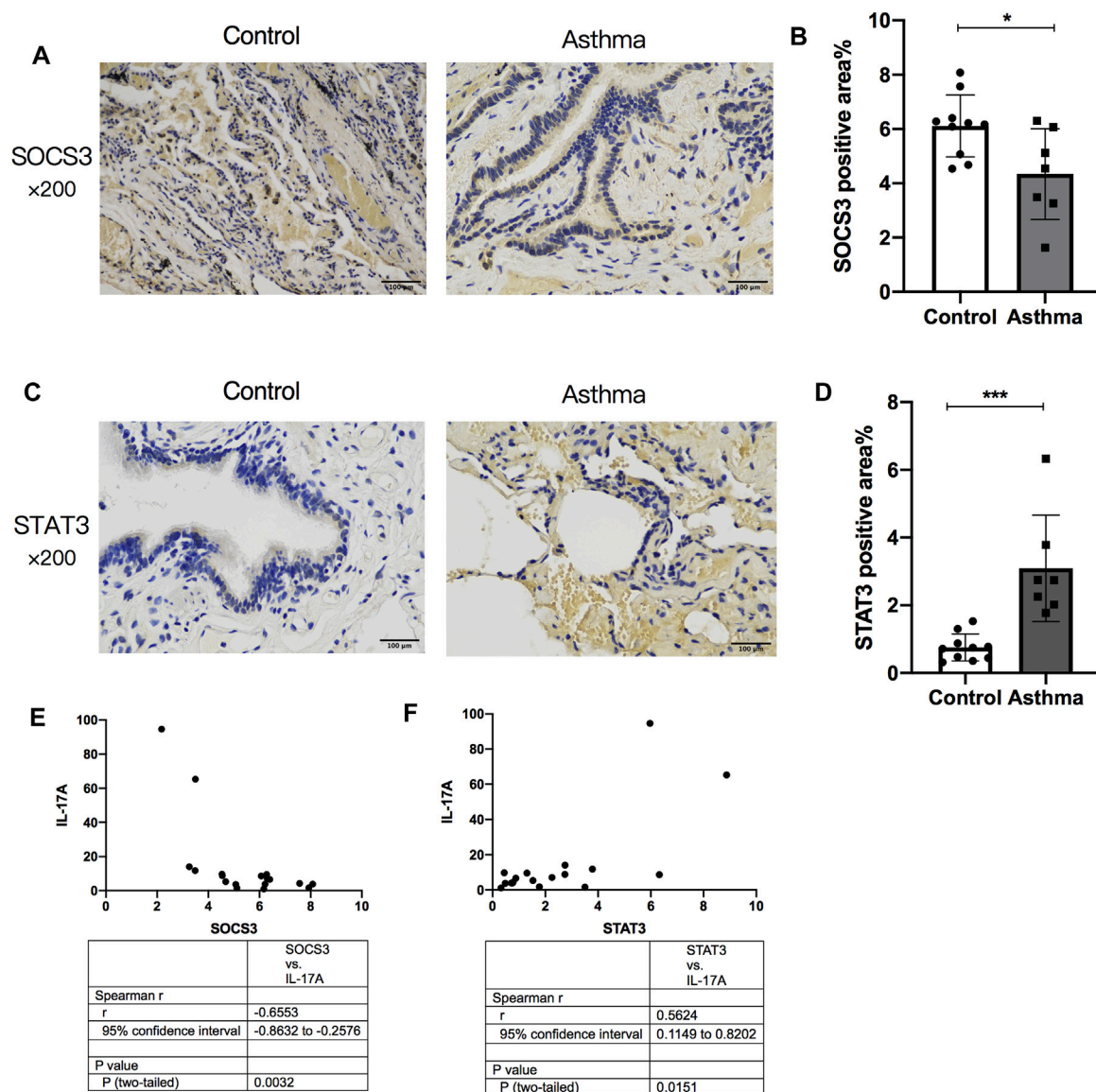


**FIGURE 7 |** Comparison of SOCS3 expression and STAT3 expression in normal lung tissue between asthma patients and healthy controls and their correlation with IL-17A expression in the lung. The expression of STAT3 and SOCS3 in lung tissues of 17 patients undergoing thoracotomy for pulmonary nodules was analyzed by immunohistochemistry. **(A)** Representative photomicrographs of immunohistochemistry of SOCS3 in lung-tissue slices of the asthma group and control group. **(B)** Percent SOCS3-positive area around airways. **(C)** Representative photomicrographs of immunohistochemistry of STAT3 in lung-tissue slices of asthma and control groups. **(D)** Percent STAT3-positive area around airways. **(E)** Correlation between the percent STAT3-positive area and the expression of IL-17A protein in human lung tissue. **(F)** Correlation between the percent SOCS3-positive area and the expression of IL-17A protein in human lung tissue. SOCS3, suppressor of cytokine signaling 3; STAT3, signal transducer and activator of transcription 3. \* $p < 0.05$ ; \*\* $p < 0.01$ ; \*\*\* $p < 0.001$ . Scale bar = 100  $\mu$ m.

group. However, a reduction of expression of the active form of GR (p-GR), which may be facilitated by HDAC2, could have led directly to corticosteroid resistance in the OVA + ozone group.

As important pathophysiological features of severe asthma, neutrophil infiltration and activation in the lung are mostly mediated by CXCL8 and CXCL1 via CXCR1 and CXCR2 (Planagumà et al., 2015). Bao, A. et al. once found increased CXCL1 mRNA expression in an ozone-exposed ovalbumin mouse model (Bao et al., 2017). Johnston, R. A. and others showed an essential role of CXCR2 in maximal neutrophil

recruitment after an acute O<sub>3</sub> exposure (Johnston et al., 2005). The ligand CXCL1 increased in our OVA + ozone-induced mouse model with neutrophil infiltration, indicating a role of chemoattractant for neutrophils in the steroid resistance of this model. The receptor CXCR2 showed a trend of increase compared with that in the control group while having no statistical difference. The difference in the mouse model and concentration or duration of ozone exposure may lead to the discrepancy of our results and Johnston, R. A. and others'. Further quantitative research should be conducted to



determine the change of chemoattractant for neutrophils in the OVA + ozone mouse model.

Ozone can induce tissue injury due to oxidative stress. Some studies have shown that the hypoxia inducer HIF-1 $\alpha$  is associated with oxidative stress and may affect asthma pathogenesis (Saini et al., 2010). HIF-1 $\alpha$  expression in the OVA + ozone group showed an increasing trend compared with that in the control group, but the difference was not significant, which may have been related to the low ozone concentration (2 ppm) used in our modeling process. This finding suggested that oxidative-stress injury may not have been the leading cause of corticosteroid insensitivity in the OVA + ozone group.

Because of high expression of Th17-related cytokines (IL-6, IL-17A, and IL-21) in the OVA + ozone group, the expression of STAT3 and SOCS3 (which are important transcription factors of Th17) was evaluated further. The role of STAT3 and SOCS3 in asthma has been discussed in relation to the T2-mediated allergic response (Seki et al., 2003; Gao and Ward, 2007). Several studies have shown that short-term ozone exposure increased levels of STAT3 or p-STAT3 (Lang et al., 2008; Mishra et al., 2016a), while our study showed an increasing trend but no statistical difference between the ozone group and the control group. Maybe, the difference in methods and the duration of ozone exposure led to this discrepancy. There is still lack of study in effects of ozone exposure on SOCS3, and few scholars have focused on the role of STAT3 and SOCS3 in the mechanism of action of T2-low asthma and corticosteroid resistance. Inhibition of STAT3 expression by C188-9 was shown to reduce airway inflammation and airway remodeling in a house dust mite-induced asthma model created by Gavino and coworkers (Gavino et al., 2016). They adopted a different type of modeling compared with our model. However, studies have demonstrated the ability of house dust mites to induce the production of Th2 cells and Th17 cells simultaneously (Lan et al., 2011), which is similar to the model induced by OVA + ozone in our study. STAT3 expression increased in the OVA + ozone group. p-STAT3 expression increased in the OVA + ozone group more than that in the OVA group. Therefore, STAT3 activated after phosphorylation may have an important role in T2-low asthma and be involved in the development of corticosteroid resistance.

The transcription suppressor SOCS3 showed an opposite trend to that of STAT3 in the OVA + ozone group. This trend has been documented in other studies related to airway inflammation. Sun and others demonstrated the inhibitory effect of SOCS3 on differentiation of Th17 cells in an asthma model (Sun et al., 2018). However, Mishra and coworkers discovered different results: the expression of SOCS3 and STAT3 increased synchronously in allergic airway inflammation (Mishra et al., 2016b). The reason for this disparity may be related to differences in the mouse model employed. Those controversial results further demonstrate the complex regulatory role of SOCS3 in asthma pathogenesis. Some studies have discussed the role of STAT3 in corticosteroid resistance (Banuelos et al., 2016; Halwani et al., 2016). However, few studies have paid attention to the potential

role of SOCS3 in corticosteroid resistance in an asthma model closely related to Th17 cells.

We showed that the expression of IL-6 and IL-17A was correlated with that of STAT3 and SOCS3. STAT3 showed a stronger correlation with the expression of Th17-related cytokines in serum (e.g., IL-6 and IL-17A) than the expression of Th2-related cytokines, which indicates its interaction with Th17 cells. The correlation between the expression of STAT3 or SOCS3 and airway inflammation indicated that STAT3 and SOCS3 are involved in asthma. A strong correlation between SOCS3 expression and asthma severity and serum IgE levels in allergic patients has been reported (Gao and Ward, 2007), which is in accordance with our findings in mouse models. Gavino and others found that blockade of Th2 and Th17 pathways by STAT3 inhibitors in a mouse model of asthma was effective in reducing lung inflammation compared with that employing blockade of one pathway alone (Gavino et al., 2016), which conformed to the correlation between STAT3 expression and IL-13 and IL-17A expressions in our study. However, we speculate that STAT3 expression may be correlated more closely with Th17 pathways than Th2 pathways in the present study due to its stronger correlation with Th17-related cytokines rather than Th2-related cytokines.

As demonstrated above, STAT3 expression is correlated with mucus secretion as well as inflammation, responsiveness, and remodeling of the airways, which suggests an important role of STAT3 in asthma pathogenesis. We found that STAT3 phosphorylation as well as the expression of IL-6 and IL-17A could not be reversed by Dex treatment, which indicates their involvement in corticosteroid resistance of OVA- and ozone-induced asthma. In an animal study, Banuelos and collaborators showed that IL-17A production was not suppressed by glucocorticoids (Banuelos et al., 2016). Previously, we found that treatment with the IL-17A monoclonal antibody reduced corticosteroid insensitivity in a mouse model of asthma (Zhang Y. et al., 2019). Here, we paid more attention to p-STAT3. It has been reported that STAT3 phosphorylation in Th17 cells is insensitive to glucocorticoid inhibition (Banuelos et al., 2016). IL-6 is involved in STAT3-regulated inflammation and may interact with STAT3 (Rottenberg and Carow, 2014). Dex and budesonide help protect human type II alveolar epithelial cells by epithelium-derived surfactant protein D in a manner that is dependent on GRs and STAT3 (an IL-6-responsive transcription factor) (Flayer et al., 2019). Thus, IL-6 and STAT3 may have important roles in an OVA- and ozone-induced corticosteroid-resistant asthma model. Our analyses in the human lung tissue of the expression of STAT3 and SOCS3 further convinced us that STAT3 and SOCS3 are involved in asthma. We analyzed the correlation between the expression of STAT3 or SOCS3 and IL-17A. The expression of IL-17A in the lung tissue of asthma patients and HCs showed a strong correlation with the expression of STAT3 and SOCS3. These findings further indicated the possible role of interaction between STAT3 or SOCS3 and Th17 cells in asthma. The expression of SOCS3 and STAT3 has been evaluated in airway inflammation in some animal models (Gao and

Ward, 2007; Santana et al., 2019; Pinheiro et al., 2020), but we are the first to observe their changes in the lung tissue of asthma patients. Though we failed to divide asthma patients to T2-high or -low endotypes, eosinophil counts in blood were  $<150/\mu\text{l}$  in the asthma group and did not show a significant difference from that in the control group (**Supplementary Table S2**).

However, there are several limitations of the current study. Firstly, increasing studies have demonstrated non-HLA antibodies such as Col-V and EGFR involved in the IL-17-related pathways in different pulmonary diseases (and may contribute to severe asthma). More attention should be paid to these pathways but not the conventional pathway. We will try to involve these non-HLA antibodies in our studies of IL-17 and its pathways. Secondly, further studies on the intervention of STAT3 and SOCS3, as well as the discussion of the mechanisms of their regulation in Th17 cells and corticosteroid resistance, should be conducted.

## CONCLUSION

We established an asthma model with neutrophil infiltration and increased expression of Th17-related cytokines by OVA sensitization/challenge and ozone exposure. The OVA + ozone group showed corticosteroid resistance with reduction of expression of HDAC2 and p-GR. STAT3 and SOCS3 appeared to be involved in asthma pathogenesis in mouse models and asthma patients. IL-6 and STAT3 may have contributed to corticosteroid resistance in the OVA + ozone group through regulation of Th17 cells. SOCS3 (a negative transcription factor) may interact with STAT3 and be involved in the corticosteroid insensitivity of the T2-low asthma model.

## DATA AVAILABILITY STATEMENT

The raw data supporting the conclusions of this article will be made available by the authors, without undue reservation.

## REFERENCES

- Alangari, A. (2014). Corticosteroids in the Treatment of Acute Asthma. *Ann. Thorac. Med.* 9, 187–192. doi:10.4103/1817-1737.140120
- Banuelos, J., Shin, S., Cao, Y., Bochner, B. S., Morales-Nebreda, L., Budinger, G. R. S., et al. (2016). BCL-2 Protects Human and Mouse Th17 Cells from Glucocorticoid-Induced Apoptosis. *Allergy* 71 (5), 640–650. doi:10.1111/all.12840
- Bao, A., Ma, A., Zhang, H., Qiao, L., Ben, S., Zhou, X., et al. (2020). Inducible Expression of Heat Shock Protein 20 Protects Airway Epithelial Cells against Oxidative Injury Involving the Nrf2-NQO-1 Pathway. *Cell Biosci.* 10, 120. doi:10.1186/s13578-020-00483-3
- Bao, A., Yang, H., Ji, J., Chen, Y., Bao, W., Li, F., et al. (2017). Involvements of P38 MAPK and Oxidative Stress in the Ozone-Induced Enhancement of AHR and Pulmonary Inflammation in an Allergic Asthma Model. *Respir. Res.* 18 (1), 216. doi:10.1186/s12931-017-0697-4
- Bao, W., Zhang, Y., Zhang, M., Bao, A., Fei, X., Zhang, X., et al. (2018). Effects of Ozone Repeated Short Exposures on the Airway/lung Inflammation, Airway Hyperresponsiveness and Mucus Production in a Mouse Model of Ovalbumin-Induced Asthma. *Biomed. Pharmacother.* 101, 293–303. doi:10.1016/j.biopha.2018.02.079

## ETHICS STATEMENT

The studies involving human participants were reviewed and approved by the Institutional Review Board at Shanghai General Hospital (No. 2018KY186) and registered on [chictr.org.cn](http://chictr.org.cn) (No. ChiCTR2000029065). The patients/participants provided their written informed consent to participate in this study. The animal study was reviewed and approved by the Ethics Committee for Animal Studies at Shanghai General Hospital, China (IACUC: 2019-A011-01).

## AUTHOR CONTRIBUTIONS

MZ designed the experiments. YX, HH, QF, LH, XZ, and XT performed the experiments. YX, WB, YZ, and MZ analyzed and interpreted the data, drafted the article, and supervised the work. All authors read and approved the final article.

## FUNDING

This work was supported by National Natural Science Foundation of China (Grant No. 81873402, 81900016 and 81800020); Appropriate technique application Program of Shanghai Municipal Health System (Grant No.2019SY042); Scientific and Technological Innovation program funded by Science and Technology Commission of Shanghai municipality (Grant No. 20Y11902400) and Program of Shanghai Municipal Health System (Grant No.201740039).

## SUPPLEMENTARY MATERIAL

The Supplementary Material for this article can be found online at: <https://www.frontiersin.org/articles/10.3389/fmolb.2021.717962/full#supplementary-material>

- Barnes, P. J. (2016). Glucocorticosteroids. *Handb. Exp. Pharmacol.* 237, 93–115. doi:10.1007/164\_2016\_62
- Bobadilla, J. L., Love, R. B., Jankowska-Gan, E., Xu, Q., Haynes, L. D., Braun, R. K., et al. (2008). Th-17, Monokines, Collagen Type V, and Primary Graft Dysfunction in Lung Transplantation. *Am. J. Respir. Crit. Care Med.* 177 (6), 660–668. doi:10.1164/rccm.200612-1901OC
- Chung, K. F. (2016). Asthma Phenotyping: a Necessity for Improved Therapeutic Precision and New Targeted Therapies. *J. Intern. Med.* 279 (2), 192–204. doi:10.1111/joim.12382
- Cosmi, L., Liotta, F., Maggi, E., Romagnani, S., and Annunziato, F. (2011). Th17 Cells: New Players in Asthma Pathogenesis. *Allergy* 66 (8), 989–998. doi:10.1111/j.1398-9995.2011.02576.x
- Farrell, A. K., Slatcher, R. B., Tobin, E. T., Imami, L., Wildman, D. E., Luca, F., et al. (2018). Socioeconomic Status, Family Negative Emotional Climate, and Anti-inflammatory Gene Expression Among Youth with Asthma. *Psychoneuroendocrinology* 91, 62–67. doi:10.1016/j.psyneuen.2018.02.011
- Flayer, C. H., Ge, M. Q., Hwang, J. W., Kokalari, B., Redai, I. G., Jiang, Z., et al. (2019). Ozone Inhalation Attenuated the Effects of Budesonide on Aspergillus Fumigatus-Induced Airway Inflammation and Hyperreactivity in Mice. *Front. Immunol.* 10, 2173. doi:10.3389/fimmu.2019.02173

- Gao, H., and Ward, P. A. (2007). STAT3 and Suppressor of Cytokine Signaling 3: Potential Targets in Lung Inflammatory Responses. *Expert Opin. Ther. Targets* 11 (7), 869–880. doi:10.1517/14728222.11.7.869
- Gavino, A. C., Nahmod, K., Bharadwaj, U., Makedonas, G., and Tweardy, D. J. (2016). STAT3 Inhibition Prevents Lung Inflammation, Remodeling, and Accumulation of Th2 and Th17 Cells in a Murine Asthma Model. *Allergy* 71 (12), 1684–1692. doi:10.1111/all.12937
- Halwani, R., Sultana, A., Al-Kufaidy, R., Jamhawi, A., Vazquez-Tello, A., and Al-Muhsen, S. (2016). Th-17 Regulatory Cytokines Inhibit Corticosteroid Induced Airway Structural Cells Apoptosis. *Respir. Res.* 17, 6. doi:10.1186/s12931-015-0307-2
- Irusen, E., Matthews, J. G., Takahashi, A., Barnes, P. J., Chung, K. F., and Adcock, I. M. (2002). p38 Mitogen-Activated Protein Kinase-Induced Glucocorticoid Receptor Phosphorylation Reduces its Activity: Role in Steroid-Insensitive Asthma. *J. Allergy Clin. Immunol.* 109 (4), 649–657. doi:10.1067/mai.2002.122465
- Irvin, C., Zafar, I., Good, J., Rollins, D., Christianson, C., Gorska, M. M., et al. (2014). Increased Frequency of Dual-Positive TH2/TH17 Cells in Bronchoalveolar Lavage Fluid Characterizes a Population of Patients with Severe Asthma. *J. Allergy Clin. Immunol.* 134 (5), 1175–1186. e7. doi:10.1016/j.jaci.2014.05.038
- Johnston, R. A., Mizgerd, J. P., and Shore, S. A. (2005). CXCR2 Is Essential for Maximal Neutrophil Recruitment and Methacholine Responsiveness after Ozone Exposure. *Am. J. Physiology-Lung Cell Mol. Physiol.* 288 (1), L61–L67. doi:10.1152/ajplung.00101.2004
- Lan, F., Liu, K., Zhang, J., Qi, Y., Li, K., and Lin, P. (2011). Th17 Response Is Augmented in OVA-Induced Asthmatic Mice Exposed to HDM. *Med. Sci. Monit.* 17 (5), BR132–BR138. doi:10.12659/msm.881759
- Lang, J. E., Williams, E. S., Mizgerd, J. P., and Shore, S. A. (2008). Effect of Obesity on Pulmonary Inflammation Induced by Acute Ozone Exposure: Role of Interleukin-6. *Am. J. Physiology-Lung Cell Mol. PhysiologyLung Cell. Mol. Physiol.* 294 (5), L1013–L1020. doi:10.1152/ajplung.00122.2007
- Last, J. A., Ward, R., Temple, L., and Kenyon, N. J. (2004). Ovalbumin-induced Airway Inflammation and Fibrosis in Mice Also Exposed to Ozone. *Inhalation Toxicol.* 16 (1), 33–43. doi:10.1080/08958370490258237
- Lee, K.-L., Lai, T.-C., Wang, Y.-C., Shih, P.-C., Yang, Y.-C., Tsao, T. C.-Y., et al. (2021). Potential Impacts of Interleukin-17A Promoter Polymorphisms on the EGFR Mutation Status and Progression of Non-small Cell Lung Cancer in Taiwan. *Genes* 12 (3), 427. doi:10.3390/genes12030427
- Li, Z., Fan, H., Chen, W., Xiao, J., Ma, X., Ni, P., et al. (2021). MicroRNA-653-5p Promotes Gastric Cancer Proliferation and Metastasis by Targeting the SOCS6-STAT3 Pathway. *Front. Mol. Biosci.* 8, 655580. doi:10.3389/fmolb.2021.655580
- Mei, D., Tan, W. S. D., and Wong, W. S. F. (2019). Pharmacological Strategies to Regain Steroid Sensitivity in Severe Asthma and COPD. *Curr. Opin. Pharmacol.* 46, 73–81. doi:10.1016/j.coph.2019.04.010
- Miossec, P., and Kolls, J. K. (2012). Targeting IL-17 and TH17 Cells in Chronic Inflammation. *Nat. Rev. Drug Discov.* 11 (10), 763–776. doi:10.1038/nrd3794
- Mishra, V., Baranwal, V., Mishra, R. K., Sharma, S., Paul, B., and Pandey, A. C. (2016a). Titanium Dioxide Nanoparticles Augment Allergic Airway Inflammation and Soc3s Expression via NF-Kb Pathway in Murine Model of Asthma. *Biomaterials* 92, 90–102. doi:10.1016/j.biomaterials.2016.03.016
- Mishra, V., DiAngelo, S. L., and Silveira, P. (2016b). Sex-specific IL-6-associated Signaling Activation in Ozone-Induced Lung Inflammation. *Biol. Sex. Differ.* 7, 16. doi:10.1186/s13293-016-0069-7
- Panettieri, R. A., Jr (2018). The Role of Neutrophils in Asthma. *Immunol. Allergy Clin. North America* 38 (4), 629–638. doi:10.1016/j.iac.2018.06.005
- Pinheiro, N. M., Miranda, C. J. C. P., Santana, F. R., Bittencourt-Mernak, M., Arantes-Costa, F. M., Olivo, C., et al. (2020). Effects of VACHT Reduction and  $\alpha$ nAChR Stimulation by PNU-282987 in Lung Inflammation in a Model of Chronic Allergic Airway Inflammation. *Eur. J. Pharmacol.* 882, 173239. doi:10.1016/j.ejphar.2020.173239
- Planagumà, A., Domènech, T., Pont, M., Calama, E., García-González, V., López, R., et al. (2015). Combined Anti CXCR2 and CXCR3 Therapy Is a Promising Anti-inflammatory Treatment for Respiratory Diseases by Reducing Neutrophil Migration and Activation. *Pulm. Pharmacol. Ther.* 34, 37–45. doi:10.1016/j.pupt.2015.08.002
- Rottenberg, M. E., and Carow, B. (2014). SOCS3 and STAT3, Major Controllers of the Outcome of Infection with *Mycobacterium tuberculosis*. *Semin. Immunol.* 26 (6), 518–532. doi:10.1016/j.smim.2014.10.004
- Saini, Y., Kim, K. Y., Lewandowski, R., Bramble, L. A., Harkema, J. R., and Lapres, J. J. (2010). Role of Hypoxia-Inducible Factor 1 $\alpha$  in Modulating Cobalt-Induced Lung Inflammation. *Am. J. Physiology-Lung Cell Mol. PhysiologyLung Cell. Mol. Physiol.* 298 (2), L139–L147. doi:10.1152/ajplung.00252.2009
- Santana, F. P. R., da Silva, R. C., Grecco, S. d. S., Pinheiro, A. J. M. C. R., Caperuto, L. C., Arantes-Costa, F. M., et al. (2019). Inhibition of MAPK and STAT3-SOCS3 by Sakuranetin Attenuated Chronic Allergic Airway Inflammation in Mice. *Mediators Inflamm.* 2019, 1–14. doi:10.1155/2019/1356356
- Seki, Y.-i., Inoue, H., Nagata, N., Hayashi, K., Fukuyama, S., Matsumoto, K., et al. (2003). SOCS-3 Regulates Onset and Maintenance of TH2-Mediated Allergic Responses. *Nat. Med.* 9 (8), 1047–1054. doi:10.1038/nm896
- Sun, W., Xiao, B., Jia, A., Qiu, L., Zeng, Q., Liu, D., et al. (2018). MBD2-mediated Th17 Differentiation in Severe Asthma Is Associated with Impaired SOCS3 Expression. *Exp. Cel. Res.* 371 (1), 196–204. doi:10.1016/j.yexcr.2018.08.010
- Svenningsen, S., and Nair, P. (2017). Asthma Endotypes and an Overview of Targeted Therapy for Asthma. *Front. Med.* 4, 158. doi:10.3389/fmed.2017.00158
- Wenzel, S. E., Schwartz, L. B., Langmack, E. L., Halliday, J. L., Trudeau, J. B., Gibbs, R. L., et al. (1999). Evidence that Severe Asthma Can Be Divided Pathologically into Two Inflammatory Subtypes with Distinct Physiologic and Clinical Characteristics. *Am. J. Respir. Crit. Care Med.* 160 (3), 1001–1008. doi:10.1164/ajrcrm.160.3.9812110
- Zhang, J.-h., Yang, X., Chen, Y.-p., Zhang, J.-f., and Li, C.-q. (2019a). Nrf2 Activator RTA-408 Protects against Ozone-Induced Acute Asthma Exacerbation by Suppressing ROS and  $\gamma$ DT17 Cells. *Inflammation* 42 (5), 1843–1856. doi:10.1007/s10753-019-01046-6
- Zhang, X., Bao, W., Fei, X., Zhang, Y., Zhang, G., Zhou, X., et al. (2018). Progesterone Attenuates Airway Remodeling and Glucocorticoid Resistance in a Murine Model of Exposing to Ozone. *Mol. Immunol.* 96, 69–77. doi:10.1016/j.molimm.2018.02.009
- Zhang, Y., Li, X., He, M., Zhang, G., Bao, W., Fei, X., et al. (2019b). The Effects of Neutralizing Anti-murine interleukin-17A Monoclonal Antibody on Ozone-Induced Inflammation and Glucocorticoids Insensitivity in a Murine Model of Asthma. *Biomed. Pharmacother.* 114, 108786. doi:10.1016/j.biopha.2019.108786
- Zhu, S.-q., Zhou, B.-h., Tan, P.-p., Chai, J., Yu, Y.-m., and Wang, H.-w. (2020). Based on G-Series Mouse TH17 Array Study the Effect of Fluoride on C2C12 Cells Cytokines Expression. *Biol. Trace Elem. Res.* doi:10.1007/s12011-020-02464-6

**Conflict of Interest:** The authors declare that the research was conducted in the absence of any commercial or financial relationships that could be construed as a potential conflict of interest.

**Publisher's Note:** All claims expressed in this article are solely those of the authors and do not necessarily represent those of their affiliated organizations, or those of the publisher, the editors and the reviewers. Any product that may be evaluated in this article, or claim that may be made by its manufacturer, is not guaranteed or endorsed by the publisher.

Copyright © 2021 Xue, Zhou, Bao, Fu, Hao, Han, Zhang, Tian and Zhang. This is an open-access article distributed under the terms of the Creative Commons Attribution License (CC BY). The use, distribution or reproduction in other forums is permitted, provided the original author(s) and the copyright owner(s) are credited and that the original publication in this journal is cited, in accordance with accepted academic practice. No use, distribution or reproduction is permitted which does not comply with these terms.



# Relationships Between Oral Microecosystem and Respiratory Diseases

Jiajia Dong<sup>1†</sup>, Wei Li<sup>2†</sup>, Qi Wang<sup>2</sup>, Jiahao Chen<sup>2</sup>, Yue Zu<sup>2</sup>, Xuedong Zhou<sup>2</sup> and Qiang Guo<sup>2\*</sup>

<sup>1</sup>Department of Pulmonary and Critical Care Medicine, West China Hospital, Sichuan University, Chengdu, China, <sup>2</sup>State Key Laboratory of Oral Diseases, National Clinical Research Center for Oral Diseases, West China Hospital of Stomatology, Sichuan University, Chengdu, China

## OPEN ACCESS

### Edited by:

Huahao Shen,  
Zhejiang University, China

### Reviewed by:

Ana Cláudia Coelho,  
University of Trás-os-Montes and Alto  
Douro, Portugal  
Kai Yang,  
First Affiliated Hospital of Guangzhou  
Medical University, China

### \*Correspondence:

Qiang Guo  
guoqiang2014@scu.edu.cn

<sup>†</sup>These authors have contributed  
equally to this work.

### Specialty section:

This article was submitted to  
Molecular Diagnostics and  
Therapeutics,  
a section of the journal  
Frontiers in Molecular Biosciences

**Received:** 31 May 2021

**Accepted:** 09 December 2021

**Published:** 04 January 2022

### Citation:

Dong J, Li W, Wang Q, Chen J, Zu Y,  
Zhou X and Guo Q (2022)  
Relationships Between Oral  
Microecosystem and  
Respiratory Diseases.  
Front. Mol. Biosci. 8:718222.  
doi: 10.3389/fmolb.2021.718222

Oral microecosystem is a very complicated ecosystem that is located in the mouth and comprises oral microbiome, diverse anatomic structures of oral cavity, saliva and interactions between oral microbiota and between oral microbiota and the host. More and more evidence from studies of epidemiology, microbiology and molecular biology is establishing a significant link between oral microecosystem and respiratory diseases. Microbiota settling down in oral microecosystem is known as the main source of lung microbiome and has been associated with the occurrence and development of respiratory diseases like pneumonia, chronic obstructive pulmonary disease, lung cancer, cystic fibrosis lung disease and asthma. In fact, it is not only indigenous oral microbes promote or directly cause respiratory infection and inflammation when inhaled into the lower respiratory tract, but also internal environment of oral microecosystem serves as a reservoir for opportunistic respiratory pathogens. Moreover, poor oral health and oral diseases caused by oral microecological dysbiosis (especially periodontal disease) are related with risk of multiple respiratory diseases. Here, we review the research status on the respiratory diseases related with oral microecosystem. Potential mechanisms on how respiratory pathogens colonize oral microecosystem and the role of indigenous oral microbes in pathogenesis of respiratory diseases are also summarized and analyzed. Given the importance of oral plaque control and oral health interventions in controlling or preventing respiratory infection and diseases, we also summarize the oral health management measures and attentions, not only for populations susceptible to respiratory infection like the elderly and hospitalized patients, but also for dentist or oral hygienists who undertake oral health care. In conclusion, the relationship between respiratory diseases and oral microecosystem has been established and supported by growing body of literature. However, etiological evidence on the role of oral microecosystem in the development of respiratory diseases is still insufficient. Further detailed studies focusing on specific mechanisms on how oral microecosystem participate in the pathogenesis of respiratory diseases could be helpful to prevent and treat respiratory diseases.

**Keywords:** oral microecosystem, respiratory disease, respiratory pathogen, oral microorganism, dental plaque, oral health care



## INTRODUCTION

Oral microecosystem is a very complicated ecosystem that is located in the mouth and comprises oral microbiome, anatomic structures of oral cavity (teeth, periodontium, tongue, oral mucosa, etc.), and saliva, in which also included interactions between oral microbiota and between oral microbiota and their hosts (Wang, 2019). As exposed to air, the mouth is in direct contact with the outside environment and is constantly challenged by microbial species present in the environment via breath and eating. The complex anatomical structure of oral cavity (as well as dental repairing materials), the presence of saliva, and other physical and chemical characteristics such as pH, oxygen content and temperature in the environment determine the organisms that settle down in oral microecosystem (Kilian, 2018). The oral microecosystem of human harbors a vast amount of highly diverse microorganisms, including bacteria, fungi, protozoa, mycoplasmas and viruses. ~700 bacterial species constitute the majority of a healthy oral microbiome and are further categorized into six major phyla by 16S rDNA profiling, viz, *Firmicutes*, *Actinobacteria*, *Proteobacteria*, *Fusobacteria*, *Bacteroidetes* and *Spirochaetes* (Verma et al., 2018). Besides, fungi (more than 100 species) also constitute the significant proportion of an oral microbiota, in which *Candida* spp. are one of the most common taxa (Seed, 2014). In oral microecosystem, microbes like bacteria and fungi attach to the tooth surface and form biofilms called dental plaques with surrounded extracellular matrix, in order to protect themselves from environmental fluctuation of oral cavity and external drug stimulations, and evade host defense mechanisms (Jhajharia et al., 2015). For the most common oral diseases, caries, the major pathogen of which is *Streptococcus mutans*, and periodontal disease, the major pathogens of which are red-complex bacteria (*Porphyromonas gingivalis*, *Treponema denticola* and *Tannerella forsythia*), dental plaques are the critical pathogenic basis (Kinane et al., 2008).

The balance of oral microecosystem not only contributes to the maintenance of oral health, but also has a potential impact on overall health. Through complicated interspecies interactions like mutualism, competition and antagonism, microbes living in oral microecosystem achieve the dynamic balance with each other, as well as with the host. However, in the condition of ecological disturbance or in occurrence of oral diseases, oral microorganisms have a chance to transfer into the circulatory system or the digestive system through oral cavity, thus affecting overall health (Hasan et al., 2014; Seedorf et al., 2014). The involvement of oral microorganisms has been observed in many diseases such as diabetes (Genco et al., 2005), bacteremia (Poveda-Roda et al., 2008), endocarditis (Parahitiyawa et al., 2009), rheumatoid arthritis (Ogrendik, 2009), atherosclerosis (Chhibber-Goel et al., 2016), preterm delivery (Teshome and Yitayeh, 2016), digestive system cancers (Seedorf et al., 2014) and other diseases.

In terms of anatomy, the oral cavity is also the gateway for the respiratory tract. In the cases of breathing with the mouth, accidentally inhaling and trachea cannula, saliva in oral microecosystem would enter the respiratory tract, and on the one hand, certain behaviors like cough could make the mucus of

the respiratory tract and other substances enter the mouth, thereby achieving the mutual exchange between the oral cavity and the respiratory tract. Extensive evidence from studies of epidemiology, microbiology and molecular biology has established a significant link between oral microbes, dental plaque, oral health, oral diseases and respiratory diseases. Oral microbiota is known as the main source of lung microbiome (Bassis et al., 2015; Pragman et al., 2018; Maddi et al., 2019). Microbes indigenous to oral microecosystem are likely to be inhaled into lower respiratory tract (Tunney et al., 2008; Worlitzsch et al., 2009; Yamasaki et al., 2013; Tan et al., 2014; Coburn et al., 2015; Yan et al., 2015; Wu et al., 2017; Muhlebach MS. et al., 2018), and may infect the lung and trachea by pathogenic virulence factors or change respiratory mucosal microenvironment conducive to the colonization of respiratory pathogens. Besides, the diverse environment inside oral microecosystem could provide latent sites for the lodging of common respiratory pathogens (Sumi et al., 2007; Heo et al., 2008; Benseal et al., 2010; Tan et al., 2014; Rivas Caldas et al., 2015; To et al., 2020), which could further invade the respiratory tract and cause diseases under the condition of low host resistance. Many studies have observed an association between oral health, oral diseases and risk of respiratory diseases like pneumonia, chronic obstructive pulmonary disease (COPD) and lung cancer (Bágyi et al., 2006; Awano et al., 2008; Prasanna, 2011; Zeng et al., 2012; Yamasaki et al., 2013; Chrysanthakopoulos, 2016; Zeng et al., 2016; Qian et al., 2020). Therefore, it is pretty critical to understand the role of oral microecosystem in pathogenesis of respiratory diseases, which would contribute to the prevention and treatment of respiratory diseases.

Here, we review and analyze the research status on the respiratory diseases related with oral microecosystem and potential mechanisms on how respiratory pathogens colonize oral microecosystem and how indigenous oral microbes participate in pathogenesis of respiratory diseases. Oral health management strategies maintaining oral hygiene and oral microbiome symbiosis are also summarized to guide oral care interventions on populations susceptible to respiratory infection like the elderly and hospitalized patients and reduce their incidence of respiratory diseases.

## THE RESPIRATORY DISEASES ASSOCIATED WITH ORAL MICROECOSYSTEM

Increasing evidence has linked oral microecosystem, as well as oral health and oral diseases, with respiratory diseases mainly pneumonia, COPD, lung cancer, cystic fibrosis (CF) lung disease and asthma (Table 1). Primary respiratory pathogens could be found in dental plaques, periodontal pockets and saliva, suggesting that oral microecosystem is a potential source of the respiratory infection and diseases (Sumi et al., 2007; Heo et al., 2008; Benseal et al., 2010; Tan et al., 2014; Rivas Caldas et al., 2015; To et al., 2020). On the other hand, the presence of orally derived bacteria in sputum and bronchoalveolar lavage (BAL) fluid have been observed by many studies (Tunney et al., 2008;

**TABLE 1 |** The relationship of oral microbes, oral infection and disease, oral health (care) with respiratory diseases.

Respiratory diseases	Oral microbes	Oral infection and disease	Oral health (care)	Respiratory pathogens detected in oral microecosystem
Pneumonia	BAL specimens (CAP patients): oral <i>streptococci</i> , <i>Neisseria</i> spp. and anaerobes ( <i>Prevotella</i> spp., <i>Fusobacterium</i> spp., <i>Veillonella</i> spp., and <i>Clostridium</i> spp.) Yamasaki et al. (2013) Saliva bacteria counts as a risk factor for AP Kikutani et al. (2015); Nishizawa et al. (2019)	Dental infection as a risk factor for pneumonia Laurence et al. (2015)  Periodontal disease as a risk factor for CAP Bágyi et al. (2006); Awano et al. (2008); Yamasaki et al. (2013)	Professional oral care reduces AP risk Quagliarello et al. (2005); Chebib et al. (2018); Khadka et al. (2021)  Brushing teeth helps control the pneumopathogens ( <i>staphylococci</i> , Enterobacteriaceae and yeasts) in resting saliva and reduce VAP risk Cecon et al. (2010); Stonecypher (2010) An increase in oral care frequency significantly reduces the NV-HAP incidence rate Giuliano et al. (2021) Preoperative oral hygiene interventions such as dental brushing and professional oral plaque control reduce incidence of POP Akutsu et al. (2010); Gonzalez-Rubio Aguilar et al. (2019); Jia et al. (2020) The elderly who wear denture during sleep are more likely to have tongue and denture plaque, gum inflammation, positive culture for <i>C. albicans</i> , higher levels of circulating IL-6, and an increased risk for incident pneumonia Iinuma et al. (2015)	Pneumonia pathogens in dental plaques (dependent elderly): <i>S. pneumoniae</i> , <i>H. influenzae</i> and <i>K. pneumoniae</i> Sumi et al. (2007)  VAP pathogens in dental plaques (VAP patients): <i>S. aureus</i> , <i>P. aeruginosa</i> , <i>Acinetobacter</i> species, and enteric species Heo et al. (2008)  Saliva (COVID-19 patients): SARS-CoV-2 To et al. (2020)
CF lung disease	Sputum and BAL specimens (CF patients): oral anaerobic bacteria Tunney et al. (2008); Worlitzsch et al. (2009); Coburn et al. (2015); Muhlebach et al. (2018a) Lower respiratory tract is dominated by oral microbiome (CF children at age 2) Muhlebach et al. (2018b)	NA	NA	Periodontal pockets (CF patients): <i>P. aeruginosa</i> , <i>S. aureus</i> Bense et al. (2010)  Saliva and subgingival plaques (CF patients): <i>P. aeruginosa</i> Rivas Caldas et al. (2015)
COPD	Tracheal aspirate specimens (COPD patients with severe acute exacerbations): <i>P. gingivalis</i> , <i>Treponema denticola</i> , <i>Tannerella forsythia</i> , <i>A. actinomycetemcomitans</i> and <i>Capnocytophaga sputigena</i> Tan et al. (2014) Lung tissues specimens (mild-moderate COPD patients): the sources of the lung tissue microbiota were 21.1% (mean) oral microbiota, 8.7% nasal microbiota, and 70.1% unknown Pragman et al. (2018) Six genera and 15 species in subgingival plaques may be associated to COPD, especially the genera <i>Dysgonomonas</i> , <i>Desulfobulbus</i> and <i>Catonella</i> with much higher proportions (COPD patients) Wu et al. (2017)	Periodontal disease as a risk factor for COPD Prasanna (2011); Zeng et al. (2012); Qian et al. (2020)	Periodontal therapy reduces the frequency of the exacerbation of COPD Kucukcoskun et al. (2013); Zhou et al. (2014)  COPD patients have significant fewer teeth, higher plaque index, poorer periodontal status and poorer oral health knowledge and behaviors, Wang et al. (2009); Gaeckle et al. (2018); Zhou et al. (2020)	Lung pathogens in subgingival plaque (COPD patients with severe acute exacerbations): <i>Acinetobacter baumannii</i> , <i>K. pneumoniae</i> , <i>P. aeruginosa</i> and <i>S. pneumoniae</i> Tan et al. (2014)
Asthma	A stronger shift in dental biofilm microbiome compared to healthy controls, with 14 different taxa (children	NA	NA	NA

(Continued on following page)

**TABLE 1 |** (Continued) The relationship of oral microbes, oral infection and disease, oral health (care) with respiratory diseases.

Respiratory diseases	Oral microbes	Oral infection and disease	Oral health (care)	Respiratory pathogens detected in oral microecosystem
	with allergic asthma) Arweiler et al. (2021)			
Lung cancer	Significant changes in saliva microbiome which are indicated by the significant increase of <i>Capnocytophaga</i> and <i>Veillonella</i> (lung cancer patients with SCC or AC) Yan et al. (2015) Lower microbial diversity and richness of salivary microbiome (non-smoking lung cancer patients) Yang et al. (2018); Hosgood et al. (2021) Salivary microbiome is related to cancer pathways, p53 signaling pathway, apoptosis and tuberculosis (non-smoking lung cancer patients) Yang et al. (2018)	Periodontal disease as a risk factor for lung cancer Chrysanthakopoulos (2016); Zeng et al. (2016)	NA	NA

BAL, bronchoalveolar lavage; CAP, community-acquired pneumonia; AP, aspiration pneumonia; VAP, ventilator-associated pneumonia; NV-HAP, nonventilator hospital-acquired pneumonia; POP, postoperative pneumonia; COVID-19, coronavirus disease 2019; SARS-CoV-2, severe acute respiratory syndrome coronavirus 2; CF, cystic fibrosis; NA, not applicable; COPD, chronic obstructive pulmonary disease; SCC, small cell carcinoma; AC, adenocarcinoma.

Worlitzsch et al., 2009; Yamasaki et al., 2013; Tan et al., 2014; Coburn et al., 2015; Yan et al., 2015; Wu et al., 2017; Muhlebach MS. et al., 2018). Oral diseases driven by dysbiosis of oral microecosystem, typically, periodontal disease (Bágyi et al., 2006; Awano et al., 2008; Prasanna, 2011; Zeng et al., 2012; Yamasaki et al., 2013; Chrysanthakopoulos, 2016; Zeng et al., 2016; Qian et al., 2020), and poor oral health status (Wang et al., 2009; Iinuma et al., 2015; Gaeckle et al., 2018; Zhou et al., 2020) are recognized as risk factors for the occurrence and progression of many respiratory diseases.

## Infectious Pulmonary Diseases Pneumonia

Pneumonia is a very common infection that inflames the air sacs in one or both lungs. Dental plaques are known to be a reservoir for common respiratory pathogens responsible for pneumonia (Sumi et al., 2007). Community-acquired pneumonia (CAP) occurs outside of hospitals or other health care facilities and the most commonly identified bacterial pathogens of CAP could be detected in dental plaques, including *Streptococcus pneumoniae* (*S. pneumoniae*), *Haemophilus influenzae* and *Klebsiella pneumoniae* (Sumi et al., 2007). In an etiology study of CAP, high rates of oral *streptococci* and anaerobes were found in the BAL specimens of CAP patients (Yamasaki et al., 2013). The level of periodontal disease has a significant association with the mortality of pneumonia and the anaerobic bacteria from the dental plaques of patients with periodontal disease could be causative agents of CAP (Bágyi et al., 2006; Awano et al., 2008; Yamasaki et al., 2013). Thus, it is suggested by a study that the presence of dental infections may worsen the symptoms of the patients who made a visit to the emergency departments because of pneumonia and increase the chance to be hospitalized (Laurence et al., 2015). In contrast to CAP, hospital-acquired pneumonia (HAP), which include ventilator-associated

pneumonia (VAP) and healthcare-associated pneumonia (HCAP), refers in particular to pneumonia occurs in hospitals (including rehabilitation hospitals, nursing homes for the elderly, etc.). The pathogenic microbial spectrum of HAP contains gram-positive cocci, such as *Staphylococcus aureus* (*S. aureus*) and *S. pneumoniae*, but more gram-negative bacteria, such as *Pseudomonas aeruginosa*, *K. pneumoniae*, *enterococci* and *Enterobacter* spp. (Miyashita et al., 2005; Cilloniz et al., 2011; Koulenti et al., 2017; Leone et al., 2018). The increasing of dental plaque is also related to the incidence of nosocomial infections of the patients in the intensive care units (ICUs) (Fourrier et al., 1998). With the aid of the molecular methods, respiratory pathogens of VAP that are isolated from dental plaque and BAL fluid from patients in ICU are found to be genetically related (Heo et al., 2008). As a form of HCAP, aspiration pneumonia increases the mortality especially in old-age people (Feng et al., 2019). Oral bacteria are recognized as a source of infection for aspiration pneumonia and oral bacteria counts are a risk factor for aspiration pneumonia (Kikutani et al., 2015; Nishizawa et al., 2019). The observation that aspiration pneumonia occurred less in older people who received professional oral care compared with no such care, indicates the importance of oral health in reducing aspiration pneumonia risk (Quagliarello et al., 2005; Chebib et al., 2018; Khadka et al., 2021).

More and more researchers are focusing on viral pneumonia, especially in the context of the current pandemic of Coronavirus disease 2019 (COVID-19), which is caused by severe acute respiratory syndrome coronavirus 2 (SARS-CoV-2). The association of COVID-19 with oral microecosystem is becoming clear. Saliva has been shown to contain infective viral loads, indicating not only its role in SARS-CoV-2 transmission but also its diagnostic value for viral RNA testing as a more easily obtainable sample (To et al., 2020; Imai and

Tanaka, 2021). The finding that angiotensin-converting enzyme II, the main host cell receptor of SARS-CoV-2, is widely expressed in salivary glands, tongue and mucosa of oral cavity (Chen et al., 2020; Xu et al., 2020), also correlates oral microecosystem with the infection and transmission of SARS-CoV-2.

### CF Lung Disease

CF lung disease is characterized by persistent airway infection with complex microbial communities which often consist of pathogens, including *S. aureus*, *H. influenzae* and *P. aeruginosa*, and endogenous microorganisms typically associated with the oral cavity (Salsgiver et al., 2016; Muhlebach M. S. et al., 2018). Oral microecosystem provides the habitats for the colonization of pathogens of CF lung disease. Identical facultative and obligate anaerobic strains, including *P. aeruginosa* and *S. aureus*, are found in CF periodontal pockets and sputum samples, suggesting that periodontal pockets is a potential source of the respiratory infection for CF patients (Bensel et al., 2010). The study of Caldas et al. also demonstrated that the primary CF pathogen *P. aeruginosa* is detected not only in the sputum samples of CF patients, but also in their saliva and subgingival plaque samples, with clonal relatedness (Rivas Caldas et al., 2015). The presence of orally derived anaerobic bacteria in sputum and BAL fluid from CF patients have been observed by many studies (Tunney et al., 2008; Worlitzsch et al., 2009; Coburn et al., 2015; Muhlebach M. S. et al., 2018). Recently, a study on succession of the CF lung microbiome in early life further revealed the role of oral bacteria on the pathophysiology of CF lung disease. It was found that CF infants had relatively sterile lower airways with a progressive shift to a microbiome dominated by aerobic and anaerobic bacteria commonly associated with the oral cavity at age two, which was correlated with a significant increase in bacterial density and inflammation, and the lung microbiome was dominated by pathogens in the majority of CF children older than four, which was associated with a further increase in inflammation and the onset of structural lung disease (Muhlebach M. S. et al., 2018). These findings suggest that oral microbes may be associated with the progression of early CF lung disease and could potentially predispose subjects to subsequent infection by pathogens (Muhlebach M. S. et al., 2018). Considering the correlation between oral bacteria and CF lung disease, the impact of oral bacteria-driven diseases especially periodontal disease, as well as the oral health management measures, on the development of CF lung disease should be further investigated.

### Obstructive Pulmonary Diseases COPD

COPD is a chronic inflammatory lung disease that causes obstructed airflow from the lungs. Metagenomic analysis shows that both periodontal pathogens (the red-complex bacteria, *Aggregatibacter actinomycetemcomitans* and *Capnocytophaga sputigena*) and lung pathogens (*Acinetobacter baumannii*, *K. pneumoniae*, *P. aeruginosa* and *S. pneumoniae*) are present in subgingival plaque biofilm and tracheal aspirate of patients with severe acute exacerbations of COPD (Tan et al., 2014), indicating that not only oral microecosystem is a reservoir

of respiratory pathogens but also periodontal pathogens may contribute to the pathology of COPD. The study of Wu et al. found that six genera and 15 species in subgingival plaques might be associated to COPD, among which the genera *Dysgonomonas*, *Desulfobulbus* and *Catonella* showed much higher proportions in COPD patients (Wu et al., 2017). To get rid of interference of upper airway microbes, a recent study surgically obtained the mild-moderate COPD lung tissues and found that the sources of the lung tissue microbiota were 21.1% (mean) oral microbiota, 8.7% nasal microbiota, and 70.1% unknown (Pragman et al., 2018). The association between oral disease and the incidence of COPD have been proved by many studies and periodontal disease is a significant risk factor for COPD (Prasanna, 2011; Zeng et al., 2012). A most recent study by Qian et al. provides substantial evidence that risks for COPD mortality increased significantly with increasing severity of periodontitis in the elderly (Qian et al., 2020). Moreover, the periodontal therapy could help COPD patients reduce the frequency of the exacerbation (Kucukcoskun et al., 2013; Zhou et al., 2014). The observations that compared with controls with normal pulmonary function, patients with COPD have significant fewer teeth, higher plaque index, poorer periodontal status and poorer oral health knowledge and behaviors, highlight the importance of oral health care and oral health knowledge in the prevention and treatment of COPD (Wang et al., 2009; Zhou et al., 2020).

### Asthma

Asthma is a chronic respiratory disease involving intermittent wheezing and airway inflammation. Although there are numerous risk factors to trigger an asthma attack or exacerbate symptoms, the main risk factor is proposed to be a hereditary predisposition to allergic inflammation of the bronchial tree that develops in response to respiratory allergens (Cherkasov et al., 2019). The hygiene hypothesis contends that fewer opportunities for infections and microbial exposures contribute to the prevalence of asthma and other allergic diseases. Consistent with the hygiene hypothesis, the high serum level of immunoglobulin G (IgG) antibodies to *P. gingivalis* corresponded with the low prevalence of asthma and it was concluded that colonization of the oral cavity by bacteria and other microbes might play a protective role in the etiology of allergic disease (Arbes et al., 2006). In fact, there are only few reports regarding the relationship between oral microbes and asthma or other allergic diseases and the few clinical findings are controversially discussed (Arweiler et al., 2021). Most recently, Arweiler et al. for the first time reported the contribution of dental biofilm to allergic health or disease. Through analysis of dental biofilm microbiome by a 16s-rRNA gene-based next-generation sequencing, it was observed that children with allergic asthma showed a stronger microbial shift compared to healthy controls, with 14 different taxa, suggesting a correlation between allergic asthma and oral bacteria (Arweiler et al., 2021). Several studies report that asthmatics presented with greater risk for caries development, worse gingival health, as well as disorders of salivary flow, composition and pH (Stensson et al., 2008; Mehta et al., 2009; Arafa et al., 2017). However, there is no



clear evidence clarifying the role of oral health status, oral diseases and specific oral pathogens on the pathophysiology of asthma. Thus, further in-depth studies on the association of asthma with oral microecosystem become necessary.

## Lung Cancers

Lung cancer is one of the most common types of cancer, with the leading cancer mortality worldwide. Besides chemical carcinogens, bacterial and viral infections are involved in the development of lung cancer. It has been verified that the microbial factors may participate in the tumorigenesis of the lung cancer through production of bacteriotoxins and other proinflammatory factors (Littman et al., 2004; Moghaddam et al., 2011; Kovaleva et al., 2019). The lung has a distinct microbiome which may influence the development of lung cancer and more and more evidence suggests that oral microbiome is one of the main sources of lung microbiome (Maddi et al., 2019). Yan et al. for the first time demonstrated the association of saliva microbiota with lung cancer. It was observed that the saliva microbiome in lung cancer patients with small cell carcinoma or adenocarcinoma had significant changes compared to the controls, which was indicated by the significant increase of *Capnocytophaga* and *Veillonella* (Yan et al., 2015). Variations in oral microbiome have been associated with future risk of lung cancer among never-smokers. Lower microbial diversity and richness of salivary microbiota are found in non-smoking lung cancer patients and the abundance of certain specific taxa is associated with altered risk (Yang et al., 2018; Hosgood et al., 2021). More specifically, a greater abundance of the *Bacilli* class and *Lactobacillales* order in saliva was associated with an increased risk of lung cancer, while a greater abundance of *Spirochaetia* and *Bacteroidetes* in saliva was associated with a decreased risk of lung cancer (Hosgood et al., 2021). Furthermore, functional analysis indicates that salivary microbiome in non-smoking female lung cancer patients is related to cancer pathways, p53 signaling pathway, apoptosis and tuberculosis (Yang et al., 2018). The relevance of periodontal disease with lung cancer are also reported. A meta-analysis of cohort studies showed that patients with periodontal disease were at increased risk of developing lung cancer (Zeng et al., 2016). In addition, the association of periodontal disease indices, including probing pocket depth, clinical attachment loss and bleeding on probing, with the risk of lung cancer is demonstrated (Chrysanthakopoulos, 2016). Oral care intervention may have their roles in the prevention and treatment of lung cancer, but relevant research is needed to provide evidence.

## COLONIZATION OF RESPIRATORY PATHOGENS IN ORAL MICROECOSYSTEM

Oral microecosystem is an important reservoir for respiratory pathogens. Various respiratory pathogens have been detected in dental plaques, periodontal pockets and saliva, including *S. pneumoniae*, *K. pneumoniae*, *S. aureus*, *P. aeruginosa*, *H. influenzae*, *Haemophilus parainfluenzae*, *Enterobacter cloacae*, *Proteus mirabilis*, *Escherichia coli*, *Acinetobacter* species and

SARS-CoV-2 (Sumi et al., 2007; Heo et al., 2008; Bense et al., 2010; Tan et al., 2014; Rivas Caldas et al., 2015; To et al., 2020). Colonization of the oral microecosystem by respiratory pathogens lays a foundation for subsequent invasion and infection by these pathogens in the lower respiratory tract while the body's immune system is weakened. Both the biological characteristics of respiratory pathogens and perturbations in oral microecosystem contribute to the adaptation and colonization of respiratory pathogens in oral microecosystem.

## Adaptation of Respiratory Pathogens to Oral Environment

When exposed to invading pathogens, oral cavity releases reactive oxygen species (ROS) and nitric oxide (NO) from neutrophils and macrophages infiltrating, which are toxic metabolites to some bacteria due to the oxidative stress they elicit (Sato et al., 2008). However, pathogens such as *K. pneumoniae* and *S. aureus* develop hydrogen ( $H_2$ ) generation to against oxidative environments in the human oral cavity (Kanazuru et al., 2010). *P. aeruginosa* is found to be killed by hydrogen peroxide ( $H_2O_2$ )-producing oral commensal streptococci in a nitrite-dependent manner through the production of reactive nitrogenous species (RNS) (Schofield and Wu, 2015). The observation that the *P. aeruginosa* strain defective in the production of nitrite reductase, which is responsible for catalyzing the reduction of nitrite to NO, showed a reduced survival rate when co-cultured with oral commensal *Streptococcus parasanguinis* (Schofield and Wu, 2016), suggests that nitrite reductase could play an important role in the interspecies interaction with oral microbes and the survival of *P. aeruginosa* in oral microecosystem. In addition to toxic metabolites from oral cavity, common oral antibacterial agents like chlorhexidine (CHX) are also challenge for respiratory pathogens. Nevertheless, it has been observed the adaptation of clinical *K. pneumoniae* isolates to CHX exposure, which is associated with mutations in the two-component regulator *phoPQ* and a putative Tet repressor gene (*smvR*), could lead to not only stable resistance to CHX, but also cross-resistance to colistin (Wand et al., 2017). Duman et al. further demonstrated decreased susceptibility to the complement-mediated serum killing within the CHX adapted strain of *K. pneumoniae*, as well as increased efflux pump expression (*cepA* and *kdeA*) (Duman et al., 2019).

Given that oral microecosystem is a complex and open environment with saliva flow and other flowing liquids from the diet, adherence is an essential step in oral colonization and subsequent respiratory infection by a respiratory pathogen. Respiratory pathogens have developed some characteristics to facilitate their adherence capacity in oral cavity. Merghni et al. found that within the twenty-one *S. aureus* strains that were isolated from the oral cavity and detected the presence of adhesins, 76.2% of strains were *icaA* and *icaD* (encoding polysaccharide intercellular adhesins) positive and 90.5% harbored both the *fmbA* and *fmbB* genes encoding fibronectin-binding proteins. Besides, the *cna* gene encoding a collagen-binding protein and *hla* gene encoding  $\alpha$ -toxin were found in 57.2 and 52.4% of the isolates, respectively, which both play an

important role in the pathogenesis of staphylococcal diseases (Merghni et al., 2015). Moreover, Wang et al. reported that *S. aureus* could activate the COX-2/PGE2 pathway in oral epithelial cell and subsequently facilitate the growth and adherence of the pathogen (Wang et al., 2017). Proteins in human saliva could modulate bacterial colonization of the oral cavity. The study of Thamadilok et al. revealed that unencapsulated *S. pneumoniae* was able to bind to low molecular-weight salivary mucin-7, presumably through a glycan-mediated mechanism which could further mediate its adherence to saliva-covered surfaces in the oral cavity (Thamadilok et al., 2016).

## Interactions of Respiratory Pathogens With Oral Microbes Facilitate Formation of Dental Plaque

Several respiratory pathogens are reported to interact with indigenous oral bacteria. Certain interspecies interactions like coaggregation would promote the formation of dental plaque biofilm. Compared with planktonically grown counterparts, microbes growing within biofilms often exhibit increased resistance to antimicrobial compounds and innate immune mechanisms. Thus, the participation of respiratory pathogens in formation of dental plaque would contribute to their oral colonization and subsequent respiratory infection. Komiyama et al. studied the interbacterial interaction between strains of *P. aeruginosa* and strains of indigenous oral bacteria, both of which were isolated from the oral cavity of CF patients, and observed coaggregation reactions between oral bacteria (*Streptococcus sanguis*, *Streptococcus mitis*, *Actinomyces naeslundii* and *Actinomyces viscosus*) and both the mucoid and nonmucoid variants of *P. aeruginosa* (Komiyama et al., 1987). These findings suggest that the diverse interbacterial interactions with indigenous oral bacteria may contribute to the oral colonization of *P. aeruginosa* in CF patients and affect the course and pathogenesis of CF. *S. aureus* is also reported to coaggregate with indigenous oral bacteria like *Streptococcus* spp., *A. naeslundii*, *A. viscosus*, *P. gingivalis* and *Fusobacterium nucleatum* (Kamaguchi et al., 2003). Further analysis of the interaction between *F. nucleatum* and *S. aureus* revealed that the outer-membrane adhesin RadD of *F. nucleatum* might partially participate in aggregation and increase the expression of the staphylococcal global regulator gene *sarA* (Lima et al., 2019). It is interesting to note that colonization of *S. aureus* also benefits other respiratory pathogens, since an interaction between the SpA protein secreted by *S. aureus* and the *P. aeruginosa* exopolysaccharide Psl has been identified, which causes aggregation of bacterial cells that leaves them resistant to tobramycin (Beaudoin et al., 2017). Complex communication and interaction within dental plaque biofilm also create a condition for further progression of virulence of pathogens. For example, *nanA*, a virulence determinant of *S. pneumoniae* that is important for colonization and infection, could be evolved by recombination of the pathogen with oral streptococci (King et al., 2005).

## Perturbation in Oral Microecosystem Favor Colonization of Respiratory Pathogens Disturbance of Oral Microecology

Normal oral microbiota plays important roles in preventing the invasion of pathogenic bacteria like *P. aeruginosa*, which is showed to fail to integrate into salivary microbial community when co-cultivated in saliva medium and whose growth is inhibited by the oral microflora via producing lactic acid (He et al., 2011). However, disturbance of oral microecology gives opportunistic respiratory pathogens chances to invade and colonize. It has widely reported that oral microbial dysbiosis or changes in oral microecosystem, such as the progression of periodontitis and denture stomatitis or the presence of dentures, promote oral colonization by *S. aureus*, *P. aeruginosa*, *Enterococcus faecalis* and *Acinetobacter* spp. and may favor the spread of more pathogenic strains (Baena-Monroy et al., 2005; Passariello et al., 2012; Colombo et al., 2013; Souto et al., 2014). Moreover, smoking is found to benefit early acquisition and colonization of respiratory pathogens including *Haemophilus* and *Pseudomonas* in dental plaque biofilms (Kumar et al., 2011).

One potential mechanism is that in the condition of oral microflora dysbiosis, the increase of some oral pathogens enhance their interaction with certain respiratory pathogens, as aforementioned, and further facilitate the oral colonization of these non-indigenous pathogens. Another mechanism could refer to the decrease of oral commensal bacteria, the function of which is to inhibit the invasion and colonization of external microorganism as well as to maintain balance of oral microecology (Tada and Hanada, 2010). Plenty of oral commensal bacteria are found to exhibit antagonistic effects against respiratory pathogens. The majority of oral *Lactobacilli* strains are reported to suppress the growth of common respiratory pathogens including *S. pneumoniae*, *P. aeruginosa*, as well as clinical isolates of Methicillin-resistant *Staphylococcus aureus* (MRSA) (Busarcevic et al., 2008; Sikorska and Smoragiewicz, 2013; Alexandre et al., 2014; Mahdi et al., 2019). Take *Lactobacillus salivarius* for example, studies revealed that it could produce LSI against the growth of *S. aureus* and *S. pneumoniae*, and salivaricin LHM against the activity of *P. aeruginosa* (Busarcevic et al., 2008; Mahdi et al., 2019). *Streptococci* are another main source of oral commensal bacteria to antagonize respiratory pathogens, particularly *Streptococcus salivarius*, which produces a variety of bacteriocins antagonizing *S. pneumoniae* (Tagg, 2004) and *Streptococcus pyogenes* (Walls et al., 2003; Tagg, 2009; Wescombe et al., 2009; Santagati et al., 2012), and block the adherence sites to reduce *S. pneumoniae* colonization (Manning et al., 2016).

## Impairment of Oral Immunity

Oral immune system functions as the foremost barrier and defense against pathogens, which depends on efficient function of oral mucosa, salivary glands and saliva, and gingival crevice. Saliva plays a key role in host defense against invading respiratory pathogens via antibody production (Aanaes et al., 2013; Mauch et al., 2017), blocking oral adherence (Lerrer et al., 2005), bacteriostatic or bactericidal activities (Geetha et al., 2003; Prokopovic et al., 2014), interfering with their interactions with oral bacteria

(Komiya and Gibbons, 1984). Internal and external factors such as aging, dysplasia, disease progression and treatment which influence salivary function or oral immunity have potential impacts on oral colonization of respiratory pathogens. Oral radiotherapy and chemotherapy, except for direct mucosal damage, both lead to decreased salivary flow and increased colonization of opportunistic pathogens such as *S. aureus* and *Candida* (Main et al., 1984; Jain et al., 2016). Natural aging, parotid and submandibular salivary gland aplasia or agenesis, medication (including anticholinergic drugs, diuretics, alpha-adrenergic agents, and antihypertensive agents) are able to change the saliva composition or affect the secretion or flow rate of saliva, and subsequently result in dry mouth and poor oral hygiene (Mathews et al., 2008), which may cause shifts from the normal oral microflora to a community that harbors a higher number of pathogens (Scannapieco, 1999).

What is noteworthy is that immunocompromise and general immunodepression also raise the risk of oral colonization by potential respiratory pathogens. Higher level of *S. aureus* in oral cavity of the elderly and institutionalized individuals was reported, including hospitalized and nursing home patients (Scannapieco et al., 1992; Tada and Hanada, 2010). Diaz et al. also found a higher prevalence of potentially opportunistic *Gammaproteobacteria* including *K. pneumoniae*, *Pseudomonas fluorescens*, *Acinetobacter* species, *Vibrio* species, *Enterobacteriaceae* species, *Staphylococcus* species, and *Enterococcus* species in the salivary bacterial microbiome of transplant recipients who were constantly on pharmacological immunosuppression (Diaz et al., 2013).

## PARTICIPATION OF INDIGENOUS ORAL MICROBES IN PATHOGENESIS OF RESPIRATORY DISEASES

The presence of oral microbes with high detectable rates in sputum and BAL specimens of patients with multiple respiratory diseases suggests a potential association of oral microbes with respiratory diseases, including oral streptococci, *Neisseria* spp. and anaerobes (*P. gingivalis*, *Treponema denticola*, *Tannerella forsythia*, *A. actinomycetemcomitans*, *Capnocytophaga sputigena*, *Prevotella* spp., *Fusobacterium* spp., *Veillonella* spp., and *Clostridium* spp.) (Tunney et al., 2008; Worlitzsch et al., 2009; Yamasaki et al., 2013; Tan et al., 2014; Coburn et al., 2015; Yan et al., 2015; Wu et al., 2017; Muhlebach MS. et al., 2018). In fact, common oral microbes such as *P. gingivalis*, *F. nucleatum*, *A. actinomycetemcomitans* and oral streptococci have been reported to be involved in the pathogenesis of respiratory diseases (Petelin et al., 2004; Pan et al., 2009; Nagaoka et al., 2013; Yamasaki et al., 2013; Whiley et al., 2014; Hayata et al., 2019). Various mechanisms have been developed to help explain how indigenous oral microorganisms may participate in the occurrence and development of respiratory diseases, based on the understanding of their virulence factors or their effects on pathogenicity of respiratory pathogens.

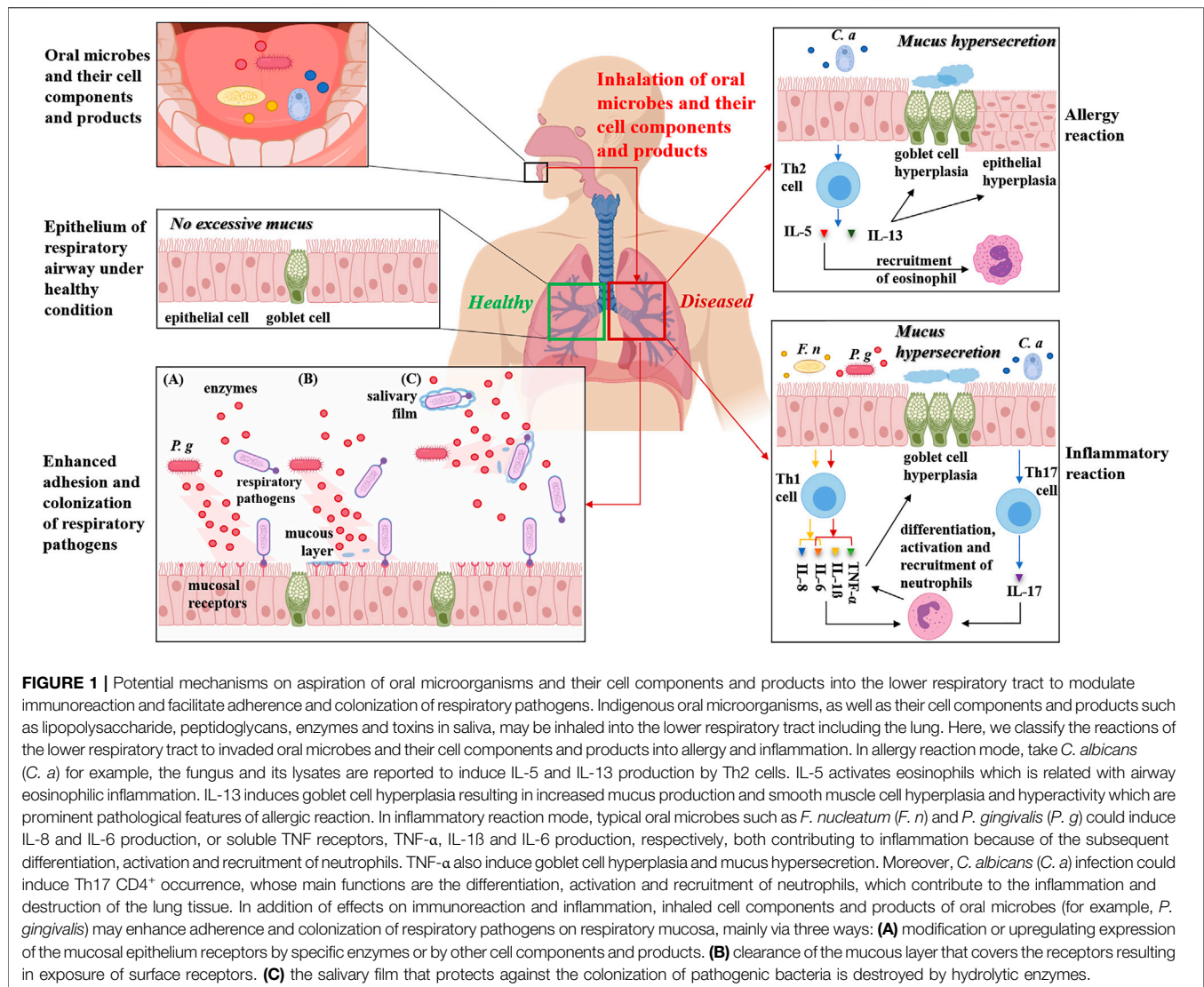
## Oral Microbes Inhaled Into the Lower Respiratory Tract Cause Infection and Regulate Immune Responses

Oral microbiome is one of the primary sources of respiratory infection and indigenous oral microbes in dental plaques, periodontal pockets or saliva could be inhaled into the lower respiratory tract to cause or aggravate respiratory infections and diseases such as aspiration pneumonia and COPD. The pathogenicity of oral microorganisms invading the lower respiratory tract is involved in different mechanisms, within which the critical one is the immunoregulation on respiratory system, including T-helper 1 (Th1) and T-helper 2 (Th2) immune responses. Regulation of the Th1/Th2 balance is a typical way by which infections of microbes influence the host immune response (Schaub et al., 2006). Effects of oral microbes on inflammatory process have been widely reported, which is characterized by Th1 immune response. The data of Scannapieco et al. revealed the potential effect of oral bacteria on inducing the release of proinflammatory cytokines from epithelial cell lines to an extent similar to that seen for respiratory pathogens (Scannapieco et al., 2001). Significantly increased production of soluble TNF receptors, TNF- $\alpha$ , IL-1 $\beta$  and IL-6 are also observed in *P. gingivalis*-infected pneumonia model (Petelin et al., 2004) (Figure 1). Recently, it was showed that some periodontopathic bacteria, especially *F. nucleatum*, strongly induced IL-6 and IL-8 production by bronchial epithelial cells, which might trigger exacerbation of COPD (Hayata et al., 2019) (Figure 1).

In addition of inflammatory reactions, oral microbes are observed to impact allergy reactions. The first direct evidence on regulatory effects of oral pathogens on allergic airway inflammation and responsiveness was reported by Card et al. Their study underlined the temporal importance of the establishment of infection since *P. gingivalis* infection established before ovalbumin (OVA) sensitization reduced airway levels of Th2 cytokines (IL-4, IL-5, IL-13) and granulocyte-macrophage colony-stimulating factor, and decreased histological inflammation, without the alteration of serum levels of OVA-specific immunoglobulin E (IgE) and airway responsiveness. Conversely, a subcutaneous infection with *P. gingivalis* initiated after allergen sensitization did not alter inflammatory end points but did reduce airway responsiveness in spite of increased serum IgE levels (Card et al., 2010). Card et al. observed a reduction of the inflammatory migrated cells in the BAL fluid (eosinophils, lymphocytes, macrophages), as well as the levels of the IL-4 and tumor necrosis factor (TNF)- $\alpha$  cytokines, in mice with asthma and periodontitis, accompanied by a decreased mucus production (Card et al., 2010). Oral microbes also have the capacity to induce Th2 immune responses. Some studies reported that *Candida albicans*, an opportunistic pathogen that colonizes oral cavity, and its extract were able to induce IL-5 production by Th2 cells which is related with eosinophilic airway inflammation (Kimura et al., 1999; Mori et al., 2001) (Figure 1).

Apoptosis, which plays an important role in immune response and tumorigenesis, is also proposed to be affected





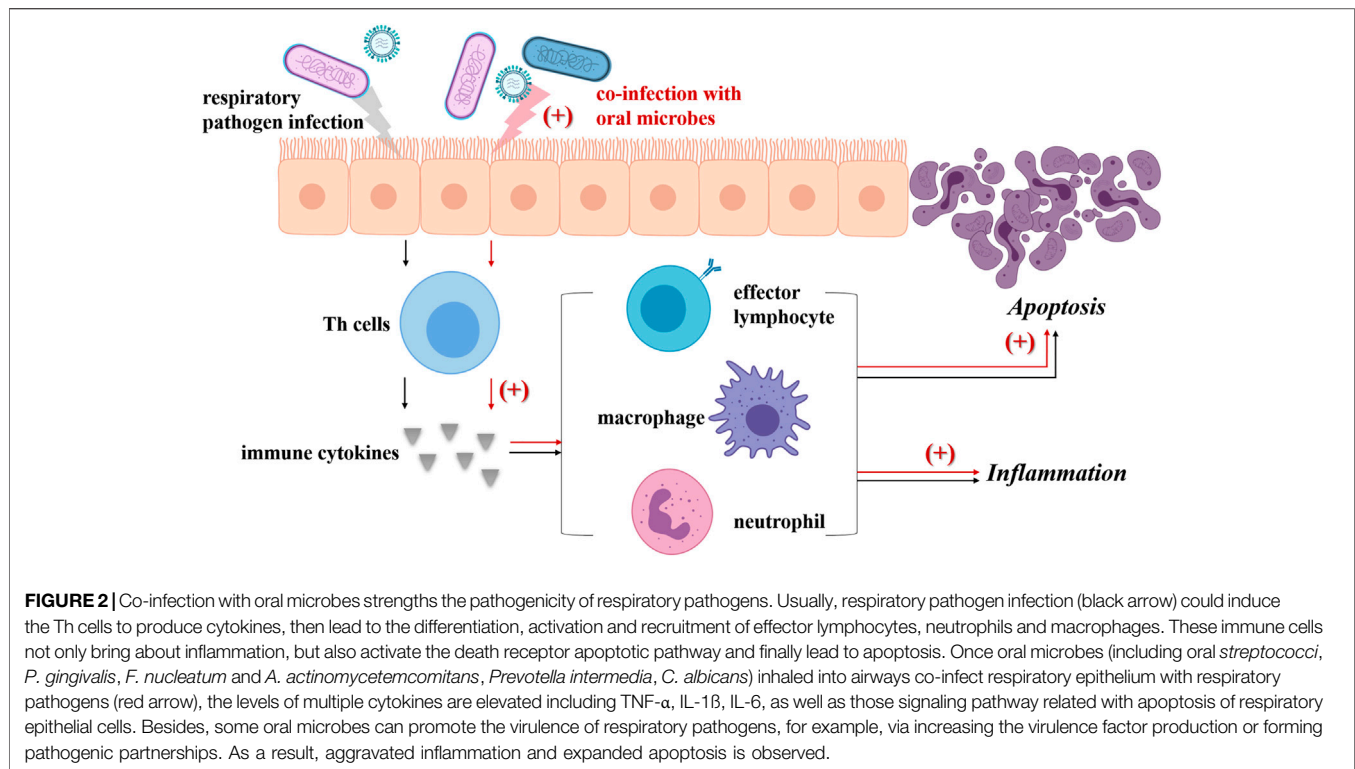
by oral bacteria. Potential regulation of lung cancer cell apoptosis by oral microbiome through p53 pathway is observed (Yang et al., 2018). Other possible mechanisms, for example, infertile defense function of tracheal mucosa causing by the invasion of oral bacteria to surface protein (fibronectin, etc.), still need exploration and evidence (Woods, 1987; Mamani et al., 2012).

## Aspiration of Oral Microbial Components and Products Alters Respiratory Mucosal Surfaces and Modulates Immune Responses

Enzymes, cytokines and other biologically active substances in saliva which are released by oral microorganisms and inflammatory periodontal tissues could be inhaled into the lower respiratory tract and potentially influence respiratory tract mucosal epithelium. In the human airway, proteases

released by invading pathogens have been associated with the regulation of the airway surface liquid layer, host defense, pathogenic infection and inflammation (Thibodeau and Butterworth, 2013). Besides proteases, it is possible for specific enzymes such as mannosidase, fucosidase, hexosaminidase and sialidase released from oral microecosystem to alter respiratory tract mucosal surfaces via modification of the mucosal epithelium or exposure of adhesion receptors located on mucosal surfaces, which would contribute to adherence and colonization by respiratory pathogens and consequent respiratory infection (Scannapieco, 1999; Gomes-Filho et al., 2010) (Figure 1). Moreover, hydrolytic enzymes from periodontal pathogens are proposed to destroy the salivary film that protects against pathogenic bacteria and leave respiratory pathogens free to enter respiratory tract, which would benefit their adherence to mucosal receptors (Scannapieco, 1999; Gomes-Filho et al., 2010) (Figure 1). Through oropharyngeal aspiration, other cell components and products of oral microbes, such as





lipopolysaccharide (LPS), peptidoglycans, lipoteichoic acids, fimbriae and toxins, as well as the cytokines released from inflammatory periodontal tissues, may also alter the respiratory epithelium and promote colonization by respiratory pathogens via the upregulation of adhesion receptor expression on the mucosal surfaces or stimulate cytokine production from respiratory epithelial cells, resulting in recruitment of inflammatory cells and inflamed epithelium that is more susceptible to respiratory infection (Scannapieco et al., 2001; Gomes-Filho et al., 2010) (**Figure 1**).

Effects of oral microbial components and products on modulating immune responses have been revealed by many studies. Take *C. albicans* for example, oropharyngeal aspiration of fungal lysates from *C. albicans* promotes the Th2 immune response, including airway eosinophilia, secretion of Th2 cytokines and mucus cell metaplasia (Allard et al., 2009) (**Figure 1**). Interestingly, oropharyngeal aspiration of *C. albicans* lysates together with *P. aeruginosa* is found to result in the shift of immune response from Th2 to Th1 in an LPS/TLR4 independent but MyD88 dependent mechanism (Allard et al., 2009). Furthermore, a soluble cell-wall  $\beta$ -glucan from *C. albicans* could facilitate OVA-induced allergic airway inflammation in mice (Inoue et al., 2009a) and induce apoptosis and oxidative stress in the lung that enhance lung inflammation and injury (Inoue et al., 2009b).

As a hallmark of chronic airway diseases including asthma, CF and COPD, mucous hypersecretion is also related with oral microbial products. Nagaoka et al. found the products of *F. nucleatum* inhibited mucus production in high concentrations, while increased mucus production in low concentrations. Thus, aspiration of saliva containing low concentrations of *F. nucleatum*

products, which is more common, might promote mucus hypersecretion in the related diseases (Nagaoka et al., 2013).

## Interactions Between Oral Microbes and Respiratory Pathogens Strengthen Respiratory Pathogenicity

Indigenous oral microbes are likely to be inhaled into the lower respiratory tract and may interact with respiratory pathogens, further modulating the pathogenicity of respiratory pathogens or both (The main mechanisms are summarized in **Figure 2**). Previous studies have reported the potential interactions between oral *streptococci* and *P. aeruginosa* which result in increased virulence and strengthened pathogenesis of the latter (Duan et al., 2003; Parkins et al., 2008; Sibley et al., 2008). Recently, Whiley et al. demonstrated that pathogenic potential of the high-virulence *P. aeruginosa* CF Liverpool Epidemic Strain (LES) could be enhanced by the presence of anginosus-group of *streptococci* (AGS) and some other viridans *streptococci* (*S. mitis*, *Streptococcus oralis*, *Streptococcus gordonii* and *Streptococcus sanguinis*), and the pathogenic partnerships between the LES and AGS were verified in the *Galleria mellonella* infection model (Whiley et al., 2014; Whiley et al., 2015). However, it should be noticed that they also pointed out the negative modulation of these oral *streptococci* to *P. aeruginosa* virulence, which was found to be dependent on inoculation sequence and environment. Instead of air cooperation within a high cell density co-culture biofilm, when co-cultured in an atmosphere containing added CO<sub>2</sub>, *S. oralis* antagonized *P. aeruginosa* LES growth via H<sub>2</sub>O<sub>2</sub> production. *S. mitis*, *S. gordonii* and *S. sanguinis* showed similar H<sub>2</sub>O<sub>2</sub> mediated inhibitory effect

when inoculated as a primary colonizer prior to introduction of the LES (Whiley et al., 2015).

There is evidence showing that co-infection of multiple periodontal pathogens and respiratory pathogens in lung epithelial cells promote the production of inflammatory cytokines and apoptosis (Pan et al., 2009; Li et al., 2014; Chen et al., 2018; Li et al., 2018). *P. gingivalis*, *F. nucleatum*, and *A. actinomycetemcomitans* are reported to foster *P. aeruginosa* invasion into HEP-2 respiratory epithelial cells and enhance host cell cytokine release and apoptosis (Pan et al., 2009). Further study showed that *P. gingivalis* modulated *P. aeruginosa*-induced apoptosis of respiratory epithelial cells through the signal transducer and activator of transcription 3 (STAT3) signaling pathway and their co-invasion led to greater cell death compared with *P. aeruginosa* challenge alone (Li et al., 2014). Recently, the study by Chen et al. revealed that co-infection of *P. gingivalis* and influenza A virus (IAV) subtype H1N1 in lung epithelial cells could induce the production of inflammatory cytokines including TNF- $\alpha$ , IL-1 $\beta$  and IL-6, as well as the production of NO, consequently promoting apoptosis in lung epithelial cells via the Bcl-2/Bax/caspase-3 signaling pathway (Chen et al., 2018). It was also observed that infection by *P. gingivalis* combined with IAV temporarily inhibited apoptosis in respiratory epithelial cells, possibly related to the initiation of autophagy (Li et al., 2018). Besides, the supernatant of *Prevotella intermedia* was found to promote pneumococcal adherence to human alveolar cells, elevate inflammatory cytokine levels in the BAL fluid, and increase platelet-activating factor receptor transcription (Nagaoka et al., 2014).

## ORAL HEALTH MANAGEMENT STRATEGIES FOR CONTROLLING RESPIRATORY DISEASES

The relationships between oral microecosystem, oral health and respiratory diseases highlight the importance of oral health management in prevention and treatment of respiratory diseases (especially pneumonia and COPD). Effective oral self-health management as well as professional oral health care, not only improve oral health, but also benefit controlling the progression or occurrence of respiratory diseases. Currently, it is clear that oral care measures maintaining oral health and oral microbiome symbiosis could reduce the incidence of pneumonia and COPD (Table 1).

### Professional Oral Health Care

Providing oral health care, including tooth, tongues and dentures, is helpful to reduce the number of microorganisms inhalable in the lower respiratory tract and control subsequent respiratory infections (Scannapieco and Shay, 2014). Professional oral health care by dentist or oral hygienists significantly benefits the populations susceptible to respiratory infection, particularly the elderly and the comatose patients. Oral health condition has been recognized as one important risk factor in the incidence of aspiration pneumonia (Quagliarello et al., 2005; Chebib et al., 2018). A systematic review conducted by Khadka et al. analyzed the articles addressing aspiration pneumonia, oral microorganisms, oral health and treatment and their results showed that professional oral hygiene care that reduces bacteria is useful in

reducing aspiration pneumonia risk (Khadka et al., 2021). For nursing home residents, a weekly professional oral care leads to a significantly lower annual prevalence of pneumonia hospitalization, especially in residents whose salivary bacterial concentration exceeded the median (Chiang et al., 2020). Brushing teeth is found to be an effective way to control the pneumopathogens (*staphylococci*, Enterobacteriaceae and yeasts) in resting saliva for reducing pulmonary infection of comatose patients and brushing twice-a-day can reduce respiratory tract infections by 69 percent in VAP (Cecon et al., 2010; Stonecypher, 2010). Most recently, a Four-Unit Cluster Randomized Study assessing the effectiveness of a standardized oral care protocol in preventing nonventilator hospital-acquired pneumonia (NV-HAP) in the acute care setting found that an increase in oral care frequency significantly reduced the NV-HAP incidence rate, suggesting that daily oral care can play a crucial role in NV-HAP prevention (Giuliano et al., 2021). Many studies also reported that preoperative oral hygiene interventions such as dental brushing and professional oral plaque control are associated with a lower incidence of postoperative pneumonia (POP) (Akutsu et al., 2010; Gonzalez-Rubio Aguilar et al., 2019; Jia et al., 2020). Therefore, oral health management is a favorable factor for preventing POP, and it could be carried out before surgery. In addition, professional oral cleansing once a week for 6 months during winter could reduce influenza infection in the elderly (Okuda et al., 2005).

Based on the current understanding of the relationship between oral microecosystem, oral health and aspiration pneumonia, it has been recommended by some scholars to use oral bacterial counts and the Oral Health Assessment Tool which assesses oral hygiene as a tool to assess the requirement of taking oral care and other preventive procedures in patients at high risk of aspiration pneumonia (Nishizawa et al., 2019). Such an oral health and oral hygiene assessment tool could be developed into a standardized oral assessment procedure and applied in the treatment of respiratory diseases related to oral bacteria and oral health.

### Personal Oral Health Care

Common oral care, such as tooth brushing, flossing and regular dental visits, has been shown to be beneficial to controlling respiratory diseases. Through comparing 20 COPD individuals with 10 healthy individuals as control, Gaeckle et al. found that the healthy controls flossed frequently as their regular dental care while COPD patients not, and the control group also visited dental clinic more regularly (Gaeckle et al., 2018). Further analysis on the observation that COPD patients have fewer teeth and higher plaque index than the controls with normal pulmonary function revealed that inappropriate tooth brushing method, lower regular supra-gingival scaling and poorer oral health knowledge were significantly associated with the risk of COPD, indicating the importance of promoting dental care and oral health knowledge that can be integrated into the prevention and treatment of COPD (Wang et al., 2009). Oral health behaviors are also related to the incidence of pneumonia. It was found that denture wearing during sleep would increase the risk of incident pneumonia in the elderly and the elderly having this behavior were more likely to have tongue and denture plaque, gum inflammation, positive culture for *C. albicans*, and

higher levels of circulating IL-6 as compared with those who remove their dentures at night, suggesting potential implications of oral hygiene programs for pneumonia prevention in the community (Iinuma et al., 2015).

## Utilization of Antimicrobial Agents and Probiotics

There has been evidence showing that mechanical oral care combined with povidone iodine (PVP-I) significantly reduced the risk of pneumonia in nursing home residents. A concentration of 0.23% PVP-I was showed rapid bactericidal activity and virucidal efficacy against *K. pneumoniae*, *S. pneumoniae*, severe acute respiratory syndrome associated coronavirus, Middle East respiratory syndrome associated coronavirus, H1N1 and rotavirus (Eggers et al., 2018). It could provide a protective oropharyngeal hygiene measure for individuals at high risk of exposure to oral and respiratory pathogens (Eggers et al., 2018). For ICU nursing, using 0.2% CHX gel three times a day to clean gingiva and dental plaque significantly decreases the colonization rate of oropharyngeal aerobic pathogens in artificially ventilated patients (Fourrier et al., 2005). A recent study showed application of oral care protocol based on the removal of secretions from the oral cavity with 0.12% CHX gluconate solution for brushing could significantly reduce the risk of development of VAP and *S. aureus* infection (Galhardo et al., 2020). In addition to the use of CHX, specific antibiotics against *P. gingivalis*, *F. nucleatum*, *A. actinomycetemcomitans* or streptococci (including *S. oralis*, *S. pyogenes*, *S. agalactiae*, *S. intermedius*, and *S. mitis*) are pointed out as a further direction in controlling respiratory infections, since these bacteria are reported to promote the colonization or virulence of respiratory pathogens (King et al., 2005; Pan et al., 2009; Li et al., 2014).

Utilization of probiotics is also proposed as a strategy to fight against respiratory infections. Multiple studies have demonstrated the negative effect of oral *lactobacilli*, *streptococci* on respiratory pathogens and the potential of these bacteria as probiotics in the future to combat various lung infections (Alexandre et al., 2014; Scofield and Wu, 2015; Kang et al., 2017; Scofield et al., 2017; Mahdi et al., 2019).

## Attentions in Dental Treatment

Patients with COPD have large amounts of mucous secretions (chronic bronchitis) with repeated coughing or dyspnea (emphysema) caused by airway destruction. If possible, it is recommended that during dental treatment, severely affected COPD patients be treated by sitting upright in dental chairs because they may experience difficulties in breathing while lying flat. At the same time, taking into account the important role of dental care and oral health knowledge in the prevention and treatment of COPD, attention should be paid to their oral hygiene guidance (Devlin, 2014).

Since an asthma attack could be triggered or exacerbated by a lot of risk factors, asthma patients should receive greater attention in dental treatment. It is suggested to assess the risk level of an asthma patient by a dental professional to decide whether the patient's health is stable enough to proceed with treatment and make sure that the patient has his or her own rescue inhaler on

hand and on the bracket table (Little et al., 2017). All dental operations as well as dental instruments and materials used during dental treatment should not trigger an asthma attack and prolonged supine positioning should be avoided (Khalifa et al., 2014; Harrington et al., 2016).

Although the number of reported cases of infection or respiratory symptoms caused by dental waterway pollution is limited, the American Dental Association requires that the routine dental treatment output water used in dental unit waterlines should meet the quality standard for drinking water (i.e.,  $\leq 500$  CFU/ml of heterotrophic water bacteria) and it is recommended to use sterile saline or sterile water as a coolant or irrigant when performing surgical procedures (Kohn et al., 2003).

## CONCLUSIONS AND FURTHER DIRECTIONS

The relationship between oral microecosystem and respiratory diseases have been proved by plenty of studies. On the one hand, indigenous oral microorganisms take a part in the occurrence and development of respiratory diseases via their pathogenicity and virulence factors when inhaled into respiratory tract or interact with respiratory pathogens. On the other hand, many respiratory pathogens are found to adapt to the fluctuational oral environment with the help of their biological characteristics and their interspecies interactions with oral residents. Although we are making continuous progresses on understanding the role of oral microecosystem in development of respiratory diseases, etiological evidence that relates respiratory diseases with oral microecosystem is still insufficient. There are a lot of aspects to be explored and studied, including: (1) the specific oral microorganisms related to different respiratory diseases, and the potential mechanisms involved in the pathogenic process; (2) the adaptation and colonization mechanisms of respiratory pathogens in oral microecosystem, influence factors and available intervention measures; (3) the specific oral health management and treatment measures for patients or susceptible populations of respiratory diseases; (4) the potential oral biomarkers or indexes such as the abundance of specific microbes to predict the progress of respiratory diseases.

## AUTHOR CONTRIBUTIONS

All authors listed have made a substantial, direct, and intellectual contribution to the work and approved it for publication.

## FUNDING

This work was supported by grants from the Youth Science Fund Project of National Natural Science Foundation of China (No. 81500842), the major scientific and technological innovation projects of Chengdu Science and Technology Bureau (No. 2020-YF08-00071-GX), and the Science and Technology Department of Sichuan Province (No. 2021YJ0133).

## REFERENCES

- Aanaes, K., Johansen, H. K., Poulsen, S. S., Pressler, T., Buchwald, C., and Høiby, N. (2013). Secretory IgA as a Diagnostic Tool for *Pseudomonas aeruginosa* Respiratory Colonization. *J. Cystic Fibrosis* 12, 81–87. doi:10.1016/j.jcf.2012.07.001
- Akutsu, Y., Matsubara, H., Shuto, K., Shiratori, T., Uesato, M., Miyazawa, Y., et al. (2010). Pre-operative Dental Brushing Can Reduce the Risk of Postoperative Pneumonia in Esophageal Cancer Patients. *Surgery* 147, 497–502. doi:10.1016/j.surg.2009.10.048
- Alexandre, Y., Le Berre, R., Barbier, G., and Le Blay, G. (2014). Screening of *Lactobacillus* Spp. For the Prevention of *Pseudomonas aeruginosa* Pulmonary Infections. *BMC Microbiol.* 14, 107. doi:10.1186/1471-2180-14-107
- Allard, J. B., Rinaldi, L., Wargo, M. J., Allen, G., Akira, S., Uematsu, S., et al. (2009). Th2 Allergic Immune Response to Inhaled Fungal Antigens Is Modulated by TLR-4-independent Bacterial Products. *Eur. J. Immunol.* 39, 776–788. doi:10.1002/eji.200838932
- Arafa, A., Aldahlawi, S., and Fathi, A. (2017). Assessment of the Oral Health Status of Asthmatic Children. *Eur. J. Dent* 11, 357–363. doi:10.4103/ejd.ejd\_65\_17
- Arbes Jr., S., Jr., Sever, M., Vaughn, B., Cohen, E., and Zeldin, D. (2006). Oral Pathogens and Allergic Disease: Results from the Third National Health and Nutrition Examination Survey. *J. Allergy Clin. Immunol.* 118, 1169–1175. doi:10.1016/j.jaci.2006.07.029
- Arweiler, N. B., Rahmel, V., Alhamwe, B. A., Alhamdan, F., Zemlin, M., Boutin, S., et al. (2021). Dental Biofilm and Saliva Microbiome and its Interplay with Pediatric Allergies. *Microorganisms* 9, 1. doi:10.3390/microorganisms9061330
- Awano, S., Ansai, T., Takata, Y., Soh, I., Akifusa, S., Hamasaki, T., et al. (2008). Oral Health and Mortality Risk from Pneumonia in the Elderly. *J. Dent Res.* 87, 334–339. doi:10.1177/154405910808700418
- Baena-Monroy, T., Moreno-Maldonado, V., Franco-Martínez, F., Aldape-Barrios, B., Quindós, G., and Sánchez-Vargas, L. O. (2005). Candida Albicans, *Staphylococcus aureus* and Streptococcus Mutans Colonization in Patients Wearing Dental Prosthesis. *Med. Oral Patol Oral Cir Bucal* 10 (Suppl. 1), E27–E39.
- Bágyi, K., Klekner, A., Hutóczki, G., and Márton, I. (2006). The Role of the Oral flora in the Pathogenesis of Aspiration Pneumonia. *Fogorv Sz* 99, 205–212.
- Bassiss, C. M., Erb-Downward, J. R., Dickson, R. P., Freeman, C. M., Schmidt, T. M., Young, V. B., et al. (2015). Analysis of the Upper Respiratory Tract Microbiotas as the Source of the Lung and Gastric Microbiotas in Healthy Individuals. *mBio* 6, e00037. doi:10.1128/mBio.00037-15
- Beaudoin, T., Yau, Y. C. W., Stapleton, P. J., Gong, Y., Wang, P. W., Guttman, D. S., et al. (2017). *Staphylococcus aureus* Interaction with *Pseudomonas aeruginosa* Biofilm Enhances Tobramycin Resistance. *NPJ Biofilms Microbiomes* 3, 25. doi:10.1038/s41522-017-0035-0
- Bensel, T., Huse, A., Borneff-Lipp, M., Wollschläger, B., Bekes, K., Setz, J., et al. (2010). Periodontal Pockets as Potential Sources of Cystic Fibrosis Lung Infection. *J. Cystic Fibrosis* 9, S38. doi:10.1016/s1569-1993(10)60147-6
- Busarcevic, M., Kojic, M., Dalgallarrondo, M., Chobert, J.-M., Haertlé, T., and Topisirovic, L. (2008). Purification of Bacteriocin LS1 Produced by Human Oral Isolate *Lactobacillus Salivarius* BGHO1. *Oral Microbiol. Immunol.* 23, 254–258. doi:10.1111/j.1399-302x.2007.00420.x
- Card, J. W., Carey, M. A., Voltz, J. W., Bradbury, J. A., Ferguson, C. D., Cohen, E. A., et al. (2010). Modulation of Allergic Airway Inflammation by the Oral Pathogen *Porphyromonas gingivalis*. *Infect. Immun.* 78, 2488–2496. doi:10.1128/iai.01270-09
- Cecon, F., Ferreira, L. E. N., Rosa, R. T., Gursky, L. C., De Paula E Carvalho, A., Samaranyake, L. P., et al. (2010). Time-related Increase of Staphylococci, Enterobacteriaceae and Yeasts in the Oral Cavities of Comatose Patients. *J. Microbiol. Immunol. Infect.* 43, 457–463. doi:10.1016/s1684-1182(10)60071-0
- Chebib, N., Müller, F., and Prendki, V. (2018). Pneumonia of the Elderly and its Link to Oral Health. *Rev. Med. Suisse* 14, 2007–2011.
- Chen, L., Zhao, J., Peng, J., Li, X., Deng, X., Geng, Z., et al. (2020). Detection of SARS-CoV-2 in Saliva and Characterization of Oral Symptoms in COVID-19 Patients. *Cell Prolif* 53, e12923. doi:10.1111/cpr.12923
- Chen, Y., Zhou, R., Yi, Z., Li, Y., Fu, Y., Zhang, Y., et al. (2018). *Porphyromonas gingivalis* Induced Inflammatory Responses and Promoted Apoptosis in Lung Epithelial Cells Infected with H1N1 via the Bcl-2/Bax/Caspase-3 S-signaling P-athway. *Mol. Med. Rep.* 18, 97–104. doi:10.3892/mmr.2018.8983
- Cherkasov, S. V., Popova, L. Y., Vitvanenko, T. V., Demina, R. R., Khlopko, Y. A., Balkin, A. S., et al. (2019). Oral Microbiomes in Children with Asthma and Dental Caries. *Oral Dis.* 25, 898–910. doi:10.1111/odi.13020
- Chhibber-Goel, J., Singhal, V., Bhowmik, D., Vivek, R., Parakh, N., Bhargava, B., et al. (2016). Linkages between Oral Commensal Bacteria and Atherosclerotic Plaques in Coronary Artery Disease Patients. *NPJ Biofilms Microbiomes* 2, 7. doi:10.1038/s41522-016-0009-7
- Chiang, T.-C., Huang, M.-S., Lu, P.-L., Huang, S.-T., and Lin, Y.-C. (2020). The Effect of Oral Care Intervention on Pneumonia Hospitalization, *Staphylococcus aureus* Distribution, and Salivary Bacterial Concentration in Taiwan Nursing home Residents: a Pilot Study. *BMC Infect. Dis.* 20, 374. doi:10.1186/s12879-020-05061-z
- Chrysanthakopoulos, N. A. (2016). Correlation between Periodontal Disease Indices and Lung Cancer in Greek Adults: a Case - Control Study. *Exp. Onc.* 38, 49–53. doi:10.31768/2312-8852.2016.38(1):49-53
- Cilloniz, C., Ewig, S., Polverino, E., Marcos, M. A., Esquinas, C., Gabarrus, A., et al. (2011). Microbial Aetiology of Community-Acquired Pneumonia and its Relation to Severity. *Thorax* 66, 340–346. doi:10.1136/thx.2010.143982
- Coburn, B., Wang, P. W., Diaz Caballero, J., Clark, S. T., Brahma, V., Donaldson, S., et al. (2015). Lung Microbiota across Age and Disease Stage in Cystic Fibrosis. *Sci. Rep.* 5, 10241. doi:10.1038/srep10241
- Colombo, A. V., Barbosa, G. M., Higashi, D., Di Micheli, G., Rodrigues, P. H., and Simionato, M. R. L. (2013). Quantitative Detection of *Staphylococcus aureus*, *Enterococcus faecalis* and *Pseudomonas aeruginosa* in Human Oral Epithelial Cells from Subjects with Periodontitis and Periodontal Health. *J. Med. Microbiol.* 62, 1592–1600. doi:10.1099/jmm.0.055830-0
- Devlin, J. (2014). Patients with Chronic Obstructive Pulmonary Disease: Management Considerations for the Dental Team. *Br. Dent J.* 217, 235–237. doi:10.1038/sj.bdj.2014.756
- Diaz, P. I., Hong, B.-Y., Frias-Lopez, J., Dupuy, A. K., Angeloni, M., Abusleme, L., et al. (2013). Transplantation-associated Long-Term Immunosuppression Promotes Oral Colonization by Potentially Opportunistic Pathogens without Impacting Other Members of the Salivary Bacteriome. *Clin. Vaccin. Immunol.* 20, 920–930. doi:10.1128/cvi.00734-12
- Duan, K., Dammal, C., Stein, J., Rabin, H., and Surette, M. G. (2003). Modulation of *Pseudomonas aeruginosa* Gene Expression by Host Microflora through Interspecies Communication. *Mol. Microbiol.* 50, 1477–1491. doi:10.1046/j.1365-2958.2003.03803.x
- Duman, G. G., Çuhadar, T., Yamak, A. S., Albakkour, K., Çağlar, K., and Kalkanci, A. (2019). Düşük Düzeyde Klorheksidin İle Karşılaştırılmış *Klebsiella pneumoniae* İzolatlarının Karakterizasyonu. *Mikrobiyol Bul* 53, 114–117. doi:10.5578/mb.67793
- Eggers, M., Koburger-Janssen, T., Eickmann, M., and Zorn, J. (2018). *In Vitro* Bactericidal and Virucidal Efficacy of Povidone-Iodine Gargle/Mouthwash against Respiratory and Oral Tract Pathogens. *Infect. Dis. Ther.* 7, 249–259. doi:10.1007/s40121-018-0200-7
- Feng, M.-C., Lin, Y.-C., Chang, Y.-H., Chen, C.-H., Chiang, H.-C., Huang, L.-C., et al. (2019). The Mortality and the Risk of Aspiration Pneumonia Related with Dysphagia in Stroke Patients. *J. Stroke Cerebrovasc. Dis.* 28, 1381–1387. doi:10.1016/j.jstrokecerebrovasdis.2019.02.011
- Fourrier, F., Dubois, D., Pronnier, P., Herbecq, P., Leroy, O., Desmettre, T., et al. (2005). Effect of Gingival and Dental Plaque Antiseptic Decontamination on Nosocomial Infections Acquired in the Intensive Care Unit: A Double-Blind Placebo-Controlled Multicenter Study\*. *Crit. Care Med.* 33, 1728–1735. doi:10.1097/01.ccm.0000171537.03493.b0
- Fourrier, F., Duvivier, B., Boutigny, H., Roussel-Delvallez, M., and Chopin, C. (1998). Colonization of Dental Plaque: a Source of Nosocomial Infections in Intensive Care Unit Patients. *Crit. Care Med.* 26, 301–308. doi:10.1097/00003246-199802000-00032
- F. Sato, E., Choudhury, T., Nishikawa, T., and Inoue, M. (2008). Dynamic Aspect of Reactive Oxygen and Nitric Oxide in Oral Cavity. *J. Clin. Biochem. Nutr.* 42, 8–13. doi:10.3164/jcfn.2008002
- Gaeckle, N. T., Heyman, B., Criner, A. J., and Criner, G. J. (2018). Markers of Dental Health Correlate with Daily Respiratory Symptoms in COPD. *J. Copd F* 5, 97–105. doi:10.15326/jcopdf.5.2.2017.0159



- Galhardo, L. F., Ruivo, G. F., Santos, F. O., Ferreira, T. T., Santos, J., L Eão, M. V., et al. (2020). Impact of Oral Care and Antisepsis on the Prevalence of Ventilator-Associated Pneumonia. *Oral Health Prev. Dent* 18, 331–336. doi:10.3290/j.ohpd.a44443
- Geetha, C., Venkatesh, S. G., Fasciotto Dunn, B. H., and Gorr, S.-U. (2003). Expression and Anti-bacterial Activity of Human Parotid Secretory Protein (PSP). *Biochem. Soc. Trans.* 31, 815–818. doi:10.1042/bst0310815
- Genco, R. J., Grossi, S. G., Ho, A., Nishimura, F., and Murayama, Y. (2005). A Proposed Model Linking Inflammation to Obesity, Diabetes, and Periodontal Infections. *J. Periodontol.* 76 (Suppl. 11S), 2075–2084. doi:10.1902/jop.2005.76.11-S.2075
- Giuliano, K. K., Penoyer, D., Middleton, A., and Baker, D. (2021). Original Research: Oral Care as Prevention for Nonventilator Hospital-Acquired Pneumonia. *Am. J. Nurs.* 121, 24–33. doi:10.1097/01.naj.0000753468.99321.93
- Gomes-Filho, I. S., Passos, J. S., and Seixas Da Cruz, S. (2010). Respiratory Disease and the Role of Oral Bacteria. *J. Oral Microbiol.* 2, 1. doi:10.3402/jom.v2i0.5811
- González-Rubio Aguilar, P., Ávalos Arenas, V., Vega Gudiño, N. A., Moreno Herrera, S. D., Villa Guillén, M., Moyao-García, D., et al. (2019). The Impact of Tooth Brushing versus Tooth Brushing and Chlorhexidine Application to Avoid Postoperative Pneumonia in Children. *Am. J. Infect. Control.* 47, 1340–1345. doi:10.1016/j.ajic.2019.05.018
- Harrington, N., Prado, N., and Barry, S. (2016). Dental Treatment in Children with Asthma - a Review. *Br. Dent J.* 220, 299–302. doi:10.1038/sj.bdj.2016.220
- Hasan, N. A., Young, B. A., Minard-Smith, A. T., Saeed, K., Li, H., Heizer, E. M., et al. (2014). Microbial Community Profiling of Human Saliva Using Shotgun Metagenomic Sequencing. *PLoS One* 9, e97699. doi:10.1371/journal.pone.0097699
- Hayata, M., Watanabe, N., Tamura, M., Kamio, N., Tanaka, H., Nodomi, K., et al. (2019). The Periodontopathic Bacterium *Fusobacterium Nucleatum* Induced Proinflammatory Cytokine Production by Human Respiratory Epithelial Cell Lines and in the Lower Respiratory Organs in Mice. *Cell Physiol Biochem* 53, 49–61. doi:10.33594/000000120
- He, X., Hu, W., He, J., Guo, L., Lux, R., and Shi, W. (2011). Community-based Interference against Integration of *Pseudomonas aeruginosa* into Human Salivary Microbial Biofilm. *Mol. Oral Microbiol.* 26, 337–352. doi:10.1111/j.2041-1014.2011.00622.x
- Heo, S. M., Haase, E. M., Lesse, A. J., Gill, S. R., and Scannapieco, F. A. (2008). Genetic Relationships between Respiratory Pathogens Isolated from Dental Plaque and Bronchoalveolar Lavage Fluid from Patients in the Intensive Care Unit Undergoing Mechanical Ventilation. *Clin. Infect. Dis.* 47, 1562–1570. doi:10.1086/593193
- Hosgood, H. D., Cai, Q., Hua, X., Long, J., Shi, J., Wan, Y., et al. (2021). Variation in Oral Microbiome Is Associated with Future Risk of Lung Cancer Among Never-Smokers. *Thorax* 76, 256–263. doi:10.1136/thoraxjnl-2020-215542
- Iinuma, T., Arai, Y., Abe, Y., Takayama, M., Fukumoto, M., Fukui, Y., et al. (2015). Denture Wearing during Sleep Doubles the Risk of Pneumonia in the Very Elderly. *J. Dent Res.* 94, 28s–36s. doi:10.1177/0022034514552493
- Imai, K., and Tanaka, H. (2021). SARS-CoV-2 Infection and Significance of Oral Health Management in the Era of "the New Normal with COVID-19. *Int. J. Mol. Sci.* 22, 1. doi:10.3390/ijms22126527
- Inoue, K.-i., Takano, H., Koike, E., Yanagisawa, R., Oda, T., Tamura, H., et al. (2009a). Candida Soluble Cell wall  $\beta$ -glucan Facilitates Ovalbumin-Induced Allergic Airway Inflammation in Mice: Possible Role of Antigen-Presenting Cells. *Respir. Res.* 10, 68. doi:10.1186/1465-9921-10-68
- Inoue, K.-i., Takano, H., Oda, T., Yanagisawa, R., Tamura, H., Adachi, Y., et al. (2009b). Soluble Cell wall  $\beta$ -glucan of candida Induces/enhances Apoptosis and Oxidative Stress in Murine Lung. *Immunopharmacology and Immunotoxicology* 31, 140–145. doi:10.1080/08923970802534678
- Jain, M., Shah, R., Chandolia, B., Mathur, A., Chauhan, Y., Chawda, J., et al. (2016). The Oral Carriage of Candida in Oral Cancer Patients of Indian Origin Undergoing Radiotherapy And/or Chemotherapy. *J. Clin. Diagn. Res.* 10, Zc17–20. doi:10.7860/JCDR/2016/15702.7180
- Jhajharia, K., Mehta, L., Parolia, A., and Shetty, K. (2015). Biofilm in Endodontics: A Review. *J. Int. Soc. Prevent Communit Dent* 5, 1–12. doi:10.4103/2231-0762.151956
- Jia, C., Sun, M., Wang, W., Li, C., Li, X., and Zhang, X. (2020). Effect of Oral Plaque Control on Postoperative Pneumonia Following Lung Cancer Surgery. *Thorac. Cancer* 11, 1655–1660. doi:10.1111/1759-7714.13448
- Kamaguchi, A., Nakayama, K., Ichiyama, S., Nakamura, R., Watanabe, T., Ohta, M., et al. (2003). Effect of *Porphyromonas Gingivalis* Vesicles on Coaggregation of *Staphylococcus aureus* to Oral Microorganisms. *Curr. Microbiol.* 47, 485–491. doi:10.1007/s00284-003-4069-6
- Kanazuru, T., Sato, E. F., Nagata, K., Matsui, H., Watanabe, K., Kasahara, E., et al. (2010). Role of Hydrogen Generation by *Klebsiella pneumoniae* in the Oral Cavity. *J. Microbiol.* 48, 778–783. doi:10.1007/s12275-010-0149-z
- Kang, M. S., Lim, H. S., Oh, J. S., Lim, Y. J., Wuertz-Kozak, K., Harro, J. M., et al. (2017). Antimicrobial Activity of *Lactobacillus Salivarius* and *Lactobacillus Fermentum* against *Staphylococcus aureus*. *Pathog. Dis.* 75, 1. doi:10.1093/femspd/ftx009
- Khadka, S., Khan, S., King, A., Goldberg, L. R., Crocombe, L., and Bettiol, S. (2021). Poor Oral hygiene, Oral Microorganisms and Aspiration Pneumonia Risk in Older People in Residential Aged Care: a Systematic Review. *Age Ageing* 50, 81–87. doi:10.1093/ageing/afaa102
- Khalifa, M. A. A. A., Abouelkheir, H. M., Khodiar, S. E.-F., and Mohamed, G. A. M. (2014). Salivary Composition and Dental Caries Among Children Controlled Asthmatics. *Egypt. J. Chest Dis. Tuberculosis* 63, 777–788. doi:10.1016/j.jejcd.2014.05.003
- Kikutani, T., Tamura, F., Tashiro, H., Yoshida, M., Konishi, K., and Hamada, R. (2015). Relationship between Oral Bacteria Count and Pneumonia Onset in Elderly Nursing home Residents. *Geriatr. Gerontol. Int.* 15, 417–421. doi:10.1111/ggi.12286
- Kilian, M. (2018). The Oral Microbiome - Friend or Foe? *Eur. J. Oral Sci.* 126, 5–12. doi:10.1111/eos.12527
- Kimura, M., Tsuruta, S., and Yoshida, T. (1999). Differences in Cytokine Production by Peripheral Blood Mononuclear Cells (PBMC) between Patients with Atopic Dermatitis and Bronchial Asthma. *Clin. Exp. Immunol.* 118, 192–196. doi:10.1046/j.1365-2249.1999.01055.x
- Kinane, D. F., Galicia, J. C., Gorr, S. U., Stathopoulou, P. G., and Benakanakere, M. (2008). P. Gingivalis Interactions with Epithelial Cells. *Front. Biosci.* 13, 966–984. doi:10.2741/2736
- King, S. J., Whatmore, A. M., and Dowson, C. G. (2005). NanA, a Neuraminidase from *Streptococcus pneumoniae*, Shows High Levels of Sequence Diversity, at Least in Part through Recombination with *Streptococcus Oralis*. *J. Bacteriol.* 187, 5376–5386. doi:10.1128/jb.187.15.5376-5386.2005
- Kohn, W. G., Collins, A. S., Cleveland, J. L., Harte, J. A., Eklund, K. J., and Malvitz, D. M. (2003). Guidelines for Infection Control in Dental Health-Care Settings--2003. *MMWR Recomm Rep.* 52, 1–61.
- Komiyama, K., and Gibbons, R. J. (1984). Interbacterial Adherence between *Actinomyces viscosus* and Strains of *Streptococcus pyogenes*, *Streptococcus agalactiae*, and *Pseudomonas aeruginosa*. *Infect. Immun.* 44, 86–90. doi:10.1128/iai.44.1.86-90.1984
- Komiyama, K., Habbick, B. F., and Gibbons, R. J. (1987). Interbacterial Adhesion between *Pseudomonas aeruginosa* and Indigenous Oral Bacteria Isolated from Patients with Cystic Fibrosis. *Can. J. Microbiol.* 33, 27–32. doi:10.1139/m87-005
- Koulenti, D., Tsigou, E., and Rello, J. (2017). Nosocomial Pneumonia in 27 ICUs in Europe: Perspectives from the EU-VAP/CAP Study. *Eur. J. Clin. Microbiol. Infect. Dis.* 36, 1999–2006. doi:10.1007/s10096-016-2703-z
- Kovaleva, O. V., Romashin, D., Zborovskaya, I. B., Davydov, M. M., Shogenov, M. S., and Gratchev, A. (2019). Human Lung Microbiome on the Way to Cancer. *J. Immunol. Res.* 2019, 1394191. doi:10.1155/2019/1394191
- Kucukcokun, M., Baser, U., Oztekin, G., Kiyan, E., and Yalcin, F. (2013). Initial Periodontal Treatment for Prevention of Chronic Obstructive Pulmonary Disease Exacerbations. *J. Periodontol.* 84, 863–870. doi:10.1902/jop.2012.120399
- Kumar, P. S., Matthews, C. R., Joshi, V., De Jager, M., and Aspiras, M. (2011). Tobacco Smoking Affects Bacterial Acquisition and Colonization in Oral Biofilms. *Infect. Immun.* 79, 4730–4738. doi:10.1128/iai.05371-11
- Laurence, B., Mould-Millman, N.-K., Scannapieco, F. A., and Abron, A. (2015). Hospital Admissions for Pneumonia More Likely with Concomitant Dental Infections. *Clin. Oral Invest.* 19, 1261–1268. doi:10.1007/s00784-014-1342-y
- Leone, M., Bouadma, L., Bouhemad, B., Brissaud, O., Dager, S., Gibot, S., et al. (2018). Hospital-acquired Pneumonia in ICU. *Anaesth. Crit. Care Pain Med.* 37, 83–98. doi:10.1016/j.accpm.2017.11.006
- Lerrer, B., Lesman-Movshovich, E., and Gilboa-Garber, N. (2005). Comparison of the Antimicrobial Adhesion Potential of Human Body Fluid Glycoconjugates Using Fucose-Binding Lectin (PA-III) of *Pseudomonas aeruginosa* and *Ulex*

- Europaeus Lectin (UEA-I). *Curr. Microbiol.* 51, 202–206. doi:10.1007/s00284-005-4571-0
- Li, Q., Pan, C., Teng, D., Lin, L., Kou, Y., Haase, E. M., et al. (2014). Porphyromonas Gingivalis Modulates Pseudomonas Aeruginosa-Induced Apoptosis of Respiratory Epithelial Cells through the STAT3 Signaling Pathway. *Microbes Infect.* 16, 17–27. doi:10.1016/j.micinf.2013.10.006
- Li, X., Li, C., Liu, J.-c., Pan, Y.-p., and Li, Y.-g. (2018). *In Vitro* effect of Porphyromonas Gingivalis Combined with Influenza A Virus on Respiratory Epithelial Cells. *Arch. Oral Biol.* 95, 125–133. doi:10.1016/j.archoralbio.2018.04.003
- Lima, B. P., Hu, L. I., Vreeman, G. W., Weibel, D. B., and Lux, R. (2019). The Oral Bacterium Fusobacterium Nucleatum Binds Staphylococcus aureus and Alters Expression of the Staphylococcal Accessory Regulator sarA. *Microb. Ecol.* 78, 336–347. doi:10.1007/s00248-018-1291-0
- Little, J. W., Miller, C., and Rhodus, N. L. (2017). *Dental Management of the Medically Compromised Patient - E-Book*. Elsevier Health Sciences.
- Littman, A. J., White, E., Jackson, L. A., Thornquist, M. D., Gaydos, C. A., Goodman, G. E., et al. (2004). Chlamydia Pneumoniae Infection and Risk of Lung Cancer. *Cancer Epidemiol. Biomarkers Prev.* 13, 1624–1630.
- Maddi, A., Sabharwal, A., Violante, T., Manuballa, S., Genco, R., Patnaik, S., et al. (2019). The Microbiome and Lung Cancer. *J. Thorac. Dis.* 11, 280–291. doi:10.21037/jtd.2018.12.88
- Mahdi, L. H., Jabbar, H. S., and Auda, I. G. (2019). Antibacterial Immunomodulatory and Antibiofilm Triple Effect of Salivarin LHM against Pseudomonas aeruginosa Urinary Tract Infection Model. *Int. J. Biol. Macromolecules* 134, 1132–1144. doi:10.1016/j.ijbiomac.2019.05.181
- Main, B. E., Calman, K. C., Ferguson, M. M., Kaye, S. B., Macfarlane, T. W., Mairs, R. J., et al. (1984). The Effect of Cytotoxic Therapy on Saliva and Oral flora. *Oral Surg. Oral Med. Oral Pathol.* 58, 545–548. doi:10.1016/0030-4220(84)90077-x
- Mamani, M., Hashemi, S. H., Hajilooi, M., Saedi, F., Niayesh, A., and Fallah, M. (2012). Evaluation of Fibronectin and C-Reactive Protein Levels in Patients with Sepsis: a Case-Control Study. *Acta Med. Iran* 50, 404–410.
- Manning, J., Dunne, E. M., Wescombe, P. A., Hale, J. D. F., Mulholland, E. K., Tagg, J. R., et al. (2016). Investigation of Streptococcus Salivarius-Mediated Inhibition of Pneumococcal Adherence to Pharyngeal Epithelial Cells. *BMC Microbiol.* 16, 225. doi:10.1186/s12866-016-0843-z
- Mathews, S. A., Kurien, B. T., and Scofield, R. H. (2008). Oral Manifestations of Sjögren's Syndrome. *J. Dent Res.* 87, 308–318. doi:10.1177/154405910808700411
- Mauch, R. M., Rossi, C. L., Aiello, T. B., Ribeiro, J. D., Ribeiro, A. F., Høiby, N., et al. (2017). Secretory IgA Response against Pseudomonas aeruginosa in the Upper Airways and the Link with Chronic Lung Infection in Cystic Fibrosis. *Pathog. Dis.* 75, 1. doi:10.1093/femspd/ftx069
- Mehta, A., Sequeira, P. S., Sahoo, R. C., and Kaur, G. (2009). Is Bronchial Asthma a Risk Factor for Gingival Diseases? A Control Study. *N. Y. State. Dent J.* 75, 44–46.
- Merghni, A., Ben Nejma, M., Helali, I., Hentati, H., Bongiovanni, A., Lafont, F., et al. (2015). Assessment of Adhesion, Invasion and Cytotoxicity Potential of Oral Staphylococcus aureus Strains. *Microb. Pathogenesis* 86, 1–9. doi:10.1016/j.micpath.2015.05.010
- Miyashita, N., Fukano, H., Mouri, K., Fukuda, M., Yoshida, K., Kobashi, Y., et al. (2005). Community-acquired Pneumonia in Japan: a Prospective Ambulatory and Hospitalized Patient Study. *J. Med. Microbiol.* 54, 395–400. doi:10.1099/jmm.0.45920-0
- Moghaddam, S. J., Ochoa, C. E., Sethi, S., and Dickey, B. F. (2011). Nontypeable Haemophilus Influenzae in Chronic Obstructive Pulmonary Disease and Lung Cancer. *Copd* 6, 113–123. doi:10.2147/copd.s15417
- Mori, A., Ikeda, Y., Taniguchi, M., Aoyama, C., Maeda, Y., Hasegawa, M., et al. (2001). IL-5 Production by Peripheral Blood Th Cells of Adult Asthma Patients in Response to Candida Albicans Allergen. *Int. Arch. Allergy Immunol.* 125 (Suppl. 1), 48–50. doi:10.1159/000053853
- Muhlebach, M. S., Hatch, J. E., Einarsson, G. G., McGrath, S. J., Gilpin, D. F., Lavelle, G., et al. (2018a). Anaerobic Bacteria Cultured from Cystic Fibrosis Airways Correlate to Milder Disease: a Multisite Study. *Eur. Respir. J.* 52, 1. doi:10.1183/13993003.00242-2018
- Muhlebach, M. S., Zorn, B. T., Esther, C. R., Hatch, J. E., Murray, C. P., Turkovic, L., et al. (2018b). Initial Acquisition and Succession of the Cystic Fibrosis Lung Microbiome Is Associated with Disease Progression in Infants and Preschool Children. *Plos Pathog.* 14, e1006798. doi:10.1371/journal.ppat.1006798
- Nagaoka, K., Yanagihara, K., Harada, Y., Yamada, K., Migiyama, Y., Morinaga, Y., et al. (2013). Macrolides Inhibit Fusobacterium Nucleatum-Induced MUC5AC Production in Human Airway Epithelial Cells. *Antimicrob. Agents Chemother.* 57, 1844–1849. doi:10.1128/aac.02466-12
- Nagaoka, K., Yanagihara, K., Morinaga, Y., Nakamura, S., Harada, T., Hasegawa, H., et al. (2014). Prevotella Intermedia Induces Severe Bacteremic Pneumococcal Pneumonia in Mice with Upregulated Platelet-Activating Factor Receptor Expression. *Infect. Immun.* 82, 587–593. doi:10.1128/iai.00943-13
- Nishizawa, T., Niikura, Y., Akasaka, K., Watanabe, M., Kurai, D., Amano, M., et al. (2019). Pilot Study for Risk Assessment of Aspiration Pneumonia Based on Oral Bacteria Levels and Serum Biomarkers. *BMC Infect. Dis.* 19, 761. doi:10.1186/s12879-019-4327-2
- Ogrendik, M. (2009). Rheumatoid Arthritis Is Linked to Oral Bacteria: Etiological Association. *Mod. Rheumatol.* 19, 453–456. doi:10.3109/s10165-009-0194-9
- Okuda, K., Kimizuka, R., Abe, S., Kato, T., and Ishihara, K. (2005). Involvement of Periodontopathic Anaerobes in Aspiration Pneumonia. *J. Periodontol.* 76 (Suppl. 11S), 2154–2160. doi:10.1902/jop.2005.76.11.S.2154
- Pan, Y., Teng, D., Burke, A. C., Haase, E. M., and Scannapieco, F. A. (2009). Oral Bacteria Modulate Invasion and Induction of Apoptosis in HEP-2 Cells by Pseudomonas aeruginosa. *Microb. Pathogenesis* 46, 73–79. doi:10.1016/j.micpath.2008.10.012
- Parahitiyawa, N. B., Jin, L. J., Leung, W. K., Yam, W. C., and Samaranyake, L. P. (2009). Microbiology of Odontogenic Bacteremia: beyond Endocarditis. *Clin. Microbiol. Rev.* 22, 46–64. doi:10.1128/cmr.00028-08
- Parkins, M. D., Sibley, C. D., Surette, M. G., and Rabin, H. R. (2008). The Streptococcus Milleri Group—An Unrecognized Cause of Disease in Cystic Fibrosis: A Case Series and Literature Review. *Pediatr. Pulmonol.* 43, 490–497. doi:10.1002/ppul.20809
- Passariello, C., Puttini, M., Iebba, V., Pera, P., and Gigola, P. (2012). Influence of Oral Conditions on Colonization by Highly Toxicogenic Staphylococcus aureus Strains. *Oral Dis.* 18, 402–409. doi:10.1111/j.1601-0825.2011.01889.x
- Petelin, M., Naruishi, K., Shiomi, N., Mineshiba, J., Arai, H., Nishimura, F., et al. (2004). Systemic Up-Regulation of sTNFR2 and IL-6 in Porphyromonas Gingivalis Pneumonia in Mice. *Exp. Mol. Pathol.* 76, 76–81. doi:10.1016/j.yexmp.2003.09.002
- Poveda-Roda, R., Jiménez, Y., Carbonell, E., Gavalda, C., Margaix-Muñoz, M. M., and Sarrión-Pérez, G. (2008). Bacteremia Originating in the Oral Cavity. A Review. *Med. Oral Patol Oral Cir Bucal* 13, E355–E362.
- Pragman, A. A., Lyu, T., Baller, J. A., Gould, T. J., Kelly, R. F., Reilly, C. S., et al. (2018). The Lung Tissue Microbiota of Mild and Moderate Chronic Obstructive Pulmonary Disease. *Microbiome* 6, 7. doi:10.1186/s40168-017-0381-4
- Prasanna, S. (2011). Causal Relationship between Periodontitis and Chronic Obstructive Pulmonary Disease. *J. Indian Soc. Periodontol.* 15, 359–365. doi:10.4103/0972-124x.92570
- Prokopovic, V., Popovic, M., Andjelkovic, U., Marsavelski, A., Raskovic, B., Gavrovic-Jankulovic, M., et al. (2014). Isolation, Biochemical Characterization and Anti-bacterial Activity of BPIFA2 Protein. *Arch. Oral Biol.* 59, 302–309. doi:10.1016/j.archoralbio.2013.12.005
- Qian, Y., Yuan, W., Mei, N., Wu, J., Xu, Q., Lu, H., et al. (2020). Periodontitis Increases the Risk of Respiratory Disease Mortality in Older Patients. *Exp. Gerontol.* 133, 110878. doi:10.1016/j.exger.2020.110878
- Quagliarello, V., Ginter, S., Han, L., Van Ness, P., Allore, H., and Tinetti, M. (2005). Modifiable Risk Factors for Nursing home-acquired Pneumonia. *Clin. Infect. Dis.* 40, 1–6. doi:10.1086/426023
- Rivas Caldas, R., Le Gall, F., Revert, K., Rault, G., Virmaux, M., Gouriou, S., et al. (2015). Pseudomonas aeruginosa and Periodontal Pathogens in the Oral Cavity and Lungs of Cystic Fibrosis Patients: a Case-Control Study. *J. Clin. Microbiol.* 53, 1898–1907. doi:10.1128/jcm.00368-15
- Salsgiver, E. L., Fink, A. K., Knapp, E. A., Lipuma, J. J., Olivier, K. N., Marshall, B. C., et al. (2016). Changing Epidemiology of the Respiratory Bacteriology of Patients with Cystic Fibrosis. *Chest* 149, 390–400. doi:10.1378/chest.15-0676
- Santagati, M., Scillato, M., Patanè, F., Aiello, C., and Stefani, S. (2012). Bacteriocin-producing Oral Streptococci and Inhibition of Respiratory Pathogens. *FEMS Immunol. Med. Microbiol.* 65, 23–31. doi:10.1111/j.1574-695x.2012.00928.x

- Scannapieco, F. A. (1999). Role of Oral Bacteria in Respiratory Infection. *J. Periodontol.* 70, 793–802. doi:10.1902/jop.1999.70.7.793
- Scannapieco, F. A., and Shay, K. (2014). Oral Health Disparities in Older Adults. *Dental Clin. North America* 58, 771–782. doi:10.1016/j.cden.2014.06.005
- Scannapieco, F. A., Stewart, E. M., and Mylotte, J. M. (1992). Colonization of Dental Plaque by Respiratory Pathogens in Medical Intensive Care Patients. *Crit. Care Med.* 20, 740–745. doi:10.1097/00003246-199206000-00007
- Scannapieco, F. A., Wang, B., and Shiau, H. J. (2001). Oral Bacteria and Respiratory Infection: Effects on Respiratory Pathogen Adhesion and Epithelial Cell Proinflammatory Cytokine Production. *Ann. Periodontol.* 6, 78–86. doi:10.1902/annals.2001.6.1.78
- Schaub, B., Lauener, R., and Von Mutius, E. (2006). The many Faces of the hygiene Hypothesis. *J. Allergy Clin. Immunol.* 117, 969–977. quiz 978. doi:10.1016/j.jaci.2006.03.003
- Scofield, J. A., Duan, D., Zhu, F., and Wu, H. (2017). A Commensal streptococcus Hijacks a *Pseudomonas aeruginosa* Exopolysaccharide to Promote Biofilm Formation. *Plos Pathog.* 13, e1006300. doi:10.1371/journal.ppat.1006300
- Scofield, J. A., and Wu, H. (2016). Nitrite Reductase Is Critical for *Pseudomonas aeruginosa* Survival during Co-infection with the Oral Commensal Streptococcus Parasanguinis. *Microbiology (Reading)* 162, 376–383. doi:10.1099/mic.0.000226
- Scofield, J. A., and Wu, H. (2015). Oral Streptococci and Nitrite-Mediated Interference of *Pseudomonas aeruginosa*. *Infect. Immun.* 83, 101–107. doi:10.1128/iai.02396-14
- Seed, P. C. (2014). The Human Mycobiome. *Cold Spring Harbor Perspect. Med.* 5, a019810. doi:10.1101/cshperspect.a019810
- Seedorf, H., Griffin, N. W., Ridaura, V. K., Reyes, A., Cheng, J., Rey, F. E., et al. (2014). Bacteria from Diverse Habitats Colonize and Compete in the Mouse Gut. *Cell* 159, 253–266. doi:10.1016/j.cell.2014.09.008
- Sibley, C. D., Parkins, M. D., Rabin, H. R., Duan, K., Norgaard, J. C., and Surette, M. G. (2008). A Polymicrobial Perspective of Pulmonary Infections Exposes an Enigmatic Pathogen in Cystic Fibrosis Patients. *Proc. Natl. Acad. Sci.* 105, 15070–15075. doi:10.1073/pnas.0804326105
- Sikorska, H., and Smoragiewicz, W. (2013). Role of Probiotics in the Prevention and Treatment of Meticillin-Resistant *Staphylococcus aureus* Infections. *Int. J. Antimicrob. Agents* 42, 475–481. doi:10.1016/j.ijantimicag.2013.08.003
- Souto, R., Silva-Boghossian, C. M., and Colombo, A. P. V. (2014). Prevalence of *Pseudomonas aeruginosa* and Acinetobacter Spp. in Subgingival Biofilm and Saliva of Subjects with Chronic Periodontal Infection. *Braz. J. Microbiol.* 45, 495–501. doi:10.1590/s1517-83822014000200017
- Stenstrom, M., Wendt, L.-K., Koch, G., Oldaesus, G., and Birkhed, D. (2008). Oral Health in Preschool Children with Asthma. *Int. J. Paediatr. Dent* 18, 243–250. doi:10.1111/j.1365-263x.2008.00921.x
- Stoney, K. (2010). Ventilator-Associated Pneumonia. *Crit. Care Nurs.* Q. 33, 339–347. doi:10.1097/cnq.0b013e3181f649a6
- Sumi, Y., Miura, H., Michiawaki, Y., Nagasawa, S., and Nagaya, M. (2007). Colonization of Dental Plaque by Respiratory Pathogens in Dependent Elderly. *Arch. Gerontol. Geriatr.* 44, 119–124. doi:10.1016/j.archger.2006.04.004
- Tada, A., and Hanada, N. (2010). Opportunistic Respiratory Pathogens in the Oral Cavity of the Elderly. *FEMS Immunol. Med. Microbiol.* 60, 1–17. doi:10.1111/j.1574-695x.2010.00709.x
- Tagg, J. R. (2004). Prevention of Streptococcal Pharyngitis by Anti-Streptococcus Pyogenes Bacteriocin-like Inhibitory Substances (BLIS) Produced by Streptococcus Salivarius. *Indian J. Med. Res.* 119 (Suppl. 1), 13–16.
- Tagg, J. R. (2009). Streptococcal Bacteriocin-like Inhibitory Substances: Some Personal Insights into the Bacteriocin-like Activities Produced by Streptococci Good and Bad. *Probiotics Antimicro. Prot.* 1, 60–66. doi:10.1007/s12602-008-9002-7
- Tan, L., Wang, H., Li, C., and Pan, Y. (2014). 16S rDNA-Based Metagenomic Analysis of Dental Plaque and Lung Bacteria in Patients with Severe Acute Exacerbations of Chronic Obstructive Pulmonary Disease. *J. Periodont Res.* 49, 760–769. doi:10.1111/jre.12159
- Teshome, A., and Yitayeh, A. (2016). Relationship between Periodontal Disease and Preterm Low Birth Weight: Systematic Review. *Pan Afr. Med. J.* 24, 215. doi:10.11604/pamj.2016.24.215.8727
- Thamadolok, S., Roche-Håkansson, H., Håkansson, A. P., and Ruhl, S. (2016). Absence of Capsule Reveals Glycan-Mediated Binding and Recognition of Salivary Mucin MUC7 by Streptococcus Pneumoniae. *Mol. Oral Microbiol.* 31, 175–188. doi:10.1111/omi.12113
- Thibodeau, P. H., and Butterworth, M. B. (2013). Proteases, Cystic Fibrosis and the Epithelial Sodium Channel (ENaC). *Cell Tissue Res* 351, 309–323. doi:10.1007/s00441-012-1439-z
- To, K. K., Tsang, O. T., Leung, W. S., Tam, A. R., Wu, T. C., Lung, D. C., et al. (2020). Temporal Profiles of Viral Load in Posterior Oropharyngeal Saliva Samples and Serum Antibody Responses during Infection by SARS-CoV-2: an Observational Cohort Study. *Lancet Infect. Dis.* 20, 565–574. doi:10.1016/S1473-3099(20)30196-1
- Tunney, M. M., Field, T. R., Moriarty, T. F., Patrick, S., Doering, G., Muhlebach, M. S., et al. (2008). Detection of Anaerobic Bacteria in High Numbers in Sputum from Patients with Cystic Fibrosis. *Am. J. Respir. Crit. Care Med.* 177, 995–1001. doi:10.1164/rccm.200708-1151oc
- Verma, D., Garg, P. K., and Dubey, A. K. (2018). Insights into the Human Oral Microbiome. *Arch. Microbiol.* 200, 525–540. doi:10.1007/s00203-018-1505-3
- Walls, T., Power, D., and Tagg, J. (2003). Bacteriocin-like Inhibitory Substance (BLIS) Production by the normal flora of the Nasopharynx: Potential to Protect against Otitis media? *J. Med. Microbiol.* 52, 829–833. doi:10.1099/jmm.0.05259-0
- Wand, M. E., Bock, L. J., Bonney, L. C., and Sutton, J. M. (2017). Mechanisms of Increased Resistance to Chlorhexidine and Cross-Resistance to Colistin Following Exposure of *Klebsiella pneumoniae* Clinical Isolates to Chlorhexidine. *Antimicrob. Agents Chemother.* 61, 16. doi:10.1128/AAC.01162-16
- Wang, Y., Ren, B., Zhou, X., Liu, S., Zhou, Y., Li, B., et al. (2017). Growth and Adherence of *Staphylococcus aureus* Were Enhanced through the PGE2 Produced by the Activated COX-2/PGE2 Pathway of Infected Oral Epithelial Cells. *PLoS One* 12, e0177166. doi:10.1371/journal.pone.0177166
- Wang, Z. M. (2019). Relationship between Oral Microecological Imbalance and General Health. *Zhonghua Kou Qiang Yi Xue Za Zhi* 54, 145–150. doi:10.3760/cma.j.issn.1002-0098.2019.03.001
- Wang, Z., Zhou, X., Zhang, J., Zhang, L., Song, Y., Hu, F. B., et al. (2009). Periodontal Health, Oral Health Behaviours, and Chronic Obstructive Pulmonary Disease. *J. Clin. Periodontol.* 36, 750–755. doi:10.1111/j.1600-051x.2009.01448.x
- Wescombe, P. A., Heng, N. C., Burton, J. P., Chilcott, C. N., and Tagg, J. R. (2009). Streptococcal Bacteriocins and the Case for Streptococcus Salivarius as Model Oral Probiotics. *Future Microbiol.* 4, 819–835. doi:10.2217/fmb.09.61
- Whiley, R. A., Fleming, E. V., Makhija, R., and Waite, R. D. (2015). Environment and Colonisation Sequence Are Key Parameters Driving Cooperation and Competition between *Pseudomonas aeruginosa* Cystic Fibrosis Strains and Oral Commensal Streptococci. *PLoS One* 10, e0115513. doi:10.1371/journal.pone.0115513
- Whiley, R. A., Sheikh, N. P., Mushtaq, N., Hagi-Pavli, E., Personne, Y., Javadi, D., et al. (2014). Differential Potentiation of the Virulence of the *Pseudomonas aeruginosa* Cystic Fibrosis liverpool Epidemic Strain by Oral Commensal Streptococci. *J. Infect. Dis.* 209, 769–780. doi:10.1093/infdis/jit568
- Woods, D. E. (1987). Role of Fibronectin in the Pathogenesis of Gram-Negative Bacillary Pneumonia. *Rev. Infect. Dis.* 9 (Suppl. 4), S386–S390. doi:10.1093/clinids/9.supplement\_4.s386
- Worlitzsch, D., Rintelen, C., Böhm, K., Wollschläger, B., Merkel, N., Borneff-Lipp, M., et al. (2009). Antibiotic-resistant Obligate Anaerobes during Exacerbations of Cystic Fibrosis Patients. *Clin. Microbiol. Infect.* 15, 454–460. doi:10.1111/j.1469-0691.2008.02659.x
- Wu, X., Chen, J., Xu, M., Zhu, D., Wang, X., Chen, Y., et al. (2017). 16S rDNA Analysis of Periodontal Plaque in Chronic Obstructive Pulmonary Disease and Periodontitis Patients. *J. Oral Microbiol.* 9, 1324725. doi:10.1080/20002297.2017.1324725
- Xu, H., Zhong, L., Deng, J., Peng, J., Dan, H., Zeng, X., et al. (2020). High Expression of ACE2 Receptor of 2019-nCoV on the Epithelial Cells of Oral Mucosa. *Int. J. Oral Sci.* 12, 8. doi:10.1038/s41368-020-0074-x
- Yamasaki, K., Kawasumi, T., Yatera, K., Fukuda, K., Noguchi, S., Nagata, S., et al. (2013). Significance of Anaerobes and Oral Bacteria in Community-Acquired Pneumonia. *PLoS One* 8, e63103. doi:10.1371/journal.pone.0063103
- Yan, X., Yang, M., Liu, J., Gao, R., Hu, J., Li, J., et al. (2015). Discovery and Validation of Potential Bacterial Biomarkers for Lung Cancer. *Am. J. Cancer Res.* 5, 3111–3122.
- Yang, J., Mu, X., Wang, Y., Zhu, D., Zhang, J., Liang, C., et al. (2018). Dysbiosis of the Salivary Microbiome Is Associated with Non-smoking Female Lung Cancer and

- Correlated with Immunocytochemistry Markers. *Front. Oncol.* 8, 520. doi:10.3389/fonc.2018.00520
- Zeng, X.-T., Tu, M.-L., Liu, D.-Y., Zheng, D., Zhang, J., and Leng, W. (2012). Periodontal Disease and Risk of Chronic Obstructive Pulmonary Disease: a Meta-Analysis of Observational Studies. *PLoS One* 7, e46508. doi:10.1371/journal.pone.0046508
- Zeng, X.-T., Xia, L.-Y., Zhang, Y.-G., Li, S., Leng, W.-D., and Kwong, J. S. W. (2016). Periodontal Disease and Incident Lung Cancer Risk: A Meta-Analysis of Cohort Studies. *J. Periodontol.* 87, 1158–1164. doi:10.1902/jop.2016.150597
- Zhou, X., Han, J., Liu, Z., Song, Y., Wang, Z., and Sun, Z. (2014). Effects of Periodontal Treatment on Lung Function and Exacerbation Frequency in Patients with Chronic Obstructive Pulmonary Disease and Chronic Periodontitis: a 2-year Pilot Randomized Controlled Trial. *J. Clin. Periodontol.* 41, 564–572. doi:10.1111/jcpe.12247
- Zhou, X., Wang, J., Liu, W., Huang, X., Song, Y., Wang, Z., et al. (2020). Periodontal Status and Microbiologic Pathogens in Patients with Chronic Obstructive Pulmonary Disease and Periodontitis: A Case-Control Study. *Copd* 15, 2071–2079. doi:10.2147/copd.s266612

**Conflict of Interest:** The authors declare that the research was conducted in the absence of any commercial or financial relationships that could be construed as a potential conflict of interest.

**Publisher's Note:** All claims expressed in this article are solely those of the authors and do not necessarily represent those of their affiliated organizations, or those of the publisher, the editors and the reviewers. Any product that may be evaluated in this article, or claim that may be made by its manufacturer, is not guaranteed or endorsed by the publisher.

Copyright © 2022 Dong, Li, Wang, Chen, Zu, Zhou and Guo. This is an open-access article distributed under the terms of the Creative Commons Attribution License (CC BY). The use, distribution or reproduction in other forums is permitted, provided the original author(s) and the copyright owner(s) are credited and that the original publication in this journal is cited, in accordance with accepted academic practice. No use, distribution or reproduction is permitted which does not comply with these terms.



# Advantages of publishing in Frontiers



## OPEN ACCESS

Articles are free to read  
for greatest visibility  
and readership



## FAST PUBLICATION

Around 90 days  
from submission  
to decision



## HIGH QUALITY PEER-REVIEW

Rigorous, collaborative,  
and constructive  
peer-review



## TRANSPARENT PEER-REVIEW

Editors and reviewers  
acknowledged by name  
on published articles

## Frontiers

Avenue du Tribunal-Fédéral 34  
1005 Lausanne | Switzerland

Visit us: [www.frontiersin.org](http://www.frontiersin.org)

Contact us: [frontiersin.org/about/contact](http://frontiersin.org/about/contact)



## REPRODUCIBILITY OF RESEARCH

Support open data  
and methods to enhance  
research reproducibility



## DIGITAL PUBLISHING

Articles designed  
for optimal readership  
across devices



## FOLLOW US

@frontiersin



## IMPACT METRICS

Advanced article metrics  
track visibility across  
digital media



## EXTENSIVE PROMOTION

Marketing  
and promotion  
of impactful research



## LOOP RESEARCH NETWORK

Our network  
increases your  
article's readership